

**Other uses, including reproduction and distribution, or selling or licensing copies, or posting to personal, institutional or third party websites are prohibited.**

**In most cases authors are permitted to post their version of the article (e.g. in Word or Tex form) to their personal website or institutional repository. Authors requiring further information regarding Elsevier's archiving and manuscript policies are encouraged to visit:**

<http://www.elsevier.com/copyright>



# KANTBP: A program for computing energy levels, reaction matrix and radial wave functions in the coupled-channel hyperspherical adiabatic approach <sup>☆</sup>

O. Chuluunbaatar <sup>a,\*</sup>, A.A. Gusev <sup>a</sup>, A.G. Abrashkevich <sup>b</sup>, A. Amaya-Tapia <sup>c</sup>, M.S. Kaschiev <sup>d</sup>,  
S.Y. Larsen <sup>e</sup>, S.I. Vinitisky <sup>a</sup>

<sup>a</sup> Joint Institute for Nuclear Research, Dubna, 141980 Moscow region, Russia

<sup>b</sup> IBM Toronto Lab, 8200 Warden Avenue, Markham, ON L6G 1C7, Canada

<sup>c</sup> Centro de Ciencias Fisicas, UNAM, Cuernavaca, Morelos, Mexico

<sup>d</sup> Institute of Mathematics and Informatics, Sofia, Bulgaria

<sup>e</sup> Temple University, Philadelphia, USA

Received 26 June 2006; accepted 20 May 2007

Available online 12 June 2007

## Abstract

A FORTRAN 77 program is presented which calculates energy values, reaction matrix and corresponding radial wave functions in a coupled-channel approximation of the hyperspherical adiabatic approach. In this approach, a multi-dimensional Schrödinger equation is reduced to a system of the coupled second-order ordinary differential equations on the finite interval with homogeneous boundary conditions of the third type. The resulting system of radial equations which contains the potential matrix elements and first-derivative coupling terms is solved using high-order accuracy approximations of the finite-element method. As a test desk, the program is applied to the calculation of the energy values and reaction matrix for an exactly solvable 2D-model of three identical particles on a line with pair zero-range potentials.

## Program summary

*Program title:* KANTBP

*Catalogue identifier:* ADZH\_v1\_0

*Program summary URL:* [http://cpc.cs.qub.ac.uk/summaries/ADZH\\_v1\\_0.html](http://cpc.cs.qub.ac.uk/summaries/ADZH_v1_0.html)

*Program obtainable from:* CPC Program Library, Queen's University, Belfast, N. Ireland

*Licensing provisions:* Standard CPC licence, <http://cpc.cs.qub.ac.uk/licence/licence.html>

*No. of lines in distributed program, including test data, etc.:* 4224

*No. of bytes in distributed program, including test data, etc.:* 31 232

*Distribution format:* tar.gz

*Programming language:* FORTRAN 77

*Computer:* Intel Xeon EM64T, Alpha 21264A, AMD Athlon MP, Pentium IV Xeon, Opteron 248, Intel Pentium IV

*Operating system:* OC Linux, Unix AIX 5.3, SunOS 5.8, Solaris, Windows XP

*RAM:* depends on (a) the number of differential equations; (b) the number and order of finite-elements; (c) the number of hyperradial points; and (d) the number of eigensolutions required. Test run requires 30 MB

*Classification:* 2.1, 2.4

*External routines:* GAULEG and GAUSSJ [W.H. Press, B.F. Flanery, S.A. Teukolsky, W.T. Vetterley, Numerical Recipes: The Art of Scientific Computing, Cambridge University Press, Cambridge, 1986]

<sup>☆</sup> This paper and its associated computer program are available via the Computer Physics Communications homepage on ScienceDirect (<http://www.sciencedirect.com/science/journal/00104655>).

\* Corresponding author.

E-mail address: [chuka@jinr.ru](mailto:chuka@jinr.ru) (O. Chuluunbaatar).

**Nature of problem:** In the hyperspherical adiabatic approach [J. Macek, J. Phys. B 1 (1968) 831–843; U. Fano, Rep. Progr. Phys. 46 (1983) 97–165; C.D. Lin, Adv. Atom. Mol. Phys. 22 (1986) 77–142], a multi-dimensional Schrödinger equation for a two-electron system [A.G. Abrashkevich, D.G. Abrashkevich, M. Shapiro, Comput. Phys. Comm. 90 (1995) 311–339] or a hydrogen atom in magnetic field [M.G. Dimova, M.S. Kaschiev, S.I. Vinitsky, J. Phys. B 38 (2005) 2337–2352] is reduced by separating the radial coordinate  $\rho$  from the angular variables to a system of second-order ordinary differential equations which contain potential matrix elements and first-derivative coupling terms. The purpose of this paper is to present the finite-element method procedure based on the use of high-order accuracy approximations for calculating approximate eigensolutions for such systems of coupled differential equations.

**Solution method:** The boundary problems for coupled differential equations are solved by the finite-element method using high-order accuracy approximations [A.G. Abrashkevich, D.G. Abrashkevich, M.S. Kaschiev, I.V. Puzynin, Comput. Phys. Comm. 85 (1995) 40–64]. The generalized algebraic eigenvalue problem  $\mathbf{A}\mathbf{F} = \mathbf{E}\mathbf{B}\mathbf{F}$  with respect to pair unknowns  $(E, \mathbf{F})$  arising after the replacement of the differential problem by the finite-element approximation is solved by the subspace iteration method using the SSPACE program [K.J. Bathe, Finite Element Procedures in Engineering Analysis, Englewood Cliffs, Prentice–Hall, New York, 1982]. The generalized algebraic eigenvalue problem  $(\mathbf{A} - \mathbf{E}\mathbf{B})\mathbf{F} = \lambda\mathbf{D}\mathbf{F}$  with respect to pair unknowns  $(\lambda, \mathbf{F})$  arising after the corresponding replacement of the scattering boundary problem in open channels at fixed energy value,  $E$ , is solved by the  $\mathbf{LDL}^T$  factorization of symmetric matrix and back-substitution methods using the DECOMP and REDBAK programs, respectively [K.J. Bathe, Finite Element Procedures in Engineering Analysis, Englewood Cliffs, Prentice–Hall, New York, 1982]. As a test desk, the program is applied to the calculation of the energy values and reaction matrix for an exactly solvable 2D-model of three identical particles on a line with pair zero-range potentials described in [Yu. A. Kuperin, P.B. Kurasov, Yu.B. Melnikov, S.P. Merkuriev, Ann. Phys. 205 (1991) 330–361; O. Chuluunbaatar, A.A. Gusev, S.Y. Larsen, S.I. Vinitsky, J. Phys. A 35 (2002) L513–L525; N.P. Mehta, J.R. Shepard, Phys. Rev. A 72 (2005) 032728-1-11; O. Chuluunbaatar, A.A. Gusev, M.S. Kaschiev, V.A. Kaschieva, A. Amaya-Tapia, S.Y. Larsen, S.I. Vinitsky, J. Phys. B 39 (2006) 243–269]. For this benchmark model the needed analytical expressions for the potential matrix elements and first-derivative coupling terms, their asymptotics and asymptotics of radial solutions of the boundary problems for coupled differential equations have been produced with help of a MAPLE computer algebra system.

**Restrictions:** The computer memory requirements depend on:

- (a) the number of differential equations;
- (b) the number and order of finite-elements;
- (c) the total number of hyperradial points; and
- (d) the number of eigensolutions required.

Restrictions due to dimension sizes may be easily alleviated by altering PARAMETER statements (see Long Write-Up and listing for details). The user must also supply subroutine POTCAL for evaluating potential matrix elements. The user should supply subroutines ASYMEV (when solving the eigenvalue problem) or ASYMSC (when solving the scattering problem) that evaluate the asymptotics of the radial wave functions at the right boundary point in case of a boundary condition of the third type, respectively.

**Running time:** The running time depends critically upon:

- (a) the number of differential equations;
- (b) the number and order of finite-elements;
- (c) the total number of hyperradial points on interval  $[0, \rho_{\max}]$ ; and
- (d) the number of eigensolutions required.

The test run which accompanies this paper took 28.48 s without calculation of matrix potentials on the Intel Pentium IV 2.4 GHz.

© 2007 Elsevier B.V. All rights reserved.

PACS: 02.30.Hq; 02.60.Jh; 02.60.Lj; 03.65.Nk; 31.15.Ja; 31.15.Pf; 34.50.-s; 34.80.Bm

**Keywords:** Eigenvalue and multi-channel scattering problems; Kantorovich method; Finite element method; R-matrix calculations; Hyperspherical coordinates; Multi-channel adiabatic approximation; Ordinary differential equations; High-order accuracy approximations

## 1. Introduction

Development of stable numerical methods for solution of elliptic partial differential equation is one of the main problems of modern computational physics. Therefore elaboration of efficient, stable and high-accurate numerical schemes for solving the Schrödinger equation in a multi-dimensional space is an important task. Numerical solution of such equation has wide applications in various quantum-mechanical problems such as the modern calculations of the weakly bound states and elastic scattering in a system of three helium atoms considered as point particles with some short range pair potentials, i.e. a trimer of helium atoms [1], or in processes of ionization and recombination of antihydrogen in magnetic trap of modern laser physics experiments [2–4]. The above mentioned experiments require computer modeling of dynamics of exotic few-body Coulomb systems in external laser pulsed fields [5–7].

There are two conditions for elaborating numerical methods: to be stable and to have a high accuracy of calculations. The resulting system of ordinary second-order differential equations obtained after reduction of a multi-dimensional boundary problem

to a one-dimensional one is solved using high-order approximations of the Finite Element Method (FEM). In order to guarantee high-order accuracy of numerical solutions, the relevant potential matrix elements should be evaluated with the same level of accuracy as approximate solutions.

One of the most popular and widely used approaches for solving the quantum-mechanical three-body problem with pair Coulomb and point interactions is the adiabatic representation method [8–10]. In the framework of the hyperspherical coordinates formulation of this method [9–14], the hyperradius  $\rho$  is treated as a slowly varying adiabatic variable, analogous to the internuclear distance in the Born–Oppenheimer approximation for molecules [8]. From the mathematical point of view this approach is well known as the Kantorovich method (KM) for the reduction of a multi-dimension boundary problem to the one-dimensional one by using a set of solutions of an auxiliary parametric eigenvalue problem [15]. These solutions are obtained for a given set of values of the adiabatic variable, which plays here a role of an external parameter. The convergence of the adiabatic expansion in the hyperspherical coordinates is higher than the ones used in most conventional approaches based on the independent electron model. This is due to the fact that collective variables such as hyperradius  $\rho = \sqrt{r_1^2 + r_2^2}$  and hyperangle  $\alpha = \arctan(r_2/r_1)$  allow for more natural and accurate accounting of electron correlations in an atomic system (see, e.g., [9,12,16–18]) than the independent electron coordinates,  $r_1$  and  $r_2$ .

An essential part in the implementation of the KM is the computation of variable coefficients (potential matrix elements) for the resulting system of the ordinary second-order differential equations. These coefficients are the integrals over eigenfunctions and their derivatives with respect to the adiabatic variable. In real applications, an efficient and stable computation of derivatives of the adiabatic eigenfunctions and the corresponding integrals with the accuracy comparable with the one achieved for adiabatic eigenfunctions presents a serious challenge for most of numerical approaches involved in various types of calculations within the adiabatic representation method [19].

This problem has been successfully solved in the paper [20]. A new method for computing variable coefficients (potential matrix elements of radial coupling) of a resulting system of ordinary second-order differential equations has been elaborated. It allows the calculation of the coefficients with the same precision as the adiabatic functions obtained as solutions of an auxiliary parametric eigenvalue problem. In the method proposed, a new boundary parametric problem with respect to unknown derivatives of eigenfunctions in the adiabatic variable (hyperradius) was formulated. An efficient, fast and stable algorithm for solving the boundary problem with the same accuracy for the adiabatic eigenfunctions and their derivatives was proposed. The method developed was tested on a parametric eigenvalue problem for a hydrogen atom on a three-dimensional sphere which has an analytical solution [21]. The accuracy, efficiency and robustness of the algorithm were studied in details. The method was also applied to the computation of the ground state energy of the helium atom and negative hydrogen ion [20], and low-excited states of a hydrogen atom in strong magnetic field [22]. The results obtained have shown an excellent agreement with the results of calculations by other methods.

The method of calculating the potential matrix elements of radial coupling suggested in paper [20] can be used in scattering calculations using some appropriate propagation scheme. In scattering calculations, in order to eliminate derivatives of the adiabatic surface eigenfunctions in hyperradius, the diabatic-by-sector approach is widely used [23]. The price for using this approximation is a slower convergence of the diabatic basis and therefore a larger number of hyperradial equations to be solved in order to get the required accuracy of the  $\mathbf{S}$ -matrix elements [24,25]. Matrix elements computed by the method [20] can be directly incorporated in the popular hyperspherical close-coupling scheme. Applications of the method to scattering problems can be very useful and promising.

In this work we present program KANTBP for solving the eigenvalue and scattering problems for the multi-dimensional Schrödinger equation using the KM approach. In this method the multi-dimensional boundary problem is reduced to a system of ordinary differential equations of the second order with variable coefficients on a semi-axis with the help of expansion of the solution over a set of orthogonal solutions of an auxiliary parametric eigenvalue problem. Reduction of the boundary problem on a finite interval is implemented in the program with help of the Dirichlet, Neumann and third type boundary conditions in calculations of the eigenvalue problem for bound states and the third type boundary condition in a form appropriate for the  $\mathbf{R}$ -matrix calculations of the multi-channel scattering problem [26–28]. Then a FEM is applied to construct numerical schemes for solving corresponding boundary problem for a system of ordinary differential equations with an accuracy of order  $O(h^{p+1})$  in the grid step  $h$ . The order of approximation,  $p$ , depends on the smoothness of required solution. Note that variable coefficients of ordinary differential equations and the corresponding solutions can have a long-range asymptotic behavior [29]. That is why one has to be very careful in the formulation of the boundary problems under consideration. As a benchmark, we consider known exactly solvable 2D-model of three identical particles on a line with pair zero-range potentials [30–32] based on an adequate formulation of spectral problems and corresponding numerical schemes. For this benchmark model the needed analytical expressions for the potential matrix elements and first-derivative coupling terms, their asymptotics and asymptotics of radial solutions of the boundary problems for coupled differential equations have been produced with help of a MAPLE computer algebra system.

The paper is organized as follows. In Section 2 we give a brief overview of the problem. The construction of the finite-element high-order schemes is discussed in Section 3. A description of the KANTBP program is given in Section 4. Subroutine units are briefly described in Section 5. Test desk is discussed in Section 6.



## 2. Statement of the problem

In many cases the solution of a multi-dimensional quantum-mechanical problem is reduced to a solution of the time-independent Schrödinger equation for wave function  $\Psi(\rho, \Omega)$

$$(\mathbf{H} + \mathbf{U}(\rho, \Omega))\Psi(\rho, \Omega) = E\Psi(\rho, \Omega), \quad (1)$$

where  $\mathbf{H}$  is the  $d > 1$  dimensional Hamiltonian,  $\mathbf{U}(\rho, \Omega)$  is the given potential,  $E$  is the energy of a system,  $\rho$  is the hyperradius, and  $\Omega$  is the set of angular coordinates which describe the internal motion of system on sphere  $S^{d-1}(\Omega)$ . In the close coupling approximation, known in mathematics as the KM [15] the partial wave function  $\Psi_i(\rho, \Omega)$  is expanded over the one-parametric basis functions  $\{B_j(\Omega; \rho)\}_{j=1}^N$ :

$$\Psi_i(\rho, \Omega) = \sum_{j=1}^N B_j(\Omega; \rho) \chi_j^{(i)}(\rho). \quad (2)$$

In Eq. (2), the vector-functions  $\chi^{(i)}(\rho) = (\chi_1^{(i)}(\rho), \dots, \chi_N^{(i)}(\rho))^T$  are unknown, and the surface functions  $\mathbf{B}(\Omega; \rho) = (B_1(\Omega; \rho), \dots, B_N(\Omega; \rho))^T$  is an orthonormal basis with respect to the set of angular coordinates  $\Omega$  for each value of hyperradius  $\rho$  which is treated here as a given parameter. In the Kantorovich approach [15], the functions  $B_j(\Omega; \rho)$  are determined as solutions of the following parametric eigenvalue problem:

$$\left(-\frac{1}{\rho^2} \hat{\mathbf{A}}_\Omega^2 + 2\mathbf{U}(\rho, \Omega)\right) B_j(\Omega; \rho) = \varepsilon_j(\rho) B_j(\Omega; \rho), \quad (3)$$

where  $\hat{\mathbf{A}}_\Omega^2$  is the generalized self-adjoint angular momentum operator. The eigenfunctions of this problem satisfy the same boundary conditions in angular variable  $\Omega$  for  $\Psi_i(\rho, \Omega)$  and are normalized as follows

$$\langle B_i(\Omega; \rho) | B_j(\Omega; \rho) \rangle_\Omega = \int B_i^*(\Omega; \rho) B_j(\Omega; \rho) d\Omega = \delta_{ij}, \quad (4)$$

where “\*” denotes the complex conjugate and  $\delta_{ij}$  is the Kroneker symbol.

After minimizing the Rayleigh–Ritz variational functional (see [20]), and using the expansion (2) equation (1) is reduced to a finite set of  $N$  ordinary second-order differential equations for the  $\chi(\rho) \equiv \chi^{(i)}(\rho)$

$$(\mathbf{L} - 2E\mathbf{I})\chi(\rho) \equiv \left(-\frac{1}{\rho^{d-1}} \mathbf{I} \frac{d}{d\rho} \rho^{d-1} \frac{d}{d\rho} + \mathbf{V}(\rho) + \mathbf{Q}(\rho) \frac{d}{d\rho} + \frac{1}{\rho^{d-1}} \frac{d\rho^{d-1} \mathbf{Q}(\rho)}{d\rho} - 2E\mathbf{I}\right) \chi(\rho) = 0. \quad (5)$$

Here  $\mathbf{I}$ ,  $\mathbf{V}(\rho)$  and  $\mathbf{Q}(\rho)$  are matrices of dimension  $N \times N$  whose elements are given by the relation

$$\begin{aligned} V_{ij}(\rho) &= H_{ij}(\rho) + \frac{\varepsilon_i(\rho) + \varepsilon_j(\rho)}{2} \delta_{ij}, \quad I_{ij} = \delta_{ij}, \\ H_{ij}(\rho) &= H_{ji}(\rho) = \left\langle \frac{\partial B_i(\Omega; \rho)}{\partial \rho} \left| \frac{\partial B_j(\Omega; \rho)}{\partial \rho} \right\rangle_\Omega, \\ Q_{ij}(\rho) &= -Q_{ji}(\rho) = -\left\langle B_i(\Omega; \rho) \left| \frac{\partial B_j(\Omega; \rho)}{\partial \rho} \right\rangle_\Omega. \end{aligned} \quad (6)$$

Let us consider the general radial homogeneous boundary conditions for the partial function  $\Psi_i(\rho, \Omega)$  at the endpoints of the finite interval  $0 < \rho < \rho_{\max} < \infty$ :

$$\mu_1 \frac{\partial \Psi_i(\rho, \Omega)}{\partial \rho} - \lambda_1 \Psi_i(\rho, \Omega) = 0, \quad \rho = 0, \quad \Omega \in S^{d-1}(\Omega), \quad (7)$$

$$\mu_2 \frac{\partial \Psi_i(\rho, \Omega)}{\partial \rho} - \lambda_2 \Psi_i(\rho, \Omega) = 0, \quad \rho = \rho_{\max}, \quad \Omega \in S^{d-1}(\Omega), \quad (8)$$

where  $\mu_1, \lambda_1$  are some constants and  $\mu_2 = \mu_2(\rho_{\max}), \lambda_2 = \lambda_2(\rho_{\max})$  are some numbers depending on the  $\rho = \rho_{\max}$ . Since the adiabatic functions form a complete set, one can alternatively require that projections of (7) and (8) onto all adiabatic functions fulfill

$$\left\langle B_j(\Omega; \rho) \left| \mu_l \frac{\partial \Psi_i(\rho, \Omega)}{\partial \rho} - \lambda_l \Psi_i(\rho, \Omega) \right\rangle_\Omega = 0, \quad l = 1, 2, \quad (9)$$

using which we obtain the following matrix homogeneous boundary conditions

$$\mu_l \left( \mathbf{I} \frac{d}{d\rho} - \mathbf{Q}(\rho) \right) \chi(\rho) - \lambda_l \chi(\rho) = 0, \quad l = 1, 2. \quad (10)$$

From here for  $l = 1$ , the left boundary condition imposed on function  $\chi(\rho)$  at  $\rho = 0$  has one of the following form:

1. if  $\lim_{\rho \rightarrow 0} \rho^{d-1} |V_{ii}(\rho)| = \infty$ , we have the Dirichlet boundary condition

$$\chi(0) = 0, \quad (11)$$

2. if  $\lim_{\rho \rightarrow 0} \rho^{d-1} |V_{ii}(\rho)| < \infty$ , we have the Neumann type boundary condition

$$\lim_{\rho \rightarrow 0} \rho^{d-1} \left( \mathbf{I} \frac{d}{d\rho} - \mathbf{Q}(\rho) \right) \chi(\rho) = 0. \quad (12)$$

### 2.1. The bound state case

For the bound state problem the energy  $E$  and radial wave function  $\chi(\rho)$  are calculated. For large  $\rho$  the radial wave function  $\chi(\rho)$  satisfies the exponentially or power decreased asymptotic behavior. From Eq. (10) for  $l = 2$ , the right boundary condition imposed on function  $\chi(\rho)$  at  $\rho = \rho_{\max}$  has one of the following form:

- if  $\mu_2 = 0$ , we have the Dirichlet boundary condition

$$\chi(\rho_{\max}) = 0, \quad (13)$$

- if  $\lambda_2 = 0$ , we have the Neumann type boundary condition

$$\left( \mathbf{I} \frac{d}{d\rho} - \mathbf{Q}(\rho) \right) \chi(\rho) = 0, \quad (14)$$

- if  $\mu_2 \neq 0$  and  $\lambda_2 \neq 0$ , we have the homogeneous third type boundary condition

$$\left( \mathbf{I} \frac{d}{d\rho} - \mathbf{Q}(\rho) \right) \chi(\rho) = \lambda \chi(\rho), \quad (15)$$

i.e.,  $\lambda \equiv \lambda(\rho) = \lambda_2(\rho)/\mu_2(\rho)$  and  $\chi(\rho)$  should be the eigenvalue and corresponding eigenvector of the above eigenvalue problem. After substituting (15) in Eq. (5) we obtain the following eigenvalue problem at  $\rho = \rho_{\max}$

$$(\mathbf{V}(\rho) + \mathbf{Q}^2(\rho)) \hat{\chi}(\rho) = \mu(\rho) \hat{\chi}(\rho), \quad \hat{\chi}(\rho) = \chi(\rho), \quad (16)$$

where eigenvalues  $\mu(\rho)$  and  $\lambda(\rho)$  satisfy the following relation

$$\mu(\rho) = \frac{1}{\rho^{d-1}} \frac{d\rho^{d-1}\lambda(\rho)}{d\rho} + \lambda^2(\rho) + 2E. \quad (17)$$

Note that, the eigenvalue  $\mu(\rho)$  should be a fixed value for the any  $E$  and  $\lambda(\rho)$  at  $\rho = \rho_{\max}$  and this condition plays a very important role in the future calculations.

### 2.2. The scattering case

Most physical matrix potentials  $\mathbf{V}(\rho)$  and  $\mathbf{Q}(\rho)$  satisfy the following asymptotic behavior at large  $\rho$

$$V_{ij}(\rho) = \sum_{l=2} \frac{v_{ij}^{(l)}}{\rho^l}, \quad Q_{ij}(\rho) = \sum_{l=1} \frac{q_{ij}^{(l)}}{\rho^l}, \quad \text{for } i \neq j, \quad (18)$$

$$V_{jj}(\rho) = \epsilon_j - \frac{2Z_j}{\rho} + \frac{l_j(l_j + d - 2)}{\rho^2} + \sum_{l=3} \frac{v_{jj}^{(l)}}{\rho^l}, \quad (19)$$

where  $\epsilon_1 \leq \dots \leq \epsilon_N$  are the threshold energy values. For the scattering problem we need to obtain the reaction matrix  $\mathbf{K}$  and radial wave functions at given momentum  $2E > \epsilon_1$ . For large  $\rho$  the radial wave functions  $\{\chi^{(i)}(\rho)\}_{i=1}^{N_o}$  satisfy the following asymptotic conditions

$$\chi_j^{(i)}(\rho) \rightarrow \frac{\sin(w_j(\rho))\delta_{ji} + \cos(w_j(\rho))K_{ji}}{\sqrt{k_j\rho^{d-1}}} + O(\rho^{-(d+1)/2}), \quad j = \overline{1, N_o}, \quad (20)$$

$$\chi_j^{(i)}(\rho) \rightarrow \frac{\exp(-v_j(\rho))}{\sqrt{q_j\rho^{d-1}}} + O(\rho^{-(d+1)/2} \exp(-v_j(\rho))), \quad j = \overline{N_o + 1, N}, \quad (21)$$

where

$$\begin{aligned} w_j(\rho) &= k_j \rho + \frac{Z_j}{k_j} \ln(2k_j \rho) - \frac{2l_j + d - 3}{4} \pi + \delta_j^c, \\ \delta_j^c &= \arg \Gamma\left(\frac{2l_j + d - 1}{2} - i \frac{Z_j}{k_j}\right), \\ v_j(\rho) &= q_j \rho - \frac{Z_j}{q_j} \ln(2q_j \rho). \end{aligned} \quad (22)$$

Here  $N_o$  is the number of open channels,  $\delta_j^c$  is the known Coulomb phase shift,  $\mathbf{K} = \{K_{ji}\}_{ji=1}^{N_o}$  is the required reaction matrix,  $k_j = \sqrt{2E - \epsilon_j}$  for  $j = \overline{1, N_o}$  and  $q_j = \sqrt{\epsilon_j - 2E}$  for  $j = \overline{N_o + 1, N}$ .

Let us consider the quadratic functional

$$\begin{aligned} \Xi(\Phi, E, \rho_{\max}) &\equiv \int_0^{\rho_{\max}} \Phi^T(\rho)(\mathbf{I} - 2E\mathbf{I})\Phi(\rho)\rho^{d-1} d\rho \\ &= \Pi(\Phi, E, \rho_{\max}) - \rho_{\max}^{d-1} \Phi^T(\rho_{\max})\Phi(\rho_{\max})\Lambda, \end{aligned} \quad (23)$$

where  $\Pi(\Phi, E, \rho_{\max})$  is the symmetric functional

$$\begin{aligned} \Pi(\Phi, E, \rho_{\max}) &= \int_0^{\rho_{\max}} \left( \frac{d\Phi^T(\rho)}{d\rho} \frac{d\Phi(\rho)}{d\rho} + \Phi^T(\rho)\mathbf{V}(\rho)\Phi(\rho) \right. \\ &\quad \left. + \Phi^T(\rho)\mathbf{Q}(\rho) \frac{d\Phi(\rho)}{d\rho} - \frac{d\Phi(\rho)^T}{d\rho} \mathbf{Q}(\rho)\Phi(\rho) - 2E\Phi^T(\rho)\Phi(\rho) \right) \rho^{d-1} d\rho, \end{aligned} \quad (24)$$

and  $\Phi(\rho) = \{\chi^{(i)}(\rho)\}_{i=1}^{N_o}$  is the matrix-solution of dimension  $N \times N_o$  which satisfies the following eigenvalue problem at  $\rho = \rho_{\max}$

$$\frac{d\Phi(\rho)}{d\rho} - \mathbf{Q}(\rho)\Phi(\rho) = \Phi(\rho)\Lambda, \quad \Lambda = \{\delta_{ij}\lambda^{(i)}\}_{ij=1}^{N_o}. \quad (25)$$

After using FEM, Eq. (23) can be approximated by the following problem at  $\rho = \rho_{\max}$  (see details in Section 3)

$$\mathbf{G}(\rho)\Phi(\rho) = \frac{d\Phi(\rho)}{d\rho} - \mathbf{Q}(\rho)\Phi(\rho), \quad (26)$$

where  $\mathbf{G}(\rho)$  is the symmetric matrix of dimension  $N \times N$ . From here, we obtain the relation between  $\Phi(\rho)$  and its derivative at  $\rho = \rho_{\max}$

$$\frac{d\Phi(\rho)}{d\rho} = \mathbf{R}(\rho)\Phi(\rho), \quad \mathbf{R}(\rho) = \mathbf{G}(\rho) + \mathbf{Q}(\rho). \quad (27)$$

After that,  $\Phi(\rho)$  and its derivative can be rewritten via the two independent fundamental regular and irregular asymptotic matrix-solutions  $\Phi_{\text{reg}}(\rho) = \{\chi_{\text{reg}}^{(i)}(\rho)\}_{i=1}^{N_o}$ ,  $\Phi_{\text{irr}}(\rho) = \{\chi_{\text{irr}}^{(i)}(\rho)\}_{i=1}^{N_o}$  of Eq. (5) and their derivatives at  $\rho = \rho_{\max}$

$$\Phi(\rho) = \Phi_{\text{reg}}(\rho) + \Phi_{\text{irr}}(\rho)\mathbf{K}, \quad \frac{d\Phi(\rho)}{d\rho} = \frac{d\Phi_{\text{reg}}(\rho)}{d\rho} + \frac{d\Phi_{\text{irr}}(\rho)}{d\rho}\mathbf{K}. \quad (28)$$

Using formula (27), we obtain the following matrix equation for the reaction matrix  $\mathbf{K}$

$$\left( \frac{d\Phi_{\text{irr}}(\rho)}{d\rho} - \mathbf{R}(\rho)\Phi_{\text{irr}}(\rho) \right) \mathbf{K} = - \left( \frac{d\Phi_{\text{reg}}(\rho)}{d\rho} - \mathbf{R}(\rho)\Phi_{\text{reg}}(\rho) \right). \quad (29)$$

In addition, it should be noted that the regular and irregular functions satisfy the generalized Wronskian relation for large  $\rho$

$$\mathbf{Wr}(\mathbf{Q}(\rho); \Phi_{\text{irr}}(\rho), \Phi_{\text{reg}}(\rho)) = \mathbf{I}_{oo}, \quad (30)$$

where  $\mathbf{Wr}(\bullet; \mathbf{a}(\rho), \mathbf{b}(\rho))$  is a generalized Wronskian with a long derivative defined as

$$\mathbf{Wr}(\bullet; \mathbf{a}(\rho), \mathbf{b}(\rho)) = \rho^{d-1} \left[ \mathbf{a}^T(\rho) \left( \frac{d\mathbf{b}(\rho)}{d\rho} - \bullet \mathbf{b}(\rho) \right) - \left( \frac{d\mathbf{a}(\rho)}{d\rho} - \bullet \mathbf{a}(\rho) \right)^T \mathbf{b}(\rho) \right]. \quad (31)$$

This Wronskian will be used to estimate a desirable accuracy of the above expansion. Here  $\mathbf{I}_{oo}$  is the unit matrix of dimension  $N_o \times N_o$  and Eq. (30) at  $\rho = \rho_{\max}$  is equivalent to

$$\mathbf{Wr}(\mathbf{R}(\rho); \Phi_{\text{irr}}(\rho), \Phi_{\text{reg}}(\rho)) = \mathbf{Wr}(\mathbf{Q}(\rho); \Phi_{\text{irr}}(\rho), \Phi_{\text{reg}}(\rho)). \quad (32)$$

Note that, when some channels are closed, the left and right matrices of Eq. (29) are rectangle matrices. Therefore, we obtain the following formula for the reaction matrix  $\mathbf{K}$

$$\mathbf{K} = -\mathbf{X}^{-1}(\rho_{\max})\mathbf{Y}(\rho_{\max}), \quad (33)$$

where

$$\begin{aligned} \mathbf{X}(\rho) &= \left( \frac{d\Phi_{\text{irr}}(\rho)}{d\rho} - \mathbf{R}(\rho)\Phi_{\text{irr}}(\rho) \right)_{oo}, \\ \mathbf{Y}(\rho) &= \left( \frac{d\Phi_{\text{reg}}(\rho)}{d\rho} - \mathbf{R}(\rho)\Phi_{\text{reg}}(\rho) \right)_{oo}, \end{aligned} \quad (34)$$

are the square matrices of dimension  $N_o \times N_o$  depended on the open–open matrix (channels).

### 2.3. Construction of the regular and irregular matrix-solutions

We can construct the regular and irregular matrix-solutions by various methods (see [33–37]). For example, we can find regular and irregular matrix-solutions  $\Phi_{\text{reg}}(\rho)$ ,  $\Phi_{\text{irr}}(\rho)$  of Eq. (5) with components  $\chi_{\text{reg}}^{(i)}(\rho) = (\chi_{1i}^{\text{reg}}(\rho), \dots, \chi_{Ni}^{\text{reg}}(\rho))^T$  and  $\chi_{\text{irr}}^{(i)}(\rho) = (\chi_{1i}^{\text{irr}}(\rho), \dots, \chi_{Ni}^{\text{irr}}(\rho))^T$  using the following asymptotic form for large  $\rho$

$$\begin{aligned} \chi_{ji}^{\text{reg}}(\rho) &= \frac{\sin(w_i(\rho))}{\sqrt{k_i \rho^{d-1}}} \sum_{l=0} \frac{s_{ji}^{(l,1)}}{\rho^l} + \frac{\cos(w_i(\rho))}{\sqrt{k_i \rho^{d-1}}} \sum_{l=0} \frac{c_{ji}^{(l,1)}}{\rho^l}, \\ \chi_{ji}^{\text{irr}}(\rho) &= \frac{\cos(w_i(\rho))}{\sqrt{k_i \rho^{d-1}}} \sum_{l=0} \frac{c_{ji}^{(l,2)}}{\rho^l} + \frac{\sin(w_i(\rho))}{\sqrt{k_i \rho^{d-1}}} \sum_{l=0} \frac{s_{ji}^{(l,2)}}{\rho^l}, \end{aligned} \quad (35)$$

with initial data

$$s_{ji}^{(0,1)} = \delta_{ji}, \quad c_{ji}^{(0,1)} = 0, \quad c_{ji}^{(0,2)} = \delta_{ji}, \quad s_{ji}^{(0,2)} = 0. \quad (36)$$

Substituting expansions (18), (19) and (35) into Eq. (5) and equating expressions of  $\sin(w_i(\rho))$ ,  $\cos(w_i(\rho))$ , and again equating coefficients of expansion for the same powers of  $\rho$ , we arrive to a set of recurrence relations with respect to unknown coefficients  $s_{ji}^{(l,1)}$ ,  $s_{ji}^{(l,2)}$  and  $c_{ji}^{(l,1)}$ ,  $c_{ji}^{(l,2)}$ . By means of initial data (36) we have a step-by-step procedure for determining of series coefficients  $s_{ji}^{(l,1)}$ ,  $s_{ji}^{(l,2)}$  and  $c_{ji}^{(l,1)}$ ,  $c_{ji}^{(l,2)}$  [38,39].

### 3. High-order approximations of the finite-element method

In order to solve numerically the Sturm–Liouville problem for Eq. (5) subject to the corresponding boundary conditions from Eqs. (11), (12) and (13), (14), (15), (25) the high-order approximations of the FEM [40,41] elaborated in our previous paper [42] have been used. Such high-order approximations of the FEM have been proved [42] to be very accurate, stable, and efficient for a wide set of quantum-mechanical problems. Computational schemes of the High-order of accuracy are derived from the Rayleigh–Ritz variational functional for the bound state problem

$$\mathcal{R}_b(\chi, E, \lambda) = \left\{ \int_0^{\rho_{\max}} \sum_{i,j=1}^N [\chi H \chi]_{ij} \rho^{d-1} d\rho - \lambda \rho_{\max}^{d-1} \sum_{j=1}^N \chi_j^2(\rho_{\max}) \right\} \left\{ \int_0^{\rho_{\max}} \sum_{j=1}^N \chi_j^2(\rho) \rho^{d-1} d\rho \right\}^{-1}, \quad (37)$$

and for the scattering problem with  $\chi(\rho) \equiv \chi^{(i)}(\rho)$  and  $\lambda \equiv \lambda^{(i)}$

$$\mathcal{R}_s(\chi, \lambda) = \left\{ \int_0^{\rho_{\max}} \sum_{i,j=1}^N [\chi(H - 2E)\chi]_{ij} \rho^{d-1} d\rho \right\} \left\{ \rho_{\max}^{d-1} \sum_{j=1}^N \chi_j^2(\rho_{\max}) \right\}^{-1}, \quad (38)$$

on the basis of the FEM. Here

$$\begin{aligned} [\chi H \chi]_{ij} &= \chi'_i(\rho) \chi'_j(\rho) \delta_{ij} + \chi_i(\rho) V_{ij}(\rho) \chi_j(\rho) + Q_{ij}(\rho) [\chi_i(\rho) \chi'_j(\rho) - \chi'_i(\rho) \chi_j(\rho)], \\ [\chi(H - 2E)\chi]_{ij} &= [\chi H \chi]_{ij} - 2E \chi_i(\rho) \chi_j(\rho) \delta_{ij}, \end{aligned} \quad (39)$$

and symbol “'” denotes a derivative in  $\rho$ .

The general idea of the FEM in one-dimensional space is to divide interval  $[0, \rho_{\max}]$  into many small domains called elements. The size of elements can be defined very freely so that physical properties can be taken into account.

Now we cover the interval  $\Delta = [0, \rho_{\max}]$  by a system of  $n$  subintervals  $\Delta_j = [\rho_{j-1}, \rho_j]$  in such a way that  $\Delta = \bigcup_{j=1}^n \Delta_j$ . In each subinterval  $\Delta_j$  the nodes

$$\rho_{j,r}^p = \rho_{j-1} + \frac{h_j}{p}r, \quad h_j = \rho_j - \rho_{j-1}, \quad r = \overline{0, p}, \quad (40)$$

and the Lagrange elements  $\{\phi_{j,r}^p(\rho)\}_{r=0}^p$

$$\phi_{j,r}^p(\rho) = \prod_{i=0, i \neq r}^p \frac{(\rho - \rho_{j,i}^p)}{(\rho_{j,r}^p - \rho_{j,i}^p)} \quad (41)$$

are determined. By means of the Lagrange elements  $\phi_{j,r}^p(\rho)$ , we define a set of local functions  $N_l(\rho)$  as follows:

$$N_l^p(\rho) = \begin{cases} \begin{cases} \phi_{1,0}^p(\rho), & \rho \in \Delta_1, \\ 0, & \rho \notin \Delta_1, \end{cases} & l = 0, \\ \begin{cases} \phi_{j,r}^p(\rho), & \rho \in \Delta_j, \\ 0, & \rho \notin \Delta_j, \end{cases} & l = r + p(j-1), \quad r = \overline{1, p-1}, \\ \begin{cases} \phi_{j,p}^p(\rho), & \rho \in \Delta_j, \\ \phi_{j+1,0}^p(\rho), & \rho \in \Delta_{j+1}, \\ 0, & \rho \notin \Delta_j \cup \Delta_{j+1}, \end{cases} & l = jp, \quad j = \overline{1, n-1}, \\ \begin{cases} \phi_{n,p}^p(\rho), & \rho \in \Delta_n, \\ 0, & \rho \notin \Delta_n, \end{cases} & l = np. \end{cases} \quad (42)$$

The functions  $\{N_l^p(\rho)\}_{l=0}^L$ ,  $L = np$ , form a basis in the space of polynomials of the  $p$ th order. Now, we approximate each function  $\chi_\mu(\rho)$  by a finite sum of local functions  $N_l^p(\rho)$

$$\chi_\mu(\rho) = \sum_{l=0}^L \chi_\mu^l N_l^p(\rho), \quad \chi_\mu^l \equiv \chi_\mu^l(\rho_{j,r}^p). \quad (43)$$

For the bound state problem, after substituting expansion (43) into the variational functional (37) and minimizing it [40,41] we obtain that vector-solution  $\chi^h$  is the eigenvector of the generalized eigenvalue problem

$$(\mathbf{A}^p - \lambda^h \mathbf{M}) \chi^h = 2E^h \mathbf{B}^p \chi^h. \quad (44)$$

Here  $\mathbf{M}$  is a diagonal matrix with zero elements, except the last  $N$  elements that are equal  $\rho_{\max}^{d-1}$ , and in case of the Dirichlet and Neumann type boundary conditions  $\lambda^h \equiv 0$ . For the third type of boundary condition we use the following additional condition (17)

$$\mu = \frac{1}{\rho^{d-1}} \frac{d\rho^{d-1}\lambda^h}{d\rho} + (\lambda^h)^2 + 2E^h, \quad (45)$$

where  $\mu$  is the first eigenvalue of the problem (16). In this case we use the following iterative scheme for solutions  $\lambda \equiv \lambda^h$ ,  $E \equiv E^h$  and  $\chi \equiv \chi^h$

$$\begin{aligned} (\mathbf{A}^p - \lambda^{(j-1)} \mathbf{M}) \chi^{(j-1)} &= 2E^{(j-1)} \mathbf{B}^p \chi^{(j-1)}, \\ (\lambda^{(j)})^2 &= \mu - \frac{d\lambda^{(j-1)}}{d\rho} - \frac{d-1}{\rho_{\max}} \lambda^{(j-1)} - 2E^{(j-1)}, \end{aligned} \quad (46)$$

with initial value  $\lambda^{(0)}$ .

To solve the scattering problem at a fixed value of energy  $E$ , after substituting expansion (43) into the variational functional (38) and minimizing it [40,41] we obtain that matrix-solution  $\Phi^h \equiv ((\chi^{(1)})^h, \dots, (\chi^{(N_o)})^h)$  is a set of eigenvectors of a special eigenvalue problem

$$\mathbf{G}^p \Phi^h \equiv (\mathbf{A}^p - 2E\mathbf{B}^p) \Phi^h = \mathbf{M} \Phi^h \Lambda^h, \quad \Lambda^h = \{\delta_{ij}(\lambda^{(i)})^h\}_{i,j=1}^{N_o}, \quad (47)$$

where  $\mathbf{M}^p$  is a diagonal matrix with zero elements except the last  $N$  elements equal to  $\rho_{\max}^{d-1}$ . Eq. (47) can be rewritten in the following form

$$\begin{pmatrix} \mathbf{G}_{aa}^p & \mathbf{G}_{ab}^p \\ \mathbf{G}_{ba}^p & \mathbf{G}_{bb}^p \end{pmatrix} \begin{pmatrix} \Phi_a^h \\ \Phi_b^h \end{pmatrix} = \rho_{\max}^{d-1} \begin{pmatrix} 0 & 0 \\ 0 & \mathbf{I} \end{pmatrix} \begin{pmatrix} \Phi_a^h \\ \Phi_b^h \end{pmatrix} \Lambda^h, \quad \Phi^h = \begin{pmatrix} \Phi_a^h \\ \Phi_b^h \end{pmatrix}, \quad (48)$$

where  $\Phi_a^h$  and  $\Phi_b^h \equiv \Phi(\rho_{\max})$  are the matrix-solutions of dimension  $(LN - N) \times N_o$  and  $N \times N_o$ , respectively. From here, we obtain the following eigenvalue problem with respect to  $\Phi_b^h$  and  $\Lambda^h$ , of nonhomogeneous problem with respect to  $\Phi_b^h$  with right-hand side



from Eq. (25)

$$(\mathbf{G}_{bb}^p - \mathbf{G}_{ba}^p (\mathbf{G}_{aa}^p)^{-1} \mathbf{G}_{ab}^p) \boldsymbol{\Phi}_b^h = \rho_{\max}^{d-1} \boldsymbol{\Phi}_b^h \boldsymbol{\Lambda}^h \equiv \rho_{\max}^{d-1} \left( \frac{d\boldsymbol{\Phi}_b^h}{d\rho} - \mathbf{Q}(\rho_{\max}) \boldsymbol{\Phi}_b^h \right), \quad (49)$$

and explicit expression for component,  $\boldsymbol{\Phi}_a^h$ ,

$$\boldsymbol{\Phi}_a^h = -(\mathbf{G}_{aa}^p)^{-1} \mathbf{G}_{ab}^p \boldsymbol{\Phi}_b^h. \quad (50)$$

From Eqs. (27) and (49) we can obtain the relation between  $\boldsymbol{\Phi}_b^h$  and its derivative

$$\begin{aligned} \frac{d\boldsymbol{\Phi}_b^h}{d\rho} &= \mathbf{R}(\rho_{\max}) \boldsymbol{\Phi}_b^h, \\ \mathbf{R}(\rho_{\max}) &= \rho_{\max}^{1-d} (\mathbf{G}_{bb}^p - \mathbf{G}_{ba}^p (\mathbf{G}_{aa}^p)^{-1} \mathbf{G}_{ab}^p) + \mathbf{Q}(\rho_{\max}), \end{aligned} \quad (51)$$

i.e. we have found the required  $\mathbf{R}(\rho_{\max})$  matrix without calculation of eigenvalue  $\boldsymbol{\Lambda}^h$  and corresponding eigenvector  $\boldsymbol{\Phi}^h$  of the eigenvalue problem (47). For calculating Eq. (51) consider the following auxiliary system of algebraic equation, as the determinant of the matrix  $\mathbf{G}^p$  nonzero,

$$\begin{pmatrix} \mathbf{G}_{aa}^p & \mathbf{G}_{ab}^p \\ \mathbf{G}_{ba}^p & \mathbf{G}_{bb}^p \end{pmatrix} \begin{pmatrix} \mathbf{F}_a^p \\ \mathbf{F}_b^p \end{pmatrix} = \rho_{\max}^{d-1} \begin{pmatrix} 0 \\ \mathbf{I} \end{pmatrix}. \quad (52)$$

The above equation has solutions

$$\mathbf{F}_a^p = -(\mathbf{G}_{aa}^p)^{-1} \mathbf{G}_{ab}^p \mathbf{F}_b^p, \quad \mathbf{F}_b^p = \rho_{\max}^{d-1} (\mathbf{G}_{bb}^p - \mathbf{G}_{ba}^p (\mathbf{G}_{aa}^p)^{-1} \mathbf{G}_{ab}^p)^{-1}. \quad (53)$$

From here, our required  $\mathbf{R}(\rho_{\max})$  matrix is equal to

$$\mathbf{R}(\rho_{\max}) = (\mathbf{F}_b^p)^{-1} + \mathbf{Q}(\rho_{\max}), \quad (54)$$

and required solution  $\boldsymbol{\Phi}$  is calculated by formulae (50) and (53)

$$\boldsymbol{\Phi}_a^h = \mathbf{F}_a^p (\mathbf{F}_b^p)^{-1} \boldsymbol{\Phi}_b^h, \quad \boldsymbol{\Phi}_b^h = \boldsymbol{\Phi}_{\text{reg}}(\rho_{\max}) + \boldsymbol{\Phi}_{\text{irr}}(\rho_{\max}) \mathbf{K}, \quad (55)$$

where reaction matrix  $\mathbf{K}$  is evaluated from (33) and asymptotics of solution  $\boldsymbol{\Phi}_{\text{reg}}(\rho) = \{\boldsymbol{\chi}_{\text{reg}}^{(i)}(\rho)\}_{i=1}^{N_o}$ ,  $\boldsymbol{\Phi}_{\text{irr}}(\rho) = \{\boldsymbol{\chi}_{\text{irr}}^{(i)}(\rho)\}_{i=1}^{N_o}$  are determined in (28).

Let  $E_m$  and  $\boldsymbol{\chi}_m(\rho)$  be the exact solutions of Eq. (44) and  $E_m^h$  and  $\boldsymbol{\chi}_m^h(\rho)$  be the corresponding numerical solutions. Then the following estimations are valid [40]

$$|E_m^h - E_m| \leq c_1 |E_m| h^{2p}, \quad \|\boldsymbol{\chi}_m^h(\rho) - \boldsymbol{\chi}_m(\rho)\|_0 \leq c_2 |E_m| h^{p+1}, \quad (56)$$

where  $h$  is the maximal step of the finite-element grid,  $m$  is the number of the corresponded solution, and the positive constants  $c_1$  and  $c_2$  do not depend on step  $h$ . Similar estimations are valid for approximate values of the eigenvalue  $(\lambda^{(i)})^h$  and corresponding solution  $(\boldsymbol{\chi}^{(i)}(\rho))^h$ . The stiffness matrix  $\mathbf{A}^p$  and the mass matrix  $\mathbf{B}^p$  are symmetric and have a banded structure, and  $\mathbf{B}^p$  matrix is positively defined. They have the following form

$$\mathbf{A}^p = \sum_{j=1}^n \mathbf{a}_j^p, \quad \mathbf{B}^p = \sum_{j=1}^n \mathbf{b}_j^p, \quad (57)$$

where the local matrices  $\mathbf{a}_j^p$  and  $\mathbf{b}_j^p$  are calculated as

$$\begin{aligned} (\mathbf{a}_j^p)_{\mu\nu}^{qr} &= \int_{-1}^{+1} \left\{ \delta_{\mu\nu} \frac{4}{h_j^2} (\phi_{j,q}^p)'(\rho) (\phi_{j,r}^p)'(\rho) + V_{\mu\nu}(\rho) \phi_{j,q}^p(\rho) \phi_{j,r}^p(\rho) \right. \\ &\quad \left. + Q_{\mu\nu}(\rho) [\phi_{j,q}^p(\rho) (\phi_{j,r}^p)'(\rho) - (\phi_{j,q}^p)'(\rho) \phi_{j,r}^p(\rho)] \frac{2}{h_j} \right\} \rho^{d-1} \frac{h_j}{2} d\eta, \end{aligned}$$

$$(\mathbf{b}_j^p)_{\mu\nu}^{qr} = \delta_{\mu\nu} \int_{-1}^{+1} \phi_{j,q}^p(\rho) \phi_{j,r}^p(\rho) \rho^{d-1} \frac{h_j}{2} d\eta, \quad (58)$$

$$\rho = \rho_{j-1} + 0.5h_j(1 + \eta), \quad q, r = \overline{0, p}, \quad \mu, \nu = \overline{1, N}.$$

Integrals (58) are evaluated using the Gaussian quadrature formulae

$$\begin{aligned} (\mathbf{a}_j^p)_{\mu\nu}^{qr} &= \sum_{g=0}^p \left\{ \delta_{\mu\nu} \frac{4}{h_j^2} (\phi_{j,q}^p)'(\rho_g) (\phi_{j,r}^p)'(\rho_g) + V_{\mu\nu}(\rho_g) \phi_{j,q}^p(\rho_g) \phi_{j,r}^p(\rho_g) \right. \\ &\quad \left. + Q_{\mu\nu}(\rho_g) [\phi_{j,q}^p(\rho_g) (\phi_{j,r}^p)'(\rho_g) - (\phi_{j,q}^p)'(\rho_g) \phi_{j,r}^p(\rho_g)] \frac{2}{h_j} \right\} \rho_g^{d-1} \frac{h_j}{2} w_g, \\ (\mathbf{b}_j^p)_{\mu\nu}^{qr} &= \sum_{g=0}^p \delta_{\mu\nu} \phi_{j,q}^p(\rho_g) \phi_{j,r}^p(\rho_g) \rho_g^{d-1} \frac{h_j}{2} w_g, \end{aligned} \quad (59)$$

where  $\rho_g = \rho_{j-1} + 0.5h_j(1 + \eta_g)$ ,  $\eta_g$  and  $w_g$ ,  $g = \overline{0, p}$  are the Gaussian nodes and weights.

This way the following solution strategy can be used: since we know functions  $\mathbf{V}(\rho)$  and  $\mathbf{Q}(\rho)$  we choose first the FEM grid, then we calculate these matrix elements in the Gaussian points and finally we evaluate the integrals. This allow us to organize the calculation scheme for a system of  $N$  equations as follows. We evaluate the values of all matrix elements for these  $N$  equations in the Gaussian nodes and store them into the external file. Then we use it to investigate the convergence rate of the Kantorovich expansion as a function of number of equations.

In order to solve the generalized eigenvalue problem (44), the subspace iteration method [40,41] elaborated by Bathe [41] for the solution of large symmetric banded matrix eigenvalue problems has been chosen. This method uses a skyline storage mode, which stores components of the matrix column vectors within the banded region of the matrix, and is ideally suited for banded finite-element matrices. The procedure chooses a vector subspace of the full solution space and iterates upon the successive solutions in the subspace (for details, see [41]). The iterations continue until the desired set of solutions in the iteration subspace converges to within the specified tolerance on the Rayleigh quotients for the eigenpairs. Generally, 10–16 iterations are required for the subspace iterations to converge the subspace to within the prescribe tolerance. If matrix  $\mathbf{A}^p - \lambda^h \mathbf{M}$  in Eq. (44) is not positively defined, problem (44) is replaced by the following problem:

$$\tilde{\mathbf{A}}^p \chi^h = \tilde{E}^h \mathbf{B}^p \chi^h, \quad \tilde{\mathbf{A}}^p = \mathbf{A}^p - \lambda^h \mathbf{M} - \alpha \mathbf{B}^p. \quad (60)$$

The number  $\alpha$  (the shift of the energy spectrum) is chosen in such a way that matrix  $\tilde{\mathbf{A}}^p$  is positive. The eigenvector of problem (44) is the same, and  $E^h = \tilde{E}^h + \alpha$ .

For the solution of Eq. (16) it is impossible to define some minimum shift, because a total set of eigenvalues,  $\mu(\rho_{\max})$ , should be depended on  $\rho = \rho_{\max}$ . But, we can use the following lower and upper bounds for the eigenvalues [43]

$$|\mu(\rho_{\max}) - f_{ii}| \leq \sum_{j=1, i \neq j}^N |f_{ij}|, \quad f_{ij} = (\mathbf{V}(\rho_{\max}) + \mathbf{Q}^2(\rho_{\max}))_{ij}, \quad i = \overline{1, N}, \quad (61)$$

and from them we can determine the minimum shift of a full set of eigenvalues  $\mu(\rho_{\max})$

$$\alpha = \min_{i=\overline{1, N}} \left( f_{ii} - \sum_{j=1, j \neq i}^N |f_{ij}| \right) - 1. \quad (62)$$

After that, we can rewrite (16) in the following form

$$\begin{aligned} (\mathbf{V}(\rho_{\max}) + \mathbf{Q}^2(\rho_{\max}) - \alpha \mathbf{I}) \hat{\chi}(\rho_{\max}) &= \tilde{\mu}(\rho_{\max}) \hat{\chi}(\rho_{\max}), \\ \mu(\rho_{\max}) &= \tilde{\mu}(\rho_{\max}) + \alpha. \end{aligned} \quad (63)$$

In this case left matrix should be positively defined, and can be diagonalized by the generalized Jacobi method.

From the estimates above one can see that we have a high accuracy for calculating the bound states and corresponding wave functions of both (eigenvalues and continuous) cases. From this point of view, the main error in the solution depends only on the number of equations  $N$  and computer precision used in calculations.

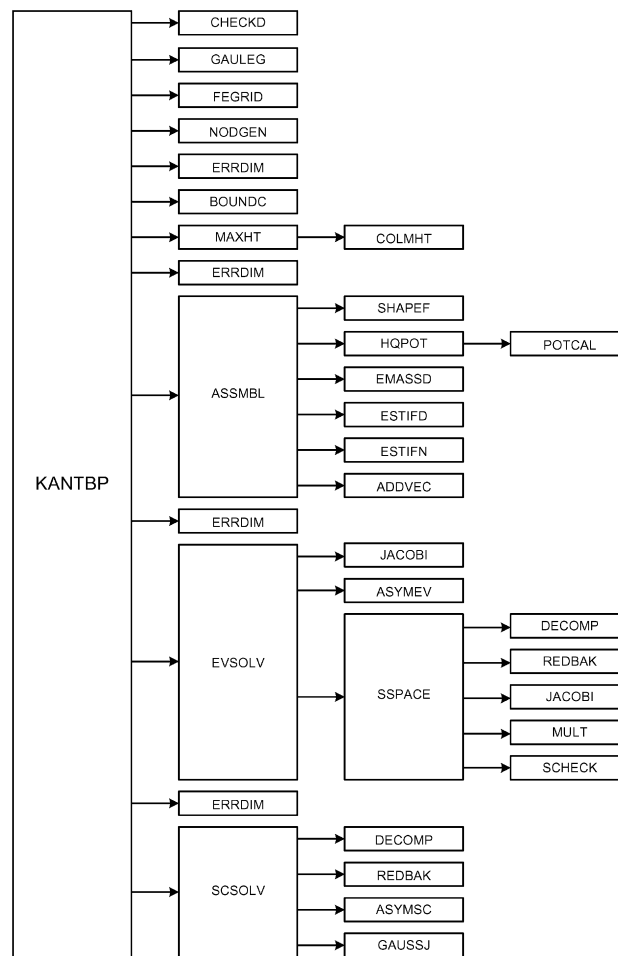


Fig. 1. Flow diagram of the KANTBP program.

#### 4. Description of the program

Fig. 1 presents a flow diagram for the KANTBP program. The function of each subroutine is described in Section 5. The KANTBP program is called from the main routine (supplied by a user) which sets dimensions of the arrays and is responsible for the input data. In the present code each array declarator is written in terms of the symbolic names of constants. These constants are defined in the following PARAMETER statement in the main routine:

PARAMETER (MTOT = 9000000, MITOT = 900000, NMESH1 = 7, MDIM1 = 6) where

- MTOT is the dimension of the working DOUBLE PRECISION array TOT.
- MITOT is the dimension of the working INTEGER array ITOT.
- NMESH1 is the dimension of the DOUBLE PRECISION array RMESH containing the information about the subdivision of the hyperradial interval  $[0, \rho_{\max}]$  on subintervals and number of elements on each one of them. NMESH1 is always odd and  $\geq 3$ .
- MDIM1 is the dimension of the DOUBLE PRECISION array THRSHL and INTEGER array NDIL containing information about a set of threshold values and numbers of coupled differential equations, respectively.

A more concrete assignment of these dimensions is discussed below. In order to change the dimensions of the code, all one has to do is to modify the single PARAMETER statement defined above in the main program unit.

The calling sequence for the subroutine KANTBP is:

```

CALL KANTBP(TITLE, IPTYPE, NROOT, MDIM, IDIM, NPOL, RTOL, NITEM,
1      SHIFT, IPRINT, IPRSTP, NMESH, RMESH, NDIR, NDIL, NMDIL,
2      THRSHL, IBOUND, FNOUT, IOUT, POTEN, IOUP, FMATR, IOUM,
3      EVWFN, IOUF, TOT, ITOT, MTOT, MITOT)

```

where the arguments have the following type and meaning:

- POTCAL is the name of the user-supplied subroutine which calculates the potential matrices  $V(\rho)$  and  $Q(\rho)$  and should be written as follows:

```

SUBROUTINE POTCAL (RHO, VV, QQ, MDIM, IOUT)
C.....
C.
C.   P R O G R A M
C.           TO CALCULATE THE POTENTIAL MATRIX ELEMENTS
C.           VV AND QQ OF DIMENSION MDIM X MDIM IN POINT
C.           RHO
C.
C.....
      IMPLICIT REAL*8 (A-H,O-Z)
      DIMENSION VV(MDIM,MDIM), QQ(MDIM,MDIM)
      RETURN
      END

```

- ASYMEV is the name of the user-supplied subroutine for the bound state problem which calculates the initial value  $\lambda^{(0)}(\rho)$  for the homogeneous third boundary condition at  $\rho = \rho_{\max}$  and should be written as follows:

```

SUBROUTINE ASYMEV (RMAX, NDIM, MDIM, SHIFT, DLAMBDA, IOUT)
C.....
C.
C.   P R O G R A M
C.           TO CALCULATE THE INITIAL VALUE DLAMBDA FOR.
C.           THE HOMOGENEOUS THIRD TYPE BOUNDARY CONDITION
C.           AT RMAX
C.
C.....
      IMPLICIT REAL*8 (A-H,O-Z)
      RETURN
      END

```

- ASYMSC is the name of the user-supplied subroutine for the scattering problem which calculates the regular, irregular asymptotic matrix-solutions  $\Phi_{\text{reg}}(\rho)$ ,  $\Phi_{\text{irr}}(\rho)$  and their derivatives at  $\rho = \rho_{\max}$  and should be written as follows:

```

SUBROUTINE ASYMSC (RMAX, NDIM, NOPEN, QR, PREG, PIRR, DREG, DIRR, IOUT)
C.....
C.
C.   P R O G R A M
C.           TO CALCULATE THE REGULAR, IRREGULAR
C.           ASYMPTOTIC MATRIX SOLUTIONS PREG, PIRR
C.           AND THEIR DERIVATIVES DREG, DIRR AT RMAX
C.
C.....
      IMPLICIT REAL*8 (A-H,O-Z)
      DIMENSION QR(NOPEN), PREG(NDIM,NOPEN), PIRR(NDIM,NOPEN),
1      DREG(NDIM,NOPEN), DIRR(NDIM,NOPEN)
      RETURN
      END

```

Here in the ASYMEV, DLAMBDA is the initial value  $\lambda^{(0)}$  and in the ASYMSC, array QR contains a set of momentum values, and NOPEN is the number of open channels. All parameters except VV, QQ, DLAMBDA, PREG, PIRR, DREG and DIRR in the subroutines POTCAL, ASYMEV and ASYMSC have the same meaning as described below and should not be changed by subroutines POTCAL, ASYMEV and ASYMSC.

#### 4.1. Input data

TITLE	CHARACTER	title of the run to be printed on the output listing. The title should be no longer than 70 characters.
IPTYPE	INTEGER	IPTYPE contains information about type of the problem solved. If IPTYPE = 0 the program calculates the eigenvalue problem; otherwise, it calculates the scattering problem.
NROOT	INTEGER	number of eigenvalues (energy levels) and eigenvectors (radial wave functions) required. NROOT should be equals to 1 in case of IBOUND > 4 and not used for the scattering problem.
MDIM	INTEGER	maximum number of coupled differential equations.
IDIM	INTEGER	dimension of the envelope space.
NPOL	INTEGER	order of finite-element shape functions (interpolating Lagrange polynomials). Usually set to 6.
RTOL	REAL*8	convergence tolerance on eigenvalues (1.D–06 or smaller). This value is not used for the scattering problem.
NITEM	INTEGER	maximum number of iterations permitted (usually set to 16). This value is not used for the scattering problem.
SHIFT	REAL*8	For the eigenvalue problem, SHIFT contains the energy spectrum. If SHIFT = 0 the value of the energy shift is determined automatically by the program; otherwise, the NROOT eigenvalues and eigenvectors closest to the shift given are calculated (the nonzero value of SHIFT is recommended since it significantly speeds up the calculation). For the scattering problem, SHIFT contains the given double energy spectrum.
IPRINT	INTEGER	level of print: = 0—minimal level of print. The initial data, short information about the numerical scheme parameters, main flags and keys, and energy values calculated are printed out; = 1—radial functions calculated are printed out with step IPRSTP additionally; = 2—potential matrix is printed out with step IPRSTP; = 3—information about nodal point distribution is printed out; = 4—global matrices <b>A</b> and <b>B</b> are printed out additionally; = 5—the highest level of print. The local stiffness and mass matrices together with all current information about the course of the subspace iteration method solution of the generalized eigenvalue problem are printed out.
IPRSTP	INTEGER	step with which potential matrix and radial wave functions are printed out.
NMESH	INTEGER	dimension of array RMESH. NMESH always should be odd and $\geq 3$ .
RMESH	REAL*8	array RMESH contains information about subdivision of interval $[0, \rho_{\max}]$ of hyperradius $\rho$ on subintervals. The whole interval $[0, \rho_{\max}]$ is divided as follows: RMESH(1) = 0, RMESH(NMESH) = $\rho_{\max}$ , and the values of RMESH(I) set the number of elements for each subinterval $[\text{RMESH}(I - 1), \text{RMESH}(I + 1)]$ , where $I = 2, 4, \dots, \text{NMESH} - 1$ .
NDIR	INTEGER	dimension of array NDIL. If NDIR > MDIM the message about the error is printed and the execution of the program is stopped.
NDIL	INTEGER	array NDIL containing information about the set of numbers of coupled differential equations and always should be $\text{NDIL}(\text{NDIR}) \leq \text{MDIM}$ .
NMDIL	INTEGER	key parameter. If NMDIL = 0 the potential matrix elements of radial coupling are calculated and written to file POTEN; otherwise, they are read from file POTEN.
THRSHL	REAL*8	array THRSHL of dimension MDIM containing values of the thresholds. This array is not used for the eigenvalue problem.
IBOUND	INTEGER	parameter defining the type of boundary conditions set in the boundary points $\rho = 0$ and $\rho = \rho_{\max}$ : = 1—the Dirichlet–Dirichlet boundary conditions: $\chi_i(0) = 0, \quad \chi_i(\rho_{\max}) = 0$ ; = 2—the Dirichlet–Neumann boundary conditions: $\chi_i(0) = 0, \quad \lim_{\rho \rightarrow \rho_{\max}} \chi'_i(\rho) = 0$ ; = 3—the Neumann–Dirichlet boundary conditions: $\lim_{\rho \rightarrow 0} \rho^n \chi'_i(\rho) = 0, \quad \chi_i(\rho_{\max}) = 0$ ; = 4—the Neumann–Neumann boundary conditions: $\lim_{\rho \rightarrow 0} \rho^n \chi'_i(\rho) = 0, \quad \lim_{\rho \rightarrow \rho_{\max}} \chi'_i(\rho) = 0$ . = 6—the Dirichlet—third type boundary conditions (only for NROOT = 1): at $\rho = 0$ the Dirichlet boundary condition



(see the case 2) is used and at  $\rho_{\max}$  the user-supplied subroutine ASYMEV for the calculation of initial value  $\lambda^{(0)}(\rho_{\max})$  or user-supplied subroutine ASYMSC for the calculation of the regular, irregular asymptotic matrix-solutions  $\Phi_{\text{reg}}(\rho)$ ,  $\Phi_{\text{irr}}(\rho)$  and their derivatives at  $\rho = \rho_{\max}$  are used;

= 8—the Neumann—third type boundary conditions (only for NROOT = 1);

at  $\rho = 0$  the Neumann boundary condition (see the case 4) is used and at  $\rho_{\max}$  the same boundary condition is used as in case 6.

Here  $n = \text{IDIM} - 1$ . IBOUND should always be equal to 6 or 8 for the scattering problem.

FNOUT	CHARACTER	name of the output file (up to 55 characters) for printing out the results of the calculation. It is system specific and may include a complete path to the file location.
IOUT	INTEGER	number of the output logical device for printing out the results of the calculation (usually set to 7).
POTEN	CHARACTER	name of the input/output file (up to 55 characters) containing potential matrix elements of radial coupling.
IOUP	INTEGER	number of the logical device for reading/storing data from/into file POTEN.
FMATR	CHARACTER	name of the scratch file (up to 55 characters) for storing stiffness matrix.
IOUM	INTEGER	number of the logical device for storing stiffness matrix.
EVWFN	CHARACTER	name of the output file (up to 55 characters) for storing the results of the calculation, namely, the energy values or reaction matrix, finite-element grid points, and radial wave functions. It is used only if IOUF > 0.
IOUF	INTEGER	number of the logical device for storing data into file EVWFN.
TOT	REAL*8	working vector of the DOUBLE PRECISION type.
ITOT	INTEGER	working vector of the INTEGER type.
MTOT	INTEGER	dimension of the DOUBLE PRECISION working array ITOT. The last address ILAST of array TOT is calculated and then compared with the given value of MTOT. If ILAST > MTOT the message about an error is printed and the execution of the program is aborted. In the last case, in order to carry out the required calculation it is necessary to increase the dimension MTOT of array TOT to the quantity ILAST taken from the message.
MITOT	INTEGER	dimension of the INTEGER working array ITOT. The last address ILAST of array ITOT is calculated and then compared with the given value of MITOT. If ILAST > MITOT the message about an error is printed and the execution of the program is aborted. In the last case, in order to carry out the required calculation it is necessary to increase the dimension MITOT of array ITOT to the quantity ILAST taken from the message.

#### 4.2. Output data

The results of the calculation of energy values or reaction matrix and radial wave functions are written using unformatted segmented records into file EVWFN, according to the following operator:

```
WRITE(IOUF)  NDIM,NN,NROOT,NGRID, (EIGV(I), I=1,NROOT)
1           , (XGRID(I), I=1,NGRID), ((R(I,J), I=1,NN), J=1,NROOT)
```

or

```
WRITE(IOUF)  NDIM,NN,NOPEN,NGRID, ((RR(I,J), I=1,NOPEN), J=1,NOPEN)
1           , (XGRID(I), I=1,NGRID), ((R(I,J), I=1,NN), J=1,NOPEN)
```

In the above, parameters presented in the WRITE statement have the following meaning:

- NDIM is the number of radial equations.
- NGRID is the number of finite-element grid points.
- NN = NGRID \* NDIM.
- NROOT is the number of roots (energy levels).
- NOPEN is the number of open channels.
- Array EIGV contains the energy values calculated.
- Array RR contains the reaction matrix values calculated.
- Array XGRID contains the values of the finite-element grid points.
- Array R contains NROOT or NOPEN eigenfunctions each per NN elements in length stored in the following way: for each of the NGRID mesh points per NDIM elements of eigenfunction (see scheme below):

1-st root	2-nd root	...	last root
1	1		1
2	2		2
1-st point .	1-st point .	...	1-st point .
.	.		.
.	.		.
NDIM	NDIM		NDIM
1	1		1
2	2		2
2-nd point .	2-nd point .	...	2-nd point .
.	.		.
.	.		.
NDIM	NDIM		NDIM
.	.		.
.	.		.
.	.		.
1	1		1
2	2		2
last point .	last point .	...	last point .
.	.		.
.	.		.
NDIM	NDIM		NDIM

## 5. Description of subprogram units

A flow diagram for the KANTBP program is presented in Fig. 1. The function of each subroutine is briefly described below. Additional details may be found in COMMENT cards within the program.

- Subroutine ADDVEC assembles the element stiffness and mass matrices into the corresponding global vector using a compact storage form.
- Subroutine ASSMBL controls the calculation of element stiffness and mass matrices and assembles them into the corresponding global matrices.
- User-supplied subroutine ASYMEV calculates the initial value  $\lambda^{(0)}(\rho_{\max})$  of the bound state problem for the homogeneous third type boundary condition.
- User-supplied subroutine ASYMSC calculates the regular, irregular asymptotic matrix-solutions  $\Phi_{\text{reg}}(\rho)$ ,  $\Phi_{\text{irr}}(\rho)$  and their derivatives at  $\rho = \rho_{\max}$  of the scattering problem.
- Subroutine BOUND C sets the Dirichlet or Neumann boundary conditions.
- Subroutine COLMHT calculates column heights in banded matrix.
- Subroutine CHECKD prints error messages when input data are incorrect and stops the execution of program KANTBP.
- Subroutine DECOMP calculates  $\mathbf{LDL}^T$  factorization of stiffness matrix. This factorization is used in subroutine REDBAK to reduce and back-substitute the iteration vectors.
- Subroutine EMASD calculates an element mass matrix.
- Subroutine ERRDIM prints error messages when high-speed storage requested by a user is exceeded and stops the execution of program KANTBP.
- Subroutine ESTIFD calculates a diagonal part of the local on element stiffness matrix.
- Subroutine ESTIFN calculates a nondiagonal part of the local on element stiffness matrix.
- Subroutine EVSOLV prepares all input data for the SSPACE program, prints out the calculated eigensolutions, and writes them into the file EVWFN, if necessary.
- Subroutine FEGRID calculates nodal points for the finite-element grid.
- Subroutine GAULEG [44] calculates nodes and weights of the Gauss–Legendre quadrature.
- Subroutine GAUSSJ [44] calculates linear equation solution by the Gauss–Jordan matrix inversion method.
- Subroutine HQPOT calculates potential matrix elements of radial coupling in the Gaussian nodes of the finite-element mesh.
- Subroutine JACOBI solves the generalized eigenproblem in subspace using the generalized Jacobi iteration.
- Subroutine MAXHT calculates addresses of diagonal elements in banded matrix.
- Subroutine MULT evaluates a product of the two vectors stored in compact form.
- Subroutine NODGEN generates a nodal point distribution for the finite-element grid.
- User-supplied subroutine POTCAL calculates the potential matrices  $\mathbf{V}(\rho)$  and  $\mathbf{Q}(\rho)$  of dimension MDIM  $\times$  MDIM.

- Subroutine SCHECK evaluates shift for Sturm sequence check (called only if SHIFT = 0).
- Subroutine SCSOLV calculates the reaction matrix and radial function, and writes them into the file EVWFN, if necessary.
- Subroutine SHAPEF calculates shape functions of the given order and their derivatives with respect to the master element coordinate  $\eta$  at a specified value of  $\rho$ .
- Subroutine SSPACE [41] finds the smallest eigenvalues and the corresponding eigenvectors in the generalized eigenproblem using the subspace iteration method [41]. We have added to this program the possibility of finding the eigensolutions closest to the energy spectrum shift given and also the possibility of using the previously calculated eigenvectors as the starting vectors for inverse iterations. The list of arguments for this program is adequately commented in the routine; so, the interested reader is referred to the program listing for further details. Warning messages will be issued if the requested accuracy RTOL is not obtained after NITEM iterations or if the stiffness matrix  $\mathbf{A}$  is not positively defined.

## 6. Test deck

The KANTBP program has been used and tested for a variety of physical problems [13,22,32,38,45–47]. Below we present exact solvable three-body benchmark for which the needed analytical expressions for the potential matrix elements and first-derivative coupling terms, their asymptotics and asymptotics of radial solutions of the boundary problems for coupled differential equations have been produced with help of a MAPLE computer algebra system.

We consider three identical particles in the center-of-mass reference frame (CMRF) described by the Jacobi coordinates,

$$\eta = \sqrt{\frac{1}{2}}(x_1 - x_2), \quad \xi = \sqrt{\frac{2}{3}}\left(\frac{x_1 + x_2}{2} - x_3\right), \quad (64)$$

in the plane  $\mathbf{R}^2$ , where  $\{(x_1, x_2, x_3) \in \mathbf{R}^3 \mid x_1 + x_2 + x_3 = 0\}$  are the Cartesian coordinates of the particles on a line. In polar coordinates

$$\eta = \rho \cos \theta, \quad \xi = \rho \sin \theta, \quad -\frac{\pi}{6} < \theta \leq 2\pi - \frac{\pi}{6}, \quad 0 \leq \rho < \infty, \quad (65)$$

the Schrödinger equation for the wave function  $\Psi(\rho, \theta)$  takes the form

$$-\frac{1}{2}\left(\frac{1}{\rho}\frac{\partial}{\partial\rho}\rho\frac{\partial}{\partial\rho} + \frac{1}{\rho^2}\frac{\partial^2}{\partial\theta^2}\right)\Psi(\rho, \theta) + \mathbf{U}(\rho, \theta)\Psi(\rho, \theta) = E\Psi(\rho, \theta), \quad (66)$$

where  $E$  is the relative energy in the CMRF. To obtain an exact solution which can be used below for a comparison with the numerical results, we involve the sum of delta-functions for describing the pair interactions with identical finite strengths. Thus,  $\mathbf{U}(\rho, \theta)$  assumes the form

$$\mathbf{U}(\rho, \theta) = g \sum_{l=-1}^1 \delta\left(\sqrt{2}\rho \left|\cos\left(\theta - \frac{2\pi}{3}l\right)\right|\right), \quad (67)$$

where  $g = \sqrt{2}c\bar{\kappa}$ , and  $\bar{\kappa} = \pi/6$  is the effective strength of the pair potential [31,48–50]. For the attractive case  $c < 0$ , we have the bound pair state  $\phi_0(\eta) = \sqrt{\bar{\kappa}} \exp(-\bar{\kappa}|\eta|)$  with the energy  $-\varepsilon_0^{(0)} = c^2\bar{\kappa}^2$ , so that  $2E = q^2 + \varepsilon_0^{(0)}$ , where  $q$  is proportional to the relative momentum of the third particle with respect to the bound pair [31,32,49,50].

Using a six-fold symmetric representation compatible with (67), we formulate the following boundary problem corresponding to equation (66) for regular and bounded solution by the radial variable  $\rho$  [31]:

$$-\left(\frac{1}{\rho}\frac{\partial}{\partial\rho}\rho\frac{\partial}{\partial\rho} + \frac{1}{\rho^2}\frac{\partial^2}{\partial\theta^2}\right)\Psi(\rho, \theta) = 2E\Psi(\rho, \theta), \quad (68)$$

with boundary conditions by the angle variable  $\theta_n \leq \theta < \theta_{n+1}$

$$\begin{aligned} \frac{1}{\rho} \frac{\partial \Psi(\rho, \theta_i)}{\partial \theta} &= (-1)^{i-n} c\bar{\kappa} \Psi(\rho, \theta_i), \\ \Psi(\rho, \theta_{n+1} - 0) &= \Psi(\rho, \theta_{n+1} + 0), \quad i = n, n+1, \end{aligned} \quad (69)$$

where  $\theta_n = \bar{\kappa}(2n - 1)$ ,  $n = \overline{0, 5}$ .

**Remark.** Problem (66), (67) is exactly solvable model. For the discrete spectrum in attractive case we have exact energies for a ground state and a half-bound state

$$2E_{\text{exact}}^b = -4c^2\bar{\kappa}^2 = -c^2\frac{\pi^2}{9}, \quad 2E_{\text{exact}}^{hb} = -c^2\bar{\kappa}^2 = -c^2\frac{\pi^2}{36}. \quad (70)$$

For the continuous spectrum in both the attractive and repulsive cases we have exact scattering matrix  $\mathbf{S}$  [30,31] that connected with reaction matrix  $\mathbf{K} = \mathbf{K}^T$  by the conventional formulae  $\mathbf{K} = \imath(\mathbf{I} + \mathbf{S})^{-1}(\mathbf{I} - \mathbf{S})$  or  $\mathbf{S} = (\mathbf{I} + \imath\mathbf{K})(\mathbf{I} - \imath\mathbf{K})^{-1}$ .

We consider here a formal expansion of the solution of Eqs. (66), (67) using a set of one-dimensional orthonormal basis functions  $B_j(\theta; \rho) \in W_2^1(-\pi/6, 2\pi - \pi/6)$ :

$$\Psi(\rho, \theta) = \sum_{j=1}^N B_j(\theta; \rho) \chi_j(\rho), \quad (71)$$

where the functions  $B_j(\theta; \rho)$  are determined as solutions of the following one-dimensional parametric eigenvalue problem:

$$\begin{aligned} -\frac{1}{\rho^2} \frac{\partial^2 B_j(\theta; \rho)}{\partial \theta^2} &= \varepsilon_j(\rho) B_j(\theta; \rho), \\ \frac{1}{\rho} \frac{\partial B_j(\theta_i; \rho)}{\partial \theta} &= (-1)^{i-n} c \bar{\kappa} B_j(\theta_i; \rho), \quad i = n, n+1, \\ B_j(\theta_{n+1} - 0; \rho) &= B_j(\theta_{n+1} + 0; \rho). \end{aligned} \quad (72)$$

After substituting the expansion (71) into the Rayleigh–Ritz variational functional and minimizing the functional, the solution of Eq. (68) is reduced to a solution of the finite set of  $N$  ordinary second-order differential equations (5).

As was shown in paper [48] the boundary problem (72) has the analytical solutions for the attractive case

$$B_1(\theta; \rho) = \sqrt{\frac{y_1^2 - x^2}{\pi(y_1^2 - x^2) - x}} \cosh \left[ 6y_1 \left( \theta - \frac{n\pi}{3} \right) \right], \quad \varepsilon_1(\rho) = -\frac{36y_1^2(\rho)}{\rho^2}, \quad (73)$$

$$B_j(\theta; \rho) = \sqrt{\frac{y_j^2 + x^2}{\pi(y_j^2 + x^2) + x}} \cos \left[ 6y_j \left( \theta - \frac{n\pi}{3} \right) \right], \quad \varepsilon_j(\rho) = \frac{36y_j^2(\rho)}{\rho^2}, \quad j \geq 2, \quad (74)$$

and for the repulsive case the index  $j$  starts from 1 in Eq. (74). The transcendental equations for the attractive case

$$\begin{aligned} y_1(\rho) \tanh(\pi y_1(\rho)) &= -x, \quad 0 \leq y_1(\rho) < \infty, \quad x = c \frac{\pi}{36} \rho, \\ y_j(\rho) \tan(\pi y_j(\rho)) &= x, \quad j - \frac{3}{2} < y_j(\rho) < j - 1, \end{aligned} \quad (75)$$

and for the repulsive case

$$y_j(\rho) \tan(\pi y_j(\rho)) = x, \quad x = c \frac{\pi}{36} \rho, \quad j - 1 < y_j(\rho) < j - \frac{1}{2}, \quad (76)$$

follow from problems (72). Roots  $y_j(\rho)$  of these equations are calculated numerically with a given accuracy for fixed values  $\rho$  from the considering interval  $\Delta = [0, \rho_{\max}]$ . The potential matrices  $\mathbf{V}(\rho)$  and  $\mathbf{Q}(\rho)$  are defined by formulas (6) and calculated by the analytical expressions using  $y_j(\rho)$  and parameter  $x$ .

For the attractive case needed matrix elements  $H_{ij}(\rho)$  and  $Q_{ij}(\rho)$  for  $i, j = \overline{1, N}$  read as follows:

$$\begin{aligned} H_{11}(\rho) &= -\left(\frac{c\pi}{36}\right)^2 \frac{1}{\tilde{y}_1^6} \left[ \frac{4\pi^2 y_1^4 - \tilde{y}_1^4}{4\tilde{y}_1^2} + \frac{\pi^2 y_1^2}{3} (\tilde{y}_1^2 + 4x) \right], \\ H_{1j}(\rho) &= H_{j1}(\rho) = \left(\frac{c\pi}{36}\right)^2 \frac{(-1)^{1+j} y_1 y_j}{\tilde{y}_1^3 \tilde{y}_j^3} \left[ 2\pi(\pi x^2 + x) \left( \frac{1}{\tilde{y}_1^2} - \frac{1}{\tilde{y}_j^2} \right) + \pi + 2\pi^2 x + \frac{4(y_1^2 \tilde{y}_j^2 + \tilde{y}_1^2 y_j^2)}{(y_1^2 + y_j^2)^2} \right], \\ Q_{1j}(\rho) &= -Q_{j1}(\rho) = -\frac{c\pi}{18} \frac{(-1)^{1+j} y_1 y_j}{(y_1^2 + y_j^2) \tilde{y}_1 \tilde{y}_j}, \\ \tilde{y}_1 &= \sqrt{\pi(y_1^2 - x^2) - x}, \end{aligned} \quad (77)$$

and

$$\begin{aligned} H_{jj}(\rho) &= -\left(\frac{c\pi}{36}\right)^2 \frac{1}{\tilde{y}_j^6} \left[ \frac{4\pi^2 y_j^4 - \tilde{y}_j^4}{4\tilde{y}_j^2} - \frac{\pi^2 y_j^2}{3} (\tilde{y}_j^2 - 4x) \right], \\ H_{ij}(\rho) &= H_{ji}(\rho) = \left(\frac{c\pi}{36}\right)^2 \frac{(-1)^{i+j} y_i y_j}{\tilde{y}_i^3 \tilde{y}_j^3} \left[ 2\pi(\pi x^2 + x) \left( \frac{1}{\tilde{y}_i^2} + \frac{1}{\tilde{y}_j^2} \right) - \pi - 2\pi^2 x + \frac{4(y_i^2 \tilde{y}_j^2 + \tilde{y}_i^2 y_j^2)}{(y_i^2 - y_j^2)^2} \right], \\ Q_{ij}(\rho) &= -Q_{ji}(\rho) = -\frac{c\pi}{18} \frac{(-1)^{i+j} y_i y_j}{(y_i^2 - y_j^2) \tilde{y}_i \tilde{y}_j}, \end{aligned}$$

$$\tilde{y}_j = \sqrt{\pi(y_j^2 + x^2)} + x, \quad i, j = \overline{2, N}. \quad (78)$$

For the repulsive case one will be used only the formula (78) but with  $i, j$  starting from 1, i.e.,  $i, j = \overline{1, N}$ .

*Comments:* The above matrix potentials are included in the subroutine POTCAL by default. Interaction constant  $c$  is accessed via general common block COMMON/IPROB/CCONST.

We consider a reduction of the boundary problem from semi-axis to finite interval using known asymptotic behavior of variable coefficients  $H_{ij}(\rho)$ ,  $Q_{ij}(\rho)$  and  $\varepsilon_j(\rho)$  and solutions  $\chi_j(\rho)$  for a large value of radial variable  $\rho$  [31,32]. For the attractive case the first threshold value  $\epsilon_1$  is equal to  $-c^2\bar{\kappa}^2$ , other threshold values are equal to zero and for the repulsive case all threshold values  $\epsilon_j$  are equal to zero. In the left boundary point we have used Neumann boundary condition (12).

### 6.1. Bound state problem with the attractive interaction

In case of the attractive interaction, the above problem has the bound state energies and corresponded wave functions  $\chi_j(\rho)$  that satisfy the following asymptotics for large  $\rho$  [32]

$$\chi_1(\rho) \rightarrow \frac{\exp(-\bar{q}\rho)}{\sqrt{\rho}}, \quad \chi_j(\rho) \rightarrow C_j \frac{\exp(-\bar{q}\rho)}{\rho^3}. \quad (79)$$

Here  $\bar{q}^2 = -2E + \epsilon_1 \geq 0$ , and  $C_j$  is the independent constant in  $\rho$ . For the calculation of the ground state energy, we have used the right boundary condition

$$\chi_j(\rho_{\max}) = 0. \quad (80)$$

The following values of numerical parameters and characters have been used in the test run via the supplied input file 3DDGSS.INP

```
&PARAM TITLE=' Ground state energy level of the 2D problem ',
IPTYPE=0, NROOT=1, MDIM=6, IDIM=2, NPOL=4, RTOL=1.D-15,
NITEM=20, SHIFT=-1.1D0, IPRINT=0, IPRSTP=100,
NMESH=5, RMESH=0.0D0, 100.D0, 10.D0, 150.D0, 50.D0,
NDIR=2, NDIL=1, 6, NMDIL=0,
IBOUND=3,
FNOUT=' 3DNGSS.LPR', IOUT=7, POTEN=' 3DNGSS.PTN', IOUP=10,
FMATR=' 3DNGSS.MAT', IOUM=11, EVWFN=' 3DNGSS.WFN', IOUF=0
&END
```

### 6.2. Half-bound state problem with the attractive interaction

From formula (79) we obtain the homogeneous third type boundary condition at  $\rho = \rho_{\max}$

$$\begin{aligned} \lim_{\rho \rightarrow \rho_{\max}} \frac{d\chi_1(\rho)}{d\rho} &= -\left(\frac{1}{2\rho_{\max}} + \bar{q}\right)\chi_1(\rho_{\max}), \\ \lim_{\rho \rightarrow \rho_{\max}} \frac{d\chi_j(\rho)}{d\rho} &= -\left(\frac{3}{\rho_{\max}} + \bar{q}\right)\chi_j(\rho_{\max}). \end{aligned} \quad (81)$$

In this case we choose initial value  $\lambda^{(0)} = -(1/(2\rho_{\max}) + \bar{q})$ , which is corrected during calculations. This function is included in the subroutine ASYMEV by default. The following values of numerical parameters and characters have been used in the test run via the supplied input file 3DDHSS.INP

```
&PARAM TITLE=' Half bound state energy level of the 2D problem ',
IPTYPE=0, NROOT=1, MDIM=6, IDIM=2, NPOL=4, RTOL=1.D-13,
NITEM=100, SHIFT=-0.2742D0, IPRINT=0, IPRSTP=100,
NMESH=5, RMESH=0.0D0, 100.D0, 10.D0, 1500.D0, 500.D0,
NDIR=2, NDIL=1, 6, NMDIL=0,
IBOUND=8,
FNOUT=' 3DNHBS.LPR', IOUT=7, POTEN=' 3DNHBS.PTN', IOUP=10,
FMATR=' 3DNHBS.MAT', IOUM=11, EVWFN=' 3DNHBS.WFN', IOUF=0
&END
```



### 6.3. Scattering problem with the attractive interaction

For scattering problem we have used the following two independent fundamental asymptotic solutions  $\chi_{ji}^{(\text{reg})}(\rho)$ ,  $\chi_{ji}^{(\text{irr})}(\rho)$  for large  $\rho$ : for  $i = 1$

$$\begin{aligned}\chi_{11}^{(\text{reg})}(\rho) &= \frac{1}{\sqrt{q\rho}} \sin(q\rho), \\ \chi_{11}^{(\text{irr})}(\rho) &= \frac{1}{\sqrt{q\rho}} \cos(q\rho), \\ \chi_{j1}^{(\text{reg})}(\rho) &= +\frac{1}{\sqrt{q}} \cos(q\rho) \frac{c_{j1}^{(3)}}{\rho^3}, \\ \chi_{j1}^{(\text{irr})}(\rho) &= -\frac{1}{\sqrt{q}} \sin(q\rho) \frac{c_{j1}^{(3)}}{\rho^3},\end{aligned}\quad (82)$$

for  $i \neq 1, j = 1$

$$\begin{aligned}\chi_{1i}^{(\text{reg})}(\rho) &= +\frac{(-1)^{1+i}}{\sqrt{k}} \cos(k\rho + \delta^{(0)}) \frac{c_{1i}^{(3)}}{\rho^3}, \\ \chi_{1i}^{(\text{irr})}(\rho) &= -\frac{(-1)^{1+i}}{\sqrt{k}} \sin(k\rho + \delta^{(0)}) \frac{c_{1i}^{(3)}}{\rho^3},\end{aligned}\quad (83)$$

and for  $i \neq 1, j \neq 1$

$$\begin{aligned}\chi_{ii}^{(\text{reg})}(\rho) &= \frac{(-1)^{i+1}}{\sqrt{k\rho}} \left( \sin(k\rho + \delta^{(0)}) \left( 1 + \frac{s_{ii}^{(2)}}{\rho^2} \right) + \cos(k\rho + \delta^{(0)}) \left( \frac{c_{ii}^{(1)}}{\rho} + \frac{c_{ii}^{(2)}}{\rho^2} \right) \right), \\ \chi_{ii}^{(\text{irr})}(\rho) &= \frac{(-1)^{i+1}}{\sqrt{k\rho}} \left( \cos(k\rho + \delta^{(0)}) \left( 1 + \frac{s_{ii}^{(2)}}{\rho^2} \right) - \sin(k\rho + \delta^{(0)}) \left( \frac{c_{ii}^{(1)}}{\rho} + \frac{c_{ii}^{(2)}}{\rho^2} \right) \right), \\ \chi_{ji}^{(\text{reg})}(\rho) &= \frac{(-1)^{i+1}}{\sqrt{k\rho}} \left( \sin(k\rho + \delta^{(0)}) \left( \frac{s_{ji}^{(1)}}{\rho} + \frac{s_{ji}^{(2)}}{\rho^2} \right) + \cos(k\rho + \delta^{(0)}) \frac{c_{ji}^{(2)}}{\rho^2} \right), \\ \chi_{ji}^{(\text{irr})}(\rho) &= \frac{(-1)^{i+1}}{\sqrt{k\rho}} \left( \cos(k\rho + \delta^{(0)}) \left( \frac{s_{ji}^{(1)}}{\rho} + \frac{s_{ji}^{(2)}}{\rho^2} \right) - \sin(k\rho + \delta^{(0)}) \frac{c_{ji}^{(2)}}{\rho^2} \right).\end{aligned}\quad (84)$$

Here  $k_1 \equiv q = \sqrt{2E - \epsilon_1}$ ,  $k_j \equiv k = \sqrt{2E}$ ,  $j = 2, \bar{N}$  and

$$\begin{aligned}c_{j1}^{(3)} &= -q \frac{72}{c^2 \pi^2} Q_{j1}^{(5/2)}, \quad c_{1i}^{(3)} = k \frac{72}{c^2 \pi^2} Q_{1i}^{(5/2)}, \\ s_{ii}^{(2)} &= -\frac{(4\epsilon_i^{(2)} - 1)(4\epsilon_i^{(2)} - 9)}{128k^2} + \frac{1}{2} \sum_{l=2, l \neq i}^N Q_{il}^{(2)} Q_{li}^{(2)}, \quad i \neq 1, \\ c_{ii}^{(1)} &= \frac{4\epsilon_i^{(2)} - 1}{8k}, \quad c_{ii}^{(2)} = \frac{\epsilon_i^{(3)}}{4k}, \\ s_{ji}^{(1)} &= -Q_{ji}^{(2)}, \quad s_{ji}^{(2)} = \frac{1}{2} \left( \sum_{l=2, l \neq j, l \neq i}^N Q_{jl}^{(2)} Q_{li}^{(2)} - Q_{ji}^{(3)} \right), \quad j \neq 1, i \neq 1, \\ c_{ji}^{(2)} &= -\frac{(2\epsilon_j^{(2)} + 2\epsilon_i^{(2)} - 1) Q_{ji}^{(2)}}{8k}, \\ Q_{j1}^{(5/2)} &= -\frac{216(-1)^{j+1}(2j-3)}{|c|^{3/2} \pi^2}, \quad Q_{1i}^{(5/2)} = \frac{216(-1)^{1+i}(2i-3)}{|c|^{3/2} \pi^2}, \\ Q_{ij}^{(2)} &= \frac{18(-1)^{i+j}(2i-3)(2j-3)}{c\pi^2(i-j)(i+j-3)}, \quad Q_{ij}^{(3)} = -\frac{36}{c\pi^2} Q_{ij}^{(2)}, \\ \epsilon_i^{(2)} &= (6i-9)^2, \quad \epsilon_i^{(3)} = -\frac{72}{c\pi^2} \epsilon_i^{(2)}.\end{aligned}\quad (85)$$

In order to compare with results [31],  $\delta^{(0)} = \pi/4$ , and  $2E = 0.085844322191962$  ( $q = 0.6$ ) have been chosen. The above matrix-solutions are included in the subroutine ASYMSC by default for  $c < 0$ . The following values of numerical parameters and characters have been used in the test run via the supplied input file 3DDSCM.INP

```
&PARAS TITLE=' Reaction matrix of the 2D problem - I ',
IPTYPE=1,MDIM=6,IDIM=2,NPOL=4,
SHIFT=0.858443221919622D-1,IPRINT=0,IPRSTP=150,
NMESH=5,RMESH=0.0D0,2000.0D0,100.0D0,4000.0D0,2000.0D0,
NDIR=2, NDIL=1,6, NMDIL=0,
THRSHL=-0.274155677808037D0,0.0D0,0.0D0,0.0D0,0.0D0,0.0D0,
IBOUND=8,
FNOUT=' 3DNSCM.LPR ', IOUT=7, POTEN=' 3DNSCM.PTN ', IOUP=10,
FMATR=' 3DNSCM.MAT ', IOUM=11, EVWFN=' 3DNSCM.WFN ', IOUF=0
&END
```

#### 6.4. Scattering problem with the repulsive interaction

In case of the repulsive interaction, we have used asymptotic solutions (84) with

$$\begin{aligned}
 s_{ii}^{(2)} &= -\frac{(4\epsilon_i^{(2)} - 1)(4\epsilon_i^{(2)} - 9)}{128k^2} + \frac{1}{2} \sum_{l \neq i, l=1}^N Q_{il}^{(2)} Q_{li}^{(2)}, \\
 c_{ii}^{(1)} &= \frac{4\epsilon_i^{(2)} - 1}{8k}, \quad c_{ii}^{(2)} = \frac{\epsilon_i^{(3)}}{4k}, \\
 s_{ji}^{(1)} &= -Q_{ji}^{(2)}, \quad s_{ji}^{(2)} = \frac{1}{2} \left( \sum_{l=1, l \neq j, l \neq i}^N Q_{jl}^{(2)} Q_{li}^{(2)} - Q_{ji}^{(3)} \right), \\
 c_{ji}^{(2)} &= -\frac{(2\epsilon_j^{(2)} + 2\epsilon_i^{(2)} - 1)Q_{ji}^{(2)}}{8k}, \\
 Q_{ij}^{(2)} &= \frac{18(-1)^{i+j}(2i-1)(2j-1)}{c\pi^2(i-j)(i+j-1)}, \quad Q_{ij}^{(3)} = -\frac{36}{c\pi^2} Q_{ij}^{(2)}, \\
 \epsilon_i^{(2)} &= (6i-3)^2, \quad \epsilon_i^{(3)} = -\frac{72}{c\pi^2} \epsilon_i^{(2)},
 \end{aligned} \tag{86}$$

and indexes  $i, j$  start from 1. In order to compare with results [31],  $\delta^{(0)} = \pi/4$ , and  $2E = 0.01$  ( $k = 0.1$ ) have been chosen. The matrix-solutions (84), (86) are included in the subroutine ASYMSC by default for  $c > 0$ . The following values of numerical parameters and characters have been used in the test run via the supplied input file 3DDSCP.INP

```
&PARAS TITLE=' Reaction matrix of the 2D problem - II ',
IPTYPE=1,MDIM=6,IDIM=2,NPOL=4,
SHIFT= 0.01D0,IPRINT=0,IPRSTP=150,
NMESH=7,RMESH=0.0D0,2000.0D0,100.0D0,4000.0D0,2000.0D0,
2000.0D0,11000.0D0,
NDIR=2, NDIL=1,6, NMDIL=0,
THRSHL= 0.0D0,0.0D0,0.0D0,0.0D0,0.0D0,0.0D0,
IBOUND=8,
FNOUT=' 3DNSCP.LPR ', IOUT=7, POTEN=' 3DNSCP.PTN ', IOUP=10,
FMATR=' 3DNSCP.MAT ', IOUM=11, EVWFN=' 3DNSCP.WFN ', IOUF=0
&END
```

These four tests run approximately for 1.01 s, 11.01 s, 7.06 s and 9.39 s without calculation of matrix potentials on the Intel Pentium IV 2.4 GHz, respectively. Total run time is 28.48 s.

#### Acknowledgements

The authors thank Prof. V.L. Derbov and Dr. V.V. Serov for a long-time collaboration. O.C. and M.S.K. acknowledge financial support from a grant I-1402/2004-2007 of the Bulgarian Foundation for Scientific Investigations and the theme 09-6-1060-2005/2009 “Mathematical support of experimental and theoretical studies conducted by JINR”.

# Appendix A. Test run output

PROBLEM: Ground state energy level of the 2D problem  
\*\*\*\*\*

## C O N T R O L I N F O R M A T I O N

```

NUMBER OF DIFFERENTIAL EQUATIONS..... (MDIM ) =      6
NUMBER OF ENERGY LEVELS REQUIRED..... (NROOT ) =      1
NUMBER OF FINITE ELEMENTS..... (NELEM ) =     250
NUMBER OF GRID POINTS..... (NGRID ) =    1001
ORDER OF SHAPE FUNCTIONS..... (NPOL ) =      4
ORDER OF GAUSS-LEGENDRE QUADRATURE... (NGQ ) =      5
NUMBER OF SUBSPACE ITERATION VECTORS.. (NC ) =      2
DIMENSION OF ENVELOPE SPACE..... (IDIM ) =      2
BOUNDARY CONDITION CODE..... (IBOUND) =      3
SHIFT OF DOUBLE ENERGY SPECTRUM..... (SHIFT ) =   -1.10000
CONVERGENCE TOLERANCE..... (RTOL ) =   0.100000E-14
    
```

## SUBDIVISION OF RHO-REGION ON THE FINITE-ELEMENT GROUPS:

\*\*\*\*\*

NO OF GROUP	NUMBER OF ELEMENTS	BEGIN OF INTERVAL	LENGTH OF ELEMENT	GRID STEP	END OF INTERVAL
1	100	0.000	0.10000	0.02500	10.000
2	150	10.000	0.26667	0.06667	50.000

## T O T A L S Y S T E M D A T A

```

TOTAL NUMBER OF ALGEBRAIC EQUATIONS.... (NN ) =    1000
TOTAL NUMBER OF MATRIX ELEMENTS..... (NWK) =    3496
MAXIMUM HALF BANDWIDTH..... (MK ) =      5
MEAN    HALF BANDWIDTH..... (MMK) =      3
    
```

NDIM, MDIM= 1 6

THERE ARE 0 ROOTS LOWER THEN SHIFT  
CONVERGENCE REACHED FOR RTOL 0.1000E-14  
I T E R A T I O N N U M B E R 6  
RELATIVE TOLERANCE REACHED ON EIGENVALUES  
0.3955E-18

\*\*\*\*\*

R O O T	N U M B E R	E I G E N V A L U E
1		-0.5482213063633842

\*\*\*\*\*

## T O T A L S Y S T E M D A T A

```

TOTAL NUMBER OF ALGEBRAIC EQUATIONS.... (NN ) =    6000
TOTAL NUMBER OF MATRIX ELEMENTS..... (NWK) =   110856
    
```

MAXIMUM HALF BANDWIDTH..... (MK ) = 30  
MEAN HALF BANDWIDTH..... (MMK) = 18

NDIM, MDIM= 6 6

THERE ARE 0 ROOTS LOWER THEN SHIFT  
CONVERGENCE REACHED FOR RTOL 0.1000E-14  
I T E R A T I O N N U M B E R 6  
RELATIVE TOLERANCE REACHED ON EIGENVALUES  
0.2729E-16

\*\*\*\*\*

R O O T	N U M B E R	E I G E N V A L U E
-----	-----	-----
1		-0.5483113526413836

\*\*\*\*\*

PROBLEM: Half bound state energy level of the 2D problem  
\*\*\*\*\*

# C O N T R O L I N F O R M A T I O N -----

NUMBER OF DIFFERENTIAL EQUATIONS..... (MDIM ) = 6  
NUMBER OF ENERGY LEVELS REQUIRED..... (NROOT ) = 1  
NUMBER OF FINITE ELEMENTS..... (NELEM ) = 1600  
NUMBER OF GRID POINTS..... (NGRID ) = 6401  
ORDER OF SHAPE FUNCTIONS..... (NPOL ) = 4  
ORDER OF GAUSS-LEGENDRE QUADRATURE... (NGQ ) = 5  
NUMBER OF SUBSPACE ITERATION VECTORS.. (NC ) = 2  
DIMENSION OF ENVELOPE SPACE..... (IDIM ) = 2  
BOUNDARY CONDITION CODE..... (IBOUND) = 8  
SHIFT OF DOUBLE ENERGY SPECTRUM..... (SHIFT ) = -0.274200  
CONVERGENCE TOLERANCE..... (RTOL ) = 0.100000E-12

SUBDIVISION OF RHO-REGION ON THE FINITE-ELEMENT GROUPS:  
\*\*\*\*\*

NO OF GROUP	NUMBER OF ELEMENTS	BEGIN OF INTERVAL	LENGTH OF ELEMENT	GRID STEP	END OF INTERVAL
-----	-----	-----	-----	-----	-----
1	100	0.000	0.10000	0.02500	10.000
2	1500	10.000	0.32667	0.08167	500.000

# T O T A L S Y S T E M D A T A -----

TOTAL NUMBER OF ALGEBRAIC EQUATIONS.... (NN ) = 6401  
TOTAL NUMBER OF MATRIX ELEMENTS..... (NWK) = 22401  
MAXIMUM HALF BANDWIDTH..... (MK ) = 5  
MEAN HALF BANDWIDTH..... (MMK) = 3

NDIM, MDIM= 1 6

THERE ARE 1 ROOTS LOWER THEN SHIFT  
 CONVERGENCE REACHED FOR RTOL 0.1000E-12  
 I T E R A T I O N N U M B E R 9  
 RELATIVE TOLERANCE REACHED ON EIGENVALUES  
 0.6835E-14  
 I T E R A T I O N N U M B E R 22  
 RELATIVE TOLERANCE REACHED ON LAMBDA  
 0.4462E-13

\*\*\*\*\*

R O O T N U M B E R	E I G E N V A L U E	L A M B D A
-----	-----	-----
1	-0.1370771705679387	-0.6232569850201794E-03

\*\*\*\*\*

# T O T A L S Y S T E M D A T A

-----

TOTAL NUMBER OF ALGEBRAIC EQUATIONS.... (NN ) = 38406  
 TOTAL NUMBER OF MATRIX ELEMENTS..... (NWK) = 710421  
 MAXIMUM HALF BANDWIDTH..... (MK ) = 30  
 MEAN HALF BANDWIDTH..... (MMK) = 18

NDIM, MDIM= 6 6

THERE ARE 1 ROOTS LOWER THEN SHIFT  
 CONVERGENCE REACHED FOR RTOL 0.1000E-12  
 I T E R A T I O N N U M B E R 9  
 RELATIVE TOLERANCE REACHED ON EIGENVALUES  
 0.1629E-13  
 I T E R A T I O N N U M B E R 15  
 RELATIVE TOLERANCE REACHED ON LAMBDA  
 0.7793E-13

\*\*\*\*\*

R O O T N U M B E R	E I G E N V A L U E	L A M B D A
-----	-----	-----
1	-0.1370777081621216	-0.1131640030879691E-02

\*\*\*\*\*

PROBLEM: Reaction matrix of the 2D problem - I  
 \*\*\*\*\*

# C O N T R O L I N F O R M A T I O N

-----

NUMBER OF DIFFERENTIAL EQUATIONS..... (MDIM ) = 6  
 NUMBER OF FINITE ELEMENTS..... (NELEM ) = 6000  
 NUMBER OF GRID POINTS..... (NGRID ) = 24001  
 ORDER OF SHAPE FUNCTIONS..... (NPOL ) = 4  
 ORDER OF GAUSS-LEGENDRE QUADRATURE... (NGQ ) = 5  
 DIMENSION OF ENVELOPE SPACE..... (IDIM ) = 2

BOUNDARY CONDITION CODE..... (IBOUND) = 8  
DOUBLE ENERGY SPECTRUM..... (SHIFT ) = 0.858443E-01

SUBDIVISION OF RHO-REGION ON THE FINITE-ELEMENT GROUPS:  
\*\*\*\*\*

NO OF GROUP	NUMBER OF ELEMENTS	BEGIN OF INTERVAL	LENGTH OF ELEMENT	GRID STEP	END OF INTERVAL
1	2000	0.000	0.05000	0.01250	100.000
2	4000	100.000	0.47500	0.11875	2000.000

T O T A L S Y S T E M D A T A  
-----

TOTAL NUMBER OF ALGEBRAIC EQUATIONS.... (NN ) = 24001  
TOTAL NUMBER OF MATRIX ELEMENTS..... (NWK) = 84001  
MAXIMUM HALF BANDWIDTH..... (MK ) = 5  
MEAN HALF BANDWIDTH..... (MMK) = 3

NDIM, MDIM= 1 6

NUMBER OF OPEN CHANNELS..... (NOPEN) = 1  
VALUE OF I-TH MOMENTUM..... (I,QR ) = 1 0.6000E+00

C H E C K W R O N S K I A N  
-----

1.00000

\*\*\*\*\*

R E A C T I O N M A T R I X  
-----

-.224884

\*\*\*\*\*

T O T A L S Y S T E M D A T A  
-----

TOTAL NUMBER OF ALGEBRAIC EQUATIONS.... (NN ) = 144006  
TOTAL NUMBER OF MATRIX ELEMENTS..... (NWK) = 2664021  
MAXIMUM HALF BANDWIDTH..... (MK ) = 30  
MEAN HALF BANDWIDTH..... (MMK) = 18

NDIM, MDIM= 6 6

NUMBER OF OPEN CHANNELS..... (NOPEN) = 6  
VALUE OF I-TH MOMENTUM..... (I,QR ) = 1 0.6000E+00  
VALUE OF I-TH MOMENTUM..... (I,QR ) = 2 0.2930E+00  
VALUE OF I-TH MOMENTUM..... (I,QR ) = 3 0.2930E+00  
VALUE OF I-TH MOMENTUM..... (I,QR ) = 4 0.2930E+00  
VALUE OF I-TH MOMENTUM..... (I,QR ) = 5 0.2930E+00  
VALUE OF I-TH MOMENTUM..... (I,QR ) = 6 0.2930E+00

C H E C K W R O N S K I A N  
-----

```

1.00000      -.497999E-09  -.320749E-07  -.160361E-06  -.466201E-06  -.105346E-05
0.202460E-08  1.00000      0.722264E-07  0.141761E-06  -.134774E-07  -.153784E-05
-.512979E-07  0.843397E-07  1.00002      0.907839E-06  0.516355E-07  -.528737E-05
-.289234E-06  0.190461E-06  0.121896E-05  1.00046      0.399782E-05  -.107733E-04
-.876239E-06  0.116431E-06  0.602785E-06  0.616311E-05  1.00545      -.838095E-06
-.203693E-05  -.125993E-05  -.427531E-05  -.816296E-05  0.764553E-05  1.03840

```

\*\*\*\*\*

# R E A C T I O N   M A T R I X

-----

```

-.126136      0.500076E-07  0.947352E-08  0.623779E-07  0.254430E-06  0.646967E-06
0.488556E-07  0.594057      0.329502E-01  0.643311E-02  0.227628E-02  0.102439E-02
-.731879E-09  0.329500E-01  0.633301      0.416376E-01  0.972776E-02  0.378363E-02
0.126927E-09  0.643288E-02  0.416358E-01  0.634932      0.430101E-01  0.103123E-01
0.647861E-08  0.227596E-02  0.972623E-02  0.429971E-01  0.625075      0.422897E-01
0.163590E-07  0.102391E-02  0.378175E-02  0.103055E-01  0.422177E-01  0.583695

```

\*\*\*\*\*

PROBLEM:    Reaction matrix of the 2D problem - II

\*\*\*\*\*

# C O N T R O L   I N F O R M A T I O N

-----

```

NUMBER OF DIFFERENTIAL EQUATIONS..... (MDIM ) =      6
NUMBER OF FINITE ELEMENTS..... (NELEM ) =    8000
NUMBER OF GRID POINTS..... (NGRID ) =   32001
ORDER OF SHAPE FUNCTIONS..... (NPOL ) =      4
ORDER OF GAUSS-LEGENDRE QUADRATURE... (NGQ ) =      5
DIMENSION OF ENVELOPE SPACE..... (IDIM ) =      2
BOUNDARY CONDITION CODE..... (IBOUND) =      8
DOUBLE ENERGY SPECTRUM..... (SHIFT ) =   0.100000E-01

```

SUBDIVISION OF RHO-REGION ON THE FINITE-ELEMENT GROUPS:

\*\*\*\*\*

NO OF GROUP	NUMBER OF ELEMENTS	BEGIN OF INTERVAL	LENGTH OF ELEMENT	GRID STEP	END OF INTERVAL
----	-----	-----	-----	-----	-----
1	2000	0.000	0.05000	0.01250	100.000
2	4000	100.000	0.47500	0.11875	2000.000
3	2000	2000.000	4.50000	1.12500	11000.000

# T O T A L   S Y S T E M   D A T A

-----

```

TOTAL NUMBER OF ALGEBRAIC EQUATIONS.... (NN ) =   32001
TOTAL NUMBER OF MATRIX ELEMENTS..... (NWK) =  112001
MAXIMUM HALF BANDWIDTH..... (MK ) =      5
MEAN      HALF BANDWIDTH..... (MMK) =      3

```

NDIM, MDIM=            1            6

NUMBER OF OPEN CHANNELS..... (NOPEN) =        1

```

VALUE OF I-TH MOMENTUM..... (I,QR ) =      1  0.1000E+00

      C H E C K   W R O N S K I A N
      -----
1.00000

*****

      R E A C T I O N   M A T R I X
      -----
-2.56560

*****

      T O T A L   S Y S T E M   D A T A
      -----

TOTAL NUMBER OF ALGEBRAIC EQUATIONS.... (NN ) =    192006
TOTAL NUMBER OF MATRIX ELEMENTS..... (NWK) =    3552021
MAXIMUM HALF BANDWIDTH..... (MK ) =         30
MEAN    HALF BANDWIDTH..... (MMK) =         18

NDIM, MDIM=          6          6

NUMBER OF OPEN CHANNELS..... (NOPEN) =         6
VALUE OF I-TH MOMENTUM..... (I,QR ) =      1  0.1000E+00
VALUE OF I-TH MOMENTUM..... (I,QR ) =      2  0.1000E+00
VALUE OF I-TH MOMENTUM..... (I,QR ) =      3  0.1000E+00
VALUE OF I-TH MOMENTUM..... (I,QR ) =      4  0.1000E+00
VALUE OF I-TH MOMENTUM..... (I,QR ) =      5  0.1000E+00
VALUE OF I-TH MOMENTUM..... (I,QR ) =      6  0.1000E+00

      C H E C K   W R O N S K I A N
      -----
1.00000      0.567061E-08  0.102062E-07  0.138098E-07  0.108079E-07  -.191238E-07
0.586799E-08  1.00000      0.349612E-07  0.436920E-07  0.312694E-07  -.679934E-07
0.110412E-07  0.401423E-07  1.00002      0.113035E-06  0.551983E-07  -.152542E-06
0.160442E-07  0.529045E-07  0.147761E-06  1.00037      0.277508E-06  -.279382E-06
0.154999E-07  0.479263E-07  0.963258E-07  0.404796E-06  1.00291      0.206195E-06
-.106373E-07  -.399516E-07  -.946524E-07  -.160079E-06  0.524729E-06  1.01472

*****

      R E A C T I O N   M A T R I X
      -----
-2.56205      -.615521E-01  -.127812E-01  -.462205E-02  -.218770E-02  -.121841E-02
-.615521E-01  -2.63648      -.789722E-01  -.196070E-01  -.805618E-02  -.418943E-02
-.127812E-01  -.789723E-01  -2.64465      -.825942E-01  -.217596E-01  -.945895E-02
-.462208E-02  -.196071E-01  -.825940E-01  -2.65580      -.850115E-01  -.231961E-01
-.218774E-02  -.805632E-02  -.217598E-01  -.850074E-01  -2.69374      -.891220E-01
-.121843E-02  -.418952E-02  -.945904E-02  -.231949E-01  -.890963E-01  -2.80482

*****

```

## References

- [1] V. Roudnev, S. Yakovlev, Chem. Phys. Lett. 328 (2000) 97–106.
- [2] A. Rotondi, M. Amoretti, et al., AIP Conf. Proc. 796 (2005) 285–290.
- [3] N. Madsen, M. Amoretti, et al., Phys. Rev. Lett. 94 (2005) 033403-1-4.
- [4] W. Bertsche, A. Boston, et al., AIP Conf. Proc. 796 (2005) 301–308.



- [5] V.L. Derbov, L.A. Melnikov, I.M. Umansky, S.I. Vinitzky, *Phys. Rev. A* 55 (1997) 3394–3400.
- [6] V.V. Serov, V.P. Kadjaeva, V.L. Derbov, S.I. Vinitzky, *Proc. SPIE* 5773 (2005) 195–206;  
V.V. Serov, V.L. Derbov, S.I. Vinitzky, *Optics and Spectroscopy* 102 (2007) 557–561.
- [7] M.V. Ryabinina, L.A. Melnikov, *Nucl. Instrum. Methods Phys. Res. Section B* 214 (2004) 35–39;  
M.V. Ryabinina, L.A. Melnikov, *AIP Conf. Proc.* 796 (2005) 325–329.
- [8] H.F. Mott, H.S.W. Massey, *The Theory of Atomic Collisions*, Oxford Univ. Press, London/New York, 1965.
- [9] J. Macek, *J. Phys. B* 1 (1968) 831–843.
- [10] S.I. Vinitzky, L.I. Ponomarev, *Sov. J. Part. Nucl.* 13 (1982) 557–587;  
L. Bracci, G. Fiorentini, *Phys. Rep.* 86 (1982) 169–216.
- [11] U. Fano, *Rep. Progr. Phys.* 46 (1983) 97–165;  
U. Fano, A.R.P. Rau, *Atomic Collisions and Spectra*, Academic Press, Florida, 1986.
- [12] C.D. Lin, *Phys. Rep.* 257 (1995) 1–83.
- [13] A.G. Abrashkevich, M.S. Kaschiev, I.V. Puzynin, S.I. Vinitzky, *Sov. J. Nucl. Phys.* 48 (1988) 602–608;  
A.G. Abrashkevich, M.I. Gajsak, V.I. Lend'el, V.Yu. Pojda, I.V. Puzynin, *Phys. Lett. A* 133 (1988) 140–143;  
A.G. Abrashkevich, D.G. Abrashkevich, M.I. Gajsak, V.I. Lendyel, I.V. Puzynin, S.I. Vinitzky, *Phys. Lett. A* 152 (1991) 467–471.
- [14] J. Bernabeu, V.M. Suslov, T.A. Strizh, S.I. Vinitzky, *Hyperfine Interactions* 101–102 (1996) 391–399.
- [15] L.V. Kantorovich, V.I. Krylov, *Approximate Methods of Higher Analysis*, Wiley, New York, 1964.
- [16] V.A. Fock, *Izv. Akad. Nauk. SSSR, Ser. Fiz.* 18 (1954) 161–172.
- [17] A.M. Ermolaev, *Quantum Theory, Part 1*, in: *Proc. of 8th UNESCO Internat. School of Physics, St Petersburg 1998*, pp. 298–315.
- [18] M.B. Kadomtsev, S.I. Vinitzky, F.R. Vukajlovic, *Phys. Rev. A* 36 (1987) 4652–4661;  
M.B. Kadomtsev, S.I. Vinitzky, *J. Phys. B* 20 (1987) 5723–5736.
- [19] A.G. Abrashkevich, D.G. Abrashkevich, M. Shapiro, *Comput. Phys. Comm.* 90 (1995) 311–339.
- [20] A.G. Abrashkevich, M.S. Kaschiev, S.I. Vinitzky, *J. Comp. Phys.* 163 (2000) 328–348.
- [21] S.I. Vinitzky, L.G. Mardoyan, G.S. Pogosyan, A.N. Sisakyan, T.A. Strizh, *Phys. At. Nucl.* 56 (1993) 321–327.
- [22] M.G. Dimova, M.S. Kaschiev, S.I. Vinitzky, *J. Phys. B* 38 (2005) 2337–2352.
- [23] J.C. Light, R.B. Walker, *J. Chem. Phys.* 65 (1976) 4272–4282;  
B. Lepetit, J.M. Launay, M. LeDourneuf, *Chem. Phys.* 106 (1986) 103–110;  
D.M. Hood, A. Kuppermann, in: D.C. Clary (Ed.), *Theory of Chemical Reaction Dynamics*, Reidel, Boston, 1986, pp. 193–214.
- [24] K. Hino, A. Igarashi, J. Macek, *Phys. Rev. A* 50 (1994) 1038–1041.
- [25] A.G. Abrashkevich, M. Shapiro, *Phys. Rev. A* 50 (1994) 1205–1217;  
A.G. Abrashkevich, M. Shapiro, *J. Phys. B* 29 (1996) 627–644.
- [26] U. Fano, C.M. Lee, *Phys. Rev. Lett.* 31 (1973) 1573–1576.
- [27] C.M. Lee, *Phys. Rev. A* 10 (1974) 584–600.
- [28] J. Macek, *Phys. Rev. A* 30 (1984) 1277–1278.
- [29] A.G. Abrashkevich, I.V. Puzynin, S.I. Vinitzky, *Comput. Phys. Comm.* 125 (2000) 259–281.
- [30] Yu.A. Kuperin, P.B. Kurasov, Yu.B. Melnikov, S.P. Merkuriev, *Ann. Phys.* 205 (1991) 330–361.
- [31] O. Chuluunbaatar, A.A. Gusev, S.Y. Larsen, S.I. Vinitzky, *J. Phys. A* 35 (2002) L513–L525.
- [32] O. Chuluunbaatar, A.A. Gusev, M.S. Kaschiev, V.A. Kaschieva, A. Amaya-Tapia, S.Y. Larsen, S.I. Vinitzky, *J. Phys. B* 39 (2006) 243–269.
- [33] P.G. Burke, H.M. Schey, *Phys. Rev.* 126 (1962) 147–162;  
P.G. Burke, D.D. McVicar, K. Smith, *Proc. Phys. Soc.* 83 (1964) 397–407.
- [34] R.J. Damburg, *Atomic Collisions*, Latvian Academy of Science, Riga, 1963.
- [35] R. McCarroll, *Proc. Phys. Soc.* 83 (1964) 409–417.
- [36] D.W. Norcross, M.J. Seaton, *J. Phys. B* 2 (1969) 731–740;  
D.W. Norcross, *Comput. Phys. Comm.* 6 (1974) 257–264.
- [37] M. Gailitis, *J. Phys. B* 9 (1975) 843–854.
- [38] O. Chuluunbaatar, A.A. Gusev, V.L. Derbov, M.S. Kaschiev, L.A. Melnikov, V.V. Serov, S.I. Vinitzky, *J. Phys. A* (2007), in press.
- [39] S.I. Vinitzky, V.P. Gerdt, A.A. Gusev, M.S. Kaschiev, V.A. Rostovtsev, V.N. Samoylov, T.V. Tupikova, O. Chuluunbaatar, *Programming and Computer Software* 33 (2007) 105–116.
- [40] G. Strang, G.J. Fix, *An Analysis of the Finite Element Method*, Prentice–Hall, Englewood Cliffs, New York, 1973.
- [41] K.J. Bathe, *Finite Element Procedures in Engineering Analysis*, Prentice–Hall, Englewood Cliffs, New York, 1982.
- [42] A.G. Abrashkevich, D.G. Abrashkevich, M.S. Kaschiev, I.V. Puzynin, *Comput. Phys. Comm.* 85 (1995) 40–64;  
A.G. Abrashkevich, D.G. Abrashkevich, M.S. Kaschiev, I.V. Puzynin, *Comput. Phys. Comm.* 85 (1995) 65–81.
- [43] F.R. Gantmacher, *The Theory of Matrices*, AMS, Providence, USA, 2000.
- [44] W.H. Press, B.F. Flannery, S.A. Teukolsky, W.T. Vetterley, *Numerical Recipes: The Art of Scientific Computing*, Cambridge University Press, Cambridge, 1986.
- [45] A.G. Abrashkevich, D.G. Abrashkevich, I.V. Khimich, I.V. Puzynin, S.I. Vinitzky, *J. Phys. B* 24 (1991) 2807–2816.
- [46] A.G. Abrashkevich, D.G. Abrashkevich, M.S. Kaschiev, V.Yu. Poida, I.V. Puzynin, S.I. Vinitzky, *J. Phys. B* 22 (1989) 3957–3963.
- [47] A.G. Abrashkevich, D.G. Abrashkevich, M.S. Kaschiev, I.V. Puzynin, S.I. Vinitzky, *Phys. Rev. A* 45 (1992) 5274–5277.
- [48] W.G. Gibson, S.Y. Larsen, J. Popiel, *Phys. Rev. A* 35 (1987) 4919–4929.
- [49] A. Amaya-Tapia, S.Y. Larsen, J. Popiel, *Few Body Systems* 23 (1997) 87–109.
- [50] N.P. Mehta, J.R. Shepard, *Phys. Rev. A* 72 (2005) 032728-1–11.



# POTMHF: A program for computing potential curves and matrix elements of the coupled adiabatic radial equations for a hydrogen-like atom in a homogeneous magnetic field <sup>☆</sup>

O. Chuluunbaatar <sup>a,\*</sup>, A.A. Gusev <sup>a</sup>, V.P. Gerdt <sup>a</sup>, V.A. Rostovtsev <sup>a</sup>, S.I. Vinitzky <sup>a</sup>,  
A.G. Abrashkevich <sup>b</sup>, M.S. Kaschiev <sup>c</sup>, V.V. Serov <sup>d</sup>

<sup>a</sup> Joint Institute for Nuclear Research, Dubna, 141980 Moscow region, Russia

<sup>b</sup> IBM Toronto Lab, 8200 Warden Avenue, Markham, ON L6G 1C7, Canada

<sup>c</sup> Institute of Mathematics and Informatics, Sofia, Bulgaria

<sup>d</sup> Saratov State University, Saratov 410012, Russia

Received 16 April 2007; received in revised form 17 September 2007; accepted 21 September 2007

Available online 29 September 2007

## Abstract

A FORTRAN 77 program is presented which calculates with the relative machine precision potential curves and matrix elements of the coupled adiabatic radial equations for a hydrogen-like atom in a homogeneous magnetic field. The potential curves are eigenvalues corresponding to the angular oblate spheroidal functions that compose adiabatic basis which depends on the radial variable as a parameter. The matrix elements of radial coupling are integrals in angular variables of the following two types: product of angular functions and the first derivative of angular functions in parameter, and product of the first derivatives of angular functions in parameter, respectively. The program calculates also the angular part of the dipole transition matrix elements (in the length form) expressed as integrals in angular variables involving product of a dipole operator and angular functions. Moreover, the program calculates asymptotic regular and irregular matrix solutions of the coupled adiabatic radial equations at the end of interval in radial variable needed for solving a multi-channel scattering problem by the generalized **R**-matrix method. Potential curves and radial matrix elements computed by the POTMHF program can be used for solving the bound state and multi-channel scattering problems. As a test desk, the program is applied to the calculation of the energy values, a short-range reaction matrix and corresponding wave functions with the help of the KANTBP program. Benchmark calculations for the known photoionization cross-sections are presented.

## Program summary

*Program title:* POTMHF

*Catalogue identifier:* AEAA\_v1\_0

*Program summary URL:* [http://cpc.cs.qub.ac.uk/summaries/AEAA\\_v1\\_0.html](http://cpc.cs.qub.ac.uk/summaries/AEAA_v1_0.html)

*Program obtainable from:* CPC Program Library, Queen's University, Belfast, N. Ireland

*Licensing provisions:* Standard CPC licence, <http://cpc.cs.qub.ac.uk/licence/licence.html>

*No. of lines in distributed program, including test data, etc.:* 8123

*No. of bytes in distributed program, including test data, etc.:* 131 396

*Distribution format:* tar.gz

*Programming language:* FORTRAN 77

*Computer:* Intel Xeon EM64T, Alpha 21264A, AMD Athlon MP, Pentium IV Xeon, Opteron 248, Intel Pentium IV

*Operating system:* OC Linux, Unix AIX 5.3, SunOS 5.8, Solaris, Windows XP

<sup>☆</sup> This paper and its associated computer program are available via the Computer Physics Communications homepage on ScienceDirect (<http://www.sciencedirect.com/science/journal/00104655>).

\* Corresponding author.

E-mail address: [chuka@jinr.ru](mailto:chuka@jinr.ru) (O. Chuluunbaatar).

RAM: Depends on

1. the number of radial differential equations;
2. the number and order of finite elements;
3. the number of radial points.

Test run requires 4 MB

Classification: 2.5

External routines: POTHMF uses some Lapack routines, copies of which are included in the distribution (see README file for details).

Nature of problem: In the multi-channel adiabatic approach the Schrödinger equation for a hydrogen-like atom in a homogeneous magnetic field of strength  $\gamma$  ( $\gamma = B/B_0$ ,  $B_0 \cong 2.35 \times 10^5$  T is a dimensionless parameter which determines the field strength  $B$ ) is reduced by separating the radial coordinate,  $r$ , from the angular variables,  $(\theta, \varphi)$ , and using a basis of the angular oblate spheroidal functions [3] to a system of second-order ordinary differential equations which contain first-derivative coupling terms [4]. The purpose of this program is to calculate potential curves and matrix elements of radial coupling needed for calculating the low-lying bound and scattering states of hydrogen-like atoms in a homogeneous magnetic field of strength  $0 < \gamma \leq 1000$  within the adiabatic approach [5]. The program evaluates also asymptotic regular and irregular matrix radial solutions of the multi-channel scattering problem needed to extract from the **R**-matrix a required symmetric shortrange open-channel reaction matrix **K** [6] independent from matching point [7]. In addition, the program computes the dipole transition matrix elements in the length form between the basis functions that are needed for calculating the dipole transitions between the low-lying bound and scattering states and photoionization cross sections [8].

Solution method: The angular oblate spheroidal eigenvalue problem depending on the radial variable is solved using a series expansion in the Legendre polynomials [3]. The resulting tridiagonal symmetric algebraic eigenvalue problem for the evaluation of selected eigenvalues, i.e. the potential curves, is solved by the **LDL**<sup>T</sup> factorization using the DSTEVR program [2]. Derivatives of the eigenfunctions with respect to the radial variable which are contained in matrix elements of the coupled radial equations are obtained by solving the inhomogeneous algebraic equations. The corresponding algebraic problem is solved by using the **LDL**<sup>T</sup> factorization with the help of the DPTTRS program [2]. Asymptotics of the matrix elements at large values of radial variable are computed using a series expansion in the associated Laguerre polynomials [9]. The corresponding matching points between the numeric and asymptotic solutions are found automatically. These asymptotics are used for the evaluation of the asymptotic regular and irregular matrix radial solutions of the multi-channel scattering problem [7]. As a test desk, the program is applied to the calculation of the energy values of the ground and excited bound states and reaction matrix of multi-channel scattering problem for a hydrogen atom in a homogeneous magnetic field using the KANTBP program [10].

Restrictions: The computer memory requirements depend on:

1. the number of radial differential equations;
2. the number and order of finite elements;
3. the total number of radial points.

Restrictions due to dimension sizes can be changed by resetting a small number of PARAMETER statements before recompiling (see Introduction and listing for details).

Running time: The running time depends critically upon:

1. the number of radial differential equations;
2. the number and order of finite elements;
3. the total number of radial points on interval  $[r_{\min}, r_{\max}]$ .

The test run which accompanies this paper took 7 s required for calculating of potential curves, radial matrix elements, and dipole transition matrix elements on a finite-element grid on interval  $[r_{\min} = 0, r_{\max} = 100]$  used for solving discrete and continuous spectrum problems and obtaining asymptotic regular and irregular matrix radial solutions at  $r_{\max} = 100$  for continuous spectrum problem on the Intel Pentium IV 2.4 GHz. The number of radial differential equations was equal to 6. The accompanying test run using the KANTBP program took 2 s for solving discrete and continuous spectrum problems using the above calculated potential curves, matrix elements and asymptotic regular and irregular matrix radial solutions. Note, that in the accompanied benchmark calculations of the photoionization cross-sections from the bound states of a hydrogen atom in a homogeneous magnetic field to continuum we have used interval  $[r_{\min} = 0, r_{\max} = 1000]$  for continuous spectrum problem. The total number of radial differential equations was varied from 10 to 18.

References:

- [1] W.H. Press, S.A. Teukolsky, W.T. Vetterling, B.P. Flannery, Numerical Recipes: The Art of Scientific Computing, Cambridge University Press, Cambridge, 1986.
- [2] <http://www.netlib.org/lapack/>.
- [3] M. Abramovits, I.A. Stegun, Handbook of Mathematical Functions, Dover, New York, 1965.
- [4] U. Fano, Colloq. Int. C.N.R.S. 273 (1977) 127;  
A.F. Starace, G.L. Webster, Phys. Rev. A 19 (1979) 1629–1640;  
C.V. Clark, K.T. Lu, A.F. Starace, in: H.G. Beyer, H. Kleinpoppen (Eds.), Progress in Atomic Spectroscopy, Part C, Plenum, New York, 1984, pp. 247–320;  
U. Fano, A.R.P. Rau, Atomic Collisions and Spectra, Academic Press, Florida, 1986.
- [5] M.G. Dimova, M.S. Kaschiev, S.I. Vinitsky, J. Phys. B 38 (2005) 2337–2352;  
O. Chuluunbaatar, A.A. Gusev, V.L. Derbov, M.S. Kaschiev, V.V. Serov, T.V. Tupikova, S.I. Vinitsky, Proc. SPIE 6537 (2007) 653706-1–18.
- [6] M.J. Seaton, Rep. Prog. Phys. 46 (1983) 167–257.

- [7] M. Gailitis, J. Phys. B 9 (1976) 843–854;  
J. Macek, Phys. Rev. A 30 (1984) 1277–1278;  
S.I. Vinitsky, V.P. Gerdt, A.A. Gusev, M.S. Kaschiev, V.A. Rostovtsev, V.N. Samoylov, T.V. Tupikova, O. Chuluunbaatar, Programming and Computer Software 33 (2007) 105–116.
- [8] H. Friedrich, Theoretical Atomic Physics, Springer, New York, 1991.
- [9] R.J. Damburg, R.Kh. Propin, J. Phys. B 1 (1968) 681–691;  
J.D. Power, Phil. Trans. Roy. Soc. London A 274 (1973) 663–702.
- [10] O. Chuluunbaatar, A.A. Gusev, A.G. Abrashkevich, A. Amaya-Tapia, M.S. Kaschiev, S.Y. Larsen, S.I. Vinitsky, Comput. Phys. Comm. 177 (2007) 649–675.

© 2007 Elsevier B.V. All rights reserved.

PACS: 02.60.Lj; 03.65.Nk; 31.15.Ja; 32.80.Fb; 33.55.Be

**Keywords:** Eigenvalue and multi-channel scattering problems; Kantorovich method; Finite element method; **R**-matrix calculation; Multi-channel adiabatic approximation; Ordinary differential equations; High-order accuracy approximation

## 1. Introduction

Nowadays the dynamics of transitional processes such as atomic scattering in the presence of an external confinement [1], channeling of light nuclei in a thin film with impurities [2], excitation, deexcitation [3], ionization and recombination of atoms and ions in magnetic traps is a subject of the experimental, theoretical and computational studies [4]. With the help of additional electric or laser pulse fields one can operate on transition rates and control the population of states in a quantum system for the above mentioned processes [5]. It is worth mentioning a recent study [6] of a new enhancement mechanism of a laser-stimulated recombination of antihydrogen in cold antiproton–positron plasma in a laboratory magnetic field  $B$  of order of few  $T$  via quasistationary states embedded in the continuum. To study optimal parameters of the laser and magnetic fields in complex cases such as when the Coulomb energy of an electron is comparable with energy of the magnetic field of strength  $\gamma$  in the axial gauge, one needs to develop really stable, inexpensive, highly efficient and accurate numerical methods and schemes required for calculations of the optical transitions between the bound and autoionization states of discrete and continuous spectra similar to the well known ones developed for the doubly-excited states of the Helium atom [7].

For an optimal account of correlations between the longitude and confined by the magnetic field transverse electron motion in cylindrical coordinates  $(z, \rho, \varphi)$  at fixed energy and azimuthal quantum number  $m$ , it is convenient to use transformation to the radial and angular variables,  $r = \sqrt{z^2 + \rho^2}$ ,  $\cos \theta = z/r$  [8]. Such transformation corresponds to the well-known change of coordinates  $(r_1, r_2)$  of the first and second electrons to hyperradius  $r = \sqrt{r_1^2 + r_2^2}$  and hyperangle  $\alpha = \arctan(r_1/r_2)$ . This allows for an adequate account of radial correlations of electrons below the threshold for the Helium atom within the multi-channel hyperspherical adiabatic approach [9]. Main problems with the known approaches for solving the above problem are related to the necessity of constructing high accurate stable numerical schemes and solving ill-conditioned and/or large-scale algebraic problems that arise as a result of applying different approximations for the singular boundary problems in the two-dimensional region [10]. In order to provide a sufficiently high accuracy of calculations, most of popular methods require a large number of basis functions and often numerical integration over a large interval [11–18]. Bound state and continuum functions are usually calculated separately by different methods and the accuracy of these functions depends strongly on the accuracy of radial matrix elements used. Hence it is important to develop numerical methods for calculating potential matrix elements for the bound state and scattering problems that combine high accuracy with calculational scheme stability and high efficiency.

In this paper we present program POTHMF that realizes the multi-channel adiabatic approach in spherical coordinates for a hydrogen-like atom problem in a homogeneous magnetic field. An attractive feature of the adiabatic approach in spherical coordinates is that the electron wave function is accurately represented near the origin irrespective of the value of field strength. However, the problem here is how to match the spherically symmetric wave functions near the origin with the wave functions of the cylindrical symmetry which are more appropriate for areas located far enough from the origin [19]. In order to lower a dimension of the algebraic problem and improve its ill-condition property we use method suggested in [20]. It is based on (i) suitable analytic parameterizations of basis functions that satisfy boundary conditions and provide reasonable convergence and accuracy of expansion for a required solution, and (ii) constructing of proper asymptotic expansions of a solution in each of two independent variables to match analytic and numerical solutions after reduction of the singular boundary problem to a regular one (in a finite two-dimensional region).

From the mathematical point of view adiabatic approach is the Kantorovich method [21] which reduces a singular boundary problem for an elliptic partial differential equation in a two-dimensional region to a regular boundary problem for a system of the close-coupled ordinary second-order differential equations of a general type (with a skew-symmetric coefficient matrix of variable coefficients at the first derivatives) for calculating the bound and regular solutions for discrete and continuous spectra [10]. For a

given azimuthal quantum number  $m$  and  $z$ -parity, a solution depending on the radial variable  $r$  and angular variable  $\eta = \cos \theta = z/r$  is expanded over the oblate angular spheroidal functions [22] in the angular variable that compose an orthogonal adiabatic basis parametrically depending on  $p = \gamma r^2/2$ . The most challenging part in realization of the Kantorovich method consists of the calculation of the coefficient matrices with the same given (machine precision) accuracy with which the eigenfunctions are computed.

In order to achieve this, the derivatives of angular functions with respect to parameter  $r$  are calculated as solutions of the nonhomogeneous boundary problem which is obtained by differentiating in parameter  $r$  the ordinary differential equation of the second order for the angular oblate spheroidal functions [22]. The corresponding algebraic eigenvalue problems (that arise as a result of the conventional representation of a solution at fixed magnetic quantum number  $m$  and  $z$ -parity by its expansion over normalized generalized Legendre polynomials [22]) are solved with the given accuracy at finite values of  $r$  by a stable symbolic–numerical algorithm [23]. Stability and economy of the numerical scheme is achieved due to the fact that for a small value of parameter  $r$  the angular functions become Legendre’s polynomials while for a large value of  $r$  in the vicinities  $\eta = \pm 1$  the angular functions become the associated Laguerre’s functions in variables  $y = 2(\gamma r^2/2)(1 \mp \eta)$ , symmetrized in accordance to the  $z$ -parity property of angular oblate spheroidal functions for all values of parameter  $r$  [24]. The latter means that the sum and difference of these functions correspond to the  $z$ -even and  $z$ -odd solutions if one replaces  $\eta$  by  $-\eta$ . Therefore, for large  $r$  one could build asymptotic expansions in the inverse powers of  $r$  needed for calculation with a given accuracy of the required set of basis functions for all values of parameter  $r$  [23]. As a consequence, at large values of the radial variable  $r$  the potential curves, radial matrix elements and dipole transition matrix elements are calculated using asymptotic formulae and matching points  $r_{\text{match}} < r_{\text{max}}$  that are found automatically from the interval of integration  $0 \leq r \leq r_{\text{max}}$ . It allows us to build a more economic algorithm for solving partial algebraic eigenvalue problem depending on parameter  $r$  with automatical choice of Wilkinson’s shift [25].

Essential economy of computer resources for numerical solution of a boundary problem for a system of the radial second-order differential equations of general type (with matrix variable coefficients at the first derivative) is achieved by reducing the interval of integration  $0 \leq r \leq r_{\text{max}}$ . In the present work, in order to do that we construct at large  $r$  ( $r \geq r_{\text{max}}$ ) an asymptotic expansion of fundamental solutions of a system of radial equations. A linear combination of Coulomb regular and irregular functions and their first derivatives is used here as a basis set. A choice of appropriate value of matching point  $r = r_{\text{max}}$  of the numerical regular solution for the radial problem on interval  $0 \leq r \leq r_{\text{max}}$  with the constructed asymptotic expansions is controlled by satisfying (with the optimal computer-dependent precision) of the conservation condition for the Wronskian with a long derivative. In the present work the KANTBP program [26] is used to calculate short-range reaction matrix  $\mathbf{K}$  in open channels. The same matrix can be used for construction of solution of the auxiliary spectral problem in closed channels by applying the multi-channel quantum-defect theory (MQDT) [12,27], including additional (with respect to direct KANTBP calculations) eigenfunctions, eigenvalues and widths of closed channels.

The POTHMF program calculates potential curves and matrix elements of the coupled adiabatic radial equations for a hydrogen-like atom in a homogeneous magnetic field. It also computes the angular part of the dipole transition matrix elements (in the length form) between the angular functions and the asymptotic regular and irregular matrix solutions of a multi-channel scattering problem. Potential curves and radial matrix elements computed by the POTHMF program are used for solving the bound state and multi-channel scattering problems with the help of the KANTBP program [26]. As a test problem, the program is applied to the calculation of the energy values, short-range reaction matrix  $\mathbf{K}$  and corresponding wave functions for a hydrogen-like atom in a homogeneous magnetic field. Benchmark calculations for the known photoionization cross-sections from the bound states ( $1s_0$ ,  $2p_{-1}$  and  $3s_0$ ) of a hydrogen atom in a homogeneous magnetic field [12,15–17] are presented.

Efficiency of the elaborated program is demonstrated here by calculating photoionization cross-sections from the ground and low-lying excited states for a hydrogen atom to continuous state with  $m = 0$ . Note, that examples of application the proposed approach for calculation the low-lying excited states of a hydrogen atom in a homogeneous magnetic field  $0 < \gamma \leq 1000$  together with analysis of convergence rate of the method using 10 radial equation are considered in [10]. Another application for calculation of continuous spectrum states and photoionization from  $3d_0$  and  $3s_0$  states to continuum at  $\gamma = 2.595 \times 10^{-5}$  together with analysis of convergence rate of the method using 35 radial equation are given in [28]. The results of high-accurate calculation of a hydrogen atom photoionization cross-sections in a strong magnetic field using the POTHMF program are discussed in details in [29].

The paper is organized as follows. In Section 2 we give a brief overview of the problem. A description of the POTHMF algorithms are in Section 3. A description of the POTHMF program is given in Section 4. The subroutine units are briefly described in Section 5. The test problem is discussed in Section 6. Benchmark calculations for the photoionization cross-sections are given in Section 7.

## 2. Statement of the problem

The Schrödinger equation for the hydrogen atom in an axially symmetric homogeneous magnetic field  $\mathbf{B} = (0, 0, B)$  in spherical coordinates  $(r, \theta, \varphi)$  can be written as the 2D-equation [8]

$$\left( -\frac{1}{r^2} \frac{\partial}{\partial r} r^2 \frac{\partial}{\partial r} + \frac{A^{(0)}(r, \theta)}{r^2} - \frac{2Z}{r} - \epsilon \right) \Psi(r, \theta) = 0 \quad (1)$$

in the region  $\Omega: 0 < r < \infty$  and  $0 < \theta < \pi$ . The operator  $A^{(0)}(r, \theta)$  is given by

$$A^{(0)}(r, \theta) = -\frac{1}{\sin \theta} \frac{\partial}{\partial \theta} \sin \theta \frac{\partial}{\partial \theta} + \frac{m^2}{\sin^2 \theta} + \gamma m r^2 + \frac{1}{4} \gamma^2 r^4 \sin^2 \theta, \quad (2)$$

where  $m = 0, \pm 1, \dots$  is the magnetic quantum number,  $\gamma = B/B_0$ ,  $B_0 \cong 2.35 \times 10^5$  T is a dimensionless parameter which determines the field strength  $B$ , and the atomic units (a.u.)  $\hbar = m_e = e = 1$  are used under the assumption of infinite mass of the nucleus with a charge  $Z$ . In these expressions,  $\epsilon = 2E$  is the doubled energy (in Rydbergs,  $1 \text{ Ry} = (1/2) \text{ a.u.}$ ) of the bound state  $|m\sigma\rangle$  at fixed values of  $m$  and  $z$ -parity;  $\sigma = \pm 1$ ; and  $\Psi \equiv \Psi_{m\sigma}(r, \theta) = (\Psi_m(r, \theta) + \sigma \Psi_m(r, \pi - \theta))/\sqrt{2}$  is the corresponding wave function. Here the sign of  $z$ -parity  $\sigma = (-1)^{N_\theta}$  is defined by the number (even or odd) of nodes  $N_\theta \equiv N_\eta$  in solution  $\Psi$  with respect to the angular variable  $\theta$  in the interval  $0 < \theta < \pi$ . We will use also the scaled variable  $\hat{r} = r\sqrt{\gamma}$ , the effective charge  $\hat{Z} = Z/\sqrt{\gamma}$  and the scaled energy  $\hat{\epsilon} = \epsilon/\gamma$ . It means that one can use unit cyclotron frequency and renormalize the initial charge  $Z$  by factor  $\sqrt{1/\gamma}$  and initial energy  $\epsilon$  by factor  $1/\gamma$  only. The wave function satisfies the following boundary conditions in each  $\mathbf{H}_{m\sigma}$  subspace of the full Hilbert space:

$$\lim_{\theta \rightarrow 0, \pi} \sin \theta \frac{\partial \Psi}{\partial \theta}(r, \theta) = 0, \quad \text{if } m = 0, \quad \text{and} \quad \Psi(r, 0) = \Psi(r, \pi) = 0, \quad \text{if } m \neq 0, \quad (3)$$

$$\lim_{r \rightarrow 0} r^2 \frac{\partial \Psi}{\partial r}(r, \theta) = 0. \quad (4)$$

The discrete spectrum wave function satisfies the asymptotic boundary condition approximated at large  $r = r_{\max}$  by a boundary condition of the first type

$$\lim_{r \rightarrow \infty} r^2 \Psi(r, \theta) = 0 \quad \rightarrow \quad \Psi(r_{\max}, \theta) = 0. \quad (5)$$

Here the energy  $\epsilon \equiv \epsilon(r_{\max})$  plays the role of eigenvalues of the boundary problem (1)–(5) on a finite interval  $0 \leq r \leq r_{\max}$  with additional normalization condition

$$\int_0^{r_{\max}} \int_0^\pi r^2 \sin \theta |\Psi(r, \theta)|^2 dr d\theta = 1. \quad (6)$$

In the Fano–Lee **R**-matrix theory [30,31] the continuum wave function  $\Psi(r, \theta)$  satisfies the boundary condition of the third type at fixed values of energy  $\epsilon$  and radial variable  $r = r_{\max}$

$$\frac{\partial \Psi(r, \theta)}{\partial r} - \mu \Psi(r, \theta) = 0. \quad (7)$$

Here the parameters  $\mu \equiv \mu(r_{\max}, \epsilon)$ , determined by the variational principle, play the role of eigenvalues of the logarithmic normal derivative matrix of the solution of the boundary problem (1)–(4), (7).

### 2.1. The KM reduction to a set of the radial differential equations

In the close coupling approximation, known in mathematics as the KM [21] the partial wave function  $\Psi_i(r, \theta)$  is expanded over the one-parametric basis functions  $\{\Phi_j^{m\sigma}(\theta; r)\}_{j=1}^N$

$$\Psi_i(r, \theta) = \sum_{j=1}^N \Phi_j^{m\sigma}(\theta; r) \chi_j^{(i)}(r). \quad (8)$$

In Eq. (8), the vector-function  $\chi^{(i)}(r) = (\chi_1^{(i)}(r), \dots, \chi_N^{(i)}(r))^T$  is unknown, and the surface functions  $\Phi^{m\sigma}(\theta; r) = (\Phi_1^{m\sigma}(\theta; r), \dots, \Phi_N^{m\sigma}(\theta; r))^T$  form an orthonormal basis with respect to the angular variable  $\theta$  for each value of radius  $r$  which is treated here as a parameter. In the Kantorovich approach [21], the functions  $\Phi_j(\theta; r) \equiv \Phi_j^{m\sigma}(\theta; r)$  are determined as solutions of the following parametric eigenvalue problem:

$$A^{(0)}(r, \theta) \Phi_j(\theta; r) = \varepsilon_j(r) \Phi_j(\theta; r). \quad (9)$$

The eigenfunctions of this problem satisfy the same boundary conditions in angular variable  $\theta$  for  $\Psi_i(r, \theta)$  and are normalized as follows

$$\langle \Phi_i(\theta; r) | \Phi_j(\theta; r) \rangle_\theta = \int_0^\pi \sin \theta \Phi_i(\theta; r) \Phi_j(\theta; r) d\theta = \delta_{ij}, \quad (10)$$

where  $\delta_{ij}$  is the Kronecker symbol.



After minimizing the Rayleigh–Ritz variational functional (see [32]) and using the expansion (8), Eq. (1) is reduced to a finite set of  $N$  ordinary second-order differential equations for the  $\chi(r) \equiv \chi^{(i)}(r)$

$$\left( -\frac{1}{r^2} \mathbf{I} \frac{d}{dr} r^2 \frac{d}{dr} + \mathbf{V}(r) + \mathbf{Q}(r) \frac{d}{dr} + \frac{1}{r^2} \frac{dr^2 \mathbf{Q}(r)}{dr} - 2E\mathbf{I} \right) \chi(r) = 0. \quad (11)$$

Here  $\mathbf{I}$ ,  $\mathbf{V}(r)$  and  $\mathbf{Q}(r)$  are  $N \times N$  matrices whose elements are given by the relation

$$\begin{aligned} V_{ij}(r) &= H_{ij}(r) + \left( \frac{\varepsilon_i(r) + \varepsilon_j(r)}{2r^2} - \frac{2Z}{r} \right) \delta_{ij}, & I_{ij} &= \delta_{ij}, \\ H_{ij}(r) &= H_{ji}(r) = \left\langle \frac{\partial \Phi_i(\theta; r)}{\partial r} \left| \frac{\partial \Phi_j(\theta; r)}{\partial r} \right\rangle_{\theta}, \\ Q_{ij}(r) &= -Q_{ji}(r) = -\left\langle \Phi_i(\theta; r) \left| \frac{\partial \Phi_j(\theta; r)}{\partial r} \right\rangle_{\theta}. \end{aligned} \quad (12)$$

The wave function  $\chi(r)$  satisfies the following boundary conditions at  $r \rightarrow 0$

$$\lim_{r \rightarrow 0} r^2 \left( \mathbf{I} \frac{d}{dr} - \mathbf{Q}(r) \right) \chi(r) = 0, \quad (13)$$

and at  $r = r_{\max}$

$$\chi(r) = 0, \quad \text{for the discrete spectrum,} \quad (14)$$

$$\left( \mathbf{I} \frac{d}{dr} - \mathbf{Q}(r) \right) \chi(r) = \mu(r) \chi(r), \quad \text{for the continuous spectrum.} \quad (15)$$

### 3. Description of the POTHMF algorithms

#### 3.1. Calculation of the angular oblate spheroidal functions

Note, that the solutions of the problem (9), (2) with the shifted eigenvalues  $\lambda_j(p) = \varepsilon_j(r) - \gamma m r^2$  correspond to the solutions of the eigenvalue problem for the angular oblate spheroidal functions [22] with respect to a variable  $\eta = \cos \theta$ :

$$-\frac{\partial}{\partial \eta} (1 - \eta^2) \frac{\partial \Phi_j(\eta; p)}{\partial \eta} + \left( \frac{m^2}{1 - \eta^2} + p^2 (1 - \eta^2) \right) \Phi_j(\eta; p) = \lambda_j(p) \Phi_j(\eta; p), \quad (16)$$

where  $p = \hat{r}^2/2 = \gamma r^2/2$ , and eigenfunctions  $\Phi_j(\eta; p)$  satisfy the orthogonality conditions (10). We obtain eigenfunctions  $\Phi_j(\eta; r) \equiv \Phi_j(\eta; p)$  in the form of a series expansion at fixed values  $\sigma = \pm 1$  and  $m$ ,

$$\Phi_j(\eta; r) = \sum_{s=(1-\sigma)/2}^{s_{\max}} c_{sj}^{m\sigma}(r) P_{|m|+s}^{(m)}(\eta). \quad (17)$$

Here  $s$  is the even (odd) integer at  $\sigma = (-1)^s = \pm 1$  up to  $s_{\max} = 2(N_{\max} - 1) + (1 - \sigma)/2$ , where  $N_{\max}$  is number of even or odd terms of expansion,  $P_{|m|+s}^{(m)}(\eta)$  are the normalized associated Legendre polynomials [22]. The coefficients  $c_{sj}^{m\sigma}(r)$  satisfy the relation

$$\sum_{s=(1-\sigma)/2}^{s_{\max}} c_{sj}^{m\sigma}(r) c_{sj'}^{m\sigma}(r) = \delta_{jj'}. \quad (18)$$

The eigenvalue problem for eigenvectors  $\mathbf{c}_j = \{c_{sj}^{m\sigma}(r)\}_{(1-\sigma)/2}^{s_{\max}}$ , and eigenvalues  $\lambda_j \equiv \lambda_j(p)$  take the form

$$\mathbf{A}^{(0)} \mathbf{c}_j = \lambda_j \mathbf{c}_j, \quad (19)$$

$$\mathbf{c}_j^T \mathbf{c}_j = \mathbf{I}, \quad (20)$$

where matrix  $\mathbf{A}^{(0)} \equiv \mathbf{A}^{(0)}(p)$  is the symmetric tridiagonal  $N_{\max} \times N_{\max}$  matrix:

$$\begin{aligned} A_{ss-2}^{(0)} &= A_{s-2s}^{(0)} = \frac{-p^2}{(2s+2|m|-1)} \sqrt{\frac{(s-1)s(s+2|m|-1)(s+2|m|)}{(2s+2|m|-3)(2s+2|m|+1)}}, \\ A_{ss}^{(0)} &= (s+|m|)(s+|m|+1) + 2p^2 \frac{(s^2+s+2s|m|+2m^2+|m|-1)}{(2s+2|m|-1)(2s+2|m|+3)}. \end{aligned} \quad (21)$$

The expansion (17) was used which provides stability of numerical calculation with the double precision arithmetic (the relative machine precision is  $\epsilon_{ps} = 2^{-52} \approx 2 \cdot 10^{-16}$ ) with the help of the subroutine DSTEVR from the LAPACK Fortran Library [33]. The orthogonality relations (18) were fulfilled with an accuracy of the order of  $\epsilon_{ps}$ .

### 3.2. Evaluation of parametric derivative of the angular functions and matrix elements

Radial matrix elements in notations of coefficient  $\mathbf{c}_j$  of decomposition (17) have the following form

$$Q_{ij}(r) = -\mathbf{c}_i^T \mathbf{c}_j^{(1)}, \quad H_{ij}(r) = (\mathbf{c}_i^{(1)})^T \mathbf{c}_j^{(1)}, \quad (22)$$

where  $\mathbf{c}_j^{(1)} = d\mathbf{c}_j/dr$ .

**Step 1.** As follows from (19), we should solve the following linear set of algebraic equations

$$\mathbf{A}^{(1)} \mathbf{c}^{(0)} - \mathbf{c}^{(0)} \lambda^{(1)} = -(\mathbf{A}^{(0)} \mathbf{c}^{(1)} - \mathbf{c}^{(1)} \lambda^{(0)}), \quad \mathbf{A}^{(1)} \equiv \frac{d\mathbf{A}^{(0)}}{dr}, \quad (23)$$

where  $\mathbf{c}^{(0)} \equiv \mathbf{c}_j$ ,  $\lambda^{(0)} \equiv \lambda_j$ ,  $\mathbf{c}^{(1)} \equiv \mathbf{c}_j^{(1)}$  and  $\lambda^{(1)} \equiv d\lambda_j/dr$ .

**Step 2.** Taking into account that  $\lambda^{(0)}$  is an eigenvalue of the operator defined in (19), the problem (23) has a solution *if and only if* the right-hand side term is orthogonal to the eigenfunction  $\mathbf{c}^{(0)}$ . Multiplying (23) by  $(\mathbf{c}^{(0)})^T$  and using the normalization condition (20), we obtain the expression for  $\lambda^{(1)}$

$$\lambda^{(1)} = (\mathbf{c}^{(0)})^T \mathbf{A}^{(1)} \mathbf{c}^{(0)} \quad (24)$$

and the set of the inhomogeneous algebraic equations for unknown vector  $\mathbf{c}^{(1)}$

$$\mathbf{L} \mathbf{c}^{(1)} \equiv \mathbf{A}^{(0)} \mathbf{c}^{(1)} - \mathbf{c}^{(1)} \lambda^{(0)} = \mathbf{b}^{(1)}, \quad \mathbf{b}^{(1)} = -\mathbf{A}^{(1)} \mathbf{c}^{(0)} + \mathbf{c}^{(0)} \lambda^{(1)}. \quad (25)$$

Now the problem (25) has a solution, but it is not unique. From the normalization condition (20) we obtain the required additional equality

$$(\mathbf{c}^{(1)})^T \mathbf{c}^{(0)} = 0, \quad (26)$$

providing the uniqueness of the solution (25). Since  $\lambda^{(0)}$  is an eigenvalue of (19), the matrix  $\mathbf{L}$  in (25) is degenerate.

Note, if matrix  $\mathbf{A}^{(0)}$  is diagonal, then the solution of system (25)–(26) can be evaluated analytically. The algorithm for numerical solution of (25) in a case of nondiagonal matrix  $\mathbf{A}^{(0)}$  can be written in three steps as follows:

**Step 3.** Calculate solutions  $\mathbf{v}^{(1)}$  and  $\mathbf{w}$  of the auxiliary inhomogeneous set algebraic equations

$$\bar{\mathbf{L}} \mathbf{v}^{(1)} = \bar{\mathbf{b}}^{(1)}, \quad \bar{\mathbf{L}} \mathbf{w} = \mathbf{d}, \quad (27)$$

with nondegenerate matrix  $\bar{\mathbf{L}}$  and right-hand sides  $\bar{\mathbf{b}}^{(1)}$  and  $\mathbf{d}$

$$\bar{L}_{ss'} = \begin{cases} L_{ss'}, & (s-S)(s'-S) \neq 0, \\ \delta_{ss'}, & (s-S)(s'-S) = 0, \end{cases} \quad (28)$$

$$\bar{b}_s^{(1)} = \begin{cases} b_s^{(1)}, & s \neq S, \\ 0, & s = S, \end{cases} \quad d_s = \begin{cases} L_{sS}, & s \neq S, \\ 0, & s = S, \end{cases} \quad (29)$$

where  $S$  is the number of the greatest absolute value element of vector  $\mathbf{c}^{(0)}$ .

**Step 4.** Evaluate coefficient  $\gamma^{(1)}$

$$\gamma^{(1)} = -\frac{\gamma_1^{(1)}}{(c_S^{(0)} - \gamma_2)}, \quad \gamma_1^{(1)} = (\mathbf{v}^{(1)})^T \mathbf{c}^{(0)}, \quad \gamma_2 = \mathbf{w}^T \mathbf{c}^{(0)}. \quad (30)$$

**Step 5.** Evaluate vector  $\mathbf{c}^{(1)}$

$$c_s^{(1)} = \begin{cases} v_s^{(1)} - \gamma^{(1)} w_s, & s \neq S, \\ \gamma^{(1)}, & s = S. \end{cases} \quad (31)$$

The above algorithm for calculation of matrix elements was implemented in the MAPLE and FORTRAN (general algorithms for evaluation of high-order derivatives of the eigenvalues, eigenvectors and corresponding matrix elements are discussed in [23]). The algorithm provides stability of numerical calculation with double precision arithmetic (the relative machine precision is  $\epsilon_{ps} = 2^{-52} \approx 2 \cdot 10^{-16}$ ) with help of the subroutine DPTTRS from the LAPACK Fortran Library [33].



### 3.3. Asymptotics of oblate angular spheroidal functions and matrix elements

At small  $r$ , asymptotic values of matrix elements  $\varepsilon_j(r)$ ,  $H_{jj'}(r)$  and  $Q_{jj'}(r)$  characterized by  $l = |m| + s = 2j - 2 + |m|$  for even states ( $\sigma = (-1)^{l-|m|} = +1$ ) and  $l = |m| + s = 2j - 1 + |m|$  for odd states ( $\sigma = (-1)^{l-|m|} = -1$ ) are the series expansion by the power of  $r$  at some finite values  $l_l, l_r$  [23]

$$\begin{aligned}\varepsilon_j(r) &= \bar{\varepsilon}_j^{(0)} + \bar{\varepsilon}_j^{(2)} r^2 + \sum_{k=1}^{k_{\max}} r^{4k} \bar{\varepsilon}_j^{(4k)}, & H_{jj'}(r) &= \sum_{k=2}^{k_{\max}} r^{4k-2} \bar{H}_{jj'}^{(4k-2)}, \\ Q_{jj'}(r) &= \sum_{k=1}^{k_{\max}} r^{4k-1} \bar{Q}_{jj'}^{(4k-1)}.\end{aligned}\quad (32)$$

The above matrix elements have been calculated analytically using the algorithm implemented in MAPLE up to  $k_{\max} = 4$ . Below we present the first few coefficients of matrix elements:

$$\begin{aligned}\bar{\varepsilon}_j^{(0)} &= \lambda_s^{m\sigma}(0) = l(l+1), & \bar{\varepsilon}_j^{(2)} &= \gamma m, & \bar{\varepsilon}_j^{(4)} &= \frac{\gamma^2}{2} \frac{l^2 + l - 1 + m^2}{(2l-1)(2l+3)}, \\ \bar{Q}_{jj+2}^{(3)} &= \frac{\gamma^2}{2} \frac{\sqrt{(l+1)^2 - m^2} \sqrt{(l+2)^2 - m^2}}{\sqrt{2l+1}(2l+3)^2 \sqrt{2l+5}}, \\ \bar{H}_{jj}^{(6)} &= \frac{\gamma^4}{2} ((16l^4 + 32l^3 + 248l^2 + 232l + 201)m^4 \\ &\quad + (-10l^2 - 224l^4 - 96l^5 + 118l - 288l^3 - 32l^6 - 195)m^2 \\ &\quad + 16l^8 + 64l^7 + 46l + 40l^6 - 127l^4 - 104l^5 + 71l^2 - 6l^3 - 6) \\ &\quad / ((2l-3)(2l-1)^4(2l+3)^4(2l+5)), \\ \bar{H}_{jj+4}^{(6)} &= \frac{-\gamma^4 \sqrt{(l+1)^2 - m^2} \sqrt{(l+2)^2 - m^2} \sqrt{(l+3)^2 - m^2} \sqrt{(l+4)^2 - m^2}}{4\sqrt{2l+1}(2l+3)^2(2l+5)(2l+7)^2 \sqrt{2l+9}}.\end{aligned}\quad (33)$$

This asymptotic behavior of effective potentials allows us to use the above boundary conditions (13) at  $r \rightarrow 0$  to find regular and bounded solutions. Note, that these asymptotic expansions have a finite radius of convergence because the parameter  $r$  has branch points in the complex plane [34–36].

Matrix elements at large  $r$  can be evaluated as series expansions by the inverse power of  $p$  up to the order of  $k_{\max}$  without taking into account the exponential small terms. For this we use the eigenfunctions  $\Phi^{m\leftarrow}(\eta; r)$  and  $\Phi^{m\rightarrow}(\eta; r)$  localized at large  $r$  in vicinity of  $\eta = \pm 1$

$$\Phi^{m\sigma=\pm 1}(\eta; r) = \frac{\Phi^{m\rightarrow}(\eta; r) \pm \Phi^{m\leftarrow}(\eta; r)}{\sqrt{2}}. \quad (34)$$

These functions have  $N_\rho \equiv n = 0, 1, 2, \dots$ , nodes in the subintervals  $0 < \eta < 1$  and  $-1 < \eta < 0$ , respectively, i.e.  $N_\rho = N_\eta/2$  for the even  $z$ -parity states,  $\sigma = +1$ , and  $N_\rho = (N_\eta - 1)/2$  for the odd  $z$ -parity states,  $\sigma = -1$ , where  $N_\eta$  is number of nodes  $\Phi^{m\sigma}(\eta; r)$  in the interval  $-1 < \eta < 1$  with parity  $\sigma = (-1)^{N_\eta}$ . Note, that  $\Phi^{m\leftarrow}(\eta; r) = \Phi^{m\rightarrow}(-\eta; r)$  and  $\Phi^{m\leftarrow}(\eta < 0; r) = \Phi^{m\rightarrow}(\eta > 0; r) = O(\exp(-p(1 + |\eta|)))$  at  $r \rightarrow \infty$  and  $|\eta| \sim 1$  and will be used in a construction of the scattering wave functions defined in (73).

Matrix elements are represented as the series expansion by the inverse power of  $r$  without the exponential terms in accordance with [23]

$$\begin{aligned}r^{-2}\varepsilon_j(r) &= \varepsilon_j^{(0)} + \sum_{k=1}^{k_{\max}} r^{-2k} \varepsilon_j^{(2k)}, & H_{jj'}(r) &= \sum_{k=1}^{k_{\max}} r^{-2k} H_{jj'}^{(2k)}, \\ Q_{jj'}(r) &= \sum_{k=1}^{k_{\max}} r^{1-2k} Q_{jj'}^{(2k-1)}.\end{aligned}\quad (35)$$

Here  $\varepsilon_{mj}^{th}(\gamma) = \varepsilon_j^{(0)}$  is an energy of the thresholds (in Ry) that corresponds to the double energy of the Landau thresholds (in a.u.).

In the present work, the calculation was performed by the algorithm implemented in MAPLE up to the  $k_{\max} = 8$ . Below we display the first several coefficients of potential curves  $\varepsilon_j(r)$  at fixed  $m$

$$\begin{aligned}\varepsilon_j^{(0)} &= \gamma(2n + m + |m| + 1), \\ \varepsilon_j^{(2)} &= -2n^2 - 2n|m| - 2n - |m| - 1,\end{aligned}\quad (36)$$

and matrix elements  $Q_{jj'}(r)$ ,  $H_{jj'}(r)$

$$\begin{aligned} Q_{jj'}^{(1)} &= (n_r - n_l) \sqrt{n+1} \sqrt{n+|m|+1} \delta_{|n_l-n_r|1}, \\ Q_{jj'}^{(3)} &= (4\gamma)^{-1} (n_r - n_l) \sqrt{n+1} \sqrt{n+|m|+1} \\ &\quad \times (2(2n+|m|+2) \delta_{|n_l-n_r|1} + \sqrt{n+2} \sqrt{n+|m|+2} \delta_{|n_l-n_r|2}), \\ H_{jj'}^{(2)} &= (2n^2 + 2n + 2|m|n + |m| + 1) \delta_{|n_l-n_r|0} \\ &\quad - \sqrt{n+1} \sqrt{n+|m|+1} \sqrt{n+2} \sqrt{n+|m|+2} \delta_{|n_l-n_r|2}. \end{aligned} \quad (37)$$

In these formulas asymptotic quantum number  $n = \min(n_l, n_r)$  denote transversal quantum number that is connected with the unified numbers  $j$  and  $j'$  by the formulas  $n_l = j - 1$  and  $n_r = j' - 1$ . Note, that  $\varepsilon_j^{(2)} + H_{jj}^{(2)} = 0$ , i.e. at large  $r$  the centrifugal terms are eliminated in Eq. (11). It means that the leading terms of radial solutions  $\chi_{jio}(r)$  have the same asymptotics as the Coulomb functions with a zero angular momentum and the effective charge  $\hat{Z}$  in terms of the scaled radial variable  $\hat{r}$ . The convergence of expansion (35) is shown in [23]. Note, that evaluating the exponential small corrections (for improving the convergence) can be done using additional series expansion of the solution in the region  $D_2 = [0, 1 - \eta_2]$ ,  $\eta_2 < \eta_1$ ,  $\eta_2 = o(p^{-1/2-\varepsilon})$  in accordance with [37].

### 3.4. Longitudinal and transversal dipole matrix elements

The longitudinal dipole matrix elements  $\mathbf{D}^{(m\sigma\sigma')}(r)$  with photon linearly polarized along  $z$  axis and transversal ones  $\mathbf{P}^{(mm'\sigma)}(r)$  with photon circularly polarized in  $XOY$  plane are expressed as

$$D_{jj'}^{(m\sigma\sigma')}(r) = \langle \Phi_j^{m\sigma}(\eta; r) | r \eta | \Phi_{j'}^{m\sigma'=-\sigma}(\eta; r) \rangle_\eta, \quad (38)$$

$$P_{jj'}^{(mm'\sigma)}(r) = \left\langle \Phi_j^{m\sigma}(\eta; r) \left| r \frac{\sqrt{1-\eta^2}}{\sqrt{2}} \right| \Phi_{j'}^{m'=m\pm 1\sigma}(\eta; r) \right\rangle_\eta. \quad (39)$$

Using expression (17) the above matrix elements can be written in the form

$$\begin{aligned} D_{jj'}^{(m\sigma\sigma')}(r) &= r \sum_{s=(1-\sigma)/2}^{s_{\max}} \sum_{s'=(1-\sigma')/2}^{s_{\max}} c_{sj}^{m\sigma}(r) c_{s'j'}^{m\sigma'}(r) \int_{-1}^1 \eta P_{|m|+s}^{(m)}(\eta) P_{|m|+s'}^{(m)}(\eta) d\eta \\ &= \delta_{|\sigma+\sigma'|0} r \sum_{s=(1-\sigma)/2}^{s_{\max}} \sum_{s'=(1-\sigma')/2}^{s_{\max}} c_{sj}^{m\sigma}(r) c_{s'j'}^{m\sigma'}(r) \delta_{|s-s'|1} \frac{\sqrt{s_>}\sqrt{s_>+2|m|}}{\sqrt{4(s_>+|m|)^2-1}}, \\ P_{jj'}^{(mm'\sigma)}(r) &= \frac{r}{\sqrt{2}} \sum_{s=(1-\sigma)/2}^{s_{\max}} \sum_{s'=(1-\sigma')/2}^{s_{\max}} c_{sj}^{m\sigma}(r) c_{s'j'}^{m'\sigma'}(r) \int_{-1}^1 \sqrt{1-\eta^2} P_{|m|+s}^{(m)}(\eta) P_{|m'|+s'}^{(m')}(\eta) d\eta \\ &= \delta_{|m-m'|1} \frac{r}{\sqrt{2}} \sum_{s=(1-\sigma)/2}^{s_{\max}} \sum_{s'=(1-\sigma')/2}^{s_{\max}} c_{sj}^{m\sigma}(r) c_{s'j'}^{m'\sigma'}(r) \\ &\quad \times \left[ \delta_{ss'+2} \sqrt{\frac{s(s-1)}{(2s+2m_<-1)(2s+2m_<+1)}} - \delta_{ss'} \sqrt{\frac{(s+2m_<+1)(s+2m_<+2)}{(2s+2m_<+1)(2s+2m_<+3)}} \right], \end{aligned} \quad (40)$$

where  $s_> = \max(s, s')$  and  $m_< = \min(|m|, |m'|)$ .

### 3.5. Asymptotics of longitudinal and transversal dipole matrix elements

We find longitudinal and transversal dipole matrix elements as the series expansion by the inverse power of  $r$  without the exponential terms

$$D_{jj'}^{(m\sigma\sigma')}(r) = r \sum_{k=0}^{k_{\max}} r^{-2k} D_{jj'}^{(2k)}, \quad P_{jj'}^{(mm'\sigma)}(r) = - \sum_{k=0}^{k_{\max}} r^{-2k} P_{jj'}^{(2k)}. \quad (42)$$

In these formulas asymptotic quantum number  $n$  denotes transversal quantum number connected with the unified numbers  $j$  and  $j'$  by the formulas  $n_l = j - 1$  and  $n_r = j' - 1$ .

The calculation was performed using the algorithm implemented in MAPLE up to  $k_{\max} = 8$ . Below we display the first few coefficients of the longitudinal dipole matrix  $\mathbf{D}^{(m\sigma\sigma')}(r)$  at fixed  $m$

$$\begin{aligned} D_{jj'}^{(0)} &= \delta_{|n_l - n_r|0}, \\ D_{jj'}^{(2)} &= \gamma^{-1} \left( -(2n + |m| + 1) \delta_{|n_l - n_r|0} + \sqrt{n} \sqrt{n + |m|} \delta_{|n_l - n_r|1} \right), \end{aligned} \quad (43)$$

and the transversal dipole matrix  $\mathbf{P}^{(mm'\sigma)}(r)$  at fixed  $|m'| = |m| + 1$

$$\begin{aligned} P_{jj'}^{(0)} &= \gamma^{-1/2} (\sqrt{n_l + |m| + 1} \delta_{n_l n_r} - \sqrt{n_l} \delta_{n_l n_r + 1}), \\ P_{jj'}^{(2)} &= 2^{-1} \gamma^{-3/2} (-\sqrt{n_l} \sqrt{n_l - 1} \sqrt{n_l + |m|} \delta_{n_l n_r + 2} \\ &\quad + \sqrt{n_l + 1} \sqrt{n_l + |m| + 1} \sqrt{n_l + |m| + 2} \delta_{n_l n_r - 1}), \end{aligned} \quad (44)$$

where  $n = \min(n_l, n_r)$ . Note, that the asymptotic longitudinal dipole matrix  $\mathbf{D}^{(m\sigma\sigma')}(r)$  is symmetric for  $\sigma$  and  $\sigma'$ , and the asymptotic transversal dipole matrix  $\mathbf{P}^{(mm'\sigma)}(r)$  is nonsymmetric but satisfies the relation  $P_{jj'}^{(mm'\sigma)}(r) = P_{j'j}^{(m'm\sigma)}(r)$ .

### 3.6. Finding optimal value of $s_{\max}$ and matching point $r_{\text{match}}$ of numerical and asymptotic solutions

At large  $s$  elements of matrix  $\mathbf{A}^{(0)}$  (21) take form

$$\begin{aligned} A_{ss}^{(0)} &= \frac{(2s + 2|m| + 1)^2 - 1}{4} + \frac{p^2}{2} + O(s^{-2}), \\ A_{ss+2}^{(0)} &= A_{ss-2}^{(0)} = -\frac{p^2}{4} + O(s^{-2}). \end{aligned} \quad (45)$$

On intervals  $s \in (s_b, s_e)$  at  $s_b, s_e \gg 1$ , we suppose that the elements of matrix  $\mathbf{A}^{(0)}$  have slow dependence on  $s$ . Therefore, for a given value of  $\lambda$  solution of algebraic problem (19), (45) will be represented in the form

$$c_s = x c_{s+2}, \quad c_{s-2} = x c_s. \quad (46)$$

From (46), (19), (45) we have algebraic equation with respect to factor  $x$

$$x + \frac{1}{x} = d \equiv \frac{(2s + 2|m| + 1)^2 - 1 - 4\lambda + 2p^2}{p^2}. \quad (47)$$

For  $s > s_2$ , where  $s_2$  is determined from Eq. (47) at  $d = 2$ ,

$$s_2 = \frac{\sqrt{4\lambda + 1} - 2|m| - 1}{2}, \quad (48)$$

Eq. (47) has two real solutions. One of them,

$$x_s = \frac{(\sqrt{(s - s_2)(s + s_2 + 2|m| + 1)} + \sqrt{p^2 + (s - s_2)(s + s_2 + 2|m| + 1)})^2}{p^2}, \quad (49)$$

is greater by absolute value than unity and the other,  $1/x_s$ , is smaller one. It means that the solution of (46) with decreased coefficients  $c_s$  at increased  $s$  exists. For  $s < s_2$  we have two solutions with oscillating coefficients  $c_s$ . Then solution of Eq. (47), allows us to determine algorithm for evaluation  $s_{\max}$ :

$$\prod_{s=s_2}^{s_{\max}-1} x_s < 1/eps, \quad \prod_{s=s_2}^{s_{\max}} x_s > 1/eps, \quad (50)$$

where  $eps = 2^{-52} \approx 2 \cdot 10^{-16}$  is the relative machine precision.

We need an approximate value of the eigenvalue  $\lambda$  for the above calculation. If we use the fact all diagonal elements  $A_{ss}^{(0)}$  of the tridiagonal matrix  $\mathbf{A}^{(0)}$  and eigenvalues  $\varepsilon_j(p)$  or  $\lambda_j(p)$  increased by number  $j$ , then we can obtain the upper bound of the eigenvalue  $\lambda_N$  with the help of Wilkinson's shift [25]

$$\text{shift} = G + A_{s_N s_N}^{(0)} + \sqrt{G^2 + (A_{s_N s_N}^{(0)})^2}, \quad G = \frac{A_{s_N - 2s_N - 2}^{(0)} - A_{s_N s_N}^{(0)}}{2}, \quad (51)$$

where  $s_N = 2(N - 1) + (1 - \sigma)/2$ . But  $\text{shift} \gg \lambda_N$  at  $p \gg 1$ . In this case we use asymptotic expression of the eigenvalue (35) at  $p \geq 2s_N$ , since the asymptotic expression gives an upper bound of the eigenvalue.

The matching point  $r_{\text{match}}$  of the numerical and asymptotic solution is calculated as follows

$$r_{\text{match}} = \max(r_\varepsilon, r_h, r_q),$$

$$r_\varepsilon = \sqrt[18]{\frac{|\varepsilon_N^{(18)}|}{\text{eps}}}, \quad r_h = \sqrt[18]{\frac{|H_{NN}^{(18)}|}{\text{eps}}}, \quad r_q = \sqrt[17]{\frac{|Q_{NN-1}^{(17)}|}{\text{eps}}}, \quad (52)$$

since  $|\varepsilon_j^{(2k)}| < \gamma |\varepsilon_j^{(2k+2)}|$ ,  $|Q_{jj'}^{(2k-1)}| < \gamma |Q_{jj'}^{(2k+1)}|$ ,  $|H_{jj'}^{(2k)}| < \gamma |H_{jj'}^{(2k+2)}|$  and  $|Q_{jj'}^{(17)}| \leq |Q_{NN-1}^{(17)}|$ ,  $|H_{jj'}^{(18)}| \leq |H_{NN}^{(18)}|$ .

The matching points  $r_{\text{match}} = r_d$  and  $r_{\text{match}} = r_p$  of the numerical and asymptotic solution are calculated follows

$$r_d = \sqrt[17]{\frac{|D_{NN}^{(18)}|}{\text{eps}}}, \quad r_p = \sqrt[18]{\frac{\max(|P_{N-1N}^{(18)}|, |P_{NN-1}^{(18)}|)}{\text{eps}}}, \quad (53)$$

since  $|D_{jj'}^{(2k)}| < \gamma |D_{jj'}^{(2k+2)}|$ ,  $|P_{jj'}^{(2k)}| < \gamma |P_{jj'}^{(2k+2)}|$ ,  $|D_{jj'}^{(18)}| \leq |D_{NN}^{(18)}|$ ,  $|P_{jj'}^{(18)}| \leq \max(|P_{N-1N}^{(18)}|, |P_{NN-1}^{(18)}|)$ .

### 3.7. Construction of regular and irregular matrix-solutions

Now let us consider the asymptotic solution following [38]

$$\chi_{ji_o}(r) = R(p_{i_o}, r)\phi_{ji_o}(r) + \frac{dR(p_{i_o}, r)}{dr}\psi_{ji_o}(r), \quad (54)$$

$$\phi_{ji_o}(r) = \sum_{k=0}^{k_{\max}} \phi_{ji_o}^{(k)} r^{-k}, \quad \psi_{ji_o}(r) = \sum_{k=0}^{k_{\max}} \psi_{ji_o}^{(k)} r^{-k}, \quad (55)$$

where  $R(p_{i_o}, r) = p_{i_o}^{-1/2} r^{-1} (t F_0(p_{i_o}, r) + G_0(p_{i_o}, r))/2$ ,  $F_0(p_{i_o}, r)$  and  $G_0(p_{i_o}, r)$  are the Coulomb regular and irregular functions, respectively [22]. These functions satisfy the condition

$$G_0(p_{i_o}, r) \frac{dF_0(p_{i_o}, r)}{dr} - \frac{dG_0(p_{i_o}, r)}{dr} F_0(p_{i_o}, r) = p_{i_o}. \quad (56)$$

After substituting the expansions (55) into Eq. (11) and equating the coefficients at the same powers of  $r$  we arrive at the set of recurrence relations with respect to the unknown coefficients  $\phi_{ji_o}^{(k)}$  and  $\psi_{ji_o}^{(k)}$ :

$$\begin{aligned} & (p_{i_o}^2 - 2E + \varepsilon_j^{(0)})\phi_{ji_o}^{(k)} - 2p_{i_o}^2(k-1)\psi_{ji_o}^{(k-1)} - (k-2)(k-3)\phi_{ji_o}^{(k-2)} \\ & - 2Z(2k-3)\psi_{ji_o}^{(k-2)} + \sum_{k'=1}^k (\varepsilon_j^{(k')} + H_{jj}^{(k')})\phi_{ji_o}^{(k-k')} \\ & = \sum_{j'=1, j' \neq j}^N \sum_{k'=1}^k [(2k-k'-3)Q_{jj'}^{(k'-1)} - H_{jj'}^{(k')}] \phi_{j'i_o}^{(k-k')} \\ & + (2p_{i_o}^2 Q_{jj'}^{(k')} + 4ZQ_{jj'}^{(k'-1)}) \psi_{j'i_o}^{(k-k')}, \end{aligned} \quad (57)$$

$$\begin{aligned} & (p_{i_o}^2 - 2E + \varepsilon_j^{(0)})\psi_{ji_o}^{(k)} + 2(k-1)\phi_{ji_o}^{(k-1)} - k(k-1)\psi_{ji_o}^{(k-2)} + \sum_{k'=1}^k (\varepsilon_j^{(k')} + H_{jj}^{(k')})\psi_{ji_o}^{(k-k')} \\ & = \sum_{j'=1, j' \neq j}^N \sum_{k'=1}^k [(2k-k'+1)Q_{jj'}^{(k'-1)} - H_{jj'}^{(k')}] \psi_{j'i_o}^{(k-k')} - 2Q_{jj'}^{(k')} \phi_{j'i_o}^{(k-k')}. \end{aligned} \quad (58)$$

We get the leading terms of the eigenfunction, the eigenvalue  $p_{i_o}^2$ , i.e. the initial data for solving the above recurrence equations from (57) and (58), as shown in [23]

$$\phi_{j_0 i_o}^{(0)} = \delta_{j_0 i_o}, \quad \psi_{j_0 i_o}^{(0)} = 0, \quad p_{i_o}^2 = 2E - \varepsilon_{i_o}^{(0)}, \quad (59)$$

that correspond to the leading term of  $\chi_{ji_o}(r)$  satisfying the asymptotic expansion at large  $r$

$$\chi_{ji_o}(r) = \frac{\exp(\imath p_{i_o} r + \imath \zeta \ln(2p_{i_o} r) + \imath \delta_{i_o}^c)}{2r \sqrt{p_{i_o}}} \delta_{ji_o}, \quad \zeta = \frac{Z}{p_{i_o}}, \quad (60)$$

where  $\zeta$  is the Sommerfeld parameter and  $\delta_{i_o}^c = \arg \Gamma(1 - \imath \zeta)$  is the Coulomb phase. Open channels have  $p_{i_o}^2 \geq 0$ , and close channels have  $p_{i_o}^2 < 0$ . Suppose that there are  $N_o \leq N$  open channels, i.e.  $p_{i_o}^2 \geq 0$  for  $i_o = 1, \dots, N_o$  and  $p_{i_o}^2 < 0$  for  $i_o = N_o + 1$ ,

$\dots, N$ . Using the explicit asymptotic expressions of the matrix elements (35) we get the explicit expression of the coefficients  $\phi_{ji_o}^{(k)}$  and  $\psi_{ji_o}^{(k)}$  via the number of the state (or of the channel)  $i_o = n_o + 1$  and the number of the current equation  $j = 1, \dots, N$ . The calculation was performed by the algorithm implemented in MAPLE up to  $k_{\max} = 15$ . For example, at  $N \geq i_o + k$  and  $k = 0, 1, 2$  such elements take the form

$$\begin{aligned}
 \phi_{i_o i_o}^{(0)} &= 1, & \psi_{i_o i_o}^{(0)} &= 0, \\
 \phi_{i_o - 1 i_o}^{(1)} &= 0, & \psi_{i_o - 1 i_o}^{(1)} &= \frac{\sqrt{n_o} \sqrt{n_o + |m|}}{\gamma}, \\
 \phi_{i_o i_o}^{(1)} &= 0, & \psi_{i_o i_o}^{(1)} &= -\frac{2n_o + |m| + 1}{\gamma}, \\
 \phi_{i_o + 1 i_o}^{(1)} &= 0, & \psi_{i_o + 1 i_o}^{(1)} &= \frac{\sqrt{n_o + 1} \sqrt{n_o + |m| + 1}}{\gamma}, \\
 \phi_{i_o - 2 i_o}^{(2)} &= -\sqrt{n_o - 1} \sqrt{n_o + |m| - 1} \sqrt{n_o} \sqrt{n_o + |m|} \left( \frac{p_{i_o}^2}{2\gamma^2} + \frac{1}{4\gamma} \right), \\
 \psi_{i_o - 2 i_o}^{(2)} &= 0, \\
 \phi_{i_o - 1 i_o}^{(2)} &= \sqrt{n_o} \sqrt{n_o + |m|} \left( \frac{p_{i_o}^2 (2n_o + |m|)}{\gamma^2} + \frac{1}{2\gamma} \right), \\
 \psi_{i_o - 1 i_o}^{(2)} &= 0, \\
 \phi_{i_o i_o}^{(2)} &= -\frac{p_{i_o}^2 (6n_o^2 + 6n_o + 2 + |m|(6n_o + 3) + |m|^2)}{2\gamma^2} - \frac{2n_o + |m| + 1}{2\gamma}, \\
 \psi_{i_o i_o}^{(2)} &= \frac{Z(2n_o + |m| + 1)}{2p_{i_o}^2 \gamma}, \\
 \phi_{i_o + 1 i_o}^{(2)} &= \sqrt{n_o + 1} \sqrt{n_o + |m| + 1} \left( \frac{p_{i_o}^2 (2n_o + |m| + 2)}{\gamma^2} + \frac{1}{2\gamma} \right), \\
 \psi_{i_o + 1 i_o}^{(2)} &= 0, \\
 \phi_{i_o + 2 i_o}^{(2)} &= -\sqrt{n_o + 1} \sqrt{n_o + |m| + 1} \sqrt{n_o + 2} \sqrt{n_o + |m| + 2} \left( \frac{p_{i_o}^2}{2\gamma^2} - \frac{1}{4\gamma} \right), \\
 \psi_{i_o + 2 i_o}^{(2)} &= 0.
 \end{aligned} \tag{61}$$

In addition, one should mention that at large  $r$  the linearly independent function (54) satisfy the Wronskian-type relation

$$\mathbf{Wr}(\mathbf{Q}(r); \chi^*(r), \chi(r)) = \frac{i}{2} \mathbf{I}_{oo}, \tag{62}$$

where  $\mathbf{Wr}(\bullet; a(r), b(r))$  is a generalized Wronskian with a long derivative defined as

$$\mathbf{Wr}(\bullet; a(r), b(r)) = r^2 \left[ a^T(r) \left( \frac{db(r)}{dr} - \bullet b(r) \right) - \left( \frac{da(r)}{dr} - \bullet a(r) \right)^T b(r) \right]. \tag{63}$$

Here “\*” denotes the complex conjugate and  $\mathbf{I}_{oo}$  is the unit matrix of dimension  $N_o \times N_o$ . These relations will be used to examine the desirable accuracy of the above expansion. Note, that in each  $k$ th order, recurrences (57) and (58) include implicitly only the factor  $Z/p_{i_o}$ . Expansion (55) holds for  $r_{\max} \gg \max(|Z/p_{i_o}|, (2i_o + |m| - 1)/\sqrt{\gamma})$ .

#### 4. Description of the POTHMF program

In order to solve radial bound state or scattering problem one needs to calculate radial matrix elements on interval  $\Delta = [r_{\min}, r_{\max}]$ . The POTHMF program calculates potential matrix elements (12) in Gaussian–Legendre nodes of order  $k + 1$  in each subinterval  $\Delta_j = [r_{j-1}, r_j]$  where  $\Delta = \bigcup_{j=1}^n \Delta_j$ . In each subinterval  $\Delta_j$  the nodes of a finite-elements grid are determined by

$$r_{j,i}^k = r_{j-1} + \frac{h_j}{k} i, \quad h_j = r_j - r_{j-1}, \quad i = \overline{0, k}, \tag{64}$$

where  $k$  order of finite-element shape functions (interpolating Lagrange polynomials) of the radial solution  $\chi(r)$ . Dipole matrix elements (38)–(39) are calculated in nodes (64), because of they are multiplied by  $\chi(r)$  given the same nodes in calculation of integral (75)–(76).

Note, that potential curves and matrix elements of radial coupling calculated by the POTHMF program can be used for solving bound state and scattering problems using appropriate programs from CPC or other available program libraries. In this paper, we use the finite-element KANTBP program [26] to solve the above mentioned problems.

Fig. 5 presents a flow diagram for the POTHMF program. The function of each subroutine is described in Section 5. The POTHMF program is called from the main routine (supplied by a user) which sets dimensions of the arrays and is responsible for the input data. In the present code each array declarator is written in terms of the symbolic names of constants. These constants are defined in the following PARAMETER statement in the main routine:

```
PARAMETER (MTOT=600 000,MITOT=70 000,NMESH1=7)
```

where

- MTOT is the dimension of the working DOUBLE PRECISION array TOT.
- MITOT is the dimension of the working INTEGER array ITOT.
- NMESH1 is the dimension of the DOUBLE PRECISION array RMESH containing the information about the subdivision of the adial interval  $[r_{\min}, r_{\max}]$  on subintervals and number of elements on each one of them. NMESH1 is always odd and  $\geq 3$ .

A more concrete assignment of these dimensions is discussed below. In order to change the dimensions of the code, all one has to do is to modify the single PARAMETER statement defined above in the main program unit.

The calling sequence for the subroutine POTHMF is:

```
CALL POTHMF (TITLE, IMATRX, IDIPOL, IFUNAS, WC, CHARGE, MDIM, NPOL,
1          SHIFTS, TOT, MTOT, ITOT, MITOT, IPRINT, IPRSTP, RMESH,
2          NMESHL, IPARTL, MQNL, POTENL, IOUPL,
3          NMESHR, IPATRR, MQNR, POTENR, IOUPR,
4          FNOUTP, IOUTP, DIPOLD, IOUDD, WFUNAS, IOUWF)
```

## Input data

TITLE	CHARACTER	title of the run to be printed on the output listing. The title should be no longer than 70 characters.
IMATRX	INTEGER	flag for performing the calculation of the potential matrix elements: = 0—calculation of potential matrices elements is not carried out; = 1—calculation of potential matrices elements is carried out only for the first atomic state, i.e. for continuum state; = 2—calculation of potential matrices elements is carried out only for the second atomic state, i.e. for bound state; = 3—calculation of potential matrices elements is carried out for both atomic states.
IDIPOL	INTEGER	flag for performing the calculation of the longitudinal/transversal dipole matrix elements: = 0—calculation of longitudinal/transversal dipole matrix elements is not carried out; = 1—calculation of longitudinal/transversal dipole matrix elements is carried out, i.e. between first and second atomic states.
IFUNAS	INTEGER	flag for performing the calculation of the asymptotic matrix solutions of the scattering problem: < 0—calculation of asymptotic matrix solutions is not carried out; $\geq 0$ and $\leq 15$ —calculation of regular and irregular asymptotic solutions and their derivatives are carried out with order IFUNAS at RMESH(NMESHL).
WC	REAL*8	cyclotron frequency > 0.
CHARGE	REAL*8	nuclear charge.
MDIM	INTEGER	number of coupled differential equations.
NPOL	INTEGER	order of finite-element shape functions (interpolating Lagrange polynomials). Usually set to 6. This is parameter corresponding to a number of nodes $k$ of subinterval (64) using in KANTBP program [26]. In case of NPOL = 0 POTHMF program calculates the matrix elements in the endpoints of subintervals and user cannot use KANTBP program [26].

SHIFTS	REAL*8	SHIFTS contains the given double energy spectrum value $\varepsilon = 2E$ (in a.u.) for scattering problem. This value should be greater than the first threshold and not equals to the open threshold values $\epsilon_{mj}^{th}(\gamma)$ from (36). Else the message about an error is printed and the execution of the program is aborted. The number of open channels $N_o$ is calculated in the program by formula $1 \leq N_o = \max_{2E > \epsilon_{mj}^{th}} j < N$ .
IPRINT	INTEGER	level of print: = 0—minimal level of print. The initial data, short information about the numerical scheme parameters, main flags and keys are printed out; = 1—matrix elements calculated are printed out in corresponding point $r$ with step IPRSTP additionally; = 2—optimal numbers $N_{\max}$ of the terms of expansion (17) calculated by the algorithm (50) are printed out in corresponding point $r$ with step IPRSTP additionally.
IPRSTP	INTEGER	step with which the calculated matrix elements are printed out.
RMESH	REAL*8	array RMESH contains information about subdivision of interval $[r_{\min}, r_{\max}]$ of radius $r$ on subintervals. The whole interval $[r_{\min}, r_{\max}]$ is divided as follows: $RMESH(1) = r_{\min}$ , $RMESH(NMESHL) = r_{\max}$ , and the values of $RMESH(I)$ set the number of elements for each subinterval $[RMESH(I-1), RMESH(I+1)]$ , where $I = 2, 4, \dots, NMESHL-1$ .
NMESHL NMESHR	INTEGER	dimensions of array RMESH of the first and second atomic states, respectively. For the calculation of longitudinal/transversal dipole matrix elements used NMESHR. These dimensions always should be odd and $NMESHL \geq NMESHR \geq 3$ .
IPARTL IPARTR	INTEGER	parities of the first and second atomic states calculated by formula $(1 - \sigma)/2$ , respectively: = 0, for even parity; = 1, for odd parity.
MQNL MQNR	INTEGER	magnetic quantum numbers of the first and second atomic states, respectively.
POTENL POTENR	CHARACTER	names of the output files (up to 55 characters) containing potential matrix elements of radial coupling for first and second atomic states calculated for a Gaussian nodes from the interval $[RMESH(1), RMESH(NMESHL)]$ and $[RMESH(1), RMESH(NMESHR)]$ , respectively.
IOUPL IOUPR	INTEGER	number of the logical device for storing data into files POTENL and POTENR, respectively.
FNOUTP	CHARACTER	name of the output file (up to 55 characters) for printing out the results of the calculation. It is system specific and may include a complete path to the file location.
IOUTP	INTEGER	number of the output logical device for printing out the results of the calculation (usually set to 7).
DIPOLD	CHARACTER	name of the output file (up to 55 characters) containing longitudinal/transversal dipole matrix elements of radial coupling for first and second atomic states calculated for a given set of radial points from the interval $[RMESH(1), RMESH(NMESHR)]$ .
IOUDD	INTEGER	number of the logical device for storing data into file DIPOLD.
WFUNAS	CHARACTER	name of the output file (up to 55 characters) containing regular and irregular asymptotic solutions and their derivatives for the scattering problem.
IOUWF	INTEGER	number of the logical device for writing data from file WFUNAS.
TOT	REAL*8	working vector of the DOUBLE PRECISION type.
ITOT	INTEGER	working vector of the INTEGER type.
MTOT	INTEGER	dimension of the DOUBLE PRECISION working array ITOT. The last address ILAST of array TOT is calculated and then compared with the given value of MTOT. If $ILAST > MTOT$ the message about an error is printed and the execution of the program is aborted. In the last case, in order to carry out the required calculation it is necessary to increase the dimension MTOT of array TOT to the ILAST value taken from the message.



**MITOT**      **INTEGER**      dimension of the **INTEGER** working array **ITOT**. The last address **ILAST** of array **ITOT** is calculated and then compared with the given value of **MITOT**. If **ILAST** > **MITOT** the message about an error is printed and the execution of the program is aborted. In the last case, in order to carry out the required calculation it is necessary to increase the dimension **MITOT** of array **ITOT** to the **ILAST** value taken from the message.

### Output data

The results of the calculation of potential matrix elements in the Gauss–Legendre nodes from the interval [**RMESH**(1), **RMESH**(**NMESH**L/**NMESH**R)] are written using unformatted segmented records into file **POTENL**/**POTENR** with number **IOUP** (**IOUPL**/**IOUPR**), according to the following operator:

```
WRITE (IOUP) L, ( (UPOT(I,J,IG), J=I, MDIM), I=1, MDIM), IG=1, NGQ),
1          ( (QPOT(I,J,IG), J=I+1, MDIM), I=1, MDIM), IG=1, NGQ)
```

The results of the calculation of potential matrix elements in the **RMESH** (**NMESH**L / **NMESH**R) are written using unformatted segmented records into the above file, according to the following operator:

```
WRITE (IOUP) NGRID, ( (H(I,J), J=I, MDIM), I=1, MDIM),
1          ( (Q(I,J), J=I+1, MDIM), I=1, MDIM)
```

The results of the calculation of longitudinal/transversal dipole matrix elements for the given set of radial points from the interval [**RMESH**(1), **RMESH** (**NMESH**R)] are written using unformatted segmented records into file **DIPOLE** with number **IOUDD**, according to the following operator:

```
WRITE (IOUDD) IG, ( (DD(I,J), J=1, MDIM), I=1, MDIM)
```

The results of the calculation of regular and irregular asymptotic matrix-solutions and their derivatives are written using unformatted segmented records into file **WFUNAS** with number **IOUWF**, according to the following operator:

```
WRITE (IOUWF) MDIM, NOPEN, (QR(I), I=1, NOPEN),
1          ( (PREG(I,J), J=1, NOPEN), I=1, MDIM),
2          ( (PIRR(I,J), J=1, NOPEN), I=1, MDIM),
3          ( (DPREG(I,J), J=1, NOPEN), I=1, MDIM),
4          ( (DPIRR(I,J), J=1, NOPEN), I=1, MDIM)
```

In the above, parameters presented in the **WRITE** statement have the following meaning:

- **L** is number of finite element.
- **NGRID** is the number of grid points.
- **IG** is the number of grid point.
- **NGQ** = **NPOL** + 1.
- **NOPEN** is the number of open channels.
- Arrays **UPOT** and **QPOT** contain the potential matrices values calculated.
- Array **DD** contains the longitudinal/transversal dipole matrix values calculated.
- Array **QR** contains the values of the momentums,  $QR(J) = \sqrt{2E - \epsilon_{mj}^{th}(\gamma)}$ .
- Arrays **PREG**, **PIRR** and **DPREG**, **DPIRR** contain the values of the regular and irregular asymptotic matrix-solutions and their derivatives, respectively.

## 5. Description of subprogram units

A flow diagram for the **POTMHF** program is presented in Fig. 5. The function of each subroutine is briefly described below. Additional details may be found in **COMMENT** cards within the program.

- Subroutine **ERRMDM** prints error messages when high-speed storage requested by a user is exceeded and stops the execution of program **POTMHF**.
- Subroutine **GAULEG** [39] calculates nodes and weights of the Gauss–Legendre quadrature. This subroutine is included in main body program.



- Subroutine FEGRID [26] calculates nodal points for the finite-element uniform grid. This subroutine is included in main body program.
- Subroutine HQPOTM calculates the potential matrix elements  $\mathbf{V}(r)$ ,  $\mathbf{Q}(r)$  of dimension  $\text{MDIM} \times \text{MDIM}$  of radial coupling in the Gaussian nodes and storing using unformatted segmented records into file POTEN.
- Subroutine MAGNET calculates the potential matrix elements  $\mathbf{V}(r)$ ,  $\mathbf{Q}(r)$  of dimension  $\text{MDIM} \times \text{MDIM}$ .
- Subroutine SPECTR evaluates the potential matrix elements  $\mathbf{H}(r)$ ,  $\mathbf{Q}(r)$  of dimension  $\text{MDIM} \times \text{MDIM}$  and the potential curves  $\epsilon(r)$  of dimension  $\text{MDIM}$  calculated via solutions of the algebraic problems (19) and (25) of dimension  $N_{\max} \times N_{\max}$ .
- INTEGER function NOPTIM calculates the optimal number  $N_{\max}$  for the calculation of the algebraic eigenvalue problem (19) with the relative machine precision.
- Subroutine SOLUTN solves the algebraic eigenvalue problem (19) and sets of inhomogeneous algebraic equations (25).
- DOUBLE PRECISION function AMKANT prepares matrix  $\mathbf{A}^{(0)}$  in the eigenvalue problem (19) and its derivatives.
- DOUBLE PRECISION function SIN2 prepares coefficients of  $p^2$  of matrix  $\mathbf{A}^{(0)}$  in the eigenvalue problem (19).
- Subroutine DSTEVR [33] solves the first  $\text{MDIM}$  eigenvalues and corresponding eigenvectors of the algebraic eigenvalue problem for the real symmetric tridiagonal matrix.
- Subroutine DBANDM calculates  $\mathbf{LDL}^T$  factorization of the tridiagonal matrix. This factorization is used in subroutine DPTTRS.
- Subroutine DPTTRS [33] solves sets of inhomogeneous algebraic equations for the real symmetric tridiagonal matrix.
- DOUBLE PRECISION function QASINF calculates the terms of the potential matrix elements  $\mathbf{Q}(r)$  in expansion (35).
- DOUBLE PRECISION function HASINF calculates the terms of the potential matrix elements  $\mathbf{H}(r)$  in expansion (35).
- DOUBLE PRECISION function SPEINF calculates the terms of the potential curve  $\epsilon(r)$  in expansion (35).
- Subroutine DIPPOT calculates the longitudinal/transversal dipole matrices elements  $\mathbf{D}^{(m\sigma\sigma')}(r)/\mathbf{P}^{(mm'\sigma)}(r)$  of dimension  $\text{MDIM} \times \text{MDIM}$  of radial coupling in the given set of radial points and stores them using unformatted segmented records into file DIPOLD.
- Subroutine DIPOLE evaluates the longitudinal dipole matrix elements  $\mathbf{D}^{(m\sigma\sigma')}(r)$  of dimension  $\text{MDIM} \times \text{MDIM}$ .
- Subroutine SPECTD evaluates the longitudinal dipole matrix elements  $\mathbf{D}^{(m-1+1)}(r)$  of dimension  $\text{MDIM} \times \text{MDIM}$  calculated via solutions of the algebraic eigenvalue problem (19) of dimension  $N_{\max} \times N_{\max}$ .
- DOUBLE PRECISION function DASINF calculates the terms of the longitudinal dipole matrix elements  $\mathbf{D}^{(m\sigma\sigma')}(r)$  of expansion (42).
- Subroutine CPOLAR evaluates the transversal dipole matrix elements  $\mathbf{P}^{(mm'\sigma)}(r)$  of dimension  $\text{MDIM} \times \text{MDIM}$ .
- Subroutine SPECTP evaluates the transversal dipole matrix elements  $\mathbf{P}^{(m<m>\sigma)}(r)$  at  $m_{<} = \min(|m|, |m'|)$ ,  $m_{>} = \max(|m|, |m'|)$  of dimension  $\text{MDIM} \times \text{MDIM}$  calculated via solutions of the algebraic eigenvalue problem (19) of dimension  $N_{\max} \times N_{\max}$ .
- DOUBLE PRECISION function CASINF calculates the terms of the transversal dipole matrix elements  $\mathbf{P}^{(m<m>\sigma)}(r)$  of expansion (42).
- Subroutine ASYMFN calculates the regular and irregular asymptotic matrix-solutions  $\chi^s(r)$ ,  $\chi^c(r)$  and their derivatives and writes them using unformatted segmented records into file WFUNAS. Also this subroutine calculates the generalized Wronskian relation by the formula (69) using DOUBLE PRECISION function QASINF.
- Subroutine MAGASC calculates the regular and irregular asymptotic matrix-solutions  $\chi^s(r)$ ,  $\chi^c(r)$  and their derivatives of the scattering problem.
- Subroutine FUNINF calculates of terms of expansion (54), (55) of asymptotics of regular and irregular solutions and their derivatives and prints a message about recommended right bound of interval  $r_{\max}$  and value of the matching point  $r_{\text{match}}$  from Eq. (52) with the given accuracy  $\text{eps}_c = 10^{-14}$ .
- Subroutine RCWFNN calculates the Coulomb regular and irregular solutions and their derivatives with the given accuracy  $\text{eps}_c = 10^{-14}$ . This subroutine is the modified version of the subroutine RCWFN [40] for DOUBLE PRECISION type. This subroutine is included in main body program.

## 6. Test desk

The test run which accompanies the POTHMF program computes the potential and longitudinal dipole matrix elements for the given atomic states (for the initial state  $\sigma = +1$  and for the final state  $\sigma = -1$ ) with  $Z = 1$ ,  $\gamma = 1$  and  $m = 0$ . After that, we applied the calculated matrix elements to the calculation of the ground state energy and reaction matrix for initial and final atomic states with help of the KANTBP program [26], respectively.

File 'INITIAL.INP' contains the initial data NAMELIST POTDAT for the calculation of the potential and longitudinal dipole matrix elements for the given atomic states for the POTHMF program. Also this file contains the initial data NAMELIST PARDIS and NAMELIST PARSCP for the calculation of the ground state energy and reaction matrix for the KANTBP program (see details in [26]), respectively. File 'INITIAL.INP' contains the following data:

```

&POTDAT TITLE=' Potential and dipole matrices elements ',
        IMATRX=3, IDIPOL=1, IFUNAS=15, WC=0.1D1, CHARGE=1.D0, MDIM=6,
        NPOL=4, SHIFTS=3.4D0, IPRINT=1, IPRSTP=1501,
        RMESH=0.0D0, 200.D0, 3.D0, 200.D0, 20.D0, 200.D0, 100.D0,
        FNOUTP=' FNOUTP.LPR ', IOUPT=7,
        NMESHL=7, IPARTL=1, MQNL=0, POTENL=' POTENL.PTN ', IOUPL=8,
        NMESHR=7, IPARTR=0, MQNR=0, POTENR=' POTENR.PTN ', IOUPR=9,
        DIPOLD=' DIPOLP.PTN ', IOUDD=10, WFUNAS=' WFUNAS.PTN ', IOUWF=1
&END
&PARDIS TITLE1=' Bound state energy levels ',
        IPTYPE=0, NROOT=1, IDIM=3, RTOL=1.D-15,
        NITEM=150, SHIFT=-0.7D0, IPRINT=2, IPRSTP=480,
        NDIR=1, NDIL=6, NMDIL=1, IBOUND=3,
        FNOUTR=' 3DNSAS.LPR ', IOUT=11, FMATRR=' 3DNSAS.MAT ', IOUM=12,
        EVWFNR=' 3DNSAS.WFN ', IOUF=0
&END
&PARSCP TITLE2=' Reaction matrix ',
        IPTYPE=1, NROOT=1, SHIFT=3.4D0, IPRINT=2, IPRSTP=480, IBOUND=8,
        THRSHL=1.D0, 3.D0, 5.D0, 7.D0, 9.D0, 11.D0,
        FNOUTL=' 3DNSSC.LPR ', NOUT=14, FMATRL=' 3DNSSC.MAT ', NOUM=15,
        EVWFNL=' 3DNSSC.WFN ', NOUF=0
&END

```

Physical parameters CHARGE, WC, MQNL and order of asymptotic solutions IFUNAS are accessed via general common block COMMON /CHARGE/ CHARGE, WC, MQNL, IFUNAS. The user subroutine ASYMSC should contain this common block and could be written as follows:

```

      SUBROUTINE ASYMSC (RMAX, NDIM, NOPEN, QR, PREG, PIRR, DREG, DIRR, IOUT)
C . . . . .
C .
C .   P R O G R A M
C .
C .           TO CALCULATE THE REGULAR, IRREGULAR
C .           ASYMPTOTIC MATRIX SOLUTIONS PREG, PIRR
C .           AND THEIR DERIVATIVES DREG, DIRR AT RMAX
C .
C .
C . . . . .
      IMPLICIT REAL*8 (A-H, O-Z)
      PARAMETER (NWOR=3000)
      DIMENSION QR (NOPEN), PREG (NDIM, NOPEN), PIRR (NDIM, NOPEN),
1      DREG (NDIM, NOPEN), DIRR (NDIM, NOPEN)
      DIMENSION WORK (NWOR)
      COMMON /CHARGE/ CHARGE, WC, MQNL, IFUNAS
      CALL MAGASC (RMAX, NDIM, NOPEN, QR, PREG, PIRR, DREG, DIRR, IFUNAS,
1      WORK, NWOR, CHARGE, WC, MQNL, IOUT)
      RETURN
      END

```

The test run which accompanies this paper took 7 s for calculation of potential curves, matrix elements and dipole transition matrix elements, and 2 s for calculation of discrete and continuous spectrum problems using the obtained potential curves and matrix elements on the Intel Pentium IV 2.4 GHz, respectively. The potential curves  $\varepsilon_j(r)$ , matrix elements  $Q_{ij}(r)$ ,  $H_{ij}(r)$ , longitudinal dipole matrix elements  $D_{ij}^{(m\sigma\sigma')}(r)$  and corresponding wave functions of continuum spectrum of this test run are presented in Figs. 1–4, 6. The finite element grid in  $r$  has been chosen as 0 (200) 3 (200) 20 (200) 100 from the initial data list (see description of array RMESH). The numbers in parentheses are the numbers of finite elements of order  $k = 4$  on each subinterval (see description value NPOL).

## 7. Benchmark calculations of the photoionization cross-sections

In this section we present calculation of photoionization cross-sections with the help of the KANTBP program using potential curves, radial matrix elements and dipole matrix elements computed by the POTHMF program. Eigenfunction of the continuum spectrum  $\Psi_i^{Em\sigma}(r, \eta)$  with the energy  $\epsilon = 2E$  describing the ejected electron above the first threshold  $\epsilon_{m1}^{th}(\gamma) = \gamma(|m| + m + 1)$  is

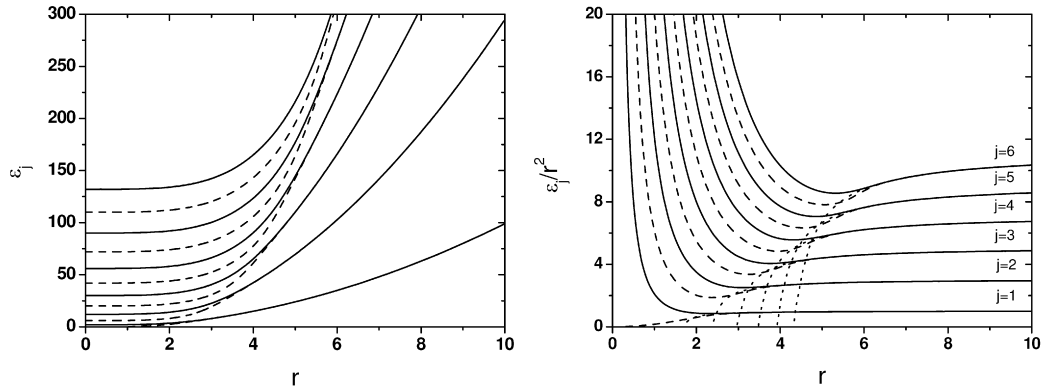


Fig. 1. Potential curves  $\varepsilon_j(r)$ , at  $m = 0$  and  $\gamma = 1$ . Full line—odd state; dashed line—even state. Dotted lines display the asymptotic behavior at large  $r$ .

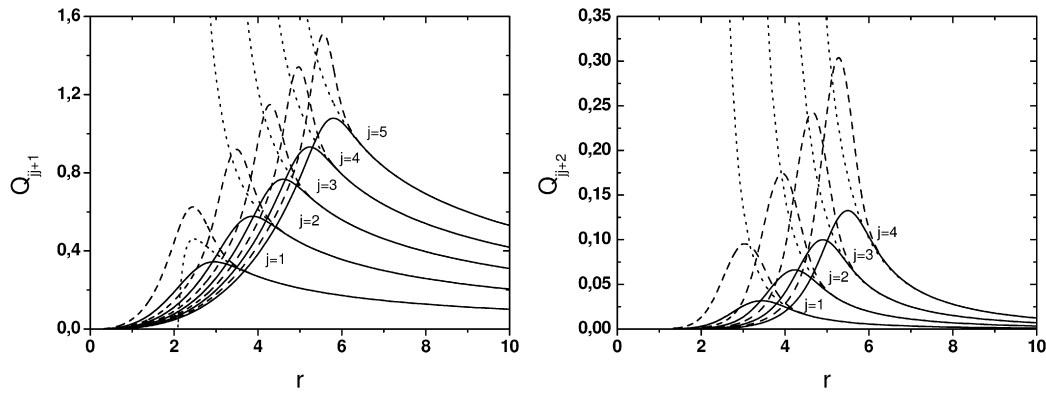


Fig. 2. Radial matrix elements  $Q_{jj+1}(r)$ ,  $Q_{jj+2}(r)$  at  $m = 0$  and  $\gamma = 1$ . Full line—odd state; dashed line—even state. Dotted lines display the asymptotic behavior at large  $r$ .

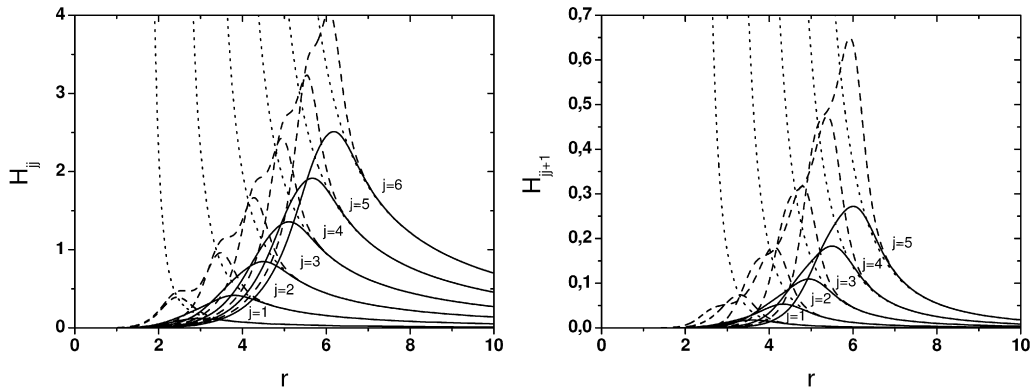


Fig. 3. Radial matrix elements  $H_{jj}(r)$ ,  $H_{jj+1}(r)$  at  $m = 0$  and  $\gamma = 1$ . Full line—odd state; dashed line—even state. Dotted lines display the asymptotic behavior at large  $r$ .

expressed as follows:

$$\Psi_i^{Em\sigma}(r, \eta) = \sum_{j=1}^N \Phi_j^{m\sigma}(\eta; r) \hat{\chi}_{ji}^{(m\sigma)}(E, r), \quad i = 1, \dots, N_o, \quad (65)$$

where solution  $\hat{\chi}^{(m\sigma)}(E, r)$  is the radial part of the “incoming” or eigenchannel wave function. In this case the eigenfunction  $\Psi_i^{Em\sigma}(r, \eta)$  is normalized by

$$\begin{aligned} \langle \Psi_i^{Em\sigma}(r, \eta) | \Psi_{i'}^{E'm'\sigma'}(r, \eta) \rangle &= \sum_{j=1}^N \int_0^\infty r^2 dr (\hat{\chi}_{ji}^{(m\sigma)}(E, r))^* \hat{\chi}_{ji'}^{(m'\sigma')}(E', r) \\ &= \delta(E - E') \delta_{mm'} \delta_{\sigma\sigma'} \delta_{ii'}. \end{aligned} \quad (66)$$

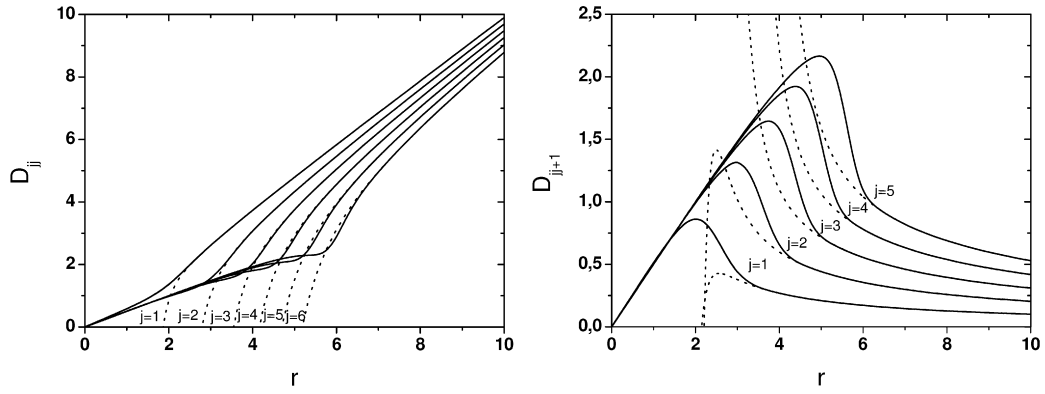


Fig. 4. Longitudinal dipole matrix elements  $D_{jj}^{(m\sigma\sigma')}(r)$ ,  $D_{jj+1}^{(m\sigma\sigma')}(r)$  at  $m=0$ ,  $\sigma=-1$ ,  $\sigma'=1$  and  $\gamma=1$ . Dotted lines display the asymptotic behavior at large  $r$ .

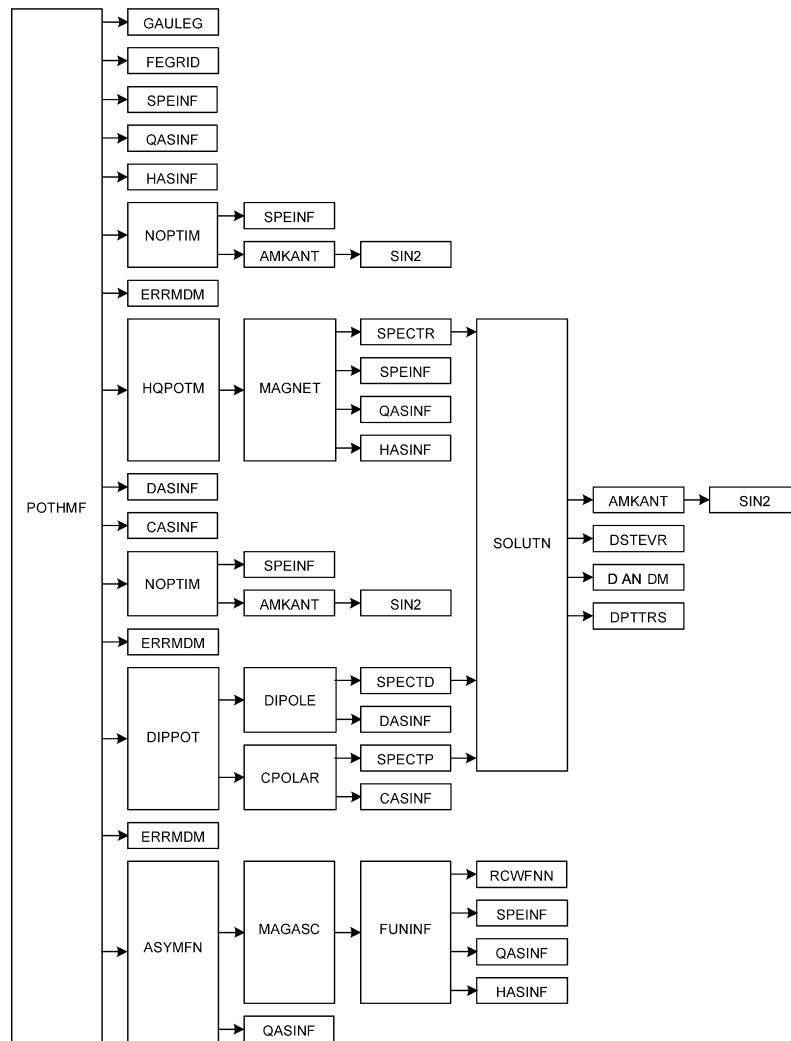


Fig. 5. Flow diagram of the POTHMF program.

The radial eigenchannel function  $\hat{\chi}^{(m\sigma)}(E, r)$  is calculated by formula

$$\hat{\chi}^{(m\sigma)}(E, r) = \sqrt{\frac{2}{\pi}} \chi^{(p)}(r) \mathbf{B} \cos \delta. \quad (67)$$

Here,  $\chi^{(p)}(r)$  is the numerical solution of Eq. (11) that satisfies the “standing” wave boundary conditions (15) and has the standard asymptotic form [26]

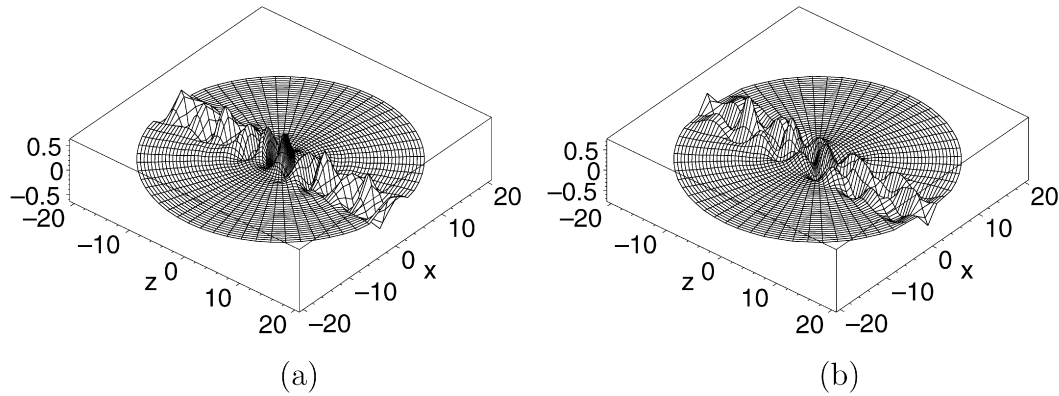


Fig. 6. The wave functions  $\Psi_1$  and  $\Psi_2$  of the first (a) and second (b) open channels of the continuum spectrum states having asymptotic (67) in the  $zx$  plane for  $\sigma = -1$ ,  $Z = 1$ ,  $\gamma = 1$  and  $m = 0$  with energy  $E = 1.7$  a.u. above the second threshold  $1/2\epsilon_{m2}^h = 1.5$ .

$$\chi^{(p)}(r) = \chi^s(r) + \chi^c(r)\mathbf{K}, \quad \mathbf{K}\mathbf{B} = \mathbf{B}\tan\delta, \quad \mathbf{B}\mathbf{B}^T = \mathbf{B}^T\mathbf{B} = \mathbf{I}_{oo}, \quad (68)$$

where  $\chi^s(r) = 2\Im(\chi(r))$  and  $\chi^c(r) = 2\Re(\chi(r))$ ,  $\mathbf{K}$  is the numerical short-range reaction matrix,  $\tan\delta$  and  $\mathbf{B}$  are the eigenvalue and the orthogonal matrix of a set of the corresponding eigenvectors. In the latter the regular and irregular functions satisfy the generalized Wronskian relation (63) at large  $r$

$$\mathbf{W}\mathbf{r}(\mathbf{Q}(r); \chi^c(r), \chi^s(r)) = \mathbf{I}_{oo}. \quad (69)$$

The radial part of the “incoming” wave function is expressed via the numerical “standing” wave function and short-range reaction matrix  $\mathbf{K}$  by the relation

$$\hat{\chi}^{(m\sigma)}(E, r) = \sqrt{\frac{2}{\pi}} \chi^-(r) = \iota \sqrt{\frac{2}{\pi}} \chi^{(p)}(r) (\mathbf{I}_{oo} + \iota \mathbf{K})^{-1} \quad (70)$$

and has the asymptotic form

$$\hat{\chi}^{(m\sigma)}(E, r) = \sqrt{\frac{2}{\pi}} (\chi(r) - \chi^*(r)\mathbf{S}^\dagger), \quad (71)$$

where  $\mathbf{S}$  is the short-range scattering matrix and

$$\mathbf{S}^\dagger \mathbf{S} = \mathbf{S} \mathbf{S}^\dagger = \mathbf{I}_{oo}, \quad \mathbf{K} = \iota (\mathbf{I}_{oo} + \mathbf{S})^{-1} (\mathbf{I}_{oo} - \mathbf{S}), \quad \mathbf{S} = (\mathbf{I}_{oo} + \iota \mathbf{K}) (\mathbf{I}_{oo} - \iota \mathbf{K})^{-1}. \quad (72)$$

The total wave function having the asymptotic form “waves going into the center + outgoing wave” [28],

$$\Psi_{Em\leftarrow}^{(-)}(r, \eta) = \frac{\Psi^{Em\sigma=+1}(r, \eta) \pm \Psi^{Em\sigma=-1}(r, \eta)}{\sqrt{2}} \exp(-\iota \delta^c). \quad (73)$$

In terms of the above definitions the cross section of photoionization  $\sigma_{m\sigma\sigma'}^d(\omega)$  by the light linearly polarized along  $z$ -axis and  $\sigma_{mm'\sigma}^p(\omega)$  by the light circularly polarized in the plane  $XOY$  are expressed as

$$\sigma_{m\sigma\sigma'}^d(\omega) = C\omega \sum_{i=1}^{N_o} |\hat{D}_{i,i',v'}^{m\sigma\sigma'}(E)|^2, \quad \sigma_{mm'\sigma}^p(\omega) = C\omega \sum_{i=1}^{N_o} |\hat{P}_{i,i',v'}^{mm'\sigma}(E)|^2. \quad (74)$$

Here  $\hat{D}_{i,i',v'}^{m\sigma\sigma'}(E)$  and  $\hat{P}_{i,i',v'}^{mm'\sigma}(E)$  are the matrix elements of the longitudinal and transversal dipole moment, respectively:

$$\begin{aligned} \hat{D}_{i,i',v'}^{m\sigma\sigma'}(E) &= \langle \Psi_i^{Em\sigma}(r, \eta) | r\eta | \Psi_{i',v'}^{m'=m, \sigma'=-\sigma}(r, \eta) \rangle \\ &= \sum_{j=1}^N \sum_{j'=1}^N \int_0^{r_{\max}} r^2 dr (\hat{\chi}_{ji}^{(m\sigma)}(E, r))^* D_{jj'}^{(m\sigma\sigma')}(r) \chi_{j'i',v'}^{(m'=m, \sigma'=-\sigma)}(r), \end{aligned} \quad (75)$$

$$\begin{aligned} \hat{P}_{i,i',v'}^{mm'\sigma}(E) &= \left\langle \Psi_i^{Em\sigma}(r, \eta) \left| r \frac{\sqrt{1-\eta^2}}{\sqrt{2}} \right| \Psi_{i',v'}^{m'=m\pm 1, \sigma'=\sigma}(r, \eta) \right\rangle \\ &= \sum_{j=1}^N \sum_{j'=1}^N \int_0^{r_{\max}} r^2 dr (\hat{\chi}_{ji}^{(m\sigma)}(E, r))^* P_{jj'}^{(mm'\sigma)}(r) \chi_{j'i',v'}^{(m'=m\pm 1, \sigma'=\sigma)}(r), \end{aligned} \quad (76)$$

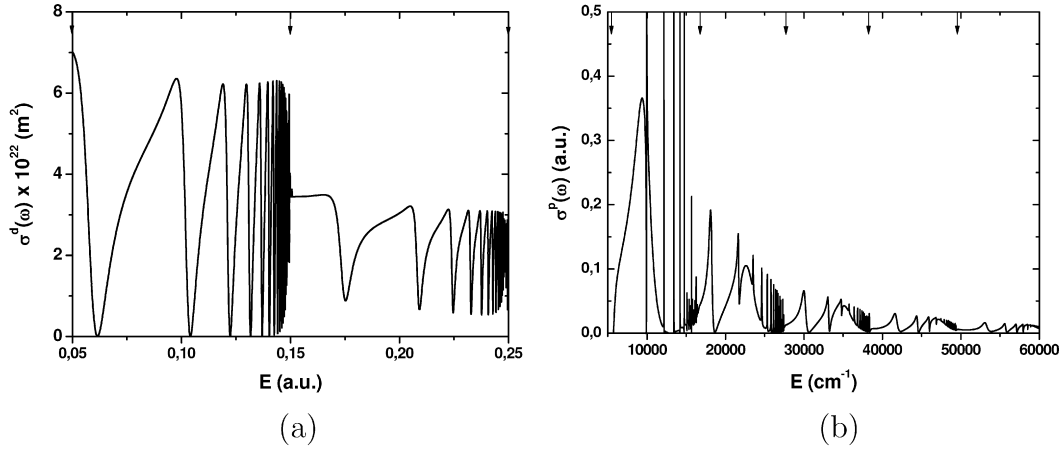


Fig. 7. Photoionization cross-sections  $\sigma_{m\sigma\sigma'}^d(\omega)$  (a) and  $\sigma_{mm'\sigma}^p(\omega)$  (b). (a) The photoionization is from the ground state  $1s_0$  with  $\gamma = 0.1$ ,  $\sigma' = 1$  and  $m = 0$  to final state with  $\sigma = -1$ . (b) The photoionization is from the excited state  $2p_{-1}$  with  $\gamma = 0.05$ ,  $\sigma = 1$  and  $m' = -1$  to final state with  $m = 0$ . The arrows indicate the successive Landau thresholds  $1/2\epsilon_{mj}^{th}$  from (35), where  $j$  runs from 1 to 2 in (a) and runs from 1 to 5 in (b).

where longitudinal  $\mathbf{D}^{(m\sigma\sigma')}(r)$  and transversal  $\mathbf{P}^{(mm'\sigma)}(r)$  dipole matrix elements are calculated by formulae (38) and (39). The cross sections (74) in terms of the  $\hat{D}_{i,i',v'}^{m\sigma\sigma'}(\hat{E})$  and  $\hat{P}_{i,i',v'}^{mm'\sigma}(\hat{E})$  expressed via  $\mathbf{D}^{(m\sigma\sigma')}(\hat{r})$  and transversal  $\mathbf{P}^{(mm'\sigma)}(\hat{r})$  in scaled variable  $\hat{r}$  and the parameters  $\hat{E}$ ,  $\hat{Z}$  reads as

$$\sigma_{m\sigma\sigma'}^d(\omega) = \frac{C\omega}{\gamma^2} \sum_{i=1}^{N_o} |\hat{D}_{i,i',v'}^{m\sigma\sigma'}(\hat{E})|^2, \quad \sigma_{mm'\sigma}^p(\omega) = \frac{C\omega}{\gamma^2} \sum_{i=1}^{N_o} |\hat{P}_{i,i',v'}^{mm'\sigma}(\hat{E})|^2. \quad (77)$$

In the above expressions,  $\omega = E - E_{m'\sigma'i'v'}$  is the frequency of radiation,  $E_{nlm} \equiv E_{m'\sigma'i'v'} < \epsilon_{mi}^{th}(\gamma)/2$  is the energy of the initial bound state  $\Psi_{i',v'}^{m'\sigma'}(r, \eta)$  with  $i' = 1$  and vibration number  $v' = 0, 1, \dots, N-1$ ,  $E$  is the energy of the final continuum state  $\Psi_i^{Em\sigma}(r, \eta)$  such that  $N_o$  is the number of the open channels,  $C = 4\pi^2\alpha a_0^2$  is a constant,  $\alpha$  is the fine-structure constant, and  $a_0$  is the Bohr radius. The continuum spectrum solution  $\chi^{(p)}(r)$  having asymptotic of “standing” wave conditions and reaction matrix  $\mathbf{K}$  required for calculation of (67) or (71), and discrete spectrum solution  $\chi_{i',v'}^{m'\sigma'}(r)$  and eigenvalue  $E_{m'\sigma'i'v'}$  have been calculated with the help of the program KANTBP [26]. One can see that using (67) or (71) for calculating the absolute value in formula (74) yields the same result. Therefore, (67) is preferable for using real arithmetics. Note, that using physical function constructed via (67) with mixed parity that has an appropriate asymptotic of the incoming wave in cylindrical coordinates on the whole axis  $z$  leads to the same result [28].

Fig. 7 displays the photoionization cross-sections  $\sigma_{m\sigma\sigma'}^d(\omega)$  and  $\sigma_{mm'\sigma}^p(\omega)$  calculated by programs POTHMF and KANTBP. The finite element grids of  $\hat{r}$  have been chosen as 0 (200) 3 (200) 20 (200) 100 for the discrete spectrum and 0 (200) 3 (200) 20 (200) 100 (1000) 1000 for the continuum one. The numbers in parentheses are the numbers of finite elements of order  $k = 4$  on each interval. In the calculations we have used the following values of physical constants [41]: the Bohr radius  $a_0 = 5.29177 \times 10^{-11}$  m, the fine-structure constant  $\alpha = 7.29735 \times 10^{-3}$  and  $1 \text{ cm}^{-1} = 4.55633 \times 10^{-6}$  a.u.

Fig. 7(a) shows the photoionization cross section from the ground state  $1s_0$  with  $\gamma = 0.1$ ,  $\sigma' = 1$  and  $m = 0$  to final state with  $\sigma = -1$ . The number of open channels is equal to 1 and 2 and dimension of the truncated system (11) is equal to  $N = 10$ . In the whole energy interval the results are in good agreement with those of  $\mathbf{R}$ -matrix calculations within the MQDT [12]. We also compared our result with those of the complex-rotation method combined with a basic set of the 10 000 complex spherical Sturmian-type expansion (CSSTE) [15] and of the 450 mixed Slater–Landau basis (MSLB) [17]. In this case the agreement is good between the thresholds, but not near them. Fig. 7(b) shows the photoionization cross section from the excited state  $2p_{-1}$  with  $\gamma = 0.05$ ,  $\sigma = 1$  and  $m' = -1$  to final state with  $m = 0$ . The number of the open channels varied from 1 to 5 and dimension of the truncated system (11) is equal to  $N = 18$ . We compared our result with those of the complex-rotation method combined with a basic set of the 10 000 CSSTE [16] and of the 288 MSLB [17]. In this case we have the some agreement between the thresholds, but not near them. So, the calculated photoionization cross sections have the true behavior above the thresholds that is one of the goal of the elaborated approach.

Fig. 8(a) displays the cross-section of photoionization by the light linearly polarized along the axis  $z$  from the rotational state  $3s_0$  at  $B_0 = 6.10 \text{ T}$  ( $\gamma = 2.595 \times 10^{-5}$ ) in the energy interval between  $E = 6.0 \text{ cm}^{-1}$  and  $E = 8.0 \text{ cm}^{-1}$ . In this case we increased  $N$  up to 35 and the finite element grids of  $\hat{r} = \sqrt{\gamma}r$  were chosen as 0 (200) 0.03 (200) 0.2 (200) 1 for the discrete spectrum and 0 (200) 0.03 (200) 0.2 (200) 1 (2000) 100 (4000) 1000 for the continuous one. The number of nodes in these grids is 2400 and 26 401, respectively. The corresponding maximal number of unknowns in Eqs. (11) is 84 000 and 924 035. Fig. 8(b) shows the absolute maximum values of the continuum wave functions  $\hat{\chi}_{j1}^{(01)}(E, \hat{r})$  at  $E = 6.0 \text{ cm}^{-1}$ . We calculated the cross-sections with the energy

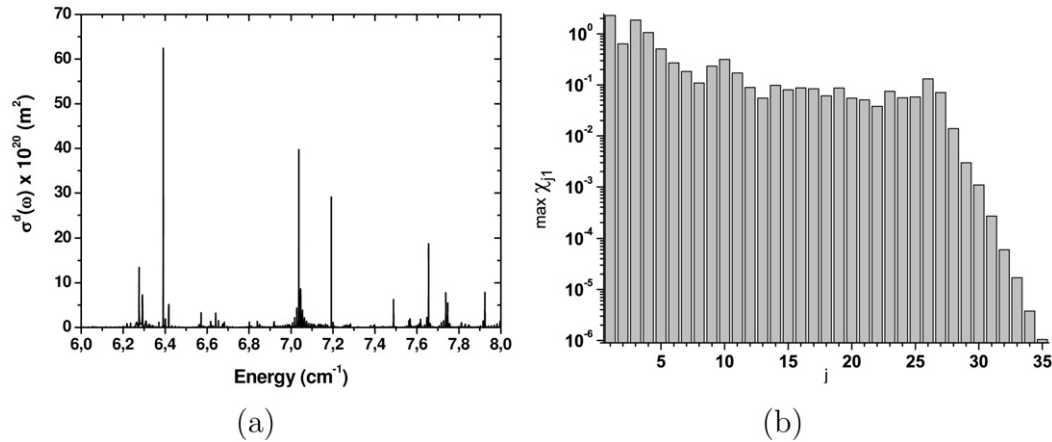


Fig. 8. (a) Cross-section of photoionization from the state  $3s_0$  versus the energy for  $\gamma = 2.595 \times 10^{-5}$  and for the final state with  $\sigma = -1$ ,  $Z = 1$ ,  $m = 0$ . (b) Absolute maximum values of the continuum wave functions  $\hat{\chi}_{j1}^{(01)}(E, \hat{r})$  at  $E = 6.0 \text{ cm}^{-1}$  and  $N = 35$  using for calculation in figure (a).

step  $5 \times 10^{-4} \text{ cm}^{-1}$  in all the region except the vicinity of peaks, where the step was  $5 \times 10^{-6} \text{ cm}^{-1}$ . Note, that states  $3d_0$ ,  $3p_0$  and  $3s_0$  with energies  $E_{320} = -0.0555555207 \text{ a.u.}$ ,  $E_{310} = -0.05555554949 \text{ a.u.}$  and  $E_{300} = -0.05555554237 \text{ a.u.}$ , respectively, are nearly degenerate. In this case we have a good agreement [15] used a basic set of the 62 500 CSSTE. More detailed discussion of results of calculation of a hydrogen atom in a strong magnetic field using the POTHMF program for calculating potential curves and matrix elements of radial coupling and dipole matrix elements is given in paper [29] where a good agreement with the results of calculations performed by other methods has been demonstrated.

## 8. Conclusions

A new efficient method of calculating both discrete and continuum spectrum wave functions of a hydrogen atom in a strong magnetic field is developed based on the Kantorovich approach to the parametric eigenvalue problems in spherical coordinates. The two-dimensional spectral problem for the Schrödinger equation with fixed magnetic quantum number and parity is reduced to a one-dimensional spectral parametric problem for the angular variable and a finite set of ordinary second-order differential equations in the radial variable. The rate of convergence of the method is examined numerically and is illustrated with a number of typical examples. The main advantage of the elaborated approach lies in the fact that calculations on all steps of the Kantorovich approach are realized with the help of stable calculation schemes and with a prescribed accuracy. The economy of computer resources is achieved with the help of calculated asymptotics for a set of adaptive basis functions, matrix elements of radial coupling and radial solutions in analytic form by means of the MAPLE computer algebra algorithms [23]. This allows one to significantly reduce the interval of integration of the corresponding boundary problems. It is shown that the calculated photoionization cross-sections has the true threshold behavior while recombination cross-sections can be recalculated using the corresponding relations presented in [6]. The approach developed provides a useful tool for calculations of threshold phenomena in the formation and ionization of (anti)hydrogen-like atoms and ions in magnetic traps.

## Acknowledgements

The authors thank Prof. V.L. Derbov for a long-time collaboration. O.C. and M.S.K. acknowledge financial support from a grant of the President of the Bulgarian Fund for Scientific Investigations under grant I-1402/2004-2007 and the theme 09-6-1060-2005/2009 “Mathematical support of experimental and theoretical studies conducted by JINR”. V.P.G. and A.A.G. acknowledge partial support from the Russian Foundation for Basic Research under grant No. 07-01-00660.

## Appendix A

```
***** BEGIN OF THE POTHMF RUN *****

PROBLEM:      Potential and dipole matrices elements
*****

                C O N T R O L   I N F O R M A T I O N
                -----
```

```

NUMBER OF DIFFERENTIAL EQUATIONS. . . . . (MDIM ) =      6
ORDER OF SHAPE FUNCTIONS. . . . . (NPOL ) =      4
ORDER OF GAUSS-LEGENDRE QUADRATURE. . . . (NGQ ) =      5
VALUE OF NUCLEAR CHARGE . . . . . (CHARGE) =     1.00000
VALUE OF CYCLOTRON FREQUENCY. . . . . (WC ) =     1.00000
VALUE OF THE RELATIVE MACHINE PRECISION . (EPSY ) =    0.222045E-15

```

#### SPECIFICATIONS OF THE FIRST ATOMIC STATE

-----

```

NUMBER OF FINITE ELEMENTS . . . . . (NELEM ) =     600
NUMBER OF GRID POINTS . . . . . (NGRID ) =    2401
PARITY OF STATE . . . . . (IPARTL) =      1
MAGNETIC QUANTUM NUMBER . . . . . (MQNL ) =      0
VALUE OF MATCHING POINT FOR EPSY. . . . . (RMATCH) =   39.0953

```

#### SUBDIVISION OF RHO-REGION ON THE FINITE-ELEMENT GROUPS:

\*\*\*\*\*

NO OF GROUP	NUMBER OF ELEMENTS	BEGIN OF INTERVAL	LENGTH OF ELEMENT	GRID STEP	END OF INTERVAL
1	200	0.000	0.01500	0.00375	3.000
2	200	3.000	0.08500	0.02125	20.000
3	200	20.000	0.40000	0.10000	100.000

LAST ADDRESS OF ARRAY ITOT USED = 3763

LAST ADDRESS OF ARRAY TOT USED = 9728

#### POTENTIAL MATRICES V(I,J) AND Q(I,J):

V-MATRIX AT THE POINT NO = 1 AND RADIUS RHO = 0.00070

0.4037D+07	0.1102D-37	-.4472D-22	-.1240D-37	-.5652D-53	-.8437D-69
0.1102D-37	0.2423D+08	0.2229D-37	-.1652D-22	-.5592D-38	-.9780D-54
-.4472D-22	0.2229D-37	0.6059D+08	0.7030D-38	-.8664D-23	-.2173D-38
-.1240D-37	-.1652D-22	0.7030D-38	0.1131D+09	0.3990D-38	-.5343D-23
-.5652D-53	-.5592D-38	-.8664D-23	0.3990D-38	0.1818D+09	-.4761D-39
-.8437D-69	-.9780D-54	-.2173D-38	-.5343D-23	-.4761D-39	0.2666D+09

Q-MATRIX AT THE POINT NO = 1 AND RADIUS RHO = 0.00070

0.0000D+00	0.9123D-11	0.2248D-26	0.2423D-42	0.2522D-57	-.6243D-73
-.9123D-11	0.0000D+00	0.4902D-11	0.5284D-27	0.3385D-42	-.8045D-58
-.2248D-26	-.4902D-11	0.0000D+00	0.3370D-11	0.8637D-27	-.1858D-42
-.2423D-42	-.5284D-27	-.3370D-11	0.0000D+00	0.2571D-11	-.4205D-27
-.2522D-57	-.3385D-42	-.8637D-27	-.2571D-11	0.0000D+00	0.2079D-11
0.6243D-73	0.8045D-58	0.1858D-42	0.4205D-27	-.2079D-11	0.0000D+00

#### POTENTIAL MATRICES V(I,J) AND Q(I,J):

V-MATRIX AT THE POINT NO = 1502 AND RADIUS RHO = 11.51962

0.8265D+00	0.1209D-03	-.1543D-01	-.3686D-03	-.9037D-05	-.2528D-06
0.1209D-03	0.2827D+01	0.6268D-03	-.4704D-01	-.1537D-02	-.4837D-04
-.1543D-01	0.6268D-03	0.4829D+01	0.1953D-02	-.9569D-01	-.4014D-02
-.3686D-03	-.4704D-01	0.1953D-02	0.6833D+01	0.4612D-02	-.1623D+00
-.9037D-05	-.1537D-02	-.9569D-01	0.4612D-02	0.8840D+01	0.9217D-02
-.2528D-06	-.4837D-04	-.4014D-02	-.1623D+00	0.9217D-02	0.1085D+02

Q-MATRIX AT THE POINT NO = 1502 AND RADIUS RHO = 11.51962

0.0000D+00	0.8748D-01	0.6854D-03	0.8256D-05	0.1360D-06	0.2879D-08
------------	------------	------------	------------	------------	------------



```

-.8748D-01  0.0000D+00  0.1764D+00  0.2124D-02  0.3501D-04  0.7408D-06
-.6854D-03  -.1764D+00  0.0000D+00  0.2668D+00  0.4396D-02  0.9302D-04
-.8256D-05  -.2124D-02  -.2668D+00  0.0000D+00  0.3589D+00  0.7592D-02
-.1360D-06  -.3501D-04  -.4396D-02  -.3589D+00  0.0000D+00  0.4528D+00
-.2879D-08  -.7408D-06  -.9302D-04  -.7592D-02  -.4528D+00  0.0000D+00

```

#### SPECIFICATIONS OF THE SECOND ATOMIC STATE

```

NUMBER OF FINITE ELEMENTS . . . . . (NELEM ) =    600
NUMBER OF GRID POINTS . . . . . (NGRID ) =   2401
PARITY OF STATE . . . . . (IPARTR) =      0
MAGNETIC QUANTUM NUMBER . . . . . (MQNR ) =      0
VALUE OF MATCHING POINT FOR EPSY. . . . . (RMATCH) =   39.0953

```

#### SUBDIVISION OF RHO-REGION ON THE FINITE-ELEMENT GROUPS:

```
*****
```

NO OF GROUP	NUMBER OF ELEMENTS	BEGIN OF INTERVAL	LENGTH OF ELEMENT	GRID STEP	END OF INTERVAL
1	200	0.000	0.01500	0.00375	3.000
2	200	3.000	0.08500	0.02125	20.000
3	200	20.000	0.40000	0.10000	100.000

LAST ADDRESS OF ARRAY ITOT USED = 3773

LAST ADDRESS OF ARRAY TOT USED = 9773

#### POTENTIAL MATRICES V(I,J) AND Q(I,J):

```

V-MATRIX AT THE POINT NO =    1  AND RADIUS RHO =    0.00070
-.2842D+04  0.4927D-37  -.1101D-21  -.4812D-37  -.7324D-53  -.4207D-68
0.4927D-37  0.1212D+08  0.1381D-36  -.2539D-22  -.4899D-38  -.2117D-53
-.1101D-21  0.1381D-36  0.4039D+08  0.7232D-38  -.1164D-22  -.3356D-38
-.4812D-37  -.2539D-22  0.7232D-38  0.8482D+08  0.4288D-38  -.6703D-23
-.7324D-53  -.4899D-38  -.1164D-22  0.4288D-38  0.1454D+09  0.2719D-38
-.4207D-68  -.2117D-53  -.3356D-38  -.6703D-23  0.2719D-38  0.2222D+09

```

```

Q-MATRIX AT THE POINT NO =    1  AND RADIUS RHO =    0.00070
0.0000D+00  0.1731D-10  0.7747D-26  0.1209D-41  0.1293D-57  0.1062D-65
-.1731D-10  0.0000D+00  0.6359D-11  0.9926D-27  0.7835D-43  0.9405D-58
-.7747D-26  -.6359D-11  0.0000D+00  0.3993D-11  0.3152D-27  0.2018D-42
-.1209D-41  -.9926D-27  -.3993D-11  0.0000D+00  0.2916D-11  0.6590D-27
-.1293D-57  -.7835D-43  -.3152D-27  -.2916D-11  0.0000D+00  0.2298D-11
-.1062D-65  -.9405D-58  -.2018D-42  -.6590D-27  -.2298D-11  0.0000D+00

```

#### POTENTIAL MATRICES V(I,J) AND Q(I,J):

```

V-MATRIX AT THE POINT NO =  1502  AND RADIUS RHO =   11.51962
0.8265D+00  0.1209D-03  -.1543D-01  -.3686D-03  -.9037D-05  -.2528D-06
0.1209D-03  0.2827D+01  0.6268D-03  -.4704D-01  -.1537D-02  -.4837D-04
-.1543D-01  0.6268D-03  0.4829D+01  0.1953D-02  -.9569D-01  -.4014D-02
-.3686D-03  -.4704D-01  0.1953D-02  0.6833D+01  0.4612D-02  -.1623D+00
-.9037D-05  -.1537D-02  -.9569D-01  0.4612D-02  0.8840D+01  0.9217D-02
-.2528D-06  -.4837D-04  -.4014D-02  -.1623D+00  0.9217D-02  0.1085D+02

```

```

Q-MATRIX AT THE POINT NO =  1502  AND RADIUS RHO =   11.51962
0.0000D+00  0.8748D-01  0.6854D-03  0.8256D-05  0.1360D-06  0.2879D-08
-.8748D-01  0.0000D+00  0.1764D+00  0.2124D-02  0.3501D-04  0.7408D-06

```

```

-.6854D-03  -.1764D+00  0.0000D+00  0.2668D+00  0.4396D-02  0.9302D-04
-.8256D-05  -.2124D-02  -.2668D+00  0.0000D+00  0.3589D+00  0.7592D-02
-.1360D-06  -.3501D-04  -.4396D-02  -.3589D+00  0.0000D+00  0.4528D+00
-.2879D-08  -.7408D-06  -.9302D-04  -.7592D-02  -.4528D+00  0.0000D+00

```

#### SPECIFICATIONS OF THE DIPOLE MATRICES

-----

```

NUMBER OF FINITE ELEMENTS . . . . . (NELEM ) =    600
NUMBER OF GRID POINTS . . . . . (NGRID ) =   2401
PARITY OF STATE . . . . . (IPARTL) =      1
MAGNETIC QUANTUM NUMBER . . . . . (MQNL ) =      0
PARITY OF STATE . . . . . (IPARTR) =      0
MAGNETIC QUANTUM NUMBER . . . . . (MQNR ) =      0
VALUE OF MATCHING POINT FOR EPSY. . . . . (RMATCH) =   41.4000

```

#### SUBDIVISION OF RHO-REGION ON THE FINITE-ELEMENT GROUPS:

\*\*\*\*\*

NO OF GROUP	NUMBER OF ELEMENTS	BEGIN OF INTERVAL	LENGTH OF ELEMENT	GRID STEP	END OF INTERVAL
1	200	0.000	0.01500	0.00375	3.000
2	200	3.000	0.08500	0.02125	20.000
3	200	20.000	0.40000	0.10000	100.000

LAST ADDRESS OF ARRAY ITOT USED = 3419

LAST ADDRESS OF ARRAY TOT USED = 9293

#### DIPOLE MATRICES D(I,J):

```

D-MATRIX AT THE POINT NO = 1 AND RADIUS RHO = 0.00000
0.0000D+00  0.0000D+00  0.0000D+00  0.0000D+00  0.0000D+00  0.0000D+00
0.0000D+00  0.0000D+00  0.0000D+00  0.0000D+00  0.0000D+00  0.0000D+00
0.0000D+00  0.0000D+00  0.0000D+00  0.0000D+00  0.0000D+00  0.0000D+00
0.0000D+00  0.0000D+00  0.0000D+00  0.0000D+00  0.0000D+00  0.0000D+00
0.0000D+00  0.0000D+00  0.0000D+00  0.0000D+00  0.0000D+00  0.0000D+00
0.0000D+00  0.0000D+00  0.0000D+00  0.0000D+00  0.0000D+00  0.0000D+00

```

#### DIPOLE MATRICES D(I,J):

```

D-MATRIX AT THE POINT NO = 1502 AND RADIUS RHO = 17.89625
0.1784D+02  0.5605D-01  0.1778D-03  0.8543D-06  0.5527D-08  0.4514D-10
0.5605D-01  0.1773D+02  0.1125D+00  0.5403D-03  0.3496D-05  0.2855D-07
0.1778D-03  0.1125D+00  0.1761D+02  0.1692D+00  0.1095D-02  0.8944D-05
0.8543D-06  0.5403D-03  0.1692D+00  0.1750D+02  0.2264D+00  0.1849D-02
0.5527D-08  0.3496D-05  0.1095D-02  0.2264D+00  0.1738D+02  0.2839D+00
0.4514D-10  0.2855D-07  0.8944D-05  0.1849D-02  0.2839D+00  0.1726D+02

```

#### SPECIFICATIONS OF THE ASYMPTOTIC SOLUTION

-----

```

NUMBER OF DIFFERENTIAL EQUATIONS. . . . . (MDIM ) =      6
NUMBER OF OPEN CHANNEL. . . . . (NOPEN ) =      2
ORDER OF CALCULATION. . . . . (IFUNAS) =     15
PARITY OF STATE . . . . . (IPARTL) =      1
MAGNETIC QUANTUM NUMBER . . . . . (MQNL ) =      0
CHARGE OF NUCLEAR . . . . . (CHARGE) =     1.00000
MAGNETIC PARAMETER. . . . . (WC ) =     1.00000

```

DOUBLE ENERGY SPECTRUM. . . . . (SHIFT ) = 3.40000  
 VALUE OF CALCULATED POINT . . . . . (RMAX ) = 100.000

LAST ADDRESS OF ARRAY TOT USED = 1166

VALUE OF I-TH THRESHOLD ENERGY (IN RY). (I,THR) = 1 0.1000E+01  
 VALUE OF I-TH THRESHOLD ENERGY (IN RY). (I,THR) = 2 0.3000E+01  
 VALUE OF I-TH MOMENTUM. . . . . (I,QR ) = 1 0.1549E+01  
 VALUE OF I-TH MOMENTUM. . . . . (I,QR ) = 2 0.6325E+00

TO HAVE REQUIRED EPSC=1.D-14  
 VALUE OF MATCHING POINT (RMATCH) = 31.6417  
 RECOMMENDED RIGHT BOUND OF  
 INTERVAL IS NOT LESS THAN (RMAX ) = 33

#### CHECK WRONSKIAN

-----  
 1.00000 -.102478E-17  
 0.197052E-17 1.00000

#### REGULAR SOLUTIONS

-----  
 0.778672E-02 -.277717E-04  
 -.281771E-04 0.117197E-01  
 -.150402E-05 -.535513E-04  
 0.243486E-08 0.289640E-06  
 -.518989E-10 -.109459E-07  
 0.515806E-12 -.195459E-09

#### IRREGULAR SOLUTIONS

-----  
 -.190795E-02 -.755766E-04  
 -.121508E-03 -.411903E-02  
 0.331762E-06 -.151932E-03  
 0.112340E-07 -.725747E-07  
 0.699426E-11 -.330613E-07  
 0.307317E-11 0.718648E-10

#### DERIVATIVE OF REGULAR SOLUTIONS

-----  
 -.304607E-02 -.484243E-04  
 -.188492E-03 -.278605E-02  
 0.561492E-06 -.974143E-04  
 0.173828E-07 -.550720E-07  
 0.134532E-10 -.210016E-07  
 0.475254E-11 0.566044E-10

#### DERIVATIVE OF IRREGULAR SOLUTIONS

-----  
 -.120955E-01 0.195204E-04  
 0.462741E-04 -.755679E-02  
 0.233031E-05 0.377738E-04  
 -.424123E-08 -.186102E-06  
 0.804558E-10 0.841921E-08  
 -.987484E-12 0.123011E-09

\*\*\*\*\* END OF THE POTHMF RUN \*\*\*\*\*

\*\*\*\*\* BEGIN OF THE KANTBP RUN \*\*\*\*\*

PROBLEM: Bound state energy levels  
 \*\*\*\*\*

# C O N T R O L I N F O R M A T I O N

```

NUMBER OF DIFFERENTIAL EQUATIONS. . . . . (MDIM ) =      6
NUMBER OF ENERGY LEVELS REQUIRED. . . . . (NROOT ) =      1
NUMBER OF FINITE ELEMENTS . . . . . (NELEM ) =     600
NUMBER OF GRID POINTS . . . . . (NGRID ) =    2401
ORDER OF SHAPE FUNCTIONS . . . . . (NPOL ) =      4
ORDER OF GAUSS-LEGENDRE QUADRATURE . . . (NGQ ) =      5
NUMBER OF SUBSPACE ITERATION VECTORS. . . (NC ) =      2
DIMENSION OF ENVELOPE SPACE . . . . . (IDIM ) =      3
BOUNDARY CONDITION CODE . . . . . (IBOUND) =      3
SHIFT OF DOUBLE ENERGY SPECTRUM . . . . . (SHIFT ) =  -0.700000
CONVERGENCE TOLERANCE . . . . . (RTOL ) =   0.100000E-14
  
```

## SUBDIVISION OF RHO-REGION ON THE FINITE-ELEMENT GROUPS:

\*\*\*\*\*

NO OF GROUP	NUMBER OF ELEMENTS	BEGIN OF INTERVAL	LENGTH OF ELEMENT	GRID STEP	END OF INTERVAL
1	200	0.000	0.01500	0.00375	3.000
2	200	3.000	0.08500	0.02125	20.000
3	200	20.000	0.40000	0.10000	100.000

LAST ADDRESS OF ARRAY ITOT USED = 64222

# T O T A L S Y S T E M D A T A

```

TOTAL NUMBER OF ALGEBRAIC EQUATIONS. . . . (NN ) =    14400
TOTAL NUMBER OF MATRIX ELEMENTS. . . . . (NWK) =   266256
MAXIMUM HALF BANDWIDTH . . . . . (MK ) =      30
MEAN    HALF BANDWIDTH . . . . . (MMK) =      18
  
```

LAST ADDRESS OF ARRAY TOT USED = 538201

NDIM, MDIM= 6 6

LAST ADDRESS OF ARRAY TOT USED = 593029

THERE ARE 0 ROOTS LOWER THEN SHIFT  
 CONVERGENCE REACHED FOR RTOL 0.1000E-14  
 I T E R A T I O N N U M B E R 9  
 RELATIVE TOLERANCE REACHED ON EIGENVALUES  
 0.1781E-15

\*\*\*\*\*

R O O T	N U M B E R	E I G E N V A L U E
1		-0.3311688955144392

\*\*\*\*\*

R                    R A D I A L    E I G E N F U N C T I O N S  
-                    - - - - -

```

0.0000  0.2406D+01 0.2984D-12 -.4758D-15 0.6931D-18 0.3585D-23 0.2470D-28
1.8000  0.3050D+00 -.1487D-01 0.5042D-03 0.1610D-04 0.4848D-06 0.1190D-07
6.4000  0.3819D-03 -.8983D-04 0.2920D-04 -.1130D-04 0.4997D-05 -.3193D-05
16.6000 0.5146D-09 -.4291D-10 0.4720D-11 -.5886D-12 0.8179D-13 -.1266D-13
52.0000 0.7291D-15 0.6787D-18 0.1469D-18 0.1157D-20 0.1846D-21 0.1947D-22

```

\*\*\*\*\*

PROBLEM:        Reaction matrix  
\*\*\*\*\*

C O N T R O L   I N F O R M A T I O N  
- - - - -

```

NUMBER OF DIFFERENTIAL EQUATIONS. . . . . (MDIM ) =      6
NUMBER OF FINITE ELEMENTS . . . . . (NELEM ) =     600
NUMBER OF GRID POINTS . . . . . (NGRID ) =    2401
ORDER OF SHAPE FUNCTIONS. . . . . (NPOL ) =      4
ORDER OF GAUSS-LEGENDRE QUADRATURE. . . . (NGQ ) =      5
DIMENSION OF ENVELOPE SPACE . . . . . (IDIM ) =      3
BOUNDARY CONDITION CODE . . . . . (IBOUND) =      8
DOUBLE ENERGY SPECTRUM. . . . . (SHIFT ) =    3.40000

```

SUBDIVISION OF RHO-REGION ON THE FINITE-ELEMENT GROUPS:  
\*\*\*\*\*

NO OF GROUP	NUMBER OF ELEMENTS	BEGIN OF INTERVAL	LENGTH OF ELEMENT	GRID STEP	END OF INTERVAL
1	200	0.000	0.01500	0.00375	3.000
2	200	3.000	0.08500	0.02125	20.000
3	200	20.000	0.40000	0.10000	100.000

LAST ADDRESS OF ARRAY ITOT USED =        64222

T O T A L   S Y S T E M   D A T A  
- - - - -

```

TOTAL NUMBER OF ALGEBRAIC EQUATIONS. . . . (NN ) =    14406
TOTAL NUMBER OF MATRIX ELEMENTS. . . . . (NWK) =   266421
MAXIMUM HALF BANDWIDTH . . . . . (MK ) =      30
MEAN        HALF BANDWIDTH . . . . . (MMK) =      18

```

LAST ADDRESS OF ARRAY TOT USED =        272110

NDIM, MDIM=                    6                    6

LAST ADDRESS OF ARRAY TOT USED =        384669

```

NUMBER OF OPEN CHANNELS. . . . . (NOPEN) =      2
VALUE OF I-TH MOMENTUM . . . . . (I,QR ) =      1  0.1549E+01
VALUE OF I-TH MOMENTUM . . . . . (I,QR ) =      2  0.6325E+00

```

```

TO HAVE REQUIRED EPSC=1.D-14
VALUE OF MATCHING POINT (RMATCH) = 31.6417
RECOMMENDED RIGHT BOUND OF
INTERVAL IS NOT LESS THAN (RMAX ) = 33

```

# C H E C K W R O N S K I A N

```

1.00000      -.102478E-17
0.197052E-17  1.00000

```

\*\*\*\*\*

# R E A C T I O N M A T R I X

```

-1.46347      2.19626
 2.19626     -8.72933

```

\*\*\*\*\*

# R R A D I A L E I G E N F U N C T I O N S

```

0.0000  0.6464D-13  0.1723D-11  0.4879D-12  -.1955D-11  -.3150D-13  0.7927D-13
        0.6148D-18  -.2533D-17  0.1684D-22  -.6326D-22  0.4306D-27  -.1633D-26
1.8000  -.2666D-01  0.6352D+00  -.8888D+00  0.2455D+01  0.1111D-01  -.4781D-01
        0.4547D-02  -.1653D-01  0.3372D-03  -.1260D-02  0.1491D-04  -.5729D-04
6.4000  -.2597D+00  0.4054D+00  0.1543D+00  -.4776D+00  -.8057D-01  0.3852D+00
        -.3576D-02  0.1317D-01  -.1418D-02  0.7051D-02  -.1987D-02  0.7691D-02
16.6000  0.5866D-01  -.1008D+00  -.1550D+00  0.6160D+00  -.4496D-02  0.1061D-01
        0.9199D-04  -.2742D-03  -.4298D-04  0.1278D-03  0.6092D-05  -.2478D-04
52.0000  0.2643D-01  -.2289D-01  -.1825D-01  0.9443D-01  -.1258D-02  0.4726D-02
        -.5400D-06  0.3805D-05  -.9910D-06  0.3781D-05  0.4891D-08  -.2518D-07
100.0000 0.1041D-01  -.3558D-02  -.8897D-02  0.4741D-01  -.3357D-03  0.1273D-02
        -.1734D-06  0.9478D-06  -.7267D-07  0.2777D-06  0.1539D-09  -.8160D-09

```

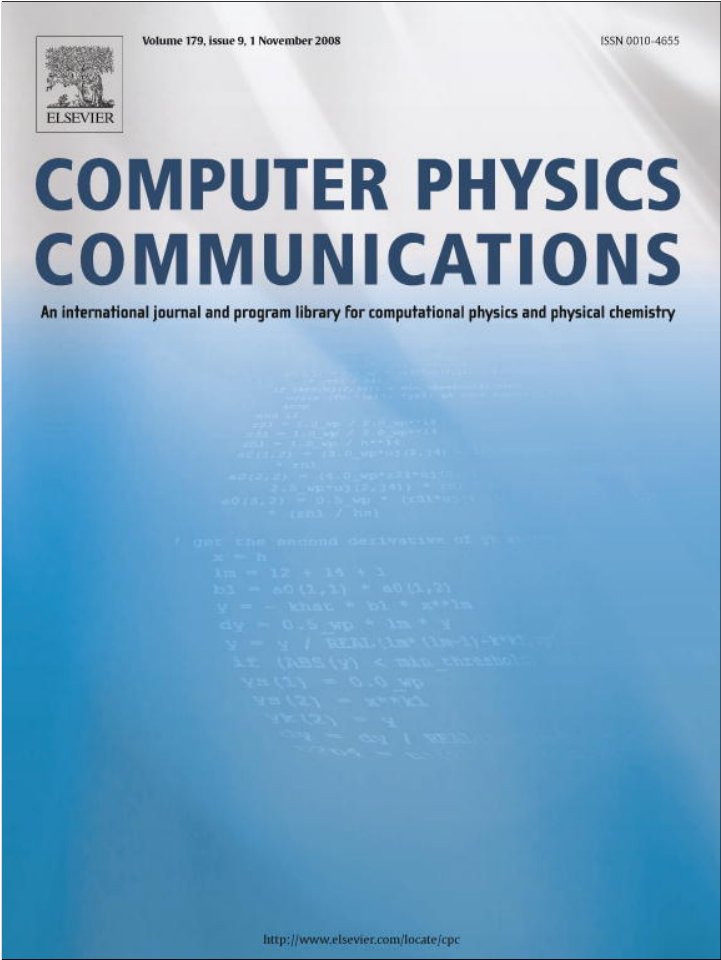
\*\*\*\*\*

\*\*\*\*\* END OF THE KANTBP RUN \*\*\*\*\*

## References

- [1] J.I. Kim, V.S. Melezhik, P. Schmelcher, Phys. Rev. Lett. 97 (2006) 193203-1–4.
- [2] Yu.N. Demkov, J.D. Meyer, Eur. Phys. J. B 42 (2004) 361–365.
- [3] A. Wetzels, A. Gurtler, L.D. Noordam, F. Robicheaux, Phys. Rev. A 73 (2006) 062507-1–8.
- [4] A. Rotondi, M. Amoretti, et al., AIP Conference Proceedings 796 (2005) 285–290.
- [5] M.V. Ryabinina, L.A. Melnikov, Nuclear Instruments and Methods in Physics Research Section B 214 (2004) 35–39;  
M.V. Ryabinina, L.A. Melnikov, AIP Conference Proceedings 796 (2005) 325–329.
- [6] V.V. Serov, V.L. Derbov, S.I. Vinitsky, Optics and Spectroscopy 102 (2007) 557–561.
- [7] A.G. Abrashkevich, M. Shapiro, Phys. Rev. A 50 (1994) 1205–1217;  
A.G. Abrashkevich, M. Shapiro, J. Phys. B 29 (1996) 627–644.
- [8] M.S. Kaschiev, S.I. Vinitsky, F.R. Vukajlovic, Phys. Rev. A 22 (1980) 557–559.
- [9] A.G. Abrashkevich, D.G. Abrashkevich, M. Shapiro, Comput. Phys. Comm. 90 (1995) 311–339.
- [10] M.G. Dimova, M.S. Kaschiev, S.I. Vinitsky, J. Phys. B 38 (2005) 2337–2352.
- [11] A. Alijah, J. Hinze, J.T. Broad, J. Phys. B 23 (1990) 45–60.
- [12] Q. Wang, C.H. Greene, Phys. Rev. A 44 (1991) 7448–7458.
- [13] U. Fano, E.Y. Sidky, Phys. Rev. A 45 (1992) 4776–4791;  
E.Y. Sidky, Phys. Rev. A 47 (1993) 2812–2818.
- [14] S. Watanabe, H.-A. Komine, Phys. Rev. Lett. 67 (1991) 3227–3230.
- [15] D. Delande, A. Bommier, J.C. Gay, Phys. Rev. Lett. 66 (1991) 141–144.
- [16] N. Merani, J. Main, G. Wunner, Astron. Astrophys. 298 (1995) 193–203.
- [17] L.B. Zhao, P.C. Stancil, Phys. Rev. A 74 (2006) 055401-1–4.
- [18] J. Eichler, Y. Yoshihama, N. Toshima, Phys. Rev. A 65 (2002) 033404-1–6.

- [19] C.V. Clark, K.T. Lu, A.F. Starace, in: H.G. Beyer, H. Kleinpoppen (Eds.), *Progress in Atomic Spectroscopy*, Part C, Plenum, New York, 1984, pp. 247–320.
- [20] O. Chuluunbaatar, A.A. Gusev, V.L. Derbov, M.S. Kaschiev, V.V. Serov, T.V. Tupikova, S.I. Vinitsky, *Proc. SPIE* 6165 (2006) 61650B-1–17.
- [21] L.V. Kantorovich, V.I. Krylov, *Approximate Methods of Higher Analysis*, Wiley, New York, 1964.
- [22] M. Abramovits, I.A. Stegun, *Handbook of Mathematical Functions*, Dover, New York, 1965.
- [23] S.I. Vinitsky, V.P. Gerdt, A.A. Gusev, M.S. Kaschiev, V.A. Rostovtsev, V.N. Samoylov, T.V. Tupikova, O. Chuluunbaatar, *Programming and Computer Software* 33 (2007) 105–116.
- [24] J.D. Power, *Phil. Trans. Roy. Soc. London A* 274 (1973) 663–702.
- [25] J.H. Wilkinson, *Lin. Algebra Appl.* 1 (1968) 409–420.
- [26] O. Chuluunbaatar, A.A. Gusev, A.G. Abrashkevich, A. Amaya-Tapia, M.S. Kaschiev, S.Y. Larsen, S.I. Vinitsky, *Comput. Phys. Comm.* 177 (2007) 649–675.
- [27] M.J. Seaton, *Rep. Prog. Phys.* 46 (1983) 167–257.
- [28] O. Chuluunbaatar, A.A. Gusev, V.L. Derbov, M.S. Kaschiev, V.V. Serov, T.V. Tupikova, S.I. Vinitsky, *Proc. SPIE* 6537 (2007) 653706-1–18.
- [29] O. Chuluunbaatar, A.A. Gusev, V.L. Derbov, M.S. Kaschiev, L.A. Melnikov, V.V. Serov, S.I. Vinitsky, *J. Phys. A* 40 (2007) 11485–11524.
- [30] U. Fano, C.M. Lee, *Phys. Rev. Lett.* 31 (1973) 1573–1576.
- [31] C.M. Lee, *Phys. Rev. A* 10 (1974) 584–600.
- [32] A.G. Abrashkevich, M.S. Kaschiev, S.I. Vinitsky, *J. Comp. Phys.* 163 (2000) 328–348.
- [33] <http://www.netlib.org/lapack/>.
- [34] A.A. Gusev, V.P. Gerdt, M.S. Kaschiev, V.A. Rostovtsev, V.N. Samoylov, T.V. Tupikova, S.I. Vinitsky, in: *Lecture Notes in Computer Science*, vol. 4194, 2006, pp. 205–218.
- [35] T. Oguchi, *Radio Sci.* 5 (1970) 1207–1214.
- [36] S.L. Skorokhodov, D.V. Khristoforov, *Comp. Math. Math. Phys.* 46 (2006) 1132–1146.
- [37] R.J. Damburg, R.Kh. Propin, *J. Phys. B* 1 (1968) 681–691.
- [38] M. Gailitis, *J. Phys. B* 9 (1976) 843–854.
- [39] W.H. Press, S.A. Teukolsky, W.T. Vetterling, B.P. Flannery, *Numerical Recipes: The Art of Scientific Computing*, Cambridge University Press, Cambridge, 1986.
- [40] A.R. Barnett, D.H. Feng, J.W. Steed, L.J.B. Goldfarb, *Comput. Phys. Comm.* 8 (1974) 377–395.
- [41] <http://physics.nist.gov/cuu/Constants/index.html>.



This article appeared in a journal published by Elsevier. The attached copy is furnished to the author for internal non-commercial research and education use, including for instruction at the authors institution and sharing with colleagues.

**Other uses, including reproduction and distribution, or selling or licensing copies, or posting to personal, institutional or third party websites are prohibited.**

**In most cases authors are permitted to post their version of the article (e.g. in Word or Tex form) to their personal website or institutional repository. Authors requiring further information regarding Elsevier's archiving and manuscript policies are encouraged to visit:**

<http://www.elsevier.com/copyright>





Contents lists available at ScienceDirect

## Computer Physics Communications

www.elsevier.com/locate/cpc



# KANTBP 2.0: New version of a program for computing energy levels, reaction matrix and radial wave functions in the coupled-channel hyperspherical adiabatic approach<sup>☆</sup>

O. Chuluunbaatar<sup>a,\*</sup>, A.A. Gusev<sup>a</sup>, S.I. Vinitzky<sup>a</sup>, A.G. Abrashkevich<sup>b</sup><sup>a</sup> Joint Institute for Nuclear Research, Dubna, 141980 Moscow region, Russia<sup>b</sup> IBM Toronto Lab, 8200 Warden Avenue, Markham, ON L6G 1C7, Canada

## ARTICLE INFO

## Article history:

Received 28 December 2007

Received in revised form 6 June 2008

Accepted 12 June 2008

Available online 17 June 2008

## PACS:

02.30.Hq

02.60.Jh

02.60.Lj

03.65.Nk

31.15.Ja

31.15.Pf

34.50.-s

34.80.Bm

## Keywords:

Eigenvalue and multi-channel scattering problems

Kantorovich method

Finite element method

R-matrix calculations

Hyperspherical coordinates

Multi-channel adiabatic approximation

Ordinary differential equations

High-order accuracy approximations

## ABSTRACT

A FORTRAN 77 program for calculating energy values, reaction matrix and corresponding radial wave functions in a coupled-channel approximation of the hyperspherical adiabatic approach is presented. In this approach, a multi-dimensional Schrödinger equation is reduced to a system of the coupled second-order ordinary differential equations on a finite interval with homogeneous boundary conditions: (i) the Dirichlet, Neumann and third type at the left and right boundary points for continuous spectrum problem, (ii) the Dirichlet and Neumann type conditions at left boundary point and Dirichlet, Neumann and third type at the right boundary point for the discrete spectrum problem. The resulting system of radial equations containing the potential matrix elements and first-derivative coupling terms is solved using high-order accuracy approximations of the finite element method. As a test desk, the program is applied to the calculation of the reaction matrix and radial wave functions for 3D-model of a hydrogen-like atom in a homogeneous magnetic field. This version extends the previous version 1.0 of the KANTBP program [O. Chuluunbaatar, A.A. Gusev, A.G. Abrashkevich, A. Amaya-Tapia, M.S. Kaschiev, S.Y. Larsen, S.I. Vinitzky, Comput. Phys. Commun. 177 (2007) 649–675].

## Program summary

Program title: KANTBP

Catalogue identifier: ADZH\_v2\_0

Program summary URL: [http://cpc.cs.qub.ac.uk/summaries/ADZH\\_v2\\_0.html](http://cpc.cs.qub.ac.uk/summaries/ADZH_v2_0.html)

Program obtainable from: CPC Program Library, Queen's University, Belfast, N. Ireland

Licensing provisions: Standard CPC licence, <http://cpc.cs.qub.ac.uk/licence/licence.html>

No. of lines in distributed program, including test data, etc.: 20 403

No. of bytes in distributed program, including test data, etc.: 147 563

Distribution format: tar.gz

Programming language: FORTRAN 77

Computer: Intel Xeon EM64T, Alpha 21264A, AMD Athlon MP, Pentium IV Xeon, Opteron 248, Intel Pentium IV

Operating system: OC Linux, Unix AIX 5.3, SunOS 5.8, Solaris, Windows XP

RAM: This depends on

1. the number of differential equations;
2. the number and order of finite elements;
3. the number of hyperradial points; and
4. the number of eigensolutions required.

The test run requires 2 MB

Classification: 2.1, 2.4

External routines: GAULEG and GAUSSJ [2]

Nature of problem: In the hyperspherical adiabatic approach [3–5], a multidimensional Schrödinger equation for a two-electron system [6] or a hydrogen atom in magnetic field [7–9] is reduced by

<sup>☆</sup> This paper and its associated computer program are available via the Computer Physics Communications homepage on ScienceDirect (<http://www.sciencedirect.com/science/journal/00104655>).

\* Corresponding author.

E-mail address: [chuka@jinr.ru](mailto:chuka@jinr.ru) (O. Chuluunbaatar).

separating radial coordinate  $\rho$  from the angular variables to a system of the second-order ordinary differential equations containing the potential matrix elements and first-derivative coupling terms. The purpose of this paper is to present the finite element method procedure based on the use of high-order accuracy approximations for calculating approximate eigensolutions of the continuum spectrum for such systems of coupled differential equations on finite intervals of the radial variable  $\rho \in [\rho_{\min}, \rho_{\max}]$ . This approach can be used in the calculations of effects of electron screening on low-energy fusion cross sections [10–12].

**Solution method:** The boundary problems for the coupled second-order differential equations are solved by the finite element method using high-order accuracy approximations [13]. The generalized algebraic eigenvalue problem  $\mathbf{A}\mathbf{F} = \mathbf{E}\mathbf{B}\mathbf{F}$  with respect to pair unknowns  $(E, \mathbf{F})$  arising after the replacement of the differential problem by the finite-element approximation is solved by the subspace iteration method using the SSPACE program [14]. The generalized algebraic eigenvalue problem  $(\mathbf{A} - \mathbf{E}\mathbf{B})\mathbf{F} = \lambda\mathbf{D}\mathbf{F}$  with respect to pair unknowns  $(\lambda, \mathbf{F})$  arising after the corresponding replacement of the scattering boundary problem in open channels at fixed energy value,  $E$ , is solved by the  $\mathbf{LDL}^T$  factorization of symmetric matrix and back-substitution methods using the DECOMP and REDBAK programs, respectively [14]. As a test desk, the program is applied to the calculation of the reaction matrix and corresponding radial wave functions for 3D-model of a hydrogen-like atom in a homogeneous magnetic field described in [9] on finite intervals of the radial variable  $\rho \in [\rho_{\min}, \rho_{\max}]$ . For this benchmark model the required analytical expressions for asymptotics of the potential matrix elements and first-derivative coupling terms, and also asymptotics of radial solutions of the boundary problems for coupled differential equations have been produced with help of a MAPLE computer algebra system.

**Restrictions:** The computer memory requirements depend on:

1. the number of differential equations;
2. the number and order of finite elements;
3. the total number of hyperradial points; and
4. the number of eigensolutions required.

Restrictions due to dimension sizes may be easily alleviated by altering PARAMETER statements (see Section 3 and [1] for details). The user must also supply subroutine POTCAL for evaluating potential matrix elements. The user should also supply subroutines ASYMEV (when solving the eigenvalue problem) or ASYMS0 and ASYMSC (when solving the scattering problem) which evaluate asymptotics of the radial wave functions at left and right boundary points in case of a boundary condition of the third type for the above problems.

**Running time:** The running time depends critically upon:

1. the number of differential equations;
2. the number and order of finite elements;
3. the total number of hyperradial points on interval  $[\rho_{\min}, \rho_{\max}]$ ; and
4. the number of eigensolutions required.

The test run which accompanies this paper took 2 s without calculation of matrix potentials on the Intel Pentium IV 2.4 GHz.

**References:**

- [1] O. Chuluunbaatar, A.A. Gusev, A.G. Abrashkevich, A. Amaya-Tapia, M.S. Kaschiev, S.Y. Larsen, S.I. Vinitsky, Comput. Phys. Commun. 177 (2007) 649–675; <http://cpc.cs.qub.ac.uk/summaries/ADZHv10.html>.
- [2] W.H. Press, S.A. Teukolsky, W.T. Vetterling, B.P. Flannery, Numerical Recipes: The Art of Scientific Computing, Cambridge University Press, Cambridge, 1986.
- [3] J. Macek, J. Phys. B 1 (1968) 831–843.
- [4] U. Fano, Rep. Progr. Phys. 46 (1983) 97–165.
- [5] C.D. Lin, Adv. Atom. Mol. Phys. 22 (1986) 77–142.
- [6] A.G. Abrashkevich, D.G. Abrashkevich, M. Shapiro, Comput. Phys. Commun. 90 (1995) 311–339.
- [7] M.G. Dimova, M.S. Kaschiev, S.I. Vinitsky, J. Phys. B 38 (2005) 2337–2352.
- [8] O. Chuluunbaatar, A.A. Gusev, V.L. Derbov, M.S. Kaschiev, L.A. Melnikov, V.V. Serov, S.I. Vinitsky, J. Phys. A 40 (2007) 11485–11524.
- [9] O. Chuluunbaatar, A.A. Gusev, V.P. Gerdt, V.A. Rostovtsev, S.I. Vinitsky, A.G. Abrashkevich, M.S. Kaschiev, V.V. Serov, Comput. Phys. Commun. 178 (2007) 301–330; <http://cpc.cs.qub.ac.uk/summaries/AEAAv10.html>.
- [10] H.J. Assenbaum, K. Langanke, C. Rolfs, Z. Phys. A 327 (1987) 461–468.
- [11] V. Melezhik, Nucl. Phys. A 550 (1992) 223–234.
- [12] L. Bracci, G. Fiorentini, V.S. Melezhik, G. Mezzorani, P. Pasini, Phys. Lett. A 153 (1991) 456–460.
- [13] A.G. Abrashkevich, D.G. Abrashkevich, M.S. Kaschiev, I.V. Puzynin, Comput. Phys. Commun. 85 (1995) 40–64.
- [14] K.J. Bathe, Finite Element Procedures in Engineering Analysis, Englewood Cliffs, Prentice-Hall, New York, 1982.

© 2008 Elsevier B.V. All rights reserved.

## 1. Introduction

In our previous paper [1] we have described the finite element method procedure based on the use of high-order accuracy approximations for calculating approximate eigensolutions of the discrete and continuum spectrum for systems of coupled differential equations on

a finite interval of the radial variable  $\rho \in [\rho_{\min}, \rho_{\max}]$  with homogeneous boundary conditions: the Dirichlet, Neumann type at  $\rho = \rho_{\min}$ ; the Dirichlet, Neumann and third type at  $\rho = \rho_{\max}$ .

The purpose of this paper is to extend the framework of work [1] for calculating approximate eigensolutions of the continuum spectrum for systems of coupled differential equations on finite intervals of the radial variable  $\rho \in [\rho_{\min}, \rho_{\max}]$  using a general homogeneous boundary condition of the third type at  $\rho = \rho_{\min}$ . The third-type boundary conditions at  $\rho = \rho_{\min}$  are formulated by using known asymptotics for a set of linear independent regular solutions for problems under consideration [2–9]. This approach can be used in calculations of effects of electron screening on low-energy fusion cross sections [10–13], channeling processes [14,15], threshold phenomena in the formation and ionization of (anti)hydrogen-like atoms and ions in magnetic traps [16], quantum dots in magnetic field [17–19] and potential scattering with confinement potentials [20].

The paper is organized as follows. In Section 2 we give a brief overview of the problem. A description of the new version of the KANTBP program is given in Section 3. Example of the asymptotic expansions of matrix elements and regular solutions at small  $\rho$  together with Test desk are discussed in Section 4.

## 2. Statement of the problem

In the Kantorovich approach [21], the  $d$ -dimensional Schrödinger equation is reduced to a finite set of  $N$  ordinary second-order differential equations on the finite interval  $[\rho_{\min}, \rho_{\max}]$  for the partial solution  $\chi(\rho) \equiv \chi^{(i)}(\rho) = (\chi_1^{(i)}(\rho), \dots, \chi_N^{(i)}(\rho))^T$

$$(\mathbf{L} - 2E\mathbf{I})\chi(\rho) \equiv \left( -\frac{1}{\rho^{d-1}} \mathbf{I} \frac{d}{d\rho} \rho^{d-1} \frac{d}{d\rho} + \mathbf{V}(\rho) + \mathbf{Q}(\rho) \frac{d}{d\rho} + \frac{1}{\rho^{d-1}} \frac{d\rho^{d-1} \mathbf{Q}(\rho)}{d\rho} - 2E\mathbf{I} \right) \chi(\rho) = 0. \quad (1)$$

Here  $\mathbf{I}$ ,  $\mathbf{V}(\rho)$  and  $\mathbf{Q}(\rho)$  are the unit, symmetric and antisymmetric matrices of dimension  $N \times N$ , respectively.

In the present work, scattering problem is solved using the homogeneous third type boundary conditions at  $\rho = \rho_{\min} > 0$  and  $\rho = \rho_{\max} \gg 1$ :

$$\frac{d\Phi(\rho)}{d\rho} = \mathbf{R}(\rho)\Phi(\rho), \quad (2)$$

where  $\Phi(\rho) = \{\chi^{(i)}(\rho)\}_{i=1}^{N_0}$  is the required matrix-solution of dimension  $N \times N_0$  and  $N_0$  is the number of open channels. Suppose that a set of linear independent regular solutions  $\tilde{\Phi}_{\text{reg}}(\rho) = \{\tilde{\chi}_{\text{reg}}^{(i)}(\rho)\}_{i=1}^N$  for a problem under consideration with components  $\tilde{\chi}_{\text{reg}}^{(i)}(\rho) = (\tilde{\chi}_{1i}^{\text{reg}}(\rho), \dots, \tilde{\chi}_{Ni}^{\text{reg}}(\rho))^T$  is known at small  $\rho$  (see, e.g., [2–9,16,22]).

Using a linear combination of these regular solutions,  $\tilde{\chi}_{\text{reg}}^{(i)}(\rho)$ , we can find required matrix solution  $\Phi(\rho)$  at  $\rho = \rho_{\min} > 0$ :

$$\Phi(\rho) = \tilde{\Phi}_{\text{reg}}(\rho)\mathbf{C}, \quad (3)$$

where  $\mathbf{C}$  is the unknown nonzero constant matrix of dimension  $N \times N_0$ . Using identity  $\mathbf{C}\mathbf{C}^{-1} = \mathbf{I}$ , the  $\mathbf{R}(\rho)$  matrix at  $\rho = \rho_{\min}$  can be easily found via the known set of linear independent regular solutions  $\tilde{\Phi}_{\text{reg}}(\rho)$

$$\mathbf{R}(\rho) \equiv \frac{d\tilde{\Phi}_{\text{reg}}(\rho)}{d\rho} \tilde{\Phi}_{\text{reg}}^{-1}(\rho) = \frac{d\Phi(\rho)}{d\rho} \Phi^{-1}(\rho). \quad (4)$$

From this we obtain the quadratic functional (compare with Eq. (23) in [1])

$$\begin{aligned} \Xi(\Phi, E, \rho_{\min}, \rho_{\max}) &\equiv \int_{\rho_{\min}}^{\rho_{\max}} \Phi^T(\rho) (\mathbf{L} - 2E\mathbf{I}) \Phi(\rho) \rho^{d-1} d\rho \\ &= \Pi(\Phi, E, \rho_{\min}, \rho_{\max}) - \rho_{\max}^{d-1} \Phi^T(\rho_{\max}) \mathbf{G}(\rho_{\max}) \Phi(\rho_{\max}), \end{aligned} \quad (5)$$

where  $\Pi(\Phi, E, \rho_{\min}, \rho_{\max})$  is the symmetric functional

$$\begin{aligned} \Pi(\Phi, E, \rho_{\min}, \rho_{\max}) &= \int_{\rho_{\min}}^{\rho_{\max}} \left[ \frac{d\Phi^T(\rho)}{d\rho} \frac{d\Phi(\rho)}{d\rho} + \Phi^T(\rho) \mathbf{V}(\rho) \Phi(\rho) \right. \\ &\quad \left. + \Phi^T(\rho) \mathbf{Q}(\rho) \frac{d\Phi(\rho)}{d\rho} - \frac{d\Phi(\rho)^T}{d\rho} \mathbf{Q}(\rho) \Phi(\rho) - 2E\Phi^T(\rho) \Phi(\rho) \right] \rho^{d-1} d\rho \\ &\quad + \rho_{\min}^{d-1} \Phi^T(\rho_{\min}) \mathbf{G}(\rho_{\min}) \Phi(\rho_{\min}), \end{aligned} \quad (6)$$

and  $\mathbf{G}(\rho) = \mathbf{R}(\rho) - \mathbf{Q}(\rho)$  is the matrix of dimension  $N \times N$  which should be symmetric according to the conventional  $\mathbf{R}$ -matrix theory. The matrix  $\mathbf{G}(\rho_{\max})$  is calculated by a procedure in the framework of the FEM described in our previous paper [1].

After numerical calculation of solution  $\Phi(\rho)$  in the nodes of the finite element grid  $\Omega$  on interval  $[\rho_{\min}, \rho_{\max}]$  using scheme implemented in [1] which takes into account Eqs. (2)–(6), matrix  $\mathbf{C}$  can be evaluated by the formula

$$\mathbf{C} = \tilde{\Phi}_{\text{reg}}^{-1}(\rho_{\min}) \Phi(\rho_{\min}). \quad (7)$$

The matrix  $\mathbf{C}$  is applied for analysis of the matrix-solution  $\Phi(\rho)$  in the vicinity of  $\rho = 0$ . For example, constant matrix  $\mathbf{C}$  satisfies ratio  $\tilde{\Phi}_{\text{reg}}^{-1}(0)\Phi(0)$  even if  $\Phi(0) \equiv \mathbf{0}$  or is very close to zero. To extract required matrix  $\mathbf{C}$  in later case, a user can use known asymptotics of the regular solutions at  $\rho_{\min}$ . Value  $\rho_{\min}$  is defined on the asymptotic domain of the  $\tilde{\Phi}_{\text{reg}}(\rho)$ .

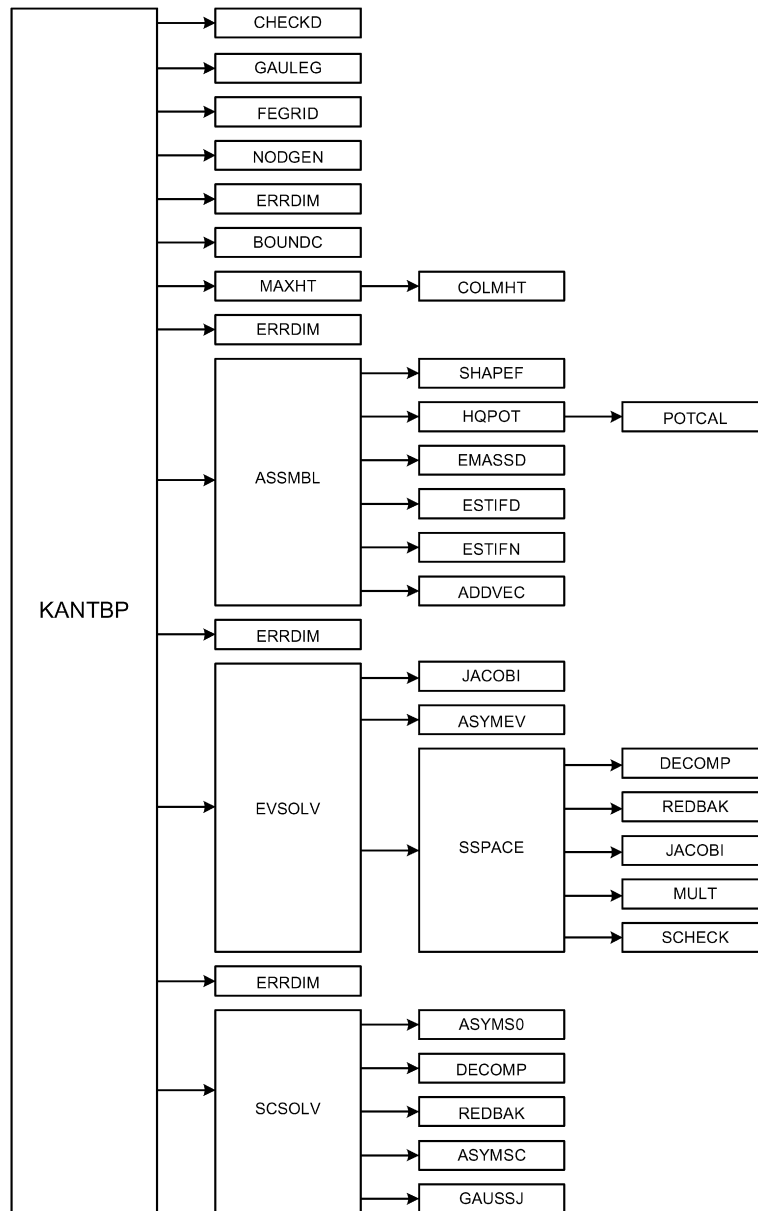


Fig. 1. Flow diagram of the new version of the KANTBP program.

### 3. Description of the program

Fig. 1 presents a flow diagram for the new version of the KANTBP program. The function of each subroutine except for a new user-supplied subroutine ASYMS0 is described in [1]. KANTBP program is called from the main routine (supplied by a user) which sets dimensions of the arrays and is responsible for the input data. In the present code each array declarator is written in terms of the symbolic names of constants. These constants are defined in the following PARAMETER statement in the main routine:

PARAMETER (MTOT=9000000,MITOT=900000,NMESH1=7,MDIM1=6)

where

- MTOT is the dimension of the working DOUBLE PRECISION array TOT.
- MITOT is the dimension of the working INTEGER array ITOT.
- NMESH1 is the dimension of the DOUBLE PRECISION array RMESH containing the information about the subdivision of the hyperradial interval  $[0, \rho_{\max}]$  on subintervals and number of elements on each one of them. NMESH1 is always odd and  $\geq 3$ .
- MDIM1 is the dimension of the DOUBLE PRECISION array THRSHL and INTEGER array NDIL containing information about a set of threshold values and numbers of coupled differential equations, respectively.

A more concrete assignment of these dimensions is discussed below. In order to change the dimensions of the code, all one has to do is to modify the single PARAMETER statement defined above in the main program unit.

The calling sequence for the subroutine KANTBP is:

```
CALL KANTBP (TITLE, IPTYPE, NROOT, MDIM, IDIM, NPOL, RTOL, NITEM,
1          SHIFT, IPRINT, IPRSTP, NMESH, RMESH, NDIR, NDIL, NMDIL,
2          THRSHL, IBOUND, FNOU, IOUT, POTEN, IOUP, FMATR, IOUM,
3          EVWFN, IOUF, TOT, ITOT, MTOT, MITOT)
```

A new user-supplied subroutine ASYMSO for calculating the regular asymptotic matrix-solution and its derivative at  $\rho = \rho_{\min}$  has been added to the scattering problem solver program. It should be written as follows:

```
SUBROUTINE ASYMSO (RMIN, NDIM, SHIFT, NOPEN, QR, PREG, DREG, IOUT)
C . . . . .
C .
C .   P R O G R A M
C .
C .   TO CALCULATE THE REGULAR ASYMPTOTIC MATRIX
C .   SOLUTION PREG AND ITS DERIVATIVE DREG
C .   AT RMIN
C .
C .
C . . . . .
IMPLICIT REAL*8 (A-H, O-Z)
DIMENSION QR (NOPEN), PREG (NDIM, NDIM), DREG (NDIM, NDIM)
RETURN
END
```

Here array QR contains a set of momentum values, SHIFT contains the given double energy spectrum value, and NOPEN is the number of open channels. To set the third type boundary conditions at both points  $\rho_{\min}$  and  $\rho_{\max}$ , flag IBOUND always should be 8. Other parameters used in the ASYMSO and also input and output data for the KANTBP program are described in [1].

#### 4. Test desk

##### 4.1. Asymptotic expansions of the matrix elements at small $\rho$

The test run which accompanies the KANTBP program computes the reaction matrix and corresponding radial wave functions for 3D-model of a hydrogen-like atom in a homogeneous magnetic field [22]. According to [16], asymptotic values of the potential curves  $E_j(\rho)$ , radial matrix elements  $H_{jj'}(\rho)$  and  $Q_{jj'}(\rho)$  at small  $\rho$  in Eq. (1) describing a hydrogen atom in a homogeneous magnetic field characterized by  $l = 2j - 2 + |m|$  for even states ( $\sigma = +1$ ) and  $l = 2j - 1 + |m|$  for odd states ( $\sigma = -1$ ) are given by expansion in powers of  $\rho$  with finite  $l, l'$

$$\begin{aligned} E_j(\rho) &= \bar{E}_j^{(0)} + \bar{E}_j^{(2)} \rho^2 + \sum_{k=1}^{[k_{\max}/4]} \rho^{4k} \bar{E}_j^{(4k)}, & H_{jj'}(\rho) &= \sum_{k=2}^{[k_{\max}/4]} \rho^{4k-2} \bar{H}_{jj'}^{(4k-2)}, \\ Q_{jj'}(\rho) &= \sum_{k=1}^{[k_{\max}/4]} \rho^{4k-1} \bar{Q}_{jj'}^{(4k-1)}, & \rho &\ll \min(l, l')/\sqrt{4\gamma}. \end{aligned} \quad (8)$$

Note, that all

$$\bar{Q}_{jj'}^{(4k-1)} \equiv 0 \quad \text{and} \quad \bar{H}_{jj'}^{(4k-2)} \equiv 0 \quad \text{if } |j - j'| > 2k. \quad (9)$$

In this work, the calculations of the above matrix elements were performed using algorithm implemented in MAPLE up to  $k_{\max} = 16$ . Below we present the first several coefficients of the matrix elements expansions:

$$\begin{aligned} \bar{E}_j^{(0)} &= l(l+1), & \bar{E}_j^{(2)} &= \gamma m, & \bar{E}_j^{(4)} &= \frac{\gamma^2}{2} \frac{l^2 + l - 1 + m^2}{(2l-1)(2l+3)}, \\ \bar{Q}_{jj+2}^{(3)} &= \frac{\gamma^2}{2} \frac{\sqrt{(l+1)^2 - m^2} \sqrt{(l+2)^2 - m^2}}{\sqrt{2l+1}(2l+3)^2 \sqrt{2l+5}}, \\ \bar{H}_{jj}^{(6)} &= \frac{\gamma^4}{2} ((16l^4 + 32l^3 + 248l^2 + 232l + 201)m^4 \\ &\quad + (-10l^2 - 224l^4 - 96l^5 + 118l - 288l^3 - 32l^6 - 195)m^2 \\ &\quad + 16l^8 + 64l^7 + 46l + 40l^6 - 127l^4 - 104l^5 + 71l^2 - 6l^3 - 6)/((2l-3)(2l-1)^4(2l+3)^4(2l+5)), \\ \bar{H}_{jj+4}^{(6)} &= \frac{-\gamma^4 \sqrt{(l+1)^2 - m^2} \sqrt{(l+2)^2 - m^2} \sqrt{(l+3)^2 - m^2} \sqrt{(l+4)^2 - m^2}}{4\sqrt{2l+1}(2l+3)^2(2l+5)(2l+7)^2 \sqrt{2l+9}}. \end{aligned} \quad (10)$$

Such asymptotic behavior of the effective potentials on the interval  $\rho \in [0, \rho_{\min}]$  allows us to find regular and bound solutions at  $\rho \rightarrow 0$  that satisfy the homogeneous third type boundary conditions (2) at  $\rho = \rho_{\min} > 0$ .

#### 4.2. Asymptotic expansions of the regular solutions at small $\rho$

The asymptotics of the regular solutions  $\tilde{\chi}_{j,\text{reg}}^{(i_0)}(\rho) \equiv \tilde{\chi}_{ji_0}(\rho)$ ,  $j = 1, \dots, N$ ,  $i_0 = 1, \dots, N$ , of Eq. (1) are sought as expansions in powers of  $\rho$  up to the finite order  $k_{\max}$

$$\tilde{\chi}_{ji,\text{reg}}(\rho) = \sum_{k=0}^{k_{\max}} \tilde{\chi}_{ji}^{(k)} \rho^{\mu_{i_0}+k}, \quad \tilde{\chi}_{ji}^{(0)} = \delta_{ji}, \quad \tilde{\chi}_{ji}^{(k<0)} \equiv 0, \quad (11)$$

where  $\mu_{i_0}$  is the unknown characteristic parameter. Substituting expansion (11) into (1) and taking into account Eqs. (8)–(10), we obtain the following system of recurrence relations for the set of the unknown coefficients  $\tilde{\chi}_{ji}^{(k)}$

$$\begin{aligned} & -(l' + 1 + \mu_{i_0} + k)(\mu_{i_0} - l' + k) \tilde{\chi}_{ji}^{(k)} \\ & = 2Z \tilde{\chi}_{ji}^{(k-1)} - (m\gamma - \epsilon) \tilde{\chi}_{ji}^{(k-2)} - \sum_{s=4}^k \tilde{E}_j^{(s)} \tilde{\chi}_{ji}^{(k-s)} - \sum_{s=4}^{k-2} \tilde{H}_{jj}^{(s)} \tilde{\chi}_{ji}^{(k-s-2)} \\ & - \sum_{s=3}^{k-1} \sum_{j'=\max(1, i-[s/4]), j' \neq j}^{\min(j_{\max}, i+[s/4])} (2l + 2k - s) \tilde{Q}_{jj'}^{(s)} \tilde{\chi}_{ji}^{(k-s-1)} - \sum_{s=4}^{k-2} \sum_{j'=\max(1, i-[s/4]), j' \neq j}^{\min(j_{\max}, i+[s/4])} \tilde{H}_{jj'}^{(s)} \tilde{\chi}_{ji}^{(k-s-2)}, \end{aligned} \quad (12)$$

where indices  $l'$  and  $l$  are defined as

$$l' = 2(j-1) + |m| + (1-\sigma)/2, \quad l = 2(i-1) + |m| + (1-\sigma)/2. \quad (13)$$

As follows from Eqs. (11) and (12) at  $k=0$ , the conventional characteristic equation gives two roots for the unknown  $\mu_{i_0}$ :  $\mu_{i_0} = -l-1$  and  $\mu_{i_0} = l$ . Value  $\mu_{i_0} = -l-1$  corresponds to irregular unbound solutions and is not considered here. Value  $\mu_{i_0} = l$  corresponds to the required regular and bound solutions and is the one we have used in our calculations.

Note that components of vector  $\{\tilde{\chi}_{ji}^{(k)}\}_{j=1}^N$  at fixed  $i$  in the left-hand side of Eq. (12) equal to zero if  $2(j-i)=k$ . In this case we can put  $\tilde{\chi}_{i+k/2,i}^{(k)} = 0$  because this term will be determined as the leading term of the asymptotic form of the  $(i+k/2)$ th solution. A more detailed analysis of (12) with the account of (9) shows that the right-hand side of Eq. (12) is equal to zero and all  $\tilde{\chi}_{ji}^{(k)}$  are equal to zero if  $|j-i| > k/2$ .

Thus, the system (12) can be solved sequentially for  $k = 1, 2, \dots, k_{\max}$ . The calculation was performed using the algorithm implemented in MAPLE up to  $k_{\max} = 16$ . Below we display the first several non-zero coefficients of the regular solutions expansions:

$$\begin{aligned} \tilde{\chi}_{ii}^{(0)} &= 1, \quad \tilde{\chi}_{ii}^{(1)} = -\frac{Z}{l+1}, \quad \tilde{\chi}_{ii}^{(2)} = -\frac{-2Z^2 + (\epsilon - m\gamma)(l+1)}{2(l+1)(2l+3)}, \\ \tilde{\chi}_{ii}^{(3)} &= \frac{Z(-2Z^2 + (\epsilon - m\gamma)(3l+4))}{6(l+1)(l+2)(2l+3)}, \\ \tilde{\chi}_{i-1i}^{(4)} &= \frac{\tilde{Q}_{i-1i}^{(3)}(2l+5)}{6(2l+3)}, \\ \tilde{\chi}_{ii}^{(4)} &= \frac{\tilde{E}_i^{(4)}}{4(2l+5)} + \frac{(\epsilon - m\gamma)^2}{8(2l+3)(2l+5)} + \frac{Z^4 - Z^2(\epsilon - m\gamma)(3l+5)}{6(l+1)(l+2)(2l+3)(2l+5)}, \\ \tilde{\chi}_{i+1i}^{(4)} &= \frac{\tilde{Q}_{i+1i}^{(3)}(2l+5)}{2(2l+7)}. \end{aligned} \quad (14)$$

The test run which accompanies the KANTBP program computes the reaction matrix and corresponding radial wave functions for 3D-model of a hydrogen-like atom in a homogeneous magnetic field with  $\sigma = -1$ ,  $Z = 1$ ,  $\gamma = 1$  and  $m = 0$  on the finite intervals of the radial variable  $\rho \in [\rho_{\min} = 0.3, \rho_{\max} = 100]$ . All needed potential elements are calculated with the help of the POTHMF program [22]. The asymptotics from Eq. (11) and needed coefficients of the matrix elements (8) are included in the subroutine ASYMS0 up to  $k_{\max} = 16$ .

File 'INPUT2.INP' contains the initial data NAMELIST POTDAT for the calculation of the potential matrix elements for the given atomic state by the POTHMF program. Also this file contains the initial data NAMELIST PARSCP for the calculation of the reaction matrix and corresponding radial wave functions for the KANTBP program. File 'INPUT2.INP' contains the following data:

```
&POTDAT TITLE='      Potential and dipole matrices elements      ',
IMATRX=1, IDIPOL=0, IFUNAS=15, WC=0.1D1, CHARGE=1.D0, MDIM=6,
NPOL=4, SHIFTS=3.4D0, IPRINT=1, IPRSTP=1501,
RMESH=0.3D0, 180.D0, 3.D0, 200.D0, 20.D0, 200.D0, 100.D0,
FNOUTP='FNOUTP.LPR', IOUTP=7, NMESHR=7, NMESHL=7,
IPARTL=1, MQNL=0, POTENL='POTENL.PTN', IOUPL=8,
WFUNAS='WFUNAS.PTN', IOUWF=0

&END

&PARSCP TITLE2='      Reaction matrix      ',
IPTYPE=1, NROOT=1, IDIM=3, SHIFT=3.4D0, IPRINT=2, IPRSTP=400,
IBOUND=8, NDIR=1, NDIL=6, NMDIL=1,
```

```

THRSHL=1.D0,3.D0,5.D0,7.D0,9.D0,11.D0,
FNOU TL='3DNSSC.LPR',NOU T=14,FMATRL='3DNSSC.MAT',NOUM=15,
EVWFNL='3DNSSC.WFN',NOUF=2
&END

```

Physical parameters CHARGE, WC, MQNL, IPARTL and order of asymptotic solutions IFUNAS are accessed via general common block COMMON /CHARGE/ CHARGE, WC, MQNL, IPARTL, IFUNAS. As an example, calculation of matrix **C** is performed by means of Eq. (7) and presented in output file. Note, that values of the partial solutions  $\chi_j^{(i)}(\rho)$  at  $\rho = 0.3$  presented in the TEST RUN OUTPUT are equal to the corresponding results presented in the TEST RUN OUTPUT of [22] which verifies and confirms the accuracy of the developed calculation scheme.

## Acknowledgements

The authors thank Profs. V.S. Melezhik, V.V. Pupyshv, F.M. Pen'kov, M. Shapiro and Dr. P.M. Krassovitskiy for useful discussions. OC, SIV and AAG acknowledge financial support from a grant I-1402/2004-2007 of the Bulgarian Foundation for Scientific Investigations, grants RFBR 07-01-00660, RFBR 08-01-00604-a and the theme 09-6-1060-2005/2010 "Mathematical support of experimental and theoretical studies conducted by JINR".

## Appendix A. TEST RUN OUTPUT

```

PROBLEM:      Reaction matrix
*****

```

### C O N T R O L I N F O R M A T I O N

```

NUMBER OF DIFFERENTIAL EQUATIONS. . . . . (MDIM ) =      6
NUMBER OF FINITE ELEMENTS . . . . . (NELEM ) =     580
NUMBER OF GRID POINTS . . . . . (NGRID ) =    2321
ORDER OF SHAPE FUNCTIONS. . . . . (NPOL ) =      4
ORDER OF GAUSS-LEGENDRE QUADRATURE. . . . (NGQ ) =      5
DIMENSION OF ENVELOPE SPACE . . . . . (IDIM ) =      3
BOUNDARY CONDITION CODE . . . . . (IBOUND) =      8
DOUBLE ENERGY SPECTRUM. . . . . (SHIFT ) =    3.40000

```

### SUBDIVISION OF RHO-REGION ON THE FINITE-ELEMENT GROUPS:

NO OF GROUP	NUMBER OF ELEMENTS	BEGIN OF INTERVAL	LENGTH OF ELEMENT	GRID STEP	END OF INTERVAL
1	180	0.300	0.01500	0.00375	3.000
2	200	3.000	0.08500	0.02125	20.000
3	200	20.000	0.40000	0.10000	100.000

```

LAST ADDRESS OF ARRAY ITOT USED =      62082

```

### T O T A L S Y S T E M D A T A

```

TOTAL NUMBER OF ALGEBRAIC EQUATIONS. . . . (NN ) =    13926
TOTAL NUMBER OF MATRIX ELEMENTS. . . . . (NWK ) =    257541
MAXIMUM HALF BANDWIDTH . . . . . (MK ) =      30
MEAN    HALF BANDWIDTH . . . . . (MMK ) =      18

```

```

LAST ADDRESS OF ARRAY TOT USED =    263150

```

```

NDIM, MDIM=      6      6

```

```

LAST ADDRESS OF ARRAY TOT USED =    371869

```

```

NUMBER OF OPEN CHANNELS . . . . . (NOPEN) =      2
VALUE OF I-TH MOMENTUM . . . . . (I,QR ) =      1  0.1549E+01
VALUE OF I-TH MOMENTUM . . . . . (I,QR ) =      2  0.6325E+00

```

```

TO HAVE REQUIRED EPSC=1.D-14
VALUE OF MATCHING POINT (RMATCH) =    31.6417
RECOMMENDED RIGHT BOUND OF
INTERVAL IS NOT LESS THAN (RMAX ) =    33

```

#### C H E C K W R O N S K I A N

```

-----
1.00000      -.102478E-17
0.197052E-17  1.00000

```

\*\*\*\*\*

#### R E A C T I O N M A T R I X

```

-----
-1.46347      2.19626
 2.19626     -8.72933

```

\*\*\*\*\*

#### R R A D I A L E I G E N F U N C T I O N S

```

-----
0.3000  0.6533D-01 0.1740D+01 -.1153D-01 0.3368D-01 -.1256D-04 0.3139D-04
        0.2082D-07 -.8510D-07 0.7188D-10 -.2697D-09 0.1034D-12 -.3923D-12
1.8000  -.2666D-01 0.6352D+00 -.8888D+00 0.2455D+01 0.1111D-01 -.4781D-01
        0.4547D-02 -.1653D-01 0.3372D-03 -.1260D-02 0.1491D-04 -.5729D-04
4.7000  0.2964D+00 -.3511D+00 0.4099D+00 -.1755D+01 0.1383D+00 -.5735D+00
        -.4163D-01 0.1528D+00 0.8703D-02 -.2809D-01 -.8857D-03 0.4631D-02
13.2000 -.1068D-01 -.4437D-01 0.1694D+00 -.6822D+00 -.7173D-02 0.3852D-01
        -.1107D-03 0.5968D-03 -.3290D-04 0.2413D-03 -.2221D-04 0.8926D-04
28.0000 0.5274D-01 -.5965D-01 -.8324D-02 -.1117D-01 0.4526D-02 -.1857D-01
        -.1015D-04 0.3768D-04 0.1217D-04 -.4945D-04 0.2971D-07 0.4214D-07
68.0000 0.2000D-01 -.1611D-01 0.3989D-01 -.1601D+00 0.6037D-04 0.8285D-04
        0.1750D-05 -.7186D-05 0.4147D-07 -.5194D-08 -.3349D-08 0.1340D-07

```

\*\*\*\*\*

\*\*\*\*\*

#### C M A T R I X

```

-----
0.261805      6.97335
-.468245      1.37416
-.574532E-02  0.144615E-01
0.976111E-04  -.402277E-03
0.382014E-05  -.143464E-04
0.611522E-07  -.231952E-06

```

\*\*\*\*\*

## References

- [1] O. Chuluunbaatar, A.A. Gusev, A.G. Abrashkevich, A. Amaya-Tapia, M.S. Kaschiev, S.Y. Larsen, S.I. Vinitsky, Comput. Phys. Comm. 177 (2007) 649–675.
- [2] V.A. Fock, Izv. Akad. Nauk SSSR, Ser. Fiz. 18 (1954) 161–172.
- [3] A.M. Ermolaev, Quantum theory, Part 1, in: Proc. of 8th UNESCO Internat. School of Physics, St. Petersburg, 1998, pp. 298–315.
- [4] M.B. Kadmets, S.I. Vinitsky, J. Phys. B 20 (1987) 5723–5736.
- [5] A.G. Abrashkevich, D.G. Abrashkevich, I.V. Puzynin, S.I. Vinitsky, J. Phys. B 24 (1991) 1615–1638.
- [6] S.I. Vinitskii, L.I. Ponomarev, Sov. J. Part. Phys. 13 (1982) 557–587.
- [7] S.I. Vinitskii, V.S. Melezhik, L.I. Ponomarev, Sov. J. Nucl. Phys. 36 (1982) 272–276.
- [8] A. Amaya-Tapia, S.Y. Larsen, J.J. Popiel, Few-Body Systems 23 (1997) 87–109.



- [9] V.V. Pupyshev, Phys. Part. Nucl. 33 (2002) 435–472.
- [10] H.J. Assenbaum, K. Langanke, C. Rolfs, Z. Phys. A 327 (1987) 461–468.
- [11] L. Bracci, G. Fiorentini, V.S. Melezhik, G. Mezzorani, P. Pasini, Phys. Lett. A 153 (1991) 456–460.
- [12] V. Melezhik, Nucl. Phys. A 550 (1992) 223–234.
- [13] V. Bystritskii, et al., Physics of Atomic Nuclei 64 (2001) 855–860.
- [14] Yu.N. Demkov, J.D. Meyer, Eur. Phys. J. B 42 (2004) 361–365.
- [15] P.M. Krassovitskiy, N.Zh. Takibaev, Bull. Russian Acad. Sci. Phys. 70 (2006) 815–818.
- [16] O. Chuluunbaatar, A.A. Gusev, V.L. Derbov, M.S. Kaschiev, L.A. Melnikov, V.V. Serov, S.I. Vinitsky, J. Phys. A 40 (2007) 11485–11524.
- [17] H.A. Sarkisyan, Mod. Phys. Lett. B 16 (2002) 835–841.
- [18] H. Voss, Comput. Phys. Comm. 174 (2006) 441–446.
- [19] W. Wang, T.-M. Hwang, J.-C. Jang, Comput. Phys. Comm. 174 (2006) 371–385.
- [20] J.I. Kim, V.S. Melezhik, P. Schmelcher, Phys. Rev. Lett. 97 (2006), 193203–1–4.
- [21] L.V. Kantorovich, V.I. Krylov, Approximate Methods of Higher Analysis, Wiley, New York, 1964.
- [22] O. Chuluunbaatar, A.A. Gusev, V.P. Gerdt, V.A. Rostovtsev, S.I. Vinitsky, A.G. Abrashkevich, M.S. Kaschiev, V.V. Serov, Comput. Phys. Comm. 178 (2007) 301–330.





Contents lists available at ScienceDirect

## Computer Physics Communications

www.elsevier.com/locate/cpc



# ODPEVP: A program for computing eigenvalues and eigenfunctions and their first derivatives with respect to the parameter of the parametric self-adjointed Sturm–Liouville problem <sup>☆</sup>

O. Chuluunbaatar <sup>a,\*</sup>, A.A. Gusev <sup>a</sup>, S.I. Vinitzky <sup>a</sup>, A.G. Abrashkevich <sup>b</sup>

<sup>a</sup> Joint Institute for Nuclear Research, Dubna, 141980 Moscow region, Russia

<sup>b</sup> IBM Toronto Lab, 8200 Warden Avenue, Markham, ON L6G 1C7, Canada

## ARTICLE INFO

## Article history:

Received 7 January 2009

Accepted 21 April 2009

Available online 22 April 2009

## PACS:

02.60.Lj

31.15.Ja

32.80.Fb

## Keywords:

Eigenvalue problems

Kantorovich method

Finite element method

Ordinary differential equations

High-order accuracy approximations

## ABSTRACT

A FORTRAN 77 program is presented for calculating with the given accuracy eigenvalues, eigenfunctions and their first derivatives with respect to the parameter of the parametric self-adjointed Sturm–Liouville problem with the parametric third type boundary conditions on the finite interval. The program calculates also potential matrix elements – integrals of the eigenfunctions multiplied by their first derivatives with respect to the parameter. Eigenvalues and matrix elements computed by the ODPEVP program can be used for solving the bound state and multi-channel scattering problems for a system of the coupled second-order ordinary differential equations with the help of the KANTBP programs [O. Chuluunbaatar, A.A. Gusev, A.G. Abrashkevich, A. Amaya-Tapia, M.S. Kaschiev, S.Y. Larsen, S.I. Vinitzky, Comput. Phys. Commun. 177 (2007) 649–675; O. Chuluunbaatar, A.A. Gusev, S.I. Vinitzky, A.G. Abrashkevich, Comput. Phys. Commun. 179 (2008) 685–693]. As a test desk, the program is applied to the calculation of the potential matrix elements for an integrable 2D-model of three identical particles on a line with pair zero-range potentials, a 3D-model of a hydrogen atom in a homogeneous magnetic field and a hydrogen atom on a three-dimensional sphere.

## Program summary

Program title: ODPEVP

Catalogue identifier: AEDV\_v1\_0

Program summary URL: [http://cpc.cs.qub.ac.uk/summaries/AEDV\\_v1\\_0.html](http://cpc.cs.qub.ac.uk/summaries/AEDV_v1_0.html)

Program obtainable from: CPC Program Library, Queen's University, Belfast, N. Ireland

Licensing provisions: Standard CPC license, <http://cpc.cs.qub.ac.uk/licence/licence.html>

No. of lines in distributed program, including test data, etc.: 3001

No. of bytes in distributed program, including test data, etc.: 24 195

Distribution format: tar.gz

Programming language: FORTRAN 77

Computer: Intel Xeon EM64T, Alpha 21264A, AMD Athlon MP, Pentium IV Xeon, Opteron 248, Intel Pentium IV

Operating system: OC Linux, Unix AIX 5.3, SunOS 5.8, Solaris, Windows XP

RAM: depends on

1. the number and order of finite elements;
2. the number of points; and
3. the number of eigenfunctions required.

Test run requires 4 MB

Classification: 2.1, 2.4

External routines: GAULEG [3]

Nature of problem: The three-dimensional boundary problem for the elliptic partial differential equation with an axial symmetry similar to the Schrödinger equation with the Coulomb and transverse oscillator potentials is reduced to the two-dimensional one. The latter finds wide applications in modeling

<sup>☆</sup> This paper and its associated computer program are available via the Computer Physics Communications homepage on ScienceDirect (<http://www.sciencedirect.com/science/journal/00104655>).

\* Corresponding author.

E-mail address: [chuka@jinr.ru](mailto:chuka@jinr.ru) (O. Chuluunbaatar).

of photoionization and recombination of oppositely charged particles (positrons, antiprotons) in the magnet-optical trap [4], optical absorption in quantum wells [5], and channeling of likely charged particles in thin doped films [6,7] or neutral atoms and molecules in artificial waveguides or surfaces [8,9]. In the adiabatic approach [10] known in mathematics as Kantorovich method [11] the solution of the two-dimensional elliptic partial differential equation is expanded over basis functions with respect to the fast variable (for example, angular variable) and depended on the slow variable (for example, radial coordinate) as a parameter. An averaging of the problem by such a basis leads to a system of the second-order ordinary differential equations which contain potential matrix elements and the first-derivative coupling terms (see, e.g., [12,13,14]). The purpose of this paper is to present the finite element method procedure based on the use of high-order accuracy approximations for calculating eigenvalues, eigenfunctions and their first derivatives with respect to the parameter of the parametric self-adjointed Sturm–Liouville problem with the parametric third type boundary conditions on the finite interval. The program developed calculates potential matrix elements – integrals of the eigenfunctions multiplied by their derivatives with respect to the parameter. These matrix elements can be used for solving the bound state and multi-channel scattering problems for a system of the coupled second-order ordinary differential equations with the help of the KANTBP programs [1,2].

**Solution method:** The parametric self-adjointed Sturm–Liouville problem with the parametric third type boundary conditions is solved by the finite element method using high-order accuracy approximations [15]. The generalized algebraic eigenvalue problem  $\mathbf{A}\mathbf{F} = \mathbf{E}\mathbf{B}\mathbf{F}$  with respect to a pair of unknown  $(\mathbf{E}, \mathbf{F})$  arising after the replacement of the differential problem by the finite-element approximation is solved by the subspace iteration method using the SSPACE program [16]. First derivatives of the eigenfunctions with respect to the parameter which contained in potential matrix elements of the coupled system equations are obtained by solving the inhomogeneous algebraic equations. As a test desk, the program is applied to the calculation of the potential matrix elements for an integrable 2D-model of three identical particles on a line with pair zero-range potentials described in [1,17,18], a 3D-model of a hydrogen atom in a homogeneous magnetic field described in [14,19] and a hydrogen atom on a three-dimensional sphere [20].

**Restrictions:** The computer memory requirements depend on:

1. the number and order of finite elements;
2. the number of points; and
3. the number of eigenfunctions required.

Restrictions due to dimension sizes may be easily alleviated by altering PARAMETER statements (see sections below and listing for details). The user must also supply DOUBLE PRECISION functions POTCCL and POTCC1 for evaluating potential function  $U(\rho, z)$  of Eq. (1) and its first derivative with respect to parameter  $\rho$ . The user should supply DOUBLE PRECISION functions F1FUNC and F2FUNC that evaluate functions  $f_1(z)$  and  $f_2(z)$  of Eq. (1). The user must also supply subroutine BOUNCF for evaluating the parametric third type boundary conditions.

**Running time:** The running time depends critically upon:

1. the number and order of finite elements;
2. the number of points on interval  $[z_{\min}, z_{\max}]$ ; and
3. the number of eigenfunctions required.

The test run which accompanies this paper took 2 s with calculation of matrix potentials on the Intel Pentium IV 2.4 GHz.

**References:**

- [1] O. Chuluunbaatar, A.A. Gusev, A.G. Abrashkevich, A. Amaya-Tapia, M.S. Kaschiev, S.Y. Larsen, S.I. Vinitsky, Comput. Phys. Comm. 177 (2007) 649–675
- [2] O. Chuluunbaatar, A.A. Gusev, S.I. Vinitsky, A.G. Abrashkevich, Comput. Phys. Comm. 179 (2008) 685–693.
- [3] W.H. Press, S.A. Teukolsky, W.T. Vetterling, B.P. Flannery, Numerical Recipes: The Art of Scientific Computing, Cambridge University Press, Cambridge, 1986.
- [4] O. Chuluunbaatar, A.A. Gusev, S.I. Vinitsky, V.L. Derbov, L.A. Melnikov, V.V. Serov, Phys. Rev. A 77 (2008) 034702–1–4.
- [5] E.M. Kazaryan, A.A. Kostanyan, H.A. Sarkisyan, Physica E 28 (2005) 423–430.
- [6] Yu.N. Demkov, J.D. Meyer, Eur. Phys. J. B 42 (2004) 361–365.
- [7] P.M. Krassovitskiy, N.Zh. Takibaev, Bull. Russian Acad. Sci. Phys. 70 (2006) 815–818.
- [8] V.S. Melezhik, J.I. Kim, P. Schmelcher, Phys. Rev. A 76 (2007) 053611–1–15.
- [9] F.M. Pen'kov, Phys. Rev. A 62 (2000) 044701–1–4.
- [10] M. Born, X. Huang, Dynamical Theory of Crystal Lattices, The Clarendon Press, Oxford, England, 1954.
- [11] L.V. Kantorovich, V.I. Krylov, Approximate Methods of Higher Analysis, Wiley, New York, 1964.
- [12] U. Fano, Colloq. Int. C.N.R.S. 273 (1977) 127;
- [13] A.F. Starace, G.L. Webster, Phys. Rev. A 19 (1979) 1629–1640.
- [14] C.V. Clark, K.T. Lu, A.F. Starace, in: H.G. Beyer, H. Kleinpoppen (eds.), Progress in Atomic Spectroscopy, Part C, Plenum, New York, 1984, pp. 247–320.
- [15] O. Chuluunbaatar, A.A. Gusev, V.L. Derbov, M.S. Kaschiev, L.A. Melnikov, V.V. Serov, S.I. Vinitsky, J. Phys. A 40 (2007) 11485–11524.
- [16] A.G. Abrashkevich, D.G. Abrashkevich, M.S. Kaschiev, I.V. Puzynin, Comput. Phys. Comm. 85 (1995) 40–64.
- [17] K.J. Bathe, Finite Element Procedures in Engineering Analysis, Englewood Cliffs, Prentice-Hall, New York, 1982.

- [17] O. Chuluunbaatar, A.A. Gusev, M.S. Kaschiev, V.A. Kaschieva, A. Amaya-Tapia, S.Y. Larsen, S.I. Vinitsky, J. Phys. B 39 (2006) 243–269.
- [18] Yu.A. Kuperin, P.B. Kurasov, Yu.B. Melnikov, S.P. Merkuriev, Ann. Phys. 205 (1991) 330–361.
- [19] O. Chuluunbaatar, A.A. Gusev, V.P. Gerdt, V.A. Rostovtsev, S.I. Vinitsky, A.G. Abrashkevich, M.S. Kaschiev, V.V. Serov, Comput. Phys. Comm. 178 (2008) 301–330.
- [20] A.G. Abrashkevich, M.S. Kaschiev, S.I. Vinitsky, J. Comp. Phys. 163 (2000) 328–348.

© 2009 Elsevier B.V. All rights reserved.

## 1. Introduction

Mathematical models of physical processes such as photoionization and laser-stimulated recombination of hydrogen like atoms in a homogeneous magnetic field under influence of a laser field, axial channeling of the charged particles in thin films, and also excitation, de-excitation of wave-packet of a hydrogen atom in a homogeneous magnetic field under influence of the sequences with ultra-short laser pulses (so-called three-dimensional kicked hydrogen atom in a magnetic field) are subjects of recent studies [1–6].

Dynamics of these processes is described in a center of mass system by three-dimensional wave functions of stationary equations of Schrödinger type. We shall emphasize, that in a vicinity of the origin of a system of coordinates or the pair impact point the attractive or repulsive Coulomb potentials dominate while in asymptotic regions it is the oscillator potential in transversal variables. Similar problems arise in quantum well with a hydrogen like impurity in study of photoabsorption processes [7].

Mathematical models of these processes used in numerical studies to describe the dynamics of few-body systems are singular spectral, boundary and evolutionary problems for multi-dimensional equation of Schrödinger type in the coordinate space. We shall emphasize, that the presence of several interaction potentials between particles or particles with external fields leads to a division of the whole region to subregions where the relevant boundary problems are solved using the corresponding dominating potential. Hence a singular problem could be reduced to a regular one on a finite region by defining asymptotic boundary conditions with the help of an appropriate asymptotic decomposition of solutions on a border of the finite region in the form of conditions of the third type.

For solving a boundary problem in the complex region, in the framework of the projective method one has to construct basic functions with nonlinear parameters in one of the subregions or in each subregion. For the coordination of compound basic functions on borders of these regions it is necessary to use conditions of the third type. Hence the amount of nonlinear parameters in a variational functional essentially increases which requires significant computer resources to calculate them.

The multi-step Kantorovich method enables one to construct an economical algorithm for calculating of parametrical basic functions which take into account all features of complex regions and conditions of the coordination between them. The use of such basis allows us to lower the dimension of an initial boundary problem by reducing it to a system of ordinary differential equations with boundary conditions of the third type [8,9]. Discretization of boundary problems by the finite-element method (FEM) [10,11] results in sequences of parametrical algebraic problems for the numerical solution of which one needs to develop economical and efficient algorithms and programs.

In this work we present an ODPEVP program for calculating with a given accuracy eigenvalues, eigenfunctions and their first derivatives with respect to the parameter of the parametric self-adjointed Sturm–Liouville problem with the parametric third type boundary conditions on the finite interval. The program calculates also potential matrix elements – integrals of the eigenfunctions multiplied by their derivatives with respect to the parameter. Eigenvalues and matrix elements computed by the ODPEVP program can be used for solving the bound state and multi-channel scattering problems for a system of the coupled second-order ordinary differential equations with the help of the KANTBP programs [8,9].

The FEM is applied to construct numerical schemes for solving the corresponding boundary problem for parametric self-adjointed ordinary differential equations with an accuracy of order  $O(h^{p+1})$  in grid step  $h$  [10,11]. The order of approximation,  $p$ , depends on the smoothness of the required solution.

As a benchmark, we present calculation with a given accuracy of eigenvalues, eigenfunctions and their first derivatives with respect to the parameter, corresponding matrix elements for Kantorovich reduction of an integrable 2D-model of three identical particles on a line with the pair zero-range potentials described in [8,12], a 3D-model of a hydrogen atom in a homogeneous magnetic field described in [1,14] and a hydrogen atom on a three-dimensional sphere [15,16]. The numeric results show that the program developed is very efficient and allows to obtain numerical solutions of the above problems with the required accuracy using very little computational resources.

The paper is organized as follows. In Section 2 we give a brief overview of the problem. The construction of the finite-element high-order schemes is discussed in Section 3. A description of the ODPEVP program is given in Section 4. Subroutine units are briefly described in Section 5. Test desk is discussed in Section 6.

## 2. Statement of the problem

Let us consider a boundary problem for a parametric self-adjointed second order ordinary differential equation

$$L(z; \rho)\psi(z; \rho) = \epsilon(\rho)\psi(z; \rho), \quad z \in [z_{\min}, z_{\max}],$$

$$L(z; \rho) \equiv -\frac{1}{f_1(z)} \frac{d}{dz} f_2(z) \frac{d}{dz} + U(\rho, z), \quad (1)$$

with parametric third type boundary conditions

$$l_1(\rho, \mu_1, \lambda_1(\rho), \psi(z; \rho)) \equiv \mu_1 f_2(z) \frac{d\psi(z; \rho)}{dz} + \lambda_1(\rho)\psi(z; \rho) = 0, \quad z = z_{\min}, \quad (2)$$

$$l_2(\rho, \mu_2, \lambda_2(\rho), \psi(z; \rho)) \equiv \mu_2 f_2(z) \frac{d\psi(z; \rho)}{dz} + \lambda_2(\rho)\psi(z; \rho) = 0, \quad z = z_{\max}. \quad (3)$$

Here  $\rho$  is a parameter, functions  $f_1(z) > 0$ ,  $f_2(z) > 0$  and  $U(\rho, z)$  are continuous on finite interval  $z \in (z_{\min}, z_{\max})$ , and function  $f_2(z)$  is differentiable by the variable on finite interval  $z \in (z_{\min}, z_{\max})$ . Also  $U(\rho, z)$ ,  $\lambda_1(\rho)$  and  $\lambda_2(\rho)$  are differentiable by parameter  $\rho$ . If  $\mu_j \lambda_j(\rho) \neq 0$ , then  $\mu_j = 1$ . The normalization condition reads for eigenfunctions  $\psi_i(z; \rho)$ ,  $\psi_j(z; \rho)$

$$\int_{z_{\min}}^{z_{\max}} f_1(z) \psi_i(z; \rho) \psi_j(z; \rho) dz = \delta_{ij}, \quad (4)$$

where  $\delta_{ij}$  is the Kronecker symbol, and  $\epsilon_1(\rho) < \epsilon_2(\rho) < \dots$ .

The main goal of this paper is to develop an efficient numerical method that will allow one to calculate  $\partial \psi_j(z; \rho) / \partial \rho$  with the same accuracy as was achieved for eigenfunctions of the boundary problem (1)–(3) and use it to compute potential matrix elements defined by formula

$$\begin{aligned} Q_{ij}(\rho) &= - \int_{z_{\min}}^{z_{\max}} f_1(z) \psi_i(z; \rho) \frac{\partial \psi_j(z; \rho)}{\partial \rho} dz, \\ H_{ij}(\rho) &= \int_{z_{\min}}^{z_{\max}} f_1(z) \frac{\partial \psi_i(z; \rho)}{\partial \rho} \frac{\partial \psi_j(z; \rho)}{\partial \rho} dz. \end{aligned} \quad (5)$$

The calculated eigenvalues and potential matrix elements can be used for solving the bound state and multi-channel scattering problems for a system of the coupled second-order ordinary differential equations with the help of the KANTBP programs [8,9].

Taking a derivative of the boundary problem (1)–(3) with respect to parameter  $\rho$ , we get that  $\partial \psi_j(z; \rho) / \partial \rho$  can be obtained as a solution of the following boundary problem

$$(L(z; \rho) - \epsilon_j(\rho)) \frac{\partial \psi_j(z; \rho)}{\partial \rho} = - \left( \frac{\partial U(\rho, z)}{\partial \rho} - \frac{\partial \epsilon_j(\rho)}{\partial \rho} \right) \psi_j(z; \rho), \quad (6)$$

$$\frac{\partial l_1(\rho, \mu_1, \lambda_1(\rho), \psi_j(z_{\min}; \rho))}{\partial \rho} = 0, \quad (7)$$

$$\frac{\partial l_2(\rho, \mu_2, \lambda_2(\rho), \psi_j(z_{\max}; \rho))}{\partial \rho} = 0. \quad (8)$$

Multiplying Eq. (6) from the left by eigenfunction  $\psi_i(z; \rho)$  and integrating over the interval  $z \in [z_{\min}, z_{\max}]$ , we obtain

$$\begin{aligned} \int_{z_{\min}}^{z_{\max}} f_1(z) \psi_i(z; \rho) (L(z; \rho) - \epsilon_j(\rho)) \frac{\partial \psi_j(z; \rho)}{\partial \rho} dz &\equiv (\epsilon_i(\rho) - \epsilon_j(\rho)) \int_{z_{\min}}^{z_{\max}} f_1(z) \psi_i(z; \rho) \frac{\partial \psi_j(z; \rho)}{\partial \rho} dz + f_{ij}(\rho, z_{\min}, z_{\max}) \\ &= - \int_{z_{\min}}^{z_{\max}} f_1(z) \psi_i(z; \rho) \left( \frac{\partial U(\rho, z)}{\partial \rho} - \frac{\partial \epsilon_j(\rho)}{\partial \rho} \right) \psi_j(z; \rho) dz, \end{aligned} \quad (9)$$

where

$$f_{ij}(\rho, z_{\min}, z_{\max}) = \begin{cases} \frac{\partial \lambda_2(\rho)}{\partial \rho} \psi_i(z_{\max}; \rho) \psi_j(z_{\max}; \rho) - \frac{\partial \lambda_1(\rho)}{\partial \rho} \psi_i(z_{\min}; \rho) \psi_j(z_{\min}; \rho), & \text{if } \mu_1 \lambda_1(\rho) \neq 0, \mu_2 \lambda_2(\rho) \neq 0, \\ \frac{\partial \lambda_2(\rho)}{\partial \rho} \psi_i(z_{\max}; \rho) \psi_j(z_{\max}; \rho), & \text{if } \mu_1 \lambda_1(\rho) = 0, \mu_2 \lambda_2(\rho) \neq 0, \\ - \frac{\partial \lambda_1(\rho)}{\partial \rho} \psi_i(z_{\min}; \rho) \psi_j(z_{\min}; \rho), & \text{if } \mu_1 \lambda_1(\rho) \neq 0, \mu_2 \lambda_2(\rho) = 0, \\ 0, & \text{if } \mu_1 \lambda_1(\rho) = 0, \mu_2 \lambda_2(\rho) = 0. \end{cases} \quad (10)$$

From here we find

$$\frac{\partial \epsilon_j(\rho)}{\partial \rho} = \int_{z_{\min}}^{z_{\max}} f_1(z) \psi_j(z; \rho) \frac{\partial U(\rho, z)}{\partial \rho} \psi_j(z; \rho) dz + f_{jj}(\rho, z_{\min}, z_{\max}). \quad (11)$$

Now the problem (6)–(8) has a solution, but it is not unique. From the normalization condition (4) we obtain the required additional condition

$$\int_{z_{\min}}^{z_{\max}} f_1(z) \psi_j(z; \rho) \frac{\partial \psi_j(z; \rho)}{\partial \rho} dz = 0. \quad (12)$$

Thus, problem (6)–(8) with additional conditions (11), (12) has now a unique solution.

In the most of applications the following formulas

$$\begin{aligned} Q_{ij}(\rho) &= \frac{1}{\epsilon_i(\rho) - \epsilon_j(\rho)} \int_{z_{\min}}^{z_{\max}} f_1(z) \psi_i(z; \rho) \frac{\partial U(\rho, z)}{\partial \rho} \psi_j(z; \rho) dz + \frac{f_{ij}(\rho, z_{\min}, z_{\max})}{\epsilon_i(\rho) - \epsilon_j(\rho)}, \quad i \neq j, \\ Q_{ii}(\rho) &= 0, \end{aligned} \quad (13)$$

and

$$H_{ij}(\rho) = - \sum_{l=1} Q_{il}(\rho) Q_{lj}(\rho), \quad (14)$$

are usually used. Note that Eq. (14) has a rather slow convergence which means that in order to get a high level of accuracy one should include a sufficiently large number of terms in a sum over  $l$ . This circumstance can present a serious problem from the computational point of view, especially in regard to demands for required computational resources and computation time. An explicit example has been given in paper [15] and can be examined with the help of *Test III* benchmark.

The continuity of eigenfunction  $\psi_j(z; \rho)$  with respect to parameter  $\rho$  is very important for calculations of the potential matrix elements (5) and their further applications for solution of a system of coupled differential equations as considered in [8]. Hence we required  $\psi_j(z; \rho) > 0$  in the vicinity of the right boundary point  $z = z_{\max}$ .

### 3. High order approximations of the finite-element method

Let us consider a numerical algorithm for the calculation of the eigenfunctions  $\psi(z; \rho)$  and their derivative with respect to the parameter  $\rho$  of the parametric boundary problem (1)–(3). Computational schemes of the high order of accuracy are derived from the Rayleigh–Ritz variational functional

$$\mathcal{R}(\psi, \epsilon) = \left\{ \int_{z_{\min}}^{z_{\max}} \left( f_2(z) \left( \frac{d\psi(z; \rho)}{dz} \right)^2 + f_1(z) U(\rho, z) \psi^2(z; \rho) \right) dz + g(\rho, z_{\min}, z_{\max}) \right\} \times \left\{ \int_{z_{\min}}^{z_{\max}} f_1(z) \psi^2(z; \rho) dz \right\}^{-1}, \quad (15)$$

on the basis of the FEM. Here

$$g(\rho, z_{\min}, z_{\max}) = \begin{cases} \lambda_2(\rho) \psi(z_{\max}; \rho) \psi(z_{\max}; \rho) - \lambda_1(\rho) \psi(z_{\min}; \rho) \psi(z_{\min}; \rho), & \text{if } \mu_1 \lambda_1(\rho) \neq 0, \mu_2 \lambda_2(\rho) \neq 0, \\ \lambda_2(\rho) \psi(z_{\max}; \rho) \psi(z_{\max}; \rho), & \text{if } \mu_1 \lambda_1(\rho) = 0, \mu_2 \lambda_2(\rho) \neq 0, \\ -\lambda_1(\rho) \psi(z_{\min}; \rho) \psi(z_{\min}; \rho), & \text{if } \mu_1 \lambda_1(\rho) \neq 0, \mu_2 \lambda_2(\rho) = 0, \\ 0, & \text{if } \mu_1 \lambda_1(\rho) = 0, \mu_2 \lambda_2(\rho) = 0. \end{cases} \quad (16)$$

The general idea of the FEM in one-dimensional space is to divide interval  $[z_{\min}, z_{\max}]$  into many small domains called elements. The size of elements can be defined very freely so that physical properties can be taken into account.

The interval  $\Delta = [z_{\min}, z_{\max}]$  is covered by a system of  $n$  subintervals  $\Delta_j = [z_{j-1}, z_j]$  in such a way that  $\Delta = \bigcup_{j=1}^n \Delta_j$ . In each subinterval  $\Delta_j$  the nodes

$$z_{j,r}^p = z_{j-1} + \frac{h_j}{p} r, \quad h_j = z_j - z_{j-1}, \quad r = \overline{0, p}, \quad (17)$$

and the Lagrange elements  $\{\phi_{j,r}^p(z)\}_{r=0}^p$

$$\phi_{j,r}^p(z) = \prod_{i=0, i \neq r}^p \frac{(z - z_{j,i}^p)}{(z_{j,r}^p - z_{j,i}^p)} \quad (18)$$

are determined. By means of the Lagrange elements  $\phi_{j,r}^p(z)$ , we define a set of local functions  $N_l(z)$  as follows:

$$N_l^p(z) = \begin{cases} \begin{cases} \phi_{1,0}^p(z), & z \in \Delta_1, \\ 0, & z \notin \Delta_1, \end{cases} & l = 0, \\ \begin{cases} \phi_{j,r}^p(z), & z \in \Delta_j, \\ 0, & z \notin \Delta_j, \end{cases} & l = r + p(j-1), \quad r = \overline{1, p-1}, \\ \begin{cases} \phi_{j,p}^p(z), & z \in \Delta_j, \\ \phi_{j+1,0}^p(z), & z \in \Delta_{j+1}, \\ 0, & z \notin \Delta_j \cup \Delta_{j+1}, \end{cases} & l = jp, \quad j = \overline{1, n-1}, \\ \begin{cases} \phi_{n,p}^p(z), & z \in \Delta_n, \\ 0, & z \notin \Delta_n, \end{cases} & l = np. \end{cases} \quad (19)$$

The functions  $\{N_l^p(z)\}_{l=0}^L$ ,  $L = np$ , form a basis in the space of polynomials of the  $p$ th order. Now, each function  $\psi(z; \rho)$  is approximated by a finite sum of local functions  $N_l^p(z)$

$$\psi(z; \rho) = \sum_{l=0}^L \psi^l(z_{j,r}^p, \rho) N_l^p(z). \quad (20)$$

After substituting expansion (20) into the variational functional (15) and minimizing it [10,11] we obtain the generalized eigenvalue problem

$$\mathbf{A}^p \boldsymbol{\psi}^h = \epsilon^h \mathbf{B}^p \boldsymbol{\psi}^h, \quad \mathbf{A}^p = \hat{\mathbf{A}}^p + \mathbf{M}. \quad (21)$$

Here  $\mathbf{A}^p$  is the stiffness matrix;  $\mathbf{B}^p$  is the mass matrix and positive definite;  $\mathbf{M}$  is the diagonal matrix with zero elements, except the first and last elements that are equal  $\lambda_2(\rho)$  (or zero) and  $-\lambda_1(\rho)$  (or zero), respectively;  $\boldsymbol{\psi}^h$  is the vector approximating solution on the finite-element grid; and  $\epsilon^h$  is the corresponding eigenvalue. The matrices  $\hat{\mathbf{A}}^p$  and  $\mathbf{B}^p$  have the following form

$$\hat{\mathbf{A}}^p = \sum_{j=1}^n \mathbf{a}_j^p, \quad \mathbf{B}^p = \sum_{j=1}^n \mathbf{b}_j^p, \quad (22)$$

where the local matrices  $\mathbf{a}_j^p$  and  $\mathbf{b}_j^p$  are calculated as

$$\begin{aligned} (\mathbf{a}_j^p)^{qr} &= \int_{-1}^{+1} \left\{ f_2(z) \frac{4}{h_j^2} \frac{d\phi_{j,q}^p(z)}{dz} \frac{d\phi_{j,r}^p(z)}{dz} + f_1(z) U(\rho, z) \phi_{j,q}^p(z) \phi_{j,r}^p(z) \right\} \frac{h_j}{2} d\eta, \\ (\mathbf{b}_j^p)^{qr} &= \int_{-1}^{+1} f_1(z) \phi_{j,q}^p(z) \phi_{j,r}^p(z) \frac{h_j}{2} d\eta, \\ z &= z_{j-1} + 0.5h_j(1 + \eta), \quad q, r = \overline{0, p}. \end{aligned} \quad (23)$$

Integrals (23) are evaluated using the Gaussian quadrature formulae

$$\begin{aligned} (\mathbf{a}_j^p)^{qr} &= \sum_{g=0}^p \left\{ f_2(z_g) \frac{4}{h_j^2} \frac{d\phi_{j,q}^p(z_g)}{dz} \frac{d\phi_{j,r}^p(z_g)}{dz} + f_1(z_g) U(\rho, z_g) \phi_{j,q}^p(z_g) \phi_{j,r}^p(z_g) \right\} \frac{h_j}{2} w_g, \\ (\mathbf{b}_j^p)^{qr} &= \sum_{g=0}^p f_1(z_g) \phi_{j,q}^p(z_g) \phi_{j,r}^p(z_g) \frac{h_j}{2} w_g, \end{aligned} \quad (24)$$

where  $z_g = z_{j-1} + 0.5h_j(1 + \eta_g)$ ,  $\eta_g$  and  $w_g$ ,  $g = \overline{0, p}$  are the Gaussian nodes and weights.

Let  $\epsilon_j(\rho)$ ,  $\psi_j(z; \rho) \in \mathcal{H}^2$  are the exact solution of (1)–(3) and  $\epsilon_j^h$ ,  $\psi_j^h \in \mathcal{H}^1$  are the numerical solution of (21). Then for  $U(\rho, z) > 0$ ,  $\lambda_1(\rho) \leq 0$  and  $\lambda_2(\rho) \geq 0$  the following estimates are valid [10]

$$|\epsilon_j(\rho) - \epsilon_j^h| \leq c_1 h^{2p}, \quad \|\psi_j(z; \rho) - \psi_j^h\|_0 \leq c_2 h^{p+1}, \quad c_1 > 0, \quad c_2 > 0, \quad (25)$$

where  $\|v(z; \rho)\|_0^2 = \int_{z_{\min}}^{z_{\max}} f_1(z) v^2(z; \rho) dz$ ,  $h$  the maximal step of the finite-element grid,  $p$  is the order of finite elements,  $j$  is the number of the corresponding eigensolution, and constants  $c_1$  and  $c_2$  do not depend on step  $h$ . It is necessary to mention that the second estimate of Eq. (25) is valid also for solution  $\partial \psi_j(z; \rho) / \partial \rho$  of problem (6)–(8), (12). This fact guarantees the same accuracy for eigenfunctions and their derivatives within the present method.

In order to solve the generalized eigenvalue problem (21), the subspace iteration method [10,11] elaborated by Bathe [11] for the solution of large symmetric banded matrix eigenvalue problems has been chosen. This method uses a skyline storage mode, which stores components of the matrix column vectors within the banded region of the matrix, and is ideally suited for banded finite element matrices. The procedure chooses a vector subspace of the full solution space and iterates upon the successive solutions in the subspace (for details, see [11]). The iterations continue until the desired set of solutions in the iteration subspace converges to within the specified tolerance on the Rayleigh quotients for the eigenpairs. If matrix  $\mathbf{A}^p$  in Eq. (21) is not positively defined, problem (21) is replaced by the following problem:

$$\tilde{\mathbf{A}}^p \boldsymbol{\phi}^h = \tilde{\epsilon}^h \mathbf{B}^p \boldsymbol{\phi}^h, \quad \tilde{\mathbf{A}}^p = \mathbf{A}^p - \alpha \mathbf{B}^p. \quad (26)$$

The number  $\alpha$  (the shift of the energy spectrum) is chosen in such a way that matrix  $\tilde{\mathbf{A}}^p$  is positive. The eigenvector of problem (21) is the same, and  $\epsilon^h = \tilde{\epsilon}^h + \alpha$ .

### 3.1. Calculations of parametric derivative of the eigenfunctions, and matrix elements

The boundary problem (6)–(8) is reduced to the linear system of inhomogeneous algebraic equations

$$\mathbf{L} \frac{\partial \boldsymbol{\psi}^h}{\partial \rho} \equiv (\mathbf{A}^p - \epsilon^h \mathbf{B}^p) \frac{\partial \boldsymbol{\psi}^h}{\partial \rho} = \mathbf{b}, \quad \mathbf{b} = - \left( \frac{\partial \mathbf{A}^p}{\partial \rho} - \frac{\partial \epsilon^h}{\partial \rho} \mathbf{B}^p \right) \boldsymbol{\psi}^h. \quad (27)$$

The normalization, orthogonalization and additional conditions are read as

$$(\boldsymbol{\psi}^h)^T \mathbf{B}^p \boldsymbol{\psi}^h = 1, \quad \left( \frac{\partial \boldsymbol{\psi}^h}{\partial \rho} \right)^T \mathbf{B}^p \boldsymbol{\psi}^h = 0, \quad \frac{\partial \epsilon^h}{\partial \rho} = (\boldsymbol{\psi}^h)^T \frac{\partial \mathbf{A}^p}{\partial \rho} \boldsymbol{\psi}^h. \quad (28)$$

From here, potential matrix elements  $Q_{ij}^h$  and  $H_{ij}^h$  have the form

$$Q_{ij}^h = -(\boldsymbol{\psi}_i^h)^T \mathbf{B}^p \frac{\partial \boldsymbol{\psi}_j^h}{\partial \rho}, \quad H_{ij}^h = \left( \frac{\partial \boldsymbol{\psi}_i^h}{\partial \rho} \right)^T \mathbf{B}^p \frac{\partial \boldsymbol{\psi}_j^h}{\partial \rho}. \quad (29)$$

Since  $\epsilon^h$  is an eigenvalue of (21), matrix  $\mathbf{L}$  in Eq. (27) is degenerate. In this case the algorithm for solving Eq. (27) can be written in three steps as follows:



**Step k1.** Calculate solutions  $\mathbf{v}$  and  $\mathbf{w}$  of the auxiliary inhomogeneous systems of algebraic equations

$$\bar{\mathbf{L}}\mathbf{v} = \bar{\mathbf{b}}, \quad \bar{\mathbf{L}}\mathbf{w} = \mathbf{d}, \quad (30)$$

with non-degenerate matrix  $\bar{\mathbf{L}}$  and right-hand sides  $\bar{\mathbf{b}}$  and  $\mathbf{d}$

$$\bar{L}_{ss'} = \begin{cases} L_{ss'}, & (s-S)(s'-S) \neq 0, \\ \delta_{ss'}, & (s-S)(s'-S) = 0, \end{cases}$$

$$\bar{b}_s = \begin{cases} b_s, & s \neq S, \\ 0, & s = S, \end{cases} \quad d_s = \begin{cases} L_{sS}, & s \neq S, \\ 0, & s = S, \end{cases} \quad (31)$$

where  $S$  is the number of the greatest absolute value element of vector  $\mathbf{B}^p \boldsymbol{\psi}^h$ .

**Step k2.** Evaluate coefficient  $\gamma$

$$\gamma = -\frac{\gamma_1}{(\mathbf{D}_S - \gamma_2)}, \quad \gamma_1 = \mathbf{v}^T \mathbf{B}^p \boldsymbol{\psi}^h, \quad \gamma_2 = \mathbf{w}^T \mathbf{B}^p \boldsymbol{\psi}^h, \quad \mathbf{D}_S = (\mathbf{B}^p \boldsymbol{\psi}^h)_S. \quad (32)$$

**Step k3.** Evaluate vector  $\partial \boldsymbol{\psi}^h / \partial \rho$

$$\frac{\partial \psi_s^h}{\partial \rho} = \begin{cases} v_s - \gamma w_s, & s \neq S, \\ \gamma, & s = S. \end{cases} \quad (33)$$

From the consideration above it is evident, that the derivative computed has the same accuracy as the calculated eigenfunction.

**Theorem.** Let  $L(z; \rho)$  from (1) is bounded positively defined operator on space  $\mathcal{H}^1$  with energy norm, and  $\lambda_1(\rho) \leq 0$ ,  $\lambda_2(\rho) \geq 0$ . Also  $\partial U(\rho, z) / \partial \rho$ ,  $\partial \lambda_1(\rho) / \partial \rho$  and  $\partial \lambda_2(\rho) / \partial \rho$  are bounded in each value of the real parameter  $\rho$ . Then for exact values of solutions,  $\partial \epsilon_j(\rho) / \partial \rho$ ,  $\partial \psi_j(z; \rho) / \partial \rho \in \mathcal{H}^2$ , from (6)–(8), (11), (12) and potential matrix elements,  $Q_{ij}(\rho)$ ,  $H_{ij}(\rho)$ , from (5), and corresponded numerical values,  $\partial \epsilon_j^h / \partial \rho$ ,  $\partial \psi_j^h / \partial \rho \in \mathcal{H}^1$ , from (27), (28) and  $Q_{ij}^h$ ,  $H_{ij}^h$ , from (29) the following estimates are valid:

$$\left| \frac{\partial \epsilon_j(\rho)}{\partial \rho} - \frac{\partial \epsilon_j^h}{\partial \rho} \right| \leq c_3 h^{2p}, \quad \left\| \frac{\partial \psi_j(z; \rho)}{\partial \rho} - \frac{\partial \psi_j^h}{\partial \rho} \right\|_0 \leq c_4 h^{p+1}, \quad |Q_{ij}(\rho) - Q_{ij}^h| \leq c_5 h^{2p}, \quad |H_{ij}(\rho) - H_{ij}^h| \leq c_6 h^{2p},$$

where  $h$  the maximal step of the finite-element grid;  $p$  is the order of finite elements;  $i, j$  are the number of the corresponding solutions; and constants  $c_3$ ,  $c_4$ ,  $c_5$  and  $c_6$  do not depend on step  $h$ .

Proof is straightforward following the scheme of proof of estimations (25) in accordance with [10].

### 3.2. Finding the lower bound for the lowest eigenvalue of the generalized eigenvalue problem

In general case it is impossible to define the lower bound for the lowest eigenvalue of Eq. (21), because the lowest eigenvalue  $\epsilon_1(\rho)$  is depended on the parameter  $\rho$ . But, we can use the following algorithm to find the lower bound for the lowest eigenvalue  $\epsilon_1(\rho)$ :

**Step 1.** Calculate  $\mathbf{LDL}^T$  factorization of  $\mathbf{A}^p - \alpha \mathbf{B}^p$ .

**Step 2.** If some elements of the diagonal matrix  $\mathbf{D}$  are less than zero then put  $\alpha = \alpha - 1$  and go to **Step 3**, else go to **Step 5**.

**Step 3.** Calculate  $\mathbf{LDL}^T$  factorization of  $\mathbf{A}^p - \alpha \mathbf{B}^p$ .

**Step 4.** If some elements of the diagonal matrix  $\mathbf{D}$  are less than zero then put  $\alpha = \alpha - 1$  and go to **Step 3**, else put  $\alpha = \alpha - 0.5$  and go to **Step 8**.

**Step 5.** Put  $\alpha = \alpha + 1$  and calculate  $\mathbf{LDL}^T$  factorization of  $\mathbf{A}^p - \alpha \mathbf{B}^p$ .

**Step 6.** If all elements of the diagonal matrix  $\mathbf{D}$  are greater than zero then put  $\alpha = \alpha + 1$  and repeat **Step 5**.

**Step 7.** Put  $\alpha = \alpha - 1.5$ .

**Step 8.** End.

After using the above algorithm one should find the lower bound for the lowest eigenvalue, and always  $\epsilon_1(\rho) - \alpha \leq 1.5$ .

## 4. Description of the program

Fig. 1 presents a flow diagram for the ODPEVP program. The function of each subroutine is described in Section 5. The ODPEVP program is called from the main routine (supplied by a user) which sets dimensions of the arrays and is responsible for the input data. In the present code each array declarator is written in terms of the symbolic names of constants. These constants are defined in the following PARAMETER statement in the main routine:

PARAMETER (MTOT=800000,MITOT=500000,NMESH1=5,NROOT1=6)

where

- MTOT is the dimension of the working DOUBLE PRECISION array TOT.
- MITOT is the dimension of the working INTEGER array ITOT.

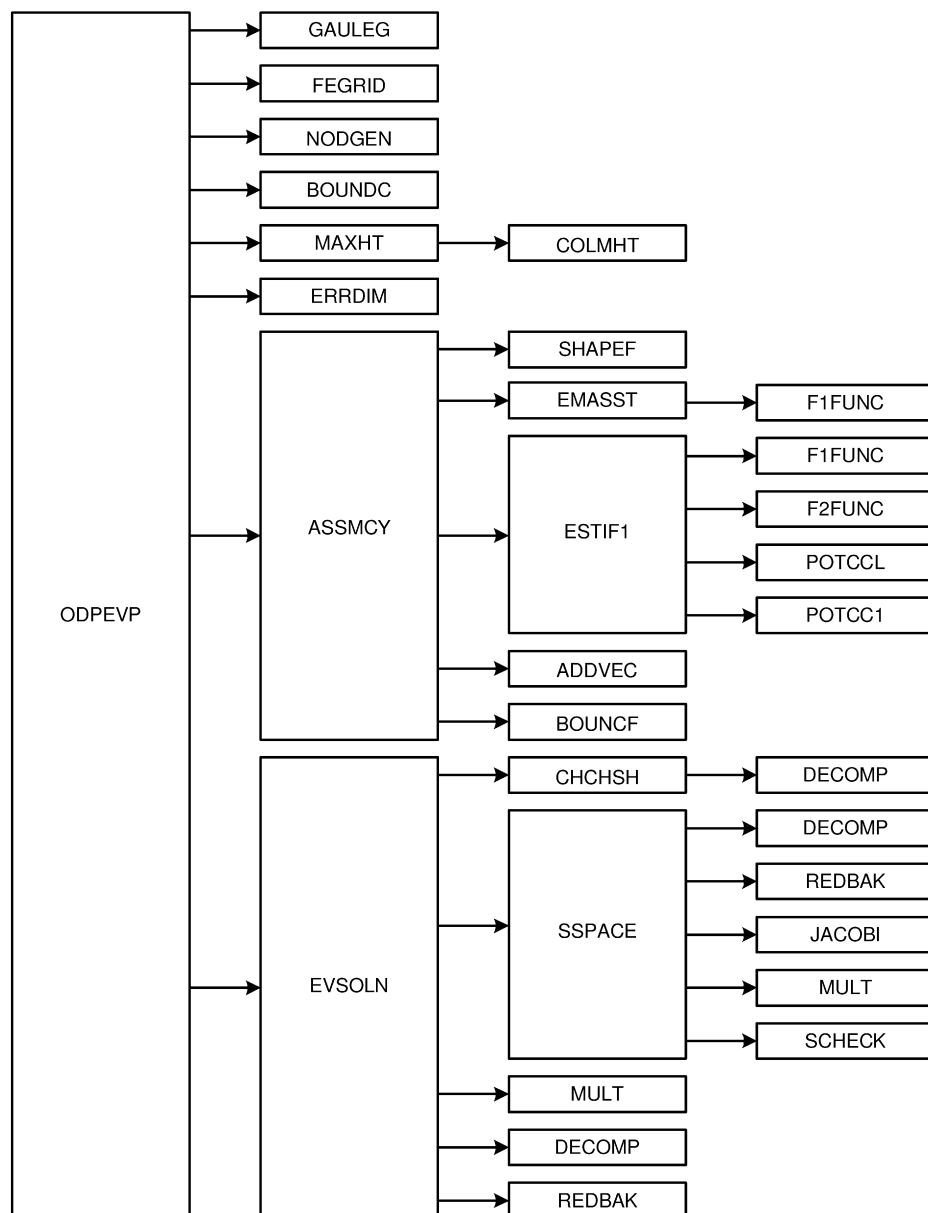


Fig. 1. Flow diagram of the ODPEVP program.

- NMESH1 is the dimension of the DOUBLE PRECISION array RMESH containing the information about the subdivision of the interval  $[z_{\min}, z_{\max}]$  on subintervals and the number of elements on each one of them. NMESH1 is always odd and  $\geq 3$ .
- NROOT1 is the number of eigenvalues and eigenvectors required, and also the dimension of the DOUBLE PRECISION arrays HH, QQ, EIGV.

A more concrete assignment of these dimensions is discussed below. In order to change the dimensions in the code, all one has to do is to modify the single PARAMETER statement defined above in the main program unit.

The calling sequence for the subroutine ODPEVP is:

```

CALL ODPEVP (TITLE, PARAM, HH, QQ, EIGV, NROOT, NPOL, RTOL, NITEM,
1          SHIFT, ICHK, IPRINT, IPRSTP, NMESH, RMESH, IBOUND,
2          FNOUT, IOUT, FMATR, IOUM, EVWFN, IOUF, TOT, ITOT, MTOT,
3          MITOT)
  
```

where the arguments have the following type and meaning:

- POTCCL is the name of the user-supplied DOUBLE PRECISION function which calculates the potential function  $U(\rho, z)$  ( $\text{PARAM} = \rho$ ,  $\text{RG} = z$ ) and should be written as follows:

```

      FUNCTION POTCCL (PARAM, RG)
C . . . . .
C .
C .   P R O G R A M
C .           TO CALCULATE THE PARAMETRIC POTENTIAL
C .           FUNCTION AT POINTS RG AND PARAM
C .
C .
C . . . . .
      IMPLICIT REAL*8 (A-H,O-Z)
      RETURN
      END

```

- POTCC1 is the name of the user-supplied DOUBLE PRECISION function which calculates first derivative of the potential function  $U(\rho, z)$  with respect to the parameter  $\rho$  (PARAM =  $\rho$ , RG =  $z$ ) and should be written as follows:

```

      FUNCTION POTCC1 (PARAM, RG)
C . . . . .
C .
C .   P R O G R A M
C .           TO CALCULATE FIRST DERIVATIVE OF PARAMETRIC
C .           POTENTIAL FUNCTION WITH RESPECT TO PARAMETER
C .           AT POINTS RG AND PARAM
C .
C .
C . . . . .
      IMPLICIT REAL*8 (A-H,O-Z)
      RETURN
      END

```

- F1FUNC is the name of the user-supplied DOUBLE PRECISION function which calculates the function  $f_1(z)$  (RG =  $z$ ) and should be written as follows:

```

      FUNCTION F1FUNC (RG)
C . . . . .
C .
C .   P R O G R A M
C .           TO CALCULATE FUNCTION F1 AT POINT RG
C .
C .
C . . . . .
      IMPLICIT REAL*8 (A-H,O-Z)
      RETURN
      END

```

- F2FUNC is the name of the user-supplied DOUBLE PRECISION function which calculates the function  $f_2(z)$  (RG =  $z$ ) and should be written as follows:

```

      FUNCTION F2FUNC (RG)
C . . . . .
C .
C .   P R O G R A M
C .           TO CALCULATE FUNCTION F2 AT POINT RG
C .
C .
C . . . . .
      IMPLICIT REAL*8 (A-H,O-Z)
      RETURN
      END

```

- BOUNCF is the name of the user-supplied subroutine which calculates the values  $\lambda_1(\rho)$ ,  $\lambda_2(\rho)$  and their first derivatives with respect to the parameter  $\rho$  (PARAM =  $\rho$ , DLMMN0 =  $\lambda_1(\rho)$ , DLMMX0 =  $\lambda_2(\rho)$ , DLMMN1 =  $\partial\lambda_1(\rho)/\partial\rho$ , DLMMX1 =  $\partial\lambda_2(\rho)/\partial\rho$ ) and should be written as follows:

```

      SUBROUTINE BOUNCF (PARAM, DLMMN0, DLMMX0, DLMMN1, DLMMX1)
C . . . . .
C .
C .   P R O G R A M
C .           TO CALCULATE DLMMN0, DLMMX0 AND THEIR
C .           FIRST DERIVATIVES WITH RESPECT TO PARAMETER
C .
C .
C . . . . .
      IMPLICIT REAL*8 (A-H,O-Z)
      RETURN
      END

```

The parameters PARAM, RG have the same meaning as described below and should not be changed by subroutine BOUNCF, and functions POTCCL, POTCC1, F1FUNC, F2FUNC.

### Input data

TITLE	CHARACTER	title of the run to be printed on the output listing. The title should be no longer than 70 characters.
PARAM	REAL*8	value of the parameter $\rho$ .
HH	REAL*8	array HH of dimension NROOT $\times$ NROOT containing values of the potential matrix $\mathbf{H}(\rho)$ .
QQ	REAL*8	array QQ of dimension NROOT $\times$ NROOT containing values of the potential matrix $\mathbf{Q}(\rho)$ .
EIGV	REAL*8	array EIGV of dimension NROOT containing values of the calculated eigenvalues $\epsilon_j(\rho)$ .
NROOT	INTEGER	number of eigenvalues and eigenvectors required.
NPOL	INTEGER	order of finite-element shape functions (interpolating Lagrange polynomials). Usually set to 6.
RTOL	REAL*8	convergence tolerance on eigenvalues (1.D-06 or smaller).
NITEM	INTEGER	maximum number of iterations permitted (usually set to 16).
SHIFT	REAL*8	contains the lower bound of lowest eigenvalue.
ICLK	INTEGER	key parameter. If ICLK $\neq 0$ the SHIFT is determined automatically by the program with help of the algorithm 3.2.
IPRINT	INTEGER	level of print: = 0 – minimal level of print. The initial data, short information about the numerical scheme parameters, main flags and keys, and eigenvalues calculated are printed out; = 1 – eigenfunctions calculated are printed out with step IPRSTP additionally; = 2 – information about nodal point distribution is printed out; = 3 – global matrices $\mathbf{A}^p$ and $\mathbf{B}^p$ are printed out additionally; = 4 – the highest level of print. The local stiffness and mass matrices together with all current information about the course of the subspace iteration method solution of the generalized eigenvalue problem are printed out.
IPRSTP	INTEGER	step with which eigenfunctions are printed out.
NMESH	INTEGER	dimension of array RMESH. NMESH always should be odd and $\geq 3$ .
RMESH	REAL*8	array RMESH contains information about subdivision of interval $[z_{\min}, z_{\max}]$ of variable $z$ on subintervals. The whole interval $[z_{\min}, z_{\max}]$ is divided as follows: $\text{RMESH}(1) = z_{\min}$ , $\text{RMESH}(\text{NMESH}) = z_{\max}$ , and the values of $\text{RMESH}(l)$ set the number of elements for each subinterval $[\text{RMESH}(l-1), \text{RMESH}(l+1)]$ , where $l = 2, 4, \dots, \text{NMESH} - 1$ .
IBOUND	INTEGER	parameter defining the type of boundary conditions set in the boundary points $z = z_{\min}$ and $z = z_{\max}$ : = 1 – the Dirichlet–Dirichlet boundary conditions: $\psi(z_{\min}; \rho) = 0$ , $\psi(z_{\max}; \rho) = 0$ ; = 2 – the Dirichlet–Neumann boundary conditions: $\psi(z_{\min}; \rho) = 0$ , $\lim_{z \rightarrow z_{\max}} f_2(z) \frac{d\psi(z; \rho)}{dz} = 0$ ; = 3 – the Neumann–Dirichlet boundary conditions: $\lim_{z \rightarrow z_{\min}} f_2(z) \frac{d\psi(z; \rho)}{dz} = 0$ , $\psi(z_{\max}; \rho) = 0$ ; = 4 – the Neumann–Neumann boundary conditions: $\lim_{z \rightarrow z_{\min}} f_2(z) \frac{d\psi(z; \rho)}{dz} = 0$ , $\lim_{z \rightarrow z_{\max}} f_2(z) \frac{d\psi(z; \rho)}{dz} = 0$ . If $\mu_1 \lambda_1(\rho) \neq 0$ the value of IBOUND equals 3 or 4. If $\mu_2 \lambda_2(\rho) \neq 0$ the value of IBOUND equals 2 or 4.
FNOUT	CHARACTER	name of the output file (up to 55 characters) for printing out the results of the calculation. It is system specific and may include a complete path to the file location.
IOUT	INTEGER	number of the output logical device for printing out the results of the calculation (usually set to 7).
FMATR	CHARACTER	name of the scratch file (up to 55 characters) for storing calculated matrices.
IOUM	INTEGER	number of the logical device for storing calculated matrices.
EVWFN	CHARACTER	name of the output file (up to 55 characters) for storing the results of the calculation, namely, the eigenvalues and eigenfunctions, their first derivatives with respect to the parameter, and finite-element grid points. It is used only if IOUF $> 0$ .
IOUF	INTEGER	number of the logical device for storing data into file EVWFN.
TOT	REAL*8	working vector of the DOUBLE PRECISION type.
ITOT	INTEGER	working vector of the INTEGER type.
MTOT	INTEGER	dimension of the DOUBLE PRECISION working array ITOT. The last address ILAST of array TOT is calculated and then compared with the given value of MTOT. If $\text{ILAST} > \text{MTOT}$ the message about an error is printed and the execution of the program is aborted. In the last case, in order to carry out the required calculation it is necessary to increase the dimension MTOT of array TOT to the quantity ILAST taken from the message.
MITOT	INTEGER	dimension of the INTEGER working array ITOT. The last address ILAST of array ITOT is calculated and then compared with the given value of MITOT. If $\text{ILAST} > \text{MITOT}$ the message about an error is printed and the execution of the program is aborted. In the last case, in order to carry out the required calculation it is necessary to increase the dimension MITOT of array ITOT to the quantity ILAST taken from the message.

### Output data

The results of the calculation of eigenvalues and eigenfunctions are written using unformatted segmented records into file EVWFN, according to the following operator:

```

WRITE(IOUF) NN, NROOT, NGRID, (EIGV(I), I=1, NROOT),
1      (BUP(I), I=1, NROOT),
2      (XGRID(I), I=1, NGRID),
3      ((R(I, J), I=1, NN), J=1, NROOT),
4      ((DR(I, J), I=1, NN), J=1, NROOT)

```

In the above, parameters presented in the WRITE statement have the following meaning:

- NGRID is the number of finite-element grid points.
- NN is the number of nodes of eigenfunctions.
- NROOT is the number of eigenvalues.
- Arrays EIGV and BUP contain the eigenvalues calculated and their first derivative with respect to the parameter  $\rho$ .
- Array XGRID contains the values of the finite-element grid points.
- Arrays R and DR contain NROOT eigenfunctions each per NN elements and their first derivative with respect to parameter  $\rho$ .

## 5. Description of subprogram units

A flow diagram for the ODPEVP program is presented in Fig. 1. The function of each subroutine is briefly described below. Additional details may be found in COMMENT cards within the program.

- Subroutine ADDVEC [8] assembles the element stiffness and mass matrices and the first derivative of stiffness matrix with respect to parameter  $\rho$  into the corresponding global vector using a compact storage form.
- Subroutine ASSMCY controls the calculation of element stiffness and mass matrices, the first derivative of stiffness matrix with respect to parameter  $\rho$ , and assembles them into the corresponding global matrices.
- User-supplied subroutine BOUNCF calculates  $\lambda_1(\rho)$ ,  $\lambda_2(\rho)$  and their first derivatives with respect to the parameter  $\rho$ .
- Subroutine BOUNDNC [8] sets the Dirichlet or Neumann boundary conditions.
- Subroutine COLMHT [8] calculates column heights in banded matrix.
- Subroutine CHCHSH calculates the lower bound of lowest eigenvalue.
- Subroutine DECOMP [11] calculates  $\mathbf{LDL}^T$  factorization of stiffness matrix. This factorization is used in subroutine REDBAK [11] to reduce and back-substitute the iteration vectors.
- Subroutine EMASST calculates an element mass matrix.
- Subroutine ERRDIM prints error messages when high-speed storage requested by a user is exceeded and stops the execution of program ODPEVP.
- Subroutine ESTIF1 calculates the local on element stiffness matrix and its first derivative with respect to the parameter  $\rho$ .
- Subroutine EVSOLN prepares all input data for the SSPACE program, prints out the calculated eigenfunctions and first derivative with respect to the parameter  $\rho$ , and writes them into the file EVWFN, if necessary. Also calculates the potential matrices  $\mathbf{H}(\rho)$  and  $\mathbf{Q}(\rho)$ .
- User-supplied DOUBLE PRECISION function F1FUNC calculates the function  $f_1(z)$ .
- User-supplied DOUBLE PRECISION function F2FUNC calculates the function  $f_2(z)$ .
- Subroutine FEGRID [8] calculates nodal points for the finite-element grid.
- Subroutine GAULEG [17] calculates nodes and weights of the Gauss–Legendre quadrature.
- Subroutine GAUSSJ [17] calculates linear equation solution by the Gauss–Jordan matrix inversion method.
- Subroutine JACOBI [11] solves the generalized eigenproblem in subspace using the generalized Jacobi iteration.
- Subroutine MAXHT [8] calculates addresses of diagonal elements in banded matrix.
- Subroutine MULT [11] evaluates a product of the two vectors stored in compact form.
- Subroutine NODGEN [8] generates a nodal point distribution for the finite-element grid.
- User-supplied DOUBLE PRECISION function POTCCL calculates the potential function  $U(\rho, z)$ .
- User-supplied DOUBLE PRECISION function POTCC1 calculates the first derivative of potential function  $U(\rho, z)$  with respect to parameter  $\rho$ .
- Subroutine SCHECK [11] evaluates shift for Sturm sequence check (called only if SHIFT = 0).
- Subroutine SHAPEF [8] calculates shape functions of the given order and their derivatives with respect to the master element coordinate  $\eta$  at a specified value of  $z$ .
- Subroutine SSPACE [11] finds the smallest eigenvalues and the corresponding eigenvectors in the generalized eigenproblem using the subspace iteration method [11]. We have added to this program the possibility of finding the eigensolutions closest to the energy spectrum shift given and also the possibility of using the previously calculated eigenvectors as the starting vectors for inverse iterations. The list of arguments for this program is adequately commented in the routine; so, the interested reader is referred to the program listing for further details. Warning messages will be issued if the requested accuracy RTOL is not obtained after NITEM iterations or if the stiffness matrix  $\mathbf{A}^p$  is not positively defined.

## 6. Test deck

### 6.1. Test I

We consider a boundary problem for the angular oblate spheroidal functions [18] with respect to a variable  $-1 < \eta = \cos \theta < 1$  in the form [1,14]:

$$-\frac{d}{d\eta}(1-\eta^2)\frac{d\Phi_j(\eta;r)}{d\eta} + \left(\frac{m^2}{1-\eta^2} + \frac{\gamma^2 r^4}{4}(1-\eta^2)\right)\Phi_j(\eta;r) = \lambda_j(r)\Phi_j(\eta;r), \quad (34)$$

with boundary conditions

$$\begin{aligned} \lim_{\eta \rightarrow \pm 1} (1-\eta^2)\frac{d\Phi_j(\eta;r)}{d\eta} &= 0, \quad \text{if } m = 0, \quad \text{and} \\ \Phi_j(\pm 1;r) &= 0, \quad \text{if } m \neq 0, \end{aligned} \quad (35)$$

where  $m = 0, \pm 1, \dots$  is the magnetic quantum number,  $\gamma = B/B_0$ ,  $B_0 \cong 2.35 \times 10^5$  T is a dimensionless parameter which determines the field strength  $B$ . The boundary problem (34), (35) has even and odd eigenfunctions.

We test only the even eigenfunctions with boundary conditions in variable  $0 \leq \eta \leq 1$  at  $m = 0$  and  $\gamma = 1$

$$\left. \frac{d\Phi_j(\eta; r)}{d\eta} \right|_{\eta=0} = 0, \quad \lim_{\eta \rightarrow 1} (1 - \eta^2) \frac{d\Phi_j(\eta; r)}{d\eta} = 0. \quad (36)$$

Here  $\lambda_1(\rho) = \lambda_2(\rho) = 0$ .

The following values of numerical parameters and characters have been used in the test run via the supplied input file MAGNET.INP

```
&PARAMS TITLE=' PARAMETRIC DIFFERENTIAL EQUATION I ',
PARAM=11.51962D0, NROOT=6, NPOL=4, RTOL=1.D-13, NITEM=100,
SHIFT=-10.D0, ICHK=1, IPRINT=2, IPRSTP=400, IBOUND=4,
NMESH=3, RMESH=0.D0, 400.D0, 1.D0,
FNOUT=' MAGNET.LPR ', IOUT=7, FMATR=' MAGNET.MAT ', IOUM=11,
EVWFN=' MAGNET.WFN ', IOUF=0
&END
```

**Remark.** To compare calculated potential matrix elements  $\mathbf{H}(\rho)$ ,  $\mathbf{Q}(\rho)$  with the results in [14] the user should recalculate diagonal matrix elements  $H_{ii}(\rho)$  by the formula

$$H_{ii}(\rho) = H_{ii}(\rho) + \frac{\epsilon_i(\rho)}{\rho^2} - \frac{2}{\rho}. \quad (37)$$

## 6.2. Test II

We consider a boundary problem

$$-\frac{\partial^2 \psi_j(\theta; \rho)}{\partial \theta^2} = \epsilon_j(\rho) \psi_j(\theta; \rho), \quad (38)$$

with boundary conditions in angular variable  $-\pi/6 \leq \theta \leq \pi/6$

$$\frac{\partial \psi_j(\theta; \rho)}{\partial \theta} - \rho c \bar{\kappa} \psi_j(\theta; \rho) = 0, \quad \theta = -\frac{\pi}{6}, \quad (39)$$

$$\frac{\partial \psi_j(\theta; \rho)}{\partial \theta} + \rho c \bar{\kappa} \psi_j(\theta; \rho) = 0, \quad \theta = \frac{\pi}{6}. \quad (40)$$

The boundary problem (38)–(40) has exact even and odd eigenfunctions, and also analytical potential matrix elements  $\mathbf{H}(\rho)$ ,  $\mathbf{Q}(\rho)$  [8,12,13].

We test only even eigenfunctions with the boundary conditions in angular variable  $-\pi/6 \leq \theta \leq 0$  at  $c = -1$  and  $\bar{\kappa} = \pi/6$

$$\frac{\partial \psi_j(\theta; \rho)}{\partial \theta} - \rho c \bar{\kappa} \psi_j(\theta; \rho) = 0, \quad \theta = -\frac{\pi}{6}, \quad (41)$$

$$\frac{\partial \psi_j(\theta; \rho)}{\partial \theta} = 0, \quad \theta = 0. \quad (42)$$

Here  $\lambda_1(\rho) = -\rho c \bar{\kappa}$  and  $\lambda_2(\rho) = 0$ .

The following values of numerical parameters and characters have been used in the test run via the supplied input file 3DELTA.INP

```
&PARAMS TITLE=' PARAMETRIC DIFFERENTIAL EQUATION II ',
PARAM=2.00469D0, NROOT=6, NPOL=4, RTOL=1.D-13, NITEM=100,
SHIFT=-10.D0, ICHK=1, IPRINT=2, IPRSTP=400, IBOUND=4,
NMESH=3, RMESH=-0.5235987755982989D0, 800.D0, 0.D0,
FNOUT=' 3DELTA.LPR ', IOUT=8, FMATR=' 3DELTA.MAT ', IOUM=12,
EVWFN=' 3DELTA.WFN ', IOUF=0
&END
```

**Remark.** To compare calculated potential matrix elements  $\mathbf{H}(\rho)$ ,  $\mathbf{Q}(\rho)$  with results in [8] the user should recalculate diagonal matrix elements  $H_{ii}(\rho)$  by the formula

$$H_{ii}(\rho) = H_{ii}(\rho) + \frac{\epsilon_i(\rho)}{\rho^2}. \quad (43)$$

## 6.3. Test III

Consider the following eigenvalue problem of hydrogen atom on a three-dimensional sphere

$$\left( -\frac{1}{\sin^2(\alpha)} \frac{d}{d\alpha} \sin^2(\alpha) \frac{d}{d\alpha} - 2r \cot(\alpha) \right) \psi(\alpha; r) = E(r) \psi(\alpha; r), \quad (44)$$

$$\lim_{\alpha \rightarrow 0} \sin^2(\alpha) \frac{d\psi(\alpha; r)}{d\alpha} = 0, \quad \lim_{\alpha \rightarrow \pi} \sin^2(\alpha) \frac{d\psi(\alpha; r)}{d\alpha} = 0. \quad (45)$$

Problem (44) has an analytical solution

$$E_n(r) = -r^2 \left( \frac{1}{n^2} - \frac{n^2 - 1}{r^2} \right), \quad n = 1, 2, \dots \quad (46)$$

with eigenfunctions  $\psi_n(\alpha; r)$  which are the radial functions of a hydrogen atom on a three-dimensional sphere [15,16]

$$\begin{aligned} \psi_n(\alpha, r) &= C_n(r) \operatorname{Re} \left\{ \exp(-i\alpha(n-1-i\sigma)) {}_2F_1(-n+1, 1+i\sigma, 2, 1-\exp(2i\alpha)) \right\}, \\ C_n(r) &= \frac{2\sqrt{\sigma(n^2+\sigma^2)}}{\sqrt{1-\exp(-2\pi\sigma)}}, \quad \sigma = \frac{r}{n}, \end{aligned} \quad (47)$$

where  ${}_2F_1$  is a full hypergeometric function [18].

The following values of numerical parameters and characters have been used in the test run via the supplied input file HYDRON.INP

```
&PARAMS TITLE='    PARAMETRIC DIFFERENTIAL EQUATION III ',
PARAM=8.D0,NROOT=6,NPOL=4,RTOL=1.D-13,NITEM=100,
SHIFT=-10.D0,ICLK=1,IPRINT=2,IPRSTP=400,IBOUND=4,
NMESH=3,RMESH=0.D0,400.D0,3.141592653589793D0,
FNOUT='ABRASH.LPR',IOUT=7,FMATR='ABRASH.MAT',IOUM=11,
EVWFN='ABRASH.WFN',IOUF=0

&END
```

## Acknowledgements

The authors thank Profs. V.P. Gerdt, V.V. Pupyshev, I.V. Puzynin and S.L. Yakovlev for useful discussions. O.C., A.A.G. and S.I.V. acknowledge financial support from the Bulgarian Foundation for Scientific Investigations, RFBR Grants Nos. 08-01-00604 and 07-01-00660, and the theme 09-6-1060-2005/2010 “Mathematical support of experimental and theoretical studies conducted by JINR”.

## Appendix A. Test run output

```
PROBLEM:    PARAMETRIC DIFFERENTIAL EQUATION I
*****

      C O N T R O L   I N F O R M A T I O N
      -----

NUMBER OF ENERGY LEVELS REQUIRED. . . . . (NROOT ) =      6
NUMBER OF FINITE ELEMENTS . . . . . (NELEM ) =     400
NUMBER OF GRID POINTS . . . . . (NGRID ) =    1601
ORDER OF SHAPE FUNCTIONS . . . . . (NPOL ) =      4
ORDER OF GAUSS-LEGENDRE QUADRATURE . . . (NGQ ) =      5
NUMBER OF SUBSPACE ITERATION VECTORS. . . (NC ) =     12
BOUNDARY CONDITION CODE . . . . . (IBOUND) =      4
SHIFT OF DOUBLE ENERGY SPECTRUM . . . . (SHIFT ) =   -10.0000
CONVERGENCE TOLERANCE . . . . . (RTOL ) =   0.100000E-12
VALUE OF PARAMETER. . . . . (PARAM ) =    11.5196

SUBDIVISION OF RHO-REGION ON THE FINITE-ELEMENT GROUPS:
*****

NO OF  NUMBER OF  BEGIN OF  LENGTH OF  GRID    END OF
GROUP  ELEMENTS   INTERVAL  ELEMENT   STEP    INTERVAL
-----
  1      400      0.00000   0.00250   0.000625  1.000

LAST ADDRESS OF ARRAY ITOT USED =      8807

      T O T A L   S Y S T E M   D A T A
      -----

TOTAL NUMBER OF ALGEBRAIC EQUATIONS. . . . (NN ) =    1601
TOTAL NUMBER OF MATRIX ELEMENTS. . . . . (NWK ) =    5601
MAXIMUM HALF BANDWIDTH . . . . . (MK ) =      5
MEAN    HALF BANDWIDTH . . . . . (MMK ) =      3

LAST ADDRESS OF ARRAY TOT USED =    12999
```

LAST ADDRESS OF ARRAY TOT USED = 45256

THERE ARE 0 ROOTS LOWER THEN SHIFT  
CONVERGENCE REACHED FOR RTOL 0.1000E-12  
I T E R A T I O N N U M B E R 27  
RELATIVE TOLERANCE REACHED ON EIGENVALUES  
0.1686E-17 0.1446E-15 0.0000E+00 0.0000E+00 0.0000E+00 0.4431E-13

\*\*\*\*\*

R O O T	N U M B E R	E I G E N V A L U E	D E R I V A T I V E
1		131.6978190423784	23.03991454532688
2		393.0465776953899	69.12818558702216
3		650.2504800146933	115.2433376999127
4		903.2033485769872	161.4069643663601
5		1151.789459036675	207.6445825421709
6		1395.882038049846	253.9865811918269

\*\*\*\*\*

R	E I G E N F U N C T I O N
0.0000	-.22274964D-23 0.89303396D-24 0.22239605D-22 -.11106591D-19 0.30880481D-16 -.11249627D-13
0.2500	0.44557304D-20 -.70037339D-18 0.52788096D-16 -.25638041D-14 0.90742591D-13 -.26726604D-11
0.5000	0.59893375D-13 -.51378822D-11 0.21053777D-09 -.54780510D-08 0.10146586D-06 -.14226801D-05
0.7500	0.82047136D-06 -.29630640D-04 0.49284800D-03 -.49838295D-02 0.34023245D-01 -.16430949D+00
1.0000	0.11475799D+02 0.11386247D+02 0.11293729D+02 0.11197966D+02 0.11098636D+02 0.10995357D+02

\*\*\*\*\*

R	I T S D E R I V A T I V E
0.0000	0.79313330D-24 0.16717921D-23 -.25982994D-21 0.24924824D-19 -.14107815D-16 0.49670201D-14
0.2500	-.38454263D-19 0.58658153D-17 -.43241464D-15 0.20512551D-13 -.70340668D-12 0.18688340D-10
0.5000	-.33974850D-12 0.28224816D-10 -.11170940D-08 0.27985656D-07 -.49719792D-06 0.66503536D-05
0.7500	-.22911857D-05 0.77342703D-04 -.11888254D-02 0.10935688D-01 -.66359810D-01 0.27458239D+00
1.0000	0.10038777D+01 0.10121499D+01 0.10212586D+01 0.10313304D+01 0.10425178D+01 0.10550076D+01

\*\*\*\*\*

P O T E N T I A L M A T R I C E S H(I,J) AND Q(I,J):

H-MATRIX AT THE PARAMETER = 11.51962

0.7653D-02	0.1209D-03	-.1543D-01	-.3686D-03	-.9037D-05	-.2528D-06
0.1209D-03	0.3876D-01	0.6268D-03	-.4704D-01	-.1537D-02	-.4837D-04
-.1543D-01	0.6268D-03	0.1023D+00	0.1953D-02	-.9569D-01	-.4014D-02
-.3686D-03	-.4704D-01	0.1953D-02	0.2000D+00	0.4612D-02	-.1623D+00
-.9037D-05	-.1537D-02	-.9569D-01	0.4612D-02	0.3339D+00	0.9217D-02
-.2528D-06	-.4837D-04	-.4014D-02	-.1623D+00	0.9217D-02	0.5064D+00

Q-MATRIX AT THE PARAMETER = 11.51962

-.1605D-16	0.8748D-01	0.6854D-03	0.8256D-05	0.1360D-06	0.2879D-08
-.8748D-01	-.4770D-16	0.1764D+00	0.2124D-02	0.3501D-04	0.7408D-06
-.6854D-03	-.1764D+00	0.2472D-16	0.2668D+00	0.4396D-02	0.9302D-04
-.8256D-05	-.2124D-02	-.2668D+00	-.9237D-16	0.3589D+00	0.7592D-02
-.1360D-06	-.3501D-04	-.4396D-02	-.3589D+00	-.6072D-17	0.4528D+00
-.2879D-08	-.7408D-06	-.9302D-04	-.7592D-02	-.4528D+00	0.6072D-17

PROBLEM: PARAMETRIC DIFFERENTIAL EQUATION II  
\*\*\*\*\*



# CONTROL INFORMATION

```

NUMBER OF ENERGY LEVELS REQUIRED. . . . (NROOT ) =      6
NUMBER OF FINITE ELEMENTS . . . . . (NELEM ) =     800
NUMBER OF GRID POINTS . . . . . (NGRID ) =    3201
ORDER OF SHAPE FUNCTIONS . . . . . (NPOL ) =      4
ORDER OF GAUSS-LEGENDRE QUADRATURE . . . (NGQ ) =      5
NUMBER OF SUBSPACE ITERATION VECTORS. . . (NC ) =     12
BOUNDARY CONDITION CODE . . . . . (IBOUND) =      4
SHIFT OF DOUBLE ENERGY SPECTRUM . . . . (SHIFT ) =   -10.0000
CONVERGENCE TOLERANCE . . . . . (RTOL ) =    0.100000E-12
VALUE OF PARAMETER. . . . . (PARAM ) =    2.00469

```

## SUBDIVISION OF RHO-REGION ON THE FINITE-ELEMENT GROUPS:

\*\*\*\*\*

NO OF GROUP	NUMBER OF ELEMENTS	BEGIN OF INTERVAL	LENGTH OF ELEMENT	GRID STEP	END OF INTERVAL
1	800	-0.52360	0.00065	0.000164	0.000

LAST ADDRESS OF ARRAY ITOT USED = 17607

# TOTAL SYSTEM DATA

```

TOTAL NUMBER OF ALGEBRAIC EQUATIONS. . . . (NN ) =    3201
TOTAL NUMBER OF MATRIX ELEMENTS. . . . . (NWK ) =   11201
MAXIMUM HALF BANDWIDTH . . . . . (MK ) =      5
MEAN    HALF BANDWIDTH . . . . . (MMK) =      3

```

LAST ADDRESS OF ARRAY TOT USED = 25799

LAST ADDRESS OF ARRAY TOT USED = 90056

THERE ARE 0 ROOTS LOWER THEN SHIFT  
CONVERGENCE REACHED FOR RTOL 0.1000E-12  
ITERATION NUMBER 15  
RELATIVE TOLERANCE REACHED ON EIGENVALUES  
0.0000E+00 0.5566E-14 0.3655E-14 0.3198E-14 0.9938E-15 0.5152E-13

\*\*\*\*\*

ROOT	NUMBER	EIGENVALUE	DERIVATIVE
1		-2.431524951096452	-1.458429440168202
2		31.91272127947840	-2.058234364971463
3		139.9725288836021	-2.012985124428196
4		319.9826816386258	-2.005659513377144
5		571.9861743548753	-2.003162124194071
6		895.9877805734652	-2.002017513522787

\*\*\*\*\*

## R EIGENFUNCTION

-0.5236	0.16689503D+01	-.19826593D+01	0.19607443D+01	-.19571733D+01	0.19559545D+01	-.19553956D+01
-0.4581	0.15627942D+01	-.17155517D+01	0.12800672D+01	-.65642720D+00	-.75119469D-01	0.80383895D+00
-0.3927	0.14729301D+01	-.12165809D+01	-.13054335D+00	0.14458929D+01	-.19567782D+01	0.13466777D+01
-0.3272	0.13984212D+01	-.55318460D+00	-.14667141D+01	0.17826097D+01	0.53663216D-01	-.18236288D+01
-0.2618	0.13384908D+01	0.18497661D+00	-.19665197D+01	-.57447142D-01	0.19573666D+01	0.34289891D-01
-0.1963	0.12925140D+01	0.89813754D+00	-.13449558D+01	-.18273543D+01	-.32200511D-01	0.17976623D+01

```
-0.1309 0.12600115D+01 0.14899118D+01 0.43542857D-01 -.13658495D+01 -.19577197D+01 -.13955940D+01
-0.0654 0.12406446D+01 0.18803190D+01 0.14072121D+01 0.76351636D+00 0.10733934D-01 -.74082992D+00
0.0000 0.12342113D+01 0.20165941D+01 0.19684461D+01 0.19605399D+01 0.19578374D+01 0.19565974D+01
```

\*\*\*\*\*

# R I T S D E R I V A T I V E

-----

```
-0.5236 0.16035732D+00 0.13094179D-02 -.60773212D-03 0.28686209D-03 -.16445461D-03 0.10614584D-03
-0.4581 0.97967070D-01 0.59195008D-01 -.53622333D-01 0.46414585D-01 -.37602731D-01 0.27780685D-01
-0.3927 0.46378558D-01 0.94296735D-01 -.66092299D-01 0.31427873D-01 -.65965486D-03 -.17886629D-01
-0.3272 0.44915769D-02 0.10617026D+00 -.41890927D-01 -.12163048D-01 0.26868776D-01 -.87796247D-02
-0.2618 -.28596841D-01 0.98927509D-01 -.52229874D-02 -.28852708D-01 0.12484460D-02 0.17146546D-01
-0.1963 -.53606702D-01 0.79908343D-01 0.19110488D-01 -.10698146D-01 -.16125139D-01 -.40659005D-02
-0.1309 -.71086469D-01 0.57828797D-01 0.22073763D-01 0.81688981D-02 -.16017773D-02 -.67842197D-02
-0.0654 -.81421778D-01 0.40772504D-01 0.12788962D-01 0.78289098D-02 0.53756919D-02 0.35489858D-02
0.0000 -.84841577D-01 0.34408945D-01 0.71690953D-02 0.30895655D-02 0.17195639D-02 0.10951726D-02
```

\*\*\*\*\*

# P O T E N T I A L M A T R I C E S H(I,J) A N D Q(I,J):

H-MATRIX AT THE PARAMETER = 2.00469

```
0.2735D-02 -.2851D-03 -.8665D-03 0.4535D-03 -.2682D-03 0.1755D-03
-.2851D-03 0.2976D-02 -.7163D-03 0.1031D-03 -.3044D-04 0.1246D-04
-.8665D-03 -.7163D-03 0.6601D-03 -.2510D-03 0.4426D-04 -.1478D-04
0.4535D-03 0.1031D-03 -.2510D-03 0.2870D-03 -.1270D-03 0.2453D-04
-.2682D-03 -.3044D-04 0.4426D-04 -.1270D-03 0.1602D-03 -.7659D-04
0.1755D-03 0.1246D-04 -.1478D-04 0.2453D-04 -.7659D-04 0.1022D-03
```

Q-MATRIX AT THE PARAMETER = 2.00469

```
-.3050D-15 -.5045D-01 0.1203D-01 -.5305D-02 0.2976D-02 -.1902D-02
0.5045D-01 0.8823D-17 -.1884D-01 0.7053D-02 -.3760D-02 0.2349D-02
-.1203D-01 0.1884D-01 0.3037D-17 -.1116D-01 0.4648D-02 -.2655D-02
0.5305D-02 -.7053D-02 0.1116D-01 -.1669D-17 -.7954D-02 0.3479D-02
-.2976D-02 0.3760D-02 -.4648D-02 0.7954D-02 0.1934D-17 -.6181D-02
0.1902D-02 -.2349D-02 0.2655D-02 -.3479D-02 0.6181D-02 0.1714D-17
```

PROBLEM: PARAMETRIC DIFFERENTIAL EQUATION III  
\*\*\*\*\*

# C O N T R O L I N F O R M A T I O N

-----

```
NUMBER OF ENERGY LEVELS REQUIRED. . . . (NROOT ) = 6
NUMBER OF FINITE ELEMENTS . . . . . (NELEM ) = 400
NUMBER OF GRID POINTS . . . . . (NGRID ) = 1601
ORDER OF SHAPE FUNCTIONS . . . . . (NPOL ) = 4
ORDER OF GAUSS-LEGENDRE QUADRATURE . . . (NGQ ) = 5
NUMBER OF SUBSPACE ITERATION VECTORS. . . (NC ) = 12
BOUNDARY CONDITION CODE . . . . . (IBOUND) = 4
SHIFT OF DOUBLE ENERGY SPECTRUM . . . . (SHIFT ) = -10.0000
CONVERGENCE TOLERANCE . . . . . (RTOL ) = 0.100000E-12
VALUE OF PARAMETER. . . . . (PARAM ) = 8.00000
```

SUBDIVISION OF RHO-REGION ON THE FINITE-ELEMENT GROUPS:

\*\*\*\*\*

NO OF GROUP	NUMBER OF ELEMENTS	BEGIN OF INTERVAL	LENGTH OF ELEMENT	GRID STEP	END OF INTERVAL
1	400	0.00000	0.00785	0.001963	3.142

LAST ADDRESS OF ARRAY ITOT USED = 8807

# T O T A L S Y S T E M D A T A

-----

TOTAL NUMBER OF ALGEBRAIC EQUATIONS. . . . (NN ) = 1601  
 TOTAL NUMBER OF MATRIX ELEMENTS. . . . . (NWK) = 5601  
 MAXIMUM HALF BANDWIDTH . . . . . (MK ) = 5  
 MEAN HALF BANDWIDTH . . . . . (MMK) = 3

LAST ADDRESS OF ARRAY TOT USED = 12999

LAST ADDRESS OF ARRAY TOT USED = 45256

THERE ARE 0 ROOTS LOWER THEN SHIFT  
 CONVERGENCE REACHED FOR RTOL 0.1000E-12  
 I T E R A T I O N N U M B E R 26  
 RELATIVE TOLERANCE REACHED ON EIGENVALUES  
 0.0000E+00 0.3826E-14 0.3197E-13 0.2584E-14 0.2651E-14 0.1134E-12

\*\*\*\*\*

R O O T N U M B E R	E I G E N V A L U E	D E R I V A T I V E
-----	-----	-----
1	-63.99999999998519	-15.99999999999546
2	-12.99999999997674	-4.000000000007500
3	0.8888888889180890	-1.777777777775382
4	11.00000000002065	-0.9999999999255478
5	21.44000000001866	-0.6400000012114990
6	33.22222222224192	-0.4444445049532144

\*\*\*\*\*

## R E I G E N F U N C T I O N

- - - - -

0.0000	0.45607017D+02	-.17888544D+02	0.13109228D+02	-.12649133D+02	0.13281250D+02	-.14196050D+02
0.7854	0.85168492D-01	0.16398529D+01	0.59790078D-01	-.61977823D+00	0.95678611D+00	-.10614438D+01
1.5708	0.15904728D-03	0.13362332D+00	0.87617699D+00	0.72882478D+00	-.68083352D+00	-.32293554D+00
2.3562	0.29701169D-06	0.51038856D-02	0.13147060D+00	0.61601006D+00	0.12401978D+01	0.13223847D+01
3.1416	0.55465260D-09	0.62383477D-04	0.30146728D-02	0.23621531D-01	0.87143859D-01	0.21527760D+00

\*\*\*\*\*

## R I T S D E R I V A T I V E

- - - - -

0.0000	0.84636099D+01	-.29068884D+01	0.15425938D+01	-.11067645D+01	0.98392782D+00	-.96904963D+00
0.7854	-.51085871D-01	-.10418382D+00	0.40991318D+00	-.31989712D+00	0.16210582D+00	0.28957439D-01
1.5708	-.22031538D-03	-.66530808D-01	-.12005277D+00	0.23307684D+00	0.17446766D+00	-.27458383D+00
2.3562	-.64469879D-06	-.46731036D-02	-.65118968D-01	-.16500181D+00	-.11862643D+00	0.11616782D+00
3.1416	-.16395611D-08	-.87854421D-04	-.28022143D-02	-.16485488D-01	-.48298137D-01	-.98023856D-01

\*\*\*\*\*

## P O T E N T I A L M A T R I C E S H(I,J) A N D Q(I,J):

H-MATRIX AT THE PARAMETER = 8.00000

0.1136D-01	-.1016D-01	-.9803D-03	0.3020D-02	-.3697D-02	0.3875D-02
-.1016D-01	0.2972D-01	-.1652D-01	-.1065D-01	0.9211D-02	-.7225D-02
-.9803D-03	-.1652D-01	0.5213D-01	-.2163D-01	-.1704D-01	0.8337D-02
0.3020D-02	-.1065D-01	-.2163D-01	0.6997D-01	-.2275D-01	-.2062D-01
-.3697D-02	0.9211D-02	-.1704D-01	-.2275D-01	0.7850D-01	-.2038D-01
0.3875D-02	-.7225D-02	0.8337D-02	-.2062D-01	-.2038D-01	0.8015D-01

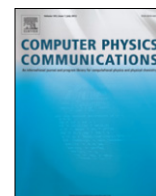
Q-MATRIX AT THE PARAMETER = 8.00000

0.1757D-15	-.7355D-01	0.3912D-01	-.3102D-01	0.2724D-01	-.2434D-01
0.7355D-01	0.4427D-16	-.1332D+00	0.5842D-01	-.3716D-01	0.2635D-01
-.3912D-01	0.1332D+00	0.1215D-15	-.1672D+00	0.5393D-01	-.3203D-01
0.3102D-01	-.5842D-01	0.1672D+00	0.7797D-16	-.1844D+00	0.4495D-01
-.2724D-01	0.3716D-01	-.5393D-01	0.1844D+00	-.4739D-16	-.1914D+00
0.2434D-01	-.2635D-01	0.3203D-01	-.4495D-01	0.1914D+00	-.2222D-16

## References

- [1] O. Chuluunbaatar, A.A. Gusev, V.L. Derbov, M.S. Kaschiev, L.A. Melnikov, V.V. Serov, S.I. Vinitsky, J. Phys. A 40 (2007) 11485–11524.
- [2] O. Chuluunbaatar, V.L. Derbov, A. Galtbayar, A.A. Gusev, M.S. Kaschiev, S.I. Vinitsky, T. Zhanlav, J. Phys. A 41 (2008) 295203-1–25.
- [3] P.M. Krassovitskiy, N.Zh. Takibaev, Bull. Russian Acad. Sci. Phys. 70 (2006) 815–818.
- [4] P.M. Krassovitskiy, S.I. Vinitsky, A.A. Gusev, O. Chuluunbaatar, Bull. Russian Acad. Sci. Phys. 73 (2009) 233–235.
- [5] Yu.N. Demkov, J.D. Meyer, Eur. Phys. J. B 42 (2004) 361–365.
- [6] M.G. Dimova, M.S. Kaschiev, S.I. Vinitsky, J. Phys. B 38 (2005) 2337–2352.
- [7] E.M. Kazaryan, A.A. Kostanyan, H.A. Sarkisyan, Physica E 28 (2005) 423–430.
- [8] O. Chuluunbaatar, A.A. Gusev, A.G. Abrashkevich, A. Amaya-Tapia, M.S. Kaschiev, S.Y. Larsen, S.I. Vinitsky, Comput. Phys. Comm. 177 (2007) 649–675.
- [9] O. Chuluunbaatar, A.A. Gusev, S.I. Vinitsky, A.G. Abrashkevich, Comput. Phys. Comm. 179 (2008) 685–693.
- [10] G. Strang, G.J. Fix, An Analysis of the Finite Element Method, Prentice-Hall, Englewood Cliffs, New York, 1973.
- [11] K.J. Bathe, Finite Element Procedures in Engineering Analysis, Prentice-Hall, Englewood Cliffs, New York, 1982.
- [12] O. Chuluunbaatar, A.A. Gusev, M.S. Kaschiev, V.A. Kaschieva, A. Amaya-Tapia, S.Y. Larsen, S.I. Vinitsky, J. Phys. B 39 (2006) 243–269.
- [13] Yu.A. Kuperin, P.B. Kurasov, Yu.B. Melnikov, S.P. Merkuriev, Ann. Phys. 205 (1991) 330–361.
- [14] O. Chuluunbaatar, A.A. Gusev, V.P. Gerdt, V.A. Rostovtsev, S.I. Vinitsky, A.G. Abrashkevich, M.S. Kaschiev, V.V. Serov, Comput. Phys. Comm. 178 (2008) 301–330.
- [15] A.G. Abrashkevich, M.S. Kaschiev, S.I. Vinitsky, J. Comp. Phys. 163 (2000) 328–348.
- [16] S.I. Vinitskii, L.G. Mardoyan, G.S. Poghosyan, A.N. Sissakian, T.A. Strizh, Phys. Atom. Nucl. 56 (1993) 321–327.
- [17] W.H. Press, S.A. Teukolsky, W.T. Vetterling, B.P. Flannery, Numerical Recipes: The Art of Scientific Computing, Cambridge University Press, Cambridge, 1986.
- [18] M. Abramowitz, I.A. Stegun, Handbook of Mathematical Functions, Dover, New York, 1965.





# POTHEA: A program for computing eigenvalues and eigenfunctions and their first derivatives with respect to the parameter of the parametric self-adjointed 2D elliptic partial differential equation<sup>☆</sup>



A.A. Gusev<sup>a</sup>, O. Chuluunbaatar<sup>a,b,\*</sup>, S.I. Vinitsky<sup>a</sup>, A.G. Abrashkevich<sup>c</sup>

<sup>a</sup> Joint Institute for Nuclear Research, Dubna, 141980 Moscow region, Russia

<sup>b</sup> National University of Mongolia, Ulaanbaatar, Mongolia

<sup>c</sup> IBM Toronto Lab, 8200 Warden Avenue, Markham, ON L6G 1C7, Canada

## ARTICLE INFO

### Article history:

Received 8 November 2013

Received in revised form

8 April 2014

Accepted 17 April 2014

Available online 2 May 2014

### Keywords:

Eigenvalue and multichannel scattering problems

Kantorovich method

Finite element method

Multichannel adiabatic approximation

Ordinary differential equations

High-order accuracy approximations

## ABSTRACT

A FORTRAN 77 program is presented for calculating with the given accuracy eigenvalues, surface eigenfunctions and their first derivatives with respect to a parameter of the parametric self-adjointed 2D elliptic partial differential equation with the Dirichlet and/or Neumann type boundary conditions on a finite two-dimensional region. The program calculates also potential matrix elements that are integrals of the products of the surface eigenfunctions and/or the first derivatives of the surface eigenfunctions with respect to a parameter. Eigenvalues and matrix elements computed by the POTHEA program can be used for solving the bound state and multi-channel scattering problems for a system of coupled second order ordinary differential equations with the help of the KANTBP program (Chuluunbaatar et al., 2007). Benchmark calculations of eigenvalues and eigenfunctions of the ground and first excited states of a Helium atom in the framework of a coupled-channel hyperspherical adiabatic approach are presented. As a test desk, the program is applied to the calculation of the eigensolutions of a 2D boundary value problem, their first derivatives with respect to a parameter and potential matrix elements used in the benchmark calculations.

### Program Summary

*Program title:* POTHEA

*Catalogue identifier:* AESX\_v1\_0

*Program summary URL:* [http://cpc.cs.qub.ac.uk/summaries/AESX\\_v1\\_0.html](http://cpc.cs.qub.ac.uk/summaries/AESX_v1_0.html)

*Program obtainable from:*

*Licensing provisions:* Standard CPC licence, <http://cpc.cs.qub.ac.uk/licence/licence.html>

*No. of bits in distributed program, including test data, etc.:* 36 929

*No. of lines in distributed program, including test data, etc.:* 3 756

*Distribution format:* tar.gz

*Programming language:* FORTRAN 77

*Computer:* Personal computer

*Operating system:* Unix/Linux, Windows

*RAM:* depends on

- (a) the number of differential equations,
- (b) the number and order of finite elements, and
- (b) the number of eigensolutions required.

<sup>☆</sup> This paper and its associated computer program are available via the Computer Physics Communication homepage on ScienceDirect (<http://www.sciencedirect.com/science/journal/00104655>).

\* Corresponding author at: Joint Institute for Nuclear Research, Dubna, 141980 Moscow region, Russia. Tel.: +7 4962162529; fax: +7 4962165084.

E-mail addresses: [gooseff@jinr.ru](mailto:gooseff@jinr.ru) (A.A. Gusev), [chuka@jinr.ru](mailto:chuka@jinr.ru) (O. Chuluunbaatar), [vinitky@theor.jinr.ru](mailto:vinitky@theor.jinr.ru) (S.I. Vinitsky), [aabrashk@ca.ibm.com](mailto:aabrashk@ca.ibm.com) (A.G. Abrashkevich).

*Classification:* 2.7

*External routine:* SSPACE [1], GAULEG [2]

*Nature of problem:* Solutions of boundary value problems (BVPs) for the elliptic partial differential equations (PDEs) of the Schrödinger type find wide application in molecular, atomic and nuclear physics, for example, in three-dimensional tunneling of a diatomic molecule incident upon a potential barrier, fission model of collision of heavy ions, fragmentation of light nuclei, a hydrogen atom in magnetic field, photoionization of Helium like atoms, one photon ionization of atoms, electron-impact ionization of molecular hydrogen and photodissociation of molecules in strong laser field [3,4]. In the coupled-channel adiabatic approach (CCAA) [4], known in mathematical physics as the Kantorovich method, the desirable solution of the original boundary value problem (BVP) is expanded over surface eigenfunctions in fast variables (for example, angular variables) of an auxiliary BVP for an appropriate PDE dependent on a slow variable (for example, radial variable) as a parameter. Averaging of the original BVP over the surface eigenfunctions leads to 1D BVP for a system of coupled second-order ordinary differential equations (SOODEs) containing the potential matrix elements and first-derivative coupling terms that are integrals of the products of the surface eigenfunctions and/or the first derivatives of the surface eigenfunctions with respect to a parameter [4]. The purpose of this paper is to present the finite element method procedure based on the use of high-order accuracy approximations for calculating eigenvalues, surface eigenfunctions and their first derivatives with respect to a parameter of the parametric BVP for self-adjointed 2D PDE with the Dirichlet and/or Neumann type boundary conditions on a finite 2D region which arise at the reduction of the 3D BVP to 1D BVP for a system of coupled SOODEs in the framework of CCAA. The program developed calculates potential matrix elements that are integrals of the products of the surface eigenfunctions and/or the first derivatives of the surface eigenfunctions with respect to a parameter. These eigenvalues and potential matrix elements can be used for solving the bound state and multi-channel scattering problems for a system of coupled SOODEs with the help of the KANTBP program [5].

*Solution method:* We seek the desirable solution of the parametric 2D BVP in the form of expansion in the basis functions of the auxiliary Sturm-Liouville problem with respect to one of the fast variables. They are chosen in analytical form or calculated by the ODPEVP program [6]. The coefficients of the expansion are vector-eigenfunctions of the parametric homogeneous 1D BVP for a system of coupled SOODEs obtained by averaging the original 2D problem over the basis functions. First derivatives with respect to the parameter of these vector-eigenfunctions and eigenvalues are solutions of the parametric inhomogeneous 1D BVP, obtained by taking a derivative of the parametric homogeneous 1D BVP with respect to the parameter [7]. Then, we solve the reduced parametric homogeneous and inhomogeneous 1D BVPs by the finite element method using high-order accuracy approximations [6]. The generalized algebraic eigenvalue problem  $\mathbf{A}\mathbf{F} = E\mathbf{B}\mathbf{F}$  with respect to a pair of unknowns ( $E$ ,  $\mathbf{F}$ ) arising after the replacement of the differential problem by the finite-element approximation is solved by the subspace iteration method using the SSPACE program [1]. First derivatives of the vector-eigenfunctions and eigenvalues with respect to the parameter are obtained by solving the inhomogeneous algebraic equations in accordance with the algorithm used in [6]. Finally, we evaluate the desirable matrix elements using the calculated eigenvalues, vector-eigenfunctions and their derivatives, which can be applied to generate the coupled system equations in the slow variable in the CCAA.

Benchmark calculations of eigenvalues and eigenfunctions of the ground and first excited states of a Helium atom in the framework of a coupled-channel hyperspherical adiabatic approach are presented. Additionally a convergence of the eigenvalues versus both the number of parametric vector-eigenfunctions and the number of their components is studied. As a test desk, the program is applied to the calculation of the eigensolutions and their first derivatives with respect to the parameter of the parametric 2D BVP including evaluation of matrix elements, which are used in the benchmark calculations.

*Restrictions:* The computer memory requirements depend on:

- (a) the number of differential equations,
- (b) the number and order of finite elements, and
- (c) the number of eigensolutions required.

Restrictions due to dimension sizes may be easily alleviated by altering PARAMETER statements (see Long Write-Up). The user must also supply subroutine POTCLC for evaluating potential matrix elements. The user must also supply additional three DOUBLE PRECISION functions (see Long Write-Up for details).

*Running time:* The running time depends critically upon:

- (a) the number of differential equations,
- (b) the number and order of finite elements, and
- (c) the number of eigensolutions required.

The test run which accompanies this paper took 15 s with calculation of matrix potentials on computer Intel Core i5 CPU 3.33 GHz, 4 GB RAM, Windows 7. This test run requires 10 MB of disk storage.

*References:*

- [1] K.J. Bathe, Finite Element Procedures in Engineering Analysis, Englewood Cliffs, Prentice Hall, New York, 1982.
- [2] W.H. Press, S.A. Teukolsky, W.T. Vetterling and B.P. Flannery, Numerical Recipes: The Art of Scientific Computing, Cambridge University Press, Cambridge, 1986.
- [3] M. Shapiro and P. Brumer, Quantum Control of Molecular Processes, Wiley VCH, Verlag GmbH & Co. KGaA, Boschstr. 12, 69469 Weinheim, Germany, 2012.

- [4] U. Fano, Rep. Progr. Phys. 46 (1983) 97–165; U. Fano and A.R.P. Rau, Atomic Collisions and Spectra, Academic Press, Florida, 1986.
- [5] O. Chuluunbaatar, A.A. Gusev, A.G. Abrashkevich, A. Amaya-Tapia, M.S. Kaschiev, S.Y. Larsen and S.I. Vinitsky, Comput. Phys. Commun. 177 (2007) 649–675.
- [6] O. Chuluunbaatar, A.A. Gusev, S.I. Vinitsky and A.G. Abrashkevich, Comput. Phys. Commun. 180 (2009) 1358–1375.
- [7] A.G. Abrashkevich, M.S. Kaschiev and S.I. Vinitsky, J. Comp. Phys. 163 (2000) 328–348.

© 2014 Elsevier B.V. All rights reserved.

## LONG WRITE-UP

### 1. Introduction

Mathematical models of few-body systems in molecular, atomic and nuclear physics, as well as physics of semiconductor nanostructures are described by boundary value problems (BVPs) for the multidimensional equation of Schrödinger type in configuration space  $\mathbf{R}^d$ , for example, in studies of spectral and optical characteristics of excited states of a Helium-like atom [1–11], photoionization and recombination of opposite charged particles (positrons, antiprotons) in the magnet-optical trap [12], optical absorption in quantum wells, quantum wires [13], and quantum dots [14], channeling of likely charged particles in thin doped films [15] and resonance tunneling of composite systems through repulsive barriers [16].

Efficient and stable algorithms for the numerical solution of such class of BVPs are based on its reduction to a system of coupled second-order ordinary differential equations (SOODEs) with respect to the slow variable (for example, radial variable) in the coupled-channel adiabatic approach (CCAA) [17,18] or the Kantorovich method (KM) [19]. It is quite natural to use the eigenfunctions dependent on the slow variable as a parameter of an auxiliary parametric BVP over the fast variables (for example, angular variables) in an appropriate region of configuration space  $\mathbf{R}^{d-1}$  as the basis for the expansion of the unknown (required) solution.

For efficient application of the CCAA (or KM) one needs to create complex programs for calculations of the following quantities with a prescribed accuracy:

- (1) parametric eigenvalues and eigenfunctions of the auxiliary parametric BVP over the fast variables,
- (2) first derivatives of the eigenvalues and eigenfunctions with respect to the parameter,
- (3) matrix elements that are integrals of products of the eigenfunctions and/or the first derivatives of the eigenfunctions with respect to the parameter that appear as variable matrix coefficients in the system of SOODEs in the slow variable,
- (4) solutions of 1D BVP for the system of coupled SOODEs in the slow variable.

Using the above approach, we leverage and elaborate programs ODPEVP [20] and POTHMF [12] for the solution of problems (1)–(3) for the parametric 1D BVP, and programs KANTBP [21,22] for the solution of problem (4).

In this paper, we present program POTHEA where we implement effective and stable algorithms developed in [7] for solving problems (1)–(3) for the parametric 2D BVP for the elliptic partial differential equation (PDE) with boundary conditions of Dirichlet and/or Neumann type on a finite two-dimensional region which arise at the reduction of the 3D BVP to a system of coupled SOODEs using the CCAA. We seek the solution of the parametric 2D BVP in the form of expansion in the basis functions of the auxiliary Sturm–Liouville problem for the SOODE with respect to one of the variables. They are chosen in analytical form or calculated by ODPEVP program [20]. The coefficients of the expansion are the parametric vector-functions which are eigensolutions of the parametric homogeneous 1D BVP for a system of coupled SOODEs obtained by averaging of the original 2D problem over the basis eigenfunctions. The required parametric derivatives of eigenvalues and vector-eigenfunctions are calculated as a solution of the parametric inhomogeneous 1D BVP which is obtained by taking a derivative of the above parametric homogeneous 1D BVP with respect to the parameter.

The finite element method (FEM) [23,24] is used to discretize both the homogeneous and inhomogeneous parametric 1D BVPs. The calculated eigenfunctions and their first derivatives with respect to the parameter are within an accuracy of the same order of  $O(h^{p+1})$ , and also the eigenvalues and matrix elements are within an accuracy of the same order of  $O(h^{2p})$  in the maximal step  $h$  of a finite element grid [23,25]. Choice of the order  $p$  of finite element approximation depends on the smoothness of the desired solutions.

The efficiency of application of the programs POTHEA and KANTBP [21,22] is demonstrated by the solution of 3D BVP for the Schrödinger equation of a Helium atom with zero total angular momentum in the body-fixed hyperspherical coordinates [7]. The corresponding benchmark calculations with a given accuracy of energies and eigenfunctions of the ground and first excited states of a Helium atom and their convergence versus both the number of parametric vector-eigenfunctions and the number of their components are presented. The numerical experiments confirm the above theoretical estimations for the eigenvalues, eigenfunctions of the parametric 2D BVP and their derivatives with respect to the parameter, and also matrix elements.

The structure of the paper is as follows. In Section 2, we present the statement of the problem and reduction of the parametric 2D BVP to the parametric 1D BVPs. The construction of the finite-element high-order schemes is discussed in Section 3. A description of the POTHEA program is given in Section 4. In Section 5, the benchmark calculations and numerical analysis of matrix elements and the eigensolutions of ground and first excited states of a Helium atom in the framework of a coupled-channel hyperspherical adiabatic approach are presented. Test desk is discussed in Section 6.



## 2. Statement of the problem

Let us consider a boundary value problem for a parametric self-adjointed 2D PDE on region  $\Omega_{x,y} = (x_{\min}, x_{\max}) \times (y_{\min}, y_{\max})$

$$\left( -\frac{1}{f_1(y)} \frac{\partial}{\partial y} f_2(y) \frac{\partial}{\partial y} - \frac{1}{f_3(y)} \frac{1}{f_4(x)} \frac{\partial}{\partial x} f_5(x) \frac{\partial}{\partial x} + U(x, y; z) - \varepsilon_i(z) \right) B_i(x, y; z) = 0, \quad (1)$$

with the Dirichlet and/or Neumann type boundary conditions

$$\begin{aligned} \lim_{y \rightarrow y_t} f_2(y) \frac{\partial B_i(x, y; z)}{\partial y} &= 0 \quad \text{or} \quad B_i(x, y_t; z) = 0, \quad x \in (x_{\min}, x_{\max}), \\ \lim_{x \rightarrow x_t} f_5(x) \frac{\partial B_i(x, y; z)}{\partial x} &= 0 \quad \text{or} \quad B_i(x_t, y; z) = 0, \quad y \in [y_{\min}, y_{\max}], \end{aligned} \quad (2)$$

where  $t = \min, \max$ . Here  $z \in \Omega_z = [z_{\min}, z_{\max}]$  is a parameter, functions  $f_1(y) > 0, f_2(y) > 0, f_3(y) > 0, f_4(x) > 0, f_5(x) > 0$ , and  $\partial_y f_2(y), \partial_x f_5(x), U(x, y; z), \partial_z U(x, y; z)$  are continuous on the  $(x, y) \in \Omega_{x,y}$ . Also assume that the parametric BVP (1), (2) has only discrete spectrum.

The program POTHEA is implemented as the sequence of the following steps:

**Step 1.** Calculates a set of  $j_{\max}$  smallest eigenvalues  $\varepsilon_1(z) < \varepsilon_2(z) < \dots < \varepsilon_N(z)$ , and  $\varepsilon_1(z) \geq \alpha(z)$ , and the corresponding eigenfunctions  $\{B_j(x, y; z)\}_{j=1}^N \in F_z \sim \mathbf{L}_2(\Omega_{x,y})$ , satisfying the orthogonality and normalization conditions

$$\int_{y_{\min}}^{y_{\max}} dy f_1(y) \int_{x_{\min}}^{x_{\max}} dx f_4(x) B_i(x, y; z) B_j(x, y; z) = \delta_{ij}, \quad (3)$$

where  $\delta_{ij}$  is the Kronecker symbol and  $\alpha(z) > -\infty$  is the lower bound of the smallest eigenvalue of  $\varepsilon_1(z)$ .

**Step 2.** Computes a set of partial derivatives of eigenvalues  $\partial_z \varepsilon_j(z)$  and partial derivatives of eigenfunctions  $\partial_z B_j(x, y; z)$  with an accuracy of the same order achieved for eigenvalues and eigenfunctions of the BVP (1)–(3), respectively.

**Step 3.** Computes elements of matrices of dimension  $N \times N$  defined by the two-dimensional integrals

$$\begin{aligned} H_{ij}(z) &= H_{ji}(z) = \int_{y_{\min}}^{y_{\max}} dy f_1(y) \int_{x_{\min}}^{x_{\max}} dx f_4(x) \frac{\partial B_i(x, y; z)}{\partial z} \frac{\partial B_j(x, y; z)}{\partial z}, \\ Q_{ij}(z) &= -Q_{ji}(z) = - \int_{y_{\min}}^{y_{\max}} dy f_1(y) \int_{x_{\min}}^{x_{\max}} dx f_4(x) B_i(x, y; z) \frac{\partial B_j(x, y; z)}{\partial z}, \end{aligned} \quad (4)$$

with an accuracy of the same order achieved for the corresponding eigenvalues of the BVP (1)–(3).

The calculated eigenvalues  $\varepsilon_i(z)$  and potential matrix elements  $H_{ij}(z), Q_{ij}(z)$  can be used for solving the bound state and multichannel scattering problems for a system of coupled SOODEs with respect to the variable  $z$  with the help of the KANTBP programs [21,22].

### 2.1. Reduction of the 2D parametric BVP to the 1D parametric BVP

**Step 1.1.** The partial wave function  $B_i(x, y; z)$  is expanded over the orthonormal basis functions  $\{\psi_j(x)\}_{j=1}^{j_{\max}}$  ( $j_{\max} \rightarrow \infty$ ):

$$B_i(x, y; z) = \sum_{j=1}^{j_{\max}} \psi_j(x) \xi_j^{(i)}(y; z). \quad (5)$$

In Eq. (5), vector-functions  $\xi^{(i)}(y; z) = \left( \xi_1^{(i)}(y; z), \dots, \xi_{j_{\max}}^{(i)}(y; z) \right)^T$  are unknown. Basis functions  $\psi_j(x)$  are determined as solutions of the following eigenvalue problem:

$$\left( -\frac{1}{f_4(x)} \frac{d}{dx} f_5(x) \frac{d}{dx} + U_0(x) \right) \psi_j(x) = \lambda_j \psi_j(x), \quad (6)$$

$$\lim_{x \rightarrow x_t} f_5(x) \frac{d\psi_j(x)}{dx} = 0 \quad \text{or} \quad \psi_j(x_t) = 0, \quad (7)$$

where  $t = \min, \max$ ,  $U_0(x)$  is a known function. Basis functions  $\psi_j(x)$  satisfy the orthogonality and normalization conditions

$$\int_{x_{\min}}^{x_{\max}} dx f_4(x) \psi_i(x) \psi_j(x) = \delta_{ij}, \quad (8)$$

and they are chosen in analytical form or calculated by the ODPEVP program [20].

**Step 1.2.** After minimizing the Rayleigh–Ritz variational functional, and using the expansion (5), the parametric BVP (1)–(3) is reduced to a finite set of  $j_{\max}$  coupled SOODEs

$$(\mathbf{D}(y; z) - \varepsilon_i(z) \mathbf{I}) \xi^{(i)}(y; z) \equiv \left( -\frac{1}{f_1(y)} \mathbf{I} \frac{\partial}{\partial y} f_2(y) \frac{\partial}{\partial y} + \mathbf{W}(y; z) - \varepsilon_i(z) \mathbf{I} \right) \xi^{(i)}(y; z) = 0, \quad (9)$$

$$\lim_{y \rightarrow y_t} f_2(y) \frac{\partial \xi^{(i)}(y; z)}{\partial y} = 0 \quad \text{or} \quad \xi^{(i)}(y_t; z) = 0, \quad (10)$$

where  $t = \min, \max$ . Here  $\mathbf{I}, \mathbf{W}(y; z)$  are symmetric matrices of dimension  $j_{\max} \times j_{\max}$

$$I_{ij} = \delta_{ij} = \int_{y_{\min}}^{y_{\max}} dy f_1(y) (\xi^{(i)}(y; z))^T \xi^{(j)}(y; z), \quad (11)$$

$$W_{ij}(y; z) = \frac{\lambda_i + \lambda_j}{2f_3(y)} \delta_{ij} + \int_{x_{\min}}^{x_{\max}} dx f_4(x) \psi_i(x) \left( U(x, y; z) - \frac{U_0(x)}{f_3(y)} \right) \psi_j(x).$$

**Step 2.1.** Taking a derivative of the boundary problem (9)–(11) with respect to parameter  $z$ , we get that  $\partial_z \xi^{(i)}(y; z)$  can be obtained as a solution of the following boundary problem

$$(\mathbf{D}(y; z) - \varepsilon_i(z) \mathbf{I}) \frac{\partial \xi^{(i)}(y; z)}{\partial z} = - \left[ \frac{\partial}{\partial z} (\mathbf{W}(y; z) - \varepsilon_i(z) \mathbf{I}) \right] \xi^{(i)}(y; z), \quad (12)$$

$$\lim_{y \rightarrow y_t} f_2(y) \frac{\partial^2 \xi^{(i)}(y; z)}{\partial y \partial z} = 0 \quad \text{or} \quad \frac{\partial \xi^{(i)}(y_t; z)}{\partial z} = 0 \quad (13)$$

where  $t = \min, \max$ . The parametric BVP (12), (13) has a unique solution, if and only if it fulfills conditions

$$\frac{\partial \varepsilon_i(z)}{\partial z} = \int_{y_{\min}}^{y_{\max}} dy f_1(y) (\xi^{(i)}(y; z))^T \frac{\partial \mathbf{W}(y; z)}{\partial z} \xi^{(i)}(y; z), \quad (14)$$

$$\int_{y_{\min}}^{y_{\max}} dy f_1(y) (\xi^{(i)}(y; r))^T \frac{\partial \xi^{(i)}(y; z)}{\partial z} = 0. \quad (15)$$

**Step 3.1.** In this case the required matrix elements (4) are represented by the one-dimensional integrals

$$H_{ij}(z) = H_{ji}(z) = \int_{y_{\min}}^{y_{\max}} dy f_1(y) \left( \frac{\partial \xi^{(i)}(y; z)}{\partial z} \right)^T \frac{\partial \xi^{(j)}(y; z)}{\partial z}, \quad (16)$$

$$Q_{ij}(z) = -Q_{ji}(z) = - \int_{y_{\min}}^{y_{\max}} dy f_1(y) (\xi^{(i)}(y; z))^T \frac{\partial \xi^{(j)}(y; z)}{\partial z}.$$

## 2.2. Continuity conditions for the eigenfunction $B_i(x, y; z)$

Since problems (1)–(3) and (9)–(11) are homogeneous, it is necessary to use an additional condition to support the continuity of vector-functions  $\xi^{(i)}(y; z)$  and matrix elements (16) with respect to parameter  $z$  on interval  $\Omega_z = [z_{\min}, z_{\max}]$ . We have used the following additional condition:

1. At the first point  $z = z_1 \in \Omega_z$ , find value  $y = y_0$ , in which eigenfunction  $B_i(x_0, y_0; z_1)$  reached an absolute maximum value and fix the sign of the value of eigenfunction  $B_i(x_0, y_0; z_1)$ . Here  $x_0 \in [x_{\min}, x_{\max}]$  is a fixed point and at least one of functions  $\psi_j(x_0)$  in expansion (5) is not equal to zero.
2. At the next points  $z \in \Omega_z$  compute the value of eigenfunction  $B_i(x_0, y_0; z)$  and compare its sign with the sign of the previous one. If they are different, change the sign of  $B_i(x_0, y_0; z)$  and again find new value  $y = y_0$ , in which eigenfunction  $B_i(x_0, y_0; z_1)$  reached an absolute maximum value, and fix the sign of the value of eigenfunction  $B_i(x_0, y_0; z)$ .

Note that if the  $\Omega_z$  grid is dense, the above algorithm works well. One can check alternatively a continuous property of the expansion  $\sum_{j=1}^{j_{\max}} \psi_j(x) \xi_j^{(i)}(y; z)$  instead of the continuous one of expansion (5).

## 3. High order approximations of the finite-element method

Let us consider a numerical algorithm for the calculation of the vector-eigenfunctions  $\xi(y; z) = \xi^{(i)}(y; z)$  of the parametric boundary problem (9)–(11) and their derivative with respect to parameter  $z$ . Computational schemes of the high order of accuracy are derived from the Rayleigh–Ritz variational functional on the basis of the finite-element method (FEM)

$$\mathcal{R}(\xi, \varepsilon) = \frac{\int_{y_{\min}}^{y_{\max}} \left( f_2(y) (\partial_y \xi(y; z))^T \partial_y \xi(y; z) + f_1(y) (\xi(y; z))^T \mathbf{W}(y, z) \xi(y; z) \right) dy}{\int_{y_{\min}}^{y_{\max}} f_1(y) (\xi(y; z))^T \xi(y; z) dy}. \quad (17)$$

The general idea of FEM in one-dimensional space is to divide interval  $[y_{\min}, y_{\max}]$  into many small domains called elements. The size of elements can be defined very freely so that physical properties or quality behavior of solutions can be taken into account. Interval  $\Delta = [y_{\min}, y_{\max}]$  is covered by a system of  $n$  subintervals  $\Delta_j = [y_{j-1}, y_j]$  in such a way that  $\Delta = \bigcup_{j=1}^n \Delta_j$ . In each subinterval  $\Delta_j$  nodes  $\{y_{j,r}^p\}_{r=0}^p$

$$y_{j,r}^p = y_{j-1} + \frac{h_j}{p} r, \quad h_j = y_j - y_{j-1}, \quad (18)$$

and the Lagrange elements  $\{\phi_{j,r}^p(y)\}_{r=0}^p$

$$\phi_{j,r}^p(y) = \prod_{i=0, i \neq r}^p \frac{(y - y_{j,i}^p)}{(y_{j,r}^p - y_{j,i}^p)} \quad (19)$$

are determined. By means of the Lagrange elements  $\phi_{j,r}^p(y)$ , we define a set of local functions  $N_l(y)$  as follows:

$$N_l^p(y) = \begin{cases} \begin{cases} \phi_{1,0}^p(y), & y \in \Delta_1, \\ 0, & y \notin \Delta_1, \end{cases} & l = 0, \\ \begin{cases} \phi_{j,r}^p(y), & y \in \Delta_j, \\ 0, & y \notin \Delta_j, \end{cases} & l = r + p(j-1), r = \overline{1, p-1}, \\ \begin{cases} \phi_{j,p}^p(y), & y \in \Delta_j, \\ \phi_{j+1,0}^p(y), & y \in \Delta_{j+1}, \\ 0, & y \notin \Delta_j \cup \Delta_{j+1}, \end{cases} & l = jp, j = \overline{1, n-1}, \\ \begin{cases} \phi_{n,p}^p(y), & y \in \Delta_n, \\ 0, & y \notin \Delta_n, \end{cases} & l = np. \end{cases} \quad (20)$$

The functions  $\{N_l^p(y)\}_{l=0}^L$ ,  $L = np$ , form a basis in the space of polynomials of the  $p$ -th order. Now, each component of the vector-functions  $\xi(y; z) \in \mathcal{F}_z^h \sim \mathcal{H}^1(\Omega_{hy})$  is approximated by a finite sum of local functions  $N_l^p(y)$

$$\xi_v(y; z) = \sum_{l=0}^L \xi_v^l(y; z) N_l^p(y), \quad (21)$$

i.e. vector-function  $\xi(y; z)$  has a generalized first-order partial derivative and belongs to the Sobolev space  $\mathcal{H}^1(\Omega_{hy})$  [23]. After substituting expansion (21) into the variational functional (17) and minimizing it [23,24] we obtain the generalized eigenvalue problem

$$\mathbf{A}^p \xi^h = \varepsilon^h \mathbf{B}^p \xi^h. \quad (22)$$

Here  $\mathbf{A}^p$  is the stiffness matrix;  $\mathbf{B}^p$  is the positive definite mass matrix;  $\xi^h$  is the vector approximating solution on the finite-element grid; and  $\varepsilon^h$  is the corresponding eigenvalue. Matrices  $\mathbf{A}^p$  and  $\mathbf{B}^p$  have the following form:

$$\mathbf{A}^p = \sum_{j=1}^n \mathbf{a}_j^p, \quad \mathbf{B}^p = \sum_{j=1}^n \mathbf{b}_j^p, \quad (23)$$

where the local matrices  $\mathbf{a}_j^p$  and  $\mathbf{b}_j^p$  are calculated as

$$(\mathbf{a}_j^p)_{\mu\nu}^{qr} = \int_{-1}^{+1} \left\{ \delta_{\mu\nu} f_2(y) \frac{4}{h_j^2} \frac{d\phi_{j,q}^p(y)}{d\eta} \frac{d\phi_{j,r}^p(y)}{d\eta} + f_1(y) W_{\mu\nu}(y; z) \phi_{j,q}^p(y) \phi_{j,r}^p(y) \right\} \frac{h_j}{2} d\eta, \quad (24)$$

$$(\mathbf{b}_j^p)_{\mu\nu}^{qr} = \delta_{\mu\nu} \int_{-1}^{+1} f_1(y) \phi_{j,q}^p(y) \phi_{j,r}^p(y) \frac{h_j}{2} d\eta, \quad y = y_{j-1} + 0.5h_j(1 + \eta), \quad q, r = \overline{0, p}.$$

Integrals (24) are evaluated using the Gaussian quadrature formulae

$$(\mathbf{a}_j^p)_{\mu\nu}^{qr} = \sum_{g=0}^p \left\{ \delta_{\mu\nu} f_2(y_g) \frac{4}{h_j^2} \frac{d\phi_{j,q}^p(y_g)}{d\eta} \frac{d\phi_{j,r}^p(y_g)}{d\eta} + f_1(y_g) W_{\mu\nu}(y_g; z) \phi_{j,q}^p(y_g) \phi_{j,r}^p(y_g) \right\} \frac{h_j}{2} w_g, \quad (25)$$

$$(\mathbf{b}_j^p)_{\mu\nu}^{qr} = \delta_{\mu\nu} \sum_{g=0}^p f_1(y_g) \phi_{j,q}^p(y_g) \phi_{j,r}^p(y_g) \frac{h_j}{2} w_g,$$

where  $y_g = y_{j-1} + 0.5h_j(1 + \eta_g)$ ,  $\eta_g$  and  $w_g$ ,  $g = \overline{0, p}$  are the Gaussian nodes and weights related to the orthogonal polynomial of order  $p + 1$ . Note in this approach maximum value of a half-band of matrices  $\mathbf{A}^p$  and  $\mathbf{B}^p$  is small compared to their dimension and is not greater than  $j_{\max} \times (p + 1)$ .

In order to solve the generalized eigenvalue problem (22), the subspace iteration method [23,24] elaborated by Bathe [24] for the solution of large symmetric banded matrix eigenvalue problems has been chosen. This method uses a skyline storage mode which stores components of the matrix column vectors within the banded region of the matrix, and is ideally suited for banded finite element matrices. The procedure chooses a vector subspace of the full solution space and iterates upon the successive solutions in the subspace (for details, see [24]). The iterations continue until the desired set of solutions in the iteration subspace converges to within the specified tolerance

on the Rayleigh quotients for the eigenpairs. If matrix  $\mathbf{A}^p$  in Eq. (22) is not positively defined, problem (22) is replaced by the following problem:

$$\tilde{\mathbf{A}}^p \phi^h = \tilde{\varepsilon}^h \mathbf{B}^p \xi^h, \quad \tilde{\mathbf{A}}^p = \mathbf{A}^p - \alpha \mathbf{B}^p. \quad (26)$$

The number  $\alpha$  (the shift of the energy spectrum) is chosen in such a way that matrix  $\tilde{\mathbf{A}}^p$  is positive defined. The eigenvector of problem (26) is the same, and  $\varepsilon^h = \tilde{\varepsilon}^h + \alpha$ .

### 3.1. Calculations of the parametric derivative of the eigenfunctions and matrix elements

The boundary problem (12)–(15) is reduced to the linear system of inhomogeneous algebraic equations

$$\mathbf{L} \frac{\partial \xi^h}{\partial z} \equiv (\mathbf{A}^p - \varepsilon^h \mathbf{B}^p) \frac{\partial \xi^h}{\partial z} = b, \quad b = - \left( \frac{\partial \mathbf{A}^p}{\partial z} - \frac{\partial \varepsilon^h}{\partial z} \mathbf{B}^p \right) \xi^h. \quad (27)$$

The normalization (11), orthogonalization (15) and additional conditions (14) read as

$$(\xi^h)^T \mathbf{B}^p \xi^h = 1, \quad \left( \frac{\partial \xi^h}{\partial z} \right)^T \mathbf{B}^p \xi^h = 0, \quad \frac{\partial \varepsilon^h}{\partial z} = (\xi^h)^T \frac{\partial \mathbf{A}^p}{\partial z} \xi^h. \quad (28)$$

From here, potential matrix elements  $H_{ij}^h(z)$  and  $Q_{ij}^h(z)$  have the form

$$H_{ij}^h(z) = \left( \frac{\partial \xi_i^h}{\partial z} \right)^T \mathbf{B}^p \frac{\partial \xi_j^h}{\partial z}, \quad Q_{ij}^h(z) = - (\xi_i^h)^T \mathbf{B}^p \frac{\partial \xi_j^h}{\partial z}. \quad (29)$$

Since  $\varepsilon^h$  is an eigenvalue of (22), matrix  $\mathbf{L}$  in Eq. (27) is degenerate. In this case the algorithm for solving Eq. (27) can be written in three steps as follows:

**Step k1.** Calculate solutions  $\mathbf{v}$  and  $\mathbf{w}$  of the auxiliary inhomogeneous systems of algebraic equations

$$\bar{\mathbf{L}} \mathbf{v} = \bar{\mathbf{b}}, \quad \bar{\mathbf{L}} \mathbf{w} = \mathbf{d}, \quad (30)$$

with non-degenerate matrix  $\bar{\mathbf{L}}$  and right-hand sides  $\bar{\mathbf{b}}$  and  $\mathbf{d}$

$$\bar{L}_{ss'} = \begin{cases} L_{ss'}, & (s-S)(s'-S) \neq 0, \\ \delta_{ss'}, & (s-S)(s'-S) = 0, \end{cases} \quad (31)$$

$$\bar{b}_s = \begin{cases} b_s, & s \neq S, \\ 0, & s = S, \end{cases} \quad d_s = \begin{cases} L_{sS}, & s \neq S, \\ 0, & s = S, \end{cases}$$

where  $S$  is the number of the greatest absolute value element of vector  $\mathbf{B}^p \xi^h$ .

**Step k2.** Evaluate coefficient  $\gamma$

$$\gamma = - \frac{\gamma_1}{(\mathbf{D}_S - \gamma_2)}, \quad \gamma_1 = \mathbf{v}^T \mathbf{B}^p \xi^h, \quad \gamma_2 = \mathbf{w}^T \mathbf{B}^p \xi^h, \quad \mathbf{D}_S = (\mathbf{B}^p \xi^h)_S. \quad (32)$$

**Step k3.** Evaluate vector  $\partial_z \xi^h$

$$\frac{\partial \xi_s^h}{\partial z} = \begin{cases} v_s - \gamma w_s, & s \neq S, \\ \gamma, & s = S. \end{cases} \quad (33)$$

From the consideration above it is evident, that the derivative computed has the same accuracy as the calculated eigenfunction.

Let  $\mathbf{D}(y; z)$  from (9) be a continuous and bounded positively defined operator on the space  $\mathcal{H}^1$  with energy norm,  $\varepsilon_i(z)$ ,  $\xi^{(i)}(y; z) \in \mathcal{H}^2$  are the exact solutions of (9)–(11), and  $\varepsilon_i^h(z)$ ,  $\xi_i^h(y; z) \in \mathcal{H}^1$  are the corresponding numerical solutions. Then the following estimates are valid [23]

$$|\varepsilon_i(z) - \varepsilon_i^h(z)| \leq c_1 h^{2p}, \quad \|\xi^{(i)}(y; z) - \xi_i^h(y; z)\|_0 \leq c_2 h^{p+1}, \quad (34)$$

where  $\|\xi^{(i)}(y; z)\|_0^2 = \int_{y_{\min}}^{y_{\max}} dy f_1(y) (\xi^{(i)}(y; z))^T \xi^{(i)}(y; z)$ ,  $h$  is the maximal step of the finite-element grid,  $p$  is the order of finite-elements,  $i$  is the number of corresponding solutions, and constants  $c_1$  and  $c_2$  do not depend on step  $h$ .

We have the following theorem.

**Theorem 1.** Let  $\mathbf{D}(y; z)$  from (9) be a continuous and bounded positively defined operator on the space  $\mathcal{H}^1$  with energy norm. Also  $\partial_z W(y; z)$  is continuous and bounded in each value of the parameter  $z$ . Then for exact values of solutions  $\partial_z \varepsilon_i(z)$ ,  $\partial_z \xi^{(i)}(y; z) \in \mathcal{H}^2$ ,  $H_{ij}(z)$ ,  $Q_{ij}(z)$

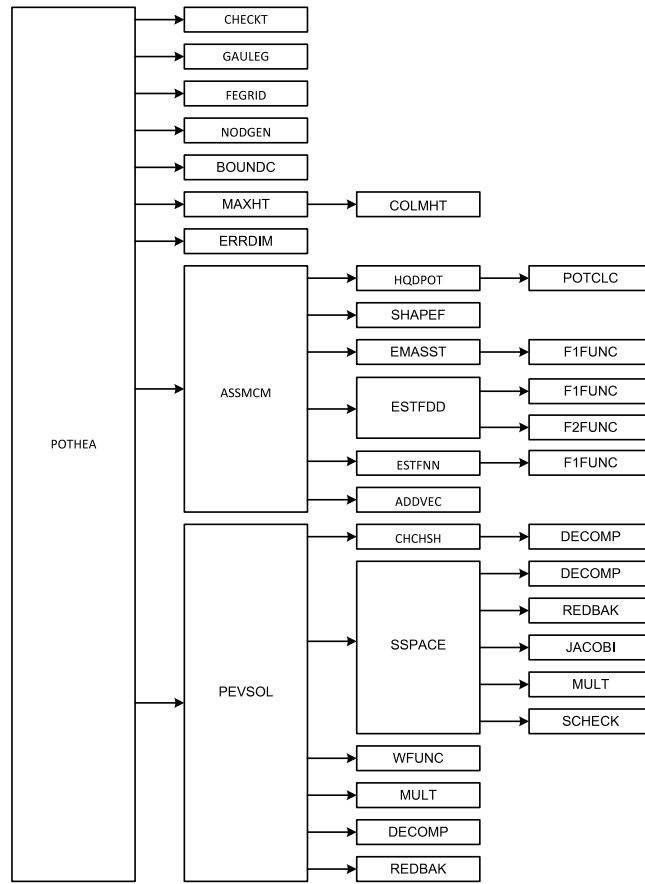


Fig. 1. Flow diagram of the POTHEA program.

from (12)–(15) and corresponding numerical values  $\partial_z \varepsilon_i^h(z)$ ,  $\partial_z \xi_i^h(y; z) \in \mathcal{H}^1$ ,  $H_{ij}^h(z)$ ,  $Q_{ij}^h(z)$  from (27)–(29) the following estimates are valid:

$$\left| \frac{\partial \varepsilon_i(z)}{\partial z} - \frac{\partial \varepsilon_i^h(z)}{\partial z} \right| \leq c_3 h^{2p}, \quad \left\| \frac{\partial \xi^{(i)}(y; z)}{\partial z} - \frac{\partial \xi_i^h(y; z)}{\partial z} \right\|_0 \leq c_4 h^{p+1}, \quad (35)$$

$$|Q_{ij}(z) - Q_{ij}^h(z)| \leq c_5 h^{2p}, \quad |H_{ij}(z) - H_{ij}^h(z)| \leq c_6 h^{2p},$$

where  $h$  is the maximal step of the finite-element grid,  $p$  is the order of finite-elements,  $i, j$  are the numbers of corresponding solutions, and constants  $c_3$ ,  $c_4$ ,  $c_5$  and  $c_6$  do not depend on step  $h$ .

Proof is straightforward following the proof schemes in accordance with [23,25].

#### 4. Description of the POTHEA program

Fig. 1 presents a flow diagram for the POTHEA program. It is called from the main routine (supplied by a user) which sets dimensions of the arrays and is responsible for the input data. The POTHEA program needs no installation. Also users can find instructions on how to compile the POTHEA in the README file.

The calling sequence for the subroutine POTHEA is:

```

1 CALL POTHEA(TITLE,PARAM,HH,QQ,EIG,ICOUN,NROOT,MDIM,NPOL,
2             RTOL,NITEM,SHIFT,ICLK,IPRINT,IPRSTP,NMESH,RMESH,
3             NDIR,NDIL,NMDIL,IBOUND,FNOUT,IOUT,POTEN,IOUP,
4             FMATR,IOUM,EVWFN,IOUF,TOT,ITOT,MTOT,MITOT)
  
```

##### Input data

CHARACTER type input data:

- TITLE is the title of the run to be printed on the output listing. The title should be no longer than 70 characters.
- FNOUT is the name of the output file (up to 55 characters) for printing out the results of the calculation. It is system specific and may include a complete path to the file location.
- POTEN is the name of the input/output file (up to 55 characters) containing potential matrix elements.

- EVWFN is the name of the output file (up to 55 characters) for storing the results of the calculation, namely, the eigenvalues and eigenfunctions, their first derivatives with respect to the parameter, and finite-element grid points.
- FMATR is the name of the scratch file (up to 55 characters) for storing calculated matrices.

DOUBLE PRECISION type input data:

- PARAM is the value of the parameter  $z$ .
- RTOL is the convergence tolerance on eigenvalues.
- SHIFT contains the lower bound of the lowest eigenvalue.
- Array RMESH contains information about subdivision of interval  $[y_{\min}, y_{\max}]$  of variable  $y$  on subintervals. The whole interval  $[y_{\min}, y_{\max}]$  is divided as follows:  $\text{RMESH}(1) = y_{\min}$ ,  $\text{RMESH}(\text{NMESH}) = y_{\max}$ , and the values of  $\text{RMESH}(I)$  set the number of elements for each subinterval  $[\text{RMESH}(I-1), \text{RMESH}(I+1)]$ , where  $I = 2, 4, \dots, \text{NMESH} - 1$ .
- TOT is the working vector of the DOUBLE PRECISION type.

INTEGER type input data:

- ICOUN is the key parameter for the continuity of eigenfunctions with respect to parameter  $z$ . For the first call of POTHEA the parameter ICOUN always 0.
- NROOT is the number of eigenvalues and eigenvectors required.
- MDIM is the maximum number of coupled differential equations.
- NPOL is the order of finite-element shape functions (interpolating Lagrange polynomials).
- NITEM is the maximum number of iterations permitted.
- ICHK is the key parameter. If  $\text{ICLK} \neq 0$  the SHIFT is determined automatically by the program with the help of the algorithm [20].
- IPRINT is the level of prints:
  - = 0—the minimal level of print. The initial data, short information about the numerical scheme parameters, main flags and keys, and eigenvalues calculated and their first derivatives with respect to the parameter are printed out;
  - = 1—eigenfunctions calculated and their first derivatives with respect to the parameter are printed out with step IPRSTP additionally;
  - = 2—potential matrix and its first derivatives with respect to the parameter are printed out with step IPRSTP;
  - = 3—information about nodal point distribution is printed out;
  - = 4—global matrices are printed out additionally;
  - = 5—the highest level of print. The local stiffness and mass matrices together with all current information about the course of the subspace iteration method solution of the generalized eigenvalue problem are printed out.
- IPRSTP is the step with which eigenfunctions are printed out.
- NMESH is the dimension of array RMESH. NMESH always should be odd and  $\geq 3$ .
- NDIR is the dimension of the INTEGER array NDIL. If  $\text{NDIR} > \text{MDIM}$  the message about the error is printed and the execution of the program is stopped.
- Array NDIL containing information about the set of numbers of coupled differential equations and always should be  $\text{NDIL}(\text{NDIR}) \leq \text{MDIM}$ .
- NMDIL is the key parameter. If  $\text{NMDIL} = 0$  the potential matrix elements of coupling are calculated and written to file POTEN; otherwise, they are read from file POTEN.
- IBOUND is the parameter defining the type of boundary conditions set in the boundary points  $y = y_{\min}$  and  $y = y_{\max}$ :
  - = 1—the Dirichlet–Dirichlet boundary conditions;
  - = 2—the Dirichlet–Neumann boundary conditions;
  - = 3—the Neumann–Dirichlet boundary conditions;
  - = 4—the Neumann–Neumann boundary conditions.
- IOUT is the number of the output logical device for printing out the calculation results.
- IOUP is the number of the logical device for reading/storing data from/into file POTEN.
- IOUM is the number of the logical device for storing calculated matrices.
- IOUF is the number of the logical device for storing data into file EVWFN.
- ITOT is the working vector of the INTEGER type.
- MTOT is the dimension of the DOUBLE PRECISION working array TOT. The last address ILAST of array TOT is calculated and then compared with the given value of MTOT. If  $\text{ILAST} > \text{MTOT}$  the message about an error is printed and the execution of the program is aborted. In the last case, in order to carry out the required calculation it is necessary to increase the dimension MTOT of array TOT to the quantity ILAST taken from the message.
- MITOT is the dimension of the INTEGER working array ITOT. The last address ILAST of array ITOT is calculated and then compared with the given value of MITOT. If  $\text{ILAST} > \text{MITOT}$  the message about an error is printed and the execution of the program is aborted. In the last case, in order to carry out the required calculation it is necessary to increase the dimension MITOT of array ITOT to the quantity ILAST taken from the message.

In the present code each array declarator is written in terms of the symbolic names of constants. These constants are defined in the following PARAMETER statement in the main routine:

```
PARAMETER (MTOT = 700000, MITOT = 40000, NMESH = 3, MDIM = 12, NROOT = 6)
```

In order to change the dimensions of the code, all one has to do is to modify the single PARAMETER statement defined above in the main program unit.

### Output data

- Array EIG of dimension NROOT containing values of the calculated eigenvalues  $\varepsilon_j(z)$ .
- Array HH of dimension NROOT  $\times$  NROOT containing values of the potential matrix  $H_{ij}(z)$ .
- Array QQ of dimension NROOT  $\times$  NROOT containing values of the potential matrix  $Q_{ij}(z)$ .

Also the results of the calculation of eigenvalues, eigenfunctions and their first derivatives with respect to parameter  $z$  from the last POTHEA call are written using unformatted segmented records into file EVWFN, according to the following operator:

```
WRITE(IOUF) NDIM,NN,NROOT,NGRID, (EIGV(I), I=1,NROOT),
1      (BUP(I), I=1,NROOT), (XGRID(I), I=1,NGRID),
2      ((R(I,J), I=1,NN), J=1,NROOT), ((DR(I,J), I=1,NN), J=1,NROOT)
```

In the above, parameters presented in the WRITE statement have the following meaning:

- Arrays EIGV and BUP contain the NROOT eigenvalues calculated and their first derivatives with respect to the parameter  $z$ , respectively.
- Array XGRID contains the NGRID values of the finite-element grid points.
- Arrays R and DR contain NROOT eigenfunctions and their first derivatives with respect to parameter  $z$ , respectively, each per NN elements in length stored in the following way: for each of the NGRID mesh points per NDIM elements of eigenfunction or its first derivative with respect to parameter  $z$ .
- NGRID is the number of finite-element grid points.
- NDIM is the number of coupled equations.
- NN = NDIM  $\times$  NGRID, if IBOIND = 4;  
NN = NDIM  $\times$  (NGRID – 1), if IBOIND = 3 or 2;  
NN = NDIM  $\times$  (NGRID – 2), if IBOIND = 1.

#### User-supplied DOUBLE PRECISION functions and subroutine

- F1FUNC is the name of the function which calculates the function  $f_1(y)$ .
- F2FUNC is the name of the function which calculates the function  $f_2(y)$ .
- WFUNC is the name of the function which calculates the basis function  $\psi_i(x)$  at fixed point  $x = x_0$ . (see Eq. (5)–(8) and Section 2.2).
- POTCLC is the name of the subroutine which calculates potential matrix elements  $WW = \mathbf{W}(y; z)$  of dimension MDIM  $\times$  MDIM and their first derivatives DW of dimension MDIM  $\times$  MDIM with respect to the parameter  $z$ .

Note that in POTHEA program we used the subroutine SSPACE which finds the smallest eigenvalues and the corresponding eigenvectors in the generalized eigenproblem using the subspace iteration method [24], and the subroutine GAULEG which calculates nodes and weights of the Gauss–Legendre quadrature [26]. The description of all subroutines can be found in comments in the program source code.

### 5. Benchmark calculation of the energies of a Helium atom

The Schrödinger equation for a Helium atom with zero total angular momentum in the conventional hyperspherical coordinates  $z \equiv R \in [0, +\infty)$ ,  $y \equiv \alpha \in [0, \pi]$ ,  $x \equiv \theta \in [0, \pi]$  can be written as the BVP for the following 3D-elliptic PDE (in atomic units  $\hbar = e = m_e = 1$ ) [7]:

$$\left( -\frac{1}{R^5} \frac{\partial}{\partial R} R^5 \frac{\partial}{\partial R} + \frac{4}{R^2} (H(\theta, \alpha; R) + V(\theta, \alpha; R)) - 2E \right) \Psi(R, \alpha, \theta) = 0, \quad (36)$$

$$H(\theta, \alpha; R) = -\frac{1}{\sin^2(\alpha)} \left( \frac{\partial}{\partial \alpha} \sin^2(\alpha) \frac{\partial}{\partial \alpha} + \frac{1}{\sin(\theta)} \frac{\partial}{\partial \theta} \sin(\theta) \frac{\partial}{\partial \theta} \right),$$

$$V(\theta, \alpha; R) = \frac{R}{2} \left( -\frac{2}{\sin(\alpha/2)} - \frac{2}{\cos(\alpha/2)} + \frac{1}{\sqrt{1 - \sin(\alpha) \cos(\theta)}} \right).$$

Total wave function  $\Psi(R, \alpha, \theta)$  satisfies the following boundary conditions:

$$\lim_{R \rightarrow 0} R^5 \frac{\partial \Psi(R, \alpha, \theta)}{\partial R} = 0, \quad \lim_{R \rightarrow \infty} R^5 \Psi(R, \alpha, \theta) = 0, \quad (37)$$

$$\lim_{\alpha \rightarrow 0, \pi} \sin^2(\alpha) \frac{\partial \Psi(R, \alpha, \theta)}{\partial \alpha} = 0, \quad \lim_{\theta \rightarrow 0, \pi} \sin(\theta) \frac{\partial \Psi(R, \alpha, \theta)}{\partial \theta} = 0, \quad (38)$$

and is normalized by condition

$$\int_0^\infty dR R^5 \int_0^\pi d\alpha \sin^2(\alpha) \int_0^\pi d\theta \sin(\theta) \Psi^2(R, \alpha, \theta) = 1. \quad (39)$$

#### 5.1. Reduction of the 3D BVP to the 1D BVP: Kantorovich expansion

Consider a formal expansion of the solution of Eqs. (36)–(39) over a set of two-dimensional parametric basis functions  $\{B_i(\alpha, \theta; R)\}_{i=1}^N$  ( $N \rightarrow \infty$ ):

$$\Psi(R, \alpha, \theta) = \sum_{j=1}^N B_j(\theta, \alpha; R) \chi_j(R). \quad (40)$$

In Eq. (40) functions  $\chi(R) = (\chi_1(R), \chi_2(R), \dots, \chi_N(R))^T$  are unknown, and adiabatic functions  $\mathbf{B}(\theta, \alpha; R) = (B_1(\alpha, \theta; R), B_2(\alpha, \theta; R), \dots, B_N(\alpha, \theta; R))^T$  form an orthonormal basis for each value of hyperradius  $R$  which is treated here as a slowly varying adiabatic parameter.



After minimizing the Rayleigh–Ritz variational functional (see [7]), and using the expansion (40), 3D BVP equation (36)–(39) is reduced to a finite set of  $N$  coupled SOODEs for  $\chi(R)$

$$\left( -\frac{1}{R^5} \mathbf{I} \frac{d}{dR} R^5 \frac{d}{dR} + \mathbf{U}(R) + \mathbf{Q}(R) \frac{d}{dR} + \frac{1}{R^5} \frac{dR^5 \mathbf{Q}(R)}{dR} - 2E \mathbf{I} \right) \chi(R) = 0, \quad (41)$$

$$\lim_{R \rightarrow 0} R^5 \frac{d\chi(R)}{dR} = 0, \quad \lim_{R \rightarrow \infty} R^5 \chi(R) = 0, \quad (42)$$

$$\int_0^\infty dR R^5 (\chi(R))^T \chi(R) = 1. \quad (43)$$

Here  $\mathbf{I}$ ,  $\mathbf{U}(R)$  and  $\mathbf{Q}(R)$  are matrices of dimension  $N \times N$ :

$$\begin{aligned} I_{ij} &= \delta_{ij}, \quad U_{ij}(R) = U_{ji}(R) = 2 \frac{\varepsilon_i(R) + \varepsilon_j(R)}{R^2} \delta_{ij} + H_{ij}(R), \\ H_{ij}(R) &= H_{ji}(R) = \int_0^\pi d\alpha \sin^2(\alpha) \int_0^\pi d\theta \sin(\theta) \frac{\partial B_i(\theta, \alpha; R)}{\partial R} \frac{\partial B_j(\theta, \alpha; R)}{\partial R}, \\ Q_{ij}(R) &= -Q_{ji}(R) = - \int_0^\pi d\alpha \sin^2(\alpha) \int_0^\pi d\theta \sin(\theta) B_i(\theta, \alpha; R) \frac{\partial B_j(\theta, \alpha; R)}{\partial R}. \end{aligned} \quad (44)$$

This problem can be solved by FEM at values  $R$  belonging to the Gauss nodes of a finite element grid  $\Omega_R$  with the help of KANTBP programs [21,22]. In the KM [19] the parametric basis functions  $B_i(\theta, \alpha; R)$  are determined as solutions of the following parametric BVP:

$$\left[ -\frac{1}{\sin^2(\alpha)} \left( \frac{\partial}{\partial \alpha} \sin^2(\alpha) \frac{\partial}{\partial \alpha} + \frac{1}{\sin(\theta)} \frac{\partial}{\partial \theta} \sin(\theta) \frac{\partial}{\partial \theta} \right) + V(\theta, \alpha; R) - \varepsilon_i(R) \right] B_i(\theta, \alpha; R) = 0, \quad (45)$$

$$\lim_{\alpha \rightarrow 0, \pi} \sin^2(\alpha) \frac{\partial B_i(\theta, \alpha; R)}{\partial \alpha} = 0, \quad \lim_{\theta \rightarrow 0, \pi} \sin(\theta) \frac{\partial B_i(\theta, \alpha; R)}{\partial \theta} = 0, \quad (46)$$

$$\int_0^\pi d\alpha \sin^2(\alpha) \int_0^\pi d\theta \sin(\theta) B_i(\theta, \alpha; R) B_j(\theta, \alpha; R) = \delta_{ij}. \quad (47)$$

## 5.2. Reduction of the 2D parametric BVP (45)–(47) to the parametric 1D BVP

Consider the following expansion of adiabatic surface function  $B_i(\alpha, \theta; R)$ :

$$B_i(\theta, \alpha; R) = \sum_{j=1}^{j_{\max}} \psi_j(\theta) \xi_j^{(i)}(\alpha; R). \quad (48)$$

Here  $\psi_j(\theta) \equiv P_{j-1}(\cos(\theta))$  is the normalized Legendre polynomial [27]:

$$-\frac{1}{\sin(\theta)} \frac{d}{d\theta} \sin(\theta) \frac{d\psi_j(\theta)}{d\theta} = \lambda_j \psi_j(\theta), \quad \lambda_j = j(j-1), \quad (49)$$

$$\lim_{\theta \rightarrow 0, \pi} \sin(\theta) \frac{d\psi_j(\theta)}{d\theta} = 0, \quad (50)$$

$$\int_0^\pi d\theta \sin(\theta) \psi_i(\theta) \psi_j(\theta) = \delta_{ij}. \quad (51)$$

After minimization of the variational functional we get that eigenfunctions  $\xi^{(i)}(\alpha; R) = \left( \xi_1^{(i)}(\alpha; R), \xi_2^{(i)}(\alpha; R), \dots, \xi_{j_{\max}}^{(i)}(\alpha; R) \right)^T$  and eigenvalues  $\varepsilon_i(R)$  satisfy the following eigenvalue problem for the set of  $j_{\max}$  coupled SOODEs

$$\left( -\frac{1}{\sin^2(\alpha)} \hat{\mathbf{I}} \frac{\partial}{\partial \alpha} \sin^2(\alpha) \frac{\partial}{\partial \alpha} + \mathbf{W}(\alpha; R) - \varepsilon_i(R) \hat{\mathbf{I}} \right) \xi^{(i)}(\alpha; R) = 0, \quad (52)$$

$$\lim_{\alpha \rightarrow 0, \pi} \sin^2(\alpha) \frac{\partial \xi^{(i)}(\alpha; R)}{\partial \alpha} = 0. \quad (53)$$

Here  $\hat{\mathbf{I}}$ ,  $\mathbf{W}(\alpha; R)$  are symmetric matrices of dimension  $j_{\max} \times j_{\max}$

$$\hat{I}_{ij} = \delta_{ij} = \int_0^\pi d\alpha \sin^2(\alpha) (\xi^{(i)}(\alpha; R))^T \xi^{(j)}(\alpha; R), \quad (54)$$

$$W_{ij}(\alpha; R) = \left[ \frac{\lambda_i + \lambda_j}{2 \sin^2(\alpha)} - \frac{R}{2} \left( \frac{2}{\sin(\alpha/2)} + \frac{2}{\cos(\alpha/2)} \right) \right] \delta_{ij} + \frac{R}{2} W_{ij}^{rep}(\alpha),$$



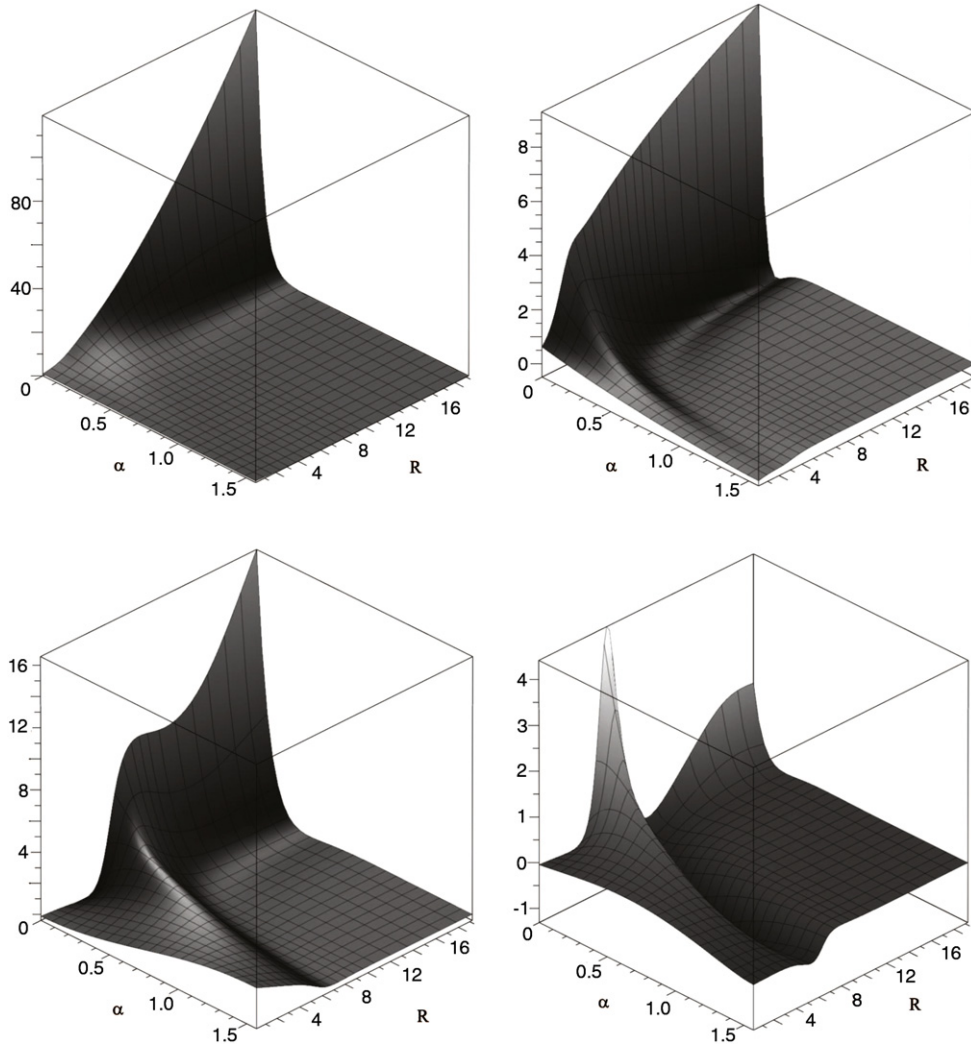


**Fig. 2.** The eigenfunctions  $B_j(\theta, \alpha, R)$  at  $\theta = \pi$  (left) and their first derivatives (right) with respect to parameter  $R$  (in a.u.) plotted vs hyperradius  $R$  (in a.u.) and variable  $\alpha$  (in rad.). Top:  $j = 1$ . Bottom:  $j = 4$ .

where

$$W_{ij}^{rep}(\alpha) = W_{ij}^{rep}(\pi - \alpha) = \int_0^\pi d\theta \sin(\theta) \frac{P_{i-1}(\cos(\theta))P_{j-1}(\cos(\theta))}{\sqrt{1 - \sin(\alpha)\cos(\theta)}} = \int_{-1}^1 d\eta \frac{P_{i-1}(\eta)P_{j-1}(\eta)}{\sqrt{1 - \sin(\alpha)\eta}}. \quad (55)$$

Because of the symmetry of matrix elements  $W_{ij}(\alpha; R)$  with respect to  $\alpha = \pi/2$ , problem (52)–(55) will be considered for  $\alpha \in [0, \pi/2]$  with the following boundary conditions for the ground and first excited states

$$\lim_{\alpha \rightarrow 0, \pi/2} \sin^2(\alpha) \frac{\partial \xi^{(i)}(\alpha; R)}{\partial \alpha} = 0. \quad (56)$$

The 1D weak singular integral (55) at  $\alpha = \pi/2$  was conventionally calculated analytically using the Clebsch–Gordan coefficients [4,5]. But this approach gives large numerical errors at large numbers  $i$  and  $j$  because of calculations of the factorial of large numbers (required factorials of numbers up to  $4j_{\max} - 3$ ). After the change of the variable in (55)

$$\eta = \eta(\alpha, \zeta) \equiv \frac{\tan(\alpha/2)}{2}(1 - \zeta^2) + \zeta, \quad \zeta \in [-1, 1], \quad \alpha \in [0, \pi/2], \quad (57)$$

we obtain a nonsingular integral

$$W_{ij}^{rep}(\alpha) = W_{ij}^{rep}(\pi - \alpha) = \frac{1}{\cos(\alpha/2)} \int_{-1}^1 d\zeta P_{i-1}(\eta(\alpha, \zeta)) P_{j-1}(\eta(\alpha, \zeta)). \quad (58)$$

The last 1D integral calculated by means of the 96-order Gauss–Legendre quadrature, and this approach gives results with accuracy  $\leq 10^{-14}$  at  $i, j \leq 120$ , i.e. with the double precision accuracy.

In Fig. 2 we plotted the first four eigenfunctions  $B_j(\theta, \alpha, R)$  at  $\theta = \pi$  and their first derivatives with respect to parameter  $R$  as functions of hyperradius  $R$  and variable  $\alpha$ . Potential curves  $4R^{-2}(\varepsilon_i(R) + 1)$ , radial diagonal and nondiagonal matrix elements  $H_{ij}(R)$ , and radial

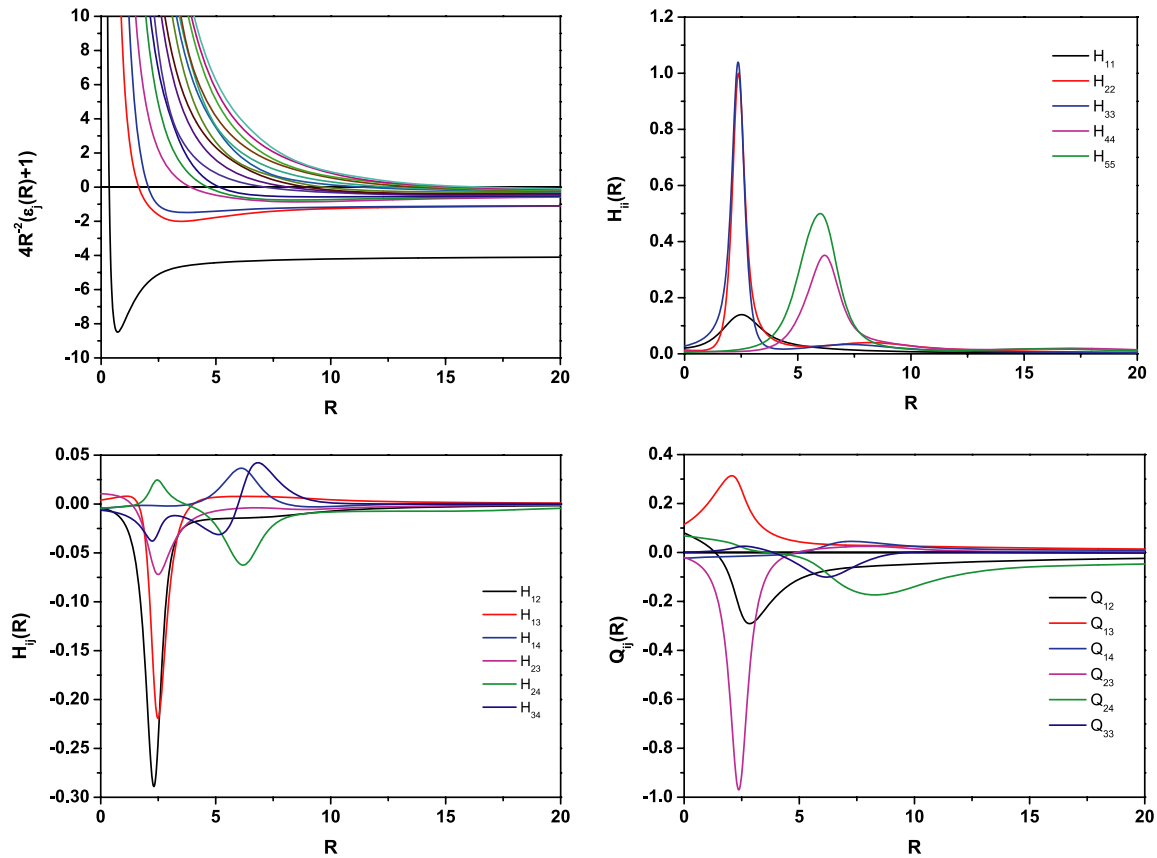


**Fig. 3.** Potential curves  $4R^{-2}(\epsilon_i(R)+1)$ ,  $i = 1, \dots, 16$  (top-left), radial diagonal (top-right) and nondiagonal (bottom-left) matrix elements  $H_{ij}(R)$ , and radial matrix elements  $Q_{ij}(R)$  (bottom-right) plotted vs hyperradius  $R$  (in a.u.).

matrix elements  $Q_{ij}(R)$  as functions of hyperradius  $R$  are displayed in Fig. 3. As can be seen from Figs. 2 and 3, our algorithm for continuity conditions from Section 2.2 for eigenfunction  $B_i(\alpha, \theta; R)$  works well. Note, that the peaks of matrix elements are result of avoiding crossing of potential curves. The classification of potential curves at small and large values of  $R$  by sets of adiabatic quantum numbers (so-called correlation diagrams), and asymptotic behavior of matrix elements are described in [3,8].

The numerical experiments show a strict correspondence with the theoretical estimations for the eigenvalues, eigenfunctions of (34) and their derivatives with respect to the parameter (35). In particular, we calculated the values of the Runge coefficients

$$\beta_l = \log_2 \left| \frac{\sigma_l^h - \sigma_l^{h/2}}{\sigma_l^{h/2} - \sigma_l^{h/4}} \right|, \quad l = 1-6, \quad (59)$$

with absolute errors on four twice condensed grids for their eigenvalues, their derivatives, and matrix elements, respectively:

$$\begin{aligned} \sigma_1^h &= |\epsilon_j^{h/8}(\rho) - \epsilon_j^h|, & \sigma_2^h &= \left| \frac{\partial \epsilon_j^{h/8}(R)}{\partial R} - \frac{\partial \epsilon_j^h}{\partial R} \right|, \\ \sigma_3^h &= \|\xi_j^{h/8}(\alpha; R) - \xi_j^h(\alpha; R)\|_0, & \sigma_4^h &= \left\| \frac{\partial \xi_j^{h/8}(\alpha; R)}{\partial R} - \frac{\partial \xi_j^h(\alpha; R)}{\partial R} \right\|_0, \\ \sigma_5^h &= |H_{ij}^{h/8}(R) - H_{ij}^h(R)|, & \sigma_6^h &= |Q_{ij}^{h/8}(R) - Q_{ij}^h(R)|. \end{aligned} \quad (60)$$

From (59) we obtained numerical estimations of the convergence order of proposed numerical schemes, i.e. theoretical estimations equal to  $\beta_l = p + 1$  for  $l = 3, 4$  and  $\beta_l = 2p$  otherwise. For the chosen approximation order  $p = 4$  for their eigenvalues, their derivatives, and matrix elements we obtain numerical estimations of Runge coefficients within 7.5–7.8, and for their eigenfunctions and their derivatives in the range 4.6–4.8, which corresponds to the theoretical error estimates at fixed number  $j_{\max}$  of Eq. (52). Calculations of (60) were performed with a specified accuracy of  $\sim 10^{-12}$  by means of POTHEA program at relative error tolerance  $\epsilon_1 = 4 \cdot 10^{-16}$ .

A convergence study of several matrix elements with respect to number  $j_{\max} = 12, 28, 40, 50, 60, 70, 80, 100, 120$  of the Legendre polynomials and the number of finite elements,  $N_{el} = 6, 12, 18, 24, 30, 36$ , of the grid  $\Omega_\alpha = \{0(N_{el})\pi/2\}$  and their order  $p = 4$  is presented in Tables 1 and 2. One can see that potential curves  $2R^{-2}(\epsilon_j(R) + 1)$  and matrix elements  $H_{ij}(R)$  converge monotonically from above, with the increasing of numbers  $N_{el}$  and  $j_{\max}$ . The absolute values of the matrix elements  $Q_{ij}(R)$  converge monotonically from above with increasing  $j_{\max}$  and from below with increasing  $N_{el}$ . As it follows from (58) and confirmed by Table 1, the convergence of eigenvalues and matrix elements vs the number of Legendre polynomials  $P_{j-1}(\eta)$ , is proportional to their order  $\sim j^{-3}$ .

**Table 1**

Convergence of potential curve  $2R^{-2}(\varepsilon_5(R) + 1)$  and matrix elements  $Q_{35}(R)$ ,  $H_{35}(R)$ ,  $H_{55}(R)$  at  $R = 7.65$  a.u. as a function of the maximum number of terms  $j_{\max}$ , numbers of finite elements  $N_{el}$  at their order  $p = 4$ .

$j_{\max}$	$N_{el}$	$2R^{-2}(\varepsilon_5(R) + 1), 10^{-1}$	$H_{55}(R), 10^{-2}$
12	6	−3.717 091 841 269 3	8.333 864 894 452
12	12	−3.717 092 590 328 6	8.333 904 465 350
12	18	−3.717 092 593 788 5	8.333 904 678 183
12	24	−3.717 092 593 920 9	8.333 904 686 599
12	30	−3.717 092 593 932 9	8.333 904 687 440
<hr/>			
12	36	−3.717 092 593 934 6	8.333 904 687 547
<hr/>			
28	36	−3.717 093 236 000 2	8.335 180 574 435
40	36	−3.717 093 288 608 1	8.335 245 600 693
50	36	−3.717 093 302 610 3	8.335 261 797 875
60	36	−3.717 093 308 887 9	8.335 268 874 497
70	36	−3.717 093 312 101 5	8.335 272 444 815
80	36	−3.717 093 313 911 2	8.335 274 437 152
100	36	−3.717 093 315 706 2	8.335 276 397 958
120	36	−3.717 093 316 498 0	8.335 277 258 259
<hr/>			
$j_{\max}$	$N_{el}$	$Q_{35}(R), 10^{-1}$	$H_{35}(R), 10^{-2}$
12	6	1.345 981 051 407 7	2.269 823 448 371
12	12	1.345 984 463 203 5	2.269 832 028 222
12	18	1.345 984 480 233 8	2.269 832 074 795
12	24	1.345 984 480 897 0	2.269 832 076 647
12	30	1.345 984 480 959 1	2.269 832 076 831
<hr/>			
12	36	1.345 984 480 970 4	2.269 832 076 853
<hr/>			
28	36	1.345 970 507 627 5	2.270 529 070 029
40	36	1.345 970 198 842 4	2.270 563 372 554
50	36	1.345 970 135 204 1	2.270 571 881 381
60	36	1.345 970 109 700 7	2.270 575 593 492
70	36	1.345 970 097 498 1	2.270 577 464 966
80	36	1.345 970 090 921 3	2.270 578 508 889
100	36	1.345 970 084 645 4	2.270 579 535 991
120	36	1.345 970 081 968 6	2.270 579 986 560

**Table 2**

Convergence of potential curve  $2R^{-2}(\varepsilon_{45}(R) + 1)$  and matrix elements  $Q_{4345}(R)$ ,  $H_{4345}(R)$ ,  $H_{4545}(R)$  at  $R = 7.65$  a.u. as a function of the maximum number of terms  $j_{\max}$ , numbers of finite elements  $N_{el}$  at their order  $p = 4$ .

$j_{\max}$	$N_{el}$	$2R^{-2}(\varepsilon_{45}(R) + 1)$	$H_{4545}(R), 10^{-3}$
28	6	4.879 922 636 381	1.034 074 714 010
28	12	4.878 939 387 221	1.037 535 372 894
28	18	4.878 936 678 011	1.037 544 063 945
28	24	4.878 936 575 214	1.037 544 380 393
28	30	4.878 936 565 567	1.037 544 409 101
<hr/>			
28	36	4.878 936 564 065	1.037 544 413 457
<hr/>			
40	36	4.878 929 789 512	1.036 946 196 503
50	36	4.878 928 117 456	1.036 806 107 806
60	36	4.878 927 388 168	1.036 746 299 243
70	36	4.878 927 020 395	1.036 716 518 763
80	36	4.878 926 815 186	1.036 700 039 417
100	36	4.878 926 613 217	1.036 683 940 956
120	36	4.878 926 524 598	1.036 676 926 529
<hr/>			
$j_{\max}$	$N_{el}$	$Q_{4345}(R), 10^{-3}$	$H_{4345}(R), 10^{-4}$
28	6	7.163 551 693 508	1.313 245 172 874
28	12	7.192 416 552 701	1.313 393 326 976
28	18	7.192 470 461 759	1.313 394 061 373
28	24	7.192 471 802 131	1.313 393 807 683
28	30	7.192 471 876 618	1.313 393 761 626
<hr/>			
28	36	7.192 471 882 307	1.313 393 751 746
<hr/>			
40	36	7.164 925 249 674	1.304 767 510 954
50	36	7.158 600 336 853	1.302 825 852 351
60	36	7.155 920 393 086	1.302 012 009 221
70	36	7.154 591 453 293	1.301 611 523 137
80	36	7.153 857 856 101	1.301 391 714 358
100	36	7.153 142 578 776	1.301 178 645 274
120	36	7.152 831 407 895	1.301 086 493 836

**Table 3**

The disk storage usage (DSU, KB) and the CPU time (min:s) scale with the number  $j_{\max}$  of Eqs. (9) and (12), the number  $n = N_{el}$  and order  $p$  of the finite-elements and the number  $N$  of eigensolutions, number of iterations NITEM, and minimal dimensions MTOT and MITOT of working arrays TOT and ITOT, respectively, and CPU time per iteration (TCPU) at the convergence tolerance on eigenvalues  $RTOL = 10^{-12}$  and the lower bound of lowest eigenvalue  $SHIFT = -1.1$ .

$j_{\max}$ NDIM	$n = N_{el}$ RMESH(2)	$p$ NPOL	$N$ NROOT	MTOT	MITOT	CPU (min:s)	DSU (KB)	NITEM	TCPU (s)
12	6	4	6	33 914	1 300	<0:01	912	45	<0.01
12	6	4	12	33 914	1 306	<0:01	3 304	52	<0.01
12	6	8	6	108 242	2 476	0:10	4 884	43	0.23
28	6	4	6	182 874	2 980	0:22	4 644	45	0.49
28	6	4	12	182 874	2 986	0:26	4 816	52	0.50
28	6	8	6	585 330	5 692	1:32	8 232	43	2.14
12	36	4	6	162 548	7 570	0:24	4 528	47	0.51
28	36	4	6	768 708	17 410	2:49	9 440	47	3.60
28	36	4	12	826 122	17 416	3:23	10 720	52	3.90

**Table 4**

Convergence of the ground state energy (in a.u.) for a Helium atom versus number  $N$  of basis functions and number  $j_{\max}$  of Legendre polynomials.

$N$	$j_{\max} = 12$ [7]	$j_{\max} = 12$	$j_{\max} = 21$	$j_{\max} = 28$
1	−2.887 911 68	−2.895 539 19	−2.895 551 19	−2.895 552 76
2	−2.891 379 91	−2.898 631 57	−2.898 643 21	−2.898 644 74
6	−2.903 004 48	−2.903 644 06	−2.903 655 96	−2.903 657 52
10	−2.903 636 13	−2.903 702 86	−2.903 714 79	−2.903 716 36
15	−2.903 705 49	−2.903 708 67	−2.903 720 60	−2.903 722 16
21	−2.903 722 64			−2.903 722 99
28	−2.903 722 66			
$N$	$j_{\max} = 35$	$j_{\max} = 40$	$j_{\max} = 45$	$j_{\max} = 50$
1	−2.895 553 32	−2.895 553 52	−2.895 553 63	−2.895 553 71
2	−2.898 645 28	−2.898 645 47	−2.898 645 58	−2.898 645 66
6	−2.903 658 08	−2.903 658 27	−2.903 658 39	−2.903 658 46
10	−2.903 716 91	−2.903 717 10	−2.903 717 22	−2.903 717 30
15	−2.903 722 72	−2.903 722 91	−2.903 723 03	−2.903 723 10
21	−2.903 723 54	−2.903 723 74	−2.903 723 85	−2.903 723 93
28	−2.903 723 55	−2.903 723 74	−2.903 723 85	−2.903 723 93
35		−2.903 723 91	−2.903 724 03	−2.903 724 10
40			−2.903 724 03	−2.903 724 10
45				−2.903 724 15
[5]				−2.903 722 99
[10]				−2.903 724 37

Table 3 shows the disk storage usage (DSU, in kilobytes) and the CPU time (in min:s) scale with the number  $j_{\max}$  of Eqs. (9) and (12), the number  $n = N_{el}$  and order  $p$  of the finite-elements and the number  $N$  of eigensolutions and minimal dimensions MTOT and MITOT of working arrays TOT and ITOT in the test run of calculations of matrix potentials with relative error tolerance  $\epsilon_2 = 10^{-12}$  in Intel Core i5 CPU 3.33 GHz, 4 GB RAM, Windows 7. One can see that the execution time linear dependent on the number of calculated solutions and quadratically dependent on the number of equations, or number of nodal points  $L + 1 = np + 1$  from (21), while disk storage usage slow depended on the number of calculated solutions and quadratically dependent on the number of equations, or number of nodal points  $L + 1 = np + 1$ . This follows from the fact that the main resources are expanded by solving the banded system of  $(N_{el} \cdot p + 1) \cdot j_{\max}$  linear algebraic equations (22) with the maximum half bandwidth  $(p + 1) \cdot j_{\max}$  and the number of arithmetic operations of the SSPACE subroutine specified in [24].

In the benchmark calculations the grids in  $R$  and  $\alpha$  have been chosen as follows:  $\Omega_R = \{0(200)10(200)30\}$  and  $\Omega_\alpha = \{0(150)\pi/2\}$ . Enclosed in parentheses are the numbers of finite elements of the order  $p = 4$  in each interval. The set of matrix elements including the eigenfunctions with number up to  $N = 45$  were calculated with an accuracy of an order of  $10^{-8}$ , using set of  $j_{\max} = 50$  Eqs. (9), (12) and the number of finite elements  $N_{el} = 150$ . The banded system of 30050 linear algebraic equations (22) with the maximum half bandwidth 250 has been solved with relative error tolerance  $\epsilon_2 = 10^{-12}$  at each value of hyperradius  $R$  belonging to the Gauss nodes of the grid  $\Omega_R$ . A convergence study of the ground and first excited state energies of a Helium atom with number  $N$  of radial equations (41) and number  $j_{\max}$  of Legendre polynomials are presented in Tables 4 and 5. One can see that the energy eigenvalues converge monotonically from above, with the  $N = 45, j_{\max} = 50$ —channel value being  $E_1 = -2.903 724 15$  a.u. and  $E_2 = -2.145 973 22$  a.u. Tables show that the obtained results agree with an accuracy of an order of  $10^{-6}$  at  $j_{\max} \sim N$  with variational estimations [10,11] and have a higher accuracy than the previous coupled-channel hyperspherical adiabatic calculations [5,7]. A similar accuracy can be achieved also in calculations of high excited states of a Helium atom, for which variational calculations were not applied, taking into account appropriate asymptotic behaviors of the matrix elements and solutions [5].

Thus, the calculation of parametric eigenvalues, eigenfunctions (parametric basis functions) and the matrix elements of the BVPs for Eqs. (9) and (12) with the help of the program POTHEA can be used for the numerical solution with the required accuracy of bound states and the scattering problem for the three dimensional equation of the Schrödinger type, including long-range potentials of the Coulomb type or for various three-dimensional elliptic equations in partial derivatives, with the help of the programs KANTBP [21,22]. The generalization of the algorithm for solving a system of parametric coupled 2D BVPs in the framework of the projection method and FEM, which can be applied for solving multidimensional boundary value problems for equations of Schrödinger type, will be given in further papers.

**Table 5**

Convergence of the first excited state energy (in a.u.) of a Helium atom versus number  $N$  of basis functions and number  $J_{\max}$  of Legendre polynomials.

$N$	$J_{\max} = 21$	$J_{\max} = 28$	$J_{\max} = 35$
1	−2.139 935 59	−2.139 935 68	−2.139 935 71
2	−2.141 664 27	−2.141 664 32	−2.141 664 34
6	−2.145 700 08	−2.145 700 17	−2.145 700 20
10	−2.145 914 95	−2.145 915 04	−2.145 915 07
15	−2.145 957 21	−2.145 957 30	−2.145 957 34
21		−2.145 968 71	−2.145 968 74
28			−2.145 970 24
$N$	$J_{\max} = 40$	$J_{\max} = 45$	$J_{\max} = 50$
1	−2.139 935 72	−2.139 935 72	−2.139 935 73
2	−2.141 664 35	−2.141 664 35	−2.141 664 36
6	−2.145 700 21	−2.145 700 21	−2.145 700 22
10	−2.145 915 09	−2.145 915 09	−2.145 915 10
15	−2.145 957 35	−2.145 957 36	−2.145 957 36
21	−2.145 968 76	−2.145 968 76	−2.145 968 77
28	−2.145 970 26	−2.145 970 26	−2.145 970 27
35	−2.145 972 10	−2.145 972 10	−2.145 972 11
40		−2.145 972 62	−2.145 972 63
45			−2.145 973 22
[5]			−2.145 956 97
[11]			−2.145 974 04

## 6. Test desk

Boundary value problems (9)–(16) for the problems considered in Section 5 and the corresponding matrix elements  $H_{ij}(z)$ ,  $Q_{ij}(z)$  at  $z = R = 7.65$  a.u. have been solved by the POTHEA program on grids  $\Omega_\alpha = \{0(150)\pi/2\}$  with input data MTOT = 700000, MITOT = 40000, NMESH = 3, MDIM = 12, NROOT = 6.

The following values of numerical parameters and characters have been used in the test run via the supplied input file POTHEA.INP

```
&PARAMS TITLE=' PARAMETRIC 2D DIFFERENTIAL EQUATION ',
      ICOUN=0,PARAM=7.65D0,NPOL=4,RTOL=1.D-12,
      NITEM=2000,SHIFT=-1.1D0,ICLK=1,IPRINT=1,IPRSTP=150,
      RMESH=0.0D0,150.D0,1.5707963267948966D0,
      NDIR=1, NDIL=12, NMDIL=0,IBOUND=4,
      FNOUT='POTHEA.LPR', IOUT=7,POTEN='POTHEA.PTN', IOUP=10,
      FMATR='POTHEA.MAT', IOUM=11,EVWFN='POTHEA.WFN', IOUF=1
&END
```

All calculation details of this problem were written into file POTHEA.LPR.

## Test run output

```
PROBLEM:  PARAMETRIC 2D DIFFERENTIAL EQUATION
*****
```

### CONTROL INFORMATION

```
NUMBER OF DIFFERENTIAL EQUATIONS. . . . (MDIM ) =    12
NUMBER OF ENERGY LEVELS REQUIRED. . . . (NROOT ) =     6
NUMBER OF FINITE ELEMENTS . . . . . (NELEM ) =   150
NUMBER OF GRID POINTS . . . . . (NGRID ) =   601
ORDER OF SHAPE FUNCTIONS . . . . . (NPOL ) =     4
ORDER OF GAUSS-LEGENDRE QUADRATURE . . . (NGQ ) =     5
NUMBER OF SUBSPACE ITERATION VECTORS. . . (NC ) =    12
BOUNDARY CONDITION CODE . . . . . (IBOUND) =     4
SHIFT OF EIGENVALUE . . . . . (SHIFT ) =  -1.10000
CONVERGENCE TOLERANCE . . . . . (RTOL ) =  0.100000E-11
VALUE OF PARAMETER. . . . . (PARAM ) =   7.65000
```

```
SUBDIVISION OF RHO-REGION ON THE FINITE-ELEMENT GROUPS:
*****
```

NO OF GROUP	NUMBER OF ELEMENTS	BEGIN OF INTERVAL	LENGTH OF ELEMENT	GRID STEP	END OF INTERVAL
1	150	0.000	0.01047	0.00262	1.571

### TOTAL SYSTEM DATA

```
TOTAL NUMBER OF ALGEBRAIC EQUATIONS. . . . (NN ) =   7212
```

TOTAL NUMBER OF MATRIX ELEMENTS. . . . . (NWK) = 262878  
 MAXIMUM HALF BANDWIDTH . . . . . (MK) = 60  
 MEAN HALF BANDWIDTH . . . . . (MMK) = 36

NDIM, MDIM= 12 12

THERE ARE 0 ROOTS LOWER THEN SHIFT  
 CONVERGENCE REACHED FOR RTOL 0.1000E-11  
 I T E R A T I O N N U M B E R 44  
 RELATIVE TOLERANCE REACHED ON EIGENVALUES  
 0.2098E-16 0.3975E-14 0.0000E+00 0.4782E-14 0.4128E-13 0.1326E-11

\*\*\*\*\*

R O O T	N U M B E R	E I G E N V A L U E	D E R I V A T I V E
1		-63.49915325624646	-15.79613618944456
2		-21.45188690752900	-3.997431891553315
3		-19.08232583432120	-4.142711985674064
4		-13.37148062340640	-3.897824374402062
5		-11.87667756641220	-3.314347679213019
6		-8.897683985407177	-2.705544197968186

\*\*\*\*\*

THERE ARE 0 ROOTS LOWER THEN SHIFT  
 THERE ARE 1 ROOTS LOWER THEN SHIFT  
 THERE ARE 2 ROOTS LOWER THEN SHIFT  
 THERE ARE 3 ROOTS LOWER THEN SHIFT  
 THERE ARE 4 ROOTS LOWER THEN SHIFT  
 THERE ARE 5 ROOTS LOWER THEN SHIFT

Y E I G E N F U N C T I O N

0.0000	0.4225D+02	-.1146D+02	-.5852D+01	0.1089D+02	-.8482D+01	0.4394D+01	0.9180D-10	-.2399D-09	0.4888D-09
	0.2768D-09	0.1720D-09	-.1439D-09	-.6736D-11	0.2973D-11	0.5036D-11	-.1174D-10	-.2842D-10	-.3904D-10
	0.2727D-12	-.1761D-12	-.1965D-12	0.1489D-12	-.1137D-11	-.3916D-11	0.1366D-13	-.2115D-13	0.7755D-13
	0.5347D-13	0.1374D-12	0.1232D-12	-.2101D-14	0.3412D-14	-.1335D-13	-.8508D-14	-.2067D-13	-.1439D-13
	-.2388D-16	0.3595D-16	-.1357D-15	-.8639D-16	-.1951D-15	-.1144D-15	-.1765D-18	0.2600D-18	-.9645D-18
	-.6132D-18	-.1328D-17	-.6915D-18	-.7617D-21	0.1631D-20	-.6517D-20	-.3980D-20	-.8757D-20	-.4118D-20
	0.5869D-20	-.1580D-20	-.8656D-21	0.1481D-20	-.1247D-20	0.5813D-21	-.4887D-21	0.1132D-21	0.1164D-21
	-.9199D-22	0.1245D-21	-.7810D-22	0.6556D-20	-.1781D-20	-.8977D-21	0.1695D-20	-.1310D-20	0.6762D-21
0.3927	0.2160D+01	0.1271D+01	0.6877D+00	-.1338D+01	0.1070D+01	-.5704D+00	-.2044D-01	-.1045D+01	0.2548D+01
	0.1532D+01	0.1190D+01	-.1095D+01	-.1775D-02	0.1345D-01	-.1037D+00	0.6894D-01	0.3425D+00	0.5857D+00
	-.2088D-03	0.7681D-03	-.5465D-02	-.3307D-02	-.1799D-01	-.5098D-01	-.2818D-04	0.7689D-04	-.5590D-03
	-.2652D-03	-.1055D-02	-.1178D-02	-.4119D-05	0.9523D-05	-.7068D-04	-.3121D-04	-.1139D-03	-.1026D-03
	-.6346D-06	0.1320D-05	-.9954D-05	-.4241D-05	-.1488D-04	-.1185D-04	-.1015D-06	0.1960D-06	-.1497D-05
	-.6242D-06	-.2141D-05	-.1573D-05	-.1668D-07	0.3052D-07	-.2355D-06	-.9670D-07	-.3271D-06	-.2268D-06
	-.2802D-08	0.4915D-08	-.3826D-07	-.1553D-07	-.5204D-07	-.3462D-07	-.4787D-09	0.8113D-09	-.6375D-08
	-.2563D-08	-.8532D-08	-.5517D-08	-.8298D-10	0.1363D-09	-.1086D-08	-.4317D-09	-.1434D-08	-.9172D-09
0.7854	0.1179D+00	0.1367D+01	0.6856D+00	-.6310D+00	0.4577D+00	-.1475D+00	-.3738D-02	-.6211D+00	0.1257D+01
	0.1603D+00	0.1082D+00	0.1203D+00	-.6788D-03	0.1087D-01	-.1608D+00	0.1644D+00	0.6513D+00	0.8656D+00
	-.1649D-03	0.4686D-03	-.1806D-01	-.6471D-02	-.6270D-01	-.2147D+00	-.4599D-04	-.3962D-05	-.3889D-02
	-.7313D-03	-.6981D-02	-.1269D-01	-.1391D-04	-.1774D-04	-.1030D-02	-.1468D-03	-.1507D-02	-.2559D-02
	-.4438D-05	-.8433D-05	-.3033D-03	-.3655D-04	-.4010D-03	-.6591D-03	-.1471D-05	-.3356D-05	-.9529D-04
	-.1023D-04	-.1185D-03	-.1912D-03	-.5018D-06	-.1274D-05	-.3128D-04	-.3079D-05	-.3734D-04	-.5954D-04
	-.1750D-06	-.4780D-06	-.1061D-04	-.9746D-06	-.1229D-04	-.1947D-04	-.6212D-07	-.1798D-06	-.3692D-05
	-.3195D-06	-.4176D-05	-.6612D-05	-.2242D-07	-.6897D-07	-.1318D-05	-.1071D-06	-.1458D-05	-.2333D-05
1.1781	0.7007D-02	0.8100D+00	0.3644D+00	0.5801D+00	-.5048D+00	0.3923D+00	-.4938D-03	-.3666D+00	0.5486D+00
	-.6731D+00	-.4216D+00	0.6695D+00	-.1391D-03	0.2280D-02	-.1611D+00	0.2277D+00	0.8125D+00	0.7350D+00
	-.5285D-04	-.1898D-02	-.2763D-01	-.3683D-02	-.8840D-01	-.4000D+00	-.2322D-04	-.1036D-02	-.9332D-02
	0.3469D-03	-.1163D-01	-.4553D-01	-.1112D-04	-.5255D-03	-.3917D-02	0.2819D-03	-.3332D-02	-.1578D-01
	-.5645D-05	-.2723D-03	-.1837D-02	0.1564D-03	-.1252D-02	-.6796D-02	-.2985D-05	-.1453D-03	-.9223D-03
	0.8450D-04	-.5423D-03	-.3253D-02	-.1628D-05	-.7968D-04	-.4853D-03	0.4629D-04	-.2565D-03	-.1662D-02
	-.9094D-06	-.4473D-04	-.2645D-03	0.2587D-04	-.1288D-03	-.8877D-03	-.5186D-06	-.2567D-04	-.1484D-03
	0.1478D-04	-.6753D-04	-.4915D-03	-.3017D-06	-.1510D-04	-.8567D-04	0.8667D-05	-.3669D-04	-.2818D-03
1.5708	0.9176D-03	0.6259D+00	0.2602D+00	0.9793D+00	-.8079D+00	0.5366D+00	-.1145D-03	-.2950D+00	0.3591D+00
	-.9164D+00	-.5359D+00	0.7541D+00	-.4206D-04	-.1909D-02	-.1584D+00	0.2483D+00	0.8699D+00	0.6095D+00
	-.2107D-04	-.3934D-02	-.3357D-01	-.1232D-02	-.8992D-01	-.5009D+00	-.1236D-04	-.2440D-02	-.1462D-01
	0.1618D-02	-.9916D-02	-.8229D-01	-.7982D-05	-.1559D-02	-.8108D-02	0.1056D-02	-.2184D-02	-.3913D-01
	-.5514D-05	-.1057D-02	-.5108D-02	0.6844D-03	-.4975D-03	-.2312D-01	-.4002D-05	-.7540D-03	-.3491D-02
	0.4685D-03	-.1856D-04	-.1527D-01	-.3019D-05	-.5609D-03	-.2526D-02	0.3376D-03	0.1279D-03	-.1083D-01
	-.2350D-05	-.4318D-03	-.1909D-02	0.2538D-03	0.1668D-03	-.8072D-02	-.1879D-05	-.3424D-03	-.1494D-02
	0.1976D-03	0.1685D-03	-.6258D-02	-.1540D-05	-.2789D-03	-.1205D-02	0.1588D-03	0.1579D-03	-.5017D-02

\*\*\*\*\*

Y I T S D E R I V A T I V E

0.0000	0.8305D+01	-.2738D+01	-.1640D+01	0.1796D+01	0.1835D+01	-.1058D+01	0.5306D-10	-.2102D-09	0.4085D-09
	0.1328D-09	0.1792D-09	-.8756D-10	-.3017D-11	0.1522D-11	0.2008D-11	-.7017D-12	-.1657D-10	-.2957D-10
	0.8393D-13	-.6855D-13	-.7260D-13	0.1507D-12	-.2009D-12	-.2170D-11	0.3195D-14	-.1136D-13	0.3155D-13

```

- .1263D-13 0.3545D-13 0.5915D-13 - .1406D-15 0.1364D-14 - .3612D-14 0.3114D-14 - .2829D-14 - .5907D-14
- .1706D-17 0.1424D-16 - .3737D-16 0.2961D-16 - .2961D-16 - .5321D-16 - .1129D-19 0.1021D-18 - .2678D-18
0.2034D-18 - .2123D-18 - .3506D-18 0.7434D-22 0.6358D-21 - .1816D-20 0.1376D-20 - .1411D-20 - .2250D-20
0.1892D-20 - .5748D-21 - .3445D-21 0.4499D-21 0.9614D-22 - .8764D-22 - .1564D-21 0.3667D-22 0.5103D-22
- .3386D-22 0.6352D-23 0.1102D-23 0.2102D-20 - .6472D-21 - .3621D-21 0.4883D-21 0.1247D-21 - .8050D-22
0.3927 - .4239D+00 0.5896D+00 0.3227D+00 - .4007D+00 - .9620D-01 0.7857D-01 0.5106D-02 - .2710D+00 0.4027D+00
- .4246D+00 0.2529D+00 0.2273D+00 0.4181D-03 0.4246D-02 - .3033D-02 - .4320D-01 0.1744D-01 0.1321D+00
0.4801D-04 0.2448D-03 - .6590D-03 0.2800D-02 0.1474D-02 - .1164D-01 0.6393D-05 0.2402D-04 - .7710D-04
0.1940D-03 0.2494D-04 - .2805D-03 0.9266D-06 0.2920D-05 - .1028D-04 0.2199D-04 0.7715D-06 - .2995D-04
0.1419D-06 0.3985D-06 - .1490D-05 0.2945D-05 - .2387D-07 - .3887D-05 0.2259D-07 0.5849D-07 - .2281D-06
0.4304D-06 - .1410D-07 - .5570D-06 0.3701D-08 0.9020D-08 - .3631D-07 0.6644D-07 - .3207D-08 - .8481D-07
0.6200D-09 0.1442D-08 - .5947D-08 0.1065D-07 - .6203D-09 - .1347D-07 0.1057D-09 0.2371D-09 - .9952D-09
0.7854 - .1756D-08 - .1116D-09 - .2206D-08 0.1830D-10 0.3989D-10 - .1695D-09 0.2963D-09 - .1828D-10 - .3721D-09
- .6952D-01 0.6128D-01 0.4800D-01 0.1842D+00 - .3575D+00 0.1918D+00 0.2330D-02 - .2599D-01 - .7033D-01
- .2571D+00 - .1716D+00 0.1822D+00 0.4148D-03 0.2555D-02 0.2318D-01 - .1004D+00 - .5479D-02 0.1104D+00
0.9998D-04 0.3003D-03 0.1044D-02 0.1009D-01 0.1502D-01 - .2996D-01 0.2775D-04 0.5818D-04 0.1699D-03
0.1326D-02 0.1692D-02 - .1355D-02 0.8368D-05 0.1411D-04 0.3925D-04 0.2993D-03 0.3830D-03 - .3285D-03
0.2665D-05 0.3886D-05 0.1067D-04 0.8126D-04 0.1052D-03 - .9249D-04 0.8820D-06 0.1160D-05 0.3188D-05
0.2430D-04 0.3182D-04 - .2828D-04 0.3005D-06 0.3664D-06 0.1013D-05 0.7714D-05 0.1020D-04 0.1212D-05
0.1047D-06 0.1207D-06 0.3367D-06 0.2551D-05 0.3408D-05 - .3055D-05 0.3715D-07 0.4115D-07 0.1163D-06
0.8695D-06 0.1176D-05 - .1055D-05 0.1340D-07 0.1453D-07 0.4173D-07 0.3040D-06 0.4189D-06 - .3765D-06
1.1781 - .6916D-02 - .1518D+00 - .6089D-01 0.2452D+00 - .4112D-01 - .1678D-01 0.5018D-03 0.6124D-01 - .1586D+00
0.5692D-02 - .2692D+00 - .1913D-02 0.1398D-03 0.1977D-02 0.4953D-01 - .1470D+00 - .2836D-01 0.4991D-01
0.5284D-04 0.7475D-03 0.6593D-02 0.1287D-01 0.3672D-01 - .2801D-01 0.2314D-04 0.3105D-03 0.2165D-02
0.1784D-02 0.7251D-02 - .1142D-03 0.1106D-04 0.1433D-03 0.9018D-03 0.4870D-03 0.2678D-02 - .8333D-04
0.5603D-05 0.7094D-04 0.4218D-03 0.1728D-03 0.1186D-02 - .4117D-04 0.2959D-05 0.3687D-04 0.2115D-03
0.7080D-04 0.5771D-03 - .2083D-04 0.1612D-05 0.1986D-04 0.1112D-03 0.3180D-04 0.2977D-03 - .1112D-04
0.8997D-06 0.1101D-04 0.6058D-04 0.1522D-04 0.1601D-03 - .6317D-05 0.5128D-06 0.6251D-05 0.3393D-04
0.7619D-05 0.8904D-04 - .3912D-05 0.2982D-06 0.3634D-05 0.1951D-04 0.3945D-05 0.5114D-04 - .2802D-05
1.5708 - .1265D-02 - .1866D+00 - .7505D-01 0.1981D+00 0.1181D+00 - .1138D+00 0.1594D-03 0.7895D-01 - .1555D+00
0.1058D+00 - .2714D+00 - .7381D-01 0.5766D-04 0.2719D-02 0.6069D-01 - .1667D+00 - .3446D-01 0.3338D-01
0.2857D-04 0.1495D-02 0.1108D-01 0.1160D-01 0.4924D-01 - .1974D-01 0.1660D-04 0.8298D-03 0.4816D-02
0.7971D-03 0.1283D-01 0.3189D-02 0.1064D-04 0.5111D-03 0.2677D-02 - .1341D-03 0.6287D-02 0.1604D-02
0.7304D-05 0.3404D-03 0.1688D-02 - .2446D-03 0.3751D-02 0.9770D-03 0.5273D-05 0.2402D-03 0.1153D-02
- .2269D-03 0.2489D-02 0.6515D-03 0.3959D-05 0.1772D-03 0.8332D-03 - .1907D-03 0.1768D-02 0.4592D-03
0.3070D-05 0.1354D-03 0.6277D-03 - .1572D-03 0.1321D-02 0.3359D-03 0.2446D-05 0.1065D-03 0.4889D-03
- .1300D-03 0.1025D-02 0.2517D-03 0.1998D-05 0.8597D-04 0.3918D-03 - .1087D-03 0.8226D-03 0.1905D-03

```

\*\*\*\*\*

#### POTENTIAL MATRICES H(I,J) AND Q(I,J):

```

H-MATRIX AT THE PARAMETER = 7.65000
0.12918038D-01 -0.12641211D-01 -0.72935879D-02 0.37629284D-02 0.10519176D-01 -0.60042850D-02
-0.12641211D-01 0.38709965D-01 0.44935643D-02 -0.18998123D-01 -0.23783442D-01 0.53965043D-02
-0.72935879D-02 0.44935643D-02 0.32704926D-01 -0.25656399D-01 0.22698321D-01 0.11990754D-01
0.37629284D-02 -0.18998123D-01 -0.25656399D-01 0.81363937D-01 -0.96634404D-02 -0.23134677D-01
0.10519176D-01 -0.23783442D-01 0.22698321D-01 -0.96634404D-02 0.83339050D-01 -0.19487269D-01
-0.60042850D-02 0.53965043D-02 0.11990754D-01 -0.23134677D-01 -0.19487269D-01 0.27420033D-01

Q-MATRIX AT THE PARAMETER = 7.65000
0.12452392D-14 -0.58590434D-01 -0.28637352D-01 0.44221163D-01 -0.33622119D-01 0.16210177D-01
0.58590434D-01 -0.35605789D-15 -0.25023025D-01 -0.16578031D+00 0.60790898D-01 -0.17278669D-01
0.28637352D-01 0.25023025D-01 -0.14683108D-15 0.45842536D-01 0.13459845D+00 -0.89786331D-01
-0.44221163D-01 0.16578031D+00 -0.45842537D-01 -0.84056152D-15 -0.20292997D+00 0.15554966D-01
0.33622119D-01 -0.60790898D-01 -0.13459845D+00 0.20292996D+00 -0.85338623D-16 -0.11414279D+00
-0.16210176D-01 0.17278664D-01 0.89786338D-01 -0.15554922D-01 0.11414281D+00 0.66845182D-17

```

## Acknowledgments

A.A.G., O.C. and S.I.V. acknowledge financial support from RFBR Grant Nos. 14-01-00420 and 13-01-00668, and the JINR theme 05-6-1119-2014/2016 “Methods, Algorithms and Software for Modeling Physical Systems, Mathematical Processing and Analysis of Experimental Data”.

## References

- [1] J. Macek, J. Phys. B 1 (1968) 831–843.
- [2] J.E. Hornos, S.W. MacDowell, C.D. Caldwell, Phys. Rev. A 33 (1986) 2212–2224.
- [3] A.G. Abrashkevich, D.G. Abrashkevich, I.V. Puzynin, S.I. Vinitzky, J. Phys. B 24 (1991) 1615–1638.
- [4] A.G. Abrashkevich, D.G. Abrashkevich, M. Shapiro, Comput. Phys. Commun. 90 (1995) 311–339.
- [5] J.J. De Groote, M. Masili, J.E. Hornos, J. Phys. B 31 (1998) 4755–4764.
- [6] J.J. De Groote, M. Masili, J.E. Hornos, J. Phys. B 33 (2000) 2641–2652.
- [7] A.G. Abrashkevich, M.S. Kaschiev, S.I. Vinitzky, J. Comput. Phys. 163 (2000) 328–348.
- [8] A.G. Abrashkevich, I.V. Puzynin, S.I. Vinitzky, Comput. Phys. Commun. 125 (2000) 259–281.
- [9] D.I. Abramov, Phys. Atom. Nucl. 76 (2013) 196–207.
- [10] O. Chuluunbaatar, I.V. Puzynin, S.I. Vinitzky, J. Phys. B 34 (2001) L425–L432.
- [11] G.W.F. Drake, Z.-C. Van, Chem. Phys. Lett. 229 (1994) 486–490.
- [12] O. Chuluunbaatar, A.A. Gusev, V.P. Gerdt, V.A. Rostovtsev, S.I. Vinitzky, A.G. Abrashkevich, M.S. Kaschiev, V.V. Serov, Comput. Phys. Commun. 178 (2008) 301–330.
- [13] A.A. Gusev, O. Chuluunbaatar, S.I. Vinitzky, E.M. Kazaryan, H.A. Sarkisyan, J. Phys. Conf. Ser. 248 (2010) 012047–1–8.
- [14] A.A. Gusev, O. Chuluunbaatar, S.I. Vinitzky, K.G. Dvovyan, E.M. Kazaryan, H.A. Sarkisyan, V.L. Derbov, A.S. Klombotskaya, V.V. Serov, Phys. Atom. Nucl. 75 (2012) 1210–1226.
- [15] O. Chuluunbaatar, A.A. Gusev, V.L. Derbov, P.M. Krassovitskiy, S.I. Vinitzky, Phys. Atom. Nucl. 72 (2009) 768–778.
- [16] G.L. Goodwin, M.R.A. Shegelski, Phys. Rev. A 72 (2005) 042713–1–7.
- [17] U. Fano, Rep. Progr. Phys. 46 (1983) 97–165.

- [18] U. Fano, A.R.P. Rau, *Atomic Collisions and Spectra*, Academic Press, Florida, 1986.
- [19] L.V. Kantorovich, V.I. Krylov, *Approximate Methods of Higher Analysis*, Wiley, New York, 1964.
- [20] O. Chuluunbaatar, A.A. Gusev, S.I. Vinitsky, A.G. Abrashkevich, *Comput. Phys. Commun.* 180 (2009) 1358–1375.
- [21] O. Chuluunbaatar, A.A. Gusev, A.G. Abrashkevich, A. Amaya-Tapia, M.S. Kaschiev, S.Y. Larsen, S.I. Vinitsky, *Comput. Phys. Commun.* 177 (2007) 649–675.
- [22] O. Chuluunbaatar, A.A. Gusev, S.I. Vinitsky, A.G. Abrashkevich, *Comput. Phys. Commun.* 179 (2008) 685–693.
- [23] G. Strang, G.J. Fix, *An Analysis of the Finite Element Method*, Prentice-Hall, Englewood Cliffs, New York, 1973.
- [24] K.J. Bathe, *Finite Element Procedures in Engineering Analysis*, Prentice Hall, Englewood Cliffs, New York, 1982.
- [25] O. Chuluunbaatar, *The Scientific Doctoral Thesis*, JINR LIBRARY, Dubna, 2010.
- [26] W.H. Press, S.A. Teukolsky, W.T. Vetterling, B.P. Flannery, *Numerical Recipes: The Art of Scientific Computing*, Cambridge University Press, Cambridge, 1986.
- [27] M. Abramovits, I.A. Stegun, *Handbook of Mathematical Functions*, Dover, New York, 1972.







# KANTBP 3.0: New version of a program for computing energy levels, reflection and transmission matrices, and corresponding wave functions in the coupled-channel adiabatic approach<sup>☆</sup>



A.A. Gusev<sup>a</sup>, O. Chuluunbaatar<sup>a,b,\*</sup>, S.I. Vinitzky<sup>a</sup>, A.G. Abrashkevich<sup>c</sup>

<sup>a</sup> Joint Institute for Nuclear Research, Dubna, 141980 Moscow region, Russia

<sup>b</sup> National University of Mongolia, Ulaanbaatar, Mongolia

<sup>c</sup> IBM Toronto Lab, 8200 Warden Avenue, Markham, ON L6G 1C7, Canada

## ARTICLE INFO

### Article history:

Received 20 May 2014

Received in revised form

24 July 2014

Accepted 3 August 2014

Available online 11 August 2014

### Keywords:

Eigenvalue and multichannel scattering problems

Kantorovich method

Finite element method

R-matrix calculations

Multichannel adiabatic approximation

Ordinary differential equations

High-order accuracy approximations

## ABSTRACT

A FORTRAN program for calculating energy values, reflection and transmission matrices, and corresponding wave functions in a coupled-channel approximation of the adiabatic approach is presented. In this approach, a multidimensional Schrödinger equation is reduced to a system of the coupled second-order ordinary differential equations on a finite interval with the homogeneous boundary conditions of the third type at the left- and right-boundary points for continuous spectrum problem. The resulting system of these equations containing the potential matrix elements and first-derivative coupling terms is solved using high-order accuracy approximations of the finite element method. As a test desk, the program is applied to the calculation of the reflection and transmission matrices and corresponding wave functions for the two-dimensional problem with different barrier potentials.

### Program summary

*Program title:* KANTBP

*Catalogue identifier:* ADZH\_v3\_0

*Program summary URL:* [http://cpc.cs.qub.ac.uk/summaries/ADZH\\_v3\\_0.html](http://cpc.cs.qub.ac.uk/summaries/ADZH_v3_0.html)

*Program obtainable from:* CPC Program Library, Queen's University, Belfast, N. Ireland

*Licensing provisions:* Standard CPC licence, <http://cpc.cs.qub.ac.uk/licence/licence.html>

*No. of lines in distributed program, including test data, etc.:* 81813

*No. of bytes in distributed program, including test data, etc.:* 276779

*Distribution format:* tar.gz

*Programming language:* FORTRAN 90/95. Compilers: Intel Fortran 8.0+, GNU Fortran 95 4.4.5+.

*Computer:* Personal computer.

*Operating system:* Unix/Linux, Window.

*RAM:* Depends on

- (a) the number of differential equations
- (b) the number and order of finite elements
- (c) the number of longitudinal points
- (d) the number of eigensolutions required.

*Classification:* 2.7.

*Does the new version supersede the previous version?:* No

<sup>☆</sup> This paper and its associated computer program are available via the Computer Physics Communication homepage on ScienceDirect (<http://www.sciencedirect.com/science/journal/00104655>).

\* Corresponding author at: Joint Institute for Nuclear Research, Dubna, 141980 Moscow region, Russia. Tel.: +7 4962162529; fax: +7 4962165084.

E-mail addresses: [gooseff@jinr.ru](mailto:gooseff@jinr.ru) (A.A. Gusev), [chuka@jinr.ru](mailto:chuka@jinr.ru) (O. Chuluunbaatar), [vinitky2008@gmail.com](mailto:vinitky2008@gmail.com) (S.I. Vinitzky), [aabrashk@ca.ibm.com](mailto:aabrashk@ca.ibm.com) (A.G. Abrashkevich).

*Catalogue identifier of previous version:* ADZH\_v2\_0

*Journal reference of previous version:* Comput. Phys. Comm. 179 (2008) 685

*Nature of problem:*

In the adiabatic approach [1], a multidimensional Schrödinger equation for quantum reflection [2], three-dimensional tunneling of a diatomic molecule incident upon a potential barrier [3], fission model of collision of heavy ions [4] or the photoionization of a hydrogen atom in magnetic field [5] is reduced by separating the longitudinal coordinate, labeled as  $z$ , from the transversal variables to a system of the second-order ordinary differential equations containing the potential matrix elements and first-derivative coupling terms. The purpose of this paper is to present the new version of the program based on the use of the finite element method of high-order accuracy approximations for calculating reflection and transmission matrices and wave functions for such systems of coupled differential equations on finite intervals of the variable  $z \in [z_{\min}, z_{\max}]$  with homogeneous boundary conditions of the third-type at the left- and right-boundary points following from the above scattering problems.

*Solution method:*

The boundary-value problems for the coupled second-order differential equations are solved by the finite element method using high-order accuracy approximations [6–8]. The generalized algebraic eigenvalue problem  $\mathbf{A}\mathbf{F} = E\mathbf{B}\mathbf{F}$  with respect to pair unknowns  $(E, \mathbf{F})$  arising after the replacement of the differential eigenvalue problem by the finite-element approximation is solved by the subspace iteration method [6]. The generalized algebraic eigenvalue problem  $(\mathbf{A} - E\mathbf{B})\mathbf{F} = \mathbf{D}\mathbf{F}$  with respect to pair unknowns  $(\mathbf{D}, \mathbf{F})$  arising after the corresponding replacement of the scattering boundary problem in open channels at fixed energy value,  $E$ , is solved by the  $\mathbf{L}\mathbf{D}\mathbf{L}^T$  factorization of symmetric matrix and back-substitution methods [6].

*Reasons for new version:*

The previous versions of KANTBP were intended only to calculate the energy levels, reaction matrix and radial wave functions of the bound state problem and scattering problem in the coupled-channel hyperspherical adiabatic approach, in which original problems were reduced to a set of coupled-channel second order differential equations with respect to radial variable in a semi-axis. However a wider range of physical scattering problems are reduced to a set of coupled-channel second order differential equations with respect to the longitudinal variable on the whole axis. In this case one needs to formulate the third-type boundary conditions for systems of coupled differential equations on a finite interval and calculate a desirable scattering matrix which is expressed via unknown reflection and transmission amplitude matrices of asymptotes of solutions in the open channels. The purpose of this new version is to provide a program for calculating the reflection and transmission amplitude matrices and corresponding wave functions of the continuous spectrum problem thus covering a wider range of physical scattering problems.

*Summary of revisions:*

The KANTBP 3.0 extends the framework of the previous versions, KANTBP 1.0 and KANTBP 2.0. It calculates the reflection and transmission amplitude matrices and corresponding wave functions of the continuous spectrum for systems of coupled differential equations on finite intervals of the variable  $z \in [z_{\min}, z_{\max}]$  using a general homogeneous boundary condition of the third-type at  $z = z_{\min} < 0$  and  $z = z_{\max} > 0$ . The third-type boundary conditions are formulated for the continuous problems under consideration by using known asymptotes for a set of linear independent asymptotic regular and irregular solutions in the open channels and a set of linear independent regular asymptotic solutions in the closed channels, respectively. The program is applied to the computation of the penetration coefficient for 2D-model of pair particles connected by the oscillator interaction potential (throughout symmetric or nonsymmetric) as well as the Coulomb-like barriers.

*Restrictions:*

The computer memory requirements depend on:

- (a) the number of differential equations
- (b) the number and order of finite elements
- (c) the total number of longitudinal points
- (d) the number of eigensolutions required.

The user must supply subroutine POTCAL for evaluating potential matrix elements. The user should also supply subroutine ASYMEV (when solving the eigenvalue problem) or ASYMSL and ASYMSR (when solving the scattering problem) which evaluate asymptotics of the wave functions at boundary points in case of a boundary condition of the third-type for the above problems.

*Running time:*

The running time depends critically upon:

- (a) the number of differential equations
- (b) the number and order of finite elements
- (c) the total number of longitudinal points on interval  $[z_{\min}, z_{\max}]$
- (d) the number of eigensolutions required.

As a test desk, the program is applied to the calculation of the reflection and transmission matrices and corresponding wave functions of the boundary-value problem for a set of  $N$  coupled-channel ordinary second order differential equations which follows from the two-dimensional problem describing a quantum tunneling of two particles  $i = 1, 2$  with masses  $m_i$  and effective charges  $Z_i$ , interacted by a harmonic oscillator potential through the repulsive Coulomb-like barrier potential  $U_i(x_i) = Z_i(x_i^s + \bar{x}_{\min}^s)^{-1/s}$  [8]. The following values of parameters were used:  $m_1 = 1$ ,  $m_2 = 3$ ,  $\bar{x}_{\min} = 0.1$ ,  $Z_1 = Z_2 = 0.1$ ,

$s = 8$ ,  $N = 4$ . The test run took 25 s with calculation of matrix potentials on the Intel Core i5 CPU 3.33 GHz, 4 GB RAM, Windows 7. This test run requires 5 MB of disk storage. The program KANTBP was tested on the JINR Central Information and Computer Complex.

The work was supported partially by RFBR Grants Nos. 14-01-00420 and 13-01-00668 and the JINR theme 05-6-1119-2014/2016 “Methods, Algorithms and Software for Modeling Physical Systems, Mathematical Processing and Analysis of Experimental Data”.

*References:*

- [1] M. Born, Festschrift Goett. Nach. Math. Phys. K1 (1951) 1–6.
- [2] H. Friedrich, Theoretical Atomic Physics, third ed., Springer, Berlin, 2006, p. 416.
- [3] G.L. Goodvin, M.R.A. Shegelski, Phys. Rev. A 72 (2005) 042713–1–7.
- [4] P. Ring, H. Massmann, J.O. Rasmussen, Nuclear Phys. A 296 (1978) 50–76.
- [5] A. Alijah, J. Hinze, J.T. Broad, J. Phys. B 23 (1990) 45–60.
- [6] K.J. Bathe, Finite Element Procedures in Engineering Analysis, Englewood Cliffs, Prentice Hall, New York, 1982.
- [7] O. Chuluunbaatar, A.A. Gusev, A.G. Abrashkevich, A. Amaya-Tapia, M.S. Kaschiev, S.Y. Larsen, S.I. Vinitsky, Comput. Phys. Comm. 177 (2007) 649–675.
- [8] A.A. Gusev, S.I. Vinitsky, O. Chuluunbaatar, V.P. Gerdt, V.A. Rostovtsev, Lect. Notes Comput. Sci. 6885 (2011) 175–191.



## ELEMENTARY PARTICLES AND FIELDS

### Theory

# Adiabatic Approach to the Problem of a Quantum Well with a Hydrogen-Like Impurity\*

A. A. Gusev<sup>1)\*\*</sup>, O. Chuluunbaatar<sup>1)</sup>, S. I. Vinitzky<sup>1)\*\*\*</sup>, V. L. Derbov<sup>2)</sup>,  
E. M. Kazaryan<sup>3),4)</sup>, A. A. Kostanyan<sup>3),4)</sup>, and H. A. Sarkisyan<sup>3),4)\*\*\*\*</sup>

Received April 17, 2009

**Abstract**—An adiabatic method is presented for solving a boundary discrete spectrum problem for a parabolic quantum well and a rectangular quantum well with infinitely-high walls in the presence of a hydrogen-like impurity. The upper and lower bounds for the energy of the ground state of the systems are obtained under the conditions of the shift of the Coulomb center in a given range of the parameter with respect to earlier variational estimates. The comparison of the rate of convergence of the adiabatic expansion of the solution in parametric bases in the cylindrical and spherical coordinates is carried out.

**DOI:** 10.1134/S1063778810020201

## 1. INTRODUCTION

In [1, 2] the optical absorption into the ground state of GaAs parabolic quantum well and rectangular quantum well with infinitely high walls in the presence of a hydrogen-like impurity was considered. The calculations of the ground state of these quantum wells were carried out using a single-parameter variational functions in the cylindrical coordinate system. The upper bounds of these energies were obtained depending on the shift of the Coulomb potential center. The analysis of more complex quantum-mechanical models leads to boundary problems in nonstandard domain of the configuration space with complex boundary, solved using multiparameter variational functions [3], finite-element method [4, 5], or by means of reducing the problem to ordinary differential equations following Kantorovich method [6], known in physics as the adiabatic approach of quantum-mechanical problems with slow and fast variables [7]. In the Kantorovich method the basis functions depend upon the slow variables as parameters and obey the boundary conditions that account for all specific features of the original problem, which provides the efficiency of the method for solving boundary problems in

a nonstandard domain, e.g., in a sector of a circle with mixed boundary conditions [7], as well as in the presence of singular potential against the background of confining potentials of the oscillator type with respect to some of the independent variables [8]. This determines the potentialities of using the method in the analysis of low-dimensional quantum-mechanical models of semiconductor nanostructures [9].

Here we present a scheme for solving the discrete-spectrum boundary problem for a parabolic quantum well and rectangular quantum well with infinitely high walls in the adiabatic representation in the cylindrical and spherical coordinates. The upper and lower bounds are obtained for the ground-state energies of the systems under the conditions of the shift of the Coulomb potential center in a given range of the parameter with respect to earlier variational estimates. It is shown that the rate of convergence of the solution expansion depends upon the choice of the adiabatic basis representation with the specific features of the problem taken into account.

## 2. ADIABATIC REPRESENTATION FOR A QUANTUM WELL IN THE CYLINDRICAL COORDINATES

For a quantum well the Schrödinger equation governing the discrete-spectrum wave function  $\psi(z, \rho, \phi) = \psi_{m_z}(z, \rho) \exp(im_z \phi) / \sqrt{2\pi}$  with the fixed magnetic quantum number  $m_z$  in the cylindrical coordinates  $(z, \rho, \phi) \in \mathbf{R}^3$  has the form [1]

$$\left[ -\frac{\hbar^2}{2m^*} \left( \frac{1}{\rho} \frac{\partial}{\partial \rho} \rho \frac{\partial}{\partial \rho} - \frac{m_z^2}{\rho^2} + \frac{\partial^2}{\partial z^2} \right) \right] \quad (1)$$

\*The text was submitted by the authors in English.

<sup>1)</sup>Joint Institute for Nuclear Research, Dubna, Russia.

<sup>2)</sup>Saratov State University, Russia.

<sup>3)</sup>Russian–Armenian (Slavonic) University, Yerevan, Armenia.

<sup>4)</sup>Yerevan State University, Armenia.

\*\*E-mail: [gooseff@jinr.ru](mailto:gooseff@jinr.ru)

\*\*\*E-mail: [vinitzky@theor.jinr.ru](mailto:vinitzky@theor.jinr.ru)

\*\*\*\*E-mail: [shayk@ysu.am](mailto:shayk@ysu.am)

# Symbolic-Numerical Algorithm for Generating Cluster Eigenfunctions: Tunneling of Clusters through Repulsive Barriers

Sergue Vinitzky<sup>1</sup>, Alexander Gusev<sup>1</sup>, Ochbadrakh Chuluunbaatar<sup>1</sup>,  
Vitaly Rostovtsev<sup>1</sup>, Luong Le Hai<sup>1,2</sup>,  
Vladimir Derbov<sup>3</sup>, and Pavel Krassovitskiy<sup>4</sup>

<sup>1</sup> Joint Institute for Nuclear Research, Dubna, Moscow Region, Russia  
vinitzky@theor.jinr.ru

<sup>2</sup> Belgorod State University, Belgorod, Russia

<sup>3</sup> Saratov State University, Saratov, Russia

<sup>4</sup> Institute of Nuclear Physics, Almaty, Kazakhstan

**Abstract.** A model for quantum tunnelling of a cluster comprising  $A$  identical particles, coupled by oscillator-type potential, through short-range repulsive potential barriers is introduced for the first time in the new symmetrized-coordinate representation and studied within the  $s$ -wave approximation. The symbolic-numerical algorithms for calculating the effective potentials of the close-coupling equations in terms of the cluster wave functions and the energy of the barrier quasistationary states are formulated and implemented using the Maple computer algebra system. The effect of quantum transparency, manifesting itself in nonmonotonic resonance-type dependence of the transmission coefficient upon the energy of the particles, the number of the particles  $A = 2, 3, 4$ , and their symmetry type, is analyzed. It is shown that the resonance behavior of the total transmission coefficient is due to the existence of barrier quasistationary states imbedded in the continuum.

## 1 Introduction

During a decade, the mechanism of quantum penetration of two bound particles through repulsive barriers [1] attracts attention from both theoretical and experimental viewpoints in relation with such problems as near-surface quantum diffusion of molecules [2–4], fragmentation in producing very neutron-rich light nuclei [5, 6], and heavy ion collisions through multidimensional barriers [7–14]. Within the general formulation of the scattering problem for ions having different masses, a benchmark model with long-range potentials was proposed in Refs. [15–17]. The generalization of the two-particle model over a quantum system of  $A$  identical particles is of great importance for the appropriate description of molecular and heavy-ion collisions. *The aim of this paper is to present the convenient formulation of the problem stated above and the calculation methods, algorithms, and programs for solving this problem.*

## Resonance tunnelling of clusters through repulsive barriers

This content has been downloaded from IOPscience. Please scroll down to see the full text.

2014 Phys. Scr. 89 054011

(<http://iopscience.iop.org/1402-4896/89/5/054011>)

View [the table of contents for this issue](#), or go to the [journal homepage](#) for more

### Download details:

This content was downloaded by: chuka

IP Address: 159.93.14.8

This content was downloaded on 30/04/2014 at 06:55

Please note that [terms and conditions apply](#).



# Resonance tunnelling of clusters through repulsive barriers

A A Gusev<sup>1</sup>, S I Vinitsky<sup>1</sup>, O Chuluunbaatar<sup>1</sup>, A Gózdź<sup>2</sup> and V L Derbov<sup>3</sup>

<sup>1</sup> Joint Institute for Nuclear Research, Dubna, Russia

<sup>2</sup> Institute of Physics, Maria Curie-Skłodowska University, Lublin, Poland

<sup>3</sup> Saratov State University, Saratov, Russia

E-mail: [gooseff@jinr.ru](mailto:gooseff@jinr.ru)

Received 1 November 2013, revised 22 November 2013

Accepted for publication 14 December 2013

Published 29 April 2014

## Abstract

Quantum tunnelling of a cluster comprised of several identical particles, coupled via an oscillator-type potential, through short-range repulsive barrier potentials is studied in the s-wave approximation of the symmetrized coordinate representation. A procedure is briefly described that allows the construction of states, symmetric or asymmetric with respect to permutations of  $A$  identical particles, from the harmonic oscillator basis functions expressed via the newly introduced symmetrized coordinates. In the coupled-channel approximation of the  $\mathcal{R}$ -matrix approach, the effect of quantum transparency is analysed; it manifests itself in non-monotonic resonance dependence of the transmission coefficient upon the energy of the particles, their number  $A = 3, 4$  and the symmetry types of their states. The total transmission coefficient is shown to demonstrate resonance behaviour with probability density growth in the vicinity of the potential energy local minima, which is a manifestation of the barrier quasi-stationary states, embedded in the continuum.

Keywords: quantum tunnelling, cluster, system of identical particles, permutation symmetry, transmission coefficient, quantum transparency, symmetrized coordinates

(Some figures may appear in colour only in the online journal)

## 1. Introduction

The mechanism of quantum penetration (tunnelling) of two bound particles through repulsive barriers is a subject of both theoretical and experimental interest in relation to such problems as those of near-surface quantum molecular diffusion, fragmentation in the production of neutron-rich light nuclei, and heavy ion collisions through multidimensional barriers [1–6]. Generalization of the two-particle model over a quantum system of  $A > 2$  identical particles is urgently needed for an appropriate description of molecular and heavy ion collisions, as well as for the study of nuclei possessing tetrahedral and octahedral symmetry [7].

Here we consider the penetration of a cluster, consisting of  $A$  identical quantum particles, coupled via the short-range oscillator-type potential, through a repulsive potential barrier. We assume that the total spin of the cluster is fixed, so only

the coordinate wavefunction is to be considered, which may be symmetric (S) or antisymmetric (A) with respect to the permutation of  $A$  identical particles. The initial problem is shown to be reduced to that of the motion of a composite system, with the internal degrees of freedom describing an  $(A - 1)d$ -dimensional oscillator, and the external degrees of freedom describing the cluster centre-of-mass motion in the  $d$ -dimensional Euclidean space. For simplicity, we restrict our consideration to the so-called s-wave approximation, in which  $d = 1$ . The reduction is provided by using appropriately chosen symmetrized coordinates, rather than the conventional Jacobi coordinates. The advantage of the symmetrized coordinates over the Jacobi ones is that they provide invariance of the resulting Hamiltonian with respect to permutations of  $A$  identical particles. This, in turn, allows the construction of basis functions that are symmetric or antisymmetric under the

permutations not only of  $A - 1$  relative coordinates, but also of  $A$  Cartesian coordinates, i.e., of  $A$  real particles that form the cluster. Using this basis to expand the solution is referred to as adopting the symmetrized coordinate representation (SCR).

In the SCR we seek the solution in the form of Galerkin or Kantorovich expansions with unknown coefficients having the form of matrix functions of the centre-of-mass variables. Thus the initial problem is reduced to a boundary-value problem (BVP) for a system of coupled-channel equations in the centre-of-mass variable with conventional asymptotic boundary conditions. The solution procedure involves combined symbolic–numeric algorithms [8, 9]. The results are analysed with particular emphasis on the quantum transparency phenomenon, i.e., the non-monotonic energy dependence of the transmission coefficient, revealing the resonance nature of quantum tunnelling of clusters in S or A states.

## 2. The setting of the problem

Consider  $A$  identical quantum particles having mass  $m$  and the set of Cartesian coordinates  $x_i \in \mathbf{R}^d$  in the  $d$ -dimensional Euclidean space, forming a vector  $\tilde{\mathbf{x}} = (\tilde{x}_1, \dots, \tilde{x}_A) \in \mathbf{R}^{A \times d}$  in the  $A \times d$ -dimensional configuration space. The particles form a cluster due to the coupling via the pair potential  $\tilde{V}^{pair}(\tilde{x}_{ij})$  depending on the relative coordinates  $\tilde{x}_{ij} = \tilde{x}_i - \tilde{x}_j$  in a similar way to the potential of a harmonic oscillator  $\tilde{V}^{hosc}(\tilde{x}_{ij}) = \frac{m\omega^2}{2}(\tilde{x}_{ij})^2$  with the frequency  $\omega$ . The particles are considered to penetrate through the repulsive potential barrier  $\tilde{V}(\tilde{x}_i)$ . Adopting the dimensionless coordinates  $x_i = \tilde{x}_i/x_{osc}$ ,  $x_{ij} = \tilde{x}_{ij}/x_{osc} = x_i - x_j$  and energy  $E = \tilde{E}/E_{osc}$ ,  $V(x_i) = \tilde{V}(x_i x_{osc})/E_{osc}$ ,  $V^{hosc}(x_{ij}) = \tilde{V}^{hosc}(x_{ij} x_{osc})/E_{osc} = x_{ij}^2/A$ , using the oscillator units (osc.u.)  $x_{osc} = \sqrt{\hbar/(m\omega\sqrt{A})}$  and  $E_{osc} = \hbar\omega\sqrt{A}/2$ , one can write the appropriate Schrödinger equation as

$$\left[ -\frac{\partial^2}{\partial \mathbf{x}^2} + \sum_{i,j=1; i < j}^A \frac{(x_{ij})^2}{A} + U(\mathbf{x}) - E \right] \Psi(\mathbf{x}) = 0, \quad (1)$$

$$U(\mathbf{x}) = \sum_{i,j=1; i < j}^A U^{pair}(x_{ij}) + \sum_{i=1}^A V(x_i),$$

where  $U^{pair}(x_{ij}) = V^{pair}(x_{ij}) - V^{hosc}(x_{ij})$  is the non-oscillator part of the coupling potential, i.e., if  $V^{pair}(x_{ij}) = V^{hosc}(x_{ij})$ , then  $U^{pair}(x_{ij}) = 0$ ,  $\mathbf{x} = (x_1, \dots, x_A) \in \mathbf{R}^{A \times d}$ .

We seek for the solutions  $\Psi(\mathbf{x})$  of equation (1), totally symmetric or antisymmetric under the permutations of  $A$  particles that belong to the permutation group  $S_n$ . A permutation of particles is nothing but a permutation of the appropriate Cartesian coordinates  $x_i \leftrightarrow x_j$ ,  $i, j = 1, \dots, A$ .

The construction of states that retain the symmetry (antisymmetry) under the permutations of  $A$  initial Cartesian coordinates (below referred to as S (A) states) is most clearly

implemented using the symmetrized relative coordinates rather than the Jacobi ones. One of the possible definitions for the symmetrized coordinates is

$$\begin{pmatrix} \xi_0 \\ \xi_1 \\ \vdots \\ \xi_{A-1} \end{pmatrix} = \frac{1}{\sqrt{A}} \begin{pmatrix} 1 & 1 & 1 & \dots & 1 \\ 1 & a_1 & a_0 & \dots & a_0 \\ 1 & a_0 & a_1 & \dots & a_0 \\ \vdots & \vdots & \vdots & \ddots & \vdots \\ 1 & a_0 & a_0 & \dots & a_1 \end{pmatrix} \begin{pmatrix} x_1 \\ x_2 \\ \vdots \\ x_A \end{pmatrix}, \quad (2)$$

where  $a_0 = 1/(1 - \sqrt{A})$ ,  $a_1 = a_0 + \sqrt{A}$ . If  $A = 2$ , then the above symmetrized coordinates are similar to the symmetrized Jacobi coordinates of [10], while for  $A = 4$  they correspond to those of [11] (up to a normalizing factor).

With the relations  $a_1 - a_0 = \sqrt{A}$ ,  $a_0 - 1 = a_0\sqrt{A}$  taken into account, the relative coordinates  $x_{ij} \equiv x_i - x_j$  of a pair of particles  $i$  and  $j$  are expressed in terms of the internal  $A - 1$  symmetrized coordinates only:

$$x_{ij} \equiv x_i - x_j = \xi_{i-1} - \xi_{j-1} \equiv \xi_{i-1, j-1}, \quad (3)$$

$$x_{i1} \equiv x_i - x_1 = \xi_{i-1} + a_0 \sum_{i'=1}^{A-1} \xi_{i'}, \quad i, j = 2, \dots, A. \quad (4)$$

In the symmetrized coordinates, equation (1) takes the form

$$\left[ -\frac{\partial^2}{\partial \xi_0^2} - \frac{\partial^2}{\partial \xi^2} + \xi^2 + U(\xi_0, \xi) - E \right] \Psi(\xi_0, \xi) = 0,$$

$$U(\xi_0, \xi) = \sum_{i,j=1; i < j}^A U^{pair}(x_{ij}(\xi)) + \sum_{i=1}^A V(x_i(\xi_0, \xi)), \quad (5)$$

with  $\xi_0 \in \mathbf{R}^d$  and  $\xi = \{\xi_1, \dots, \xi_{A-1}\} \in \mathbf{R}^{(A-1) \times d}$ , which is invariant under the permutations  $\xi_i \leftrightarrow \xi_j$  with  $i, j = 1, \dots, A - 1$ , i.e., the invariance of equation (1) under the permutations  $x_i \leftrightarrow x_j$  with  $i, j = 1, \dots, A$  survives the symmetrizing coordinate transformation (2). This remarkable fact is one of the most prominent features of the proposed approach.

## 3. The symmetrized coordinate representation

We restrict ourselves to considering  $V^{pair}(x_{ij}) = V^{hosc}(x_{ij})$  in the s-wave approximation ( $d = 1$ ). We define the set of SCR cluster functions  $\langle \xi | j \rangle^{S(A)} \equiv \Phi_j^{S(A)}(\xi)$  and the corresponding energy eigenvalues  $\epsilon_j^{S(A)}$  as a solution of the BVP for the equation

$$\left( -\frac{\partial^2}{\partial \xi^2} + \xi^2 - \epsilon_j^{S(A)} \right) \Phi_j^{S(A)}(\xi) = 0. \quad (6)$$

The solution is sought for in the form of an expansion:

$$\Phi_j^{S(A)}(\xi) = \sum_{\{i_1, \dots, i_{A-1}\} \in \Delta_j} \alpha_{j[i_1, \dots, i_{A-1}]}^{S(A)} \Phi_{[i_1, \dots, i_{A-1}]}^{osc}(\xi). \quad (7)$$

Here the set  $\Delta_j \equiv \{i_1, \dots, i_{A-1}\}$  is defined by the condition

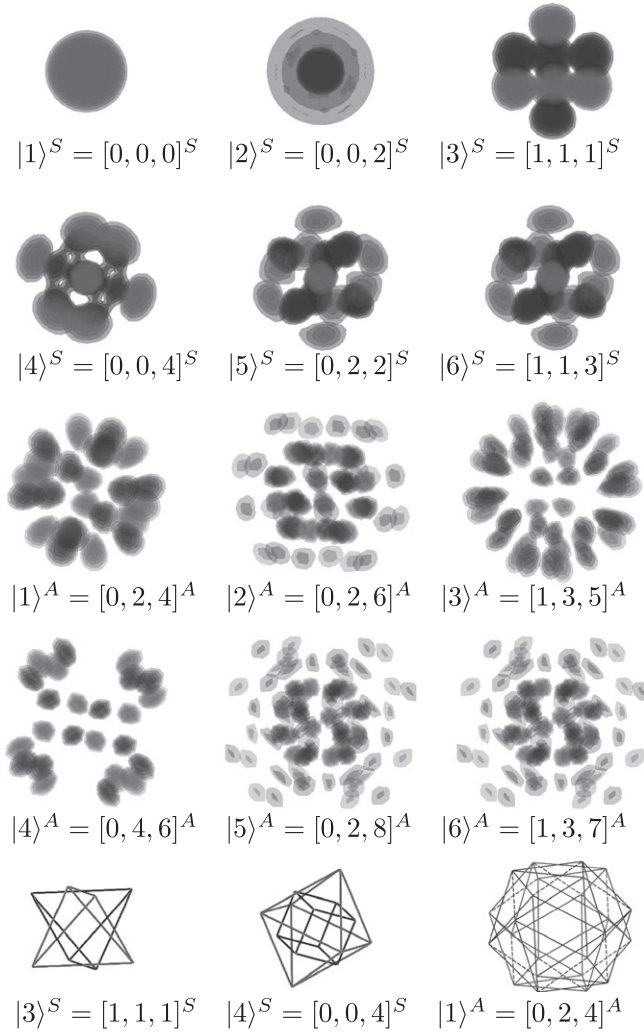


**Figure 1.** Profiles of the first six 3D oscillator eigenfunctions  $\langle \xi | j \rangle^{S(A)}$  symmetric and antisymmetric under a permutation of  $A = 4$  particles in the internal 3D space  $(\xi_1, \xi_2, \xi_3)$ . The vertices of the figures illustrate the positions of maxima (black) and minima (grey) for the eigenfunctions  $|3\rangle^S$ ,  $|4\rangle^S$ , and  $|1\rangle^A$ .

$\Delta_j = \left\{ i_1, \dots, i_{A-1} \mid \left( 2 \sum_{k=1}^{A-1} i_k + A - 1 \right) = \epsilon_j^{S(A)} \right\}$ , and  $\Phi_{[i_1, \dots, i_{A-1}]}^{osc}(\xi) = \prod_{k=1}^{A-1} \frac{\exp(-\xi_k^2/2) H_{i_k}(\xi_k)}{4/\pi \sqrt{2}^k \sqrt{i_k!}}$  is the eigenfunction, corresponding to the energy eigenvalue  $\epsilon_{[i_1, \dots, i_{A-1}]}^{osc} \equiv \epsilon_f^{osc} = 2f + A - 1$ ,  $f = \sum_{k=1}^{A-1} i_k$ , of the  $(A - 1)$ -dimensional oscillator. The energy levels are degenerate with the degeneracy multiplicity (DM)  $p = (A + f - 2)! / f! (A - 2)!$  [12]. The coefficients  $\alpha_j^{S(A)}$  of the orthonormal eigenfunctions  $\Phi_j^{S(A)}(\xi)$ , symmetric (S) (or antisymmetric (A)) under the permutations of  $A$  particles and the corresponding eigenvalues  $\epsilon_j^{S(A)}$  with the DM  $p^{S(A)} \ll p$  are calculated using the SCR algorithm [8] in two steps. First, the eigenfunctions symmetric (or antisymmetric) under the permutations of  $\xi_i$  (see equation (3)) are constructed in a standard way. These

eigenfunctions are symmetric (antisymmetric) under the permutation of  $A - 1$  particles. Second, the eigenfunctions symmetric (antisymmetric) under the permutation of a single pair  $x_i \leftrightarrow x_1$ , e.g.,  $x_2 \leftrightarrow x_1$  (see equation (4)), are constructed and orthonormalized using the Gram–Schmidt procedure.

In the particular case  $A = 3$ ,  $d = 1$ , the S (or A) functions can be expressed in polar coordinates  $\xi_1 = \rho \cos \varphi$ ,  $\xi_2 = \rho \sin \varphi$  as

$$\Phi_{k,m}^{S(A)}(\rho, \varphi, A = 3) = R_{km}(\rho) Y_m^{S(A)}(3m(\varphi + \pi/12)),$$

$$R_{km}(\rho) = \sqrt{2k!/(k+3m)!} (\rho^2)^{3m/2} e^{-\rho^2/2} L_k^{3m}(\rho^2),$$

where  $k = 0, 1, \dots$ , and  $L_k^{3m}(\rho^2)$  are the generalized Laguerre polynomials [13],  $Y_m^S(\varphi) = \cos(\varphi)/\sqrt{(1 + \delta_{m0})\pi}$ ,  $m = 0, 1, \dots$ , for S states, and  $Y_m^A(\varphi) = \sin(\varphi)/\sqrt{\pi}$ ,  $m = 1, 2, \dots$ , for A states, that are classified in terms of irreducible representations of the  $D_{3m}$  symmetry group. The corresponding energy levels  $\epsilon_{k,m}^{S(A)} = 2(2k + 3m + 1)$  have the DM  $p^{S(A)} = K + 1$  if the energy  $\epsilon_{k,m}^{S(A)} - \epsilon_{ground}^{S(A)} = 12K + K'$ , where  $K' = 0, 4, 6, 8, 10, 14$ ,  $\epsilon_{ground}^{S(A)} = 2$  and  $\epsilon_{ground}^A = 8$ .

For  $A = 4$ ,  $d = 1$ , the energy levels  $\epsilon_{i_1, i_2, i_3}^{S(A)} = 2(i_1 + i_2 + i_3 + 3/2)$  have the DM  $p^{S(A)} = 3K^2 + (3 + K')$   $K + K' + \delta_{0, K'}$  if the energy  $\epsilon_{i_1, i_2, i_3}^{S(A)} - \epsilon_{ground}^{S(A)} = 4(6K + K') + K''$ , where  $K' = 0, 1, 2, 3, 4, 5$ ,  $K'' = 0, 6$ ,  $\epsilon_{ground}^S = 3$ ,  $\epsilon_{ground}^A = 15$ . Here  $i_1 = 0, 1, \dots$ ,  $i_2 = i_1 + 2, \dots$ ,  $i_3 = i_2 + 2, \dots$  for S states and  $i_2 = i_1 + 2, i_1 + 4, \dots$ ,  $i_3 = i_2 + 2, i_2 + 4, \dots$  for A states. The S states with even values of the quantum numbers  $i_1, i_2, i_3$  and the A states with odd ones have the octahedral  $O_h$  symmetry, while the A states with even values of  $i_1, i_2, i_3$  and the S states with odd ones have the tetrahedral  $T_d$  symmetry. Figure 1 shows example profiles of S and A oscillator eigenfunctions for  $A = 4$ ,  $d = 1$ . Note that four maxima (black) and four minima (grey) of  $|3\rangle^S$  are positioned at the vertices of two tetrahedra forming a *stella octangula*. Eight maxima and six outer minima for  $|4\rangle^S$  are positioned at the vertices of a cube and an octahedron. The positions of twelve maxima of  $|1\rangle^A$  coincide with the vertices of a polyhedron with 20 triangle faces (only 8 of them being equilateral triangles) and 30 edges, 6 of them having the length 2.25 and the other having the length 2.66 (in oscillator units (osc.u.)).

#### 4. Coupled-channel equations in the SCR

We restrict our consideration to the so-called s-wave approximation ( $d = 1$ ). The asymptotic boundary conditions for the solution  $\Psi^{S(A)}(\xi_0, \xi) = \left\{ \Psi_{i_0}^{S(A)}(\xi_0, \xi) \right\}_{i_0=1}^{N_0}$ , describing the incident wave and outgoing waves at  $\xi_0^+ \rightarrow +\infty$  and

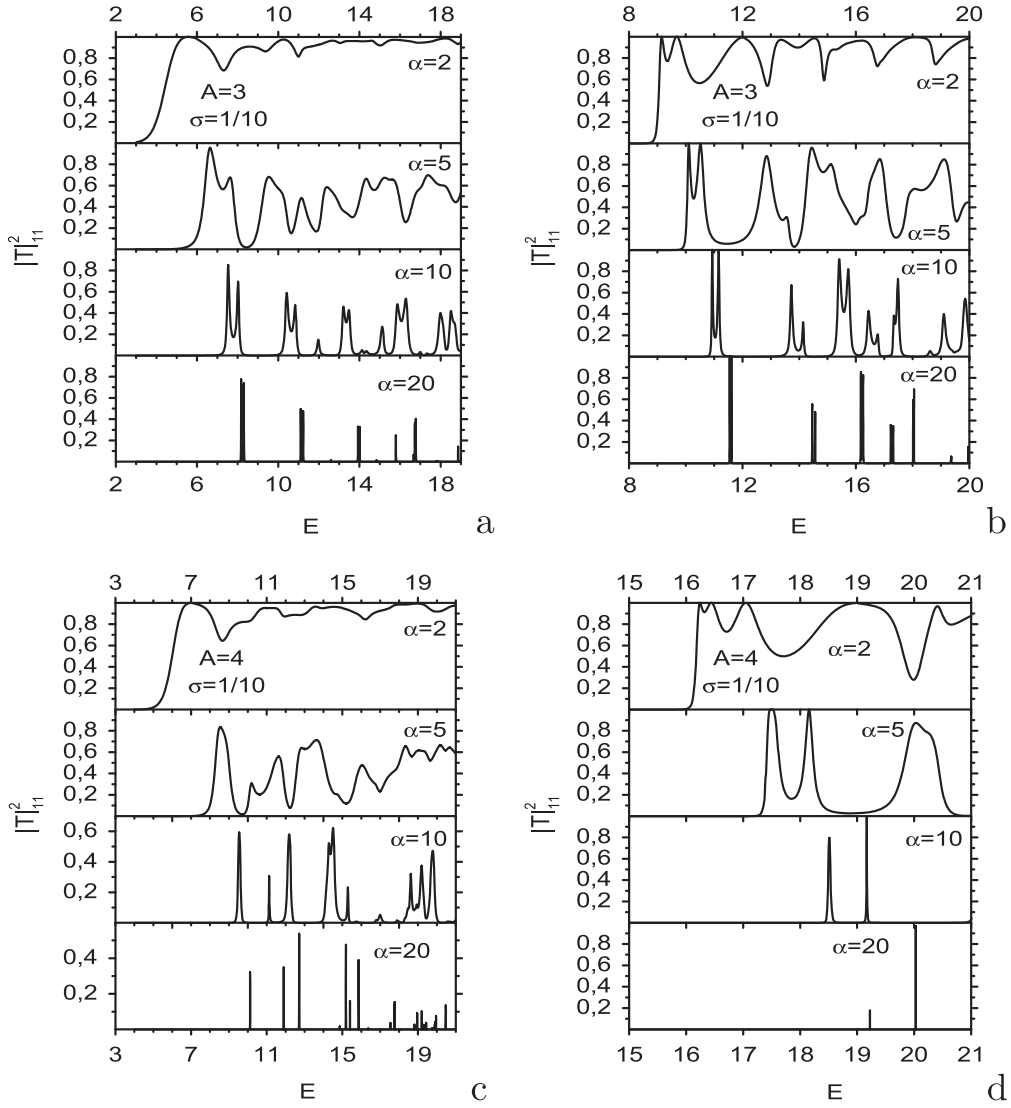


**Figure 2.** The total probabilities of transmission through the repulsive Gaussian barrier for the system of  $A = 3, 4$  particles, coupled by the oscillator potential and initially in the ground symmetric (left) or antisymmetric (right) state, versus the energy  $E$  (in osc.u.).

$\xi_0^- \rightarrow -\infty$ , can be written in the matrix form  $\Psi^{S(A)} = \Phi^{S(A)T} F$ , where

$$\begin{pmatrix} F_{\rightarrow}(\xi_0^+) & F_{\leftarrow}(\xi_0^+) \\ F_{\rightarrow}(\xi_0^-) & F_{\leftarrow}(\xi_0^-) \end{pmatrix} = \begin{pmatrix} \mathbf{0} & \mathbf{X}^{(-)}(\xi_0^+) \\ \mathbf{X}^{(+)}(\xi_0^-) & \mathbf{0} \end{pmatrix} + \begin{pmatrix} \mathbf{0} & \mathbf{X}^{(+)}(\xi_0^+) \\ \mathbf{X}^{(-)}(\xi_0^-) & \mathbf{0} \end{pmatrix} \mathbf{S}. \quad (8)$$

Here  $\mathbf{X}_{i_0}^{(\mp)}(\xi_0) = \frac{\exp(\mp i(p_{i_0}\xi_0))}{\sqrt{p_{i_0}}}$ ,  $v = \leftarrow, \rightarrow$  indicates the initial direction of the particle motion along the  $\xi_0$  axis, and  $N_0$  is the number of open channels with the fixed energy  $E$  and momentum  $p_{i_0}^2 = E - \epsilon_{i_0}^{S(A)} > 0$ . The quantities  $R_{j_0}^{\leftarrow} = R_{j_0}^{\leftarrow}(E)$ ,  $R_{j_0}^{\rightarrow} = R_{j_0}^{\rightarrow}(E)$ ,  $T_{j_0}^{\leftarrow} = T_{j_0}^{\leftarrow}(E)$ , and  $T_{j_0}^{\rightarrow} =$

$T_{j_0}^{\rightarrow}(E)$  are the unknown amplitudes of the reflected and transmitted waves.  $\mathbf{S}$  is the scattering matrix, which is unitary and symmetric [6]:

$$\mathbf{S} = \begin{pmatrix} \mathbf{R}_{\rightarrow} & \mathbf{T}_{\leftarrow} \\ \mathbf{T}_{\rightarrow} & \mathbf{R}_{\leftarrow} \end{pmatrix}, \quad \mathbf{S}^\dagger \mathbf{S} = \mathbf{S} \mathbf{S}^\dagger = \mathbf{I}. \quad (9)$$

Now we proceed to seek for the solution of the problem (5) in symmetrized coordinates in the form

$$\Psi_{i_0}^{S(A)}(\xi_0, \xi) = \sum_{j=1}^{j_{\max}} \Phi_j^{S(A)}(\xi) \chi_{j_0}^{S(A)}(\xi_0), \quad (10)$$

where  $\chi_{j_0}^{S(A)}(\xi_0)$  are the unknown functions and  $\Phi_j^{S(A)}(\xi)$  are the SCR cluster functions (7).

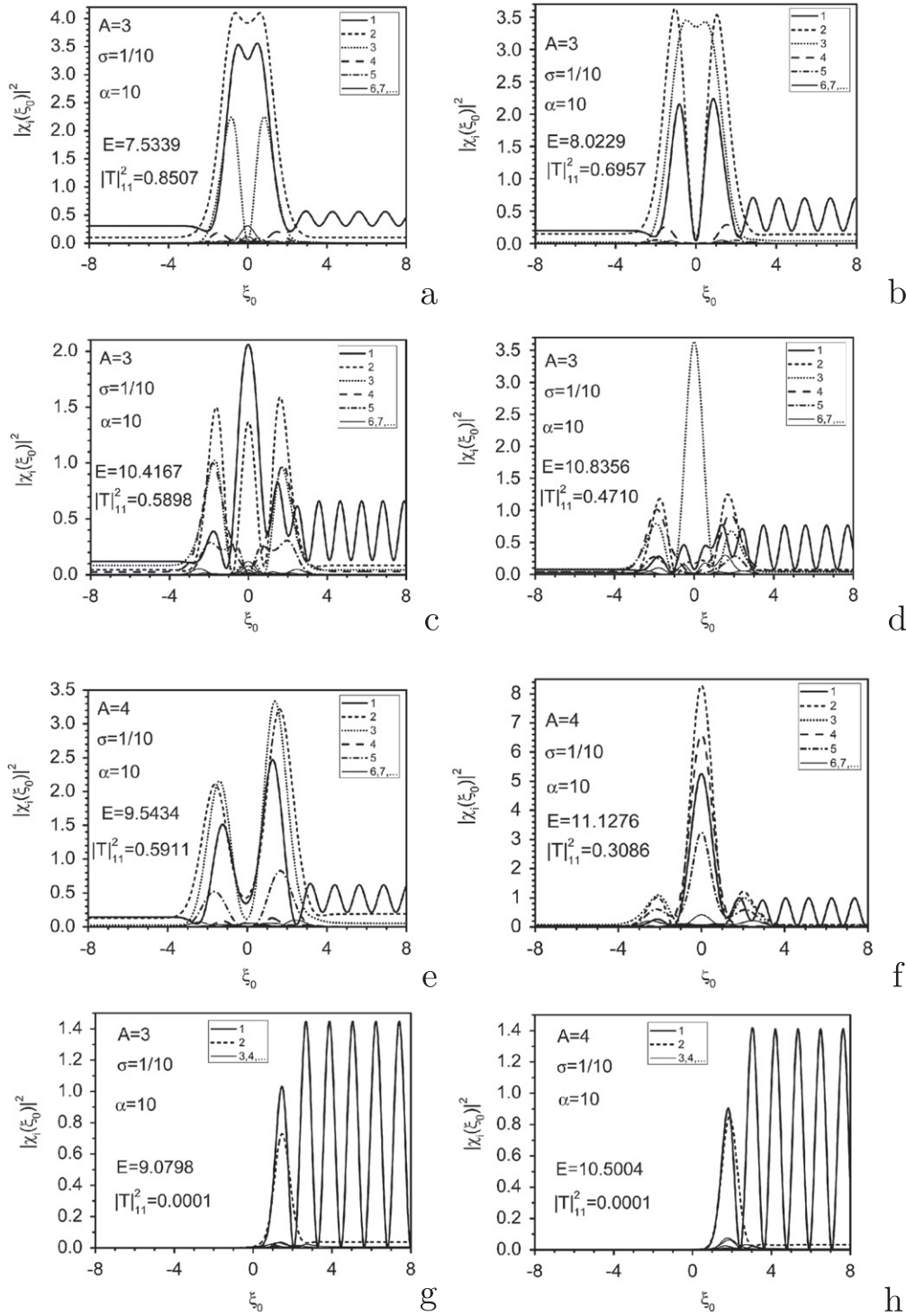


**Figure 3.** The probability densities  $|\chi_i(\xi_0)|^2$  for the coefficient functions of the decomposition (10), representing the incident wavefunction of the ground S state of the particles at the values of the collision energy  $E$  corresponding to individual maxima and minima of the transmission coefficient in figure 2. The parameters of the Gaussian barrier are  $\alpha = 10$  and  $\sigma = 0.1$ .

In the SCR the set of coupled-channel Galerkin-type equations in the centre-of-mass variable has the form

$$\sum_{j=1}^{j_{\max}} \left[ \left( -\frac{d^2}{d\xi_0^2} - p_i^2 \right) \delta_{ij} + V_{ij}^{S(A)}(\xi_0) \right] \chi_{j_{i_0}}^{S(A)}(\xi_0) = 0, \quad (11)$$

where  $V_{ij}^{S(A)}(\xi_0)$  are the effective potentials defined as

$$V_{ij}^{S(A)}(\xi_0) = \int d\xi \Phi_i^{S(A)}(\xi) \left( \sum_{k=1}^A V(x_k) \right) \Phi_j^{S(A)}(\xi). \quad (12)$$

The boundary conditions at  $\xi_0 = \xi_t$  and  $t = \min, \max$  have



**Table 1.** Comparison of the resonance energy values  $E_S$  and  $E_A$  (in osc.u.) for S and A states with the approximate eigenvalues  $E_i^D$ , for the first ten quasi-stationary states  $i = 1, \dots, 10$ , at  $A = 3, 4$  ( $\sigma = 1/10$ ,  $\alpha = 20$ ).

$i$	$A = 3$				$A = 4$			
	$E_S$		$E_A$		$E_i^D$	$E_S$	$E_i^{D31}$	$E_i^{D22}$
1	8.18	8.31			8.19	10.12	10.03	
2	11.11	11.23			11.09	11.89		11.76
3			11.55	11.61	11.52	12.71	12.60	
4	12.60				12.51	14.86	14.71	
5	13.93	14.00			13.86	15.19	15.04	
6			14.46	14.56	14.42	15.41		15.21
7	14.84	14.88			14.74	15.86		15.64
8	15.79				15.67	16.37	16.18	
9			16.18	16.25	16.11	17.54	17.34	
10	16.67	16.73			16.53	17.76	17.56	

the form

$$\left. \frac{dF(\xi_0)}{d\xi_0} \right|_{\xi_0=\xi_i} = \mathcal{R}(\xi_i) F(\xi_i). \quad (13)$$

Here  $\mathcal{R}(\xi)$  is an unknown  $j_{\max} \times j_{\max}$   $\mathcal{R}$ -matrix function and  $F(\xi_0) = \{\chi_{i_0}(\xi_0)\}_{i_0=1}^{N_0} = \{\{\chi_{j_0}(\xi_0)\}_{j_0=1}^{j_{\max}}\}_{i_0=1}^{N_0}$  is the required  $j_{\max} \times N_0$  ( $j_{\max} \geq N_0$ ) matrix solution of the BVP (11)–(13) with asymptotes (8)–(9).

## 5. Results

Consider the repulsive barrier  $V(x_i)$  in (12) described by the Gaussian potential  $V(x_i) = \frac{\alpha}{\sqrt{2\pi}\sigma} \exp(-\frac{x_i^2}{\sigma^2})$ . Figure 2 shows the energy dependence of the total transmission probability  $|T|_{ii}^2 = \sum_{j=1}^{N_0} |T_{ji}(E)|^2$ . This is the probability of a transition from a chosen state  $i$  into any of the  $N_0$  states, found from (8)–(9) by solving the BVP (11)–(13) [6]. For this purpose we solve the BVP at  $A = 3, 4$ :  $j_{\max} = 21, 39$  ( $j_{\max} = 16, 15$ ) for S (A) states with an accuracy of about four significant figures, using the KANTBP program [9] on the finite-element grid  $\Omega_\xi \{-\xi_0^{\max}, \xi_0^{\max}\}$ ,  $\xi_0^{\max} = 10.5, 12.8$ , with  $N_{\text{elem}} = 800, 976$  the fourth-order Lagrange elements between the nodes. Figure 2 illustrates the non-monotonic dependence of the transmission probability upon the energy; the observed resonances are manifestations of the quantum transparency effect. With the barrier height increasing, the peaks become narrower and their positions shift towards higher energies. The multiplet structures of the peaks are similar for symmetric and antisymmetric states.

The effect of quantum transparency, accompanied with the enhancement of the probability density in the vicinity of the potential energy local minima, is due to the existence of barrier quasi-stationary states, embedded in the continuum. Figure 3 shows that in the case of resonance transmission the wavefunctions, depending on the centre-of-mass variable  $\xi_0$ ,

are localized in the vicinity of the potential barrier centre ( $\xi_0 = 0$ ). The correspondence between the probability density distributions shown in figure 3 and the transmission probability features in figure 2 is the following: figures 3(a)–(d) correspond to the first four peaks in figure 2(a), the third panel from the top; figures 3(e), (f) correspond to the first two peaks in figure 2(c), the third panel from the top; figure 3(g) corresponds to the dip between the second and the third peaks in figure 2(a), the third panel from the top; figure 3(h) corresponds to the dip between the first and second peaks in figure 2(c), the third panel from the top.

Table 1 presents the resonance values of the energy  $E_S$  ( $E_A$ ) calculated by solving the BVP (11)–(13) for S (A) states at  $A = 3, 4$   $\sigma = 1/10$ ,  $\alpha = 20$ , which correspond to the maxima of the transmission coefficients  $|T|_{ii}^2$  in figure 2 for  $E < 18$ , and the corresponding approximate energy eigenvalues  $E_i^D$  of the quasi-stationary states of the BVP for equation (1), calculated using the Galerkin sets of 816, 1820 basis functions of the truncated  $A$ -dimensional oscillator at  $A = 3, 4$ , calculated by means of the DC algorithm [8]. The approximation of a narrow barrier with impermeable walls used in the DC algorithm is seen to provide a good approximation  $E_i^D$  of the above high-accuracy results  $E_S$  and  $E_A$ , with the error smaller than 2%.

When  $A = 3$  there are six similar wells, three of them on each side of the plane  $\xi_0 = 0$ . The symmetry with respect to the plane  $\xi_0 = 0$  explains the presence of doublets. The presence of states with definite symmetry is associated with the fact that the axis  $\xi_0$  is a third-order symmetry axis.

When  $A = 4$  there are 14 wells. Six wells in the centre correspond to the case where two particles are located on one side of the barrier and the other two are on the other side. The corresponding energy eigenvalue is denoted by  $E_i^{D22}$ . The remaining eight wells correspond to the case where one particle is located on one side of the barrier and the remaining three are on the other side. The corresponding energy eigenvalue is denoted by  $E_i^{D31}$ . For these states, one expects doublets to be observed, like for the case of three particles.

However, the separation between the energy levels is much smaller, because the four-well groups are strongly separated by two barriers, rather than only one barrier as for the case  $A = 3$ .

## 6. Conclusion

A cluster model consisting of  $A$  identical particles bound by an oscillator-type potential in the external field of a target was formulated in new symmetrized coordinates. Typical examples of clusters with  $A = 3$  and  $A = 4$  identical particles were analysed in the  $s$ -wave approximation, and the correspondence was revealed between the representations of the symmetry groups  $D_3$  for  $A = 3$  SCR cluster function shapes, and  $T_d$  and  $O_h$  for  $A = 4$  ones. We demonstrated the quantum transparency effect that manifests itself in a non-monotonic resonance-type dependence of the transmission coefficient upon the energy of the particles, their number  $A = 3, 4$ , and the symmetry types of their states. We found that this effect accompanies an enhancement of the probability density in the vicinity of local potential minima and is related to the existence of sub-barrier quasi-stationary states, embedded in the continuum.

The proposed approach can be adapted to analyse nuclei having tetrahedral and octahedral symmetry, the quantum diffusion of molecules and microscopic clusters through surfaces, and the fragmentation mechanism involved in the production of neutron-rich light nuclei.

## Acknowledgments

The work was supported by grants 13-602-02 JINR, 11-01-00523 and 14-01-00420 RFBR and the Bogoliubov–Infeld program.

## References

- [1] Hofmann H 1974 *Nucl. Phys. A* **224** 116
- [2] Ring R, Rasmussen J and Massman H 1976 *Sov. J. Part. Nucl.* **7** 916
- [3] Hagino K, Rowley N and Kruppa A T 1999 *Comput. Phys. Commun.* **123** 143
- [4] Pen'kov F M 2000 *JETP* **91** 698
- [5] Ahsan N and Volya A 2010 *Phys. Rev. C* **82** 064607
- [6] Gusev A *et al* 2011 *Lecture Notes in Computer Science* vol 6885 (Berlin: Springer) p 175
- [7] Dobrowolski A *et al* 2011 *Int. J. Mod. Phys. E* **20** 500
- [8] Gusev A *et al* 2013 *Lecture Notes in Computer Science* vol 8136 (Berlin: Springer) p 155  
Vinitisky S *et al* 2013 *Lecture Notes in Computer Science* vol 8136 (Berlin: Springer) p 427
- [9] Chuluunbaatar O *et al* 2008 *Comput. Phys. Commun.* **179** 685  
<http://www.info.jinr.ru/programs/jinrlib/kantbp/indexe.html>
- [10] Kamuntavičius G P *et al* 2001 *Nucl. Phys. A* **695** 191
- [11] Kramer P and Moshinsky M 1966 *Nucl. Phys.* **82** 241
- [12] Baker G A Jr 1956 *Phys. Rev.* **103** 1119
- [13] Abramowitz M and Stegun I A 1972 *Handbook of Mathematical Functions* (New York: Dover)

# Models of quantum tunneling of a diatomic molecule affected by laser pulses through repulsive barriers

S. Vinitzky<sup>a</sup>, A. Gusev<sup>a</sup>, O. Chuluunbaatar<sup>a</sup>, L.L. Hai<sup>a</sup>, V. Derbov<sup>b</sup>, P.M. Krassovitskiy<sup>c</sup>

<sup>a</sup>Joint Institute for Nuclear Research, 6 Joliot-Curie St., 141980, Dubna, Moscow region, Russia;

<sup>b</sup>Saratov State University, 83 Astrakhanskaya St., Saratov, 410012, Russia;

<sup>c</sup>Institute of Nuclear Physics, 1 Ibragimov St., Almaty, 050032, Kazakhstan.

## ABSTRACT

The model for quantum tunneling of a diatomic homonuclear molecule is formulated as a 2D boundary-value problem (2D BVP) for the Schrödinger equation with homogeneous boundary conditions of the third type. The molecule is considered as a pair of identical particles coupled via the effective potential. For short-range barrier potentials the Galerkin reduction to BVP for a set of closed-channel second-order ordinary differential equations (ODEs) is obtained by expanding the solution in a basis of transverse variable functions. Benchmark calculations of quantum tunneling through Gaussian barriers are presented for a pair of identical nuclei coupled by Morse potential. The results are compared with the direct numerical solution of the original 2D BVP obtained using the Numerov scheme. The effect of quantum transparency, i.e., the resonance behavior of the transmission coefficient versus the energy of the molecule, is shown to be a manifestation of the barrier metastable states, embedded in the continuum below the dissociation threshold, as well as quantum diffusion. The possibility of controlling the dynamics of atom-ion collisions by laser pulses is analyzed using a 1D BVP two-center model with Pöschl-Teller potentials.

**Keywords:** tunneling, interatomic potentials, diatomic molecules, quantum diffusion, laser pulses, time-dependent Schrödinger equation

## 1. INTRODUCTION

The study of tunneling coupled particles through repulsive barriers<sup>1</sup> has revealed the effect of resonance quantum transparency: when the cluster size is comparable with the spatial width of the barrier, there are mechanisms that lead to greater transparency of the barrier. These mechanisms are related to the formation of the barrier resonances, provided that the potential energy of the composite system has local minima giving rise to metastable states of the moving cluster.<sup>2</sup> Currently this effect and its possible applications are a subject of extensive study in relation with different quantum-physical problems, e.g., sub-barrier tunneling of light nuclei,<sup>3</sup> quantum diffusion of molecules,<sup>4</sup> exciton resonance passage through a quantum heterostructure barrier,<sup>5</sup> resonant formation of molecules from individual atoms,<sup>6</sup> controlling the direction of diffusion in solids,<sup>7</sup> and tunnelling of ions and clusters through repulsive barriers.<sup>8,9</sup> One more important problem is the possibility to control the tunneling of molecules by means of laser pulses, which can allow the enhancement of desired chemical reactions.<sup>10</sup> For the analysis of these effects it is useful to develop model approaches based on approximations, providing a realistic description of interactions between the atoms in the molecule, as well as with the barriers and/or external fields.

In this paper we formulate and study the model of a diatomic molecule with the nuclei coupled via the effective Morse potential, tunneling through a Gaussian repulsive barrier. We present the comparison of the close-coupling approximate results with those of the direct numerical solution of the original 2D BVP using the Numerov scheme below the dissociation threshold. The effect of quantum transparency, i.e., the resonance behavior of the transmission coefficient versus the energy of the molecule, as well as quantum diffusion are analyzed. Atom-ion collisions, as well as the dynamics of an ion in the field of a laser pulse, are studied on the base of a two-center model with Pöschl-Teller potentials.

---

Further author information: (Send correspondence to A.G.)

A.G.: E-mail: gooseff@jinr.ru

S.V.: E-mail: vinitzky@theor.jinr.ru



## 2. MODEL I. TRANSMISSION OF A DIATOMIC MOLECULE THROUGH A BARRIER

We consider a 2D model of two identical particles with mass  $m$ , coupled by pair interaction  $\tilde{V}(x_2 - x_1)$  and interacting with barrier potentials  $\tilde{V}_b(x_1)$  and  $\tilde{V}_b(x_2)$ . The relevant stationary Schrödinger equation for the wave function  $\Psi(x_1, x_2)$  in the s-wave approximation has the form:

$$\left( \frac{\hbar^2}{2m} \frac{\partial^2}{\partial x_1^2} - \frac{\hbar^2}{2m} \frac{\partial^2}{\partial x_2^2} + \tilde{V}(x_2 - x_1) + \tilde{V}_b(x_1) + \tilde{V}_b(x_2) - \tilde{E} \right) \Psi(x_1, x_2) = 0, \quad (1)$$

where  $\tilde{E}$  is total energy of the system and  $\hbar$  is Plank constant. Using the change of variables  $x = x_2 - x_1$ ,  $y = x_2 + x_1$ , we can rewrite Eq. (1) in the form

$$\left( -\frac{\hbar^2}{m} \frac{\partial^2}{\partial y^2} - \frac{\hbar^2}{m} \frac{\partial^2}{\partial x^2} + \tilde{V}(x) + \tilde{V}_b\left(\frac{x+y}{2}\right) + \tilde{V}_b\left(\frac{x-y}{2}\right) - \tilde{E} \right) \Psi(y, x) = 0. \quad (2)$$

The equation describing the molecular subsystem has the form

$$\left( -\frac{\hbar^2}{m} \frac{d^2}{dx^2} + \tilde{V}(x) - \tilde{\varepsilon} \right) \phi(x) = 0. \quad (3)$$

The molecular subsystem considered is assumed to possess the continuous energy spectrum with the eigenvalues  $\tilde{\varepsilon} \geq 0$  and eigenfunctions  $\phi_{\tilde{\varepsilon}}(x)$  and the discrete energy spectrum with the finite number  $n$  of bound states with the eigenfunctions  $\phi_j(x)$  and the eigenvalues  $\tilde{\varepsilon}_j = -|\tilde{\varepsilon}_j|$ ,  $j = 1, n$ .

The asymptotic boundary conditions imposed on the solution for the 2D model in the s-wave approximation  $\Psi(y, x) = \{\Psi_j(y, x)\}_{j=1}^{N_o}$  with the direction  $v \rightarrow$  can be written in the obvious form

$$\begin{aligned} \Psi_j(y \rightarrow -\infty, x) &\rightarrow \phi_j(x) \frac{\exp(ik_j y)}{\sqrt{k_j}} + \sum_{l=1}^{N_o} \phi_l(x) \frac{\exp(-ik_l y)}{\sqrt{k_l}} R_{lj}, \\ \Psi_j(y \rightarrow +\infty, x) &\rightarrow \sum_{l=1}^{N_o} \phi_l(x) \frac{\exp(ik_l y)}{\sqrt{k_l}} T_{lj}, \\ \Psi_j(y, x \rightarrow \pm\infty) &\rightarrow 0, \end{aligned} \quad (4)$$

where  $R_{lj}$  and  $T_{lj}$  are the reflection and transmission amplitudes,  $N_o$  is the number of open channels,  $k_i$  is the wave number,  $k_i = \sqrt{(m/\hbar^2)(\tilde{E} - \tilde{\varepsilon}_i)} > 0$ , below dissociation threshold  $\tilde{E} < 0$ ,  $\phi_i(x)$  and  $\varepsilon_i$  are the eigenfunctions and eigenvalues of the BVP for Eq. (3).

The solution of Eq. (2) is sought for in the form of Galerkin expansion

$$\Psi(y, r) = \sum_{j=1}^{j_{\max}} \phi_j(r) \chi_{ji_o}(y), \quad (5)$$

Here  $\chi_{ji_o}(y)$  are unknown functions and the orthonormalized basis functions  $\phi_j(r)$  in the interval  $0 \leq r \leq r_{\max}$  are defined as eigenfunctions of the BVP for the equation

$$\left( -\frac{d^2}{dr^2} + V(r) - \varepsilon_j \right) \phi_j(r) = 0, \quad \phi_j(0) = \phi_j(r_{\max}) = 0, \quad \int_0^{r_{\max}} dr \phi_i(r) \phi_j(r) = \delta_{ij}, \quad (6)$$

where  $V(r) = (m/\hbar^2)\tilde{V}(x)$ ,  $\varepsilon_j = (m/\hbar^2)\tilde{\varepsilon}_j$ . The desirable set of numerical solutions of this BVP is calculated with the given accuracy by means of the program ODPEVP.<sup>11</sup> Hence, we calculate the set of  $n$  bound states having the eigenfunctions  $\phi_j(x)$  and the eigenvalues  $\varepsilon_j$ ,  $j = 1, n$  and the desirable set of pseudostates with the eigenfunctions  $\phi_j(x)$  and the eigenvalues  $\varepsilon_j \geq 0$ ,  $j = n+1, j_{\max}$ . The latter approximate the set of continuum eigensolutions  $\varepsilon \geq 0$  of the BVP for Eq. (3).

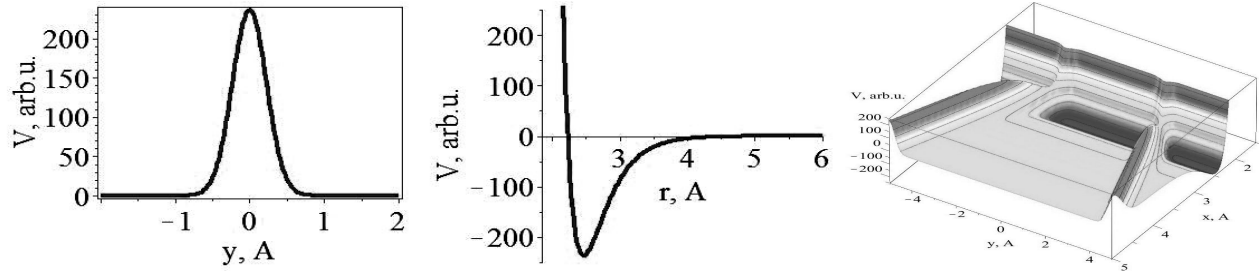


Figure 1. Gaussian-type barrier  $V_b(x_i) = \hat{D} \exp\left(-\frac{x_i^2}{2\sigma}\right)$ , at  $\hat{D} = 236.510003758401 \text{ \AA}^{-2} = (m/\hbar^2)\tilde{V}_0 = (m/\hbar^2)D$ ,  $\tilde{V}_0 = D = 1280\text{K}$ ,  $\sigma = 5.23 \cdot 10^{-2} \text{ \AA}^2$ , the two-particle interaction potential,  $V(r) = \hat{D}\{\exp[-2(r - \hat{r}_{eq})\hat{\rho}] - 2\exp[-(r - \hat{r}_{eq})\hat{\rho}]\}$ ,  $\hat{r}_{eq} = 2.47 \text{ \AA}$ ,  $\hat{\rho} = 2.96812423381643 \text{ \AA}^{-1}$  and the corresponding 2D potential.

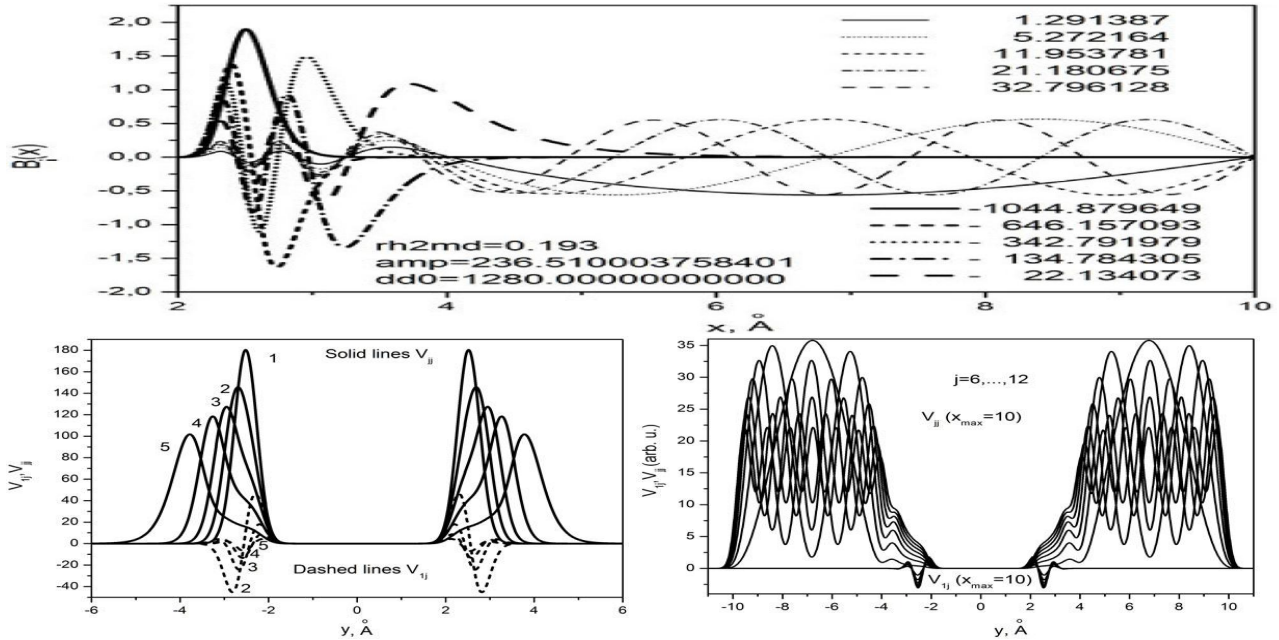


Figure 2. The wave functions  $\phi_j(r)$  of the bound states  $j = 1, 5$  (solid lines) and pseudostates  $j = 6, \dots, 15$  (dashed lines). The matrix elements  $V_{jj}(y)$  (solid lines) and  $V_{j1}(y)$  (dashed lines).

The set of closed-channel Galerkin equations has the form

$$\left[-\frac{d^2}{dy^2} + \varepsilon_i - E\right] \chi_{ii_o}(y) + \sum_{j=1}^{j_{\max}} V_{ij}(y) \chi_{ji_o}(y) = 0. \quad (7)$$

Thus, the scattering problem (2)–(3) with the asymptotic boundary conditions (4) is reduced to the boundary-value problem for the set of close-coupling equations in the Galerkin form (7) with the boundary conditions at  $y = y_{\min}$  and  $y = y_{\max}$  (from ref.<sup>9</sup>):

$$\left.\frac{d\mathbf{F}(y)}{dy}\right|_{y=y_{\min}} = \mathcal{R}(y_{\min})\mathbf{F}(y_{\min}), \quad \left.\frac{d\mathbf{F}(y)}{dy}\right|_{y=y_{\max}} = \mathcal{R}(y_{\max})\mathbf{F}(y_{\max}), \quad (8)$$

where  $\mathcal{R}(y)$  is an unknown  $j_{\max} \times j_{\max}$  matrix function,  $\mathbf{F}(y) = \{\chi_{ii_o}(y)\}_{i_o=1}^{N_o} = \{\{\chi_{ji_o}(y)\}_{j=1}^{j_{\max}}\}_{i_o=1}^{N_o}$  is the required  $j_{\max} \times N_o$  matrix solution, and  $N_o$  is the number of open channels,  $N_o = \max_{E \geq \varepsilon_j} j \leq j_{\max}$ , calculated using the third version of the program KANTBP.<sup>12</sup>

In Eq. (7) the effective potentials  $V_{ij}(y)$  are expressed by the integrals

$$V_{ij}(y) = \int_0^{r_{\max}} dr \phi_i(r) (V_b(\frac{r+y}{2}) + V_b(\frac{r-y}{2})) \phi_j(r). \quad (9)$$

For example let us take the parameters of the molecule  $\text{Be}_2$ , namely, the reduced mass  $\mu = m/2 = 4.506\text{Da}$ , the average distance between the atoms  $2.47\text{\AA}$ , the frequency of molecular vibrations expressed in temperature units  $\hbar\omega = 398.72\text{K}$ , the ground state of molecule  $^1\Sigma_u^+$ , the wave number of the order of  $277.124\text{cm}^{-1}$  for the observable excited-to-ground state transitions (we use relationship  $1\text{K} = 0.69503476\text{cm}^{-1}$  from<sup>13</sup>). These values were used to determine the parameters of the Morse potential

$$\tilde{V} = D\{\exp[-2(r - \hat{r}_{eq})\hat{\rho}] - 2\exp[-(r - \hat{r}_{eq})\hat{\rho}]\}, \quad (10)$$

where  $D$  is the depth of the interaction potential well and  $\hat{\rho}$  describes the width of the potential well. The values of  $D$  and  $\hat{\rho}$  are determined from the known spectrum

$$-\tilde{\varepsilon}_n = D \left[ 1 - \varsigma(n + 1/2) \right]^2. \quad (11)$$

Having the average size of the molecule and the separation between the energy levels taken into account, one can parametrize the molecular potential to fit the observable quantities, namely,  $D = 1280\text{K}$ ,  $\hat{r}_{eq} = 2.47\text{\AA}$ ,  $\hat{\rho} = 2.968\text{\AA}^{-1}$  is determined from the condition  $(\tilde{\varepsilon}_2 - \tilde{\varepsilon}_1)/(2\pi\hbar c) = 277.124\text{cm}^{-1}$ , at  $\varsigma = \frac{\hat{\rho}\hbar}{\sqrt{mD}} = 0.193$  is the dimensionless constant of the problem and  $\hat{D} = (\frac{\sqrt{mD}}{\hbar})^2 = (\hat{\rho}/0.193)^2 = (2.968\text{\AA}^{-1}/0.193)^2 = 236.5\text{\AA}^{-2}$ . In accordance with (11), the ground state energy of the molecule  $\text{Be}_2$  is equal to  $-\tilde{\varepsilon}_n = -1044.88\text{K}$ . Since the bond in the molecule  $\text{Be}_2$  is of the Van der Waals type, one can consider each constituent atom independently interacting with the external barrier potential. The latter should be chosen to have the height and the width typical for barriers in a real crystal lattice. Moreover, this potential should be a smooth function having the second derivative to apply high-accuracy numerical methods, like the Numerov method or the finite element method, for solving the BVP for the systems of second-order ordinary differential equations. Therefore, we choose the Gaussian repulsive barrier potential

$$\tilde{V}_b(x_i) = \tilde{V}_0 \exp\left(-\frac{x_i^2}{2\sigma}\right), \quad V_b(x_i) = \frac{m}{\hbar^2} \tilde{V}_b(x_i) = \hat{D} \exp\left(-\frac{x_i^2}{2\sigma}\right). \quad (12)$$

Here the parameters  $\tilde{V}_0 = 1280\text{K}$ ,  $\hat{D} = 236.510003758401\text{\AA}^{-2} = (m/\hbar^2)\tilde{V}_0$ ,  $\sigma = 5.23 \cdot 10^{-2}\text{\AA}^2$  are determined by the model requirement that the width of repulsive potential at the kinetic energy equal to that of the ground state is  $1\text{\AA}$ , so that the average distance  $2.47\text{\AA}$  between the atoms of Be is less than the distance  $2.56\text{\AA}$  between Cu atoms in the plane (111) of the crystal lattice cell. The potential barrier height  $\tilde{V}_0$  of the order of 200 meV was estimated following the experimental observation of quantum diffusion of hydrogen atoms.<sup>14</sup> Fig. 1 illustrates the Gaussian and Morse potentials, and the corresponding 2D potential. Fig. 2 presents the calculated eigenfunctions of the BVP (6) and the effective potentials  $V_{ij}(y)$  of Eq. (9), calculated using these functions. Note, that the wave functions  $\phi_j(r)$  and the eigenvalues  $\varepsilon_j(r)$  of the bound states  $j = 1, 5$  (solid lines) approximate the known analytical ones of the BVP for Eq. (3) with the Morse potential (10) with four and seven significant digits, respectively, the states being localized in the well, while the pseudostates  $j = 6, \dots, 15$  are approximated with the same accuracy and localized outside the well. The matrix elements between the bound states are localized in the vicinity of the barriers and the matrix elements between the pseudostates are localized beyond the barriers. The matrix elements between the bound states and pseudostates are small. The expansion of the desirable solution (5) over such orthogonal basis at ( $j_{\max} = 15$ ) with only ten closed channels taken into account allows the calculation of approximate solutions of the original 2D problem (2) at  $E < 0$  with the required accuracy of  $h^{p+1}$  for the eigenfunctions and  $h^{2p}$  for the eigenvalues with respect to the maximum step  $h$  of the finite-element grid,  $p$  being the order of approximation. The solutions of the BVPs (6)-(12) were performed on the finite-element grids  $\Omega_r = \{0(N_{elem} = 800)12\}$ , and  $\Omega_y = \{-12(N_{elem} = 120)12\}$ , respectively, with  $N_{elem}$  fourth-order Lagrange elements  $p = 4$  between the nodes, using the program KANTBP 3.0.<sup>15</sup>

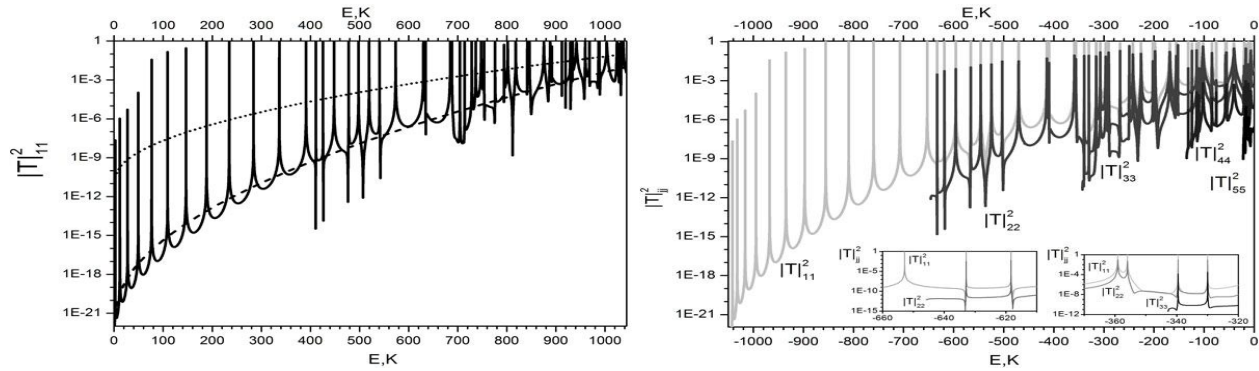


Figure 3. Left panel: Comparison of the total probability of penetration from the first channel to all five open channels simulated by the Galerkin expansion and Numerov calculations ; dotted and dashed curves are probabilities of penetration of one particle through one barrier and one particle through a sequence of two barriers, i.e., upper and lower average, respectively. Right panel: The total probability of penetration from the first channels with the energies  $E_1 = -1044.879649$ ,  $E_2 = -646.1570935$ ,  $E_3 = -342.7919791$ ,  $E_4 = -134.7843058$ ,  $E_5 = -22.13407384$  (in K) to all five open channels, simulated by the Galerkin expansion.

The left panel of Fig. 3 illustrates the comparison of the total probability of penetration from the first channel to all five open channels simulated by Galerkin expansion and Numerov calculations. One can see that the position of resonances calculated with accuracy of order of  $10^{-6}$  by the Galerkin expansion and Numerov procedure (at steps  $h_x = 0.05$ ,  $h_y = 0.05$  with accuracy  $< 10^{-3}$ ) are in good agreement, the difference in height is explained by the crudeness of the energy grid used in the latter case. Probabilities of penetration of one particle through one barrier, one particle through a sequence of two barriers, and one particles with double mass through one barrier give approximations of upper, lower and average estimations. In the right panel of Fig. 3 we show the resonance behavior of the total probability of penetration with the transition from the first channels with the energies  $E_1 = -1044.879649$ ,  $E_2 = -646.1570935$ ,  $E_3 = -342.7919791$ ,  $E_4 = -134.7843058$ ,  $E_5 = -22.13407384$  (in K) to all five open channels, simulated by the Galerkin expansion. The total transmission probability is seen to demonstrate the resonance behavior. Some peaks are high and narrow, and the position of peaks corresponding to transitions from different bound states are similar. As the energy of the initial excited state increases, the transmission peaks demonstrate a shift towards higher energies, the set of peak positions keeping approximately the same as for the transitions from the ground state and the peaks just replacing each other, like it was observed in the model calculations.<sup>16</sup> For example, the left epure shows that the positions of the 13th and 14th peaks for transitions from the first state coincide with the positions of the 1st and 2nd peaks for the transitions from the second state, while the right epure shows that the positions of the 25th and 26th peaks for transitions from the first state coincide with the positions of the 13th and 14th peaks for transitions from the second state and with the positions of the 1st and 2nd peaks for the transitions from the third state.

One can suppose that a better fit of the Morse potential to the observable upper part of the discrete spectrum of Be molecule, containing six more Val der Waals bound states, will increase the density of peaks near the dissociation threshold.<sup>17–20</sup> As one can see from right panels of Fig. 2, the diagonal potentials  $V_{jj}(y)$  have shapes of double barriers and nondiagonal matrix elements  $V_{ij}$  have size less then four time. It means that positions of peaks are real part of energy of the quasistationary states imbedded in continuum that are predominately localized between double barriers. It is confirmed by behavior of probability density of coefficient functions  $\chi_{ji_o}(y)$ . The examples from Fig. 4 shows that in the case of resonance transmission the wave functions, depending on the center-of-mass variable  $y$ , are localized in the vicinity of the potential barrier center ( $y = 0$ ), and in the case of total reflection the wave functions are localized at the barrier side, on which the wave is incident, and decrease to zero within the effective range of the barrier action. For the energy values, corresponding to some of the transmission coefficient peaks in Fig. 3 at within the effective range of barrier potential action the wave functions demonstrate considerable increase (till  $10^6$  times, see Fig. 4) of the probability density in comparison with the incident unit flux. This is a fingerprint of quasistationary states, which is not a quantitative definition, but a clear evidence in favour of their presence in the system.<sup>21,22</sup>

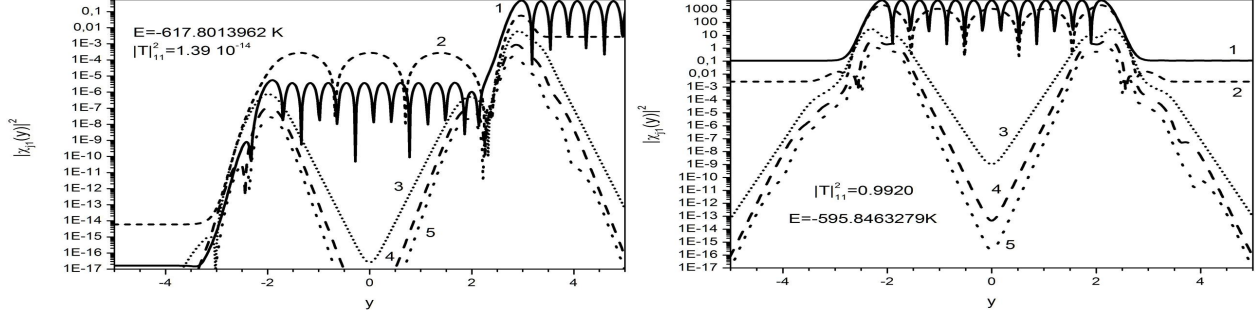


Figure 4. The examples of probability  $|\chi_{j1}(y)|^2$  of component of vector-functions in the case of total reflection (left) and resonance transmission (right).

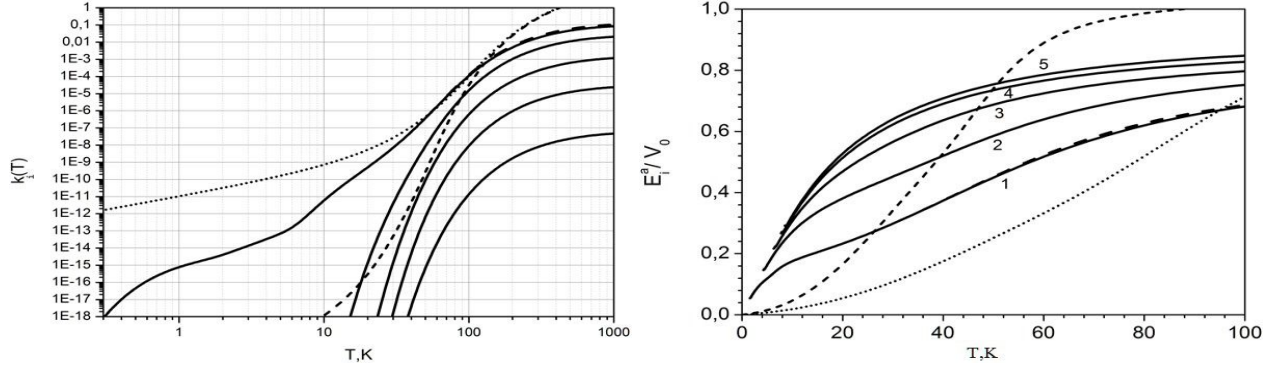


Figure 5. Left panel: Thermal rate constants vs. temperature: partial  $k_i(T)$  (solid curve) and total  $\hat{k}(T)$  (dashed lines) and their upper (dotted curves) and lower (short dashed) estimations. Right panel: The temperature-dependent activation energy: partial  $E_i^a(T)$  (solid curve) and total  $E^a(T)$  (dashed lines) activation energy, and its approximation of lower (dotted curves) and upper (short dashed) estimations that produced by corresponding upper and lower estimations of  $k(T)$  of the left panel.

For a quantum particle, the possibility of tunneling makes the concept of activation barrier ill defined and therefore deviations from Arrhenius behavior may be expected. Normalized total thermal rate constant  $\hat{k}^{qn}/k_{(0)}^{qn}$  have of the form:<sup>4,23</sup>

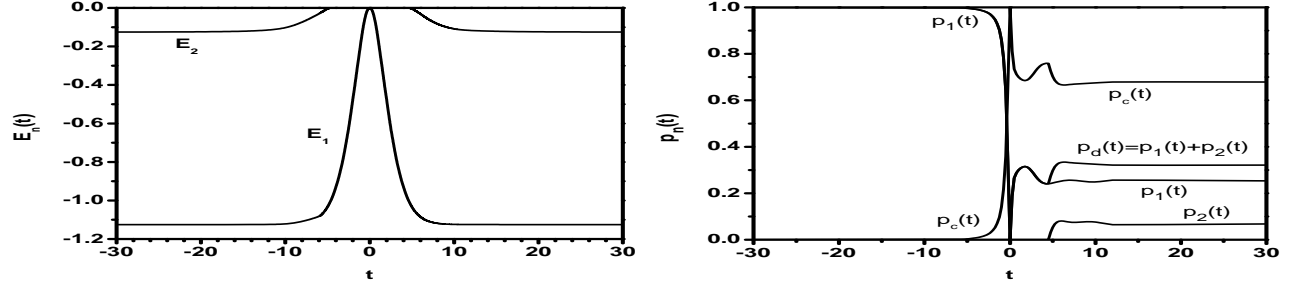
$$\hat{k}^{qn}/k_{(0)}^{qn} = \sum_{i=1}^{N_o} \hat{k}_i(T), \quad \hat{k}_i(T) = \frac{e^{-\tilde{\epsilon}_i/T}}{Q_{vib}} k_i(T), \quad Q_{vib} = \sum_{i=1}^{N_o} e^{-\tilde{\epsilon}_i/T}, \quad (13)$$

$$k_i(T) = \frac{1}{\sqrt{T}} \int_0^{\tilde{E}_y^{\max}} W_{ii}(\tilde{E}_y) e^{-\tilde{E}_y/T} d\tilde{E}_y + \frac{1}{\sqrt{T}} \int_{\tilde{E}_y^{\max}}^{\infty} W_{ii}(\tilde{E}_y) e^{-\tilde{E}_y/T} d\tilde{E}_y. \quad (14)$$

where  $\hat{k}_i(T)$  are weighed thermal rate constants,  $Q_{vib}$  is vibrational energy counted of the bottom of the Morse potential and  $k_i(T)$  is partial thermal rate constant in initial vibrational state  $i$ ,  $W_{ii}(\tilde{E}) = |T|_{ii}^2(\tilde{E})$  is the total transmission probability for initial state  $i$ . Fig. 5a displays the comparison of partial  $k_i(T)$  and total  $\hat{k}(T)$  thermal rate constant vs temperature  $T$  and with their upper and lower estimations. Diffusion can still be approximately described by using a temperature-dependent activation energy, often much lower than the classical energy barrier. The temperature-dependent activation energy: total  $\hat{E}^a(T)$  and partial  $E_i^a(T)$  are defined by

$$\hat{E}^a(T) = -\frac{1}{\sqrt{\beta \hat{k}(T)}} \frac{d\sqrt{\beta \hat{k}(T)}}{d\beta}, \quad E_i^a(T) = -\frac{1}{\sqrt{\beta k_i(T)}} \frac{d\sqrt{\beta k_i(T)}}{d\beta}, \quad \beta = 1/T.$$

Fig. 5a displays the comparison of partial  $E_i^a(T)$  and total  $\hat{E}^a(T)$  activation energy vs temperature  $T$  and with their upper and lower estimations in restricted interval till  $T_{\max} = 100K$ . So, activation energy  $E^a$  for a composite system less then two noninteracted particles. With increasing temperature  $T$  contribution of high energies  $E_y$ , will be taking into account.



a) b)  
Figure 6. a) Eigenenergies  $E_n(t)$  of the instant Hamiltonian depending on time as a parameter  $t$ . b) The bound state probabilities  $p_1(t)$ ,  $p_2(t)$  and the ionization probability  $p_e(t)$  versus the time  $t$ . Here  $A_0 = -15/8$ ,  $A_1 = 15/8$ ,  $v = 1/2$ ,  $x_0(t_0) = vt_0 = -15$ , and  $t_0 = -30$ .

### 3. MODEL II. IONIZATION OF A PÖSCHL-TELLER ATOM

Let us consider simplified model of collision of antiproton ( $\bar{p}+H$ ) or proton ( $p+H$ ) on hydrogen atom where incident nucleus moves by straight line classical trajectory with the velocity  $v$ , which describe by the TDSE on the finite time interval  $t \in [t_0, T]$  for the two-center problem<sup>24</sup> with Pöschl-Teller potentials, similar to the ionization problem.<sup>25</sup> We consider a particular case of a resting well,  $A_0 < 0$ , and a barrier,  $A_1 > 0$ , (or a well at  $A_1 < 0$ ) moving with the velocity  $v$  with respect to the resting well in units  $\hbar = m_e = 1$ :

$$i\frac{\partial\psi(x,t)}{\partial t} = H(x,t)\psi(x,t),$$

$$H(x,t) = -\frac{1}{2}\frac{\partial^2}{\partial x^2} + \frac{A_0}{\cosh^2(x)} + \frac{A_1}{\cosh^2(x-x_0(t))}, \quad (15)$$

where  $H(x,t)$  is the instant Hamiltonian and  $x_0(t) = vt$  is the position of the moving barrier center. For numerical calculation **with required accuracy** the initial infinite-axis boundary problem is reduced to a sufficiently large finite interval  $x \in (x_{\min}, x_{\max})$  with the boundary and normalization conditions

$$\psi(x_{\min}, t) = 0, \quad \psi(x_{\max}, t) = 0, \quad \|\psi(x, t)\|^2 = \int_{x_{\min}}^{x_{\max}} |\psi(x, t)|^2 dx = 1. \quad (16)$$

We consider an example of the wave packet evolution in the time interval  $t \in [t_0, T]$ , induced by the barrier ( $A_1 = 15/8$ ) moving with the velocity  $v$  with respect to the motionless well ( $A_0 = -15/8$ ) that supports two bound states  $n_0 = 2$  with the energies  $E_1(t = t_0) \cong E_1^W = -9/8 = -1.125$  and  $E_2(t = t_0) \cong E_2^W = -1/8 = -0.125$ .

For  $v > 0$  we choose the initial time  $t_0$  and the final time  $T$  to correspond to the initial  $x_0(t_0) = vt_0 = -15$  and the final  $x_0(T) = vT = 15$  positions of the moving barrier center with the aim to preserve with required accuracy the discrete spectrum states supported by the resting well at both  $t_0$  and  $T$ . We start from the initial state that corresponds with required accuracy to the ground state supported by the resting well

$$\psi(x, t_0) \cong \psi_1^W(x) = N_1(\cosh x)^{-(\sqrt{1-8A_0}-1)/2}. \quad (17)$$

Note that in the case  $A_1 + A_0 = 0$  at  $t = 0$  the potential of the problem (15) is equal to zero on the entire axis and the instant Hamiltonian  $H(x, t)$  at  $t = 0$  has purely continuous spectrum that provides the complete ionization of the considered quantum system and the capture to the discrete spectrum states during further evolution.

The calculations were performed using the program TIME6T<sup>26</sup> within the spatial interval  $x \in (-512, 512)$ , which was sufficient to avoid reflection from the boundaries within the considered time interval  $t \in [t_0, T]$ . The wave functions  $\psi_n(x; t)$  of the discrete spectrum  $E_n < 0$  and the wave functions  $\psi_E^\nu(x; t) \equiv \psi_E^{\leftarrow}(x; t)$  of the continuous spectrum  $E \geq 0$  of the instant Hamiltonian  $H(x, t)$  depend on  $t$  as a parameter, as follows from Eq.

(15). They were calculated in the spatial interval  $x \in (x_{\min}, x_{\max})$  with the homogeneous third-type boundary conditions by mean of the modified<sup>15</sup> KANTBP program<sup>12</sup> using the appropriate asymptotic expressions. The subscript  $\nu$  equals  $\rightarrow$  or  $\leftarrow$  for the positive or negative direction of the final momentum  $q = \pm\sqrt{2E}$ , respectively. After joining the asymptotic expressions on the entire axis  $x \in (-\infty, +\infty)$ , these functions satisfy the conventional relations

$$\int_{-\infty}^{+\infty} dx (\psi_E^{\nu'}(x; t))^* \psi_E^{\nu}(x; t) = (2\pi) \delta(E - E') \delta_{\nu\nu'}, \quad (18)$$

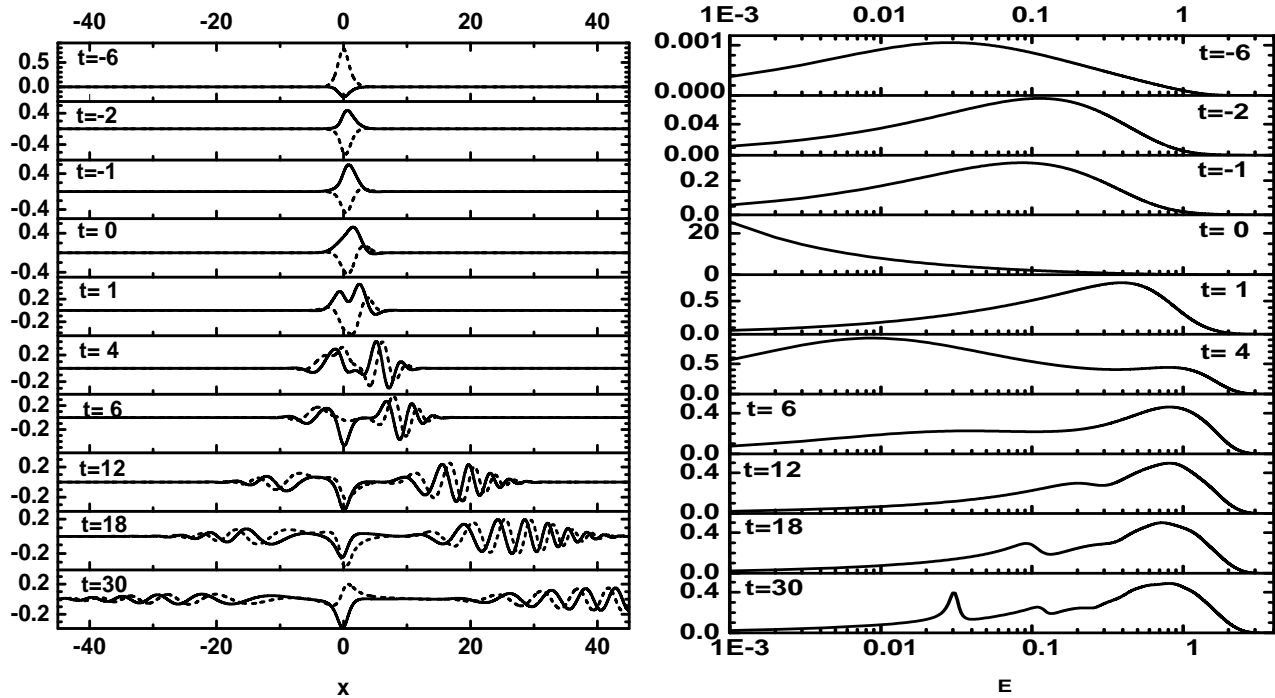
$$\int_{-\infty}^{+\infty} dx (\psi_E^{\nu}(x; t))^* \psi_n(x; t) = 0, \quad (19)$$

$$\sum_{n=1}^{n_0} \psi_n(x; t) \psi_n(x'; t) + \sum_{\nu=\pm} \int_0^{+\infty} dE (\psi_E^{\nu}(x; t))^* \psi_E^{\nu}(x'; t) = \delta(x - x'). \quad (20)$$

An example of the dependence of eigenenergies  $E_n < 0$  of the instant Hamiltonian upon the time parameter  $t$  is shown in Fig. 6a. In the vicinity of  $t = 0$  the Hamiltonian is seen to have only one eigenvalue  $E_1 < 0$  and at  $t = 0$  it has only a continuous spectrum.

The probabilities  $p_n(t)$  and  $p_c(t)$  of transitions to the bound and continuum states and the energy distribution of probability  $p_E(t)$  in the continuous spectrum  $E \geq 0$  in the above capture and ionization processes are calculated using the expressions

$$p_n(t) = |t_{n0}(t)|^2, \quad t_n(t) = \int_{x_{\min}}^{x_{\max}} dx (\psi_n(x, t))^* \psi(x, t) \quad (21)$$



a) Figure 7. a) The real part (solid line) and the imaginary part (dashed line) of the wave function; b) the energy distribution of ionization probability  $p_E(t)$  at different moments of time  $t$  for the fixed values of parameters  $v = 1/2$ ,  $A_0 = -15/8$ ,  $A_1 = 15/8$  and the initial position of the moving barrier  $x_0(t_0) = vt_0 = -15$ ,  $t_0 = -30$ .



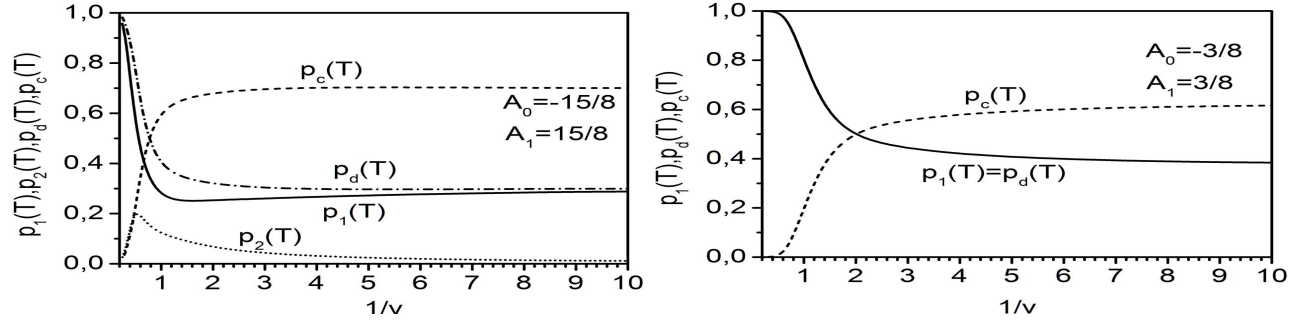


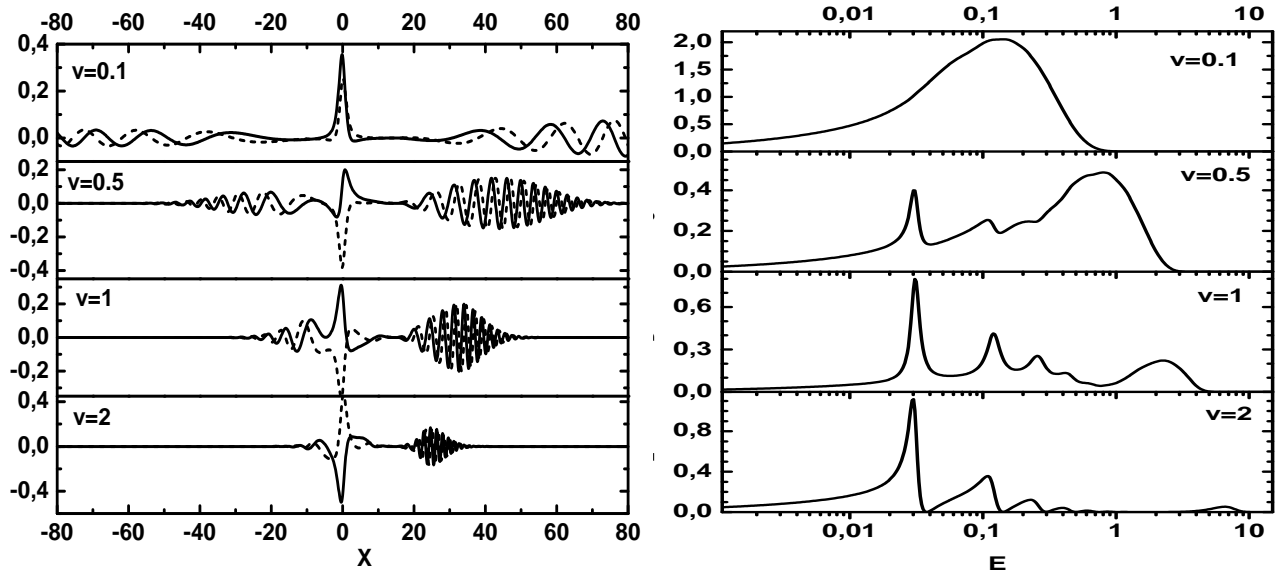
Figure 8. The probabilities  $p_1(T)$ ,  $p_2(T)$  of the ground state and lower excited states, and the ionization probability  $p_c(T)$  versus the inverse velocity  $1/v$  for the time  $T = 15/v$  and the initial time  $t_0 = -15/v$ , when the position of the center of barrier is  $x_0(T) = 15$  and  $x_0(t_0) = -15$ , respectively.

$$p_E(t) = \frac{|t_E^{\rightarrow}(t)|^2 + |t_E^{\leftarrow}(t)|^2}{2\pi}, \quad t_E^{\rightarrow}(t) = \int_{x_{\min}}^{x_{\max}} dx (\psi_E^{\rightarrow}(x, t))^* \psi(x, t). \quad (22)$$

As follows from Eq. (20), they satisfy with the required accuracy the condition at  $E_{\max} \gg 1$ :

$$\sum_{n=1}^{n_0} p_n(t) + p_c(t) = 1, \quad p_c(t) = \int_0^{E_{\max}} p_E(t) dE. \quad (23)$$

As mentioned above, at  $t = 0$  the effective potential is zero, and the eigenfunctions of the instant Hamiltonian correspond to the continuous spectrum. Then the effective potential becomes nonzero again and the capture to the excited and ground states become possible, which is seen from the evolution of probabilities  $p_E(t)$  and  $p_c(t)$  in Figs. 6b and 7. Fig. 7 shows that at  $t \geq 1$  the maxima of the energy distribution  $p_{E \sim 1} \sim 0.5$  correspond to the forward and backward ionization waves with similar frequencies. The maxima of  $p_c(t)$  at  $t \sim 4$  in Fig. 6b correspond to the maxima of  $p_{E \sim 0.01} \sim 1$  at  $t = 4$  in Fig. 7b and correlate with ionization and capture processes. With increasing velocity the probability densities of the excited states tend to zero (see Fig. 8). The



a) Figure 9. a) The real part (solid line) and the imaginary part (dashed line) of the wave function; b) the energy distribution of ionization probability  $p_E(T)$  for the fixed velocity values  $v = 0.1, 0.5, 1, 2$  at  $A_0 = -15/8$ ,  $A_1 = 15/8$ .



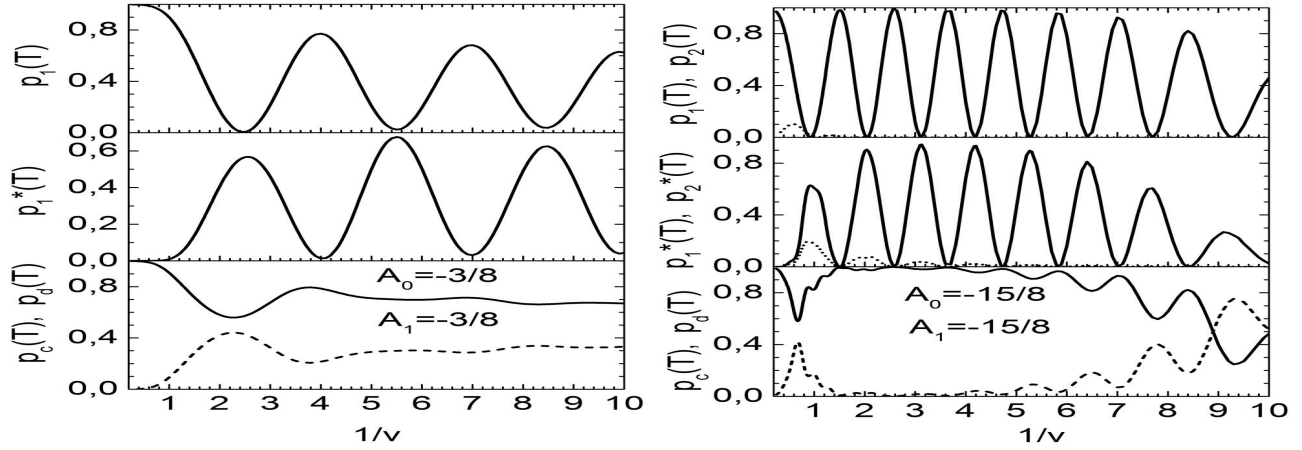
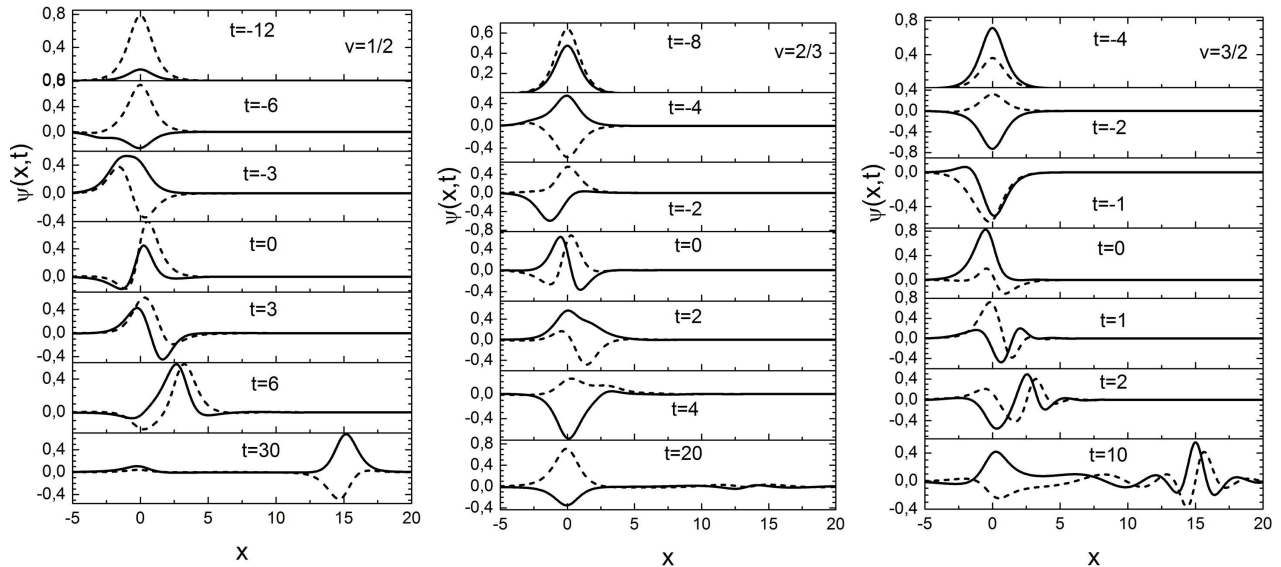


Figure 10. The probabilities  $p_1(T)$ ,  $p_2(T)$  of the ground and lower excited states in a resting well, the probabilities  $p_1^*(T)$ ,  $p_2^*(T)$  of the ground and lower excited states in a moving well, and the ionization probability  $p_c(T)$  versus the inverse velocity  $1/v$  for the time  $T = 15/v$  and the initial time  $t_0 = -15/v$ , when the position of the barrier center is  $x_0(T) = 15$  and  $x_0(t_0) = -15$ , respectively.

wave function and the distribution of ionization probability  $p_E(t)$  for some particular values of the velocity are shown in Fig. 9. As seen from Fig. 9, with increasing  $v$  the forward ionization waves become dominant and their energy increases.

Consider another example of the evolution of the wave packet in the time interval  $t \in [t_0, T]$ , induced by the barrier ( $A_1 = 3/8$ ) moving with the velocity  $v$  with respect to the fixed well ( $A_0 = -3/8$ ), supporting a single bound state  $n_0 = 1$  with energy  $E_1(t = t_0) \cong E_1^W = -1/8 = -0.125$ . Fig. 8 shows that, generally, the velocity distribution of the probability has the similar structure. Note, that the probability of detecting the system in the excited states is substantially smaller than that in the ground state.

For two cases discussed above let us consider an example of the wave packet evolution, induced by the well



a) b)  
Figure 11. a) The real part (solid line) and the imaginary part (dashed line) of the wave function for three fixed values of velocity  $v = 1/2, 2/3, 3/2$  at different moments of time  $t$  and  $A_0 = A_1 = -15/8$ .

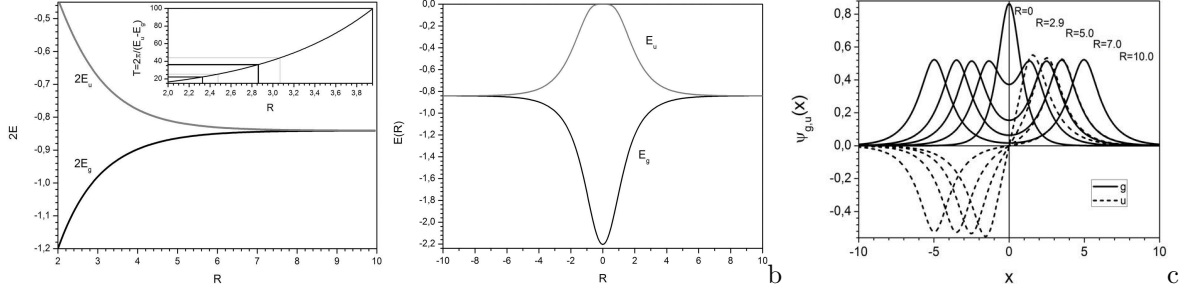


Figure 12. The potential curves (a,b) and the wave functions (c) of the ground (gerade  $g$ ) and excited (ungerade  $u$ ) states of the electron at different values of the internuclear distance  $R$ . The inset in Fig. (a) shows the dependence of the free oscillation period upon  $R$ . The values of  $R$  corresponding to the maxima of ionization probability are shown by vertical lines.

( $A_1 = A_0$ ), moving with the velocity  $v$ , in the time interval  $t \in [t_0, T]$ . An example of the dependence of eigenenergies  $E_n < 0$  and eigenfunctions of the instant Hamiltonian, having also a continuous spectrum, upon the time parameter  $t$  is shown in Fig. 12b,c as a function of  $R = vt$ . At  $t = 0$ , i.e. at  $R = 0$ , the Hamiltonian is seen to have only one eigenvalue  $E_1(R = 0) < 0$  because in this point  $E_2(R = 0) = 0$ , i.e. second eigenvalue touch boundary of continuous spectrum and after that go to unphysical sheet of energy. At  $t > 0$  the bound state corresponding second eigenvalue appears again and its settlement occurs by capture of ionized particles to discrete spectrum  $E_2(R \neq 0) < 0$ . Fig. 10 shows the dependence of probabilities  $p_1(T)$ ,  $p_2(T)$  of detecting the system in the ground and first excited states in the resting well and the probabilities  $p_1^*(T)$ ,  $p_2^*(T)$  for the ground and first excited states in the moving well versus the inverse velocity  $1/v$ . The Figure 10 shows that the probability to remain in the resting well or to go to the moving one is rapidly oscillating at small  $v$ , which is due to multiple reflection of the wave packet from the walls of the wells. The probability of transition to the continuum is also a rapidly oscillating functions at  $v \rightarrow 0$ , due to the reflection from the walls of the wells. There is also a peak at  $v \sim 0.5$  in the case of  $A_0 = -3/8$  and at  $v \sim 1.5$  in the case of  $A_0 = -15/8$ , which are associated with the appearance of the barrier, separating the wells starting from the time  $t = \ln(2 + \sqrt{3})/v$ .

Figure 11 shows the time dependence of the wave function  $\psi(x, t)$  at the velocities of the well  $v = 1/2$ ,  $v = 2/3$ , and  $v = 3/2$ , when the wave packet passes to the moving well, remains localized in the resting well, and is partially converted into the continuum, respectively. At low velocities the wave packet is seen to oscillate. At high velocities the mutual influence of the wells becomes negligible, and in the limit  $v \rightarrow \infty$  the scattering becomes purely elastic.

The considered models allow the description of composite systems in transient effective potentials that may cause not only the excitation and ionization processes, but also the capture to bound states. The models are advantageous for demonstrating the efficiency of computational unitary schemes, implemented in the applied program TIME6.

#### 4. MODEL III. IONIZATION DYNAMICS OF A MOLECULAR ION

Now consider a simplified one-dimensional model of molecular ion with two nuclei fixed at the points  $\pm R/2$ , attracting an electron at the point  $x$  via a superposition of two identical PöschlTeller (PT) potentials. The system is affected by the electric field of a laser pulse. The Schrödinger equation describing the ionization dynamics of this model (in atomic units) reads

$$\begin{aligned} i \frac{\partial \psi(x, t)}{\partial t} &= H(x, t) \psi(x, t), \\ H(x, t) &= H_0(x) + V(x, t) \\ H_0(x) &= -\frac{1}{2} \frac{\partial^2}{\partial x^2} - \frac{V_0}{\cosh^2((x - R/2)/L)} - \frac{V_0}{\cosh^2((x + R/2)/L)}, \end{aligned} \quad (24)$$

Here  $V(x, t)$  is the potential induced by the laser pulse

$$V(x, t) = F_0 f(t) \sin(\omega_L t), \quad (25)$$

with the amplitude  $F_0$  and the frequency  $\omega_L$ . We choose the envelope function  $f(t)$  of the laser pulse in the form  $f(t) = \sin^2(\pi t/T_{pulse})$ , where  $T_{pulse}$  is the pulse duration.

The BVP for Eq. (24) was solved with the boundary and normalization conditions (16) and the initial state  $\psi(x, 0) = (\psi_g + \psi_u)/\sqrt{2}$  localized in the right-hand well of the double-well potential. The finite spatial interval  $x \in (-128, 128)$  was sufficient to avoid reflection from the boundaries within the considered time interval  $t \in [t_0, T]$  using the program TIME6T.<sup>26</sup>

Figures 12–15 present the results of calculations performed using the following parameters. The magnitude and the width of the PT potentials were  $V_0 = 2.216E_h$  and  $L = 2/3a_B$ , respectively, where  $E_h \equiv Ry = \hbar^2/2/m_e/a_B$  and  $a_B = \hbar^2/m_e/e^2$  is the Bohr radius. The laser frequency  $\omega_L = 0.16546$  corresponded to the wavelength  $\lambda = 300$  nm and the period  $T_{oc} = 2\pi/\omega_L = 37.973$ ; the pulse duration was taken to be  $T_{pulse} = 32T_{oc}$ .

For the fixed values of the parameter  $R > R_0 \approx 0.1$  the Hamiltonian  $H_0(x; R)$  has two eigenvalues, corresponding to the ground and excited state that vary with the distance between wells as shown in Fig. 12a. The eigenstates possess the symmetry with respect to permutations of identical nuclei, namely, the ground state is even (gerade,  $g$ ) and the excited state is odd (ungerade,  $u$ ). With respect to the center of symmetry the wave function is symmetric for  $g$  state and antisymmetric for  $u$  state. The wider is the barrier, the smaller is the separation between the energy levels. In the process of evolution, the wave function of the initial state  $\psi_a(x) = (\psi_g + \psi_u)/\sqrt{2}$  localized in the well (a) turns into the wave function  $\psi_b(x) = (\psi_g - \psi_u)/\sqrt{2}$ , localized in the well (b), and then returns to the initial state. In the absence of external fields the evolution of the initial state  $\psi(x, 0) = \psi_a(x)$  (Fig. 13 at  $R = 2.9$ ) can be described by the formula

$$\begin{aligned} \psi(x, t) &= \frac{1}{2}(\psi_g(t) + \psi_u(t)) = \frac{1}{2}(\psi_g \exp(iE_g t) + \psi_u(t) \exp(iE_u t)) \\ &= \frac{\exp(iE_g t)}{2}[\psi_a(x)(1 + \exp(i(E_u - E_g)t) + \psi_b(x)(1 - \exp(i(E_u - E_g)t)]. \end{aligned}$$

The period of free oscillation  $T \equiv T_{gu} = 2\pi/(E_u - E_g)$  versus the distance  $R$  is shown in the inset of Fig. 12a. At  $R = 2.9$  the frequency of free oscillation is equal to the wave frequency.

In Fig. 14 the probability  $P_+$  of the particle localization in the right-hand well and the total discrete spectrum probability  $P$  at  $T_{fin} = 36T_{oc}$  are shown as functions of  $R$  (left) and the free oscillation frequency  $\omega_{gu}$  (right).

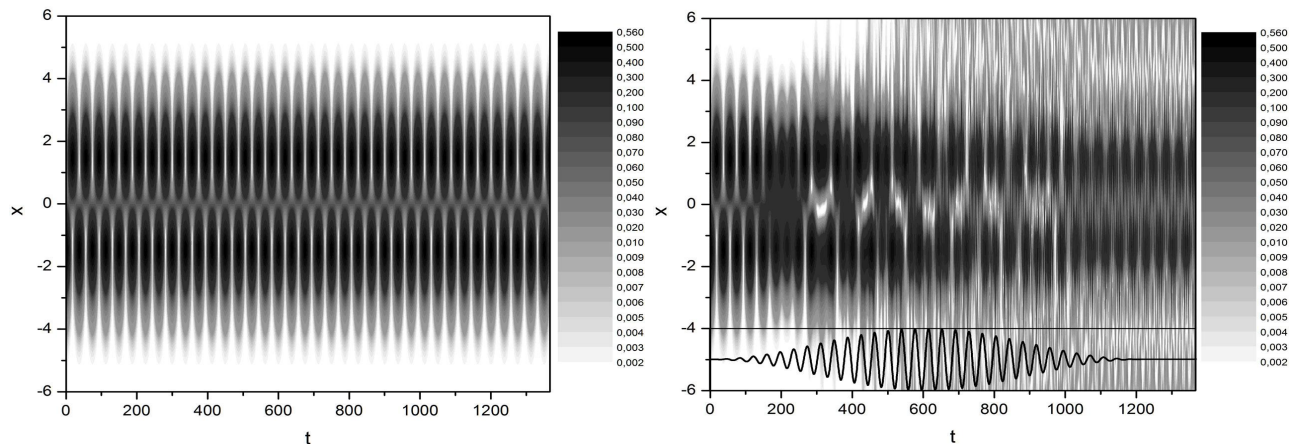


Figure 13. Temporal dynamics of the wave function without the laser pulse (left) and with the laser pulse (right).  $R = 2.9$ , the line plots the laser pulse  $f(t) \sin(\omega_L t)$ ,  $\omega_L = 0.16546$ ,  $F_0 = 0.05$  a.u. Note that the laser frequency is close to the resonance 1:1, i.e.  $\omega_L = \omega_{gu}$ .

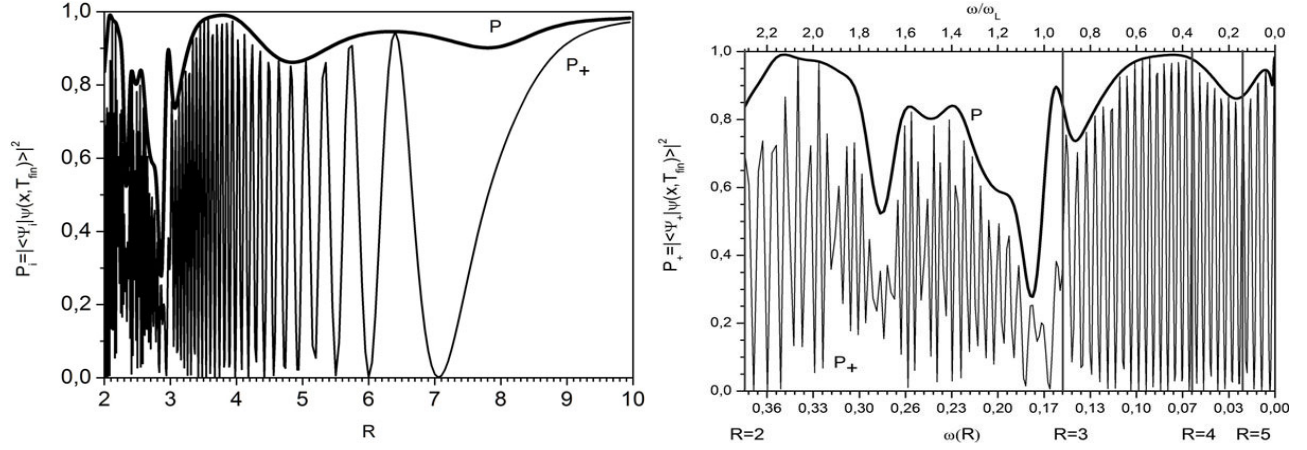


Figure 14. The probability  $P_+$  of the particle localization in the right-hand well and the total discrete spectrum probability  $P$  at the time  $T_{fin} = 36T_{oc}$  as functions of the internuclear distance  $R$  (left) and the free oscillation frequency  $\omega$  (right).

From Fig. 14 the probability of electron localization in the initial state  $\psi_a(x, T_{fin})$  at the moment of time  $T_{fin}$  at  $R \ll 10$  is seen to be a fast oscillating function of  $R$ . The total discrete spectrum probability  $P$  is a slow varying function everywhere except the interval  $R \in (2.2, 4.2)$ , in which  $P$  has four peaks. These peaks are clearly seen in the right panel of Fig. 14. The values of  $R$  corresponding to the resonance periods  $T_{gu}$  and frequencies  $\omega_{gu}$  are indicated by straight lines in the inset of Fig. 12a. The greatest peak is located in the vicinity of  $R \approx 2.86$  for which the free oscillation frequency  $\omega_{gu} \approx 0.173$  ( $T_{gu} \approx 36.2$ ) is approximately equal to the laser pulse frequency  $\omega_L = 0.16546$ ,  $\omega_{gu} \approx \omega_L$ , and the second peak is located at  $R \approx 2.33$ , for which the free oscillation frequency  $\omega_{gu} \approx 0.282$  ( $T_{gu} \approx 22.2$ ) is approximately by 3/2 times larger than  $\omega_L$ ,  $\omega_{gu}/\omega_L \approx 3/2$ . Thus, the resonances 1 : 1 (the evolution of which is shown in Fig. 13) and 3 : 2 are observed, the small deviations being due to the small pulse duration and the variation of its envelope.

The time dependence of the probability  $P_+$  of the particle localization in the right-hand well and of the total

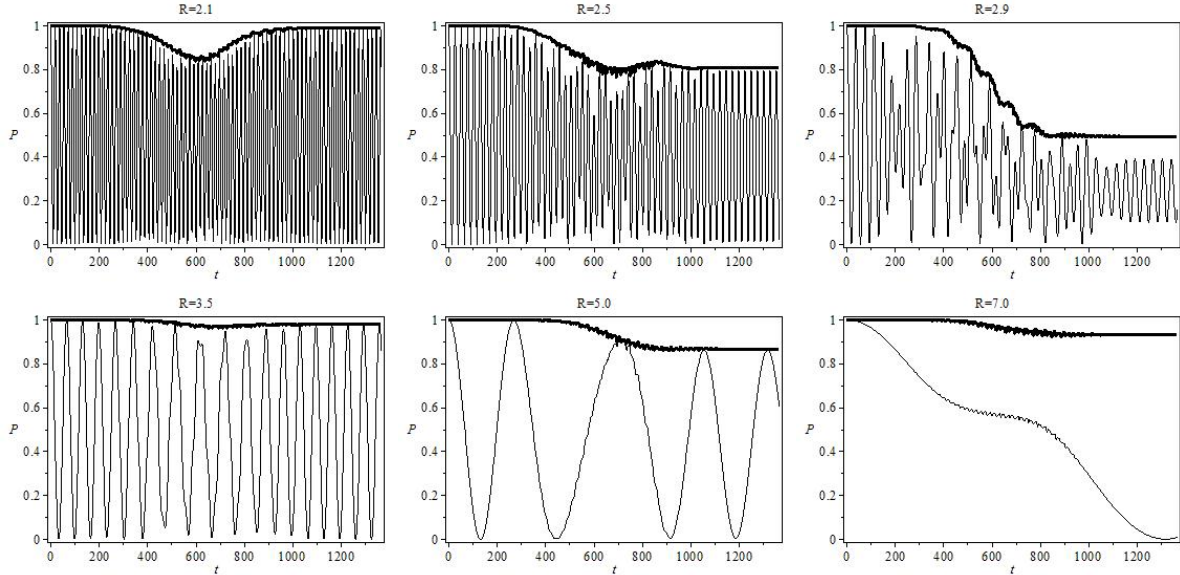


Figure 15. The probability  $P_+$  of the particle localization in the right-hand well and the total discrete spectrum probability  $P$  as functions of time  $t$  at different values of  $R$ .

discrete spectrum probability  $P$  at different values of  $R$  is shown in Fig. 15. It is seen that at large distance between the wells the period of free oscillation is large, and the ionization occurs from a definite well. Decreasing the separation between the wells gives rise to the additional resonance ionization when the resonance frequency conditions are satisfied and the capture from the continuum otherwise.

## 5. CONCLUSIONS

The effect of quantum transparency in resonance tunneling of diatomic molecules through repulsive potential barriers is demonstrated and shown to lead to quantum diffusion by the example of diatomic low-dimensional model systems, coupled via realistic molecular potentials. The proposed models and approach, the quantum transparency effect itself and the developed software can find further applications in barrier heavy-ion reactions and molecular quantum diffusion. They can be also applied in the studies of laser control of molecular tunneling, aimed at enhancing the rate of chemical reactions and quantum diffusion.

### 5.1 Acknowledgments

The work was supported partially by grants RFBR14-01-00420 and 13-01-00668, 13-602-02 JINR and 0602/GF MES RK. Authors thank profs. F.M. Penkov and A.V. Mitin for collaboration.

## REFERENCES

- [1] Pen'kov, F.M., "Quantum transmittance of barriers for composite particles," JETP 91, 698–705 (2000).
- [2] Pen'kov, F.M., "Metastable states of a coupled pair on a repulsive barrier," Phys. Rev. A 62, 044701–1–4 (2000).
- [3] Shotter, A.C. and Shotter, M.D., "Quantum mechanical tunneling of composite particle systems: Linkage to sub-barrier nuclear reactions," Phys. Rev. C 83, 054621–1–11 (2011).
- [4] Pijper, E. and Fasolino, A., "Quantum surface diffusion of vibrationally excited molecular dimers," J. Chem. Phys. 126, 014708–1–10 (2007).
- [5] Kavka, J.J., Shegelski, M.R.A. and Hong, W.P., "Tunneling and reflection of an exciton incident upon a quantum heterostructure barrier," J. Phys.: Condens. Matter. 24, 365802–1–13 (2012).
- [6] Shegelski MRA, Hnybida J., Vogt R. "Formation of a molecule by atoms incident upon an external potential," Phys.Rev. A. 78, 062703–1–5 (2007).
- [7] Bondar, D.I., Liu, W.-Ki, Ivanov, M.Yu., "Enhancement and suppression of tunneling by controlling symmetries of a potential barrier," Phys. Rev. A 82, 052112–1–9 (2010).
- [8] Gusev, A., Vinitsky, S., Chuluunbaatar, O., Rostovtsev, V.A., Hai, L.L., Derbov, V. and Krassovitskiy, P., "Symbolic-numerical algorithm for generating cluster eigenfunctions: tunneling of clusters through repulsive barriers," Lecture Notes in Computer Science 8136, 427–442 (2013).
- [9] Gusev, A.A., Vinitsky, S.I., Chuluunbaatar, O., Gerdt, V.P., Rostovtsev V.A., "Symbolic-numerical algorithms to solve the quantum tunneling problem for a coupled pair of ions," Lecture Notes in Computer Science 6885, 175–191 (2011).
- [10] Shapiro, M. and Brumer, P., [Quantum Control of Molecular Processes] Wiley-VCH, Weinheim, 2012.
- [11] Chuluunbaatar, O., Gusev, A.A., Vinitsky, S.I. and Abrashkevich, A.G., "A program for computing eigenvalues and eigenfunctions and their first derivatives with respect to the parameter of the parametric self-adjoint Sturm-Liouville problem", Computer Physics Communications, 180, 1358-1375 (2009).
- [12] Chuluunbaatar, O., Gusev, A.A., Vinitsky, S.I. and Abrashkevich, A.G., "KANTBP 2.0: New version of a program for computing energy levels, reaction matrix and radial wave functions in the coupled-channel hyperspherical adiabatic approach," Comput. Phys. Commun. 179, 685–693 (2008).
- [13] Fundamental Physical Constants <http://physics.nist.gov/constants>
- [14] Lauhon, L.J. and Ho, W., "Direct observation of the quantum tunneling of single hydrogen atoms with a scanning tunneling microscope," Phys. Rev. Lett. 85, 4566–4569 (2000).
- [15] "A program package for solution of two-dimensional discrete and continuum spectra boundary-value problems in kantorovich (adiabatic) approach," Program library "JINRLIB" <http://wwwinfo.jinr.ru/programs/jinrlib/kantbp/indexe.html>

- [16] Ahsan, N., and Volya, A., "Quantum tunneling and scattering of a composite object reexamined," *Phys. Rev. C* **82**, 064607–1–19 (2010)
- [17] Merritt, J.M., Bondybey, V.E. and Heaven, M.C., "Beryllium Dimer — Caught in the Act of Bonding" *Science* **326**, 1548–1551 (2009).
- [18] Patkowski, K., Špirko V., and Szalewicz, K. "On the Elusive Twelfth Vibrational State of Beryllium Dimer" *Science* **326**, 1382–1384 (2009).
- [19] Mitin, A. V., "Accurate calculations of dissociation energies of weakly bonded He<sub>2</sub> and Be<sub>2</sub> molecules by MRCI method," *Russ. J. Phys. Chem. A.* **84**, 2314–2319 (2010).
- [20] Mitin, A. V., "Ab initio calculations of weakly bonded He<sub>2</sub> and Be<sub>2</sub> molecules by MRCI method with pseudo-natural molecular orbitals," *Int. J. Quantum Chem.* **111**, 2560–2567 (2011) .
- [21] Baz', A.I., Zel'dovich, Ya.B. and Perelomov, A.M., [Scattering, Reactions, and Decay in Nonrelativistic Quantum Mechanics], Jerusalem, 1969; Nauka, Moscow, 1971.
- [22] de Carvalho, C.A.A. and Nussenzveig, H.M., "Time delay," *Phys. Rept.* **364**, 83–174 (2002).
- [23] Miller, W.H. "Quantum mechanical transition state theory and a new semiclassical model for reaction rate constants", *J. Chem.Phys.* **61**, 1823–1834 (1974).
- [24] Soloviev, E.A. and Vinitsky, S.I. "Suitable coordinates for the three-body problem in the adiabatic representation", *J. Phys. B* **18**, L557-L562 (1985).
- [25] Corso, P.P., Fiordilino, E. and Persico, F., "Ionization dynamics of a model molecular ion," *J. Phys. B: At. Mol. Opt. Phys.* **38**, 1015–1028 (2005).
- [26] Vinitsky, S.I., Gusev, A.A. and Chuluunbaatar, O., "Program complex for the numerical solution of the Cauchy problem for the time-dependent Schroedinger equation," Program library "JINRLIB" <http://wwwinfo.jinr.ru/programs/jinrlib/time6t/indexe.html>





# Calculation of a hydrogen atom photoionization in a strong magnetic field by using the angular oblate spheroidal functions

O Chuluunbaatar<sup>1</sup>, A A Gusev<sup>1</sup>, V L Derbov<sup>2</sup>, M S Kaschiev<sup>3</sup>,  
L A Melnikov<sup>2</sup>, V V Serov<sup>2</sup> and S I Vinitsky<sup>1</sup>

<sup>1</sup> Joint Institute for Nuclear Research, Dubna, Moscow Region 141980, Russia

<sup>2</sup> Saratov State University, Russia

<sup>3</sup> Institute of Mathematics and Informatics, BAS, Sofia, Bulgaria

Received 7 June 2007, in final form 9 August 2007

Published 4 September 2007

Online at [stacks.iop.org/JPhysA/40/11485](http://stacks.iop.org/JPhysA/40/11485)

## Abstract

A new efficient method for calculating the photoionization of a hydrogen atom in a strong magnetic field is developed based on the Kantorovich approach to the parametric boundary problems in spherical coordinates using the orthogonal basis set of angular oblate spheroidal functions. The progress as compared with our previous paper (Dimova M G, Kaschiev M S and Vinitsky S I 2005 *J. Phys. B: At. Mol. Opt. Phys.* **38** 2337–52) consists of the development of the Kantorovich method for calculating the wavefunctions of a continuous spectrum, including the quasi-stationary states imbedded in the continuum. Resonance transmission and total reflection effects for scattering processes of electrons on protons in a homogenous magnetic field are manifested. The photoionization cross sections found for the ground and excited states are in good agreement with the calculations by other authors and demonstrate correct threshold behavior. The estimates using the calculated photoionization cross section show that due to the quasi-stationary states the laser-stimulated recombination may be enhanced by choosing the optimal laser frequency.

PACS numbers: 31.15.Ja, 31.15.Pf, 34.50.Pi, 32.80.Fb

## 1. Introduction

In recent decades the dynamics of transient processes in magnetic traps, such as excitation, de-excitation, ionization, recombination of ions and atoms, became a subject of intense experimental and theoretical studies [1–4]. Recently a new mechanism of formation of metastable positive-energy atoms via quasi-stationary states [5] due to the magnetic field was revealed. The most complicated case when the magnetic energy is comparable to that of Coulomb interaction requires new approaches to provide really stable numerical schemes



for the states of both discrete and continuous spectra, including the quasi-stationary states, analogous to the well-known doubly excited states of a helium atom [6–10]. In the known approaches serious problems arise, for example, concerned with reproducing true threshold behavior in the variational complex rotation method [8, 11] or with constructing efficient and stable numerical schemes [11]. In doing so, this method does not describe the difference in physical asymptotics of scattering states for a different choice of a gauge of magnetic field [12]. The **R**-matrix approach [13–16] using the combined nonorthogonal basis of Landau and Sturmian functions in both cylindrical and spherical coordinates leads to the ill-conditioned matrix problems [6, 17]. The method of diabatic sector basis functions requires a huge interval for the integration of the closed set of radial equations, because the overlap matrix between the pure physical asymptotic solutions in cylindrical coordinates and the numerical basis functions at large  $r$  can be calculated only numerically [7, 10]. The Kantorovich method (KM) [18] has been shown to provide strong mathematical background for consequent development of the adiabatic approach in spherical coordinates [19] using the orthogonal basis set of angular oblate spheroidal functions (AOSF) [20]. This approach yields stable calculation schemes for boundary problems, however, heretofore it has been elaborated only for the discrete spectrum problem [9].

In the present paper we develop the KM (i.e., the reduction of the boundary problem for elliptical partial differential equation in a 2D domain to a regular boundary problem for a set of ordinary second-order differential equations with variable coefficients with the boundary conditions of the third kind) in the form, appropriate for **R**-matrix calculations of the continuous spectrum and photoionization of atomic hydrogen in a strong magnetic field [21]. The solution depending on the radial variable  $r$  and the angular variable  $\eta = \cos \theta = z/r$  with fixed values of the magnetic quantum number  $m$  and the  $z$ -parity  $\sigma$  is expanded using the basis set of the AOSF, which is orthogonal at fixed values of the radial variable. A matter of principle in the implementation of KM is how to calculate the matrix of the variable coefficients, expressed as angular integrals involving the derivatives of the angular functions with respect to a parameter, keeping the accuracy the same as for the angular functions themselves. This is achieved by calculating the mentioned derivatives as solutions of the inhomogenous boundary problem that results from differentiation of the ordinary second-order differential equation for the spheroidal functions with respect to the parameter and the corresponding algebraic eigenvalue problem, for which a stable symbolic-numerical algorithm is developed [22, 23]. The stability of the computational scheme is achieved using the fact that at small  $r$  (in the vicinity of pair collision point) the angular functions turn into the associated Legendre polynomials, while at large  $r$  near  $\eta = \pm 1$  they turn into the associated Laguerre functions [24, 25]. This makes it possible to construct asymptotic expansions in powers of  $r^{-2}$ , necessary for computer-accuracy calculation of the basis set of functions at all values of the parameter  $r$ . Substantial economy of computer resource in the numerical solution of the boundary problem for the set of radial equations is achieved by decreasing the integration interval  $0 \leq r \leq r_{\max}$ . With this aim in the present paper for large  $r \geq r_{\max}$  new asymptotic expansions of the fundamental solutions of the radial equations are constructed in the basis of linear combinations of Coulomb regular and irregular functions and their derivatives. The corresponding matrix of asymptotic expansions of fundamental solutions is derived in the analytic form and is related to the overlap matrix between the physical asymptotic form of fundamental solutions in the cylindrical coordinates,  $z = r \cos \theta$ ,  $\rho = r \sin \theta$  and the asymptotic form of the basis functions of the independent variable  $\eta = \cos \theta$  at large values of  $r$ . The presented recurrence relations for expressing this matrix in the analytic form are the key to calculating the reaction matrix **K** via the matrix of logarithmic derivative of the radial solution in the joining point of numerical and asymptotic solutions in the inner and outer regions. The capabilities of the elaborated method and the

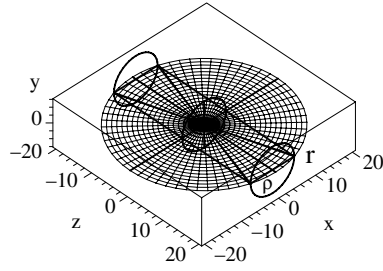


**Figure 1.** Projections of cylindrical and spherical coordinate systems in the  $zx$  plane for a hydrogen atom or scattering of an electron with a proton in a homogenous magnetic field  $\vec{B} = (0, 0, B)$ .

computational scheme are demonstrated by the example of photoionization cross section of a hydrogen atom in the magnetic field. Using the previously derived relation between the photoionization cross section and the laser-induced radiative recombination rate, it is shown that the latter can be increased by tuning the laser frequency to resonances that arise due to quasi-stationary states.

The paper is organized as follows. In section 2 the 2D-eigenvalue problem for the Schrödinger equation, describing a hydrogen atom in an axially symmetric magnetic field, is considered in the cylindrical coordinates together with the appropriate classification of states. The reduction of the 2D-eigenvalue problem to a 1D-eigenvalue problem for a set of closed longitude equations via both the Kantorovich and Galerkin methods is described briefly. It is shown that the Galerkin expansion follows from the Kantorovich expansion at  $z \rightarrow \pm\infty$ . In section 2.3 the relation between the function with given parity and the function having the physical scattering asymptotic form in the cylindrical coordinates is established. In section 3 the same problem as in section 2 is considered in the spherical coordinates. The reduction of the 2D-eigenvalue problem to a 1D-eigenvalue problem for a set of closed radial equations via four steps of the KM is described briefly in section 3.1. The asymptotic forms of the matrix element and radial solutions are considered in sections 3.2–3.5. The asymptotic expressions using regular and irregular Coulomb functions needed to find the solutions and the reaction matrix by means of the **R**-matrix method are presented in section 3.6. The correspondence of asymptotic total wavefunctions at large  $r$  and  $|z|$  is shown explicitly in section 3.7. The method is applied to the ionization of low-lying states of a hydrogen atom in section 4. In section 5 the numerical results obtained within the framework of the finite-element method are discussed. The estimates of the laser-induced recombination rate based on the calculated photoionization cross sections are also presented. In conclusion we outline the perspectives of further applications of this approach. The detailed analysis of asymptotic calculations is given in appendix A, B and C.

## 2. Statement of the problem in cylindrical coordinates

In the cylindrical coordinates  $(\rho, z, \varphi)$  (see figure 1) the wavefunction

$$\hat{\Psi}(\rho, z, \varphi) = \Psi(\rho, z) \frac{\exp(im\varphi)}{\sqrt{2\pi}} \quad (1)$$

of a hydrogen atom in an axially symmetric magnetic field  $\vec{B} = (0, 0, B)$  satisfies the 2D Schrödinger equation

$$-\frac{\partial^2}{\partial z^2} \Psi(\rho, z) + \left( \hat{A}_c - \frac{2Z}{\sqrt{\rho^2 + z^2}} \right) \Psi(\rho, z) = \epsilon \Psi(\rho, z), \quad (2)$$

$$\hat{A}_c = -\frac{1}{\rho} \frac{\partial}{\partial \rho} \rho \frac{\partial}{\partial \rho} + \frac{m^2}{\rho^2} + m\gamma + \frac{\gamma^2 \rho^2}{4}, \quad (3)$$

in the region  $\Omega_c$ :  $0 < \rho < \infty$  and  $-\infty < z < \infty$ . Here  $m = 0, \pm 1, \dots$  is the magnetic quantum number,  $\gamma = B/B_0$ ,  $B_0 \cong 2.35 \times 10^5 T$  is a dimensionless parameter which determines the field strength  $B$ . We use the atomic units (au)  $\hbar = m_e = e = 1$  and assume the mass of the nucleus with a charge  $Z$  to be infinite. In these expressions  $\epsilon = 2E$  is the twice energy (expressed in Rydbergs,  $1 \text{ Ry} = (1/2) \text{ au}$ ) of the bound state  $|m\sigma\rangle$  with fixed values of  $m$  and  $z$ -parity  $\sigma = \pm 1$  and  $\Psi(\rho, z) \equiv \Psi^{m\sigma}(\rho, z) = \sigma \Psi^{m\sigma}(\rho, -z)$  is the corresponding wavefunction. The boundary conditions in each  $m\sigma$  subspace of the full Hilbert space have the form

$$\lim_{\rho \rightarrow 0} \rho \frac{\partial \Psi(\rho, z)}{\partial \rho} = 0, \quad \text{for } m = 0, \quad \text{and} \quad \Psi(0, z) = 0, \quad \text{for } m \neq 0, \quad (4)$$

$$\lim_{\rho \rightarrow \infty} \Psi(\rho, z) = 0. \quad (5)$$

The wavefunction of the discrete spectrum obeys the asymptotic boundary condition. Approximately this condition is replaced by the boundary condition of the first type at large, but finite  $|z| = z_{\max} \gg 1$ , namely,

$$\lim_{z \rightarrow \pm\infty} \Psi(\rho, z) = 0 \quad \rightarrow \quad \Psi(\rho, \pm z_{\max}) = 0. \quad (6)$$

These functions satisfy the additional normalization condition

$$\int_{-z_{\max}}^{z_{\max}} \int_0^\infty |\Psi(\rho, z)|^2 \rho d\rho dz = 1. \quad (7)$$

The asymptotic boundary condition for the continuum wavefunction will be considered in section 2.3.

### 2.1. Kantorovich expansion

Consider a formal expansion of the partial solution  $\Psi_i^{Em\sigma}(\rho, z)$  of equations (2)–(5), corresponding to the eigenstate  $|m\sigma i\rangle$ , expanded in the finite set of one-dimensional basis functions  $\{\hat{\Phi}_j^m(\rho; z)\}_{j=1}^{j_{\max}}$

$$\Psi_i^{Em\sigma}(\rho, z) = \sum_{j=1}^{j_{\max}} \hat{\Phi}_j^m(\rho; z) \hat{\chi}_j^{(m\sigma i)}(E, z). \quad (8)$$

In equation (8) the functions  $\hat{\chi}^{(i)}(z) \equiv \hat{\chi}^{(m\sigma i)}(E, z)$ ,  $(\hat{\chi}^{(i)}(z))^T = (\hat{\chi}_1^{(i)}(z), \dots, \hat{\chi}_{j_{\max}}^{(i)}(z))$  are unknown and the surface functions  $\hat{\Phi}(\rho; z) \equiv \hat{\Phi}^m(\rho; z) = \hat{\Phi}^m(\rho; -z)$ ,  $(\hat{\Phi}(\rho; z))^T = (\hat{\Phi}_1(\rho; z), \dots, \hat{\Phi}_{j_{\max}}(\rho; z))$  form an orthonormal basis for each value of the variable  $z$  which is treated as a parameter.

In the Kantorovich approach the wavefunctions  $\hat{\Phi}_j(\rho; z)$  and the potential curves  $\hat{E}_j(z)$  (in Ry) are determined as the solutions of the following one-dimensional parametric eigenvalue problem

$$\left( \hat{A}_c - \frac{2Z}{\sqrt{\rho^2 + z^2}} \right) \hat{\Phi}_j(\rho; z) = \hat{E}_j(z) \hat{\Phi}_j(\rho; z), \quad (9)$$

with the boundary conditions

$$\lim_{\rho \rightarrow 0} \rho \frac{\partial \hat{\Phi}_j(\rho; z)}{\partial \rho} = 0, \quad \text{for } m = 0, \quad \text{and} \quad \hat{\Phi}_j(0; z) = 0, \quad \text{for } m \neq 0, \quad (10)$$

$$\lim_{\rho \rightarrow \infty} \hat{\Phi}_j(\rho; z) = 0. \quad (11)$$

Since the operator in the left-hand side of equation (9) is self-adjoint, its eigenfunctions are orthonormal

$$\langle \hat{\Phi}_i(\rho; z) | \hat{\Phi}_j(\rho; z) \rangle_\rho = \int_0^\infty \hat{\Phi}_i(\rho; z) \hat{\Phi}_j(\rho; z) \rho \, d\rho = \delta_{ij}, \quad (12)$$

where  $\delta_{ij}$  is the Kronecker symbol. Therefore, we transform the solution of the above problem into the solution of an eigenvalue problem for a set of  $j_{\max}$  ordinary second-order differential equations that determines the energy  $\epsilon$  and the coefficients  $\hat{\chi}^{(i)}(z)$  of expansion (8)

$$\left( -\mathbf{I} \frac{d^2}{dz^2} + \hat{\mathbf{U}}(z) + \hat{\mathbf{Q}}(z) \frac{d}{dz} + \frac{d\hat{\mathbf{Q}}(z)}{dz} \right) \hat{\chi}^{(i)}(z) = \epsilon_i \mathbf{I} \hat{\chi}^{(i)}(z). \quad (13)$$

Here  $\mathbf{I}$ ,  $\hat{\mathbf{U}}(z) = \hat{\mathbf{U}}(-z)$  and  $\hat{\mathbf{Q}}(z) = -\hat{\mathbf{Q}}(-z)$  are the  $j_{\max} \times j_{\max}$  matrices whose elements are expressed as

$$\begin{aligned} \hat{U}_{ij}(z) &= \frac{\hat{E}_i(z) + \hat{E}_j(z)}{2} \delta_{ij} + \hat{H}_{ij}(z), \quad I_{ij} = \delta_{ij}, \\ \hat{H}_{ij}(z) &= \hat{H}_{ji}(z) = \int_0^\infty \frac{\partial \hat{\Phi}_i(\rho; z)}{\partial z} \frac{\partial \hat{\Phi}_j(\rho; z)}{\partial z} \rho \, d\rho, \\ \hat{Q}_{ij}(z) &= -\hat{Q}_{ji}(z) = - \int_0^\infty \hat{\Phi}_i(\rho; z) \frac{\partial \hat{\Phi}_j(\rho; z)}{\partial z} \rho \, d\rho. \end{aligned} \quad (14)$$

The discrete spectrum solutions obey the asymptotic boundary condition and the orthonormality conditions

$$\lim_{z \rightarrow \pm\infty} \hat{\chi}^{(i)}(z) = 0 \quad \rightarrow \quad \hat{\chi}^{(i)}(\pm z_{\max}) = 0, \quad \int_{-z_{\max}}^{z_{\max}} (\hat{\chi}^{(i)}(z))^T \hat{\chi}^{(j)}(z) \, dz = \delta_{ij}. \quad (15)$$

The application of this approach to the calculation of low-excited bound states of the hydrogen atom for  $\gamma > 1$  and  $-m = 0, \dots, 10$  will be presented in the forthcoming paper [26] for  $j_{\max} \sim 10$ , while the cases of laboratory fields of  $\gamma \sim 6$  T and  $-m < 150$  were considered in [27].

## 2.2. Galerkin expansion

Consider a formal expansion of the partial solution  $\Psi_i^{Em\sigma}(\rho, z)$  of equations (2)–(5) corresponding to the eigenstate  $|m\sigma i\rangle$ , in terms of the finite set of one-dimensional basis functions  $\{\tilde{\Phi}_j^m(\rho)\}_{j=1}^{j_{\max}}$

$$\Psi_i^{Em\sigma}(\rho, z) = \sum_{j=1}^{j_{\max}} \tilde{\Phi}_j^m(\rho) \tilde{\chi}_j^{(m\sigma i)}(E, z). \quad (16)$$

In the Galerkin approach the wavefunctions  $\tilde{\Phi}_j(\rho) = \tilde{\Phi}_j^m(\rho)$  and the potential curves  $\tilde{E}_j$  (in Ry) are determined as the solutions of the following one-dimensional eigenvalue problem

$$\hat{A}_c \tilde{\Phi}_j(\rho) = \tilde{E}_j \tilde{\Phi}_j(\rho), \quad (17)$$

with the boundary conditions

$$\lim_{\rho \rightarrow 0} \rho \frac{\partial \tilde{\Phi}_j(\rho)}{\partial \rho} = 0, \quad \text{for } m = 0, \quad \text{and} \quad \tilde{\Phi}_j(0) = 0, \quad \text{for } m \neq 0, \quad (18)$$

$$\lim_{\rho \rightarrow \infty} \tilde{\Phi}_j(\rho) = 0. \quad (19)$$

The above eigenvalue problem has the exact solution at fixed  $m$ , normalized like (12)

$$\tilde{\Phi}_j(\rho) = \sqrt{\frac{\gamma N_\rho!}{(N_\rho + |m|)!}} \exp\left(-\frac{\gamma \rho^2}{4}\right) \left(\frac{\gamma \rho^2}{2}\right)^{\frac{|m|}{2}} L_{N_\rho}^{|m|}\left(\frac{\gamma \rho^2}{2}\right), \quad (20)$$

$$\tilde{E}_j = \gamma(2N_\rho + |m| + m + 1),$$

where  $N_\rho = j - 1$  is the transversal quantum number and  $L_{N_\rho}^{|m|}(x)$  is the associated Laguerre polynomial [20]. Note that the Galerkin expansion follows from the Kantorovich expansion at  $z \rightarrow \pm\infty$ , i.e.,

$$\tilde{\Phi}_j(\rho) = \lim_{z \rightarrow \pm\infty} \hat{\Phi}_j(\rho; z), \quad \lim_{z \rightarrow \pm\infty} \hat{E}_j(z) = \tilde{E}_j = \epsilon_{mj}^{\text{th}}(\gamma) = \gamma(2N_\rho + |m| + m + 1). \quad (21)$$

Therefore, we transform the solution of the above problem into the solution of an eigenvalue problem for a set of  $j_{\text{max}}$  ordinary second-order differential equations that determines the energy  $\epsilon$  and the coefficients  $\tilde{\chi}^{(i)}(z)$  of expansion (16)

$$\left(-\mathbf{I} \frac{d^2}{dz^2} + \tilde{\mathbf{U}}(z)\right) \tilde{\chi}^{(i)}(z) = \epsilon_i \mathbf{I} \tilde{\chi}^{(i)}(z), \quad (22)$$

and the matrix  $\tilde{\mathbf{U}}(z) = \tilde{\mathbf{U}}(-z)$  is expressed as

$$\tilde{U}_{ij}(z) = \frac{\tilde{E}_i + \tilde{E}_j}{2} \delta_{ij} - \int_0^\infty \tilde{\Phi}_i(\rho) \frac{2Z}{\sqrt{\rho^2 + z^2}} \tilde{\Phi}_j(\rho) \rho d\rho. \quad (23)$$

The discrete spectrum solutions obey the asymptotic boundary condition and the orthonormality condition

$$\lim_{z \rightarrow \pm\infty} \tilde{\chi}^{(i)}(z) = 0 \quad \rightarrow \quad \tilde{\chi}^{(i)}(\pm z_{\text{max}}) = 0, \quad \int_{-z_{\text{max}}}^{z_{\text{max}}} (\tilde{\chi}^{(i)}(z))^T \tilde{\chi}^{(j)}(z) dz = \delta_{ij}. \quad (24)$$

The application of this approach to the calculation of bound states of the hydrogen atom for  $\gamma > 1$  is well known in [28]. The calculation of photoionizations of hydrogen in a strong magnetic field of  $B \sim 600\text{--}2000$  T was considered within the frameworks of the multichannel quantum defect theory [29], while for the cases of laboratory fields of  $B \sim 6$  T such a type of calculations is of course not practicable, because  $j_{\text{max}} \sim 200$ .

### 2.3. Relation between the parity functions and the functions having physical scattering asymptotic form in cylindrical coordinates

The asymptotic form of the coefficients  $\tilde{\chi}^{(n)}(z)$  of expansion (16) (or  $\hat{\chi}^{(n)}(z)$  of expansion (8)) with fixed  $m$ ,  $\sigma$  and  $\epsilon = 2E$  for the  $n$ th solution in open channels is

$$\chi_{E\sigma n'n}(z \rightarrow \pm\infty) = \begin{cases} \frac{a_{+1n'n}}{\sqrt{p_{n'}}} \cos\left(p_{n'}z + \frac{Z}{p_{n'}} \frac{z}{|z|} \ln(2p_{n'}|z|) + \frac{z}{|z|} \delta_{+1n}\right), & \sigma = +1, \\ \frac{a_{-1n'n}}{\sqrt{p_{n'}}} \sin\left(p_{n'}z + \frac{Z}{p_{n'}} \frac{z}{|z|} \ln(2p_{n'}|z|) + \frac{z}{|z|} \delta_{-1n}\right), & \sigma = -1, \end{cases} \quad (25)$$

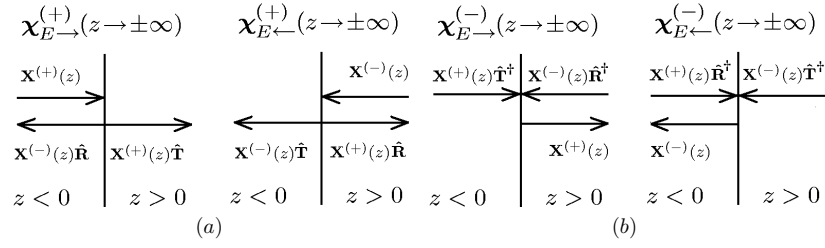


**Figure 2.** Schematic diagrams of the continuum spectrum states' waves having the asymptotic form: (a) 'incident wave + outgoing wave', (b) 'incident wave + ingoing wave'.

where  $p_n = \sqrt{2E - \epsilon_{mn}^{\text{th}}} \geq 0$  and  $n, n' = 1, \dots, N_o$ ,  $\delta_{\sigma n} = \delta_n^{\sigma} + \delta_n^c - (\sigma + 1)\pi/4$  are the phase shifts,  $\delta_n^{\sigma}$  and  $\delta_n^c$  are the eigenchannel short-range and Coulomb phase shifts,  $a_{\sigma n'n} = C_{n'n}^{\sigma}$  are the amplitudes or mixed parameters defined in section 4 and  $N_o = \max_{2E \geq \epsilon_{mn}^{\text{th}}} n$  is the number of open channels. Equation (25) may be rewritten in the matrix form, so that

$$\chi_{E\sigma}(z \rightarrow \pm\infty) = \begin{cases} \begin{cases} \frac{1}{2}\mathbf{X}^{(+)}(z)\mathbf{A}_{+1} + \frac{1}{2}\mathbf{X}^{(-)}(z)\mathbf{A}_{+1}^*, & \sigma = +1, \\ \frac{1}{2l}\mathbf{X}^{(+)}(z)\mathbf{A}_{-1} - \frac{1}{2l}\mathbf{X}^{(-)}(z)\mathbf{A}_{-1}^*, & \sigma = -1, \end{cases} & , \quad z > 0, \\ \begin{cases} \frac{1}{2}\mathbf{X}^{(+)}(z)\mathbf{A}_{+1}^* + \frac{1}{2}\mathbf{X}^{(-)}(z)\mathbf{A}_{+1}, & \sigma = +1, \\ \frac{1}{2l}\mathbf{X}^{(+)}(z)\mathbf{A}_{-1}^* - \frac{1}{2l}\mathbf{X}^{(-)}(z)\mathbf{A}_{-1}, & \sigma = -1, \end{cases} & , \quad z < 0, \end{cases} \quad (26)$$

where coefficients of matrices  $\mathbf{X}^{(\pm)}(z)$  and  $\mathbf{A}_{\pm 1}$  take the form

$$X_{n'n}^{(\pm)}(z) = p_{n'}^{-1/2} \exp\left(\pm i p_{n'} z \pm i \frac{Z}{p_{n'}} \frac{z}{|z|} \ln(2p_{n'}|z|)\right) \delta_{n'n}, \quad (27)$$

$$A_{\sigma n'n} = a_{\sigma n'n} \exp(i\delta_{\sigma n}). \quad (28)$$

On the other hand, the function that describes the incidence of the particle and its scattering, having the asymptotic form 'incident wave + outgoing wave' (see figure 2(a)), is

$$\chi_{E\hat{v}}^{(+)}(z \rightarrow \pm\infty) = \begin{cases} \begin{cases} \mathbf{X}^{(+)}(z)\hat{\mathbf{T}}, & z > 0, \\ \mathbf{X}^{(+)}(z) + \mathbf{X}^{(-)}(z)\hat{\mathbf{R}}, & z < 0, \end{cases} & , \quad \hat{v} = \rightarrow, \\ \begin{cases} \mathbf{X}^{(-)}(z) + \mathbf{X}^{(+)}(z)\hat{\mathbf{R}}, & z > 0, \\ \mathbf{X}^{(-)}(z)\hat{\mathbf{T}}, & z < 0, \end{cases} & , \quad \hat{v} = \leftarrow, \end{cases} \quad (29)$$

where  $\hat{\mathbf{T}}$  and  $\hat{\mathbf{R}}$  are the transmission and reflection amplitude matrices,  $\hat{\mathbf{T}}^\dagger \hat{\mathbf{T}} + \hat{\mathbf{R}}^\dagger \hat{\mathbf{R}} = \mathbf{I}_{oo}$ ,  $\hat{v}$  denotes the initial direction of the particle motion along the  $z$  axis and  $\mathbf{I}_{oo}$  is the unit  $N_o \times N_o$  matrix. Note that due to the symmetry of the scattering potential the transmission and reflection coefficients are independent of the direction of the incident wave vector.

This wavefunction may be presented as a linear combination of the solutions having positive and negative parities:

$$\chi_{E\hat{v}}^{(+)}(z) = \chi_{E,+1}(z)\mathbf{B}_{+1} \pm i\chi_{E,-1}(z)\mathbf{B}_{-1}. \quad (30)$$

It is easy to show that  $\mathbf{B}_\sigma = [\mathbf{A}_\sigma^*]^{-1}$ , and  $\hat{\mathbf{T}}$  and  $\hat{\mathbf{R}}$  are defined by

$$\begin{aligned} \hat{\mathbf{T}} &= \frac{1}{2}(\mathbf{A}_{+1}\mathbf{B}_{+1} + \mathbf{A}_{-1}\mathbf{B}_{-1}) = \frac{1}{2}(-\check{\mathbf{S}}_{+1} + \check{\mathbf{S}}_{-1}), \\ \hat{\mathbf{R}} &= \frac{1}{2}(\mathbf{A}_{+1}\mathbf{B}_{+1} - \mathbf{A}_{-1}\mathbf{B}_{-1}) = \frac{1}{2}(-\check{\mathbf{S}}_{+1} - \check{\mathbf{S}}_{-1}), \end{aligned} \quad (31)$$

where  $\check{S}_\sigma$  is the scattering matrix at fixed  $\sigma$  defined by (28). However, to calculate the ionization cross section it is necessary to use the function having the reverse asymptotic form ‘incident wave + ingoing wave’ (see figure 2(b)), that is

$$\chi_{E\hat{v}}^{(-)}(z \rightarrow \pm\infty) = \begin{cases} \begin{cases} \mathbf{X}^{(+)}(z) + \mathbf{X}^{(-)}(z)\hat{\mathbf{R}}^\dagger, & z > 0, \\ \mathbf{X}^{(+)}(z)\hat{\mathbf{T}}^\dagger, & z < 0, \end{cases} & \hat{v} = \rightarrow, \\ \begin{cases} \mathbf{X}^{(-)}(z)\hat{\mathbf{T}}^\dagger, & z > 0, \\ \mathbf{X}^{(-)}(z) + \mathbf{X}^{(+)}(z)\hat{\mathbf{R}}^\dagger, & z < 0, \end{cases} & \hat{v} = \leftarrow, \end{cases} \quad (32)$$

or

$$\chi_{E\hat{v}}^{(-)}(z) = \chi_{E,+1}(z)\mathbf{B}_{+1}^* \pm \iota \chi_{E,-1}(z)\mathbf{B}_{-1}^*. \quad (33)$$

Note that  $(\chi_{E\hat{v}}^{(-)}(z))^* = \chi_{E\hat{v}}^{(+)}(z)$ . The functions are normalized so that

$$\sum_{n''=1}^{j_{\max}} \int_{-\infty}^{\infty} (\chi_{E'm\hat{v}'n''n'}^{(\pm)}(z))^* \chi_{Em\hat{v}n'n}^{(\pm)}(z) dz = 2\pi \delta(E' - E) \delta_{\hat{v}'\hat{v}} \delta_{n'n}. \quad (34)$$

The  $\hat{\mathbf{S}}$ -matrix may be composed of the transmission and reflection amplitudes

$$\hat{\mathbf{S}} = \begin{pmatrix} \hat{\mathbf{T}} & \hat{\mathbf{R}} \\ \hat{\mathbf{R}} & \hat{\mathbf{T}} \end{pmatrix}. \quad (35)$$

This matrix is unitary, since  $\hat{\mathbf{T}}^\dagger \hat{\mathbf{T}} + \hat{\mathbf{R}}^\dagger \hat{\mathbf{R}} = \mathbf{I}_{oo}$  and  $\hat{\mathbf{R}}^\dagger \hat{\mathbf{T}} + \hat{\mathbf{T}}^\dagger \hat{\mathbf{R}} = \mathbf{0}$ . These conditions will be used to check the accuracy of numerical multichannel calculations of continuous spectrum wavefunctions in section 5.

To calculate the ionization it is convenient to use the function renormalized to  $\delta(E' - E)$ , i.e., divided by  $\sqrt{2\pi}$  :

$$|E\hat{v}mN_\rho\rangle = \frac{\exp(\iota m\varphi)}{2\pi} \sum_{n'=1}^{j_{\max}} \tilde{\Phi}_{n'}(\rho) \tilde{\chi}_{Em\hat{v}n'n}^{(-)}(z) \quad (36)$$

or

$$|E\hat{v}mN_\rho\rangle = \frac{\exp(\iota m\varphi)}{2\pi} \sum_{n'=1}^{j_{\max}} \hat{\Phi}_{n'}(\rho; z) \hat{\chi}_{Em\hat{v}n'n}^{(-)}(z), \quad (37)$$

where  $N_\rho = n - 1$ . The expression for the cross section of ionization by the light linearly polarized along the axis  $z$  is

$$\sigma_{Nlm}^d(\omega) = 4\pi^2 \alpha \omega \sum_{N_\rho=0}^{N_o-1} \sum_{\hat{v}} |\langle E\hat{v}mN_\rho | z | Nlm \rangle|^2 a_0^2. \quad (38)$$

In the above expressions  $\omega = E - E_{Nlm}$  is the frequency of radiation,  $E_{Nlm}$  is the energy of the initial bound state  $|Nlm\rangle$  specified by the spherical quantum numbers  $N, l, m$  defined in section 3,  $\alpha$  is the fine-structure constant,  $a_0$  is the Bohr radius.

For recombination the wavefunction should be renormalized to one particle per unit length in the incident wave

$$|vmN_\rho\rangle = \sqrt{p_n} \frac{\exp(\iota m\varphi)}{\sqrt{2\pi}} \sum_{n'=1}^{j_{\max}} \tilde{\Phi}_{n'}(\rho) \tilde{\chi}_{Em\hat{v}n'n}^{(+)}(z) \quad (39)$$

or

$$|vmN_\rho\rangle = \sqrt{p_n} \frac{\exp(\iota m\varphi)}{\sqrt{2\pi}} \sum_{n'=1}^{j_{\max}} \hat{\Phi}_{n'}(\rho; z) \hat{\chi}_{Em\hat{v}n'n}^{(+)}(z), \quad (40)$$

where  $v = \hat{v} p_n$  and  $N_\rho = n - 1$ . The expression for the rate of recombination induced by the light linearly polarized along the axis  $z$  for the particle, initially moving in the channel  $N_\rho$  with the velocity  $v$  has the form

$$\lambda_{NN_\rho}^{rec}(v) = 4\pi^2 \alpha I \sum_{l=0}^{N-1} \sum_{m=-l}^0 |\langle Nlm | z | v m N_\rho \rangle|^2 \delta(E - E_{Nlm} - \omega) a_0^2, \quad (41)$$

$I$  being the intensity of the incident light.

For the light circularly polarized in the plane  $xOy$  the above expressions read as

$$\sigma_{Nlm}^p(\omega) = 4\pi^2 \alpha \omega \sum_{N_\rho=0}^{N_o-1} \sum_{\hat{v}} |\langle E \hat{v} m \pm 1 N_\rho | \vec{e}_\pm \vec{r} | Nlm \rangle|^2 a_0^2, \quad (42)$$

$$\lambda_{NN_\rho}^{rec}(v) = 4\pi^2 \alpha I \sum_{l=0}^{N-1} \sum_{m=-l}^0 |\langle Nlm \pm 1 | \vec{e}_\pm \vec{r} | v m N_\rho \rangle|^2 \delta(E - E_{Nlm} - \omega) a_0^2, \quad (43)$$

where the complex unit vectors are  $\vec{e}_\pm = \frac{1}{\sqrt{2}} \vec{i} \pm \frac{i}{\sqrt{2}} \vec{j}$ .

### 3. Statement of the problem in spherical coordinates

In the spherical coordinates  $(r, \theta, \varphi)$  (see figure 1) equation (2) can be rewritten as [31]

$$\left( -\frac{1}{r^2} \frac{\partial}{\partial r} r^2 \frac{\partial}{\partial r} + \frac{1}{r^2} \hat{A}(p) - \frac{2Z}{r} \right) \Psi(r, \eta) = \epsilon \Psi(r, \eta) \quad (44)$$

in the domain  $\Omega$ :  $0 < r < \infty$  and  $-1 < \eta = \cos \theta < 1$ . Here  $\hat{A}(p)$  is the parametric Hamiltonian

$$\hat{A}(p) = -\frac{\partial}{\partial \eta} (1 - \eta^2) \frac{\partial}{\partial \eta} + \frac{m^2}{1 - \eta^2} + 2pm + p^2(1 - \eta^2), \quad (45)$$

$p = \gamma r^2/2$  and  $\Psi(r, \eta) \equiv \Psi^{m\sigma}(r, \eta) = \sigma \Psi^{m\sigma}(r, -\eta)$ . The sign of  $z$ -parity  $\sigma = (-1)^{N_\eta}$  is defined by the number of nodes  $N_\eta$  of the solution  $\Psi(r, \eta)$  as a function of  $\eta$ . We will also use the scaled radial variable  $\hat{r} = r\sqrt{\gamma}$ , the effective charge  $\hat{Z} = Z/\sqrt{\gamma}$  and the scaled energy  $\hat{\epsilon} = \epsilon/\gamma$  or  $\hat{E} = E/\gamma$ . Practically it means replacing  $\gamma$  with 1 and multiplying  $Z$  by  $1/\sqrt{\gamma}$  and  $\epsilon$  or  $E$  by  $1/\gamma$  in all equations above.

The boundary conditions in each  $m\sigma$  subspace of the full Hilbert space have the form

$$\lim_{\eta \rightarrow \pm 1} (1 - \eta^2) \frac{\partial \Psi(r, \eta)}{\partial \eta} = 0, \quad \text{for } m = 0, \quad \text{and } \Psi(r, \pm 1) = 0, \quad \text{for } m \neq 0, \quad (46)$$

$$\lim_{r \rightarrow 0} r^2 \frac{\partial \Psi(r, \eta)}{\partial r} = 0. \quad (47)$$

The wavefunction of the discrete spectrum obeys the asymptotic boundary condition. Approximately this condition is replaced by the boundary condition of the first type at large, but finite  $r = r_{\max}$ , namely,

$$\lim_{r \rightarrow \infty} r^2 \Psi(r, \eta) = 0 \quad \rightarrow \quad \Psi(r_{\max}, \eta) = 0. \quad (48)$$



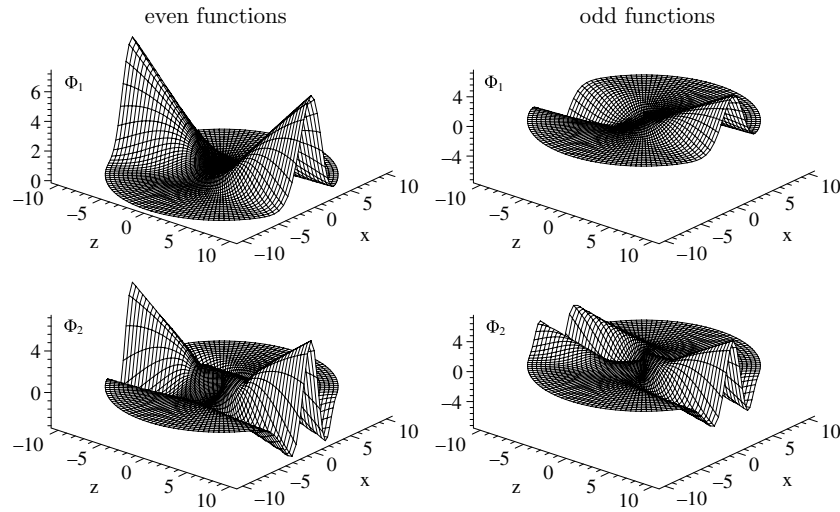


**Figure 3.** Profiles of the even  $\Phi_i \equiv \Phi^{m\sigma=+1}(\eta; r)$  and odd  $\Phi_i \equiv \Phi^{m\sigma=-1}(\eta; r)$  basis functions at  $m = 0$  and  $\gamma = 1$  for  $i = 1, 2$  in the  $zx$  plane.

In the Fano-Lee **R**-matrix theory [14, 15] the wavefunction of the continuum  $\Psi(r, \eta)$  obeys the boundary condition of the third type at fixed values of the energy  $\epsilon$  and the radial variable  $r = r_{\max}$

$$\frac{\partial \Psi(r, \eta)}{\partial r} - \mu \Psi(r, \eta) = 0. \quad (49)$$

Here the parameters  $\mu \equiv \mu(r_{\max}, \epsilon)$ , determined by the variational principle, play the role of eigenvalues of the logarithmic normal derivative matrix of the solution of the boundary problem (44)–(47) and (49).

### 3.1. Kantorovich expansion

Consider a formal expansion of the partial solution  $\Psi_i^{Em\sigma}(r, \eta)$  of equations (44)–(47) with conditions (48) and (49), corresponding to the eigenstate  $|m\sigma i\rangle$ , in terms of the finite set of one-dimensional basis functions  $\{\Phi_j^{m\sigma}(\eta; r)\}_{j=1}^{j_{\max}}$

$$\Psi_i^{Em\sigma}(r, \eta) = \sum_{j=1}^{j_{\max}} \Phi_j^{m\sigma}(\eta; r) \chi_j^{(m\sigma i)}(E, r). \quad (50)$$

In equation (50) the functions  $\chi^{(i)}(r) \equiv \chi^{(m\sigma i)}(E, r)$ ,  $(\chi^{(i)}(r))^T = (\chi_1^{(i)}(r), \dots, \chi_{j_{\max}}^{(i)}(r))$  are unknown and the surface functions  $\Phi(\eta; r) \equiv \Phi^{m\sigma}(\eta; r) = \sigma \Phi^{m\sigma}(-\eta; r)$ ,  $(\Phi(\eta; r))^T = (\Phi_1(\eta; r), \dots, \Phi_{j_{\max}}(\eta; r))$  form an orthonormal basis for each value of  $r$  which is treated as a parameter (see figure 3).

In the Kantorovich approach the wavefunctions  $\Phi_j(\eta; r)$  and the potential curves  $E_j(r)$  (in Ry) are determined as the solutions of the following one-dimensional parametric eigenvalue problem

$$\hat{A}(p)\Phi_j(\eta; r) = E_j(r)\Phi_j(\eta; r), \quad (51)$$

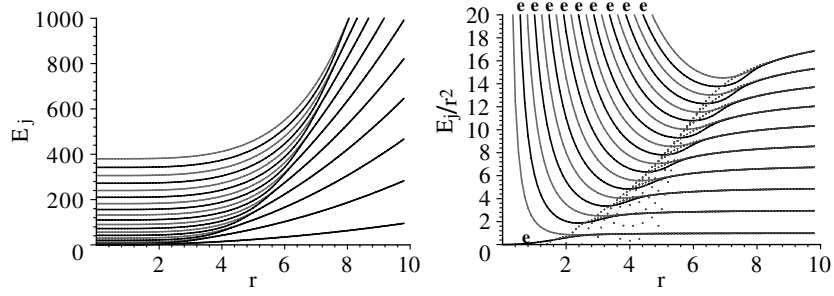


**Figure 4.** Potential curves  $E_j(r)$ ,  $j = 1, 2, \dots$  at  $m = 0$  and  $\gamma = 1$  for some first even  $j = (l - |m|)/2 + 1$  (marked by 'e') and odd  $j = (l - |m| + 1)/2$  states. Dotted lines display the asymptotic behavior at large  $r$ .

with the boundary conditions

$$\lim_{\eta \rightarrow \pm 1} (1 - \eta^2) \frac{\partial \Phi_j(\eta; r)}{\partial \eta} = 0, \quad \text{for } m = 0 \quad \text{and} \quad \Phi_j(\pm 1; r) = 0, \quad \text{for } m \neq 0. \quad (52)$$

Since the operator in the left-hand side of equation (51) is self-adjoint, its eigenfunctions are orthonormal,

$$\langle \Phi_i(\eta; r) | \Phi_j(\eta; r) \rangle_\eta = \int_{-1}^1 \Phi_i(\eta; r) \Phi_j(\eta; r) d\eta = \delta_{ij}. \quad (53)$$

Note that the solutions of this problem with shifted eigenvalues,  $\check{E}_j(r) = E_j(r) - 2pm$ , correspond to the solutions of the eigenvalue problem for the AOSF [20]

$$A(p) \Phi_j(\eta; r) = \check{E}_j(r) \Phi_j(\eta; r), \quad (54)$$

where  $A(p) = \hat{A}(p) - 2pm$ . At fixed values  $\sigma = \pm 1$  and  $|m|$  the eigenfunctions  $\Phi_j(\theta; r)$  are sought in the form of a series expansion over the normalized associated Legendre polynomials  $P_{|m|+s}^{|m|}(\eta)$  [20] with unknown coefficients  $c_{sj}^{|m|\sigma}(r)$ ,

$$\Phi_j(\eta; r) = \sum_{s=(1-\sigma)/2}^{s_{\max}} c_{sj}^{|m|\sigma}(r) P_{|m|+s}^{|m|}(\eta), \quad (55)$$

where  $s$  is an even (odd) integer at  $\sigma = (-1)^s = \pm 1$ . The calculations of eigenfunctions  $\Phi_j(\theta; r)$  and of eigenvalues  $E_i(r)$  were performed by a special choice of value  $s_{\max}$  to achieve a relative computer accuracy using the code POTHMF realizing in FORTRAN [23]. Their plots are presented in figures 3 and 4. For small  $p$  the asymptotic behavior of the eigenvalues  $E_j(r)$ ,  $j = 1, 2, \dots$  at fixed values of  $m$  and  $\sigma$  is determined by the values of the orbital quantum number  $l$  labeled by a conventional sequences of  $\{s, p, d, f, g, h, i, k, l, \dots\}$ :  $E_j(0) = l(l+1)$ ,  $l = 0, 1, \dots$ , where  $j = (l - |m|)/2 + 1$  for even states,  $\sigma = +1 = (-1)^{l-|m|}$  and  $j = (l - |m| + 1)/2$  for odd states,  $\sigma = -1 = (-1)^{l-|m|}$ , defined by  $\Phi_j(\eta; 0) = P_l^{|m|}(\eta)$ . Taking into account the fact that the number of nodes  $N_\eta$  of the eigenfunction  $\Phi_j(\eta; r)$  at fixed  $m$  and  $\sigma = (-1)^{N_\eta}$  does not depend on the parameter  $p$ , we find a one-to-one correspondence between these sets, i.e.,  $N_\eta = l - |m|$ .

For large  $r$  the asymptotic behavior of the eigenfunctions  $\Phi_j(\eta; r)$  and eigenvalues  $E_j(r)$  at fixed values of  $m$  and  $\sigma$  is determined by the value of the transversal quantum number,

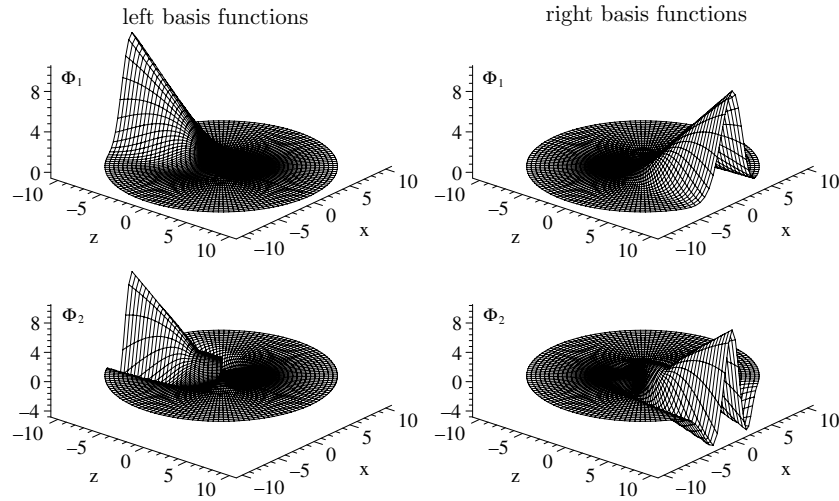


**Figure 5.** Profiles of the left  $\Phi_i \equiv \Phi^{m \rightarrow}(\eta; r)$  and right  $\Phi_i \equiv \Phi^{m \leftarrow}(\eta; r)$  basis functions at  $m = 0$  and  $\gamma = 1$  for  $i = 1, 2$  in the  $zx$  plane.

$N_\rho = j - 1$  (see equations (20) and (21) and section 3.4)

$$\begin{aligned} \tilde{\Phi}_j(\rho) &= \lim_{r \rightarrow \infty, |\eta| \sim 1} r^{-1} \Phi_j(|\eta|; r), \\ \lim_{r \rightarrow \infty} r^{-2} E_j(r) &= \epsilon_{mj}^{\text{th}}(\gamma) = \gamma(2N_\rho + |m| + m + 1). \end{aligned} \quad (56)$$

The transversal quantum number  $N_\rho$ , i.e., the number of nodes of the eigenfunction  $\Phi^{m\sigma}(\eta; r)$  in the subinterval  $0 < \eta < 1$  or  $-1 < \eta < 0$ , can be expressed via  $N_\eta$  as follows:  $N_\rho = N_\eta/2$  for the even states,  $\sigma = +1$  and  $N_\rho = (N_\eta - 1)/2$  for the odd states,  $\sigma = -1$ . It means that the eigenfunctions

$$\Phi^{m\hat{v}}(\eta; r) = \frac{\Phi^{m\sigma=+1}(\eta; r) \pm \Phi^{m\sigma=-1}(\eta; r)}{\sqrt{2}}, \quad (57)$$

labeled by  $\hat{v} = \overset{\leftarrow}{\rightarrow}$  at large  $r$  are localized in the vicinity of  $\eta = \pm 1$  (i.e., at  $z \rightarrow +\infty$  and  $z \rightarrow -\infty$ ) and have  $N_\rho$  nodes in the subintervals  $0 < \eta < 1$  and  $-1 < \eta < 0$ , respectively (see figure 5). Such asymptotic functions  $\Phi^{m\hat{v}}(\eta; r)$  correspond to  $\tilde{\Phi}^m(\rho)$  in equations (20) and (21). Their asymptotic behavior is considered in section 3.4. Taking into account the above-mentioned correspondence rules between the quantum numbers  $N_\eta$  and  $N_\rho$  and number  $j$  at fixed values  $m$  and  $\sigma$ , we will use the unified number,  $j$ , without pointing out explicitly a concrete type of quantum numbers.

From here on we transform the solution of problem (44) into the solution of an eigenvalue problem for a set of  $j_{\text{max}}$  ordinary second-order differential equations that determine the energy  $\epsilon$  and the coefficients  $\chi^{(i)}(r)$  of expansion (50) (the radial wavefunctions):

$$\left( -\mathbf{I} \frac{1}{r^2} \frac{d}{dr} r^2 \frac{d}{dr} + \frac{\mathbf{U}(r)}{r^2} + \mathbf{Q}(r) \frac{d}{dr} + \frac{1}{r^2} \frac{dr^2 \mathbf{Q}(r)}{dr} \right) \chi^{(i)}(r) = \epsilon_i \mathbf{I} \chi^{(i)}(r), \quad (58)$$

$$\lim_{r \rightarrow 0} r^2 \left( \frac{d\chi^{(i)}(r)}{dr} - \mathbf{Q}(r) \chi^{(i)}(r) \right) = 0. \quad (59)$$

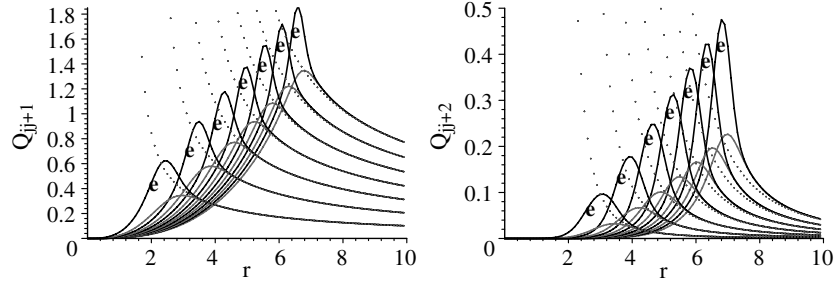


**Figure 6.** Radial matrix elements  $Q_{ij}(r)$  for even (marked by 'e') and odd parities at  $m = 0$  and  $\gamma = 1$ . Dotted lines display the asymptotic behavior at large  $r$ .

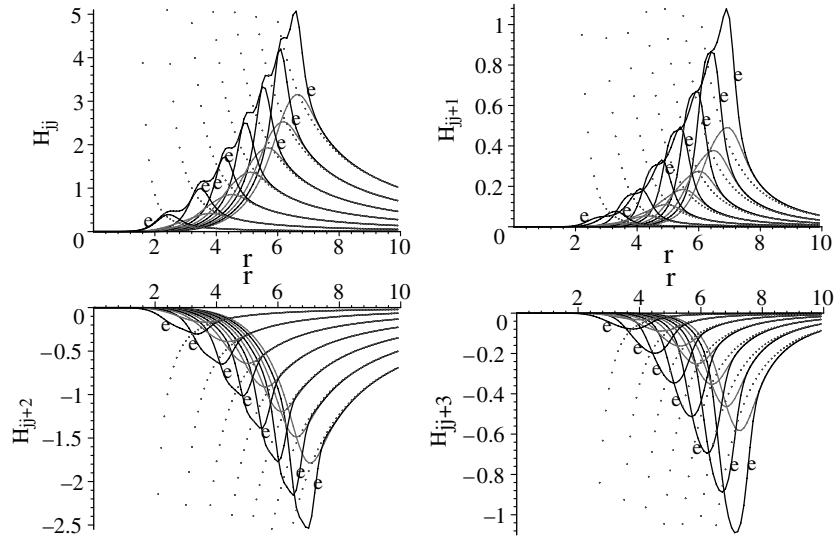


**Figure 7.** Radial matrix elements  $H_{ij}(r)$  for even (marked by 'e') and odd parities at  $m = 0$  and  $\gamma = 1$ . Dotted lines display the asymptotic behavior at large  $r$ .

Here  $\mathbf{U}(r)$  and  $\mathbf{Q}(r)$  are  $j_{\max} \times j_{\max}$  matrices with the elements expressed as

$$\begin{aligned}
 U_{ij}(r) &= \frac{E_i(r) + E_j(r)}{2} \delta_{ij} - 2Zr \delta_{ij} + r^2 H_{ij}(r), \\
 H_{ij}(r) &= H_{ji}(r) = \int_{-1}^1 \frac{\partial \Phi_i(\eta; r)}{\partial r} \frac{\partial \Phi_j(\eta; r)}{\partial r} d\eta, \\
 Q_{ij}(r) &= -Q_{ji}(r) = - \int_{-1}^1 \Phi_i(\eta; r) \frac{\partial \Phi_j(\eta; r)}{\partial r} d\eta.
 \end{aligned} \tag{60}$$

The calculations of radial coupling matrix elements  $H_{ij}(r)$  and  $Q_{ij}(r)$  were performed by a special choice of value of matching point  $r_{\text{match}}$  of their asymptotic form from section 3.4 to achieve a relative computer accuracy using the code POTHMF realizing in FORTRAN [23]. Their plots are presented in figures 6 and 7. The peculiarities of behavior of the plots and the corresponding asymptotics are considered in section 3.4.

The discrete spectrum solutions obey the asymptotic boundary condition and the orthonormality conditions

$$\lim_{r \rightarrow \infty} r^2 \chi^{(i)}(r) = 0 \quad \rightarrow \quad \chi^{(i)}(r_{\max}) = 0, \quad \int_0^{r_{\max}} r^2 (\chi^{(i)}(r))^T \chi^{(j)}(r) dr = \delta_{ij}. \quad (61)$$

The continuous spectrum solution  $\chi^{(i)}(r)$  satisfies the third-type boundary condition

$$\frac{d\chi(r)}{dr} = \mathbf{R}\chi(r), \quad r = r_{\max}, \quad (62)$$

where the nonsymmetrical matrix  $\mathbf{R}$  is calculated using the method of [21].

Thus, within the framework of the Kantorovich approach the original problem is reduced to the following steps.

- The calculation of the potential curves  $E_j(r)$  and eigenfunctions  $\Phi_j(\theta; r)$  of the spectral problem (51)–(53) for a given set of  $r \in \omega_r$  at fixed values  $m$  and  $\gamma = 1$ .
- The calculation of the derivatives  $\partial \Phi(\theta; r)/\partial r$  and the corresponding integrals (see (60)) for the radial coupling matrices  $\mathbf{U}(r)$  and  $\mathbf{Q}(r)$ .
- The calculation of the scaled energies  $\hat{\epsilon}$  and radial wavefunctions  $\chi^{(i)}(r)$  as solutions of 1D-eigenvalue problem (58)–(60) with the conditions (61) at fixed  $m$ ,  $\gamma = 1$  and the effective charge  $\hat{Z} = Z/\sqrt{\gamma}$ . Analysis of the convergence of the solutions depending on the number of channels  $j_{\max}$ . Recalculation of the scaled energies into the initial ones  $\epsilon = \hat{\epsilon}\gamma$  or  $E = \hat{E}\gamma$ .
- The calculation of the matrix  $\mathbf{R}$  and the reaction matrix  $\mathbf{K}$  (equations (62) and (100)), corresponding to the radial wavefunctions  $\chi^{(i)}(r)$ , as solutions of 1D-eigenvalue problem (58)–(60) with the condition (62) at fixed  $m$ ,  $\gamma = 1$ , the effective charge  $\hat{Z} = Z/\sqrt{\gamma}$  and the scaled energy  $\hat{\epsilon}$  or  $\hat{E}$ . The analysis of the convergence of the solutions depends on the number of channels  $j_{\max}$ .

Taking into account the above rules of correspondence and the asymptotic behavior of the eigenvalues  $E_i(r)$  at large  $r$  (see also section 3.4), we can express the values of the binding energy  $\mathcal{E}$  via the eigenvalues  $\epsilon_i$  of the problem (58)–(61) numbered by a vibration quantum number,  $v = 0, 1, 2, \dots$ , in ascending order  $\epsilon_i = \epsilon_{iv}$ :  $\epsilon_{i0} < \epsilon_{i1} < \epsilon_{i2} < \dots$ , as  $\mathcal{E} = (\epsilon_{mi}^{\text{th}}(\gamma) - \epsilon_{iv})/2$  (in au), where  $\epsilon_{m\sigma i}^{\text{th}}(\gamma)$  is the true threshold shift (56) or the reduced one  $\epsilon_m^{\text{th}}(\gamma) = \gamma(|m| + m + 1)$ . Then for  $\gamma \rightarrow 0$  one can mark eigenvalues  $\epsilon_i = \epsilon_{iv}$  by a set of quantum numbers  $(NN_r m \sigma)$ , where  $N$  is a principal quantum number of a free-hydrogen-like atom and  $N_r$  is an integer that numerates in ascending order the zero-order degenerate perturbation theory energy,  $\epsilon_{iv} = 2E_N^{(0)} + 2E_{NN_r m \sigma}^{(1)}\gamma^2 + O(\gamma^4)$  at fixed  $N$ . The corresponding zero-order approximation states,  $|NN_r m \sigma\rangle$ , are determined by a linear combination of free-hydrogen atom states  $|Nlm\rangle$  and are labeled by  $N_r = 0, 2, \dots, 2[(N-1-|m|)/2]$  for  $\sigma = +1$  and  $N_r = 1, 3, \dots, 2[(N-|m|)/2] - 1$  for  $\sigma = -1$ . The latter can be marked also by a set of spherical quantum numbers  $(Nlm)$  because of the correspondence of the number of radial nodes,  $N_r = N - l - 1$ , of the free-hydrogen states and the number of changing sign,  $[N_r/2]$ , of coefficients of the linear combination  $|NN_r m \sigma\rangle$ . To show this correspondence visually, we display in figures 8 and 9, as an example, a comparison of the three-dimensional plots of the normalized wavefunctions in the  $zx$  plane of the free-hydrogen atom spherical states  $|Nlm\rangle$  and anisotropic zero-order approximation states  $|NN_r m \sigma\rangle$  separated by parity  $\sigma = \pm 1$  for a manifold with  $N = 9$  and  $m = 0$ , for which the convergence of the method for

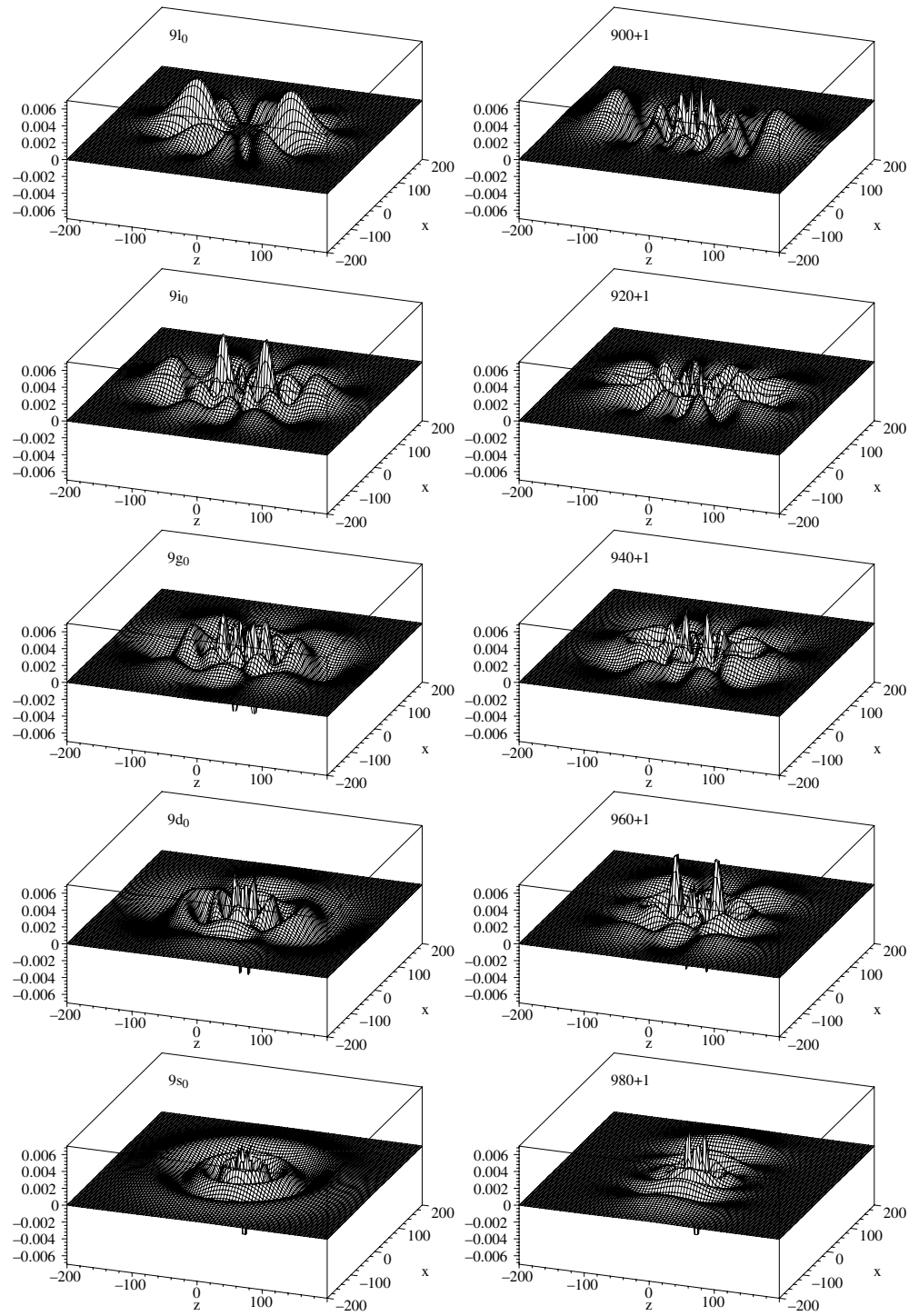


**Figure 8.** The three-dimensional plots of the normalized even wavefunctions ( $\sigma = +1$ ) in the  $zx$  plane of free-hydrogen atom states  $|Nlm\rangle$  and zero-order approximation states  $|NN_r m \sigma\rangle$  for a manifold with  $N = 9$  and  $m = 0$ .

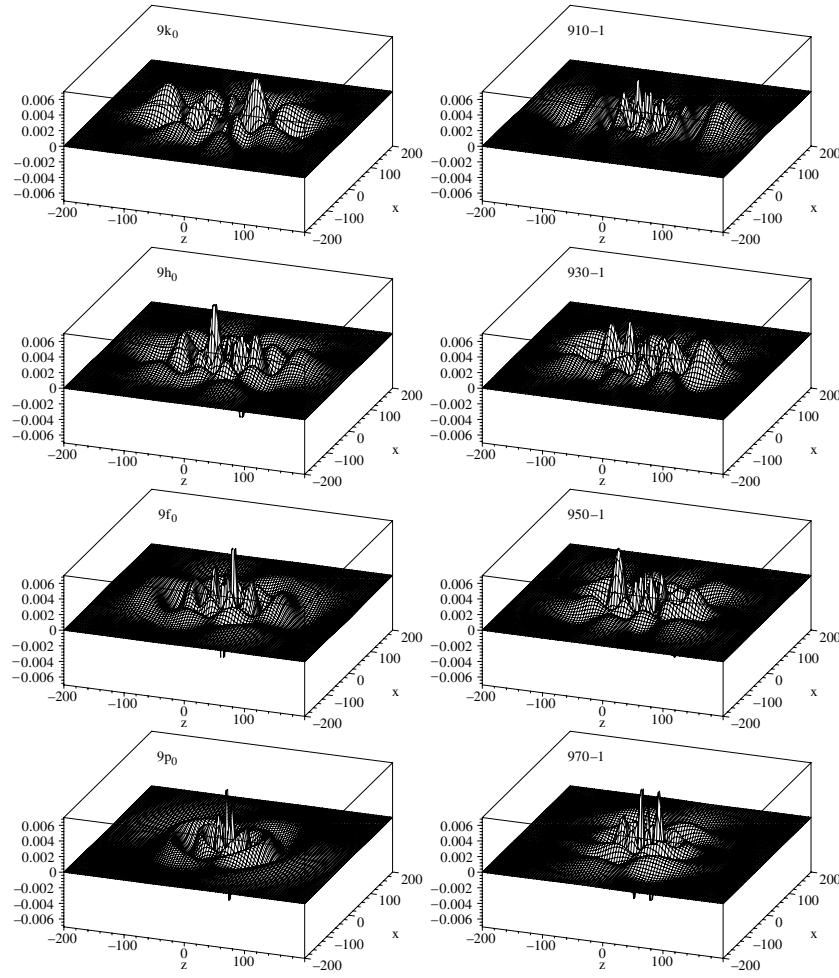


**Figure 9.** Same as in figure 8 but odd wavefunctions ( $\sigma = -1$ ).

the energy of states by  $j_{\max}$  has been studied in paper [9]. One can see that for anisotropic states belong to the lower part of the spectrum the so-called vibrational states (with minimum energy corrections  $E_{NN_r m \sigma}^{(1)}$ ) are distributed mainly along the  $z$ -axis while for anisotropic states belong to the upper part of the spectrum the so-called rotational states (with maximum energy corrections  $E_{NN_r m \sigma}^{(1)}$ ) are distributed mainly across the  $z$ -axis. An appearance of anisotropy of such states in the photoionization cross-section calculations will be shown explicitly in section 5. Indeed, for  $\gamma \rightarrow 0$  it is sufficient to cut  $j_{\max} \geq 2[(N - |m|)/2]$  in (58)–(61), while for  $\gamma \rightarrow \infty$  a diagonal approximation of equations (16) and (8) or an effective approximation of equations (58)–(61) given in appendix B is sufficient to yield the known adiabatic classification by  $[N_\rho N_z]$  or  $[N_\rho N_{|z|}]$  with fixed  $m, \sigma$ . Here adiabatic quantum numbers  $N_z = 2N_{|z|} + (1 - \sigma)/2$  and  $N_{|z|}$  can be determined as a sum of the number of nodes,  $N_r$ , and the number of changing sign of coefficients of the linear combination  $|NN_r m \sigma\rangle$ , i.e.  $N_{|z|} = [(N + 1 - |m| - (1 - \sigma)/2)/2][(N - |m| - (1 - \sigma)/2)/2] + [N_r/2]$ .



### 3.2. Expansion of the matrix elements at small $r$

In accordance with [22] the asymptotic values of the potential curves  $E_j(r)$ , radial matrix elements  $H_{jj'}(r)$  and  $Q_{jj'}(r)$  at small  $r$  characterized by  $l = 2j - 2 + |m|$  for even states ( $\sigma = +1$ ) and  $l = 2j - 1 + |m|$  for odd states ( $\sigma = -1$ ) are given by expansion in powers of  $r$  with finite  $l, l'$ :

$$\begin{aligned} E_j(r) &= \bar{E}_j^{(0)} + \bar{E}_j^{(2)} r^2 + \sum_{k=1}^{[k_{\max}/4]} r^{4k} \bar{E}_j^{(4k)}, & H_{jj'}(r) &= \sum_{k=2}^{[k_{\max}/4]} r^{4k-2} \bar{H}_{jj'}^{(4k-2)}, \\ Q_{jj'}(r) &= \sum_{k=1}^{[k_{\max}/4]} r^{4k-1} \bar{Q}_{jj'}^{(4k-1)}, & r &\ll \min(l, l')\gamma/2. \end{aligned} \quad (63)$$

Note that all

$$\bar{Q}_{jj'}^{(4k-1)} \equiv 0 \quad \text{and} \quad \bar{H}_{jj'}^{(4k-2)} \equiv 0 \quad \text{if} \quad |j - j'| > 2k. \quad (64)$$

The calculation was performed using the algorithm implemented in MAPLE up to  $k_{\max} = 36$ . Below we display several first coefficients of the matrix elements expansions:

$$\begin{aligned} \bar{E}_j^{(0)} &= l(l+1), & \bar{E}_j^{(2)} &= \gamma m, & \bar{E}_j^{(4)} &= \frac{\gamma^2}{2} \frac{l^2 + l - 1 + m^2}{(2l-1)(2l+3)}, \\ \bar{Q}_{jj+2}^{(3)} &= \frac{\gamma^2}{2} \frac{\sqrt{(l+1)^2 - m^2} \sqrt{(l+2)^2 - m^2}}{\sqrt{2l+1}(2l+3)^2 \sqrt{2l+5}}, \\ \bar{H}_{jj}^{(6)} &= \frac{\gamma^4}{2} ((16l^4 + 32l^3 + 248l^2 + 232l + 201)m^4 \\ &\quad + (-10l^2 - 224l^4 - 96l^5 + 118l - 288l^3 - 32l^6 - 195)m^2 + 16l^8 + 64l^7 \\ &\quad + 46l + 40l^6 - 127l^4 - 104l^5 + 71l^2 - 6l^3 - 6)/((2l-3)(2l-1)^4(2l+3)^4(2l+5)), \\ \bar{H}_{jj+4}^{(6)} &= \frac{-\gamma^4 \sqrt{(l+1)^2 - m^2} \sqrt{(l+2)^2 - m^2} \sqrt{(l+3)^2 - m^2} \sqrt{(l+4)^2 - m^2}}{4\sqrt{2l+1}(2l+3)^2(2l+5)(2l+7)^2 \sqrt{2l+9}}. \end{aligned} \quad (65)$$

Such asymptotic behavior of the effective potentials allows us to find regular and bound solutions at  $r \rightarrow 0$  that satisfied the boundary conditions (59).

### 3.3. Expansion of the regular solutions in power series

The asymptotics of the regular solutions  $\chi_j^{(i_o)}(r) \equiv \chi_{ji_o}(r)$ ,  $j = 1, \dots, j_{\max}$ ,  $i_o = 1, \dots, N_o \leq j_{\max}$  of equation (58) are sought as expansions in powers of  $r$  up to an finite order  $k_{\max}$ :

$$\chi_{ji_o}(r) = c_{i_o} \sum_{k=0}^{k_{\max}} \chi_{ji_o}^{(k)} r^{\mu_{i_o} + k}, \quad \chi_{ji_o}^{(0)} = \delta_{ji_o}, \quad \chi_{ji_o}^{(k < 0)} \equiv 0, \quad (66)$$

where  $c_{i_o}$  are normalized constants,  $\mu_{i_o}$  is an unknown characteristic parameter. Substituting expansion (66) into (58) with equations (63)–(65) taken into account, we obtain the following



system of recurrence relations for the set of the unknown coefficients  $\chi_{ji_o}^{(k)}$ :

$$\begin{aligned}
 & -(l' + 1 + \mu_{i_o} + k)(\mu_{i_o} - l' + k)\chi_{ji_o}^{(k)} = 2Z\chi_{ji_o}^{(k-1)} - (m\gamma - \epsilon)\chi_{ji_o}^{(k-2)} \\
 & - \sum_{s=4}^k \bar{E}_j^{(s)} \chi_{ji_o}^{(k-s)} - \sum_{s=4}^{k-2} \bar{H}_{jj}^{(s)} \chi_{ji_o}^{(k-s-2)} \\
 & - \sum_{s=3}^{k-1} \sum_{j'=\max(1, i_o - [s/4]), j' \neq j}^{\min(j_{\max}, i_o + [s/4])} (2l + 2k - s) \bar{Q}_{jj'}^{(s)} \chi_{j'i_o}^{(k-s-1)} \\
 & - \sum_{s=4}^{k-2} \sum_{j'=\max(1, i_o - [s/4]), j' \neq j}^{\min(j_{\max}, i_o + [s/4])} \bar{H}_{jj'}^{(s)} \chi_{j'i_o}^{(k-s-2)},
 \end{aligned} \tag{67}$$

where the indices  $l'$  and  $l$  are defined by

$$l' = 2(j - 1) + |m| + (1 - \sigma)/2, \quad l = 2(i_o - 1) + |m| + (1 - \sigma)/2. \tag{68}$$

As follows from equations (66) and (67) at  $k = 0$ , the conventional characteristic equation gives two roots for the unknown  $\mu_{i_o}$ :  $\mu_{i_o} = -l - 1$  and  $\mu_{i_o} = l$ . The value  $\mu_{i_o} = -l - 1$  corresponds to irregular unbound solutions and is not considered here. The value  $\mu_{i_o} = l$  corresponds to the required regular and bound solutions.

Note that the components of the vector  $\{\chi_{ji_o}^{(k)}\}_{j=1}^{j_{\max}}$  at fixed  $i_o$  in the lhs of equation (67) is equal to zero if  $j - i_o = k$ . In this case we can put  $\chi_{i_o+ki_o}^{(k)} = 0$ , because this term will be determined as the leading term of the asymptotic form of the  $(i_o + k)$ th solution. A more detailed analysis of (67) with the account of (64) shows that the rhs of equation (67) is equal to zero and all  $\chi_{ji_o}^{(k)}$  are equal to zero if  $|j - i_o| > k/2$ .

Thus, the system (67) can be solved sequentially for  $k = 1, 2, \dots, k_{\max}$ . Below we display several first non-zero coefficients of the regular solutions expansions:

$$\begin{aligned}
 \chi_{i_o i_o}^{(0)} &= 1, \quad \chi_{i_o i_o}^{(1)} = -\frac{Z}{l+1}, \quad \chi_{i_o i_o}^{(2)} = -\frac{-2Z^2 + (\epsilon - m\gamma)(l+1)}{2(l+1)(2l+3)}, \\
 \chi_{i_o i_o}^{(3)} &= \frac{Z(-2Z^2 + (\epsilon - m\gamma)(3l+4))}{6(l+1)(l+2)(2l+3)}, \\
 \chi_{i_o-2i_o}^{(4)} &= \frac{\bar{Q}_{i_o-2i_o}^{(3)}(2l+5)}{6(2l+3)}, \\
 \chi_{i_o i_o}^{(4)} &= \frac{\bar{E}_{i_o}^{(4)}}{4(2l+5)} + \frac{(\epsilon - m\gamma)^2}{8(2l+3)(2l+5)} + \frac{Z^4 - Z^2(\epsilon - m\gamma)(3l+5)}{6(l+1)(l+2)(2l+3)(2l+5)}, \\
 \chi_{i_o+2i_o}^{(4)} &= \frac{\bar{Q}_{i_o+2i_o}^{(3)}(2l+5)}{2(2l+7)}.
 \end{aligned} \tag{69}$$

In the case of  $\gamma = 0$  these coefficients transform into conventional ones for the expansion of the free regular Coulomb function  $F_l(r)$  up to the factor  $r^{-1}$  with a known value of the coefficient  $c_{i_o}(\gamma = 0) = c_l$  from [20]. The latter gives us the opportunity to estimate the ratio  $|c_{i_o}(\gamma)/c_{i_o}(0)|^2$  of a probability density,  $|c_{i_o}(\gamma)|^2$ , extracted from the calculated solution of equations (58)–(60) with boundary conditions (61) (or (62)) using asymptotic (66) and a free probability density,  $|c_{i_o}(0)|^2$ , in the vicinity of  $r = 0$ .

### 3.4. Asymptotic form of basis functions and matrix elements at large $r$

Let us describe briefly the evaluation of the matrix elements at large  $r$  as expansions in powers of  $p^{-1}$  till the order of  $k_{\max}$ . For this purpose we use the eigenfunctions labeled by  $\hat{v} = \overleftrightarrow{\leftarrow}$  and localized at large  $r$  in the vicinity of  $\eta = \pm 1$  (see figure 3)

$$\Phi^{m\sigma=\pm 1}(\eta; r) = \frac{\Phi^{m\rightarrow}(\eta; r) \pm \Phi^{m\leftarrow}(\eta; r)}{\sqrt{2}}. \quad (70)$$

These functions have  $N_\rho \equiv n = 0, 1, 2, \dots$ , nodes in the subintervals  $0 < \eta < 1$  and  $-1 < \eta < 0$ ,  $N_\rho = N_\eta/2$  for even states,  $\sigma = +1$  and  $N_\rho = (N_\eta - 1)/2$  for the odd states,  $\sigma = -1$ ,  $N_\eta$  being the number of nodes of  $\Phi^{m\sigma}(\eta; r)$  in the interval  $-1 < \eta < 1$  and the parity  $\sigma = (-1)^{N_\eta}$ . Note that  $\Phi^{m\leftarrow}(\eta; r) = \Phi^{m\rightarrow}(-\eta; r)$  and  $\Phi^{m\leftarrow}(\eta < 0; r) = \Phi^{m\rightarrow}(\eta > 0; r) = O(\exp(-p(1 + |\eta|)))$  at  $r \rightarrow \infty$  and  $|\eta| \sim 1$  which will be used in the construction of the scattering wavefunctions defined by equation (105).

We find the matrix elements expanded in inverse powers of  $r$  with finite  $j = n_l - 1$ ,  $j' = n_r - 1$  and with the exponential terms omitted [22]

$$\begin{aligned} r^{-2} E_j(r) &= E_j^{(0)} + \sum_{k=1}^{k_{\max}} r^{-2k} E_j^{(2k)}, & H_{jj'}(r) &= \sum_{k=1}^{k_{\max}} r^{-2k} H_{jj'}^{(2k)}, \\ Q_{jj'}(r) &= \sum_{k=1}^{k_{\max}} r^{-2k+1} Q_{jj'}^{(2k-1)}, & r &\gg \max(n_l, n_r) \gamma / 2. \end{aligned} \quad (71)$$

The calculation was performed using the algorithm describing in appendix A and implemented in MAPLE up to  $k_{\max} = 8$ . Below we display the first several coefficients of the potential curves  $E_j(r)$  at fixed  $m$ :

$$\begin{aligned} E_j^{(0)} &= \gamma(2n + |m| + m + 1), \\ E_j^{(2)} &= -2n^2 - 2n - 1 - 2|m|n - |m|, \\ E_j^{(4)} &= (2\gamma)^{-1}(-4n^3 - 6n^2 - 4n - 6|m|n^2 - 6|m|n - 2m^2n - 2|m| - m^2 - 1), \end{aligned} \quad (72)$$

and the matrix elements  $Q_{jj'}(r)$ ,  $H_{jj'}(r)$ :

$$\begin{aligned} Q_{jj'}^{(1)} &= (n_r - n_l) \sqrt{n+1} \sqrt{n+|m|+1} \delta_{|n_l-n_r|,1}, \\ Q_{jj'}^{(3)} &= (4\gamma)^{-1} (n_r - n_l) \sqrt{n+1} \sqrt{n+|m|+1} (2(2n+|m|+2) \delta_{|n_l-n_r|,1} \\ &\quad + \sqrt{n+2} \sqrt{n+|m|+2} \delta_{|n_l-n_r|,2}), \\ H_{jj'}^{(2)} &= (2n^2 + 2n + 2|m|n + |m| + 1) \delta_{|n_l-n_r|,0} \\ &\quad - \sqrt{n+1} \sqrt{n+|m|+1} \sqrt{n+2} \sqrt{n+|m|+2} \delta_{|n_l-n_r|,2}, \end{aligned} \quad (73)$$

$$\begin{aligned} H_{jj'}^{(4)} &= \gamma^{-1} ((2n+|m|+1)(2n^2+2n+2|m|n+|m|+2) \delta_{|n_l-n_r|,0} \\ &\quad + \sqrt{n+1} \sqrt{n+|m|+1} (n^2+2n+|m|n+|m|+2) \delta_{|n_l-n_r|,1} \\ &\quad - \sqrt{n+1} \sqrt{n+|m|+1} \sqrt{n+2} \sqrt{n+|m|+2} (2n+|m|+3) \delta_{|n_l-n_r|,2} \\ &\quad - \sqrt{n+1} \sqrt{n+|m|+1} \sqrt{n+2} \sqrt{n+|m|+2} \sqrt{n+3} \sqrt{n+|m|+3} \delta_{|n_l-n_r|,3}), \end{aligned} \quad (74)$$

where  $n = \min(n_l, n_r)$ . Note that all  $Q_{jj'}^{(2k+1)} \equiv 0$  and  $H_{jj'}^{(2k)} \equiv 0$  if  $|j - j'| > k + 1$ . Moreover, for second-order coefficients the identity  $E_j^{(2)} + H_{jj}^{(2)} = 0$  takes place, i.e., at large  $r$  the centrifugal terms are eliminated from equation (58). It means that the leading terms

of the radial solutions  $\chi_{ji_o}(r)$  have the asymptotic form of the Coulomb functions with zero angular momentum. If the scaled radial variable  $\hat{r}$  is used, we put  $\gamma = 1$  and use the effective charge  $\hat{Z}$  and the scaled energy  $\hat{\epsilon} = \epsilon/\gamma$  or  $\hat{E} = E/\gamma$  in the above expressions. Note that the convergence domain of expansions (63) and (71) at small and large  $r$  is limited to the range of avoided crossing of the eigenvalues and maxima of the matrix elements versus  $r$  (see figures 4–7), that correspond to the known branching points in the complex plane of the parameter  $p$  [30]. This remark can be taken into account in the construction of the corresponding asymptotic solutions. To show explicitly the region where expansion (71) is valid the asymptotic values of potentials and matrix elements are displayed by dotted lines in figures 4–7. One can compare them with the corresponding numerical values calculated as mentioned above by the computer relative accuracy in the finite interval of the radial variable. The exponentially small corrections improving the convergence can be calculated by means of the additional series expansion of the solution in the region  $D_2 = [0, 1 - \eta_2]$ ,  $\eta_2 < \eta_1$ ,  $\eta_2 = o(p^{-1/2-\varepsilon})$  [24].

### 3.5. Asymptotic radial solution with exponential and inverse power series

The radial solutions  $\chi_j^{(i_o)}(r) \equiv \chi_{ji_o}(r)$ ,  $j = 1, \dots, j_{\max}$ ,  $i_o = 1, \dots, N_o \leq j_{\max}$  of equation (58) at large  $r$  without the centrifugal terms (i.e., with zero angular momentum) have the asymptotic form

$$\chi_{ji_o}^{(as)}(r) = \frac{\exp(\iota p_{i_o} r + \iota \zeta \ln(2p_{i_o} r) + \iota \delta_{i_o}^c)}{2r \sqrt{p_{i_o}}} \delta_{ji_o}, \quad (75)$$

where  $p_{i_o}$  is the relative momentum in the channel,  $\zeta \equiv \zeta_{i_o}$  is a Zommerfeld-type parameter,  $\delta_{i_o}^c = \arg \Gamma(1 - \iota \zeta)$  is the phase defined by the known Coulomb phase shift. The values of these characteristic parameters will be adapted to find the formal asymptotic solutions expanding the functions  $\phi_{ji_o}(r)$  in inverse powers of  $r$ :

$$\chi_{ji_o}(r) = \phi_{ji_o}(r) \chi_{i_o i_o}^{(as)}(r), \quad \phi_{ji_o}(r) = \sum_{k=0}^{k_{\max}} \phi_{ji_o}^{(k)} r^{-k}. \quad (76)$$

Substituting expansion (76) into equation (58) and equating the coefficients at the same powers of  $r$  we arrive at the recurrence relations for the unknown coefficients  $\phi_{ji_o}^{(k)}$  [22]

$$\begin{aligned} & (p_{i_o}^2 - 2E + E_j^{(0)}) \phi_{ji_o}^{(k)} + (2p_{i_o} \zeta - 2Z + 2\iota p_{i_o} (k-1)) \phi_{ji_o}^{(k-1)} \\ & + (\zeta - 2\iota + \iota k)(\zeta - \iota + \iota k) \phi_{ji_o}^{(k-2)} + \sum_{k'=1}^k (E_j^{(k')} + H_{jj}^{(k')}) \phi_{ji_o}^{(k-k')} \\ & = \sum_{j'=1, j' \neq j}^{j_{\max}} \sum_{k'=1}^k (-2\iota p_{i_o} Q_{jj'}^{(k')} + (2k - k' - 1 - 2\iota \zeta) Q_{jj'}^{(k'-1)} - H_{jj'}^{(k')}) \phi_{j'i_o}^{(k-k')}. \end{aligned} \quad (77)$$

From the first three equations of the set (77) for  $\phi_{i_o i_o}^{(0)}$ ,  $\phi_{j_0 i_o}^{(0)}$ ,  $\phi_{i_o i_o}^{(1)}$  we get the leading terms of the eigenfunction, the eigenvalue of the relative momentum,  $p_{i_o}$ , and the characteristic parameter,  $\zeta$ , i.e., the initial data for solving the recurrence equations (77),

$$\phi_{j_0 i_o}^{(0)} = \delta_{j_0 i_o}, \quad p_{i_o}^2 = 2E - E_{i_o}^{(0)} \rightarrow p_{i_o} = \sqrt{2E - E_{i_o}^{(0)}}, \quad \zeta = \frac{Z}{p_{i_o}}. \quad (78)$$

For open channels  $p_{i_o}^2 \geq 0$ , while for closed channels  $p_{i_o}^2 < 0$ . Suppose there are  $N_o \leq j_{\max}$  open channels, i.e.,  $p_{i_o}^2 \geq 0$  for  $i_o = 1, \dots, N_o$  and  $p_{i_o}^2 < 0$  for  $i_o = N_o + 1, \dots, j_{\max}$ . Substituting these initial data into the sequent equations of the set (77), we get a step-by-step

procedure for determining the coefficients  $\phi_{ji_o}^{(k)}$  till  $k = k_{\max}$ . For example, for  $k = 1$  the coefficients have the form

$$\phi_{ji_o}^{(1)} = \frac{2\iota p_{i_o} Q_{ji_o}^{(1)}}{E_{i_o}^{(0)} - E_{j_1}^{(0)}}, \quad \phi_{i_o i_o}^{(1)} = \frac{\iota(Z^2 + \iota Z p_{i_o})}{2p_{i_o}^3} - \sum_{j_1=\max(1, i_o-1), j_1 \neq i_o}^{\min(j_{\max}, i_o+1)} Q_{i_o j_1}^{(1)} \phi_{j_1 i_o}^{(1)}. \quad (79)$$

Substituting the asymptotic expressions (71) into equation (79), one can express the coefficients  $\phi_{ji_o}^{(k)}$  explicitly via the number of the state (or of the channel)  $i_o = n_o + 1$  and the number of the current equation  $j = 1, \dots, j_{\max}$ . Note that if  $j_{\max} \geq i_o + k$ , then all nonzero terms in the sums in equations (79) will be included into the evaluation of each nonzero element  $\phi_{ji_o}^{(k)}$  of the order  $k$ . The calculation was performed using the algorithm implemented in MAPLE up to  $k_{\max} = 15$ . For example, at  $j_{\max} \geq i_o + k$  and  $k = 0, 1$  the substitution of (73) into (79) yields

$$\begin{aligned} \phi_{i_o i_o}^{(0)} &= 1, \\ \phi_{i_o-1 i_o}^{(1)} &= \iota \frac{p_{i_o} \sqrt{n_o} \sqrt{n_o + |m|}}{\gamma}, \\ \phi_{i_o i_o}^{(1)} &= \left[ \iota \frac{Z^2}{2p_{i_o}^3} - \frac{Z}{2p_{i_o}^2} \right] - \iota \frac{p_{i_o} (2n_o + |m| + 1)}{\gamma}, \\ \phi_{i_o+1 i_o}^{(1)} &= \iota \frac{p_{i_o} \sqrt{n_o + 1} \sqrt{n_o + |m| + 1}}{\gamma}. \end{aligned} \quad (80)$$

If we use the scaled radial variable  $\hat{r}$ , we put  $\gamma = 1$  and use the effective charge  $\hat{Z}$ , the scaled energy  $\hat{\epsilon} = \epsilon/\gamma$  and the momentum  $\hat{p}_{i_o} = p_{i_o}/\sqrt{\gamma}$ , ( $\zeta = \hat{\zeta} = \hat{Z}/\hat{p}_{i_o}$ ) in the above expressions. For  $\hat{r}_{\max} \gg \max(\hat{Z}^2/(2\hat{p}_{i_o}^2), n_o/2)$  we can use expansion (75).

### 3.6. Asymptotic radial solution with Coulomb functions and inverse power series

Now let us consider the asymptotic solution  $\chi_j^{(i_o)}(r) \equiv \chi_{ji_o}(r)$ ,  $j = 1, \dots, j_{\max}$ ,  $i_o = 1, \dots, N_o \leq j_{\max}$  of equation (58) following [32]:

$$\chi_{ji_o}(r) = R(p_{i_o}, r) \phi_{ji_o}(r) + \frac{dR(p_{i_o}, r)}{dr} \psi_{ji_o}(r), \quad (81)$$

where  $R(p_{i_o}, r) = p_{i_o}^{-1/2} r^{-1} (\iota F_0(p_{i_o}, r) + G_0(p_{i_o}, r))/2$ ,  $F_0(p_{i_o}, r)$  and  $G_0(p_{i_o}, r)$  are the Coulomb regular and irregular functions, respectively [20], that satisfy the condition

$$G_0(p_{i_o}, r) \frac{dF_0(p_{i_o}, r)}{dr} - \frac{dG_0(p_{i_o}, r)}{dr} F_0(p_{i_o}, r) = p_{i_o}. \quad (82)$$

The function  $R(p_{i_o}, r)$  satisfies the differential equation

$$\frac{d^2 R(p_{i_o}, r)}{dr^2} + \frac{2}{r} \frac{dR(p_{i_o}, r)}{dr} + \left( p_{i_o}^2 + \frac{2Z}{r} \right) R(p_{i_o}, r) = 0. \quad (83)$$

Substituting function (81) into equation (58), using equation (83) and extracting the coefficients for the Coulomb function and its derivative, we arrive at an axillary set of two coupled differential equations with respect to the unknown functions  $\phi_{ji_o}(r) \psi_{ji_o}(r)$  and the relative momentum  $p_{i_o}$  [22]. Then we expand the functions  $\phi_{ji_o}(r)$  and  $\psi_{ji_o}(r)$  in inverse powers of  $r$ :

$$\phi_{ji_o}(r) = \sum_{k=0}^{k_{\max}} \phi_{ji_o}^{(k)} r^{-k}, \quad \psi_{ji_o}(r) = \sum_{k=0}^{k_{\max}} \psi_{ji_o}^{(k)} r^{-k}. \quad (84)$$

After substituting expansions (84) into these axillary equations and equating the coefficients at the same powers of  $r$  we arrive at the recurrence relations for the unknown coefficients  $\phi_{ji_o}^{(k)}$  and  $\psi_{ji_o}^{(k)}$ :

$$\begin{aligned} & (p_{i_o}^2 - 2E + E_j^{(0)})\phi_{ji_o}^{(k)} - 2p_{i_o}^2(k-1)\psi_{ji_o}^{(k-1)} - (k-2)(k-3)\phi_{ji_o}^{(k-2)} \\ & - 2Z(2k-3)\psi_{ji_o}^{(k-2)} + \sum_{k'=1}^k (E_j^{(k')} + H_{jj}^{(k')})\phi_{ji_o}^{(k-k')} \\ & = \sum_{j'=1, j' \neq j}^{j_{\max}} \sum_{k'=1}^k [(2k-k'-3)Q_{jj'}^{(k'-1)} - H_{jj'}^{(k')}] \phi_{j'i_o}^{(k-k')} \\ & + (2p_{i_o}^2 Q_{jj'}^{(k')} + 4ZQ_{jj'}^{(k'-1)}) \psi_{j'i_o}^{(k-k')}, \end{aligned} \quad (85)$$

$$\begin{aligned} & (p_{i_o}^2 - 2E + E_j^{(0)})\psi_{ji_o}^{(k)} + 2(k-1)\phi_{ji_o}^{(k-1)} - k(k-1)\psi_{ji_o}^{(k-2)} + \sum_{k'=1}^k (E_j^{(k')} + H_{jj}^{(k')})\psi_{ji_o}^{(k-k')} \\ & = \sum_{j'=1, j' \neq j}^{j_{\max}} \sum_{k'=1}^k [(2k-k'+1)Q_{jj'}^{(k'-1)} - H_{jj'}^{(k')}] \psi_{j'i_o}^{(k-k')} - 2Q_{jj'}^{(k')} \phi_{j'i_o}^{(k-k')}. \end{aligned} \quad (86)$$

The summation indices  $j_k, k = 0, 1, \dots, k_{\max}$  possess integer values, except  $i_o$  and  $j_{k+1}$ , i.e.,  $j_k = 1, 2, \dots, j_{\max}$ ,  $j_k \neq i_o$ ,  $j_k \neq j_{k+1}$ . From the first four equations of the set (85) and (86) for  $\phi_{i_o i_o}^{(0)}, \phi_{j_0 i_o}^{(0)}, \psi_{i_o i_o}^{(0)}, \psi_{j_0 i_o}^{(0)}$  we get the leading terms of the eigenfunction and eigenvalue of the relative momentum,  $p_{i_o}$ , i.e., the initial data for solving the recurrence equations (85) and (86),

$$\phi_{j_0 i_o}^{(0)} = \delta_{j_0 i_o}, \quad \psi_{j_0 i_o}^{(0)} = 0, \quad p_{i_o}^2 = 2E - E_{i_o}^{(0)}, \quad (87)$$

that correspond to the leading term of  $\chi_{ji_o}(r)$  satisfying the asymptotic expansion (75) at large  $r$ . Substituting these initial data into equations (85) and (86), we get a step-by-step procedure for the coefficients  $\phi_{ji_o}^{(k)}$  and  $\psi_{ji_o}^{(k)}$  till  $k = k_{\max}$ . For example, for  $k = 1$  these coefficients have the form

$$\begin{aligned} \phi_{j_1 i_o}^{(1)} &= 0, \quad \psi_{j_1 i_o}^{(1)} = \frac{2Q_{j_1 i_o}^{(1)}}{E_{i_o}^{(0)} - E_{j_1}^{(0)}}, \\ \phi_{i_o i_o}^{(1)} &= 0, \quad \psi_{i_o i_o}^{(1)} = - \sum_{j_0=\max(1, i_o-1), j_0 \neq i_o}^{\min(j_{\max}, i_o+1)} Q_{i_o j_0}^{(1)} \psi_{j_0 i_o}^{(1)}. \end{aligned} \quad (88)$$

Substituting the asymptotic expressions (71) into equation (88), we get the explicit expression of the coefficients  $\phi_{ji_o}^{(k)}$  and  $\psi_{ji_o}^{(k)}$  via the number of the state (or of the channel)  $i_o = n_o + 1$  and the number of the current equation  $j = 1, \dots, j_{\max}$ . The calculation was performed using the algorithm implemented in MAPLE up to  $k_{\max} = 15$ . For example, at  $j_{\max} \geq i_o + k$  and  $k = 0, 1$ , substituting (73) into (88) such elements take the form

$$\begin{aligned} \phi_{i_o i_o}^{(0)} &= 1, \quad \psi_{i_o i_o}^{(0)} = 0, \\ \phi_{i_o-1 i_o}^{(1)} &= 0, \quad \psi_{i_o-1 i_o}^{(1)} = \frac{\sqrt{n_o} \sqrt{n_o + |m|}}{\gamma}, \\ \phi_{i_o i_o}^{(1)} &= 0, \quad \psi_{i_o i_o}^{(1)} = -\frac{2n_o + |m| + 1}{\gamma}, \\ \phi_{i_o+1 i_o}^{(1)} &= 0, \quad \psi_{i_o+1 i_o}^{(1)} = \frac{\sqrt{n_o + 1} \sqrt{n_o + |m| + 1}}{\gamma}. \end{aligned} \quad (89)$$

If we use the scaled radial variable  $\hat{r}$ , we put  $\gamma = 1$  and use the effective charge  $\hat{Z}$  and the scaled momentum  $\hat{p}_{i_o}$  ( $\zeta = \hat{Z}/\hat{p}_{i_o}$ ) in the above expressions.

Similar to [32], in each order  $k$  the recurrence relation (85) includes implicitly only the factor  $Z/p_{i_o}$ , while the recurrence relation (77) includes explicitly the quadratic factor  $(Z/p_{i_o})^2$ . This allows us to expect that for small values of  $\hat{p}_{i_o}$  or large values of the effective charge  $\hat{Z}$  and, therefore, of the parameter  $|\zeta| = |\hat{Z}/\hat{p}_{i_o}| \gg 1$ , one can use expansion (81) at as substantially smaller distance  $\hat{r}_{\max}/|\zeta|$  rather than expansion (75) at the essentially larger distance  $\hat{r}_{\max}$ .

Taking the convergence domain of the matrix elements into account, we find that the convergence domain of expansion (81) is  $\hat{r}_{\max} \gg n_o/2$  and  $\hat{r}_{\max} \gg \hat{Z}/\hat{p}_{i_o}(2n_o + |m| + 1)$ , as follows from the asymptotic behavior of the matrix elements which does not depend on  $p_{i_o}$ . This is the main goal of expansion (81).

In addition, it should be noted that at large  $r$  the linearly independent matrix functions  $\chi(r) \equiv \{\chi^{(i_o)}(r)\}_{i_o=1}^{N_o}$  of (76) and (81) satisfy the Wronskian-type relation

$$\mathbf{Wr}(\mathbf{Q}(r); \chi^*(r), \chi(r)) = \frac{i}{2} \mathbf{I}_{oo}, \quad (90)$$

where  $\mathbf{Wr}(\bullet; \chi^*(r), \chi(r))$  is a generalized Wronskian with the long derivative defined as

$$\mathbf{Wr}(\bullet; \chi^*(r), \chi(r)) = r^2 \left[ (\chi^*(r))^T \left( \frac{d\chi(r)}{dr} - \bullet \chi(r) \right) - \left( \frac{d\chi^*(r)}{dr} - \bullet \chi^*(r) \right)^T \chi(r) \right]. \quad (91)$$

These relations are used to analyze the desirable accuracy of the above expansion [23].

### 3.7. Correspondence of asymptotic total wavefunctions at large $r$ and $|z|$

To clarify the geometric sense of expansion (81) and (84) we recalculate the first four coefficients (88) and (89) for  $j_{\max} \geq i_o + 1$  using the functions  $|j\rangle = \tilde{\Phi}_j(\rho) = \lim_{r \rightarrow \infty, |\eta| \sim 1} r^{-1} \Phi_j(|\eta|; r)$  from (56):

$$\begin{aligned} \phi_{j_1 i_o}^{(1)} &= 0, \\ \psi_{j_1 i_o}^{(1)} &= -\frac{1}{2} \langle j_1 | \rho^2 | i_o \rangle = \frac{\sqrt{n_o} \sqrt{n_o + |m|}}{\gamma} \delta_{j_1, i_o-1} + \frac{\sqrt{n_o + 1} \sqrt{n_o + |m| + 1}}{\gamma} \delta_{j_1, i_o+1}, \\ \phi_{i_o i_o}^{(1)} &= 0, \quad \psi_{i_o i_o}^{(1)} = -\frac{1}{2} \langle i_o | \rho^2 | i_o \rangle = -\frac{2n_o + |m| + 1}{\gamma}. \end{aligned} \quad (92)$$

Taking into account the orthogonality  $\langle j | i_o \rangle = \langle \tilde{\Phi}_j^m(\rho) | \tilde{\Phi}_{i_o}^m(\rho) \rangle = \delta_{ji_o}$  and completeness  $\sum_j |\tilde{\Phi}_j^m(\rho') \rangle \langle \tilde{\Phi}_j^m(\rho) | = \delta(\rho' - \rho)$  of the basis functions (56), the asymptotic form of the total wavefunction at  $p_{i_o} \rho^2 / (2r) \ll 1$  can be written as

$$\begin{aligned} \Psi^{m\hat{v}}(r, \eta) &= r \sum_j |\tilde{\Phi}_j^m(\rho)\rangle \left[ \langle \tilde{\Phi}_j^m(\rho) | \tilde{\Phi}_{i_o}^m(\rho) \rangle - \frac{1}{2r} \langle \tilde{\Phi}_j^m(\rho) | \rho^2 | \tilde{\Phi}_{i_o}^m(\rho) \rangle \frac{d}{dr} \right] \chi_{i_o i_o}^{(as)}(p_{i_o}, r) \\ &= r \sum_j |\tilde{\Phi}_j^m(\rho)\rangle \langle \tilde{\Phi}_j^m(\rho) | \left[ |\tilde{\Phi}_{i_o}^m(\rho)\rangle - \frac{1}{2r} \rho^2 |\tilde{\Phi}_{i_o}^m(\rho)\rangle \frac{d}{dr} \right] \chi_{i_o i_o}^{(as)}(p_{i_o}, r) \\ &\approx r \tilde{\Phi}_{i_o}^m(\rho) \chi_{i_o i_o}^{(as)}(p_{i_o}, r(1 - \rho^2/(2r^2))) \approx \frac{1}{2} \tilde{\Phi}_{i_o}^m(\rho) X_{i_o i_o}^{(+)}(|z|) \exp(i\delta_{i_o}^c). \end{aligned} \quad (93)$$

In the last transformation we use the relation  $|z| = r(1 - \rho^2/(2r^2)) + O(r^{-2})$  and the definitions (21), (57) and (27). Thus, the matrix of coefficients (81), (84) and (89) corresponds to the

overlap matrix between the asymptotic fundamental solutions (16) and (27) of equation (2) in cylindrical coordinates  $z = r \cos \theta$ ,  $\rho = r \sin \theta$  at large  $|z|$  and the asymptotic basis functions of the independent variable  $\eta = \cos \theta$  at large  $r$ . In appendix B we present detailed explanation of the effective approximation in the KM including the explicit construction of the corresponding effective mass and potentials versus the radial variable  $r$  and the results of calculation of their asymptotic values up to the order of  $r^{-4}$ .

#### 4. Scattering states and photoionization cross sections

Consider the ejected electron above the first threshold  $\epsilon_{m1}^{\text{th}}(\gamma) = \epsilon_m^{\text{th}}(\gamma) = \gamma(|m| + m + 1)$ . We express the corresponding eigenfunction  $\Psi_i^{Em\sigma}(r, \eta)$  of the continuous spectrum with the energy  $\epsilon = 2E$  as

$$\Psi_i^{Em\sigma}(r, \eta) = \sum_{j=1}^{j_{\max}} \Phi_j^{m\sigma}(\eta; r) \hat{\chi}_{ji}^{(m\sigma)}(E, r), \quad i = 1, \dots, N_o, \quad (94)$$

where  $\hat{\chi}^{(m\sigma)}(E, r)$  is the radial part of the ‘incoming’ or eigenchannel wavefunction. The normalization condition for  $\Psi_i^{Em\sigma}(r, \eta)$  is

$$\begin{aligned} \langle \Psi_i^{Em\sigma}(r, \eta) | \Psi_{i'}^{E'm'\sigma'}(r, \eta) \rangle &= \sum_{j=1}^{j_{\max}} \int_0^\infty r^2 dr (\hat{\chi}_{ji}^{(m\sigma)}(E, r))^* \hat{\chi}_{ji'}^{(m'\sigma')}(E', r) \\ &= \delta(E - E') \delta_{mm'} \delta_{\sigma\sigma'} \delta_{ii'}. \end{aligned} \quad (95)$$

The function  $\hat{\chi}^{(m\sigma)}(E, r)$  is expressed as

$$\hat{\chi}^{(m\sigma)}(E, r) = \sqrt{\frac{2}{\pi}} \chi^{(p)}(r) \mathbf{C} \cos \delta. \quad (96)$$

The function  $\chi^{(p)}(r)$  is a numerical solution of equation (58) that satisfies the ‘standing-wave’ boundary conditions (62) and has the standard asymptotic form [33]

$$\chi^{(p)}(r) = \chi^s(r) + \chi^c(r) \mathbf{K}, \quad \mathbf{K} \mathbf{C} = \mathbf{C} \tan \delta, \quad \mathbf{C} \mathbf{C}^T = \mathbf{C}^T \mathbf{C} = \mathbf{I}_{oo}. \quad (97)$$

Here  $\chi^s(r) = 2 \text{Im}(\chi(r))$  and  $\chi^c(r) = 2 \text{Re}(\chi(r))$ ,  $\chi(r)$  is the asymptotic solution defined in section 3.5 or 3.6,  $\mathbf{K} \equiv \mathbf{K}_\sigma$  is the numerical short-range reaction matrix with the eigenvalue  $\tan \delta$  and the orthogonal matrix  $\mathbf{C}$  of the corresponding eigenvectors. The regular and irregular functions satisfy the generalized Wronskian relation (91) at large  $r$

$$\mathbf{W}(\mathbf{Q}(r); \chi^c(r), \chi^s(r)) = \mathbf{I}_{oo}. \quad (98)$$

Using  $\mathbf{R}$ -matrix calculus [21], we obtain the equation expressing the reaction matrix  $\mathbf{K}$  via the matrix  $\mathbf{R}$  at  $r = r_{\max}$

$$\left( \mathbf{R} \chi^c(r) - \frac{d\chi^c(r)}{dr} \right) \mathbf{K} = \left( \frac{d\chi^s(r)}{dr} - \mathbf{R} \chi^s(r) \right). \quad (99)$$

When some channels are closed, the matrices in equation (99) are rectangular. Hence, the reaction matrix  $\mathbf{K}$  may be presented as

$$\mathbf{K} = -\mathbf{X}^{-1}(r_{\max}) \mathbf{Y}(r_{\max}), \quad (100)$$

where

$$\mathbf{X}(r) = \left( \frac{d\chi^c(r)}{dr} - \mathbf{R} \chi^c(r) \right)_{oo}, \quad \mathbf{Y}(r) = \left( \frac{d\chi^s(r)}{dr} - \mathbf{R} \chi^s(r) \right)_{oo}, \quad (101)$$

are square  $N_o \times N_o$  matrices.

The radial part of the ‘incoming’ wavefunction is expressed via the numerical ‘standing’ wavefunction and the short-range reaction matrix  $\mathbf{K}$  by the relation

$$\hat{\chi}^{(m\sigma)}(E, r) = \sqrt{\frac{2}{\pi}} \chi^-(r) = \iota \sqrt{\frac{2}{\pi}} \chi^{(p)}(r) (\mathbf{I}_{oo} + \iota \mathbf{K})^{-1}, \quad (102)$$

and has the asymptotic form

$$\hat{\chi}^{(m\sigma)}(E, r) = \sqrt{\frac{2}{\pi}} (\chi(r) - \chi^*(r) \mathbf{S}^\dagger). \quad (103)$$

Here  $\mathbf{S}$  is the short-range scattering matrix, expressed via the scattering matrix  $\check{\mathbf{S}}_\sigma$  (31) and Coulomb phase shift  $\delta^c$  as  $\mathbf{S} \equiv \mathbf{S}_\sigma = \exp(-\iota \delta^c) \check{\mathbf{S}}_\sigma \exp(-\iota \delta^c)$ , for which

$$\mathbf{S}^\dagger \mathbf{S} = \mathbf{S} \mathbf{S}^\dagger = \mathbf{I}_{oo}, \quad \mathbf{K} = \iota (\mathbf{I}_{oo} + \mathbf{S})^{-1} (\mathbf{I}_{oo} - \mathbf{S}), \quad \mathbf{S} = (\mathbf{I}_{oo} + \iota \mathbf{K}) (\mathbf{I}_{oo} - \iota \mathbf{K})^{-1}. \quad (104)$$

The total wavefunction has the asymptotic form reverse to the common scattering problem, namely, ‘incident wave + ingoing wave’,

$$\Psi_{Em\hat{v}}^{(-)}(r, \eta) \equiv \Psi_{Em\hat{\leftarrow}}^{(-)}(r, \eta) = \frac{1}{\sqrt{2}} (\Psi^{Em\sigma=+1}(r, \eta) \pm \Psi^{Em\sigma=-1}(r, \eta)) \exp(-\iota \delta^c), \quad (105)$$

that corresponds to the function (36) (see details in appendix C). Now the expression (38) for the cross section  $\sigma_{Nlm}^d(\omega)$  of photoionization by the light linearly polarized along the axis  $z$  can be written as

$$\sigma_{Nlm}^d(\omega) = 4\pi^2 \alpha \omega \sum_{i=1}^{N_o} |D_{i,N,l}^{m\sigma\sigma'}(E)|^2 a_0^2, \quad (106)$$

where  $D_{i,N,l}^{m\sigma\sigma'}(E) \equiv D_{i,i',v'}^{m\sigma\sigma'}(E)$  are the matrix elements of the dipole moment

$$D_{i,i',v'}^{m\sigma\sigma'}(E) = \langle \Psi_i^{Em\sigma=\mp 1}(r, \eta) | r \eta | \Psi_{i',v'}^{m\sigma'=\pm 1}(r, \eta) \rangle = \sum_{j=1}^{j_{\max}} \int_0^{r_{\max}} r^2 dr \hat{\chi}_{ji}^{(m\sigma=\mp 1)}(E, r) d_{ji',v'}^{(m\sigma\sigma')}(r), \quad (107)$$

and  $d_{ji',v'}^{(m\sigma\sigma')}(r)$  are the matrix elements of the partial dipole moments

$$d_{ji',v'}^{(m\sigma\sigma')}(r) = \sum_{j'=1}^{j_{\max}} \langle \Phi_j^{m\sigma=\mp 1}(\eta; r) | r \eta | \Phi_{j'}^{m\sigma'=\pm 1}(\eta; r) \rangle_\eta \chi_{ji',v'}^{(m\sigma'=\pm 1)}(r). \quad (108)$$

In the above expressions  $\omega = E - E_{Nlm}$  is the frequency of radiation,  $E_{Nlm} \equiv E_{m\sigma'i'v'}$  is the energy of the initial bound state  $|Nlm\rangle = \Psi_{i',v'}^{m\sigma'}(r, \eta)$  below half of the first true threshold shift  $\epsilon_{m1}^{\text{th}}(\gamma)/2$  from formula (56) at  $i' = 1$ . The continuous spectrum solution  $\chi^{(p)}(r)$  having the asymptotic form of a ‘standing’ wave and the reaction matrix  $\mathbf{K}$  required for calculating (96) or (103), as well as the discrete spectrum solution  $\chi(r)$  and the eigenvalue  $E_{m\sigma'i'=1v'}$ , can be calculated using the program KANTBP [33]. Figure 10 shows an example of the wavefunctions of the continuous spectrum calculated using equations (94)–(96) in the basis of functions (51) shown in figure 3 for  $\sigma = -1$ ,  $Z = 1$ ,  $m = 0$  and  $\gamma = 1$  with the energy  $E = 1.7$  au above the second threshold  $1/2\epsilon_{m2}^{\text{th}} = 1.5$ . One can see that equations (96) and (103) yield the same result when used to calculate the absolute value in equation (106), as well as equation (105) performing the summation over  $\hat{v}$  in accordance with equation (38). Hence, equation (96) is preferable for using real arithmetic. For the light circularly polarized in the plane  $xOy$  similar expression can be written using (42) with  $(\vec{e}_\pm \vec{r}) = \frac{r}{\sqrt{2}} \sqrt{1 - \eta^2} \exp(\pm \iota \varphi)$ .



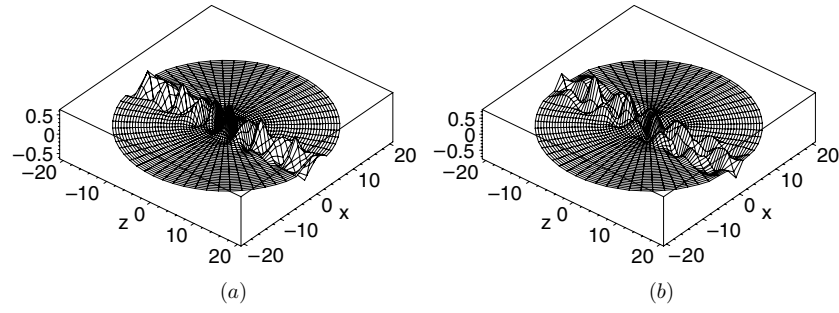


**Figure 10.** Profiles of wavefunctions  $\Psi_1$  and  $\Psi_2$  in the  $zx$  plane of the first (a) and the second (b) open channels having the asymptotic form (96) for  $\sigma = -1$ ,  $Z = 1$ ,  $m = 0$  and  $\gamma = 1$  with the energy  $E = 1.7$  au above the second threshold  $1/2\epsilon_{m2}^{\text{th}} = 1.5$ .

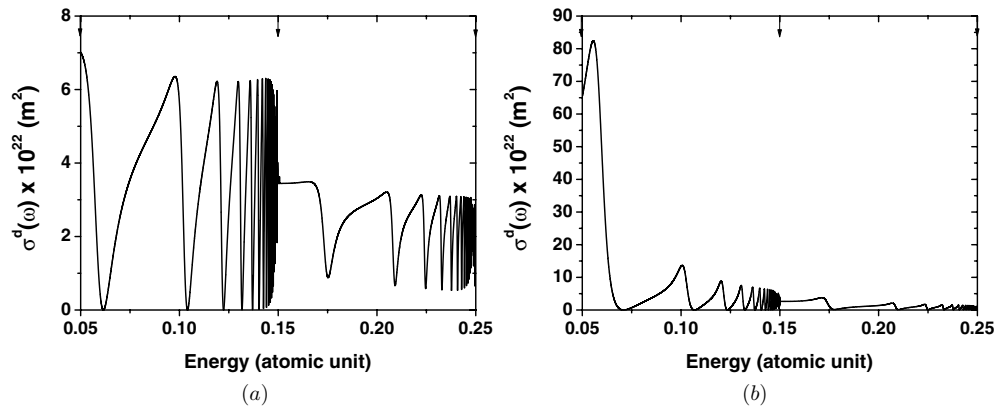


**Figure 11.** Cross sections of photoionization from the states  $1s_0$  (a) and  $3d_0$  (b) versus the energy for  $\gamma = 1 \times 10^{-1}$ , and for the final state with  $\sigma = -1$ ,  $Z = 1$ ,  $m = 0$ . The arrows indicate the successive Landau thresholds  $E_j = 1/2\epsilon_{mj}^{\text{th}}$  (71).

## 5. Numerical results and discussion

In our calculations we used the following values of the physical constants [34]:  $1 \text{ cm}^{-1} = 4.55633 \times 10^{-6} \text{ au}$ , the Bohr radius  $a_0 = 5.29177 \times 10^{-11} \text{ m}$  and the fine-structure constant  $\alpha = 7.29735 \times 10^{-3}$ .

Figure 11 displays the calculated photoionization cross section from the states  $1s_0$  and  $3d_0$  at  $B_0 = 2.35 \times 10^4 T$  ( $\gamma = 1 \times 10^{-1}$ ) in the energy interval from  $E = 0.05 \text{ au}$  to  $E = 0.25 \text{ au}$  with the final state  $\sigma = -1$ ,  $m = 0$ . We used ten eigenfunctions ( $j_{\text{max}} = 10$ ) of the problem (51)–(53) which requires to solve ten equations of the system (58). The finite element grids of  $\hat{r} = \sqrt{\gamma}r$  have been chosen as 0 (200) 3 (200) 20 (200) 100 for the discrete spectrum and 0 (200) 3 (200) 20 (200) 100 (1000) 1000 for the continuous one. Enclosed in parentheses are the numbers of finite elements of the order  $k = 4$  in each interval. The number of nodes in the grids is 2400 and 6401, so that the maximum number of unknowns in equation (58) is 24 000 and 64 010, respectively. Figure 12 displays the continuous spectrum states (in scaled coordinates) with the energies  $E = 0.0596 \text{ au}$  and  $E = 0.0903 \text{ au}$  that correspond to  $\delta_o = 0$  and  $\delta_o = \pi/2$ , respectively. The corresponding series of quasi-stationary states imbedded in the continuum,

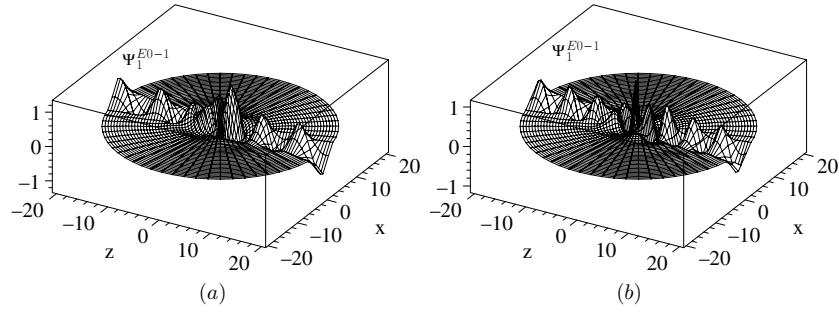


**Figure 12.** Profiles of the eigenfunctions  $\Psi_1^{Em\sigma}$  in the  $zx$  plane of the continuous spectrum with  $\sigma = -1$ ,  $Z = 1$ ,  $m = 0$  and  $\gamma = 1 \times 10^{-1}$ . The states with the energies  $E = 0.0596$  au and  $E = 0.0903$  au correspond to  $\delta_o = 0$  and  $\delta_o = \pi/2$ , respectively.

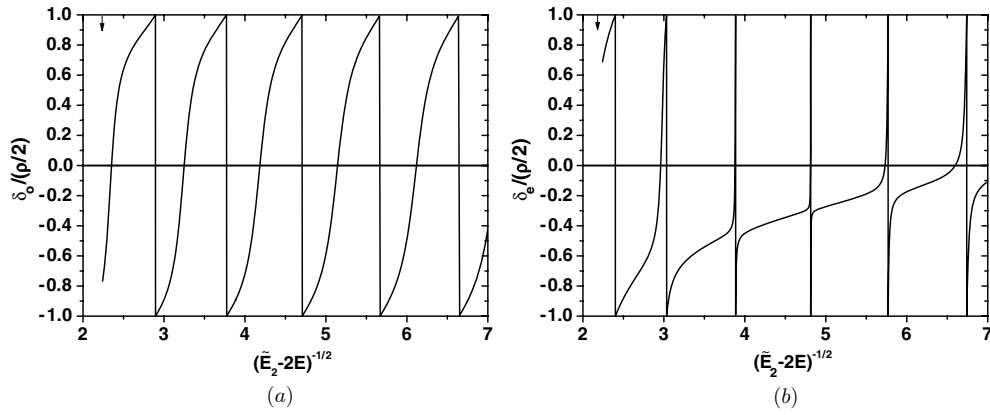


**Figure 13.** Phase shift  $\delta$  of odd (a) and even (b) continuum states for  $Z = 1$ ,  $m = 0$  and  $\gamma = 1 \times 10^{-1}$  versus  $(\tilde{E}_2 - 2E)^{-1/2}$ . The arrow points at the energy of the first Landau threshold  $(\tilde{E}_2 - \tilde{E}_1)^{-1/2} = 5^{1/2} \approx 2.236$ .

defined by the short-range phase shifts  $\delta_o = n_o\pi + \pi/2$ , are plotted in figure 13(a) versus  $(\tilde{E}_2 - 2E)^{-1/2} = n_o + \Delta_{n_o}$ , where  $\tilde{E}_j = \epsilon_{mj}^{\text{th}}$ . The existence of such states allows one to explain the nonmonotonic dependence of the photoionization cross section upon the energy between the thresholds. The short-range phase shifts  $\delta_e = n_e\pi + \pi/2$  of the even continuum states are plotted in figure 13(b) versus  $(\tilde{E}_2 - 2E)^{-1/2} = n_e + \Delta_{n_e}$ . The corresponding transmission  $|\hat{\mathbf{T}}|^2 = \sin^2(\delta_e - \delta_o)$  and reflection  $|\hat{\mathbf{R}}|^2 = \cos^2(\delta_e - \delta_o)$  coefficients (31) versus the energy  $E$  (a) and  $(\tilde{E}_2 - 2E)^{-1/2}$  (b) are shown in figure 14. Nonmonotonic behavior of  $|\hat{\mathbf{T}}|$  and  $|\hat{\mathbf{R}}|$  is seen to include the cases of resonance transmission  $|\hat{\mathbf{T}}| = 1$  and  $|\hat{\mathbf{R}}| = 0$  and total reflection  $|\hat{\mathbf{T}}| = 0$  and  $|\hat{\mathbf{R}}| = 1$ . As an example, we display the absolute values of the total wavefunctions (105) of the continuous spectrum  $\Psi_{Em\rightarrow}^{(-)}$  and  $\Psi_{Em\leftarrow}^{(-)}$  in figure 15 (in scaled coordinates). The profiles of the states with the energy  $E = 0.05885$  au and  $E = 0.11692$  au demonstrate the resonance transmission and total reflection, respectively. They agree with appendix C and with the proper longitudinal solutions combined with the left and right basis functions (see figures 2(b) and 5).

Figure 16 demonstrates the dependence on the energy  $E$  (a) and  $(\tilde{E}_2 - 2E)^{-1/2}$  (b) of the following quantities: the squared modulus of the matrix element (SMME)  $\tilde{T}_{11} = S_{11} - 1$ ,

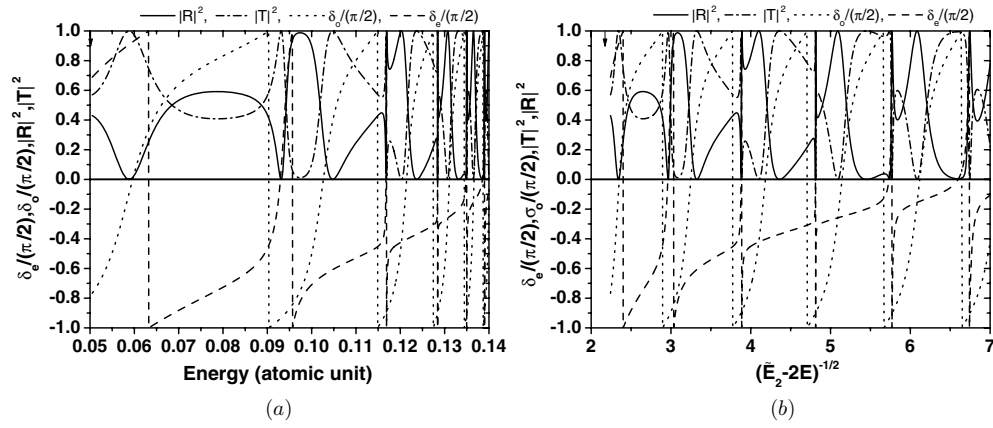


**Figure 14.** Transmission  $|\hat{T}|^2$  and reflection  $|\hat{R}|^2$  coefficients, even  $\delta_e$  and odd  $\delta_o$  phase shifts versus the energy  $E$  (a) and  $(E_2 - 2E)^{-1/2}$  (b) for continuum states with  $Z = 1$ ,  $m = 0$  and  $\gamma = 1 \times 10^{-1}$ .

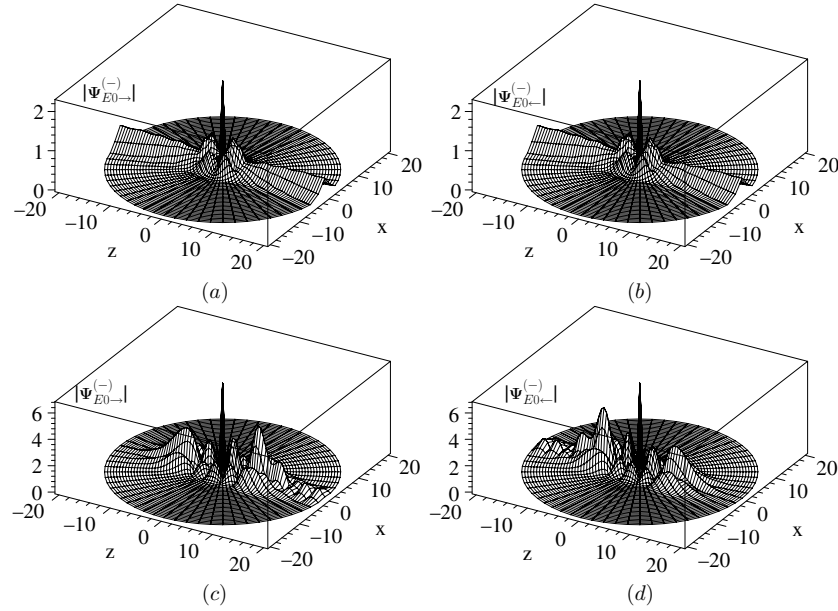


**Figure 15.** Profiles of total wavefunctions  $|\Psi_{Em\rightarrow}^{(-)}|$  (a, c) and  $|\Psi_{Em\leftarrow}^{(-)}|$  (b, d) in the  $zx$  plane of the continuous spectrum with  $Z = 1$ ,  $m = 0$  and  $\gamma = 1 \times 10^{-1}$ . The states with the energy  $E = 0.05885$  au (a, b) correspond to the resonance transmission, while those with the energy  $E = 0.11692$  au (c, d) correspond to the total reflection.

characterizing the elastic scattering of the electron, the odd phase shift (OPS)  $\delta_o$ , and the cross section  $\sigma^d(\omega)$  (106) of photoionization from the initial even state  $1s_0$  ( $(Nlm) = (100)$ ) with the energy  $E_{100} = -0.497\,526\,480\,40$  au,  $\omega = E - E_{100}$  being the frequency of radiation. The final scattering state with  $\sigma = -1$  and  $m = 0$  in the magnetic field  $B_0 = 2.35 \times 10^4$  T ( $\gamma = 1 \times 10^{-1}$ ) is considered. The first two quantities are normalized to fit the plot

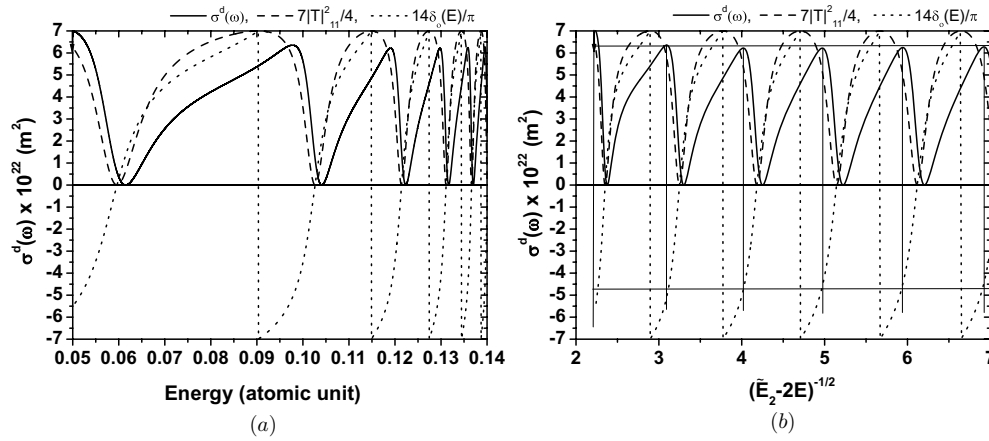


**Figure 16.** Squared modulus of the matrix element  $\tilde{T}_{11}$ , multiplied by  $7/4$ , odd phase shift  $\delta_o$  multiplied by  $14/\pi$  and cross section  $\sigma^d(\omega)$  (106) of photoionization from the initial state  $1s_0$  versus the energy  $E$  (a) and  $(\tilde{E}_2 - 2E)^{-1/2}$  (b) for the final scattering state with  $\sigma = -1$ ,  $Z = 1$ ,  $m = 0$  and  $\gamma = 1 \times 10^{-1}$ .

range. The comparison of the three curves shows that the maxima of the SMME of elastic scattering coincide with the jumps of the OPS. The minima of SMME coincide with zeros of OPS exactly, while the minima of the photoionization cross section (PCS) occur with some delay. Figure 16(b) shows that in the scale  $(\tilde{E}_2 - 2E)^{-1/2}$  SMME is periodical, while PCS is quasi-periodical. The maxima of PCS occur after each phase jump when the OPS has approximately the same value of  $-0.35/\pi$ , while the maxima of SMME coincide exactly with these jumps that, as mentioned above, correspond to quasi-stationary states imbedded in the continuum. The minima of PCS correspond approximately to the same value  $0.1/\pi$  of the phase. The figures show only the first fragment of the infinite sequence of maxima and minima that corresponds to the existence of the infinite and countable series of Coulomb quasi-stationary states below the second threshold, induced by the confinement potential of the magnetic field, in accordance with the multichannel quantum defect theory.

For the initial state  $1s_0$  in the whole energy interval the results are in good agreement with those of **R**-matrix calculations within the frameworks of the multichannel quantum defect theory [6]. We also compared our results with those of the complex-rotation method using the expansion over the basic set of 10 000 complex spherical Sturmian-type functions [11] and the basic set of 450 mixed Slater-Landau functions [8]. In this case the agreement is good only between the thresholds, but not near them. The agreement with [6] proves that our method is valid to describe the true threshold behavior of the photoionization cross section, i.e., one of the goals of elaborating the new approach is achieved.

Figure 17 displays the cross section of photoionization by the light linearly polarized along the axis  $z$  from the vibrational state  $3d_0$  (a) and the rotational state  $3s_0$  (b) at  $B_0 = 6.10$  T ( $\gamma = 2.595 \times 10^{-5}$ ) in the energy interval between  $E = 6.0$  cm $^{-1}$  and  $E = 8.0$  cm $^{-1}$ . In this case we increased  $j_{\max}$  up to 35 and the finite element grids of  $\hat{r} = \sqrt{\gamma}r$  were chosen as 0 (200) 0.03 (200) 0.2 (200) 1 for the discrete spectrum and 0 (200) 0.03 (200) 0.2 (200) 1 (2000) 100 (4000) 1000 for the continuous one. The number of nodes in these grids is 2400 and 26 401, respectively. The corresponding maximal number of unknowns in equation (58) is 84 000 and 924 035. Figure 18(a) shows the absolute maximum values of the continuum wavefunctions  $\hat{\chi}_{j1}^{(01)}(E, \hat{r})$  at  $E = 6.0$  cm $^{-1}$ . We calculated the cross sections with the

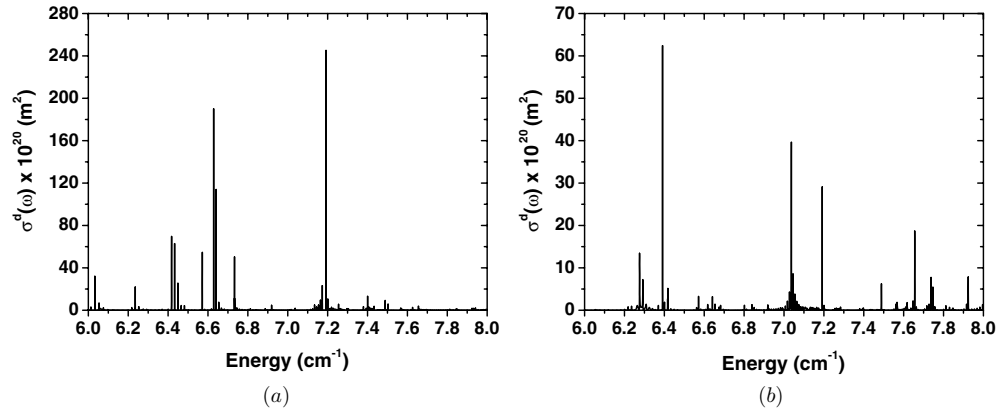


**Figure 17.** The cross section of photoionization from the states  $3d_0$  (a) and  $3s_0$  (b) versus the energy for  $\gamma = 2.595 \times 10^{-5}$  and for the final state with  $\sigma = -1$ ,  $Z = 1$ ,  $m = 0$ .

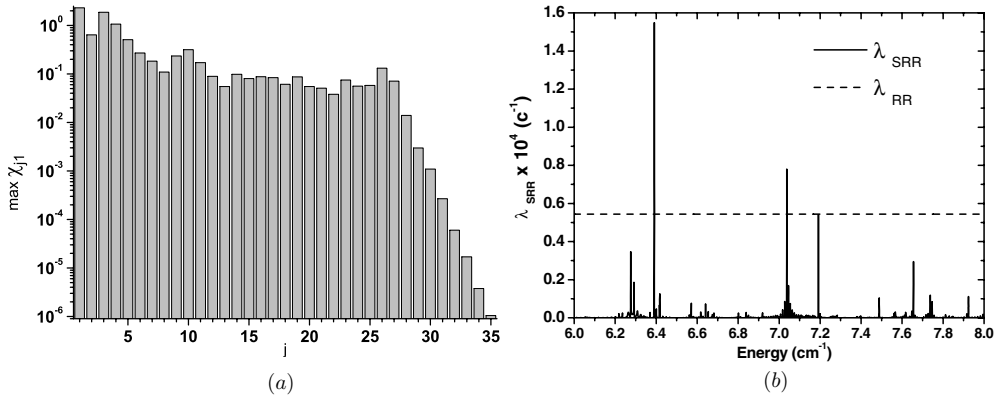


**Figure 18.** (a) Absolute maximum values,  $\max \chi_{j1}$ , of the continuum wavefunctions  $\hat{\chi}_{j1}^{(01)}(E, \hat{r})$  at  $\gamma = 2.595 \times 10^{-5}$ ,  $E = 6.0 \text{ cm}^{-1}$  and  $j_{\max} = 35$ . (b) Laser-stimulated radiative recombination rate into the bound state  $N' = 3$ ,  $l' = 0$ ,  $m' = 0$  versus the energy of the initially free positron.

energy step  $5 \times 10^{-4} \text{ cm}^{-1}$  in all the region except the vicinity of peaks, where the step was  $5 \times 10^{-6} \text{ cm}^{-1}$ .

The relation between the photoionization cross section and the induced radiative recombination rate [5] makes it possible to apply the results of this section to an urgent problem of the production of cold antihydrogen atoms in magnetic traps [3]. The idea is to use the resonances due to the quasi-stationary states arising in the magnetic field in order to enhance the laser-induced radiative recombination into a given bound state by choosing the proper laser frequency. Let us consider the recombination into the state  $N' = 3$ ,  $l' = 0$ ,  $m' = 0$ , that may be stimulated by a titanium-sapphire laser, under the conditions typical for positron-antiproton plasma in magnetic traps used for antihydrogen production, namely, the temperature of the plasma  $T = 4 \text{ K}$ , the positron density  $n_e = 1 \times 10^8 \text{ cm}^{-3}$ , the magnetic induction  $B = 6.10 \text{ T}$ . The laser intensity is taken such that at  $4 \text{ K}$  without the magnetic field the rate of induced recombination is equal to that of the spontaneous one. In particular, for  $N = 3$

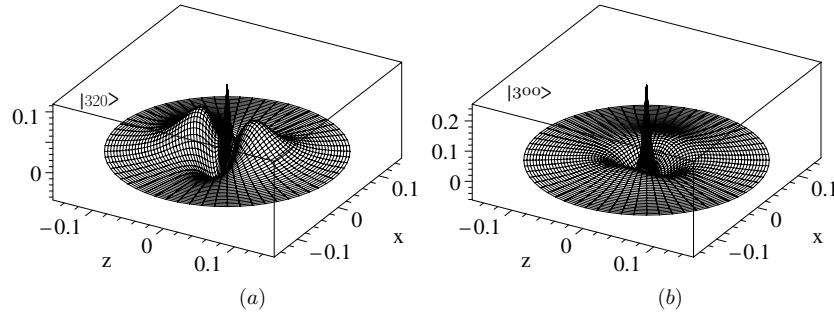


**Figure 19.** Profiles of the wavefunctions in the  $xz$  plane of the bound states  $|Nlm\rangle$  with  $\sigma = +1$ ,  $Z = 1$  and  $\gamma = 2.595 \times 10^{-5}$ : (a) the vibrational state  $|320\rangle$  with the minimal energy correction; (b) the rotational state  $|300\rangle$  with the maximal energy correction.

this intensity is  $I = 24 \text{ W cm}^{-2}$  [4]. Figure 18(b) shows the dependence of the laser-stimulated recombination rate per one antiproton  $\lambda_{\text{SRR}}$  upon the initial energy of the positron  $E = E_{Nlm} + \omega$ . For comparison the horizontal dashed line displays the rate  $\lambda_{\text{RR}}$  of the spontaneous radiative recombination into all the states with  $N = 3$ , which at the intensity considered is equal to the rate of the laser-stimulated recombination without the magnetic field. Obviously, there are narrow resonances for which the rate of recombination into the state with fixed  $l = 0, m = 0$  in magnetic field is appreciably higher than the rate of recombination into all nine states with different  $l$  and  $m$  possible for  $N = 3$  without the magnetic field.

Note that states  $3d_0$ ,  $3p_0$  and  $3s_0$  with energies  $E_{320} = -0.055\,555\,552\,07 \text{ au}$ ,  $E_{310} = -0.055\,555\,549\,49 \text{ au}$  and  $E_{300} = -0.055\,555\,542\,37 \text{ au}$ , respectively, are nearly degenerate. To calculate these energies we used three equations of the system (58) ( $j_{\text{max}} = 3$ ); increasing  $j_{\text{max}}$  keeps them stable. We also compared the energies with those calculated by means of the second-order algebraic perturbation theory [35]. The results coincide with each other to the 13th digit. The wavefunctions of the bound states  $|Nlm\rangle$  with even parity  $\sigma = +1$  in a homogenous magnetic field are shown in figure 19. Values of functions scaled by factor  $\gamma^{3/4}$  versus scaled coordinates  $\hat{r}$ . From here one can find an evident explanation of the fact that the cross section of photoionization by the light linearly polarized along the axis  $z$  (see figure 17) from the vibrational state  $3d_0$  distributed along the  $z$  axis exceeds in four times the cross section from the rotational state  $3s_0$  distributed along the  $x$  axis.

## 6. Conclusions

A new efficient method for calculating both the discrete and the continuous spectrum wavefunctions of a hydrogen atom in a strong magnetic field is developed based on the Kantorovich approach to the parametric eigenvalue problems in spherical coordinates. The 2D spectral problem for the Schrödinger equation with fixed magnetic quantum number and parity is reduced to a 1D spectral parametric problem for the angular variable and a finite set of ordinary second-order differential equations for the radial variable. The rate of convergence is analyzed numerically and is illustrated with a number of typical examples. The results are in good agreement with calculations of photoionization cross sections by other authors. It is shown that the calculated photoionization cross sections has the true threshold behavior and that the recombination cross sections can be recalculated using the relations presented. The recurrence relations for the calculation of the coefficients of asymptotic expansions of

fundamental solutions of a set of the radial equations or the overlap matrix open the way to study the threshold phenomena using the known asymptotic expansion of Coulomb functions [36, 37].

The main advantages of the elaborated approach from the calculation and the theoretical viewpoints consist of the following.

The calculations on all steps of the Kantorovich approach are realized with the help of stable calculation schemes and with prescribed accuracy. The economy of computer resources is achieved by means of analytic calculation of all needed asymptotic forms of adaptive basis functions, matrix elements of radial coupling and radial solutions, which makes it possible to reduce the interval of integration in the corresponding boundary problems.

For the first time resonance transmission and total reflection effects for scattering processes of electrons on protons in a homogenous magnetic field are manifested.

The approach developed provides a useful tool for calculations of threshold phenomena in the formation and ionization of (anti)hydrogen-like atoms and ions in magnetic traps, quantum dots in magnetic field [38], channeling processes [39] and potential scattering with confinement potentials [40].

### Acknowledgments

The authors thank Professors A G Abrashkevich, A M Ermolaev, V S Melezhik and V V Pupyshv for an useful discussion. This work was partly supported by Grant I-1402/2004-2007 of the Bulgarian Foundation for Scientific Investigations, the theme 09-6-1060-2005/2009 ‘Mathematical support of experimental and theoretical studies conducted by JINR’ and Scientific Center for Applied Research of JINR. A part of this work was carried out within the framework of the Russian Analytical Departmental Objective Program ‘Development of the Scientific Potential of the Higher School’ (2006–2008), project RNP.2.1.1.4473 ‘Mesooptics’ and supported by the grant CRDF BRHE REC-006 SR-006-X1/B75M06 Y3-P-06-08.

### Appendix A. Asymptotic expansions of basis functions and matrix elements at large $r$

Following [20, 24], at step 1 we change the coordinate  $\eta \in [0, 1]$  (or  $\eta \in [-1, 0]$ ) for the new coordinate  $y$  according to

$$y = 2p(1 - \eta) \quad (\text{or } y = 2p(1 + \eta)). \quad (\text{A.1})$$

For our purposes it is sufficient to consider  $\eta \in [0, 1]$ . We suppose that the coordinate  $y$  lies in the interval corresponding to  $\eta \in D_1$ ,  $D_1 = [1 - \eta_1, 1]$ ,  $\eta_1 = o(p^{1/2-\epsilon})$ ,  $0 < \epsilon < 1/2$ . Now the eigenvalue problem (54) takes the form

$$\left[ (y^2 - 4py) \frac{\partial^2}{\partial y^2} + (2y - 4p) \frac{\partial}{\partial y} - \left( \frac{16p^2(m^2 + y^2) + y^3(y - 8p)}{4y(y - 4p)} + \lambda_n \right) \right] \Phi_j(y) = 0. \quad (\text{A.2})$$

The corresponding matrix elements (60) read as

$$Q_{jj'}(r) = -I_{01;jj'}(r), \quad H_{jj'}(r) = I_{11;jj'}(r). \quad (\text{A.3})$$

where the integrals  $I_{dd';jj'}(r)$  with  $d, d' = 0, 1$  are calculated as follows:

$$I_{dd';jj'}(r) = \frac{1}{2p} \int_0^{2p} dy \left[ \left( \frac{\partial}{\partial r} + \frac{2y}{r} \frac{\partial}{\partial y} \right)^d \Phi_j(y) \right] \left[ \left( \frac{\partial}{\partial r} + \frac{2y}{r} \frac{\partial}{\partial y} \right)^{d'} \Phi_{j'}(y) \right]. \quad (\text{A.4})$$



In these expressions the asymptotic quantum number  $n$  denotes the transversal quantum numbers that are connected with the unified numbers  $j$  and  $j'$  as  $n_l = j - 1$  and  $n_r = j' - 1$ . At steps 2–3 from the set of functions  $\Phi_j(y)$  we turn to the set of functions  $F_n(y)$

$$\Phi_j(y) = f_m(y)F_n(y), \quad f_m(y) = \exp\left(-\frac{y}{2}\right)y^{|m|/2}\left(1 - \frac{y}{4p}\right)^{|m|/2}, \quad (\text{A.5})$$

the latter presented as a sum of the associated Laguerre polynomials [20]

$$F_n(y) = (2p)^{1/2} \sum_s C_n(s, r) L_{n+s}^{|m|}(y). \quad (\text{A.6})$$

Using the knowing properties of the associated Laguerre polynomials [20], we find that the coefficients  $C_n(s, r)$  satisfy the recurrence relations

$$\begin{aligned} &\left(n + s + \frac{|m| + 1}{2} - \frac{\lambda_n + 2(n + s)^2 + 2(n + s)(|m| + 1) + |m| + 1}{4p}\right) C_n(s, r) \\ &+ \frac{(n + s + 1)(s + 1 + n + |m|)}{4p} C_n(s + 1, r) \\ &+ \frac{(s + n)(s + |m| + n)}{4p} C_n(s - 1, r) = 0. \end{aligned} \quad (\text{A.7})$$

As a result of this step we get the matrix elements as a sum of integrals with the associated Laguerre polynomials

$$I_{dd';jj'}(r) = \sum_{s_l s_r} \int_0^{2p} dy f_m^2(y) \tilde{C}_{n_l, s_l}^{(d)} \tilde{C}_{n_r, s_r}^{(d')}, \quad (\text{A.8})$$

where the coefficients  $\tilde{C}_{n_r, s_r}^{(d)}$  are obtained by differentiation of (A.5) and (A.6) and formation of a given weight factor,  $f_m^2(y)$ , such that

$$\begin{aligned} \tilde{C}_{n_l, s_l}^{(0)} &= C_{n_l}(s_l, r) L_{n_l + s_l}^{|m|}(y), \quad \tilde{C}_{n_r, s_r}^{(0)} = C_{n_r}(s_r, r) L_{n_r + s_r}^{|m|}(y), \\ \tilde{C}_{n_r, s_r}^{(1)} &= \frac{dC_{n_r}(s_r, r)}{dr} L_{n_r + s_r}^{|m|}(y) + \frac{C_{n_r}(s_r, r)}{r} [(n_r + s_r + 1) L_{n_r + s_r + 1}^{|m|}(y) \\ &\quad - (n_r + s_r + |m|) L_{n_r + s_r - 1}^{|m|}(y)]. \end{aligned} \quad (\text{A.9})$$

At step 4 for the evaluation of the integrals (A.8) we change the domain from  $[0, 2p]$  to  $[0, \infty)$  and then omit the exponentially small terms. Using the approximated relation up to the order of  $k_{\max} < |m|$ , that is exact if  $k_{\max} \geq |m|$

$$\left(1 - \frac{y}{4p}\right)^{|m|} = \sum_{k=0}^{k_{\max}} \frac{|m|!}{k!(|m| - k)!} \left(\frac{y}{4p}\right)^k + O((4p)^{-k_{\max}-1}), \quad (\text{A.10})$$

and the orthonormality condition for the associated Laguerre polynomials

$$\int_0^\infty dy \exp(-y) y^{|m|} L_{n_l + s_l}^{|m|}(y) L_{n_r + s_r}^{|m|}(y) = \frac{(n_l + s_l + |m|)!}{(n_l + s_l)!} \delta_{n_l + s_l, n_r + s_r}, \quad (\text{A.11})$$

we obtain the matrix elements in the algebraic form. For example, if  $k_{\max} = 1$  the matrix element  $I_{00;jj} \equiv I_{jj} \equiv 1$  takes the form

$$I_{00;jj}(r) = \sum_s \left[1 - \frac{|m|(2n + 2s + |m| + 1)}{4p}\right] C_n(s, r)^2 \frac{(n + s + |m|)!}{(n + s)!}. \quad (\text{A.12})$$



At step 5 we expand  $C_n(s, r)$  and  $\lambda_n$  as

$$C_n(s, r) = c_{s,n}^{(0)} + \sum_{k=1}^{k_{\max}} \left( \frac{1}{4p} \right)^k c_{s,n}^{(k)}, \quad \lambda_n = 4p \left[ \frac{|m|+1}{2} + \beta_n^{(0)} + \sum_{k=1}^{k_{\max}} \left( \frac{1}{4p} \right)^k \beta_n^{(k)} \right]. \quad (\text{A.13})$$

Substituting (A.13) into (A.7) and equating the coefficients at equal powers of  $p$ , we arrive at the set of recurrence relations for evaluating the coefficients  $\beta_n^{(k)}$  and  $c_{s,n}^{(k)}$  (except  $c_{0,n}^{(k)}$ )

$$s c_{s,n}^{(k)} = ((n+s+|m|+1)(2n+2s+|m|+1) - (n+s+|m|)(|m|+1)) c_{s,n}^{(k-1)} \\ - (n+s)(n+s+|m|) c_{s-1,n}^{(k-1)} - (n+s+|m|+1)(n+s+1) c_{s+1,n}^{(k-1)} + \sum_{k'=1}^{k-|s|} \beta_n^{(k')} c_{s,n}^{(k-k')}, \quad (\text{A.14})$$

with the initial conditions

$$\beta_n^{(0)} = n, \quad c_{s,n}^{(0)} = \delta_{s0} \sqrt{\frac{n!}{(n+|m|)!}}. \quad (\text{A.15})$$

Note that all  $c_{s,n}^{(k)} \equiv 0$  if  $|s| > k$ . For  $k_{\max} = 1$  the output is the following:

$$c_{-1,n}^{(1)} = n(n+|m|) c_{0,n}^{(0)}, \quad \beta_n^{(1)} = -1 - 2n - 2|m|n - 2n^2 - |m|, \\ c_{1,n}^{(1)} = -(n+1)(n+|m|+1) c_{0,n}^{(0)}. \quad (\text{A.16})$$

Substituting (A.13) into (A.12) and equating it to unity, we find the coefficients  $c_{0,j}^{(k)}$

$$c_{0,n}^{(1)} = \frac{|m|(2n+|m|+1)}{2} c_{0,n}^{(0)}. \quad (\text{A.17})$$

At step 6, substituting (A.13) with the coefficients  $c_{s,j}^{(k)}$  evaluated at step 5 into the expressions of the matrix elements, evaluated at step 4 by means of equation (A.3), we easily find the matrix elements expanded in inverse powers of  $r$  with finite  $j = n_l - 1$ ,  $j' = n_r - 1$  and with the exponential terms omitted [22] in the form (71).

## Appendix B. The effective approximation for the Kantorovich method

Consider the set of close-coupled radial equations (58) and neglect the coupling of the states  $|j\rangle$  and  $|j'\rangle$  disconnected from the open channel  $|i_o\rangle$ . This can be useful for sufficiently large effective charge  $\hat{Z} = Z/\sqrt{\gamma}$ , when the contribution of the adiabatic correction is sufficiently small. From the physical viewpoint this may help to understand the asymptotic boundary conditions in the open channel. We introduce the so-called effective adiabatic approximation, in which we project the radial equations onto the open channel  $|i\rangle = |i_o\rangle$  by means of a canonical transformation. The new solution  $\chi_{ii}^{\text{new}} \equiv \chi_{ii}^{\text{new}}(r)$  is related to the old solutions  $\chi_{ji} \equiv \chi_{ji}(r)$  of equations (58) as

$$\chi_{ii}^{\text{new}} = \sum_j T_{ij} \chi_j \approx \sum_{j,j'=1}^{j_{\max}} \langle i | \exp(iS^{(2)}) | j' \rangle \langle j' | \exp(iS^{(1)}) | j \rangle \chi_{ji}. \quad (\text{B.1})$$

Restricting the expansion of the exponentials to the second order  $\exp(iS^{(1)}) \approx 1 + iS^{(1)} + (iS^{(1)})^2/2$  and  $\exp(iS^{(2)}) \approx 1 + iS^{(2)}$ , we define the nondiagonal matrix elements of the

generators  $S^{(1)}$  and  $S^{(2)}$  in the following way:

$$\begin{aligned}\iota S_{ij}^{(1)} &= (1 - \delta_{ij}) \Delta_{ij}^{-1} \left( H_{ij} + Q_{ij} \frac{d}{dr} + \frac{1}{r^2} \frac{d}{dr} r^2 Q_{ij} \right), \\ \iota S_{ij}^{(2)} &= (1 - \delta_{ij}) 2 \Delta_{ij}^{-2} Q_{ij} V'_{jj}, \\ \Delta_{ij} &= \Delta_{ij}(r) = V_{ii} - V_{jj}, \quad V_{ii} = U_{ii} r^{-2}.\end{aligned}\tag{B.2}$$

This approximation eliminates the rhs of equation (58) with the accuracy  $O(\max_{ij} |\Delta_{ij}^{-3}|)$  and generates the inverse operator for the open channel  $|i_o\rangle$

$$\begin{aligned}\chi_j &= T_{ji_o}^{-1} \chi_{i_o}^{\text{new}}, \quad \chi_{i_o}^{\text{new}} = \sum_j T_{i_o j} \chi_j, \\ \langle i_o | T | i_o \rangle &= \langle i_o | T^{-1} | i_o \rangle = 1 = \langle i_o | i_o \rangle.\end{aligned}\tag{B.3}$$

As a result we get the projection of equations (58) onto the channel  $|i_o\rangle$

$$\sum_{ij} T_{i_o i} (H_{ij}^{\text{old}} - 2E)_{ij} T_{ji_o}^{-1} \chi_{i_o}^{\text{new}} = (H_{i_o i_o}^{\text{new}} - 2E) \chi_{i_o}^{\text{new}} = 0,\tag{B.4}$$

where

$$H_{i_o i_o}^{\text{new}} = H_{i_o i_o}^{\text{old}} + \frac{1}{2} [\iota S^{(1)}, H^{\text{old}}]_{i_o i_o} + \frac{1}{2} [\iota S^{(1)} + \iota S^{(2)}, H^1]_{i_o i_o},\tag{B.5}$$

and  $H_{ij}^1 = \Delta_{ij} \iota S_{ij}^{(2)}$ . We can write equation (B.4) in the explicit form

$$-\frac{1}{r^2} \frac{d}{dr} \frac{r^2}{\mu(r)} \frac{d\chi_{i_o}^{\text{new}}(r)}{dr} + \frac{\mu'(r)}{\mu^2(r)r} \chi_{i_o}^{\text{new}}(r) + [\hat{U}_{\text{eff}} - 2E] \chi_{i_o}^{\text{new}}(r) = 0.\tag{B.6}$$

The new solution  $\psi \equiv \mu^{-1/2} \chi_{ii}^{\text{new}}(r)$  in such a diagonal representation satisfies the following equation

$$-\frac{1}{r^2} (r^2 \psi')' + \mu^{1/2} (\mu^{-1/2})'' \psi + \mu [\hat{U}_{\text{ad}} + \delta U - 2E] \psi = 0, \quad \lim_{r \rightarrow 0} r^2 \frac{d\psi}{dr} = 0,\tag{B.7}$$

where the modified scalar product and the adiabatic potential are defined as

$$\langle \psi | \psi \rangle = \int_0^\infty dr r^2 \mu \psi \psi, \quad \hat{U}_{\text{ad}} = V_{ii}.$$

The effective potential  $\hat{U}_{\text{eff}}(r)$  is the sum of the adiabatic potential  $\hat{U}_{\text{ad}}(r)$  and the *effective non-adiabatic correction*  $\delta U(r)$ .  $\mu(r)$  can be considered as the *effective mass*, expressed as

$$\begin{aligned}\mu^{-1}(r) &= 1 + W_{ii}(r), \quad W_{ii}(r) = -4 \sum_{j \neq i}^{j_{\text{max}}} Q_{ij}(r) Q_{ji}(r) \Delta_{ij}^{-1}(r), \\ \delta U(r) &= \sum_{j \neq i}^{j_{\text{max}}} (\Delta_{ij}^{-1} V_{ij}^{(1)} + \Delta_{ij}^{-2} V_{ij}^{(2)} + \Delta_{ij}^{-3} V_{ij}^{(3)}).\end{aligned}\tag{B.8}$$

Here  $W_{ii}(r)$  is the effective mass correction and

$$\begin{aligned}V_{ij}^{(1)} &= H_{ij}^2 - (Q'_{ij})^2 + 2Q_{ij} H'_{ij} - 2Q_{ij} Q''_{ij}, \\ V_{ij}^{(2)} &= H_{ij} Q_{ij} (\Sigma'_{ij} - \Delta'_{ij}) + Q_{ij} Q'_{ij} (\Sigma'_{ij} + 3\Delta'_{ij}) + Q_{ij}^2 (\Sigma''_{ij} + \Delta''_{ij}), \\ V_{ij}^{(3)} &= Q_{ij}^2 (\Sigma'_{ij} + \Delta'_{ij}) (\Sigma'_{ij} - 2\Delta'_{ij}), \\ \Sigma_{ij} &= \Sigma_{ij}(r) = V_{ii} + V_{jj}.\end{aligned}\tag{B.9}$$

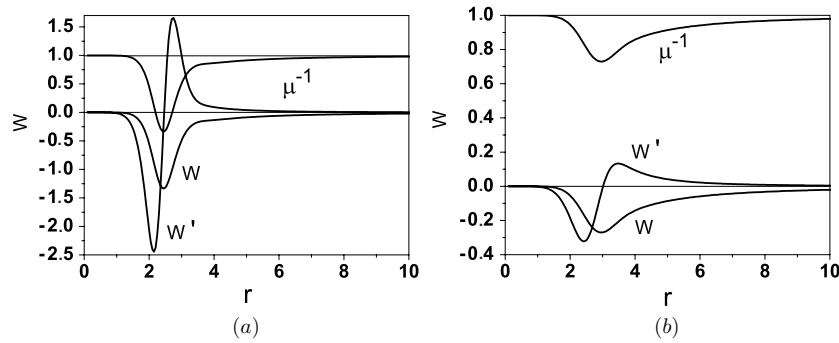


**Figure B1.** The effective mass correction  $W_{11}$ , its derivative  $W'_{11}$  and the inverse effective mass  $\mu^{-1}$  at  $\gamma = 1$  and  $m = 0$  for the first even (a) and odd (b) states.

In the above expressions all terms are functions of  $r$ ; the dash denotes the derivative with respect to  $r$ . At large  $r$  the leading terms of  $W_{ii}(r)$  and  $\delta U(r)$  calculated using the asymptotic basis functions read as

$$W_{ii}(r) = W_{ii}^{as} r^{-2} + O(r^{-4}), \quad \delta U(r) = \delta U^{as} r^{-4} + O(r^{-6}), \quad (\text{B.10})$$

where the effective mass correction

$$-W_{ii}^{as} = \langle i | \rho^2 | i \rangle = 2(2n + |m| + 1) \gamma^{-1} \quad (\text{B.11})$$

is the mean value of the transversal variable,  $\rho^2 = (r \sin \theta)^2$ , characterizing the electron precession around the  $z$  axis in the magnetic field  $\gamma$  (see figure 1), while

$$\delta U^{as} = -(4n^3 + 5n^2 - 4n - 3 + |m|(6n^2 + 5n - 2) + m^2(2n + 1))(2\gamma)^{-1} \quad (\text{B.12})$$

is the asymptotic value correction of the electron polarizability,

$$U = U^{as} r^{-4} = (E^{(4)} + H^{(4)}) r^{-4}, \quad (\text{B.13})$$

where coefficients  $E^{(4)}$  and  $H^{(4)}$  are given by (72) and (74). The plots of the above effective mass and effective potentials having essentially nonmonotonic behavior in a reaction region and given asymptotic form for large  $r$  are shown in figures B1 and B2.

For elastic scattering states with given  $2E(p_{i_o}) = p_{i_o}^2 + E_{i_o}^{(0)}$  we reformulate the problem as

$$(\hat{H}_{\text{eff}} - p_{i_o}^2) \psi \equiv -\frac{1}{r^2} (r^2 \psi')' + \mu^{1/2} (\mu^{-1/2})'' \psi + \mu [\hat{U}_{\text{eff}} - 2E(p_{i_o})] \psi = 0. \quad (\text{B.14})$$

For the function  $\chi^{\text{eff}} = r \mu^{1/2} \psi$  this equation has the conventional form

$$\left( \frac{d}{dr} \mu^{-1}(r) \frac{d}{dr} - U_{\text{eff}}(r) + p_{i_o}^2 \right) \chi_{i_o i_o}^{\text{eff}}(r) = 0, \quad (\text{B.15})$$

where the effective potential is given by

$$U_{\text{eff}}(r) = V_{i_o i_o}(r) + \delta U(r) - \frac{2Z}{r} - E_{i_o}^{(0)}. \quad (\text{B.16})$$

For large  $r$ , using the asymptotic values  $W_{i_o i_o}^{(j_{\text{max}})}$  of  $r^2 W(r)$  and  $\delta U_{i_o i_o}^{(j_{\text{max}})}$  of  $r^4 \delta U(r)$  from (B.8) we have

$$\left( -\frac{d}{dr} \left( 1 + \frac{W_{i_o i_o}^{(j_{\text{max}})}}{r^2} \right) \frac{d}{dr} - \frac{2Z}{r} + \frac{\delta U_{i_o i_o}^{(j_{\text{max}})}}{r^4} - p_{i_o}^2 \right) \bar{\chi}_{i_o i_o}^{as}(r) = 0, \quad (\text{B.17})$$

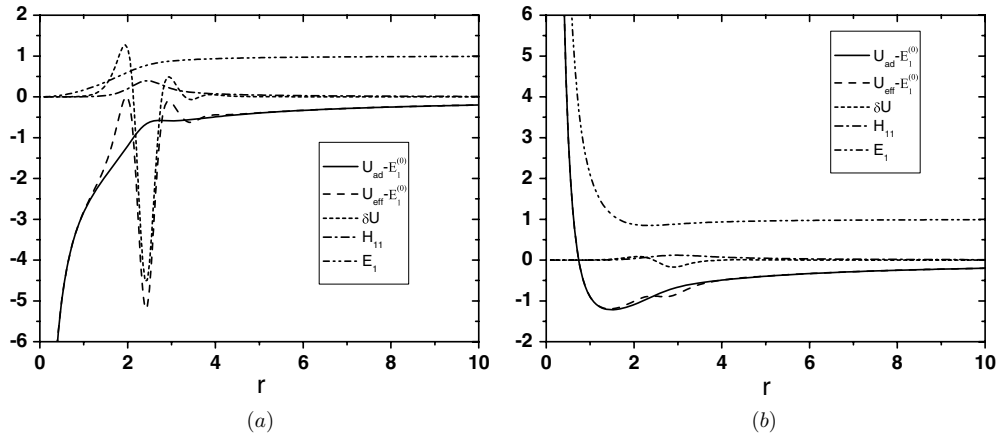


**Figure B2.** The adiabatic potential  $\hat{U}_{\text{ad}}(r)$ , the effective adiabatic potential  $\hat{U}_{\text{eff}}(r)$ , the effective non-adiabatic correction  $\delta U$ , the potential curve  $E_1(r)$  and the radial potential  $H_{11}$  at  $\gamma = 1$  and  $m = 0$  for the first even (a) and odd (b) states.

and to the order of  $O(r^{-3})$  equation (B.15) may be written as

$$\left( \frac{d^2}{dr^2} - \frac{2W_{i_o i_o}^{(j_{\text{max}})}}{r^3} \frac{d}{dr} + \left( \frac{2Z}{r} + p_{i_o}^2 \right) \left( 1 - \frac{W_{i_o i_o}^{(j_{\text{max}})}}{r^2} \right) \right) \bar{\chi}_{i_o i_o}^{as}(r) = 0. \quad (\text{B.18})$$

For  $p_{i_o} W_{i_o i_o}^{(j_{\text{max}})} / (2r) \ll 1$  the solutions belonging to the continuous spectrum can be written in the form

$$\begin{aligned} \bar{\chi}_{i_o i_o}^{as}(r) &\approx \frac{1}{\sqrt{2\pi p_{i_o}}} \sin \left( p_{i_o} r_1 + \frac{Z}{p_{i_o}} \ln(2p_{i_o} r_1) + \delta^c + \delta^{(j_{\text{max}})} \right) \\ &\approx \frac{1}{\sqrt{2\pi p_{i_o}}} \left[ \sin \left( p_{i_o} r + \frac{Z}{p_{i_o}} \ln(2p_{i_o} r) + \delta^c + \delta^{(j_{\text{max}})} \right) \right. \\ &\quad \left. + p_{i_o} \frac{W_{i_o i_o}^{(j_{\text{max}})}}{2r} \cos \left( p_{i_o} r + \frac{Z}{p_{i_o}} \ln(2p_{i_o} r) + \delta^c + \delta^{(j_{\text{max}})} \right) \right], \end{aligned} \quad (\text{B.19})$$

where  $r_1 = r(1 + W_{i_o i_o}^{(j_{\text{max}})} / (2r^2))$  and  $r_1 = r(1 - \langle i_o | \rho^2 | i_o \rangle / (2r^2))$  at  $j_{\text{max}} \geq i_o + 1$  and  $\delta^{(j_{\text{max}})} \equiv \delta^{(j_{\text{max}})}(p_{i_o})$  is the required phase shift of the elastic scattering in the open channel  $|i_o\rangle$  count off the known Coulomb phase shift  $\delta^c = \arg \Gamma(1 - iZ/p_{i_o})$ .

Remembering that  $r^2 = \rho^2 + z^2$  and  $|z| \sim r(1 - \rho^2 / (2r^2))$  in the asymptotic region  $\rho/r \ll 1$  one can introduce the *mean position* operator in the new representation  $\chi^{\text{new}} = T\chi$   $r_{\text{mean}}^{\text{new}} = \langle \chi^{\text{new}} | \hat{r}_{\text{mean}}^{\text{new}} | \chi^{\text{new}} \rangle = \langle \chi | T^{-1} \hat{r}_{\text{mean}}^{\text{new}} T | \chi \rangle = \langle \chi | \hat{r}_{\text{mean}} | \chi \rangle = r_{\text{mean}}$ . (B.20)

The *mean position* operator  $\hat{r}_{\text{mean}}^{\text{new}} = r$  plays the role of the longitudinal coordinate  $z$  in the new representation  $\chi^{\text{new}}$ . In other words, the  $z$ -delocalization is accounted for in the new radial functions  $\chi^{\text{new}} = T\chi$ . In the old representation  $\chi$  the mean position operator  $\hat{r}_{\text{mean}}$  is defined as

$$\hat{r}_{\text{mean}} = T^{-1} \hat{r}_{\text{mean}}^{\text{new}} T = T^{-1} r T = r + \delta \hat{r}, \quad (\text{B.21})$$

where  $\delta \hat{r}$  is the delocalization of the longitudinal coordinate  $z$  that has the order of  $\rho^2 / (2r)$  in the asymptotic region  $\rho/r \ll 1$  (see figure 1)

$$\hat{r}_{\text{mean}} \rightarrow T^{-1} r T \approx \langle z \rangle. \quad (\text{B.22})$$

Note that the transformation affects only the form of the radial solutions and the longitudinal coordinate  $z$  enters only the total expansion of the wavefunction. If we omit the non-adiabatic terms, the solution takes the adiabatic form

$$\chi^{\text{ad}} \sim \sin \left( p_{i_o} r + \frac{Z}{p_{i_o}} \ln(2p_{i_o} r) + \delta^c + \delta^{\text{ad}} \right). \quad (\text{B.23})$$

Then the difference between the true phase shift  $\delta$ ,  $j_{\text{max}}$  th approximation  $\delta^{(j_{\text{max}})}$  and the adiabatic phase shift  $\delta^{\text{ad}}$  can be expressed as

$$\delta^{(j_{\text{max}})} = \delta^{\text{ad}} - p_{i_o} \frac{W_{i_o i_o}^{(j_{\text{max}})}}{2r}, \quad \delta = \lim_{j_{\text{max}} \rightarrow \infty} \delta^{(j_{\text{max}})} = \delta^{\text{ad}} + p_{i_o} \frac{\langle i_o | \rho^2 | i_o \rangle}{2r}. \quad (\text{B.24})$$

The asymptotic solutions  $\bar{\chi}_j(r)$  of equations (58) are related to the solution  $\bar{\chi}_{i_o i_o}^{\text{new}}(r)$  of the effective equation (B.7) via the inverse asymptotic transformation that reveals weak asymptotic coupling of the closed channels

$$\bar{\chi}_{j i_o}^{\text{as}}(r) = T_{j i_o}^{-1} \bar{\chi}_{i_o i_o}^{\text{new}}(r) \sim \exp \left[ -\frac{\langle j | \rho^2 | i_o \rangle (1 - \delta_{j i_o})}{2r} \frac{d}{dr} \right] \bar{\chi}_{i_o i_o}^{\text{new}}(r). \quad (\text{B.25})$$

Making use of equation (B.25), we arrive at the asymptotic solutions for equations (58)

$$\begin{aligned} \bar{\chi}_{i_o i_o}^{\text{as}}(r) &= \bar{\chi}_{i_o i_o}^{\text{new}}(r), \quad \bar{\chi}_{j i_o}^{\text{as}}(r) = T_{j 0}^{-1} \bar{\chi}_{i_o i_o}^{\text{new}}(r) \\ &\approx -\frac{\langle j | \rho^2 | i_o \rangle (1 - \delta_{j i_o})}{2\sqrt{2\pi p_{i_o} r}} p_{i_o} \cos \left( p_{i_o} r + \frac{Z}{p_{i_o}} \ln(2p_{i_o} r) + \delta^c + \delta^{(j_{\text{max}})} \right). \end{aligned} \quad (\text{B.26})$$

The expansion of the partial wavefunction  $\Psi_{i_o}$  in the open channel  $|i_o\rangle$  over the set of asymptotic angular functions  $\Phi_j(\theta; r) = r^{-1} \tilde{\Phi}_j(\rho)(1 + o(1))$  for  $\rho/r \ll 1$ ,

$$\Psi_{i_o} = \left( |\tilde{\Phi}_{i_o}\rangle \langle \tilde{\Phi}_{i_o}| + \sum_{j \neq i_o}^{j_{\text{max}} \rightarrow \infty} |\tilde{\Phi}_j\rangle \langle \tilde{\Phi}_j| T^{-1} |\tilde{\Phi}_{i_o}\rangle \right) \bar{\chi}_{i_o i_o}^{\text{new}}(r), \quad (\text{B.27})$$

subject to the completeness condition takes the form

$$\begin{aligned} \Psi_{i_o} &\approx \frac{\tilde{\Phi}_{i_o}(\rho)}{\sqrt{2\pi p_{i_o}}} \left[ \sin \left( p_{i_o} r + \frac{Z}{p_{i_o}} \ln(2p_{i_o} r) + \delta^c + \delta \right) \right. \\ &\quad \left. - p_{i_o} \frac{\rho^2}{2r} \cos \left( p_{i_o} r + \frac{Z}{p_{i_o}} \ln(2p_{i_o} r) + \delta^c + \delta \right) \right]. \end{aligned} \quad (\text{B.28})$$

For  $p_{i_o} \rho^2 / (2r) \ll 1$ , to the accuracy of  $O(r^{-1})$ , we have the true separable representation in cylindrical coordinates  $(\rho, z)$

$$\begin{aligned} \Psi_{i_o}(r, \rho) &\sim \frac{\tilde{\Phi}_{i_o}(\rho)}{\sqrt{2\pi p_{i_o}}} \sin \left( p_{i_o} \left( r - \frac{\rho^2}{2r} \right) + \frac{Z}{p_{i_o}} \ln \left( 2p_{i_o} \left( r - \frac{\rho^2}{2r} \right) \right) + \delta(p_{i_o}) \right) \\ &\rightarrow \frac{\tilde{\Phi}_{i_o}(\rho)}{\sqrt{2\pi p_{i_o}}} \sin \left( p_{i_o} |z| + \frac{Z}{p_{i_o}} \ln 2p_{i_o} |z| + \delta(p_{i_o}) \right) \sim \frac{\tilde{\Phi}_{i_o}(\rho)}{\sqrt{2\pi p_{i_o}}} \bar{\chi}_{i_o i_o}^{(0)}(|z|). \end{aligned} \quad (\text{B.29})$$

Taking equation (56) and  $|z| \sim r(1 - \rho^2/2r^2)$  into account, one can see that it is compatible with asymptotic expressions (75) and (81) to the order  $k_{\text{max}}$  of truncation of expansions (76) and (84).

### Appendix C. Asymptotic function ‘incident wave + ingoing wave’

Let us express the wavefunction (105) as

$$\Psi_{Em\leftarrow}^{(-)}(r, \eta) = \frac{1}{\sqrt{2}} \left( (\Phi^{m\sigma=+1}(\eta; r))^T \hat{\chi}^{(m\sigma=+1)}(E, r) \pm (\Phi^{m\sigma=-1}(\eta; r))^T \hat{\chi}^{(m\sigma=-1)}(E, r) \right) \exp(-i\delta^c). \quad (C.1)$$

As mentioned above, asymptotically this function consists of waves going into the center and an outgoing plane wave (reverse to the case of an incident plane wave and waves going out of the center in scattering theory). Using (57) equation (C.1) can be rewritten in the form

$$\Psi_{Em\leftarrow}^{(-)}(r, \eta) = \frac{1}{2} \left( (\Phi^{m\leftarrow}(\eta; r))^T [\hat{\chi}^{(m\sigma=+1)}(E, r) \pm \hat{\chi}^{(m\sigma=-1)}(E, r)] + (\Phi^{m\rightarrow}(\eta; r))^T [\hat{\chi}^{(m\sigma=+1)}(E, r) \mp \hat{\chi}^{(m\sigma=-1)}(E, r)] \right) \exp(-i\delta^c). \quad (C.2)$$

At  $r \rightarrow \infty$ ,  $|\eta| \sim 1$  it has the asymptotic form

$$\Psi_{Em\rightarrow}^{(-)}(r, \eta) \rightarrow \sqrt{\frac{2}{\pi}} \left( (\Phi^{m\leftarrow}(\eta; r))^T [\check{\chi}(r) + \check{\chi}^*(r) \hat{\mathbf{R}}^\dagger] + (\Phi^{m\rightarrow}(\eta; r))^T \check{\chi}^*(r) \hat{\mathbf{T}}^\dagger \right), \quad (C.3)$$

$$\Psi_{Em\leftarrow}^{(-)}(r, \eta) \rightarrow \sqrt{\frac{2}{\pi}} \left( (\Phi^{m\leftarrow}(\eta; r))^T \check{\chi}^*(r) \hat{\mathbf{T}}^\dagger + (\Phi^{m\rightarrow}(\eta; r))^T [\check{\chi}(r) + \check{\chi}^*(r) \hat{\mathbf{R}}^\dagger] \right), \quad (C.4)$$

where  $\hat{\mathbf{T}}^\dagger$  and  $\hat{\mathbf{R}}^\dagger$  are the conjugate transmission and reflection amplitude matrices from (31), and the fundamental solutions  $\check{\chi}(r)$  are related to the asymptotic solutions  $\chi(r)$  from (76) or (81)

$$\hat{\mathbf{T}}^\dagger = \frac{1}{2}(-\check{\mathbf{S}}_{+1}^\dagger + \check{\mathbf{S}}_{-1}^\dagger), \quad \hat{\mathbf{R}}^\dagger = \frac{1}{2}(-\check{\mathbf{S}}_{+1}^\dagger - \check{\mathbf{S}}_{-1}^\dagger), \quad \check{\chi}(r) = \chi(r) \exp(-i\delta^c). \quad (C.5)$$

Note that  $\Phi^{m\leftarrow}(\eta; r) = \Phi^{m\rightarrow}(-\eta; r)$  and  $\Phi^{m\leftarrow}(\eta < 0; r) = \Phi^{m\rightarrow}(\eta > 0; r) = O(\exp(-p(1 + |\eta|)))$  at  $r \rightarrow \infty$  and  $|\eta| \sim 1$ . Equations (C.3) and (C.4) may be rewritten in the matrix form

$$\begin{pmatrix} \Psi_{Em\rightarrow}^{(-)}(r, \eta_+) & \Psi_{Em\leftarrow}^{(-)}(r, \eta_+) \\ \Psi_{Em\rightarrow}^{(-)}(r, \eta_-) & \Psi_{Em\leftarrow}^{(-)}(r, \eta_-) \end{pmatrix} \rightarrow \sqrt{\frac{2}{\pi}} \begin{pmatrix} \Phi^{m\leftarrow}(\eta_+; r) & 0 \\ 0 & \Phi^{m\rightarrow}(\eta_-; r) \end{pmatrix}^T \times \left[ \begin{pmatrix} \check{\chi}(r) & 0 \\ 0 & \check{\chi}(r) \end{pmatrix} + \begin{pmatrix} 0 & \check{\chi}^*(r) \\ \check{\chi}^*(r) & 0 \end{pmatrix} \hat{\mathbf{S}}^\dagger \right], \quad (C.6)$$

where  $\eta_\pm = \pm|\eta|$ ,  $|\eta| \sim 1$  and  $\hat{\mathbf{S}}^\dagger = \hat{\mathbf{S}}^{-1}$  is the inverse of the scattering matrix corresponding to (35):

$$\hat{\mathbf{S}}^\dagger = \begin{pmatrix} \hat{\mathbf{T}}^\dagger & \hat{\mathbf{R}}^\dagger \\ \hat{\mathbf{R}}^\dagger & \hat{\mathbf{T}}^\dagger \end{pmatrix}. \quad (C.7)$$

### References

- [1] Rotondi A *et al* 2005 *AIP Conf. Proc.* **796** 285–90  
Madsen N *et al* 2005 *Phys. Rev. Lett.* **94** 033403-1–4
- [2] Wetzels A, Gurtler A, Noordam L D and Robicheaux F 2006 *Phys. Rev. A* **73** 062507-1–8
- [3] Menshikov L I and Landua R 2003 *Phys. Uspekhi* **46** 227–58
- [4] Ryabinina M V and Melnikov L A 2005 *AIP Conf. Proc.* **796** 325–9  
Ryabinina M V and Melnikov L A 2004 *Nucl. Instrum. Methods Phys. Res. B* **214** 35–9
- [5] Serov V V, Derbov V L and Vinitsky S I 2007 *Opt. Spectrosc.* **102** 557–61
- [6] Wang Q and Greene C H 1991 *Phys. Rev. A* **44** 7448–58
- [7] Watanabe S and Komine H-A 1991 *Phys. Rev. Lett.* **67** 3227–30

- [8] Zhao L B and Stancil P C 2006 *Phys. Rev. A* **74** 055401-1-4
- [9] Dimova M G, Kaschiev M S and Vinitzky S I 2005 *J. Phys. B: At. Mol. Opt. Phys.* **38** 2337-52
- [10] Abrashkevich A G and Shapiro M 1994 *Phys. Rev. A* **50** 1205-17
- [11] Delande D, Bommier A and Gay J C 1991 *Phys. Rev. Lett.* **66** 141-4
- [12] Eichler J, Yoshihama Y and Toshima N 2002 *Phys. Rev. A* **65** 033404-1-6
- [13] Burke P G 1977 *Potential Scattering in Atomic Physics* (New York: Plenum)
- [14] Fano U and Lee C M 1973 *Phys. Rev. Lett.* **31** 1573-6
- [15] Lee C M 1974 *Phys. Rev. A* **10** 584-600
- [16] Seaton M J 1983 *Rep. Prog. Phys.* **46** 167-257
- [17] Greene C H 1983 *Phys. Rev. A* **28** 2209-16
- [18] Kantorovich L V and Krylov V I 1964 *Approximate Methods of Higher Analysis* (New York: Wiley)
- [19] Fano U 1977 *Colloq. Int. C. N. R. S.* **273** 127
- Starace A F and Webster G L 1979 *Phys. Rev. A* **19** 1629-40
- Clark C V, Lu K T and Starace A F 1984 *Progress in Atomic Spectroscopy* ed H G Beyer and H Kleinpoppen (New York: Plenum) Part C pp 247-320
- [20] Abramovits M and Stegun I A 1972 *Handbook of Mathematical Functions* (New York: Dover) p 1037
- [21] Chuluunbaatar O, Gusev A A, Derbov V L, Kaschiev M S, Serov V V, Tupikova T V and Vinitzky S I 2006 *Proc. SPIE* **6165** 61650B-1-17
- [22] Vinitzky S I, Gerdt V P, Gusev A A, Kaschiev M S, Rostovtsev V A, Samoylov V N, Tupikova T V and Chuluunbaatar O 2007 *Program. Comput. Softw.* **33** 105-16
- [23] Chuluunbaatar O, Gusev A A, Gerdt V P, Rostovtsev V A, Vinitzky S I, Abrashkevich A G, Kaschiev M S and Serov V V 2007 accepted in *Comput. Phys. Commun.*
- [24] Damburg R J and Propin R Kh 1968 *J. Phys. B: At. Mol. Phys.* **1** 681-91
- [25] Power J D 1973 *Phil. Trans. R. Soc. A* **274** 663-702
- [26] Chuluunbaatar O, Gusev A A, Gerdt V P, Kaschiev M S, Rostovtsev V A, Samoylov V N, Tupikova T V and Vinitzky S I 2007 *Lect. Notes Comput. Sci.* at press
- [27] Guest J R, Choi J-H and Raithel 2003 *Phys. Rev. A* **68** 022509-1-9
- [28] Fridrich H 1982 *Phys. Rev. A* **46** 1827-38
- [29] Aljiah A, Hinze J and Broad J T 1990 *J. Phys. B: At. Mol. Opt. Phys.* **23** 45-60
- [30] Gusev A A, Gerdt V P, Kaschiev M S, Rostovtsev V A, Samoylov V N, Tupikova T V and Vinitzky S I 2006 *Lecture Notes Comput. Sci.* **4194** 205-18
- [31] Kaschiev M S, Vinitzky S I and Vukajlovic F R 1980 *Phys. Rev. A* **22** 557-559
- [32] Gailitis M 1976 *J. Phys. B: At. Mol. Phys.* **9** 843-54
- [33] Chuluunbaatar O, Gusev A A, Abrashkevich A G, Amaya-Tapia A, Kaschiev M S, Larsen S Y and Vinitzky S I 2007 *Comput. Phys. Commun.* (at press)
- [34] <http://physics.nist.gov/cuu/Constants/index.html>
- [35] Gusev A A, Samoilov V N, Rostovtsev V A and Vinitzky S I 2001 *CASC-2001: Proc. 4th Workshop on Computer Algebra in Scientific Computing* (Berlin: Springer) pp 309-22
- [36] Seaton M J 2002 *Comput. Phys. Commun.* **146** 225-49
- [37] Pupyshev V V 1995 *J. Phys. A: Math. Gen.* **28** 3305-18
- Pupyshev V V 1997 *Phys. Part. Nucl.* **28** 586-614
- [38] Sarkisyan H A 2002 *Mod. Phys. Lett. B* **16** 835-41
- [39] Demkov Yu N and Meyer J D 2004 *Eur. Phys. J. B* **42** 361-5
- [40] Kim J I, Melezhik V S and Schmelcher P 2006 *Phys. Rev. Lett.* **97** 193203-1-4

# Photoionization and recombination of a hydrogen atom in a magnetic field

O. Chuluunbaatar,<sup>1</sup> A. A. Gusev,<sup>1</sup> S. I. Vinitzky,<sup>1</sup> V. L. Derbov,<sup>2</sup> L. A. Melnikov,<sup>2</sup> and V. V. Serov<sup>2</sup>

<sup>1</sup>Joint Institute for Nuclear Research, Dubna, Russia

<sup>2</sup>Saratov State University, Saratov, 410012, Russia

(Received 18 December 2007; published 21 March 2008)

Application of the adiabatic method and program packages for solving the boundary problem for a discrete and continuous spectrum of a hydrogenlike atom in a homogeneous magnetic field is presented. Based on this the estimation of the photoionization cross section and laser-induced recombination rate is carried out. Effects of resonance transmission and total reflection of oppositely charged particles in a homogeneous magnetic field are demonstrated.

DOI: 10.1103/PhysRevA.77.034702

PACS number(s): 32.80.Fb

In a recent paper [1] an alternative mechanism of laser-induced recombination of antihydrogen from cold anti-proton-positron plasma in a magnetic trap was revealed. This resonance mechanism makes use of quasistationary states embedded in the continuum. These states arise due to the transverse confinement potential induced by the magnetic field. The optimization of laser and magnetic field parameters in the case when the Coulomb energy is comparable with that of the magnetic field can be studied by means of the adiabatic approach in spherical coordinates using the basis of angular oblate spheroidal functions [2]. An attractive feature of this approach is that the electron wave function is accurately evaluated near the origin irrespective of the field strength [3,4]. However, the key point for the scattering problem is how to match the spherically symmetric wave functions near the origin with the wave functions possessing the cylindrical symmetry which are more appropriate in the area located far enough from the origin [5]. This problem was resolved in the appropriate calculation scheme and program packages aimed at the solution of the boundary problems for discrete and continuous spectrum of a hydrogenlike atom in a homogeneous magnetic field developed by the authors earlier [6–8].

In this Brief Report we apply this approach to the calculation of the optical transitions between the bound and the autoionization states both of discrete and continuous spectrum. Our analysis revealed the effects of resonance transmission and total reflection of oppositely charged particles in a homogeneous magnetic field related to the existence of quasistationary states embedded in the continuum.

The Schrödinger equation for the wave function  $\hat{\Psi}(\Omega) = \Psi(r, \eta) \exp(im\varphi) / \sqrt{2\pi}$  of a hydrogen atom with the charge  $Z$  of the nucleus in the axially symmetric magnetic field  $\mathbf{B} = (B_x=0, B_y=0, B_z=B)$  written in spherical coordinates  $\Omega = (r, \eta = \cos \theta, \varphi)$  is reduced to the two-dimensional (2D) equation for the partial component  $\Psi(r, \eta) \equiv \Psi^{m\sigma}(r, \eta) = \sigma \Psi^{m\sigma}(r, -\eta)$  at fixed values of the magnetic quantum number  $m=0, \pm 1, \dots$  and  $z$  parity  $\sigma = \pm 1$ ,

$$\left( -\frac{1}{r^2} \frac{\partial}{\partial r} r^2 \frac{\partial}{\partial r} + \frac{1}{r^2} \hat{A}(p) - \frac{2Z}{r} \right) \Psi(r, \eta) = \epsilon \Psi(r, \eta). \quad (1)$$

Here we use the atomic units (a.u.)  $\hbar = m_e = e = 1$  and put the mass of the nucleus to be infinite,  $\epsilon = 2E$ ,  $E$  is the energy

[expressed in Rydbergs,  $1 \text{ Ry} = (1/2) \text{ a.u.}$ ] of the state  $|m\sigma\rangle$ .

The operator  $\hat{A}(p)$  is defined by

$$\hat{A}(p) = -\frac{\partial}{\partial \eta} (1 - \eta^2) \frac{\partial}{\partial \eta} + \frac{m^2}{1 - \eta^2} + 2pm + p^2(1 - \eta^2),$$

where  $p = \gamma r^2/2$  is the confinement potential induced by the magnetic field,  $\gamma = B/B_0$  is a dimensionless parameter determined by the field  $B$ , and  $B_0 \equiv 2.35 \times 10^5 \text{ T}$ .

Let us consider a formal adiabatic expansion of the partial solution  $\Psi_i^{Em\sigma}(r, \eta)$  of Eq. (1) in terms of one-dimensional basis functions  $\{\Phi_j^{m\sigma}(\eta; r)\}_{j=1}^{j_{\max}}$ ,

$$\Psi_i^{Em\sigma}(r, \eta) = \sum_{j=1}^{j_{\max}} \Phi_j^{m\sigma}(\eta; r) \chi_j^{(m\sigma i)}(E, r). \quad (2)$$

The radial wave functions  $\chi^{(i)}(r) \equiv \chi^{(m\sigma i)}(E, r)$ ,  $[\chi^{(i)}(r)]^T = (\chi_1^{(i)}(r), \dots, \chi_{j_{\max}}^{(i)}(r))$  are unknown, the orthonormal basis wave functions  $\Phi_j(r, \eta) \equiv \Phi_j^{m\sigma}(\eta; r) = \sigma \Phi_j^{m\sigma}(-\eta; r)$  and the potential curves  $E_j(r)$  (in Ry) are the solutions of the parametric eigenvalue problem

$$\hat{A}(p) \Phi_j(\eta; r) = E_j(r) \Phi_j(\eta; r). \quad (3)$$

The solutions of this problem with shifted eigenvalues  $\check{E}_j(r) = E_j(r) - 2pm$  correspond to the angular oblate spheroidal functions [9].

By using the expansion (2) we reduce the initial problem (1) to a boundary problem for a set of  $j_{\max}$  coupled second-order ordinary differential equations that determine the radial wave functions  $\chi^{(i)}(r)$  of the expansion (2) in the finite interval  $r \in [0, r_{\max}]$ ,

$$\left( -\frac{1}{r^2} \mathbf{I} \frac{d}{dr} r^2 \frac{d}{dr} + \frac{\mathbf{U}(r)}{r^2} + \mathbf{Q}(r) \frac{d}{dr} + \frac{1}{r^2} \frac{dr^2 \mathbf{Q}(r)}{dr} \right) \chi^{(i)}(r) = \epsilon \mathbf{I} \chi^{(i)}(r), \quad (4)$$

with the boundary condition at  $r=0$ ,

$$\lim_{r \rightarrow 0} r^2 \left( \frac{d\chi^{(i)}(r)}{dr} - \mathbf{Q}(r) \chi^{(i)}(r) \right) = 0. \quad (5)$$

Here  $\mathbf{I}$ ,  $\mathbf{U}(r)$ , and  $\mathbf{Q}(r)$  are  $j_{\max} \times j_{\max}$  matrices with the elements

$$U_{ij}(r) = \frac{E_i(r) + E_j(r) - 4Zr}{2} \delta_{ij} + r^2 H_{ij}(r), \quad I_{ij} = \delta_{ij},$$



$$H_{ij}(r) = H_{ji}(r) = \int_{-1}^1 \frac{\partial \Phi_i(\eta; r)}{\partial r} \frac{\partial \Phi_j(\eta; r)}{\partial r} d\eta, \\ Q_{ij}(r) = -Q_{ji}(r) = - \int_{-1}^1 \Phi_i(\eta; r) \frac{\partial \Phi_j(\eta; r)}{\partial r} d\eta, \quad (6)$$

where  $\delta_{ij}$  is the Kronecker symbol. The eigenfunctions  $\Phi_j(\eta; r)$ , potential curves  $E_j(r)$ , and radial coupling matrix elements  $H_{ij}(r)$  and  $Q_{ij}(r)$  were calculated using the program POTHMF [8].

The discrete spectrum solutions  $\chi^{(i)}(r)$  obey the first-type boundary condition,  $\chi^{(i)}(r_{\max})=0$ , which makes it possible to calculate the energy eigenvalues  $E \equiv E_{m\sigma v}$ ,  $v=0, v_{\max}$  and the corresponding eigenfunctions  $\Psi_{iv}^{m\sigma}(r, \eta) \equiv \Psi_i^{Em\sigma}(r, \eta)$  of Eq. (2) at  $i=1$  using the program KANTBP [7]. The orthogonality and normalization condition for  $\hat{\Psi}_{iv}^{m\sigma}(\Omega)$  is

$$\langle \hat{\Psi}_{iv}^{m\sigma}(\Omega) | \hat{\Psi}_{i'v'}^{m'\sigma'}(\Omega) \rangle = \delta_{vv'} \delta_{mm'} \delta_{\sigma\sigma'} \delta_{ii'}. \quad (7)$$

The continuous-spectrum solutions  $\chi^{(i)}(r)$  obey the third-type boundary condition at fixed energy  $\epsilon=2E$  above the first Landau threshold  $E_j(\infty) \equiv \epsilon_{mj}^{th}(\gamma) = \gamma(2j-1+m+|m|)$  with  $j=1$ ,

$$\frac{d\chi(r)}{dr} = \mathbf{R}\chi(r), \quad r = r_{\max}, \quad (8)$$

where  $\mathbf{R}$  is a nonsymmetric  $j_{\max} \times j_{\max}$  matrix which was calculated using the program KANTBP [7]. The orthogonality and normalization condition for  $\hat{\Psi}_i^{Em\sigma}(\Omega)$  is

$$\langle \hat{\Psi}_i^{Em\sigma}(\Omega) | \hat{\Psi}_{i'}^{E'm'\sigma'}(\Omega) \rangle = \delta(E-E') \delta_{mm'} \delta_{\sigma\sigma'} \delta_{ii'}. \quad (9)$$

We express the corresponding eigenfunction  $\Psi_i^{Em\sigma}(r, \eta)$  of the continuous spectrum with the energy  $\epsilon=2E$  in open channels,  $i=1, N_o$ ,  $N_o = \max_{2E \geq \epsilon_{mj}^{th}} j < j_{\max}$ , in the form of Eq. (2), where  $\hat{\chi}^{(m\sigma)}(E, r) \equiv \{\chi^{(i\sigma)}(r)\}_{i=1}^{N_o}$  is now the radial part of the eigenchannel or “incoming” wave function. The eigenchannel wave function  $\hat{\chi}^{(m\sigma)}(E, r)$  is expressed as

$$\hat{\chi}^{(m\sigma)}(E, r) = (2/\pi)^{1/2} \chi^{(p)}(r) \mathbf{C} \cos \delta. \quad (10)$$

The function  $\chi^{(p)}(r)$  is a numerical solution of Eq. (4) that satisfies the “standing-wave” boundary conditions (8) and has the standard asymptotic form [7]

$$\chi^{(p)}(r) = \chi^s(r) + \chi^c(r) \mathbf{K}, \quad \mathbf{K} \mathbf{C} = \mathbf{C} \tan \delta. \quad (11)$$

Here  $\mathbf{K} \equiv \mathbf{K}_{\sigma}$  is the symmetric numerical *short-range reaction matrix* with the diagonal eigenvalue matrix  $\tan \delta \equiv \{\delta_{ij} \tan \delta_j\}_{i,j=1}^{N_o}$  depending on the *short-range even or odd phase shift vector*  $\delta \equiv \delta_{\sigma} = \{\delta_j\}_{j=1}^{N_o}$ , and the orthogonal matrix  $\mathbf{C}^T \mathbf{C} = \mathbf{I}_{oo}$  of the corresponding eigenvectors  $\mathbf{C}$ , where  $\mathbf{I}_{oo}$  is the unit  $N_o \times N_o$  matrix. Note that in Eq. (10)  $\cos \delta$  is the diagonal matrix defined in the same terms. The regular  $\chi^s(r) = 2 \operatorname{Im}[\chi(r)]$  and irregular  $\chi^c(r) = 2 \operatorname{Re}[\chi(r)]$  asymptotic functions are expressed via the fundamental asymptotic solution  $\chi(r)$  with the leading terms at  $r \rightarrow \infty$ ,

$$\chi_{ji_o}(r) = \frac{\exp[ip_{i_o} r + i\zeta \ln(2p_{i_o} r) + i\delta_{i_o}^c]}{2r\sqrt{p_{i_o}}} \delta_{ji_o}, \quad (12)$$

where  $p_{i_o}$  is the relative momentum in the channel  $i_o$ ,  $\zeta \equiv \xi_{i_o} = Z/p_{i_o}$  is a Sommerfeld-type parameter,  $\delta_{i_o}^c = \arg \Gamma(1-i\zeta)$  is the known Coulomb phase shift [9]. Using **R**-matrix calculus [7], we obtain the equation expressing the reaction matrix  $\mathbf{K}$  via the matrix  $\mathbf{R}$  at  $r=r_{\max}$ ,

$$\mathbf{K} = -\mathbf{X}^{-1}(r_{\max}) \mathbf{Y}(r_{\max}), \quad (13)$$

where  $\mathbf{X}(r)$  and  $\mathbf{Y}(r)$  are square  $N_o \times N_o$  matrices depending on the open-open matrix (channels)

$$\mathbf{X}(r) = \left( \frac{d\chi^c(r)}{dr} - \mathbf{R}\chi^c(r) \right)_{oo}, \\ \mathbf{Y}(r) = \left( \frac{d\chi^s(r)}{dr} - \mathbf{R}\chi^s(r) \right)_{oo}. \quad (14)$$

The radial part of the “incoming” wave function  $\hat{\chi}^{(m\sigma)}(E, r) = (2/\pi)^{1/2} \chi^-(r)$  is expressed via the numerical “standing” wave function and the short-range reaction matrix  $\mathbf{K}$  by the relation

$$\chi^-(r) = i\chi^{(p)}(r)(\mathbf{I}_{oo} + i\mathbf{K})^{-1} \quad (15)$$

and has the asymptotic form

$$\hat{\chi}^{(m\sigma)}(E, r) = (2/\pi)^{1/2} [\chi(r) - \chi^*(r) \mathbf{S}^\dagger]. \quad (16)$$

Here  $\mathbf{S} \equiv \mathbf{S}_{\sigma}$  is the unitary short-range scattering matrix,  $\mathbf{S}^\dagger \mathbf{S} = \mathbf{S} \mathbf{S}^\dagger = \mathbf{I}_{oo}$ , which can be expressed via the calculated  $\mathbf{K}$  matrix as

$$\mathbf{S} = (\mathbf{I}_{oo} + i\mathbf{K})(\mathbf{I}_{oo} - i\mathbf{K})^{-1}. \quad (17)$$

The ionization wave function  $\Psi_{Em\hat{v}}^{(-)}(r, \eta) \equiv \Psi_{Em\hat{v}}^{(-)}(r, \eta)$  has the asymptotic form reverse to the common scattering problem, namely, “incident wave+ingoing wave”

$$\Psi_{Em\hat{v}}^{(-)}(r, \eta) = \frac{\Psi_{Em,+1}^{(-)}(r, \eta) \pm \Psi_{Em,-1}^{(-)}(r, \eta)}{\sqrt{2}} \exp(-i\delta^r). \quad (18)$$

The function  $\Psi_{Em\hat{v}}^{(-)}(r, \eta)$  corresponds to the function  $|E\hat{v}mN_p\rangle$  defined in the cylindrical coordinates  $(\rho, z, \varphi)$ ,

$$|E\hat{v}mN_p\rangle = \frac{\exp(im\varphi)}{2\pi} \sum_{n'=1}^{j_{\max}} \Phi_{n'}(\rho) \chi_{Em\hat{v}n'}^{(-)}(z). \quad (19)$$

Here  $N_p = n-1$ ,  $\hat{v}$  denotes the initial direction of the particle motion along the  $z$  axis, and  $\Phi_{n'}(\rho)$  is the eigenfunction of a two-dimensional oscillator that corresponds to  $\Phi_j^{m\hat{v}}(r, \eta) = [\Phi_j^{m,+1}(r, \eta) \pm \Phi_j^{m,-1}(r, \eta)]/\sqrt{2}$  at  $r \rightarrow \infty$ . At  $z \rightarrow \pm \infty$  the function  $\chi_{Em\hat{v}n'}^{(-)}(z)$  has the following asymptotic form:

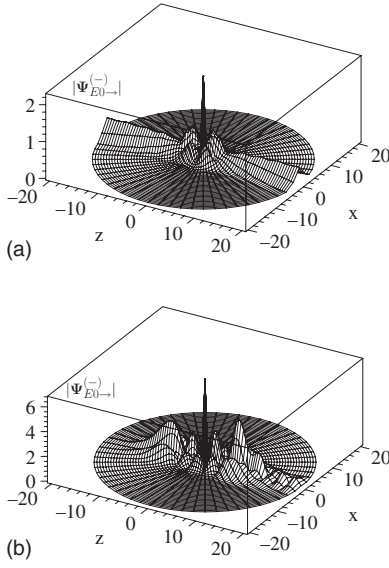


FIG. 1. Profiles  $|\Psi_{Em\rightarrow}^{(-)}|$  of the total wave function (18) in the  $xz$  plane with  $Z=1$ ,  $m=0$ ,  $\gamma=0.1$  and the energies  $E=0.058\ 85$  a.u. (a) and  $E=0.116\ 92$  a.u. (b), demonstrating resonance transmission and total reflection, respectively.

$$\chi_{E\hat{v}}^{(-)}(z) = \begin{cases} \begin{cases} \mathbf{X}^{(+)}(z) + \mathbf{X}^{(-)}(z)\hat{\mathbf{R}}^{\dagger}, & z > 0, \\ \mathbf{X}^{(+)}(z)\hat{\mathbf{T}}^{\dagger}, & z < 0, \end{cases} & \hat{v} = \rightarrow, \\ \begin{cases} \mathbf{X}^{(-)}(z)\hat{\mathbf{T}}^{\dagger}, & z > 0, \\ \mathbf{X}^{(-)}(z) + \mathbf{X}^{(+)}(z)\hat{\mathbf{R}}^{\dagger}, & z < 0, \end{cases} & \hat{v} = \leftarrow, \end{cases} \quad (20)$$

where the matrix elements of  $\mathbf{X}^{(\pm)}(z)$  are

$$X_{n'n}^{(\pm)}(z) = \exp\left(\pm i p_{n'} z \pm i \zeta_{n'} \frac{z}{|z|} \ln(2p_{n'}|z|)\right) \frac{\delta_{n'n}}{\sqrt{p_{n'}}}, \quad (21)$$

$\hat{\mathbf{T}}$  and  $\hat{\mathbf{R}}$  are the transmission and reflection amplitude matrices,  $\hat{\mathbf{T}}^{\dagger}\hat{\mathbf{T}} + \hat{\mathbf{R}}^{\dagger}\hat{\mathbf{R}} = \mathbf{I}_{oo}$ . It is easy to show that  $\hat{\mathbf{T}}$  and  $\hat{\mathbf{R}}$  may be expressed in terms of the long-range scattering matrices  $\check{\mathbf{S}}_{\sigma} = \exp(i\delta_{\sigma})\mathbf{S}_{\sigma}\exp(i\delta_{\sigma}^*)$  as

$$\begin{aligned} \hat{\mathbf{T}} &= 2^{-1}(-\check{\mathbf{S}}_{+1} + \check{\mathbf{S}}_{-1}), \\ \hat{\mathbf{R}} &= 2^{-1}(-\check{\mathbf{S}}_{+1} - \check{\mathbf{S}}_{-1}). \end{aligned} \quad (22)$$

Therefore the cross section  $\sigma_{Nlm}^d(\omega)$  of photoionization of the atom by the light, linearly polarized along the axis  $z$ , is expressed as

$$\sigma_{Nlm}^d(\omega) = 4\pi^2\alpha\omega \sum_{i=1}^{N_o} |D_{i,N,l}^{m\sigma\sigma'}(E)|^2 a_0^2, \quad (23)$$

where  $\alpha$  is the fine-structure constant,  $a_0$  is the Bohr radius, and  $D_{i,N,l}^{m\sigma\sigma'}(E) \equiv D_{i,i',v'}^{m\sigma\sigma'}(E)$  are the dipole moment matrix elements

$$D_{i,i',v'}^{m\sigma\sigma'}(E) = \langle \Psi_i^{Em\sigma=\mp 1}(r, \eta) | r | \eta \rangle \langle \Psi_{i',v'}^{m\sigma'=\pm 1}(r, \eta) \rangle. \quad (24)$$

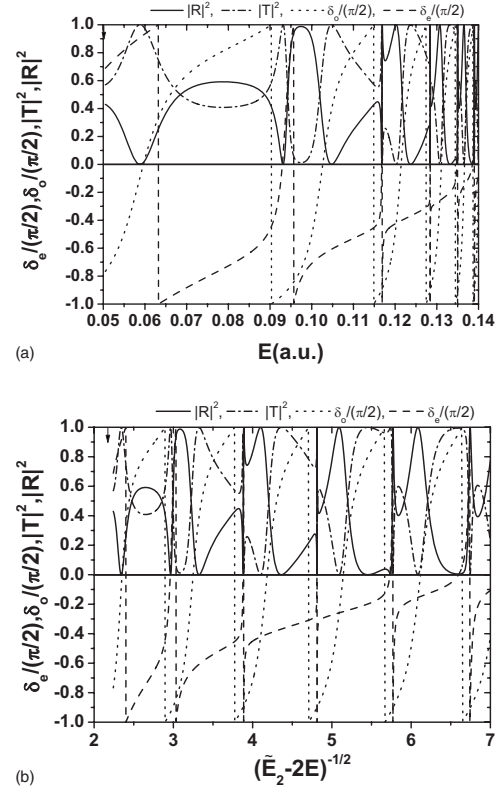


FIG. 2. Transmission  $|\hat{\mathbf{T}}|^2$  and reflection  $|\hat{\mathbf{R}}|^2$  coefficient (22), even  $\delta_e$  and odd  $\delta_o$  short-range phase shifts (11) versus the energy  $E$  (a) and  $(\tilde{E}_2 - 2E)^{-1/2}$  (b) for  $Z=1$ ,  $m=0$ ,  $\gamma=0.1$ . Arrow marks the first threshold  $E_1 = \gamma/2$ .

In the above expressions  $\omega = E - E_{Nlm}$  is the frequency of radiation and  $E_{Nlm} \equiv E_{m\sigma' i' v'}$  is the energy of the initial bound state  $|Nlm\rangle = \Psi_{i' v'}^{m\sigma'}(r, \eta)$  below the first threshold shift  $\epsilon_{m1}^{th}(\gamma)/2$  at  $i'=1$ . The continuous spectrum solution  $\chi^{(p)}(r)$  having the asymptotic form of a “standing” wave and the reaction matrix  $\mathbf{K}$  required for using Eq. (10) or Eq. (16), as well as the discrete spectrum solution  $\chi(r)$  and the eigenvalue  $E_{m\sigma' i' v'}$ , were calculated using the program KANTBP [7].

Profiles of the wave function (18) for  $Z=1$ ,  $m=0$ ,  $\gamma=0.1$ ,  $j_{\max}=10$ , and  $N_o=1$  are shown in Fig. 1 at two fixed values of energy  $E$ , corresponding to resonance transmission  $|\hat{\mathbf{T}}|^2 = \sin^2(\delta_e - \delta_o) = 1$  and total reflection  $|\hat{\mathbf{R}}|^2 = \cos^2(\delta_e - \delta_o) = 1$ . Here  $\delta_e \equiv \delta_1^{+1}$  and  $\delta_o \equiv \delta_1^{-1}$  are the *short-range phase shifts* for even and odd states from Eq. (11), respectively. The transmission and reflection coefficients are explicitly shown in Fig. 2 together with the even  $\delta_e$  and odd  $\delta_o$  phase shifts versus the energy  $E$  [Fig. 2(a)] and  $(\tilde{E}_2 - 2E)^{-1/2}$  [Fig. 2(b)], where  $\tilde{E}_2 = \epsilon_{m2}^{th}(\gamma)$  is the second threshold shift. The quasistationary states imbedded in the continuum correspond to the *short-range phase shifts*  $\delta_{o(e)} = n_{o(e)}\pi + \pi/2$  at  $(\tilde{E}_2 - 2E)^{-1/2} = n_{o(e)} + \Delta_{n_{o(e)}}$ . Nonmonotonic behavior of  $|\hat{\mathbf{T}}|$  and  $|\hat{\mathbf{R}}|$  is seen to include the cases of resonance transmission and total reflection, related to the existence of these quasistationary states.

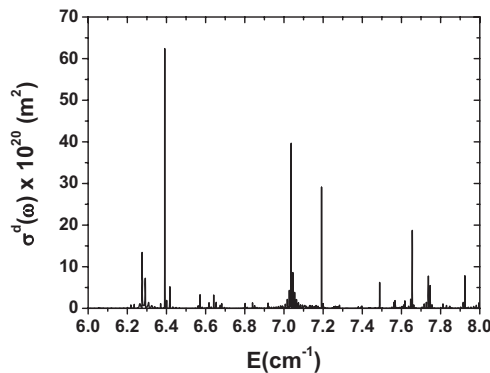


FIG. 3. Cross section of photoionization from the state  $3s_0$  versus the energy  $E$  for  $\gamma=2.595 \times 10^{-5}$  and the final state with  $\sigma=-1$ ,  $Z=1$ ,  $m=0$ .

Figure 3 clarifies the behavior of the cross section of photoionization by the light, linearly polarized along the axis  $z$ , from the rotational state  $3s_0$  at  $B_0=6.1$  T ( $\gamma=2.595 \times 10^{-5}$ ) in the energy interval  $E=6.0$ – $8.0$   $\text{cm}^{-1}$  at  $j_{\text{max}}=35$ . The cross sections have been calculated with the energy step  $5 \times 10^{-4}$   $\text{cm}^{-1}$  in all the regions except the vicinity of peaks, where the step was  $5 \times 10^{-6}$   $\text{cm}^{-1}$ . From our numerical experiments it follows that the absolute maximal values of the continuum wave functions  $\hat{\chi}_{jl}^{(01)}(E, r)$  decrease from  $10^{-4}$  to  $10^{-6}$  when the number of components  $j$  is increased from 30 to 35, thus demonstrating the linear rate of convergence of the expansion (2) in the energy interval considered. The relation between the photoionization cross section and the induced radiative recombination rate [1] makes it possible to apply the above results to the urgent problem of production of cold antihydrogen atoms in magnetic traps [10].

As an example, consider the recombination into the state  $N'=3$ ,  $l'=0$ ,  $m'=0$  that may be stimulated by a titanium-sapphire laser, under the conditions typical for positron-antiproton plasma in magnetic traps used for antihydrogen production, namely, the temperature of the plasma  $T=4$  K, the positron density  $n_e=1 \times 10^8$   $\text{cm}^{-3}$ , and the magnetic induction  $B=6.10$  T. The laser intensity is taken such that at 4 K without the magnetic field the rate of induced recombination is equal to that of the spontaneous one. In particular, for  $N=3$  this intensity is  $I=24$   $\text{W/cm}^2$  [11]. Figure 4(b) shows

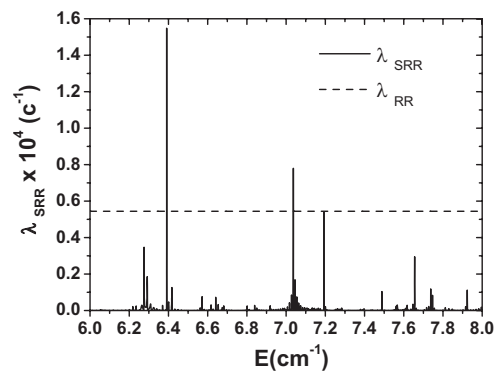


FIG. 4. Laser-stimulated radiative recombination rate into the bound state  $N'=3$ ,  $l'=0$ ,  $m'=0$  versus the energy  $E$  of the initially free positron.

the dependence of the laser-stimulated recombination rate  $\lambda_{\text{SRR}}$  per one antiproton upon the initial energy  $E=E_{Nlm}+\omega$  of the positron. For comparison the horizontal dashed line displays the rate  $\lambda_{\text{RR}}$  of the spontaneous radiative recombination into all the states with  $N=3$ , which at the intensity considered is equal to the rate of the laser-stimulated recombination without the magnetic field [11]. One can see narrow resonances for which the rate of recombination into the state with fixed  $l=0$ ,  $m=0$  in the magnetic field is appreciably higher than the rate of recombination into all nine states with different  $l$  and  $m$  possible for  $N=3$  without the magnetic field. Thus we demonstrated the efficiency of the proposed approach and program packages in calculations of photoionization and laser-induced recombination of a (anti)hydrogen atom in the magnetic field and the effects of resonance transmission and total reflection of oppositely charged particles in the magnetic field.

Further applications of the method may be associated with calculations of laser-induced recombination of antihydrogen in magnetic traps [1,6], channeling of light nuclei in thin doped films [12], and potential scattering with confinement potentials [13].

The authors thank Professor A.G. Abrashkevich, Professor A. M. Ermolaev, Professor V. S. Melezhik, Professor M. S. Kaschiev, and Professor V. V. Pupyshev for useful discussions. This work was partly supported by Grants No. CRDF BRHE REC-006 SR-006-X1/B75M06 Y3-P-06-08 and No. 07-01-00660, and JINR theme 09-6-1060-2005/2009.

- [1] V. V. Serov *et al.*, Opt. Spectrosc. **102**, 557 (2007).
- [2] U. Fano, Colloq. Int. C. N. R. S. **273**, 127 (1977); A. F. Starace and G. L. Webster, Phys. Rev. A **19**, 1629 (1979).
- [3] M. S. Kaschiev, S. I. Vinitsky, and F. R. Vukajlovic, Phys. Rev. A **22**, 557 (1980).
- [4] M. G. Dimova, M. S. Kaschiev, and S. I. Vinitsky, J. Phys. B **38**, 2337 (2005).
- [5] C. V. Clark, K. T. Lu, and A. F. Starace, in *Progress in Atomic Spectroscopy, Part C*, edited by H. G. Beyer and H. Kleinpoppen (Plenum, New York, 1984), p. 247.
- [6] O. Chuluunbaatar *et al.*, J. Phys. A **40**, 11485 (2007).
- [7] O. Chuluunbaatar *et al.*, Comput. Phys. Commun. **177**, 649

- (2007).
- [8] O. Chuluunbaatar *et al.*, Comput. Phys. Commun. **178**, 301 (2008).
- [9] M. Abramovits and I. A. Stegun, *Handbook of Mathematical Functions* (Dover, New York, 1972).
- [10] L. I. Men'shikov and R. Landua, Phys. Usp. **46**, 227 (2003).
- [11] M. V. Ryabinina and L. A. Melnikov, Nucl. Instrum. Methods Phys. Res. B **214**, 35 (2004).
- [12] Yu. N. Demkov and J. D. Meyer, Eur. Phys. J. B **42**, 361 (2004).
- [13] J. I. Kim, V. S. Melezhik, and P. Schmelcher, Phys. Rev. Lett. **97**, 193203 (2006).

# The Cross Section of Reaction of Two Charged Particles in a Channel of a Crystal

P. M. Krassovitskiy<sup>a</sup>, S. I. Vinit'skiy<sup>b</sup>, A. A. Gusev<sup>b</sup>, and O. Chuluunbaatar<sup>b</sup>

<sup>a</sup> Institute of Nuclear Physics NNC RK, Almaty, 050035 Kazakhstan

<sup>b</sup> Joint Institute for Nuclear Research, Dubna, Moscow oblast, 141980 Russia

E-mail: pavel.Kras@inp.kr

**Abstract**—The problem of interaction of two channeling similarly charged particles in the center-of-mass system has been reduced to the Schrödinger equation in spherical coordinates with an additional oscillator potential. Preliminary estimations have been obtained and nonmonotonic behavior of the multiplication factor of nuclear reactions on the collision energy is established.

**DOI:** 10.3103/S1062873809020208

## INTRODUCTION

The interaction of channeling particles is considered as a possible solution to the problem of synthesis of light elements and interaction of low-energy nuclei [1, 2]. It is suggested that the effect of focusing of a channeling beam can significantly change the behavior of the nuclear reaction cross section, depending on the energy of colliding particles and lattice parameters. To estimate the cross section, it is necessary to calculate the wave function of the continuous spectrum, which describes the interaction of channeling particles at the point of their pair collision rather than only the reflectances and transmittances within the model [3, 4]. One of known approaches to solving such problems was proposed in [5, 6] and applied in [7] to calculate the quasi-stationary states, providing total reflection and resonant transmission of electrons and protons in a uniform magnetic field at resonant energies [7].

In this study, the approach of [5–7] is used to solve the problem of scattering of channeling similarly charged particles in a crystal within the model [3, 4] in order to calculate the wave function of continuous spectrum and estimate the energy dependence on the nuclear reaction multiplication factor: the ratio of the probability densities of the wave functions at the point of pair collision with an additional confinement potential and without it.

## STATEMENT OF THE PROBLEM

We use the model of two similarly charged particles in the channeling mode, which are described by the Schrödinger equation

$$\left( -\frac{1}{2M}\Delta_{\mathbf{R}} - \frac{1}{2\mu}\Delta_{\mathbf{r}} + U_{12}(|\mathbf{r}_1 - \mathbf{r}_2|) + U_1(\mathbf{r}_1) + U_2(\mathbf{r}_2) \right)_{(1)} \times \Psi(\mathbf{r}_1, \mathbf{r}_2) = E_G \Psi(\mathbf{r}_1, \mathbf{r}_2),$$

where  $\mathbf{r}_1$ , and  $\mathbf{r}_2$  are the radius vectors of the particles with masses  $m_1$  and  $m_2$  and charges  $z_1$  and  $z_2$ , respectively;  $M$  and  $\mu$  are the total and reduced masses of the two particles and  $\mathbf{R}$  and  $\mathbf{r}$  are the Jacobian radius vectors. The potentials  $U_1(\mathbf{r}_1)$ ,  $U_2(\mathbf{r}_2)$ , and  $U_{12}(|\mathbf{r}_1 - \mathbf{r}_2|)$  determine the interaction of particles with the crystal and their Coulomb interaction in atomic units. Approximation of the interaction potential of the particles and crystal by a continuous potential, its expansion in a series in powers of distance from the channeling axis ( $\rho$ ), and consideration of only the main term [8], provided that the ratios of charges and masses of the interacting particles are equal, make it possible to separate the part corresponding to the center-of-mass motion in Eq. (1) [3, 4]. Then, the wave function directly describing the interaction between the particles obeys the 3D Schrödinger equation in atomic units:

$$\left( -\frac{1}{2\mu}\Delta_{\mathbf{r}} + U_{12}(|\mathbf{r}|) + \alpha'\rho^2 \right) \Psi(\mathbf{r}) = E_{int} \Psi(\mathbf{r}). \quad (2)$$

Here,  $\mathbf{r} = \mathbf{r}_1 - \mathbf{r}_2$ ,  $\alpha' = \alpha(m_2^2 z_1 + m_1^2 z_2)/(m_1 + m_2)^2$ ,  $\alpha$  is the expansion parameter of the particle–crystal interaction potential, and  $U_{12}(|\mathbf{r}|) = z_1 z_2 / r$  is the Coulomb potential of particle interaction.

In Eq. (2), we can perform partial separation of variables, specifically, separate the dependence on the angle  $\varphi$  in cylindrical ( $z$ ,  $\rho$ ,  $\varphi$ ) or spherical ( $r$ ,  $\theta$ ,  $\varphi$ ) coordinates (the distance from the channeling axis coincides with the coordinate  $\rho$ ).

Numerical analysis showed that the scattering problem for Eq. (2) can be solved in the cylindrical coordinate system in the range  $\Omega = (0 \leq \rho \leq \rho_{\max}, 0 \leq |z| \leq z_{\max})$  if the solution must be calculated in the asymptotic region  $\Omega_{as} = \left( \rho, |z| \frac{\rho}{|z|} \ll 1 \right)$ ; however, in the range

$\Omega\Omega_{as}$ , the solution to the problem is unstable. In [4], this problem was solved using a matrix sweep with discretization of the initial equation according to the Numerov method. The transmittances and reflectances were obtained by direct sweep for the corresponding scattering problem on specified grids of energy values. However, the reverse sweep, successfully reconstructing the wave function in the larger part of  $\Omega$ , fails to yield a solution in the region  $\Omega_0 = |z^2 + \rho^2| < 1$ , because it is necessary to take into account a large number of rapidly oscillating functions in this region. With due regard to the fact that the wave function in  $\Omega_0$  is determined by the dominant spherically symmetric Coulomb potential, one can obtain an estimate for the steps  $\Delta z$  and  $\Delta \rho$  of the crowding grid  $\Omega$ :

$$\frac{(l_{\max} + l_z)\sqrt{(\Delta z)^2 + (\Delta \rho)^2}}{2\pi} \ll \sqrt{z^2 + \rho^2}, \quad (3)$$

where  $l_{\max}$  and  $l_z$  are, respectively, the maximum angular momentum (taken into account) and its conserved projection on the  $z$  axis. The alternative method [5–7], which makes it possible to solve the problem in spherical coordinates and takes into account the cylindrical symmetry in the asymptotic region  $\Omega_{as}$ , is described below.

### KANTOROVICH METHOD

Equation (2) in spherical coordinates, at a fixed magnetic quantum number  $m$  and  $z$  parity, can be written as

$$\left(-\frac{1}{r^2}\frac{\partial}{\partial r}r^2\frac{\partial}{\partial r} + \frac{A^{(0)}(r, \theta)}{r^2} + \frac{2Z}{r} - 2E\right)\Psi(r, \theta) = 0, \quad (4)$$

where the operator  $A^{(0)}(r, \theta)$ , dependent on the parameter  $r$ , has the form

$$\begin{aligned} A^{(0)}(r, \theta) \\ = -\frac{1}{\sin\theta}\frac{\partial}{\partial\theta}\sin\theta\frac{\partial}{\partial\theta} + \frac{m^2}{\sin^2\theta} + \frac{1}{4}\gamma^2r^4\sin^2\theta. \end{aligned} \quad (5)$$

Here, the quantities  $\gamma^2 = 8\mu\alpha'$ ,  $Z = \mu z_1 z_2$  and  $E = \mu E_{\text{int}}$  are determined from Eq. (2). Furthermore, we use the scale transformation  $r \rightarrow \sqrt{\gamma}r$ ,  $Z \rightarrow Z/\sqrt{\gamma}$ , and  $E \rightarrow E/\gamma$ . The solution to Eq. (4) is sought in the form of a Kantorovich expansion of the function  $\Psi(r, \theta)$  in angular oblate spheroidal functions  $\Phi_i(r, \theta)$  of the operator  $A^{(0)}(r, \theta)$ , which are calculated using the POTHMF program on the specified grid  $r \in \Omega_r$  of radial variables [6].

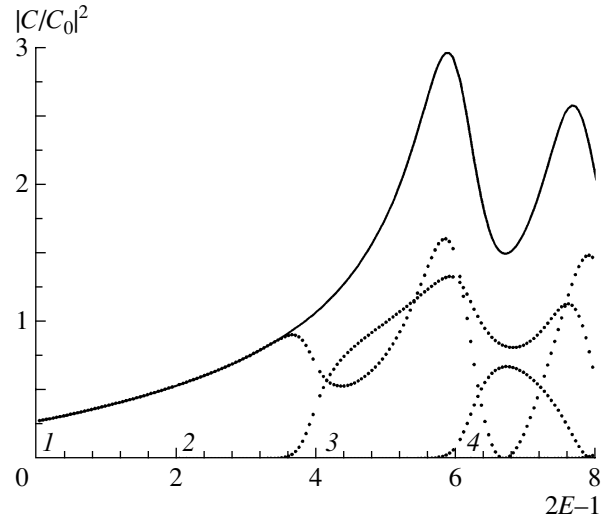
The expansion coefficients  $\chi_{ij}(r)$  of the function  $\Psi(r, \theta)$  satisfy the system of  $N$  differential equations

$$\begin{aligned} &\left(-\frac{1}{r^2}\mathbf{I}\frac{d}{dr}r^2\frac{d}{dr} + \mathbf{V}(r) + \frac{2Z}{r} \right. \\ &\left. + \mathbf{Q}(r)\frac{d}{dr} + \frac{1}{r^2}\frac{dr^2\mathbf{Q}(r)}{dr} - 2E\mathbf{I}\right)\chi(r) = 0, \end{aligned} \quad (6)$$

where  $\mathbf{I}$  is the unit matrix;  $\mathbf{V}$  and  $\mathbf{Q}$  are matrices with a dimension of  $N \times N$ , calculated on the specified grid  $r \in \Omega_r$  using the POTHMF program [6]; and  $\chi(r) = \{\chi_i(r)\}_{i=1}^{N_0}$  is a rectangular  $N \times N_0$  matrix, composed of columns  $\chi_i(r) = \{\chi_{ji}(r)\}_{j=1}^N$  ( $N_0$  is the number of open channels with the energy  $2E > E_i(\infty) = 2i - 1 + |m| > 0$ ,  $i = 1, \dots, N_0$ ). The boundary-value problems of continuous spectrum for the system of  $N$  equations (6) with  $N_0$  open channels are solved using the KANTBP program [5], which implements the finite-element method of high accuracy on the grid  $\Omega_r$ , including the vicinity of  $r = 0$ .

### PRELIMINARY ESTIMATIONS OF THE MULTIPLICATION FACTOR

Using the KANTBP and POTHMF programs at different energies  $E$  and effective charges  $Z$ , we calculated the multiplication factors  $|C(2E)/C_0(2E)|^2 = \sum_{i=1}^{N_0} |C_i(2E)/C_0(2E)|^2$ , where  $C_i(2E) = \chi_{1i}(r=0)$  are the numerical values of solutions to Eq. (6) at the pair impact point and  $C_0(2E) = \chi_{11}(r=0)$  is the Coulomb function with the effective charge  $Z$  at energy  $2E - 1$ .



Dependence of the total multiplication factor (solid line) and the multiplication factor in each open channel (1–4, dotted lines) on the doubled energy  $2E$ , counted from the first threshold  $E_1 = 1$ , i.e.  $2E - 1$  at the effective charge  $Z = 6$ . The doubled barrier height is  $2U_0 = 6.24$ .

Figure shows the estimate of the total multiplication factor and the multiplication factors in each open channel (1–4) as functions of the energy  $2E - 1$ , counted from the first threshold, at the effective charge  $Z = 6$  for the even solution component at  $m = 0$ . The maximum total multiplication factor is obtained at  $2E - 1 = 5.9$ , between the third and fourth channels at transmission through the barrier  $2U_0 = 6.24$  and almost total reflection. Such behavior is a consequence of superstrong focusing effects, accompanying astrophysical magnetic fields. The interaction of particles in a channel involves two competing processes: defocusing (Coulomb interaction) and focusing (oscillator interaction, effectively decreasing the dimension of the problem); therefore, there is the energy range where the probability density of the wave function at the pair collision point has a maximum for quasi-stationary continuous-spectrum states. To study the interaction of channeling particles at real values of the effective charge  $Z$ , for example, for identical particles with the mass and charge of deuteron nucleus, it is necessary to set the effective charge  $Z \approx 100$  and solve the problem with a large number of open channels  $N_0 \approx U_0 = 3(Z/2)^{2/3}$ , which requires significant computational resources.

### CONCLUSIONS

We have determined the optimal conditions under which the problem of interaction of channeling particles can be solved. Preliminary estimates of the multiplication factor are obtained. The energy dependence of the multiplication factor is nonmonotonic, which is explained by the presence of two potentials: defocusing

Coulomb potential (interaction between similarly charged particles) and focusing oscillator potential (interaction of particles with the crystal). These potentials maintain quasi-stationary continuous-spectrum states and provide almost total reflection.

### ACKNOWLEDGMENTS

We are grateful to Prof. F.M. Penkov for his help.

This study was supported in part by the Russian Foundation for Basic Research, project nos. 08-01-00604 and 07-01-00660.

### REFERENCES

1. Demkov, Yu.N. and Meyer, J.D., *Eur. Phys. J. B*, 2004, vol. 42, p. 361.
2. Takibaev, N.Zh. et al., *Vestn. NYaTs RK: Yad. Fiz. Radiat. Materialovedenie*, 2003, no. 4, p. 75.
3. Krassovitskiy, P.M., *Vestn. NYaTs RK*, 2005, no. 4(24), p. 18.
4. Krassovitskiy, P.M. and Takibaev, N.Zh., *Izv. Ross. Akad. Nauk, Ser. Fiz.*, 2006, vol. 70, no. 5, p. 709.
5. Chuluunbaatar, O. et al., *Comput. Phys. Commun.*, 2007, vol. 177, p. 649.
6. Chuluunbaatar, O. et al., *Comput. Phys. Commun.*, 2008, vol. 178, p. 301.
7. Chuluunbaatar, O. et al., *Phys. Rev. A*, 2008, vol. 77, 034 702.
8. Kumakhov, M.A. and Shimmer, G., *Atomnye stolknoveniya v kristallakh*, Moscow: Atomizdat, 1980, Kumakhov, M.A. and Shimmer, G., *Atomic Collisions in Crystals*, New York: Gordon and Breach, 1989.

We consider a *new method* for the description of the penetration of  $A$  identical quantum particles, coupled by short-range oscillator-like interaction, through a repulsive potential barrier. We assume that the spin part of the wave function is known, so that only the spatial part of the wave function is to be considered, which may be symmetric or antisymmetric with respect to a permutation of  $A$  identical particles. The initial problem is reduced to the penetration of a composite system with the internal degrees of freedom, describing an  $(A-1) \times d$ -dimensional oscillator, and the external degrees of freedom describing the center-of-mass motion of  $A$  particles in  $d$ -dimensional Euclidian space. For simplicity, we restrict our consideration to the so-called  $s$ -wave approximation [1] corresponding to one-dimensional Euclidean space ( $d = 1$ ).

We seek for the solution in the form of Galerkin expansion in terms of cluster functions in the *new symmetrized coordinate representation* (SCR) [18] with unknown coefficients having the form of matrix functions of the center-of-mass variable. As a result, the problem is reduced to a boundary-value problem for a system of ordinary second-order differential equations with respect to the center-of-mass variable. Conventional asymptotic boundary conditions involving unknown amplitudes of reflected and transmitted waves are imposed on the desired matrix solution. Solving the problem was implemented as a complex of the *symbolic-numeric algorithms and programs* in CAS MAPLE and FORTRAN environment. The results of calculations are analyzed with particular emphasis on the effect of quantum transparency that manifests itself as nonmonotonic energy dependence of the transmission coefficient due to resonance tunnelling of the bound particles in  $S(A)$  states through the repulsive potential barriers.

The paper is organized as follows. In Section 2, we present the problem statement in symmetrized coordinates. In Section 3, we introduce the SCR of the cluster functions of the considered problem and the asymptotic boundary conditions involving unknown amplitudes of reflected and transmitted waves. In Section 4, we formulate the boundary-value problem for the close-coupling equations in the Galerkin form using the SCR. In Section 5, we analyze the results of numerical experiment on the resonance transmission of a few coupled identical particles in  $S(A)$  states, whose energies coincide with the resonance eigenenergies of the barrier quasi-stationary states embedded in the continuum. In Conclusion, we sum up the results and discuss briefly the perspectives of application of the developed approach.

## 2 Problem Statement

We consider a system of  $A$  identical quantum particles having the mass  $m$  and a set of the Cartesian coordinates  $x_i \in \mathbf{R}^d$  in  $d$ -dimensional Euclidian space, considered as vector  $\tilde{\mathbf{x}} = (\tilde{x}_1, \dots, \tilde{x}_A) \in \mathbf{R}^{A \times d}$  in  $A \times d$ -dimensional configuration space. The particles are coupled by the pair potentials  $\tilde{V}^{pair}(\tilde{x}_{ij})$  depending upon the relative coordinates,  $\tilde{x}_{ij} = \tilde{x}_i - \tilde{x}_j$ , similar to a harmonic oscillator potential  $\tilde{V}^{hosc}(\tilde{x}_{ij}) = \frac{m\omega^2}{2}(\tilde{x}_{ij})^2$  with the frequency  $\omega$ . The resulting clusters are subject to the influence of the potentials  $\tilde{V}(\tilde{x}_i)$  describing the external field

of a target. The appropriate Schrödinger equation takes the form

$$\left[ -\frac{\hbar^2}{2m} \sum_{i=1}^A \frac{\partial^2}{\partial \tilde{x}_i^2} + \sum_{i,j=1;i < j}^A \tilde{V}^{pair}(\tilde{x}_{ij}) + \sum_{i=1}^A \tilde{V}(\tilde{x}_i) - \tilde{E} \right] \tilde{\Psi}(\tilde{\mathbf{x}}) = 0,$$

where  $\tilde{E}$  is the total energy of the system of  $A$  particles, and  $\tilde{P}^2 = 2m\tilde{E}/\hbar^2$ ,  $\tilde{P}$  is the total momentum of the system, and  $\hbar$  is Planck constant. Using the oscillator units  $x_{osc} = \sqrt{\hbar/(m\omega\sqrt{A})}$ ,  $p_{osc} = \sqrt{(m\omega\sqrt{A})/\hbar} = x_{osc}^{-1}$ , and  $E_{osc} = \hbar\omega\sqrt{A}/2$  to introduce the dimensionless coordinates  $x_i = \tilde{x}_i/x_{osc}$ ,  $x_{ij} = \tilde{x}_{ij}/x_{osc} = x_i - x_j$ ,  $E = \tilde{E}/E_{osc} = P^2$ ,  $P = \tilde{P}/p_{osc} = \tilde{P}x_{osc}$ ,  $V^{pair}(x_{ij}) = \tilde{V}^{pair}(x_{ij}x_{osc})/E_{osc}$ ,  $V^{hosc}(x_{ij}) = \tilde{V}^{hosc}(x_{ij}x_{osc})/E_{osc} = \frac{1}{A}(x_{ij})^2$  and  $V(x_i) = \tilde{V}(x_ix_{osc})/E_{osc}$ , one can rewrite the above equation in the form

$$\left[ -\sum_{i=1}^A \frac{\partial^2}{\partial x_i^2} + \sum_{i,j=1;i < j}^A \frac{1}{A}(x_{ij})^2 + \sum_{i,j=1;i < j}^A U^{pair}(x_{ij}) + \sum_{i=1}^A V(x_i) - E \right] \Psi(\mathbf{x}) = 0, \quad (1)$$

where  $U^{pair}(x_{ij}) = V^{pair}(x_{ij}) - V^{hosc}(x_{ij})$ , i.e., if  $V^{pair}(x_{ij}) = V^{hosc}(x_{ij})$ , then  $U^{pair}(x_{ij}) = 0$ .

The problem of tunnelling of a cluster of  $A$  identical particles in the symmetrized coordinates  $(\xi_0, \boldsymbol{\xi})$ , where  $\boldsymbol{\xi} = \{\xi_1, \dots, \xi_{A-1}\}$ :

$$\xi_0 = \frac{1}{\sqrt{A}} \left( \sum_{t=1}^A x_t \right), \quad \xi_s = \frac{1}{\sqrt{A}} \left( x_1 + \sum_{t=2}^A a_0 x_t + \sqrt{A} x_{s+1} \right), \quad s = 1, \dots, A-1, \quad (2)$$

in terms of total potential  $U(\xi_0, \boldsymbol{\xi}) = V(\xi_0, \boldsymbol{\xi}) + U^{eff}(\xi_0, \boldsymbol{\xi})$  reads as [18]

$$\left[ -\frac{\partial^2}{\partial \xi_0^2} + \sum_{i=1}^{A-1} \left( -\frac{\partial^2}{\partial \xi_i^2} + (\xi_i)^2 \right) + U(\xi_0, \boldsymbol{\xi}) - E \right] \Psi(\xi_0, \boldsymbol{\xi}) = 0, \quad (3)$$

$$U^{eff}(\xi_0, \boldsymbol{\xi}) = \sum_{i,j=1;i < j}^A U^{pair}(x_{ij}(\boldsymbol{\xi})), \quad V(\xi_0, \boldsymbol{\xi}) = \sum_{i=1}^A V(x_i(\xi_0, \boldsymbol{\xi})),$$

which is invariant under permutations  $\xi_i \leftrightarrow \xi_j$  at  $i, j = 1, \dots, A-1$ , i.e., the invariance of Eq. (1) under permutations  $x_i \leftrightarrow x_j$  at  $i, j = 1, \dots, A$  survives the transformation.

### 3 Cluster Functions and Asymptotic Boundary Conditions

For simplicity we restrict our consideration to the so-called  $s$ -wave approximation [1], i.e., one-dimensional Euclidian space ( $d = 1$ ). Cluster functions  $\tilde{\Phi}_j(\xi_0, \boldsymbol{\xi})$ ,



where  $\boldsymbol{\xi} = \{\xi_1, \dots, \xi_{A-1}\}$ , corresponding to the threshold energies  $\tilde{\epsilon}_j(\xi_0)$  dependent on  $\xi_0$  as a parameter, are solutions of the parametric eigenvalue problem

$$\left(-\frac{\partial^2}{\partial \boldsymbol{\xi}^2} + \boldsymbol{\xi}^2 + U(\xi_0, \boldsymbol{\xi}) - \tilde{\epsilon}_j(\xi_0)\right) \tilde{\Phi}_j(\xi_0, \boldsymbol{\xi}) = 0, \quad \int_{-\infty}^{+\infty} \tilde{\Phi}_i(\xi_0, \boldsymbol{\xi}) \tilde{\Phi}_j(\xi_0, \boldsymbol{\xi}) d^{A-1} \boldsymbol{\xi} = \delta_{ij}, \quad (4)$$

where  $U(\xi_0, \boldsymbol{\xi}) = V(\xi_0, \boldsymbol{\xi}) + U^{eff}(\xi_0, \boldsymbol{\xi})$  is the total potential that enters Eq. (3). The effective potential  $U^{eff}(\xi_0, \boldsymbol{\xi})$  can be approximated also by the deformed Wood–Saxon potential in the single-particle oscillator approximation [9]. We seek for the cluster functions  $\Phi_i(\xi_0, \boldsymbol{\xi})$  in the form of an expansion over the eigenfunctions  $\Phi_{j'}^{S(A)}(\boldsymbol{\xi})$ , symmetric (S) or antisymmetric (A) with respect to a permutation of the initial  $A$  Cartesian coordinates of  $A$  identical particles. These functions correspond to eigenenergies  $E_i^{S(A)}$  of the  $(A-1)$ -dimensional oscillator, generated by the algorithm SCR [18], with unknown coefficients  $\tilde{\alpha}_{j'}^{(i)}(\xi_0)$ :

$$\tilde{\Phi}_i(\xi_0, \boldsymbol{\xi}) = \sum_{j'=1}^{j'_{\max}} \tilde{\alpha}_{j'}^{(i)}(\xi_0) \Phi_{j'}^{S(A)}(\boldsymbol{\xi}). \quad (5)$$

Thus, the eigenvalue problem (4) is reduced to a linearized version of the Hartree–Fock algebraic eigenvalue problem

$$\sum_{j'=1}^{j'_{\max}} \left( \delta_{ij'} E_i^{S(A)} + U_{ij'}(\xi_0) - \delta_{ij'} \tilde{\epsilon}_i(\xi_0) \right) \tilde{\alpha}_{j'}^{(i)}(\xi_0) = 0, \quad \sum_{j'=1}^{j'_{\max}} \tilde{\alpha}_{j'}^{(i')}(\xi_0) \tilde{\alpha}_{j'}^{(i)}(\xi_0) = \delta_{ii'}, \quad (6)$$

where the potentials  $U_{ij'}^{pair}$  and  $V_{ij'}(\xi_0)$  are expressed in terms of the integrals

$$U_{ij'}^{pair} = \int d^{A-1} \boldsymbol{\xi} \Phi_i^{S(A)}(\boldsymbol{\xi}) U^{eff}(\boldsymbol{\xi}) \Phi_{j'}^{S(A)}(\boldsymbol{\xi}), \quad (7)$$

$$V_{ij'}(\xi_0) = \int d^{A-1} \boldsymbol{\xi} \Phi_i^{S(A)}(\boldsymbol{\xi}) \left( \sum_{k=1}^A V(x_k(\xi_0, \boldsymbol{\xi})) \right) \Phi_{j'}^{S(A)}(\boldsymbol{\xi}). \quad (8)$$

The parametric *algorithm SCR*, i.e., *algorithm PSCR*, for solving the above parametric eigenvalue problem was implemented by means of subroutines [19, 20], or in the single-particle approximation by means of the subroutine [9] in CAS MAPLE and FORTRAN environment.

(G) If  $U_{ij'}(\xi_0) = U_{ij'}^{pair}$  are independent on  $\xi_0$ , then  $\tilde{\epsilon}_i(\xi_0) = \tilde{\epsilon}_i$  and  $\tilde{\alpha}_{j'}^{(i)}(\xi_0) = \tilde{\alpha}_{j'}^{(i)}$  are also independent of  $\xi_0$ , and (5) reduces to  $\tilde{\Phi}_i(\boldsymbol{\xi}) = \sum_{j'=1}^{j'_{\max}} \tilde{\alpha}_{j'}^{(i)} \Phi_{j'}^{S(A)}(\boldsymbol{\xi})$ .

(O) If  $V^{pair}(x_{ij}) = V^{hosc}(x_{ij})$  and  $U_{ij'}^{pair} = 0$ , then  $\tilde{\epsilon}_i = E_i^{S(A)}$  and  $\tilde{\alpha}_{j'}^{(i)} = \delta_{ij'}$ .

For the short-range barrier potentials  $V(\xi_0, x_i(\boldsymbol{\xi}))$  in terms of the asymptotic cluster functions  $\tilde{\Phi}_j(\boldsymbol{\xi}) \rightarrow \tilde{\Phi}_j(\xi_0, \boldsymbol{\xi})$  at  $|\xi_0| \rightarrow \infty$  the asymptotic boundary conditions for the solution  $\Psi(\xi_0, \boldsymbol{\xi}) = \{\Psi_{i_o}(\xi_0, \boldsymbol{\xi})\}_{i_o=1}^{N_o}$  in the asymptotic region  $|\boldsymbol{\xi}|/|\xi_0| \ll 1$  have the form [16]

$$\Psi_{i_o}^{\leftrightarrow}(\xi_0 \rightarrow \pm\infty, \boldsymbol{\xi}) \rightarrow \tilde{\Phi}_{i_o}(\boldsymbol{\xi}) \frac{\exp(\mp i(p_{i_o}\xi_0))}{\sqrt{p_{i_o}}} + \sum_{j=1}^{N_o} \tilde{\Phi}_j(\boldsymbol{\xi}) \frac{\exp(\pm i(p_j\xi_0))}{\sqrt{p_j}} R_{j i_o}^{\leftrightarrow}(E),$$

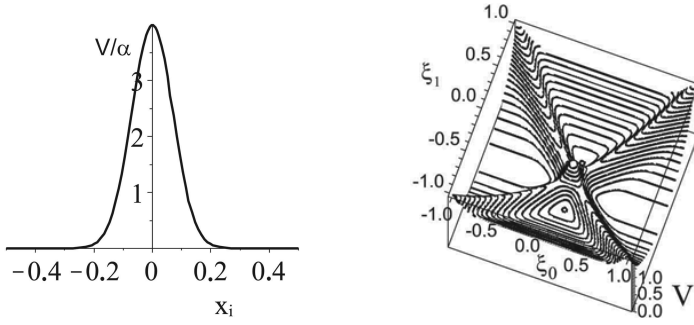


**Fig. 1.** The Gaussian-type potential (16) at  $\sigma = 0.1$  (in oscillator units) and the corresponding 2D barrier potential at  $\alpha = 1/10$ ,  $\sigma = 0.1$

$$\Psi_{i_o}^{\leftrightarrow}(\xi_0 \rightarrow \mp\infty, \xi) \rightarrow \sum_{j=1}^{N_o} \tilde{\Phi}_j(\xi) \frac{\exp(\mp i(p_j \xi_0))}{\sqrt{p_j}} T_{ji_o}^{\leftrightarrow}(E), \quad (9)$$

$$\Psi_{i_o}^{\leftrightarrow}(\xi_0, |\xi| \rightarrow \infty) \rightarrow 0.$$

Here  $v = \leftarrow, \rightarrow$  indicates the initial direction of the particle motion along the  $\xi_0$  axis,  $N_o$  is the number of open channels at the fixed energy  $E$  and momentum  $p_{i_o}^2 = E - E_{i_o} > 0$  of cluster;  $R_{ji_o}^{\leftarrow} = R_{ji_o}^{\leftarrow}(E)$ ,  $R_{ji_o}^{\rightarrow} = R_{ji_o}^{\rightarrow}(E)$  and  $T_{ji_o}^{\leftarrow} = T_{ji_o}^{\leftarrow}(E)$ ,  $T_{ji_o}^{\rightarrow} = T_{ji_o}^{\rightarrow}(E)$  are the unknown amplitudes of the reflected and transmitted waves. We can rewrite Eqs. (9) in the matrix form  $\Psi = \tilde{\Phi}^T \mathbf{F}$  describing the incident wave and the outgoing waves at  $\xi_0^+ \rightarrow +\infty$  and  $\xi_0^- \rightarrow -\infty$  as

$$\begin{pmatrix} \mathbf{F}_{\rightarrow}(\xi_0^+) & \mathbf{F}_{\leftarrow}(\xi_0^+) \\ \mathbf{F}_{\rightarrow}(\xi_0^-) & \mathbf{F}_{\leftarrow}(\xi_0^-) \end{pmatrix} = \begin{pmatrix} \mathbf{0} & \mathbf{X}^{(-)}(\xi_0^+) \\ \mathbf{X}^{(+)}(\xi_0^-) & \mathbf{0} \end{pmatrix} + \begin{pmatrix} \mathbf{0} & \mathbf{X}^{(+)}(\xi_0^+) \\ \mathbf{X}^{(-)}(\xi_0^-) & \mathbf{0} \end{pmatrix} \mathbf{S}. \quad (10)$$

Here the unitary and symmetric scattering matrix  $\mathbf{S}$

$$\mathbf{S} = \begin{pmatrix} \mathbf{R}_{\rightarrow} & \mathbf{T}_{\leftarrow} \\ \mathbf{T}_{\rightarrow} & \mathbf{R}_{\leftarrow} \end{pmatrix}, \quad \mathbf{S}^\dagger \mathbf{S} = \mathbf{S} \mathbf{S}^\dagger = \mathbf{I}, \quad (11)$$

where  $\mathbf{S}^\dagger$  is the conjugate transpose of  $\mathbf{S}$ . It is composed of the matrices, whose elements are reflection and transmission amplitudes that enter Eqs. (9) and possess the following properties[16, 17]:

$$\begin{aligned} \mathbf{T}_{\rightarrow}^\dagger \mathbf{T}_{\rightarrow} + \mathbf{R}_{\rightarrow}^\dagger \mathbf{R}_{\rightarrow} &= \mathbf{I}_{oo} = \mathbf{T}_{\leftarrow}^\dagger \mathbf{T}_{\leftarrow} + \mathbf{R}_{\leftarrow}^\dagger \mathbf{R}_{\leftarrow}, \\ \mathbf{T}_{\rightarrow}^\dagger \mathbf{R}_{\leftarrow} + \mathbf{R}_{\rightarrow}^\dagger \mathbf{T}_{\leftarrow} &= \mathbf{0} = \mathbf{R}_{\leftarrow}^\dagger \mathbf{T}_{\rightarrow} + \mathbf{T}_{\leftarrow}^\dagger \mathbf{R}_{\rightarrow}, \\ \mathbf{T}_{\rightarrow}^T &= \mathbf{T}_{\leftarrow}, \quad \mathbf{R}_{\rightarrow}^T = \mathbf{R}_{\leftarrow}, \quad \mathbf{R}_{\leftarrow}^T = \mathbf{R}_{\rightarrow}. \end{aligned} \quad (12)$$

## 4 Close-Coupling Equations in the SCR

We seek for the solution of problem (3) in the symmetrized coordinates in the form of Galerkin (G) expansion over the asymptotic cluster functions  $\tilde{\Phi}_j(\xi)$

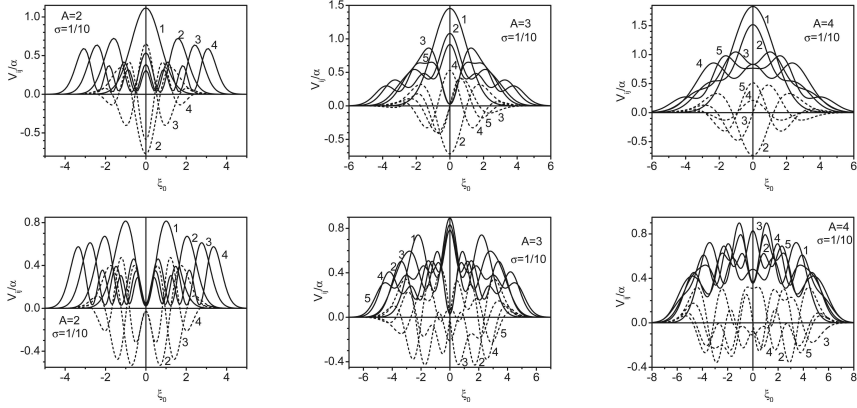


**Fig. 2.** Diagonal  $V_{jj}$  (solid lines) and nondiagonal  $V_{j1}$ , (dashed lines) effective potentials for  $A = 2$ ,  $A = 3$  and  $A = 4$  of the S- (upper panels) and A- (lower panels) of the particles at  $\sigma = 1/10$

corresponding to the eigenvalues  $\tilde{\epsilon}_i$ , which are also independent of  $\xi_0$ , from (6) under the (G) condition, with unknown coefficient functions  $\chi_{ji_o}(\xi_0)$ :

$$\Psi_{i_o}(\xi_0, \xi) = \sum_{j=1}^{j_{\max}} \tilde{\Phi}_j(\xi) \chi_{ji_o}(\xi_0), \quad \chi_{ji_o}(\xi_0) = \int d^{A-1} \xi \tilde{\Phi}_j(\xi) \Psi_{i_o}(\xi_0, \xi). \quad (13)$$

The set of close-coupling Galerkin equations in the symmetrized coordinates has the form

$$\left[ -\frac{d^2}{d\xi_0^2} + \tilde{\epsilon}_i - E \right] \chi_{ii_o}(\xi_0) + \sum_{j=1}^{j_{\max}} \tilde{V}_{ij}(\xi_0) \chi_{ji_o}(\xi_0) = 0, \quad (14)$$

where the effective potentials  $\tilde{V}_{ij}(\xi_0)$  are calculated using the set of eigenvectors  $\tilde{\alpha}_{j'}^{(i)}$  of the nonparametric algebraic problem (6) under the above condition (G):  $U_{ij'}(\xi_0) = U_{ij'}^{pair} \neq 0$ ,

$$\tilde{V}_{ij}(\xi_0) = \sum_{j'=1}^{j'_{\max}} \sum_{j''=1}^{j''_{\max}} \tilde{\alpha}_{j'}^{(i)} V_{j'j''}(\xi_0) \tilde{\alpha}_{j''}^{(j)}, \quad (15)$$

and the integrals  $V_{ij'}(\xi_0)$  are defined in (8) and calculated in CAS MAPLE. In the examples considered below, we put  $U_{ij'}(\xi_0) = U_{ij'}^{pair} = 0$  in (6), then we have the (O) condition:  $\tilde{\epsilon}_i = E_i^{S(A)}$ ,  $\tilde{\alpha}_{j'}^{(i)} = \delta_{ij'}$  and  $\tilde{V}_{ij}(\xi_0) = V_{ij}(\xi_0)$ . The repulsive barrier is chosen to have the Gaussian shape

$$V(x_i) = \frac{\alpha}{\sqrt{2\pi}\sigma} \exp\left(-\frac{x_i^2}{\sigma^2}\right). \quad (16)$$

**Table 1.** Resonance values of the energy  $E_S$  ( $E_A$ ) for S (A) states for  $A = 2, 3, 4$  ( $\sigma = 1/10$ ,  $\alpha = 20$ ) with approximate eigenvalues  $E_i^D$ , for the first ten states  $i = 1, \dots, 10$ , calculated using the truncated oscillator basis (D) till  $j_{\max} = 136, 816, 1820$  at  $A = 2, 3, 4$ . The asterisk labels two overlapping peaks of transmission probability

$i$	1	2	3	4	5	6	7	8	9	10
$A = 2$										
$E_S$	5.72	9.06	9.48	12.46	12.57	13.46	15.74	15.78	16.65	17.41
$E_A$	5.71	9.06	9.48	12.45	12.57	13.45	15.76*	15.76*	16.66	17.40
$E_i^D$	5.76	9.12	9.53	12.52	12.64	13.52	15.81	15.84	16.73	17.47
$A = 3$										
$E_S$	8.18	11.11		12.60	13.93		14.84	15.79		16.67
	8.31	11.23			14.00		14.88			16.73
$E_A$			11.55			14.46			16.18	
			11.61			14.56			16.25	
$E_i^D$	8.19	11.09	11.52	12.51	13.86	14.42	14.74	15.67	16.11	16.53
$A = 4$										
$E_S$	10.12	11.89	12.71	14.86	15.19	15.41	15.86	16.37	17.54	17.76
$E_i^{D31}$	10.03		12.60	14.71	15.04			16.18	17.34	17.56
$E_i^{D22}$		11.76				15.21	15.64			

Figure 1 illustrates the Gaussian potential and the corresponding barrier potentials in the symmetrized coordinates at  $A = 2$ . This potential has the oscillator-type shape, and two barriers are crossing at the right angle. In the case  $A \geq 3$ , the hyperplanes of barriers are crossing at the right angle, too.

The effective potentials  $V_{ij}(\xi_0)$  calculated using the *algorithm SCR* [18] and *algorithm DC* (see Section 5), are shown in Fig. 2. In comparison with the symmetric basis, for antisymmetric one the increase of the numbers  $i$  and/or  $j$  results in stronger oscillation of the effective potentials  $V_{ij}$  and weaker decrease of them to zero at  $\xi_0 \rightarrow \infty$ . At  $A = 2$ , all effective potentials are even functions, and at  $A \geq 3$ , some effective potentials are odd functions.

Thus, the scattering problem (3) with the asymptotic boundary conditions (9) is reduced to the boundary-value problem for the set of close-coupling equations in the Galerkin form (14) under the boundary conditions at  $d = 1$ ,  $\xi_0 = \xi_{\min}$  and  $\xi_0 = \xi_{\max}$ :

$$\left. \frac{d\mathbf{F}(\xi_0)}{d\xi_0} \right|_{\xi_0=\xi_{\min}} = \mathcal{R}(\xi_{\min})\mathbf{F}(\xi_{\min}), \quad \left. \frac{d\mathbf{F}(\xi_0)}{d\xi_0} \right|_{\xi_0=\xi_{\max}} = \mathcal{R}(\xi_{\max})\mathbf{F}(\xi_{\max}), \quad (17)$$

where  $\mathcal{R}(\xi)$  is an unknown  $j_{\max} \times j_{\max}$  matrix function,  $\mathbf{F}(\xi_0) = \{\chi_{i_o}(\xi_0)\}_{i_o=1}^{N_o} = \{\{\chi_{ji_o}(\xi_0)\}_{j=1}^{j_{\max}}\}_{i_o=1}^{N_o}$  is the required  $j_{\max} \times N_o$  matrix solution, and  $N_o$  is the number of open channels,  $N_o = \max_{2E \geq \bar{\epsilon}_j} j \leq j_{\max}$ , calculated using the third version of KANTBP 3.0 program [21, 22], implemented in CAS MAPLE and FORTRAN environment and described in [16, 17].

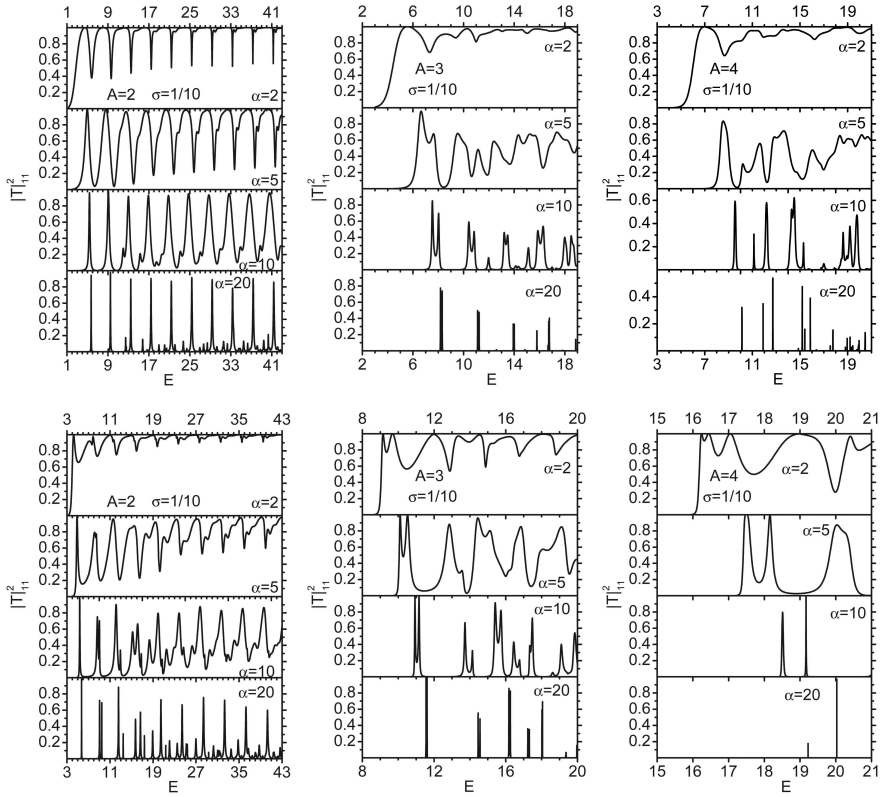


**Fig. 3.** The total transmission probability  $|T|_{11}^2$  vs energy  $E$  (in oscillator units) for the system of  $A = 2, 3, 4$  S- (upper panels) and A- (lower panels) particles coupled by the oscillator potential and being initially in the ground cluster state penetrating through the repulsive Gaussian-type potential barriers (16) with  $\sigma = 0.1$  and  $\alpha = 2, 5, 10, 20$

## 5 Resonance Transmission of a Few Coupled Particles

In the (O) case, i.e.,  $V^{pair}(x_{ij}) = V^{hosc}(x_{ij})$ , the solution of the scattering problem described above yields the reflection and transmission amplitudes  $R_{ji_o}(E)$  and  $T_{ji_o}(E)$  that enter the asymptotic boundary conditions (9) as unknowns.  $|R_{ji_o}(E)|^2$  ( $|T_{ji_o}(E)|^2$ ) is the probability of a transition to the state described by the reflected (transmitted) wave and, hence, will be referred as the reflection (transmission) coefficient. Note that  $|R_{ji_o}(E)|^2 + |T_{ji_o}(E)|^2 = 1$ .

In Figs. 3 and 4, we show the energy dependence of the total transmission probability  $|T|_{ii}^2 = \sum_{j=1}^{N_o} |T_{ji}(E)|^2$ . This is the probability of a transition from a chosen state  $i$  into any of  $N_o$  states found from Eq. (13) by solving the boundary-value problem in the Galerkin form, (14) and (17), using the KANTBP 3.0 program [21, 22] on the finite-element grid  $\Omega_\xi\{-\xi_0^{\max}, \xi_0^{\max}\}$  with  $N_{\text{elem}}$  fourth-order Lagrange elements between the nodes. For S-solutions at  $A = 2, 3, 4$

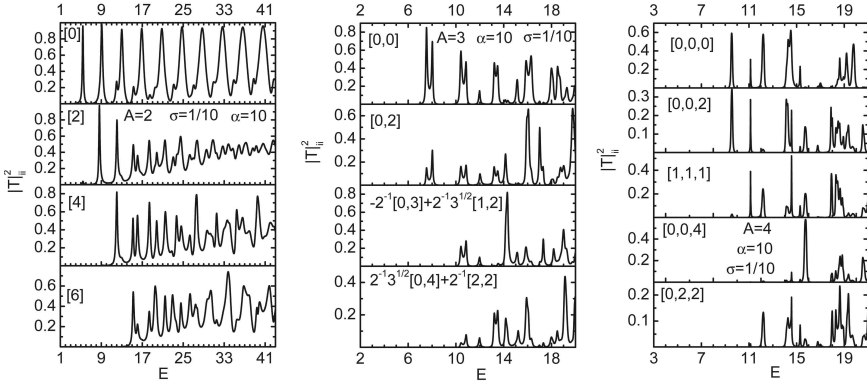


**Fig. 4.** The total transmission probability  $|T|_{ii}^2$  vs the energy  $E$  (in oscillator units) for the system of  $A = 2, 3, 4$  particles, coupled by the oscillator potential and being initially in the ground and excited S-states, penetrating through the repulsive Gaussian-type potential barriers (16) with  $\sigma = 0.1$  and  $\alpha = 10$ . We use the notation of the S-states,  $[i_1, \dots, i_{A-1}] = 1/\sqrt{N_\beta} \sum_{i'_1, \dots, i'_{A-1}} \prod \hat{\Phi}_{i'_k}(\xi_k)$ , with summation over all ( $N_\beta$ ) multiset permutations of  $i_1, \dots, i_{A-1}$  of  $A - 1$ -dimensional oscillator functions [18]

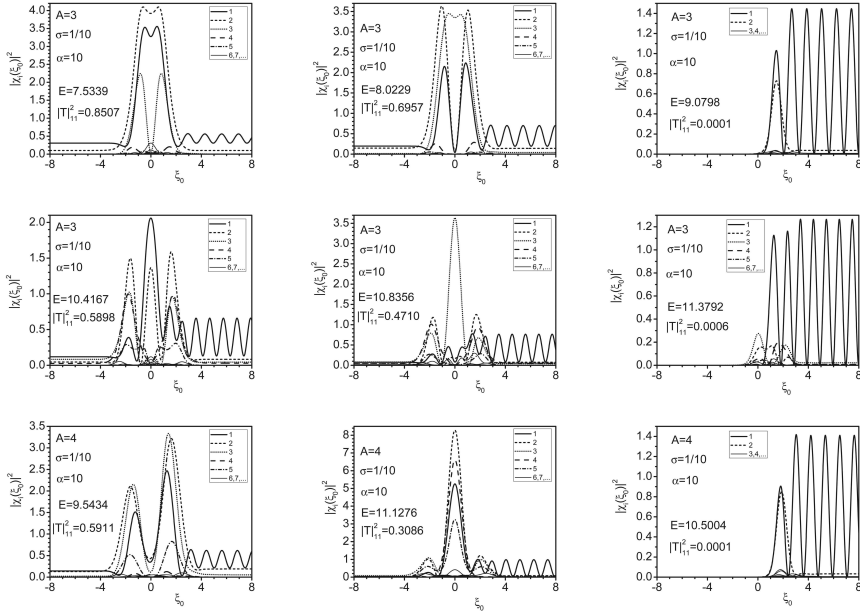
the following parameters were used:  $j_{\max} = 13, 21, 39$ ,  $\xi_0^{\max} = 9.3, 10.5, 12.8$ ,  $N_{\text{elem}} = 664, 800, 976$ , while for A-solutions we used  $j_{\max} = 13, 16, 15$ ,  $\xi_0^{\max} = 9.3, 10.5, 12.2$ ,  $N_{\text{elem}} = 664, 800, 976$  that yield an accuracy of the solutions of an order of the fourth significant figures.

Figure 3 demonstrates non-monotonic behavior of the total transmission probability versus the energy, and the observed resonances are manifestations of the quantum transparency effect. With the barrier height increasing, the peaks become narrower, and their positions shift to higher energies. The multiplet structure of the peaks in the symmetric case is similar to that in the antisymmetric case. For three particles, the major peaks are double, while for two and four particles, they are single. For  $A = 2$  and  $\alpha = 10, 20$ , one can observe the additional multiplets of small peaks.

Figure 4 illustrates the energy dependence of the total transmission probabilities from the excited states. As the energy of the initial excited state increases, the transmission peaks demonstrate a shift towards higher energies, the set of peak positions keeping approximately the same as for the transitions from the ground state and the peaks just replacing each other, like it was observed in the model calculations [12]. For example, for  $A = 3$ , the position of the third peak for transitions from the first two states ( $E = 10.4167$  and  $E = 10.4156$ ) coincides with the position of the first peak for the transitions from the second two states ( $E = 10.4197$  and  $E = 10.4298$ ).

### Calculation of Energy Position of the Barrier Quasistationary States.

In the considered case, the potential barrier  $V(x_i)$  is narrow, and  $V^{\text{pair}}(x_{ij}) = V^{\text{hosc}}(x_{ij})$ , so that we solve Eq. (1) in the Cartesian coordinates  $x_1, \dots, x_A$  in one



**Fig. 5.** The probability densities  $|\chi_i(\xi_0)|^2$  for the coefficient functions of the decomposition (13), representing the incident wave function of the ground S-state of the particles at the values of the collision energy  $E$  corresponding to individual maxima and minima of the transmission coefficient in Fig. 3. The parameters of the Gaussian barrier are  $\alpha = 10$  and  $\sigma = 0.1$

of the  $2^A - 2$  subdomains, defined as  $p_i x_i > 0, p_i = \pm 1$ , under the Dirichlet conditions (DC):  $\Psi(x_1, \dots, x_A)|_{\cup_{i=1}^A \{x_i=0\}} = 0$  at the internal boundaries  $\cup_{i=1}^A \{x_i = 0\}$ . Here the value  $p_i = \pm 1$  indicates the location of the  $i^{th}$  particle at the right or left side of the barrier, respectively. Thus, in the DC procedure we seek for the solution in the form of a Galerkin expansion over the orthogonal truncated oscillator basis,  $\Psi_i^D(\mathbf{x}) = \sum_{j=1}^{j_{max}} \bar{\Phi}_j(\mathbf{x}) \Psi_{ji}^D$  composed of  $A$ -dimensional harmonic oscillator functions  $\bar{\Phi}_j(\mathbf{x})$ , odd in each of the Cartesian coordinates  $x_1, \dots, x_A$  in accordance with the above DCs, with unknown coefficients  $\Psi_{ji}^D$ . As a result, we arrive at the algebraic eigenvalue problem  $D\Psi^D = \Psi^D E^D$  with a dense real-symmetric  $j_{max} \times j_{max}$  matrix. So, in the DC procedure we seek for an approximate solution in one of the potential wells, i.e., we neglect the tunnelling through the barriers between wells. Therefore, we cannot observe the splitting inherent in exact eigenvalues corresponding to S and A eigenstates, differing in permutation symmetry. However, we can explain the mechanism of their appearance and give their classification, which is important, too. This *algorithm DC* was implemented in CAS MAPLE and FORTRAN environment.

*Remark.* The DC procedure is similar to solving Eq. (3) in the symmetrized coordinates  $\xi_0, \xi$  related to the Cartesian ones by Eq. (2), implemented the following two steps:

- (i) we approximate the narrow barriers by impenetrable walls  $x_k(\xi_0, \xi) = 0$ ;
- (ii) we superpose these mutually perpendicular walls with the coordinate hyperplanes using rotations.

Actually, the two approaches yield the same boundary-value problem formulated in different coordinates (1), (3).

### The algorithm DC:

---

#### Input:

$A$  is the number of identical particles;

$x_k, k = 1, \dots, A$  are the Cartesian coordinates of the identical particles;

$p_k = \pm 1$  indicates the location of the  $k^{th}$  particle ;

$j_{max}$  is the number of the eigenfunctions of A-dimensional harmonic oscillator;

#### Output:

$D = \{D_{j'j}\}$  is the  $j_{max} \times j_{max}$  matrix ;

$E_i^D$  and  $\Psi_{ji}^D$  are the real-value eigenenergies and eigenvectors;

---

#### Local:

$$\Phi_j = \sqrt{2^A} \prod_{k=1}^A \bar{\Phi}_{i_k}(x_k);$$

$$I(i'_k, i_k) = \int_0^\infty \bar{\Phi}_{i'_k}(x) \bar{\Phi}_{i_k}(x) dx = \frac{2^{(i'_k + i_k)/2} {}_2F_1(i'_k, i_k; (2 - i'_k - i_k)/2; 1/2)}{\Gamma((2 - i'_k - i_k)/2) \sqrt{i'_k! i_k!}};$$

$\Gamma(*)$  is the gamma-function,  ${}_2F_1(*, *; *, *)$  is the hypergeometric function;

---

1:  $Eq := (-\Delta + \sum (p_k x_k - p_{k'} x_{k'})/2A)$ ;

2:  $Eq := \sqrt{A/(A-1)}(Eq, \Delta \rightarrow \Delta/(A/(A-1))), x_k \rightarrow x_k \sqrt[4]{A/(A-1)}$ ;

3:  $Eq := Eq, p_k^2 \rightarrow 1, \Delta = \sum_k (x_k^2 - (2n_k + 1))$ ;

4:  $Eq := Eq \prod \bar{\Phi}_{i_k}(x_k)$ ;

5:  $Eq := x_k = (\sqrt{i_k + 1} \bar{\Phi}_{i_k+1}(x_k) + \sqrt{i_k} \bar{\Phi}_{i_k-1}(x_k)) / (\sqrt{2} \bar{\Phi}_{i_k}(x_k))$ ;

6: **for**  $j, j' = 1, \dots, j_{max}$  **do**

$D_{j'j} := \Phi_{i_k}(x_k) \rightarrow I(i'_k, i_k)$ ;

**end for**

7:  $D\Psi_{ji}^D = \Psi_{ji}^D E_i^D \rightarrow E_i^D$  and  $\Psi_{ji}^D$ ;

---

In Table 1, we present the resonance values of the energy  $E_S$  ( $E_A$ ) calculated by solving the boundary-value problem (14) and (17), using the KANTBP 3.0 program, for S (A) states at  $A = 2, 3, 4$   $\sigma = 1/10$ ,  $\alpha = 20$  that correspond to the maxima of transmission coefficients  $|T|_{ii}^2$  in Fig. 3 up to values of energy  $E < 18$  and corresponding resonance values of the energy  $E_D$  calculated by means of the algorithm DC. One can see that the accepted approximation of the narrow barrier with impermeable walls using in the algorithm DC provides the appropriate approximations  $E_i^D$  of the above high accuracy results  $E_S$  ( $E_A$ ) with the error smaller than 2%. Below we give a comparison and qualitative analysis of the obtained results.



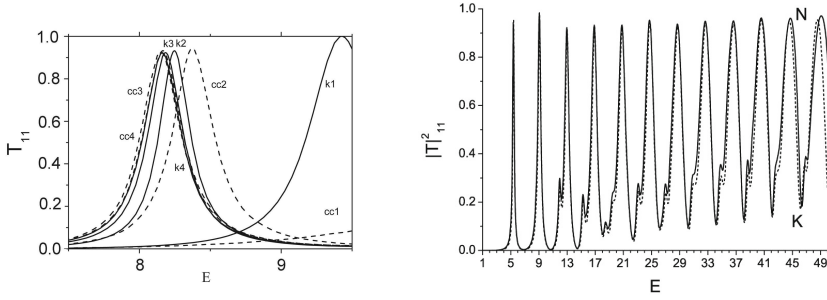


**Fig. 6.** a. The comparison of convergence rate of Galerkin (cc\*) and Kantorovich (k\*) close-coupling expansions in calculations of transmission coefficient  $|T_{11}|^2$  for the S-states,  $A = 2$  at  $\alpha = 10$ ,  $\sigma = 0.1$ , like epure of the first peak from Fig. 3. b. The comparison of Galerkin and Kantorovich methods (G=K) with Finite-Difference Numerov method (N)

For two particles,  $A = 2$  (see Fig. 1), there are two symmetric potential wells. In each of them both symmetric and asymmetric wave functions are constructed. Since the potential barrier separating the wells is sufficiently high, the appropriate energies are closely spaced, so that each level describes the states of both S and A type. The lower energy levels form a sequence “singlet-doublet-triplet, etc.”, which is seen in Fig. 3. The resonance transmission energies for a pair of particles in S states are lower than that for a pair of those in A states. This is due to the fact that in the vicinity of the collision point, the wave function is zero. When  $A = 3$  there are six similar wells, three of them at each side of the plane  $\xi_0 = 0$ . The symmetry with respect to the plane  $\xi_0 = 0$  explains the presence of doublets. The presence of states with definite symmetry is associated with the fact that the axis  $\xi_0$  is a third-order symmetry axis. However, in contrast to the case  $A = 2$ , one can obtain either S or A combinations of states. For example, the first four solutions of the problem, in one of the wells (e.g., the one restricted with the pair-collision planes “13” and “23”) possess the dominant components  $2\sqrt{2}\bar{\Phi}_1(x_1)\bar{\Phi}_1(x_2)\bar{\Phi}_1(x_3)$ ,  $2(\bar{\Phi}_1(x_1)\bar{\Phi}_3(x_2) + \bar{\Phi}_3(x_1)\bar{\Phi}_1(x_2))\bar{\Phi}_1(x_3)$ ,  $2(\bar{\Phi}_1(x_1)\bar{\Phi}_3(x_2) - \bar{\Phi}_3(x_1)\bar{\Phi}_1(x_2))\bar{\Phi}_1(x_3)$ ,  $2\sqrt{2}\bar{\Phi}_1(x_1)\bar{\Phi}_1(x_2)\bar{\Phi}_3(x_3)$ . Note that the first, second, and fourth of these functions are symmetric with respect to the permutation  $x_1 \leftrightarrow x_2$ , while the third one is antisymmetric. Hence, in all six wells using the first four solutions one can obtain six S and two A states.

When  $A = 4$  there are 14 wells. Six wells at the center correspond to the case when two particles are located at one side of the barrier and the rest two at the other side. The corresponding eigenenergy is denoted  $E_i^{D22}$ . The rest eight wells correspond to the case when one particle is located at one side of the barrier and the rest three at the other side. The corresponding eigenenergy is denoted  $E_i^{D31}$ . For these states, doublets must be observed, similar to the case of three particles. However, the separation between the energy levels is much smaller, because the 4-well groups are strongly separated by two barriers, instead of only one barrier in the case  $A = 3$ .

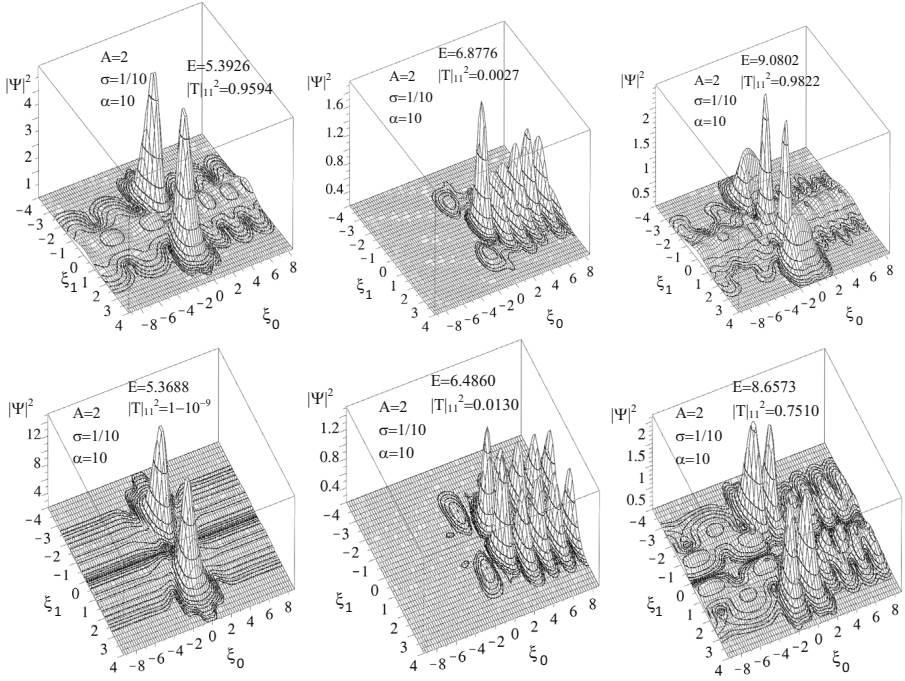


**Fig. 7.** The profiles of probability densities  $|\Psi(\xi_0, \xi_1)|^2$  for the S- (upper panel) and A- (lower panel) states of  $A = 2$  particles, revealing resonance transmission and total reflection at resonance energies, shown in Figs. 3

The necessary condition for the quasi-stationary state being symmetric (anti-symmetric) is that the wave functions must be symmetric (antisymmetric) with respect to those coordinates  $x_i$  and  $x_j$ , for which  $p_i = p_j$ .

The effect of quantum transparency is caused by the existence of barrier quasi-stationary states imbedded in the continuum. Fig. 5 shows that in the case of resonance transmission, the wave functions depending on the center-of-mass variable  $\xi_0$  are localized in the vicinity of the potential barrier center ( $\xi_0 = 0$ ).

For the energy values corresponding to some of the transmission coefficient peaks in Fig. 3 at  $\alpha = 10$  within the effective range of barrier potential action, the wave functions demonstrate considerable increase (from two to ten times) of the probability density in comparison with the incident unit flux. This is a fingerprint of quasistationary states, which is not a quantitative definition, but a clear evidence in favor of their presence in the system[23]. In the case of total reflection, the wave functions are localized at the barrier side, on which the wave is incident, and decrease to zero within the effective range of the barrier action.

Note that the explicit explanation of the quantum transparency effect is achieved in the framework of Kantorovich close-coupling equations because of the multi-barrier potential structure of the effective potential, appearing explicitly even in the diagonal or adiabatic approximation, in particular, in the S case

for  $A = 2$  [1, 16]. Nevertheless, in Galerkin close-coupling equations, the multi-barrier potential structure of the effective potential is observed explicitly in the A case (see Fig. 2).

As an example, Fig. 6a, which is an epure of Fig. 3, shows the comparison of convergence rates of Galerkin (13) and Kantorovich close-coupling expansions in calculations of transmission coefficient  $|T|_{11}^2$  for S wave functions,  $A = 2$  at  $\alpha = 10$ ,  $\sigma = 0.1$ . One can see that the diagonal approximation of the Kantorovich method provides better approximations of the positions of the transmission coefficient  $|T|_{11}^2$  resonance peaks. With the increasing number of basis functions, i.e., the number  $j_{\max}$  of close-coupling equations with respect to the center-of-mass coordinates in Galerkin (14) and Kantorovich form, respectively, the convergence rates are similar and confirm the results obtained by solving the problem by means of the Finite-Difference Numerov method in 2D domain [1], see Fig. 6 b. This is true for the considered short-range potentials (16), while for long-range potentials of the Coulomb type, the Kantorovich method can be more efficient [16].

Figure 7 shows the profiles of  $|\Psi|^2 \equiv |\Psi_{Em \rightarrow}^{(-)}|^2$  for the S and A total wave functions of the continuous spectrum in the  $(\xi_0, \xi_1)$  plane with  $A = 2$ ,  $\alpha = 10$ ,  $\sigma = 1/10$  at the resonance energies of the first and the second maximum and the first minimum of the transmission coefficient demonstrating *resonance transmission* and *total reflection*, respectively. It is seen that in the case of resonance transmission, the redistribution of energy from the center-mass degree of freedom to the internal (transverse) ones takes place, i.e., the transverse oscillator undergoes a transition from the ground state to the excited state, while in the total reflection, the redistribution of energy is extremely small, and the transverse oscillator returns to infinity in the same state.

## 6 Conclusion

We considered a model cluster of  $A$  identical particles bound by the oscillator-type potential that undergo quantum tunnelling through the short-range repulsive barrier potentials. The model was formulated in the new representation, which we referred as the Symmetrized Coordinate Representation (SCR, see forthcoming paper [18]), that implies construction of symmetric (asymmetric) combinations of oscillator wave functions in new coordinates. The approach was implemented as a complex of the symbolic-numeric algorithms and programs.

For clarity, a system of several identical particles was considered in one-dimensional Euclidian space ( $d = 1$ ). We calculated only the spatial part of the wave function, symmetric or antisymmetric under permutation of  $A$  identical particles. If necessary, the spin part of the wave function can be introduced using the conventional procedure for more rigorous calculation.

We analyzed the effect of quantum transparency, i.e., the resonance tunnelling of several bound particles through repulsive potential barriers. We demonstrated that this effect is due to the existence of sub-barrier quasistationary states imbedded in the continuum. For the considered type of symmetric Gaussian barrier

potential, the energies of the S and A quasistationary states are slightly different because of the similarity of the multiplet structure of oscillator energy levels at a fixed number of particles. This fact explains a similar behavior of transmission coefficients for S and A states shifted by threshold energies. The multiplet structure of these states is varied with increasing the number of particles, e.g., for three particles, the major peaks are double, while for two and four particles, they are single. Our calculations have also shown that with increasing the energy of the initial excited state of few-body clusters, the transmission peaks demonstrate a shift towards higher energies, the set of peak positions keeping approximately the same as for the transitions from the ground state and the peaks just skipping from one position to another.

The proposed approach can be adapted and applied to tetrahedral-symmetric nuclei, quantum diffusion of molecules and micro-clusters through surfaces, and fragmentation mechanism in producing very neutron-rich light nuclei. In connection with the intense search for superheavy nuclei, a particularly significant application of the proposed approach is the mathematically correct analysis of mechanisms of sub-barrier fusion of heavy nuclei and the study of fusion rate enhancement by means of resonance tunnelling.

The authors thank Professors V.P. Gerdt, A. Góźdz, and F.M. Penkov for collaboration. The work was supported by grants 13-602-02 JINR, 11-01-00523 and 13-01-00668 RFBR, 0602/GF MES RK and the Bogoliubov-Infeld program.

## References

1. Pen'kov, F.M.: Quantum transmittance of barriers for composite particles. JETP 91, 698–705 (2000)
2. Pijper, E., Fasolino, A.: Quantum surface diffusion of vibrationally excited molecular dimers. J. Chem. Phys. 126, 014708-1–014708-10 (2007)
3. Bondar, D.I., Liu, W.-K., Ivanov, M.Y.: Enhancement and suppression of tunneling by controlling symmetries of a potential barrier. Phys. Rev. A 82, 052112-1–052112-9 (2010)
4. Shegelski, M.R.A., Pittman, J., Vogt, R., Schaan, B.: Time-dependent trapping of a molecule. European Phys. J. Plus 127, 17-1–17-13 (2012)
5. Ershov, S.N., Danilin, B.V.: Breakup of two-neutron halo nuclei. Phys. Part. Nucl. 39, 1622–1720 (2008)
6. Nesterov, A.V., Arickx, F., Broeckhove, J., Vasilevsky, V.S.: Three-cluster description of properties of light nuclei with neutron and proton access within the algebraic version of the resonating group method. Phys. Part. Nucl. 41, 1337–1426 (2010)
7. Hofmann, H.: Quantummechanical treatment of the penetration through a two-dimensional fission barrier. Nucl. Phys. A 224, 116–139 (1974)
8. Krappe, H.J., Möhring, K., Nemes, M.C., Rossner, H.: On the interpretation of heavy-ion sub-barrier fusion data. Z. Phys. A 314, 23–31 (1983)
9. Cwiok, S., Dudek, J., Nazarewicz, W., Skalski, J., Werner, T.: Single-particle energies, wave functions, quadrupole moments and g-factors in an axially deformed Woods-Saxon potential with applications to the two-centre-type nuclear problems. Comput. Phys. Communications 46, 379–399 (1987)

10. Hagino, K., Rowley, N., Kruppa, A.T.: A program for coupled-channel calculations with all order couplings for heavy-ion fusion reactions. *Comput. Phys. Commun.* 123, 143–152 (1999)
11. Zagrebaev, V.I., Samarin, V.V.: Near-barrier fusion of heavy nuclei: coupling of channels. *Phys. Atom. Nucl.* 67, 1462–1477 (2004)
12. Ahsan, N., Volya, A.: Quantum tunneling and scattering of a composite object reexamined. *Phys. Rev. C* 82, 064607-1–064607-19 (2010)
13. Shotter, A.C., Shotter, M.D.: Quantum mechanical tunneling of composite particle systems: Linkage to sub-barrier nuclear reactions. *Phys. Rev. C* 83, 054621-1–054621-11 (2011)
14. Shilov, V.M.: Sub-barrier fusion of intermediate and heavy nuclear systems. *arXiv:1012.3683 [nucl-th]* *Phys. Atom. Nucl.* 75, 485–490 (2012)
15. Chuluunbaatar, O., Gusev, A.A., Derbov, V.L., Krassovitskiy, P.M., Vinitsky, S.I.: Channeling problem for charged particles produced by confining environment. *Phys. Atom. Nucl.* 72, 768–778 (2009)
16. Gusev, A.A., Vinitsky, S.I., Chuluunbaatar, O., Gerdt, V.P., Rostovtsev, V.A.: Symbolic-numerical algorithms to solve the quantum tunneling problem for a coupled pair of ions. In: Gerdt, V.P., Koepf, W., Mayr, E.W., Vorozhtsov, E.V. (eds.) *CASC 2011. LNCS*, vol. 6885, pp. 175–191. Springer, Heidelberg (2011)
17. Gusev, A.A., Chuluunbaatar, O., Vinitsky, S.I.: Computational scheme for calculating reflection and transmission matrices, and corresponding wave functions of multichannel scattering problems. In: Uvarova, L.A. (ed.) *Proc. Second International Conference “The Modeling of Non-linear Processes and Systems”*, Yanus, Moscow, pp. 978–975 (2011)
18. Gusev, A., Vinitsky, S., Chuluunbaatar, O., Rostovtsev, V., Hai, L., Derbov, V., Gózdź, A., Klimov, E.: Symbolic-numerical algorithm for generating cluster eigenfunctions: identical particles with pair oscillator interactions. In: Gerdt, V.P., Koepf, W., Mayr, E.W., Vorozhtsov, E.V. (eds.) *CASC 2013. LNCS*, vol. 8136, pp. 155–168. Springer, Heidelberg (2013)
19. Vinitsky, S.I., Gerdt, V.P., Gusev, A.A., Kaschiev, M.S., Rostovtsev, V.A., Samoilov, V.N., Tupikova, T.V., Chuluunbaatar, O.: A symbolic-numerical algorithm for the computation of matrix elements in the parametric eigenvalue problem. *Programming and Computer Software* 33, 105–116 (2007)
20. Bunge, C.F.: Fast eigensolver for dense real-symmetric matrices. *Comput. Phys. Communications* 138, 92–100 (2001)
21. Chuluunbaatar, O., Gusev, A.A., Vinitsky, S.I., Abrashkevich, A.G.: KANTBP 2.0: New version of a program for computing energy levels, reaction matrix and radial wave functions in the coupled-channel hyperspherical adiabatic approach. *Comput. Phys. Commun.* 179, 685–693 (2008)
22. Chuluunbaatar, O., Gusev, A.A., Vinitsky, S.I., Abrashkevich, A.G.: KANTBP 3.0 - New version of a program for computing energy levels, reflection and transmission matrices, and corresponding wave functions in the coupled-channel adiabatic approach, Program library “JINRLIB”, <http://wwwinfo.jinr.ru/programs/jinrllib/kantbp/indexe.html>
23. de Carvalho, C.A.A., Nussenzweig, H.M.: Time delay. *Phys. Rept.* 364, 83–174 (2002)

# Symbolic-Numerical Algorithms for Solving Parabolic Quantum Well Problem with Hydrogen-Like Impurity

S.I. Vinitsky, O. Chuluunbaatar, V.P. Gerdt, A.A. Gusev, and V.A. Rostovtsev

Joint Institute for Nuclear Research, Dubna, Russia  
vinitsky@theor.jinr.ru

**Abstract.** For parabolic quantum well problem with hydrogen-like impurity a two-dimensional boundary-value problem is formulated in spherical coordinates at fixed magnetic quantum number. Computational scheme using *modified* angular prolate spheroidal functions is presented. Symbolic-numerical algorithms for solving the problem are elaborated. The efficiency of the algorithms and their implementation is demonstrated by solving typical test examples and proving the compatibility conditions for asymptotic solutions of scattering problems in spherical and cylindrical coordinates.

**Keywords:** Symbolic-numerical algorithms, parabolic quantum well, hydrogen-like impurity, modified prolate angular spheroidal functions.

## 1 Introduction

In [1] optical absorption into the ground state of GaAs parabolic quantum well and rectangular quantum well with infinitely high walls in the presence of a hydrogen-like impurity was considered. Calculation of the ground state of these quantum wells was carried out using single-parameter variational functions in the cylindrical coordinate system. The upper bounds of these energies were obtained depending on the shift of the Coulomb potential center. The analysis of more complex quantum mechanical models leads to boundary-value problems in a non-standard domain of the configuration space with complex boundary, solved using finite-element method [2,3], or by means of reducing the problem to ordinary differential equations following Kantorovich method [4], known in physics as the adiabatic approach to quantum mechanical problems with slow and fast variables. In the Kantorovich method, the basis functions depend upon the slow variables as parameters and obey the boundary conditions that account for all specific features of the original problem. This provides the efficiency of the method for solving boundary-value problems in a non-standard domain, e.g., in a sector of a circle with mixed boundary conditions [5], as well as in the presence of singular potential against the background of confining potentials of the oscillator type with respect to some independent variables [6,7]. The latter determines the potentialities of using the method to analyze low-dimensional quantum mechanical models of semiconductor nanostructures [8].

In this paper we present a scheme for solving the boundary-value problem for a parabolic quantum well in the adiabatic representation and in the spherical coordinates. For efficient application of the Kantorovich method we elaborated the following symbolic-numerical algorithms to compute the appropriate quantities to a prescribed accuracy:

- numerical solution of the parametric self-adjointed Sturm-Liouville problem on a bounded interval of the parameter values and calculation of derivatives with respect to the parameter of the eigenfunctions and of the matrix elements (integrals of the eigenfunctions multiplied by their derivatives with respect to the parameter) that appear as variable coefficients in the system of second-order ordinary differential equations (ODPEVP, implemented in FORTRAN [9]),
- asymptotic forms of the eigenfunctions and of the matrix elements that appear as variable coefficients in asymptotic solutions of the boundary-value problem under consideration and in the asymptotic forms of the system of second-order ordinary differential equations (MATRA, implemented in MAPLE),
- asymptotic forms of the solutions of the system of second-order ordinary differential equations for small and large values of the radial variable needed for solving the corresponding boundary-value problem with the third-type boundary conditions (ASYMRS, implemented in MAPLE),
- numerical solutions of the boundary-value problem for a system of second-order ordinary differential equations (KANTBP, implemented in FORTRAN[5]).

The paper is organized as follows. In Section 2, the statement of the boundary-value problem is given. In Section 3, the procedure MATRA for analytic calculation of asymptotic form of basis functions and matrix elements at large values of the radial variable is described. In Section 4, the procedure ASYMRS for the calculation of asymptotic forms of fundamental solutions of a system of radial equations at large values of radial variable in the analytic form is presented. In Section 5, a test example of numerical calculation of the ground state energy and wave functions with the help of ODPEVP and KANTBP programs is given. The Conclusion outlines further applications of the above set of symbolic-numerical algorithms and programs.

## 2 Problem Statement

The Schrödinger equation describing the parabolic quantum well problem with shifted hydrogen-like impurity in the reduced atomic units and in the spherical coordinates  $(r, \eta = \cos \theta, \phi)$  at a fixed magnetic quantum number  $m$  reads as [4]

$$\left(-\frac{1}{r^2} \frac{\partial}{\partial r} r^2 \frac{\partial}{\partial r} + \frac{1}{r^2} A(c, b) - \frac{2q}{r}\right) \psi_m(r, \eta) = 2E \psi_m(r, \eta). \quad (1)$$

Here  $A(c, b) \equiv A^{(0)}(c, b) + c^2 + f$  is the operator of the modified angular functions, which at  $b = f = 0$  correspond to the angular prolate spheroidal functions [10]

$$A^{(0)}(c, b) = -\frac{\partial}{\partial \eta} (1 - \eta^2) \frac{\partial}{\partial \eta} + \frac{m^2}{1 - \eta^2} + c^2 (\eta^2 - 1) - b\eta, \quad (2)$$

where  $c = \omega r^2$ ,  $b = -2\omega^2 z_c r^3$ , and  $f = (\omega z_c r)^2$  are real parameters depending on the harmonic oscillator frequency  $\omega$  and the shift  $z_c$  of the Coulomb charge  $q$  along  $z$ -axis from the origin of the cylindrical frame  $(\rho, z, \phi)$  in  $\mathbf{R}^3$ , i.e.,  $r = \sqrt{\rho^2 + (z - z_c)^2}$ . The wave functions  $\psi_m(r, \eta, b) \equiv \psi_{mi}(r, \eta, b) \equiv \psi_{mi}(r, \eta, z_c)$  at fixed  $m$  obey the following conditions at the boundary of the domain  $\Omega_{r, \eta} = \Omega(0 \leq r < \infty, -1 \leq \eta \leq 1)$ :

$$\lim_{\eta \rightarrow \pm 1} (1 - \eta^2) \frac{\partial \psi_m(r, \eta)}{\partial \eta} = 0, \text{ for } m = 0, \text{ and } \psi_m(r, \pm 1) = 0, \text{ for } m \neq 0,$$

$$\lim_{r \rightarrow 0} r^2 \frac{\partial \psi_m(r, \eta)}{\partial r} = 0.$$

At large  $r = r_{\max} \gg 1$  the discrete-spectrum wave functions obey the Dirichlet boundary condition that follows from the asymptotic behavior of the solution

$$\lim_{r \rightarrow +\infty} r^2 \psi_m(r, \eta) = 0 \quad \rightarrow \quad \psi_m(r_{\max}, \eta) = 0,$$

and also the orthonormality condition

$$\int_0^{r_{\max}} \int_{-1}^1 \psi_{mi}(r, \eta) \psi_{mj}(r, \eta) r^2 dr d\eta = \delta_{ij}. \quad (3)$$

The solution of (1)–(3) at fixed  $m$  is sought in the form of the Kantorovich expansion with respect to the single-parameter functions  $\Phi_j(\eta; r) \equiv \Phi_{mj}(\eta; r)$ :

$$\psi_{mi}(r, \eta) = \sum_{j=1}^{j_{\max}} \Phi_{mj}(\eta; r) \chi_{ji}(r), \quad (4)$$

Here the functions  $\chi_{ji}(r)$  are to be found, while the basis functions  $\Phi_j(\eta; r) \in F_r \sim L_2[-1, 1]$  are solutions of the eigenvalue problem:

$$A(c, b) \Phi_{mj}(\eta; r) = E_j(r) \Phi_{mj}(\eta; r). \quad (5)$$

The eigenfunctions  $\Phi_{mj}(\eta; r) \equiv \Phi_{mj}(r, \eta, z_c)$  at fixed  $m$  obey the symmetry condition  $\Phi_{mj}(r, \eta, z_c) = \exp(i\pi\nu_{mq}) \Phi_{mj}(r, -\eta, -z_c)$ , where  $\nu_{mq} \equiv \nu_{mq}(r, z_c)$  is the real phase,  $q$  is the number of zeros in  $\eta \in [-1, 1]$ , in particular,  $\nu_{mq}(r, 0) = q$  at  $z_c = 0$ ,  $E_j(r, z_c) = E_j(r, -z_c)$ , and the boundary conditions with respect to the angular variable  $\eta$  at each fixed value of the parameter  $r \in \mathbf{R}_+^1$

$$\lim_{\eta \rightarrow \pm 1} (1 - \eta^2) \frac{\partial \Phi_{mj}(\eta; r)}{\partial \eta} = 0, \text{ for } m = 0, \text{ and } \Phi_{mj}(r, \pm 1) = 0, \text{ for } m \neq 0, \quad (6)$$

as well as the orthonormality conditions in the interval  $\Omega_\eta = [-1, 1]$ :

$$\langle \Phi_{mi}(\eta; r) | \Phi_{mj}(\eta; r) \rangle_{\Omega_\eta} = \int_{-1}^1 \Phi_{mi}(\eta; r) \Phi_{mj}(\eta; r) d\eta = \delta_{ij}. \quad (7)$$

Note that the eigenvalues  $E_j(r)$  of the operator  $A(c, b)$  from (5) are related to the eigenvalues  $\lambda_j(r)$  of the operator  $A^{(0)}(c, b)$  from (2) by the equality



$E_j(r) = \lambda_j(r) + c^2 + f$ . The projection of Eq. (1), using expansion (4), is reduced to the set of  $j_{\max}$  ordinary second-order differential equations with respect to the unknown vector function  $\chi^{(i)}(r) \equiv (\chi_{1i}(r), \dots, \chi_{j_{\max}i}(r))$ :

$$\left( -\frac{1}{r^{d-1}} \mathbf{I} \frac{d}{dr} r^{d-1} \frac{d}{dr} + \frac{\mathbf{U}(r)}{r^2} + \mathbf{Q}(r) \frac{d}{dr} + \frac{1}{r^{d-1}} \frac{d r^{d-1} \mathbf{Q}(r)}{dr} - 2E \mathbf{I} \right) \chi^{(i)}(r) = 0. \quad (8)$$

Here  $d = 3$  is the dimension of the above space  $\mathbf{R}^3$ ,  $\mathbf{I}$ ,  $\mathbf{U}(r)$ , and  $\mathbf{Q}(r)$  are  $j_{\max} \times j_{\max}$  matrices whose entries are defined by the following relations:

$$\begin{aligned} U_{ij}(r) &= r^2 H_{ij}(r) + \frac{E_i(r) + E_j(r)}{2} \delta_{ij} - 2qr \delta_{ij} \quad I_{ij} = \delta_{ij}, \\ H_{ij}(r) &= H_{ji}(r) = \left\langle \frac{\partial \Phi_i(\eta; r)}{\partial r} \left| \frac{\partial \Phi_j(\eta; r)}{\partial r} \right\rangle_{\Omega_\eta}, \\ Q_{ij}(r) &= -Q_{ji}(r) = - \left\langle \Phi_i(\eta; r) \left| \frac{\partial \Phi_j(\eta; r)}{\partial r} \right\rangle_{\Omega_\eta}. \end{aligned} \quad (9)$$

The discrete-spectrum solutions obey the asymptotic boundary conditions and the orthonormality condition

$$\lim_{r \rightarrow 0} r^{d-1} \frac{d\chi^{(i)}(r)}{dr} = 0, \quad \lim_{r \rightarrow \infty} r^{d-1} \chi^{(i)}(r) = 0 \quad \rightarrow \quad \chi^{(i)}(r_{\max}) = 0, \quad (10)$$

$$\int_0^{r_{\max}} r^{d-1} \left( \chi^{(i)}(r) \right)^T \chi^{(j)}(r) dr = \delta_{ij}. \quad (11)$$

**Remark 1.** The continuity of the eigenfunction  $\Phi_j(\eta; r)$  with respect to the parameter  $r$  is very important for calculations of the potential matrix elements (9) and their further applications for solution of boundary problems for a system of coupled differential equations (8) as considered in [5]. Hence we required  $\Phi_j(\eta; r) > 0$  in the vicinity of the right boundary point  $\eta = 1$  [9].

**Remark 2.** The formulation of the boundary-value problem of continuous spectrum for the set of Eqs. (8) using asymptotic expansions of the solutions presented below is given in [5,7].

### 3 Symbolic Algorithm for Evaluating the Asymptotic Forms of Matrix Elements

The procedure MATRA computes the asymptotic forms of solutions of the eigenvalue problem (5) together with the matrix elements (9) as expansions in powers of  $r$  and  $1/r$  for small and large values of  $r$ , respectively. Here we consider the case of large  $r$ .

In **step 1** we go from the coordinate  $\eta \in [-1, 1]$  to the new coordinate  $\hat{z} \in [\sqrt{\omega}(-r + z_c), \sqrt{\omega}(r + z_c)]$  using the formula  $r\eta \equiv z' = z - z_c = (\hat{z} - z_c \sqrt{\omega})/\sqrt{\omega}$ .

In **step 2** we construct the asymptotic expansion defined in the domain  $\eta \in [-\eta_1, \eta_1]$ , where  $\eta_1 = O((\omega r^2)^{-1/2+\epsilon})$ ,  $0 < \epsilon < 1/2$ . It means that in

the evaluation of the corresponding integrals we omit exponentially small terms and change the domain from the finite interval  $[\sqrt{\omega}(-r + z_c), \sqrt{\omega}(r + z_c)]$  to the infinite one  $(-\infty, +\infty)$ .

In **step 3** we find the asymptotic solution  $\Phi_j^{as}(\hat{z}; r)$  and  $r^{-2}E_j(r) = r^{-2}(\lambda_j(r) + c^2 + f) = \omega\beta_j(r)$  as an expansion with  $j = n + 1$

$$\Phi_j^{as}(\hat{z}; r) = \sqrt[4]{\omega}\sqrt{r} \sum_{k=0}^{k_{\max}} \frac{\Phi_n^{(2k)}(\hat{z})}{r^{2k}}, \quad E_j(r) = \sum_{k=0}^{k_{\max}} \frac{E_n^{(2k)}}{r^{2k}}, \quad \beta_j(r) = \sum_{k=0}^{k_{\max}} \frac{\beta_n^{(2k)}}{r^{2k}}. \quad (12)$$

Substituting Eq. (12) into Eq. (5) and equating the coefficients at the same powers of  $r$ , we arrive at a system of recurrence differential equations for evaluating the coefficients  $\Phi_n^{(2k)}(\hat{z})$  and  $\beta_n^{(2k)}$ ,  $k = 1, \dots, k_{\max}$ :

$$L(n)\Phi_n^{(2k)} = f_n^{(2k)}(\hat{z}), \quad L(n) = -\frac{d^2}{d\hat{z}^2} - (2n+1) + \hat{z}^2, \quad (13)$$

with the initial data  $\beta_n^{(0)} = 2n+1$ , and  $\Phi_n^{(0)}(\hat{z})$  is a known solution of the problem

$$L(n)\Phi_n^{(0)}(\hat{z}) = 0, \quad \int_{-\infty}^{+\infty} \Phi_n^{(0)}(\hat{z})\Phi_{n'}^{(0)}(\hat{z})d\hat{z} = \delta_{nn'}. \quad (14)$$

In Eqs. (13) the right-hand sides  $f_n^{(2k)}(\hat{z})$  are defined by the relations

$$f_n^{(2k)}(\hat{z}) = \frac{(\hat{z} - z_c\sqrt{\omega})^2}{\omega} \frac{d^2\Phi_n^{(2k-2)}(\hat{z})}{d\hat{z}^2} + \frac{2(\hat{z} - z_c\sqrt{\omega})}{\omega} \frac{d\Phi_n^{(2k-2)}(\hat{z})}{d\hat{z}} + \sum_{j=1}^k (a^{(2j)}(\hat{z}, z_c) - \beta_n^{(2j)})\Phi_n^{(2k-2j)}(\hat{z}) = 0,$$

where the coefficients  $a^{(2j)}(\hat{z}, z_c)$  are defined by Taylor expansion at large  $\omega r^2$

$$\frac{m^2}{1 - \eta^2} = m^2 \left( 1 - \frac{(\hat{z} - z_c\sqrt{\omega})^2}{\omega r^2} \right)^{-1} = \sum_{j=0}^{k_{\max}} \frac{a^{(2j)}(\hat{z}, z_c)}{r^{2j}}. \quad (15)$$

Note that the coefficients  $a^{(2j)}(\hat{z}, z_c)$  contain the terms of the order of  $\hat{z}^{2l}$  till  $l = j$ . The orthogonality and normalization conditions follow from (7) and (12)

$$I_{jj'}^{(2k)} = \sum_{l=0}^k \int_{-\infty}^{\infty} \Phi_{n_l}^{(2l)}(\hat{z})\Phi_{n_r}^{(2k-2l)}(\hat{z})d\hat{z} = \delta_{k0}\delta_{n_l n_r} \quad (16)$$

where  $n_l = j - 1$ ,  $n_r = j' - 1$ .

We find the asymptotic expressions of the matrix elements  $H_{jj'}(r)$  and  $Q_{jj'}(r)$  from (9) in the form of expansions

$$Q_{jj'}(r) = \sum_{k=1}^{k_{\max}} \frac{Q_{jj'}^{(2k-1)}}{r^{2k-1}}, \quad H_{jj'}(r) = \sum_{k=1}^{k_{\max}} \frac{H_{jj'}^{(2k)}}{r^{2k}}. \quad (17)$$

**Table 1.** Values of the partial sums (27) for  $r^{-2}E_j(r)$  depending on  $k_{\max}$  for  $\omega = 3$ ,  $m = 0$ ,  $z_c = 0.4$ , and  $r = 8$ . The last row contains the corresponding numerical values (n.v.) calculated by means of ODPEVP [9].

$j$	$r^{-2}E_1$	$r^{-2}E_2$	$r^{-2}E_3$	$r^{-2}E_4$
$r^{-0}E_j^{(0)}$	3	9	15	21
$+r^{-2}E_j^{(2)}$	2.9845312	8.9614062	14.922656	20.868281
$+r^{-4}E_j^{(4)}$	2.9844843	8.9611764	14.922034	20.866998
$+r^{-6}E_j^{(6)}$	2.9844838	8.9611729	14.922022	20.866966
$+r^{-8}E_j^{(8)}$	2.9844838	8.9611729	14.922022	20.866965
$+r^{-10}E_j^{(10)}$	2.9844838	8.9611729	14.922022	20.866965
(n.v.)	2.9844838	8.9611729	14.922022	20.866965

Here the coefficients  $Q_{jj'}^{(2k+1)}$  and  $H_{jj'}^{(2k+2)}$  are defined by the relations

$$\begin{aligned}
 Q_{jj'}^{(2k+1)} &= - \sum_{l=0}^k \int_{-\infty}^{+\infty} \Phi_{n_l}^{(2l)}(\hat{z}) \hat{Q} \Phi_{n_r}^{(2k-2l)}(\hat{z}) d\hat{z}, \\
 H_{jj'}^{(2k+2)} &= \sum_{l=0}^k \int_{-\infty}^{+\infty} \hat{Q} \Phi_{n_l}^{(2l)}(\hat{z}) \hat{Q} \Phi_{n_r}^{(2k-2l)}(\hat{z}) d\hat{z}, \\
 \hat{Q} \Phi_{n_l}^{(2l)}(\hat{z}) &= \left( \frac{1}{2} - 2l \right) \Phi_{n_l}^{(2l)}(\hat{z}) + (\hat{z} - z_c \sqrt{\omega}) \frac{d\Phi_{n_l}^{(2l)}(\hat{z})}{d\hat{z}}.
 \end{aligned} \tag{18}$$

In **step 4** we construct  $\Phi_n^{(2k)}(\hat{z})$  as the expansion with unknown coefficients  $b_{n;s}^{(2k)}$

$$\Phi_n^{(2k)}(\hat{z}) = \sum_{s=-M(k)}^{M(k)} b_{n;s}^{(2k)} \Phi_{n+s}^{(0)}(\hat{z}). \tag{19}$$

Here the basis functions  $\Phi_v^{(0)}(\hat{z})$  are solutions of (14) expressed in terms of the Hermite polynomials [10]

$$\Phi_v^{(0)}(\hat{z}) = \frac{H_v(\hat{z}) \exp(-\hat{z}^2/2)}{\sqrt[4]{\pi} \sqrt{2^v} \sqrt{v!}}.$$

Using the known recurrence relation for Hermite polynomials  $H_v(\hat{z})$

$$\hat{z} H_v(\hat{z}) = \frac{H_{v+1}(\hat{z})}{2} + v H_{v-1}(\hat{z}), \quad \frac{dH_v(\hat{z})}{d\hat{z}} = 2v H_{v-1}(\hat{z}), \tag{20}$$

we obtain the recurrence relations for the basis functions  $\Phi_v^{(0)}(\hat{z})$ :

$$\begin{aligned}
 \hat{z} \Phi_v^{(0)}(\hat{z}) &= + \frac{\sqrt{v+1}}{\sqrt{2}} \Phi_{v+1}^{(0)}(\hat{z}) + \frac{\sqrt{v}}{\sqrt{2}} \Phi_{v-1}^{(0)}(\hat{z}), \\
 \frac{d\Phi_v^{(0)}(\hat{z})}{d\hat{z}} &= - \frac{\sqrt{v+1}}{\sqrt{2}} \Phi_{v+1}^{(0)}(\hat{z}) + \frac{\sqrt{v}}{\sqrt{2}} \Phi_{v-1}^{(0)}(\hat{z}),
 \end{aligned} \tag{21}$$

**Table 2.** The same as in Table 1, but for  $Q_{ij}(r)$  at  $i \neq j$ 

$i, j$	$Q_{12}, 10^{-2}$	$Q_{23}, 10^{-2}$	$Q_{34}, 10^{-1}$	$Q_{13}, 10^{-2}$	$Q_{24}, 10^{-1}$	$Q_{14}, 10^{-4}$
$r^{-1}Q_{ij}^{(1)}$	6.1237243	8.6602540	1.0606601	-8.8388347	-1.5309310	0
$+r^{-3}Q_{ij}^{(3)}$	6.2072876	8.8911941	1.1027551	-8.8450495	-1.5340009	-5.5338541
$+r^{-5}Q_{ij}^{(5)}$	6.2085282	8.8962122	1.1040117	-8.8447852	-1.5339440	-5.6676737
$+r^{-7}Q_{ij}^{(7)}$	6.2085518	8.8963403	1.1040530	-8.8447748	-1.5339400	-5.6710585
$+r^{-9}Q_{ij}^{(9)}$	6.2085523	8.8963441	1.1040545	-8.8447745	-1.5339398	-5.6711548
(n.v.)	6.2085523	8.8963442	1.1040546	-8.8447745	-1.5339398	-5.6711580

$$\hat{z} \frac{d\Phi_v^{(0)}(\hat{z})}{d\hat{z}} = -\frac{1}{2}\Phi_v^{(0)}(\hat{z}) - \frac{\sqrt{v+1}\sqrt{v+2}}{2}\Phi_{v+2}^{(0)}(\hat{z}) + \frac{\sqrt{v-1}\sqrt{v}}{2}\Phi_{v-2}^{(0)}(\hat{z}),$$

$$L(n)\Phi_{n+s}^{(0)}(\hat{z}) \equiv \left(-\frac{d^2}{d\hat{z}^2} - (2n+1) + \hat{z}^2\right)\Phi_{n+s}^{(0)}(\hat{z}) = 2s\Phi_{n+s}^{(0)}(\hat{z}).$$

From (13), (15), and (21) we obtain the needed value of  $M(k) = 2k + 1$  in the expansion (19) to provide the calculation of nonzero terms only.

Substituting Eq. (19) into Eq. (13), using Eq. (21) and equating coefficients at the same powers of  $r$ , we arrive at a set of recurrence relations for evaluating the coefficients  $\beta_n^{(2k)}$  and  $b_{n;s}^{(2k)}$

$$2sb_{n;s}^{(2k)} = f_{n;s}^{(2k)}, \quad (22)$$

$$f_{n;s}^{(2k)} = -\sum_{t=-4}^4 h_{n;s-t,t} b_{n;s-t}^{(2k-2)} - \sum_{j=1}^k \sum_{t=-2j}^{2j} a_{n;s-t,t}^{(2j)} b_{n;s-t}^{(2k-2j)} + \sum_{j=1}^k \beta_n^{(2j)} b_{n;s}^{(2k-2j)},$$

$$I_{jj'}^{(2k)} = \sum_{l=0}^k \sum_{s=-2k-1}^{2k+1} b_{n_l;s}^{(2l)} b_{n_r;s+n_l-n_r}^{(2k-2l)} = \delta_{k0} \delta_{n_l n_r}, \quad (23)$$

with the initial data  $\beta_n^{(0)} = 2n + 1$  and  $b_{n;s}^{(0)} = \delta_{s0}$ . The coefficients  $h_{n;s,t}$  and  $a_{n;s,t}^{(2j)}$  in the relations (22) are calculated using (15), (21) from the relations

$$\frac{(\hat{z} - z_c \sqrt{\omega})^2}{\omega} \frac{d^2 \Phi_{n+s}^{(0)}(\hat{z})}{d\hat{z}^2} + \frac{2(\hat{z} - z_c \sqrt{\omega})}{\omega} \frac{d\Phi_{n+s}^{(0)}(\hat{z})}{d\hat{z}} = \sum_{t=-4}^4 h_{n;s,t} \Phi_{n+s+t}^{(0)}(\hat{z}),$$

$$a^{(2j)}(\hat{z}, z_c) \Phi_{n+s}^{(0)}(\hat{z}) = \sum_{t=-2j}^{2j} a_{n;s,t}^{(2j)} \Phi_{n+s+t}^{(0)}(\hat{z}). \quad (24)$$

The corresponding coefficients  $Q_{jj'}^{(2k+1)}$  and  $H_{jj'}^{(2k+2)}$  from Eq. (18) have the following explicit form:

$$Q_{jj'}^{(2k+1)} = -\sum_{l=0}^k \sum_{s=-2k-1}^{2k+1} b_{n_l;s}^{(2l)} \left( (-2k+2l) b_{n_r;s+n_l-n_r}^{(2k-2l)} \right. \quad (25)$$

**Table 3.** The same as in Table 1, but for  $H_{ij}(r)$  at  $i \neq j$ 

$i, j$	$H_{12}, 10^{-3}$	$H_{23}, 10^{-2}$	$H_{34}, 10^{-2}$	$H_{13}, 10^{-3}$	$H_{24}, 10^{-2}$	$H_{14}, 10^{-2}$
$r^{-2} H_{ij}^{(2)}$	-7.6546554	-2.1650635	-3.9774756	-5.3033008	-0.9185586	1.8750000
$+r^{-4} H_{ij}^{(4)}$	-7.7794422	-2.2165683	-4.1102192	-5.6189439	-1.0089114	1.9299804
$+r^{-6} H_{ij}^{(6)}$	-7.7817944	-2.2178064	-4.1142837	-5.6289351	-1.0129576	1.9313221
$+r^{-8} H_{ij}^{(8)}$	-7.7818496	-2.2178410	-4.1144203	-5.6292488	-1.0131247	1.9313584
$+r^{-10} H_{ij}^{(10)}$	-7.7818511	-2.2178422	-4.1144255	-5.6292592	-1.0131316	1.9313595
(n.v.)	-7.7818512	-2.2178422	-4.1144257	-5.6292596	-1.0131319	1.9313596

$$\begin{aligned}
& + \frac{z_c \sqrt{\omega} \sqrt{n_l + s}}{\sqrt{2}} b_{n_r; s+n_l-n_r-1}^{(2k-2l)} - \frac{z_c \sqrt{\omega} \sqrt{n_l + s + 1}}{\sqrt{2}} b_{n_r; s+n_l-n_r+1}^{(2k-2l)} \\
& - \frac{\sqrt{n_l + s - 1} \sqrt{n_l + s}}{2} b_{n_r; s+n_l-n_r-2}^{(2k-2l)} + \frac{\sqrt{n_l + s + 1} \sqrt{n_l + s + 2}}{2} b_{n_r; s+n_l-n_r+2}^{(2k-2l)} \Big), \\
H_{jj'}^{(2k+2)} &= \sum_{l=0}^k \sum_{s=-2k-1}^{2k+1} b_{n_l; s}^{(2l)} \left( \left\{ 2l(2k-2l) + \frac{(n_l + s)^2 + n_l + s + 1}{2} \right. \right. \\
& + \frac{z_c^2 \omega}{2} (2n_l + 2s + 1) \Big\} b_{n_r; s+n_l-n_r}^{(2k-2l)} \\
& + \frac{z_c \sqrt{\omega} \sqrt{n_l + s}}{\sqrt{2}} (-4l + 2k - n_l - s) b_{n_r; s+n_l-n_r-1}^{(2k-2l)} \\
& + \frac{z_c \sqrt{\omega} \sqrt{n_l + s + 1}}{\sqrt{2}} (4l - 2k - n_l - s - 1) b_{n_r; s+n_l-n_r+1}^{(2k-2l)} \\
& - \frac{\sqrt{n_l + s - 1} \sqrt{n_l + s}}{2} (-4l + 2k + z_c^2 \omega) b_{n_r; s+n_l-n_r-2}^{(2k-2l)} \\
& - \frac{\sqrt{n_l + s + 1} \sqrt{n_l + s + 2}}{2} (4l - 2k + z_c^2 \omega) b_{n_r; s+n_l-n_r+2}^{(2k-2l)} \\
& + \frac{z_c \sqrt{\omega} \sqrt{n_l + s - 2} \sqrt{n_l + s - 1} \sqrt{n_l + s}}{\sqrt{2}} b_{n_r; s+n_l-n_r-3}^{(2k-2l)} \\
& + \frac{z_c \sqrt{\omega} \sqrt{n_l + s + 1} \sqrt{n_l + s + 2} \sqrt{n_l + s + 3}}{\sqrt{2}} b_{n_r; s+n_l-n_r+3}^{(2k-2l)} \\
& - \frac{\sqrt{n_l + s - 3} \sqrt{n_l + s - 2} \sqrt{n_l + s - 1} \sqrt{n_l + s}}{4} b_{n_r; s+n_l-n_r-4}^{(2k-2l)} \\
& - \frac{\sqrt{n_l + s + 1} \sqrt{n_l + s + 2} \sqrt{n_l + s + 3} \sqrt{n_l + s + 4}}{4} b_{n_r; s+n_l-n_r+4}^{(2k-2l)} \Big). \tag{26}
\end{aligned}$$

In **step 5** we sequentially evaluate the solutions  $b_{n;s}^{(2k)}$  and  $\beta_n^{(2k)}$  of the set of recurrence relations (22), (23) in each  $k$ th order ( $k = 1, \dots, k_{\max}$ ):

$$\begin{aligned}
f_{n;0}^{(2k)} &= 0 \rightarrow \beta_n^{(2k)}; \\
b_{n;s \neq 0}^{(2k)} &= f_{n;s}^{(2k)} / (2s); \\
I_{ii}^{(2k)} &= \delta_{k0} \rightarrow b_{n;0}^{(2k)}.
\end{aligned}$$

**Table 4.** The same as in Table 1, but for  $H_{jj}(r)$ 

$j, j$	$H_{11}, 10^{-2}$	$H_{22}, 10^{-2}$	$H_{33}, 10^{-2}$	$H_{44}, 10^{-1}$
$r^{-2} H_{jj}^{(2)}$	1.1562500	3.4687500	7.3437500	1.2781250
$+r^{-4} H_{jj}^{(4)}$	1.1675830	3.5283837	7.5051513	1.3110092
$+r^{-6} H_{jj}^{(6)}$	1.1677930	3.5299856	7.5110492	1.3125245
$+r^{-8} H_{jj}^{(8)}$	1.1677976	3.5300324	7.5112738	1.3125967
$+r^{-10} H_{jj}^{(10)}$	1.1677977	3.5300339	7.5112827	1.3126002
(n.v.)	1.1677977	3.5300339	7.5112831	1.3126004

In **step 6**, by substituting (12) with the coefficients  $b_{n;s}^{(2k)}$  calculated at **step 5** into the expressions for the matrix elements evaluated at **step 4** and taking into account the above definition  $r^{-2} E_j(r) = r^{-2}(\lambda_j(r) + c^2 + f) = \omega \beta_j(r)$ , i.e.  $E_j^{(2k)} = \omega \beta_j^{(2k)}$ , we produce the **output** containing the matrix elements as an expansion in inverse powers of  $r$  for  $k = 0, 1, \dots, k_{\max}$  at  $j, j' = 1, \dots, j_{\max}$ :

$$r^{-2} E_j(r) = \sum_{k=0}^{k_{\max}} \frac{E_j^{(2k)}}{r^{2k}}, \quad H_{jj'}(r) = \sum_{k=1}^{k_{\max}} \frac{H_{jj'}^{(2k)}}{r^{2k}}, \quad Q_{jj'}(r) = \sum_{k=1}^{k_{\max}} \frac{Q_{jj'}^{(2k-1)}}{r^{2k-1}}. \quad (27)$$

The calculation described above was performed by the algorithm implemented in MAPLE up to  $k_{\max} = 8$ . For example, the explicit expression of the desirable nonzero coefficients  $E_j^{(2k)}$ ,  $H_{ij}^{(2k)} = H_{ji}^{(2k)}$  and  $Q_{ij}^{(2k-1)} = -Q_{ji}^{(2k-1)}$  reads as ( $j = n + 1$ ):

$$\begin{aligned} E_j^{(0)} &= \omega(2n+1), \quad E_j^{(2)} = m^2 - \frac{1}{4} - \frac{z_c^2 \omega}{2}(2n+1) - \frac{n^2 + n + 1}{2}, \\ H_{jj}^{(2)} &= \frac{z_c^2 \omega}{2}(2n+1) + \frac{n^2 + n + 1}{2}, \\ H_{jj-1}^{(2)} &= -\frac{z_c \sqrt{\omega} \sqrt{n}}{\sqrt{2}}, \quad H_{jj-2}^{(2)} = -\frac{\omega z_c^2 \sqrt{n-1} \sqrt{n}}{2}, \\ Q_{jj-1}^{(1)} &= -\frac{z_c \sqrt{\omega} \sqrt{n}}{\sqrt{2}}, \quad Q_{jj-2}^{(1)} = \frac{\sqrt{n-1} \sqrt{n}}{2}. \end{aligned} \quad (28)$$

Tables 1–4 demonstrate the convergence of partial sums in the asymptotic expansions (27) of effective potentials  $Q_{ij}(r)$  and  $H_{ij}(r)$  calculated by the algorithm MATRA to the corresponding numerical values calculated by means of ODPEVP [9].

**Remark 3.** As follows from Eq. (28), the reduction of the problem (1) under the axial symmetry at fixed  $m$  by means of the modified angular prolate spheroidal functions (4) at large  $r$  leads to the asymptotic centrifugal term  $(E_j^{(2)} + H_{jj}^{(2)})r^{-2} = (m^2 - 1/4)r^{-2}$  in the effective potentials (9) of the set of radial equations (8). The latter term is characterized by the integer magnetic quantum number  $m$ .

#### 4 Symbolic Algorithm for Evaluation the Asymptotic Forms of Radial Solutions

In the procedure ASYMRS, using the above asymptotic expressions of the matrix elements, the asymptotic forms of the fundamental radial solutions  $\chi_{ji_o}(r)$  of Eqs. (8) at small and large values of  $r$  are calculated, and the needed boundary conditions for the reduced interval  $[r_{\min}, r_{\max}]$  are generated. Here we consider the case of large  $r$ .

We find the asymptotic solution  $\chi_{ji_o}^{as}(r)$  at large  $r \geq r_{\max}$  in the form

$$\chi_{ji_o}^{as}(r) = \left( \phi_{ji_o}(r) + \psi_{ji_o}(r) \frac{d}{dr} \right) R(p_{i_o}, r), \quad (29)$$

where  $p_{i_o}^2 = 2E - \varepsilon_{i_o}^{th}$  is the relative energy with respect to the threshold value  $\varepsilon_{i_o}^{th} = E_{i_o}^{(0)}$ , and the function  $R(p_{i_o}, r) \equiv R(p_{i_o}, r)$  satisfies the differential equation

$$\frac{d^2 R(p_{i_o}, r)}{dr^2} + \frac{2}{r} \frac{dR(p_{i_o}, r)}{dr} + \left( p_{i_o}^2 + \frac{2q}{r} - \frac{M_2}{r^2} \right) R(p_{i_o}, r) = 0 \quad (30)$$

In (30) the asymptotic centrifugal term  $M_2/r^2$  with the factor  $M_2 = m^2 - 1/4$  determines the order  $\nu$  of the desirable solution

$$R(p_{i_o}, r) \equiv R_\nu(p_{i_o}, r) = p_{i_o}^{-1/2} r^{-1} ({}_1F_\nu(p_{i_o}, r) + G_\nu(p_{i_o}, r))/2,$$

where  $F_\nu(p_{i_o}, r)$  and  $G_\nu(p_{i_o}, r)$  are the regular and irregular Coulomb functions of the half-integer order  $\nu = m - 1/2$  [11].

**Remark 4.** In the conventional 3D problem under spherical symmetry using the angular spherical harmonic functions leads to integer  $M_2 = l(l+1)$  and  $\nu = l$  [12], whereas in the 3D problem under axial symmetry the angular oblate spheroidal functions at large  $r$  lead to  $M_2 = 0$  and  $\nu = 0$  [6]. However, at small  $r$  in both cases we have  $M_2 = l(l+1)$  and  $\nu = l$ .

In the case of  $p_{i_o} = 0$  and  $q \neq 0$  the function  $R(p_{i_o}, r)$  has the form

$$R(p_{i_o}, r) = \pi^{1/2} r^{-1/2} ({}_1J_{\nu'}(\sqrt{8qr}) - Y_{\nu'}(\sqrt{8qr}))/2,$$

while in the case of  $p_{i_o} \neq 0$  and  $q = 0$  it reads as

$$R(p_{i_o}, r) = \pi^{1/2} 2^{-1/2} r^{-1/2} ({}_1J_{\nu'/2}(p_{i_o} r) - Y_{\nu'/2}(p_{i_o} r))/2.$$

Here  $J_{\nu'}$  and  $Y_{\nu'}$  are Bessel functions of the first and the second kind [10] of the order  $\nu' = \sqrt{1+4M_2}$ ,  $\nu' = 2m$  at  $M_2 = m^2 - 1/4$  and  $\nu' = 2l+1$  at  $M_2 = l(l+1)$ .

In **step 1** substituting the function (29) into Eq. (8), using (30) and extracting the coefficients for the Coulomb function and its derivative, we arrive at two coupled differential equations with respect to the unknown functions  $\phi_{ji_o}(r)$  and  $\psi_{ji_o}(r)$ .

In **step 2** we expand the functions  $\phi_{ji_o}(r)$  and  $\psi_{ji_o}(r)$  in inverse powers of  $r$ :

$$\phi_{ji_o}(r) = \sum_{k=0}^{k_{\max}} \phi_{ji_o}^{(k)} r^{-k}, \quad \psi_{ji_o}(r) = \sum_{k=0}^{k_{\max}} \psi_{ji_o}^{(k)} r^{-k}. \quad (31)$$

After substituting the expansions (27), (31) into Eqs. (8) and equating the coefficients at the same powers of  $r$ , we compute a set of recurrence relations with respect to the unknown coefficients  $\phi_{ji_o}^{(k)}$  and  $\psi_{ji_o}^{(k)}$

$$\left(p_{i_o}^2 - 2E + E_j^{(0)}\right) \phi_{ji_o}^{(k)} = f_{ji_o}^{(k)}, \quad \left(p_{i_o}^2 - 2E + E_j^{(0)}\right) \psi_{ji_o}^{(k)} = g_{ji_o}^{(k)}, \quad (32)$$

where the right-hand sides  $f_{ji_o}^{(k)}$  and  $g_{ji_o}^{(k)}$  are defined by the relations

$$f_{ji_o}^{(k)} = 2p_{i_o}^2(k-1)\psi_{ji_o}^{(k-1)} \quad (33)$$

$$\begin{aligned} & + \left((k-2)(k-3) + M_2 - \left(E_j^{(2)} + H_{jj}^{(2)}\right)\right) \phi_{ji_o}^{(k-2)} + 2q(2k-3)\psi_{ji_o}^{(k-2)} \\ & - M_2(k-2)\psi_{ji_o}^{(k-3)} - \sum_{k'=3}^k \left(E_j^{(k')} + H_{jj}^{(k')}\right) \phi_{ji_o}^{(k-k')} \\ & + \sum_{j'=1, j' \neq j}^{j_{\max}} \sum_{k'=1}^k \left[ \left((2k-k'-3)Q_{jj'}^{(k'-1)} - H_{jj'}^{(k')}\right) \phi_{j'i_o}^{(k-k')} \right. \\ & \left. + \left(2p_{i_o}^2 Q_{jj'}^{(k')} + 4qQ_{jj'}^{(k'-1)}\right) \psi_{j'i_o}^{(k-k')} \right], \end{aligned}$$

$$g_{ji_o}^{(k)} = -2(k-1)\phi_{ji_o}^{(k-1)} \quad (34)$$

$$\begin{aligned} & + M_2\phi_{ji_o}^{(k-2)} + \left(k(k-1) - \left(E_j^{(2)} + H_{jj}^{(2)}\right)\right) \psi_{ji_o}^{(k-2)} \\ & - 2M_2(k-2)\psi_{ji_o}^{(k-3)} - \sum_{k'=1}^k \left(E_j^{(k')} + H_{jj}^{(k')}\right) \psi_{ji_o}^{(k-k')} \\ & + \sum_{j'=1, j' \neq j}^{j_{\max}} \sum_{k'=1}^k \left[ \left((2k-k'+1)Q_{jj'}^{(k'-1)} - H_{jj'}^{(k')}\right) \psi_{j'i_o}^{(k-k')} - 2Q_{jj'}^{(k')} \phi_{j'i_o}^{(k-k')} \right]. \end{aligned}$$

It should be noted that these relations differ from the case of  $M_2 = 0$  [6] only by the terms containing  $M_2 = E_{i_o}^{(2)} + H_{i_o i_o}^{(2)}$ .

In **step 3** from equations (32) at  $k = 0$  we get the initial data for the recurrence procedure, including the special threshold case  $2E = E_{i_o}^{(0)}$  ( $p_{i_o}^2 = 0$ )

$$\phi_{j_0 i_o}^{(0)} = \delta_{j_0 i_o}, \quad \psi_{j_0 i_o}^{(0)} = 0, \quad p_{i_o}^2 = 2E - E_{i_o}^{(0)}. \quad (35)$$

The open channels have  $p_{i_o}^2 \geq 0$  whereas the close channels have  $p_{i_o}^2 < 0$ . Suppose that there are  $N_o \leq j_{\max}$  open channels, i.e.,  $p_{i_o}^2 \geq 0$  for  $i_o = 1, \dots, N_o$  and  $p_{i_o}^2 < 0$  for  $i_o = N_o + 1, \dots, j_{\max}$ . After substitution of (35) into (32) the recurrence relations for  $k = 1, 2, \dots, k_{\max}$  take the form

$$\left(E_j^{(0)} - E_{i_o}^{(0)}\right) \phi_{ji_o}^{(k)} = f_{ji_o}^{(k)}, \quad \left(E_j^{(0)} - E_{i_o}^{(0)}\right) \psi_{ji_o}^{(k)} = g_{ji_o}^{(k)}. \quad (36)$$



**Step 4** performs the calculation of the coefficients  $\phi_{ji_o}^{(k)}$  and  $\psi_{ji_o}^{(k)}$  by a step-by-step procedure of solving equations (36) with r.h.s. determined by (33), (34), for  $k = 1, 2, \dots, k_{\max}$ :

$$\begin{aligned} \phi_{ji_o}^{(k)} &= \frac{f_{ji_o}^{(k)}}{E_j^{(0)} - E_{i_o}^{(0)}}, \quad \psi_{ji_o}^{(k)} = \frac{g_{ji_o}^{(k)}}{E_j^{(0)} - E_{i_o}^{(0)}}, \quad j \neq i_o, \\ \{f_{i_o i_o}^{(k+1+\delta p_{i_o})} = 0, g_{i_o i_o}^{(k+1)} = 0\} &\rightarrow \{\phi_{i_o i_o}^{(k)}, \psi_{i_o i_o}^{(k)}\}, \end{aligned}$$

where  $\delta p_{i_o} = 1$  at  $p_{i_o} = 0$  (threshold case) and  $\delta p_{i_o} = 0$  at  $p_{i_o} \neq 0$ .

The calculation was performed by means of the algorithm, implemented in MAPLE up to  $k_{\max} = 8$ . Its **output** contains the elements at  $k = 0, 1, \dots, k_{\max}$ . For example, for  $k_{\max} = 1$  we have the coefficients  $\phi_{ji_o}^{(k)}$  and  $\psi_{ji_o}^{(k)}$  in the form

$$\begin{aligned} \phi_{ji_o}^{(1)} &= 0, \quad \psi_{ji_o}^{(1)} = \frac{2Q_{ji_o}^{(1)}}{E_{i_o}^{(0)} - E_j^{(0)}}, \\ \phi_{i_o i_o}^{(1)} &= 0, \quad \psi_{i_o i_o}^{(1)} = -\left(1 - \frac{\delta p_{i_o}}{3}\right) \sum_{j_0=\max(1, i_o-2), j_0 \neq i_o}^{\min(j_{\max}, i_o+2)} Q_{i_o j_0}^{(1)} \psi_{j_0 i_o}^{(1)}, \end{aligned} \quad (37)$$

and substituting the asymptotic expressions (27) into the above equation, we arrive at the explicit expression of the desirable nonzero coefficients  $\phi_{ji_o}^{(k)}$  and  $\psi_{ji_o}^{(k)}$  (for  $j_{\max} \geq i_o + 2k$ ,  $i_o = n_o + 1$ ,  $\langle \hat{z} | i_o \rangle = \sqrt[4]{\omega} \Phi_{n_o}^{(0)}(\hat{z})$ ,  $z' = z - z_c = \frac{\hat{z}}{\sqrt{\omega}} - z_c$ ):

$$\begin{aligned} \psi_{i_o-2i_o}^{(1)} &= -\frac{1}{2} \frac{\sqrt{n_o-1} \sqrt{n_o}}{2\omega} = -\frac{1}{2} \left\langle i_o - 2 \left| (z - z_c)^2 \right| i_o \right\rangle_z, \\ \psi_{i_o-1i_o}^{(1)} &= \frac{z_c \sqrt{n_o}}{\sqrt{2} \sqrt{\omega}} = -\frac{1}{2} \left\langle i_o - 1 \left| (z - z_c)^2 \right| i_o \right\rangle_z, \\ \psi_{i_o i_o}^{(1)} &= -\frac{1}{2} \left(1 - \frac{\delta p_{i_o}}{3}\right) \left(\frac{2n_o + 1}{2\omega} + z_c^2\right) = -\frac{1}{2} \left(1 - \frac{\delta p_{i_o}}{3}\right) \left\langle i_o \left| (z - z_c)^2 \right| i_o \right\rangle_z, \\ \psi_{i_o+1i_o}^{(1)} &= \frac{z_c \sqrt{n_o+1}}{\sqrt{2} \sqrt{\omega}} = -\frac{1}{2} \left\langle i_o + 1 \left| (z - z_c)^2 \right| i_o \right\rangle_z, \\ \psi_{i_o+2i_o}^{(1)} &= -\frac{1}{2} \frac{\sqrt{n_o+1} \sqrt{n_o+2}}{2\omega} = -\frac{1}{2} \left\langle i_o + 2 \left| (z - z_c)^2 \right| i_o \right\rangle_z. \end{aligned} \quad (38)$$

**Remark 5.** The obtained results correspond to the asymptotic transformation of the arguments  $r, \eta$  of the total function  $\psi_{mi_o}^{as}$  in terms of the asymptotic basis functions  $\Phi_j^{as}(\hat{z}; r)$  from (12) at fixed magnetic quantum number  $m$ :

$$\begin{aligned} \psi_{mi_o}^{as}(r, \eta) &= \sum_{j=1}^{j_{\max}} \Phi_j^{as}(\hat{z}; r) \chi_{ji_o}^{as}(r) = \sum_{j=1}^{j_{\max}} \Phi_j^{as}(\hat{z}; r) \left( \phi_{ji_o}(r) + \psi_{ji_o}(r) \frac{d}{dr} \right) R(p_{i_o}, r) \\ &= \sqrt[4]{\omega} \sqrt{r} \sum_{k=0}^{k_{\max}} r^{-k} \sum_{p=0}^k \sum_{j=1}^{j_{\max}} \Phi_j^{(p)}(\hat{z}) \left( \phi_{ji_o}^{(k-p)} + \psi_{ji_o}^{(k-p)} \frac{d}{dr} \right) R(p_{i_o}, r). \end{aligned}$$

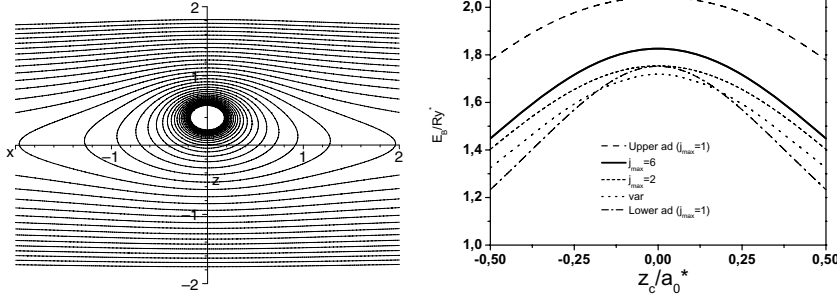


**Fig. 1.** Isolines of the potential energy surface as a function of two independent variables  $\rho, z$  with shift of center of Coulomb potential along the variable  $z$  on  $z_c = 0.4$  (left panel). The binding energy  $-E_B = 2E - \varepsilon_1^{th}$  ( $\text{Ry}^* = 5.2 \text{ meV}$ ) versus position shift of Coulomb center of impurity by variable  $z$  in interval  $z_c \in [-0.5, 0.5]$  ( $a_0^* = 102 \text{ \AA}$ ) at  $q = 1$ ,  $\omega = 3$  and  $m = 0$  (right panel). Dotted line is variational calculations [1], dash-dotted line is the adiabatic approximation ( $j_{max} = 1$ ), short-dashed line is the Kantorovich approximation (4) at  $j_{max} = 2$  basis functions, solid line is the Kantorovich approximation (4) at  $j_{max} = 6$  basis functions, dashed line is the crude adiabatic approximation ( $j_{max} = 1$ , when the diagonal adiabatic positive correction  $H_{11}(r) = 0$  is neglected).

Taking into account the orthogonality (14) and completeness  $\sum_j \langle \hat{z}' | j \rangle \langle j | \hat{z} \rangle = \delta(\hat{z}' - \hat{z})$  relations for the asymptotic basis functions  $\Phi_j^{(0)}(\hat{z}; r)$ , we obtain the desirable asymptotic form of the total wave function at  $p_{i_o} \hat{z} / (2r) \ll 1$  and  $k_{max} = 1$ :

$$\begin{aligned} \psi_{mi_o}^{(as)}(r, \eta) &= \sqrt[4]{\omega} \sqrt{r} \sum_j \langle \hat{z} | j \rangle \left[ \langle j | i_o \rangle - \frac{1}{2r} \langle j | (z - z_c)^2 | i_o \rangle \frac{d}{dr} \right] R(p_{i_o}, r) \\ &\approx \sqrt[4]{\omega} \sqrt{r} \Phi_{i_o}^{(0)}(\hat{z}) \chi_{i_o i_o}^{(as)} \left( r - \frac{(z - z_c)^2}{2r} \right) \\ &\approx \frac{\sqrt[4]{\omega}}{2(p_{i_o} \rho)^{1/2}} \Phi_{i_o}^{(0)}(\hat{z}) ({}_1F_\nu(p_{i_o}, \rho) + G_\nu(p_{i_o}, \rho)). \end{aligned} \quad (39)$$

Thus, we obtain the needed compatibility conditions for the asymptotic solutions of scattering problems in the spherical coordinates  $(r, \eta, \varphi)$  shifted by  $z_c$  along  $z$  axis and in the cylindrical coordinates  $(\rho, z, \varphi)$

$$\rho = r \sqrt{1 - (z - z_c)^2 / r^2} = r - (z - z_c)^2 / (2r) + O(r^{-2}),$$

including the regular  $F_\nu$  and irregular  $G_\nu$  Coulomb functions of the half-integer order  $\nu = m - 1/2$  from Eq. (30).

It should be noted that at large  $r$  the linearly independent functions (29) satisfy the Wronskian-type relation

$$\mathbf{W}(\mathbf{Q}(r); \chi^*(r), \chi(r)) = \frac{l}{2} \mathbf{I}_{oo}, \quad (40)$$

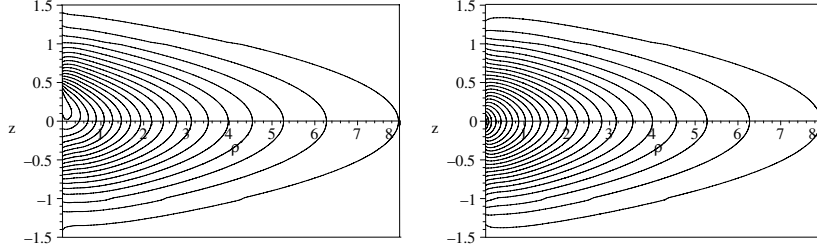


**Fig. 2.** Isolines of the ground-state wave function for the values of parameters  $q = 1$ ,  $\omega = 3$  and  $m = 0$ . Left panel:  $z_c = 0.4$ , Right panel:  $z_c = 0$ .

where  $\mathbf{W}(\bullet; \chi^*(r), \chi(r))$  is the generalized Wronskian with the long derivative defined as

$$\mathbf{W}(\bullet; \chi^*(r), \chi(r)) = r^2 \left[ (\chi^*)^T \left( \frac{d\chi}{dr} - \bullet \chi \right) - \left( \frac{d\chi^*}{dr} - \bullet \chi^* \right)^T \chi \right].$$

These relations will be used to examine the desirable accuracy of the above expansion till  $k_{\max}$  using KANTBP program implemented in FORTRAN [5,7] for numerical solving the boundary problem of discrete or continuous spectrum. The symbolic calculations of the above asymptotic expressions were performed using the codes MATRA and ASYMRS implemented in MAPLE, that generate FORTRAN codes of subroutines POTCAL and ASYMSC in KANTBP [5,7].

## 5 Test Example

The calculation for the GaAs parabolic quantum well was carried out with the values of parameters  $q = 1$ ,  $\omega = 3$ ,  $m = 0$ , and  $z_c \in [-0.5, 0.5]$  in the reduced atomic units from [1,4] by applying the programs KANTBP [5] and ODPEVP [9]. These programs implementing the finite-element method to solve the boundary-value problems (8)–(11) and (5)–(7) were applied respectively on the grids  $\Omega_r = \{0(200)1(200)5(200)100\}$  and  $\Omega_\eta = \{-1(800)1\}$  with the Lagrange elements of the order  $p = 4$  between the nodes. In the above grids  $\Omega_r$  and  $\Omega_\eta$ , the number of grid elements is shown in the parentheses.

As follows from the theorem [13], for the ground state the adiabatic approximation ( $j_{\max} = 1$ ) gives the upper bound for the energy, while in the so-called crude adiabatic approximation, when the diagonal adiabatic positive correction  $H_{11}(r) = 0$  is neglected, one gets the lower bound for the energy. The corresponding inverse estimators for the binding energy  $-E_B = 2E - \varepsilon_1^{th}$  (in units  $Ry^* = 5.2$  meV) in spherical coordinates are presented in Fig. 1. As one can see, these values are upper and lower estimates of the binding energy from the variational calculation [1]. The corresponding inverse lower estimators of the binding energy for increasing number of single-parameter basis functions  $j_{\max}$

allow one to analyze the convergence rate of the method used for solving the boundary-value problem in the two-dimensional domain (see Fig. 2). In particular, the Kantorovich approximation (4) at  $j_{max} = 10$  basis functions leads to the following inverse lower estimation of the binding energy  $E_B/Ry^* = 1.82774$ .

## 6 Conclusion

We presented the scheme for solving the boundary-value problem with discrete spectrum for a parabolic quantum well in the adiabatic representation. The upper and lower bounds for the energy of the ground state of the systems are obtained under the conditions of the shift of the Coulomb center in a given range of the parameter with respect to earlier variational estimates. It is shown that the rate of convergence depends significantly on the appropriate choice of the adiabatic basis parameterization taking the specific features of the considered problem into account. The presented results allow one to estimate the efficiency of the method and to prove the compatibility conditions (39) for asymptotic solutions of scattering problems in spherical and cylindrical coordinates. The software package developed is applicable to the investigation of semiconductor nanostructure models. Further development of the method and the software package is planned for solving the quasi-2D and quasi-1D boundary-value problems with both discrete and continuous spectrum, which are necessary for calculating the optical transition rates, channelling and transport characteristics in the models like quantum wells and quantum wires.

The authors thank Profs. V.L. Derbov, E.M. Kazaryan, A.A. Kostanyan and H.A. Sarkisyan for collaboration. The work was supported partially by RFBR (grants 07-01-00660 and 08-01-00604).

## References

1. Kazaryan, E.M., Kostanyan, A.A., Sarkisyan, H.: Impurity optical absorption in parabolic quantum well. *Physica E* 28, 423–430 (2005)
2. Voss, H.: Numerical calculation of the electronic structure for three-dimensional quantum dots. *Comput. Phys. Commun.* 174, 441–446 (2006)
3. Wang, W., Hwang, T.-M., Jang, J.-C.: A second-order finite volume scheme for three dimensional truncated pyramidal quantum dot. *Comput. Phys. Commun.* 174, 371–385 (2006)
4. Gusev, A.A., Chuluunbaatar, O., Vinitisky, S.I., Derbov, V.L., Kazaryan, E.M., Kostanyan, A.A., Sarkisyan, H.A.: Adiabatic approach to the problem of a quantum well with a hydrogen – like impurity. *Phys. Atomic Nuclei* 72, 1600–1608 (2010)
5. Chuluunbaatar, O., Gusev, A.A., Abrashkevich, A.G., Amaya-Tapia, A., Kaschiev, M.S., Larsen, S.Y., Vinitisky, S.I.: KANTBP: A program for computing energy levels, reaction matrix and radial wave functions in the coupled-channel hyperspherical adiabatic approach. *Comput. Phys. Commun.* 177, 649–675 (2007)
6. Chuluunbaatar, O., Gusev, A.A., Gerdt, V.P., Rostovtsev, V.A., Vinitisky, S.I., Abrashkevich, A.G., Kaschiev, M.S., Serov, V.V.: POTHMF: A program for computing potential curves and matrix elements of the coupled adiabatic radial equations for a hydrogen-like atom in a homogeneous magnetic field. *Comput. Phys. Commun.* 178, 301–330 (2008)

7. Chuluunbaatar, O., Gusev, A.A., Vinitsky, S.I., Abrashkevich, A.G.: KANTBP 2.0: New version of a program for computing energy levels, reaction matrix and radial wave functions in the coupled-channel hyperspherical adiabatic approach. *Comput. Phys. Commun.* 179, 685–693 (2008)
8. Gusev, A.I., Rempel, A.A.: *Nanocrystalline materials*. Cambridge Int. Sci, Cambridge (2004)
9. Chuluunbaatar, O., Gusev, A.A., Vinitsky, S.I., Abrashkevich, A.G.: ODPEVP: A program for computing eigenvalues and eigenfunctions and their first derivatives with respect to the parameter of the parametric self-adjointed Sturm-Liouville problem. Accepted in *Comput. Phys. Commun.* (2009), 10.1016/j.cpc.2009.04.017
10. Abramowitz, M., Stegun, I.A.: *Handbook of Mathematical Functions*. Dover, New York (1972)
11. Barnett, A.R.: KLEIN: Coulomb functions for real  $\lambda$  and positive energy of high accuracy. *Comput. Phys. Commun.* 24, 141–159 (1981)
12. Barnett, A.R., Feng, D.H., Steed, J.W., Goldfarb, L.J.B.: Coulomb wave functions for all real  $\eta$  and  $\rho$ . *Comput. Phys. Comm.* 8, 377–395 (1974)
13. Epstein, S.T.: Ground state energy of a molecule in adiabatic approximation. *J. Chem. Phys.* 144, 836–837 (1965)

# Symbolic-Numerical Algorithms to Solve the Quantum Tunneling Problem for a Coupled Pair of Ions

A.A. Gusev, S.I. Vitsky, O. Chuluunbaatar,  
V.P. Gerdt, and V.A. Rostovtsev

Joint Institute for Nuclear Research, Dubna, Russia  
{gooseff,chuka,gerdt,rost}@jinr.ru, vitsky@theor.jinr.ru

**Abstract.** Symbolic-numerical algorithms for solving a boundary value problem (BVP) for the 2D Schrödinger equation with homogeneous third type boundary conditions to study the quantum tunneling model of a coupled pair of nonidentical ions are described. The Kantorovich reduction of the above problem with non-symmetric long-range potentials to the BVPs for sets of the second order ordinary differential equations (ODEs) is given by expanding solution over the one-parametric set of basis functions. Symbolic algorithms for evaluation of asymptotics of the basis functions, effective potentials, and linear independent solutions of the ODEs in the form of inverse power series of independent variable at large values are given by using appropriate etalon equations. Benchmark calculation of quantum tunneling problem of coupled pair of identical ions through Coulomb-like barrier is presented.

## 1 Introduction

Quantum mechanical treatment on the basis of adiabatic description of penetration through a two-dimensional fission barrier has been studied for a long period of time [1,2]. Current interest is stimulated by the prominent papers in which the model of quantum tunneling problem of coupled pair of ions through truncated Coulomb barrier were investigated for identical mass and charges of ions [3,4]. Study of quantum tunneling problem for a coupled pair of ions with distinct mass and charges for their penetration through a nontruncated Coulomb barrier is an important problem.

The aim of this paper is to develop a symbolic-numerical algorithm (SNA) for solving the 2D boundary value problem (BVP) with homogeneous third type boundary conditions to analyze the above problem. In the framework of Kantorovich method (KM) [5], we search for a solution by means of expansion over the solution to the one-parametric eigenvalue problem calculated by program ODPEVP [6]. This way the BVP is reduced to a set of second order differential equations (ODEs) on the whole axis with homogeneous third type boundary conditions of general type. The main task here is to formulate these boundary conditions which are not invariant under reflection with respect to the  $x$ -axis.

This is because the conventionally used symmetric conditions are applicable only for identical particles. To apply the finite element method (FEM) to solving the BVP on a finite interval we need not only the adaptation of KANTBP 2.0 code [7], but also the elaboration of new symbolic algorithms to evaluate coefficients of the asymptotic expansion of both effective potential and solution to ODEs. These coefficients are needed to match evaluated asymptotic solutions with numerical ones at boundary points and extract the required matrix of transmission and the reflections amplitudes from numerical solutions.

In this paper, we present algorithms for calculation of the asymptotic expansions for solution to the eigenvalue problem with a long-range potential of general type. These asymptotic expansions are applied to evaluate the effective potentials of ODEs. The next step is to design a new algorithm for evaluation of the asymptotic expansion of linear independent solutions to ODEs. This distinguish algorithm is substantially different from the previously elaborated one [8]. Instead of applying an expansion over the solution to an etalon equation, we propose to use an appropriate etalon equation with a long-range potential in the form of the inverse power series that provides a more economical and universal way to generate relevant recurrence relations and the corresponding FORTRAN subroutines.

The paper is organized as follows. In Section 2, the problem statement is done. In Section 3, the BVP is formulated for ODEs. Here the symbolic algorithms for the evaluation of asymptotic expansions of solutions to parametric BVP, for calculation of the corresponding integrals, and for the asymptotic expansion of linear independent solutions to ODEs together with their implementation in Maple are described. Section 4 is devoted to the benchmark calculation of the penetration coefficients for tunneling of the identical ions through long-range Coulomb like barriers. In Conclusion, we summarize the results and discuss the future applications of our SNAs.

## 2 Problem Statement

Wave function  $\Psi(x, y)$  of model of heavy ion pair connected with oscillator potential scattering in the center mass coordinate system through Coulomb barriers satisfies the two-dimensional (2D) Schrödinger equation [3]:

$$\left\{ -\frac{\partial^2}{\partial y^2} - \frac{\partial^2}{\partial x^2} + x^2 + 2(U_1(x_1) + U_2(x_2) - E) \right\} \Psi(x, y) = 0, \quad (1)$$

where  $x_1 = s_2 y + s_1 x$ ,  $x_2 = s_2 y - s_3 x$  are variables in the laboratory coordinate system, parameters  $s_2 = \frac{\sqrt{m_1 m_2}}{M}$ ,  $s_1 = \frac{m_2}{M}$ ,  $s_3 = \frac{m_1}{M}$  are defined via masses of ions  $m_1$  and  $m_2$  and total mass  $M = m_1 + m_2$  and reduced mass  $\mu = \frac{m_1 m_2}{M}$  in the oscillator units of length  $x_{osc} = \sqrt{\frac{\hbar}{\mu \omega}}$  and energy  $E_{osc} = \hbar \omega$  ( $\omega$  is oscillator frequency). We choose barrier potential  $U_i(x_i)$  of ions labelled by  $i = 1, 2$  with charges  $\tilde{Z}_i > 0$  in the form of the truncated Coulomb potential cut off on small  $0 < \bar{x}_{min} < 1$  and large  $\bar{x}_{max} > 1$  distances from origin,

$$U_i(x_i) = \left\{ \frac{\hat{Z}_i}{\bar{x}_{\min}} - \frac{\hat{Z}_i}{\bar{x}_{\max}}, |x_i| \leq \bar{x}_{\min}; \frac{\hat{Z}_i}{|x_i|} - \frac{\hat{Z}_i}{\bar{x}_{\max}}, |x_i| > \bar{x}_{\min}; 0, |x_i| > \bar{x}_{\max} \right\}, \quad (2)$$

or the Coulomb-like potentials that depend on the integer parameter  $s \geq 2$  and truncation parameter  $\bar{x}_{\min} > 0$  and defined as

$$U_i(x_i) = \hat{Z}_i(|x_i|^s + \bar{x}_{\min}^s)^{-1/s}. \quad (3)$$

In both cases, the sum of barrier potential functions  $U(x, y) = U_1(x_1) + U_2(x_2)$  has asymptotic form

$$U(x, y) \rightarrow \sigma_y \frac{Z_{12}}{y} + O(y^{-3}), \quad y \rightarrow \pm\infty, \quad (4)$$

where  $\sigma_y = 1$  if  $y > 0$  and  $\sigma_y = -1$  if  $y < 0$ ;  $Z_{12} = 0$  for Eq. (2) and  $Z_{12} = (\hat{Z}_1 + \hat{Z}_2)/s_2$  for Eq. (3).

The asymptotic boundary conditions for the solution  $\Psi(y, x) = \{\Psi_{i_o}(y, x)\}_{i_o=1}^{N_o}$  with direction  $v = \rightarrow$  can be written in the obvious form

$$\begin{aligned} \Psi_{i_o}(y \rightarrow -\infty, x) &\rightarrow B_{i_o}^{(0)}(x) \frac{\exp\left(i\left(p_{i_o}y - \sigma_y \frac{Z_{12}}{p_{i_o}} \ln(2p_{i_o}|y|)\right)\right)}{\sqrt{p_{i_o}}} \\ &+ \sum_{j=1}^{N_o} B_j^{(0)}(x) \frac{\exp\left(-i\left(p_jy - \sigma_y \frac{Z_{12}}{p_j} \ln(2p_j|y|)\right)\right)}{\sqrt{p_j}} R_{ji_o}, \\ \Psi_{i_o}(y \rightarrow +\infty, x) &\rightarrow \sum_{j=1}^{N_o} B_j^{(0)}(x) \frac{\exp\left(i\left(p_jy - \sigma_y \frac{Z_{12}}{p_j} \ln(2p_j|y|)\right)\right)}{\sqrt{p_j}} T_{ji_o}, \\ \Psi_{i_o}(y, x \rightarrow \pm\infty) &\rightarrow 0. \end{aligned} \quad (5)$$

Here  $N_o$  is the number of open channels at fixed energy  $2E = p^2 + \varepsilon_{i_o}^{(0)} > 0$ ,  $T_{ji_o}$  and  $R_{ji_o}$  are unknown transition and reflections amplitudes,  $B_j^{(0)}(x)$  are the basis functions of oscillator with energy  $\varepsilon_j^{(0)} = 2n + 1$  at  $n \geq 0$ ,  $j = n + 1$

$$\left\{ -\frac{\partial^2}{\partial x^2} + x^2 - \varepsilon_j^{(0)} \right\} B_j^{(0)}(x) = 0, \quad \int_{-\infty}^{+\infty} B_j^{(0)}(x) B_{j'}^{(0)}(x) dx = \delta_{jj'}. \quad (6)$$

### 3 Formulation of BVP for a Set of the Kantorovich ODEs

We construct a desired solution of the BVP in the form of Kantorovich's expansion:

$$\Psi_{i'}(x, y) = \sum_{j=1}^N B_j(x; y) \chi_{ji'}(y). \quad (7)$$



The basis functions  $B_j(x; y)$  of the fast variable  $x$  and the potential curves  $E_i(y)$  that depend continuously on the slow variable  $y$  as a parameter are chosen as solutions of the BVPs for the equation on grid  $\Omega_x\{x_{\min}(y), x_{\max}(y)\}$

$$\left\{ -\frac{d^2}{dx^2} + x^2 + 2U(x, y) - \varepsilon_j(y) \right\} B_j(x; y) = 0, \quad (8)$$

which are subject to the boundary, normalization, and orthogonality conditions

$$B_j(x_{\min}(y); y) = B_j(x_{\max}(y); y) = 0, \quad \langle B_i | B_j \rangle = \int_{x_{\min}(y)}^{x_{\max}(y)} B_i(x; y) B_j(x; y) dx = \delta_{ij}. \quad (9)$$

By substituting (7) into (1)–(5) and by taking average over (9), we obtain the BVP for a set of  $N$  coupled ODEs that describes the slow subsystem for the partial solutions  $\chi^{(i')}(y) = (\chi_1^{(i')}, \dots, \chi_N^{(i')})^T$ :

$$\{\mathbf{H} - 2E\mathbf{I}\} \chi^{(i')}(y) = 0, \quad \mathbf{H} = -\mathbf{I} \frac{d^2}{dy^2} + \mathbf{V}(y) + \mathbf{Q}(y) \frac{d}{dy} + \frac{d\mathbf{Q}(y)}{dy}. \quad (10)$$

Here  $\mathbf{I}$  is the unit matrix,  $\mathbf{V}(y)$  and  $\mathbf{Q}(y)$  are the effective potential  $N \times N$  matrices:

$$V_{ij}(y) = \varepsilon_j(y) \delta_{ij} + H_{ij}(y), \quad H_{ij}(y) = \int_{x_{\min}(y)}^{x_{\max}(y)} \frac{\partial B_i(x; y)}{\partial y} \frac{\partial B_j(x; y)}{\partial y} dx, \quad (11)$$

$$Q_{ij}(y) = - \int_{x_{\min}(y)}^{x_{\max}(y)} B_i(x; y) \frac{\partial B_j(x; y)}{\partial y} dx.$$

that is calculated numerically by means of program ODPEVP [6]. The boundary conditions at  $y = y_{\min} \ll -1$  and  $y = y_{\max} \gg 1$  are given by

$$\left. \frac{d\Phi(y)}{dy} \right|_{y=y_{\min}} = \mathcal{R}(y_{\min}) \Phi(y_{\min}), \quad \left. \frac{d\Phi(y)}{dy} \right|_{y=y_{\max}} = \mathcal{R}(y_{\max}) \Phi(y_{\max}), \quad (12)$$

where  $\mathcal{R}(y)$  is an unknown  $N \times N$  nonsymmetric matrix-function,  $\Phi(y) = \{\chi^{(i_o)}(y)\}_{i_o=1}^{N_o}$  is the required  $N \times N_o$  matrix solution, and  $N_o$  is the number of open channels,  $N_o = \max_{2E \geq \varepsilon_j} j \leq N$  that is calculated numerically by means of the program KANTBP 3.0. It is a modified version of the program KANTBP 2.0 [7] including matching asymptotic solutions evaluated in the next sections with numerical ones at boundary points  $y = y_{\min} \ll -1$  and  $y = y_{\max} \gg 1$  in (12).

The matrix solution  $\Phi_v(y) = \Phi(y)$  that describes the incidence of the particle and its scattering, having the asymptotic form “incident wave + outgoing waves”, is

$$\Phi_v(y \rightarrow \pm\infty) = \begin{cases} \begin{cases} \mathbf{X}^{(+)}(y)\mathbf{T}_v, & y > 0, \\ \mathbf{X}^{(+)}(y) + \mathbf{X}^{(-)}(y)\mathbf{R}_v, & y < 0, \end{cases} & v = \rightarrow, \\ \begin{cases} \mathbf{X}^{(-)}(y) + \mathbf{X}^{(+)}(y)\mathbf{R}_v, & y > 0, \\ \mathbf{X}^{(-)}(y)\mathbf{T}_v, & y < 0, \end{cases} & v = \leftarrow, \end{cases} \quad (13)$$

with  $\mathbf{R}_v$  and  $\mathbf{T}_v$  being the reflection and transmission  $N_o \times N_o$  matrices,  $v$  denotes the initial direction of the particle motion along the  $y$ -axis. Here the leading term of the asymptotic rectangle-matrix functions  $\mathbf{X}^{(\pm)}(y)$  has the form

$$X_{ji_o}^{(\pm)}(y) \rightarrow p_j^{-1/2} \exp\left(\pm i\left(p_j y - \sigma_y \frac{Z_{12}}{p_j} \ln(2p_j|y|)\right)\right) \delta_{ji_o}, \quad (14)$$

$$p_{i_o} = \sqrt{2E - \varepsilon_{i_o}}, \quad j = 1, \dots, N, \quad i_o = 1, \dots, N_o.$$

The matrix solution  $\Phi_v(y, E)$  is normalized so that

$$\int_{-\infty}^{\infty} \Phi_{v'}^\dagger(y, E') \Phi_v(y, E) dy = 2\pi \delta(E' - E) \delta_{v'v} \mathbf{I}_{o_o}, \quad (15)$$

where  $\mathbf{I}_{o_o}$  is the identity  $N_o \times N_o$  matrix.

Suppose that a set of linear independent regular square-solutions  $\Phi_v^{\text{reg}}(y) = \{\chi_{i'}^{\text{reg}}(y)\}_{i'=1}^N$  for a problem under consideration with components  $\chi_{\text{reg}}^{(i')}(y) = (\chi_{1i'}^{\text{reg}}(y), \dots, \chi_{Ni'}^{\text{reg}}(y))^T$  is known at  $y > 0, v = \rightarrow$  or  $y < 0, v = \leftarrow$ , i.e.,

$$\begin{aligned} \Phi_{\rightarrow}^{\text{reg}}(y) &= \tilde{\mathbf{X}}^{(+)}(y), \quad y > 0, \quad \Phi_{\leftarrow}^{\text{reg}}(y) = \tilde{\mathbf{X}}^{(-)}(y), \quad y < 0. \\ \tilde{X}_{ji_o}^{(\pm)}(y) &= X_{ji_o}^{(\pm)}(y), \quad j = 1, \dots, N, \quad i_o = 1, \dots, N_o. \end{aligned} \quad (16)$$

In a case of some channels are closed, we must use additional leading terms of regular asymptotic functions correspondingly at  $z > 0$  and  $z < 0$

$$\begin{aligned} \tilde{X}_{ji_c}^{(\pm)}(y) &\rightarrow q_j^{-1/2} \exp\left(\mp \left(q_j y + \sigma_y \frac{Z_{12}}{q_j} \ln(2q_j|y|)\right)\right) \delta_{ji_c}, \\ q_{i_c} &= \sqrt{\varepsilon_{i_c} - 2E}, \quad j = 1, \dots, N, \quad i_c = N_o + 1, \dots, N. \end{aligned} \quad (17)$$

In this case, the required part of  $\mathcal{R}_{\rightarrow}(y)$  at  $y = y_{\max} > 0$  and  $\mathcal{R}_{\rightarrow}(y)$  matrix  $y = y_{\min} < 0$  can be found via the known set of linear independent regular solutions  $\Phi_v^{\text{reg}}(y)$

$$\mathcal{R}_v(y) = \frac{d\Phi_v^{\text{reg}}(y)}{dy} (\Phi_v^{\text{reg}}(y))^{-1}. \quad (18)$$

These matrix-functions  $\mathcal{R}_v(y)$  by dimension of  $N \times N$  are used for calculating numerical solutions  $\Phi_v^h(y)$  of BVP (10)–(12).

By using  $\Phi_{\rightarrow}^h(y_{\max})$  and  $\mathcal{R}_{\rightarrow}(y)$  numerically calculated with KANTBP 3.0, we obtain the following matrix equations for the reflection  $\mathbf{R}_{\rightarrow}$  and transmission  $\mathbf{T}_{\rightarrow}$  matrices

$$\begin{aligned}\mathbf{Y}_{\rightarrow}^{(-)}(y_{\min})\mathbf{R}_{\rightarrow} &= -\mathbf{Y}_{\rightarrow}^{(+)}(y_{\min}), \quad \mathbf{X}^{(+)}(y_{\max})\mathbf{T}_{\rightarrow} = \boldsymbol{\Phi}_{\rightarrow}^h(y_{\max}), \\ \mathbf{Y}_{\rightarrow}^{(\pm)}(y) &= \frac{d\mathbf{X}^{(\pm)}(y)}{dy} - \mathcal{R}_{\rightarrow}(y)\mathbf{X}^{(\pm)}(y).\end{aligned}\quad (19)$$

Note that, when some channels are closed, the  $\mathbf{Y}_{\rightarrow}^{(\pm)}(y)$  and  $\mathbf{X}^{(-)}(y)$  are rectangular  $N \times N_o$  matrices. The reflection  $\mathbf{R}_{\rightarrow}$  and transmission  $\mathbf{T}_{\rightarrow}$  matrices are evaluated in terms of the pseudoinverse matrices of  $\mathbf{Y}_{\rightarrow}^{(-)}(y_{\min})$  and  $\mathbf{X}^{(+)}(y_{\max})$

$$\begin{aligned}\mathbf{R}_{\rightarrow} &= -\left(\left(\mathbf{Y}_{\rightarrow}^{(-)}(y_{\min})\right)^T \mathbf{Y}_{\rightarrow}^{(-)}(y_{\min})\right)^{-1} \left(\mathbf{Y}_{\rightarrow}^{(-)}(y_{\min})\right)^T \mathbf{Y}_{\rightarrow}^{(+)}(y_{\min}), \\ \mathbf{T}_{\rightarrow} &= \left(\left(\mathbf{X}^{(+)}(y_{\max})\right)^T \mathbf{X}^{(+)}(y_{\max})\right)^{-1} \left(\mathbf{X}^{(+)}(y_{\max})\right)^T \boldsymbol{\Phi}_{\rightarrow}^h(y_{\max}).\end{aligned}\quad (20)$$

Having  $\boldsymbol{\Phi}_{\leftarrow}^h(y_{\min})$  and  $\mathcal{R}_{\leftarrow}(y)$  numerically calculated with KANTBP 3.0, we obtain the following matrix equations for the reflection  $\mathbf{R}_{\leftarrow}$  and transmission  $\mathbf{T}_{\leftarrow}$  matrices:

$$\begin{aligned}\mathbf{Y}_{\leftarrow}^{(+)}(y_{\max})\mathbf{R}_{\leftarrow} &= -\mathbf{Y}_{\leftarrow}^{(-)}(y_{\max}), \quad \mathbf{X}^{(-)}(y_{\min})\mathbf{T}_{\leftarrow} = \boldsymbol{\Phi}_{\leftarrow}^h(y_{\min}), \\ \mathbf{Y}_{\leftarrow}^{(\pm)}(y) &= \frac{d\mathbf{X}^{(\pm)}(y)}{dy} - \mathcal{R}_{\leftarrow}(y)\mathbf{X}^{(\pm)}(y).\end{aligned}\quad (21)$$

Therefore, using the pseudoinverse matrices of  $\mathbf{Y}_{\leftarrow}^{(+)}(y)$  and  $\mathbf{X}^{(-)}(y)$ , we obtain the following formulae:

$$\begin{aligned}\mathbf{R}_{\leftarrow} &= -\left(\left(\mathbf{Y}_{\leftarrow}^{(+)}(y_{\max})\right)^T \mathbf{Y}_{\leftarrow}^{(+)}(y_{\max})\right)^{-1} \left(\mathbf{Y}_{\leftarrow}^{(+)}(y_{\max})\right)^T \mathbf{Y}_{\leftarrow}^{(-)}(y_{\max}), \\ \mathbf{T}_{\leftarrow} &= \left(\left(\mathbf{X}^{(-)}(y_{\min})\right)^T \mathbf{X}^{(-)}(y_{\min})\right)^{-1} \left(\mathbf{X}^{(-)}(y_{\min})\right)^T \boldsymbol{\Phi}_{\leftarrow}^h(y_{\min}).\end{aligned}\quad (22)$$

Let us now rewrite Eq. (13) in the matrix form at  $y_{\pm} \rightarrow \pm\infty$

$$\begin{pmatrix} \boldsymbol{\Phi}_{\rightarrow}(y_{+}) & \boldsymbol{\Phi}_{\leftarrow}(y_{+}) \\ \boldsymbol{\Phi}_{\rightarrow}(y_{-}) & \boldsymbol{\Phi}_{\leftarrow}(y_{-}) \end{pmatrix} = \begin{pmatrix} \mathbf{0} & \mathbf{X}^{(-)}(y_{+}) \\ \mathbf{X}^{(+)}(y_{-}) & \mathbf{0} \end{pmatrix} + \begin{pmatrix} \mathbf{0} & \mathbf{X}^{(+)}(y_{+}) \\ \mathbf{X}^{(-)}(y_{-}) & \mathbf{0} \end{pmatrix} \mathbf{S}, \quad (23)$$

where the symmetric and unitary scattering matrix  $\mathbf{S}$  is composed of the transmission and reflection matrices from (20) and (22)

$$\mathbf{S} = \begin{pmatrix} \mathbf{R}_{\rightarrow} & \mathbf{T}_{\leftarrow} \\ \mathbf{T}_{\rightarrow} & \mathbf{R}_{\leftarrow} \end{pmatrix}, \quad \mathbf{S}\mathbf{S}^{\dagger} = \mathbf{S}^{\dagger}\mathbf{S} = \mathbf{I}. \quad (24)$$

In addition, it should be noted that the functions  $\mathbf{X}^{(\pm)}(y)$  satisfy relations

$$\mathbf{Wr}(\mathbf{Q}(y); \mathbf{X}^{(\mp)}(y), \mathbf{X}^{(\pm)}(y)) = \pm 2i\mathbf{I}_{oo}, \quad \mathbf{Wr}(\mathbf{Q}(y); \mathbf{X}^{(\pm)}(y), \mathbf{X}^{(\pm)}(y)) = 0, \quad (25)$$

where  $\mathbf{Wr}(\bullet; \mathbf{a}(y), \mathbf{b}(y))$  is a generalized Wronskian with a long derivative defined as

$$\mathbf{Wr}(\bullet; \mathbf{a}(y), \mathbf{b}(y)) = \mathbf{a}^T(y) \left( \frac{d\mathbf{b}(y)}{dy} - \bullet \mathbf{b}(y) \right) - \left( \frac{d\mathbf{a}(y)}{dy} - \bullet \mathbf{a}(y) \right)^T \mathbf{b}(y). \quad (26)$$

*Remark 1.* This Wronskian will be used below to estimate a desirable precision of the above expansion as well as the symmetry and unitarity properties of the scattering matrix  $\mathbf{S}$  in (24).

## Algorithm 1. Evaluating Effective Potential Asymptotics

**Input.** We evaluate the asymptotics of effective potentials (11) at large  $|y|$  via the asymptotics of solutions to the eigenvalue problem (8), (9) at  $|y/x| \gg 1$ ,

$$\left( \frac{d^2}{dx^2} + x^2 + 2U(x, y) - \varepsilon_j(y) \right) B_j(x; y) = 0, \quad \int_{x_{\min}(y)}^{x_{\max}(y)} B_i(x; y) B_j(x; y) dx = \delta_{ij} \quad (27)$$

with the Coulomb-like potential

$$2U(x, y) = 2\hat{Z}_1 / \sqrt[5]{(s_2 y + s_1 x)^s + \bar{x}_{\min}^s} + 2\hat{Z}_2 / \sqrt[5]{(s_2 y - s_3 x)^s + \bar{x}_{\min}^s}. \quad (28)$$

At **step 1** we find  $B_j(x; y)$  and  $\varepsilon_j(y)$  as a series expansion with  $j = n + 1$

$$B_j(x; y) = \sum_{k=0}^{k_{\max}} \frac{B_n^{(k)}(x)}{y^k}, \quad \varepsilon_j(y) = \sum_{k=0}^{k_{\max}} \frac{\varepsilon_n^{(k)}}{y^k}. \quad (29)$$

Substituting (29) to (27) and equating coefficients of the same powers of  $y$ , we arrive at a system of recurrence differential equations for evaluating coefficients  $B_n^{(k)}(x)$  and  $\varepsilon_n^{(k)}$ ,  $k = 1, \dots, k_{\max}$ :

$$L(n)B_n^{(k)}(x) = f_n^{(k)}(x), \quad L(n) = -\frac{d^2}{dx^2} - (2n+1)x^2, \quad (30)$$

with the initial data  $\varepsilon_n^{(0)} = 2n+1$  and with  $B_n^{(0)}(x)$  as the known solution of the problem

$$L(n)B_n^{(0)}(x) = 0, \quad \int_{-\infty}^{+\infty} B_n^{(0)}(x) B_{n'}^{(0)}(x) dx = \delta_{nn'}. \quad (31)$$

In Eqs. (30), the right-hand sides  $f_n^{(k)}(x)$  are defined by relations

$$f_n^{(k)}(x) = \sum_{p=1}^k (U^{(p)}(x) - \varepsilon_n^{(p)}) B^{(k-p)}(x),$$

**Table 1.** Values of the partial sums (41) for  $V_{jj} \equiv V_{jj}(y)$  from (11) depending on  $k_{\max}$  for  $s_1 = s_2 = s_3 = 1/2$ ,  $\bar{x}_{\min} = 0.1$ ,  $s = 8$ ,  $\hat{Z}_1 = \hat{Z}_2 = 1$ ,  $y = y_2^{\text{match}} = 12.5$ . The last row contains the corresponding numerical values (n.v.).

$k_{\max}$	$V_{11}$	$V_{22}$	$V_{33}$	$V_{44}$	$V_{55}$	$V_{66}$
0	1.000000000	3.000000000	5.000000000	7.000000000	9.000000000	11.00000000
1	1.640000000	3.640000000	5.640000000	7.640000000	9.640000000	11.64000000
2	1.640000000	3.640000000	5.640000000	7.640000000	9.640000000	11.64000000
3	1.642048000	3.646144000	5.650240000	7.654336000	9.658432000	11.66252800
4	1.642048000	3.646144000	5.650240000	7.654336000	9.658432000	11.66252800
5	1.642067661	3.646242304	5.650495590	7.654827520	9.659238093	11.66372731
6	1.642065564	3.646236013	5.650485105	7.654812840	9.659219218	11.66370424
7	1.642065878	3.646238215	5.650492969	7.654832658	9.659259798	11.66377691
8	1.642065798	3.646237812	5.650491922	7.654830645	9.659256497	11.66377199
9	1.642065809	3.646237888	5.650492232	7.654831584	9.659258797	11.66377684
10	1.642065806	3.646237868	5.650492158	7.654831394	9.659258408	11.66377614
11	1.642065807	3.646237871	5.650492174	7.654831450	9.659258560	11.66377650
12	1.642065807	3.646237870	5.650492169	7.654831434	9.659258520	11.66377642
nv	1.642065807	3.646237871	5.650492170	7.654831437	9.659258529	11.66377644

where the coefficients  $U^{(j)}(x)$  are determined by Taylor expansion of (28) at large  $y$

$$2U(x, y) = \sum_{k=1}^{k_{\max}} \frac{U^{(k)}(x)}{y^k}, \quad (32)$$

$$\begin{aligned}
U^{(1)}(x) &= \sigma_y 2(\hat{Z}_1 + \hat{Z}_2)/s_2, & U^{(2)}(x) &= \sigma_y 2x(\hat{Z}_1 s_1 - \hat{Z}_2 s_3)/s_2^2, \\
U^{(3)}(x) &= \sigma_y 2x^2(\hat{Z}_1 s_1^2 + \hat{Z}_2 s_3^2)/s_2^3, & U^{(4)}(x) &= \sigma_y 2x^3(\hat{Z}_1 s_1^3 - \hat{Z}_2 s_3^3)/s_2^4, \\
U^{(5)}(x) &= \sigma_y 2x^4(\hat{Z}_1 s_1^4 + \hat{Z}_2 s_3^4)/s_2^5, & U^{(6)}(x) &= \sigma_y 2x^5(\hat{Z}_1 s_1^5 - \hat{Z}_2 s_3^5)/s_2^6, \\
U^{(7)}(x) &= \sigma_y 2x^6(\hat{Z}_1 s_1^6 + \hat{Z}_2 s_3^6)/s_2^7, & U^{(8)}(x) &= \sigma_y 2x^7(\hat{Z}_1 s_1^7 - \hat{Z}_2 s_3^7)/s_2^8, \\
U^{(9)}(x) &= \sigma_y 2x^8(\hat{Z}_1 s_1^8 + \hat{Z}_2 s_3^8)/s_2^9 - \sigma_y \bar{x}_{\min}^8(\hat{Z}_1 + \hat{Z}_2)/(4s_2^9), \\
U^{(10)}(x) &= \sigma_y 2x^9(\hat{Z}_1 s_1^9 - \hat{Z}_2 s_3^9)/s_2^{10} - \sigma_y 9x\bar{x}_{\min}^8(\hat{Z}_1 - \hat{Z}_2)/(8s_2^{10}).
\end{aligned}$$

The orthogonality and normalization conditions follow from (27) and (29)

$$I_{jj'}^{(k)} = \sum_{l=0}^k \int_{-\infty}^{\infty} B_{n_l}^{(l)}(x) B_{n_r}^{(k-l)}(x) dx = \delta_{k0} \delta_{n_l n_r} \quad (33)$$

where  $n_l = j - 1$ ,  $n_r = j' - 1$ .

We find the asymptotics of matrix elements  $H_{jj'}(y)$  and  $Q_{jj'}(y)$  from (11) in the form of expansions

$$Q_{jj'}(y) = \sum_{k=1}^{k_{\max}} \frac{Q_{jj'}^{(k)}}{y^k}, \quad H_{jj'}(y) = \sum_{k=2}^{k_{\max}} \frac{H_{jj'}^{(k)}}{y^k}. \quad (34)$$

**Table 2.** The same as in Table 1, but for  $Q_{jj'} \equiv Q_{jj'}(y)$  at  $j \neq j'$ 

$k_{\max}$	$Q_{13}, 10^{-4}$	$Q_{15}, 10^{-6}$	$Q_{24}, 10^{-4}$	$Q_{26}, 10^{-6}$	$Q_{35}, 10^{-4}$	$Q_{46}, 10^{-4}$
3	0.00000000	0.000000	0.00000000	0.000000	0.00000000	0.00000000
4	1.73778562	0.000000	3.00993299	0.000000	4.25668806	5.49536066
5	1.73778562	0.000000	3.00993299	0.000000	4.25668806	5.49536066
6	1.79339476	1.605297	3.17046275	3.589554	4.57452077	6.02291528
7	1.78627679	1.605297	3.15813407	3.589554	4.55708537	6.00040628
8	1.78814526	1.713173	3.16568539	3.927259	4.57691814	6.04176657
9	1.78761568	1.705283	3.16415663	3.909616	4.57389135	6.03674256
10	1.78771659	1.711496	3.16457995	3.934625	4.57519301	6.03996585
11	1.78768515	1.710423	3.16444912	3.931266	4.57484597	6.03923893
12	1.78769198	1.710818	3.16447978	3.933127	4.57494688	6.03951537
nv	1.78769041	1.710734	3.16447143	3.932815	4.57491909	6.03944626

Here the coefficients  $Q_{jj'}^{(k)}$  and  $H_{jj'}^{(k)}$  are defined by the relations

$$\begin{aligned}
 Q_{jj'}^{(k)} &= - \sum_{l=0}^{k-1} \int_{-\infty}^{+\infty} B_{n_l}^{(l)}(x) \hat{Q} B_{n_r}^{(k-1-l)}(x) dx, \quad \hat{Q} B_{n_l}^{(l)}(x) = l B_{n_l}^{(l)}(x), \\
 H_{jj'}^{(k)} &= \sum_{l=0}^{k-2} \int_{-\infty}^{+\infty} \hat{Q} B_{n_l}^{(l)}(x) \hat{Q} B_{n_r}^{(k-2-l)}(x) dx.
 \end{aligned} \tag{35}$$

At **step 2**, we construct  $B_n^{(k)}(x)$  as the expansion with unknown coefficients  $b_{n;s}^{(k)}$

$$B_n^{(k)}(x) = \sum_{s=-M(k)}^{M(k)} b_{n;s}^{(k)} B_{n+s}^{(0)}(y). \tag{36}$$

Here  $B_v^{(0)}(x)$  are solutions to (31) in terms of the Hermite polynomials [9]

$$B_v^{(0)}(x) = \frac{H_v(x) \exp(-x^2/2)}{\sqrt[4]{\pi} \sqrt{2^v v!}}.$$

By means of the well-known recurrence relation for Hermite polynomials  $H_v(x)$  we obtain the recurrence relations for basis functions  $B_v^{(0)}(x)$ :

$$\begin{aligned}
 x B_v^{(0)}(x) &= + \frac{\sqrt{v+1}}{\sqrt{2}} B_{v+1}^{(0)}(x) + \frac{\sqrt{v}}{\sqrt{2}} B_{v-1}^{(0)}(x), \\
 L(n) B_{n+s}^{(0)}(x) &\equiv \left( -\frac{d^2}{dx^2} - (2n+1)x^2 \right) B_{n+s}^{(0)}(x) = 2s B_{n+s}^{(0)}(x).
 \end{aligned} \tag{37}$$

From (30), (32), and (37) we have the needed value of  $M(k) = 2k+1$  in expansion (36) to provide calculation of nonzero terms only.

Substituting (36) to (30), taking into account (37), and equating coefficients of the identical powers of  $y$ , we arrive at a set of recurrence relations for evaluation of coefficients  $E_n^{(k)}$  and  $b_{n;s}^{(k)}$

$$2sb_{n;s}^{(k)} = f_{n;s}^{(k)}, \quad I_{jj'}^{(k)} = \sum_{l=0}^k \sum_{s=-2k-1}^{2k+1} b_{n_l;s}^{(l)} b_{n_r;s+n_l-n_r}^{(k-l)} = \delta_{k0} \delta_{n_l n_r}, \quad (38)$$

with initial data  $\varepsilon_n^{(0)} = 2n + 1$  and  $b_{n;s}^{(0)} = \delta_{s0}$ .

The corresponding coefficients  $Q_{jj'}^{(k)}$  and  $H_{jj'}^{(k)}$  in (35) have the following explicit form:

$$Q_{jj+t}^{(k)}(y) = - \sum_{k'=0}^{k-1} \sum_{s=\max(-k+1, k'-k+1-t)}^{\min(k-1, k-1-k'-t)} (k-1-k') b_{n;n+s}^{(k')} b_{n+t;n+s}^{(k-1-k')},$$

$$H_{jj+t}^{(k)}(y) = \sum_{k'=0}^{k-2} \sum_{s=\max(-k+2, k'-k+2-t)}^{\min(k-2, k-2-k'-t)} k'(k-2-k') b_{n;n+s}^{(k')} b_{n+t;n+s}^{(k-2-k')}. \quad (39)$$

At **step 3**, we evaluate sequentially the solutions  $b_{n;s}^{(k)}$  and  $\varepsilon_n^{(k)}$  to the set of recurrence relations (38) for each  $k$ th order ( $k = 1, \dots, k_{\max}$ ):

$$f_{n;0}^{(k)} = 0 \rightarrow \varepsilon_n^{(k)}; \quad b_{n;s \neq 0}^{(k)} = f_{n;s}^{(k)} / (s); \quad I_{ii}^{(k)} = \delta_{k0} \rightarrow b_{n;0}^{(k)}. \quad (40)$$

At **step 4**, we substitute coefficients  $b_{n;s}^{(k)}$  calculated in (40) into the expressions for the matrix elements (34), (39) evaluated at **step 2** and taking into account coefficients  $\varepsilon_j^{(k)}$  calculated in (40). In doing so we produce the **output** containing the matrix elements as a series expansion of inverse powers of  $y$  for  $k = 0, 1, \dots, k_{\max}$  at  $j, j' = 1, \dots, N$  ( $\varepsilon_j^{(k < 0)} = H_{jj'}^{(k < 2)} = Q_{jj'}^{(k < 1)} = 0$ ):

$$\varepsilon_j(y) = \sum_{k=0}^{k_{\max}} \frac{\varepsilon_j^{(k)}}{y^k}, \quad H_{jj'}(y) = \sum_{k=2}^{k_{\max}} \frac{H_{jj'}^{(k)}}{y^k}, \quad Q_{jj'}(y) = \sum_{k=1}^{k_{\max}} \frac{Q_{jj'}^{(k)}}{y^k}. \quad (41)$$

The above described calculation was performed by the algorithm implemented in MAPLE up to  $k_{\max} = 12$ . For example, the explicit expression of the desirable nonzero coefficients  $\varepsilon_j^{(k)}$ ,  $H_{ij}^{(k)} = H_{ji}^{(k)}$  and  $Q_{ij}^{(k)} = -Q_{ji}^{(k)}$  reads as ( $j = n + 1$ ):

$$\begin{aligned} \varepsilon_j^{(0)} &= (2n + 1), \quad \varepsilon_j^{(1)} = \sigma_y \frac{2(\hat{Z}_2 + \hat{Z}_1)}{s_2}, \quad \varepsilon_j^{(3)} = \sigma_y \frac{(2n + 1)(\hat{Z}_2 s_3^2 + \hat{Z}_1 s_1^2)}{s_2^3}, \\ \varepsilon_j^{(4)} &= -\frac{(\hat{Z}_2 s_3 - \hat{Z}_1 s_1)^2}{s_2^4}, \quad \varepsilon_j^{(5)} = \sigma_y \frac{3(2n^2 + 2n + 1)(\hat{Z}_2 s_3^4 + \hat{Z}_1 s_1^4)}{2s_2^5}, \\ Q_{jj-3}^{(5)} &= -\sigma_y \frac{\sqrt{n-2}\sqrt{n-1}\sqrt{2}\sqrt{n}(\hat{Z}_2 s_3^3 - \hat{Z}_1 s_1^3)}{3s_2^4}, \\ Q_{jj-2}^{(4)} &= -\sigma_y \frac{3\sqrt{n-1}\sqrt{n}(\hat{Z}_2 s_3^2 + \hat{Z}_1 s_1^2)}{4s_2^3}, \end{aligned} \quad (42)$$

**Table 3.** The same as in Table 1, but for  $H_{jj'} \equiv H_{jj'}(y)$  at  $j \neq j'$ 

$k_{\max}$	$H_{13}, 10^{-10}$	$H_{15}, 10^{-8}$	$H_{24}, 10^{-9}$	$H_{26}, 10^{-6}$	$H_{35}, 10^{-9}$	$H_{46}, 10^{-8}$
8	0.000	-7.3972	0.000	-1.65406	0.000	0.0000
9	0.000	-7.3972	0.000	-1.65406	0.000	0.0000
10	0.683	-8.1862	1.972	-1.90107	4.463	0.8643
11	0.683	-8.1256	1.972	-1.88752	4.463	0.8643
12	0.780	-8.1839	2.347	-1.91203	5.488	1.0969
nv	0.782	-8.1763	2.376	-1.91042	5.608	1.1334

$$\begin{aligned}
Q_{jj-1}^{(3)} &= -\sigma_y \frac{\sqrt{2}\sqrt{n}(-\hat{Z}_1 s_1 + \hat{Z}_2 s_3)}{s_2^2}, \quad Q_{jj-1}^{(5)} = -\sigma_y \frac{3\sqrt{2}n\sqrt{n}(\hat{Z}_2 s_3^3 - \hat{Z}_1 s_1^3)}{s_2^4}, \\
H_{jj-3}^{(7)} &= -\frac{3\sqrt{2}\sqrt{n}\sqrt{n-1}\sqrt{n-2}(\hat{Z}_2 s_3^2 + \hat{Z}_1 s_1^2)(-\hat{Z}_1 s_1 + \hat{Z}_2 s_3)}{2s_2^5}, \\
H_{jj-2}^{(6)} &= -\frac{2\sqrt{n}\sqrt{n-1}(\hat{Z}_2 s_3 - \hat{Z}_1 s_1)^2}{s_2^4}, \\
H_{jj-1}^{(7)} &= \frac{3n\sqrt{2}\sqrt{n}(\hat{Z}_2 s_3^2 + \hat{Z}_1 s_1^2)(\hat{Z}_2 s_3 - \hat{Z}_1 s_1)}{2s_2^5}, \\
H_{jj}^{(6)} &= \frac{2(2n+1)(\hat{Z}_2 s_3 - \hat{Z}_1 s_1)^2}{s_2^4}.
\end{aligned}$$

*Remark 2.* In the case of  $\hat{Z}_1 = \hat{Z}_2$ ,  $s_1 = s_3$  (i.e., for equal masses and charges), the set of equations (10) has even and odd parity solutions that are calculated separately: for the even solutions  $n = 2j - 2$  and for the odd solutions  $n = 2j - 1$ . In this case, the above coefficients which contain terms like  $(-\hat{Z}_1 s_1 + \hat{Z}_2 s_3)$  vanish when they have no terms  $(\hat{Z}_1 s_1 + \hat{Z}_2 s_3)$ .

## Algorithm 2. Evaluation of the Asymptotic Solutions

**Input.** We calculate the asymptotic solution to the set of  $N$  ODEs at large values of the independent variable  $|y| \gg 1$

$$\begin{aligned}
&\left[ -\frac{1}{y^{d-1}} \frac{d}{dy} y^{d-1} \frac{d}{dy} + \varepsilon_i(y) + H_{ii}(y) - 2E \right] \chi_{ii'}(y) \\
&= \sum_{j=1, j \neq i}^N \left[ -Q_{ij}(y) \frac{d}{dy} - \frac{1}{y^{d-1}} \frac{d}{dy} y^{d-1} Q_{ij}(y) - H_{ij}(y) \right] \chi_{ji'}(y).
\end{aligned} \tag{43}$$

Here  $d \geq 1$  is the dimension of configuration space of a general scattering problem [7] while in the considered case (10), we put  $d = 1$  and calculate asymptotic solution on two intervals  $-\infty < y \leq y_{\min}$  and  $y_{\max} \leq y < \infty$ . We suppose that



coefficients of Eqs. (43) are present in the general form (41) and, in particular, in the form (42).

**Step 1.** We construct the solution to Eqs. (43) in the form:

$$\chi_{ji'}(y) = \left( \phi_{ji'}(y) + \psi_{ji'}(y) \frac{d}{dy} \right) R_{i'}(y), \quad (44)$$

where  $\phi_{ji'}(y)$  and  $\psi_{ji'}(y)$  are unknown functions,  $R_{i'}(y)$  is known function. We choose  $R_{i'}(y)$  as solutions of the auxiliary problem treated like etalon equation ( $Z_{i'}^{(k<1)} = Z_{i'}^{(k>k'_{\max})} = 0$ ):

$$\left[ -\frac{1}{y^{d-1}} \frac{d}{dy} y^{d-1} \frac{d}{dy} + \sum_{k=1}^{k'_{\max}} \frac{Z_{i'}^{(k)}}{y^k} - p_{i'}^2 \right] R_{i'}(y) = 0. \quad (45)$$

*Remark 3.* If  $Z_{i'}^{(k \geq 3)} = 0$  then solutions to the last equation are presented via hypergeometric functions, exponential, trigonometric, Bessel, Coulomb functions, etc. For example, if the leading terms of the asymptotic solutions are given by formula

$$R_{i'}(y) = \frac{1}{\sqrt{p_{i'} y^{d-1}}} \exp \left( \pm i \left( p_{i'} y - \frac{Z_{i'}^{(1)}}{2p_{i'}} \ln(2p_{i'} |y|) \right) \right), \quad (46)$$

the coefficient  $Z_{i'}^{(2)}$  of potential in the etalon equation (45) has the form:

$$Z_{i'}^{(2)} = -\frac{(d-3)(d-1)}{4} \pm i \frac{Z_{i'}^{(1)}}{p_{i'}} - \frac{(Z_{i'}^{(1)})^2}{p_{i'}^2}. \quad (47)$$

**Step 2.** At this step, we compute the coefficients  $\phi_{i'}(y)$  and  $\psi_{i'}(y)$  of the expansion (44) in the form of series by inverse powers of  $y$  ( $\phi_{ji'}^{(k'<0)} = \psi_{ji'}^{(k'<0)} = 0$ ):

$$\phi_{ji'}(y) = \phi_{ji'}^{(0)} + \sum_{k'=1}^{k_{\max}} \frac{\phi_{ji'}^{(k')}}{y^{k'}}, \quad \psi_{ji'}(y) = \psi_{ji'}^{(0)} + \sum_{k'=1}^{k_{\max}} \frac{\psi_{ji'}^{(k')}}{y^{k'}}. \quad (48)$$

After substitution of (44), (48) into (43) with the use of Eq. (45), we arrive at the set of recurrence relations at  $k' \leq k_{\max}$ :

$$\begin{aligned} \left( \varepsilon_i^{(0)} - 2E + p_{i'}^2 \right) \phi_{ii'}^{(k')} + \left( \varepsilon_i^{(1)} - Z_{i'}^{(1)} \right) \phi_{ii'}^{(k'-1)} - 2p_{i'}^2 (k' - 1) \psi_{ii'}^{(k'-1)} &= -f_{ii'}^{(k')}, \\ \left( \varepsilon_i^{(0)} - 2E + p_{i'}^2 \right) \psi_{ii'}^{(k')} + 2(k' - 1) \phi_{ii'}^{(k'-1)} + \left( \varepsilon_i^{(1)} - Z_{i'}^{(1)} \right) \psi_{ii'}^{(k'-1)} &= -g_{ii'}^{(k')}, \end{aligned} \quad (49)$$

where the right-hand sides  $f_{ii'}^{(k)}$  and  $g_{ii'}^{(k)}$  are defined by relations

$$f_{ii'}^{(k')} = -(k' - 2)(k' - d) \phi_{ii'}^{(k'-2)} + \sum_{k=2}^{k'} \left( V_{ii}^{(k)} - Z_{i'}^{(k)} \right) \phi_{ii'}^{(k'-k)}$$

$$+ \sum_{k=1}^{k'} \left( Z_{i'}^{(k)} (2k' - 2 - k) \psi_{ii'}^{(k' - k - 1)} + \sum_{j=1, j \neq i}^N \left( \sum_{k''=1}^{k'} 2Q_{ij}^{(k)} Z_{i'}^{(k'')} \psi_{ji'}^{(k' - k - k'')} \right. \right. \\ \left. \left. - 2p_{i'}^2 Q_{ij}^{(k)} \psi_{ji'}^{(k' - k)} + Q_{ij}^{(k)} (-2k' + k + d + 1) \phi_{ji'}^{(k' - k - 1)} + V_{ij}^{(k)} \phi_{ji'}^{(k' - k)} \right) \right); \quad (50)$$

$$g_{ii'}^{(k)} = -(k' - 1)(k' - 3 + d) \psi_{ii'}^{(k' - 2)} + \sum_{k=2}^{k'} \left( V_{ii}^{(k)} - Z_{i'}^{(k)} \right) \psi_{ii'}^{(k' - k)} \\ + \sum_{j=1, j \neq i}^N \sum_{k=1}^{k'} \left( 2Q_{ij}^{(k)} \phi_{ji'}^{(k' - k)} - Q_{ij}^{(k)} (2k' + d - 3 - k) \psi_{ji'}^{(k' - k - 1)} + V_{ij}^{(k)} \psi_{ji'}^{(k' - k)} \right)$$

with initial conditions  $p_{i'}^2 = 2E - \varepsilon_{i'}^{(0)}$ ,  $\phi_{ii'}^{(0)} = \delta_{ii'}$ ,  $\psi_{ii'}^{(0)} = 0$ , at  $i' = i_o$  run the open channels  $i_o = 1, \dots, N_o$  and  $p_{i'} = iq_{i'}$ ,  $q_{i'} > 0$ ,  $q_{i'}^2 = \varepsilon_{i'}^{(0)} - 2E$  at  $i' = i_c$  run the closed channels  $i_c = N_o + 1, \dots, N$  that follow from (14) and (17). Also from Eq. (49) at  $k' = 1$  and  $i = i'$ ,

$$\left( \varepsilon_{i'}^{(1)} - Z_{i'}^{(1)} \right) \phi_{ii'}^{(0)} = 0, \quad \left( \varepsilon_{i'}^{(1)} - Z_{i'}^{(1)} \right) \psi_{ii'}^{(0)} = 0, \quad (51)$$

we obtain condition  $Z_{i'}^{(1)} = \varepsilon_{i'}^{(1)}$ .

**Step 3.** Here we perform calculation of the coefficients  $\phi_{ii'}^{(k')}$  and  $\psi_{ii'}^{(k')}$  by a step-by-step procedure of solving Eqs. (49) for  $2E \neq \varepsilon_{i'}^{(0)}$ ,  $i \neq i'$  and  $k' = 2, \dots, k_{\max}$ :

$$\phi_{ii'}^{(k')} = \left[ \varepsilon_i^{(0)} - \varepsilon_{i'}^{(0)} \right]^{-1} \left[ -f_{ii'}^{(k')} - \left( \varepsilon_i^{(1)} - Z_{i'}^{(1)} \right) \phi_{ii'}^{(k' - 1)} + 2p_{i'}^2 (k' - 1) \psi_{ii'}^{(k' - 1)} \right], \\ \psi_{ii'}^{(k')} = \left[ \varepsilon_i^{(0)} - \varepsilon_{i'}^{(0)} \right]^{-1} \left[ -g_{ii'}^{(k')} - 2(k' - 1) \phi_{ii'}^{(k' - 1)} - \left( \varepsilon_i^{(1)} - Z_{i'}^{(1)} \right) \psi_{ii'}^{(k' - 1)} \right], \\ \phi_{ii'}^{(k' - 1)} = -[2(k' - 1)]^{-1} g_{ii'}^{(k)}, \\ \psi_{ii'}^{(k' - 1)} = \left[ 2(k' - 1) \left( 2E - \varepsilon_{i'}^{(0)} \right) \right]^{-1} f_{ii'}^{(k)}. \quad (52)$$

The above described algorithm has been implemented in MAPLE and FORTRAN to calculate the desirable  $\phi_{ii'}^{(k')}$  and  $\psi_{ii'}^{(k')}$  in the **output** up to  $k_{\max} - 1 = 11$  order.

*Remark 4.* The choice of appropriate values  $y_{\min}$  and  $y_{\max}$  for the constructed expansions of the linearly independent solutions for  $p_{i_o} > 0$  is controlled by the fulfillment of the Wronskian condition (26)

$$y^{d-1} W r(\mathbf{Q}(y); \chi^*(y), \chi(y)) = \pm 2i \mathbf{I}_{oo} \quad (53)$$

up to the prescribed precision  $\varepsilon_{Wr}$ .

As a result, Algorithms 1 and 2 generate required asymptotic solution (5) up to the order  $O(|y|^{-k_{\max}})$  at  $|y|/|x| \gg 1$  that reduce the BVP (1) from plane  $\mathbf{R}^2$

$$\psi_{i'}^{as}(x, y) = \sum_{j=1}^N \sum_{k=0}^{k_{\max}} y^{-k} \sum_{s=\min(1-j, -M(k))}^{M(k)} B_{j-1+s}^{(0)}(x) b_{j-1;s}^{(k)} \left( \phi_{ji'}^{(k-p)} + \psi_{ji'}^{(k-p)} \frac{d}{dy} \right) R_{i'}(y) \quad (54)$$

to a finite domain  $\Omega_{xy} = [\Omega_x \{x_{\min}, x_{\max}\} \times \Omega_y \{y_{\min}, y_{\max}\}]$ .

## 4 Benchmark Calculation of Penetration Coefficient

As a benchmark calculation we consider the BVPs (1)–(6) that model the quantum tunneling problem for a coupled pair of identical ions with the following values of parameters:  $\bar{x}_{\max} = 5$  for Eq. (2) and  $s = 8$  for Eq. (3),  $s_1 = s_2 = s_3 = 1/2$ ,  $\bar{x}_{\min} = 0.1$ ,  $\hat{Z}_1 = \hat{Z}_2 = 0.5$  and  $\hat{Z}_1 = \hat{Z}_2 = 1$  in oscillator units. For given number  $N$  of ODES (10), the values  $x_{\min}$  and  $x_{\max}$  of grid  $\Omega_x\{x_{\min}, x_{\max}\}$  are chosen in the region  $|x| > x_0 = \sqrt{2N+1}$  where the Hermite polynomial [9] (or of wave function in a general case) has none zeros. These values are computed with prescribed precision  $eps > 0$  from the condition

$$\exp\left(\int_{x_0}^x dx \sqrt{x^2 - x_0^2}\right) \leq eps,$$

which in the given case leads to inequality

$$\exp\left(-x\sqrt{x^2 - x_0^2}/2\right)\left(x + \sqrt{x^2 - x_0^2}\right)^{x_0^2/2} x_0^{-x_0^2/2} \leq eps. \quad (55)$$

To find an approximate solution, at the first step we choose the initial approximation  $x_{\max} = x_0$ , after that it is increased with step equal 1 until (55) is satisfied. Values  $y_{\min} < x_{\min}$  and  $y_{\max} > x_{\max}$  were chosen from the condition that potential (2) or (3) is negligible on the interval  $x_{\min} < x < x_{\max}$ .

The matching points  $y_1^{match}$  and  $y_2^{match}$  of the numerical (11) and asymptotic (41) effective potential were calculated as follows:

$$y_1^{match} = \min\{y_1^E, y_1^Q, y_1^H\}, \quad y_2^{match} = \max\{y_2^E, y_2^Q, y_2^H\},$$

$$y_t^E = \sigma_y \sqrt[k_{\max}]{\frac{|E_N^{(k_{\max})}|}{eps}}, \quad y_t^Q = \sigma_y \sqrt[k_{\max}]{\frac{|Q_{NN-1}^{(k_{\max})}|}{eps}}, \quad y_t^H = \sigma_y \sqrt[k_{\max}]{\frac{|H_{NN}^{(k_{\max})}|}{eps}},$$

since  $|E_j^{(k_{\max})}| < |E_N^{(k_{\max})}|$ ,  $|Q_{jj'}^{(k_{\max})}| < |Q_{NN-1}^{(k_{\max})}|$ ,  $|H_{jj'}^{(k_{\max})}| < |H_{NN}^{(k_{\max})}|$ . So, the values  $y_{\min}$  and  $y_{\max}$  are chosen from the inequalities  $y_{\min} < y_1^{match} < x_{\min}$  and  $y_{\max} > y_2^{match} > x_{\max}$  taking into account. This gives

$$y_{\min} = \min \left[ y_1^{match}, \min_j \left( - \sqrt[k_{\max}]{\frac{|\phi_{ji_o}^{(k_{\max})}|}{eps}} \right), \min_j \left( - \sqrt[k_{\max}]{\frac{|\psi_{ji_o}^{(k_{\max})}|}{eps}} \right) \right],$$

$$y_{\max} = \max \left[ y_2^{match}, \max_j \left( \sqrt[k_{\max}]{\frac{|\phi_{ji_o}^{(k_{\max})}|}{eps}} \right), \max_j \left( \sqrt[k_{\max}]{\frac{|\psi_{ji_o}^{(k_{\max})}|}{eps}} \right) \right]. \quad (56)$$

In the considered examples, we used the grids  $\Omega_x\{x_{\min}, x_{\max}\} = \{-10(768)10\}$  and  $\Omega_y\{y_{\min}, y_{\max}\} = \{-125(200)-25(100)-6(200)6(100)25(200)125\}$  with the Lagrange elements of the order  $p = 4$  between the nodes. In the above grids  $\Omega_x$  and  $\Omega_y$ , the number of grid elements is shown in the parentheses.

To illustrate Remark 2 by an example, we can point out the lines for  $k_{\max} = 3$  (containing only zero values) in Table 2. Other zero values in Tables 2 and 3 point out different leading terms in the inverse power series expansion of matrix elements between various eigenfunctions. The numerical values of effective potentials calculated by ODPEVP [6] with a given precision  $\epsilon_{ps}$  of order of  $10^{-10}$  in the last line of the Tables 1, 2 and 3 are in a good agreement with the asymptotic values from (41) in the matching points  $y = y_t^{match}$ .

In the calculation of solutions, we used the etalon equation (45) at  $d = 1$  with the two sets of parameters taken in the first case as in Remark 3 and in second case as  $k'_{\max} = 1$ ,  $Z_{i'}^{(1)} = 2\sigma_y Z_{12}$ , that corresponds to the known solutions on the open channels

$$R_{i_o}^{\pm}(p_{i_o}, y) = p_{i_o}^{-1/2} \begin{cases} (G_0(p_{i_o}, +y) \pm iF_0(p_{i_o}, +y)) \exp(\mp i\sigma_{i_o})/2, & y > 0, \\ (G_0(p_{i_o}, -y) \mp iF_0(p_{i_o}, -y)) \exp(\pm i\sigma_{i_o})/2, & y < 0, \end{cases} \quad (57)$$

and on the closed channels

$$R_{i_c}(q_{i_c}, y) = q_{i_c}^{-1/2} t \exp(-t/2) U(1 + Z_{12}/q_{i_c}, 2, t), \quad t = 2q_{i_c}|y|. \quad (58)$$

Here  $F_0(p_{i_o}, y)$  and  $G_0(p_{i_o}, y)$  are regular and irregular continuum zero order Coulomb functions;  $\sigma_{i_o} = \arg \Gamma(1 + iZ_{12}/p_{i_o})$  is the Coulomb phase shift [9]; and  $U(a, b, c)$  is the confluent hypergeometric function of second kind.

*Remark 5.* In the numerical calculation, the exponential small factor  $\exp(-t/2)$  in  $R_{i_c}(q_{i_c}, y)$  and its first derivative was neglected since this factor is canceled during evaluation of  $\mathcal{R}(y)$  matrix in Eq. (18).

Required reflection  $\mathbf{R}_{\rightarrow}$  and transmission  $\mathbf{T}_{\rightarrow}$  matrixes calculated by formulas (20) via matrix of logarithmic derivatives  $\mathcal{R}_{\rightarrow}(y)$  and solution  $\Phi_{\rightarrow}^h(y_{\max})$  calculated numerically on the above grid  $\Omega_y\{y_{\min}, y_{\max}\}$  by means of the program KANTBP 3.0, including matching in the boundary points  $y_{\min}$  and  $y_{\max}$  of (12) with asymptotic solution evaluated in first case has the error of order 0.1% in comparison with a more accurate result obtained with asymptotic solution evaluated in the second case.

According to Remarks 1 and 4, the Wronskian condition depends on the number  $N$  of ODEs, on the value of threshold energy, on the type of etalon equation, etc. At the boundary points  $y_{\min}$  and  $y_{\max}$  of the above grid  $\Omega_y\{y_{\min}, y_{\max}\}$ , the absolute values  $\varepsilon_{Wr}$  of components of difference between the calculated Wronskian and its theoretical value (53) are less than  $10^{-11}$ .

The total probabilities  $T \equiv T_{11} = \sum_{j=1}^{N_o} |T_{1j}|^2$  of penetration through Truncated Coulomb (2) and Coulomb-like (3) potential barriers are shown in Fig. 1. The first of them is in a good agreement with results obtained by solving the BVP (1), (2), (5), and (6) in the 2D domain using Numerov method in papers [3,4]. These pictures illustrate the important peculiarity that a more realistic nontruncated Coulomb-like barrier having a more wide than truncated one, leads to a set of the probability maximums having a bigger half-width. It can be used for verification of the models and quantum transparency effect.

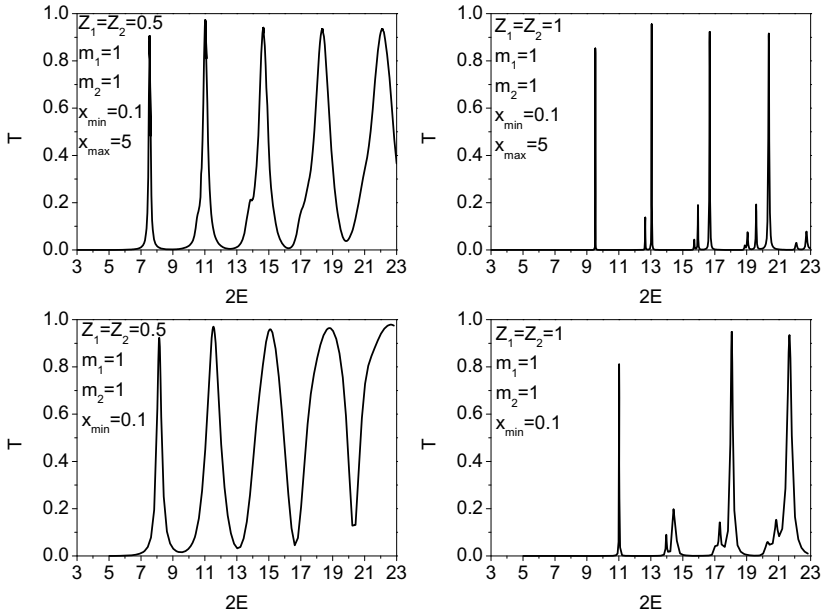


**Fig. 1.** The total probabilities  $T \equiv T_{11} = \sum_{j=1}^{N_o} |T_{1j}|^2$  of penetration through Truncated Coulomb (2) at  $x_{\max} = 5$  (upper panel), and Coulomb-like (3) (lower panel), potential barriers:  $x_{\min} = 0.1$ ,  $m_1 = m_2 = 1$ , left panel:  $\hat{Z}_1 = \hat{Z}_2 = 0.5$ , right panel:  $\hat{Z}_1 = \hat{Z}_2 = 1$ .

## 5 Conclusion

The BVP for the 2D Schrödinger equation with long-range potentials from the 2D plane is reduced to sets of the BVPs for the ODEs in a finite 2D domain with help of the presented symbolic algorithms for evaluation of asymptotics of solutions and effective potentials of the ODEs. The BVPs for the resulting system of equations containing effective potentials, which are calculated by program ODPEVP [6], are solved by the new version of program KANTBP 2.0 using high-order precision approximations of the FEM [7]. The computational efficiency of the SNAs proposed is demonstrated by the benchmark calculation of quantum transmittance of long-range barriers for composite particles. The further development of the SNAs and software for solving the BVPs of the Schrödinger equation with long-range potentials can serve as a useful tool to study quantum transparency effects not only in heavy ion physics but also in quantum chemistry [11] and atomic physics [12].

Authors thank Profs. F.M. Pen'kov and P.M. Krassovitskiy for useful discussion. This work was done within the framework of the Protocols No. 4028-3-10/12 of collaboration between JINR and INP (Almaty) in dynamics of few-body systems and quantum transparency of barriers for structure particles and ions. The work was supported partially by RFBR (grants 10-01-00200 and 11-01-00523).

## References

1. Hofmann, H.: Quantum mechanical treatment of the penetration through a two-dimensional fission barrier. *Nucl. Phys. A* 224, 116–139 (1974)
2. Hagino, K., Rowley, N., Kruppa, A.T.: A program for coupled-channel calculations with all order couplings for heavy-ion fusion reactions. *Comput. Phys. Commun.* 123, 143–152 (1999)
3. Pen'kov, F.M.: Metastable states of a coupled pair on a repulsive barrier. *Phys. Rev. A* 62, 044701-1-4 (2000)
4. Pen'kov, F.M.: Quantum Transmittance of Barriers for Composite Particles. *JETP* 91, 698–705 (2000)
5. Kantorovich, L.V., Krylov, V.I.: *Approximate Methods of Higher Analysis*. Wiley, New York (1964)
6. Chuluunbaatar, O., Gusev, A.A., Vinitsky, S.I., Abrashkevich, A.G.: ODPEVP: A program for computing eigenvalues and eigenfunctions and their first derivatives with respect to the parameter of the parametric self-adjointed Sturm–Liouville problem. *Comput. Phys. Commun.* 180, 1358–1375 (2009)
7. Chuluunbaatar, O., Gusev, A.A., Vinitsky, S.I., Abrashkevich, A.G.: KANTBP 2. 0: New version of a program for computing energy levels, reaction matrix and radial wave functions in the coupled-channel hyperspherical adiabatic approach. *Comput. Phys. Commun.* 179, 685–693 (2008)
8. Chuluunbaatar, O., Gusev, A., Gerdt, V., Kaschiev, M., Rostovtsev, V., Samoylov, V., Tupikova, T., Vinitsky, S.: A Symbolic-numerical algorithm for solving the eigenvalue problem for a hydrogen atom in the magnetic field: cylindrical coordinates. In: Ganzha, V.G., Mayr, E.W., Vorozhtsov, E.V. (eds.) *CASC 2007. LNCS*, vol. 4770, pp. 118–133. Springer, Heidelberg (2007)
9. Abramowitz, M., Stegun, I.A.: *Handbook of Mathematical Functions*. Dover, New York (1965)
10. Barnett, A.R., Feng, D.H., Steed, J.W., Goldfarb, L.J.B.: Coulomb wave functions for all real  $\eta$  and  $\rho$ . *Comput. Phys. Comm.* 8, 377–395 (1974)
11. Goodvin, G.L., Shegelski, M.R.A.: Three-dimensional tunneling of a diatomic molecule incident upon a potential barrier. *Phys. Rev. A* 72, 042713-1-7 (2005)
12. Giannakeas, P., Melezhik, V.S., Schmelcher, P.: D-wave confinement-induced resonances in harmonic waveguides. *arXiv:1102.5686v1* (2011)



# Symbolic-Numerical Calculations of High- $|m|$ Rydberg States and Decay Rates in Strong Magnetic Fields<sup>\*</sup>

Alexander Gusev, Sergue Vinitsky, Ochbadrakh Chuluunbaatar,  
Vladimir Gerdt, Luong Le Hai, and Vitaly Rostovtsev <sup>\*\*</sup>

Joint Institute for Nuclear Research, Dubna, Moscow Region, Russia  
`gooseff@jinr.ru`, `vinitsky@theor.jinr.ru`

**Abstract.** Symbolic-numeric solving of the boundary value problem for the Schrödinger equation in cylindrical coordinates is given. This problem describes the impurity states of a quantum wire or a hydrogen-like atom in a strong homogeneous magnetic field. It is solved by applying the Kantorovich method that reduces the problem to the boundary-value problem for a set of ordinary differential equations with respect to the longitudinal variables. The effective potentials of these equations are given by integrals over the transverse variable. The integrands are products of the transverse basis functions depending on the longitudinal variable as a parameter and their first derivatives. To solve the problem at high magnetic quantum numbers  $|m|$  and study its solutions we present an algorithm implemented in Maple that allows to obtain *analytic expressions* for the effective potentials and for the transverse dipole moment matrix elements. The efficiency and accuracy of the derived algorithm and that of Kantorovich numerical scheme are confirmed by calculating eigenenergies and eigenfunctions, dipole moments and decay rates of low-excited Rydberg states at high  $|m| \sim 200$  of a hydrogen atom in the laboratory homogeneous magnetic field  $\gamma \sim 2.35 \times 10^{-5}$  ( $B \sim 6T$ ).

## 1 Introduction

In earlier papers, we considered the application of the Kantorovich method for solving the discrete- and continuous-spectrum boundary-value problems (BVP) [1] for hydrogen-like atoms in magnetic field and the ion axial channelling problem in a crystal. The approach implies the use of a parametric basis of oblate spheroidal angular functions in spherical coordinates where the radial variable runs a semi-axis [2,3,4,5]. The method has been further developed in connection with calculations of spectral and optical characteristics of model semiconductor nanostructures, namely, quantum dots(QD), quantum wells(QW) and quantum

---

<sup>\*</sup> This work was partially supported by the RFBR Grants Nos. 10-02-00200 and 11-01-00523.

<sup>\*\*</sup> The coauthors (AG, SV, OC, VG, and LH) congratulate Vitaly Rostovtsev on turning 20 for the fourth time.



wires(QWr) [6,7,8,9]. For this purpose we used different parametric basis functions in appropriate coordinate systems. The functions were calculated by solving parametric eigenvalue problems by means of the program ODPEVP [10].

Taking into account the growing interest in problems possessing axial symmetry, like impurity states of QWr's or high-angular-momentum Rydberg states and quasi-stationary states imbedded in continuum of a hydrogen atom in magneto-optical traps [11,12,13], it is imperative to implement the Kantorovich scheme for solving the BVP for the longitudinal variable running the whole axis of a cylindrical coordinate system[8,9]. This would allow direct calculation of the main characteristics of a multichannel scattering problem, such as reflection and transmission coefficients matrices, recombination rates and ionization cross-sections for Rydberg states, and decay rates of the lowest bound states of manifolds with high values of the magnetic quantum number  $|m|$  [11,12,13].

For the Schrödinger equation describing a hydrogen-like atom in a strong homogeneous magnetic field, the boundary-value problem (BVP) in cylindrical coordinates is reduced to solving a set of the longitudinal equations in the framework of the Kantorovich method. The effective potentials of these equations are given by integrals over the transverse variable, the integrands being products of transverse basis functions, depending on the longitudinal variable as a parameter, and their first derivatives with respect to the parameter. One can say that at high  $|m|$ , the discrete-spectrum problem is described by a system of two coupled 2D- and 1D-oscillators corresponding to the transverse  $\rho$  and longitudinal  $z$  variables, with the frequencies  $\omega_\rho$  and  $\omega_z$ , respectively. To analyze the low-excited Rydberg states of such system it is useful to have the solution *in an analytic form*. Indeed, for high  $|m|$  we can consider the Coulomb potential as a perturbation with respect to the transversal centrifugal potential and the oscillator potential with the frequency  $\omega_\rho = \gamma/2$ . For the laboratory magnetic field  $B = B_0\gamma \sim 6T$ , i.e.,  $\gamma \sim 2.35 \times 10^{-5}$ , this is true at the *adiabatic parameter* values  $\tilde{m} \sim 5.89$ , where  $\tilde{m}$  is defined as  $\tilde{m} = (\omega_\rho/\omega_z)^{4/3} = |m|\gamma^{1/3}$ . Under the condition  $|m| \geq 6\gamma^{-1/3}$  we can approximate the Coulomb potential by a Taylor expansion in powers of the auxiliary transverse variable with respect to a specially chosen point with given accuracy in the region of its convergence. Then we can find the approximate transversal eigenvalues and eigenfunctions depending parametrically on the longitudinal variable, in the framework of a perturbation scheme and by using the eigenvalues and eigenfunctions of the 2D oscillator as unperturbed ones. To express *analytically* the transverse basis functions and eigenvalues, the corresponding effective potentials, and the transverse dipole moment matrix elements as well as perturbation solution of the BVP, we elaborate a symbolic-numerical algorithm (SNA) implemented in Maple. The efficiency and accuracy of the algorithm and that of the derived Kantorovich numerical scheme are confirmed by computation of eigenenergies and eigenfunctions, dipole moments and decay rates for the manifolds of high- $|m|$  low-excited Rydberg states of a hydrogen atom in the laboratory homogeneous magnetic field, and by comparison with the results obtained by other methods.

The paper is organized as follows. In Section 2, we briefly describe the reduction by the KM of the 3D eigenvalue problem at fixed values  $|m|$  of magnetic quantum number to the 1D eigenvalue problem for a set of close-coupled longitudinal equations. In Sections 3 and 4, the algorithm for calculating the effective potentials and the transverse dipole moment matrix elements *in the analytic form* at large values of  $|m|$  is presented. The algorithm has been implemented in Maple. To find the validity range of the method, in Section 5 we compare our results with the known ones obtained in the cylindrical coordinates. Decay rates of the lowest bound states of manifolds with high magnetic quantum number  $|m|$  are also presented here. In Section 6, we conclude and discuss possible future applications of the described method.

## 2 Problem Statement in Cylindrical Coordinates

The component  $\Psi(\rho, z)$  of the wave function  $\Psi(\rho, z, \varphi) = \Psi(\rho, z) \exp(i m \varphi) / \sqrt{2\pi}$  of a hydrogen atom in an axially symmetric magnetic field  $\mathbf{B} = (0, 0, B)$  in the cylindrical coordinates  $(\rho, z, \varphi)$  satisfies the 2D Schrödinger equation in the region  $\Omega_c = \{0 < \rho < \infty \text{ and } -\infty < z < \infty\}$ :

$$-\frac{\partial^2}{\partial z^2} \Psi(\rho, z) + A_c \Psi(\rho, z) = \epsilon \Psi(\rho, z), \quad A_c = -\frac{1}{\rho} \frac{\partial}{\partial \rho} \rho \frac{\partial}{\partial \rho} + m\gamma + U(\rho, z), \quad (1)$$

$$U(\rho, z) = \frac{m^2}{\rho^2} + \frac{\gamma^2 \rho^2}{4} + V_c(\rho, z), \quad V_c(\rho, z) = -\frac{2q}{\sqrt{\rho^2 + z^2}}. \quad (2)$$

Here  $m = 0, \pm 1, \dots$  is the magnetic quantum number,  $\gamma = B/B_0 = \hbar\omega_c/(2Ry)$ ,  $B_0 \cong 2.35 \times 10^5 T$  is a dimensionless parameter which determines the field strength  $B$ ,  $\omega_c = eB/(m_e c) = eB_0\gamma/(m_e c)$  is the cyclotron frequency, and  $U(\rho, z)$  is the potential energy (see Fig. 1a),  $q$  is Coulomb charge of nucleus. We use the atomic units (*a.u.*)  $\hbar = m_e = e = 1$  and assume the mass of the nucleus to be infinite. In these expressions,  $\epsilon = 2E$ ,  $E$  is the energy (expressed in Rydbergs,  $1 Ry = (1/2) a.u.$ ) of the bound state  $|m\sigma\rangle$  with fixed values of  $m$  and  $z$ -parity  $\sigma = \pm 1$ , and  $\Psi(\rho, z) \equiv \Psi^{m\sigma}(\rho, z) = \sigma \Psi^{m\sigma}(\rho, -z)$  is the corresponding wave function. The boundary conditions in each  $m\sigma$  subspace  $L_2(\Omega)$  of the complete Hilbert space have the form

$$\lim_{\rho \rightarrow 0} \rho \frac{\partial \Psi(\rho, z)}{\partial \rho} = 0, \quad \text{for } m = 0, \quad \text{and } \Psi(0, z) = 0, \quad \text{for } m \neq 0, \quad (3)$$

$$\lim_{\rho \rightarrow \infty} \Psi(\rho, z) = 0. \quad (4)$$

The eigenfunction  $\Psi(\rho, z) \equiv \Psi_t(\rho, z) \in L_2(\Omega)$  of the discrete real-valued spectrum  $\epsilon : \epsilon_1 < \epsilon_2 < \dots < \epsilon_t < \dots < \gamma$  obeys the asymptotic boundary condition. Approximately this condition is replaced by the boundary condition of the second and/or first type at small and large  $|z|$ , but finite  $|z| = z_{\max} \gg 1$ ,

$$\lim_{z \rightarrow 0} \frac{\partial \Psi(\rho, z)}{\partial z} = 0, \quad \sigma = +1, \quad \Psi(\rho, 0) = 0, \quad \sigma = -1, \quad (5)$$

$$\lim_{z \rightarrow \pm\infty} \Psi(\rho, z) = 0 \quad \rightarrow \quad \Psi(\rho, \pm|z_{\max}|) = 0. \quad (6)$$

In numerical calculation of the eigenvalues and eigenfunctions with given accuracy by programs KANTBP2 and ODPEVP realizing the finite element method, we used computational schemes derived from the Rayleigh–Ritz variational functional [1,10]

$$\mathcal{R}(\Psi_t, \epsilon_t) = \left( \int_{-z_{\max}}^{z_{\max}} dz \int_0^\infty \rho d\rho \frac{\partial \Psi_t(\rho, z)}{\partial z} \frac{\partial \Psi_t(\rho, z)}{\partial z} + \frac{\partial \Psi_t(\rho, z)}{\partial \rho} \frac{\partial \Psi_t(\rho, z)}{\partial \rho} \right. \\ \left. + \Psi_t(\rho, z)(m\gamma + U(\rho, z))\Psi_t(\rho, z) \right) / \int_{-z_{\max}}^{z_{\max}} dz \int_0^\infty \rho d\rho \Psi_t(\rho, z) \Psi_{t'}(\rho, z) \quad (7)$$

with the additional normalization and orthogonality conditions

$$\langle t | t' \rangle = \int_{-z_{\max}}^{z_{\max}} dz \int_0^\infty \rho d\rho \Psi_t(\rho, z) \Psi_{t'}(\rho, z) = 2 \int_0^{z_{\max}} dz \int_0^\infty \rho d\rho \Psi_t(\rho, z) \Psi_{t'}(\rho, z) = \delta_{tt'}. \quad (8)$$

For  $m \neq 0$  eigenfunctions  $\Psi_t(\rho, z) \sim \rho^{|m|/2}$  at small  $\rho$ . So, in numerical calculations, a reduced interval  $[0 < \rho_{\min}, \rho_{\max} \gg 1]$  is conventionally used [8].

## 2.1 Kantorovich Reduction

Consider a formal expansion of the partial solution  $\Psi_t^{m\sigma}(\rho, z)$  of Eqs. (1)–(4) corresponding to the eigenstate  $|m\sigma t\rangle$  expanded in the finite set of one-dimensional basis functions  $\{B_j^m(\rho; z)\}_{j=1}^{j_{\max}}$

$$\Psi_t^{m\sigma}(\rho, z) = \sum_{j=1}^{j_{\max}} B_j^m(\rho; z) \chi_j^{(m\sigma t)}(z). \quad (9)$$

In Eq. (9), the functions  $\chi^{(t)}(z) \equiv \chi^{(m\sigma t)}(z)$ ,  $(\chi^{(t)}(z))^T = (\chi_1^{(t)}(z), \dots, \chi_{j_{\max}}^{(t)}(z))$  are unknown, and the surface functions  $\mathbf{B}(\rho; z) = \mathbf{B}^m(\rho; -z)$ ,  $(\mathbf{B}(\rho; z))^T = (B_1(\rho; z), \dots, B_{j_{\max}}(\rho; z))$  form an orthonormal basis for each value of the variable  $z \in \mathcal{R}$  which is treated as a parameter.

In KM, the wave functions  $B_j(\rho; z)$  (see Fig. 2) and the potential curves  $E_j(z)$  (in  $Ry$ ) are determined as solutions of the following eigenvalue problem

$$A_c B_j(\rho; z) = E_j(z) B_j(\rho; z), \quad (10)$$

with the operator  $A_c$  from (1)–(2) and the boundary conditions (3), (4) at each fixed  $z \in \mathcal{R}$ . Since the operator in the left-hand side of Eq. (10) is self-adjoint, its eigenfunctions are orthonormal

$$\left\langle B_i(\rho; z) \left| B_j(\rho; z) \right\rangle_\rho = \int_0^\infty B_i(\rho; z) B_j(\rho; z) \rho d\rho = \delta_{ij}, \quad (11)$$

where  $\delta_{ij}$  is the Kronecker symbol. Therefore, we transform the solution of the above problem into the solution of an eigenvalue problem for a set of  $j_{\max}$

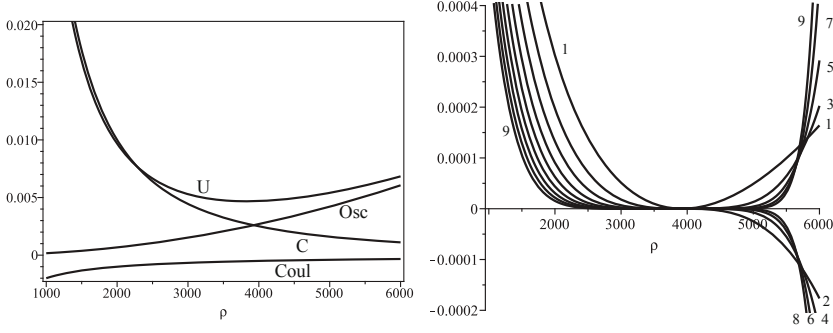


**Fig. 1.** Left panel: the profile of potential energy  $U(\rho, z) = m^2/\rho^2 + \gamma^2 \rho^2/4 + V_c(\rho, z)$  ( $U$ ) in the plane  $z = 0$  and its components, namely, the centrifugal ( $C$ ), oscillator ( $Osc$ ), and Coulomb ( $Coul$ ) potentials. Right panel: the approximation errors  $\delta U^{(j_{\max})}(\rho, z) \equiv \sum_{i=1}^{j_{\max}} U^{(i)}(\rho, z) - U(\rho, z)$  ( $j_{\max} = 1, \dots, 9$ ) of the potential energy  $U(\rho, z = 0)$ . Here  $q = -1$ ,  $m = -200$ ,  $\gamma = 2.553191 \cdot 10^{-5}$  ( $B = 6T$ ,  $\tilde{m} \approx 5.89$ )

ordinary second-order differential equations that determines the energy  $\epsilon$  and the coefficients  $\chi^{(i)}(z)$  of the expansion (9)

$$\left( -\mathbf{I} \frac{d^2}{dz^2} + \mathbf{U}(z) + \mathbf{Q}(z) \frac{d}{dz} + \frac{d\mathbf{Q}(z)}{dz} \right) \chi^{(t)}(z) = \epsilon_t \mathbf{I} \chi^{(t)}(z). \quad (12)$$

Here  $\mathbf{I}$ ,  $\mathbf{U}(z) = \mathbf{U}(-z)$ , and  $\mathbf{Q}(z) = -\mathbf{Q}(-z)$  are the  $j_{\max} \times j_{\max}$  matrices whose elements are expressed as

$$U_{ij}(z) = E_i(z) \delta_{ij} + H_{ij}(z), \quad H_{ij}(z) = \int_0^\infty \frac{\partial B_i(\rho; z)}{\partial z} \frac{\partial B_j(\rho; z)}{\partial z} \rho d\rho, \quad (13)$$

$$I_{ij}(z) = \delta_{ij}, \quad Q_{ij}(z) = -Q_{ji}(z) = - \int_0^\infty B_i(\rho; z) \frac{\partial B_j(\rho; z)}{\partial z} \rho d\rho.$$

The discrete spectrum solutions  $\epsilon : \epsilon_1 < \epsilon_2 < \dots < \epsilon_t < \dots < \gamma$  at fixed  $m$  and parity  $\sigma = \pm 1$  obey the asymptotic boundary condition and are orthonormal

$$\lim_{z \rightarrow 0} \left( \frac{d}{dz} - \mathbf{Q}(z) \right) \chi^{(t)}(z) = 0, \quad \sigma = +1, \quad \chi^{(t)}(0) = 0, \quad \sigma = -1, \quad (14)$$

$$\lim_{z \rightarrow \pm\infty} \chi^{(t)}(z) = 0 \quad \rightarrow \quad \chi^{(t)}(\pm z_{\max}) = 0, \quad (15)$$

$$\int_{-z_{\max}}^{z_{\max}} \left( \chi^{(t)}(z) \right)^T \chi^{(t')}(z) dz = 2 \int_0^{z_{\max}} \left( \chi^{(t)}(z) \right)^T \chi^{(t')}(z) dz = \delta_{tt'}. \quad (16)$$

*Remark 1.* In diagonal adiabatic approximation

$$\left( -\frac{d^2}{dz^2} + U_{jj}(z) \right) \chi_j^{(v)}(z) = \epsilon_{jv} \chi_j^{(v)}(z) \quad (17)$$

discrete spectrum  $\epsilon : \epsilon_{j1} < \epsilon_{j2} < \dots < \epsilon_{jv} < \dots < \gamma$  numerated by number  $v$  that determines the number  $v - 1$  of nodes of the solution  $\chi_j^{(v)}(z)$  at fixed value  $j$ .

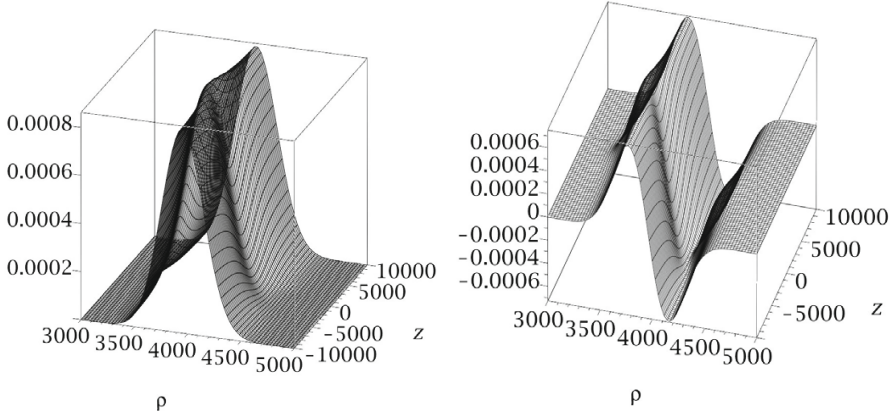


**Fig. 2.** The basis functions  $B_1$  and  $B_2$  for  $m = -200$ ,  $q = 1$ ,  $\gamma = 2.553191 \cdot 10^{-5}$

### 3 Solving the Parametric Eigenvalue Problem at Large $|m|$

**Step 1.** In (10), (11) apply the transformation to a scaled variable  $x$

$$x = \frac{\gamma \rho^2}{2}, \quad \rho = \frac{\sqrt{x}}{\sqrt{\gamma/2}}, \quad (18)$$

and put  $\lambda_j(z) = E_j(z)/(2\gamma) = \lambda_j^{(0)} + m/2 + \delta\lambda_j(z)$ , where  $\lambda_j^{(0)} = n + (|m| + 1)/2$ . The eigenvalue problem reads

$$\left( -\frac{\partial}{\partial x} x \frac{\partial}{\partial x} + \frac{m^2}{4x} + \frac{x}{4} + \frac{m}{2} - \frac{q}{\gamma \sqrt{\frac{2x}{\gamma} + z^2}} - \lambda_j \right) B_j(x; z) = 0, \quad (19)$$

with a normalization condition

$$\frac{1}{\gamma} \int_0^\infty B_j(x; z)^2 dx = 1. \quad (20)$$

At  $q = 0$ , Eq. (19) without  $m/2$  takes the form

$$L(n)B_j^{(0)}(x) = 0, \quad L(n) = -\frac{\partial}{\partial x} x \frac{\partial}{\partial x} + \frac{m^2}{4x} + \frac{x}{4} - \lambda_j^{(0)}, \quad (21)$$

and has the regular and bounded solutions at

$$\lambda_j^{(0)} = n + (|m| + 1)/2, \quad (22)$$

where the transverse quantum number  $n \equiv N_\rho = j - 1 = 0, 1, \dots$  determines the number of nodes of the solution  $B_j^{(0)}(x) \equiv B_{nm}^{(0)}(x)$  with respect to the variable  $x$ . The normalized solutions of Eq. (21) take the form

$$B_j^{(0)}(x) = C_{n|m|} e^{-\frac{x}{2}} x^{\frac{|m|}{2}} L_n^{|m|}(x), \quad C_{n|m|} = \left[ \gamma \frac{n!}{(n+|m|)!} \right]^{\frac{1}{2}}, \quad (23)$$

$$\frac{1}{\gamma} \int_0^\infty B_{nm}^{(0)}(x) B_{n'm}^{(0)}(x) dx = \delta_{nn'}, \quad (24)$$

where  $L_n^{|m|}(x)$  are Laguerre polynomials [14].

**Step 2.** Substituting the notation  $\delta\lambda_j(z) = \lambda_j(z) - \lambda_j^{(0)} - m/2 \equiv E_j(z)/(2\gamma) - (n + (m + |m| + 1)/2)$ , and the Taylor expansion in the vicinity of the point  $x_0 = x_s\gamma$ :

$$V_c(x, z) = -\frac{q}{\gamma \sqrt{\frac{2x}{\gamma} + z^2}} = -\sum_{k=1}^{j_{\max}} V^{(k)}(x, z) \varepsilon^k = -\frac{\varepsilon q}{\gamma(z^2 + 2x_s)^{1/2}} \quad (25)$$

$$+ \frac{\varepsilon q(x - x_s\gamma)}{\gamma^2(z^2 + 2x_s)^{3/2}} - \frac{3\varepsilon^2 q(x - x_s\gamma)^2}{2\gamma^3(z^2 + 2x_s)^{5/2}} + \frac{5\varepsilon^3 q(x - x_s\gamma)^3}{2\gamma^4(z^2 + 2x_s)^{7/2}} + O\left(\frac{\varepsilon^4}{(z^2 + 2x_s)^{9/2}}\right),$$

into Eq. (19) at  $q \neq 0$ , transform it to the following form

$$L(n)B_j(x; z) + \left( \sum_{k=1}^{j_{\max}} V^{(k)}(z) \varepsilon^k - \delta\lambda_j(z) \right) B_j(x; z) = 0. \quad (26)$$

Here  $\varepsilon$  is a formal parameter that will be put to be 1 in the final expression. The parameters  $x_s = \rho_s^2/2$  and  $\rho_s$  approximately correspond to the minimum of the potential energy (2). In so doing, the Coulomb term is neglected. In the calculations we choose  $\rho_s = \sqrt{2|m|/\gamma}$  under assumption that the condition  $\gamma^2 \rho^2/4 + m^2/\rho^2 \gg 2|q|/\rho$  is valid. The approximation errors  $\delta U^{(j_{\max})}(\rho, z)$  at  $j_{\max} = 1, \dots, 9$  are illustrated in Fig. 1b. One can see that in the localization interval  $\rho \in [3000, 5000]$  of the eigenfunction (19), the errors decrease with increasing order  $j_{\max}$  (see Fig. 2). Performing Taylor expansion at  $|z|/\rho_s \gg 1$ , we arrive at the inverse power series that gives the same results as the perturbation theory in powers of  $1/|z|$  [8].

**Step 3.** The solution of Eq. (26) is found in the form of perturbation expansion in powers of  $\varepsilon$

$$\delta\lambda_j(z) = \sum_{k=1}^{k_{\max}} \varepsilon^k \lambda_n^{(k)}(z), \quad B_j(x; z) = B_n^{(0)}(x) + \sum_{k=0}^{k_{\max}} \varepsilon^k B_n^{(k)}(x, z). \quad (27)$$

Equating coefficients at the same powers of  $\varepsilon$ , we arrive at the system of inhomogeneous differential equations with respect to corrections  $\lambda_n^{(k)}(z)$  and  $B_n^{(k)}(x, z)$ :

$$L(n)B_n^{(0)}(x) = 0 \equiv f_n^{(0)}(z), \quad (28)$$

$$L(n)B_n^{(k)}(x, z) = (\lambda_n^{(k)}(z) - V^{(k)}(z))B_n^{(0)}(x)$$

$$+ \sum_{p=1}^{k-1} (\lambda_n^{(k-p)}(z) - V^{(k-p)}(z))B_n^{(p)}(x, z) \equiv f_n^{(k)}(z), \quad k \geq 1.$$

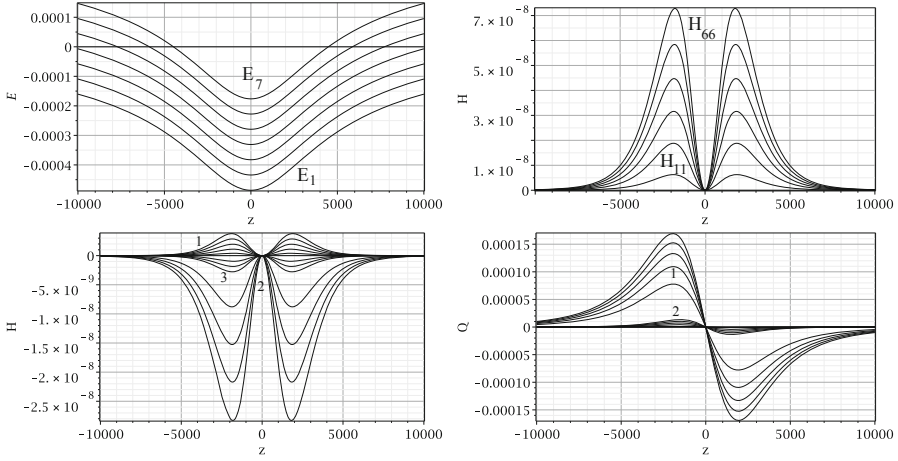


**Fig. 3.** The eigenvalues  $E_j(z)$  and the effective potentials  $H_{jj}(z)$ ,  $H_{jj'}(z)$  (curves  $H_{jj-1}(z)$ ,  $j = 2, \dots, 6$ , are marked by number 1, curves  $H_{jj-2}(z)$ ,  $j = 3, \dots, 6$ , are marked by number 2 and curves  $H_{jj-3}(z)$ ,  $j = 4, \dots, 6$ , are marked by number 3) and  $Q_{jj'}(z)$  (curves  $Q_{jj-1}(z)$ ,  $j = 2, \dots, 6$ , are marked by number 1, and curves  $Q_{jj-2}(z)$ ,  $j = 3, \dots, 6$ , are marked by number 2) for  $m = -200$ ,  $q = 1$ ,  $\gamma = 2.553191 \cdot 10^{-5}$

To solve Eqs. (26) we used the *nonnormalized* orthogonal basis

$$B_{n+s}(x) = C_{n|m|} e^{-\frac{x}{2}} x^{\frac{|m|}{2}} L_{n+s}^{|m|}(x) = C_{n|m|} C_{n+s|m|}^{-1} B_{n+s,m}^{(0)}(x), \quad (29)$$

$$\langle s|s' \rangle = \int_0^\infty B_{n+s}(x) B_{n+s'}(x) dx = \delta_{ss'} \gamma \frac{n!}{(n+|m|)!} \frac{(n+s+|m|)!}{(n+s)!}.$$

The action of the operators  $L(n)$  and  $x$  on the functions  $B_{n+s}(x)$  is defined by the relations

$$\begin{aligned} L(n)B_{n+s}(x) &= sB_{n+s}(x), \\ xB_{n+s}(x) &= -(n+s+|m|)B_{n+s-1}(x) + (2(n+s)+|m|+1)B_{n+s}(x) \\ &\quad -(n+s+1)B_{n+s+1}(x) \end{aligned} \quad (30)$$

that involve no fractional powers of quantum numbers  $n$  and  $m$ .

**Step 4.** Applying Eqs. (30), the right-hand side  $f_n^{(k)}(z)$  and the solutions  $B_n^{(k)}(x, z)$  of the system (28) are expanded over the *nonnormalized* basis states  $B_{n+s}(x)$

$$B_n^{(k)}(x, z) = \sum_{s=-s_{\max}}^{s_{\max}} b_{n;s}^{(k)}(z) B_{n+s}(x), \quad f_n^{(k)}(z) = \sum_{s=-s_{\max}}^{s_{\max}} f_{n;s}^{(k)}(z) B_{n+s}(x). \quad (31)$$

Then the recurrent set of linear algebraic equations for unknown *nonnormalized* coefficients  $b_{n;s}^{(k)}(z)$  and corrections  $\lambda_n^{(k)}(z)$  is obtained

$$s b_{n;s}^{(k)}(z) - f_{n;s}^{(k)}(z) = 0, \quad s = -s_{\max}, \dots, s_{\max},$$

which is solved sequentially for  $k = 1, 2, \dots, k_{\max}$ :

$$f_{n;0}^{(k)}(z) = 0 \rightarrow \lambda_n^{(k)}(z); \quad b_{n;s}^{(k)}(z) = f_{n;s}^{(k)}(z)/s, \quad s = -s_{\max}, \dots, s_{\max}, \quad s \neq 0.$$

The initial conditions (22) and  $b_{n;s}^{(0)}(z) = \delta_{s0}$  follow from Eqs. (21) and (24).

**Step 5.** To obtain the normalized wave function  $B_j(x; z)$  up to the  $k$ th order, the coefficient  $b_0^{(k)}$  are defined by the following relation:

$$b_{n;0}^{(k)}(z) = -\frac{1}{2\gamma} \sum_{p=1}^{k-1} \sum_{s'=-s_{\max}}^{s_{\max}} \sum_{s=-s_{\max}}^{s_{\max}} b_{n;s}^{(k-p)}(z) \langle s|s' \rangle b_{n;s'}^{(p)}(z), \quad b_{n;0}^{(k=1)}(z) = 0.$$

As an example of the output file at steps 1–5, we display nonzero coefficients  $\lambda_n^{(k)}(z)$ ,  $b_{n;s}^{(k)}(z)$  of the expansions (27), (31) over the *nonnormalized* basis functions (29) up to  $O(\varepsilon^2)$ :

$$\begin{aligned} \lambda_n^{(0)} &= n + (|m| + 1)/2, \\ \lambda_n^{(1)}(z) &= -\frac{q}{\gamma\sqrt{z^2 + 2x_s}} + \frac{q(2n + |m| + 1)}{\gamma^2(z^2 + 2x_s)^{3/2}} - \frac{x_s q}{\gamma(z^2 + 2x_s)^{3/2}}, \\ \lambda_n^{(2)}(z) &= -q^2(2n + |m| + 1)/(\gamma^4(z^2 + 2x_s)^3) - 3q[|m|^2 + 2 + 6n|m| \\ &\quad + 6n^2 + 6n + 3|m| - 2\gamma(2n + |m| + 1)x_s + x_s^2\gamma^2]/(2\gamma^3(z^2 + 2x_s)^{5/2}), \\ b_{n;0}^{(0)}(z) &= 1, \\ b_{n;-1}^{(1)}(z) &= -q(n + |m|)/(\gamma^2(z^2 + 2x_s)^{3/2}), \quad b_{n;1}^{(1)}(z) = q(n + 1)/(\gamma^2(z^2 + 2x_s)^{3/2}), \\ b_{n;-2}^{(2)}(z) &= q(n + |m|)(n + |m| - 1)(2q - 3\gamma\sqrt{(z^2 + 2x_s)})/(4\gamma^4(z^2 + 2x_s)^3), \\ b_{n;-1}^{(2)}(z) &= q(n + |m|)(2q + 3\gamma(2n + |m| - \gamma x_s)\sqrt{(z^2 + 2x_s)})/(\gamma^4(z^2 + 2x_s)^3), \\ b_{n;0}^{(2)}(z) &= q^2(2n^2 + 2n + 2n|m| + |m| + 1)/(2\gamma^4(z^2 + 2x_s)^3), \\ b_{n;1}^{(2)}(z) &= -q(n + 1)(2q + 3\gamma(2n + |m| + 2 - \gamma x_s)\sqrt{(z^2 + 2x_s)})/(\gamma^4(z^2 + 2x_s)^3), \\ b_{n;2}^{(2)}(z) &= q(n + 1)(n + 2)(2q + 3\gamma\sqrt{(z^2 + 2x_s)})/(4\gamma^4(z^2 + 2x_s)^3). \end{aligned} \quad (32)$$

These expansions involve parameters  $x_s = \rho_s^2/2$  and  $\rho_s$  that approximately corresponded to the minimum of the potential energy (2) and determined the point  $x_0 = \gamma x_s$  of expansion of (25) of Coulomb potential  $V_c(x, z)$ .

**Step 6.** In terms of the scaled variable  $x$ , the expressions of the effective potentials  $H_{ij}(z) = H_{ji}(z)$  and  $Q_{ij}(z) = -Q_{ji}(z)$  take the form

$$H_{ij}(z) = \frac{1}{\gamma} \int_0^\infty dx \frac{\partial B_i(x; z)}{\partial z} \frac{\partial B_j(x; z)}{\partial z}, \quad Q_{ij}(z) = -\frac{1}{\gamma} \int_0^\infty dx B_i(x; z) \frac{\partial B_j(x; z)}{\partial z}. \quad (33)$$

To calculate them we expand the solution (26) over the *normalized* orthogonal basis  $B_{n+s;m}^{(0)}(x)$  with the *normalized* coefficients  $b_{n;n+s;m}^{(k)}(z)$ ,

$$B_j(x; z) \equiv B_j^m(x; z) = \sum_{k=0}^{k_{\max}} \varepsilon^k \sum_{s=-s_{\max}}^{s_{\max}} b_{n;n+s;m}^{(k)}(z) B_{n+s;m}^{(0)}(x). \quad (34)$$



The normalized coefficients  $b_{n;n+s;m}^{(k)}(z)$  are expressed via  $b_{n;s}^{(k)}(z)$ ,

$$b_{n;n+s;m}^{(k)}(z) = b_{n;s}^{(k)}(z) \sqrt{\frac{n!}{(n+|m|)!} \frac{(n+s+|m|)!}{(n+s)!}} \quad (35)$$

as follows from Eqs. (31), (34), and (29).

**Step 7.** As a result of substituting Eqs. (34) into Eq. (33), the matrix elements take the form

$$\begin{aligned} Q_{jj+t}(z) &= -\sum_{k=0}^{k_{\max}} \varepsilon^k \sum_{k'=0}^k \sum_{s=\max(-s_{\max}, -s_{\max}+t)}^{\min(s_{\max}, s_{\max}+t)} b_{n;n+s;m}^{(k')}(z) \frac{db_{n+t;n+s;m}^{(k-k')}(z)}{dz}, \\ H_{jj+t}(z) &= \sum_{k=0}^{k_{\max}} \varepsilon^k \sum_{k'=0}^k \sum_{s=\max(-s_{\max}, -s_{\max}+t)}^{\min(s_{\max}, s_{\max}+t)} \frac{db_{n;n+s;m}^{(k')}(z)}{dz} \frac{db_{n+t;n+s;m}^{(k-k')}(z)}{dz}. \end{aligned} \quad (36)$$

By collecting the coefficients at similar powers of  $\varepsilon$  in Eq. (36) the algorithm yields the final expansions of eigenvalues and effective potentials available in the output file

$$E_j(z) = \sum_{k=0}^{k_{\max}} E_j^{(k)}(z), \quad H_{ij}(z) = \sum_{k=2}^{k_{\max}} H_{ij}^{(k)}(z), \quad Q_{ij}(z) = \sum_{k=1}^{k_{\max}} Q_{ij}^{(k)}(z). \quad (37)$$

Successful runs of the Maple implementation of the algorithm were performed up to  $k_{\max} = 6$  (the run time 30 s using Intel Core i5, 3.36 GHz, 4 GB). Below we present a few first nonzero coefficients derived *in the analytic form* ( $j = n+1$ ):

$$\begin{aligned} E_j^{(0)} &= 2\gamma(n + (m + |m| + 1)/2), \\ E_j^{(1)}(z) &= -\frac{2q}{\sqrt{z^2 + \rho_s^2}} + \frac{2q(2n + |m| + 1)}{\gamma(z^2 + \rho_s^2)^{3/2}} - \frac{\rho_s^2 q}{(z^2 + \rho_s^2)^{3/2}}, \\ E_j^{(2)}(z) &= -\frac{2q^2(2n + |m| + 1)}{\gamma^3(z^2 + \rho_s^2)^3} \\ &\quad - \frac{3q[|m|^2 + 2 + 6n|m| + 6n^2 + 6n + 3|m| - \gamma(2n + |m| + 1)\rho_s^2 + \rho_s^4\gamma^2/4]}{\gamma^2(z^2 + \rho_s^2)^{5/2}}, \\ Q_{jj-1}^{(1)}(z) &= -\sqrt{n}\sqrt{n+|m|} \frac{3zq}{\gamma^2(z^2 + \rho_s^2)^{5/2}}, \\ Q_{jj-1}^{(2)}(z) &= -\sqrt{n}\sqrt{n+|m|} \left[ \frac{15zq(2|m| + 4n - \rho_s^2\gamma)}{2\gamma^3(z^2 + \rho_s^2)^{7/2}} + \frac{12zq^2}{\gamma^4(z^2 + \rho_s^2)^4} \right], \\ Q_{jj-2}^{(2)}(z) &= -\sqrt{n}\sqrt{n-1}\sqrt{n+|m|}\sqrt{n+|m|-1} \frac{15qz}{4\gamma^3(z^2 + \rho_s^2)^{7/2}}, \\ H_{jj}^{(2)}(z) &= 9q^2(2n^2 + 2n|m| + 2n + |m| + 1) \left[ \frac{1}{\gamma^4(z^2 + \rho_s^2)^4} - \frac{\rho_s^2}{\gamma^4(z^2 + \rho_s^2)^5} \right], \\ H_{jj-2}^{(2)}(z) &= -9q^2\sqrt{n}\sqrt{n-1}\sqrt{n+|m|}\sqrt{n+|m|-1} \left[ \frac{1}{\gamma^4(z^2 + \rho_s^2)^4} + \frac{\rho_s^2}{\gamma^4(z^2 + \rho_s^2)^5} \right]. \end{aligned}$$

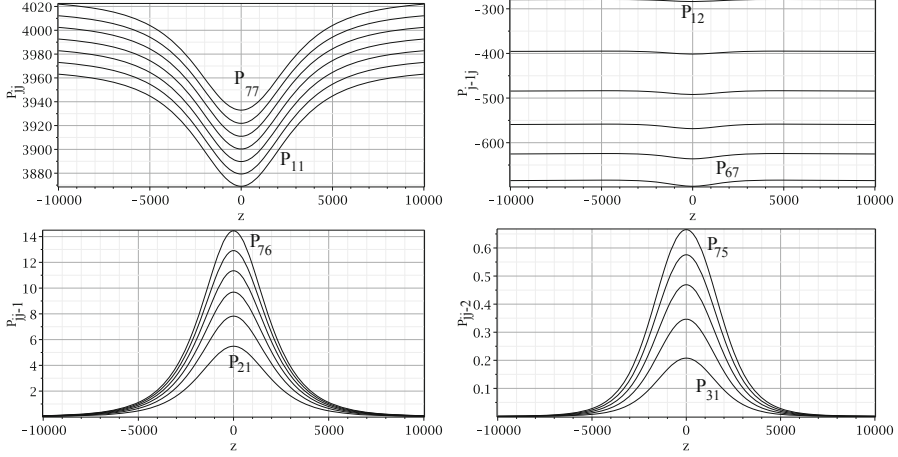


**Fig. 4.** Transverse dipole matrix elements  $P_{nn'}^{(0);|m||m|±1}$  (subscripts  $n, n'$  run 0, 1, 2, 3, 4, 5, 6) for  $m = -200$ ,  $q = 1$ ,  $\gamma = 2.553191 \cdot 10^{-5}$

As an example, Fig. 3 shows the eigenvalues and effective potentials (37), which agree with those calculated numerically using ODPEVP [10] with the accuracy of the order of  $10^{-10}$ . We used finite element grid on the interval  $\rho \in [\rho_{\min} = 2000, \rho_{\max} = 6000]$  with the Lagrange elements of fourth order. Expanding (37) into the Taylor series at  $|z|/\rho_s \gg 1$ , we arrive at perturbation expansion in powers of  $1/z$  [8].

#### 4 Calculations of the Transversal Dipole Matrix Elements

Using the scaled variable  $x$  defined by Eq. (18) one can express the transverse dipole matrix elements  $P_{ij}^{(0);|m||m|±1}(z) = \langle |m|, n | \rho e^{\pm i\varphi} | |m| \mp 1, n' \rangle$  and  $P_{ij}^{(0);-|m|,-|m|±1}(z) = \langle -|m|, n | \rho e^{\mp i\varphi} | -|m| \pm 1, n' \rangle$  possessing the property

$$\langle |m|, n | \rho \exp(\pm i\varphi) | |m| \mp 1, n' \rangle^* = \langle |m| \mp 1, n' | \rho \exp(\mp i\varphi) | |m|, n \rangle,$$

where  $i = n + 1$  and  $j = n' + 1$ , in the following form

$$P_{ij}^{(0);-|m|,-|m|±1}(z) = P_{ij}^{(0);|m||m|±1}(z) = \sqrt{\frac{2}{\gamma^3}} \int_0^\infty dx B_i^{|m|}(x; z) \sqrt{x} B_j^{|m|±1}(x; z). \quad (38)$$

According to Eqs. (22.7.12), (33.7.30), and (22.7.31) of [14], the dipole moment matrix elements calculated with normalized basis functions  $||m|, n\rangle = B_{n|m|}^{(0)}(x) e^{i|m|\varphi} / \sqrt{2\pi}$  by means of Eq. (23) are expressed as

$$P_{ij}^{(0);|m||m|±1} = \sqrt{\frac{2}{\gamma^3}} \langle |m|, n | \sqrt{x} e^{\pm i\varphi} | |m| \mp 1, n' \rangle$$

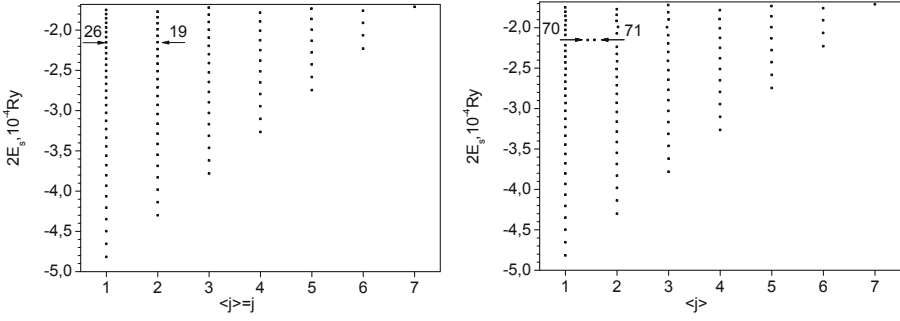


**Fig. 5.** Energy eigenvalues  $2E_s$  for even ( $\sigma = +1$ ) lower eigenstates vs the state number  $\langle j \rangle$  calculated in the diagonal adiabatic approximation (left) and in the Kantorovich approximation at  $j_{\max} = 6$  with given accuracy (right). Here  $m = -200$ ,  $\gamma = 2.553191 \cdot 10^{-5}$ ,  $q = 1$ ,  $\sigma = +1$ . The quantity  $\langle j \rangle = \sum_j \int j \chi_{j,s}(z)^2 dz$  is the averaged quantum number,  $s$  is the eigenvalue number in the ascending energy sequence  $E_1 < E_2 < \dots < E_s < \dots < \gamma/2$ , corresponding to the number  $v$  of the eigenvalue  $E_{j1} < E_{j2} < \dots < E_{jv} < \dots < \gamma/2$  counted at each  $\langle j \rangle = j$  in diagonal approximation (17) of Eqs. (12)

$$\begin{aligned}
 &= \sqrt{\frac{2}{\gamma^3}} \frac{1}{2\pi} \int_0^{2\pi} d\varphi \int_0^\infty e^{-i|m|\varphi} B_{i,|m|}^{(0)}(x) e^{\pm i\varphi} \sqrt{x} e^{i(|m|\mp 1)\varphi} B_{i,|m|\mp 1}^{(0)}(x) dx \\
 &= \sqrt{\frac{2}{\gamma}} \left[ \delta_{nn'} \sqrt{n + |m| + 1/2 \mp 1/2} - \delta_{n\mp 1, n'} \sqrt{n + 1/2 \mp 1/2} \right]. \quad (39)
 \end{aligned}$$

As a result of substituting Eqs. (34) and (39) into Eq. (38), the matrix elements take the following *analytic* form ( $j = n + 1$ )

$$\begin{aligned}
 P_{jj+t}^{|m|, |m|-1}(z) &= \sum_{k=0}^{k_{\max}} P_{jj+t}^{(k); |m|, |m|-1}(z), \\
 P_{jj+t}^{(k); |m|, |m|-1}(z) &= \sqrt{\frac{2}{\gamma}} \sum_{k'=0}^k \sum_{s=\max(-k, k'-k-t)}^{\min(k, k-k'-t)} \left[ b_{n;n+s;|m|}^{(k')}(z) b_{n+t;n+s;|m|-1}^{(k-k')}(z) \right. \\
 &\quad \times \left. \sqrt{n+s+|m|+1} - b_{n;n+s;|m|}^{(k')}(z) b_{n+t;n+s+1;|m|-1}^{(k-k')}(z) \sqrt{n+s+1} \right]. \quad (40)
 \end{aligned}$$

Successful run of the Maple-implemented algorithm was performed up to  $k_{\max} = 6$  (run time 90 s with Intel Core i5, 3.36 GHz, 4 GB). A few first nonzero coefficients derived *in the analytic form* are presented below ( $j = n + 1$ ):

$$\begin{aligned}
 P_{jj}^{(0); |m|, |m|-1}(z) &= + \frac{\sqrt{2}\sqrt{n+|m|+1}}{\sqrt{\gamma}}, \quad P_{jj}^{(1); |m|, |m|-1}(z) = - \frac{\sqrt{2}\sqrt{n+|m|}q}{\gamma^{5/2}(\rho_s^2 + z^2)^{3/2}}, \\
 P_{j-1j}^{(0); |m|, |m|-1}(z) &= - \frac{\sqrt{n}\sqrt{2}}{\sqrt{\gamma}}, \\
 P_{j-1j}^{(1); |m|, |m|-1}(z) &= - \frac{\sqrt{n}\sqrt{2}\sqrt{n+|m|}(\sqrt{n+|m|-1} - \sqrt{n+|m|+1})q}{(\rho_s^2 + z^2)^{3/2}\gamma^{5/2}}, \quad (41)
 \end{aligned}$$

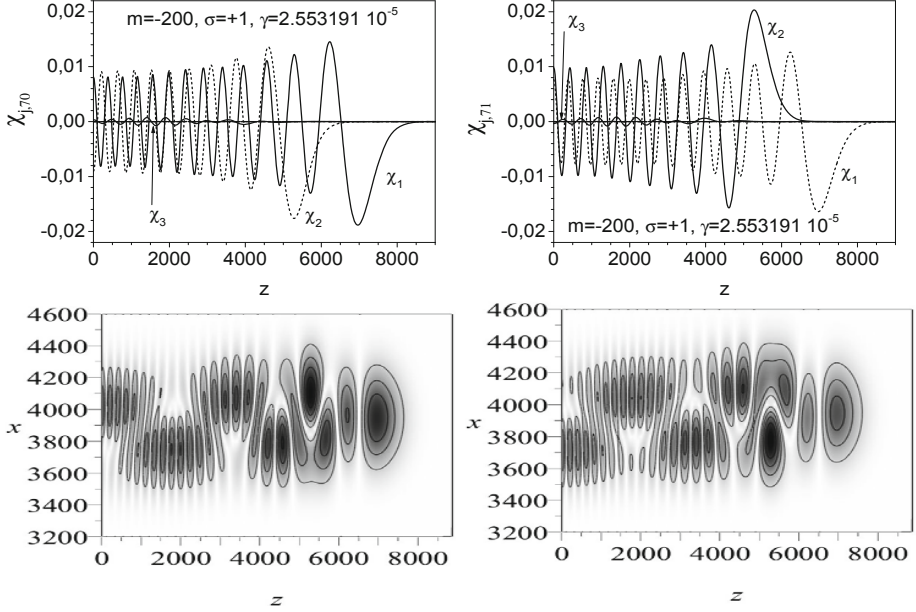


**Fig. 6.** Upper panels: the first three components of the eigenfunctions  $\chi_{j,70}$  and  $\chi_{j,71}$  ( $j = 1, 2, 3$ ). The dominant components are  $j = 1$  ( $\langle j \rangle = 1.43$ ) with  $v - 1 = 25$  nodes and  $j = 2$  ( $\langle j \rangle = 1.56$ ) with  $v - 1 = 18$  nodes, respectively. Lower panels: the profile of the wave function  $\Psi_{s=70}^{m=-200, \sigma=+1}(\rho, z)$  and  $\Psi_{s=71}^{m=-200, \sigma=+1}(\rho, z)$  of the resonance states in the  $zx$  plane with the energies  $2E_{s=70}^{m=-200, \sigma=+1} = -2.151832 \cdot 10^{-4} \text{ Ry}$  and  $2E_{s=71}^{m=-200, \sigma=+1} = -2.150977 \cdot 10^{-4} \text{ Ry}$  pointed by arrows in the right panel of Fig. 5

$$P_{jj-1}^{(1); |m||m|-1}(z) = \frac{\sqrt{n}\sqrt{2}(\sqrt{n+|m|-1}\sqrt{n+|m|+1} - n - |m|)q}{(\rho_s^2 + z^2)^{3/2}\gamma^{5/2}}.$$

The comparison of our analytical numerical results with those obtained numerically using the program ODPEVP [10] shows the convergence of the perturbation series expansion up to  $k_{\text{max}} = 6$  with four significant digits. Expanding (40) into a Taylor series at  $|z|/\rho_s \gg 1$ , we arrive at the inverse power series for the dipole matrix elements. To obtain the leading terms at  $|z| \rightarrow \infty$  it is sufficiently to put  $\rho_s = 0$  in (41).

## 5 Calculations of Rydberg States and Decay Rates

In Fig. 5 we present an example of the lower part of discrete spectrum calculated in the diagonal adiabatic and Kantorovich approximations with the effective potentials (37) by means of the program KANTBP2 [1]. In numerical calculations at  $q = -1$ ,  $\gamma = 2.553191 \cdot 10^{-5}$  for  $|m| \sim 200$ , we use finite element grid on the interval  $z \in [0, z_{\text{max}} = 11000]$  with the Lagrange elements of fourth order. In

Fig. 6, we show an example of resonance states formed by coupling of the quasi-degenerate states with the energies  $2E_{j=1,v=26}^{m=-200,\sigma=+1} = -2.151260 \cdot 10^{-4} \text{ Ry}$  and  $2E_{j=2,v=19}^{m=-200,\sigma=+1} = -2.151202 \cdot 10^{-4} \text{ Ry}$  in the diagonal adiabatic approximation (17) pointed by arrows in the left panel of Fig. 5.

The partial transition decay rates  $\Gamma_{\tilde{s} \rightarrow \tilde{s}'}$  are calculated as

$$\Gamma_{\tilde{s} \rightarrow \tilde{s}'} = \frac{4}{3} \frac{e^2 \omega_{\tilde{s}\tilde{s}'}^3}{4\pi\epsilon_0 \hbar c^3} |\langle \tilde{s}' | \mathbf{r} | \tilde{s} \rangle|^2, \quad \omega_{\tilde{s}\tilde{s}'} = (\bar{E}_{\tilde{s}'} - \bar{E}_{\tilde{s}}) / \hbar. \quad (42)$$

In the above expressions,  $\epsilon_0 = 8.854187817 \cdot 10^{-12} \text{ F/m}$  is the dielectric constant, the energy  $\bar{E}_{\tilde{s}'} = E_{\tilde{s}'} E_B$  and the dipole moment  $\langle \tilde{s}' | \mathbf{r} | \tilde{s} \rangle = a_B \langle \tilde{s}' | \mathbf{r} | \tilde{s} \rangle$  are expressed in the atomic units  $E_B = 2 \text{ Ry} = 4.35974434 \cdot 10^{-18} \text{ J}$ ,  $a_B = 0.52917721092 \cdot 10^{-10} \text{ m}$ , i.e.

$$\Gamma_{\tilde{s} \rightarrow \tilde{s}'} = 2.142 \cdot 10^{10} (E_{\tilde{s}'} - E_{\tilde{s}})^3 |\langle \tilde{s}' | \mathbf{r} | \tilde{s} \rangle|^2 \times \text{s}^{-1}. \quad (43)$$

Here  $|\langle \tilde{s}' | \mathbf{r} | \tilde{s} \rangle|^2$  defined by the expression

$$|\langle \tilde{s}' | \mathbf{r} | \tilde{s} \rangle|^2 = (1/2) |\langle \tilde{s}' | \rho e^{-i\varphi} | \tilde{s} \rangle|^2 + |\langle \tilde{s}' | z | \tilde{s} \rangle|^2 + (1/2) |\langle \tilde{s}' | \rho e^{+i\varphi} | \tilde{s} \rangle|^2, \quad (44)$$

where  $\langle \tilde{s}' | z | \tilde{s} \rangle$  and  $\langle \tilde{s}' | \rho e^{\pm i\varphi} | \tilde{s} \rangle$  are the longitudinal and transverse dipole moment, respectively. As follows from Eq. (40),

$$\langle \tilde{s}' | z | \tilde{s} \rangle = \delta_{m'm} \delta_{-\sigma'\sigma} \sum_{i,j=1}^{j_{\max}} \int_{z_{\min}}^{z_{\max}} dz \chi_{i\tilde{s}'}^{m\sigma'}(z) z \chi_{j\tilde{s}}^{m\sigma}(z), \quad (45)$$

$$\langle \tilde{s}' | \rho e^{\pm i\varphi} | \tilde{s} \rangle = \delta_{m'm \mp 1} \delta_{\sigma'\sigma} \sum_{i,j=1}^{j_{\max}} \int_{z_{\min}}^{z_{\max}} dz \chi_{i\tilde{s}'}^{m'\sigma}(z) P_{ij}^{m',m}(z) \chi_{j\tilde{s}}^{m\sigma}(z). \quad (46)$$

In Table 1 we show our present results for partial decay rates (43) and dipole moments (45) and (46). The results were obtained numerically by means of the program KANTBP 2.0 [1] using the analytically derived effective potentials (37) and matrix elements of transversal dipole moments (40), i.e.,  $M_{\tilde{s}'\tilde{s}} = \langle \tilde{s}' | \rho e^{-i\varphi} | \tilde{s} \rangle$  for cyclotron decay (C) ( $q \rightarrow q' = q$ , where  $q = j - m$  is magnetron quantum number,  $m \rightarrow m' = m - 1$ ,  $\sigma \rightarrow \sigma' = \sigma$ ,  $j \rightarrow j' = j - 1$ ,  $v \rightarrow v' = v$ );  $M_{\tilde{s}'\tilde{s}} = \langle \tilde{s}' | z | \tilde{s} \rangle$  for the bounce decay (B) ( $q \rightarrow q' = q$ ,  $m \rightarrow m' = m$ ,  $\sigma \rightarrow \sigma' = -\sigma$ ,  $j \rightarrow j' = j$ ,  $v \rightarrow v' = v - 1$ ), and  $M_{\tilde{s}'\tilde{s}} = \langle \tilde{s}' | \rho e^{+i\varphi} | \tilde{s} \rangle$  for the magnetron decay (M) ( $q \rightarrow q' = q - 1$ ,  $m \rightarrow m' = m + 1$ ,  $\sigma \rightarrow \sigma' = \sigma$ ,  $j \rightarrow j' = j$ ,  $v \rightarrow v' = v$ ). The results agree with the numerical ones from [12] within the required accuracy.

In Table 1 we also show the energy values  $2E_{|\tilde{s}}|$  calculated in the Kantorovich approximation (K) at  $j_{\max} = 6$ , and obtained by the aid of the diagonal approximation (17) in the *analytical form*

$$2E_{|\tilde{s}}| \approx 2E_{i,v}^{m,\sigma} = U_{ii}^{(0)} + \mathcal{E}_{i,v}^{(0)} + \sum_{\kappa=2}^{\kappa_{\max}} \mathcal{E}_{i,v}^{(\kappa-1)}, \quad (47)$$

$$\mathcal{E}_{i,v}^{(0)} = \omega_{z,i}(2v+1), \quad \mathcal{E}_{i,v}^{(1)} = \frac{3U_i^{(4)}(2v^2+2v+1)}{4\omega_{z,i}^2},$$

$$\mathcal{E}_{i,v}^{(2)} = -\frac{(2v+1)(17v^2+17v+21)(U_i^{(4)})^2}{16\omega_{z,i}^5} + \frac{5(2v+1)(2v^2+2v+3)U_i^{(6)}}{8\omega_{z,i}^3}.$$

**Table 1.** The partial transition decay rates  $\Gamma_{\tilde{s} \rightarrow \tilde{s}'}$  evaluated using Eq. (43) from the state  $|\tilde{s}\rangle = |j, v, \sigma, m\rangle$  to  $|\tilde{s}'\rangle = |j', v', \sigma', m'\rangle$  with energies  $2E_{|\tilde{s}\rangle}$  and  $2E_{|\tilde{s}'\rangle}$  calculated using the Kantorovich approximation (K) at  $j_{\max} = 6$  and the corresponding dipole moments  $M_{\tilde{s}'\tilde{s}}$ . In square brackets, numerical results of [12] are given. The energies calculated in *analytical form* using the crude diagonal approximation with the Taylor series of  $U_{ii}(z) = E_i(z)$  up to harmonic (H) and anharmonic (A) terms of order of  $z^2$  and  $z^{10}$ , respectively. The corresponding energies in the diagonal approximation with Taylor series of  $U_{ii}(z) = E_i(z) + H_{ii}(z)$  differing only in two last digits, are shown in parentheses.

	$\tilde{s}$	$\tilde{s}'$	$ j, v, \sigma, m\rangle$	$ j', v', \sigma', m'\rangle$	$\Gamma_{\tilde{s} \rightarrow \tilde{s}'},$ $s^{-1}$	$M_{\tilde{s}'\tilde{s}},$ $a_B$	$2E_{\tilde{s}},$ $10^{-4}\text{Ry}$	$2E_{\tilde{s}'},$ $10^{-4}\text{Ry}$
C	5	1	$ 2, 1, +1, -200\rangle$	$ 1, 1, +1, -201\rangle$	13.1 [13.7]	276.4 [283]	K -4.29933 H -4.29978(76) A -4.30019(18)	-4.80384 -4.80384(83) -4.80424(23)
C	13	5	$ 3, 1, +1, -200\rangle$	$ 2, 1, +1, -201\rangle$	26.3 [27.5]	390.9 [401]	K -3.78171 H -3.78299(95) A -3.78342(38)	-4.28632 -4.28688(86) -4.28729(27)
B	1	1	$ 1, 2, -1, -200\rangle$	$ 1, 1, +1, -200\rangle$	0.180 [0.178]	349.4 [350]	K -4.73499 H -4.73329(27) A -4.73531(29)	-4.81688 -4.81683(83) -4.81724(23)
B	2	1	$ 1, 3, +1, -200\rangle$	$ 1, 2, -1, -200\rangle$	0.345 [0.342]	499.0 [500]	K -4.65469 H -4.64974(71) A -4.65497(94)	-4.73499 -4.73329(27) -4.73531(29)
M	1	1	$ 1, 1, +1, -200\rangle$	$ 1, 1, +1, -199\rangle$	0.045 [0.044]	3870 [3872]	K -4.81688 H -4.81683(83) A -4.81724(23)	-4.83003 -4.82993(93) -4.83034(33)

The latter was obtained using SNA like in Section 3, but for a perturbed 1D oscillator with *adiabatic frequency*  $\omega_{z,i}$ . It was accomplished with the help of a Taylor expansion up to  $z^{2\kappa_{\max}}$  of effective potentials  $U_{ii}(z) = E_i(z) + H_{ii}(z)$  from Eq. (37) for the harmonic (H) and anharmonic (A) terms, i.e.,  $2\kappa_{\max} = 2$  and  $2\kappa_{\max} = 10$ , respectively,

$$U_{ii}(z) = U_{ii}(0) + \omega_{z,i}^2 z^2 + \sum_{\kappa=2}^{\kappa_{\max}} U_i^{(2\kappa)} z^{2\kappa}. \quad (48)$$

Moreover, in Table 1 we present also the results for the energies (47) in the crude and adiabatic approximations obtained without and with the diagonal potential  $H_{ii}$ , respectively. One can see that the energies in crude adiabatic and adiabatic approximations differ only in two last significant figures, i.e., are the same within the accuracy of  $\sim 10^{-8}$ . One can see from Table 1 that the adiabatic harmonic (H) diagonal approximation and the crude anharmonic (A) one provide the *upper and lower estimations of the energy values of low-excited Rydberg states* with  $j = 1$ , respectively.

*Remark 2.* In the expansions (47) and (48), the coefficients are calculated using  $U_{ii}^{(0)} = U_{ii}(0)$ ,  $\omega_{z,i}^2 = (d^2 U_{ii}(z)/dz^2)_{z=0}/2$ ,  $U_i^{(2\kappa)} = (d^{2\kappa} U_{ii}(z)/dz^{2\kappa})_{z=0}/((2\kappa)!)$ .

In the harmonic approximation  $\omega_{z,i}^2 = \sum_{k=1}^{k_{\max}} \omega_{z,i,E}^{(k)} + \sum_{k=2}^{k_{\max}} \omega_{z,i,H}^{(k)}$ , where  $\omega_{z,i,E}^{(k)} = (d^2 E_i^{(k)}(z)/dz^2)_{z=0}/2$  and  $\omega_{z,i,H}^{(k)} = (d^2 H_{ii}^{(k)}(z)/dz^2)_{z=0}/2$ , the leading terms are:

$$\begin{aligned} \omega_{z,i,E}^{(1)} &= \frac{5q}{2\rho_s^3} - \frac{3q(2n+|m|+1)}{\gamma\rho_s^5}, & \omega_{z,i,H}^{(2)} &= \frac{9q^2(2n^2+2n|m|+2n+|m|+1)}{\rho_s^{10}\gamma^4}, \\ \omega_{z,i,E}^{(2)} &= \frac{15q}{8\rho_s^3} - \frac{15q(2n+|m|+1)}{2\gamma\rho_s^5} + \frac{15q(6n^2+6n|m|+6n+m^2+3|m|+2)}{2\gamma^2\rho_s^7} \\ &\quad + \frac{6q^2(2n+|m|+1)}{\gamma^3\rho_s^8}. \end{aligned}$$

The substitution of  $\rho_s = \sqrt{2|m|/\gamma}$  into the leading term  $\omega_{z,i}^2 \approx \omega_{z,i,E}^{(1)}$  at  $n = 0$  yields  $\omega_{z,i}^2 \approx (q\sqrt{\gamma}(2|m|-3))/(4m^2\sqrt{2|m|})$ . At  $q = 1$  we obtain the *adiabatic parameter*  $(\omega_\rho/\omega_{z,i=1})^{4/3} = |m|\gamma^{1/3}$ , where  $\omega_\rho = \gamma/2$ , in agreement with [13].

## 6 Conclusions

A new efficient method to calculate wave functions and decay rates of high- $|m|$  Rydberg states of a hydrogen atom in a magnetic field is developed. It is based on the KM application to parametric eigenvalue problems in cylindrical coordinates. The results are in a good agreement with the calculations executed in spherical coordinates at fixed  $|m| > 140$  for  $\gamma \sim 2.553 \cdot 10^{-5}$ . The elaborated SNA for calculation of the effective potentials, dipole moment matrix elements, and the perturbation solutions *in analytic form* allows us to generate effective approximations for a finite set of longitudinal equations. This provides benchmark calculations for the new version KANTBP3 of our earlier program KANTBP2 [1] announced in [9]. The developed approach is a useful tool for calculating the threshold phenomena in formation, decay, and ionization of (anti)hydrogen-like atoms and ions in magneto-optical traps [11,12,13], and channelling of ions in thin films [4].

The authors thank Prof. V.L. Derbov for valuable discussions.

## References

1. Chuluunbaatar, O., Gusev, A.A., Vinitsky, S.I., Abrashkevich, A.G.: KANTBP 2.0: New version of a program for computing energy levels, reaction matrix and radial wave functions in the coupled-channel hyperspherical adiabatic approach. Phys. Commun. 179, 685–693 (2008)
2. Gusev, A., Gerdt, V., Kaschiev, M., Rostovtsev, V., Samoylov, V., Tupikova, T., Vinitsky, S.: A Symbolic-Numerical Algorithm for Solving the Eigenvalue Problem for a Hydrogen Atom in Magnetic Field. In: Ganzha, V.G., Mayr, E.W., Vorozhtsov, E.V. (eds.) CASC 2006. LNCS, vol. 4194, pp. 205–218. Springer, Heidelberg (2006)
3. Chuluunbaatar, O., Gusev, A.A., Derbov, V.L., Kaschiev, M.S., Melnikov, L.A., Serov, V.V., Vinitsky, S.I.: Calculation of a hydrogen atom photoionization in a strong magnetic field by using the angular oblate spheroidal functions. J. Phys. A 40, 11485–11524 (2007)

4. Gusev, A.A., Derbov, V.L., Krassovitskiy, P.M., Vinitsky, S.I.: Channeling problem for charged particles produced by confining environment. *Phys. At. Nucl.* 72, 768–778 (2009)
5. Chuluunbaatar, O., Gusev, A.A., Gerdt, V.P., Rostovtsev, V.A., Vinitsky, S.I., Abrashkevich, A.G., Kaschiev, M.S., Serov, V.V.: POTHMF: A program for computing potential curves and matrix elements of the coupled adiabatic radial equations for a hydrogen-like atom in a homogeneous magnetic field. *Comput. Phys. Commun.* 178, 301–330 (2008)
6. Gusev, A.A., Chuluunbaatar, O., Gerdt, V.P., Rostovtsev, V.A., Vinitsky, S.I., Derbov, V.L., Serov, V.V.: Symbolic-Numeric Algorithms for Computer Analysis of Spheroidal Quantum Dot Models. In: Gerdt, V.P., Koepf, W., Mayr, E.W., Vorozhtsov, E.V. (eds.) *CASC 2010. LNCS*, vol. 6244, pp. 106–122. Springer, Heidelberg (2010); arXiv:1104.2292
7. Vinitsky, S.I., Chuluunbaatar, O., Gerdt, V.P., Gusev, A.A., Rostovtsev, V.A.: Symbolic-Numerical Algorithms for Solving Parabolic Quantum Well Problem with Hydrogen-Like Impurity. In: Gerdt, V.P., Mayr, E.W., Vorozhtsov, E.V. (eds.) *CASC 2009. LNCS*, vol. 5743, pp. 334–349. Springer, Heidelberg (2009)
8. Chuluunbaatar, O., Gusev, A., Gerdt, V., Kaschiev, M., Rostovtsev, V., Samoylov, V., Tupikova, T., Vinitsky, S.: A Symbolic-Numerical Algorithm for Solving the Eigenvalue Problem for a Hydrogen Atom in the Magnetic Field: Cylindrical Coordinates. In: Ganzha, V.G., Mayr, E.W., Vorozhtsov, E.V. (eds.) *CASC 2007. LNCS*, vol. 4770, pp. 118–133. Springer, Heidelberg (2007)
9. Gusev, A.A., Vinitsky, S.I., Chuluunbaatar, O., Gerdt, V.P., Rostovtsev, V.A.: Symbolic-Numerical Algorithms to Solve the Quantum Tunneling Problem for a Coupled Pair of Ions. In: Gerdt, V.P., Koepf, W., Mayr, E.W., Vorozhtsov, E.V. (eds.) *CASC 2011. LNCS*, vol. 6885, pp. 175–191. Springer, Heidelberg (2011)
10. Chuluunbaatar, O., Gusev, A.A., Vinitsky, S.I., Abrashkevich, A.G.: ODPEVP: A program for computing eigenvalues and eigenfunctions and their first derivatives with respect to the parameter of the parametric self-adjointed Sturm-Liouville problem. *Comput. Phys. Commun.* 180, 1358–1375 (2009)
11. Chuluunbaatar, O., Gusev, A.A., Vinitsky, S.I., Derbov, V.L., Melnikov, L.A., Serov, V.V.: Photoionization and recombination of a hydrogen atom in a magnetic field. *Phys. Rev. A* 77, 034702–1–034702–4 (2008)
12. Guest, J.R., Choi, J.-H., Raithel, G.: Decay rates of high- $|m|$  Rydberg states in strong magnetic fields. *Phys. Rev. A* 68, 022509–1–022509–9 (2003)
13. Guest, J.R., Raithel, G.: High- $|m|$  Rydberg states in strong magnetic fields. *Phys. Rev. A* 68, 052502–1–052502–9 (2003)
14. Abramovits, M., Stegun, I.A.: *Handbook of Mathematical Functions*. Dover, New York (1972)





# Symbolic-Numerical Solution of Boundary-Value Problems with Self-adjoint Second-Order Differential Equation Using the Finite Element Method with Interpolation Hermite Polynomials

Alexander A. Gusev<sup>1</sup>, Ochbadrakh Chuluunbaatar<sup>1,2</sup>, Sergue I. Vinitsky<sup>1</sup>,  
Vladimir L. Derbov<sup>3</sup>, Andrzej Gózdź<sup>4</sup>, Luong Le Hai<sup>1,5</sup>,  
and Vitaly A. Rostovtsev<sup>1</sup>

<sup>1</sup> Joint Institute for Nuclear Research, Dubna, Russia,  
gooseff@jinr.ru

<sup>2</sup> National University of Mongolia, UlaanBaatar, Mongolia

<sup>3</sup> Saratov State University, Saratov, Russia

<sup>4</sup> Institute of Physics, Maria Curie-Skłodowska University, Lublin, Poland

<sup>5</sup> Belgorod State University, Belgorod, Russia

**Abstract.** We present a symbolic algorithm generating finite-element schemes with interpolating Hermite polynomials intended for solving the boundary-value problems with self-adjoint second-order differential equation and implemented in the Maple computer algebra system. Recurrence relations for the calculation in analytical form of the interpolating Hermite polynomials with nodes of arbitrary multiplicity are derived. The integrals of interpolating Hermite polynomials are used for constructing the stiffness and mass matrices and formulating a generalized algebraic eigenvalue problem. The algorithm is used to generate Fortran routines that allow solution of the generalized algebraic eigenvalue problem with matrices of large dimension. The efficiency of the programs generated in Maple and Fortran is demonstrated by the examples of exactly solvable quantum-mechanical problems with continuous and piecewise continuous potentials.

## 1 Introduction

The study of mathematical models that describe tunneling and channeling of composite quantum systems through multidimensional barriers, photo-ionization and photo-absorption in molecular, atomic, nuclear, and quantum-dimensional semiconductor systems, requires high-accuracy efficient algorithms and programs for solving boundary-value problems (BVPs) [7,5,8,9,13].

In this direction, using the variation-projection BVP formulation and finite element method (FEM) with Lagrange interpolation elements [12,2,1], the symbolic-numeric algorithms (SNAs) and programs have been elaborated [5,6,4]. This implementation of FEM using the interpolation Lagrange polynomials (ILPs) was such that it preserved only the continuity of the solution itself in

the course of its numerical approximation on a finite-element grid. However, in the above class of problems, particularly, in quantum-dimensional semiconductor systems, the continuity should be preserved not only for the solution (wave function) itself, but also for the probability current [2,10]. The required continuity of the solution derivatives can be preserved in FEM numerical approximation using the interpolation Hermite polynomials (IHPs) [3,11].

This motivated the aim of the present work, namely, the use of FEM with IHPs to elaborate SNAs implemented in Maple-Fortran for the solution of the BVPs with self-adjoint second order differential equation, and the analysis of the approximate numerical solutions in benchmark calculations.

In this paper, we present a symbolic algorithm implemented in Maple computer algebra system (CAS) that generates finite-element calculation schemes for solving BVPs for the self-adjoint second-order differential equation using interpolating Hermite polynomials. We derived recurrence relations for the calculation of the IHPs with nodes of arbitrary multiplicity. The stiffness and mass matrices are expressed via the integrals of products of the BVP coefficient functions, the IHPs and their derivatives. The result is used to formulate a generalized algebraic eigenvalue problem solved in Maple for matrices of small dimension. We use the symbolic algorithm to generate Fortran routines that allow the solution of the generalized algebraic eigenvalue problem with matrices of large dimension. We demonstrate the efficiency of the programs generated in Maple and Fortran for  $100 \times 100$  and higher-order matrices, respectively, in benchmark calculations for exactly solvable quantum-mechanical problems with continuous and piecewise continuous potentials.

The paper is organized as follows. In Section 2, the formulation of BVPs and variational functional is presented. Section 3 describes the algorithm that generates algebraic problems using the finite element method with interpolation Hermite polynomials. In Section 4, the benchmark calculations are analysed. The obtained results and further development of SNA are discussed in Conclusion.

## 2 Formulation of BVPs

We consider a self-adjoint second-order differential equation with respect to the unknown solution  $\Phi(z)$  in the region  $z \in \Omega_z = (z^{\min}, z^{\max})$  [4]

$$(D - 2E)\Phi(z) = 0, \quad D = -\frac{1}{f_1(z)} \frac{\partial}{\partial z} f_2(z) \frac{\partial}{\partial z} + V(z). \quad (1)$$

If no additional restrictions are explicitly specified, we assume  $f_1(z) > 0$ ,  $f_2(z) > 0$ , and  $V(z)$  to be continuous functions that have derivatives up to the order of  $\kappa^{\max} \geq 1$  in the domain  $z \in \bar{\Omega}_z = [z^{\min}, z^{\max}]$ . In quantum mechanics, Eq. (1) is actually the Schrödinger equation that describes a particle with the wave function  $\Phi(z)$  and the energy  $E$ .

For a discrete-spectrum problem, the eigenfunctions  $\Phi(z) = \Phi_m(z) \in \mathcal{H}_2^2$  in the Sobolev space  $\mathcal{H}_2^2$  corresponding to the eigenvalues  $E_1 < E_2 < \dots < E_m <$

... are to satisfy the boundary condition of the first (I) and/or the second (II) and/or the third (III) kind at given values of parameters  $\mathcal{R}(z^t)$

$$(I) : \Phi_m(z^t) = 0, \quad t = \min \text{ and/or } \max, \quad (2)$$

$$(II) : f_1(z) \frac{d\Phi_m(z)}{dz} \Big|_{z=z^t} = 0, \quad t = \min \text{ and/or } \max, \quad (3)$$

$$(III) : \frac{d\Phi_m(z)}{dz} \Big|_{z=z^t} = \mathcal{R}(z^t) \Phi_m(z^t), \quad t = \min \text{ and/or } \max \quad (4)$$

along with the normalization and orthogonality condition

$$\langle \Phi_m(z) | \Phi_{m'}(z) \rangle = \int_{z^{\min}}^{z^{\max}} f_1(z) (\Phi_m(z))^* \Phi_{m'}(z) dz = \delta_{mm'}. \quad (5)$$

The solution of the above BPVs can be reduced to the calculation of stationary points of a variational functional [12,6]

$$\begin{aligned} \Xi(\Phi, E, z^{\min}, z^{\max}) &\equiv \int_{z^{\min}}^{z^{\max}} \Phi^*(z) (D - 2E) \Phi(z) dz = \Pi(\Phi, E, z^{\min}, z^{\max}) \\ &- f_2(z^{\max}) \Phi^*(z^{\max}) \mathcal{R}(z^{\max}) \Phi(z^{\max}) + f_2(z^{\min}) \Phi^*(z^{\min}) \mathcal{R}(z^{\min}) \Phi(z^{\min}), \end{aligned} \quad (6)$$

where the symmetric functional  $\Pi(\Phi, E, z^{\min}, z^{\max})$  is expressed as

$$\begin{aligned} \Pi(\Phi, E, z^{\min}, z^{\max}) &= \int_{z^{\min}}^{z^{\max}} \left[ f_2(z) \frac{d\Phi^*(z)}{dz} \frac{d\Phi(z)}{dz} + f_1(z) \Phi^*(z) V(z) \Phi(z) \right. \\ &\quad \left. - f_1(z) 2E \Phi^*(z) \Phi(z) \right] dz. \end{aligned} \quad (7)$$

Here  $\mathcal{R}(z) \rightarrow \infty$  and  $\mathcal{R}(z) = 0$  for discrete spectrum problem with BCs (I) and BCs (II), Eqs. (2) and (3), respectively.

### 3 FEM Generation of Algebraic Problems

High-accuracy computational schemes for solving the BVP (1)–(4) can be derived from the variational functional (6), (7) basing on the FEM. The general idea of the FEM in one-dimensional space is to divide the interval  $[z^{\min}, z^{\max}]$  into many small domains referred to as elements. The size of the elements can be defined free enough to account for physical properties or qualitative behavior of the desired solutions, such as smoothness.

The interval  $\Delta = [z^{\min}, z^{\max}]$  is covered by a set of  $n$  elements  $\Delta_j = [z_j^{\min}, z_j^{\max}] \equiv [z_{j+1}^{\min}]$  in such a way that  $\Delta = \bigcup_{j=1}^n \Delta_j$ . Thus, we obtain the grid

$$\begin{aligned} \Omega^{h_j(z)}[z^{\min}, z^{\max}] &= \{z^{\min} = z_1^{\min}, z_j^{\max} = z_j^{\min} + h_j, j = 1, \dots, n-1, \\ &z_n^{\max} = z_n^{\min} + h_n = z^{\max}\}, \end{aligned} \quad (8)$$

where  $z_j^{\min} \equiv z_{j-1}^{\max}$ ,  $j = 2, \dots, n$  are the mesh points, and the steps  $h_j = z_j^{\max} - z_j^{\min}$  are the lengths of the elements  $\Delta_j$ .

### 3.1 Interpolation Hermite Polynomials

In each element  $\Delta_j$  we define the equidistant sub-grid  $\Omega_j^{h_j(z)}[z_j^{\min}, z_j^{\max}] = \{z_{(j-1)p} = z_j^{\min}, z_{(j-1)p+r}, r = 1, \dots, p-1, z_{jp} = z_j^{\max}\}$  with the nodal points  $z_r \equiv z_{(j-1)p+r}$  determined by the formula

$$z_{(j-1)p+r} = ((p-r)z_j^{\min} + rz_j^{\max})/p, \quad r = 0, \dots, p. \quad (9)$$

As a set of basis functions  $\{N_l(z, z_j^{\min}, z_j^{\max})\}_{l=0}^{l^{\max}}, l^{\max} = \sum_{r=0}^p \kappa_r^{\max}$  we will use the IHPs  $\{\{\varphi_r^\kappa(z)\}_{r=0}^p\}_{\kappa=0}^{\kappa_r^{\max}-1}$  in the nodes  $z_r, r = 0, \dots, p$  of the grid (9). The values of the functions  $\varphi_r^\kappa(z)$  with their derivatives up to the order  $(\kappa_r^{\max} - 1)$ , i.e.  $\kappa = 0, \dots, \kappa_r^{\max} - 1$ , where  $\kappa_r^{\max}$  is referred to as the multiplicity of the node  $z_r$ , are determined by the expressions [3]

$$\varphi_r^\kappa(z_{r'}) = \delta_{rr'}\delta_{\kappa 0}, \quad \left. \frac{d^{\kappa'}}{dz^{\kappa'}} \varphi_r^\kappa(z) \right|_{z=z_{r'}} = \delta_{rr'}\delta_{\kappa\kappa'}. \quad (10)$$

To calculate the IHPs we introduce the auxiliary weight function

$$w_r(z) = \prod_{r'=0, r' \neq r}^p \left( \frac{z - z_{r'}}{z_r - z_{r'}} \right)^{\kappa_{r'}^{\max}}, \quad w_r(z_r) = 1. \quad (11)$$

The weight function derivatives can be presented as a product

$$\frac{d^\kappa w_r(z)}{dz^\kappa} = w_r(z) g_r^\kappa(z),$$

where the factor  $g_r^\kappa(z)$  is calculated by means of the recurrence relations

$$g_r^\kappa(z) = \frac{dg_r^{\kappa-1}(z)}{dz} + g_r^1(z)g_r^{\kappa-1}(z), \quad (12)$$

with the initial conditions

$$g_r^0(z) = 1, \quad g_r^1(z) \equiv \frac{1}{w_r(z)} \frac{dw_r(z)}{dz} = \sum_{r'=0, r' \neq r}^p \frac{\kappa_{r'}^{\max}}{z - z_{r'}}.$$

We will seek for the IHPs  $\varphi_r^\kappa(z)$  in the following form:

$$\varphi_r^\kappa(z) = w_r(z) \sum_{\kappa'=0}^{\kappa_r^{\max}-1} a_r^{\kappa, \kappa'}(z - z_r)^{\kappa'}. \quad (13)$$

Differentiating the function (13) by  $z$  at the point of  $z_r$  and using Eq. (11), we obtain

$$\left. \frac{d^{\kappa'}}{dz^{\kappa'}} \varphi_r^\kappa(z) \right|_{z=z_r} = \sum_{\kappa''=0}^{\kappa'} \frac{\kappa'!}{\kappa''!(\kappa' - \kappa'')!} g_r^{\kappa' - \kappa''}(z_r) a_r^{\kappa, \kappa''} \kappa''!. \quad (14)$$

Hence we arrive at the expression for the coefficients  $a_r^{\kappa, \kappa'}$

$$a_r^{\kappa, \kappa'} = \left( \frac{d^{\kappa'} \varphi_r^{\kappa}(z)}{dz^{\kappa'}} \Big|_{z=z_r} - \sum_{\kappa''=0}^{\kappa'-1} \frac{\kappa'!}{\kappa''!(\kappa' - \kappa'')!} g_r^{\kappa' - \kappa''}(z_r) a_r^{\kappa, \kappa''} \kappa''! \right) / \kappa'!. \quad (15)$$

Taking Eq. (10) into account, we finally get:

$$a_r^{\kappa, \kappa'} = \begin{cases} 0, & \kappa' < \kappa, \\ 1/\kappa'!, & \kappa' = \kappa, \\ - \sum_{\kappa''=\kappa}^{\kappa'-1} \frac{1}{(\kappa' - \kappa'')!} g_r^{\kappa' - \kappa''}(z_r) a_r^{\kappa, \kappa''}, & \kappa' > \kappa. \end{cases}$$

Note that all degrees of interpolation Hermite polynomials  $\varphi_r^{\kappa}(z)$  do not depend on  $\kappa$  and equal  $p' = \sum_{r=0}^p \kappa_r^{\max} - 1$ . Below we consider only the IHPs with the nodes of identical multiplicity  $\kappa_r^{\max} = \kappa^{\max}$ ,  $r = 0, \dots, p$ . In this case, the degree of the polynomials is equal to  $p' = \kappa^{\max}(p + 1) - 1$ . We introduce the following notation for such polynomials:

$$N_{\kappa^{\max}p + \kappa}(z, z_j^{\min}, z_j^{\max}) = \varphi_r^{\kappa}(z), \quad r = 0, \dots, p, \quad \kappa = 0, \dots, \kappa^{\max} - 1. \quad (16)$$

These IHPs form a basis in the space of polynomials having the degree  $p' = \kappa^{\max}(p + 1) - 1$  in the element  $z \in [z_j^{\min}, z_j^{\max}]$  that have continuous derivatives up to the order  $\kappa^{\max} - 1$  at the boundary points  $z_j^{\min}$  and  $z_j^{\max}$  of the element  $z \in [z_j^{\min}, z_j^{\max}]$ . The IHPs at  $\kappa^{\max} = 1, 2, 3$  and  $p = 4$  are shown in Fig. 1. It is seen that the values of IHP  $N_{\kappa^{\max}p + \kappa}(z, z_j^{\min}, z_j^{\max})$  and  $N_{\kappa}(z, z_{j+1}^{\min}, z_{j+1}^{\max})$  (at  $r = p$  and  $r = 0$ ) and their derivatives up to the order  $\kappa^{\max} - 1$  coincide at the mutual point  $z_j^{\max} = z_{j+1}^{\min}$  of the adjacent elements. Moreover, the boundary points are nodes (zeros) of multiplicity  $\kappa^{\max}$  of other IHPs, irrespective of the length of elements of  $[z_j^{\min}, z_j^{\max}]$  and  $[z_{j+1}^{\min}, z_{j+1}^{\max}]$ . This allows construction of a basis of piecewise and polynomial functions having continuous derivatives to the order of  $\kappa^{\max} - 1$  in any set  $\Delta = \bigcup_{j=1}^n \Delta_j = [z_j^{\min}, z_j^{\max}]$  of elements  $\Delta_j = [z_j^{\min}, z_j^{\max}] \equiv z_{j+1}^{\min}$ . The **Algorithm 1** of the IHP construction is presented in Appendix A and implemented in the CAS Maple.

### 3.2 Generation of Algebraic Eigenvalue Problems

We consider a discrete representation of the solutions  $\Phi(z)$  of the problem (1), (5), (4) reduced by means of the FEM to the variational functional (6), (7) on the finite-element grid,

$$\Omega_{h_j(z)}^p[z^{\min}, z^{\max}] = [z_0 = z^{\min}, z_l, l = 1, \dots, np - 1, z_{np} = z^{\max}],$$

with the mesh points  $z_l = z_{jp} = z_j^{\max} \equiv z_{j+1}^{\min}$  of the grid  $\Omega^{h_j(z)}[z^{\min}, z^{\max}]$  determined by Eq. (8) and the nodal points  $z_l = z_{(j-1)p+r}$ ,  $r = 0, \dots, p$  of the sub-grids  $\Omega_j^{h_j(z)}[z_j^{\min}, z_j^{\max}]$ ,  $j = 1, \dots, n$ , determined by Eq. (9). The solutions

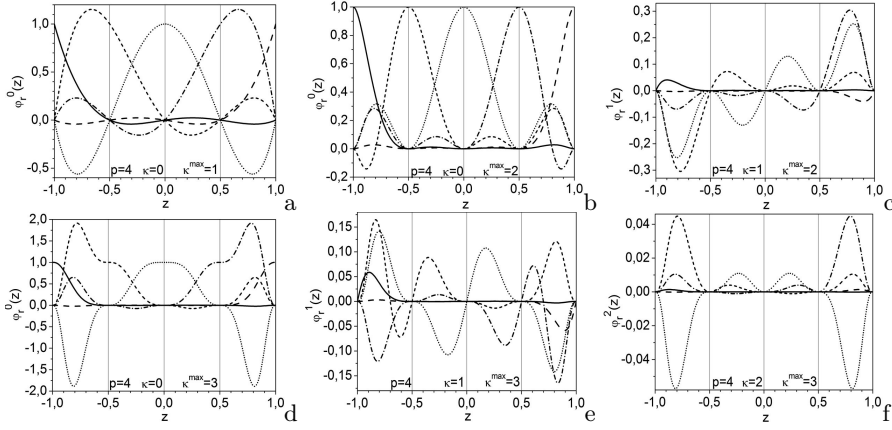


**Fig. 1.** The IHP coinciding at  $\kappa^{\max} = 1$  with the ILP (a) and IHPs at  $\kappa^{\max} = 2$  (b, c) and  $\kappa^{\max} = 3$  (d, e, f). Here  $p + 1 = 5$  is the number of nodes in the subinterval,  $\Delta_j = [z_j^{\min} = -1, z_j^{\max} = 1]$ . The grid nodes  $z_r$  are shown by vertical lines.

$\Phi^h(z) \approx \Phi(z)$  are sought for in the form of a finite sum over the basis of local functions  $N_\mu^g(z)$  at each nodal point  $z = z_k$  of the grid  $\Omega_{h_j}^p[z^{\min}, z^{\max}]$ :

$$\Phi^h(z) = \sum_{\mu=0}^{L-1} \Phi_\mu^h N_\mu^g(z), \quad \Phi^h(z_l) = \Phi_{l\kappa^{\max}}^h, \quad \left. \frac{d^\kappa \Phi^h(z)}{dz^\kappa} \right|_{z=z_l} = \Phi_{l\kappa^{\max}+\kappa}^h \quad (17)$$

where  $L = (pn+1)\kappa^{\max}$  is the number of local functions and  $\Phi_\mu^h$  at  $\mu = l\kappa^{\max} + \kappa$  are the nodal values of the  $\kappa$ th derivatives of the function  $\Phi^h(z)$  (including the function  $\Phi^h(z)$  itself for  $\kappa = 0$ ) at the points  $z_l$ .

The local functions  $N_\mu^g(z) \equiv N_{l\kappa^{\max}+\kappa}^g(z)$  are piecewise polynomials of the given order  $p'$ , their derivative of the order  $\kappa$  at the node  $z_l$  equals one, and the derivative of the order  $\kappa' \neq \kappa$  at this node equals zero, while the values of the function  $N_\mu^g(z)$  with all its derivatives up to the order  $(\kappa^{\max} - 1)$  equal zero at all other nodes  $z_{l'} \neq z_l$  of the grid  $\Omega_{h_j}(z)$ , i.e.,  $\left. \frac{d^\kappa N_{l'\kappa^{\max}+\kappa'}^g}{dz^\kappa} \right|_{z=z_l} = \delta_{ll'} \delta_{\kappa\kappa'}$ ,  $l = 0, \dots, np$ ,  $\kappa = 0, \dots, \kappa^{\max} - 1$ .

For the nodes  $z_l$  of the grid that do not coincide with the mesh points  $z_j^{\max}$ , i.e., at  $l \neq jp$ ,  $j = 1 \dots n-1$ , the polynomial  $N_\mu^g$  at  $\mu = ((j-1)p+r)\kappa^{\max} + \kappa$  has the form

$$N_{(p(j-1)+r)\kappa^{\max}+\kappa}^g = \begin{cases} N_{\kappa^{\max}r+\kappa}(z, z_j^{\min}, z_j^{\max}), & z \in \Delta_j; \\ 0, & z \notin \Delta_j, \end{cases} \quad (18)$$

i.e., it is defined as the IHP  $N_{\kappa^{\max}r+\kappa}(z, z_j^{\min}, z_j^{\max})$  in the interval  $z \in \Delta_j$  and zero otherwise. Since the points  $z_j^{\min}$  and  $z_j^{\max}$  are nodes of multiplicity  $\kappa^{\max}$ , such piecewise polynomial functions and their derivatives up to the order  $\kappa^{\max} - 1$

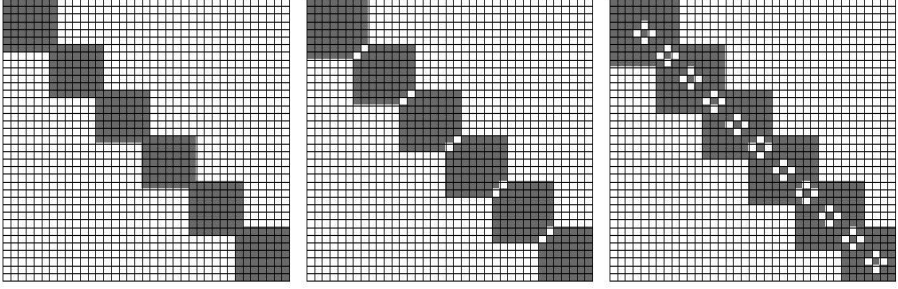


**Fig. 2.** The structure of matrices  $B_{L_1 L_2}$  and  $A_{L_1 L_2}$  for the potential  $V(z) = 0$ , the number of elements  $n = 6$  in the entire interval  $(z^{\min}, z^{\max})$ , and different values of the multiplicity of nodes  $\kappa^{\max}$  and the number of subintervals  $p$ . From left to right:  $(\kappa^{\max}, p) = (1, 6)$ ,  $(\kappa^{\max}, p) = (2, 3)$ ,  $(\kappa^{\max}, p) = (3, 2)$ . The dimensions of matrices are  $L \times L$ ,  $L = \kappa^{\max}(np + 1)$ :  $37 \times 37$ ,  $38 \times 38$ ,  $39 \times 39$ .

are continuous in the entire interval  $\Delta$ . In Fig. 1 such IHPs are plotted by dotted, short-dashed and dot-dashed lines.

For the nodal points of the grid  $z_l$  that coincide with one of the mesh points  $z_j^{\max}$  belonging to two elements  $\Delta_j$  and  $\Delta_{j+1}$ ,  $j = 1 \dots n - 1$ , i.e., for  $l = jp$ , the polynomial, whose derivative of the order  $\kappa$  equals one at the node  $z_l$ , has the form

$$N_{p\kappa^{\max}j+\kappa}^g = \begin{cases} N_{\kappa^{\max}p+\kappa}(z, z_j^{\min}, z_j^{\max}), & z \in \Delta_j; \\ N_{\kappa}(z, z_{j+1}^{\min}, z_{j+1}^{\max}), & z \in \Delta_{j+1}; \\ 0, & z \notin \Delta_j \cup \Delta_{j+1}, \end{cases} \quad (19)$$

In other words, it is constructed by joining the polynomial  $N_{p\kappa^{\max}+\kappa}(z, z_j^{\min}, z_j^{\max})$  defined in the element  $\Delta_j$  with the polynomial  $N_{\kappa}(z, z_{j+1}^{\min}, z_{j+1}^{\max})$  defined in the element  $\Delta_{j+1}$ . This polynomial is also continuous with all its derivatives of the order  $\kappa^{\max} - 1$  in the interval  $z \in \Delta$ . The corresponding IHPs are plotted in Fig. 1 by solid and long-dashed lines.

The substitution of the expansion (17) into the variational functional (6), (7) reduces the solution of the problem (1)–(5) to the solution of the generalized algebraic eigenvalue problem with respect to the desired set of eigenvalues  $E$  and eigenvectors  $\Phi^h = \{\Phi_{\mu}^h\}_{\mu=0}^{L-1}$ :

$$(\tilde{\mathbf{A}} - 2E\mathbf{B})\Phi^h = 0. \quad (20)$$

Here  $\tilde{\mathbf{A}} = \mathbf{A} + \mathbf{M}_{\min} - \mathbf{M}_{\max}$  and  $\mathbf{B}$  are symmetric  $L \times L$  stiffness and mass matrices,  $L = \kappa^{\max}(np + 1)$ ,  $\mathbf{M}_{\max}$  and  $\mathbf{M}_{\min}$  are  $L \times L$  matrices with zero elements except  $M_{11} = f_2(z^{\min})R(z^{\min})$  and  $M_{L+1-\kappa^{\max}, L+1-\kappa^{\max}} = f_2(z^{\max})R(z^{\max})$ , respectively. The **Algorithm 2** that generates the local functions  $N_{\mu}^g(z)$  defined by (18), (19) and the matrices  $\mathbf{A}$  and  $\mathbf{B}$  is described in Appendix B and implemented in the CAS Maple.



**Table 1.** Runge coefficients (24) for the eigenvalues (Runge Eigv) and the eigenfunction (Runge EigF) of the first three lower-energy states calculated for schemes with different  $\kappa^{\max}$  and  $p$  up to order  $p' = \kappa^{\max}(p+1) - 1 = 8$  at  $h = 0.125$  for schemes with  $p' = 7$ ,  $p' = 8$ , and at  $h = 0.0625$  for the rest of the schemes. Theoretical estimates of Runge coefficient for the convergence of eigenvalues and eigenfunctions are  $2p'$  and  $(p' + 1)$ , respectively. The execution time  $T_h$  (in seconds) for the mesh step  $h = 1/32$  is presented in the last column.

$\kappa^{\max}$	$p$	$p'$	Runge Eigv			$2p'$	Runge EigF			$p' + 1$	$T_h$
1	1	1	2.00	2.00	1.99	2	1.99	1.99	2.00	2	9.36
1	2	2	4.00	3.99	3.99	4	2.99	2.98	3.02	3	19.5
1	3	3	5.99	6.00	5.99	6	3.98	3.99	3.97	4	33.4
2	1	3	5.97	5.96	5.96	6	3.95	3.95	3.94	4	21.8
1	4	4	7.99	8.00	8.00	8	4.99	4.98	5.00	5	48.6
1	5	5	9.99	9.99	9.99	10	5.98	6.01	5.97	6	65.6
2	2	5	9.97	9.97	9.97	10	5.96	5.98	5.95	6	47.6
3	1	5	10.05	10.05	10.06	10	6.01	6.04	6.02	6	38.0
1	6	6	12.00	12.00	12.00	12	6.99	6.97	6.99	7	88.9
1	7	7	13.98	13.98	13.98	14	7.85	8.03	7.85	8	111.
2	3	7	13.88	13.87	13.87	14	7.77	7.95	7.77	8	82.3
4	1	7	13.59	13.58	13.57	14	7.61	7.57	7.59	8	59.6
1	8	8	16.13	16.00	15.99	16	9.00	8.82	9.09	9	139.
3	2	8	15.75	15.75	15.74	16	8.83	8.67	8.86	9	99.1

To solve equation (20) we have chosen the subspace iteration method [12,1] elaborated by Bathe [1] for the solution of large symmetric banded matrix eigenvalue problems. This method uses a skyline storage mode, which stores the components of the matrix column vectors within the nonzero band of the matrix and, therefore, is perfectly suitable for the banded FEM matrices. The procedure chooses a vector subspace of the full solution space and iterates upon the successive solutions in the subspace (for details, see [1]). Using the Rayleigh quotients for the eigenpairs, the iterations are repeated until the desired set of solutions in the iteration subspace converges to within the specified tolerance. Generally, 10–24 iterations are enough to converge the subspace to within the prescribed tolerance. If the matrix  $\mathbf{A}$  in Eq. (20) is not positive-definite, the problem (20) is replaced with the following problem:  $\check{\mathbf{A}}\check{\Phi}^h = \check{E}^h \mathbf{B}\Phi^h$ ,  $\check{\mathbf{A}} = \mathbf{A} - \alpha\mathbf{B}$ . The number  $\alpha$  (the shift of the energy spectrum) is chosen such that the matrix  $\check{\mathbf{A}}$  is positive-definite. The eigenvector of this problem is the same, and  $E^h = \check{E}^h + \alpha$ .

The theoretical estimate for the  $\mathbf{H}^0$  norm of the difference between the exact solution  $\Phi_m(z) \in \mathcal{H}_2^2$  and the numerical one  $\Phi_m^h(z) \in \mathbf{H}^{\kappa^{\max}}$  has the order of

$$|E_m^h - E_m| \leq c_1 h^{2p'}, \quad \|\Phi_m^h(z) - \Phi_m(z)\|_0 \leq c_2 h^{p'+1}, \quad (21)$$

where  $h = \max_{1 \leq j \leq n} h_j$  is the maximal step of the grid [12].

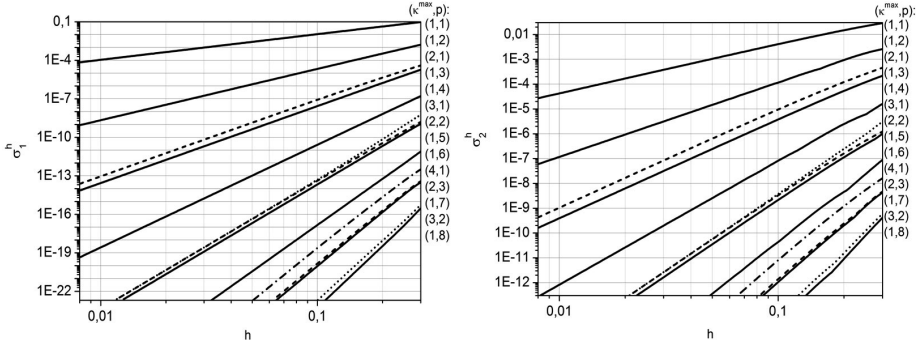


**Fig. 3.** Absolute errors  $\sigma_1^h = |\varepsilon_1^{exact} - \varepsilon_1^h|$  and  $\sigma_2^h = \max_{z \in \Omega^h(z)} |\chi_1^{exact}(z) - \chi_1^h(z)|$  for the ground state vs the grid step  $h$  calculated using approximation by IHPs with different  $\kappa^{\max}$  and  $p$

## 4 Benchmark Calculations

### 4.1 Modified Pöschl–Teller Potential

As an example, we consider the exactly solvable eigenvalue problem for Schrödinger equation in the units  $\hbar = m = 1$ :

$$\left( -\frac{d^2}{dz^2} + 2V(z) - 2E \right) \Phi(z) = 0, \quad (22)$$

with the modified Pöschl–Teller potential on the axis  $z \in (-\infty, +\infty)$ :

$$V(z) = -\frac{\alpha^2}{2} \frac{\lambda(\lambda-1)}{(\cosh(\alpha z))^2}, \quad (23)$$

where  $\alpha > 0$  and  $\lambda > 0$  are real-value parameters. The parameters  $\lambda = 11/2$  and  $\alpha = 1$  were chosen such that the discrete spectrum problem for Eq. (22) with the potential (23) had five eigenvalues  $2E_m = [-20.25, -12.25, -6.25, -2.25, -0.25]$  with the corresponding five eigenfunctions  $\psi_m(x)$  known in the analytical form.

The numerical experiments using the finite-element grid  $\Omega_{h_j(z)}^p [z^{\min} = -40, z^{\max} = 40]$  demonstrated strict correspondence to the theoretical estimations (21) for eigenvalues and eigenfunctions. In particular, we calculated the Runge coefficients

$$\beta_l = \log_2 \left| \frac{\sigma_l^h - \sigma_l^{h/2}}{\sigma_l^{h/2} - \sigma_l^{h/4}} \right|, \quad l = 1, 2, \quad (24)$$

on three twice condensed grids with the absolute errors

$$\sigma_1^h = |E_m^{exact} - E_m^h|, \quad \sigma_2^h = \max_{z \in \Omega^h(z)} |\Phi_m^{exact}(z) - \Phi_m^h(z)| \quad (25)$$

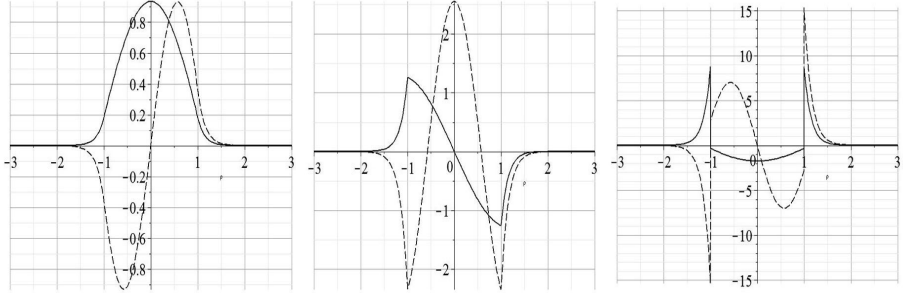


**Fig. 4.** The solutions and their first and second derivatives for the ground state (solid curves) and the first excited state (dashed curves) of the rectangular well potential problem

for the eigenvalues and eigenfunctions, respectively. From Eq. (25) we obtained the numerical estimations of the convergence order of the proposed numerical schemes, the theoretical estimates being  $\beta_1 = 2p'$  and  $\beta_2 = p' + 1$ .

In Table 1, we show the Runge coefficients (24) for the eigenvalues (Runge Eigv) and the eigenfunction (Runge EigF) of the first three lower-energy states calculated for schemes with different  $\kappa^{\max}$  and  $p$  up to order  $p' = \kappa^{\max}(p+1) - 1 = 8$ . One can see that for the chosen  $p' = 1 \div 8$ , the numerical estimates of Runge coefficients lie within  $2p' \pm 0.06$  for  $p' = 1, \dots, 6$  and  $2p' \pm 0.56$  for  $p' = 7, 8$  in the case of eigenvalues and within  $(p' + 1) \pm 0.2$  in the case of eigenfunctions, which strongly corresponds to the theoretical error estimates (21). In Fig. 3, we show the dependence of absolute errors  $\sigma_1^h = |\varepsilon_1^{\text{exact}} - \varepsilon_1^h|$  for eigenvalues and  $\sigma_2^h = \max_{z \in \Omega^h(z)} |\chi_1^{\text{exact}}(z) - \chi_1^h(z)|$  for eigenfunctions of the ground state vs. the grid step  $h$  calculated using approximation by IHPs with different  $\kappa^{\max}$  and  $p$ . In the double logarithmic scale, the errors lie on lines with different slopes that explicitly show the desirable order of approximation  $p' = \kappa^{\max}(p + 1) - 1$  by IHPs with different  $\kappa^{\max}$  and  $p$ .

For calculations, we used the program KANTBP 1.1 with the specified accuracy of  $\sim 10^{-34}$  and the relative error tolerance of the eigenvalues  $\epsilon_1 = 4 \cdot 10^{-34}$ , implemented in Intel Fortran 77 on the computer 2 x Xeon 3.2 GHz, 4 GB RAM. The data type QUADRUPLE PRECISION provided 32 significant digits. The running time  $T_h$  for  $h = 1/32 = 0.03125$  is presented in the last column of Table 1.

## 4.2 Rectangular Well Potential

For piecewise continuous potentials (or potentials with discontinuous derivatives), the approximation by IHPs does not converge to the desired solution with increasing number of nodes. Within the FEM approach, the following technique is used. Let the potential have the form  $V(z) = \{V_i(z), z \in (\zeta_i^{\min}, \zeta_i^{\max})\}$ ,  $\zeta_{i+1}^{\min} = \zeta_i^{\max}$ , where  $V_i(z)$  are  $(p' + 1)$ -times differentiable functions. The interval of the problem definition is divided into a set of subintervals  $[z_j^{\min}, z_j^{\max}]$

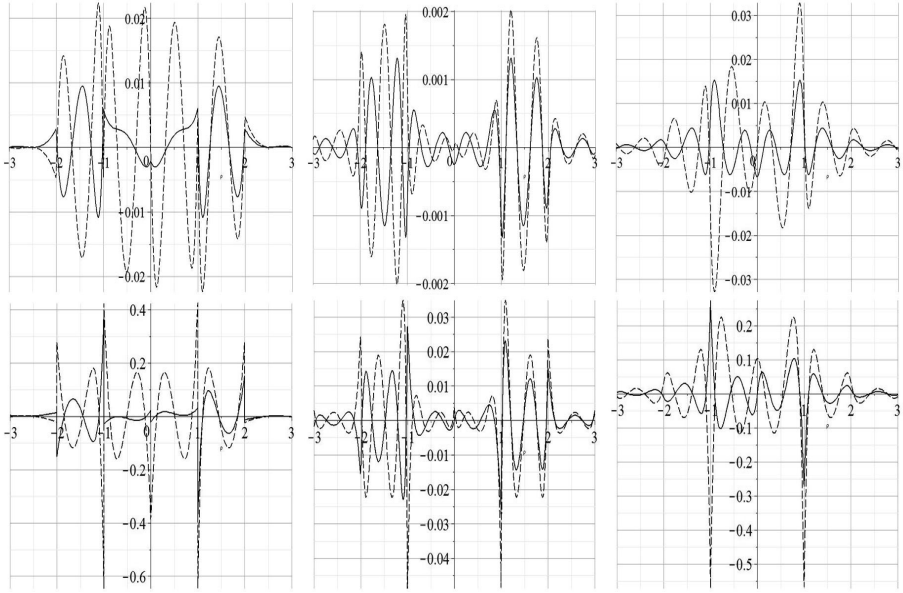


**Fig. 5.** The difference of numerical and exact eigenfunctions  $D_{swp,0}^{\kappa^{\max},p} = \psi_0^{\kappa^{\max},p}(z) - \psi_0(z)$  (solid curves) and  $D_{swp,1}^{\kappa^{\max},p} = \psi_1^{\kappa^{\max},p}(z) - \psi_1(z)$  (dashed curves) (upper panels) and their first derivatives (lower panels) for rectangular well potential for  $n = 10$  elements in the interval  $(-5, 5)$  and different values of the multiplicity of nodes  $\kappa^{\max}$  and the number of subinterval divisions  $p$ . >From left to right:  $(\kappa^{\max}, p) = (1, 3)$ ,  $(\kappa^{\max}, p) = (2, 1)$ ,  $(\kappa^{\max}, p) = (3, 1)$ .

$(z_j^{\max} \equiv z_{j+1}^{\min})$ , such that every point  $\zeta_i^{\min}$ , in which the second derivative of the solution is discontinuous, coincides with some boundary point  $z_j^{\min}$ .

Consider, e.g., the exactly solvable discrete-spectrum problem for Eq. (22) with the rectangular well potential  $2V(z) = V_0$ , if  $|z| \leq a$ , and  $2V(z) = 0$  otherwise. At  $a = 1$ ,  $2V_0 = -50$  the discrete-spectrum problem has five eigenfunctions (see Fig. 4), expressed in the analytical form via five eigenvalues  $2E_m = [-48.109146, -42.474904, -33.232792, -20.714111, -5.965365]$ .

Since the first two eigenfunctions rapidly decrease, it is sufficient to use the finite-element grid  $\Omega_{h_j(z)}^p[z^{\min} = -5, z^{\max} = 5]$ . The calculation error for the first two eigenvalues is presented in Table 2. It is seen that the scheme with  $\kappa^{\max} = 1$  and  $\kappa^{\max} = 2$  having the same order of accuracy  $p' = 3$  and  $p' = 5$  ( $p' = \kappa^{\max}(p + 1) - 1$ ) yield nearly the same error (at  $n = 20$ ,  $h = 1/2$  the error is about  $10^{-2}$  and  $4 \cdot 10^{-6}$ , respectively), while for  $\kappa^{\max} = 3$ , the error is much higher (about  $10^{-2}$  at  $n = 20$ ,  $h = 1/2$ ). In Table 2, we show the Runge coefficients (24) for the eigenvalues of the first two lower-energy states calculated for schemes with different  $\kappa^{\max}$  and  $p$  with order  $p' = \kappa^{\max}(p + 1) - 1 = 3$  and  $p' = \kappa^{\max}(p + 1) - 1 = 5$ . One can see that for the chosen  $p' = 3, 5$ , the numerical estimates of Runge coefficients lie within  $2p' \pm 0.5$  for schemes with  $\kappa^{\max} = 1, 2$

**Table 2.** The absolute errors  $\sigma_1^h(E_0)$  and  $\sigma_1^h(E_1)$  of eigenvalues of ground and first excited state for square well potential for  $a = 1$  and  $2V_0 = -50$ . The Runge coefficient (Ru) from (24) for the eigenvalues at  $h = 1/4$ ,  $n = 40$  and its theoretical estimates ( $2p'$ ) are given in last two columns.

$(\kappa^{\max}, p)$	$p'$	$\sigma_1^{h=1}(E_0)$	$\sigma_1^{h=1/2}(E_0)$	$\sigma_1^{h=1/4}(E_0)$	$\sigma_1^{h=1/8}(E_0)$	$\sigma_1^{h=1/16}(E_0)$	Ru	$2p'$
(1,3)	3	1.93e-02	1.39e-03	4.44e-05	8.83e-07	1.48e-08	5.65	6
(2,1)	3	5.70e-02	3.15e-03	1.00e-04	2.21e-06	4.14e-08	5.50	6
(1,5)	5	2.47e-04	1.67e-06	3.82e-09	5.26e-12	2.22e-12	10.3	10
(2,2)	5	4.01e-04	2.59e-06	6.12e-09	8.59e-12	2.20e-13	9.51	10
(3,1)	5	1.48e-02	2.66e-03	3.51e-04	4.40e-05	5.50e-06	2.99	10
$(\kappa^{\max}, p)$	$p'$	$\sigma_1^{h=1}(E_1)$	$\sigma_1^{h=1/2}(E_1)$	$\sigma_1^{h=1/4}(E_1)$	$\sigma_1^{h=1/8}(E_1)$	$\sigma_1^{h=1/16}(E_1)$	Ru	$2p'$
(1,3)	3	9.96e-02	4.38e-03	1.25e-04	2.40e-06	3.96e-08	5.70	6
(2,1)	3	2.92e-01	1.14e-02	3.08e-04	6.33e-06	1.14e-07	5.60	6
(1,5)	5	6.44e-04	3.75e-06	7.93e-09	1.04e-11	2.63e-12	9.99	10
(2,2)	5	9.40e-04	5.66e-06	1.27e-08	1.74e-11	2.06e-13	9.53	10
(3,1)	5	6.70e-02	1.07e-02	1.39e-03	1.74e-04	2.17e-05	3.01	10

which strongly corresponds to the theoretical error estimates (21). While the scheme with  $\kappa^{\max} = 3$ ,  $p = 1$  of fifth order  $p' = 5$  gives Runge coefficient  $\beta_1 = 3$ . Maximal discrepancies arise in the vicinities of discontinuity of the potential well (at  $z = \pm 1$ ) because of a worse approximation of function with discontinuous second derivative by means of functions with continuous one.

It is due to the fact that the first derivative of the solution has a discontinuity at  $z = \pm a$  displayed in Fig 4. To illustrate this fact, we display in Fig. 5 the discrepancies of eigenfunctions and their first derivatives. It is seen that the scheme with  $\kappa^{\max} = 2$ ,  $p = 1$  provides better approximation for eigenfunctions among schemes of third order  $p' = 3$ . The scheme of fifth order  $p' = 5$  with  $\kappa^{\max} = 3$ ,  $p = 1$  leads to worse approximation in comparison with schemes of third order.

## 5 Conclusion

We presented the SNAs for solving the BVPs with self-adjoint second order differential equation using the FEM with interpolation Hermite polynomials. The proposed approach preserves the property of continuity of derivatives of the desired solutions. We demonstrated the efficiency of the programs generated in Maple and Fortran for  $100 \times 100$  and greater-order matrices, respectively, in benchmark calculations for exactly solvable quantum-mechanical problems with continuous and piecewise continuous potentials. The analysis of approximate numerical solutions in benchmark calculations with smooth potentials shows

that the order  $p' = \kappa^{\max}(p + 1) - 1$  of the elaborated FEM schemes strongly corresponds to the theoretical error estimates. Schemes of higher order  $p'$  allow high-accuracy results at larger step of the finite-element grid, provided that the derivative of the  $p'$ th order is a smooth function. Schemes with the fixed order  $p'$  have similar rate convergence, the execution time being smaller for greater  $\kappa^{\max}$  due to smaller dimension of matrices used in the calculations. However, if the  $\kappa$ th derivative of the desired solution has discontinuity points, i.e., for potentials having a discontinuous derivative of the order  $\kappa - 2$ , the schemes with  $\kappa^{\max} \geq \kappa$  operate worse, because in this case, the solution having discontinuous  $\kappa^{th}$  derivatives is approximated by functions having no such discontinuities.

In future, the elaborated calculation schemes, algorithms, and programs will be applied to the analysis of models of molecular, atomic, and nuclear systems, as well as to quantum-dimensional systems such as quantum dots, wires, and wells in bulk semiconductors, and smooth irregular wave-guide structures with piecewise continuous potentials.

The authors thank Professor V.P. Gerdt for collaboration. The work was partially supported by the Russian Foundation for Basic Research (RFBR) (grants No. 14-01-00420 and 13-01-00668) and the Bogoliubov–Infeld program.

## A Algorithm 1. Generation of IHPs

### Input:

$z^{\min}, z^{\max}$ , (formal parameters) the boundary points of the interval;  
 $p$  is the number of subintervals:  $p + 1$  is the number of nodes of IHPs;  
 $\kappa^{\max}$  is the multiplicity of nodes;  
 $f_1(z)$  and  $f_2(z)$  are coefficient functions from (1);

### Output:

$N_{l_1}(z, z^{\min}, z^{\max})$  are IHPs,  $l_1 = 0, \dots, l_{\max}$ , i.e.  $l_{\max} + 1$  is number of IHPs;  
 $A_{l_1; l_2}(z^{\min}, z^{\max})$  and  $B_{l_1; l_2}(z^{\min}, z^{\max})$  are auxiliary integrals;

### Local:

$l_{\max} = \kappa^{\max}(p + 1) - 1$  is largest index of IHPs,  $l_{\max} + 1$  is number of IHPs;  
 $z_r$  are nodes in subinterval;  
 $w_r(z)$  are weight functions;  
 $g_r^{\kappa}(z)$  are derivatives of order  $\kappa$  divided by weight function;  
 $a_r^{\kappa, \kappa'}$  are coefficients of expansion (13);

---



---

1: generation of IHPs and calculation of integrals in the interval  $[z^{\min}, z^{\max}]$

1.1.: for  $r:=0$  to  $p$  do

$z_r = ((p - r)z^{\min} + rz^{\max})/p$ ;

end for;

1.2.: for  $r:=0$  to  $p$  do

1.2.1: auxiliary weight function

$$w_r(z) = \prod_{r'=0, r' \neq r}^p \left( \frac{z - z_{r'}}{z_r - z_{r'}} \right)^{\kappa^{\max}};$$

1.2.2: recurrence relation for calculating the function  $g_r^{\kappa}(z)$

$$g_r^0(z) = 1;$$

```


$$g_r^1(z) = \sum_{r'=0, r' \neq r}^p \frac{\kappa^{\max}}{z - z_{r'}};$$

for  $\kappa := 2$  to  $\kappa^{\max} - 1$  do
  
$$g_r^\kappa(z) = \frac{dg_r^{\kappa-1}(z)}{dz} + g_r^1(z)g_r^{\kappa-1}(z);$$

end for;
1.2.3: recurrence relation for calculation of coefficients  $a_r^{\kappa, \kappa'}$ 
for  $\kappa := 0$  to  $\kappa^{\max} - 1$  do
  
$$a_r^{\kappa, \kappa} = 1/\kappa!;$$

  for  $\kappa' := \kappa + 1$  to  $\kappa^{\max} - 1$  do
    
$$a_r^{\kappa, \kappa'} = - \sum_{\kappa''=\kappa}^{\kappa'-1} \frac{1}{(\kappa' - \kappa'')!} g_r^{\kappa' - \kappa''}(z_r) a_r^{\kappa, \kappa''};$$

  end for;
1.2.4: calculation of IHP

$$N_{\kappa^{\max} r + \kappa}(z, z^{\min}, z^{\max}) \equiv \varphi_r^\kappa(z) = w_r(z) \sum_{\kappa'=\kappa}^{\kappa^{\max}-1} a_r^{\kappa, \kappa'}(z - z_r)^{\kappa'};$$

end for;
end for;

$$l_{\max} = \kappa^{\max}(p + 1) - 1;$$

1.3: calculation of the auxiliary integrals
for  $l_1 := 0$  to  $l_{\max}$  do
  for  $l_2 := l_1$  to  $l_{\max}$  do
    
$$A_{l_1; l_2}(z^{\min}, z^{\max}) = \int_{z^{\min}}^{z^{\max}} f_2(z) \frac{dN_{l_1}(z, z^{\min}, z^{\max})}{dz} \frac{dN_{l_2}(z, z^{\min}, z^{\max})}{dz} dz;$$

    
$$B_{l_1; l_2}(z^{\min}, z^{\max}) = \int_{z^{\min}}^{z^{\max}} f_1(z) N_{l_1}(z, z^{\min}, z^{\max}) N_{l_2}(z, z^{\min}, z^{\max}) dz;$$

  end for;
end for;

```

**Remarks.** 1. In commonly used coordinates, the integrals in Step 1.3. are calculated analytically. If  $f_1(z)$  or  $f_2(z)$  are such that these integrals cannot be calculated analytically, then one can apply the expansion over the interpolation polynomials.

2. The auxiliary integrals  $A_{l_1; l_2}(z^{\min}, z^{\max})$  and  $B_{l_1; l_2}(z^{\min}, z^{\max})$  are symmetric with respect to permutations of their indexes.

## B Algorithm 2: FEM Generation of Algebraic Eigenvalue Problem

### Input:

$n$  is the number of subintervals  $\Delta_j = [z_j^{\min}, z_j^{\max} = z_j^{\min} + h_j];$

$\Delta_j = [z_j^{\min}, z_j^{\max}]$  are sets of subintervals ( $z_j^{\max} \equiv z_{j+1}^{\min}$ );

$p$  is the number of divisions of subintervals:  $p + 1$  is the number of nodes of IHP;

$\kappa^{\max}$  is the multiplicity of nodes;

$N_{l_1}(z, z^{\min}, z^{\max})$  are IHP;

$A_{l_1; l_2}(z^{\min}, z^{\max})$  and  $B_{l_1; l_2}(z^{\min}, z^{\max})$  are auxiliary integrals from the **Algorithm 1**;

$V(z)$  is coefficient function from (1);

**Output:**

$z_l$  are nodes in the whole interval,  $l = 0, \dots, np$ ;

$N_l^g$  are piecewise polynomials;

$A_{L_1 L_2}$  and  $B_{L_1 L_2}$  are matrices of algebraic eigenvalue problem (20);

**Local:**

$l_{\max} = \kappa^{\max}(p+1) - 1$  where  $l_{\max} + 1$  is number of IHP;

$L = \kappa^{\max}(np+1)$  is the dimension of the algebraic eigenvalue problem.

## 2.1. calculation of grid points

```

 $z_0 = z_1^{\min};$ 
for  $j := 1$  to  $n$  do
  for  $r := 1$  to  $p-1$  do
     $z_{(j-1)p+r} = ((p-r)z_j^{\min} + rz_j^{\max})/p;$ 
  end for;
   $z_{jp} = z_j^{\max};$ 
end for;
```

## 2.2. calculation of piecewise polynomials

```

for  $\kappa := 0$  to  $\kappa^{\max} - 1$  do
   $N_{\kappa}^g = \{N_{\kappa}(z, z_1^{\min}, z_1^{\max}), z \in \Delta_1\};$ 
  for  $j := 1$  to  $n$  do
    for  $r := 1$  to  $p-1$  do
       $N_{((j-1)p+r)\kappa^{\max}+\kappa}^g = \{N_{\kappa^{\max}r+\kappa}(z, z_j^{\min}, z_j^{\max}), z \in \Delta_j; 0, z \notin \Delta_j\};$ 
    end for;
    if  $(j < n)$  then
       $N_{jp\kappa^{\max}+\kappa}^g := \{N_{\kappa^{\max}p+\kappa}(z, z_j^{\min}, z_j^{\max}), z \in \Delta_j;$ 
       $N_{\kappa}(z, z_{j+1}^{\min}, z_{j+1}^{\max}), z \in \Delta_{j+1}; 0, z \notin \Delta_j \cup \Delta_{j+1}\};$ 
    else
       $N_{np\kappa^{\max}+\kappa}^g := \{N_{\kappa^{\max}p+\kappa}(z, z_n^{\min}, z_n^{\max}), z \in \Delta_n; 0, z \notin \Delta_n\};$ 
    end if;
  end for;
end for;
```

2.3. Generation of matrices **A** and **B**

```

for  $j := 1$  to  $n$  do
  for  $l_1 := 0$  to  $l_{\max} - 1$  do
     $L_1 = p\kappa^{\max}(j-1) + l_1 + 1;$ 
    for  $l_2$  from  $l_1$  to  $l_{\max} - 1$  do
       $L_2 = p\kappa^{\max}(j-1) + l_2 + 1;$ 
       $A_{L_1 L_2} = A_{L_1 L_2} + A_{l_1; l_2}(z_j^{\min}, z_j^{\max})$ 
       $+ \int_{z_j^{\min}}^{z_j^{\max}} f_1(z) dz N_{L_1}(z, z_j^{\min}, z_j^{\max}) V(z) N_{L_2}(z, z_j^{\min}, z_j^{\max});$ 
       $B_{L_1 L_2} = B_{L_1 L_2} + B_{l_1; l_2}(z_j^{\min}, z_j^{\max});$ 
    end for  $(j, l_1, l_2)$ 
  end for
```



**Remarks.** 1. If the coefficients of the equation (1) are given in the tabular form, then we use the following matrix elements in Step 1.3 of Algorithm 1 and Step 2.3 of Algorithm 2:

$$\begin{aligned} & \int_{z_j^{\min}}^{z_j^{\max}} f_1(z) dz N_{L_1}(z, z_j^{\min}, z_j^{\max}) V(z) N_{L_2}(z, z_j^{\min}, z_j^{\max}) \\ &= \sum_{r=0}^p \sum_{\kappa=0}^{\kappa^{\max}-1} V^{(\kappa)}(z_{(j-1)p+r}) V_{l_1;l_2;\kappa^{\max}r+\kappa}(z_j^{\min}, z_j^{\max}), \end{aligned} \quad (26)$$

where  $V_{l_1;l_2;l_3}(z^{\min}, z^{\max})$  are determined by integrals with IHPs

$$\begin{aligned} V_{l_1;l_2;l_3}(z_j^{\min}, z_j^{\max}) &= \int_{z_j^{\min}}^{z_j^{\max}} f_1(z) N_{l_1}(z, z_j^{\min}, z_j^{\max}) \\ &\quad \times N_{l_2}(z, z_j^{\min}, z_j^{\max}) N_{l_3}(z, z_j^{\min}, z_j^{\max}) dz. \end{aligned} \quad (27)$$

The obtained expression will be exact for polynomial potentials of the degree smaller than  $p'$ . Generally this decomposition leads to numerical eigenfunctions and eigenvalues with the accuracy of order about  $p' + 1$ . If the integrals in Step 1.3 of Algorithm 1 and Step 2.3 of Algorithm 2 cannot be calculated in the analytical form, then the Gauss integration rule [1,6] with  $p' + 1$  nodes is applied and held the theoretical estimations (21).

2. Using the local coordinate  $\eta \in [-1, 1]$  related to the absolute coordinate  $z$  as  $z = z_j^{\min} + h_j(1 + \eta)/2$ ,  $\frac{dz}{d\eta} = h_j/2$ , one should exploit the following expansions of the function and its first derivative

$$\begin{aligned} \hat{\Phi}(z) &= \sum_{r=0}^p \sum_{\kappa=0}^{\kappa^{\max}-1} \hat{\Phi}_{\kappa^{\max}r+\kappa} N_{\kappa^{\max}r+\kappa}(\eta, -1, 1) \left( \frac{dz}{d\eta} \right)^{\kappa}, \\ \frac{d\hat{\Phi}(z)}{dz} &= \sum_{r=0}^p \sum_{\kappa=0}^{\kappa^{\max}-1} \hat{\Phi}_{\kappa^{\max}r+\kappa} \frac{dN_{\kappa^{\max}r+\kappa}(\eta, -1, 1)}{d\eta} \left( \frac{dz}{d\eta} \right)^{\kappa-1}. \end{aligned}$$

3. The matrices  $A_{L_1 L_2}$  and  $B_{L_1 L_2}$  are symmetric, their dimension is  $L \times L$ , where  $L = \kappa^{\max}(np + 1)$ . They consist of  $n$  sub-matrices with the dimension  $\kappa^{\max}(p + 1) \times \kappa^{\max}(p + 1)$ . The intersections of these sub-matrices are blocks having the dimension  $\kappa^{\max} \times \kappa^{\max}$ . These blocks include elements that equal zero in both matrices  $B_{L_1 L_2}$  and  $A_{L_1 L_2}$  for  $V(z) = 0$  and become nonzero in the matrix  $A_{L_1 L_2}$ , when  $V(z) \neq 0$ . The existence of such elements is a manifestation of the IHPs symmetry. The total number of elements in all these blocks is  $(n(p^2 + 2p) + 1)(\kappa^{\max})^2$ . Examples of banded matrix structures are shown in Fig. 2.

4. To impose the BC (III) in  $z^{\min}$  one should apply  $A_{11} = A_{11} + f_2(z^{\min})R(z^{\min})$ , while to impose the BC (III) in  $z^{\max}$  one should apply  $A_{L+1-\kappa^{\max}, L+1-\kappa^{\max}} = A_{L+1-\kappa^{\max}, L+1-\kappa^{\max}} - f_2(z^{\max})R(z^{\max})$ . To impose the BC (I) in  $z^{\min}$  one should drop first row and first column, while to apply the BC (I) in  $z^{\max}$  one should drop row and column with number  $L + 1 - \kappa^{\max}$ .

5. For small matrix dimensions  $\sim 100$ , the desired solution of the problem generated at Step 2.3 is performed using the built-in procedures of the Maple LinearAlgebra package. For large matrix dimensions  $\sim 100 \div 1000000$ , the subspace iteration method is used, implemented in the Fortran program SSPACE [1].

## References

1. Bathe, K.J.: *Finite Element Procedures in Engineering Analysis*, Englewood Cliffs. Prentice Hall, New York (1982)
2. Becker, E.B., Carey, G.F., Tinsley Oden, J.: *Finite elements. An introduction*, vol. I. Prentice-Hall, Inc., Englewood Cliffs (1981)
3. Berezin, I.S., Zhidkov, N.P.: *Computing Methods*, vol. I. Pergamon Press, Oxford (1965)
4. Chuluunbaatar, O., Gusev, A.A., Vinitsky, S.I., Abrashkevich, A.G.: ODPEVP: A program for computing eigenvalues and eigenfunctions and their first derivatives with respect to the parameter of the parametric self-adjointed Sturm-Liouville problem. *Comput. Phys. Commun.* 180, 1358–1375 (2009)
5. Chuluunbaatar, O., Gusev, A.A., Gerdt, V.P., Kaschiev, M.S., Rostovtsev, V.A., Samoylov, V., Tupikova, T., Vinitsky, S.I.: A symbolic-numerical Algorithm for solving the eigenvalue problem for a hydrogen atom in the magnetic field: cylindrical coordinates. In: Ganzha, V.G., Mayr, E.W., Vorozhtsov, E.V. (eds.) *CASC 2007. LNCS*, vol. 4770, pp. 118–133. Springer, Heidelberg (2007)
6. Chuluunbaatar, O., et al.: KANTBP: A program for computing energy levels, reaction matrix and radial wave functions in the coupled-channel hyperspherical adiabatic approach. *Comput. Phys. Commun.* 177, 649–675 (2007)
7. Cwiok, S., et al.: Single-particle energies, wave functions, quadrupole moments and g-factors in an axially deformed Woods-Saxon potential with applications to the two-centre-type nuclear problems. *Comput. Phys. Communications* 46, 379–399 (1987)
8. Gusev, A.A., Chuluunbaatar, O., Gerdt, V.P., Rostovtsev, V.A., Vinitsky, S.I., Derbov, V.L., Serov, V.V.: Symbolic-numeric algorithms for computer analysis of spheroidal quantum dot models. In: Gerdt, V.P., Koepf, W., Mayr, E.W., Vorozhtsov, E.V. (eds.) *CASC 2010. LNCS*, vol. 6244, pp. 106–122. Springer, Heidelberg (2010)
9. Gusev, A.A., Vinitsky, S.I., Chuluunbaatar, O., Gerdt, V.P., Rostovtsev, V.A.: Symbolic-numerical algorithms to solve the quantum tunneling problem for a coupled pair of ions. In: Gerdt, V.P., Koepf, W., Mayr, E.W., Vorozhtsov, E.V. (eds.) *CASC 2011. LNCS*, vol. 6885, pp. 175–191. Springer, Heidelberg (2011)
10. Ramdas Ram-Mohan, L.: *Finite Element and Boundary Element Applications in Quantum Mechanics*. Oxford University Press, New York (2002)
11. Samarski, A.A., Gulin, A.V.: *Numerical methods*, Nauka, Moscow (1989) (in Russian)
12. Strang, G., Fix, G.J.: *An Analysis of the Finite Element Method*. Prentice-Hall, Englewood Cliffs (1973)
13. Vinitsky, S., Gusev, A., Chuluunbaatar, O., Rostovtsev, V., Le Hai, L., Derbov, V., Krassovitskiy, P.: Symbolic-numerical algorithm for generating cluster eigenfunctions: quantum tunneling of clusters through repulsive barriers. In: Gerdt, V.P., Koepf, W., Mayr, E.W., Vorozhtsov, E.V. (eds.) *CASC 2013. LNCS*, vol. 8136, pp. 427–442. Springer, Heidelberg (2013)



# Symbolic-Numeric Algorithm for Solving the Problem of Quantum Tunneling of a Diatomic Molecule through Repulsive Barriers

Sergue Vinitzky<sup>1</sup>, Alexander Gusev<sup>1</sup>, Ochbadrakh Chuluunbaatar<sup>1,2</sup>,  
Luong Le Hai<sup>1,3</sup>, Andrzej Gózdź<sup>4</sup>, Vladimir L. Derbov<sup>5</sup>,  
and Pavel Krassovitskiy<sup>6</sup>

<sup>1</sup> Joint Institute for Nuclear Research, Dubna, Moscow Region, Russia  
`vinitzky@theor.jinr.ru`

<sup>2</sup> National University of Mongolia, UlaanBaatar, Mongolia

<sup>3</sup> Belgorod State University, Belgorod, Russia

<sup>4</sup> Institute of Physics, Maria Curie-Skłodowska University, Lublin, Poland

<sup>5</sup> Saratov State University, Saratov, Russia

<sup>6</sup> Institute of Nuclear Physics, Almaty, Kazakhstan

**Abstract.** Symbolic-numeric algorithm for solving the boundary-value problems that describe the model of quantum tunneling of a diatomic molecule through repulsive barriers is described. Two boundary-value problems (BVPs) in Cartesian and polar coordinates are formulated and reduced to 1D BVPs for different systems of coupled second-order differential equations (SCSODEs) that contain potential matrix elements with different asymptotic behavior. A symbolic algorithm implemented in CAS Maple to calculate the required asymptotic behavior of adiabatic basis, the potential matrix elements, and the fundamental solutions of the SCSODEs is elaborated. Comparative analysis of the potential matrix elements calculated in the Cartesian and polar coordinates is presented. Benchmark calculations of quantum tunneling of a diatomic molecule with the nuclei coupled by Morse potential through Gaussian barriers below dissociation threshold are carried out in Cartesian and polar coordinates using the finite element method, and the results are discussed.

**Keywords:** Symbolic-numeric algorithm, quantum tunneling problem, diatomic molecule, repulsive barriers, boundary-value problem, adiabatic representation, asymptotic solutions, finite element method.

## 1 Introduction

The study of tunneling of coupled particles through repulsive barriers [11] has revealed the effect of resonance quantum transparency: when the cluster size is comparable with the spatial width of the barrier, there are mechanisms that lead to greater transparency of the barrier. These mechanisms are related to the formation of the barrier resonances, provided that the potential energy of the composite system has local minima giving rise to metastable states of the moving cluster [10]. Currently this effect and its possible applications are a

subject of extensive study in relation with different quantum-physical problems, e.g., quantum diffusion of molecules [12], exciton resonance passage through a quantum heterostructure barrier [8], resonant formation of molecules from individual atoms [13], controlling the direction of diffusion in solids [1], and tunnelling of ions and clusters through repulsive barriers [7,6]. For the analysis of these effects, it is useful to develop model approaches based on approximations providing a realistic description of interactions between the atoms in the molecule as well as with the barriers, and to elaborate symbolic-numeric algorithms and software.

In this paper, we formulate and study the model of a diatomic molecule with the nuclei coupled via the effective Morse potential that penetrates through a Gaussian repulsive barrier, using Galerkin and Kantorovich expansion of the desired solution in Cartesian and polar coordinates, respectively. We formulate two boundary-value problems (BVP) and use different sets of basis functions to reduce the original problem to 1D BVPs for different systems of coupled second-order differential equations (SCSODEs) that contain potential matrix elements with different asymptotic behavior. In the first case, the potential matrix elements decrease exponentially, and in the second case, they decrease as inverse powers of the independent variable. In the second case, we must calculate the asymptotic behavior of the potential matrix elements to solve the boundary value problem. For this goal, we develop symbolic algorithms implemented in CAS Maple to calculate the required asymptotic behavior of the potential matrix elements as well as the fundamental solutions of SCSODEs. We present a comparative analysis of the potential matrix elements calculated in the Cartesian and polar coordinates, which are used to solve the quantum tunneling problem below the dissociation threshold. The necessity for two statements of the problem follows from the important practical applications of further self-consistent study of the system above the dissociation threshold, which is convenient in polar coordinates. The effect of quantum transparency, i.e., the resonance behavior of the transmission coefficient versus the energy of the molecule is analyzed.

The paper is organized as follows. In Sections 2 and 3, we formulate and solve the BVPs in Cartesian and polar coordinates. In Section 4, the leading terms of the asymptotic expressions of effective potentials and fundamental solutions are calculated using the elaborated algorithms in CAS Maple. In Section 5, we analyze the solution of the quantum tunneling problem below the dissociation threshold. In Conclusion, the prospects of future studies are discussed.

## 2 Model I. Quantum Tunneling in Cartesian Coordinates

We consider a 2D model of two identical particles with the mass  $m$  coupled by the pair potential  $\tilde{V}(x_2 - x_1)$  and interacting with the external barrier potentials  $\tilde{V}^b(x_1)$  and  $\tilde{V}^b(x_2)$ . Using the change of variables  $x = x_2 - x_1$ ,  $y = x_2 + x_1$ ,

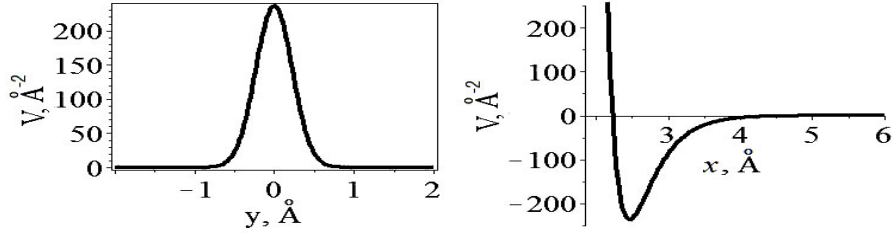


**Fig. 1.** Gaussian-type barrier  $V^b(x_i) = \hat{D} \exp\left(-\frac{x_i^2}{2\sigma}\right)$ , at  $\hat{D} = 236.510003758401 \text{Å}^{-2} = (m/\hbar^2)\tilde{V}_0 = (m/\hbar^2)D$ ,  $\tilde{V}_0 = D = 1280\text{K}$ ,  $\sigma = 5.23 \cdot 10^{-2} \text{Å}^2$ , and the two-particle interaction potential,  $V^M(x) = \hat{D}\{\exp[-2(x - \hat{x}_{eq})\hat{\rho}] - 2\exp[-(x - \hat{x}_{eq})\hat{\rho}]\}$ ,  $\hat{x}_{eq} = 2.47 \text{Å}$ ,  $\hat{\rho} = 2.96812423381643 \text{Å}^{-1}$

$y \in (-\infty, \infty)$ ,  $x \in (-\infty, \infty)$ , we arrive at the Schrödinger equation for the wave function  $\Psi(x, y)$  in the s-wave approximation

$$\left( -\frac{\hbar^2}{m} \frac{1}{f_1(y)} \frac{\partial}{\partial y} f_2(y) \frac{\partial}{\partial y} - \frac{\hbar^2}{m} \frac{1}{f_3(x)} \frac{\partial}{\partial x} f_4(x) \frac{\partial}{\partial x} + \tilde{V}(x, y) - \tilde{E} \right) \Psi(y, x) = 0. \quad (1)$$

where  $\hbar$  is the Planck constant,  $\tilde{E}$  is the total energy of the system, and the potential function  $V(x, y)$  is defined by the formula

$$\tilde{V}(x, y) = \tilde{V}^M(x) + \tilde{V}^b(x_1) + \tilde{V}^b(x_2). \quad (2)$$

The equation describing the molecular subsystem has the form

$$\left( -\frac{\hbar^2}{m} \frac{1}{f_3(x)} \frac{\partial}{\partial x} f_4(x) \frac{\partial}{\partial x} + \tilde{V}^M(x) - \tilde{\varepsilon} \right) \phi(x) = 0. \quad (3)$$

The molecular subsystem is assumed to possess the continuous energy spectrum with the eigenvalues  $\tilde{\varepsilon} \geq 0$  and eigenfunctions  $\phi_{\tilde{\varepsilon}}(x)$  and the discrete energy spectrum, consisting of the finite number  $n$  of bound states with the eigenfunctions  $\phi_j(x)$  and the eigenvalues  $\tilde{\varepsilon}_j = -|\tilde{\varepsilon}_j|$ ,  $j = 1, n$ .

The asymptotic boundary conditions imposed on the solution for the 2D model in the s-wave approximation  $\Psi(y, x) = \{\Psi_j(y, x)\}_{j=1}^{N_o}$  in the asymptotic region  $\Omega_j^{as} = \{(x, y) | |x|/|y| \ll 1\}$  with the direction  $v \Rightarrow$  can be written in the obvious form

$$\begin{aligned} \Psi_j(y \rightarrow -\infty, x) &\rightarrow \phi_j(x) \frac{\exp(ip_j y)}{\sqrt{p_j f_2(y)}} + \sum_{l=1}^{N_o} \phi_l(x) \frac{\exp(-ip_l y)}{\sqrt{p_l f_2(y)}} R_{lj}, \\ \Psi_j(y \rightarrow +\infty, x) &\rightarrow \sum_{l=1}^{N_o} \phi_l(x) \frac{\exp(ip_l y)}{\sqrt{p_l f_2(y)}} T_{lj}, \\ \Psi_j(y, x \rightarrow \pm\infty) &\rightarrow 0, \end{aligned} \quad (4)$$

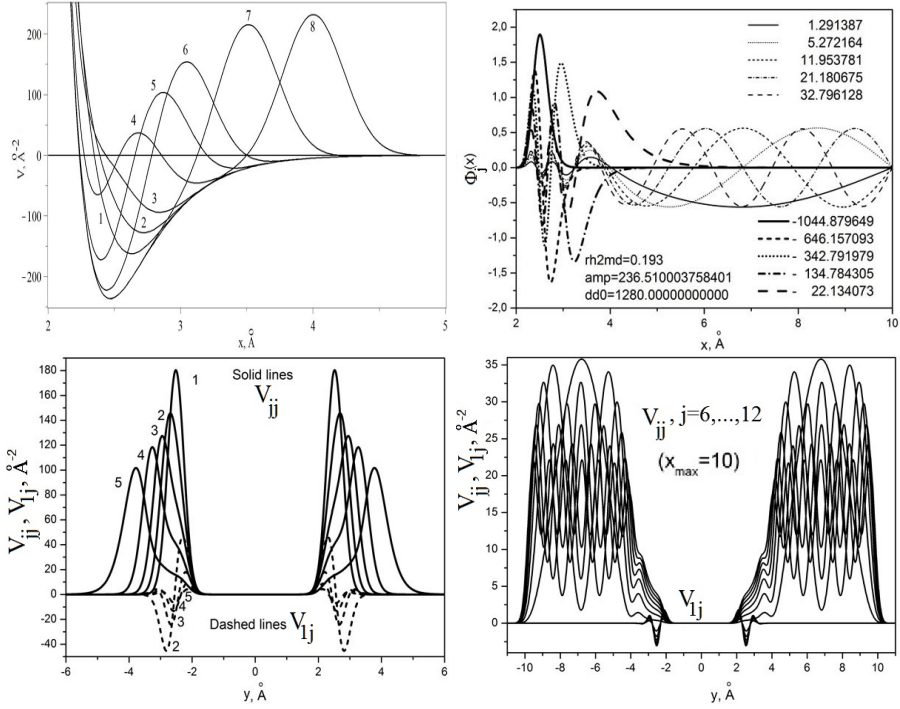


**Fig. 2.** Sections of the total potential energy  $V(y; x) = V^M(y; x) + V^b(y; x)$  at  $y = 2.2, 2.3, 2.4, 2.6, 2.8, 3, 3.5, 4$  (curves are noted by 1,...,8). The wave functions  $\phi_j(r)$  of the bound states  $j = 1, 5$  (solid lines) and pseudostates  $j = 6, \dots, 12$  (dashed lines) (corresponding energy eigenvalues given in K). The matrix elements  $V_{jj}(y)$  (solid lines) and  $V_{j1}(y)$  (dashed lines) (in  $\text{\AA}^{-2}$ )

where  $f_1(y) = f_2(y) = 1$ ,  $R_{lj}(\tilde{E})$  and  $T_{lj}(\tilde{E})$  are the reflection and transmission amplitudes,  $N_o \leq n$  is the number of open channels,  $p_i$  is the wave number,  $p_i = \sqrt{(m/\hbar^2)(\tilde{E} - \tilde{\varepsilon}_i)} > 0$ , below dissociation threshold  $\tilde{E} < 0$ ,  $\phi_j(x)$  and  $\varepsilon_j < 0$  at  $j = 1, n$  are the eigenfunctions and eigenvalues of the BVP for Eq. (3).

The solution of Eq. (1) is sought for in the form of Galerkin expansion

$$\Psi_{i_o}(y, x) = \sum_{j=1}^{j_{\max}} \phi_j(x) \chi_{ji_o}(y). \quad (5)$$

Here  $\chi_{ji_o}(y)$  are unknown functions and the orthonormalized basis functions  $\phi_j(x)$  in the interval  $0 \leq x \leq x_{\max}$  are defined as eigenfunctions of the BVP for the equation

$$\left( -\frac{1}{f_3(x)} \frac{\partial}{\partial x} f_4(x) \frac{\partial}{\partial x} + V^M(x) - \varepsilon_j \right) \phi_j(x) = 0, \quad (6)$$

with the boundary and orthonormalization conditions

$$\phi_j(0) = \phi_j(x_{\max}) = 0, \quad \int_0^{x_{\max}} f_3(x) dx \phi_i(x) \phi_j(x) = \delta_{ij}, \quad (7)$$

where  $f_3(x) = f_4(x) = 1$ ,  $V(x) = (m/\hbar^2)\tilde{V}(x)$ ,  $\varepsilon_j = (m/\hbar^2)\tilde{\varepsilon}_j$ . The desired set of numerical solutions of this BVP is calculated with the given accuracy by means of the program ODPEVP [4]. Hence, we calculate the set of  $n$  bound states having the eigenfunctions  $\phi_j(x)$  and the eigenvalues  $\varepsilon_j$ ,  $j = 1, n$  and the desired set of pseudostates with the eigenfunctions  $\phi_j(x)$  and the eigenvalues  $\varepsilon_j \geq 0$ ,  $j = n+1, j_{\max}$ . The latter approximate the set of continuum eigensolutions  $\varepsilon \geq 0$  of the BVP for Eq. (3).

The set of closed-channel Galerkin equations has the form

$$\left[ -\frac{1}{f_1(y)} \frac{\partial}{\partial y} f_2(y) \frac{\partial}{\partial y} + \varepsilon_i - E \right] \chi_{ii_o}(y) + \sum_{j=1}^{j_{\max}} V_{ij}^b(y) \chi_{ji_o}(y) = 0. \quad (8)$$

Thus, the scattering problem (1)–(3) with the asymptotic boundary conditions (4) is reduced to the boundary-value problem for the set of close-coupling equations in the Galerkin form (8) for  $f_1(y) = f_2(y) = 1$  with the boundary conditions at  $y = y_{\min}$  and  $y = y_{\max}$  [6]:

$$\left. \frac{d\mathbf{F}(y)}{dy} \right|_{y=y_t} = \mathcal{R}(y_t) \mathbf{F}(y_t), \quad t = \min, \max, \quad (9)$$

where  $\mathcal{R}(y_{\min})$  and  $\mathcal{R}(y_{\max})$  are  $j_{\max} \times j_{\max}$  symmetric matrix function of  $E$ ,  $\mathbf{F}(y) = \{\chi_{i_o}(y)\}_{i_o=1}^{N_o} = \{\{\chi_{ji_o}(y)\}_{j=1}^{j_{\max}}\}_{i_o=1}^{N_o}$  is the required  $j_{\max} \times N_o$  matrix solution at the number of open channels  $N_o = \max_{E \geq \varepsilon_j} j \leq j_{\max}$ . These matrices

and the sought-for  $N_o \times N_o$  matrices of the reflection and transmission amplitudes  $\mathbf{R}$  and  $\mathbf{T}$  are calculated using the third version of the program KANTBP [3].

In Eq. (8), the effective potentials  $V_{ij}(y)$  are expressed by the integrals

$$V_{ij}^b(y) = \int_0^{x_{\max}} f_1(x) dx \phi_i(x) (V^b(\frac{x+y}{2}) + V^b(\frac{x-y}{2})) \phi_j(x). \quad (10)$$

For example, let us take the parameters of the molecule Be<sub>2</sub>, namely, the reduced mass  $\mu = m/2 = 4.506\text{Da}$ , the average distance between the nuclei  $2.47\text{\AA}$ , the frequency of molecular vibrations expressed in temperature units  $\hbar\omega = 398.72\text{K}$ , the ground state of molecule  $^1\Sigma_u^+$ , the wave number of the order of  $277.124\text{cm}^{-1}$  for the observable excited-to-ground state transitions (we use the relation  $1\text{K} = 0.69503476\text{cm}^{-1}$  from [5]). These values were used to determine the parameters of the Morse potential  $\tilde{V}^M(x)$  and  $V^M(x) = (m/\hbar^2)\tilde{V}^M(x)$  of Eqs. (3) and (6)

$$\tilde{V}^M(x) = D\{\exp[-2(x - \hat{x}_{eq})\hat{\rho}] - 2\exp[-(x - \hat{x}_{eq})\hat{\rho}]\}, \quad (11)$$

where  $D$  is the depth of the interaction potential well and  $\hat{\rho}$  describes the potential well width. The values of  $D$  and  $\hat{\rho}$  are determined from the discrete spectrum



of the BVP (6)–(7) which is approximated by the known discrete spectrum of Eq. (3)

$$\tilde{\varepsilon}_j = -D \left[ 1 - \varsigma(j - 1/2) \right]^2, \quad j = 1, \dots, n = \left[ \varsigma^{-1} + \frac{1}{2} \right]. \quad (12)$$

The discrete spectrum eigenfunctions  $\phi_j(x)$  of the BVP (6)–(7) are approximated by the solutions  $\tilde{\phi}_j(\varsigma)$  of equation (3) in the new variable  $\varsigma$ :

$$\frac{d^2 \tilde{\phi}_j(\varsigma)}{d\varsigma^2} + \frac{1}{\varsigma} \frac{d\tilde{\phi}_j(\varsigma)}{d\varsigma} + \left( -\frac{1}{4} + \frac{j + s_j - 1/2}{\varsigma} - \frac{s_j^2}{\varsigma^2} \right) \tilde{\phi}_j(\varsigma) = 0,$$

where  $s_j = \sqrt{-\varepsilon_j}/\hat{\rho} = \sqrt{\hat{D}}/\hat{\rho} - j + 1/2$  and  $\varsigma = 2\sqrt{\hat{D}} \exp[-(x - \hat{x}_{eq})\hat{\rho}]/\hat{\rho}$ , at  $\varsigma \in (0, +\infty)$  corresponding to the extended interval  $x \in (-\infty, +\infty)$  and have the form

$$\tilde{\phi}_j(\varsigma) = N_j \exp(-\frac{\varsigma}{2}) \varsigma^{s_j} {}_1F_1(1 - j, 2s_j + 1, \varsigma), \quad N_j^2 = \frac{\hat{\rho} \Gamma(2s_j + j)}{(j - 1)! \Gamma(2s_j) \Gamma(2s_j + 1)}. \quad (13)$$

Having the average size of the molecule and the separation between the energy levels taken into account, one can parameterize the molecular potential to fit the observable quantities, namely,  $D = 1280\text{K}$ ,  $\hat{x}_{eq} = 2.47\text{\AA}$ ,  $\hat{\rho} = 2.968\text{\AA}^{-1}$  is determined from the condition  $(\tilde{\varepsilon}_2 - \tilde{\varepsilon}_1)/(2\pi\hbar c) = 277.124\text{ cm}^{-1}$ ,  $\varsigma = \frac{\hat{\rho}\hbar}{\sqrt{mD}} = 0.193$  is the dimensionless constant of the problem, and  $\hat{D} = (\frac{\sqrt{mD}}{\hbar})^2 = (\hat{\rho}/0.193)^2 = (2.968\text{\AA}^{-1}/0.193)^2 = 236.5\text{\AA}^{-2}$ . In accordance with (12), the ground state energy of the molecule  $\text{Be}_2$  is equal to  $-\tilde{\varepsilon}_1 = -1044.88\text{K}$ .

The set of pseudostates with the eigenfunctions  $\phi_j(x)$  and the eigenvalues  $\varepsilon_j \geq 0$ ,  $j = n + 1, j_{\max}$ , approximated by the set of continuous spectrum solutions  $\tilde{\phi}_k(\varsigma)$  with fixed  $k = \sqrt{\varepsilon} > 0$  that satisfy Eq. (3) written in the new variable  $\varsigma$ , i.e., the equation

$$\frac{d^2 \tilde{\phi}_k(\varsigma)}{d\varsigma^2} + \frac{1}{\varsigma} \frac{d\tilde{\phi}_k(\varsigma)}{d\varsigma} + \left( -\frac{1}{4} + \frac{\sqrt{\hat{D}}/\hat{\rho}}{\varsigma} + \frac{s_k^2}{\varsigma^2} \right) \tilde{\phi}_k(\varsigma) = 0.$$

At fixed  $s_k = \frac{k}{\hat{\rho}}$ , these solutions take the form

$$\begin{aligned} \tilde{\phi}_k(\varsigma) = & \frac{N_k \exp(-\varsigma/2)}{2i} (\exp(iw) \varsigma^{-ik/\hat{\rho}} {}_1F_1(-\frac{\sqrt{D}}{\hat{\rho}} + \frac{1}{2} - \frac{ik}{\hat{\rho}}, 1 - \frac{2ik}{\hat{\rho}}, \varsigma) \\ & - \exp(-iw) \varsigma^{ik/\hat{\rho}} {}_1F_1(-\frac{\sqrt{D}}{\hat{\rho}} + \frac{1}{2} + \frac{ik}{\hat{\rho}}, 1 + \frac{2ik}{\hat{\rho}}, \varsigma)), \\ w = & \arg(\Gamma(1 + \frac{2ik}{\hat{\rho}})) + \arg(\Gamma(-\frac{\sqrt{D}}{\hat{\rho}} + \frac{1}{2} - \frac{ik}{\hat{\rho}})). \end{aligned} \quad (14)$$

Asymptotically  $\tilde{\phi}_k^{as}(x \rightarrow \infty) = \sin(kx + \delta(k))$ ,  $\delta(k) = -kx_{eq} - s_k \ln(2\sqrt{\hat{D}}/\hat{\rho}) + w$  corresponds to the scattering phase.

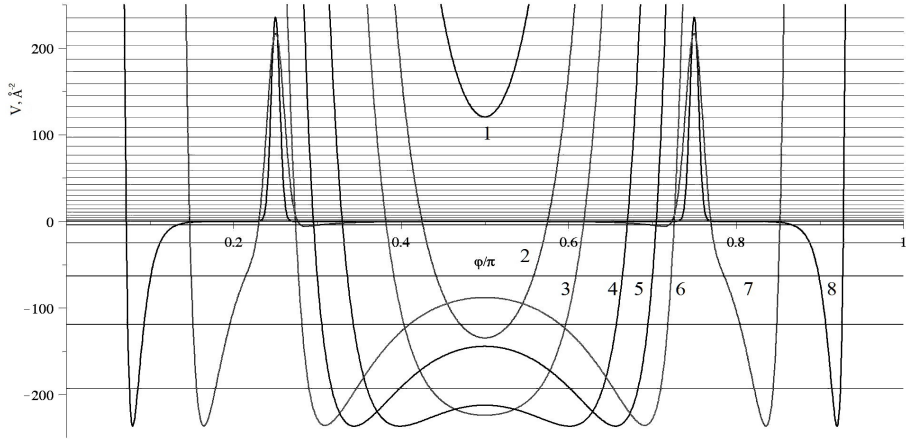


**Fig. 3.** Sections of the total potential energy  $V(\rho; \varphi) = V^M(\rho; \varphi) + V^b(\rho; \varphi)$  in polar coordinates at  $\rho = 2.2, 2.3, 2.4, 2.6, 2.8, 3, 5, 10$  (curves are noted by 1,...,8). Straight lines are energy levels at  $\rho = 10$ .

Since the bond in the molecule  $\text{Be}_2$  is of the Van der Waals type, one can consider each constituent atom independently interacting with the external barrier potential. The latter should be chosen to have the height and the width typical of barriers in a real crystal lattice. Moreover, this potential should be a smooth function having the second derivative to apply high-accuracy numerical methods, like the Numerov method or the finite element method, for solving the BVP for the systems of second-order ordinary differential equations. We choose the repulsive barrier potential to be Gaussian:

$$\tilde{V}^b(x_i) = \tilde{V}_0 \exp\left(-\frac{x_i^2}{2\sigma}\right), \quad V^b(x_i) = \frac{m}{\hbar^2} \tilde{V}^b(x_i) = \hat{D} \exp\left(-\frac{x_i^2}{2\sigma}\right). \quad (15)$$

Here the parameters  $\tilde{V}_0 = 1280K$ ,  $\hat{D} = 236.510003758401\text{\AA}^{-2} = (m/\hbar^2)\tilde{V}_0$ ,  $\sigma = 5.23 \cdot 10^{-2}\text{\AA}^2$  are determined by the model requirement that the width of the repulsive potential at the kinetic energy equal to that of the ground state is  $1\text{\AA}$ , so that the average distance  $2.47\text{\AA}$  between the atoms of Be is smaller than the distance  $2.56\text{\AA}$  between Cu atoms in the plane (111) of the crystal lattice cell. The potential barrier height  $\tilde{V}_0$  of the order of 200 meV was estimated following the experimental observation of quantum diffusion of hydrogen atoms [9]. Fig. 1 illustrates the Gaussian and Morse potentials.

Figure 2 presents the sections of the total potential energy, the calculated eigenfunctions of the BVP (6) and the effective potentials  $V_{ij}(y)$  of Eq. (10) calculated using these functions. Note that the wave functions  $\phi_j(x)$  and the eigenvalues  $\varepsilon_j(x)$  of the bound states  $j = 1, 5$  (solid lines) approximate the known analytical ones of the BVP for Eq. (3) with the Morse potential (11) with four and seven significant digits, respectively. The states are localized in the well,

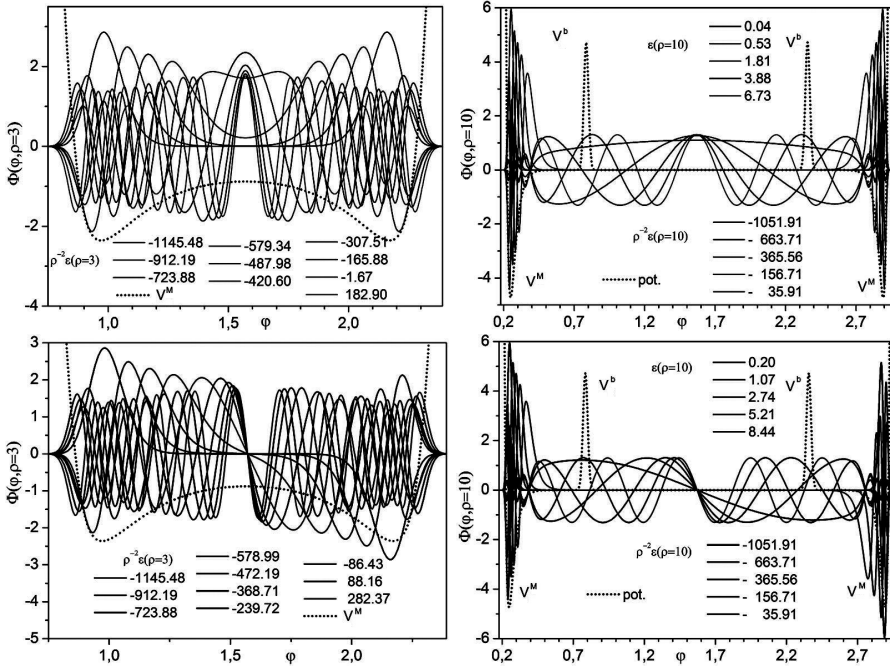


**Fig. 4.** Even and odd eigenfunctions of the parametric eigenvalue problem for the fast subsystem at  $\rho = 3$  and  $\rho = 10$  (corresponding energy eigenvalues given in K)

while the pseudostates  $j = 6, \dots, 12$  are approximated with the same accuracy and localized outside the well. The matrix elements between the bound states are localized in the vicinity of the barriers and the matrix elements between the pseudostates are localized beyond the barriers. The matrix elements between the bound states and pseudostates are small. The solution of the BVP (6), (7) was performed on the finite-element grids  $\Omega_x = \{0(N_{elem} = 800)12\}$ , with  $N_{elem}$  fourth-order Lagrange elements  $p = 4$  between the nodes, using the program ODPEVP [4].

### 3 Model II. Quantum Tunneling in Polar Coordinates

Using the change of variables  $x = \rho \sin \varphi$ ,  $y = \rho \cos \varphi$ , we can rewrite Eq. (1) in polar coordinates  $(\rho, \varphi)$   $\Omega_{\rho, \varphi} = (\rho \in (0, \infty), \varphi \in [0, \pi])$  in the dimensionless form

$$\left( -\frac{1}{\rho} \frac{d}{d\rho} \rho \frac{d}{d\rho} - \frac{1}{\rho^2} \frac{\partial^2}{\partial \varphi^2} + V(\rho, \varphi) - E \right) \Psi(\rho, \varphi) = 0, \quad (16)$$

where the potential function  $V(\rho, \varphi) = V^M(\rho, \varphi) + V^b(\rho, \varphi)$  is defined by the formula in term of potentials (11) and (15)

$$V^M(\rho, \varphi) = V(\rho \sin \varphi), \quad V^b(\rho, \varphi) = V^b\left(\rho \frac{\sin(\varphi + \pi/4)}{\sqrt{2}}\right) + V^b\left(\rho \frac{\sin(\varphi - \pi/4)}{\sqrt{2}}\right). \quad (17)$$

Sections of the potential function  $V(\rho, \varphi)$  at a set of slow variable values  $\rho$  are shown in Fig. 3. One can see that at large  $\rho$ , the width of the potential wells decreases as  $\rho$  increases. Therefore, at large  $\rho$ , the potential of two-center problem, symmetric with respect to  $\varphi = \pi/2$ , transforms into two one-center Morse potentials.

The asymptotic boundary conditions imposed on the solution for the 2D model in the s-wave approximation  $\Psi(\rho, \varphi) = \{\Psi_j(\rho, \varphi)\}_{j=1}^{N_o}$  in the asymptotic region  $\Omega_j^{as} = \{(\varphi, \rho) | \varphi/\rho \ll 1\}$  can be written in the obvious form

$$\Psi(\rho, \varphi, \varphi_0) = \sum_{i_o=1}^{N_o} \Psi_{ji_o}(\rho, \phi) \phi_{i_o}(-\varphi_0; \rho \rightarrow +\infty) \quad (18)$$

$$\Psi_{i_o}(\rho \rightarrow +\infty, \varphi) \rightarrow \sqrt{\frac{2}{\pi}} \sum_{j=1}^{N_o} \phi_j(\varphi; \rho) [\chi_{ji_o}^*(\rho) \delta_{ji_o} - \chi_{ji_o}(\rho) S_{ji_o}(E)], \quad (19)$$

$$\Psi_{i_o}(\rho, \phi \rightarrow 0) \rightarrow 0, \quad \Psi_{i_o}(\rho, \phi \rightarrow \pi) \rightarrow 0, \quad \chi_{ji_o}(\rho) = \frac{\exp(i(p_j \rho - \frac{\pi}{4}))}{2\sqrt{p_j \rho}},$$

where the angle  $\varphi_0$  determines the direction of the incident wave propagation, in particular,  $\varphi_0 = 0$  corresponds to  $v \rightarrow$  and  $\varphi_0 = \pi$  corresponds to  $v \leftarrow$ .  $S_{ji_o}(E)$  are the elements of the  $N_o \times N_o$  **S**-matrix,  $N_o$  is the number of open channels,  $p_i$  is the wave number,  $p_i = \sqrt{(m/\hbar^2)(\tilde{E} - \tilde{\varepsilon}_i(\rho \rightarrow +\infty))} > 0$ , below the dissociation threshold  $\tilde{E} < 0$ ,  $\phi_i(\varphi, \rho \rightarrow +\infty) = \sqrt{\rho} \phi_i(x)$ , and  $\varepsilon_i(\rho \rightarrow \infty)/\rho^2 = \varepsilon_i^{(0)} < 0$  are the eigenfunctions localized in the asymptotic region  $\Omega_j^{as}$ , and the eigenvalues of the BVP for Eq. (21).

The solution of Eq. (16) is sought for in the form of Kantorovich expansion

$$\Psi_{i_o}(\rho, \varphi) = \sum_{j=1}^{j_{\max}} \phi_j(\varphi; \rho) \chi_{ji_o}(\rho). \quad (20)$$

Here  $\chi_{ji_o}(\rho)$  are unknown functions and the orthonormalized basis functions  $\phi_j(\varphi; \rho)$  in the interval  $\varphi \in [0, \pi]$  are defined as eigenfunctions of the BVP for the equation

$$\left( -\frac{\partial^2}{\partial \varphi^2} + \rho^2 (V^M(\rho \sin \varphi) + V^b(\rho, \phi)) - \varepsilon_j(\rho) \right) \phi_j(\varphi; \rho) = 0, \quad (21)$$

with orthonormalization conditions

$$\int_0^\pi d\varphi \phi_i(\varphi; \rho) \phi_j(\varphi; \rho) = \delta_{ij}. \quad (22)$$

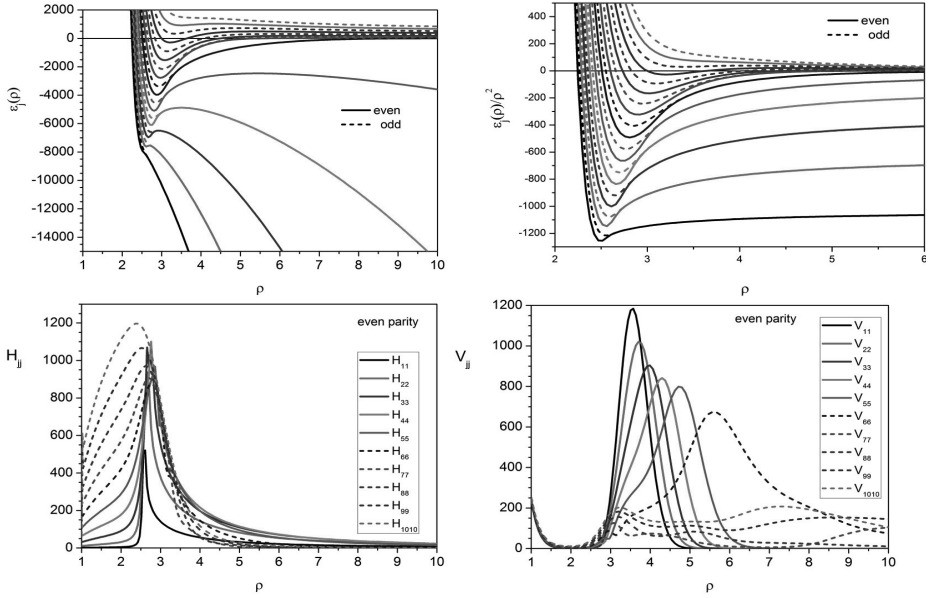


**Fig. 5.** Potential curves  $\varepsilon_j(\rho)$  and even diagonal effective potentials  $H_{jj}(\rho)$  and  $V_{jj}^b(\rho)$  vs  $\rho$  (Å)

The solution of the BVPs (21), (22) was performed on the finite-element grids  $\Omega_\varphi = \{\varphi_1(N_{elem} = 800)\pi/2\}$ , if  $\varphi_3 = (8 + \varphi x_{eq})/(\varphi\rho) > \pi/4$ ,  $\Omega_\varphi = \{\varphi_1(N_{elem} = 300)\varphi_2(N_{elem} = 60)\varphi_4(N_{elem} = 40)\varphi_5(N_{elem} = 100)\pi/2\}$  with  $N_{elem}$  fourth-order Lagrange elements  $p = 4$  between the nodes, using the program ODPEVP [4]. Here angles  $\varphi_1 = (-3 + \varphi x_{eq})/(\varphi\rho)$  and  $\varphi_2 = (4 + \varphi x_{eq})/(\varphi\rho)$  are marked left and right bounds of well (17) and angles  $\varphi_4 = \pi/4 - 4\sqrt{\sigma}/\rho$  and  $\varphi_5 = \pi/4 + 4\sqrt{\sigma}/\rho$  are marked left and right bounds of potential barrier (17).

First, let us put  $V^b(\rho, \varphi) = 0$  in Eq. (21). In this case, we calculate the set of  $n$  bound states having the eigenfunctions  $\phi_j(\varphi; \rho)$  and the eigenvalues  $\varepsilon_j(\rho) < 0$  at  $j = 1, 2, \dots, n$ , and the desired set of pseudostates with the eigenfunctions  $\phi_j(\varphi; \rho)$  and the eigenvalues  $\varepsilon_j(\rho) \geq 0$  at  $j = n + 1, \dots, j_{max}$ . The latter approximate the set of continuum eigensolutions  $\varepsilon(\rho) \geq 0$  of the BVP for Eq. (3). The eigenvalues have the following asymptotes:  $\varepsilon_j(\rho \rightarrow \infty)/\rho^2 = \varepsilon_j$  at  $j = 1, 2, \dots, n$  and  $\varepsilon_j(\rho \rightarrow \infty)/\rho^2 = (j - n)^2/\rho^2 + O(1/\rho^3)$  at  $j = n + 1, \dots, j_{max}$ .

The eigenfunctions  $\phi_j(\varphi; \rho)$ ,  $j = 1, 20$  are shown in Fig. 4 at  $\rho = 3$  and  $\rho = 10$ . Taking the above symmetry  $V(\varphi, \rho) = V(\pi - \varphi, \rho)$  of the potential into account, the eigenfunctions are separated into two subsets, namely, the even  $\phi_j^{\sigma=1}(\varphi; \rho)$  and odd  $\phi_j^{\sigma=-1}(\varphi; \rho)$  ones. The linear combinations

$$\phi_j^{\rightarrow\leftarrow}(\varphi; \rho) = (\phi_j^{\sigma=1}(\varphi; \rho) \pm \phi_j^{\sigma=-1}(\varphi; \rho))/\sqrt{2}$$

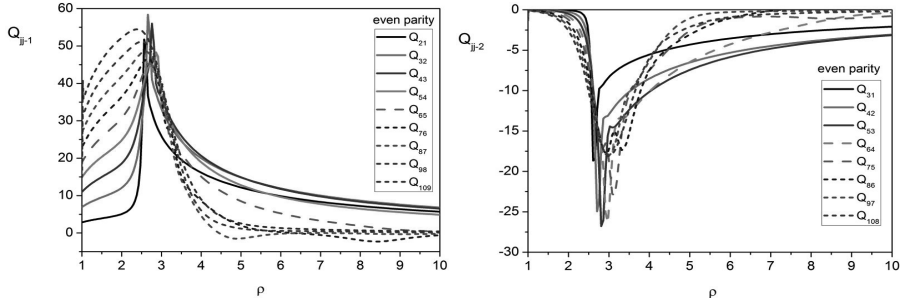


**Fig. 6.** Even effective potentials  $Q_{ij}(\rho)$  vs  $\rho$  (Å)

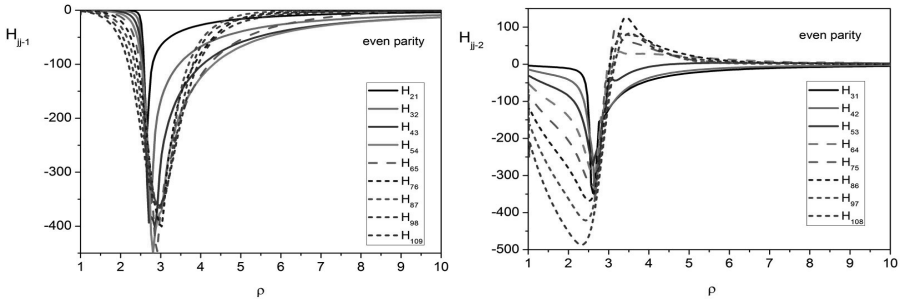


**Fig. 7.** Even effective potentials  $H_{ij}(\rho)$  vs  $\rho$  (Å)

at large  $\rho$  have maxima in the vicinity of  $\varphi = 0$  and  $\varphi = \pi$ , respectively, such that they correspond to the functions presented in Fig. 2. Taking this property into account, we arrive at the expressions [2]

$$\tilde{\mathbf{T}} = (-\tilde{\mathbf{S}}_{+1} + \tilde{\mathbf{S}}_{-1})/2, \quad \tilde{\mathbf{R}} = (-\tilde{\mathbf{S}}_{+1} - \tilde{\mathbf{S}}_{-1})/2, \quad (23)$$

which relate the even  $\tilde{\mathbf{S}}_{+1}$  and odd  $\tilde{\mathbf{S}}_{-1}$  elements of the matrix  $\tilde{\mathbf{S}} = e^{i\pi/4} \mathbf{S} e^{i\pi/4}$  from Eq. (19) to the transmission  $\tilde{\mathbf{T}}$  and reflection  $\tilde{\mathbf{R}}$  amplitudes from Eq. (4).

The set of closed-channel Kantorovich self-adjoint equations has the form

$$\left[ -\frac{1}{\rho} \frac{d}{d\rho} \rho \frac{d}{d\rho} + \frac{\varepsilon_i(\rho)}{\rho^2} - E \right] \chi_{ii_o}(\rho) + \sum_{j=1}^{j_{\max}} W_{ij}(\rho) \chi_{ji_o}(\rho) = 0. \quad (24)$$

where the potential matrix operator  $W_{ij}(\rho)$  has the form

$$W_{ij}(\rho) = V_{ij}^b(\rho) + H_{ji}(\rho) + \frac{1}{\rho} \frac{d}{d\rho} \rho Q_{ji}(\rho) + Q_{ji}(\rho) \frac{d}{d\rho}. \quad (25)$$

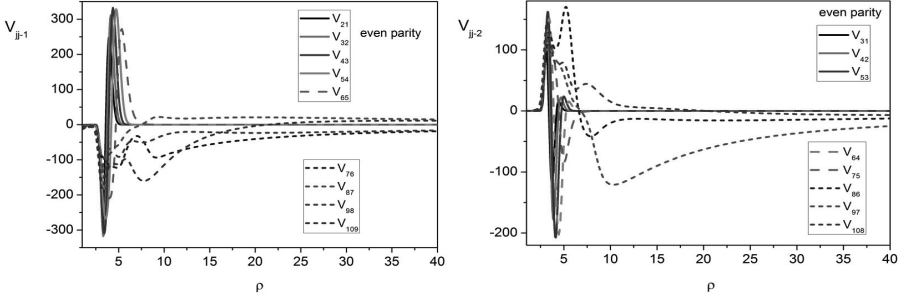


**Fig. 8.** Even effective potentials  $V_{ij}(\rho)$  vs  $\rho$  (Å)

The potential curves  $\varepsilon_j(\rho)$  (see Fig. 5) and the effective potentials  $Q_{ij}(\rho) = -Q_{ji}(\rho)$ ,  $H_{ij}(\rho) = H_{ji}(\rho)$  and  $V_{ij}^b(\rho)$  (see Figs. 6–8) are determined by the integrals calculated using the program ODPEVP

$$Q_{ij}(\rho) = - \int_0^\pi d\varphi \phi_i(\varphi; \rho) \frac{d\phi_j(\varphi; \rho)}{d\rho}, H_{ij}(\rho) = \int_0^\pi d\varphi \frac{d\phi_i(\varphi; \rho)}{d\rho} \frac{d\phi_j(\varphi; \rho)}{d\rho}, \quad (26)$$

$$V_{ij}^b(\rho) = \int_0^\pi d\varphi \phi_i(\varphi; \rho) \left( V^b\left(\rho \frac{\sin(\varphi + \pi/4)}{\sqrt{2}}\right) + V^b\left(\rho \frac{\sin(\varphi - \pi/4)}{\sqrt{2}}\right) \right) \phi_j(\varphi; \rho).$$

If we take the potential  $V^b(\rho, \phi)$  in Eq. (21) into account by using the matrix elements  $V_{ij}^b(\rho)$  from Eq.(26), then we put  $V_{ij}^b(\rho) = 0$  in Eq.(25). Thus, the scattering problem for Eq. (16) with the asymptotic boundary conditions (19) is reduced to the boundary-value problem for the set of close-coupling equations in the Kantorovich form (18) with the boundary conditions at  $\rho = \rho_{\min}$  and  $\rho = \rho_{\max}$  [6]:

$$\left. \frac{d\mathbf{F}(\rho)}{d\rho} \right|_{\rho=\rho_t} = (\mathcal{R}(\rho_t) + \mathbf{Q}(\rho_t))\mathbf{F}(\rho_t), \quad t = \min, \max, \quad (27)$$

where  $\mathcal{R}(\rho)$  is an unknown  $j_{\max} \times j_{\max}$  symmetric matrix function,  $\mathbf{F}(\rho) = \{\chi_{i_o}(\rho)\}_{i_o=1}^{N_o} = \{\{\chi_{ji_o}(\rho)\}_{j=1}^{j_{\max}}\}_{i_o=1}^{N_o}$  is the required  $j_{\max} \times N_o$  matrix solution, and  $N_o$  is the number of open channels,  $N_o = \max_{E \geq \varepsilon_j} j \leq j_{\max}$ , calculated using the program KANTBP 3.0 [3].

## 4 Asymptotic Form of Effective Potentials and Solutions

**Algorithm 1.** At large  $\rho$ , the width of the potential well is decreasing with increasing  $\rho$  (see Fig. 3). This allows linearization of the argument  $\rho \sin \varphi - \hat{x}_{eq} \rightarrow \rho(\varphi - \arcsin(\hat{x}_{eq}/\rho))$  at  $|x - \hat{x}_{eq}|/\rho \ll 1$  in the expression of the potential function  $V^M(\rho \sin \varphi)$  and reformulation of Eq. (21) on the interval  $\varphi = (0, \pi)$

$$\left( -\frac{\partial^2}{\partial \varphi^2} + \rho^2 V^M(\rho(\varphi - \arcsin(\hat{x}_{eq}/\rho))) - \varepsilon_j(\rho) \right) \phi_j(\varphi; \rho) = 0. \quad (28)$$

**Table 1.** The calculated coefficients  $Q_{ij}^{(1)}$   $H_{ij}^{(2)}$  of expansions (31) (up rows) and corresponding numerical values  $Q_{ij}$  and  $H_{ij}$  at  $\rho = 100$ (down rows)

$Q_{ij}^{(1)}$ $Q_{ij}$	1	2	3	4	5
1	0 0	55.852657 0.55 863277	-20.662584 -0.20 664572	9.913235 0.09 914008	-4.888752 -0.04 891971
2	-55.852657 -0.55 863277	0 0	66.253422 0.66 270932	-30.004416 -0.30 010937	14.557626 0.14 568965
3	20.662584 0.20 664572	-66.253422 -0.66 270932	0 0	62.290358 0.62 317875	-28.724086 -0.28 751980
4	-9.913235 -0.09 914008	30.004416 0.30 010937	62.290358 0.62 317875	0 0	43.265811 0.43 320993
5	4.888752 0.04 891971	-14.557626 -0.14 568966	28.724086 0.28 751983	-43.265811 -0.43 321006	0 0
$H_{ij}^{(2)}$ $H_{ij}$	1	2	3	4	5
1	692.635 0.0692 859	-364.132 -0.0364 209	-462.085 -0.0462 371	397.196 0.0397 441	-240.775 -0.0241 084
2	-364.132 -0.0364 209	1718.621 0.1719 273	-873.970 -0.0874 195	-219.292 -0.0219 721	253.669 0.0254 209
3	-462.085 -0.0462 371	-873.970 -0.0874 195	2210.843 0.2211 927	-1250.672 -0.1251 191	244.905 0.0244 755
4	397.196 0.0397 441	-219.292 -0.0219 721	-1250.672 -0.1251 191	2088.603 0.2090 243	-1167.908 -0.1169 414
5	-240.775 -0.0241 084	253.669 0.0254 209	244.905 0.0244 755	-1167.908 -0.1169 414	1209.648 0.1212 568

This equation coincides with Eq. (6), (11), taking the notations

$$\hat{D} \rightarrow \hat{D}\rho^2, \hat{\rho} \rightarrow \hat{\rho}\rho, \hat{x}_{eq} \rightarrow \arcsin(\hat{x}_{eq}/\rho) \quad (29)$$

into account.

As a result, we obtain the approximate eigenvalues  $\varepsilon_j(\rho)$  that depend on  $\rho$  as a parameter, expressed as

$$\varepsilon_j(\rho) = \rho^2 \varepsilon_j^{(0)}, \quad \varepsilon_j^{(0)} = -\hat{D} \left[ 1 - \frac{\hat{\rho}(j - \frac{1}{2})}{\sqrt{\hat{D}}} \right]^2, \quad j = 1, \dots, n = \left\lceil \frac{\sqrt{\hat{D}}}{\hat{\rho}} + \frac{1}{2} \right\rceil. \quad (30)$$

These eigenvalues demonstrate correct asymptotic behavior  $\tilde{\varepsilon}_j(\rho)/\rho^2 = \tilde{\varepsilon}_j$  describing the lower part of the discrete spectrum of problem (3). In the considered case, they correspond to the first five ( $n = 5$ ) eigenvalues  $\tilde{\varepsilon}_1, \dots, \tilde{\varepsilon}_5$ . The corresponding eigenfunctions  $\phi_j(\varphi; \rho)$  at  $j = 1, \dots, n$ , parametrically depending



on the slow variable  $\rho$  via the new independent variable  $\zeta = \zeta(\varphi; \rho) = 2\rho\sqrt{\hat{D}}\exp[-\hat{\rho}\rho(\varphi - \arcsin(\hat{x}_{eq}/\rho))]/\hat{\rho}$ ,  $\zeta \in [0, +\infty)$  have the form

$$\tilde{\phi}_j(\zeta; \rho) = N_j(\rho) \exp\left(-\frac{\zeta}{2}\right) \zeta^{s_j} {}_1F_1(1-j, 2s_j+1, \zeta),$$

$$N_j^2(\rho) = \frac{\rho \hat{\rho} \Gamma(2s_j+j)}{(j-1)! \Gamma(2s_j) \Gamma(2s_j+1)},$$

where  $s_j = \sqrt{\hat{D}}/\hat{\rho} - j + 1/2$  is a positive parameter. In the considered case, the wave function outside the well at  $|x - \hat{x}_{eq}|/\rho \gg 1$  is exponentially decreasing. This makes it possible to integrate the product of functions  $\tilde{\psi}_j(\zeta(\varphi; \rho); \rho)$  and/or  $\partial \tilde{\psi}_j(\zeta(\varphi; \rho); \rho)/\partial \rho|_{\phi=\text{const}}$  by  $\zeta$  in the interval  $\zeta \in (0, +\infty)$ . The calculated eigenfunctions with  $\rho = 10$  for  $j = 1, \dots, 5$  shown in Fig. 4 qualitatively agree with the bound states in Fig. 2. The matrix elements between the states of the lower part of the discrete spectrum  $i, j = 1, \dots, n = 5$  with the eigenvalues  $\varepsilon_j(\rho)/\rho^2 = \varepsilon_j^{(0)}$  are expanded in inverse powers of  $\rho$ :

$$Q_{ij}(\rho) = \sum_{k=1}^{k_{\max}} \frac{Q_{ij}^{(2k-1)}}{\rho^{2k-1}}, \quad H_{ij}(\rho) = \sum_{k=1}^{k_{\max}} \frac{H_{ij}^{(2k)}}{\rho^{2k}}, \quad V_{ij}(\rho) = O(\exp(-\rho)), \quad (31)$$

and calculated up to the desired order  $k_{\max}$  in CAS MAPLE. As an example, the calculated coefficients  $Q_{ij}^{(1)}$  and  $H_{ij}^{(2)}$  of expansions (31) are presented in Table 1. For comparison, the numerical values of matrix elements  $Q_{ij}$  and  $H_{ij}$  at  $\rho = 100$  are also given in Table 1. One can see that with the first nonzero coefficients of these expansions, one gets the numerical approximation of the matrix elements with three significant digits.

For the states  $i, j = n+1, \dots, j_{\max}$  with the eigenvalues  $\varepsilon_j(\rho \rightarrow \infty) = (j-n)^2 + O(1/\rho) = \varepsilon_j^{(2)} + O(1/\rho) = k^2 + O(1/\rho)$  corresponding to pseudo states of the BVP (6), (7) we consider the approximation by the eigenfunctions of continuous spectrum (see Eq. (14) with the notations (29)) reduced to the finite interval  $\varphi \in (0, \pi/2)$  by means of the procedure implemented in CAS MAPLE. The energy spectrum of even and odd states is evaluated basing on the conditions

$$\left. \frac{d\tilde{\phi}_k(\varphi; \rho)}{d\varphi} \right|_{\varphi=\pi/2} = 0 \quad \text{and} \quad \tilde{\phi}_k(\pi/2; \rho) = 0$$

for even and odd states, respectively. The calculated eigenfunctions at  $\rho = 10$  for  $i = 6, \dots, 10$  are in quantitative agreement with the numerical ones shown in Fig. 4 and in qualitative agreement with pseudo-states displayed in Fig. 2. Thus, the basis eigenfunctions of Galerkin expansion (5) correspond to the asymptotic ones for Kantorovich expansion (20) at large values of the parameter  $\rho$ .

The diagonal and nondiagonal barrier matrix elements  $V_{ij}(\rho)$  shown in Figs. 5 and 8 should be compared with the corresponding ones displayed in Fig. 2. From this comparison, one can see that the matrix elements  $V_{ij}(\rho)$  from (26) between discrete-spectrum states of BVP (21), (22) and the matrix elements

$V_{ij}(y)$  from (10) between a discrete spectrum state and a pseudo-state (6), (7) demonstrate qualitatively similar behavior in the coordinates  $y$  and  $\rho$ . Since  $\rho = \sqrt{x^2 + y^2} > y$ , the potentials  $V_{ij}(\rho)$  are delocalized with respect to  $V_{ij}(y)$ . Due to slowly decreasing kinematic behavior of the potentials  $Q_{ij}(\rho)$  and  $H_{ij}(\rho)$  as  $\rho^{-1}$  and  $\rho^{-2}$ , respectively, compared to the exponentially decreasing  $V_{ij}(y)$ , one should take into account the leading terms of their asymptotic expressions in solving the BVP (24)-(26) generated by the Kantorovich expansion (18) in the calculation of scattering with five open channels.

## Algorithm 2. Evaluation of the Asymptotic Solutions

**Input.** We calculate the asymptotic solution of the set of  $N$  ODEs at high values of the independent variable  $\rho \gg 1$

$$\begin{aligned} & \left[ -\frac{1}{\rho} \frac{d}{d\rho} \rho \frac{d}{d\rho} + \frac{\varepsilon_i(\rho)}{\rho^2} + \mathcal{H}_{ii}(\rho) - 2E \right] \chi_{ii'}(\rho) \\ &= \sum_{j=1, j \neq i}^N \left[ -Q_{ij}(\rho) \frac{d}{d\rho} - \frac{1}{\rho} \frac{d}{d\rho} \rho Q_{ij}(\rho) - \mathcal{H}_{ij}(\rho) \right] \chi_{ji'}(\rho). \end{aligned} \quad (32)$$

The coefficients of Eqs. (32), where  $\mathcal{H}_{ij} = V_{ij}^b + H_{ij}$  are presented in the form of the inverse power series (31). In particular,  $\varepsilon_i(\rho)/\rho^2 = \varepsilon_i^{(0)} + \varepsilon_i^{(2)}/\rho^2$ .

**Step 1.** We construct the solution of Eqs. (32) in the form:

$$\chi_{ji'}(\rho) = \left( \phi_{ji'}(\rho) + \psi_{ji'}(\rho) \frac{d}{d\rho} \right) R_{i'}(\rho), \quad (33)$$

where  $\phi_{ji'}(\rho)$  and  $\psi_{ji'}(\rho)$  are unknown functions,  $R_{i'}(\rho)$  is a known function. We choose  $R_{i'}(\rho)$  as solutions of the auxiliary problem treated like an etalon equation:

$$\left[ -\frac{1}{\rho} \frac{d}{d\rho} \rho \frac{d}{d\rho} + \frac{Z_{i'}^{(2)}}{\rho^2} - p_{i'}^2 \right] R_{i'}(\rho) = 0, \quad (34)$$

where  $Z_{i'}^{(2)} = \varepsilon_{i'}^{(2)}$ .

**Step 2.** At this step, we compute the coefficients  $\phi_{i'}(\rho)$  and  $\psi_{i'}(\rho)$  of the expansion (33) in the form of truncated expansion in inverse powers of  $\rho$

$$(\phi_{ji'}^{(k' < 0)} = \psi_{ji'}^{(k' < 0)} = 0):$$

$$\phi_{ji'}(\rho) = \phi_{ji'}^{(0)} + \sum_{k'=1}^{k_{\max}} \frac{\phi_{ji'}^{(k')}}{\rho^{k'}}, \quad \psi_{ji'}(\rho) = \psi_{ji'}^{(0)} + \sum_{k'=1}^{k_{\max}} \frac{\psi_{ji'}^{(k')}}{\rho^{k'}}. \quad (35)$$

After the substitution of Eqs.(33)–(35) into Eq. (32) with the use of Eq.(34), we arrive at the set of recurrence relations at  $k' \leq k_{\max}$ :

$$\begin{aligned} & \left( \varepsilon_i^{(0)} - 2E + p_{i'}^2 \right) \phi_{ii'}^{(k')} - 2p_{i'}^2(k' - 1) \psi_{ii'}^{(k'-1)} = -f_{ii'}^{(k')}, \\ & \left( \varepsilon_i^{(0)} - 2E + p_{i'}^2 \right) \psi_{ii'}^{(k')} + 2(k' - 1) \phi_{ii'}^{(k'-1)} = -g_{ii'}^{(k')}, \end{aligned} \quad (36)$$

where the right-hand sides  $f_{ii'}^{(k)}$  and  $g_{ii'}^{(k)}$  are defined by the relations

$$\begin{aligned}
 f_{ii'}^{(k')} &= -(k' - 2)^2 - Z_{i'}^{(2)} \phi_{ii'}^{(k'-2)} + \sum_{k=2}^{k'} \mathcal{H}_{ii}^{(k)} \phi_{ii'}^{(k'-k)} \\
 &+ Z_{i'}^{(2)} (2k' - 4) \psi_{ii'}^{(k'-3)} + \sum_{k=1}^{k'} \sum_{j=1, j \neq i}^N \left( 2Q_{ij}^{(k)} Z_{i'}^{(2)} \psi_{ji'}^{(k'-k-2)} \right. \\
 &\left. - 2p_{i'}^2 Q_{ij}^{(k)} \psi_{ji'}^{(k'-k)} + Q_{ij}^{(k)} (-2k' + k + 3) \phi_{ji'}^{(k'-k-1)} + \mathcal{H}_{ij}^{(k)} \phi_{ji'}^{(k'-k)} \right); \\
 g_{ii'}^{(k)} &= -(k' - 1)^2 - Z_{i'}^{(2)} \psi_{ii'}^{(k'-2)} + \sum_{k=2}^{k'} \mathcal{H}_{ii}^{(k)} \psi_{ii'}^{(k'-k)} \\
 &+ \sum_{j=1, j \neq i}^N \sum_{k=1}^{k'} \left( 2Q_{ij}^{(k)} \phi_{ji'}^{(k'-k)} - Q_{ij}^{(k)} (2k' - 1 - k) \psi_{ji'}^{(k'-k-1)} + \mathcal{H}_{ij}^{(k)} \psi_{ji'}^{(k'-k)} \right)
 \end{aligned} \tag{37}$$

with the initial conditions  $p_{i'}^2 = 2E - \varepsilon_{i'}^{(0)}$ ,  $\phi_{ii'}^{(0)} = \delta_{ii'}$ ,  $\psi_{ii'}^{(0)} = 0$ .

**Step 3.** Here we calculate the coefficients  $\phi_{ii'}^{(k')}$  and  $\psi_{ii'}^{(k')}$  using the step-by-step procedure of solving Eqs. (36) for  $2E \neq \varepsilon_{i'}^{(0)}$ ,  $i \neq i'$  and  $k' = 2, \dots, k_{\max}$ :

$$\begin{aligned}
 \phi_{ii'}^{(k')} &= \left[ \varepsilon_i^{(0)} - \varepsilon_{i'}^{(0)} \right]^{-1} \left[ -f_{ii'}^{(k')} + 2p_{i'}^2 (k' - 1) \psi_{ii'}^{(k'-1)} \right], \\
 \psi_{ii'}^{(k')} &= \left[ \varepsilon_i^{(0)} - \varepsilon_{i'}^{(0)} \right]^{-1} \left[ -g_{ii'}^{(k')} - 2(k' - 1) \phi_{ii'}^{(k'-1)} \right], \\
 \phi_{i'i'}^{(k'-1)} &= -[2(k' - 1)]^{-1} g_{i'i'}^{(k)}, \\
 \psi_{i'i'}^{(k'-1)} &= \left[ 2(k' - 1) (2E - \varepsilon_{i'}^{(0)}) \right]^{-1} f_{i'i'}^{(k)}.
 \end{aligned} \tag{38}$$

The above described algorithm was implemented in MAPLE and FORTRAN to calculate the desired  $\phi_{ii'}^{(k')}$  and  $\psi_{ii'}^{(k')}$  in the **output** up to needed order of  $k_{\max}$ .

The choice of appropriate values  $\rho_{\min}$  and  $\rho_{\max}$  for the constructed expansions of the linearly independent solutions for  $p_{i_o} > 0$  is controlled by the fulfilment of the Wronskian condition to the prescribed precision  $\varepsilon_{W\tau}$ :

$$\begin{aligned}
 Wr(\mathbf{Q}(\rho); \chi^*(\rho), \chi(\rho)) &= \frac{2n}{\pi} \mathbf{I}_{oo}, \\
 W(\mathbf{Q}, \chi^*, \chi) &\equiv \rho \left( \chi^{*T} \left( \frac{d\chi}{d\rho} - \mathbf{Q}\chi \right) - \chi^T \left( \frac{d\chi^*}{d\rho} - \mathbf{Q}\chi^* \right) \right).
 \end{aligned} \tag{39}$$

## 5 Analysis of Quantum Tunneling Problem

The solutions of the BVPs (8)–(15) and (24)–(27) were performed on the finite-element grids  $\Omega_y = \{-12(N_{elem} = 120)12\}$  and  $\Omega_\rho = \{0(N_{elem} = 1200)120\}$ , respectively, with  $N_{elem}$  fourth-order Lagrange elements  $p = 4$  between the

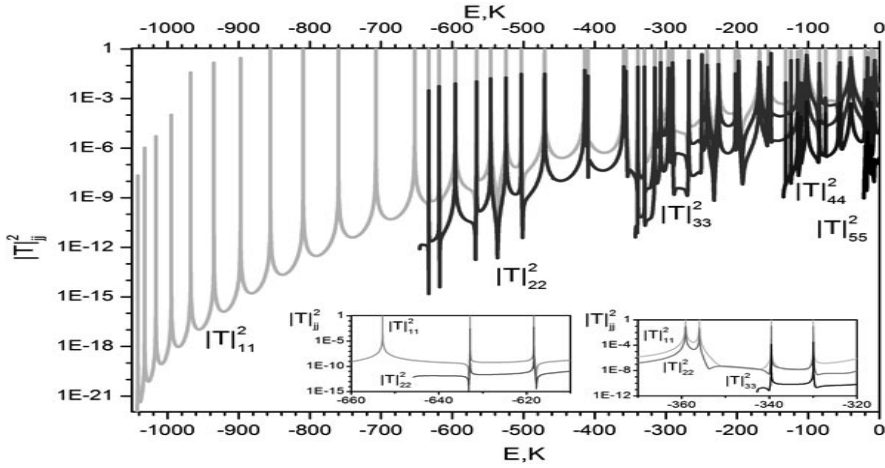


**Fig. 9.** The total probability of penetration from the first channels with the energies  $E_1 = -1044.879649$ ,  $E_2 = -646.1570935$ ,  $E_3 = -342.7919791$ ,  $E_4 = -134.7843058$ ,  $E_5 = -22.13407384$  (in K) to all five open channels simulated by the Galerkin and Kantorovich expansions

nodes using the program KANTBP 3.0. The expansion of the desirable solution (5) over such orthogonal basis at ( $j_{max} = 15$ ) with only ten closed channels taken into account allows the calculation of approximate solutions of the original 2D problem (1) at  $E < 0$  with the required accuracy. Fig. 9 shows the resonance behavior of the total penetration probability with the transition from the first channels having the energies  $E_1 = -1044.879649$ ,  $E_2 = -646.1570935$ ,  $E_3 = -342.7919791$ ,  $E_4 = -134.7843058$ ,  $E_5 = -22.13407384$  (in K) to all five open channels, simulated using the Galerkin expansion (5) as well as the Katorovich one (18). The total transmission probability is seen to demonstrate the resonance behavior, i.e., effect of quantum transparency. Some peaks are high and narrow, and the positions of peaks corresponding to transitions from different bound states are similar.

As the energy of the initial excited state increases, the transmission peaks demonstrate a shift towards higher energies, the set of peak positions keeping approximately the same as for the transitions from the ground state and the peaks just replacing each other. For example, the left epure shows that the positions of the 13th and 14th peaks for transitions from the first state coincide with the positions of the 1st and 2nd peaks for the transitions from the second state, while the right epure shows that the positions of the 25th and 26th peaks for transitions from the first state coincide with the positions of the 13th and 14th peaks for transitions from the second state and with the positions of the 1st and 2nd peaks for the transitions from the third state.

As one can see from Fig. 2, the diagonal matrix elements of the potential  $V_{jj}^b(y)$  have the shapes of double barriers, and the nondiagonal matrix elements

$V_{ij}^b(y)$  are by more than four times smaller than  $V_{jj}^b(\rho)$  and  $V_{ij}^b(\rho)$  in Figs. 5 and 8. It means that the position of peaks corresponds to the real part of energy of the metastable states embedded in the continuum, which are mainly localized between double barriers.

## 6 Conclusions

We have demonstrated efficiency of symbolic-numeric algorithms for solving the boundary-value problems that describe the quantum tunneling of diatomic low-dimensional model systems, coupled via realistic molecular potentials, through repulsive barriers below a dissociation threshold. We presented a comparative analysis of the potential matrix elements and solutions with different asymptotic behavior calculated in the Cartesian and polar coordinates. The necessity for two statements of the problem follows from the important practical applications of further self-consistent study of the system above the dissociation threshold, which is convenient in polar coordinates. The effect of quantum transparency in resonance tunneling of diatomic molecules through repulsive potential barriers was revealed that produced by metastable states imbedded in continuum. The proposed models and elaborated symbolic-numerical algorithms, the quantum transparency effect itself, and the developed software can find further applications in barrier heavy-ion reactions and molecular quantum diffusion. The authors thank Prof. F.M. Penkov for collaboration. The work was supported partially by grants RFBR 14-01-00420 and 13-01-00668 and 0602/GF MES RK.

## References

1. Bondar, D.I., Liu, W.-K., Ivanov, M.Y.: Enhancement and suppression of tunneling by controlling symmetries of a potential barrier. *Phys. Rev. A* 82, 052112–1–9 (2010)
2. Chuluunbaatar, O., Gusev, A.A., Derbov, V.L., Kaschiev, M.S., Melnikov, L.A., Serov, V.V., Vinitsky, S.I.: Calculation of a hydrogen atom photoionization in a strong magnetic field by using the angular oblate spheroidal functions. *J. Phys. A* 40, 11485–11524 (2007)
3. Chuluunbaatar, O., Gusev, A.A., Vinitsky, S.I., Abrashkevich, A.G.: KANTBP 2.0: New version of a program for computing energy levels, reaction matrix and radial wave functions in the coupled-channel hyperspherical adiabatic approach. *Comput. Phys. Commun.* 179, 685–693 (2008)
4. Chuluunbaatar, O., Gusev, A.A., Vinitsky, S.I., Abrashkevich, A.G.: ODPEVP: A program for computing eigenvalues and eigenfunctions and their first derivatives with respect to the parameter of the parametric self-adjointed Sturm-Liouville problem. *Comput. Phys. Commun.* 180, 1358–1375 (2009)
5. Fundamental Physical Constants, <http://physics.nist.gov/constants>
6. Gusev, A.A., Vinitsky, S.I., Chuluunbaatar, O., Gerdt, V.P., Rostovtsev, V.A.: Symbolic-numerical algorithms to solve the quantum tunneling problem for a coupled pair of ions. In: Gerdt, V.P., Koepf, W., Mayr, E.W., Vorozhtsov, E.V. (eds.) CASC 2011. LNCS, vol. 6885, pp. 175–191. Springer, Heidelberg (2011)

7. Vinitsky, S., Gusev, A., Chuluunbaatar, O., Rostovtsev, V., Le Hai, L., Derbov, V., Krassovitskiy, P.: Symbolic-numerical algorithm for generating cluster eigenfunctions: tunneling of clusters through repulsive barriers. In: Gerdt, V.P., Koepf, W., Mayr, E.W., Vorozhtsov, E.V. (eds.) *CASC 2013. LNCS*, vol. 8136, pp. 427–442. Springer, Heidelberg (2013)
8. Kavka, J.J., Shegelski, M.R.A., Hong, W.P.: Tunneling and reflection of an exciton incident upon a quantum heterostructure barrier. *J. Phys.: Condens. Matter.* 24, 365802–1–13 (2012)
9. Lauhon, L.J., Ho, W.: Direct observation of the quantum tunneling of single hydrogen atoms with a scanning tunneling microscope. *Phys. Rev. Lett.* 85, 4566–4569 (2000)
10. Pen'kov, F.M.: Metastable states of a coupled pair on a repulsive barrier. *Phys. Rev. A* 62, 044701–1–4 (2000)
11. Pen'kov, F.M.: Quantum transmittance of barriers for composite particles. *JETP* 91, 698–705 (2000)
12. Pijper, E., Fasolino, A.: Quantum surface diffusion of vibrationally excited molecular dimers. *J. Chem. Phys.* 126, 014708–1–10 (2007)
13. Shegelski, M.R.A., Hnybida, J., Vogt, R.: Formation of a molecule by atoms incident upon an external potential. *Phys. Rev. A.* 78, 062703–1–5 (2007)



# Symbolic-Numeric Algorithms for Computer Analysis of Spheroidal Quantum Dot Models

A.A. Gusev<sup>1,2</sup>, O. Chuluunbaatar<sup>1</sup>, V.P. Gerdt<sup>1</sup>, V.A. Rostovtsev<sup>1,2</sup>,  
S.I. Vinitsky<sup>1</sup>, V.L. Derbov<sup>3</sup>, V.V. Serov<sup>3</sup>

<sup>1</sup> Joint Institute for Nuclear Research, Dubna, Russia

<sup>2</sup> Dubna International University of Nature, Society & Man, Dubna, Russia

<sup>3</sup> Saratov State University, Saratov, Russia

gooseff@jinr.ru

**Abstract.** A computational scheme for solving elliptic boundary value problems with axially symmetric confining potentials using different sets of one-parameter basis functions is presented. The efficiency of the proposed symbolic-numerical algorithms implemented in Maple is shown by examples of spheroidal quantum dot models, for which energy spectra and eigenfunctions versus the spheroid aspect ratio were calculated within the conventional effective mass approximation. Critical values of the aspect ratio, at which the discrete spectrum of models with finite-wall potentials is transformed into a continuous one in strong dimensional quantization regime, were revealed using the exact and adiabatic classifications.

## 1 Introduction

To analyze the geometrical, spectral and optical characteristics of quantum dots in the effective mass approximation and in the regime of strong dimensional quantization following [1], many methods and models were used, including the exactly solvable model of a spherical impermeable well [2], the adiabatic approximation for a lens-shaped well confined to a narrow wetting layer [3] and a hemispherical impermeable well [4], the model of strongly oblate or prolate ellipsoidal impermeable well [5], as well as numerical solutions of the boundary value problems (BVPs) with separable variables in the spheroidal coordinates for wells with infinite and finite wall heights [6,7,8]. However, thorough comparative analysis of spectral characteristics of models with different potentials, including those with non-separable variables, remains to be a challenging problem. This situation stimulates the study of a wider class of model well potentials with application of symbolic-numerical algorithms (SNA) and problem-oriented software developed by the authors of the present paper during years [9,10,11,12,13,14].

Here we analyse the spectral characteristics of the following models: a spherical quantum dot (SQD), an oblate spheroidal quantum dot (OSQD), and a prolate spheroidal quantum dot (PSQD). We make use of the Kantorovich method that reduces the problem to a set of ordinary differential equations (ODE) [15]. In contrast to the well-known method of adiabatic representation [16], this method



implies neither adiabatic separation of fast and slow variables nor the presence of a small parameter. We present a calculation scheme for solving elliptical BVPs with axially-symmetric potentials in cylindrical coordinates (CC), spherical coordinates (SC), oblate spheroidal coordinates (OSC), and prolate spheroidal coordinates (PSC). Basing on the SNA developed for axially-symmetric potentials, different sets of solutions are constructed for the parametric BVPs related to the fast subsystem, namely, the eigenvalue problem solutions (the terms and the basis functions), depending upon the slow variable as a parameter, as well as the matrix elements, i.e., the integrals of the products of basis functions and their derivatives with respect to the parameter, which are calculated analytically by means of elaborated SNA MATRA implemented in MAPLE, or numerically using the program ODPEVP [13] implementing the finite-element method (FEM). These terms and matrix elements form the matrices of variable coefficients in the set of second-order ODE with respect to the slow variable. The BVP for this set of ODEs is solved by means of the program KANTBP [11], also implementing the FEM. The efficiency of the calculation scheme and the SNA used is demonstrated by comparison of the spectra versus the ellipticity of the prolate or oblate spheroid in the models of quantum dots with different confining potentials, such as the isotropic and anisotropic harmonic oscillator, the spherical and spheroidal well with finite or infinite walls approximated by smooth short-range potentials as well as by constructing the adiabatic classification of the states.

The paper is organized as follows. In Section 2, the calculation scheme for solving elliptic BVPs with axially-symmetric confining potentials is presented. In Section 3, SNA MATRA for solving parametric BVP and corresponding integrals implemented in Maple is described. Section 4 is devoted to the analysis of the spectra of quantum dot models with three types of axially-symmetric potentials, including the benchmark exactly solvable models. In Conclusion we summarize the results and discuss the future applications of our calculation scheme and the SNA project presented.

## 2 Problem Statement

Within the effective mass approximation under the conditions of strong dimensional quantization, the Schrödinger equation for the slow envelope of the wave function  $\tilde{\Psi}(\tilde{\mathbf{r}})$  of a charge carrier (electron  $e$  or hole  $h$ ) in the models of a spherical, prolate or oblate spheroidal quantum dot (SQD, PSQD or OSQD) has the form

$$\{\tilde{H} - \tilde{E}\}\tilde{\Psi}(\tilde{\mathbf{r}}) = \{(2\mu_p)^{-1}\tilde{\mathbf{P}}^2 + \tilde{U}(\tilde{\mathbf{r}}) - \tilde{E}\}\tilde{\Psi}(\tilde{\mathbf{r}}) = 0, \quad (1)$$

where  $\tilde{\mathbf{r}} \in \mathbf{R}^3$  is the position vector of the particle having the effective mass  $\mu_p = \mu_e$  (or  $\mu_p = \mu_h$ ),  $\tilde{\mathbf{P}} = -i\hbar\nabla_{\tilde{\mathbf{r}}}$  is the momentum operator,  $\tilde{E}$  is the energy of the particle,  $\tilde{U}(\tilde{\mathbf{r}})$  is the axially-symmetric potential confining the particle motion in SQD, PSQD or OSQD. In Model A,  $\tilde{U}(\tilde{\mathbf{r}})$  is chosen to be the potential of an

isotropic or anisotropic axially-symmetric harmonic oscillator with the angular frequency  $\tilde{\omega} = \gamma_{\tilde{r}_0} \hbar / (\mu_p \tilde{r}_0^2)$ ,  $\gamma_{\tilde{r}_0} \sim \pi^2/3$  being an adjustable parameter:

$$\tilde{U}^L(\tilde{\mathbf{r}}) = \mu_p \tilde{\omega}^2 (\zeta_1 (\tilde{x}^2 + \tilde{y}^2) + \zeta_3 \tilde{z}^2) / 2, \quad (2)$$

$r_0 = \sqrt{\zeta_1 (\tilde{x}_0^2 + \tilde{y}_0^2) + \zeta_3 \tilde{z}_0^2}$  is the radius of a spherical QD ( $\zeta_1 = 1, \zeta_3 = 1$ ) or that of a spheroidal QD ( $\zeta_1 = (\tilde{r}_0/\tilde{a})^4, \zeta_3 = (\tilde{r}_0/\tilde{c})^4$ ), inscribed into a spherical one, where  $\tilde{a}$  and  $\tilde{c}$  are the semiaxes of the ellipse which transforms into a sphere at  $\tilde{a} = \tilde{c} = \tilde{r}_0$ . For Model B,  $\tilde{U}(\tilde{\mathbf{r}})$  is the potential of a spherical or axially-symmetric well

$$\tilde{U}^B(\tilde{\mathbf{r}}) = \{0, 0 \leq (\tilde{x}^2 + \tilde{y}^2)/\tilde{a}^2 + \tilde{z}^2/\tilde{c}^2 < 1; \tilde{U}_0, (\tilde{x}^2 + \tilde{y}^2)/\tilde{a}^2 + \tilde{z}^2/\tilde{c}^2 \geq 1\}, \quad (3)$$

with walls of finite or infinite height  $1 \ll \tilde{U}_0 < \infty$ . For Model C,  $\tilde{U}(\tilde{\mathbf{r}})$  is taken to be a spherical or axially-symmetric diffuse potential

$$\tilde{U}^C(\tilde{\mathbf{r}}) = \tilde{U}_0 [1 + \exp(((\tilde{x}^2 + \tilde{y}^2)/\tilde{a}^2 + \tilde{z}^2/\tilde{c}^2 - 1)/s)]^{-1}, \quad (4)$$

where  $s$  is the edge diffusiveness parameter of the function smoothly approximating the vertical walls of finite height  $\tilde{U}_0$ . Below we restrict ourselves by considering Model B with infinite walls  $\tilde{U}_0 \rightarrow \infty$  and Model C with walls of finite height  $\tilde{U}_0$ . We make use of the reduced atomic units:  $a_B^* = \kappa \hbar^2 / \mu_p e^2$  is the reduced Bohr radius,  $\kappa$  is the DC permittivity,  $E_R \equiv Ry^* = \hbar^2 / (2\mu_p a_B^{*2})$  is the reduced Rydberg unit of energy, and the following dimensionless quantities are introduced:  $\tilde{\Psi}(\tilde{\mathbf{r}}) = a_B^{*-3/2} \Psi(\mathbf{r})$ ,  $2\hat{H} = \hat{H}/Ry^*$ ,  $2E = \tilde{E}/Ry^*$ ,  $2U(\mathbf{r}) = \tilde{U}(\tilde{\mathbf{r}})/Ry^*$ ,  $\mathbf{r} = \tilde{\mathbf{r}}/a_B^*$ ,  $a = \tilde{a}/a_B^*$ ,  $\tilde{c} = c/a_B^*$ ,  $r_0 = \tilde{r}_0/a_B^*$ ,  $\omega = \gamma_{r_0}/r_0^2 = \hbar\tilde{\omega}/(2Ry^*)$ . For an electron with the reduced mass  $\mu_p \equiv \mu_e = 0.067m_0$  at  $\kappa = 13.18$  in GaAs:  $a_B^* = 102\text{\AA} = 10.2 \text{ nm}$ ,  $Ry^* = E_R = 5.2 \text{ meV}$ .

Since the Hamiltonian  $\hat{H}$  in (1)–(4) commutes with the  $z$ -parity operator ( $z \rightarrow -z$  or  $\eta \rightarrow -\eta$ ), the solutions are divided into even ( $\sigma = +1$ ) and odd ( $\sigma = -1$ ) ones. The solution of Eq. (1), periodical with respect to the azimuthal angle  $\varphi$ , is sought in the form of a product  $\Psi(x_f, x_s, \varphi) = \Psi^{m\sigma}(x_f, x_s) e^{im\varphi} / \sqrt{2\pi}$ , where  $m = 0, \pm 1, \pm 2, \dots$  is the magnetic quantum number. Then the function  $\Psi^{m\sigma}(x_f, x_s)$  satisfies the following equation in the two-dimensional domain  $\Omega = \Omega_{x_f}(x_s) \cup \Omega_{x_s} \subset \mathbf{R}^2 \setminus \{0\}$ ,  $\Omega_{x_f}(x_s) = (x_f^{\min}(x_s), x_f^{\max}(x_s))$ ,  $\Omega_{x_s} = (x_s^{\min}, x_s^{\max})$ :

$$\left( \hat{H}_1(x_f; x_s) + \hat{H}_2(x_s) + V(x_f, x_s) - 2E \right) \Psi^{m\sigma}(x_f, x_s) = 0. \quad (5)$$

The Hamiltonian of the slow subsystem  $\hat{H}_2(x_s)$  is expressed as

$$\hat{H}_2(x_s) = \check{H}_2(x_s) = -\frac{1}{g_{1s}(x_s)} \frac{\partial}{\partial x_s} g_{2s}(x_s) \frac{\partial}{\partial x_s} + \check{V}_s(x_s), \quad (6)$$

and the Hamiltonian of the fast subsystem  $\hat{H}_1(x_f; x_s)$  is expressed via the reduced Hamiltonian  $\check{H}_f(x_f; x_s)$  and the weighting factor  $g_{3s}(x_s)$ :

$$\begin{aligned} \hat{H}_1(x_f; x_s) &= g_{3s}^{-1}(x_s) \check{H}_f(x_f; x_s), \\ \check{H}_f(x_f; x_s) &= -\frac{1}{g_{1f}(x_f)} \frac{\partial}{\partial x_f} g_{2f}(x_f) \frac{\partial}{\partial x_f} + \check{V}_f(x_f) + \check{V}_{fs}(x_f, x_s). \end{aligned} \quad (7)$$

**Table 1.** The values of conditionally fast  $x_f$  and slow  $x_s$  independent variables, the coefficients  $g_{is}(x_s)$ ,  $g_{jf}(x_f)$ , and the potentials  $\tilde{V}_f(x_f)$ ,  $\tilde{V}_s(x_s)$ ,  $\tilde{V}_{fs}(x_f, x_s)$ , in Eqs.(5)–(7) for SQD, OSQD and PSQD in cylindrical (CC), spherical (SC), and oblate & prolate spheroidal (OSC & PSC) coordinates with  $(d/2)^2 = \pm(a^2 - c^2)$ , + for OSC, – for PSC.

	CC		SC	OSC & PSC
	OSQD	PSQD	SQD	OSQD & PSQD
$x_f$	$z$	$\rho$	$\eta$	$\eta$
$x_s$	$\rho$	$z$	$r$	$\xi$
$g_{1f}$	1	$\rho$	1	1
$g_{2f}$	1	$\rho$	$1 - \eta^2$	$1 - \eta^2$
$g_{1s}$	$\rho$	1	$r^2$	1
$g_{2s}$	$\rho$	1	$r^2$	$\xi^2 \pm 1$
$g_{3s}$	1	1	$r^2$	1
$\tilde{V}_f(x_f)$	$\omega^2 \zeta_3 z^2$	$m^2/\rho^2 + \omega^2 \zeta_1 \rho^2$	$m^2/g_{2f}$	$m^2/g_{2f} \pm (d/2)^2 g_{2f} 2E$
$\tilde{V}_s(x_s)$	$m^2/\rho^2 + \omega^2 \zeta_1 \rho^2$	$\omega^2 \zeta_3 z^2$	0	$\mp m^2/g_{2s} - ((d/2)^2 g_{2s} - 1) 2E$
$\tilde{V}_{fs}(x_f, x_s)$	0	0	$\tilde{V}(r, \eta)$	$V(\xi, \eta)$

Table 1 contains the values of conditionally fast  $x_f$  and slow  $x_s$  independent variables, the coefficients  $g_{1s}(x_s)$ ,  $g_{2s}(x_s)$ ,  $g_{3s}(x_s)$ ,  $g_{1f}(x_f)$ ,  $g_{2f}(x_f)$ , and the reduced potentials  $\tilde{V}_f(x_f)$ ,  $\tilde{V}_s(x_s)$ ,  $\tilde{V}_{fs}(x_f, x_s)$ , entering Eqs. (5)–(7) for SQD, OSQD, and PSQD in cylindrical ( $\mathbf{x} = (z, \rho, \varphi)$ ), spherical ( $\mathbf{x} = (r, \eta = \cos \theta, \varphi)$ ), and oblate/prolate spheroidal ( $\mathbf{x} = (\xi, \eta, \varphi)$ ) coordinates [17]. In spherical coordinates, the potential  $\tilde{V}(r, \eta)$  in Table 1 using the definitions (2), (4) in the reduced atomic units, for Model A is expressed as

$$\tilde{V}(r, \eta) = 2r^2 V(r, \eta) = \omega^2 r^4 (\zeta_1 (1 - \eta^2) + \zeta_3 \eta^2),$$

and for Model C as

$$\tilde{V}(r, \eta) = 2r^2 V(r, \eta) = 2r^2 U_0 [1 + \exp((r^2((1 - \eta^2)/a^2 + \zeta_3 \eta^2/c^2) - 1)/s)]^{-1},$$

both having zero first derivatives in the vicinity of the origin  $r = 0$  (equilibrium point). For Model B. the potentials  $\tilde{V}_{fs}$  are zero, since the potential (3) is reformulated below in the form of boundary conditions with respect to the variables  $x_f$  and  $x_s$ . The solution  $\Psi_i^{m\sigma}(x_f, x_s) \equiv \Psi_i^{Em\sigma}(x_f, x_s)$  of the problem (5)–(7) is sought in the form of Kantorovich expansion [15]

$$\Psi_i^{Em\sigma}(x_f, x_s) = \sum_{j=1}^{j_{\max}} \Phi_j^{m\sigma}(x_f; x_s) \chi_j^{(m\sigma i)}(E, x_s), \quad (8)$$

using as a set of trial functions the eigenfunctions  $\Phi_j^{m\sigma}(x_f; x_s)$  of the Hamiltonian  $\tilde{H}_f(x_f; x_s)$  from (7), i.e., the solutions of the parametric BVP

$$\{\tilde{H}_f(x_f; x_s) - \tilde{\lambda}_i(x_s)\} \Phi_i^{m\sigma}(x_f; x_s) = 0, \quad (9)$$

in the interval  $x_f \in \Omega_{x_f}(x_s)$  depending on the conditionally slow variable  $x_s \in \Omega_{x_s}$  as on a parameter. These solutions obey the boundary conditions

$$\lim_{x_f \rightarrow x_f^t(x_s)} \left( N_f^{(m\sigma)}(x_s) g_{2f}(x_f) \frac{d\Phi_j^{m\sigma}(x_f; x_s)}{dx_f} + D_f^{(m\sigma)}(x_s) \Phi_j^{m\sigma}(x_f; x_s) \right) = 0 \quad (10)$$

at the boundary points  $\{x_f^{\min}(x_s), x_f^{\max}(x_s)\} = \partial\Omega_{x_f}(x_s)$ , of the interval  $\Omega_{x_f}(x_s)$ . In Eq. (10),  $N_f^{(m\sigma)}(x_s) \equiv N_f^{(m\sigma)}$ ,  $D_f^{(m\sigma)}(x_s) \equiv D_f^{(m\sigma)}$ , unless specially declared, are determined by the relations  $N_f^{(m\sigma)} = 1$ ,  $D_f^{(m\sigma)} = 0$  at  $m = 0$ ,  $\sigma = +1$  (or at  $\sigma = 0$ , i.e., without parity separation),  $N_f^{(m\sigma)} = 0$ ,  $D_f^{(m\sigma)} = 1$  at  $m = 0$ ,  $\sigma = -1$  or at  $m \neq 0$ . The eigenfunctions satisfy the orthonormality condition with the weighting function  $g_{1f}(x_f)$  in the same interval  $x_f \in \Omega_{x_f}(x_s)$ :

$$\langle \Phi_i^{m\sigma} | \Phi_j^{m\sigma} \rangle = \int_{x_f^{\min}(x_s)}^{x_f^{\max}(x_s)} \Phi_i^{m\sigma}(x_f; x_s) \Phi_j^{m\sigma}(x_f; x_s) g_{1f}(x_f) dx_f = \delta_{ij}. \quad (11)$$

Here  $\tilde{\lambda}_1(x_s) < \dots < \tilde{\lambda}_{j_{\max}}(x_s) < \dots$  is the desired set of real eigenvalues. The corresponding set of potential curves  $2E_1(x_s) < \dots < 2E_{j_{\max}}(x_s) < \dots$  of Eqs. (7) is determined by  $2E_j(x_s) = g_{3s}^{-1}(x_s) \tilde{\lambda}_j(x_s)$ . Note that for OSC and PSC, the desired set of real eigenvalues  $\tilde{\lambda}_j(x_s)$  depends on a combined parameter,  $x_s \rightarrow p^2 = (d/2)^2 2E$ , the product of spectral  $2E$  and geometrical  $(d/2)^2$  parameters of the problem (5). The solutions of the problem (9)–(11) for Models A and B are calculated in the analytical form, while for Model C this is done using the program ODPEVP [13].

Substituting the expansion (8) into Eq. (5) in consideration of (9) and (11), we get a set of ODEs for the slow subsystem with respect to the unknown vector functions  $\chi^{(m\sigma i)}(x_s, E) \equiv \chi^{(i)}(x_s) = (\chi_1^{(i)}(x_s), \dots, \chi_{j_{\max}}^{(i)}(x_s))^T$ :

$$\begin{aligned} & \left( -\frac{1}{g_{1s}(x_s)} \mathbf{I} \frac{d}{dx_s} g_{2s}(x_s) \frac{d}{dx_s} + 2\mathbf{E}(x_s) + \mathbf{I} \tilde{V}_s(x_s) - 2\mathbf{I}E \right) \chi^{(i)}(x_s) = \\ & = - \left( \frac{g_{2s}(x_s)}{g_{1s}(x_s)} \mathbf{W}(x_s) + \frac{1}{g_{1s}(x_s)} \frac{dg_{2s}(x_s)}{dx_s} \mathbf{Q}(x_s) + \frac{g_{2s}(x_s)}{g_{1s}(x_s)} \mathbf{Q}(x_s) \frac{d}{dx_s} \right) \chi^{(i)}(x_s). \end{aligned} \quad (12)$$

Here  $2\mathbf{E}(x_s) = \text{diag}(g_{3s}^{-1}(x_s) \tilde{\lambda}_j(x_s))$ ,  $\mathbf{W}(x_s)$ , and  $\mathbf{Q}(x_s)$  are matrices of the dimension  $j_{\max} \times j_{\max}$ ,

$$\begin{aligned} W_{ij}(x_s) &= W_{ji}(x_s) = \int_{x_f^{\min}(x_s)}^{x_f^{\max}(x_s)} g_{1f}(x_f) \frac{\partial \Phi_i(x_f; x_s)}{\partial x_s} \frac{\partial \Phi_j(x_f; x_s)}{\partial x_s} dx_f, \\ Q_{ij}(x_s) &= -Q_{ji}(x_s) = - \int_{x_f^{\min}(x_s)}^{x_f^{\max}(x_s)} g_{1f}(x_f) \Phi_i(x_f; x_s) \frac{\partial \Phi_j(x_f; x_s)}{\partial x_s} dx_f, \end{aligned} \quad (13)$$

calculated analytically for Model B and by means of the program ODPEVP [13] for Model C. Note that for Model A in SC or CC and Model B in OSC or PSC, the variables  $x_f$  and  $x_s$  are separated so that the matrix elements  $W_{ij}(x_s) = Q_{ij}(x_s) \equiv 0$  are put into the r.h.s. of Eq. (12), and  $\tilde{V}_s(x_s)$  are substituted from Table 1. The discrete spectrum solutions  $2E : 2E_1 < 2E_2 < \dots < 2E_t < \dots$  that obey the boundary conditions at points  $x_s^t = \{x_s^{\min}, x_s^{\max}\} = \partial\Omega_{x_s}$  bounding the interval  $\Omega_{x_s}$ :

$$\lim_{x_s \rightarrow x_s^t} \left( N_s^{(m\sigma)} g_{2s}(x_s) \frac{d\chi^{(m\sigma p)}(x_s)}{dx_s} + D_s^{(m\sigma)} \chi^{(m\sigma p)}(x_s) \right) = 0, \quad (14)$$

where  $N_s^{(m\sigma)} = 1$ ,  $D_s^{(m\sigma)} = 0$  at  $m = 0, \sigma = +1$  (or at  $\sigma = 0$ , i.e. without parity separation),  $N_s^{(m\sigma)} = 0$ ,  $D_s^{(m\sigma)} = 1$  at  $m = 0, \sigma = -1$  or at  $m \neq 0$ , and the orthonormality conditions

$$\int_{x_s^{\min}}^{x_s^{\max}} (\chi^{(i)}(x_s))^T \chi^{(j)}(x_s) g_{1s}(x_s) dx_s = \delta_{ij}, \quad (15)$$

are calculated by means of the program KANTBP [11]. To ensure the prescribed accuracy of calculation of the lower part of the spectrum discussed below with eight significant digits we used  $j_{\max} = 16$  basis functions in the expansion (8) and the discrete approximation of the desired solution by Lagrange finite elements of the fourth order with respect to the grid pitch  $\Omega_{h^s(x_s)}^p = [x_{\min}^s, x_k^s = x_{k-1}^s + h_k^s, x_{\max}^s]$ .

### 3 SNA MATRA for Calculation of the BVP and Integrals

To calculate the effective potentials of the problem (12)–(15) for each value  $x_s = x_k^s$  of the FEM grid  $\Omega_{h^s(x_s)}^p = [x_{\min}^s, x_{\max}^s]$  we consider a discrete representation of solutions  $\Phi(x_f; x_s) \equiv \Phi^{m\sigma}(x_f; x_s)$  of the problem (9) by means of the FEM on the grid,  $\Omega_{h^f(x_f)}^p(x_s) = [x_0^f = x_{\min}^f(x_s), x_k^f = x_{k-1}^f + h_k^f, x_{\bar{n}}^f = x_{\max}^f(x_s)]$ , in a finite sum:

$$\Phi(x_f; x_s) = \sum_{\mu=0}^{\bar{n}p} \Phi_{\mu}^h(x_s) N_{\mu}^p(x_f) = \sum_{k=1}^{\bar{n}} \sum_{r=0}^p \Phi_{r+p(k-1)}^h(x_s) N_{r+p(k-1)}^p(x_f), \quad (16)$$

where  $N_{\mu}^p(x_f)$  are local functions, and  $\Phi_{\mu}^h(x_s)$  are node values of  $\Phi(x_{\mu}^f; x_s)$ . The local functions  $N_{\mu}^p(x_f)$  are piece-wise polynomials of the given order,  $p$  equals one only in the node  $x_{\mu}^f$  and equals zero in all other nodes  $x_{\nu}^f \neq x_{\mu}^f$  of the grid  $\Omega_{h^f(x_f)}^p(x_s)$ , i.e.,  $N_{\nu}^p(x_{\mu}^f) = \delta_{\nu\mu}$ ,  $\mu, \nu = 0, 1, \dots, \bar{n}p$ . The coefficients  $\Phi_{\nu}(x_s)$  are formally connected with the solution  $\Phi(x_{k,r}^{fp}; x_s)$  in a node  $x_{\nu}^f = x_{k,r}^{fp}$ ,  $k = 1, \dots, \bar{n}$ ,  $r = 0, \dots, p$ :

$$\Phi_{\nu}^h(x_s) = \Phi_{r+p(k-1)}^h(x_s) \approx \Phi(x_{k,r}^{fp}; x_s), \quad x_{k,r}^{fp} = x_{k-1}^f + \frac{h_k^f}{p} r.$$

The theoretical estimate for the  $\mathbf{H}^0$  norm between the exact and numerical solution has the order of

$$|\check{\lambda}_j(x_s) - \check{\lambda}_j^h(x_s)| \leq c_1 h^{2p}, \quad \left\| \Phi_j(x_f; x_s) - \Phi_j^h(x_s) \right\|_0 \leq c_2 h^{p+1}, \quad (17)$$

where  $h^f = \max_{1 < j < \bar{n}} h_j^f$  is the maximal step of the grid, and the constants  $c_1 > 0$ ,  $c_2 > 0$  do not depend on the step  $h^f$  [19]. It has been shown possible to construct schemes for solving the BVPs and integrals with high order of accuracy comparable with that of the computer in accordance with the following estimations [13]

$$\left| \frac{\partial \check{\lambda}_j(x_s)}{\partial x_s} - \frac{\partial \check{\lambda}_j^h(x_s)}{\partial x_s} \right| \leq c_3 h^{2p}, \quad \left\| \frac{\partial \Phi_j(x_f; x_s)}{\partial x_s} - \frac{\partial \Phi_j^h(x_s)}{\partial x_s} \right\|_0 \leq c_4 h^{p+1}, \quad (18)$$

$$|Q_{ij}(x_s) - Q_{ij}^h(x_s)| \leq c_5 h^{2p}, \quad |W_{ij}(x_s) - W_{ij}^h(x_s)| \leq c_6 h^{2p}, \quad (19)$$

where  $h^f$  is the grid step,  $p$  is the order of finite elements,  $i, j$  are the numbers of the corresponding solutions, and the constants  $c_3$ ,  $c_4$ ,  $c_5$ , and  $c_6$  do not depend on the step  $h^f$ . The proof is straightforward following the scheme of the proof of estimations (17) in accordance with [19,20]. Verification of the above estimations is provided by numerical analysis on condensed grids and by comparison with examples of exact solvable models A and B.

Let us consider the reduction of BVP (9), (11) in the interval  $\Delta: x_{\min}^f(x_s) < x_f < x_{\max}^f(x_s)$  with the boundary conditions (10) at points  $x_{\min}^f(x_s)$  and  $x_{\max}^f(x_s)$  rewritten in the form

$$\mathbf{A}(x_s)\Phi_j(x_f; x_s) = \check{\lambda}_j(x_s)\mathbf{B}(x_s)\Phi_j(x_f; x_s), \quad (20)$$

where  $\mathbf{A}(x_s)$  is a differential operator, and  $\mathbf{B}(x_s)$  is a multiplication operator, differentiable with respect to the parameter  $x_s \in \Omega_{x_s}$ . Substituting the expansion (16) into (20) and performing integration with respect to  $x_f$  by parts in the interval  $\Delta = \cup_{k=1}^{\bar{n}} \Delta_k$ , we arrive at a set of linear algebraic equations

$$\mathbf{a}_{\mu\nu}^p(x_s)\Phi_{j,\mu}^h(x_s) = \check{\lambda}_j^h(x_s)\mathbf{b}_{\mu\nu}^p(x_s)\Phi_{j,\mu}^h(x_s), \quad (21)$$

in the framework of the briefly described FEM. Using the  $p$ -order Lagrange elements [19], we present below Algorithm 1 for constructing the algebraic problem (21) by the FEM in the form of conventional pseudocode. Its MAPLE realization allows us to show explicitly the recalculation of indices  $\mu, \nu$  and to test the corresponding modules of the parametric matrix problems, derivatives of solutions by parameter, and calculation of integrals.

**Algorithm 1.** Generation of parametric algebraic problems**Input:**

$\Delta = \cup_{k=1}^{\bar{n}} \Delta_k = [x_{\min}^f(x_s), x_{\max}^f(x_s)]$  is the interval of changing of the independent variable  $x_f$ , whose boundaries depend on the parameter  $x_s = x_{k'}^s$ ;

$h_k^f = x_k^f - x_{k-1}^f$  is the grid step;

$\bar{n}$  is the number of subintervals  $\Delta_k = [x_{k-1}^f, x_k^f]$ ;

$p$  is the order of finite elements;

$\mathbf{A}(x_s), \mathbf{B}(x_s)$  are the differential operators in Eq. (20);

**Output:**

$N_\mu^p(x_f)$  are the basis functions in (16);

$\mathbf{a}_{\mu\nu}^p(x_s), \mathbf{b}_{\mu\nu}^p(x_s)$  are the matrix elements in the system of algebraic equations (21);

**Local:**

$x_{k,r}^{fp}$  are the nodes;  $\phi_{k,r}^p(x_f)$  are the Lagrange elements;  $\mu, \nu = 0, 1, \dots, \bar{n}p$ ;

---

```

1: for k:=1 to  $\bar{n}$  do
    for r:=0 to p do
         $x_{k,r}^{fp} = x_{k-1}^f + \frac{h_k^f}{p}r$ 
    end for;
end for;
2:  $\phi_{k,r}^p(x_f) = \prod_{r' \neq r} [(x_f - x_{k,r'}^{fp})(x_{k,r}^{fp} - x_{k,r'}^{fp})^{-1}]$ 
3:  $N_0^p(x_f) :=$  if  $x_f \in \Delta_1$  then  $\phi_{1,0}^p(x_f)$  else 0;
   for k:=1 to  $\bar{n}$  do
       for r:=1 to p-1 do
            $N_{r+p(k-1)}^p(x_f) :=$  if  $x_f \in \Delta_k$  then  $\phi_{k,r}^p(x_f)$  else 0;
       end for;
        $N_{kp}^p(x_f) :=$  if  $x_f \in \Delta_k$  then  $\phi_{k,p}^p(x_f)$ 
           else if  $x_f \in \Delta_{k+1}$  then  $\phi_{k+1,0}^p(x_f)$  else 0;
       end for;
        $N_{\bar{n}p}^p(x_f) :=$  if  $x_f \in \Delta_{\bar{n}}$  then  $\phi_{\bar{n},p}^p(x_f)$  else 0;
4: for  $\mu, \nu := 0$  to  $\bar{n}p$  do
     $\mathbf{a}_{\mu\nu}^p(x_s) := \int_{\Delta} g_1(x_f) N_\mu^p(x_f) \mathbf{A}(x_s) N_\nu^p(x_f) dx_f$ ;
     $\mathbf{b}_{\mu\nu}^p(x_s) := \int_{\Delta} g_1(x_f) N_\mu^p(x_f) \mathbf{B}(x_s) N_\nu^p(x_f) dx_f$ ;
end for;
```

---

**Remarks:**

1. For equation (9), the matrix elements of the operator (7), and  $V(x_f; x_s) = \check{V}_{fs}(x_f, x_s) + \check{V}_f(x_f)$  between the local functions  $N_\mu(x_f)$  and  $N_\nu(x_f)$  defined in the same interval  $\Delta_j$  calculated by formula using  $x_f = x_{k-1}^f + 0.5h_k^f(1 + \eta_f)$ ,  $q, r = \bar{0}, p$ :

$$\begin{aligned}
(\mathbf{a}(x_s))_{\mu,\nu} &= \int_{-1}^{+1} \left\{ \frac{4}{(h_k^f)^2} g_{2f}(x_f) (\phi_{k,q}^p)' (\phi_{k,r}^p)' + g_{1f}(x_f) V(x_f; x_s) \phi_{k,q}^p \phi_{k,r}^p \right\} \frac{h_k^f}{2} d\eta_f, \\
(\mathbf{b}(x_s))_{\mu,\nu} &= \int_{-1}^{+1} g_{1f}(x_f) \phi_{k,q}^p \phi_{k,r}^p \frac{h_k^f}{2} d\eta_f, \quad \mu = q + p(k-1), \quad \nu = r + p(k-1).
\end{aligned}$$

2. If the integrals can not be calculated analytically (see, e.g., section 4), then they are calculated by numerical methods [19], namely, by means of the Gauss quadrature formulae of the order  $p+1$ .

3. For OSQD&PSQD model C, the problem (9)–(11) has been solved using the grid  $\Omega_{h^f(x_f)}^p(x_s)[x_{\min}^f, x_{\max}^f] = -1(20)1$  (the number in parentheses denotes the number of finite elements of order  $p=4$  in each interval).

Generally, 10-16 iterations are required for the subspace iterations to converge the subspace to within the prescribed tolerance. If the matrix  $\mathbf{a}^p \equiv \mathbf{a}^p(x_s)$  in Eq. (21) is not positively defined, the problem (21) is replaced by the following problem:

$$\tilde{\mathbf{a}}^p \Phi^h = \tilde{\lambda}^h \mathbf{b}^p \Phi^h, \quad \tilde{\mathbf{a}}^p = \mathbf{a}^p - \alpha \mathbf{b}^p. \quad (22)$$

The number  $\alpha$  (the shift of the energy spectrum) is chosen in such a way that the matrix  $\tilde{\mathbf{a}}^p$  is positive. The eigenvector of the problem (22) is the same, and  $\tilde{\lambda}^h = \lambda^h + \alpha$ , where the shift  $\alpha$  is evaluated by Algorithm 2.

**Algorithm 2.** Evaluating the lower bound for the lowest eigenvalue of the generalized eigenvalue problem

Generally it is impossible to define the lower bound for the lowest eigenvalue of Eq. (22) because the eigenvalues  $\tilde{\lambda}_1^h(x_s) < \dots < \tilde{\lambda}_i^h(x_s) < \dots < \tilde{\lambda}_{j_{max}}^h(x_s)$  depend upon the parameter  $x_s$ . However, we can use the following algorithm to find the lower bound for the lowest eigenvalue  $\tilde{\lambda}_1^h(x_s)$  at a fixed value of  $x_s$ :

- Step 1.** Calculate  $\mathbf{L} \mathbf{D} \mathbf{L}^T$  factorization of  $\mathbf{A}^p - \alpha \mathbf{B}^p$ .
- Step 2.** If some elements of the diagonal matrix  $\mathbf{D}$  are less than zero then put  $\alpha = \alpha - 1$  and go to **Step 3**, else go to **Step 5**.
- Step 3.** Calculate  $\mathbf{L} \mathbf{D} \mathbf{L}^T$  factorization of  $\mathbf{A}^p - \alpha \mathbf{B}^p$ .
- Step 4.** If some elements of the diagonal matrix  $\mathbf{D}$  are less than zero then put  $\alpha = \alpha - 1$  and go to **Step 3**, else put  $\alpha = \alpha - 0.5$  and go to **Step 8**.
- Step 5.** Put  $\alpha = \alpha + 1$  and calculate  $\mathbf{L} \mathbf{D} \mathbf{L}^T$  factorization of  $\mathbf{A}^p - \alpha \mathbf{B}^p$ .
- Step 6.** If all elements of the diagonal matrix  $\mathbf{D}$  are greater than zero then go to **Step 5**.
- Step 7.** Put  $\alpha = \alpha - 1.5$ .
- Step 8.** End.

After using the above algorithm one should find the lower bound for the lowest eigenvalue, and always  $\tilde{\lambda}_1^h(x_s) - \alpha \leq 1.5$ .



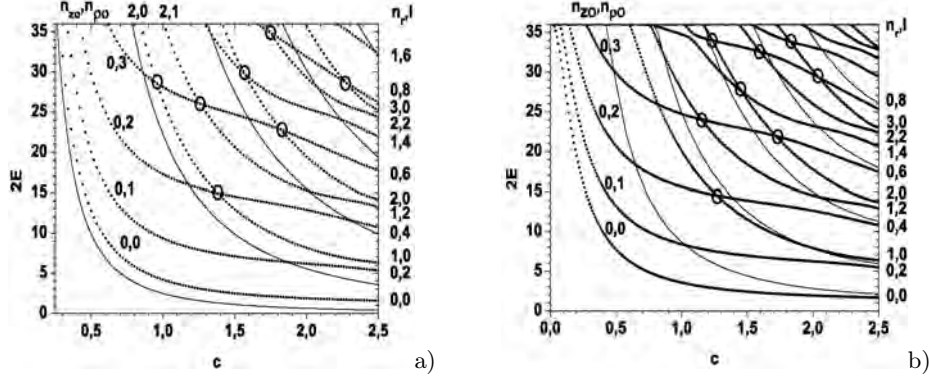


**Fig. 1.** The energies  $2E = \tilde{E}/E_R$  of even  $\sigma = +1$  lower states for OSQD versus the minor  $c$ ,  $\zeta_{ca} = c/a \in (1/5, 1)$  being the spheroid aspect ratio: a) well with impermeable walls, b) diffusion potential with  $2U_0 = 36$ ,  $s = 0.1$ , the major semiaxis  $a = 2.5$  and  $m = 0$ . Tine lines are minimal values  $2E_i^{min} \equiv 2E_i(x_s = 0)$  of potential curves.

#### 4 Spectral Characteristics of Spheroidal QDs

**Models B and C for Oblate Spheroidal QD.** At fixed coordinate  $x_s$  of the slow subsystem, the motion of the particle in the fast degree of freedom  $x_f$  is localized within the potential well having the effective width

$$\tilde{L}(x_s) = 2c\sqrt{1 - x_s^2/a^2}, \quad (23)$$

where  $L = \tilde{L}/a_B^*$ . The parametric BVP (9)–(11) at fixed values of the coordinate  $x_s$ ,  $x_s \in (0, a)$ , is solved in the interval  $x_f \in (-L(x_s)/2, L(x_s)/2)$  for Model C using the program ODPEVP, and for Model B the eigenvalues  $\tilde{E}_{n_o}(x_s)/E_R \equiv 2E_i(x_s)$ ,  $n_o = i = 1, 2, \dots$ , and the corresponding parametric eigenfunctions  $\Phi_i^\sigma(x_f; x_s)$ , obeying the boundary conditions (10) and the normalization condition (11), are expressed in the analytical form:

$$2E_i(x_s) = \frac{\pi^2 n_o^2}{L^2(x_s)}, \quad \Phi_i^\sigma(x_f; x_s) = \sqrt{\frac{2}{L(x_s)}} \sin\left(\frac{\pi n_o}{2} \left(\frac{x_f}{L(x_s)/2} - 1\right)\right), \quad (24)$$

where the even solutions  $\sigma = +1$  are labelled with odd  $n_o = n_{zo} + 1 = 2i - 1$ , and the odd ones  $\sigma = -1$  with even  $n_o = n_{zo} + 1 = 2i$ ,  $i = 1, 2, 3, \dots$ . The effective potentials (13) in Eq. (12) for the slow subsystem are expressed analytically via the integrals over the fast variable  $x_f$  of the basis functions (24) and their derivatives with respect to the parameter  $x_s$  including states with both parities  $\sigma = \pm 1$ :

$$2E_i(x_s) = \frac{a^2 \pi^2 n_o^2}{4c^2(a^2 - x_s^2)}, \quad W_{ii}(x_s) = \frac{3 + \pi^2 n_o^2}{12} \frac{x_s^2}{(a^2 - x_s^2)^2}, \quad (25)$$

$$W_{ij}(x_s) = \frac{2n_o n'_o (n_o^2 + n_o'^2)(1 + (-1)^{n_o + n'_o})}{(n_o^2 - n_o'^2)^2} \frac{x_s^2}{(a^2 - x_s^2)^2},$$

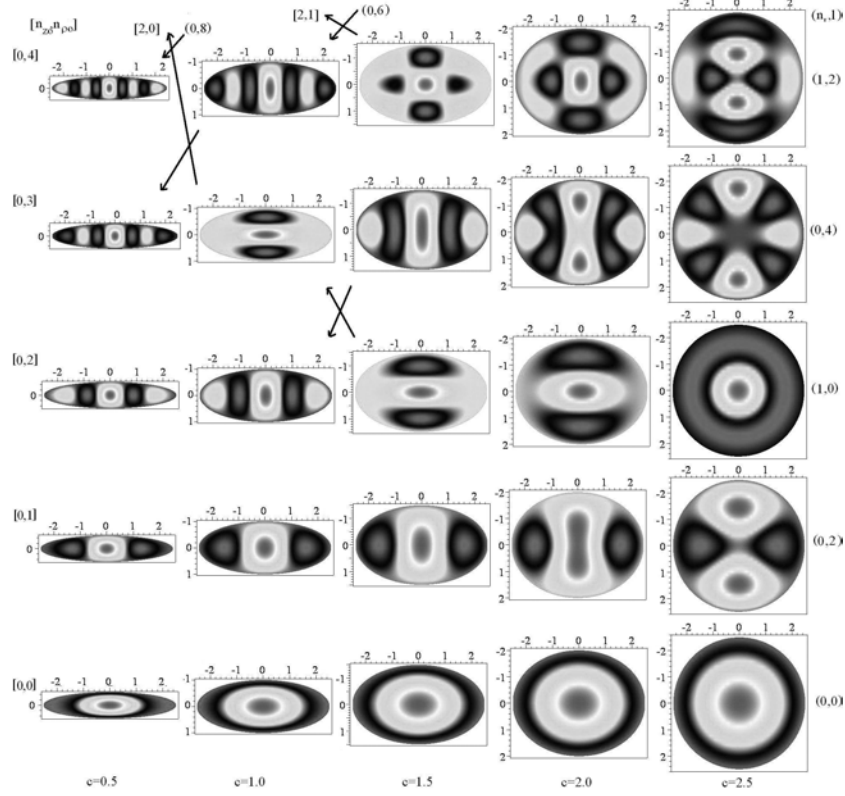


**Fig. 2.** Contour lines of the first five even-parity wave functions  $\sigma = +1$  in the  $xz$  plane of Model B of OSQD for the major semiaxis  $a = 2.5$  and different values of the minor semiaxis  $c$  ( $\zeta_{ca} = c/a \in (1/5, 1)$ )

$$Q_{ij}(x_s) = \frac{n_o n'_o (1 + (-1)^{n_o + n'_o})}{(n_o^2 - n_o'^2)^2} \frac{x_s}{a^2 - x_s^2}, \quad n'_o \neq n_o.$$

For Model B at  $c = a = r_0$  the OSQD turns into SQD with known analytically expressed energy levels  $E_t \equiv E_{nlm}^{sp}$  and the corresponding eigenfunctions

$$2E_{nlm}^{sp} = \frac{\alpha_{n_r+1, l+1/2}^2}{r_0^2}, \quad \Phi_{nlm}^{sp}(r, \theta, \varphi) = \frac{\sqrt{2} J_{l+1/2}(\sqrt{2E_{nlm}^{sp}} r)}{r_0 \sqrt{r} |J_{l+3/2}(\alpha_{n_r+1, l+1/2})|} Y_{lm}(\theta, \varphi), \quad (26)$$

where  $\alpha_{n_r+1, l+1/2}$  are zeros of the Bessel function of semi-integer index  $l + 1/2$ , numbered in ascending order  $0 < \alpha_{11} < \alpha_{12} < \dots < \alpha_{iv} < \dots$  by the integer  $i, v = 1, 2, 3, \dots$ . Otherwise one can use equivalent pairs  $iv \leftrightarrow \{n_r, l\}$  with  $n_r = 0, 1, 2, \dots$  numbering the zeros of Bessel function and  $l = 0, 1, 2, \dots$  being the orbital quantum number that determines the parity of states  $\hat{\sigma} = (-1)^l = (-1)^m \sigma$ ,  $\sigma = (-1)^{l-m} = \pm 1$ . At fixed  $l$ , the energy levels  $\tilde{E}_{nlm}/E_R = 2E_t$  degenerate with respect to the magnetic quantum number  $m$ , are labelled with

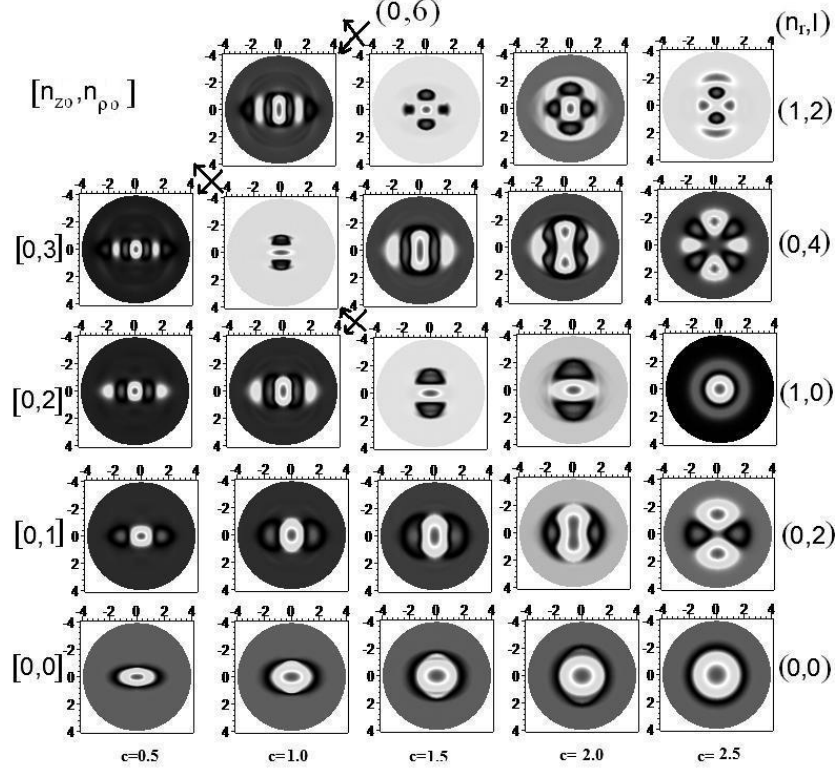


**Fig. 3.** Contour lines of the first five even-parity wave functions  $\sigma = +1$  in the  $xz$  plane of Model C of OSQD with  $2U_0 = 36$  and  $s = 0.1$  for the major semiaxis  $a = 2.5$  and different values of the minor semiaxis  $c$  ( $\zeta_{ca} = c/a \in (1/5, 1)$ )

the quantum number  $n = n_r + 1 = i = 1, 2, 3, \dots$ , in contrast to the spectrum of a spherical oscillator, degenerate with respect to the quantum number  $\lambda = 2n_r + l$ . Figures 1, 2, and 3 show the lower part of non-equidistant spectrum  $\tilde{E}(\zeta_{ca})/E_R = 2E_t$  and the eigenfunctions  $\Psi_t^{m\sigma}$  from Eq. (8) for even states OSQD Models B and C at  $m = 0$ . There is a one-to-one correspondence rule  $n_o = n_{zo} + 1 = 2n - (1 + \sigma)/2$ ,  $n = 1, 2, 3, \dots$ ,  $n_\rho = (l - |m| - (1 - \sigma)/2)/2$ , between the sets of spherical quantum numbers  $(n, l, m, \hat{\sigma})$  of SQD with radius  $r_0 = a = c$  and spheroidal ones  $(n_\xi = n_r, n_\eta = l - |m|, m, \sigma)$  of OSQD with the major  $a$  and the minor  $c$  semiaxes, and the adiabatic set of cylindrical quantum numbers  $(n_{zo}, n_\rho, m, \sigma)$  at continuous variation of the parameter  $\zeta_{ca} = c/a$ . The presence of crossing points of the energy levels of similar parity under the symmetry change from spherical  $\zeta_{ca} = 1$  to axial, i.e., under the variation of the parameter  $0 < \zeta_{ca} < 1$ , in the BVP with two variables at fixed  $m$  for Model B is caused by the possibility of variable separation in the OSC [17], i.e., the r.h.s. of Eq. (12) equals zero. The transformation of eigenfunctions occurring in the course of a transition through the crossing points (marked by circles) in Fig. 1, is shown in Fig. 2 for model B and in Fig. 3 for model C (marked by arrows). From

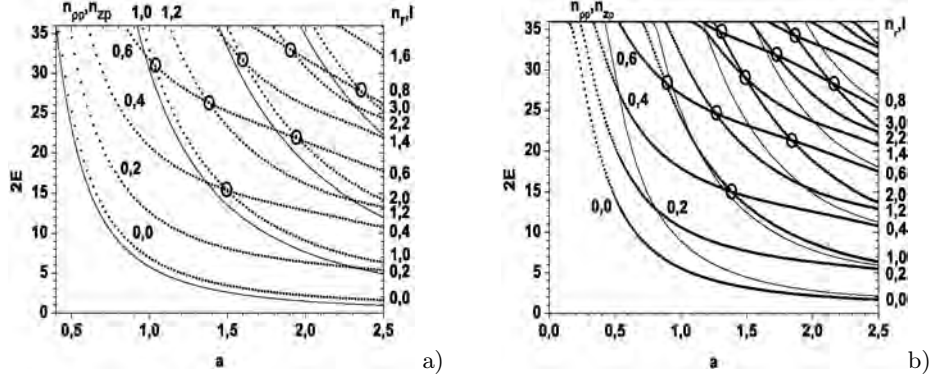


**Fig. 4.** The energies  $2E = \tilde{E}/E_R$  of even  $\sigma = +1$  lowest states for PSQD depending on the minor semiaxis  $a$  ( $\zeta_{ac} = a/c \in (1/5, 1)$  is the spheroid aspect ratio): a) well with impermeable walls, b) diffusion potential,  $2U_0 = 36$ ,  $s = 0.1$ , for the major semiaxis  $c = 2.5$  and  $m = 0$ . Tine lines are minimal values  $2E_i^{min} \equiv 2E_i(x_s = 0)$  of potential curves.

comparison of these Figures one can see that if the eigenfunctions are ordered according to increasing eigenvalues of the BVPs, then for both Models B and C, the number of nodes [18] is invariant under the variation of parameter  $c$  from  $c = a = 2.5$  to  $c = 0.5$  of potentials (3) and (4). For Model B, such a behavior follows from the fact of separation of variables of the BVP with potential (3) in the OSC (see Table 1), while for Model C, further investigation is needed because the coordinate system, where the variables of the BVP with potential (4) are separated, is unknown. So, at small value of deformation parameter ( $\zeta_{ca}$  for OSQD or  $\zeta_{ac}$  for PSQD) there are nodes only along corresponding major axis. For Model C, at each value of the parameter  $a$  there is a finite number of discrete energy levels limited by the value  $2U_0$  of the well walls height. As shown in Fig. 1b, the number of levels of OSQD, equal to that of SQD at  $a = c = r_0$ , is reduced with the decrease of the parameter  $c$  (or  $\zeta_{ca}$ ), in contrast to Models A and B that have countable spectra, and avoided crossings appear just below the threshold.

**Models B and C for Prolate Spheroidal QD.** In contrast to OSQD, for PSQD at fixed coordinate  $x_s$  of the slow subsystem the motion of the particle is confined to a 2D potential well with the effective variable radius

$$\rho_0(x_s) = a\sqrt{1 - x_s^2/c^2}, \quad (27)$$

where  $\rho_0(x_s) = \tilde{\rho}_0(x_s)/a_B$ . The parametric BVP (9)–(11) at fixed values of the coordinate  $x_s$  from the interval  $x_s \in (-c, c)$  is solved in the interval  $x_f \in (0, \rho_0(x_s))$  for Model C using the program ODPEVP, while for Model B the eigenvalues  $\tilde{E}_{n_{pp}+1}(x_s)/E_R \equiv 2E_i(x_s)$ ,  $n_{pp} + 1 = i = 1, 2, \dots$ , and the corresponding parametric basis functions  $\Phi_i^{m\sigma=0}(x_f; x_s) \equiv \Phi_i^m(x_f; x_s)$  without

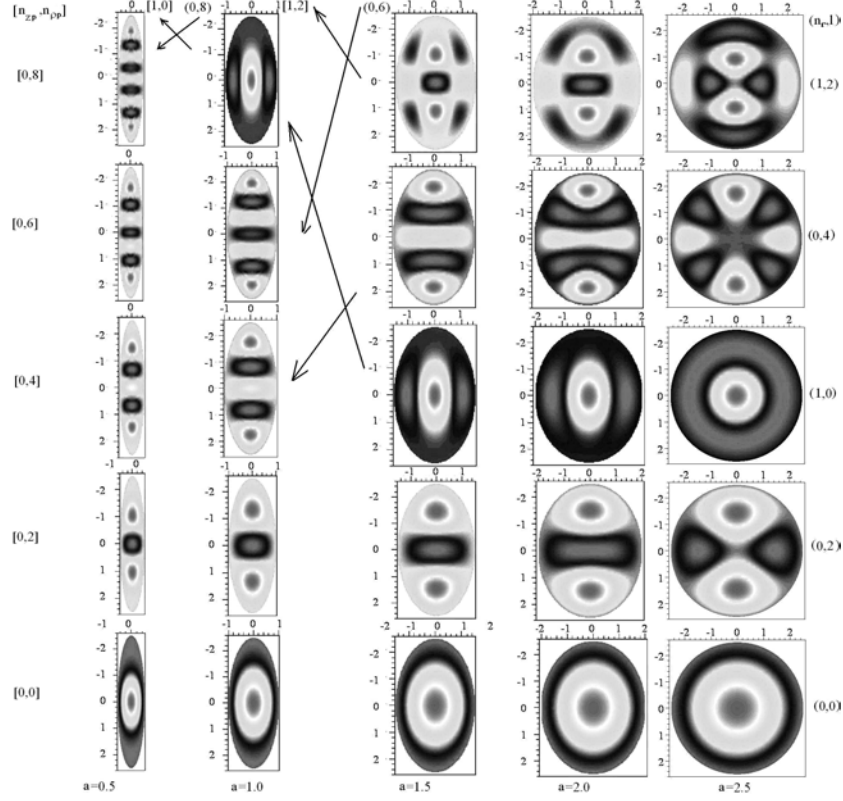


**Fig. 5.** Contour lines of the first five even-parity wave functions  $\sigma = +1$  in the  $xz$  plane of Model B of PSQD for the major semiaxis  $c = 2.5$  and different values of the minor semiaxis  $a$  ( $\zeta_{ac} = a/c \in (1/5, 1)$ )

parity separation obeying the boundary conditions (10) and the normalization condition (11) are expressed in the analytical form:

$$2E_i(x_s) = \frac{\alpha_{n_{pp}+1,|m|}^2}{\rho_0^2(x_s)}, \quad \Phi_{n_{pp}}^m(x_s) = \frac{\sqrt{2}}{\rho_0(x_s)} \frac{J_{|m|}(\sqrt{2E_{n_{pp}+1,|m|}}(x_s)x_f)}{|J_{|m|+1}(\alpha_{n_{pp}+1,|m|})|}, \quad (28)$$

where  $\alpha_{n_{pp}+1,|m|} = \bar{J}_{|m|}^{n_{pp}+1}$  are positive zeros of the Bessel function of the first kind  $J_{|m|}(x_f)$  labeled in the ascending order with the quantum number  $n_{pp}+1 = i = 1, 2, \dots$ . The effective potentials (13) in Eq.(12) for the slow subsystem are calculated numerically in quadratures via the integrals over the fast variable  $x_f$  of the basis functions(28) and their derivatives with respect to the parameter  $x_s$  using SNA MATRA from Section 2. Figures 4 and 5 illustrate the lower part of the non-equidistant spectrum  $E(\zeta_{ac})/E_R = 2\tilde{E}_t$  and the eigenfunctions  $\Psi_t^{m\sigma}$  from Eq. (8) of even states of PSQD Models B and C. There is a one-to-one correspondence rule  $n_{pp} + 1 = n_p = i = n = n_r + 1$ ,  $i = 1, 2, \dots$  and  $n_{zp} = l - |m|$  between the sets of quantum numbers  $(n, l, m, \hat{\sigma})$  of SQD with the

radius  $r_0 = a = c$  and spheroidal ones ( $n_\xi = n_r, n_\eta = l - |m|, m, \sigma$ ) of PSQD with the major  $c$  and the minor  $a$  semiaxes, and the adiabatic set of quantum numbers ( $n = n_{\rho\rho} + 1, n_{zp}, m, \sigma$ ) under the continuous variation of the parameter  $\zeta_{ac} = a/c$ . The presence of crossing points of similar-parity energy levels in Fig. 4 under the change of symmetry from spherical  $\zeta_{ac} = 1$  to axial, i.e., under the variation of the parameter  $0 < \zeta_{ac} < 1$ , in the BVP with two variables at fixed  $m$  for Model B is caused by the possibility of variable separation in the PSC [17], i.e., r.h.s. of Eq. (12) equals zero. For Model C, at each value of the parameter  $c$  there is also only a finite number of discrete energy levels limited by the value  $2U_0$  of the well walls height. As shown in Fig. 4b, the number of energy levels of PSQD, equal to that of SQD at  $a = c = r_0$ , which is determined by the product of mass  $\mu_e$  of the particle, the well depth  $\tilde{U}_0$ , and the square of the radius  $\tilde{r}_0$ , is reduced with the decrease of the parameter  $\tilde{a}$  (or  $\zeta_{ac}$ ) because of the promotion of the potential curve (lower bound) into the continuous spectrum, in contrast to Models A and B having countable spectra. Note that the spectrum of Model C for PSQD or OSQD should approach that of Model B with the growth of the walls height  $U_0$  of the spheroidal well. However, at critical values of the ellipsoid aspect ratio it is shown that in the effective mass approximation, both the terms (lower bound) and the discrete energy eigenvalues in models of the B type move into the continuum. Therefore, when approaching the critical aspect ratio values, it is necessary to use models such as the lens-shaped self-assembled QDs with a quantum well confined to a narrow wetting layer [3] or if a minor semiaxis becomes comparable with the lattice constant to consider models (see, e.g. [21]), different from the effective mass approximation.

## 5 Conclusion

By examples of the analysis of energy spectra of SQD, PSQD, and OSQD models with three types of axially symmetric potentials, the efficiency of the developed computational scheme and SNA is demonstrated. Only Model A (anisotropic harmonic oscillator potential) is shown to have an equidistant spectrum, while Models B and C (wells with infinite and finite walls height) possess non-equidistant spectra. In Model C, there is a finite number of energy levels. This number becomes smaller as the parameter  $a$  or  $c$  ( $\zeta_{ac}$  or  $\zeta_{ca}$ ) is reduced because the potential curve (lower bound) moves into the continuum. Models A and B have countable discrete spectra. This difference in spectra allows verification of SQD, PSQD, and OSQD models using experimental data [2], e.g., photoabsorption, from which not only the energy level spacing, but also the mean geometric dimensions of QD may be derived [5,7,8]. It is shown that there are critical values of the ellipsoid aspect ratio, at which in the approximation of effective mass the discrete spectrum of models with finite-wall potentials turns into a continuous one. Hence, using experimental data, it is possible to verify different QD models like the lens-shaped self-assembled QDs with a quantum well confined to a narrow wetting layer [3], or to determine the validity domain of the effective mass approximation, if a minor semiaxis becomes comparable with the lattice constant and to proceed opportunely to more adequate models such as [21].

Note *a posteriori* that the diagonal approximation of the slow-variable ODE (12) without the diagonal matrix element  $W_{ii}$  (so-called rude adiabatic approximation) provides the lower estimate of the calculated energy levels. With this matrix element taken into account (adiabatic approximation), the upper estimate of energy is provided, unless in the domain of the energy level crossing points. Therefore, the Born–Oppenheimer (BO) approximation is generally applicable only for estimating the ground state at an appropriate value of the small parameter. For Model B in the first BO approximation  $2E_i \approx E_i^{(0)} + E_i^{(1)}$  is given by the minimal value of the slow subsystem energy  $E_1^{\min}(x_s)$  at the equilibrium points  $x_s = 0$  (namely,  $E_i^{(0)} = \pi^2 n_o^2 / (2c)^2$  from Eq. (24) for OSQD and  $E_i^{(0)} = \alpha_{n_{pp}+1}^2 / a^2$  from Eq. (28) for PSQD), and by the corresponding energy values  $E_i^{(1)} = \pi(ac)^{-1} n_o(2n_\rho + |m| + 1)$  and  $E_i^{(1)} = 2(ac)^{-1} \alpha_{n_{pp}+1, |m|} (n_z + 1/2)$  of the 2D and 1D harmonic oscillator, respectively. It is shown in [4] that the terms  $E_i(x_s)$  allow high-precision approximation by the Hulten potential. This can be accomplished by means of computer algebra software, e.g., Maple, Mathematica, which allows (in the rude adiabatic approximation) to obtain the lower bound of the spectrum by solving transcendental equations expressed analytically in terms of known special functions, and to use this approach for further development of our SNA project.

The software package developed is applicable to the investigation of impurity and exciton states in semiconductor nanostructure models. Further development of the method and the software package is planned for solving the quasi-2D and quasi-1D BVPs with both discrete and continuous spectrum, which are necessary for calculating the optical transition rates, channeling and transport characteristics in the models like quantum wells and quantum wires.

Authors thank Profs. K.G. Dvovyan, E.M. Kazaryan, and H.A. Sarkisyan for collaboration in the field and Profs. T. Sturm and C. Philips for support of our SNA project. This work was done within the framework of the Protocol No. 3967-3-6-09/11 of collaboration between JINR and RAU in dynamics of finite-dimensional quantum models and nanostructures in external fields. The work was supported partially by RFBR (grants 10-01-00200 and 08-01-00604), and by the grant No. MK-2344.2010.2 of the President of Russian Federation.

## References

1. Harrison, P.: Quantum Well, Wires and Dots. In: Theoretical and Computational Physics of Semiconductor Nanostructures. Wiley, New York (2005)
2. Gambaryan, K.M.: Interaction and Cooperative Nucleation of InAsSbP Quantum Dots and Pits on InAs(100) Substrate. *Nanoscale. Res. Lett.* (2009), doi:10.1007/s11671-009-9510-8
3. Wojs, A., Hawrylak, P., Fafard, S., Jacak, L.: Electronic structure and magneto-optics of self-assembled quantum dots. *Phys. Rev. B* 54, 5604–5608 (1996)
4. Juharyan, L.A., Kazaryan, E.M., Petrosyan, L.S.: Electronic states and interband light absorption in semi-spherical quantum dot under the influence of strong magnetic field. *Solid State Comm.* 139, 537–540 (2006)
5. Dvovyan, K.G., Hayrapetyan, D.B., Kazaryan, E.M., Tshantshapanyan, A.A.: Electron States and Light Absorption in Strongly Oblate and Strongly Prolate Ellipsoidal Quantum Dots in Presence of Electrical and Magnetic Fields. *Nanoscale Res. Lett.* 2, 601–608 (2007)

6. Cantele, G., Ninno, D., Iadonisi, G.: Confined states in ellipsoidal quantum dots. *J. Phys. Condens. Matt.* 12, 9019–9036 (2000)
7. Trani, F., Cantele, G., Ninno, D., Iadonisi, G.: Tight-binding calculation of the optical absorption cross section of spherical and ellipsoidal silicon nanocrystals. *Phys. Rev. B* 72, 075423 (2005)
8. Lepadatu, A.-M., Stavarache, I., Ciurea, M.L., Iancu, V.: The influence of shape and potential barrier on confinement energy levels in quantum dots. *J. Appl. Phys.* 107, 033721 (2010)
9. Vinitsky, S.I., Gerdt, V.P., Gusev, A.A., Kaschiev, M.S., Rostovtsev, V.A., Samoilov, V.N., Tupikova, T.V., Chuluunbaatar, O.: A symbolic-numerical algorithm for the computation of matrix elements in the parametric eigenvalue problem. *Programming and Computer Software* 33, 105–116 (2007)
10. Chuluunbaatar, O., Gusev, A., Gerdt, V., Kaschiev, M., Rostovtsev, V., Samoylov, V., Tupikova, T., Vinitsky, S.: A Symbolic-numerical algorithm for solving the eigenvalue problem for a hydrogen atom in the magnetic field: cylindrical coordinates. In: Ganzha, V.G., Mayr, E.W., Vorozhtsov, E.V. (eds.) *CASC 2007. LNCS*, vol. 4770, pp. 118–133. Springer, Heidelberg (2007)
11. Chuluunbaatar, O., Gusev, A.A., Abrashkevich, A.G., Amaya-Tapia, A., Kaschiev, M.S., Larsen, S.Y., Vinitsky, S.I.: KANTBP: A program for computing energy levels, reaction matrix and radial wave functions in the coupled-channel hyperspherical adiabatic approach. *Comput. Phys. Commun.* 177, 649–675 (2007)
12. Chuluunbaatar, O., Gusev, A.A., Gerdt, V.P., Rostovtsev, V.A., Vinitsky, S.I., Abrashkevich, A.G., Kaschiev, M.S., Serov, V.V.: POTHMF: A program for computing potential curves and matrix elements of the coupled adiabatic radial equations for a hydrogen-like atom in a homogeneous magnetic field. *Comput. Phys. Commun.* 178, 301–330 (2008)
13. Chuluunbaatar, O., Gusev, A.A., Vinitsky, S.I., Abrashkevich, A.G.: ODPEVP: A program for computing eigenvalues and eigenfunctions and their first derivatives with respect to the parameter of the parametric self-adjointed Sturm-Liouville problem. *Comput. Phys. Commun.* 180, 1358–1375 (2009)
14. Vinitsky, S.I., Chuluunbaatar, O., Gerdt, V.P., Gusev, A.A., Rostovtsev, V.A.: Symbolic-numerical algorithms for solving parabolic quantum well problem with hydrogen-like impurity. In: Gerdt, V.P., Mayr, E.W., Vorozhtsov, E.V. (eds.) *CASC 2009. LNCS*, vol. 5743, pp. 334–349. Springer, Heidelberg (2009)
15. Kantorovich, L.V., Krylov, V.I.: *Approximate Methods of Higher Analysis*. Wiley, New York (1964)
16. Born, M., Huang, X.: *Dynamical Theory of Crystal Lattices*. The Clarendon Press, Oxford (1954)
17. Abramowitz, M., Stegun, I.A.: *Handbook of Mathematical Functions*. Dover, New York (1965)
18. Courant, R., Hilbert, D.: *Methods of Mathematical Physics*, vol. 1. Wiley, Chichester (1989)
19. Strang, G., Fix, G.J.: *An Analysis of the Finite Element Method*. Prentice-Hall, Englewood Cliffs (1973)
20. Schultz, M.H.:  $L^2$  Error Bounds for the Rayleigh-Ritz-Galerkin Method. *SIAM J. Numer. Anal.* 8, 737–748 (1971)
21. Harper, P.G.: Single Band Motion of Conduction Electrons in a Uniform Magnetic Field. *Proc. Phys. Soc. A* 68, 874–878 (1955)





# Symbolic-Numeric Solution of Boundary-Value Problems for the Schrödinger Equation Using the Finite Element Method: Scattering Problem and Resonance States

A.A. Gusev<sup>1</sup>, L. Le Hai<sup>1,2</sup>, O. Chuluunbaatar<sup>1,3</sup>, V. Ulziibayar<sup>4</sup>,  
S.I. Vinitsky<sup>1</sup>, V.L. Derbov<sup>5</sup>, A. Gózdź<sup>6</sup>, and V.A. Rostovtsev<sup>1</sup>

<sup>1</sup> Joint Institute for Nuclear Research, Dubna, Russia  
gooseff@jinr.ru

<sup>2</sup> Belgorod State University, Belgorod, Russia

<sup>3</sup> National University of Mongolia, UlaanBaatar, Mongolia

<sup>4</sup> Mongolian University of Science and Technology, UlaanBaatar, Mongolia

<sup>5</sup> Saratov State University, Saratov, Russia

<sup>6</sup> Institute of Physics, Maria Curie-Skłodowska University, Lublin, Poland

**Abstract.** We present new symbolic-numeric algorithms for solving the Schrödinger equation describing the scattering problem and resonance states. The boundary-value problems are formulated and discretized using the finite element method with interpolating Hermite polynomials which provide the required continuity of the derivatives of the approximated solutions. The efficiency of the algorithms and programs implemented in the Maple computer algebra system is demonstrated by analysing the scattering problems and resonance states for the Schrödinger equation with continuous (piecewise continuous) real (complex) potentials like single (double) barrier (well).

## 1 Introduction

High-accuracy efficient algorithms and programs for solving boundary-value problems are presently indispensable for studying important mathematical models, describing wave propagation in smoothly irregular waveguides, tunnelling and channelling of compound quantum systems through multidimensional potential barriers, photoionization, photoabsorption, and transport in atomic, molecular, and quantum-dimensional semiconductor systems [1–15].

For this class of problems not only the solution itself, but also its first derivative must be continuous, which is of particular importance in the case of quantum-dimensional semiconductor systems and smoothly irregular waveguides, described by partial differential equations with piecewise-continuous coefficient functions [2, 16–18]. As shown by the example of solving an eigenvalue problem for the Schrödinger equation [19], the required continuity of the derivatives can be efficiently implemented in the approximating numerical solution on a finite-element grid using the Hermite interpolating elements [17, 20]. The reduction of the initial

boundary-value problems to the corresponding algebraic problems is a cumbersome problem of the Finite-Element Method using high-order approximation. The generation of the local functions using the high-order Hermite interpolation polynomials and the elements of mass and stiffness matrices is performed in the analytic form using the algorithm elaborated by the authors and implemented in CAS Maple. Using CAS Maple is a key point of the approach. Now it is possible to work with multiprocessor computers that implement parallel computations of algebraic problem with high-dimension matrices using the LinearAlgebra package of CAS Maple. Moreover, in our previous paper [19] we also used the symbolic algorithm to generate Fortran routines that allow the solution of the generalized algebraic eigenvalue problem with high-dimension matrices for real-valued potentials. Further development of this approach for solving the scattering problem and calculating the resonance metastable states for real-valued and complex potentials is an important problem that constitutes the goal of the present paper.

In this paper we present a new approach to the study of the resonance scattering problem and the metastable states for both continuous and piecewise continuous real-valued and complex potentials. The discretization of the corresponding boundary-value problem reformulated in terms of symmetric quadratic functionals is implemented using the Hermite interpolation polynomials which provide the required continuity of the derivatives of the approximated solutions. The continuity of the approximate solutions derivatives is the key point in the problems of quantum mechanics, waveguide theory, etc. For the scattering problem with the fixed real energy value  $E = \Re E$ ,  $\Re E > 0$  we formulate the boundary-value problem for the Schrödinger equation in the finite interval  $|z| \leq |z^{\max}|$  with the conditions of the third kind at the boundary points of the interval and construct the appropriate variational functional. The asymptotic solutions of the scattering problem at  $|z^{\max}| \leq |z| < \infty$  comprise the incident wave and the unknown amplitudes of transmitted  $T(E)$  and reflected  $R(E)$  waves, which are calculated together with the desired numerical solution in the finite interval and its logarithmic derivatives at the boundary points of the interval. To calculate the resonance state with the unknown complex eigenvalue of energy  $E_r = \Re E_r + i \Im E_r$ ,  $\Re E_r > 0$ ,  $\Im E_r < 0$  we formulate the boundary-value problem for the Schrödinger equation in the finite interval with the conditions of the third kind at the boundary points of the interval and construct the appropriate variational functional. In contrast to the scattering problem, in the asymptotic solutions of this problem the amplitude of the incident waves is zero, i.e., only the outgoing waves are present,  $\exp(i\sqrt{E_r}|z|)$ , that meet the radiation condition [23] and are considered within the sufficiently large but finite interval  $|z| \leq |z^{\max}|$ .

The constructed stiffness and mass matrices for the variational functionals, comprising the boundary conditions of the first, second, or third kind, are used to formulate the generalized algebraic eigenvalue problem. To calculate the resonance states with unknown complex energy eigenvalues  $E_r$  we use the Newton iteration scheme, in which the initial approximation is chosen as the solution of the scattering problem with the boundary conditions of the third kind and the real values of energy  $E = \Re E > 0$ , close to the resonance ones,  $E_r = \Re E_r + i \Im E_r$ , and corresponding to the maximal value of the transmission coefficient  $|T(E)|^2$ .

We also used the appropriate solutions of the eigenvalue problem with the boundary conditions of the first or the second kind.

The efficiency (the order of approximation with respect to the finite element grid step) and the capability of time saving (the execution time for the Maple algorithms for banded matrices with the dimension up to 300) is demonstrated by the test calculations of scattering and resonance states for the Schrödinger equation with continuous (piecewise continuous) real (complex) barrier (double barrier) or well (double well) potential functions.

The paper is organized as follows. In Section 2 the formulation of the boundary-value problems with the boundary conditions of the first, second, and third kind is presented, as well as the appropriate variational functionals. Section 3 presents the finite-element scheme with the interpolating Hermite polynomials and describes the algorithm of reducing the boundary-value problems to the algebraic ones. Section 4 is devoted to test calculations that demonstrate the efficiency and time-saving capability of the proposed computational schemes, implemented as a Maple program. In the Conclusion we discuss the results and the possible applications of the proposed computational schemes and computer programs.

## 2 Formulation of Boundary-Value Problems

Consider the second-order differential equation with respect to the unknown function  $\Phi(z)$  in the interval  $z \in \Omega_z = (z^{\min}, z^{\max})$  [19]

$$(D-2E)\Phi(z) = 0, \quad D = -\frac{1}{f_1(z)}\frac{\partial}{\partial z}f_2(z)\frac{\partial}{\partial z} + V(z). \quad (1)$$

The coefficient functions  $f_1(z) > 0$ ,  $f_2(z) > 0$  and the real or complex potential function  $V(z)$  are assumed to be continuous and to possess derivatives up to the order  $\kappa^{\max} - 1 \geq 1$  in the domain  $z \in \bar{\Omega}_z = [z^{\min}, z^{\max}]$ . Alternative assumptions for piecewise continuous functions will be also considered below.

Depending on the physical problem, the desired solution is to obey the appropriate boundary conditions at the end points  $z^{\min}$  and  $z^{\max}$  of the interval  $\bar{\Omega}_z$ :

$$(I) : \quad \Phi_m(z^t) = 0, \quad t = \min \text{ and/or } \max, \quad (2)$$

$$(II) : \quad d\Phi_m(z)/dz|_{z=z^t} = 0, \quad t = \min \text{ and/or } \max, \quad (3)$$

$$(III) : \quad d\Phi_m(z)/dz|_{z=z^t} = \mathcal{R}(z^t)\Phi_m(z^t), \quad t = \min \text{ and/or } \max. \quad (4)$$

The solution of the boundary-value problem can be reduced to the determination of stationary point (or minimal value) of the variational functional [21]

$$\begin{aligned} \Xi(\Phi, E, z^{\min}, z^{\max}) &\equiv \int_{z^{\min}}^{z^{\max}} \Phi(z) (D-2E)\Phi(z) f_1(z) dz = \Pi(\Phi, E, z^{\min}, z^{\max}) + C, \\ C &= -f_2(z^{\max})\Phi(z^{\max})\mathcal{R}(z^{\max})\Phi(z^{\max}) + f_2(z^{\min})\Phi(z^{\min})\mathcal{R}(z^{\min})\Phi(z^{\min}), \end{aligned} \quad (5)$$

where  $\Pi(\Phi, E, z^{\min}, z^{\max})$  is the symmetric functional

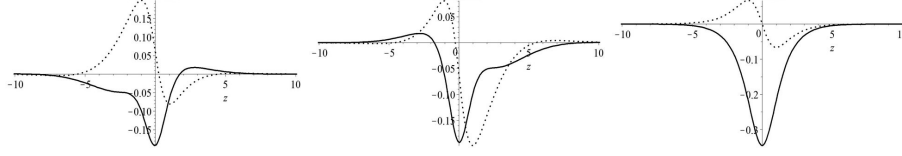


**Fig. 1.** Real (solid line) and imaginary (dotted line) parts of the eigenfunctions  $\Phi_1^+(z)$ ,  $\Phi_1^-(z)$  and  $\Phi_1(z)$  with eigenvalues  $E_1^\pm$  and  $E_1$ , respectively, given in Table 1.

$$\begin{aligned} \Pi(\Phi, E, z^{\min}, z^{\max}) = & \int_{z^{\min}}^{z^{\max}} [f_2(z) d\Phi(z)/dz d\Phi(z)/dz \\ & + f_1(z) \Phi(z) V(z) \Phi(z) - f_1(z) 2E \Phi(z) \Phi(z)] dz. \end{aligned} \quad (6)$$

*Problem 1.* For bound states the eigenfunctions are considered that obey the boundary conditions of the second kind (3) or the first kind (2) for  $\mathcal{R}(z) = 0$  or  $\mathcal{R}(z) \rightarrow \infty$  in the functional (5), (6), respectively.

In the case (a) of the complex potential and complex eigenvalues  $E_m = \Re E_m + i \Im E_m$  the eigenfunctions  $\Phi_m(z)$  obey the normalization and orthogonality conditions

$$\langle \Phi_m | \Phi_{m'} \rangle = \int_{z^{\min}}^{z^{\max}} \Phi_m(z) \Phi_{m'}(z) f_1(z) dz = \delta_{mm'}. \quad (7)$$

In the case (b) of the real eigenvalues  $E_m$ , i.e.,  $E_m = E_m^*$ ,  $\Im E = 0$ , the left-hand function  $\Phi_m(z)$  in the scalar product (7) and the functional (5), (6) is replaced with the complex conjugate function  $\Phi_m^*(z)$ , corresponding to the same eigenvalue  $E_m^* = E_m$ .

*Problem 2.* For solving the scattering problem with fixed real eigenvalues  $E$  the eigenfunctions  $\Phi(E, z)$  are to satisfy the boundary conditions of the third kind (4). The asymptotic solutions of the scattering problem at  $|z^{\max}| \leq |z| < \infty$  comprise the incident wave and the unknown amplitudes of transmitted  $T(E)$  and reflected  $R(E)$  waves, which are calculated together with the desired numerical solution in the finite interval and its logarithmic derivatives  $\mathcal{R}(z^t)$  at the boundary points of the interval. The unknown eigenvalues  $\mathcal{R}(z^{\min})$  (or  $\mathcal{R}(z^{\max})$ ) are determined by solving the problem (19) with the boundary conditions (4) taken into account in a way similar to [9]. The parameter  $\mathcal{R}(z^t)$ ,  $t = \max$  (or  $t = \min$ ), in the functional (5), (6) is determined from the asymptotic boundary conditions,  $\mathcal{R}(z^t) = \left. \frac{d\Phi_{as}(E, z)}{dz} \right|_{z=z^t} \frac{1}{\Phi_{as}(E, z^t)}$ , where the asymptotic solutions  $\Phi_{as}(E, z)$  are  $\delta$ -function normalized.

In the case (a) of the complex potential the eigenfunctions  $\Phi(E, z)$  obey the normalization and orthogonality conditions

$$\begin{aligned} \langle \Phi(E) | \Phi(E') \rangle &= \int_{z^{\min}}^{z^{\max}} \Phi(E, z) \Phi(E', z) f_1(z) dz + C(E, E') = 2\pi \delta(E - E'), \quad (8) \\ C(E, E') &= \int_{-\infty}^{z^{\min}} \Phi_{as}(E, z) \Phi_{as}(E', z) f_1(z) dz + \int_{z^{\max}}^{+\infty} \Phi_{as}(E, z) \Phi_{as}(E', z) f_1(z) dz. \end{aligned}$$

In the case (b) of the real potential the left-hand function  $\Phi(E, z)$  in the scalar product (8) and in the functional (5), (6) is replaced with the complex conjugate eigenfunction  $\Phi^*(E, z)$ . The detailed consideration of the asymptotic functions  $\Phi_{as}(E, z)$  will be presented below.

*Problem 3.* For metastable states the solution satisfies the boundary conditions of the third kind (4), where the parameter  $\mathcal{R}(z^t)$  depends upon the complex energy value  $E = \Re E + i\Im E$  in the lower semiplane:  $\mathcal{R}(z^{\min}) = -\sqrt{-2E}$ ,  $\mathcal{R}(z^{\max}) = \sqrt{-2E}$ , with  $\Re E > 0$  and  $\Im E < 0$ . In this case for the real (b) and complex (a) potentials (provided that the real and imaginary parts of the latter are specifically chosen, see [13]) the solution satisfies the normalization condition

$$(\Phi_m | \Phi_m) = 2\sqrt{-2E_m} \left( \int_{z^{\min}}^{z^{\max}} \Phi_m(z) \Phi_m(z) f_1(z) dz - 1 \right) + C_{mm} = 0, \quad (9)$$

$$C_{mm} = -f_2(z^{\max}) \Phi_m(z^{\max}) \Phi_m(z^{\max}) + f_2(z^{\min}) \Phi_m(z^{\min}) \Phi_m(z^{\min}),$$

and the orthogonality condition

$$(\Phi_m | \Phi_{m'}) = (\sqrt{-2E_m} + \sqrt{-2E_{m'}}) \int_{z^{\min}}^{z^{\max}} \Phi_m(z) \Phi_{m'}(z) f_1(z) dz + C_{mm'} = 0, \quad (10)$$

$$C_{mm'} = -f_2(z^{\max}) \Phi_m(z^{\max}) \Phi_{m'}(z^{\max}) + f_2(z^{\min}) \Phi_m(z^{\min}) \Phi_{m'}(z^{\min}),$$

that follows from calculating the difference of the functionals (5) with the eigenvalues  $E_m, E_{m'}$  and the corresponding eigenfunctions  $\Phi_m(z), \Phi_{m'}(z)$  substituted into them and with  $\imath p_m = \imath \sqrt{2E_m}$  and  $\imath p_{m'} = \imath \sqrt{2E_{m'}}$  substituted into the parameter  $\mathcal{R}(z^{\max})$  and with inverse sign into the parameter  $\mathcal{R}(z^{\min})$ , respectively. Similar orthogonality condition for real potentials was derived earlier using the Green function of the semiaxis [22].

## 2.1 Scattering Problem: The Physical Asymptotic Solutions in Longitudinal Coordinates and the Scattering Matrix

The solutions of the scattering problem with the fixed energy value  $E > 0$  normalized by the condition (8) on the axis  $z \in (-\infty, +\infty)$  possess the “incident wave + outgoing waves” asymptotic form

$$\Phi_v(z \rightarrow \pm\infty) = \begin{cases} \begin{cases} X^{(+)}(z)T_v, & z > 0, \\ X^{(+)}(z) + X^{(-)}(z)R_v, & z < 0, \end{cases} & v = \rightarrow, \\ \begin{cases} X^{(-)}(z) + X^{(+)}(z)R_v, & z > 0, \\ X^{(-)}(z)T_v, & z < 0, \end{cases} & v = \leftarrow, \end{cases} \quad (11)$$

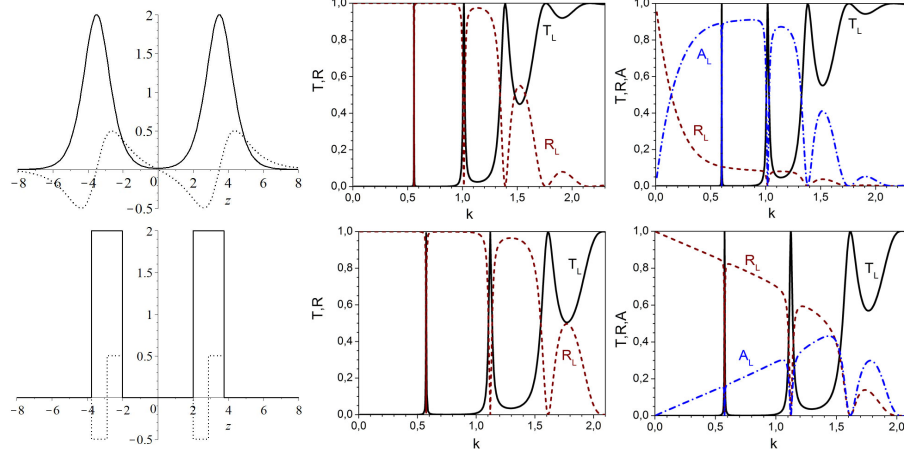


**Fig. 2.** The system of two complex Scarf potentials with  $V_1 = 2$ ,  $V_2 = 1$  separated by the distance  $d = 7/2$ , and the system of two complex rectangular potential barriers. The solid line shows the real part and the dotted line shows the imaginary part (left-hand panel). The coefficients of transmission  $T_L = |T_{\rightarrow}|^2$  (solid line), reflection  $R_L = |R_{\rightarrow}|^2$  (dotted line), and absorption  $A_L$  (dash-dotted line) versus the wave number  $k = \sqrt{2E}$  for the systems of two purely real potentials (center panel) and complex potentials (right-hand panel).

where  $T_v$  and  $R_v$  are the transmission and reflection amplitudes,  $v$  is the initial direction of the particle motion along the  $z$  axis. For example, for  $f_1(z) = f_2(z) = 1$  and rapidly decreasing  $V(z \rightarrow \pm\infty) \rightarrow 0$  the asymptotic solutions  $X^{(\pm)}(z) \equiv X^{(\pm)}(z, E)$  have the form

$$X^{(\pm)}(z) \rightarrow (p)^{-1/2} \exp(\pm ipz), p = \sqrt{2E} \quad (12)$$

with the normalization condition

$$\int_{-\infty}^{\infty} (X^{(\pm)}(z, E'))^* X^{(\pm)}(z, E) dz = 2\pi\delta(E' - E). \quad (13)$$

Generally, the functions  $X^{(\pm)}(z)$  satisfy the conditions with the Wronskian

$$\begin{aligned} \text{Wr}(X^{(\mp)}(z), X^{(\pm)}(z)) &= \pm 2i, \quad \text{Wr}(X^{(\pm)}(z), X^{(\pm)}(z)) = 0, \\ \text{Wr}(a(z), b(z)) &= f_2(z) (a(z)db(z)/dz - da(z)/dz b(z)). \end{aligned} \quad (14)$$

For real-valued potentials the Wronskian is constant, which yields the following properties of the reflection and transmission amplitudes

$$\begin{aligned} T_{\rightarrow}^* T_{\rightarrow} + R_{\rightarrow}^* R_{\rightarrow} &= T_{\leftarrow}^* T_{\leftarrow} + R_{\leftarrow}^* R_{\leftarrow} = 1, & T_{\rightarrow} &= T_{\leftarrow} \\ T_{\rightarrow}^* R_{\leftarrow} + R_{\rightarrow}^* T_{\leftarrow} &= R_{\leftarrow}^* T_{\rightarrow} + T_{\leftarrow}^* R_{\rightarrow} = 0, \end{aligned} \quad (15)$$

as well as the symmetric and unitary properties of the scattering matrix

$$\mathbf{S} = \begin{pmatrix} R_{\rightarrow} & T_{\leftarrow} \\ T_{\rightarrow} & R_{\leftarrow} \end{pmatrix}, \quad \mathbf{S}^\dagger \mathbf{S} = \mathbf{S} \mathbf{S}^\dagger = 1. \quad (16)$$

### 3 Generation of Algebraic Problems

First, the initial interval  $[z^{\min}, z^{\max}]$  is divided into  $n'$  subintervals  $\tilde{\Omega}_i = [z'_{i-1}, z'_i]$ , each of them being divided into  $n_i$  finite elements of different length  $h_i = (z'_i - z'_{i-1})/n_i$ . As a result we arrive at the following partitioning of the domain into  $n = n_1 + \dots + n_i + \dots + n_{n'} \geq n'$  finite elements

$$\begin{aligned} \Omega_{h_j(z)}^p[z^{\min}, z^{\max}] &= \cup_{j=1}^n \Omega_j = \cup_{i=1}^{n'} \bar{\Omega}_i, & \bar{\Omega}_i &= \cup_{j=n_1+\dots+n_{i-1}+1}^{n_1+\dots+n_{i-1}+n_i} \Omega_j, \\ \Omega_j &= [z_j^{\min}, z_j^{\max}] \equiv [z_{j+1}^{\min}], & j &= 0, \dots, n, \\ z_{j=i'+n_1+\dots+n_{i-1}}^{\max} &= (z'_{i-1}(n_i - i') + z'_i i')/n_i, & i' &= 0, \dots, n_i, \quad i = 1, \dots, n'. \end{aligned} \quad (17)$$

Each of the finite elements is then divided into  $p$  similar intervals, thus forming the finite-element grid  $\Omega_{h_j(z)}^p[z^{\min}, z^{\max}] = \{z_0, z_1, \dots, z_{np}\}$ , where  $z_{p(j-1)+r} = (z_j^{\min}(p-r) + z_j^{\max}r)/p$ ,  $r = 0, \dots, p$ .

The solutions  $\hat{\Phi}(z)$  are sought for in the form of a finite sum over the basis of local functions  $N_\mu^g(z)$  at each nodal point  $z = z_k$  of the grid  $\Omega_{h_j(z)}^p[z^{\min}, z^{\max}]$ :

$$\hat{\Phi}(z) = \sum_{\mu=0}^{L-1} \Phi_\mu^h N_\mu^g(z), \quad \hat{\Phi}(z_l) = \Phi_{l\kappa^{\max}}^h, \quad d^\kappa \hat{\Phi}(z)/dz^\kappa|_{z=z_l} = \Phi_{l\kappa^{\max}+\kappa}^h \quad (18)$$

where  $L = (pn+1)\kappa^{\max}$  is the number of local functions and  $\Phi_\mu^h$  at  $\mu = l\kappa^{\max} + \kappa$  are the nodal values of the  $\kappa$ -th derivatives of the function  $\hat{\Phi}(z)$  (including the function  $\hat{\Phi}(z)$  itself for  $\kappa = 0$ ) at the points  $z_l$ .

The local functions  $N_\mu^g(z) \equiv N_{l\kappa^{\max}+\kappa}^g(z)$  are piecewise polynomials of the given order  $p' = \kappa^{\max}(p+1)-1$  constructed in our previous paper [19]. Their derivative of the order  $\kappa$  at the node  $z_l$  equals one, and the derivative of the order  $\kappa' \neq \kappa$  at this node equals zero, while the values of the function  $N_\mu^g(z)$  with all its derivatives up to the order  $(\kappa^{\max}-1)$  equal zero at all other nodes  $z_{l'} \neq z_l$  of the grid  $\Omega_{h_j(z)}^p[z^{\min}, z^{\max}]$ , i.e.,  $d^\kappa N_{l'\kappa^{\max}+\kappa'}^g/dz^\kappa|_{z=z_l} = \delta_{ll'} \delta_{\kappa\kappa'}$ ,  $l = 0, \dots, np$ ,  $\kappa = 0, \dots, \kappa^{\max}-1$ .

The substitution of the expansion (18) into the variational functional (5), (6) reduces the solution of the eigenvalue *problem 1 or 3* (1)–(4) with the normalization condition (7)) or (9), or the scattering *problem 2* (1)–(4) with the fixed energy  $E$  to the solution of the algebraic problem with respect to the desired set  $\Phi^h = \{\Phi_\mu^h\}_{\mu=0}^{L-1}$ :

$$(\mathbf{A} - \mathbf{M}_{\max} + \mathbf{M}_{\min} - 2E\mathbf{B})\Phi^h = 0. \quad (19)$$



Here  $\mathbf{A}$  and  $\mathbf{B}$  are the symmetric  $L \times L$  stiffness and mass matrices,  $L = \kappa^{\max}(np + 1)$ ,

$$A_{\mu_1; \mu_2} = \int_{z^{\min}}^{z^{\max}} f_2(z) \frac{dN_{\mu_1}^g(z)}{dz} \frac{dN_{\mu_2}^g(z)}{dz} dz + \int_{z^{\min}}^{z^{\max}} f_1(z) dz N_{\mu_1}^g(z) V(z) N_{\mu_2}^g(z),$$

$$B_{l_1; l_2} = \int_{z^{\min}}^{z^{\max}} f_1(z) N_{\mu_1}^g(z) N_{\mu_2}^g(z) dz,$$

$\mathbf{M}_{\max}$  and  $\mathbf{M}_{\min}$  are  $L \times L$  the matrices with zero elements except  $M_{11} = f_2(z^{\min}) \mathcal{R}(z^{\min})$  and  $M_{L+1-\kappa^{\max}, L+1-\kappa^{\max}} = f_2(z^{\max}) \mathcal{R}(z^{\max})$ , respectively. The unknown eigenvalues  $\mathcal{R}(z^{\min})$  or  $\mathcal{R}(z^{\max})$  are determined by solving the problem (19) with the boundary conditions (4) taken into account in a way similar to [9].

The theoretical estimate for the  $\mathbf{H}^0$  norm of the difference between the exact solution  $\Phi_m(z) \in \mathcal{H}_2^2$  and the numerical one  $\Phi_m^h(z) \in \mathbf{H}^{\kappa^{\max}}$  has the order of

$$|E_m^h - E_m| \leq c_1 h^{2p'}, \quad \|\Phi_m^h(z) - \Phi_m(z)\|_0 \leq c_2 h^{p'+1}, \quad (20)$$

where  $h = \max_{1 \leq j \leq n} h_j$  is the maximal step of the grid [21].

*Remark.* To obtain the eigenvalue estimate of the order  $2p'$  the integrals are to be calculated with the same order of accuracy  $2p'$ . If the integrals are calculated with the accuracy  $p' + 1$ , then we get the estimate of the same order  $p' + 1$  both for eigenvalues and for eigenfunctions.

### 3.1 The Calculation Scheme for the Solution Matrix $\Phi^h = \Phi_{\leftarrow}^h$

In this case Eq. (19) can be written in the following form

$$(\mathbf{G} + \mathbf{M}_{\min}) \begin{pmatrix} \Phi_{\leftarrow}^a \\ \Phi_{\leftarrow}^b \end{pmatrix} \equiv \begin{pmatrix} \mathbf{G}_{\leftarrow}^{aa} & \mathbf{G}_{\leftarrow}^{ab} \\ \mathbf{G}_{\leftarrow}^{ba} & \mathbf{G}_{\leftarrow}^{bb} \end{pmatrix} \begin{pmatrix} \Phi_{\leftarrow}^a \\ \Phi_{\leftarrow}^b \end{pmatrix} = \begin{pmatrix} \mathbf{0} & \mathbf{0} \\ \mathbf{0} & \mathbf{G}(z^{\max}) \end{pmatrix} \begin{pmatrix} \Phi_{\leftarrow}^a \\ \Phi_{\leftarrow}^b \end{pmatrix}, \quad (21)$$

where  $(\mathbf{M}_{\min})_{11} = M_{11} = f_2(z^{\min}) \mathcal{R}(z^{\min})$ ,  $\mathcal{R}(z^{\min}) = \iota \sqrt{2E}$ , the solutions  $\Phi_{\leftarrow}^a$  and  $\Phi_{\leftarrow}^b \equiv \Phi_{\leftarrow}(z^{\max})$  are vectors with the dimension  $(L-1)$  and 1, respectively.

Hence the explicit expressions follow

$$\Phi_{\leftarrow}^a = -(\mathbf{G}_{\leftarrow}^{aa})^{-1} \mathbf{G}_{\leftarrow}^{ab} \Phi_{\leftarrow}^b, \quad \mathbf{G}(z^{\max}) = \mathbf{G}_{\leftarrow}^{bb} - \mathbf{G}_{\leftarrow}^{ba} (\mathbf{G}_{\leftarrow}^{aa})^{-1} \mathbf{G}_{\leftarrow}^{ab}. \quad (22)$$

Form Eqs. (21) and (22) the relation between  $\Phi_{\leftarrow}^b$  and its derivative follows

$$d\Phi_{\leftarrow}^b/dz = \mathcal{R}(z^{\max}) \Phi_{\leftarrow}^b, \quad \mathcal{R}(z^{\max}) = \mathbf{G}(z^{\max}). \quad (23)$$

Note, that the matrix  $\mathbf{G}(z^{\max})$  is defined as the inverse of the submatrix  $\mathbf{G}_{\leftarrow}^{aa}$ , the calculation of which requires significant computer resources. To solve Eq. (23) without inverting  $\mathbf{G}_{\leftarrow}^{aa}$ , let us consider the set of algebraic equations with respect to the vectors  $\mathbf{F}_{\leftarrow}^a$  и  $\mathbf{F}_{\leftarrow}^b$

$$\begin{pmatrix} \mathbf{G}_{\leftarrow}^{aa} & \mathbf{G}_{\leftarrow}^{ab} \\ \mathbf{G}_{\leftarrow}^{ba} & \mathbf{G}_{\leftarrow}^{bb} \end{pmatrix} \begin{pmatrix} \mathbf{F}_{\leftarrow}^a \\ \mathbf{F}_{\leftarrow}^b \end{pmatrix} = f_2(z^{\max}) \begin{pmatrix} \mathbf{0} \\ \mathbf{I} \end{pmatrix}. \quad (24)$$

Since the determinant of the matrix  $\mathbf{G} + \mathbf{M}_{\min}$  is nonzero, the set of equations has the unique solution

$$\mathbf{F}_{\leftarrow}^a = -(\mathbf{G}_{\leftarrow}^{aa})^{-1} \mathbf{G}_{\leftarrow}^{ab} \mathbf{F}_{\leftarrow}^b, \quad \mathbf{F}_{\leftarrow}^b = f_2(z^{\max}) (\mathbf{G}_{\leftarrow}^{bb} - \mathbf{G}_{\leftarrow}^{ba} (\mathbf{G}_{\leftarrow}^{aa})^{-1} \mathbf{G}_{\leftarrow}^{ab})^{-1}. \quad (25)$$

Then the expression for  $\mathcal{R}(z^{\max})$  follows

$$\mathcal{R}(z^{\max}) = (\mathbf{F}_{\leftarrow}^b)^{-1}. \quad (26)$$

From Eqs. (23) and (11) we get the equation for the reflection amplitude  $R_{\leftarrow}$ :

$$Y_{\leftarrow}^{(+)}(z^{\max}) R_{\leftarrow} = -Y_{\leftarrow}^{(-)}(z^{\max}), \quad Y_{\leftarrow}^{(\pm)}(z) = dX^{(\pm)}(z)/dz - \mathcal{R}(z) X^{(\pm)}(z). \quad (27)$$

Having solved this equation, we find the reflection amplitude  $R_{\leftarrow}$

$$R_{\leftarrow} = -(Y_{\leftarrow}^{(+)}(z^{\max}))^{-1} Y_{\leftarrow}^{(-)}(z^{\max}). \quad (28)$$

Then the desired solution  $\Phi_{\leftarrow}^h$  is calculated from Eqs. (11), (22), and (25)

$$\Phi_{\leftarrow}^b = X^{(-)}(z^{\max}) + X^{(+)}(z^{\max}) R_{\leftarrow}, \quad \Phi_{\leftarrow}^a = F_{\leftarrow}^a (F_{\leftarrow}^b)^{-1} \Phi_{\leftarrow}^b. \quad (29)$$

The transmission amplitude  $T_{\leftarrow}$  is determined by solving the equation

$$X^{(-)}(z^{\min}) T_{\leftarrow} = \Phi_{\leftarrow}^h(z^{\min}), \quad T_{\leftarrow} = (X^{(-)}(z^{\min}))^{-1} \Phi_{\leftarrow}^h(z^{\min}).$$

### 3.2 The Calculation Scheme for the Solution Matrix $\Phi^h = \Phi_{\rightarrow}^h$

In this case Eq. (19) can be written as follows:

$$(\mathbf{G} - \mathbf{M}_{\max}) \begin{pmatrix} \Phi_{\rightarrow}^a \\ \Phi_{\rightarrow}^b \end{pmatrix} \equiv \begin{pmatrix} \mathbf{G}_{\rightarrow}^{aa} & \mathbf{G}_{\rightarrow}^{ab} \\ \mathbf{G}_{\rightarrow}^{ba} & \mathbf{G}_{\rightarrow}^{bb} \end{pmatrix} \begin{pmatrix} \Phi_{\rightarrow}^a \\ \Phi_{\rightarrow}^b \end{pmatrix} = \begin{pmatrix} -\mathbf{G}(z^{\min}) & \mathbf{0} \\ \mathbf{0} & \mathbf{0} \end{pmatrix} \begin{pmatrix} \Phi_{\rightarrow}^a \\ \Phi_{\rightarrow}^b \end{pmatrix}, \quad (30)$$

where  $(\mathbf{M}_{\max}^p)_{LL} = M_{L+1-\kappa^{\max}, L+1-\kappa^{\max}} = f_2(z^{\max}) \mathcal{R}(z^{\max})$ ,  $\mathcal{R}(z^{\max}) = -i\sqrt{2E}$ , the solutions  $\Phi_{\rightarrow}^a$  and  $\Phi_{\rightarrow}^b \equiv \Phi_{\rightarrow}(z_{\min})$  are vectors with the dimension 1 and  $(L-1)$ , respectively.

The desired matrix  $\mathbf{G}(z^{\min}) = \mathcal{R}(z^{\min})$  is expressed as

$$\mathcal{R}(z^{\min}) = (\mathbf{F}_{\rightarrow}^a)^{-1}, \quad (31)$$

and the desired solution  $\Phi_{\rightarrow}^h$  is calculated as

$$\Phi_{\rightarrow}^b = \mathbf{F}_{\rightarrow}^b (\mathbf{F}_{\rightarrow}^a)^{-1} \Phi_{\rightarrow}^a, \quad \Phi_{\rightarrow}^a = X^{(+)}(z^{\min}) + X^{(-)}(z^{\min}) R_{\rightarrow}. \quad (32)$$

Here  $\Phi_{\rightarrow}^a \equiv \Phi_{\rightarrow}(z^{\min})$  and  $\Phi_{\rightarrow}^b$  are vectors with the dimension 1 and  $(L-1)$ . The column vectors  $\mathbf{F}_{\rightarrow}^a$  and  $\mathbf{F}_{\rightarrow}^b$  with the dimension 1 and  $(L-1)$  are solutions of the sets of algebraic equations

$$(\mathbf{G} - \mathbf{M}_{\max}) \begin{pmatrix} \mathbf{F}_{\rightarrow}^a \\ \mathbf{F}_{\rightarrow}^b \end{pmatrix} \equiv \begin{pmatrix} \mathbf{G}_{\rightarrow}^{aa} & \mathbf{G}_{\rightarrow}^{ab} \\ \mathbf{G}_{\rightarrow}^{ba} & \mathbf{G}_{\rightarrow}^{bb} \end{pmatrix} \begin{pmatrix} \mathbf{F}_{\rightarrow}^a \\ \mathbf{F}_{\rightarrow}^b \end{pmatrix} = -f_2(z^{\min}) \begin{pmatrix} \mathbf{I} \\ \mathbf{0} \end{pmatrix}. \quad (33)$$

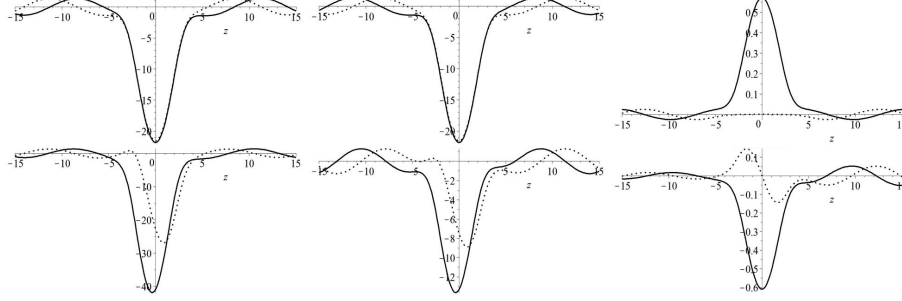


**Fig. 3.** Wave functions of the scattering problem for the first resonance value of energy  $2E_1^{\max T}$ , corresponding to the full transparency, i.e., the maximal transmission coefficient, for  $\Phi_{\rightarrow}$  (left-hand panels) and  $\Phi_{\leftarrow}$  (central panels); the functions of resonance metastable states with the energies  $2E_1^T$  (right-hand panels), respectively, given in Table 3. The upper panels refer to the system of two real Scarf potentials with  $V_1 = 2$ ,  $V_2 = 0$ , the lower panels refer to the system of two complex Scarf potentials with  $V_1 = 2$ ,  $V_2 = 1$ . Solid and dotted lines show the real and imaginary parts of the wave functions, respectively.

Finally, we arrive at the following equations for the amplitudes of reflection  $R_{\rightarrow}$  and transmission  $T_{\rightarrow}$ :

$$Y_{\rightarrow}^{(-)}(z^{\min})R_{\rightarrow} = -Y_{\rightarrow}^{(+)}(z^{\min}), \quad X^{(+)}(z^{\max})T_{\rightarrow} = \Phi_{\rightarrow}^h(z^{\max}). \quad (34)$$

$$Y_{\rightarrow}^{(\pm)}(z) = \frac{dX^{(\pm)}(z)}{dz} - \mathcal{R}(z)X^{(\pm)}(z), \quad (35)$$

The amplitudes of reflection  $R_{\rightarrow}$  and transmission  $T_{\rightarrow}$  take the form

$$R_{\rightarrow} = -\left(Y_{\rightarrow}^{(-)}(z^{\min})\right)^{-1} Y_{\rightarrow}^{(+)}(z^{\min}), \quad T_{\rightarrow} = \left(X^{(+)}(z^{\max})\right)^{-1} \Phi_{\rightarrow}^h(z^{\max}).$$

### 3.3 Algorithm for Calculating the Complex Eigenvalues and Eigenfunctions of Metastable States

To calculate a complex eigenvalue and the corresponding eigenfunction a discrete problem is solved for the equation

$$\mathcal{F}(u) = 0, \quad \Leftrightarrow \quad \{ \mathcal{F}_1(u) = 0, \quad \mathcal{F}_2(u) = 0 \} \quad (36)$$

with respect to the pair of unknowns  $u = \{E^h, \Phi^h\}$ , where  $\mathcal{F}_1(u)$  and  $\mathcal{F}_2(u)$  are given by the expressions

$$\mathcal{F}_1(u) = [\mathbf{A} - 2E^h\mathbf{B} + \mathbf{M}_{\min}(E^h) - \mathbf{M}_{\max}(E^h)] \Phi^h, \quad \mathcal{F}_2(u) = (\Phi^h)^T \mathcal{F}_1(u).$$

The transition from the approximate solution  $u_k$  to the approximate solution  $u_{k+1}$  is given by the formulas

$$\begin{aligned} 2E_{k+1}^h &= 2E_k^h + \mu_k \tau_k, \quad \Phi_{k+1}^h = \Phi_k^h + \mathbf{v}_k \tau_k, \\ \mathbf{v}_k &= \mathbf{v}_k^{(1)} + \mathbf{v}_k^{(2)} \mu_k, \quad \Phi_{k+1}^h = \Phi_{k+1}^h ((\Phi_{k+1}^h)^T \mathbf{B} \Phi_{k+1}^h)^{-1/2}, \end{aligned} \quad (37)$$

where  $2E_{k=0} = 2E_0$ ,  $\Phi_{k=0}^h = \Phi_0$  is the initial approximation from the vicinity of the solution  $2E = 2E_*$ ,  $\Phi^h = \Phi_*$ . The iteration corrections  $\mathbf{v}_k^{(1)}$ ,  $\mathbf{v}_k^{(2)}$  are found by solving the inhomogeneous algebraic problems

$$\mathcal{F}_1(E_k^h, \mathbf{v}_k^{(1)}) = -\mathcal{F}_1(E_k^h, \Phi_k^h) = -\mathcal{F}_1(u_k), \quad \Rightarrow \quad \mathbf{v}_k^{(1)} = -\Phi_k^h, \quad (38)$$

$$\mathcal{F}_1(E_k^h, \mathbf{v}_k^{(2)}) = \left( \mathbf{B} - \frac{d\mathbf{M}_{\min}(E_k^h)}{2dE_k^h} + \frac{d\mathbf{M}_{\max}(E_k^h)}{2dE_k^h} \right) \Phi_k^h, \quad (39)$$

and the correction  $\mu_k$  to the eigenvalue  $E_k^h$  is found using the formula

$$\mu_k = \frac{\mathcal{F}_2(E_k^h, \Phi_k^h)}{(\Phi_k^h)^T \mathbf{B} \Phi_k^h} = \frac{(\Phi_k^h)^T \mathcal{F}_1(E_k^h, \Phi_k^h)}{(\Phi_k^h)^T \mathbf{B} \Phi_k^h}.$$

that follows from Eq. (36). The expressions for nonzero elements of  $\mathbf{M}_{\min}(E_k^h)$ ,  $\mathbf{M}_{\max}(E_k^h)$ , and their derivatives by  $2E_k^h$  have the form ( $L' = L + 1 - \kappa^{\max}$ )

$$\begin{aligned} (\mathbf{M}_{\min}(E_k^h))_{11} &= -f_2(z^{\min})\sqrt{-2E_k^h}, \quad (\mathbf{M}_{\max}(E_k^h))_{L',L'} = f_2(z^{\max})\sqrt{-2E_k^h}, \\ \frac{d(\mathbf{M}_{\min}(E_k^h))_{11}}{d(2E_k^h)} &= \frac{f_2(z^{\min})}{2\sqrt{-2E_k^h}}, \quad \frac{d(\mathbf{M}_{\max}(E_k^h))_{L',L'}}{d(2E_k^h)} = -\frac{f_2(z^{\max})}{2\sqrt{-2E_k^h}}. \end{aligned}$$

The iteration step  $\tau_k$  in the vicinity of the solution is equal to one, and the optimal step  $\tau_k$  is calculated using the formula [24]

$$\tau_k = \max(\theta, \delta_k(0)/(\delta_k(0) + \delta_k(1))), \quad \theta = 0.1.$$

Here  $\delta_k(0) = |\mathcal{F}_1(E_k^h, \Phi_k^h)|^2$  and  $\delta_k(1) = |\mathcal{F}_1(E_{k+1}^h, \Phi_{k+1}^h)|^2$  are the residuals and  $E_{k+1}$  и  $\Phi_{k+1}^h$  are calculated using Eqs. (37) at  $\tau_k = 1$ . In all cases  $\theta < \tau_k < 1$ . The iteration process (37) is terminated when the condition  $|\mathcal{F}_2(E_k^h, \Phi_k^h)|^2 < \varepsilon$  becomes valid, where  $\varepsilon > 0$  is the predetermined accuracy of the approximate solution calculation.

## 4 Benchmark Calculations

As an example, let us consider the Schrödinger equation (1) at  $f_1(z) = f_2(z) = 1$  with the complex Scarf potential on the axis  $z \in (-\infty, +\infty)$ :

$$V_{Scarf}(z) = V_1 \cosh^{-2} z + iV_2 \sinh z \cosh^{-2} z. \quad (40)$$

*Problem 1.* For  $V_1 < 0$  and  $V_2^2 \in \mathcal{R}$  the bound state problem has a finite set of known analytic solutions [12]. At  $|V_2| < 1/4 - V_1$  the eigenvalues are essentially complex conjugate pairs:

$$E_n^\pm = -\left(n - (g_+^* \pm i g_-^* - 1)/2\right)^2, \quad g_\pm^* = \sqrt{1/4 - V_1 \mp V_2}, \quad n=0, 1, \dots, (g_+^* - 1)/2. \quad (41)$$

At  $|V_2| > 1/4 - V_1$  (or when  $V_2$  is imaginary) the eigenvalues are real:

$$E_n = -\left(n - (g_+^* + g_-^* - 1)/2\right)^2, \quad n=0, 1, \dots, (g_+^* + g_-^* - 1)/2. \quad (42)$$

**Table 1.** Eigenvalues  $E_1^\pm$ ,  $E_1$  and their differences from the corresponding analytic values calculated using the grid  $(-20(N_1) - 4(N_2)4(N_3)20)$  with the number  $N_1=N_2=N_3$  of the eighth-order finite elements ( $\kappa_{\max}=3$ ,  $p=2$ ) in each of the subintervals, depending on  $N_1$ . The last row presents the analytic values and the Runge coefficient (43).

$N_1$	$V_1 = -2, V_2 = -3$		$V_1 = -2, V_2 = -1$	
4	$-0.229080666 \pm 0.559461207^*I$	$2.8E-4 \mp 3.1E-4^*I$	$-0.921836165$	$5.4E-4 + 6E-14^*I$
8	$-0.229357025 \pm 0.559142713^*I$	$-9.5E-7 \pm 1.3E-6^*I$	$-0.922378370$	$-9.6E-7 - 6E-13^*I$
16	$-0.229356076 \pm 0.559144037^*I$	$3E-10 \pm 2.5E-9^*I$	$-0.922377406$	$-6E-10 - 3E-11^*I$
ext	$-0.229356076 \pm 0.559144040^*I$	$Ru = 8.005$	$-0.922377405$	$Ru = 9.130$

**Table 2.** Dependence of the coefficients of transmission  $T$ , reflection  $R$ , and absorption  $A$  calculated using the grid  $(-20(N_1)20)$  upon the number  $N_1$  of the eighth-order finite elements ( $\kappa_{\max} = 3$ ,  $p = 2$ ) for  $V_1 = 2$ ,  $V_2 = 2$ ,  $k = 2E = 1$ . The last two rows present the analytical solution and the Runge coefficient (43).

$N_1$	Digits	$T_{\rightarrow}$	$R_{\rightarrow}$	$A_{\rightarrow}$
20	16	0.6005954018870188	0.0007394643169153872	0.3986651337960658
40	16	0.5984475588608321	0.0007498888028424546	0.4008025523363254
80	16	0.5984514912751766	0.0007498689244704378	0.4007986398003530
80	8	0.59845983	0.00074979961	0.4007903704
ext		0.5984515130037975	0.0007498688034693990	0.4007986181927332
$Ru$	16	9.088	9.029	9.088

The numerical experiments using the finite-element grid  $\Omega_{h_j(z)}^p[z^{\min}, z^{\max}]$  demonstrated strict correspondence to the theoretical estimations (20) for both eigenvalues and eigenfunctions. In particular, we calculated the Runge coefficients

$$\beta_l = \log_2 \left| (\sigma_l^h - \sigma_l^{h/2}) / (\sigma_l^{h/2} - \sigma_l^{h/4}) \right|, \quad l = 1, 2, \quad (43)$$

on three twice condensed grids with the absolute errors

$$\sigma_1^h = |F(E_m^{exact}) - F(E_m^h)|, \quad \sigma_2^h = \max_{z \in \Omega^h(z)} |\Phi_m^{exact}(z) - \Phi_m^h(z)| \quad (44)$$

for the eigenvalues and eigenfunctions, respectively. From Eq. (44) we obtained the numerical assessment of the convergence order  $Ru \sim 8 \div 9$  of the proposed numerical schemes (shown for  $F(E) = E$  in Table 1 and for  $F(E) = T_{\rightarrow}, R_{\rightarrow}, A_{\rightarrow}$  in Table 2), the theoretical estimates being  $\beta_1 = p' + 1$  and  $\beta_2 = p' + 1$ , in accordance with the *Remark* following Eq. (20).

*Problem 2.* For the scattering problem with fixed real-valued energy  $2E = k^2 > 0$  and the complex Scarf potential (40) the coefficients of transmission  $|T|^2$  and reflection  $|R|^2$  are expressed as

$$\begin{aligned}
|R_{\rightarrow}|^2 &= D_{\rightarrow}/D, \quad |R_{\leftarrow}|^2 = D_{\leftarrow}/D, \quad |T_{\rightarrow}|^2 = |T_{\leftarrow}|^2 = \sinh^2(2\pi k)/D, \\
D_{\rightarrow} &= (2 \cosh(\pi g_+) \cosh(\pi g_-) + \cosh^2(\pi g_+) e^{-2\pi k} + \cosh^2(\pi g_-) e^{2\pi k}), \\
D_{\leftarrow} &= (2 \cosh(\pi g_+) \cosh(\pi g_-) + \cosh^2(\pi g_+) e^{2\pi k} + \cosh^2(\pi g_-) e^{-2\pi k}), \\
D &= \sinh^2(2\pi k) + 2 \cosh(2\pi k) \cosh(\pi g_+) \cosh(\pi g_-) + \cosh^2(\pi g_+) + \cosh^2(\pi g_-).
\end{aligned} \tag{45}$$

Here the notation  $g_{\pm} = \sqrt{V_1 \pm V_2 - 1/4}$  is used. It has been proved [11] that when the potential is complex and spatially non-symmetric, the reflectivity depends on whether the particle is incident from the left or the right side. For the complex potential scattering with the fixed real  $E > 0$  the conditions (15) are modified as follows:

$$|R_{\rightarrow}|^2 + |T_{\rightarrow}|^2 = 1 - A_{\rightarrow}, \quad |R_{\leftarrow}|^2 + |T_{\leftarrow}|^2 = 1 - A_{\leftarrow}, \quad T_{\rightarrow} = T_{\leftarrow} \equiv T.$$

For the complex Scarf potential  $A_{\rightarrow}$  and  $A_{\leftarrow}$  are expressed as

$$A_{\rightarrow} = \frac{s_+ s_- - s_-^2}{1 + s_+ s_-}, \quad A_{\leftarrow} = \frac{s_+ s_- - s_+^2}{1 + s_+ s_-}, \quad s_{\pm} = \frac{\cosh(\pi g_+) e^{\pm \pi k} + \cosh(\pi g_-) e^{\mp \pi k}}{\sinh(2\pi k)}. \tag{46}$$

Here we consider only positive values  $A_{\rightarrow} > 0$  (or  $A_{\leftarrow} > 0$ ), commonly interpreted as the probability of absorption [11, 13].

The *Problem 1* of determining the eigenvalues  $E_m^h$  and the corresponding eigenfunctions  $\Phi_m^h(z)$  for Eq. (19) was solved using the built-in package LinearAlgebra of the Maple system. Table 1 presents the dependence of the eigenvalues calculated using the grid  $(-20(N_1) - 4(N_2)4(N_3)20)$  with the number  $N_1 = N_2 = N_3$  of the eighth-order finite elements ( $\kappa_{\max} = 3$ ,  $p = 2$ ) in each of the subintervals upon  $N_1$ . One can see that these sequences converge to the analytical results (41) and (42). The behaviour of the eigenfunctions  $\Phi_m^h(z)$  is illustrated by Fig. 1. The time of computing the auxiliary integrals is nearly 42 seconds, the time of constructing the matrices and solving the algebraic eigenvalue problem at  $N = 16$  amounts to 4.5 seconds. Table 2 illustrates the dependence of the coefficients of transmission  $T$ , reflection  $R$ , and absorption  $A$  calculated using the grid  $(-20(N_1)20)$  upon the number  $N_1$  of the eighth-order finite elements ( $\kappa_{\max} = 3$ ,  $p = 2$ ). One can see that these sequences converge to the analytical results (45) and (46). The time of constructing the matrices and solving the algebraic problem for  $N_1 = 20$  and  $N_1 = 80$  (Digits:=16) amounts to 5 and 22 seconds, respectively, and for  $N_1 = 80$  Digits:=8 this time is 5 seconds.

For a system of multiple barrier Scarf potentials separated from each other the approximate analytic expressions for the coefficients of transmission, reflection, and absorption are also available. In particular, for a system of two Scarf potential the analytic expressions are presented in Ref. [13].

The scattering *Problem 2* with Eqs. (21) and (30) was solved following the algorithm of Sections 3.1 and 3.2 and using the built-in package LinearAlgebra of the Maple system using the finite-element grid  $(-8(N_1 = 40)8)$  c  $N_1$  with Hermite eighth-order finite elements ( $\kappa_{\max} = 3$ ,  $p = 2$ ). The dependence upon  $k$  for the coefficients of transmission, reflection, and absorption, calculated with the absolute accuracy 0.001, in the system of two Scarf potentials with  $V_1 = 2$ ,

**Table 3.** The first resonance energy values  $2E_i^{\max T}$  for the maximal transmission coefficient (full transparency) and the eigenvalues  $2E_i^r$  of resonance metastable states.

Scarf	$V_1 = 2$	$2E_1^{\max T} = 0.310918$	$2E_1^r = 0.31093782 - i0.00069129$
	$V_2 = 0$	$2E_2^{\max T} = 1.025359$	$2E_2^r = 1.02413913 - i0.01733149$
	$V_1 = 2$	$2E_1^{\max T} = 0.360240$	$2E_1^r = 0.36025570 - i0.00103794$
	$V_2 = 1$	$2E_2^{\max T} = 1.036324$	$2E_2^r = 1.03383748 - i0.02383030$
Steps/ wells	$V_1 = 2$	$2E_1^{\max T} = 0.329476$	$2E_1^r = 0.32921557 - i0.00247662$
	$V_2 = 0$	$2E_2^{\max T} = 1.254400$	$2E_2^r = 1.25175270 - i0.03351010$
	$V_1 = 2$	$2E_1^{\max T} = 0.331776$	$2E_1^r = 0.33292316 - i0.00247662$
	$V_2 = 1/2$	$2E_2^{\max T} = 1.263376$	$2E_2^r = 1.26054650 - i0.03359483$

$V_2 = 1$  separated by the interval  $d = 7/2$ , is presented in the upper panel of Fig. 2. The resonance structure of the transmission coefficient is due to the presence of metastable states submerged in the continuous spectrum.

*Problem 3.* The complex eigenvalues and the corresponding eigenfunctions of the metastable states are calculated by means of the Newton iteration algorithm of Section 3.3 using the built-in package LinearAlgebra of the Maple system. For the initial approximation we used both the solutions of the bound-state *Problem 1* and the solutions of the scattering *Problem 2* with the resonance values of energy  $E = E^r$ , corresponding to the peaks of the transmission coefficient.

For the system of two real- and complex-valued Scarf potentials Fig. 3 presents the wave functions of the scattering problem for the first resonance state, corresponding to the maximal transmission coefficient (full transparency), and the functions of a resonance metastable state. The first resonance energy values  $2E_i^{\max T}$  corresponding to the maximal transmission coefficient (full transparency) and the eigenvalues  $2E_i^r$  of the resonance metastable states are shown in Table 3. The calculations were performed using the grid  $(-8(N_1 = 40)8)$  with  $N_1$  Hermite eighth-order finite elements ( $\kappa_{\max} = 3$ ,  $p = 2$ ).

In a similar way the piecewise continuous potentials are considered, in particular, the systems of potential steps/wells with rectangular-shaped walls. The latter problem can be solved analytically. The lower panel of Fig. 2 presents the approximation of the system of two Scarf potentials with a system of potential steps/wells. As seen from Fig. 2, with the increase of the wave number  $k$  the transmission, reflection, and absorption coefficients differ stronger. The calculations were performed using the grid  $(-7(N_1=10)-2-7/4(N_2=3)-2-7/8(N_3=3)-2(N_4=20)2(N_5=3)2+7/8(N_6=3)2+7/4(N_7=10)7)$  with  $N_i$  ( $i = 1, \dots, 7$ ) Hermite seventh-order finite elements ( $\kappa_{\max}=2$ ,  $p = 3$ ). The eigenvalues for the system of real and complex potential steps/wells (see Table 3) qualitatively agree with the results presented in the above paragraph. The scattering wave functions for the first two resonance energy values and for the resonance metastable states behave qualitatively similar to those of the system of Scarf potentials, and for this reason are not presented here.

## 5 Conclusion

The presented analysis of solving the eigenvalue problem, the scattering problem, and the calculation of resonance metastable states for the Schrödinger equation with continuous and piecewise continuous real-valued and complex potentials demonstrated the efficiency of the developed algorithms and programs, implemented in the Maple computer algebra system. The algorithm conserves the derivative continuity property, inherent in the desired solution, in the approximating numeric solution, defined on the finite-element grid using the Hermite interpolating elements.

Further development of the proposed algorithms and programs is targeted at the solution of the problems that describe the scattering processes in the quantum-dimensional semiconductor systems and smoothly irregular waveguides with piecewise continuous real-valued and complex coefficient functions in the partial differential equations, which require the continuity of not only the solution itself, but also of its first derivative.

The authors thank Prof. V.P. Gerdt for collaboration and support of this work. The work was partially supported by the Russian Foundation for Basic Research (RFBR) (grants No. 14-01-00420 and 13-01-00668) and the Bogoliubov-Infeld program.

## References

1. Kotlyar, V.V., Kovalev, A.A., Nalimov, A.G.: Gradient microoptical elements for achieving superresolution. *Kompyuternaya optika* **33**, 369–378 (2009). (in Russian)
2. Rezanur Rakhman, K.M., Sevastyanov, L.A.: One-dimensional scattering problem at stepwise potential with non-coincident asymptotic forms. *Vestnik RUDN, ser. Fizika* No. 5 (1), 35–38 (1997) (in Russian)
3. Sevastyanov, L.A., Sevastyanov, A.L., Tyutyunnik, A.A.: Analytical calculations in maple to implement the method of adiabatic modes for modelling smoothly irregular integrated optical waveguide structures. In: Gerdt, V.P., Koepf, W., Seiler, W.M., Vorozhtsov, E.V. (eds.) *CASC 2014. LNCS*, vol. 8660, pp. 419–431. Springer, Heidelberg (2014)
4. Chuluunbaatar, O., Gusev, A.A., Gerdt, V.P., Kaschiev, M.S., Rostovtsev, V.A., Samoylov, V., Tupikova, T., Vinitsky, S.I.: A symbolic-numerical algorithm for solving the eigenvalue problem for a hydrogen atom in the magnetic field: cylindrical coordinates. In: Ganzha, V.G., Mayr, E.W., Vorozhtsov, E.V. (eds.) *CASC 2007. LNCS*, vol. 4770, pp. 118–133. Springer, Heidelberg (2007)
5. Gusev, A.A., Chuluunbaatar, O., Gerdt, V.P., Rostovtsev, V.A., Vinitsky, S.I., Derbov, V.L., Serov, V.V.: Symbolic-numeric algorithms for computer analysis of spheroidal quantum dot models. In: Gerdt, V.P., Koepf, W., Mayr, E.W., Vorozhtsov, E.V. (eds.) *CASC 2010. LNCS*, vol. 6244, pp. 106–122. Springer, Heidelberg (2010)
6. Gusev, A.A., Vinitsky, S.I., Chuluunbaatar, O., Gerdt, V.P., Rostovtsev, V.A.: Symbolic-numerical algorithms to solve the quantum tunneling problem for a coupled pair of ions. In: Gerdt, V.P., Koepf, W., Mayr, E.W., Vorozhtsov, E.V. (eds.) *CASC 2011. LNCS*, vol. 6885, pp. 175–191. Springer, Heidelberg (2011)



7. Vinitzky, S., Gusev, A., Chuluunbaatar, O., Rostovtsev, V., Le Hai, L., Derbov, V., Krassovitskiy, P.: Symbolic-numerical algorithm for generating cluster eigenfunctions: tunneling of clusters through repulsive barriers. In: Gerdt, V.P., Koepf, W., Mayr, E.W., Vorozhtsov, E.V. (eds.) CASC 2013. LNCS, vol. 8136, pp. 427–442. Springer, Heidelberg (2013)
8. Vinitzky, S., Gusev, A., Chuluunbaatar, O., Le Hai, L., Gózdź, A., Derbov, V., Krassovitskiy, P.: Symbolic-numeric algorithm for solving the problem of quantum tunneling of a diatomic molecule through repulsive barriers. In: Gerdt, V.P., Koepf, W., Seiler, W.M., Vorozhtsov, E.V. (eds.) CASC 2014. LNCS, vol. 8660, pp. 472–490. Springer, Heidelberg (2014)
9. Gusev, A.A., Chuluunbaatar, O., Vinitzky, S.I., Abrashkevich, A.G.: KANTBP 3.0: New version of a program for computing energy levels, reflection and transmission matrices, and corresponding wave functions in the coupled-channel adiabatic approach. *Comput. Phys. Commun.* **185**, 3341–3343 (2014)
10. Molinàs-Mata, P., Molinàs-Mata, P.: Electron absorption by complex potentials: One-dimensional case. *Phys. Rev. A* **54**, 2060–2065 (1996)
11. Ahmed, Z.: Schrödinger transmission through one-dimensional complex potentials. *Phys. Rev. A* **64**, 042716 (2001)
12. Ahmed, Z.: Real and complex discrete eigenvalues in an exactly solvable one-dimensional complex PT -invariant potential. *Phys. Lett. A* **282**, 343–348 (2001)
13. Cerveró, J.M., Rodríguez, A.: Absorption in atomic wires. *Phys. Rev. A* **70**, 052705 (2004)
14. Muga, J.G., Palao, J.P., Navarro, B., Egusquiza, I.L.: Complex absorbing potentials. *Phys. Reports* **395**, 357–426 (2004)
15. Cannata, F., Dedonder, J.-P., Ventura, A.: Scattering in PT-symmetric quantum mechanics. *Annals of Physics* **322**, 397–433 (2007)
16. Becker, E.B., Carey, G.F., Oden, T.J.: *Finite elements. An introduction*, vol. I. Prentice-Hall Inc., Englewood Cliffs (1981)
17. Ram-Mohan, R.L.: *Finite Element and Boundary Element Applications in Quantum Mechanics*. Oxford University Press, New York (2002)
18. Amodio, P., Blinkov, Y., Gerdt, V., La Scala, R.: On consistency of finite difference approximations to the navier-stokes equations. In: Gerdt, V.P., Koepf, W., Mayr, E.W., Vorozhtsov, E.V. (eds.) CASC 2013. LNCS, vol. 8136, pp. 46–60. Springer, Heidelberg (2013)
19. Gusev, A.A., Chuluunbaatar, O., Vinitzky, S.I., Derbov, V.L., Gózdź, A., Le Hai, L., Rostovtsev, V.A.: Symbolic-numerical solution of boundary-value problems with self-adjoint second-order differential equation using the finite element method with interpolation hermite polynomials. In: Gerdt, V.P., Koepf, W., Seiler, W.M., Vorozhtsov, E.V. (eds.) CASC 2014. LNCS, vol. 8660, pp. 138–154. Springer, Heidelberg (2014)
20. Berezin, I.S., Zhidkov, N.P.: *Computing Methods*, vol. I. Pergamon Press, Oxford (1965)
21. Strang, G., Fix, G.J.: *An Analysis of the Finite Element Method*. Prentice-Hall, Englewood Cliffs (1973)
22. Kukulin, V.I., Krasnopol'sky, V.M., Horáček, J.: *Theory of Resonances*, pp. 107–112. Academia, Praha (1989)
23. Siegert, A.J.F.: On the derivation of the dispersion formula for nuclear reactions. *Phys. Rev.* **56**, 750–752 (1939)
24. Ermakov, V.V., Kalitkin, N.N.: The optimal step and regularization for Newton's method. *USSR Computational Mathematics and Mathematical Physics* **21**, 235–242 (1981)

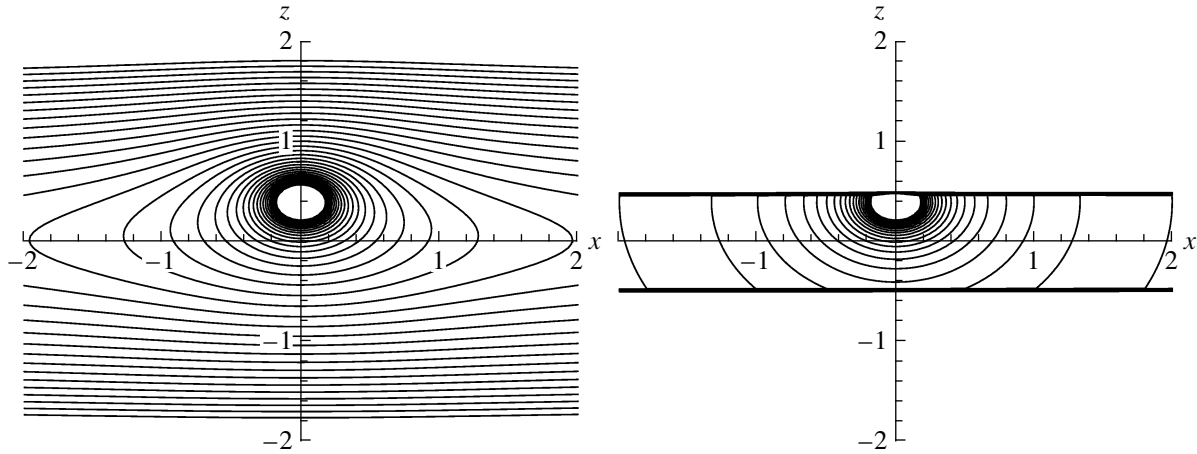


**Fig. 1.** Isolines of potential energy surface as function of two independent variables  $\bar{\rho}, \bar{z}$  with shift of center of Coulomb potential along variable  $\bar{z}$  on  $\bar{z}_c = 0.4$ . Left panel: Model A for values of parameters  $m_z = 0, Z = 1$  and  $\bar{\omega} = 3$ . Right panel: Model B for values of parameters  $m_z = 0, Z = 1$ , and  $\bar{L} = 1$ .

$$+ U(z, \rho) \Big] \psi_{m_z}(z, \rho) = E \psi_{m_z}(z, \rho).$$

Here,  $E$  is the energy of the discrete spectrum,  $U(z, \rho)$  is the quantum well potential taken as the sum of the confining potential  $V_{\text{conf}}(z)$ , depending on the longitudinal coordinate  $z$ , and the Coulomb potential (see Fig. 1)

$$U(z, \rho) = V_{\text{conf}}(z) - \frac{Ze^2}{\varepsilon_d \sqrt{(z - z_c)^2 + \rho^2}},$$

where  $m^* = \beta m_e$  is the reduced mass,  $Z$  is the reduced Coulomb charge,  $z_c$  is the shift of the Coulomb center along  $z$ ,  $\varepsilon_d$  is the relative dielectric constant. The confining potential is chosen as the potential  $V_A(z)$  of a harmonic oscillator having the frequency  $\omega$  (Model A):

$$V_{\text{conf}}(z) = V_A(z) = \frac{m^* \omega^2}{2} z^2$$

or as an infinitely deep potential well with vertical wall  $V_B(z)$  (Model B):

$$V_{\text{conf}}(z) = V_B(z) = \begin{cases} 0, & |z| < L/2, \\ +\infty, & |z| \geq L/2. \end{cases}$$

At a fixed value of the magnetic quantum number  $m_z$  the wave functions  $\psi_{m_z}(z, \rho) \equiv \psi_{m_z i}(z, \rho) \in W_2^1(\Omega)$  [10] of the discrete spectrum satisfy the normalization condition

$$\begin{aligned} & \langle \psi_{m_z i}(z, \rho) | \psi_{m_z j}(z, \rho) \rangle_{\Omega_{\bar{z}}} \\ &= \int_0^{+\infty} \int_{-\infty}^{+\infty} \psi_{m_z i}(z, \rho) \psi_{m_z j}(z, \rho) \rho d\rho dz = \delta_{ij}. \end{aligned} \quad (2)$$

Let us introduce the new independent variables  $\bar{\rho} = \rho/a_0^*$ ,  $\bar{z} = z/a_0^*$  and the notations  $\bar{z}_c = z_c/a_0^*$ ,  $2\bar{E} = E/R_0^*$ , where  $a_0^* = (\varepsilon_d/\beta)a_0$  and  $R_0^* \equiv \text{Ry}^* = m^* e^4 / (2\hbar^2) = \text{Ry} \beta / (\varepsilon_d^2)$  are the reduced atomic units,  $m^* = \beta m_e$  is the effective mass,  $e^* = e/\sqrt{\varepsilon_d}$  is the effective charge,  $a_0 = \hbar^2 / (m_e e^2)$ ,  $\omega = \gamma \hbar / (m_e \beta L^2)$ ,  $L = a_0^* \bar{L}$ ,  $\bar{\omega} = \gamma / \bar{L}^2$ ,  $\bar{\omega} = \hbar / (a_0^{*2} m^*) \bar{\omega}$ ,  $\text{Ry} = m_e e^4 / (2\hbar^2)$ .

In the reduced atomic units the Schrödinger equation, describing the Models A and B, takes the form

$$\left[ -\frac{1}{\bar{\rho}} \frac{\partial}{\partial \bar{\rho}} \bar{\rho} \frac{\partial}{\partial \bar{\rho}} + \frac{m_z^2}{\bar{\rho}^2} - \frac{\partial^2}{\partial \bar{z}^2} + \bar{\omega}^2 (\bar{z})^2 \right. \quad (3)$$

$$\left. - \frac{2Z}{\sqrt{(\bar{z} - \bar{z}_c)^2 + \bar{\rho}^2}} - 2\bar{E} \right] \psi_{m_z}(\bar{z}, \bar{\rho}) = 0,$$

$$\left[ -\frac{1}{\bar{\rho}} \frac{\partial}{\partial \bar{\rho}} \bar{\rho} \frac{\partial}{\partial \bar{\rho}} + \frac{m_z^2}{\bar{\rho}^2} - \frac{\partial^2}{\partial \bar{z}^2} \right. \quad (4)$$

$$\left. - \frac{2Z}{\sqrt{(\bar{z} - \bar{z}_c)^2 + \bar{\rho}^2}} - 2\bar{E} \right] \psi_{m_z}(\bar{z}, \bar{\rho}) = 0,$$

where the wave function  $\psi_{m_z}(\bar{z}, \bar{\rho}) \equiv \psi_{m_z i}(\bar{z}, \bar{\rho}; \bar{z}_c)$  at fixed  $m_z$  obeys the conditions at the boundary of the domain  $\Omega_{\bar{z}, \bar{\rho}} = \Omega(\bar{z}, \bar{\rho})$

$$\lim_{\bar{\rho} \rightarrow 0} \bar{\rho} \frac{\partial \psi_{m_z}(\bar{z}, \bar{\rho})}{\partial \bar{\rho}} = 0, \quad \text{if } m = 0, \quad (5)$$

$$\text{and } \psi_{m_z}(\bar{z}, 0) = 0, \quad \text{if } m \neq 0,$$

$$\lim_{\bar{z} \rightarrow \pm \infty} \psi_{m_z}(\bar{z}, \bar{\rho}) = 0 \rightarrow \leftarrow \psi_{m_z}(\bar{z}_{\min}, \bar{\rho}) = 0, \quad (6)$$

$$\psi_{m_z}(\bar{z}_{\max}, \bar{\rho}) = 0,$$

$$\psi_{m_z}(\bar{z}_{\min} = -\bar{L}/2, \bar{\rho}) = 0, \quad (7)$$

$$\psi_{m_z}(\bar{z}_{\max} = \bar{L}/2, \bar{\rho}) = 0.$$

The wave functions of the discrete spectrum at large  $\bar{\rho} = \bar{\rho}_{\max} \gg 1$  satisfy the Dirichlet boundary condition following the asymptotic form of the solution

$$\lim_{\bar{\rho} \rightarrow +\infty} \bar{\rho} \psi_{m_z}(\bar{z}, \bar{\rho}) = 0 \rightarrow \psi_{m_z}(\bar{z}, \bar{\rho}_{\max}) = 0 \quad (8)$$

and the normalization condition

$$(a_0^*)^3 \int_{\bar{z}_{\min}}^{\bar{z}_{\max}} \int_0^{\bar{\rho}_{\max}} \psi_{m_z i}(\bar{z}, \bar{\rho}) \psi_{m_z j}(\bar{z}, \bar{\rho}) \bar{\rho} d\bar{\rho} d\bar{z} = \delta_{ij}. \quad (9)$$

The solution of the problem (1), (2) is sought in the form of the expansion with respect to the set of single-parameter functions  $B_j(\bar{z}; \bar{\rho})$ :

$$\psi_{m_z i}(\bar{z}, \bar{\rho}) = \sum_{j=1}^{j_{\max}} B_j(\bar{z}; \bar{\rho}) \chi_{ji}(\bar{\rho}). \quad (10)$$

Here the vector functions  $\chi_{ji}(\bar{\rho})$  are to be found, while the basis functions  $B_j(\bar{z}; \bar{\rho})$  are defined as the solutions of the boundary-value problem

$$\left[ -\frac{\partial^2}{\partial \bar{z}^2} + \bar{\omega}^2 \bar{z}^2 - \frac{2Z}{\sqrt{(\bar{z} - \bar{z}_c)^2 + \bar{\rho}^2}} \right] \quad (11)$$

$$\times B_j(\bar{z}; \bar{\rho}) = \bar{E}_j(\bar{\rho}) B_j(\bar{z}; \bar{\rho}),$$

$$\left[ -\frac{\partial^2}{\partial \bar{z}^2} - \frac{2Z}{\sqrt{(\bar{z} - \bar{z}_c)^2 + \bar{\rho}^2}} \right] B_j(\bar{z}; \bar{\rho}) = \bar{E}_j(\bar{\rho}) B_j(\bar{z}; \bar{\rho}). \quad (12)$$

The eigenfunctions  $B_j(\bar{z}; \bar{\rho})$  at each fixed value of the parameter  $\bar{\rho} \in \mathbf{R}_+^1$ , obey the Dirichlet boundary conditions with respect to the variable  $\bar{z}$ :

$$B_j(\bar{z}; \bar{\rho})|_{\bar{z}=\bar{z}_{\min}} = 0, \quad B_j(\bar{z}; \bar{\rho})|_{\bar{z}=\bar{z}_{\max}} = 0, \quad (13)$$

and satisfy the orthogonality and normalization conditions in the interval  $\Omega_{\bar{z}} = [\bar{z}_{\min}, \bar{z}_{\max}]$ :

$$\begin{aligned} & \langle B_i(\bar{z}; \bar{\rho}) | B_j(\bar{z}; \bar{\rho}) \rangle_{\Omega} \\ &= a_0^* \int_{\bar{z}_{\min}}^{\bar{z}_{\max}} B_i(\bar{z}; \bar{\rho}) B_j(\bar{z}; \bar{\rho}) d\bar{z} = \delta_{ij}. \end{aligned} \quad (14)$$

Note, that due to the singular behavior of the one-dimensional Coulomb potential in the vicinity of  $\bar{z} = \bar{z}_c$  the eigenfunctions  $B_j(\bar{z}; \bar{\rho}) \in F_{\bar{\rho}} \sim L_2[\bar{z}_{\min}, \bar{z}_{\max}]$  of the problem (11)–(14) at  $\bar{\rho} = 0$  have only generalized partial derivatives of the first order, i.e., belong to Sobolev space  $B_j(\bar{z}; \bar{\rho}) \in W_2^1[\bar{z}_{\min}, \bar{z}_{\max}]$  [10, 11]. The Model A is considered in configuration space  $\mathbf{R}^3$  with an additional oscillator potential providing a confinement along  $z$ -axis and is known in literature as *parabolic quantum well* [1], while the Model B is considered explicitly in quasi-2D space  $\mathbf{R}^2 \otimes$

$[-\bar{L}/2, \bar{L}/2]$ , and is known in literature as *quantum well* [2, 9]. As one can see, potential surface of the Model A can be considered as some approximation of potential surface of the Model B by means of appropriate variation of parameters  $\bar{\omega}$  and  $\bar{L}$ , and  $\bar{z}_c \in (-\bar{L}/2, \bar{L}/2)$  (see Fig. 1). In limits  $\bar{\omega} \rightarrow \infty$  and  $\bar{L} \rightarrow 0$  both models transfer to exact solvable model of planar hydrogen-like atom with known eigenfunction and eigenenergies  $E_n/R_0^* = -Z^2/(n + 1/2)^2$ ,  $n = 0, 1, 2, \dots$  [12].

At  $\bar{\rho} \rightarrow +\infty$  the eigenfunctions  $B_j(\bar{z}; \bar{\rho})$  in the domain  $\Omega_{\text{as}} : \frac{\bar{z}^2}{\bar{\rho}^2} \ll 1$  for Model B are expressed via the eigenfunctions of a one-dimensional oscillator  $B_j^{(0)}(\bar{z}; \bar{\rho} \rightarrow \infty) \equiv B_j^{(0)}(\bar{z})$  depending on the scaled variable  $\xi$ :  $\bar{z} = a_{\bar{\omega}} \xi$ , where  $a_{\bar{\omega}} = (\bar{\omega})^{-1/2}$ , normalized by the condition (14):

$$B_j^{(0)}(\bar{z}) = \frac{1}{(a_0^*)^{1/2} (a_{\bar{\omega}})^{1/2} \pi^{1/4} (2^n n!)^{1/2}} \times \exp\left(-\frac{1}{2} \left(\frac{\bar{z}}{a_{\bar{\omega}}}\right)^2\right) H_n\left(\frac{\bar{z}}{a_{\bar{\omega}}}\right), \quad (15)$$

where  $H_n$  are the Hermite polynomials, and the eigenvalues  $\bar{E}_j(\bar{\rho} \rightarrow \infty) = \bar{E}_j^{\text{th}}$  are expressed via the corresponding eigenvalues of the energy of one-dimensional harmonic oscillator  $\bar{E}_j^{\text{th}} = \bar{\omega}(2j - 1) = \bar{\omega}(2n + 1)$ ,  $j = n + 1 = 1, 2, \dots, j_{\max}$  ( $n = j - 1 = 0, 1, \dots, j_{\max} - 1$ ). This follows from the fact that at  $\bar{\rho} \rightarrow \infty$  the correction  $\Delta \bar{E}_j(\bar{\rho} \rightarrow \infty)$  to the eigenvalues  $\bar{E}_j^{\text{th}}$ , calculated using the asymptotic basis functions, has the order of smallness

$$\begin{aligned} \Delta \bar{E}_j(\bar{\rho} \rightarrow \infty) &= -\frac{2Z}{\bar{\rho}} \int_{\bar{z}_{\min}}^{\bar{z}_{\max}} B_j^{(0)}(\bar{z}; \bar{\rho} \rightarrow \infty) \\ &\times \frac{1}{\sqrt{1 + \frac{(\bar{z} - \bar{z}_c)^2}{\bar{\rho}^2}}} B_j^{(0)}(\bar{z}; \bar{\rho} \rightarrow \infty) d\bar{z} \\ &= -\frac{2Z}{\bar{\rho}} + O(\bar{\rho}^{-3}). \end{aligned}$$

For Model B at  $\bar{\rho} \rightarrow +\infty$  the eigenfunctions  $B_j(\bar{z}; \bar{\rho})$  in the domain  $\Omega_{\text{as}} : \frac{\bar{z}^2}{\bar{\rho}^2} \ll 1$  are expressed via the eigenfunctions of the one-dimensional rectangular potential well  $B_j^{(0)}(\bar{z}; \bar{\rho} \rightarrow \infty) \equiv B_j^{(0)}(\bar{z})$ , normalized by the condition (14):

$$B_j^{(0)}(\bar{z}) = \frac{1}{(a_0^*)^{1/2} \sqrt{\frac{2}{L}}} \begin{cases} \sin \frac{\pi j}{L} \bar{z}, & \text{even } j \geq 2, \\ \cos \frac{\pi j}{L} \bar{z}, & \text{odd } j \geq 1, \end{cases}$$

while the eigenvalues  $\bar{E}_j(\bar{\rho} \rightarrow \infty) = \bar{E}_j^{\text{th}}$  are expressed via the corresponding eigenvalues of the energy of a particle in a one-dimensional rectangular potential well  $\bar{E}_j^{\text{th}} = \pi^2 j^2 / \bar{L}^2$ ,  $j = 1, 2, \dots, j_{\text{max}}$ .

Under the variable change  $\bar{z}' = \bar{z} - \bar{z}_c$  the eigenvalue problem (11)–(14) takes the form

$$\left[ -\frac{\partial^2}{\partial \bar{z}'^2} + \bar{\omega}^2(\bar{z}' + \bar{z}_c)^2 - \frac{2Z}{\sqrt{\bar{z}'^2 + \bar{\rho}^2}} \right] \quad (16)$$

$$\times \Phi_j(\bar{z}'; \bar{\rho}) = \bar{E}_j(\bar{\rho}) \Phi_j(\bar{z}'; \bar{\rho}),$$

$$\left[ -\frac{\partial^2}{\partial \bar{z}'^2} - \frac{2Z}{\sqrt{\bar{z}'^2 + \bar{\rho}^2}} \right] \Phi_j(\bar{z}'; \bar{\rho}) \quad (17)$$

$$= \bar{E}_j(\bar{\rho}) \Phi_j(\bar{z}'; \bar{\rho}).$$

The eigenfunctions

$$\Phi_j(\bar{z}'; \bar{\rho}) = \exp(-i\bar{z}_c \bar{p}_{\bar{z}}) B_j(\bar{z}; \bar{\rho})$$

$$= \exp\left(\bar{z}_c \frac{d}{d\bar{z}}\right) B_j(\bar{z}; \bar{\rho})$$

form a complete orthogonal basis, obey the symmetry conditions

$$B_j(\bar{z}; \bar{\rho}, \bar{z}_c) = \exp(i\pi\nu_{m_z q}) B_j(-\bar{z}; \bar{\rho}, -\bar{z}_c)$$

and

$$\bar{E}_j(\bar{\rho}, \bar{z}_c) = \bar{E}_j(\bar{\rho}, -\bar{z}_c),$$

where  $\nu_{m_z q}$  is the real phase,  $q$  is the number of zeros in  $\bar{z} \in \mathbf{R}$  for Model A and  $\bar{z} \in [\bar{z}_{\text{min}}, \bar{z}_{\text{max}}]$  for Model B, and the Dirichlet boundary conditions with respect to the variable  $\bar{z}'$  at each fixed value of the parameter  $\bar{\rho} \in \mathbf{R}_+^1$ :

$$\Phi_j(\bar{z}'_{\text{min}}; \bar{\rho}) = 0, \quad \Phi_j(\bar{z}'_{\text{max}}; \bar{\rho}) = 0, \quad (18)$$

$$\bar{z}'_{\text{min}} = \bar{z}_{\text{min}} - \bar{z}_c, \quad \bar{z}'_{\text{max}} = \bar{z}_{\text{max}} - \bar{z}_c.$$

They also satisfy the orthonormality conditions in the interval  $\Omega'_{\bar{z}} = [\bar{z}'_{\text{min}} = \bar{z}_{\text{min}} - \bar{z}_c, \bar{z}'_{\text{max}} = \bar{z}_{\text{max}} - \bar{z}_c]$ :

$$\langle \Phi_i(\bar{z}'; \bar{\rho}) | \Phi_j(\bar{z}'; \bar{\rho}) \rangle_{\Omega'} \quad (19)$$

$$= a_0^* \int_{\bar{z}'_{\text{min}}}^{\bar{z}'_{\text{max}}} \Phi_i(\bar{z}'; \bar{\rho}) \Phi_j(\bar{z}'; \bar{\rho}) d\bar{z}' = \delta_{ij}.$$

By means of the variation of the corresponding Rayleigh–Ritz functional [7] using the expansion (10), Eq. (1) is reduced to the set of  $j_{\text{max}}$  ordinary differential equations of the second order with respect to the unknown functions  $\chi(\bar{\rho}) \equiv \chi^{(i)}(\bar{\rho})$ :

$$\left( -\frac{1}{\bar{\rho}^{d-1}} \mathbf{I} \frac{d}{d\bar{\rho}} \bar{\rho}^{d-1} \frac{d}{d\bar{\rho}} + \mathbf{V}(\bar{\rho}) + \mathbf{Q}(\bar{\rho}) \frac{d}{d\bar{\rho}} \right) \quad (20)$$

$$+ \frac{1}{\bar{\rho}^{d-1}} \frac{d\bar{\rho}^{d-1} \mathbf{Q}(\bar{\rho})}{d\bar{\rho}} - 2\bar{E} \mathbf{I} \chi(\bar{\rho}) = 0.$$

Here,  $d = 2$  is the dimensionality of the space,  $\mathbf{I}$ ,  $\mathbf{V}(\bar{\rho})$ , and  $\mathbf{Q}(\bar{\rho})$  are  $j_{\text{max}} \times j_{\text{max}}$  matrices, the elements of which are defined by the relations

$$V_{ij}(\bar{\rho}) = H_{ij}(\bar{\rho}) + \frac{\bar{E}_i(\bar{\rho}) + \bar{E}_j(\bar{\rho})}{2} \delta_{ij} \quad (21)$$

$$+ \frac{m_z^2}{\bar{\rho}^2} \delta_{ij}, \quad I_{ij} = \delta_{ij},$$

$$H_{ij}(\bar{\rho}) = H_{ji}(\bar{\rho}) = \left\langle \frac{\partial B_i(\bar{z}'; \bar{\rho})}{\partial \bar{\rho}} \left| \frac{\partial B_j(\bar{z}'; \bar{\rho})}{\partial \bar{\rho}} \right\rangle_{\Omega_{\bar{z}'}} ,$$

$$Q_{ij}(\bar{\rho}) = -Q_{ji}(\bar{\rho}) = - \left\langle B_i(\bar{z}'; \bar{\rho}) \left| \frac{\partial B_j(\bar{z}'; \bar{\rho})}{\partial \bar{\rho}} \right\rangle_{\Omega_{\bar{z}'}} .$$

Due to (5)–(9) the discrete spectrum solutions obey the asymptotic boundary and orthonormality conditions

$$\lim_{\bar{\rho} \rightarrow 0} \bar{\rho}^{d-1} \frac{d\chi(\bar{\rho})}{d\bar{\rho}} = 0, \quad \text{if } m_z = 0, \quad (22)$$

$$\text{and } \chi(0) = 0, \quad \text{if } m_z \neq 0,$$

$$\lim_{\bar{\rho} \rightarrow \infty} \bar{\rho}^{d-1} \chi^{(i)}(\bar{\rho}) = 0 \rightarrow \chi^{(i)}(\bar{\rho}_{\text{max}}) = 0, \quad (23)$$

$$(a_0^*)^d \int_0^{\bar{\rho}_{\text{max}}} \bar{\rho}^{d-1} \left( \chi^{(i)}(\bar{\rho}) \right)^T \chi^{(j)}(\bar{\rho}) d\bar{\rho} = \delta_{ij}. \quad (24)$$

Since the equation (16) (or (17)) is linear and the boundary conditions (18) are homogeneous, the sign of the phase of the basis functions is arbitrary. Hence, the sign of the phase at the point  $\bar{z}'_{\text{min}}$  was fixed by imposing the condition

$$\frac{\partial}{\partial \bar{z}'} \Phi_j(\bar{z}'; \bar{\rho}) \Big|_{\bar{z}' = \bar{z}'_{\text{min}}} > 0,$$

which is necessary for the calculation of integrals (21), including the basis functions and their derivatives with respect to the parameter  $\bar{\rho}$ , i.e., the variables coefficients in Eq. (20).

### 3. ADIABATIC REPRESENTATION FOR THE PARABOLIC QUANTUM WELL IN SPHERICAL COORDINATES

Using the reduced atomic units the Schrödinger equation (1) in the spherical coordinates  $(\bar{r}, \eta = \cos \theta, \phi)$  takes the form

$$\left( -\frac{1}{\bar{r}^2} \frac{\partial}{\partial \bar{r}} \bar{r}^2 \frac{\partial}{\partial \bar{r}} + \frac{1}{\bar{r}^2} \hat{A}(c) - \frac{2Z}{\bar{r}} \right) \quad (25)$$

$$\times \psi_{m_z}(\bar{r}, \eta) = 2\bar{E} \psi_{m_z}(\bar{r}, \eta).$$

Here  $\hat{A}(c) \equiv \hat{A}(c, b) = \hat{A}^{(0)}(c) + c^2 + f$ ,  $\hat{A}^{(0)}(c)$  is the operator of modified angular functions [13] that at  $b = 0$  corresponds to prolate spheroidal functions [14]

$$\hat{A}^{(0)}(c) = -\frac{\partial}{\partial \eta}(1 - \eta^2)\frac{\partial}{\partial \eta} \quad (26)$$

$$+ \frac{m_z^2}{1 - \eta^2} + c^2(\eta^2 - 1) - b\eta,$$

where  $c = \bar{\omega}\bar{r}^2$ ,  $b = -2\bar{\omega}^2\bar{z}_c\bar{r}^3$ , and  $f = (\bar{\omega}\bar{z}_c\bar{r})^2$  are the parameter depending on  $\bar{\omega}$ ,  $\bar{z}_c$ , and  $\bar{r} \in \mathbf{R}_+^1$ . The wave functions  $\psi_{m_z}(\bar{r}, \eta, b) \equiv \psi_{m_z i}(\bar{r}, \eta, b) \equiv \psi_{m_z i}(\bar{r}, \eta, \bar{z}_c)$  at fixed  $m_z$  obey the conditions at the boundary of the domain  $\Omega_{\bar{r}, \eta} = \Omega(\bar{r}, \eta)$

$$\lim_{\eta \rightarrow \pm 1} (1 - \eta^2) \frac{\partial \psi_{m_z}(\bar{r}, \eta)}{\partial \eta} = 0, \quad \text{if } m_z = 0,$$

$$\text{and } \psi_{m_z}(\bar{r}, \pm 1) = 0, \quad \text{if } m_z \neq 0,$$

$$\lim_{\bar{r} \rightarrow 0} \bar{r}^2 \frac{\partial \psi_{m_z}(\bar{r}, \eta)}{\partial \bar{r}} = 0.$$

At large  $\bar{r} = \bar{r}_{\max} \gg 1$  the discrete-spectrum wave functions obey the Dirichlet boundary condition that follows from the asymptotic behavior of the solution

$$\lim_{\bar{r} \rightarrow +\infty} \bar{r}^2 \psi_{m_z}(\bar{r}, \eta) = 0$$

$$\rightarrow \psi_{m_z}(\bar{r}_{\max}, \eta) = 0,$$

and also the orthonormality condition

$$(a_0^*)^3 \int_0^{\bar{r}_{\max}} \int_{-1}^1 \psi_{m_z i}(\bar{r}, \eta) \quad (27)$$

$$\times \psi_{m_z j}(\bar{r}, \eta) \bar{r}^2 d\bar{r} d\eta = \delta_{ij}.$$

The solution of (25)–(27) at fixed  $m_z$  is sought in the form of the expansion with respect to single-parameter functions  $\Phi_j(\eta; \bar{r}) \equiv \Phi_{m_z j}(\eta; \bar{r})$ :

$$\psi_{m_z i}(\bar{r}, \eta) = \sum_{j=1}^{j_{\max}} \Phi_{m_z j}(\eta; \bar{r}) \chi_{ji}(\bar{r}). \quad (28)$$

Here the vector functions  $\chi_{ji}(\bar{r})$  are to be found, while the basis functions  $\Phi_j(\eta; \bar{r}) \in F_{\bar{r}} \sim L_2[-1, 1]$  are defined as a set of regular solutions of the eigenvalue problem:

$$\hat{A}(c)\Phi_{m_z j}(\eta; \bar{r}) = \bar{E}_j(\bar{r})\Phi_{m_z j}(\eta; \bar{r}). \quad (29)$$

The eigenfunctions  $\Phi_{m_z j}(\eta; \bar{r}) \equiv \Phi_{m_z j}(\bar{r}, \eta, \bar{z}_c)$  at fixed  $m_z$  obey the symmetry condition  $\Phi_{m_z j}(\bar{r}, \eta, \bar{z}_c) = \exp(i\pi\nu_{m_z q})\Phi_{m_z j}(\bar{r}, -\eta, -\bar{z}_c)$ , where  $\nu_{m_z q}$  is the real phase,  $q$  is the number of zeros in  $\eta \in [-1, 1]$ ,  $\bar{E}_j(\bar{r}, \bar{z}_c) = \bar{E}_j(\bar{r}, -\bar{z}_c)$ , and the boundary conditions with respect to the variable  $\eta$ , analogous to those

imposed on the wave function  $\psi_j(\eta, \bar{r})$  at each fixed value of the parameter  $\bar{r} \in \mathbf{R}_+^1$

$$\lim_{\eta \rightarrow \pm 1} (1 - \eta^2) \frac{\partial \Phi_{m_z j}(\eta; \bar{r})}{\partial \eta} = 0, \quad \text{if } m_z = 0, \quad (30)$$

$$\text{and } \Phi_{m_z j}(\bar{r}, \pm 1) = 0, \quad \text{if } m_z \neq 0,$$

as well as the orthonormality conditions in the interval  $\Omega_{\eta} = [-1, 1]$ :

$$\langle \Phi_{m_z i}(\eta; \bar{r}) | \Phi_{m_z j}(\eta; \bar{r}) \rangle_{\Omega_{\eta}} \quad (31)$$

$$= \int_{-1}^1 \Phi_{m_z i}(\eta; \bar{r}) \Phi_{m_z j}(\eta; \bar{r}) d\eta = \delta_{ij}.$$

By means of the variation of the corresponding Rayleigh–Ritz functional [7, 8] using the expansion (28) Eq. (25) is reduced to the set of  $j_{\max}$  ordinary differential equations of the second order with respect to the unknown functions  $\chi(\bar{r}) \equiv \chi^{(i)}(\bar{r})$ :

$$\left( -\frac{1}{\bar{r}^{d-1}} \mathbf{I} \frac{d}{d\bar{r}} \bar{r}^{d-1} \frac{d}{d\bar{r}} + \frac{\mathbf{U}(\bar{r})}{\bar{r}^2} + \mathbf{Q}(\bar{r}) \frac{d}{d\bar{r}} \right. \quad (32)$$

$$\left. + \frac{1}{\bar{r}^{d-1}} \frac{d\bar{r}^{d-1} \mathbf{Q}(\bar{r})}{d\bar{r}} - 2\bar{E} \mathbf{I} \right) \chi(\bar{r}) = 0.$$

Here,  $d = 3$  is the dimensionality of the space,  $\mathbf{I}$ ,  $\mathbf{U}(\bar{r})$ , and  $\mathbf{Q}(\bar{r})$  are  $j_{\max} \times j_{\max}$  matrices with the elements defined by the relations similar to (21) with  $\mathbf{V}(\bar{r})$  replaced with  $\mathbf{U}(\bar{r})$ , the Coulomb potential  $-2Z\bar{r}\delta_{ij}$  added and with additional division by  $\bar{r}^2$  due to the definition of  $\hat{A}(c)$ :

$$U_{ij}(\bar{r}) = \bar{r}^2 H_{ij}(\bar{r}) + \frac{\bar{E}_i(\bar{r}) + \bar{E}_j(\bar{r})}{2} \delta_{ij} \quad (33)$$

$$- 2Z\bar{r}\delta_{ij}, \quad I_{ij} = \delta_{ij},$$

$$H_{ij}(\bar{r}) = H_{ji}(\bar{r}) = \left\langle \frac{\partial \Phi_i(\eta; \bar{r})}{\partial \bar{r}} \left| \frac{\partial \Phi_j(\eta; \bar{r})}{\partial \bar{r}} \right\rangle_{\Omega_{\eta}},$$

$$Q_{ij}(\bar{r}) = -Q_{ji}(\bar{r}) = - \left\langle \Phi_i(\eta; \bar{r}) \left| \frac{\partial \Phi_j(\eta; \bar{r})}{\partial \bar{r}} \right\rangle_{\Omega_{\eta}}.$$

Note, that Eq. (29) is linear and the boundary conditions (31) are homogeneous, the sign of the phase of the basis functions  $\Phi_j(\eta; \bar{r})$  is arbitrary. Hence, we fix the phase sign at the point  $\eta = +1$  by the condition

$$\left. \frac{\partial}{\partial \eta} \Phi_{m_z j}(\eta; \bar{r}) \right|_{\eta=+1} > 0,$$

which is necessary to calculate the integrals (33) involving the basis functions and their derivatives with respect to the parameter  $\bar{r}$ , i.e., the variable coefficients in Eq. (32).

**Table 1.** Dependence of the calculated binding energy  $E_B/R_0^* = -(2\bar{E}(\bar{z}_c) - \bar{E}_i(\infty))$  of the parabolic quantum well upon the number of the basis functions  $j_{\max}$ , compared with the energy obtained by means of the crude adiabatic approximation (C) and variation calculation (V) from [1]

$j_{\max}$	$\bar{z}_c = 0$	$\bar{z}_c = \pm 0.2$	$\bar{z}_c = \pm 0.3$	$\bar{z}_c = \pm 0.5$
Cylindrical coordinates				
C	1.86807	1.80379	1.72781	1.51517
1	1.53006	1.44930	1.35848	1.13252
4	1.71971	1.67525	1.60682	1.40688
8	1.77801	1.71637	1.63800	1.42465
12	1.79548	1.72927	1.64846	1.43391
16	1.80389	1.73567	1.65399	1.43763
20	1.80878	1.73948	1.65764	1.43958
24	1.81194	1.74201	1.66020	1.44081
V	1.72040	1.63506	1.54708	1.32406
Spherical coordinates				
C	2.04328	2.00216	1.94853	1.77774
1	1.75493	1.62950	1.50485	1.23289
2	1.75493	1.69037	1.61395	1.40265
4	1.82171	1.75050	1.66764	1.44490
6	1.82758	1.75567	1.67215	1.44803
8	1.82773	1.75581	1.67228	1.44813
10	1.82774	1.75582	1.67229	1.44814

The discrete-spectrum solutions obey the asymptotic boundary conditions and the orthonormality condition

$$\lim_{\bar{r} \rightarrow 0} \bar{r}^{d-1} \frac{d\chi(\bar{r})}{d\bar{r}} = 0, \quad (34)$$

$$\lim_{\bar{r} \rightarrow \infty} \bar{r}^{d-1} \chi^{(i)}(\bar{r}) = 0 \rightarrow \chi^{(i)}(\rho_{\max}) = 0, \quad (35)$$

$$(a_0^*)^d \int_0^{\bar{r}_{\max}} \bar{r}^{d-1} \left( \chi^{(i)}(\bar{r}) \right)^T \chi^{(j)}(\bar{r}) d\bar{r} = \delta_{ij}.$$

#### 4. ANALYSIS AND DISCUSSION OF NUMERICAL RESULTS

Solving the boundary problems (20)–(24) and (32)–(35), the eigenfunctions  $\chi(\bar{\rho})$  and  $\chi(\bar{r})$ , as well as the corresponding energy eigenvalues  $2\bar{E}$  are calculated, in terms of which the total energy  $E$  in reduced Rydbergs  $E/R_0^* = 2\bar{E}$ , the relative energy  $\bar{\varepsilon}_i = 2\bar{E} - \bar{E}_i(\infty)$  with respect to the threshold  $\bar{E}_i(\infty) =$

**Table 2.** Dependence of the calculated binding energy  $E_B/R_0^* = -(2\bar{E}(\bar{z}_c) - \bar{E}_i(\infty))$  of the rectangular quantum well with infinitely high walls upon the number of the basis functions  $j_{\max}$ , compared with the energy obtained by means of the crude adiabatic approximation (C) and variation calculation (V) from [16]

$j_{\max}$	$\bar{z}_c = 0$	$\bar{z}_c = \pm 0.1$	$\bar{z}_c = \pm 0.2$	$\bar{z}_c = \pm 0.3$	$\bar{z}_c = \pm 0.4$
C	2.38323	2.30772	2.10042	1.81957	1.55033
1	2.13116	2.02095	1.75055	1.46353	1.28534
2	2.13117	2.16691	2.02381	1.76819	1.51999
3	2.32502	2.23095	2.02692	1.78287	1.52827
4	2.32502	2.26106	2.04603	1.78449	1.52974
8	2.35034	2.27160	2.05932	1.78818	1.53035
12	2.35281	2.27363	2.06042	1.78852	1.53038
16	2.35338	2.27409	2.06065	1.78863	1.53041
20	2.35356	2.27422	2.06074	1.78869	1.53042
24	2.35366	2.27430	2.06079	1.78871	1.53042
V	2.31025	2.21933	1.99129	1.72052	1.48128

$\bar{E}_i^{\text{th}}$  and the binding energy  $\bar{\varepsilon}_i^B = -(2\bar{E} - \bar{E}_i(\infty))$  or  $E_B/R_0^* = -(2\bar{E}(\bar{z}_c) - \bar{E}_i(\infty))$  are expressed. For GaAs we use the following parameters:  $a_0^* = 102 \text{ \AA}$ ,  $R_0^* = 5.2 \text{ meV}$ ,  $\beta = 0.067$ ,  $\varepsilon_d = 13.18$ ,  $L = 102 \text{ \AA}$ ,  $\gamma = 3$ .

**Model A.** The calculations for the parabolic quantum well were carried out with  $Z = 1$ ,  $\bar{\omega} = 3$ ,  $m_z = 0$ , and  $\bar{z}_c \in [-0.5, 0.5]$  using the software package, based on the program KANTBP [7], implementing the finite-element method for solving the boundary problems (11), (13), (14) (or (16), (18), (19)) and (29)–(31) on the grids  $\Omega_{\bar{z}} = \{-12(70) - 5(100) - 1(200)1(100)5(70)12\}$  and  $\Omega_{\eta} = \{-1(800)1\}$  with the Lagrange elements of the order  $p = 4$  between the nodes, respectively (the number of elements given in parentheses). For the problems (20)–(24) and (32)–(35) we used the finite-element grid  $\Omega_{\bar{\rho}} = \Omega_{\bar{r}} = \{0(200)1(200)5(200)100\}$  with the Lagrange elements of the order  $p = 4$  between the nodes,  $\bar{\rho} = \bar{\rho}_{\max}$ .

As follows from the theorem [15], for the ground state the adiabatic approximation ( $j_{\max} = 1$ ) gives the upper bound for the energy, while in the so-called crude adiabatic approximation, when the diagonal adiabatic positive correction  $H_{jj}(\bar{\rho}) = 0$  is neglected, one gets the lower bound for the energy. The corresponding inverse estimators for the binding energy  $E_B/R_0^*$  in cylindrical and spherical coordinates are presented in Table 1. From this table it fol-

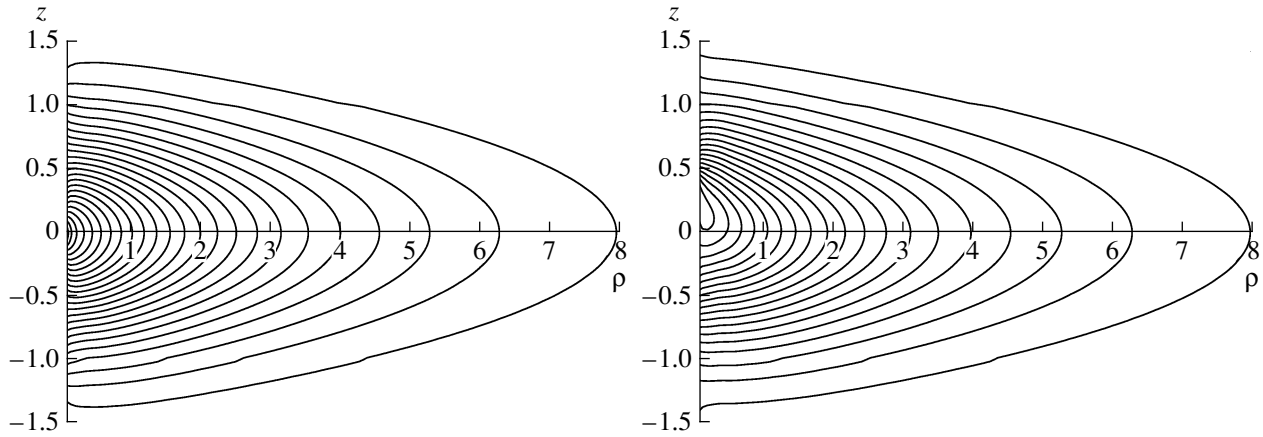


**Fig. 2.** Isolines of ground-state wave function of Model A for values of parameters  $m_z = 0$ ,  $Z = 1$ , and  $\bar{\omega} = 3$ . Left panel:  $\bar{z}_c = 0$ , right panel:  $\bar{z}_c = 0.4$ .

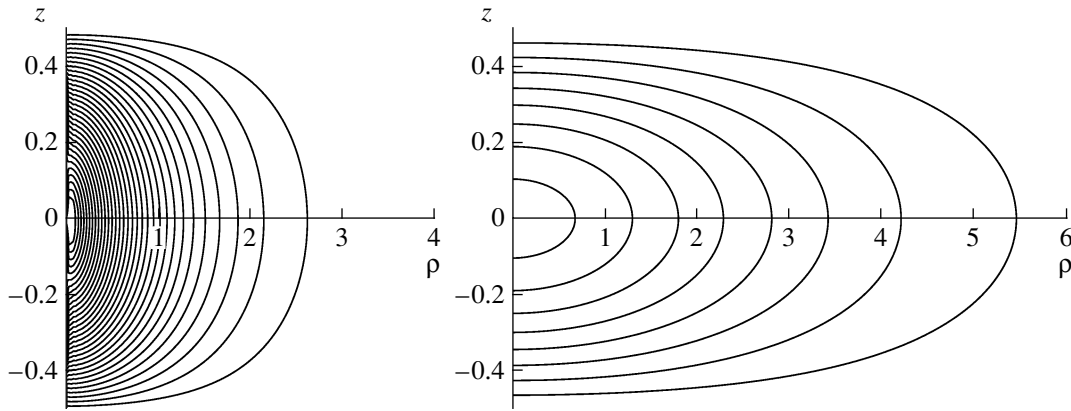


**Fig. 3.** Isolines of ground-state wave function of Model B for values of parameters  $m_z = 0$ ,  $Z = 1$ , and  $\bar{L} = 1$ . Left panel:  $\bar{z}_c = 0$ , right panel:  $\bar{z}_c = 0.4$ .

lows that these values are upper and lower estimates of the binding energy from the variational calculation [1]. The corresponding inverse lower estimators of the binding energy for increasing number of single-parameter basis functions  $j_{\max}$  allow one to analyze the convergence rate of the method used for the solution of the boundary problem in the two-dimensional domain (for example, see Fig. 2). As seen from table 1, the lower estimate of the binding energy, calculated in the cylindrical coordinates at  $j_{\max} = 4$ , is closest to the variational calculation. This is because in the variational calculation at all values of  $\bar{\rho} \in \mathbf{R}_1^+$  the function  $B_1^{(0)}$  of the ground state of the oscillator with the threshold energy  $\bar{E}_1^{\text{th}} = \bar{\omega}$ , corresponding to the single-parameter basis function  $B_1(\bar{z}; \bar{\rho} \rightarrow \infty)$  at  $\bar{\rho} \rightarrow \infty$ , was used. From Table 1 it is seen that the rate of convergence with respect to the basis functions' number in the spherical parameterization (29) is considerably higher than that in the cylindrical one (11), (16). This is due to the singular behavior

of the Coulomb potential, which for the choice of the basis in the cylindrical parameterization leads to the solution of the problem in the class of generalized functions belonging to the Sobolev space  $W_2^1$ .

**Model B.** The calculations for the rectangular quantum well with infinitely high walls were carried out with  $Z = 1$ ,  $\bar{L} = 1$ ,  $m_z = 0$  and  $\bar{z}_c \in (-0.5, 0.5)$  using the above-mentioned software package implementing the finite-element method for solving the boundary problems (12), (13), (14) (or (17), (18), (19)) on the grid  $\Omega_{\bar{z}} = \{-0.5(200)0.25(200)0.25(200)0.5\}$  with the Lagrange elements of the order  $p = 4$  between the nodes (the number of elements given in parentheses). For the problem (20)–(24) we used the finite-element grid  $\Omega_{\bar{\rho}} = \Omega_{\bar{r}} = \{0(50)1(50)5(50)100\}$  with the Lagrange elements of the order  $p = 4$  between the nodes.  $\bar{\rho} = \bar{\rho}_{\max}$ .

The corresponding inverse estimators of the binding energy  $E_B/R_0^*$ , calculated in the cylindrical co-

ordinates, are presented in Table 2. From this table it follows that these values are upper and lower estimates of the binding energy from the variational calculations, carried out in [2]. The corresponding inverse lower estimates of the binding energy for increasing number  $j_{\max}$  of single-parameter basis functions allow one to analyze numerically the rate of convergence of the method of solving the boundary problem in the two-dimensional domain (for example, see Fig. 3). As seen from Table 2, the lower estimate of the binding energy, calculated in the cylindrical coordinates at  $j_{\max} = 4$  is closest to the variational calculation. This is because in the variational calculation at all values of  $\bar{\rho} \in \mathbf{R}_1^+$  the function  $B_1^{(0)}$  of the ground state of the rectangular well with the threshold energy  $\bar{E}_1^{\text{th}} = \pi^2/L^2$ , corresponding to the single-parameter basis function  $B_1(\bar{z}; \bar{\rho} \rightarrow \infty)$  at  $\bar{\rho} \rightarrow \infty$  was used.

## 5. CONCLUSION

We presented the scheme of the solution of the boundary problem with discrete spectrum for a parabolic quantum well and a rectangular quantum well with infinitely high walls in the adiabatic representation. The upper and lower bounds for the energy of the ground state of the systems are obtained under the conditions of the shift of the Coulomb center in a given range of the parameter with respect to earlier variational estimates. It is shown that the rate of convergence depends significantly on the appropriate choice of the adiabatic basis parameterization taking the specific features of the considered problem into account. The presented results allow one to estimate the efficiency of the method and the software package developed for the investigation of the semiconductor nanostructure models. Further development of the method and the software package is planned in relation with solving the quasi-2D and quasi-1D boundary problems with both discrete and continuous spectrum, which are necessary for calculating the optical transition rates and transport characteristics in the models like quantum wells and quantum wires.

The work was carried out in the framework of the Collaboration Protocol JINR-YeSU 3720 of May 26, 2006 and the National Program of the Republic of Armenia "Semiconductor micro- and nanoelectronics" and supported partially by RFBR (grants nos. 07-01-00660 and 08-01-00604) and CRDF-NFSAT (grant no. UC-06/07).

## REFERENCES

1. E. M. Kazaryan, A. A. Kostanyan, and H. A. Sarkisyan, *Physica E* **28**, 423 (2005).
2. M. S. Atoyan, E. M. Kazaryan, and H. A. Sarkisyan, *Physica E* **22**, 860 (2004); A. M. Kazaryan and E. M. Kazaryan, *Fiz. Tekh. Poluprovodnikov* **7**, 1983 (1977) [*Sov. Phys. Semicond.* **7**, 1322 (1977)]; G. Bastard, *Phys. Rev. B* **24**, 4714 (1981).
3. A. N. Vasilyev, S. I. Vinitzky, and D. A. Tarkhov, in *Computer Modeling* (Polytechn. Univ., Saint-Petersburg, 2007), p. 90 [in Russian].
4. H. Voss, *Comput. Phys. Commun.* **174**, 441 (2006).
5. W. Wang, T.-M. Hwang, and J.-C. Jang, *Comput. Phys. Commun.* **174**, 371 (2006).
6. L. V. Kantorovich and V. I. Krylov, *Approximate Methods of Higher Analysis* (Interscience, New York, 1964).
7. O. Chuluunbaatar et al., *Comput. Phys. Commun.* **177**, 649 (2007).
8. O. Chuluunbaatar et al., *Comput. Phys. Commun.* **178**, 301 (2008).
9. A. I. Gusev, and A. A. Rempel, *Nanocrystalline Materials* (Cambridge Int. Sci., Cambridge, 2004); A. I. Gusev, *Nanomaterials, Nanostructures, Nanotechnologies* (Fizmatlit, Moscow, 2007) [in Russian].
10. A. N. Tikhonov and A. A. Samarskii, *Equations of Mathematical Physics* (Dover, New York, 1990), p. 777.
11. R. Loudon, *Am. J. Phys.* **27**, 649 (1959); S. I. Vinitzky, G. S. Pogosyan, A. N. Sissakian, and V. M. Ter-Antonyan, Preprint no. P2-86-571, JINR (Dubna, 1986); L. D. Landau and E. M. Lifshitz, *Quantum Mechanics*, 3rd ed. (Pergamon, Oxford, 1977).
12. L. G. Mardoyan, G. S. Pogosyan, A. N. Sissakian, and V. M. Ter-Antonyan, *Quantum Systems with Hidden Symmetry. Interbasis Expansions* (Fizmatlit, Moscow, 2006) [in Russian].
13. S. Yu. Slavyanov and W. Lay, *Special Functions* (Oxford Univ., Oxford, 2000).
14. M. Abramowitz and I. A. Stegun, *Handbook of Mathematical Functions* (Dover, New York, 1972).
15. F. D. Bratsev, *Dokl. Akad. Nauk SSSR* **160**, 570 (1965) [*Sov. Phys. Dokl.* **10**, 44 (1965)].
16. A. A. Kostanyan, PhD Thesis (Russ.-Armen. (Slavonic) Univ., Yerevan, 2007).



Resonant Tunneling of a Few-Body Cluster  
Through Repulsive Barriers\*A. A. Gusev<sup>1)\*\*</sup>, S. I. Vinitsky<sup>1)</sup>, O. Chuluunbaatar<sup>1),2)</sup>,  
L. L. Hai<sup>1)</sup>, V. L. Derbov<sup>3)</sup>, A. Góźdz<sup>4)</sup>, and P. M. Krassovitskiy<sup>5)</sup>

Received April 18, 2013

**Abstract**—A model for quantum tunnelling of a cluster comprised of  $A$  identical particles, interacting via oscillator-type potential, through short-range repulsive barrier potentials is introduced for the first time in symmetrized-coordinate representation and numerically studied in the  $s$ -wave approximation. A constructive method for symmetrizing or antisymmetrizing the  $(A - 1)$ -dimensional harmonic oscillator basis functions in the new symmetrized coordinates with respect to permutations of coordinates of  $A$  identical particles is described. The effect of quantum transparency, manifesting itself in nonmonotonic resonance-type dependence of the transmission coefficient upon the energy of the particles, their number  $A = 2, 3, 4$  and the type of their symmetry, is analyzed. It is shown that the total transmission coefficient demonstrates the resonance behavior due to the existence of barrier quasi-stationary states, embedded in the continuum.

DOI: 10.1134/S1063778814030107

## 1. INTRODUCTION

During a decade the mechanism of quantum penetration of two bound particles through repulsive barriers, manifested in [1], attracts attention from both theoretical and experimental viewpoints in relation with such problems as near-surface quantum diffusion of molecules [2–5], fragmentation in producing very neutron-rich light nuclei [6–9], and heavy-ion collisions through multidimensional barriers [10–16]. In a general formulation of the scattering problem for ions having different masses a benchmark model with long-range potentials was proposed in [17, 18]. The generalization of the two-particle model over a quantum system of  $A$  identical particles is of great importance for appropriate description of molecular and heavy-ion collisions as well as a microscopic study of tetrahedral-symmetric nuclei [19, 20]. *The aim of this paper is to present a suitable formulation of the problem stated above and calculation methods for solving it.*

We consider the penetration of  $A$  identical quantum particles, coupled by short-range oscillator-like

interaction, through a repulsive potential barrier. We assume that the spin part of the wave function is known, so that only the spatial part of the wave function is to be considered, which may be symmetric or antisymmetric with respect to a permutation of  $A$  identical particles [21–24]. The initial problem is reduced to penetration of a composite system with the internal degrees of freedom, describing an  $(A - 1) \times d$ -dimensional oscillator, and the external degrees of freedom, describing the center-of-mass motion of  $A$  particles in  $d$ -dimensional Euclidean space. For simplicity, we restrict our consideration to the so-called  $s$ -wave approximation [1], corresponding to one-dimensional Euclidean space ( $d = 1$ ). It is shown that the reduction is provided by using appropriately chosen symmetrized coordinates, rather than the conventional Jacobi coordinates. The main goal of introducing the symmetrized coordinates is to provide invariance of the Hamiltonian with respect to permutations of  $A$  identical particles. This allows construction not only of basis functions, symmetric or antisymmetric under permutations of  $A - 1$  relative coordinates, but also of basis functions, symmetric (S) or antisymmetric (A) under permutations of  $A$  Cartesian coordinates. We refer the expansion of the solution in the basis of such type as symmetrized coordinate representation (SCR).

We seek for the solution in the form of Galerkin or Kantorovich expansions [25] with unknown coefficients having the form of matrix functions of the center-of-mass variables in the SCR. As a result, the problem is reduced to a boundary-value problem for a

\*The text was submitted by the authors in English.

<sup>1)</sup>Joint Institute for Nuclear Research, Dubna, Russia.<sup>2)</sup>National University of Mongolia, Ulaanbaatar.<sup>3)</sup>Saratov State University, Russia.<sup>4)</sup>Department of Mathematical Physics, Institute of Physics, University of Maria Curie-Skłodowska, Lublin, Poland.<sup>5)</sup>Institute of Nuclear Physics, Almaty, Kazakhstan.\*\*E-mail: [gooseff@jinr.ru](mailto:gooseff@jinr.ru)

system of ordinary second-order differential equations with respect to the center-of-mass variable. Conventional asymptotic boundary conditions are imposed on the desired matrix solution. The results of calculations are analyzed with particular emphasis on the effect of quantum transparency that manifests itself as nonmonotonic energy dependence of the transmission coefficient due to resonance tunnelling of the bound particles in S (A) states through the repulsive potential barriers.

The paper is organized as follows. In Section 2 we present the statement of the problem in conventional Jacobi and symmetrized coordinates. In Section 3 we introduce the SCR of the solution of the considered problem. In Section 4 we formulate the boundary-value problem for close-coupling equations in Galerkin and Kantorovich forms using conventional and parametric SCRs, respectively. In Section 5 we analyze the results of a numerical experiment on resonance transmission of a few coupled identical particles in S (A) states. In Conclusion we sum up the results and discuss briefly the perspectives of application of the developed approach.

## 2. THE STATEMENT OF THE PROBLEM

The problem of penetration of  $A$  identical quantum particles with the mass  $m$  and a set of the Cartesian coordinates  $x_i \in \mathbf{R}^d$  in  $d$ -dimensional Euclidean space, considered as vector  $\tilde{\mathbf{x}} = (\tilde{x}_1, \dots, \tilde{x}_A) \in \mathbf{R}^{A \times d}$  in  $A \times d$ -dimensional configuration space, coupled by the pair potential  $\tilde{V}^{\text{pair}}(\tilde{x}_{ij})$  of relative coordinates,  $\tilde{x}_{ij} = \tilde{x}_i - \tilde{x}_j$ , similar to a harmonic oscillator  $\tilde{V}^{\text{hosc}}(\tilde{x}_{ij}) = \frac{m\omega^2}{2}(\tilde{x}_{ij})^2$  with frequency  $\omega$ , through the repulsive potential barriers  $\tilde{V}(\tilde{x}_i)$  is described by the Schrödinger equation

$$\left[ -\frac{\hbar^2}{2m} \sum_{i=1}^A \frac{\partial^2}{\partial \tilde{x}_i^2} + \sum_{i,j=1; i < j}^A \tilde{V}^{\text{pair}}(\tilde{x}_{ij}) + \sum_{i=1}^A \tilde{V}(\tilde{x}_i) - \tilde{E} \right] \tilde{\Psi}(\tilde{x}_1, \dots, \tilde{x}_A) = 0,$$

where  $\tilde{E}$  is the total energy of the system of  $A$  particles and  $\tilde{P}^2 = 2m\tilde{E}/\hbar^2$ ,  $\tilde{P}$  is the total momentum of the system of  $A$  particles. Using the oscillator units  $x_{\text{osc}} = \sqrt{\hbar/(m\omega\sqrt{A})}$ ,  $p_{\text{osc}} = \sqrt{(m\omega\sqrt{A})/\hbar} = x_{\text{osc}}^{-1}$ , and  $E_{\text{osc}} = \hbar\omega\sqrt{A}/2$  to introduce the dimensionless coordinates  $x_i = \tilde{x}_i/x_{\text{osc}}$ ,  $x_{ij} = \tilde{x}_{ij}/x_{\text{osc}} = x_i - x_j$ ,  $E = \tilde{E}/E_{\text{osc}} = P^2$ ,  $P = \tilde{P}/p_{\text{osc}} = \tilde{P}x_{\text{osc}}$ ,  $V^{\text{pair}}(x_{ij}) = \tilde{V}^{\text{pair}}(x_{ij}x_{\text{osc}})/E_{\text{osc}}$ ,  $V^{\text{hosc}}(x_{ij}) = \tilde{V}^{\text{hosc}}(x_{ij}x_{\text{osc}})/E_{\text{osc}} = \frac{1}{A}(x_{ij})^2$ , and  $V(x_i) = \tilde{V}(x_ix_{\text{osc}})/E_{\text{osc}}$ , one can rewrite the above equation in the form

$$\left[ -\sum_{i=1}^A \frac{\partial^2}{\partial x_i^2} + \sum_{i,j=1; i < j}^A \frac{1}{A}(x_{ij})^2 + \sum_{i,j=1; i < j}^A U^{\text{pair}}(x_{ij}) + \sum_{i=1}^A V(x_i) - E \right] \times \Psi(x_1, \dots, x_A) = 0, \quad (1)$$

where  $U^{\text{pair}}(x_{ij}) = V^{\text{pair}}(x_{ij}) - V^{\text{hosc}}(x_{ij})$ , i.e., if  $V^{\text{pair}}(x_{ij}) = V^{\text{hosc}}(x_{ij})$ , then  $U^{\text{pair}}(x_{ij}) = 0$ .

Our goal is to find the solutions  $\Psi(x_1, \dots, x_A)$  of Eq. (1), totally symmetric (or antisymmetric) with respect to the permutations of  $A$  particles that belong to the permutation group  $S_n$ . The permutation of particles is nothing but a permutation of the Cartesian coordinates  $x_i \leftrightarrow x_j$ ,  $i, j = 1, \dots, A$ .

First, we introduce the Jacobi coordinates following one of the possible definitions [7]

$$y_0 = \frac{1}{\sqrt{A}} \left( \sum_{t=1}^A x_t \right), \quad (2)$$

$$y_s = \frac{1}{\sqrt{s(s+1)}} \left( \sum_{t=1}^s x_t - s x_{s+1} \right),$$

$$s = 1, \dots, A-1.$$

In the matrix form Eqs. (2) read as

$$\begin{pmatrix} y_0 \\ y_1 \\ y_2 \\ y_3 \\ \vdots \\ y_{A-1} \end{pmatrix} = J \begin{pmatrix} x_1 \\ x_2 \\ x_3 \\ \vdots \\ x_{A-1} \\ x_A \end{pmatrix}, \quad J = \begin{pmatrix} 1/\sqrt{A} & 1/\sqrt{A} & 1/\sqrt{A} & 1/\sqrt{A} & \cdots & 1/\sqrt{A} \\ 1/\sqrt{2} & -1/\sqrt{2} & 0 & 0 & \cdots & 0 \\ 1/\sqrt{6} & 1/\sqrt{6} & -2/\sqrt{6} & 0 & \cdots & 0 \\ 1/\sqrt{12} & 1/\sqrt{12} & 1/\sqrt{12} & -3/\sqrt{12} & \cdots & 0 \\ \vdots & \vdots & \vdots & \vdots & \ddots & \vdots \\ \frac{1}{\sqrt{(A-1)A}} & \frac{1}{\sqrt{(A-1)A}} & \frac{1}{\sqrt{(A-1)A}} & \frac{1}{\sqrt{(A-1)A}} & \cdots & -\frac{A-1}{\sqrt{(A-1)A}} \end{pmatrix}.$$

The inverse coordinate transformation is implemented using the transposed matrix  $J^{-1} = J^T$ , i.e.  $J$  is an orthogonal matrix with pairs of complex conjugate eigenvalues, the absolute values of which are equal to one.

The Jacobi coordinates have the property  $\sum_{i=0}^{A-1} (y_i \cdot y_i) = \sum_{i=1}^A (x_i \cdot x_i) = r^2$ . Consequently,

$$\begin{aligned} \sum_{i,j=1}^A (x_{ij})^2 &= 2A \sum_{i=0}^{A-1} (y_i)^2 \\ -2 \left( \sum_{i=1}^A x_i \right)^2 &= 2A \sum_{i=1}^{A-1} (y_i)^2, \end{aligned}$$

so that Eq. (1) takes the form

$$\begin{aligned} &\left[ -\frac{\partial^2}{\partial y_0^2} + \sum_{i=1}^{A-1} \left( -\frac{\partial^2}{\partial y_i^2} + (y_i)^2 \right) \right. \\ &\quad \left. + U(y_0, \dots, y_{A-1}) - E \right] \Psi(y_0, \dots, y_{A-1}) = 0, \\ &\quad U(y_0, \dots, y_{A-1}) \\ &= \sum_{i,j=1; i < j}^A U^{\text{pair}}(x_{ij}(y_1, \dots, y_{A-1})) \\ &\quad + \sum_{i=1}^A V(x_i(y_0, \dots, y_{A-1})), \end{aligned}$$

which, as follows from Eq. (2), is *not invariant* with respect to permutations  $y_i \leftrightarrow y_j$  at  $i, j = 1, \dots, A-1$ .

The construction of desirable solutions of Eq. (1) in the form of linear combinations of the solutions of Eq. (3), totally symmetric (antisymmetric) with respect to permutations of coordinates  $x_i \leftrightarrow x_j$  (at  $i, j = 1, \dots, A$ ) of  $A$  identical particles is implemented using various special procedures (see, e.g., [26–35]).

### Symmetrized Coordinates

As will be shown below, a simple and clear way to construct the states keeping the symmetry (antisymmetry) under the permutations of  $A$  initial Cartesian coordinates, which we refer as S (A) states, is to use the symmetrized relative coordinates rather than the Jacobi coordinates.

The transformation from the Cartesian coordinates to one of the possible choices of symmetrized ones  $\xi_i$  has the form:

$$\xi_0 = \frac{1}{\sqrt{A}} \left( \sum_{t=1}^A x_t \right), \quad (3)$$

$$\xi_s = \frac{1}{\sqrt{A}} \left( x_1 + \sum_{t=2}^A a_0 x_t + \sqrt{A} x_{s+1} \right),$$

$$s = 1, \dots, A-1,$$

$$x_1 = \frac{1}{\sqrt{A}} \left( \sum_{t=0}^{A-1} \xi_t \right),$$

$$x_s = \frac{1}{\sqrt{A}} \left( \xi_0 + \sum_{t=1}^{A-1} a_0 \xi_t + \sqrt{A} \xi_{s-1} \right),$$

$$s = 2, \dots, A,$$

or, in the matrix form,

$$\begin{pmatrix} \xi_0 \\ \xi_1 \\ \xi_2 \\ \vdots \\ \xi_{A-2} \\ \xi_{A-1} \end{pmatrix} = C \begin{pmatrix} x_1 \\ x_2 \\ x_3 \\ \vdots \\ x_{A-1} \\ x_A \end{pmatrix}, \quad (4)$$

$$\begin{pmatrix} x_1 \\ x_2 \\ x_3 \\ \vdots \\ x_{A-1} \\ x_A \end{pmatrix} = C^{-1} \begin{pmatrix} \xi_0 \\ \xi_1 \\ \xi_2 \\ \vdots \\ \xi_{A-2} \\ \xi_{A-1} \end{pmatrix},$$

$$C = \frac{1}{\sqrt{A}} \begin{pmatrix} 1 & 1 & 1 & 1 & \cdots & 1 & 1 \\ 1 & a_1 & a_0 & a_0 & \cdots & a_0 & a_0 \\ 1 & a_0 & a_1 & a_0 & \cdots & a_0 & a_0 \\ 1 & a_0 & a_0 & a_1 & \cdots & a_0 & a_0 \\ \vdots & \vdots & \vdots & \vdots & \ddots & \vdots & \vdots \\ 1 & a_0 & a_0 & a_0 & \cdots & a_1 & a_0 \\ 1 & a_0 & a_0 & a_0 & \cdots & a_0 & a_1 \end{pmatrix},$$

where  $a_0 = 1/(1 - \sqrt{A}) < 0$ ,  $a_1 = a_0 + \sqrt{A}$ . The inverse coordinate transformation is performed using the same matrix  $C^{-1} = C$ ,  $C^2 = I$ , i.e.  $C = C^T$  is a symmetric orthogonal matrix with the eigenvalues  $\lambda_1 = -1$ ,  $\lambda_2 = 1$ ,  $\dots$ ,  $\lambda_A = 1$  and  $\det C = -1$ . At  $A = 2$  the symmetrized variables (4) are similar up to normalization factors to the symmetrized Jacobi coordinates (2) considered in [36], while at  $A = 4$  they correspond to another choice of symmetrized co-

ordinates  $(\ddot{x}_4, \ddot{x}_1, \ddot{x}_2, \ddot{x}_3)^T = C(x_4, x_1, x_2, x_3)^T$  considered in [26, 37], and mentioned earlier in [38]. We could not find a general definition of symmetrized coordinates for  $A$  identical particles like (4) in the available literature, so we believe that in the present paper it is introduced for the first time.

With the relations  $a_1 - a_0 = \sqrt{A}$ ,  $a_0 - 1 = a_0\sqrt{A}$  taken into account, the relative coordinates  $x_{ij} \equiv x_i - x_j$  of a pair of particles  $i$  and  $j$  are expressed in terms of the internal  $A - 1$  symmetrized coordinates only:

$$\begin{aligned} x_{ij} &\equiv x_i - x_j = \xi_{i-1} - \xi_{j-1} \equiv \xi_{i-1,j-1}, \quad (5) \\ x_{i1} &\equiv x_i - x_1 = \xi_{i-1} + a_0 \sum_{i'=1}^{A-1} \xi_{i'}, \\ i, j &= 2, \dots, A. \end{aligned}$$

So, if only the absolute values of  $x_{ij}$  are to be considered, then there are  $(A - 1)(A - 2)/2$  old relative coordinates transformed into new relative ones and  $A - 1$  old relative coordinates expressed in terms of  $A - 1$  internal symmetrized coordinates. These important relations essentially simplify the procedures of symmetrization (or antisymmetrization) of the oscillator basis functions and the calculations of the corresponding pair-interaction integrals  $V^{\text{pair}}(x_{ij})$ . Note that the symmetrized coordinates are related with the Jacobi ones as

$$\begin{pmatrix} y_0 \\ y_1 \\ y_2 \\ \vdots \\ y_{A-2} \\ y_{A-1} \end{pmatrix} = B \begin{pmatrix} \xi_0 \\ \xi_1 \\ \xi_2 \\ \vdots \\ \xi_{A-2} \\ \xi_{A-1} \end{pmatrix}, \quad B = JC$$

$$= \begin{pmatrix} 1 & 0 & 0 & 0 & 0 & \cdots & 0 & 0 \\ 0 & b_1^0 & b_1^- & b_1^- & b_1^- & \cdots & b_1^- & b_1^- \\ 0 & b_2^+ & b_2^0 & b_2^- & b_2^- & \cdots & b_2^- & b_2^- \\ 0 & b_3^+ & b_3^+ & b_3^0 & b_3^- & \cdots & b_3^- & b_3^- \\ 0 & b_4^+ & b_4^+ & b_4^+ & b_4^0 & \cdots & b_4^- & b_4^- \\ \vdots & \vdots & \vdots & \vdots & \vdots & \ddots & \vdots & \vdots \\ 0 & b_{A-1}^+ & b_{A-1}^+ & b_{A-1}^+ & b_{A-1}^+ & \cdots & b_{A-1}^+ & b_{A-1}^0 \end{pmatrix},$$

where  $b_s^+ = 1/((\sqrt{A} - 1)\sqrt{s(s+1)})$ ,  $b_s^- = \sqrt{A}/((\sqrt{A} - 1)\sqrt{s(s+1)})$ , and  $b_s^0 = (1 + s - s\sqrt{A})/((\sqrt{A} - 1)\sqrt{s(s+1)})$ . One can see that

for the center of mass the symmetrized and Jacobi coordinates are equal,  $y_0 = \xi_0$ , while the relative coordinates are related via the  $(A - 1) \times (A - 1)$  matrix  $M$  with the elements  $M_{ij} = B_{i+1,j+1}$  and  $\det M = (-1)^{A \times d}$ , i.e. the matrix, obtained by cancelling the first row and the first column. The inverse transformation is given by the matrix  $B^{-1} = (JC)^{-1} = CJ^T = B^T$ , i.e.,  $B$  is also an orthogonal matrix.

Note, that for  $A = 3$  and  $d = 1$  the relation between the Jacobi coordinates

$$y_1 = 1/\sqrt{2}(x_1 - x_2), \quad y_2 = 1/\sqrt{6}(x_1 + x_2 - 2x_3)$$

and the symmetrized ones

$$\begin{aligned} \xi_1 &= 1/\sqrt{3}(x_1 + 1/2(\sqrt{3} - 1)x_2 - 1/2(\sqrt{3} + 1)x_3), \\ \xi_2 &= 1/\sqrt{3}(x_1 - 1/2(\sqrt{3} + 1)x_2 + 1/2(\sqrt{3} - 1)x_3) \end{aligned}$$

is given by the orthogonal matrix  $M$ :

$$\begin{aligned} M &= \begin{pmatrix} b_1^0 & b_1^- \\ b_2^+ & b_2^0 \end{pmatrix} \quad (6) \\ &= \begin{pmatrix} (\sqrt{6} - \sqrt{2})/4 & (\sqrt{6} + \sqrt{2})/4 \\ (\sqrt{6} + \sqrt{2})/4 & -(\sqrt{6} - \sqrt{2})/4 \end{pmatrix} \\ &= \begin{pmatrix} \sin \phi_1 & \cos \phi_1 \\ \cos \phi_1 & -\sin \phi_1 \end{pmatrix} \\ &= \begin{pmatrix} 0 & 1 \\ 1 & 0 \end{pmatrix} \begin{pmatrix} \cos \phi_1 & -\sin \phi_1 \\ \sin \phi_1 & \cos \phi_1 \end{pmatrix} \\ &= \begin{pmatrix} \cos \phi_1 & \sin \phi_1 \\ -\sin \phi_1 & \cos \phi_1 \end{pmatrix} \begin{pmatrix} 0 & 1 \\ 1 & 0 \end{pmatrix} \\ &= M_1(\phi_1)M_0. \end{aligned}$$

This transformation is a product of the permutation of coordinates  $(\xi_1, \xi_2) \rightarrow (\xi_2, \xi_1)$  and the counterclockwise rotation by the angle  $\phi_1 = \pi/12$ . A schematic 3D image in the left panel of Fig. 1 shows the coordinate planes (marked with  $\boxed{1}$ ,  $\boxed{2}$ ,  $\boxed{3}$ ) and the center-of-mass plane in  $\mathbf{R}^3$  (its visible part having the shape of a hexagon), together with the lines of intersection of these planes with pair-collision planes ( $x_i = x_j$ ), which correspond to pair-collision lines ( $\{x_i = x_j, x_1 + x_2 + x_3 = 0\}$ ) (marked with 12, 23, 13) in the center-of-mass plane  $x_1 + x_2 + x_3 = 0$ , belonging to  $\mathbf{R}^2$ . Different projections of this geometry clarify the nature of the Jacobi ( $y_1, y_2$ ) and the symmetric ( $\xi_1, \xi_2$ ) coordinates (middle and right

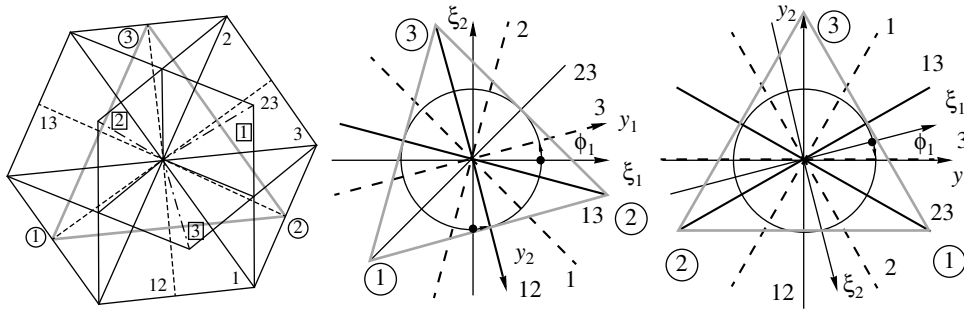


**Fig. 1.** (Left panel) The coordinate planes 1, 2, 3, labelled with boxes, the center-of-mass plane in  $\mathbf{R}^3$ , and the lines of intersection of these planes with the pair-collision planes  $x_i = x_j$ , corresponding to pair-collision lines  $\{x_i = x_j, x_1 + x_2 + x_3 = 0\}$  (labelled 12, 23, 13) in the center-of-mass plane  $x_1 + x_2 + x_3 = 0$ , belonging to  $\mathbf{R}^2$ . (Middle and right panels) The equilateral triangle showing the isomorphism between the group of its symmetry operations  $D_3$  in  $\mathbf{R}^2$  and the group of permutations  $S_3$  of three objects 1, 2, 3, labelled with circles. The symmetric  $(\xi_1, \xi_2)$  and Jacobi  $(y_1, y_2)$  coordinates, related via the transformation (6) in the center-of-mass plane  $\mathbf{R}^2$ , respectively.

panels, respectively), related by the above transformation in the center-of-mass plane  $\mathbf{R}^2$ . This illustrates the isomorphism between the symmetry group of an equilateral triangle  $D_3$  in  $\mathbf{R}^2$  and the 3-body permutation group  $S_3$  ( $A = 3$ ), discussed in [34, 39, 40] in a different context.

At  $A = 4$  and  $d = 1$  the relation between the Jacobi coordinates

$$\begin{aligned} y_1 &= 1/\sqrt{2}(x_1 - x_2), \\ y_2 &= 1/\sqrt{6}(x_1 + x_2 - 2x_3), \\ y_3 &= 1/\sqrt{12}(x_1 + x_2 + x_3 - 3x_4) \end{aligned}$$

and the symmetrized ones

$$\begin{aligned} \xi_1 &= 1/2(x_1 + x_2 - x_3 - x_4), \\ \xi_2 &= 1/2(x_1 - x_2 + x_3 - x_4), \\ \xi_3 &= 1/2(x_1 - x_2 - x_3 + x_4) \end{aligned}$$

is given by the orthogonal matrix  $M$ :

$$\begin{aligned} M &= \begin{pmatrix} b_1^0 & b_1^- & b_1^- \\ b_2^+ & b_2^0 & b_2^- \\ b_3^+ & b_3^+ & b_3^0 \end{pmatrix} \\ &= \begin{pmatrix} 0 & \sqrt{2}/2 & \sqrt{2}/2 \\ \sqrt{6}/3 & -\sqrt{6}/6 & \sqrt{6}/6 \\ \sqrt{3}/3 & \sqrt{3}/3 & -\sqrt{3}/3 \end{pmatrix}. \end{aligned}$$

One of the possible decompositions  $M = M_3(\phi_3) \times M_2(\phi_2)M_1(\phi_1)$  of this matrix is

$$M = \begin{pmatrix} 1 & 0 & 0 \\ 0 & \cos \phi_3 & \sin \phi_3 \\ 0 & -\sin \phi_3 & \cos \phi_3 \end{pmatrix} \quad (7)$$

$$\times \begin{pmatrix} \cos \phi_2 & \sin \phi_2 & 0 \\ -\sin \phi_2 & \cos \phi_2 & 0 \\ 0 & 0 & 1 \end{pmatrix} \begin{pmatrix} 1 & 0 & 0 \\ 0 & \cos \phi_1 & \sin \phi_1 \\ 0 & -\sin \phi_1 & \cos \phi_1 \end{pmatrix}.$$

This transformation is a product of three counter-clockwise rotations: the first of them by the angle  $\phi_1 = 3\pi/4$  about the first old axis, the second one by the angle  $\phi_2 = \pi - \arctan(\sqrt{2}) \approx 16\pi/23$  about the third new axis, and the third one by the angle  $\phi_3 = \pi/3$  about the first new axis. Note, that the second angle  $\phi_2$  is supplementary to the angle between an edge and a face of a regular tetrahedron, associated with the system of symmetrized coordinates  $\{\xi_1, \xi_2, \xi_3\} \in \mathbf{R}^3$ . This transformation illustrates the isomorphism between the tetrahedron group  $T_d$  in  $\mathbf{R}^3$  and the 4-particle permutation group  $S_4$  ( $A = 4$ ), discussed in [26] in the case of  $d = 3$ . The three transformations  $M = M_3(\phi_3)M_2(\phi_2)M_1(\phi_1)$  are illustrated in Fig. 2.

Note, that the transformations from the initial coordinates to Jacobi coordinates are rotations in  $A \times d$ -configuration space, while the transformations from the initial coordinates to the symmetrized ones involve also permutations or reflections. The transformations between Jacobi and symmetrized coordinates in the center-of-mass hyperplane are rotations in the  $(A - 1) \times d$ -configuration space, but for odd  $A \times d$  they involve also a permutation or reflection. The key point of using the symmetrized coordinates is that in these coordinates the symmetry with respect to a permutation of two identical particles coincides with the symmetry with respect to a geometrical reflection in the  $(A - 2) \times d$ -dimensional plane  $\xi_i - \xi_j = 0$ . For example, at  $A = 3$  and  $d = 1$ , such  $((A - 2) \times d = 1)$ -dimensional objects are lines  $\xi_i - \xi_j = 0$ , see Fig. 1, while at  $A = 4$  and  $d = 1$ , such  $((A -$

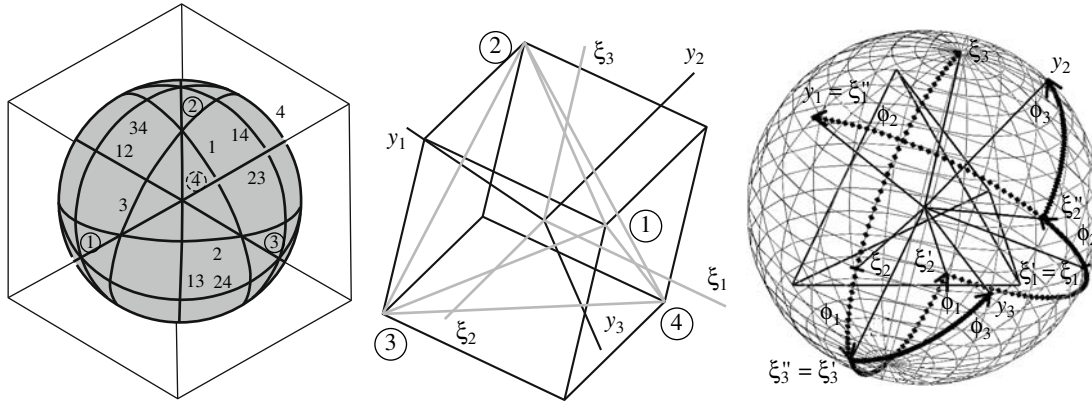


**Fig. 2.** (Left panel) Intersections in  $\mathbf{R}^4$  of the coordinate spaces  $\mathbf{R}^3$  (labelled 1, 2, 3, 4) and the spaces  $\mathbf{R}^3$  of pair collisions (labelled 12, etc.) with the sphere  $\mathbf{S}^2$  in the center-of-mass space  $\mathbf{R}^3$ . (Middle and right panels) The tetrahedron showing the isomorphism between the group of its symmetry operations  $T_d$  in  $\mathbf{R}^3$  and the group of permutations  $S_4$  of four objects 1, 2, 3, 4, labelled with circles. The two systems of coordinates,  $(y_1, y_2, y_3)$  and  $(\xi_1, \xi_2, \xi_3)$ , are related via the transformation (7), i.e. via three counterclockwise rotations by the angles  $\phi_1 = 3\pi/4$ ,  $\phi_2 = \pi - \arctan\sqrt{2}$ , and  $\phi_3 = \pi/3$  about the axes  $\xi_1$ ,  $\xi'_3$ , and  $y_1 = \xi''_1$ , respectively, are used in the text.

$2) \times d = 2$ )-dimensional objects are 2D planes. The lines in  $\mathbf{R}^4$ , corresponding to the intersection of the coordinate spaces  $\mathbf{R}^3$  (labelled 1, 2, 3, 4) and the pair-collision spaces  $\mathbf{R}^3$  (labelled 12, etc.) with the sphere  $\mathbf{S}^2$  in the center-of-mass space  $\mathbf{R}^3$  are shown in Fig. 2.

In the symmetrized coordinates Eq. (1) takes the form

$$\left[ -\frac{\partial^2}{\partial \xi_0^2} + \sum_{i=1}^{A-1} \left( -\frac{\partial^2}{\partial \xi_i^2} + (\xi_i)^2 \right) + U(\xi_0, \dots, \xi_{A-1}) - E \right] \Psi(\xi_0, \dots, \xi_{A-1}) = 0, \quad (8)$$

$$U(\xi_0, \dots, \xi_{A-1}) = \sum_{i,j=1; i < j}^A U^{\text{pair}}(x_{ij}(\xi_1, \dots, \xi_{A-1})) + \sum_{i=1}^A V(x_i(\xi_0, \dots, \xi_{A-1})),$$

which is *invariant* under permutations  $\xi_i \leftrightarrow \xi_j$  at  $i, j = 1, \dots, A-1$ , as follows from Eq. (4), i.e., the *invariance* of Eq. (1) under permutations  $x_i \leftrightarrow x_j$  at  $i, j = 1, \dots, A$  survives. This remarkable fact is one of the most prominent features of the proposed approach.

Here and below we use the oscillator units introduced above.

#### Asymptotic Boundary Conditions

For simplicity we restrict our consideration to the so-called *s*-wave approximation [1], i.e., one-

dimensional Euclidean space ( $d = 1$ ). The asymptotic boundary conditions for the solution  $\Psi(\xi_0, \xi) = \{\Psi_{i_o}(\xi_0, \xi)\}_{i_o=1}^{N_o}$  ( $\xi_0, \xi = \{\xi_1, \dots, \xi_{A-1}\}$ ) have the form

$$\begin{aligned} & \Psi_{i_o}^{\leftarrow}(\xi_0 \rightarrow \pm\infty, \xi) \quad (9) \\ & \rightarrow \tilde{\Phi}_{i_o}(\xi) \frac{\exp(\mp i(p_{i_o}\xi_0))}{\sqrt{p_{i_o}}} \\ & + \sum_{j=1}^{N_o} \tilde{\Phi}_j(\xi) \frac{\exp(\pm i(p_j\xi_0))}{\sqrt{p_j}} R_{ji_o}^{\leftarrow}(E), \\ & \Psi_{i_o}^{\leftarrow}(\xi_0 \rightarrow \mp\infty, \xi) \\ & \rightarrow \sum_{j=1}^{N_o} \tilde{\Phi}_j(\xi) \frac{\exp(\mp i(p_j\xi_0))}{\sqrt{p_j}} T_{ji_o}^{\leftarrow}(E), \\ & \Psi_{i_o}^{\leftarrow}(\xi_0, |\xi| \rightarrow \infty) \rightarrow 0. \end{aligned}$$

Here,  $v = \leftarrow, \rightarrow$  indicates the initial direction of the particle motion along the  $\xi_0$  axis,  $N_o$  is the number of open channels at the fixed energy  $E$  and relative momentum  $p_{i_o}^2 = E - E_{i_o} > 0$  of the cluster;  $R_{ji_o}^{\leftarrow} = R_{ji_o}^{\leftarrow}(E)$ ,  $R_{ji_o}^{\rightarrow} = R_{ji_o}^{\rightarrow}(E)$  and  $T_{ji_o}^{\leftarrow} = T_{ji_o}^{\leftarrow}(E)$ ,  $T_{ji_o}^{\rightarrow} = T_{ji_o}^{\rightarrow}(E)$  are unknown amplitudes of the reflected and transmitted waves. We can rewrite Eqs. (9) in the matrix form  $\Psi = \Phi^T \mathbf{F}$ , describing the incident wave and outgoing waves at  $\xi_0^+ \rightarrow +\infty$  and  $\xi_0^- \rightarrow -\infty$  as

$$\begin{pmatrix} \mathbf{F}_{\rightarrow}(\xi_0^+) & \mathbf{F}_{\leftarrow}(\xi_0^+) \\ \mathbf{F}_{\rightarrow}(\xi_0^-) & \mathbf{F}_{\leftarrow}(\xi_0^-) \end{pmatrix} \quad (10)$$

$$= \begin{pmatrix} \mathbf{0} & \mathbf{X}^{(-)}(\xi_0^+) \\ \mathbf{X}^{(+)}(\xi_0^-) & \mathbf{0} \end{pmatrix} + \begin{pmatrix} \mathbf{0} & \mathbf{X}^{(+)}(\xi_0^+) \\ \mathbf{X}^{(-)}(\xi_0^-) & \mathbf{0} \end{pmatrix} \mathbf{S},$$

where the unitary and symmetric scattering matrix  $\mathbf{S}$

$$\mathbf{S} = \begin{pmatrix} \mathbf{R}_{\rightarrow} & \mathbf{T}_{\leftarrow} \\ \mathbf{T}_{\rightarrow} & \mathbf{R}_{\leftarrow} \end{pmatrix}, \quad \mathbf{S}^\dagger \mathbf{S} = \mathbf{S} \mathbf{S}^\dagger = \mathbf{I} \quad (11)$$

is composed of the matrices, whose elements are reflection and transmission amplitudes that enter Eqs. (9). These matrices possess the following properties (see [41] for details):

$$\mathbf{T}_{\rightarrow}^\dagger \mathbf{T}_{\rightarrow} + \mathbf{R}_{\rightarrow}^\dagger \mathbf{R}_{\rightarrow} = \mathbf{I}_{oo} \quad (12)$$

$$= \mathbf{T}_{\leftarrow}^\dagger \mathbf{T}_{\leftarrow} + \mathbf{R}_{\leftarrow}^\dagger \mathbf{R}_{\leftarrow},$$

$$\mathbf{T}_{\rightarrow}^\dagger \mathbf{R}_{\leftarrow} + \mathbf{R}_{\rightarrow}^\dagger \mathbf{T}_{\leftarrow} = \mathbf{0} = \mathbf{R}_{\leftarrow}^\dagger \mathbf{T}_{\rightarrow} + \mathbf{T}_{\leftarrow}^\dagger \mathbf{R}_{\rightarrow},$$

$$\mathbf{T}_{\rightarrow}^T = \mathbf{T}_{\leftarrow}, \quad \mathbf{R}_{\rightarrow}^T = \mathbf{R}_{\leftarrow}, \quad \mathbf{R}_{\leftarrow}^T = \mathbf{R}_{\rightarrow}.$$

If  $V^{\text{pair}}(x_{ij}) = V^{\text{hosc}}(x_{ij})$ , then the basis functions of  $(A-1)$ -dimensional oscillator  $\Phi_j(\boldsymbol{\xi})$  corresponding to the energy  $E_i = (2 \sum_{k=1}^{A-1} i_k + A - 1)$  have the form:

$$\left( -\frac{\partial^2}{\partial \boldsymbol{\xi}^2} + \boldsymbol{\xi}^2 - E_j \right) \Phi_j(\boldsymbol{\xi}) = 0, \quad (13)$$

$$\int_{-\infty}^{+\infty} \Phi_i(\boldsymbol{\xi}) \Phi_j(\boldsymbol{\xi}) d^{A-1} \boldsymbol{\xi} = \delta_{ij}.$$

In the next section we describe the procedure of constructing the required sets of basis functions that depend on  $A-1$  symmetrized internal coordinates and are symmetric (S) or antisymmetric (A) with respect to permutation of the initial  $A$  Cartesian coordinates of  $A$  identical particles and the corresponding eigenvalues for a cluster of  $A$  identical particles in the center-of-mass system (CMS), which we refer as *symmetrized coordinates representation*.

### 3. SYMMETRIZED COORDINATES REPRESENTATION

For simplicity, consider the solutions of Eq. (8) in the internal symmetrized coordinates  $\{\xi_1, \dots, \xi_{A-1}\} \in \mathbf{R}^{A-1}$ ,  $x_i \in \mathbf{R}^1$ , in the case of 1D Euclidean space ( $d=1$ ). The relevant equation describes an  $(A-1)$ -dimensional oscillator with the eigenfunctions  $\Phi_j(\xi_1, \dots, \xi_{A-1})$  and the energy eigenvalues  $E_j$ :

$$\left[ \sum_{i=1}^{A-1} \left( -\frac{\partial^2}{\partial \xi_i^2} + (\xi_i)^2 \right) - E_j \right] \quad (14)$$

$$\times \Phi_j(\xi_1, \dots, \xi_{A-1}) = 0,$$

$$E_j = 2 \sum_{k=1}^{A-1} i_k + A - 1,$$

where the numbers  $i_k$ ,  $k=1, \dots, A-1$ , are integer,  $i_k=0, 1, 2, 3, \dots$ . The eigenfunctions  $\Phi_j(\xi_1, \dots, \xi_{A-1})$  can be expressed in terms of the conventional eigenfunctions of individual 1D oscillators as

$$\Phi_j(\xi_1, \dots, \xi_{A-1}) \quad (15)$$

$$= \sum_{2 \sum_{k=1}^{A-1} i_k + A - 1 = E_j} \beta_{j[i_1, i_2, \dots, i_{A-1}]}$$

$$\times \bar{\Phi}_{[i_1, i_2, \dots, i_{A-1}]}(\xi_1, \dots, \xi_{A-1}),$$

$$\bar{\Phi}_{[i_1, i_2, \dots, i_{A-1}]}(\xi_1, \dots, \xi_{A-1}) = \prod_{k=1}^{A-1} \bar{\Phi}_{i_k}(\xi_k),$$

$$\bar{\Phi}_{i_k}(\xi_k) = \frac{\exp(-\xi_k^2/2) H_{i_k}(\xi_k)}{\sqrt{4\pi} \sqrt{2^{i_k}} \sqrt{i_k!}},$$

where  $H_{i_k}(\xi_k)$  are Hermite polynomials [42]. Generally, the energy level  $E_f = 2f + A - 1$ ,  $f = \sum_{k=1}^{A-1} i_k$ , of an  $(A-1)$ -dimensional oscillator is known [43] to possess the degeneracy multiplicity  $p = (A + f - 2)!/f!/(A-2)!$  with respect to the conventional oscillator eigenfunctions  $\bar{\Phi}_{[i_1, i_2, \dots, i_{A-1}]}(\xi_1, \dots, \xi_{A-1})$ . This degeneracy allows further symmetrization by choosing the appropriate coefficients  $\beta_{[i_1, i_2, \dots, i_{A-1}]}^{(j)}$ . Degeneracy multiplicity  $p$  of all states with the given energy  $E_j$  is defined by formula

$$p = \sum_{2 \sum_{k=1}^{A-1} i_k + A - 1 = E_j} N_\beta, \quad (16)$$

$$N_\beta = (A-1)! / \prod_{k=1}^{N_v} v_k!,$$

where  $N_\beta$  is the number of multiset permutations (m.p.) of  $[i_1, i_2, \dots, i_{A-1}]$ , and  $N_v \leq A-1$  is the number of different values  $i_k$  in the multiset  $[i_1, i_2, \dots, i_{A-1}]$ , and  $v_k$  is the number of repetitions of the given value  $i_k$ .

#### Step 1. Symmetrization with Respect to Permutation of $A-1$ Particles

For the states  $\Phi_j^s(\xi_1, \dots, \xi_{A-1}) \equiv \Phi_{[i_1, i_2, \dots, i_{A-1}]}^s \times (\xi_1, \dots, \xi_{A-1})$ , symmetric with respect to permutation of  $A-1$  particles  $i = [i_1, i_2, \dots, i_{A-1}]$ , the coefficients  $\beta_{i[i'_1, i'_2, \dots, i'_{A-1}]}$  in Eq. (15) are

$$\beta_{i[i'_1, i'_2, \dots, i'_{A-1}]} \quad (17)$$

**Table 1.** The eigenvalues  $E_j^s = E_{[i_1, i_2, \dots, i_{N-1}]}^s$  for the first oscillator symmetric eigenfunctions  $\Phi_j^s(\xi_1, \dots, \xi_{N-1}) = |[i_1, i_2, \dots, i_{A-1}] \rangle = \Phi_{[i_1, i_2, \dots, i_{A-1}]}^s(\xi_1, \dots, \xi_{A-1})$  with  $E_j^s - E_1^s = 2 \sum_{k=1}^{A-1} i_k \leq 10$ ,  $E_1^s = A - 1$  and corresponding number  $N_\beta$  of a multiset permutations  $[i_1, i_2, \dots, i_{A-1}]$  of quantum numbers  $i_1, i_2, \dots, i_{A-1}$  from (16) (see (17))

$A = 3$			$A = 4$			$A = 5$			$A = 6$			$E_j^s - E_1^s$
$j$	$ [i_1, i_2] \rangle$	$N_\beta$	$j$	$ [i_1, i_2, i_3] \rangle$	$N_\beta$	$j$	$ [i_1, i_2, i_3, i_4] \rangle$	$N_\beta$	$j$	$ [i_1, i_2, i_3, i_4, i_5] \rangle$	$N_\beta$	
1	$ [0, 0] \rangle$	1	1	$ [0, 0, 0] \rangle$	1	1	$ [0, 0, 0, 0] \rangle$	1	1	$ [0, 0, 0, 0, 0] \rangle$	1	0
2	$ [0, 1] \rangle$	2	2	$ [0, 0, 1] \rangle$	3	2	$ [0, 0, 0, 1] \rangle$	4	2	$ [0, 0, 0, 0, 1] \rangle$	5	2
3	$ [0, 2] \rangle$	2	3	$ [0, 0, 2] \rangle$	3	3	$ [0, 0, 0, 2] \rangle$	4	3	$ [0, 0, 0, 0, 2] \rangle$	5	
4	$ [1, 1] \rangle$	1	4	$ [0, 1, 1] \rangle$	3	4	$ [0, 0, 1, 1] \rangle$	6	4	$ [0, 0, 0, 1, 1] \rangle$	10	4
5	$ [0, 3] \rangle$	2	5	$ [0, 0, 3] \rangle$	3	5	$ [0, 0, 0, 3] \rangle$	4	5	$ [0, 0, 0, 0, 3] \rangle$	5	
6	$ [1, 2] \rangle$	2	6	$ [0, 1, 2] \rangle$	6	6	$ [0, 0, 1, 2] \rangle$	12	6	$ [0, 0, 0, 1, 2] \rangle$	20	6
			7	$ [1, 1, 1] \rangle$	1	7	$ [0, 1, 1, 1] \rangle$	4	7	$ [0, 0, 1, 1, 1] \rangle$	10	
7	$ [0, 4] \rangle$	2	8	$ [0, 0, 4] \rangle$	3	8	$ [0, 0, 0, 4] \rangle$	4	8	$ [0, 0, 0, 0, 4] \rangle$	5	
8	$ [1, 3] \rangle$	2	9	$ [0, 1, 3] \rangle$	6	9	$ [0, 0, 1, 3] \rangle$	12	9	$ [0, 0, 0, 1, 3] \rangle$	20	
9	$ [2, 2] \rangle$	1	10	$ [0, 2, 2] \rangle$	3	10	$ [0, 0, 2, 2] \rangle$	6	10	$ [0, 0, 0, 2, 2] \rangle$	10	8
			11	$ [1, 1, 2] \rangle$	3	11	$ [0, 1, 1, 2] \rangle$	12	11	$ [0, 0, 1, 1, 2] \rangle$	30	
						12	$ [1, 1, 1, 1] \rangle$	1	12	$ [0, 1, 1, 1, 1] \rangle$	5	
10	$ [0, 5] \rangle$	2	12	$ [0, 0, 5] \rangle$	3	13	$ [0, 0, 0, 5] \rangle$	4	13	$ [0, 0, 0, 0, 5] \rangle$	5	
11	$ [1, 4] \rangle$	2	13	$ [0, 1, 4] \rangle$	6	14	$ [0, 0, 1, 4] \rangle$	12	14	$ [0, 0, 0, 1, 4] \rangle$	20	
12	$ [2, 3] \rangle$	2	14	$ [0, 2, 3] \rangle$	6	15	$ [0, 0, 2, 3] \rangle$	12	15	$ [0, 0, 0, 2, 3] \rangle$	20	
			15	$ [1, 1, 3] \rangle$	3	16	$ [0, 1, 1, 3] \rangle$	12	16	$ [0, 0, 1, 1, 3] \rangle$	30	10
			16	$ [1, 2, 2] \rangle$	3	17	$ [0, 1, 2, 2] \rangle$	12	17	$ [0, 0, 1, 2, 2] \rangle$	30	
						18	$ [1, 1, 1, 2] \rangle$	4	18	$ [0, 1, 1, 1, 2] \rangle$	20	
									19	$ [1, 1, 1, 1, 1] \rangle$	1	

$$= \begin{cases} \frac{1}{\sqrt{N_\beta}}, & \text{if } [i'_1, i'_2, \dots, i'_{A-1}] \text{ is a multiset} \\ & \text{permutation of } [i_1, i_2, \dots, i_{A-1}]; \\ 0, & \text{otherwise.} \end{cases}$$

In Table 1 we demonstrate the rules of correspondence between the multisets of quantum numbers  $[i_1, i_2, \dots, i_{A-1}]$  and the numbers  $j$  of the eigenfunctions  $\Phi_j^s(\xi_1, \dots, \xi_{A-1})$  for symmetric states of an  $(A - 1)$ -dimensional harmonic oscillator with the energy eigenvalues  $E_j^s$ , enumerated in nondecreasing order,  $E_1^s = A - 1 < E_2^s \leq E_3^s \leq E_4^s \leq \dots$ , for  $A$  particles with the degenerate spectrum  $E_j^s = 2 \sum_{k=1}^{A-1} i_k + A - 1$ . The corresponding isolines of the first eight symmetric oscillator eigenfunctions  $\Phi_{[i_1, i_2]}^s(\xi_1, \xi_2)$  for  $A = 3$  are shown in Fig. 3.

With increasing  $A$  for given  $E' = E_j^s - E_1^s$  the multiplicity of degeneracy, i.e., the number  $p_s \leq p$

of symmetric eigenfunctions, corresponding to the same eigenvalue, sharply increases and reaches a plateau. At fixed  $A$  with increasing  $E'$  the multiplicity increases faster, when  $A$  is larger. For example, the eigenvalue  $E' = 6$  at  $A = 2$  is nondegenerate ( $p_s = 1$ ), at  $A = 3$  it is doubly degenerate ( $p_s = 2$ ), and at large  $A \geq 4$  it is triply degenerate ( $p_s = 3$ ). For  $A = 4$ , when the eigenvalue increases from  $E' = 8$  to  $E' = 10$ , the multiplicity increases from  $p_s = 4$  to  $p_s = 5$ , while for  $A = 6$  under the same conditions the multiplicity increases from  $p_s = 5$  to  $p_s = 7$ .

For example, we can construct the states, antisymmetric with respect to permutation of  $A - 1$  particles with spin  $1/2$ , in a conventional way as a product of two determinants of  $K \times K$  and  $[(A - 1)K] \times [(A - 1)K]$  matrices, involving  $K$  and  $[(A - 1)K]$  states of pairs of particles with compensated and noncompensated spins, respectively, such that the total spin equals  $(A - 1)/2 - K$  [22, 23]. For



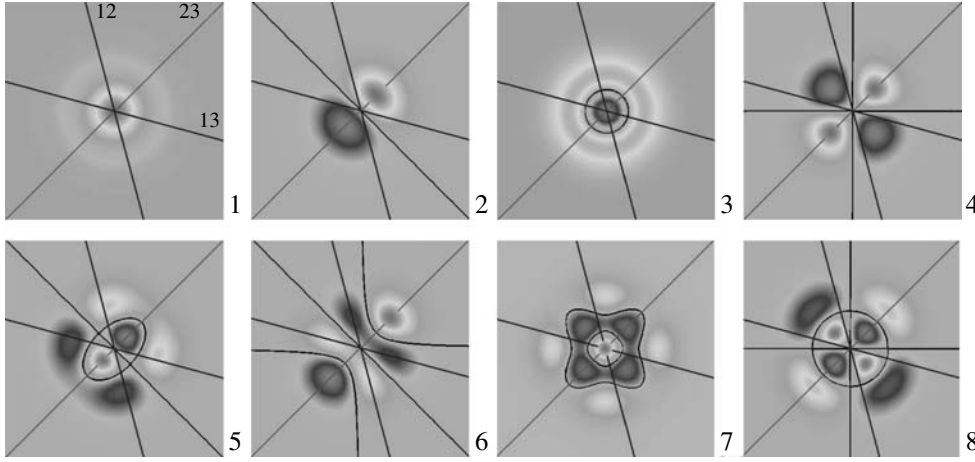


**Fig. 3.** Profiles of the first eight oscillator s eigenfunctions  $\Phi_{[i_1, i_2]}^s(\xi_1, \xi_2)$ , at  $A = 3$  in the coordinate frame  $(\xi_1, \xi_2)$ . The lines correspond to pair collision  $x_2 = x_3$ ,  $x_1 = x_2$  and  $x_1 = x_3$  of projection  $(x_1, x_2, x_3) \rightarrow (\xi_1, \xi_2)$  marked only in the left upper panel by 23, 12, and 13, respectively. The additional lines are nodes of the eigenfunctions  $\Phi_{[i_1, i_2]}^s(\xi_1, \xi_2)$ .

simplicity we consider a restricted case. The states  $\Phi_j^a(\xi_1, \dots, \xi_{A-1}) \equiv \Phi_{[i_1, i_2, \dots, i_{A-1}]}^a(\xi_1, \dots, \xi_{A-1})$ , antisymmetric with respect to permutation of  $A - 1$  particles, are constructed in a conventional way

$$\Phi_{[i_1, i_2, \dots, i_{A-1}]}^a(\xi_1, \dots, \xi_{A-1}) = \frac{1}{\sqrt{(A-1)!}} \quad (18)$$

$$\times \begin{vmatrix} \bar{\Phi}_{i_1}(\xi_1) & \bar{\Phi}_{i_2}(\xi_1) & \cdots & \bar{\Phi}_{i_{A-1}}(\xi_1) \\ \bar{\Phi}_{i_1}(\xi_2) & \bar{\Phi}_{i_2}(\xi_2) & \cdots & \bar{\Phi}_{i_{A-1}}(\xi_2) \\ \vdots & \vdots & \ddots & \vdots \\ \bar{\Phi}_{i_1}(\xi_{A-1}) & \bar{\Phi}_{i_2}(\xi_{A-1}) & \cdots & \bar{\Phi}_{i_{A-1}}(\xi_{A-1}) \end{vmatrix},$$

i.e., the coefficients  $\beta_{i[i'_1, i'_2, \dots, i'_{A-1}]}$  in Eq. (15) are expressed as  $\beta_{i[i'_1, i'_2, \dots, i'_{A-1}]} = \varepsilon_{i'_1, i'_2, \dots, i'_{A-1}} / \sqrt{(A-1)!}$ , where  $\varepsilon_{i'_1, i'_2, \dots, i'_{A-1}}$  is a totally antisymmetric tensor. This tensor is defined as follows:  $\varepsilon_{i'_1, i'_2, \dots, i'_{A-1}} = +1(-1)$  if  $i'_1, i'_2, \dots, i'_{A-1}$  is an even (odd) permutation of the numbers  $i_1 < i_2 < \dots < i_{A-1}$  and  $\varepsilon_{i'_1, i'_2, \dots, i'_{A-1}} = 0$  otherwise, i.e., when some two numbers in the set  $i'_1, i'_2, \dots, i'_{A-1}$  are equal. Therefore, for antisymmetric states the indices  $i_k$  in Eq. (14) take the integer values  $i_k = k - 1, k, k + 1, \dots; k = 1, \dots, A - 1$ .

Table 2 demonstrates the rules of correspondence between the multisets of quantum numbers  $[i_1, i_2, \dots, i_{A-1}]$  and the numbers  $j$  of the eigenfunctions  $\Phi_j^a(\xi_1, \dots, \xi_{A-1})$  for antisymmetric states of an  $(A - 1)$ -dimensional harmonic oscillator with the energy eigenvalues  $E_j^a$ , enumerated in nondecreasing order,  $E_1^a = (A - 1)^2 < E_2^a \leq E_3^a \leq E_4^a \leq \dots$ , for  $A$  particles with the degenerate spectrum

$E_j^a = 2 \sum_{k=1}^{A-1} i_k + A - 1$ . For given  $E' = E_j^a - E_1^a$  the number  $p_a < p$  of degenerate antisymmetric eigenfunctions is seen to equal the number  $p_s^{A-1} \leq p$  of symmetric eigenfunctions with the same  $E' = E_j^s - E_1^s$ . Note, that the multisets, characterizing symmetric states, are related with the sets, characterizing antisymmetric states, by the following rule: the first number is left unchanged, from the second number we subtract one, from the third one we subtract two, and so on. The corresponding isolines of the first eight oscillator antisymmetric eigenfunctions  $\Phi_{[i_1, i_2]}^a(\xi_1, \xi_2)$  for  $A = 3$  are shown in Fig. 4.

Here and below the indexes  $s$  and  $a$  are used for the functions, symmetric (antisymmetric) under permutations of  $A - 1$  relative coordinates, constructed at the first step of the procedure. On the contrary, indexes  $S$  and  $A$  are used for functions, symmetric (asymmetric) under permutations of  $A$  initial Cartesian coordinates. This is actually a symmetry with respect to permutation of identical particles themselves; in this sense  $S$  and  $A$  states may be attributed to boson- and fermion-like particles. However, we prefer to use the  $S(A)$  notation as more rigorous.

### Step 2. Symmetrization with Respect to Permutation of $A$ Particles

For  $A = 2$  the symmetrized coordinate  $\xi_1$  corresponds to the difference  $x_2 - x_1$  of Cartesian coordinates, so that a function even (odd) with respect to  $\xi_1$  appears to be symmetric (antisymmetric) with respect to the permutation of two particles  $x_2 \leftrightarrow x_1$ . Hence, even (odd) eigenfunctions with corresponding eigenvalues  $E_j^s = 2(2n) + 1$  ( $E_j^a = 2(2n + 1) + 1$ ) describe  $S(A)$  solutions.

**Table 2.** The eigenvalues  $E_j^a = E_{[i_1, i_2, \dots, i_{A-1}]}^a$  for the first oscillator antisymmetric eigenfunctions  $\Phi_j^a(\xi_1, \dots, \xi_{A-1}) = |[i_1, i_2, \dots, i_{A-1}] = \Phi_{[i_1, i_2, \dots, i_{A-1}]}^a(\xi_1, \dots, \xi_{A-1})$  from (18) with  $E_j^a - E_1^a \leq 10$ ,  $E_1^a = (A-1)^2$

$A = 3, E_1^a = 4$		$A = 4, E_1^a = 9$		$A = 5, E_1^a = 16$		$E_j^a - E_1^a$
$j$	$ [i_1, i_2]\rangle$	$j$	$ [i_1, i_2, i_3]\rangle$	$j$	$ [i_1, i_2, i_3, i_4]\rangle$	
1	$ [0, 1]\rangle$	1	$ [0, 1, 2]\rangle$	1	$ [0, 1, 2, 3]\rangle$	0
2	$ [0, 2]\rangle$	2	$ [0, 1, 3]\rangle$	2	$ [0, 1, 2, 4]\rangle$	2
3	$ [1, 2]\rangle$	3	$ [0, 2, 3]\rangle$	3	$ [0, 1, 3, 4]\rangle$	
4	$ [0, 3]\rangle$	4	$ [0, 1, 4]\rangle$	4	$ [0, 1, 2, 5]\rangle$	4
5	$ [1, 3]\rangle$	5	$ [1, 2, 3]\rangle$	5	$ [0, 2, 3, 4]\rangle$	
6	$ [0, 4]\rangle$	6	$ [0, 2, 4]\rangle$	6	$ [0, 1, 3, 5]\rangle$	6
		7	$ [0, 1, 5]\rangle$	7	$ [0, 1, 2, 6]\rangle$	
7	$ [2, 3]\rangle$	8	$ [1, 2, 4]\rangle$	8	$ [1, 2, 3, 4]\rangle$	
8	$ [1, 4]\rangle$	9	$ [0, 3, 4]\rangle$	9	$ [0, 2, 3, 5]\rangle$	
9	$ [0, 5]\rangle$	10	$ [0, 2, 5]\rangle$	10	$ [0, 1, 4, 5]\rangle$	8
		11	$ [0, 1, 6]\rangle$	11	$ [0, 1, 3, 6]\rangle$	
				12	$ [0, 1, 2, 7]\rangle$	
10	$ [2, 4]\rangle$	12	$ [1, 3, 4]\rangle$	13	$ [1, 2, 3, 5]\rangle$	
11	$ [1, 5]\rangle$	13	$ [1, 2, 5]\rangle$	14	$ [0, 2, 4, 5]\rangle$	
12	$ [0, 6]\rangle$	14	$ [0, 3, 5]\rangle$	15	$ [0, 2, 3, 6]\rangle$	10
		15	$ [0, 2, 6]\rangle$	16	$ [0, 1, 4, 6]\rangle$	
		16	$ [0, 1, 7]\rangle$	17	$ [0, 1, 3, 7]\rangle$	
				18	$ [0, 1, 2, 8]\rangle$	

For  $A \geq 3$  the functions symmetric (antisymmetric) with respect to permutations of Cartesian coordinates  $x_{i+1} \leftrightarrow x_{j+1}$ ,  $i, j = 0, \dots, A-1$ :  $\Phi^{S(A)}(\dots, x_{i+1}, \dots, x_{j+1}, \dots) \equiv \Phi^{S(A)}(\xi_1(x_1, \dots, x_A), \dots, \xi_{A-1}(x_1, \dots, x_A)) = \pm \Phi^{S(A)}(\dots, x_{j+1}, \dots, x_{i+1}, \dots)$  become symmetric (antisymmetric) with respect to permutations of symmetrized coordinates  $\xi_i \leftrightarrow \xi_j$ ,  $i, j = 1, \dots, A-1$ :  $\Phi^{S(A)}(\dots, \xi_i, \dots, \xi_j, \dots) = \pm \Phi^{S(A)}(\dots, \xi_j, \dots, \xi_i, \dots)$ , as follows from Eq. (5). However, the converse statement is not valid,  $\Phi^{s(a)}(\dots, \xi_i, \dots, \xi_j, \dots) = \pm \Phi^{s(a)}(\dots, \xi_j, \dots, \xi_i, \dots) \not\equiv \Phi^{s(a)}(x_1, \dots, x_{i+1}, \dots) = \pm \Phi^{s(a)}(x_{i+1}, \dots, x_1, \dots)$ , because we deal with a projection map  $(\xi_1, \dots, \xi_{A-1})^T = \hat{C}(x_1, \dots, x_A)^T$ , which is implemented by the  $(A-1) \times A$  matrix  $\hat{C}$  with the matrix elements  $\hat{C}_{ij} = C_{i+1,j}$ , obtained from (4) by cancelling the first row. Hence, the functions, symmetric (antisymmetric) with respect to permutations of

symmetrized coordinates, are divided into two types, namely, the S (A) solutions, symmetric (antisymmetric) with respect to permutations  $x_1 \leftrightarrow x_{j+1}$  at  $j = 1, \dots, A-1$ :

$$\begin{aligned} & \Phi^{S(A)}(x_1, \dots, x_{i+1}, \dots) \\ & \equiv \Phi^{S(A)}(\xi_1(x_1, \dots, x_A), \dots, \xi_{A-1}(x_1, \dots, x_A)) \\ & = \pm \Phi^{S(A)}(x_{i+1}, \dots, x_1, \dots), \end{aligned}$$

and the other s (a) solutions,  $\Phi^{s(a)}(x_1, \dots, x_{i+1}, \dots) \neq \pm \Phi^{s(a)}(x_{i+1}, \dots, x_1, \dots)$ , which should be eliminated. These requirements are equivalent to only one permutation  $x_1 \leftrightarrow x_2$ , as follows from (5), which simplifies their practical implementation. With these requirements taken into account in the Gram–Schmidt process, implemented in a *symbolic algorithm SCR*, we obtained the required characteristics of S and A eigenfunctions

$$\Phi_i^{S(A)}(\xi_1, \dots, \xi_{A-1}) \quad (19)$$

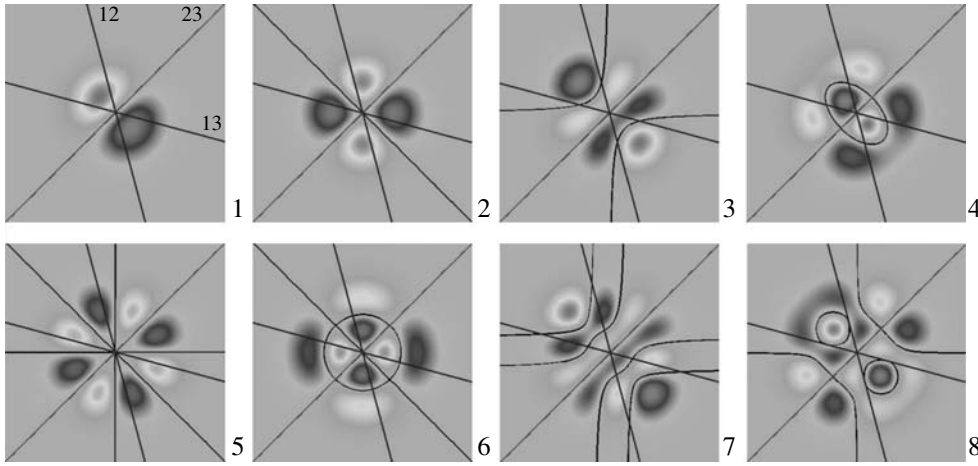


**Fig. 4.** The same as in Fig. 3, but for the first eight oscillator A eigenfunctions  $\Phi_{[i_1, i_2]}^A(\xi_1, \xi_2)$ , at  $A = 3$ .

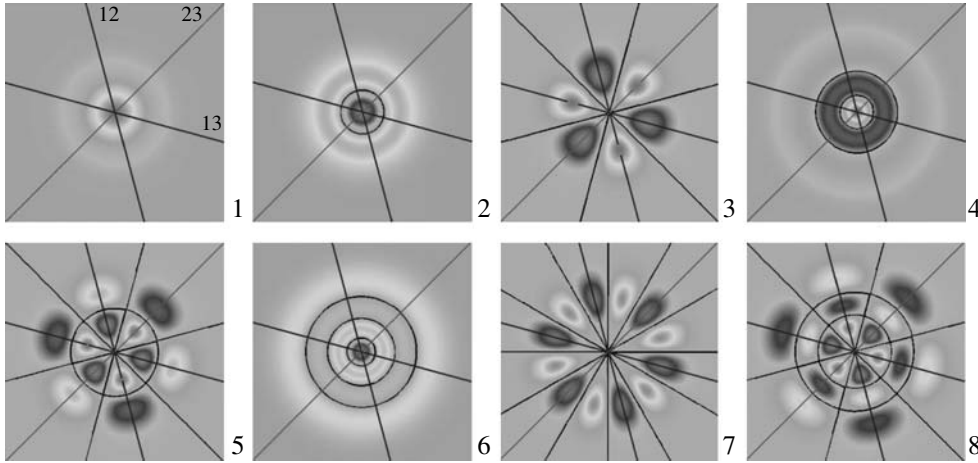


**Fig. 5.** The same as in Fig. 3, but for the first eight oscillator S eigenfunctions  $\Phi_{[i_1, i_2]}^S(\xi_1, \xi_2)$ , at  $A = 3$ .

$$= \sum_{2 \sum_{k=1}^{A-1} i_k + A - 1 = E_i^{s(a)}} \alpha_{i_{[i_1, i_2, \dots, i_{A-1}]}^{S(A)}} \times \Phi_{[i_1, i_2, \dots, i_{A-1}]}^{s(a)}(\xi_1, \dots, \xi_{A-1})$$

with respect to permutations of  $A$  identical particles, the examples of which are presented in Tables 3 and 4. Note, that for  $A = 4$  the first four states from Table 3 are similar to those of the translation-invariant model without excitation of the center-of-mass variable[37]. This SCR algorithm was implemented in Maple and published in [44].

As an example, in Figs. 5 and 6 we show isolines of the first eight S and A oscillator eigenfunctions  $\Phi_{[i_1, i_2]}^S(\xi_1, \xi_2)$  and  $\Phi_{[i_1, i_2]}^A(\xi_1, \xi_2)$  for  $A = 3$ , calculated at the second step of the algorithm. One can see that the S (A) oscillator eigenfunctions are symmetric (antisymmetric) with respect to reflections from three straight lines. The first line (labelled 23) corresponds

to the permutation  $(x_2, x_3)$  and is rotated by  $\pi/4$  counterclockwise with respect to the axis  $\xi_1$ . The second and the third lines (labelled 12 and 13) correspond to the permutations  $(x_1, x_2)$  and  $(x_1, x_3)$  and are rotated by  $\pi/3$  clockwise and counterclockwise with respect to the first line. These lines divide the plane into six sectors, while the symmetric (antisymmetric) oscillator eigenfunctions, calculated at the first step of the algorithm, which are symmetric (or antisymmetric) with respect to reflections from the first line, generate the division of the plane into two parts.

The Jacobi coordinates  $(y_1, y_2)$  are related to the symmetrized coordinates  $(\xi_1, \xi_2)$  via the orthogonal transformation (6), i.e., the permutation of coordinates  $(\xi_1, \xi_2) \rightarrow (\xi_2, \xi_1)$  and the clockwise rotation by the angle  $\phi_1 = \pi/12$ . Therefore, in the Jacobi coordinates the lines, corresponding to pair collisions of the particles  $(x_2, x_3)$ ,  $(x_1, x_2)$ , and  $(x_1, x_3)$ , will be also clockwise rotated by the angle  $\phi_1 = \pi/12$ .

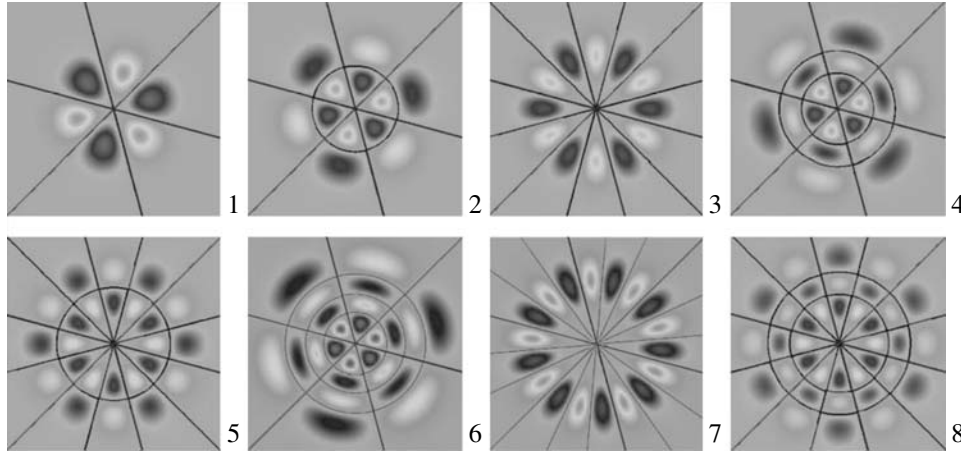


**Fig. 6.** The same as in Fig. 3, but for the first eight oscillator A eigenfunctions  $\Phi_{[i_1, i_2]}^A(\xi_1, \xi_2)$ , at  $A = 3$ .

Counterclockwise rotation of the coordinate system  $(\xi_2, \xi_1)$  to  $(y_1, y_2)$  by the angle  $\phi_1 = \pi/12$  induces a unitary transformation of the corresponding  $(A = 2)$ -oscillator functions  $\langle \xi_2, \xi_1 | i_2, i_1 \rangle = \bar{\Phi}_{[i_2, i_1]}(\xi_2, \xi_1)$  with  $j = (i_2 + i_1)/2$ :

$$\begin{aligned} & \langle j + m', j - m' | y_1, y_2 \rangle \\ &= \sum_{m=-j}^{m=j} \langle j + m', j - m' | G_{21}(\phi_1) | j + m, j - m \rangle \\ & \quad \times \langle j + m, j - m | \xi_2, \xi_1 \rangle. \end{aligned}$$

The matrix elements  $\langle j + m', j - m' | G_{21}(\phi_1) | j + m, j - m \rangle$  are expressed as the integrals [45]:

$$\begin{aligned} & \langle j + m', j - m' | G_{21}(\phi) | j + m, j - m \rangle \\ &= d_{m'm}^j(2\phi_1) = \int_{-\infty}^{\infty} \int_{-\infty}^{\infty} d\xi_2 d\xi_1 \langle j + m', \\ & \quad j - m' | \xi_2 \cos \phi_1 + \xi_1 \sin \phi_1, \\ & \quad -\xi_2 \sin \phi_1 + \xi_1 \cos \phi_1 \rangle \\ & \quad \times \langle \xi_2, \xi_1 | j + m, j - m \rangle, \end{aligned}$$

where

$$\begin{aligned} & d_{m'm}^j(2\phi_1) = N_{m'm}^j \sin^{|m'-m|} \phi_1 \\ & \quad \times \cos^{|m'+m|} \phi_1 P_{j-(|m'-m|+|m'+m|)/2}^{|m'-m|, |m'+m|}(\cos(2\phi_1)) \end{aligned}$$

are Wigner functions [46],  $N_{m'm}^j$  are the normalization factors,  $P_s^{\mu\nu}(x)$  are Jacobi polynomials [42]. This is the simplest integral representation of the oscillator Wigner functions [47].

Figure 7 shows examples of profiles of S and A oscillator eigenfunctions  $\Phi_{[i_1, i_2, i_3]}^{S,A}(\xi_1, \xi_2, \xi_3)$  for  $A = 4$ . Note that four maxima (black) and four minima

(grey) of the S eigenfunction  $\Phi_{[1,1,1]}^S(\xi_1, \xi_2, \xi_3)$  are positioned at the vertices of two tetrahedrons forming a *stella octangula*, with the edges shown by black and grey lines, respectively. Eight maxima and six outer minima for S eigenfunction  $\Phi_{[0,0,4]}^S(\xi_1, \xi_2, \xi_3)$  are positioned at the vertices of a cube and an octahedron, the edges of which are shown by black and grey lines, respectively. The positions of twelve maxima of the A oscillator eigenfunction,  $\Phi_{[0,2,4]}^A(\xi_1, \xi_2, \xi_3)$  coincide with the vertices of a polyhedron with 20 triangle faces (only 8 of them being equilateral triangles) and 30 edges, 6 of them having the length 2.25 and the other having the length 2.66.

For  $A = 4$  the 3D rotation (7), reducing the coordinate system  $(\xi_1, \xi_2, \xi_3)$  to  $(y_1, y_2, y_3)$ , can be presented as a product of three counterclockwise rotations  $M = M_3(\phi_3)M_2(\phi_2)M_1(\phi_1)$  in separate coordinate planes: by the angle  $\phi_1 = 3\pi/4$  about the first old axis,  $\xi_1$ , by the angle  $\phi_2 = \pi - \arctan(\sqrt{2}) \approx 16\pi/23$  about the third new axis,  $\xi'_3$ , and by the angle  $\phi_3 = \pi/3$  about the first new axis,  $y_1 = \xi'_1$  (see Fig. 2). This 3D rotation induces a unitary transformation of the corresponding  $(A = 3)$ -oscillator functions  $\langle \xi_1, \xi_2, \xi_3 | i_1, i_2, i_3 \rangle = \bar{\Phi}_{[i_1, i_2, i_3]}(\xi_1, \xi_2, \xi_3)$ ,  $n = i_1 + i_2 + i_3$ :

$$\begin{aligned} & \langle j' + m', j' - m', n - 2j' | y_1, y_2, y_3 \rangle \\ &= \sum_{j=0}^{n/2} \sum_{m=-j}^{m=j} \langle j' + m', j' - m', \\ & \quad n - 2j' | G(3) | j + m, j - m, n - 2j \rangle \\ & \quad \times \langle j + m, j - m, n - 2j | \xi_1, \xi_2, \xi_3 \rangle. \end{aligned}$$

Here the matrix elements  $\langle j' + m', j' - m', n - 2j' | G(3) | j + m, j - m, n - 2j \rangle$  are defined as [45]

$$\langle j' + m', j' - m',$$

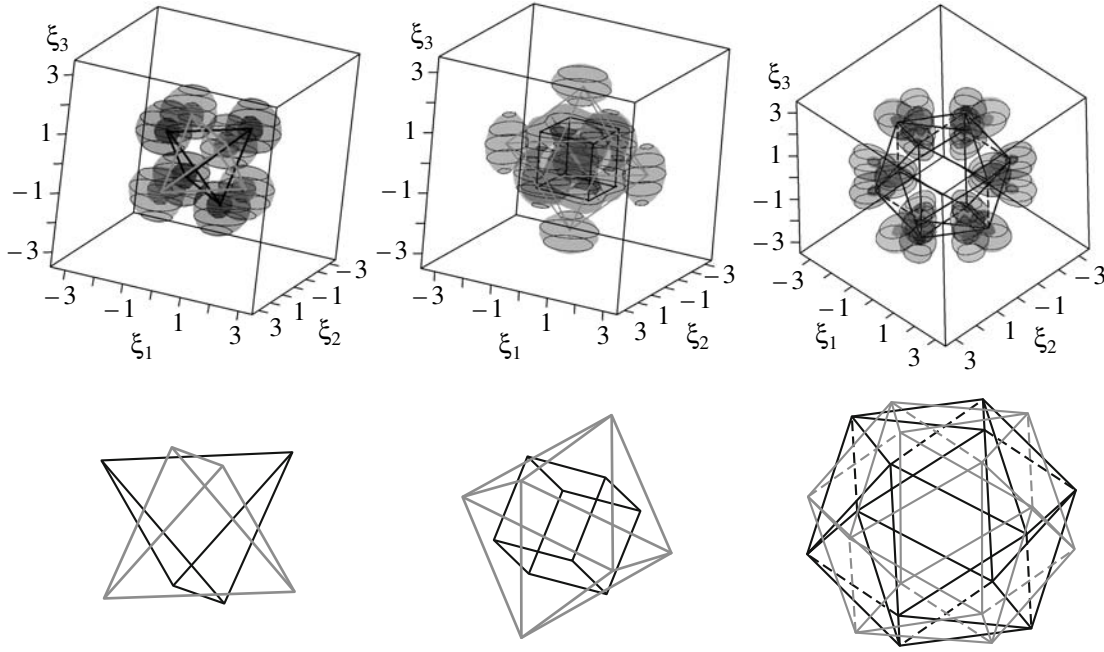


**Fig. 7.** (Upper panels) Profiles of the oscillator S eigenfunctions  $\Phi_{[1,1,1]}^S(\xi_1, \xi_2, \xi_3)$ ,  $\Phi_{[0,0,4]}^S(\xi_1, \xi_2, \xi_3)$  and A eigenfunction  $\Phi_{[0,2,4]}^A(\xi_1, \xi_2, \xi_3)$ , at  $A = 4$  (left, middle, and right panels, respectively). (Lower panels) Some maxima and minima positions of these functions are connected by black and gray lines and duplicated: two tetrahedrons forming a *stella octangula* for  $\Phi_{[1,1,1]}^S(\xi_1, \xi_2, \xi_3)$ , a cube and an octahedron for  $\Phi_{[0,0,4]}^S(\xi_1, \xi_2, \xi_3)$ , and a polyhedron with 20 triangle faces (only 8 of them being equilateral triangles) and 30 edges, 6 of them having the length 2.25 and the other having the length 2.66 for  $\Phi_{[0,2,4]}^A(\xi_1, \xi_2, \xi_3)$ .

$$\begin{aligned}
 & n - 2j' |G_{2,3}(\phi_3)G_{1,2}(\phi_2)G_{2,3}(\phi_1)|j + m, \\
 & \quad j - m, n - 2j \rangle \\
 & = \sum_t^{\min(j, j')} d_{t-j', m'}^{j'} (2\phi_3) d_{2j'-(n+t)/2, 2j-(n+t)/2}^{(n-t)/2} \\
 & \quad \times (2\phi_2) d_{m, t-j}^j (2\phi_1),
 \end{aligned}$$

where the values of  $t$  are such that the absolute values of all  $t$ -dependent subscripts in the Wigner  $d$  functions do not exceed those of the superscripts.

In the general case, the transformations of  $(A - 1)$ -dimensional oscillator functions induced by permutation of coordinates and  $(A - 1)$ -dimensional finite rotation, presented as a product of  $(A - 1)(A - 2)/2$  rotations in separate coordinate planes, can be constructed using the diagram method, which reduces the analytic calculations of the  $(A - 1)$ -dimensional *oscillator Wigner functions* to simple geometric operations [47].

The degeneracy multiplicity (16), i.e., the number  $p$  of all states with the given energy  $E_j$ , the numbers  $p_s$  ( $p_a$ ) of the states, symmetric (antisymmetric) under permutations of  $A - 1$  relative coordinates together with the total numbers  $p_S$  ( $p_A$ ) of the states, symmetric (antisymmetric) under permutations of  $A$

initial Cartesian coordinates are summarized in Table 5 for the bottom part of the energy spectrum.

Note that the S and A states with  $E' = E_1^{S,A} + 2$  do not exist. The numbers  $p_s$  ( $p_a$ ) are essentially smaller than the total number  $p$  of all states, which simplifies the procedure of constructing S (A) states with possible excitation of the center-of-mass degree of freedom and allows the use of a compact basis with the reduced degeneracy  $p_S$  ( $p_A$ ) of the S (A) states in our final calculations. For clarity, in the case  $A = 3$ ,  $d = 1$ , the S (A)-type functions generated by the SCR algorithm, in polar coordinates  $\xi_1 = \rho \cos \varphi$ ,  $\xi_2 = \rho \sin \varphi$  are expressed as:

$$\begin{aligned}
 & \Phi_{k,m}^{S(A)}(\rho, \varphi) = C_{km}(\rho^2)^{3m/2} \\
 & \quad \times \exp(-\rho^2/2) L_k^{3m}(\rho^2) \frac{\cos}{\sin}(3m(\varphi + \pi/12)),
 \end{aligned} \tag{20}$$

where  $C_{km}$  is the normalization constant,  $L_k^{3m}(\rho^2)$  are the Laguerre polynomials [42],  $k = 0, 1, \dots$ ,  $m = 0, 1, \dots$  for S states, while  $m = 1, 2, \dots$  for A states, that are classified by irreducible representations of the  $D_{3m}$  symmetry group. The corresponding energy levels  $E_{k,m}^{S(A)} = 2(2k + 3m + 1) = E_{[i_1, i_2]}^{s(a)} = 2(i_1 + i_2 + 1)$  have the degeneracy multiplicity  $K + 1$ , if the energy  $E_{k,m}^{S(A)} - E_1^{S(A)} = 12K + K'$ , where  $K' =$

**Table 3.** The first few eigenvalues  $E_j^S$  and the oscillator S eigenfunctions (19) at  $E_j^S - E_1^S \leq 10$ ,  $E_1^S = A - 1$  (We use the notations  $[[i_1, i_2, \dots, i_{A-1}]] \equiv \Phi_{[i_1, i_2, \dots, i_{A-1}]}^s(\xi_1, \dots, \xi_{A-1})$  from Eqs. (15) and (17), i.e.  $[i_1, i_2, \dots, i_{A-1}]$  assumes the summation over permutations of  $[i_1, i_2, \dots, i_{A-1}]$  in the layer  $2 \sum_{k=1}^{A-1} i_k + A - 1 = E_i^{s(a)}$ )

$A = 2$		$A = 3$		$A = 4$		$A = 5$		$E_j^S - E_1^S$
$j$	$\Phi_j^S(\xi_1)$	$j$	$\Phi_j^S(\xi_1, \xi_2)$	$j$	$\Phi_j^S(\xi_1, \xi_2, \xi_3)$	$j$	$\Phi_j^S(\xi_1, \xi_2, \xi_3, \xi_4)$	
1	$[[0]]$	1	$[[0, 0]]$	1	$[[0, 0, 0]]$	1	$[[0, 0, 0, 0]]$	0
2	$[[2]]$	2	$[[0, 2]]$	2	$[[0, 0, 2]]$	2	$[[0, 0, 0, 2]]$	4
		3	$\frac{1}{2}[[0, 3]] - \frac{\sqrt{3}}{2}[[1, 2]]$	3	$[[1, 1, 1]]$	3	$\approx -0.27[[0, 0, 0, 3]] + 0.27[[0, 0, 1, 2]] - 0.93[[0, 1, 1, 1]]$	6
3	$[[4]]$	4	$\frac{\sqrt{3}}{2}[[0, 4]] + \frac{1}{2}[[2, 2]]$	4	$[[0, 0, 4]]$	4	$\frac{\sqrt{2}}{2}[[0, 0, 0, 4]] + \frac{\sqrt{2}}{2}[[0, 0, 2, 2]]$	8
				5	$[[0, 2, 2]]$	5	$\approx -0.32[[0, 0, 0, 4]] - 0.39[[0, 0, 1, 3]] + 0.32[[0, 0, 2, 2]] + 0.67[[0, 1, 1, 2]] - 0.44[[1, 1, 1, 1]]$	
		5	$\frac{\sqrt{5}}{4}[[0, 5]] - \frac{3}{4}[[1, 4]] - \frac{\sqrt{2}}{4}[[2, 3]]$	6	$[[1, 1, 3]]$	6, 7	Two functions	10

**Table 4.** The first few eigenvalues  $E_j^A$  and the oscillator A eigenfunctions (19) at  $E_j^A - E_1^A \leq 10$ ,  $E_1^A = A^2 - 1$  (We use the notations  $[[i_1, i_2, \dots, i_{A-1}]] \equiv \Phi_{[i_1, i_2, \dots, i_{A-1}]}^a(\xi_1, \dots, \xi_{A-1})$  from Eq. (18), i.e.  $[i_1, i_2, \dots, i_{A-1}]$  assumes the summation over the multiset permutations of  $[i_1, i_2, \dots, i_{A-1}]$  in the layer  $2 \sum_{k=1}^{A-1} i_k + A - 1 = E_i^{s(a)}$ )

$A = 2, E_1^A = 3$		$A = 3, E_1^A = 8$		$A = 4, E_1^A = 15$		$E_j^A - E_1^A$
$j$	$\Phi_j^A(\xi_1)$	$j$	$\Phi_j^A(\xi_1, \xi_2)$	$j$	$\Phi_j^A(\xi_1, \xi_2, \xi_3)$	
1	$[[1]]$	1	$\frac{1}{2}[[0, 3]] + \frac{\sqrt{3}}{2}[[1, 2]]$	1	$[[0, 2, 4]]$	0
2	$[[3]]$	2	$\frac{\sqrt{5}}{4}[[0, 5]] + \frac{3}{4}[[1, 4]] - \frac{\sqrt{2}}{4}[[2, 3]]$	2	$[[0, 2, 6]]$	4
		3	$\frac{1}{4}[[0, 6]] - \frac{\sqrt{15}}{4}[[2, 4]]$	3	$[[1, 3, 5]]$	6
3	$[[5]]$	4	$\frac{\sqrt{21}}{8}[[0, 7]] + \frac{3\sqrt{3}}{8}[[1, 6]] - \frac{1}{8}[[2, 5]] + \frac{\sqrt{5}}{8}[[3, 4]]$	4	$[[0, 4, 6]]$	8
		5	$\frac{\sqrt{2}}{4}[[0, 8]] - \frac{\sqrt{14}}{4}[[2, 6]]$	5	$[[0, 2, 8]]$	
				6	$[[1, 3, 7]]$	10

0, 4, 6, 8, 10, 14. For example, in Figs. 5 and 6 we show the wave functions  $\Phi_{3,0}^S(\rho, \varphi)$  and  $\Phi_{0,2}^S(\rho, \varphi)$  (or  $\Phi_{3,1}^A(\rho, \varphi)$  and  $\Phi_{0,3}^A(\rho, \varphi)$ ) labelled with 6 and 7, corresponding to the energy levels  $E_{k,m}^{S(A)} - E_1^{S(A)} = 12$  with the degeneracy  $K = 2$ , while the functions labelled with 1, 2, 3, 4, 5, 8 are nondegenerate ( $K = 1$ ). From our calculation we conclude that the eigenfunctions of the  $A$  identical particle system in one dimension are degenerate like in [48], and this result disagrees with [49]. The latter can be presented

as a linear combination of the above S (A)-type functions.

#### The Parametric Symmetrized Coordinates Representation

Now let us introduce the basis of orthonormalized eigenfunctions  $\tilde{\Phi}_i(\xi; \xi_0)$ ,  $\xi = \{\xi_1, \dots, \xi_{A-1}\}$  of a parametric  $(A - 1)$ -dimensional oscillator with the energy eigenvalues  $\tilde{\epsilon}_i(\xi_0)$ :

$$\left[ \sum_{i=1}^{A-1} \left( -\frac{\partial^2}{\partial \xi_i^2} + (\xi_i)^2 \right) + U(\xi_0, \xi) \right] \tilde{\Phi}_i(\xi; \xi_0) = \tilde{\epsilon}_i(\xi_0) \tilde{\Phi}_i(\xi; \xi_0) \quad (21)$$

$$\begin{aligned}
 & -\tilde{\epsilon}_i(\xi_0) \Big] \tilde{\Phi}_i(\xi; \xi_0) = 0, \\
 U(\xi_0, \xi) &= \sum_{i,j=1; i < j}^A U^{\text{pair}}(x_{ij}(\xi)) + \sum_{i=1}^A V(x_i(\xi_0, \xi)).
 \end{aligned}$$

We choose the parametric SCR (PSCR) basis functions as linear combinations of the S and A eigenfunctions  $\Phi_{j'}^{S(A)}(\xi)$  constructed above:

$$\tilde{\Phi}_i(\xi; \xi_0) = \sum_{j'=1}^{j'_{\max}} \tilde{\alpha}_{j'}^{(i)}(\xi_0) \Phi_{j'}^{S(A)}(\xi). \quad (22)$$

Thus, the eigenvalue problem (21) is reduced to a parametric linearized version of the Hartree–Fock algebraic eigenvalue problem

$$\begin{aligned}
 & \sum_{j'=1}^{j'_{\max}} (\delta_{ij'} E_i + U_{ij'}(\xi_0)) \tilde{\alpha}_{j'}^{(i)}(\xi_0) = 0, \\
 & -\delta_{ij'} \tilde{\epsilon}_i(\xi_0) \tilde{\alpha}_{j'}^{(i)}(\xi_0) = 0, \\
 & \sum_{j'=1}^{j'_{\max}} \tilde{\alpha}_{j'}^{(i')}(\xi_0) \tilde{\alpha}_{j'}^{(i)}(\xi_0) = \delta_{ii'},
 \end{aligned} \quad (23)$$

where the effective potentials  $U_{ij'}(\xi_0) = U_{ij'}^{\text{pair}} + V_{ij'}(\xi_0)$  are expressed in terms of the integrals

$$\begin{aligned}
 U_{ij'}^{\text{pair}} &= \int d^{A-1} \xi \Phi_i^{S(A)}(\xi) \Phi_{j'}^{S(A)}(\xi) \\
 & \times \left( \sum_{k,k'=1; k < k'}^A U^{\text{pair}}(x_{kk'}(\xi)) \right) \Phi_{j'}^{S(A)}(\xi), \\
 V_{ij'}(\xi_0) &= \int d^{A-1} \xi \Phi_i^{S(A)}(\xi) \\
 & \times \left( \sum_{k=1}^A V(x_k(\xi_0, \xi)) \right) \Phi_{j'}^{S(A)}(\xi).
 \end{aligned} \quad (24)$$

Taking Eqs. (15) and (19) into account, integrals (24) are expressed via basis integrals

$$\begin{aligned}
 & U_{ij'}^{\text{pair}} \\
 &= \sum_{i' [i_1'', \dots, i_{A-1}''] [j_1'', \dots, j_{A-1}''] j'} \alpha_{ii'}^{S(A)} \beta_{i' [i_1'', \dots, i_{A-1}'']}^{s(a)} \\
 & \times \bar{U}_{[i_1'', \dots, i_{A-1}''] [j_1'', \dots, j_{A-1}'']}^{\text{pair}} \beta_{j' [i_1'', \dots, i_{A-1}'']}^{s(a)} \alpha_{jj'}^{S(A)}, \\
 & V_{ij'}(\xi_0) \\
 &= \sum_{i' [i_1'', \dots, i_{A-1}''] [j_1'', \dots, j_{A-1}''] j'} \alpha_{ii'}^{S(A)} \beta_{i' [i_1'', \dots, i_{A-1}'']}^{s(a)}
 \end{aligned} \quad (25)$$

$$\begin{aligned}
 & \times \bar{V}_{[i_1'', \dots, i_{A-1}''] [j_1'', \dots, j_{A-1}'']}(\xi_0) \beta_{j' [i_1'', \dots, i_{A-1}'']}^{s(a)} \alpha_{jj'}^{S(A)}, \\
 \bar{U}_{[i_1'', \dots, i_{A-1}''] [j_1'', \dots, j_{A-1}'']}^{\text{pair}} &= \int d^{A-1} \xi \bar{\Phi}_{[i_1'', \dots, i_{A-1}'']}(\xi) \\
 & \times \left( \sum_{k,k'=1; k < k'}^A U^{\text{pair}}(x_{kk'}(\xi)) \right) \bar{\Phi}_{[j_1'', \dots, j_{A-1}'']}(\xi), \\
 \bar{V}_{[i_1'', \dots, i_{A-1}''] [j_1'', \dots, j_{A-1}'']}(\xi_0) &= \int d^{A-1} \xi \bar{\Phi}_{[i_1'', \dots, i_{A-1}'']}(\xi) \\
 & \times \left( \sum_{k=1}^A V(x_k(\xi_0, \xi)) \right) \bar{\Phi}_{[j_1'', \dots, j_{A-1}'']}(\xi).
 \end{aligned}$$

If  $U_{ij'}(\xi_0) = U_{ij'}^{\text{pair}}$  are independent of  $\xi_0$ , then  $\tilde{\epsilon}_i(\xi_0) = \tilde{\epsilon}_i$  and  $\tilde{\alpha}_{j'}^{(i)}(\xi_0) = \tilde{\alpha}_{j'}^{(i)}$  are also independent of  $\xi_0$ , and Eq. (22) reduces to

$$\tilde{\Phi}_i(\xi) = \sum_{j'=1}^{j'_{\max}} \tilde{\alpha}_{j'}^{(i)} \Phi_{j'}^{S(A)}(\xi). \quad (26)$$

Moreover, if  $U_{ij'}^{\text{pair}} = 0$ , then  $\tilde{\epsilon}_i = E_i^{S(A)}$  and  $\tilde{\alpha}_{j'}^{(i)} = \delta_{ij'}$ , and Eq. (26) reduces to Eq. (19). The solutions of the parametric eigenvalue problem (23) and their derivatives with respect to parameter  $\xi_0$  are calculated by means of algorithms [50, 51].

An example of such parametric basis of S type at  $A = 2$  was considered earlier [1, 18]. The case  $A \geq 3$  will be considered elsewhere. The algebraic problem in symmetrized coordinates can be rewritten also in terms of the integrals that involve the eigenfunctions of  $(A - 1)$ -dimensional harmonic oscillator in Jacobi coordinates, making use of the interbasis coefficients, generated by the transformations with  $(A - 1)$ -dimensional *oscillator Wigner functions*, described in the previous subsection.

#### 4. CLOSE-COUPLING EQUATIONS IN THE SCR

Now we proceed to seeking the solution of the problem (8) in the symmetrized coordinates in the form of Galerkin expansion

$$\Psi_{i_o}(\xi_0, \xi) = \sum_{j=1}^{j_{\max}} \tilde{\Phi}_j(\xi) \chi_{ji_o}(\xi_0), \quad (27)$$

where  $\chi_i(\xi_0)$  are unknown functions

$$\chi_{ji_o}(\xi_0) = \int d^{A-1} \xi \tilde{\Phi}_j(\xi) \Psi_{i_o}(\xi_0, \xi),$$

and  $\tilde{\Phi}_j(\xi)$  are the orthonormalized basis eigenfunctions (26) of the  $(A - 1)$ -dimensional oscillator with

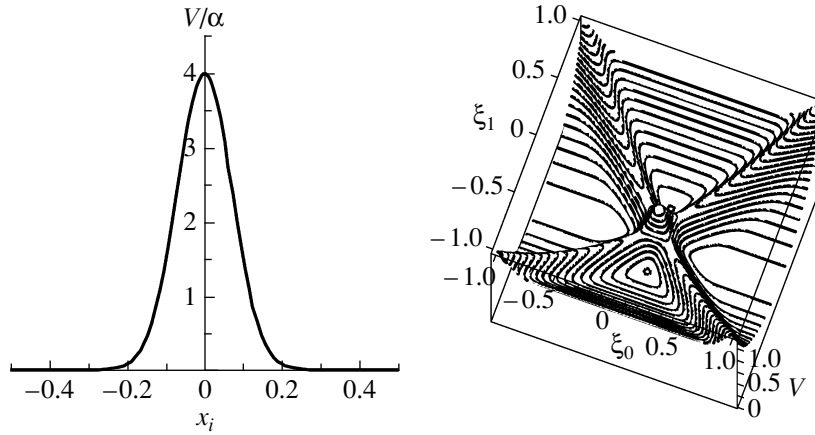


**Fig. 8.** (Left panel) Gaussian-type potential (30) at  $\sigma = 0.1$  (in oscillator units). (Right panel) Corresponding 2D barrier potential at  $\alpha = 1/10$ ,  $\sigma = 0.1$ .

the energy eigenvalues  $E_i$ , Eq. (14), constructed in the SCR.

The set of close-coupling Galerkin equations in the symmetrized coordinates has the form

$$\left[ -\frac{d^2}{d\xi_0^2} + \tilde{\epsilon}_i - E \right] \chi_{ii_0}(\xi_0) + \sum_{j=1}^{j_{\max}} \tilde{V}_{ij}(\xi_0) \chi_{ji_0}(\xi_0) = 0, \quad (28)$$

where the effective potentials  $\tilde{V}_{ij}(\xi_0)$  are calculated by means of  $V_{ij}(\xi_0)$  from (24)

$$\tilde{V}_{ij}(\xi_0) = \sum_{j'=1}^{j'_{\max}} \sum_{j''=1}^{j''_{\max}} \tilde{\alpha}_{j'}^{(i)} V_{j'j''}(\xi_0) \tilde{\alpha}_{j''}^{(j)}, \quad (29)$$

and a set of the eigenvectors  $\tilde{\alpha}_{j'}^{(i)}$  of the nonparametric algebraic problem (23) under the above condition  $U_{ij'}(\xi_0) = U_{ij'}^{\text{pair}} \neq 0$ . In the examples considered below we put  $U_{ij'}(\xi_0) = U_{ij'}^{\text{pair}} = 0$  in (23), then we have  $\tilde{\epsilon}_i = E_i^{S(A)}$ ,  $\tilde{\alpha}_{j'}^{(i)} = \delta_{ij'}$  and  $\tilde{V}_{ij}(\xi_0) = V_{ij}(\xi_0)$ .

The repulsive barrier is chosen to be Gaussian

$$V(x_i) = \frac{\alpha}{\sqrt{2\pi}\sigma} \exp\left(-\frac{x_i^2}{\sigma^2}\right). \quad (30)$$

Figure 8 illustrates the Gaussian potential and the corresponding barrier potentials in symmetrized coordinates at  $A = 2$ . This potential has the oscillator-type shape, and two barriers are crossing at the right angle. In the case  $A \geq 3$  the hyperplanes of barriers are crossing at the right angle, too. The effective potentials  $V_{ij}(\xi_0)$  calculated using *symbolic algorithm* SCR described in the previous section are shown in Figs. 9 and 10. In comparison with the symmetric

basis, for antisymmetric one the increase of the numbers  $i$  and/or  $j$  results in stronger oscillation of the effective potentials  $V_{ij}$  and weaker decrease of them to zero at  $\xi_0 \rightarrow \infty$ . At  $A = 2$  all effective potentials are even functions, and at  $A \geq 3$  some effective potentials are odd functions.

We can also seek for the solution of the problem (8) in symmetrized coordinates in the form of the Kantorovich expansion

$$\Psi_{i_0}(\xi_0, \xi) = \sum_{j=1}^{j_{\max}} \tilde{\Phi}_j(\xi; \xi_0) \tilde{\chi}_{ji_0}(\xi_0). \quad (31)$$

Here  $\tilde{\chi}_{ii_0}(\xi_0)$  are unknown functions

$$\tilde{\chi}_{ji_0}(\xi_0) = \int d^{A-1} \xi \tilde{\Phi}_j(\xi; \xi_0) \Psi_{i_0}(\xi_0, \xi),$$

and  $\tilde{\Phi}_i(\xi; \xi_0)$  are the orthonormalized basis eigenfunctions of the parametric  $(A - 1)$ -dimensional oscillator with eigenenergies  $\tilde{E}_i(\xi_0)$  from Eq. (21) in the PSCR. Taking Eqs. (15) and (13) into account, the set of the close-coupling equations in the Kantorovich form reads as

$$\left[ -\frac{d^2}{d\xi_0^2} + \tilde{\epsilon}_i(\xi_0) - E \right] \tilde{\chi}_{ii_0}(\xi_0) + \sum_{j=1}^{j_{\max}} \left[ H_{ij}(\xi_0) + \frac{d}{d\xi_0} Q_{ij}(\xi_0) + Q_{ij}(\xi_0) \frac{d}{d\xi_0} \right] \tilde{\chi}_{ji_0}(\xi_0) = 0, \quad (32)$$

where the effective potentials  $H_{ij}(\xi_0)$  and  $Q_{ij}(\xi_0)$  are calculated

$$H_{ij}(\xi_0) = \sum_{j'=1}^{j'_{\max}} \frac{d\tilde{\alpha}_{j'}^{(i)}(\xi_0)}{d\xi_0} \frac{d\tilde{\alpha}_{j'}^{(j)}(\xi_0)}{d\xi_0}, \quad (33)$$



**Table 5.** The degeneracy multiplicities  $p$  from (16),  $p_s = p_a$  and  $p_S = p_A$  of s, a, S, and A eigenfunctions of the oscillator energy levels  $\Delta E_j = E_j^\bullet - E_1^\bullet$  ( $\bullet = 0, s, a, S, A$ )

$A = 3$			$A = 4$			$A = 5$			$A = 6$			$\Delta E_j$
$p$	$p_s, p_a$	$p_S, p_A$	$p$	$p_s, p_a$	$p_S, p_A$	$p$	$p_s, p_a$	$p_S, p_A$	$p$	$p_s, p_a$	$p_S, p_A$	
1	1	1	1	1	1	1	1	1	1	1	1	0
2	1	0	3	1	0	4	1	0	5	1	0	2
3	2	1	6	2	1	10	2	1	15	2	1	4
4	2	1	10	3	1	20	3	1	35	3	1	6
5	3	1	15	4	2	35	5	2	70	5	2	8
6	3	1	21	5	1	56	6	2	126	7	2	10
7	4	2	28	7	3	84	9	3	210	10	4	12

**Table 6.** Resonance values of the energy  $E_S$  ( $E_A$ ) (in oscillator units) for S (A) states for  $A = 2, 3, 4$  ( $\sigma = 1/10, \alpha = 20$ ) with approximate eigenvalues  $E_i^D$ , for the first ten states  $i = 1, \dots, 10$ , calculated using the truncated oscillator basis (D) till  $j_{\max} = 136, 816, 1820$  at  $A = 2, 3, 4$ 

$i$	1	2	3	4	5	6	7	8	9	10
$A = 2$										
$E_S$	5.72	9.06	9.48	12.46	12.57	13.46	15.74	15.78	16.65	17.41
$E_A$	5.71	9.06	9.48	12.45	12.57	13.45	15.76*	15.76*	16.66	17.40
$E_i^D$	5.76	9.12	9.53	12.52	12.64	13.52	15.81	15.84	16.73	17.47
$A = 3$										
$E_S$	8.18	11.11		12.60	13.93		14.84	15.79		16.67
	8.31	11.23			14.00		14.88			16.73
$E_A$			11.55			14.46			16.18	
			11.61			14.56			16.25	
$E_i^D$	8.19	11.09	11.52	12.51	13.86	14.42	14.74	15.67	16.11	16.53
$A = 4$										
$E_S$	10.12	11.89	12.71	14.86	15.19	15.41	15.86	16.37	17.54	17.76
$E_i^{D31}$	10.03		12.60	14.71	15.04			16.18	17.34	17.56
$E_i^{D22}$		11.76				15.21	15.64			

\* Two overlapping peaks of transmission probability.

$$Q_{ij}(\xi_0) = - \sum_{j'=1}^{j'_{\max}} \tilde{\alpha}_{j'}^{(i)}(\xi_0) \frac{d\tilde{\alpha}_{j'}^{(j)}(\xi_0)}{d\xi_0},$$

using the solutions  $\tilde{\epsilon}_i(\xi_0)$  and  $\tilde{\alpha}_{j'}^{(i)}(\xi_0)$ , and their first derivatives of the parametric algebraic eigenvalue problem (23). Note, that the PSCR constructed in the above form with the long derivative  $D_{ij} = \delta_{ij} d/d\xi_0 - Q_{ij}(\xi_0)$  can be treated as an *alternative version* [52] of the method of generator coordinates

with velocity-dependent effective potential [53, 54]. Indeed, equations (32) can be rewritten in the terms of long derivatives  $D_{ij}$ , which apply in some adiabatic calculations

$$\sum_{j=1}^{j_{\max}} [-D_{ij}^2 + \mathcal{F}_{ij}(\xi_0) + (\tilde{\epsilon}_i(\xi_0) - E)\delta_{ij}] \quad (34)$$

$$\times \tilde{\chi}_{jio}(\xi_0) = 0.$$

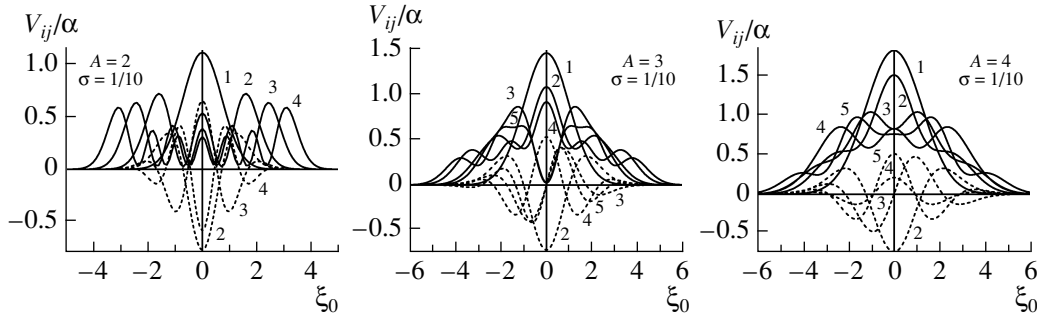


**Fig. 9.** Diagonal  $V_{jj}$  (solid lines) and nondiagonal  $V_{j1}$  (dashed lines) effective potentials for  $A = 2$ ,  $A = 3$ , and  $A = 4$  of the S states of the particles at  $\sigma = 0.1$ .  $j$  is the number of the state in Table 3.

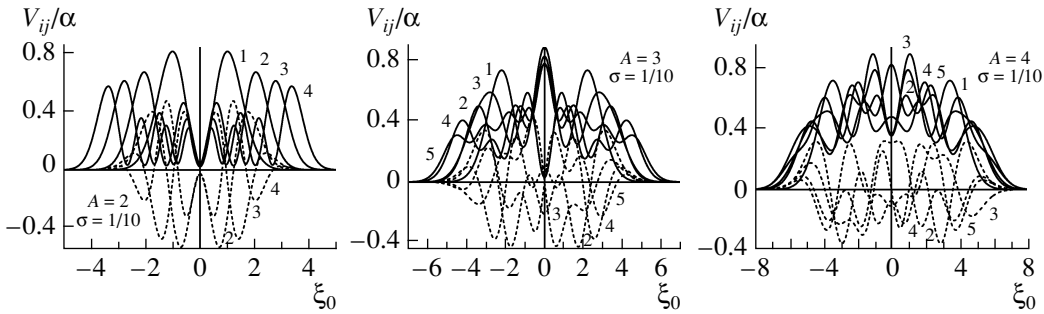


**Fig. 10.** The same as in Fig. 9 but for A states.  $j$  is the number of state in Table 4.

However, the curvature matrix elements

$$\mathcal{F}_{ij}(\xi_0) = H_{ij}(\xi_0) - \sum_{j''=1}^{j''_{\max}} Q_{ij''}(\xi_0) Q_{j''j}(\xi_0)$$

tend to zero only at  $j''_{\max} \gg j'_{\max} \gg j_{\max}$ . This fact explains the different rate of convergence of approximate solutions to exact ones with increasing  $j_{\max}$  in different calculations. The asymptotic form of the matrix solution  $\tilde{\chi}_{jio}(\xi_0)$ , compatible with (9), was derived earlier in [18].

Thus, the scattering problem (8) with the asymptotic boundary conditions (9) is reduced to the boundary-value problem for the set of close-coupling equations in Galerkin or Kantorovich form, (28) or (32), with the boundary conditions at  $d = 1$ ,  $\xi_0 = \xi_{\min}$  and  $\xi_0 = \xi_{\max}$ :

$$\begin{aligned} \left. \frac{d\mathbf{F}(\xi_0)}{d\xi_0} \right|_{\xi_0=\xi_{\min}} &= \mathcal{R}(\xi_{\min})\mathbf{F}(\xi_{\min}), \\ \left. \frac{d\mathbf{F}(\xi_0)}{d\xi_0} \right|_{\xi_0=\xi_{\max}} &= \mathcal{R}(\xi_{\max})\mathbf{F}(\xi_{\max}), \end{aligned} \quad (35)$$

where  $\mathcal{R}(\xi)$  is an unknown  $j_{\max} \times j_{\max}$  matrix function,  $\mathbf{F}(\xi_0) = \{\chi_{i_o}(\xi_0)\}_{i_o=1}^{N_o} = \{\{\chi_{jio}(\xi_0)\}_{j=1}^{j_{\max}}\}_{i_o=1}^{N_o}$  is the required  $j_{\max} \times N_o$  matrix solution, and  $N_o$  is the number of open channels,  $N_o = \max_{2E \geq E_j} j \leq$

$j_{\max}$ , calculated using the third version of KANTBP program [55], described in [18, 41].

## 5. RESONANCE TRANSMISSION OF A FEW COUPLED PARTICLES

In the case of  $V^{\text{pair}}(x_{ij}) = V^{\text{hosc}}(x_{ij})$ , the solution of the scattering problem described above yields the reflection and transmission amplitudes  $R_{jio}(E)$  and  $T_{jio}(E)$  that enter the asymptotic boundary conditions (9) as unknowns.  $|R_{jio}(E)|^2$  ( $|T_{jio}(E)|^2$ ) is the probability of a transition to the state, described by the reflected (transmitted) wave and, hence, will be referred as the reflection (transmission) coefficient. Note that  $|R_{jio}(E)|^2 + |T_{jio}(E)|^2 = 1$ .

In Figs. 11, 12, and 13 we show the energy dependence of the total transmission probability  $|T|_{ii}^2 = \sum_{j=1}^{N_o} |T_{jio}(E)|^2$ . This is the probability of a transition from a chosen state  $i$  into any of  $N_o$  states, found from Eq. (27) by solving the boundary-value problem in the Galerkin form, (28) and (35), with the KANTBP program [55] on the finite-element grid  $\Omega_{\xi} \{-\xi_0^{\max}, \xi_0^{\max}\}$  with  $N_{\text{elem}}$  fourth-order Lagrange elements between the nodes. For S solutions at  $N = 2, 3, 4$  the following parameters are used:  $j_{\max} = 13, 21, 39$ ,  $\xi_0^{\max} = 9.3, 10.5, 12.8$ ,  $N_{\text{elem}} = 664, 800, 976$ , while for A solutions  $j_{\max} = 13, 16, 15$ ,  $\xi_0^{\max} = 9.3, 10.5, 12.2$ ,

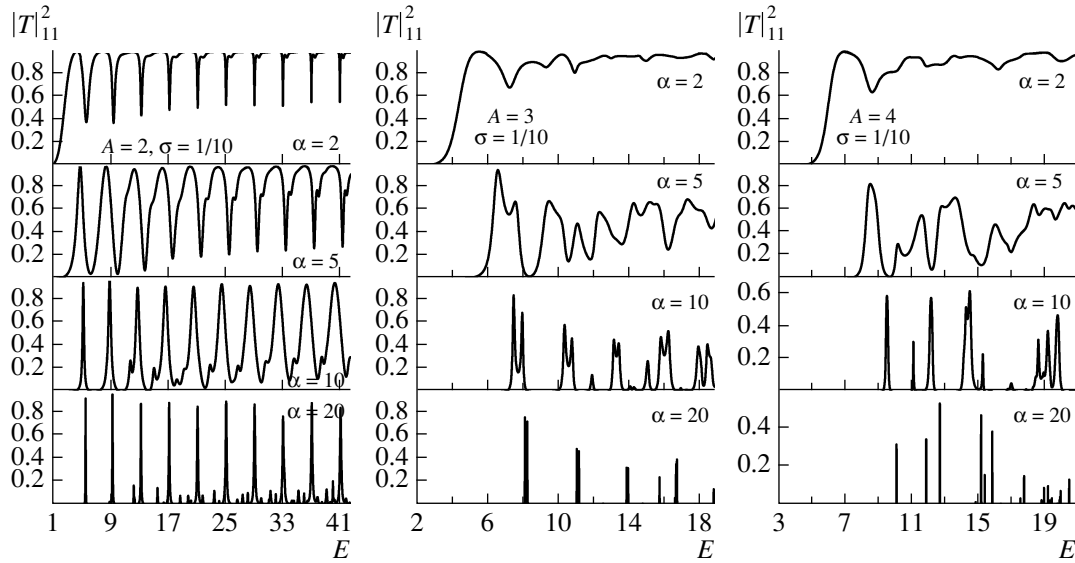


**Fig. 11.** The total transmission probabilities  $|T|_{11}^2$  vs energy  $E$  (in oscillator units) from the ground state of the system of  $A = 2, 3, 4$  of the S states of the particles, coupled by the oscillator potential, through the repulsive Gaussian-type potential barriers (30) at  $\sigma = 0.1$  and  $\alpha = 2, 5, 10, 20$ .

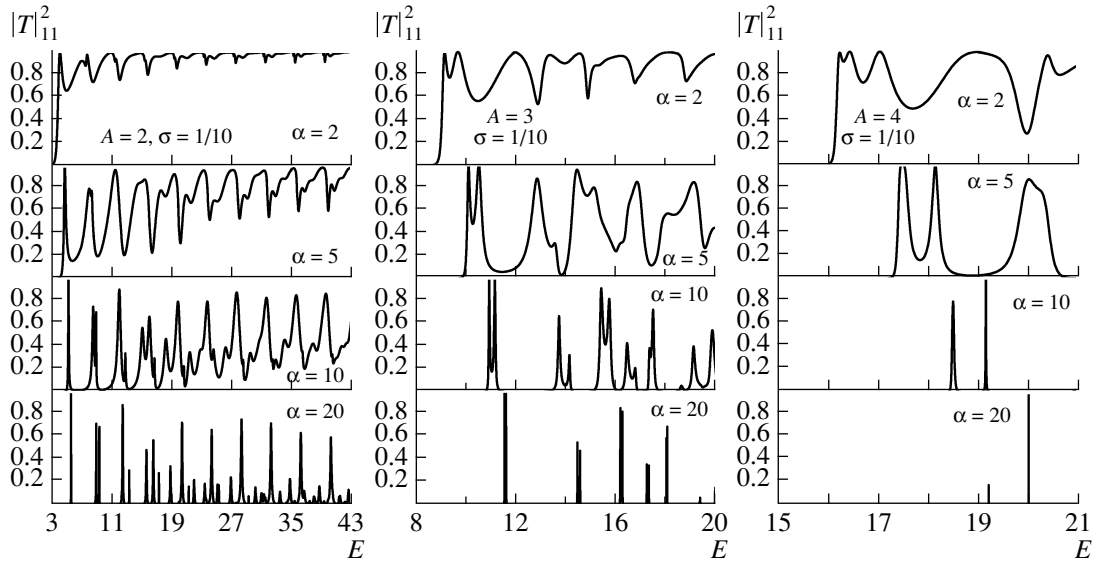


**Fig. 12.** The same as in Fig. 11 but for A states of the particles.

$N_{\text{elem}} = 664, 800, 976$ . Figures 11 and 12 demonstrate the nonmonotonic behavior of the probability versus the energy, and the observed resonances are manifestations of the quantum transparency effect. With the barrier height increasing, the peaks become narrower and their positions shift to higher energies. The multiplet structure of the peaks in the symmetric case is similar to that in the antisymmetric case. For three particles the major peaks are double, while for two and four particles they are single. For  $A = 2$  and  $\alpha = 10, 20$  one can observe additional multiplets

of small peaks. Figure 13 illustrates the energy dependence of transmission probabilities from the excited states. As the energy of the initial excited state increases, the transmission peaks demonstrate a shift towards higher energies, the set of peak positions keeping approximately the same as for the transitions from the ground state and the peaks just changing one position for another, like it was observed in the model calculations [14]. For example, for  $A = 3$  the position of the third peak for transitions from the first two states ( $E = 10.4167$  and  $E = 10.4156$ )

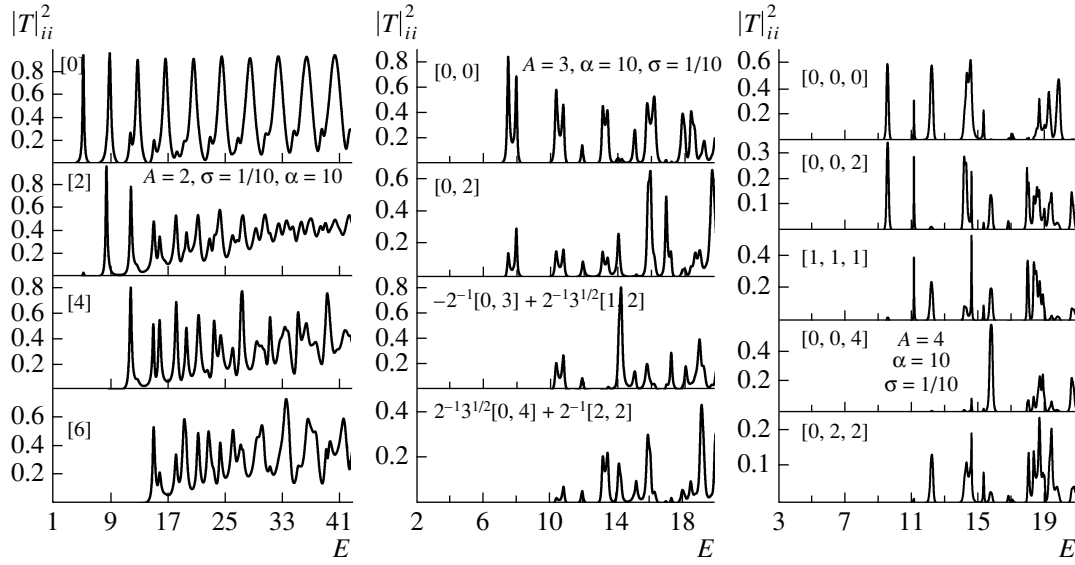


**Fig. 13.** The total penetration probabilities  $|T_{ii}|^2$  vs energy  $E$  (in oscillator units) from the ground and excited states of the system of  $A = 2, 3, 4$  of the S states of the particles, coupled by the oscillator potential, through the repulsive Gaussian-type potential barriers (30) at  $\sigma = 0.1$  and  $\alpha = 10$ .

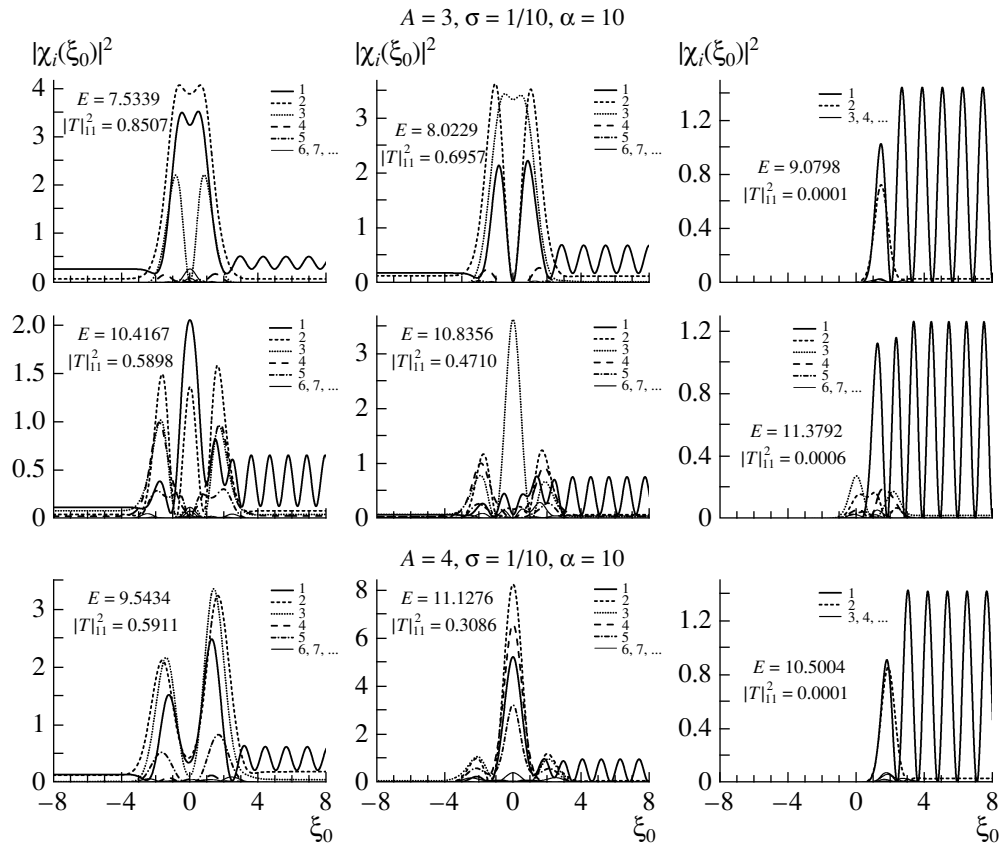


**Fig. 14.** The probability densities  $|\chi_i(\xi_0)|^2$  of coefficient functions of decomposition (27), representing the incident wave function of the ground S state of the particles at the values of the collision energy  $E$ , corresponding to some maxima and minima of the transmission coefficient in Fig. 11 for the parameters of the Gaussian barrier  $\alpha = 10$  and  $\sigma = 0.1$ .

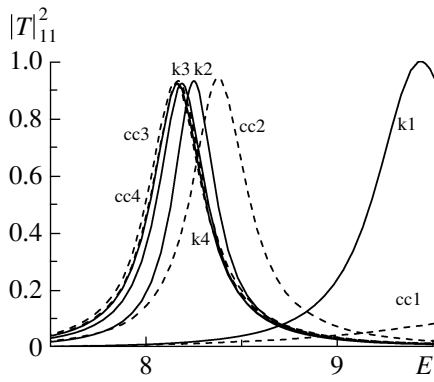


**Fig. 15.** The epures of the first peak in Fig. 11 illustrating the convergence of Galerkin (cc\*) and Kantorovich (k\*) close-coupling expansions in calculations of transmission coefficient  $|T|_{11}^2$  for the S-states,  $A = 2$  at  $\alpha = 10$ ,  $\sigma = 0.1$  ( $E$  in oscillator units).

coincides with the position of the first peak for the transitions from the second two states ( $E = 10.4197$  and  $E = 10.4298$ ).

The effect of quantum transparency is caused by the existence of barrier quasistationary states, embedded in the continuum. Figure 14 shows that in the case of resonance transmission the wave functions, depending on the center-of-mass variable  $\xi_0$ , are localized in the vicinity of the potential barrier center ( $\xi_0 = 0$ ).

For the energy values, corresponding to some of the transmission coefficient peaks in Fig. 11 at  $\alpha = 10$  within the effective range of barrier potential action, the wave functions demonstrate considerable increase (from two to ten times) of the probability density in comparison with the incident unit flux. This is a fingerprint of quasistationary states, which is not a quantitative definition, but a clear evidence in favor of their presence in the system [56, 57].

In the case of total reflection the wave functions are localized at the barrier side, on which the wave is incident, and decrease to zero within the effective range of the barrier action.

Note that the explicit explanation of quantum transparency effect is achieved in the frame of Kantorovich close-coupling equations (32) because of the multi-barrier potential structure of the effective potential (33), appearing explicitly even in the diagonal or adiabatic approximation, in particular, in the S case for  $A = 2$  [1, 18]. Nevertheless, in Galerkin close-coupling equations the multi-barrier potential structure of the effective potential is observed explicitly in the A case (see Fig. 10).

As an example, Fig. 15, which is an epure of Fig. 11, shows the comparison of convergence rates of Galerkin (27) and Kantorovich (31) close-coupling expansions in calculations of transmission coefficient

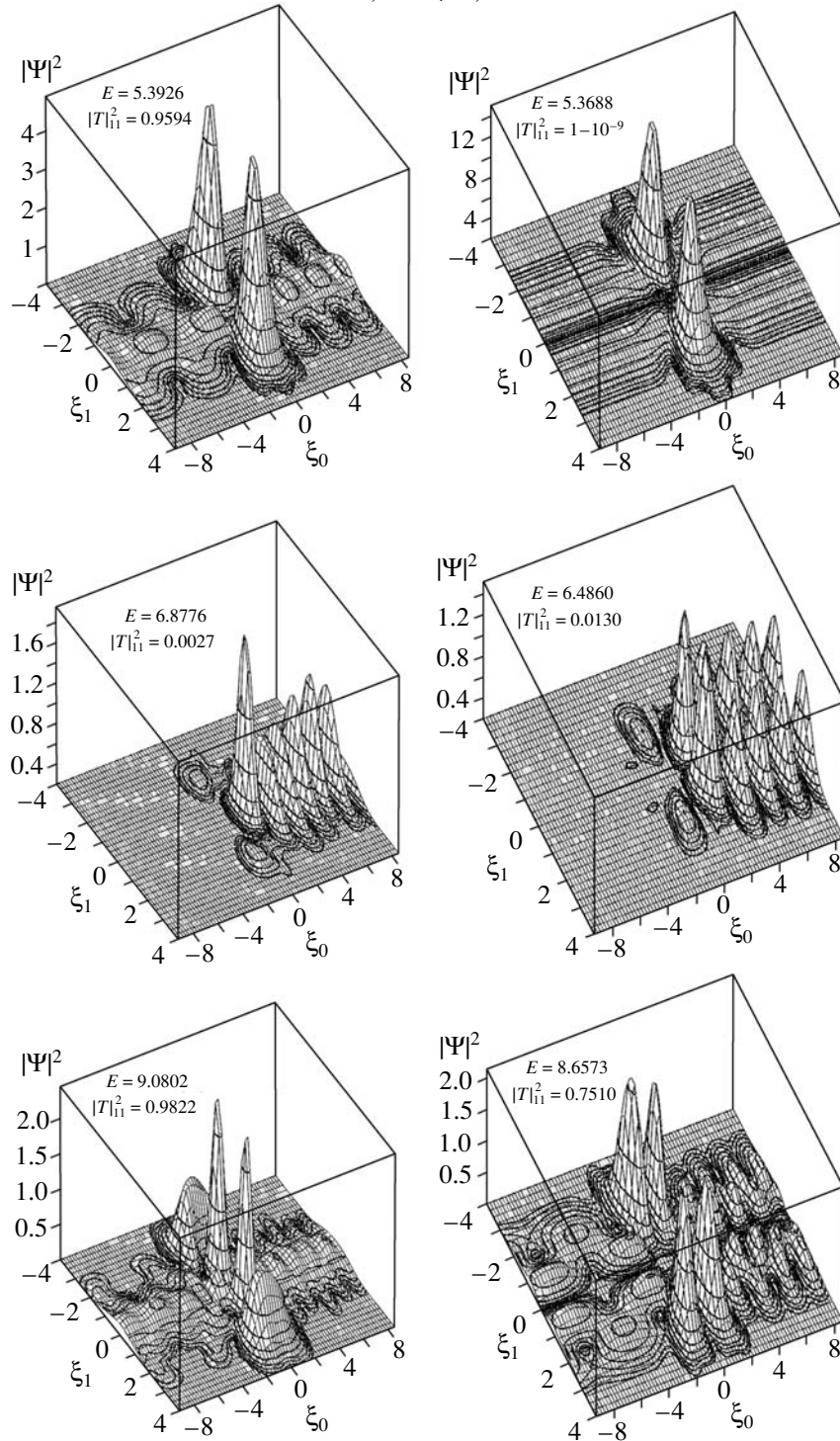
$|T|_{11}^2$  for S wave functions,  $A = 2$  at  $\alpha = 10$ ,  $\sigma = 0.1$ . One can see that the diagonal approximation of the Kantorovich method provides better approximations of the positions of the transmission coefficient  $|T|_{11}^2$  resonance peaks. With the increasing number of basis functions, i.e., the number  $j_{\max}$  of close-coupling equations with respect to the center-of-mass coordinates in Galerkin (28) and Kantorovich (32) form, respectively, the convergence rates are similar and confirm the results obtained by solving the problem by means of the Finite-Difference Numerov method in 2D domain [1]. This is true for the considered short-range potentials (30), while for long-range potentials of the Coulomb type the Kantorovich method can be more efficient [18].

Figure 16 shows the profiles of  $|\Psi|^2 \equiv |\Psi_{Em \rightarrow}^{(-)}|^2$  for the S and A total wave functions of the continuous spectrum in the  $(\xi_0, \xi_1)$  plane with  $A = 2$ ,  $\alpha = 10$ ,  $\sigma = 1/10$  at the resonance energies of the first and the second maximum and the first minimum of the transmission coefficient demonstrating *resonance transmission* and *total reflection*, respectively. It is seen that in the case of resonance transmission the redistribution of energy from the center-of-mass degree of freedom to the internal (transverse) ones takes place, i.e., the transverse oscillator undergoes a transition from the ground state to the excited state, while in the total reflection the redistribution of energy is extremely small and the transverse oscillator returns to infinity in the same state.

In Table 6 we present the resonance values of the energy  $E_S$  ( $E_A$ ) calculated by solving the boundary-value problem (28) and (35), using the KANTBP 3.0 program, for S (A) states at  $A = 2, 3, 4$ ,  $\sigma = 1/10$ ,  $\alpha = 20$  that correspond to the maxima of transmission coefficients  $|T|_{ii}^2$  in Fig. 11 up to the values of energy  $E < 18$  and the corresponding resonance values of the energy  $E_D$  calculated by means of the Dirichlet conditions (DC) algorithm. One can see, that the accepted approximation of narrow barrier with impermeable walls using in the DC algorithm provides an appropriate approximation  $E_i^D$  of the above high accuracy results  $E_S$  ( $E_A$ ) with the error smaller than 2%. Below we give a comparison and qualitative analysis of the obtained results.

In the considered case the potential barrier  $V(x_i)$  is narrow and  $V^{\text{pair}}(x_{ij}) = V^{\text{hosc}}(x_{ij})$ , so that we solve Eq. (1) in the Cartesian coordinates  $x_1, \dots, x_A$  in one of the  $2^A - 2$  subdomains, defined as  $p_i x_i > 0$ ,  $p_i = \pm 1$ , with the DC:  $\Psi(x_1, \dots, x_A)|_{\cup_{i=1}^A \{x_i=0\}} = 0$  at the internal boundaries  $\cup_{i=1}^A \{x_i = 0\}$ . Here, the value  $p_i = \pm 1$  indicates the location of the  $i$ th particle at the right or left side of the barrier, respectively. Thus, in the DC procedure we seek for the solution in

$$A = 2, \sigma = 1/10, \alpha = 10$$



**Fig. 16.** The profiles of probability densities  $|\Psi(\xi_0, \xi_1)|^2$  for the S (left panels) and A (right panels) states of  $A = 2$  particles, revealing resonance transmission and total reflection at resonance energies, depicted in Figs. 11 and 12.

the form of a Galerkin expansion over the orthogonal truncated oscillator basis,  $\Psi_i^D(\mathbf{x}) = \sum_{j=1}^{j_{\max}} \bar{\Phi}_j(\mathbf{x}) \Psi_{ji}^D$  composed of  $A$ -dimensional harmonic oscillator functions  $\bar{\Phi}_j(\mathbf{x})$ , odd in each of the Cartesian coordi-

nates  $x_1, \dots, x_A$  in accordance with the above DCs, with unknown coefficients  $\Psi_{ji}^D$ . As a result, we arrive at the algebraic eigenvalue problem  $\mathbf{D}\Psi^D = \Psi^D \mathbf{E}^D$  with a dense real-symmetric  $j_{\max} \times j_{\max}$  matrix. So,

in the DC procedure we seek for an approximate solution in one of the potential wells, i.e., we neglect the tunnelling through the barriers between wells. Therefore, we cannot observe the splitting, inherent in exact eigenvalues, corresponding to S and A eigenstates, differing in permutation symmetry. However, we can explain the mechanism of their appearance and give their classification, which is important, too. The DC algorithm was implemented in CAS Maple and Fortran environment and published in [58].

*Remark.* The DC procedure is similar to solving Eq. (8) in the symmetrized coordinates  $\xi_0, \xi$  related to the Cartesian ones via Eq. (3), implemented by the following two steps:

- (i) we approximate the narrow barriers by impenetrable walls  $x_k(\xi_0, \xi) = 0$ ;
- (ii) we superpose these mutually perpendicular walls with the coordinate hyperplanes using rotations.

Actually, the two approaches yield the same boundary-value problem, formulated in different coordinates (1), (8).

Below we give a comparison and qualitative analysis of the obtained results. For two particles,  $A = 2$  (see Fig. 8), there are two symmetric potential wells. In each of them both symmetric and asymmetric wave functions are constructed. Since the potential barrier, separating the wells, is sufficiently high, the appropriate energies are closely spaced, so that each level describes the states of both S and A type. The lower energy levels form a sequence “singlet–doublet–triplet, etc.”, which is seen in Fig. 11. The resonance transmission energies for a pair of particles in S states is lower than that for a pair of those in A states. This is due to the fact that in the vicinity of the collision point the wave function is zero.

When  $A = 3$ , there are six similar wells, three of them at each side of the plane  $\xi_0 = 0$ . The symmetry with respect to the plane  $\xi_0 = 0$  explains the presence of doublets. The presence of states with definite symmetry is associated with the fact that the axis  $\xi_0$  is a third-order symmetry axis. However, in contrast to the case  $A = 2$ , one can obtain either S or A combinations of states. For example, the first four solutions of the problem, in one of the wells (e.g., the one restricted with the pair-collision planes “13” and “23”) possess the dominant components  $2\sqrt{2}\bar{\Phi}_1(x_1)\bar{\Phi}_1(x_2)\bar{\Phi}_1(x_3)$ ,  $2(\bar{\Phi}_1(x_1)\bar{\Phi}_3(x_2) + \bar{\Phi}_3(x_1)\bar{\Phi}_1(x_2))\bar{\Phi}_1(x_3)$ ,  $2(\bar{\Phi}_1(x_1)\bar{\Phi}_3(x_2) - \bar{\Phi}_3(x_1)\bar{\Phi}_1(x_2))\bar{\Phi}_1(x_3)$ ,  $2\sqrt{2}\bar{\Phi}_1(x_1)\bar{\Phi}_1(x_2)\bar{\Phi}_3(x_3)$ . Note, that the first, second, and fourth of these functions are symmetric with respect to the permutation  $x_1 \leftrightarrow x_2$ , while the third one is antisymmetric. Hence, in all six wells using the first four solutions one can obtain six S and two A states.

When  $A = 4$  there are 14 wells. Six wells in the center correspond to the case when two particles are located at one side of the barrier and the rest two at the other side. The corresponding eigenenergy is denoted as  $E_i^{D22}$ . The rest eight wells correspond to the case when one particle is located at one side of the barrier and the rest three at the other side. The corresponding eigenenergy is denoted as  $E_i^{D31}$ . For these states doublets must be observed, similar to the case of three particles. However, the separation between the energy levels is much smaller, because the 4-well groups are strongly separated by two barriers, instead of only one barrier in the case  $A = 3$ .

The necessary condition for the quasi-stationary state being symmetric (antisymmetric) is that the wave functions must be symmetric (antisymmetric) with respect to those coordinates  $x_i$  and  $x_j$ , for which  $p_i = p_j$ .

## 6. CONCLUSION

We considered a model of  $A$  identical particles bound by the oscillator-type potential that undergo quantum tunnelling through the short-range repulsive barrier potentials. The model was formulated in the new representation, which we referred as symmetrized coordinate representation (SCR). The constructive method of symmetrizing or antisymmetrizing the harmonic oscillator basis functions in the new symmetrized coordinates was described. We had shown that the transformations of  $(A - 1)$ -dimensional oscillator basis functions from the symmetrized coordinates to the Jacobi coordinates, reducible to permutations of coordinates and  $(A - 1)$ -dimensional finite rotation, are implemented by means of the  $(A - 1)$ -dimensional *oscillator Wigner functions* [45], while the reduction of the SCR in the Cartesian coordinates to the hyperspherical ones is given by means of the *Clebsch–Gordan coefficients of the interbasis expansions* [47]. One can use the above transformations to recalculate the SCR,  $(A - 1)$ -harmonic oscillator functions of symmetric or antisymmetric type with respect to permutations of Cartesian coordinates of  $A$  identical particles, in desirable sets of Jacobi and/or hyperspherical coordinates.

For clarity a system of several identical particles in one-dimensional Euclidean space ( $d = 1$ ) was considered with a discrete spectrum of relative motion in the center-of-mass coordinate system, described by the internal symmetrized variables, and a continuous spectrum of the center-of-mass motion, described by the external variable. We calculated only the spatial part of the wave function, symmetric or antisymmetric under permutation of  $A$  identical particles. If

necessary, the spin part of the wave function can be determined using the conventional procedure and included in a more rigorous calculation.

The multichannel scattering problem for the Schrödinger equation with several short-range repulsive barriers was formulated. The problem was reduced to the boundary-value problem for a set of the close-coupling second-order differential equations with respect to the longitudinal variable on the whole axis. This was implemented by expanding the wave function over the oscillator basis of several bound particles possessing symmetry or antisymmetry under permutations of  $A$  initial Cartesian coordinates.

We analyzed the effect of quantum transparency, i.e., the resonance tunnelling of several bound particles through repulsive potential barriers. We demonstrated that this effect is due to the existence of the sub-barrier quasi-stationary states, embedded in the continuum. For the considered type of symmetric Gaussian barrier potential the positions of the energies of the S and A quasi-stationary states have a small difference, because of the similar multiplet structure of oscillator energy levels at a fixed number of particles. This fact explains the similar behavior of transmission coefficients from S and A states shifted by the threshold energies. However, the multiplet structure of energy positions of these states is varied with increasing number of particles such that for three particles the major peaks are double, while for two and four particles they are single. Our calculations also show that with the increasing energy of the initial excited state of few-body clusters, the transmission peaks demonstrate a shift towards higher energies, the set of peak positions keeping approximately the same as for the transitions from the ground state and the peaks just skipping from one position for another.

The proposed approach can be adapted and applied to the analysis of tetrahedral-symmetric nuclei, the study of quantum diffusion of molecules and micro-clusters through surfaces and the fragmentation mechanism in producing very neutron-rich light nuclei. In connection with the intense search for superheavy nuclei, a particularly significant application of the proposed approach is the mathematically correct analysis of mechanisms of sub-barrier fusion of heavy nuclei and the study of fusion rate enhancement by means of resonance tunnelling.

The authors thank Profs. A. Amaya Tapia, V.B. Belyaev, A. Dobrowolski, S.N. Ershov, V.P. Gerdt, G.P. Kamuntavičius, F.M. Pen'kov, G.S. Pogosyan, and V.V. Pupyshev for useful discussions. The work was supported partially by grants nos. 13-602-02 JINR, 11-01-00523 and 13-01-00668 RFBR, 0602/GF MES RK and the Bogoliubov–Infeld program.

## REFERENCES

1. F. M. Pen'kov, J. Exp. Theor. Phys. **91**, 698 (2000); Phys. Rev. A **62**, 044701 (2000).
2. T. Sato and Y. Kayanuma, Europhys. Lett. **60**, 331 (2002).
3. E. Pijper and A. Fasolino, J. Chem. Phys. **126**, 014708 (2007).
4. D. I. Bondar, W.-Ki Liu, and M. Yu. Ivanov, Phys. Rev. A **82**, 052112 (2010).
5. M. R. A. Shegelski et al., Eur. Phys. J. Plus **127**, 17 (2012).
6. S. N. Ershov and B. V. Danilin, Phys. Part. Nucl. **39**, 835 (2008).
7. P. Navrátil, G. P. Kamuntavičius, and B. R. Barrett, Phys. Rev. C **61**, 044001 (2000).
8. B. E. Grinyuk and I. V. Simenog, Phys. At. Nucl. **72**, 6 (2009).
9. A. V. Nesterov et al., Phys. Part. Nucl. **41**, 716 (2010).
10. H. Hofmann, Nucl. Phys. A **224**, 116 (1974).
11. H. J. Krappe et al., Z. Phys. A **314**, 23 (1983).
12. K. Hagino, N. Rowley, and A. T. Kruppa, Comput. Phys. Commun. **123**, 143 (1999).
13. V. I. Zagrebaev and V. V. Samarin, Phys. At. Nucl. **67**, 1462 (2004).
14. N. Ahsan and A. Volya, Phys. Rev. C **82**, 064607 (2010).
15. A. C. Shotter and M. D. Shotter, Phys. Rev. C **83**, 054621 (2011).
16. V. M. Shilov, Phys. At. Nucl. **75**, 449 (2012).
17. O. Chuluunbaatar et al., Phys. At. Nucl. **72**, 768 (2009).
18. A. A. Gusev et al., Lect. Notes Comp. Sci. **6885**, 175 (2011).
19. M. Dobrowolski et al., Int. J. Mod. Phys. E **20**, 500 (2011).
20. Sh. Tagami, Yo. R. Shimizu, and J. Dudek, arXiv:1301.3279v1 [nucl-th].
21. Yo. Kanada-En'yo and Yo. Hidaka, Phys. Rev. C **84**, 014313 (2011).
22. V. A. Fock, Z. Phys. **61**, 126 (1930); Usp. Fiz. Nauk **93**, 342 (1967); *Fundamentals of Quantum Mechanics* (Mir, Moscow, 1978) [in Russian].
23. M. Hamermesh, *Group Theory and Its Application to Physical Problems* (Dover, 1989).
24. C. Lubich, *From Quantum to Classical Molecular Dynamics: Reduced Models and Numerical Analysis* (European Mathematical Society Publ., Zürich, 2008).
25. L. V. Kantorovich and V. I. Krylov, *Approximate Methods of Higher Analysis* (Wiley, New York, 1964).
26. P. Kramer and M. Moshinsky, Nucl. Phys. **82**, 241 (1966).
27. M. Kretzschmar, Z. Phys. **157**, 433, 558 (1960); Z. Phys. **158**, 284 (1960).
28. V. G. Neudatchin and Yu. F. Smirnov, *Nucleon Clusters in the Light Nuclei* (Nauka, Moscow, 1969) [in Russian].



29. M. Moshinsky and Y. F. Smirnov, *The Harmonic Oscillator in Modern Physics* (Informa Health Care, Amsterdam, 1996).
30. K. Wildermuth and Y. C. Tang, *A Unified Theory of the Nucleus* (Vieweg, Braunschweig, 1977).
31. A. Novoselsky and J. Katriel, *Ann. Phys. (N.Y.)* **196**, 135 (1989).
32. G. P. Kamuntavičius, *Few-Body Syst.* **1**, 91 (1986).
33. G. Kamuntavičius, *Sov. J. Part. Nucl.* **20**, 109 (1989); A. Deveikis and G. Kamuntavičius, *Lithuanian Phys. J.* **37**, 371 (1997).
34. V. V. Pupyshev, *Phys. Part. Nucl.* **30**, 689 (1999).
35. V. V. Kornyak, *Phys. At. Nucl.* **76**, 240 (2013); arXiv:1208.5734.
36. G. P. Kamuntavičius et al., *Nucl. Phys. A* **695**, 191 (2001).
37. V. C. Aguilara-Navarro, M. Moshinsky, and W. W. Yeh, *Ann. Phys. (N.Y.)* **51**, 312 (1969); V. C. Aguilara-Navarro, M. Moshinsky, and P. Kramer, *Ann. Phys. (N.Y.)* **54**, 379 (1969); J.-M. Lévy-Leblond, *J. Math. Phys.* **7**, 2217 (1966).
38. D. W. Jepsent and J. O. Hirschfelder, *Proc. Natl. Acad. Sci. USA* **45**, 249 (1959); J. O. Hirschfelder, *Int. J. Quantum Chem.* **3** (Suppl. S3a), 17 (1969).
39. R. T. Pack and G. A. Parker, *J. Chem. Phys.* **87**, 3888 (1987).
40. V. S. Buslaev et al., *Phys. At. Nucl.* **76**, 208 (2013).
41. A. A. Gusev, O. Chuluunbaatar, and S. I. Vinitzky, in *Proceedings of the 2nd International Conference on The Modeling of Non-Linear Processes and Systems*, Ed. L. A. Uvarova (Yanus, Moscow, 2011).
42. M. Abramowitz and I. A. Stegun, *Handbook of Mathematical Functions* (Dover, New York, 1965).
43. G. A. Baker, Jr., *Phys. Rev.* **103**, 1119 (1956).
44. A. Gusev et al., *Lect. Notes Comp. Sci.* (accepted).
45. G. S. Pogosyan, Ya. A. Smorodinsky, and V. M. Ter-Antonyan, *J. Phys. A* **14**, 769 (1981).
46. D. A. Varshalovich, A. N. Moskalev, and V. K. Chersonsky, *Quantum Theory of Angular Momentum: Irreducible Tensors, Spherical Harmonics, Vector Coupling Coefficients, 3nj Symbols* (Nauka, Leningrad, 1975; World Scientific, Singapore, 1988).
47. L. G. Mardoyan, G. S. Pogosyan, A. N. Sissakyan, and V. M. Ter-Antonyan, *Quantum System with Hidden Symmetry. Interbasis Expansion* (Fizmatlit, Moscow, 2006) [in Russian].
48. J. M. Lévy-Leblond, *Phys. Lett. A* **26**, 540 (1968).
49. Zh. Wang et al., arXiv:1108.1607v4 [math-ph].
50. S. I. Vinitzky, V. P. Gerdt, A. A. Gusev, et al., *Progr. Computer Software* **33**, 105 (2007).
51. C. F. Bunge, *Comput. Phys. Commun.* **138**, 92 (2001).
52. V. M. Dubovik et al., *Bulgarian J. Phys.* **17**, 1 (1990).
53. J. J. Griffin and J. A. Wheeler, *Phys. Rev.* **108**, 311 (1957).
54. D. Baye, P.-H. Heenen, and M. Libert-Heinemann, *Nucl. Phys. A* **291**, 230 (1977).
55. O. Chuluunbaatar et al., *Comput. Phys. Commun.* **179**, 685 (2008).
56. A. I. Baz', Ya. B. Zel'dovich, and A. M. Perelomov, *Scattering, Reactions, and Decay in Nonrelativistic Quantum Mechanics* (Jerusalem, 1969; Nauka, Moscow, 1971).
57. C. A. A. de Carvalho and H. M. Nussenzveig, *Phys. Rep.* **364**, 83 (2002).
58. S. Vinitzky et al., *Lect. Notes Comp. Sci.* (accepted).



# ELEMENTARY PARTICLES AND FIELDS

## Theory

### Channeling Problem for Charged Particles Produced by Confining Environment\*

O. Chuluunbaatar<sup>1)</sup>, A. A. Gusev<sup>1)</sup>, V. L. Derbov<sup>2)</sup>, P. M. Krassovitskiy<sup>3)</sup>, and S. I. Vinitzky<sup>1)</sup>

Received October 14, 2008

**Abstract**—Channeling problem produced by confining environment that leads to resonance scattering of charged particles via quasistationary states imbedded in the continuum is examined. Nonmonotonic dependence of physical parameters on collision energy and/or confining environment due to resonance transmission and total reflection effects is confirmed that can increase the rate of recombination processes. The reduction of the model for two identical charged ions to a boundary problem is considered together with the asymptotic behavior of the solution in the vicinity of pair-collision point and the results of  $R$ -matrix calculations. Tentative estimations of the enhancement factor and the total reflection effect are discussed.

PACS numbers: 31.15.Ja, 31.15.Pf, 34.50.-s, 34.50.Pi

DOI: 10.1134/S1063778809050044

#### 1. INTRODUCTION

The interaction of channelled particles is considered as one of the possible ways to solve the problem of synthesis of light elements and study the interactions of nuclei at low energies [1–3]. It is supposed [3], that the effect of superfocusing beam channelling can essentially change the behavior of a nuclear reaction cross section as a function of the energy of colliding particles and the parameters of the crystal lattice. To estimate the cross section it is necessary to calculate the wave function of the continuous spectrum describing the interaction of channelled particles in a vicinity of the point of their pair impact, rather than the reflection and transmission coefficients within the framework of the model [4]. One of the known approaches to solve such type of problems has been proposed in [5, 6]. It was also applied to calculate the quasistationary states, providing the full reflection and resonant transmission of electrons and protons in a homogeneous magnetic field at resonant energies [7]. Here this approach is applied to the scattering of similarly charged particles channelled in a crystal in the framework of the model of [4]. We calculate the wave function of the continuous spectrum and estimate the dependence of the reaction enhancement coefficient on the energy by calculating a ratio of the probability density in the vicinity of the pair-collision

point in the presence of an additional confining potential and without it.

The paper is organized as follows. In Section 2 the axis channelling model of two identical charged ions is briefly described. In Section 3 the nonrelativistic problem of an ion in the Coulomb field and the uniform magnetic field is recalled. In Section 4 the details of the  $R$ -matrix-calculation scheme of the continuous spectrum problem on a finite interval with the third-type boundary conditions are described together with the brief analysis of an example of quasistationary states. In Section 5 the asymptotic expansions of the continuous spectrum solutions in open channels at small values of the radial variable (i.e., in the vicinity of the pair-collision point) are presented. In Section 6 preliminary estimations of the enhancement factor are discussed. In Conclusion the prospects of further application of the proposed approach and the expected results are discussed.

#### 2. THE CHANNELLING MODEL OF TWO IDENTICAL CHARGED IONS

The nonrelativistic model of two positive ions labelled by  $i = 1, 2$  with the effective masses  $m_i$  and charges  $q_i$  under the axis channelling condition with the energy  $E_t$  in the laboratory frame is described by the  $6D$  equation

$$(H_t - E_t)\Psi_t(\mathbf{r}_1, \mathbf{r}_2) = 0, \quad (1)$$

$$H_t = -\frac{1}{2m_1}\Delta_{\mathbf{r}_1}^{(3)} - \frac{1}{2m_2}\Delta_{\mathbf{r}_2}^{(3)} + U_1(\mathbf{r}_1) + U_2(\mathbf{r}_2) + U_{12}(\mathbf{r}_1 - \mathbf{r}_2), \quad (2)$$

\*The text was submitted by the authors in English.

<sup>1)</sup>Joint Institute for Nuclear Research, Dubna, Russia.

<sup>2)</sup>Saratov State University, Russia.

<sup>3)</sup>Institute of Nuclear Physics, Almaty, Kazakhstan.

where  $\mathbf{r}_i$  are the position vectors of ions in  $R^3$ ,  $\Delta_{\mathbf{r}_i}^{(3)}$  are the Laplace operators in  $R^3$ ,  $U_i(\mathbf{r}_i)$  is the energy of interaction between the particles and the crystal and  $U_{12}(\mathbf{r}_1 - \mathbf{r}_2) = q_1 q_2 / |\mathbf{r}_1 - \mathbf{r}_2|$  is their mutual Coulomb interaction energy in atomic units.

The potentials of interaction between the particles and the crystals are approximated by the known continuous potentials [8] of the form  $U_i(\mathbf{r}_i) \equiv \sum_s U_i(|\mathbf{r}_i - \mathbf{R}_s|)$ , where  $\mathbf{R}_s$  are position of crystal atomic chains formed a channel, and their expansions in powers of the distance from channelling axis coincided with the axis  $Z$  of a laboratory frame. Their leading approximation yield  $2D$  harmonic oscillators  $U_i(\mathbf{r}_i) = m_i \omega_i^2 \rho_i^2 / 2$  with frequencies  $\omega_1 \neq \omega_2$  with respect to the transverse variables  $\rho_i$ :  $\mathbf{r}_i = (z_i, \rho_i, \varphi_i) \in R^3$ , where  $\omega_i^2 = 2\alpha_i q_i / m_i$ , and  $\alpha_i \approx \alpha$  are constants of particle–crystal interaction.

The motion of a system of two particles with total mass  $M = m_1 + m_2$  and reduced mass  $\mu = m_1 m_2 / (m_1 + m_2)$  in Jacobi variables  $\mathbf{R} = (m_1 \mathbf{r}_1 + m_2 \mathbf{r}_2) / (m_1 + m_2)$  and  $\mathbf{r} = \mathbf{r}_1 - \mathbf{r}_2$  is averaged in the plane-wave approximation with the momentum  $K_Z$  along the axis  $Z$ , which yields the  $5D$  equation [4]

$$(H - E)\Psi(\mathbf{R}_\perp, \mathbf{r}) = 0, \quad (3)$$

$$\begin{aligned} \Psi(\mathbf{R}_\perp, \mathbf{r}) &= \Psi_t(\mathbf{R}, \mathbf{r}) \exp(iK_Z Z), \\ H &= -\frac{1}{2M} \Delta_{\mathbf{R}_\perp}^{(2)} - \frac{1}{2\mu} \Delta_{\mathbf{r}}^{(3)} \\ &+ U(\mathbf{R}_\perp, \mathbf{r}_\perp) + U_{12}(\mathbf{r}), \end{aligned} \quad (4)$$

where  $E = E_t - K_Z^2 / 2M$  is the energy,  $\mathbf{R}_\perp = (X_\perp, Y_\perp)$  and  $\mathbf{r}_\perp = (x_\perp, y_\perp)$  are transverse components of radius-vectors of the center-of-mass and relative motion of ions,  $\Delta_{\mathbf{R}_\perp}^{(2)}$  is the Laplace operator in the transversal space  $R^2$  and  $U(\mathbf{R}_\perp, \mathbf{r}_\perp)$  is the effective potential of the system of two particles

$$\begin{aligned} U(\mathbf{R}_\perp, \mathbf{r}_\perp) &= \frac{m_1 \omega_1^2 + m_2 \omega_2^2}{2} \mathbf{R}_\perp^2 \\ &+ \mu(\omega_1^2 - \omega_2^2) \mathbf{r}_\perp \mathbf{R}_\perp + \frac{\mu^2}{2} \left( \frac{\omega_1^2}{m_1} + \frac{\omega_2^2}{m_2} \right) \mathbf{r}_\perp^2. \end{aligned}$$

Under the condition  $\omega_1^2 - \omega_2^2 = 0$ , namely,  $q_1 m_2 - q_2 m_1 = 0$ , the variables can be separated:  $\Psi(\mathbf{R}_\perp, \mathbf{r}) = \Psi_\perp(\mathbf{R}_\perp) \Psi_{\text{int}}(\mathbf{r})$ , so that the  $5D$  problem is split into the  $2D$  equation describing the center-of-mass motion with the energy  $E_{a_\perp}$ ,

$$\begin{aligned} \left( -\frac{1}{2\mu} \Delta_{\mathbf{R}_\perp}^{(2)} + \frac{m_1 \omega_1^2 + m_2 \omega_2^2}{2} \mathbf{R}_\perp^2 \right) \\ \times \Psi_\perp(\mathbf{R}_\perp) = E_{a_\perp} \Psi_\perp(\mathbf{R}_\perp), \end{aligned} \quad (5)$$

and the  $3D$  equation that describes the relative motion,

$$\left( -\frac{1}{2\mu} \Delta_{\mathbf{r}}^{(3)} + \frac{\mu^2}{2} \left( \frac{\omega_1^2}{m_1} + \frac{\omega_2^2}{m_2} \right) \mathbf{r}_\perp^2 + U_{12}(\mathbf{r}) \right) \quad (6)$$

$$\times \Psi_{\text{int}}(\mathbf{r}) = E_{\text{int}} \Psi_{\text{int}}(\mathbf{r}),$$

where  $E_{\text{int}} = E - E_{a_\perp}$  is the energy in the center-of-mass frame. Note, that in accordance with the Kohn theorem [9], the generalization of the above model onto a similar  $n$ -particle system is also possible. Such setting of the problem can be also used if the frequencies  $\omega_i$  are considered as phenomenological parameters induced by a certain environment like artificial waveguides and if  $U_{12}(\mathbf{r})$  is the screening Coulomb potential for the scattering model of neutral atoms with confining potentials [10, 11].

We can rewrite Eq. (6) in the explicit form with respect to Coulomb interaction

$$\left( -\Delta_{\mathbf{r}}^{(3)} + \frac{2Z}{r} + \frac{\gamma^2}{4} \mathbf{r}_\perp^2 \right) \Psi_{\text{int}}(\mathbf{r}) = \epsilon \Psi_{\text{int}}(\mathbf{r}), \quad (7)$$

where  $Z = \mu q_1 q_2$  is the reduced charge,  $\gamma^2 = 8\mu\alpha\tilde{q}$ ,  $\tilde{q} = (q_1 m_2^2 + q_2 m_1^2) / (m_1 + m_2)^2$ , is the interaction constant, and  $\epsilon = 2\mu E_{\text{int}}$  is the reduced energy. Further, we use the scale transformation  $r \rightarrow \sqrt{\gamma} r$ ,  $Z \rightarrow Z / \sqrt{\gamma}$ ,  $E_{\text{int}} \rightarrow E_{\text{int}} / \gamma$ :

$$\left( -\Delta_{\mathbf{r}}^{(3)} + \frac{2\hat{Z}}{r} + \frac{1}{4} \mathbf{r}_\perp^2 \right) \Psi_{\text{int}}(\mathbf{r}) = \hat{\epsilon} \Psi_{\text{int}}(\mathbf{r}), \quad (8)$$

where  $\hat{Z} = Z / \sqrt{\gamma}$  and  $\hat{\epsilon} = \epsilon / \gamma$ .

### 3. AN ION IN COULOMB AND UNIFORM MAGNETIC FIELDS

Equation (8) is similar to the Schrödinger equation describing the motion of a particle with mass  $m_1$  and charge  $q_1$  in Coulomb field of the particle with the infinite mass  $m_2$  and charge  $q_2$ , and in an axially symmetric magnetic field  $\mathbf{B} = (0, 0, B = \gamma B_0)$ ,  $B_0 = 2.35 \times 10^5$  T [6]. In spherical coordinates  $(r, \eta = \cos \theta, \varphi)$  the later can be written in atomic units for the wave function  $\Psi(r, \eta, \phi) = \Psi_m(r, \eta) \exp(i m \varphi) / (2\pi)^{1/2}$  as the  $2D$  equation for the fixed magnetic quantum number  $m$  in the region  $\Omega = \{0 < r < \infty, -1 < \eta < 1\}$ :

$$\left( -\frac{1}{r^2} \frac{\partial}{\partial r} r^2 \frac{\partial}{\partial r} + \frac{\hat{A}^{(0)}(\eta; r)}{r^2} + \frac{2Z}{r} - \epsilon \right) \quad (9)$$

$$\times \Psi_m(r, \eta) = 0.$$

The operator  $\hat{A}^{(0)}(\eta; r) = A^{(0)}(\eta; r) - (\text{sign}q_1)\gamma mr^2$ , where  $(\text{sign}q_1) = -(+)$ , for example, for electron (positron), and  $A^{(0)}(r, \eta)$  is given by

$$A^{(0)}(\eta; r) = -\frac{\partial}{\partial \eta}(1 - \eta^2)\frac{\partial}{\partial \eta} + \frac{m^2}{1 - \eta^2} + \left(\frac{\gamma r^2}{2}\right)^2 (1 - \eta^2). \quad (10)$$

Here,  $Z = m_1 q_1 q_2$  is the reduced charge and  $\epsilon = 2m_1 E$  is the reduced energy. Thus, Eq. (8) with proper definitions for  $Z$ ,  $\epsilon$ , and  $\gamma$  formally corresponds to Eq. (9) if we put  $\hat{A}^{(0)}(\eta; r) = A^{(0)}(\eta; r)$ , i.e., if we omit  $\gamma mr^2$ . The wave function satisfies the following boundary conditions in each  $m\sigma$  subspace ( $\sigma$  is  $z$  parity  $\Psi_m(r, -\eta) = \sigma\Psi_m(r, \eta)$ ) of the full Hilbert space:

$$\begin{aligned} \lim_{\eta \rightarrow \pm 1} (1 - \eta^2) \frac{\partial \Psi_m(r, \eta)}{\partial \eta} &= 0, \quad \text{if } m = 0, \\ \Psi_m(r, \pm 1) &= 0, \quad \text{if } m \neq 0, \\ \left. \frac{\partial \Psi_m(r, \eta)}{\partial \eta} \right|_{\eta=0} &= 0, \quad \text{if } \sigma = +1, \\ \Psi_m(r, 0) &= 0, \quad \text{if } \sigma = -1. \end{aligned}$$

We consider the Kantorovich expansion of the partial solution  $\Psi_i^{m\sigma}(r, \eta)$  using the set of one-dimensional parametric basis functions  $\phi_j(\eta; r) \equiv \phi_j^{m\sigma}(\eta; r)$ :

$$\Psi_i^{m\sigma}(r, \eta) = \sum_{j=1}^{j_{\max}} \phi_j^{m\sigma}(\eta; r) \chi_j^{(i)}(r). \quad (11)$$

The matrix-valued functions  $\chi(r) \equiv \{\chi^{(i)}(r)\}_{i=1}^{j_{\max}}$  composed from vector functions  $(\chi^{(i)})^T = (\chi_1^{(i)}(r), \dots, \chi_{j_{\max}}^{(i)}(r))$  are unknown. The vector angular functions  $(\phi(\eta; r))^T = (\phi_1(\eta; r), \dots, \phi_{j_{\max}}(\eta; r))$  form an orthonormal basis for each value of the radius  $r$  which is treated here as a parameter. The *angular oblate spheroidal functions*  $\phi_i(\eta; r) \in \mathcal{F}_r \sim L_2([-1, 1])$  and the corresponding *potential curves*  $E_i(r)$  (in  $\text{Ry} = 1/2$  a.u.) are determined as the solutions of the following one-dimensional parametric eigenvalue problem:

$$\begin{aligned} \hat{A}^{(0)}(\eta; r) \phi_j(\eta; r) &= E_j(r) \phi_j(\eta; r), \\ \int_{-1}^1 \phi_i(\eta; r) \phi_j(\eta; r) d\eta &= \delta_{ij}. \end{aligned}$$

By substituting expansion (11) into the above boundary-value problem (9)–(11), we arrive at an eigenvalue problem for a system of  $j_{\max}$  ordinary second-order differential equations that determines the coefficients (radial wave functions) at the fixed energy  $\epsilon$   $(\chi^{(i)}(r))^T = (\chi_1^{(i)}(r), \chi_2^{(i)}(r), \dots, \chi_{j_{\max}}^{(i)}(r))$  in the expansion (11):

$$\begin{aligned} \left( -\mathbf{I} \frac{1}{r^2} \frac{d}{dr} r^2 \frac{d}{dr} + \frac{\mathbf{U}(r)}{r^2} + \mathbf{Q}(r) \frac{d}{dr} + \frac{1}{r^2} \frac{dr^2 \mathbf{Q}(r)}{dr} \right) \chi^{(i)}(r) &= \epsilon_i \mathbf{I} \chi^{(i)}(r), \end{aligned} \quad (12)$$

Here,  $\mathbf{I}$ ,  $\mathbf{U}(r)$ , and  $\mathbf{Q}(r)$  are finite  $j_{\max} \times j_{\max}$  matrices whose elements are given by the relations

$$U_{ij}(r) = \frac{E_i(r) + E_j(r) + 4Zr}{2} \delta_{ij} + r^2 H_{ij}(r), \quad (13)$$

$$H_{ij}(r) = \int_{-1}^1 \frac{\partial \phi_i(\eta; r)}{\partial r} \frac{\partial \phi_j(\eta; r)}{\partial r} d\eta,$$

$$Q_{ij}(r) = - \int_{-1}^1 \phi_i(\eta; r) \frac{\partial \phi_j(\eta; r)}{\partial r} d\eta.$$

The continuum wave function  $\Psi(r, \theta)$  satisfies the boundary condition of the third type:

$$\frac{d\Phi(r)}{dr} = \mathbf{R}(r) \Phi(r), \quad (14)$$

$$\mathbf{R}(r) \equiv \frac{d\Phi(r)}{dr} \Phi^{-1}(r),$$

at fixed values of the energy  $\epsilon$  and the radial variable  $r = r_{\min} > 0$  and  $r = r_{\max} \gg 1$ , where  $\Phi(r) = \{\chi^{(i)}(r)\}_{i=1}^{N_o}$  is an unknown  $j_{\max} \times N_o$  matrix and  $N_o = \max_{2E \geq \epsilon_j^{\text{th}}} j < j_{\max}$  is the number of open channels with Landau threshold  $\epsilon_{mj}^{\text{th}}(\gamma) = \lim_{r \rightarrow \infty} r^{-2} E_j(r) = \gamma(2j - 1 + |m| - (\text{sign}q_1)m)$ .

#### 4. THE CONTINUOUS SPECTRUM PROBLEM

The continuous spectrum solutions  $\chi^{(i)}(r)$  obey the third-type boundary condition at fixed energy  $\epsilon = 2E$  above the first Landau threshold  $\epsilon_{mj}^{\text{th}}(\gamma)$  with  $j = 1$ :

$$\frac{d\chi(r)}{dr} = \mathbf{R}\chi(r), \quad r = r_{\max}, \quad (15)$$

where  $\mathbf{R}$  is a nonsymmetric  $j_{\max} \times j_{\max}$  matrix which was calculated using the program KANTBP [5]. The orthogonality/normalization condition for  $\hat{\Psi}_i^{Em\sigma}(\Omega)$  at  $m = m'$  is

$$\langle \hat{\Psi}_i^{Em\sigma}(\Omega) | \hat{\Psi}_{i'}^{E'm'\sigma'}(\Omega) \rangle = \delta(E - E') \delta_{mm'} \delta_{\sigma\sigma'} \delta_{ii'}. \quad (16)$$

We express the corresponding eigenfunction  $\Psi_i^{Em\sigma}(r, \eta)$  of the continuous spectrum with the energy  $\epsilon = 2E$  in open channels  $i = \overline{1, N_o}$  in the form of Eq. (11), where  $\hat{\chi}^{(m\sigma)}(E, r) \equiv \{\chi^{(i_o)}(r)\}_{i_o=1}^{N_o}$  is now the radial part of the eigenchannel or “incoming” and “outgoing” wave function. The eigenchannel wave function  $\hat{\chi}^{(m\sigma)}(E, r)$  is expressed as

$$\hat{\chi}^{(m\sigma)}(E, r) = (2/\pi)^{1/2} \chi^{(p)}(r) \mathbf{C} \cos \delta. \quad (17)$$

The function  $\chi^{(p)}(r)$  is a numerical solution of Eq. (12) that satisfies the “standing-wave” boundary conditions (15) and has the standard asymptotic form [5]

$$\chi^{(p)}(r) = \chi^s(r) + \chi^c(r) \mathbf{K}, \quad (18)$$

$$\mathbf{K} \mathbf{C} = \mathbf{C} \tan \delta.$$

Here,  $\mathbf{K} \equiv \mathbf{K}_\sigma$  is the symmetric numerical *short-range reaction matrix* with the diagonal eigenvalue matrix  $\tan \delta \equiv \{\delta_{ij} \tan \delta_j\}_{ij=1}^{N_o}$  depending on the *short-range even/odd phase shift vector*  $\delta \equiv \delta_\sigma = \{\delta_j^\sigma\}_{j=1}^{N_o}$ , and the orthogonal matrix  $\mathbf{C}^T \mathbf{C} = \mathbf{I}_{oo}$  of the corresponding eigenvectors  $\mathbf{C}$ , where  $\mathbf{I}_{oo}$  is the unit  $N_o \times N_o$  matrix. Note, that in Eq. (17),  $\cos \delta$  is a diagonal matrix defined in the same terms. The regular  $\chi^s(r) = 2\Im(\chi(r))$  and irregular  $\chi^c(r) = 2\Re(\chi(r))$  asymptotic functions are expressed via the fundamental asymptotic solution  $\chi(r)$  with the leading terms at  $r \rightarrow \infty$ :

$$\chi_{jio}(r) = \frac{\exp(ip_{i_o}r + i\zeta \ln(2p_{i_o}r) + i\delta_{i_o}^c)}{2r\sqrt{p_{i_o}}} \delta_{jio}, \quad (19)$$

where  $p_{i_o}$  is the relative momentum in the channel  $i_o$ ,  $\zeta \equiv \zeta_{i_o} = Z/p_{i_o}$  is a Sommerfeld-type parameter,  $\delta_{i_o}^c = \arg \Gamma(1 - i\zeta)$  is the known Coulomb phase shift [12]. Using the  $\mathbf{R}$ -matrix calculus [5], we obtain the equation expressing the reaction matrix  $\mathbf{K}$  via the matrix  $\mathbf{R}$  at  $r = r_{\max}$

$$\mathbf{K} = -\mathbf{X}^{-1}(r_{\max}) \mathbf{Y}(r_{\max}), \quad (20)$$

where  $\mathbf{X}(r)$  and  $\mathbf{Y}(r)$  are square  $N_o \times N_o$  matrices depending on the open-open matrix (channels)

$$\mathbf{X}(r) = \left( \frac{d\chi^c(r)}{dr} - \mathbf{R} \chi^c(r) \right)_{oo}, \quad (21)$$

$$\mathbf{Y}(r) = \left( \frac{d\chi^s(r)}{dr} - \mathbf{R} \chi^s(r) \right)_{oo}.$$

The radial part of the “incoming” and “outgoing” wave functions  $\hat{\chi}^{(m\sigma)}(E, r) = (2/\pi)^{1/2} \chi^\mp(r)$  is expressed via the numerical “standing” wave function and the short-range reaction matrix  $\mathbf{K}$  by the relation

$$\begin{aligned} \chi^-(r) &= i\chi^{(p)}(r)(\mathbf{I}_{oo} + i\mathbf{K})^{-1}, \\ \chi^+(r) &= -i\chi^{(p)}(r)(\mathbf{I}_{oo} - i\mathbf{K})^{-1}, \end{aligned} \quad (22)$$

and have the asymptotic forms

$$\begin{aligned} \hat{\chi}^{(m\sigma)}(E, r) &= (2/\pi)^{1/2} (\chi(r) - \chi^*(r) \mathbf{S}^\dagger), \\ \hat{\chi}^{(m\sigma)}(E, r) &= (2/\pi)^{1/2} (\chi^*(r) - \chi(r) \mathbf{S}). \end{aligned} \quad (23)$$

Here,  $\mathbf{S} \equiv \mathbf{S}_\sigma$  is the symmetric unitary short-range scattering matrix,  $\mathbf{S}^\dagger \mathbf{S} = \mathbf{S} \mathbf{S}^\dagger = \mathbf{I}_{oo}$ , which can be expressed via the calculated  $\mathbf{K}$  matrix as

$$\mathbf{S} = (\mathbf{I}_{oo} + i\mathbf{K})(\mathbf{I}_{oo} - i\mathbf{K})^{-1}. \quad (24)$$

The ionization wave function  $\Psi_{Em\hat{v}}^{(-)}(r, \eta) \equiv \Psi_{Em\hat{v}}^{(-)}(r, \eta)$  has the asymptotic form reverse to the common scattering problem, namely, “incident wave + ingoing wave”

$$\begin{aligned} \Psi_{Em\hat{v}}^{(-)}(r, \eta) &= 2^{-1/2} (\Psi^{Em,+1}(r, \eta) \\ &\pm \Psi^{Em,-1}(r, \eta)) \exp(-i\delta^c). \end{aligned} \quad (25)$$

The function  $\Psi_{Em\hat{v}}^{(-)}(r, \eta)$  corresponds to the function  $|E\hat{v}mN_\rho\rangle$  defined in the cylindrical coordinates  $(\rho, z, \varphi)$

$$|E\hat{v}mN_\rho\rangle = \frac{\exp(im\varphi)}{2\pi} \sum_{n'=1}^{j_{\max}} \Phi_{n'}(\rho) \chi_{Em\hat{v}n'}^{(-)}(z). \quad (26)$$

Here,  $N_\rho = n - 1$ ,  $\hat{v}$  denotes the initial direction of the particle motion along the  $z$  axis,  $\Phi_{n'}(\rho)$  is the eigenfunction of a two-dimensional oscillator that corresponds to  $\Phi_j^{m\hat{v}}(r, \eta) = (\Phi_j^{m,+1}(r, \eta) \pm \Phi_j^{m,-1}(r, \eta))/\sqrt{2}$  at  $r \rightarrow \infty$ . At  $z \rightarrow \pm\infty$  the function  $\chi_{Em\hat{v}n'}^{(-)}(z)$  has the following asymptotic form:

$$\chi_{E\hat{v}}^{(-)}(z) \quad (27)$$

$$= \begin{cases} \begin{cases} \mathbf{X}^{(+)}(z) + \mathbf{X}^{(-)}(z) \hat{\mathbf{R}}^\dagger, & z > 0, \\ \mathbf{X}^{(+)}(z) \hat{\mathbf{T}}^\dagger, & z < 0, \end{cases} & \hat{v} = \rightarrow, \\ \begin{cases} \mathbf{X}^{(-)}(z) \hat{\mathbf{T}}^\dagger, & z > 0, \\ \mathbf{X}^{(-)}(z) + \mathbf{X}^{(+)}(z) \hat{\mathbf{R}}^\dagger, & z < 0, \end{cases} & \hat{v} = \leftarrow, \end{cases}$$



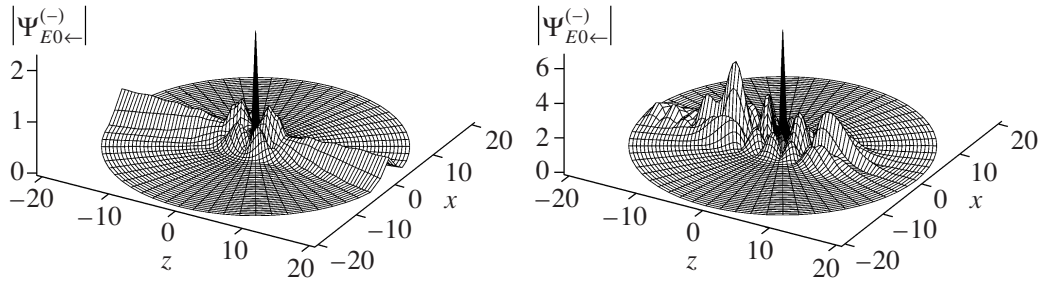


**Fig. 1.** Profiles of total wave functions (25) of the continuous spectrum in the  $z, x$  plane with  $Z = -1$ ,  $m = 0$ , and  $\gamma = 0.1$ . The states with the energy  $E = 0.05885$  a.u. (left) correspond to the resonance transmission, while those with the energy  $E = 0.11692$  a.u. (right) correspond to the total reflection.

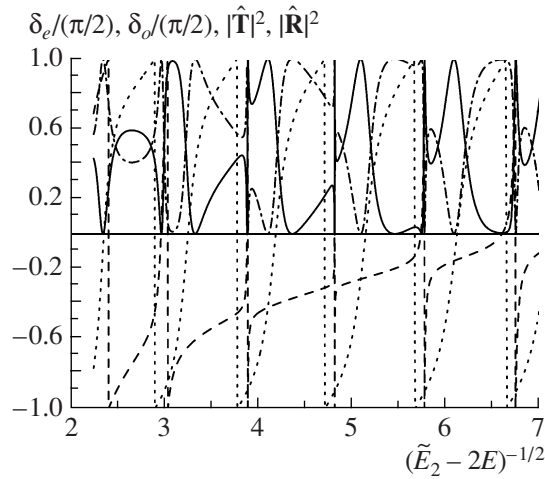


**Fig. 2.** Transmission  $|\hat{\mathbf{T}}|^2$  (dash-dotted curve) and reflection  $|\hat{\mathbf{R}}|^2$  (solid curve) coefficients (29), even  $\delta_e$  (dashed curve) and odd  $\delta_o$  (dotted curve) short-range phase shifts (18) versus  $(\tilde{E}_2 - 2E)^{-1/2}$  for  $Z = -1$ ,  $m = 0$ ,  $\gamma = 0.1$ . Here, the position of the first threshold  $2E = E_1 = \gamma = 0.1$  corresponds to  $(E_2 - 2E)^{-1/2} \approx 2.23$ .

where the matrix elements of  $\mathbf{X}^{(\pm)}(z)$  are

$$X_{n'n}^{(\pm)}(z) = \exp\left(\pm i p_{n'} z \pm i \zeta_{n'} \frac{z}{|z|} \ln(2 p_{n'} |z|)\right) \frac{\delta_{n'n}}{\sqrt{p_{n'}}}, \quad (28)$$

$\hat{\mathbf{T}}$  and  $\hat{\mathbf{R}}$  are the transmission and reflection amplitude matrices,  $\hat{\mathbf{T}}^\dagger \hat{\mathbf{T}} + \hat{\mathbf{R}}^\dagger \hat{\mathbf{R}} = \mathbf{I}_{oo}$ . It is easy to show that  $\hat{\mathbf{T}}$  and  $\hat{\mathbf{R}}$  may be expressed in terms of the long-range scattering matrices  $\hat{\mathbf{S}}_\sigma = \exp(i\delta^c) \mathbf{S}_\sigma \exp(i\delta^c)$  as

$$\begin{aligned} \hat{\mathbf{T}} &= 2^{-1}(-\hat{\mathbf{S}}_{+1} + \hat{\mathbf{S}}_{-1}), \\ \hat{\mathbf{R}} &= 2^{-1}(-\hat{\mathbf{S}}_{+1} - \hat{\mathbf{S}}_{-1}). \end{aligned} \quad (29)$$

Note, that the scattering wave function  $\Psi_{Em\leftarrow}^{(+)}(r, \eta)$

is defined by the formula  $\Psi_{Em\leftarrow}^{(+)}(r, \eta) = \left(\Psi_{Em\rightarrow}^{(-)}(r, \eta)\right)^*$  having the asymptotic form “incident wave + outgoing wave”. For recombination the above wave function should be renormalized to one particle per unit length in the incident wave by factor  $\sqrt{p_{i_o}}$  in each partial wave functions.

The continuous spectrum solution  $\chi^{(p)}(r)$  having the asymptotic form of a “standing” wave and the reaction matrix  $\mathbf{K}$  from (18) were calculated using the program KANTBP [5]. As an example, the profiles of the wave function (25) using Eq. (22) for  $Z = -1$ ,  $m = 0$ ,  $\gamma = 0.1$ ,  $j_{\max} = 10$ , and  $N_o = 1$  are shown in Fig. 1 at two fixed values of energy  $E$ , corresponding to resonance transmission  $|\hat{\mathbf{T}}|^2 = \sin^2(\delta_e - \delta_o) = 1$  and total reflection  $|\hat{\mathbf{R}}|^2 = \cos^2(\delta_e - \delta_o) = 1$ . One can see that the probability density of the wave function around a point of pair impact in the case of reflection is greater than in the case of transmission. Here,  $\delta_e \equiv \delta_1^{+1}$  and  $\delta_o \equiv \delta_1^{-1}$  are the *short-range phase shifts* for even and odd states from Eq. (18), respectively. The transmission and reflection coefficients are explicitly shown in Fig. 2 together with the even  $\delta_e$  and odd  $\delta_o$  phase shifts versus the inverse square root of energy  $(\tilde{E}_2 - 2E)^{-1/2}$  relative to the second threshold shift  $\tilde{E}_2 = \epsilon_{m2}^{\text{th}}(\gamma)$ . The countable series of quasistationary states imbedded in the continuum corresponds to the *short-range phase shifts*  $\delta_{o(e)} = n_{o(e)}\pi + \pi/2$  at  $(\tilde{E}_2 - 2E)^{-1/2} = n_{o(e)} + \Delta_{n_{o(e)}}$  (the first  $n_{o(e)} = 1-6$  of them are presented in Fig. 2). Nonmonotonic behavior of  $|\hat{\mathbf{T}}|$  and  $|\hat{\mathbf{R}}|$  is seen to include the cases of resonance transmission and total reflection, related to the existence of these quasistationary states.

One can fit the obtained numerical results for a finite number of quasistationary states using the appropriate analytic parametrization [13] to extrapolate them from above the  $i_o$ th threshold to below the  $(i_o +$

1)th threshold and, as a result, to estimate the countable set of quasistationary states between the thresholds. Such a procedure provides a considerable reduction of the computer facilities required and allows one to select the appropriate energy subregions for further numerical calculations aimed at the determination of the resonance frequencies of photoionization and the induced or spontaneous recombination [14].

## 5. ASYMPTOTIC SOLUTION AT SMALL VALUES OF THE RADIAL VARIABLE

Let us suppose that the set of linearly independent solutions  $\tilde{\Phi}_{\text{reg}}(r) = \{\tilde{\chi}_{\text{reg}}^{(i)}(r)\}_{i=1}^{j_{\text{max}}}$ , where  $\tilde{\chi}_{\text{reg}}^{(i)}(r) = (\tilde{\chi}_{1i}^{\text{reg}}(r), \dots, \tilde{\chi}_{j_{\text{max}}i}^{\text{reg}}(r))^T$ , is constructed. Using a linear combination of these regular solutions,  $\tilde{\chi}_{\text{reg}}^{(i)}(r)$ , we can find the required matrix solution  $\Phi(r)$  at  $r = r_{\text{min}} > 0$ :

$$\Phi(r) = \tilde{\Phi}_{\text{reg}}(r)\mathbf{C}, \quad (30)$$

$$\chi_{ji_o}(r) = \sum_{i=1}^{j_{\text{max}}} \tilde{\chi}_{ji}^{\text{reg}}(r) C_{ii_o},$$

where  $\mathbf{C}$  is an unknown nonzero constant  $j_{\text{max}} \times N_o$  matrix. Using the identity  $\mathbf{C}\mathbf{C}^{-1} = \mathbf{I}$ , the  $\mathbf{R}(r)$  matrix at  $r = r_{\text{min}}$  can be easily found via the known set of linear independent regular solutions  $\tilde{\Phi}_{\text{reg}}(r)$ :

$$\mathbf{R}(r) \equiv \frac{d\tilde{\Phi}_{\text{reg}}(r)}{dr} \tilde{\Phi}_{\text{reg}}^{-1}(r), \quad (31)$$

$$R_{ji}(r) = \sum_{i'=1}^{j_{\text{max}}} \frac{d\tilde{\chi}_{ji'}^{\text{reg}}(r)}{dr} (\tilde{\chi}^{\text{reg}}(r))_{i'i}^{-1}.$$

After the numerical calculation of the solution  $\Phi(r) = \Phi^h(r)$  in the nodes of the finite-element grid  $\Omega_r^h$  within the interval  $[r_{\text{min}}, r_{\text{max}}]$ , taking Eqs. (14)–(31) into account, the matrix  $\mathbf{C}$  can be evaluated using the formula at  $j = 1, \dots, j_{\text{max}}$  and  $i_o = 1, \dots, N_o$ :

$$\mathbf{C} = \tilde{\Phi}_{\text{reg}}^{-1}(r_{\text{min}}) \Phi(r_{\text{min}}), \quad (32)$$

$$C_{ji_o} = \sum_{i=1}^{j_{\text{max}}} (\tilde{\chi}_{\text{reg}}^{-1})_{ji}(r_{\text{min}}) \chi_{ii_o}(r_{\text{min}}).$$

The matrix  $\mathbf{C}$  is applied to the analysis of the matrix solution  $\Phi(r)$  in the vicinity of  $r = 0$ . For example, a constant matrix  $\mathbf{C}$  keeps the ratio  $\tilde{\Phi}_{\text{reg}}^{-1}(0)\Phi(0)$  finite and nonzero even if  $\Phi(0) \equiv \mathbf{0}$  or is very close to zero. To extract the required matrix  $\mathbf{C}$  in this case, one can use the known asymptotic form of the regular solutions at  $r_{\text{min}}$ . The value  $r_{\text{min}}$  is defined in the asymptotic domain of the  $\tilde{\Phi}_{\text{reg}}(r)$ . As a result, we

obtain the total wave function in each open channel  $r \leq r_{\text{min}}$ :

$$\psi_{i_o}(\eta, r) = \sum_{j=1}^{j_{\text{max}}} \sum_{i=1}^{j_{\text{max}}} \phi_j^{m\sigma}(\eta; r) \chi_{ji}^{\text{reg}}(r) C_{ii_o}.$$

At small  $r$  we find the asymptotic solutions of the problem (12)–(14) as an expansion in powers of  $r$  and Legendre polynomials  $P_{l+s}^{|m|}(\eta; r)$  with  $l = 2(j-1) + |m| + (1-\sigma)/2$ :

$$E_j(r) = E_j^{(0)} + E_j^{(2)}r^2 + \sum_{k=1}^{k_{\text{max}}/4} r^{4k} E_j^{(4k)}, \quad (33)$$

$$\phi_j(\eta; r) = \phi_j^{(0)}(\eta; r) + \sum_{k=1}^{k_{\text{max}}} r^{4k} \phi_j^{(k)}(\eta; r),$$

$$\phi_j^{(k)}(\eta; r) = \sum_{s=-2k}^{2k} P_{l+s}^{|m|}(\eta; r) b_{sj}^{(k)}.$$

The substitution of Eq. (33) into Eq. (12) leads to the recursive relations for the unknowns  $b_{sj}^{(k)}$  for  $s \neq 0$  and  $E_j^{(4k)}$ :

$$(s^2 + (2l+1)s)b_{sj}^{(k)} = - \sum_{s'=-2}^2 v_{s;s'}^{(1)} b_{s-s'j}^{(k-1)} + \sum_{p=0}^{k-1} E_j^{(4k-4p)} b_{sj}^{(p)}, \quad (34)$$

where the matrix elements are defined by the relations with the notation  $t = l + s$ :

$$v_{-2;t}^{(k)} = \delta_{1k} \frac{1}{4(2|m| + 2t - 1)}$$

$$\times \sqrt{\frac{(t-1)t(2|m| + t - 1)(2|m| + t)}{(2|m| + 2t - 3)(2|m| + 2t + 1)}},$$

$$v_{0;t}^{(k)} = \delta_{1k} \frac{2(t^2 + t + 2|m|t + 2|m|^2 + |m| - 1)}{(2|m| + 2t - 1)(2|m| + 2t + 3)},$$

$$v_{2;t}^{(k)} = \delta_{1k} \frac{1}{4(2|m| + 2t + 3)}$$

$$\times \sqrt{\frac{(t+1)(t+2)(2|m| + t + 1)(2|m| + t + 2)}{(2|m| + 2t + 1)(2|m| + 2t + 5)}}.$$

These equations were solved at given initial data  $E_j^{(0)} = l(l+1)$  and  $b_{sj}^{(0)} = \delta_{s0}$ . The coefficients  $b_{0j}^{(k)}$  at  $s = 0$  were calculated from the normalization condi-



tion (12):

$$b_{0j}^{(k)} = - \sum_{p=0}^k \sum_{s'=-2k}^{2k} \sum_{s=-2k}^{2k} b_{sj}^{(k-p)} \langle s|s' \rangle b_{s'j}^{(p)}. \quad (35)$$

Thus, the asymptotic expansions of the matrix elements take the form

$$\begin{aligned} H_{jj'}(r) &= \sum_{k=1}^{k_{\max}/4} r^{4k-2} \bar{H}_{jj'}^{(4k-2)}, \\ Q_{jj'}(r) &= \sum_{k=1}^{k_{\max}/4} r^{4k-1} \bar{Q}_{jj'}^{(4k-1)}, \\ \bar{H}_{jj'}^{(4k-2)} &= \sum_{p=0}^k \sum_{s'=-2k}^{2k} \sum_{s=-2k}^{2k} b_{sj}^{(k-p)} \\ &\quad \times 16p(k-p) \delta_{s+j s'+j'} b_{s'j'}^{(p)}, \end{aligned}$$

$$\begin{aligned} \bar{Q}_{jj'}^{(4k-1)} &= \sum_{p=0}^k \sum_{s'=-2k}^{2k} \sum_{s=-2k}^{2k} b_{sj}^{(k-p)} \\ &\quad \times 4(k-p) \delta_{s+j s'+j'} b_{s'j'}^{(p)}. \end{aligned}$$

The calculation was performed using the algorithm implemented in MAPLE up to  $k_{\max} = 16$ . Below we display the first few coefficients of the matrix elements with  $l = 2(j-1) + |m| + (1-\sigma)/2$ :

$$\begin{aligned} \bar{E}_j^{(0)} &= l(l+1), \quad \bar{E}_j^{(2)} = \gamma m, \\ \bar{E}_j^{(4)} &= \frac{\gamma^2(l^2 + l - 1 + |m|^2)}{2(2l-1)(2l+3)}, \end{aligned}$$

$$\bar{Q}_{jj-2}^{(3)} = - \frac{\gamma^2(l + |m|)^{1/2}(l - |m|)^{1/2}(l - 1 - |m|)^{1/2}(l - 1 + |m|)^{1/2}}{2(2l-3)^{1/2}(2l+1)^{1/2}(2l-1)^2}.$$

At small  $r$  we find the asymptotic solutions of the problem (12)–(14) in the form of an expansion in powers of  $r$ :

$$\tilde{\chi}_{ji}(r) = \sum_{k=0}^{k_{\max}} \tilde{\chi}_{ji}^{(k)} r^{\mu_i + k}, \quad \tilde{\chi}_{ji}^{(0)} = \delta_{ji}, \quad (36)$$

where  $\mu_0$  is the unknown characteristic parameter. The substitution of Eq. (36) into Eq. (12) leads to the recursive relations for the unknowns  $\tilde{\chi}_{ji}^{(k)}$  with  $l' = 2(j-1) + |m| + (1-\sigma)/2$ ,  $l = 2(i-1) + |m| + (1-\sigma)/2$ :

$$\begin{aligned} &-(l' + 1 + \mu_i + k)(\mu_i - l' + k) \tilde{\chi}_{ji}^{(k)} \\ &= 2Z \tilde{\chi}_{ji}^{(k-1)} - (m\gamma - \epsilon) \tilde{\chi}_{ji}^{(k-2)} - \sum_{s=4}^k \bar{E}_j^{(s)} \tilde{\chi}_{ji}^{(k-s)} \\ &\quad - \sum_{s=4}^{k-2} \bar{H}_{jj}^{(s)} \tilde{\chi}_{ji}^{(k-s-2)} \\ &\quad - \sum_{s=3}^{k-1} \sum_{j'=\max(1, i-[s/4]), j' \neq j}^{\min(j_{\max}, i+[s/4])} (2l + 2k - s) \bar{Q}_{jj'}^{(s)} \tilde{\chi}_{j'i}^{(k-s-1)} \end{aligned} \quad (37)$$

$$- \sum_{s=4}^{k-2} \sum_{j'=\max(1, i-[s/4]), j' \neq j}^{\min(j_{\max}, i+[s/4])} \bar{H}_{jj'}^{(s)} \tilde{\chi}_{j'i}^{(k-s-2)}.$$

As follows from Eq. (37) at  $k = 0$ , the conventional characteristic equation yields two roots for the unknown  $\mu_i$ :  $\mu_i = -l' - 1$  and  $\mu_i = l'$ . The value  $\mu_i = -l' - 1$  corresponds to irregular unbound solutions and is not considered here. The value  $\mu_i = l'$  corresponds to the required regular and bound solutions and is the one we have used in our calculations. In this case (37) the coefficients of the asymptotic expansion of the regular solution (36) are

$$\begin{aligned} \tilde{\chi}_{ii}^{(0)} &= 1, \quad \tilde{\chi}_{ii}^{(1)} = \frac{Z}{l+1}, \\ \tilde{\chi}_{ii}^{(2)} &= - \frac{-2Z^2 + (\epsilon - m\gamma)(l+1)}{2(l+1)(2l+3)}, \\ \tilde{\chi}_{ii}^{(3)} &= - \frac{Z(-2Z^2 + (\epsilon - m\gamma)(3l+4))}{6(l+1)(l+2)(2l+3)}, \\ \tilde{\chi}_{i-1i}^{(4)} &= \frac{\bar{Q}_{i-1i}^{(3)}(2l+5)}{6(2l+3)}, \end{aligned} \quad (38)$$

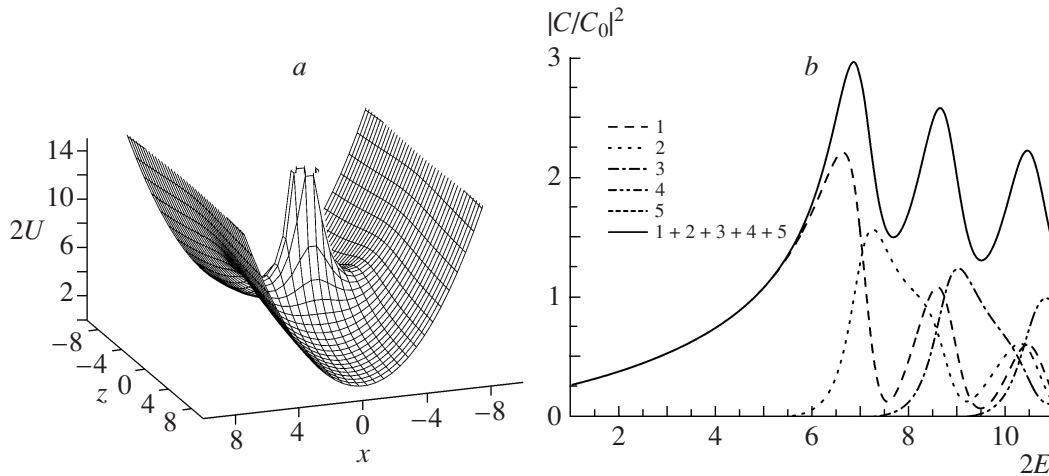


**Fig. 3.** (a) Effective potential  $2U$  in the  $z, x$  plane; (b) the full enhancement coefficient (solid line) and partial enhancement coefficients in each open channel ( $i = 1-5$ ) versus the threshold energy  $2E$ , for the effective charge  $Z = +6$  and  $\gamma = 1$  (in scaled variables).

$$\begin{aligned}\tilde{\chi}_{ii}^{(4)} &= \frac{\bar{E}_i^{(4)}}{4(2l+5)} + \frac{(\epsilon - m\gamma)^2}{8(2l+3)(2l+5)} \\ &+ \frac{Z^4 - Z^2(\epsilon - m\gamma)(3l+5)}{6(l+1)(l+2)(2l+3)(2l+5)}, \\ \tilde{\chi}_{i+1i}^{(4)} &= \frac{\bar{Q}_{i+1i}^{(3)}(2l+5)}{2(2l+7)}.\end{aligned}$$

As a result, we get the required expansion of  $2D$ -solution in the Kantorovich form:

$$\psi_{i_o}^{(as)}(\eta, r)$$

$$\begin{aligned}&= \sum_{i=1}^{j_{\max}} \sum_{k=0}^{k_{\max}} \sum_{p=0}^{k_{\max}-k} \sum_{j=1}^{j_{\max}} r^{\mu_i+k} \phi_j^{(k-p)}(\eta) \tilde{\chi}_{ji}^{(p)\text{reg}} C_{ii_o}, \\ \phi_j^{(k-p)}(\eta) &= \sum_{s=\max(-l, -2k+2p)}^{2k-2p} P_{l+s}^{[m]}(\eta) b_{sj}^{(k-p)},\end{aligned}$$

where  $l = 2(i-1) + |m| + (1-\sigma)/2$ ,  $\mu_i = l$ . The above asymptotic form of the Kantorovich expansion is equivalent to the Galerkin one over the basis of Legendre polynomials:

$$\begin{aligned}&\psi_{i_o}^{(as)}(\eta, r) \\ &= \sum_{i=1}^{j_{\max}} \sum_{k=0}^{k_{\max}} \sum_{s=\max(-l, -2k+2p)}^{2k-2p} f_s^{(k)}(r, \eta) g_{si}^{(k_{\max}-k)} C_{ii_o}, \\ f_s^{(k)}(r, \eta) &= r^{\mu_i+k} P_{l+s}^{[m]}(\eta), \\ g_{si}^{(k_{\max}-k)} &= \sum_{p=0}^{k_{\max}-k} \sum_{j=1}^{j_{\max}} b_{sj}^{(k-p)} \tilde{\chi}_{ji}^{(p)\text{reg}}.\end{aligned}$$

Moreover, using the substitution  $r = (\rho^2 + z^2)^{1/2}$  and  $\eta = z(\rho^2 + z^2)^{-1/2}$ , one gets the asymptotic series for the regular solution in the Galerkin form in cylindrical coordinates  $(\rho, z)$  over the homogeneous polynomials of the degree  $(\mu_i + k)$  with respect to the variables  $(\rho, z)$ :

$$f_s^{(k)}(\rho, z) = (\rho^2 + z^2)^{(\mu_i+k)/2} P_{l+s}^{[m]}(z(\rho^2 + z^2)^{-1/2}).$$

Note, that one can also derive the above asymptotic expansion in Galerkin form with the help of the direct calculation scheme [15]. The above asymptotic expansions can be applied to set the third-type boundary condition around the point of pair impact in different calculation schemes.

## 6. PRELIMINARY ESTIMATIONS OF THE ENHANCEMENT COEFFICIENT

The solution of the channelling problem (8) with the help of calculation schemes described in Sections 4 and 5 was found using the programs KANTBP 2.0 and POTHMF at various values of the scaled energy  $E$  and the effective charge  $Z$ . As a result, the values of the enhancement coefficient have been calculated by means of the formula  $|C(2E)/C_0(2E)|^2 = \sum_{i=1}^{N_o} |C_i(2E)/C_0(2E)|^2$ , where  $C_i(2E) = \chi_{1i}(r=0)$  are the numerical values of the solution at the point of pair impact from Eq. (12) and  $C_0(2E) = \chi_{11}(r=0)$  is the Coulomb function with the effective charge  $Z$  at the energy  $2E - 1$ .

Figure 3 illustrates the estimations of the total enhancement coefficient and the enhancement coefficients in each open channel (1–5) as functions of the energy  $2E$ , related to the zero energy of free threshold, at the effective charge  $Z = 6$  for even components of

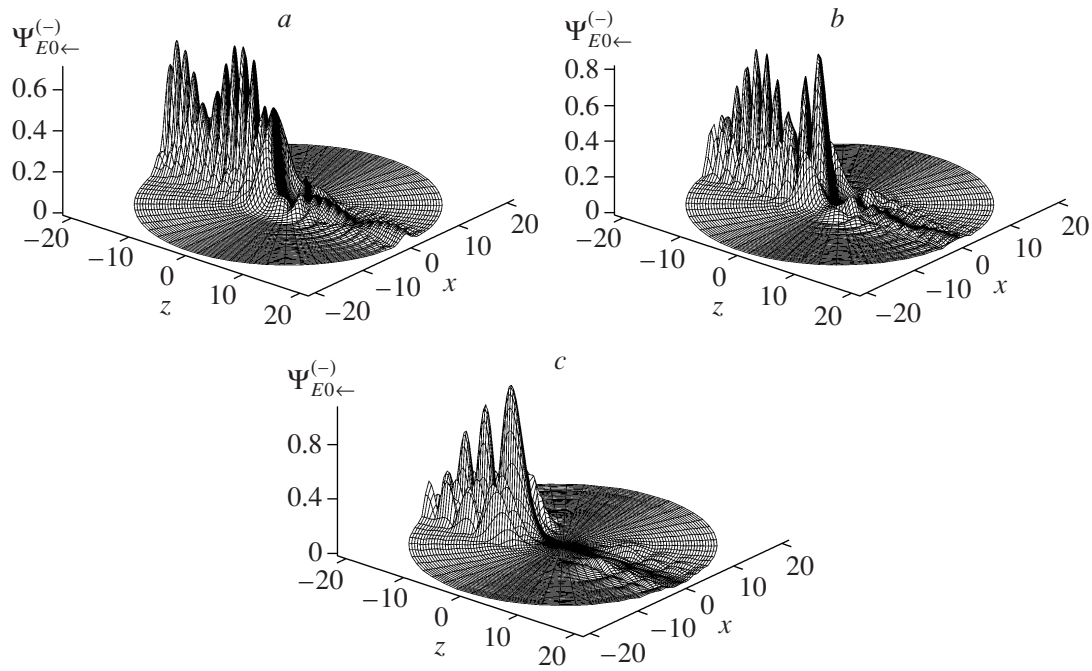


**Fig. 4.** Profiles of total wave functions  $|\Psi_{i_o;E0\leftarrow}^{(-)}|$  of the continuous spectrum in the  $z, x$  plane for the first, second, and third ( $a$ – $c$ ) open channels at  $2E = 6.552$ ,  $Z = +6$ ,  $\gamma = 1$  (in scaled variables).

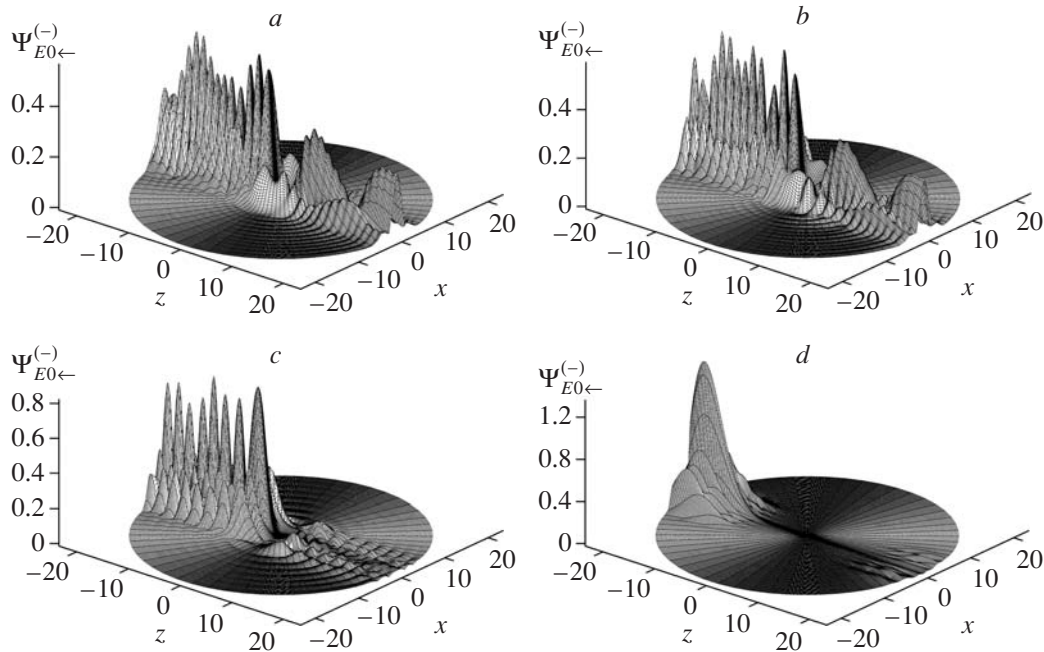


**Fig. 5.** Profiles of total wave functions  $|\Psi_{i_o;E0\leftarrow}^{(-)}|$  in the  $z, x$  plane of the continuous spectrum of first, second, third, and fourth ( $a$ – $d$ ) open channels at  $2E = 7.70$ ,  $Z = +6$ ,  $\gamma = 1$  (in scaled variables).

the solution at  $m = 0$ . The maximum of the total enhancement coefficient is achieved at the value  $2E = 6.9$ , between the third and the fourth channel at passing the minimum of the barrier  $2U_0 = 6.24$ , where

$2U_0 = 2U(\rho, z) = 2Z/(\rho^2 + z^2)^{1/2} + (1/4)\rho^2$  at the saddle point with coordinates  $z = 0$  and  $\rho = \rho_0$  under the condition  $\partial U(\rho, z)/\partial \rho|_{\rho} = 0$  (see Fig. 3b). The reflection is practically total, indeed, at  $2E = 6.552$

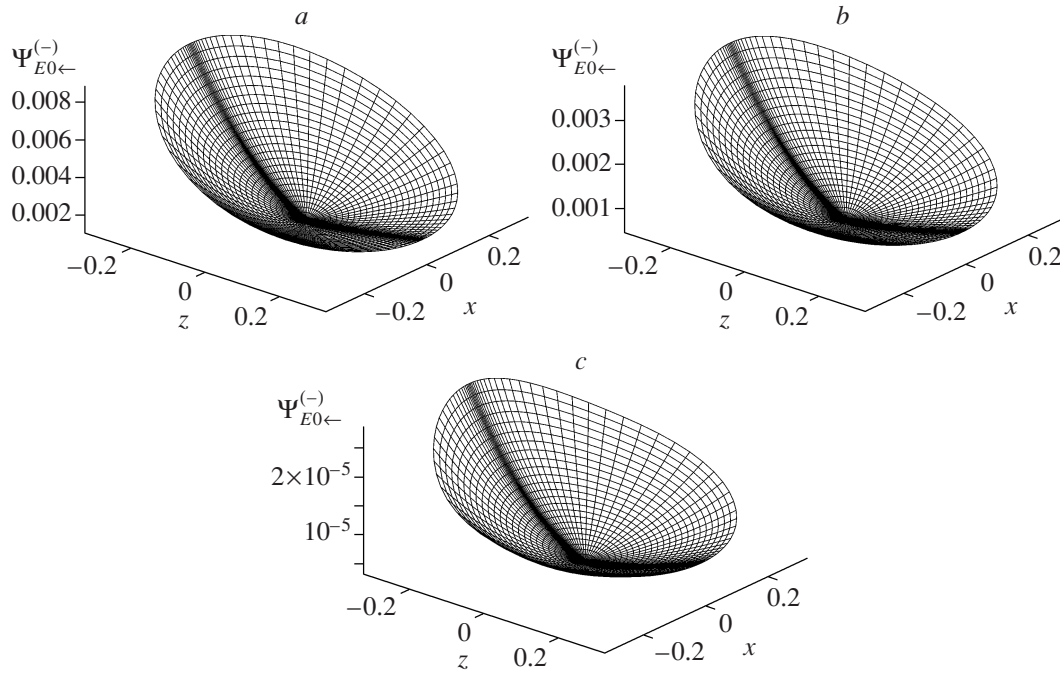


**Fig. 6.** Asymptotic behavior of the total wave functions  $|\Psi_{E0\leftarrow}^{(-)}|$  of the continuous spectrum in the  $z, x$  plane for the first, second, and third ( $a$ – $c$ ) open channels at  $2E = 6.552$ ,  $Z = +6$ ,  $\gamma = 1$  (in scaled variables).

the matrix of reflections coefficients is

$$|\hat{\mathbf{R}}|^2 = \begin{pmatrix} 0.967329 & 0.004785 & -0.000094 \\ 0.004785 & 0.990368 & 0.000074 \\ -0.000094 & 0.000074 & 0.999999 \end{pmatrix}.$$

Similar to the case of attraction (see Fig. 1), the

first local minimum of the total enhancement coefficient appears with increasing energy above the fourth threshold energy to  $2E = 7.70$ , where the diagonal elements of the transition coefficient matrix increases to approximately  $\sim 0.5$  in the first and the second channels:

$$|\hat{\mathbf{R}}|^2 = \begin{pmatrix} 0.473201 & 0.235919 & 0.043577 & -4 \times 10^{-7} \\ 0.235919 & 0.555215 & -0.003336 & 1 \times 10^{-7} \\ 0.043577 & -0.003336 & 0.995355 & 4 \times 10^{-8} \\ -4 \times 10^{-7} & 1 \times 10^{-7} & 4 \times 10^{-8} & 1.00000 \end{pmatrix}.$$

Such a behavior is a consequence of the effects of superstrong focusing, corresponding to astrophysical magnetic fields. At interaction of particles in the channel the competition of two processes occur: the defocusing due to Coulomb interactions and the focusing due to the oscillator interaction [3], effectively lowering the dimension of the problem. Hence, there exists a region of energy, where the probability density at the point of pair impact has a

maximum for quasistationary states of the continuous spectrum. For example, the first component of the *short-range even phase-shift vector*  $\delta \equiv \delta_e = \{\delta_j^e\}_{j=1}^{N_o=3} = (-1.5707, 0.7717, 0.5343)^T$  of the even state equals  $-\pi/2$  at  $2E = 6.552$  (see Fig. 3). Figures 4–6 present the partial ionization wave functions  $|\Psi_{E0\leftarrow}^{(-)}|$  and their asymptotic behavior versus the coordinates  $(x, z)$  in the plane  $y = 0$ .

To study the interaction of channelled particles at real values of an effective charge,  $Z$ , for example, for identical particles with masses and charges of a deuterium nucleus, it is necessary to set an effective charge,  $Z \sim 100$ , and to solve the problem with a large number of open channels,  $N_o \sim U_0 \sim 3(Z/2)^{2/3}/2$ , that requires significant computer resource.

## 7. CONCLUSIONS

In the present paper the optimal conditions have been determined under which it is possible to solve the problem of interaction of channelled particles. Tentative estimations of the enhancement factor were obtained without additional short-range nuclear potentials. The dependence of the enhancement factor upon the energy is nonmonotonic, which is a manifestation of two potentials, the defocusing Coulomb potential of interaction between identical charged particles and the focusing oscillator potential, responsible for the interaction of particles with the crystal, supporting the quasistationary states in the continuous spectrum and providing the practically total reflection. In the framework of the proposed approach one can obtain improved estimations of the enhancement factor taking into account the known parametrizations of the  $R$  matrix of nuclear reactions at an appropriate point  $r_{\min} = r_0$  in the vicinity of the pair impact point.

The presented approach and the programs that allow one to study the threshold peculiarities of photoionization and recombination of particles with the opposite-sign charges (positrons, antiprotons) in a magneto-optical trap [16], the optical absorption in quantum wells [17], and the channelling of similarly charged particles in thin doped films [3] or neutral atoms and molecules in artificial waveguides or surfaces [10, 11].

The application of the total reflection effect to oppositely charged particles in a homogeneous magnetic field can give a new mechanism of jumps in a magneto-optical trap [16, 18] after each pair collision without any additional external confinement in the longitudinal direction under the resonance conditions (the temperature and the axial magnetic field parameter  $\gamma$  or the frequency and the polarization of the additional laser field [14, 19]), provided that the collision integral in the Boltzmann equation will be properly taken into account [20, 21].

## ACKNOWLEDGMENTS

The authors are grateful to Prof. Yu. N. Demkov, Prof. V. S. Melezhik, Prof. F.M. Pen'kov, Prof.

V.V. Pupyshev, and Prof. N.Zh. Takibaev for useful discussions.

This work was partly supported by RFBR grants nos. 08-01-00604 and 07-01-00660, CRDF BRHE grant no. REC-006 and JINR theme no. 05-6-1060-2005/2010.

## REFERENCES

1. Vit. M. Bystritskiĭ et al., Phys. At. Nucl. **64**, 855 (2001).
2. F. Raiola et al., Eur. Phys. A **13**, 377 (2002); J. Phys. G **31**, 1141 (2005).
3. Yu. N. Demkov and J. D. Meyer, Eur. Phys. J. B **42**, 361 (2004).
4. P. M. Krassovitskiy and N. Zh. Takibaev, Bull. Russ. Acad. Sci., Phys. Ser. **70**, 815 (2006).
5. O. Chuluunbaatar et al., Comput. Phys. Commun. **177**, 649 (2007); **179**, 685 (2008).
6. O. Chuluunbaatar et al., Comput. Phys. Commun. **178**, 301 (2008); Phys. At. Nucl. **71**, 844 (2008).
7. O. Chuluunbaatar et al., Phys. Rev. A **77**, 034702 (2008).
8. A. H. Sorencen, Nucl. Instrum. Methods Phys. Res. B **119**, 1 (1996).
9. W. Kohn, Phys. Rev. **123**, 1242 (1961).
10. V. S. Melezhik, J. I. Kim, and P. Schmelcher, Phys. Rev. A **76**, 053611 (2007).
11. F. M. Pen'kov, Phys. Rev. A **62**, 044701 (2000).
12. M. Abramowitz and I. A. Stegun, *Handbook of Mathematical Functions* (Dover, New York, 1972).
13. A. I. Baz, Ya. B. Zeldovich, and A. M. Perelomov, *Scattering, Reactions and Decays in Nonrelativistic Quantum Mechanics* (Nauka, Moscow, 1971) [in Russian].
14. V. V. Serov, V. L. Derbov, and S. I. Vinitsky, Opt. Spectrosc. **102**, 557 (2007).
15. V. V. Pupyshev, Theor. Math. Phys. **136**, 970 (2003); **156**, 1058 (2008).
16. M. C. Fujiwara et al., Phys. Rev. Lett. **101**, 053401 (2008).
17. E. M. Kazaryan, A. A. Kostanyan, and H. A. Sarkisyan, Physica E **28**, 423 (2005).
18. A. Yu. Voronin and P. Froelich, J. Phys. B **38**, L301 (2005).
19. M. V. Ryabinina and L. A. Melnikov, Nucl. Instrum. Methods Phys. Res. B **214**, 35 (2004).
20. V. L. Saveliev and K. Nanbu, Phys. Rev. E **65**, 051205 (2002).
21. D. Benedetto, F. Castella, R. Esposito, and M. Pulvirenti, Commun. Math. Phys. **277**, 1 (2008).



# Adiabatic Representation for a Hydrogen Atom Photoionization in a Uniform Magnetic Field\*

O. Chuluunbaatar<sup>1)\*\*</sup>, A. A. Gusev<sup>1)\*\*\*</sup>, V. L. Derbov<sup>2)</sup>, M. S. Kaschiev<sup>†3)</sup>,  
L. G. Mardoyan<sup>4)</sup>, V. V. Serov<sup>2)</sup>, T. V. Tupikova<sup>1)</sup>, and S. I. Vinitsky<sup>1)\*\*\*\*</sup>

Received August 20, 2007

**Abstract**—A new effective method of calculating wave functions of discrete and continuous spectra of a hydrogen atom in a strong magnetic field is developed on the basis of the adiabatic approach to parametric eigenvalue problems in spherical coordinates. The two-dimensional spectral problem for the Schrödinger equation at a fixed magnetic quantum number and parity is reduced to a spectral parametric problem for a one-dimensional angular equation and a finite set of ordinary second-order radial differential equations. The results are in good agreement with the photoionization calculations by other authors and have a true threshold behavior.

PACS numbers: 31.15.Ja, 31.15.Pf, 34.50.-s, 34.50.Pi

DOI: 10.1134/S1063778808050128

## 1. INTRODUCTION

Recent Monte Carlo estimations of the influence of a strong magnetic field on the spontaneous recombination of the anti-hydrogen in the cold positron–antiproton plasma conditions of the ATHENA [1, 2] and ALPHA [3] experiments (CERN) have shown that further quantum mechanical analysis is needed [4]. We can draw attention to a new enhancement mechanism of a laser-stimulated recombination of anti-hydrogen in cold antiproton–positron plasma in a laboratory magnetic field via quasistationary states embedded in the continuum that has been revealed recently [5]. At the first stage of such an analysis, the adiabatic representation known in mathematics as a Kantorovich method is developed for solving the problem of low-lying excited states of the hydrogen atom in a magnetic field in spherical coordinates [6] and the benchmark three-body scattering problem on a line [7].

Indeed, the adiabatic representation in cylindrical coordinates was applied recently to revive the

basic decay mechanisms of Rydberg states with high magnetic quantum numbers in the magnetic traps [8]. It has been shown that the exhaustive analysis of the complex dynamics of the electron with decreasing module of magnetic number is impossible without taking the nonadiabatic coupling into consideration [9]. However, high-accuracy calculations in cylindrical coordinates is a rather cumbersome problem except the cases of high magnetic numbers or a dominating magnetic field [10]. So, using spherical coordinates is preferable when Coulomb and magnetic fields have comparable contributions in the average potential energy [11] but leads to nontrue threshold behavior of the photoionization cross section calculated by the complex rotation–variational method [12].

In this paper, we develop the Kantorovich approach with a boundary condition of the third type in a form appropriate for the  $\mathbf{R}$ -matrix calculations of atomic hydrogen photoionization in a strong magnetic field using a uniform orthogonal parametric basis of the angular oblate spheroidal functions [13] in spherical coordinates only, instead of the combined nonorthogonal basis of Landau and Sturmian functions in both cylindrical and spherical coordinates [14, 15]. The efficiency of the elaborated approach which provides true threshold behavior of photoionization cross sections of a hydrogen atom from the ground state to the different continuous-spectrum states is demonstrated.

The paper is organized as follows. The 2D eigenvalue problem for the Schrödinger equation for the hydrogen atom in an axially symmetric magnetic field,

\*The text was submitted by the authors in English.

†Deceased.

<sup>1)</sup>Joint Institute for Nuclear Research, Dubna, Russia.

<sup>2)</sup>Saratov State University, Saratov, Russia.

<sup>3)</sup>Institute of Mathematics and Informatics, BAS, Sofia, Bulgaria.

<sup>4)</sup>Yerevan State University, Yerevan, Armenia.

\*\*E-mail: [chuka@jinr.ru](mailto:chuka@jinr.ru)

\*\*\*E-mail: [gooseff@jinr.ru](mailto:gooseff@jinr.ru)

\*\*\*\*E-mail: [vinitsky@theor.jinr.ru](mailto:vinitsky@theor.jinr.ru)



written in spherical coordinates, is considered in Section 2 together with the appropriate classification of states. The reduction of the 2D eigenvalue problem to a 1D eigenvalue problem for a set of closed radial equations via four steps of the Kantorovich method is described briefly in Section 3. All the asymptotic expressions needed to find the solutions and the reaction matrix using the **R**-matrix method, are presented in Section 4. The method is applied to the calculation of ionization from the ground state to the different continuous-spectrum states in Section 5. In the Conclusions, we outline the prospects for further applications of this approach.

## 2. STATEMENT OF THE PROBLEM

The Schrödinger equation for the wave function  $\hat{\Psi}(r, \theta, \varphi) = \Psi(r, \theta) \exp(im\varphi)/\sqrt{2\pi}$  in the spherical coordinates  $(r, \theta, \phi)$  of the hydrogen atom in an axially symmetric magnetic field  $\vec{B} = (0, 0, B)$  can be written as the 2D equation

$$\left( -\frac{1}{r^2} \frac{\partial}{\partial r} r^2 \frac{\partial}{\partial r} - \frac{1}{r^2 \sin \theta} \frac{\partial}{\partial \theta} \sin \theta \frac{\partial}{\partial \theta} + U(r, \theta) \right) \Psi(r, \theta) = \epsilon \Psi(r, \theta), \quad (1)$$

in the region  $\Omega$ :  $0 < r < \infty$  and  $0 < \theta < \pi$ . The potential function  $U(r, \theta)$  is given by

$$U(r, \theta) = -\frac{2Z}{r} + V(r, \theta), \quad (2)$$

$$V(r, \theta) = \frac{m^2}{r^2 \sin^2 \theta} + \gamma m + \frac{\gamma^2 r^2}{4} \sin^2 \theta,$$

where  $m = 0, \pm 1, \dots$  is the magnetic quantum number,  $\gamma = B/B_0$ ,  $B_0 \cong 2.35 \times 10^5$  T is a dimensionless parameter which determines the field strength  $B$ , and the atomic units (a.u.)  $\hbar = m_e = e = 1$  are used under the assumption of infinite mass of the nucleus. In these expressions,  $\epsilon = 2E$  is the doubled energy (in units of rydbergs,  $1\text{Ry} = (1/2)$  a.u.) of the bound state  $|m\sigma\rangle$  at fixed values of  $m$  and  $z$  parity;  $\sigma = \pm 1$ ;  $\Psi \equiv \Psi_{m\sigma}(r, \theta) = (\Psi_m(r, \theta) + \sigma \Psi_m(r, \pi - \theta))/\sqrt{2}$  is the corresponding wave function. Here, the sign of  $z$  parity  $\sigma = (-1)^{N_\theta}$  is defined by the (even or odd) number of nodes  $N_\theta$  in the solution  $\Psi$  with respect to the angular variable  $\theta$  in the interval  $0 < \theta < \pi$ . The wave function satisfies the following boundary conditions in each  $\mathbf{H}_{m\sigma}$  subspace of the full Hilbert space:

$$\lim_{\theta \rightarrow 0} \sin \theta \frac{\partial \Psi(r, \theta)}{\partial \theta} = 0, \quad \text{for } m = 0, \quad (3)$$

$$\text{and } \Psi(r, 0) = 0, \quad \text{for } m \neq 0,$$

$$\frac{\partial \Psi}{\partial \theta} \left( r, \frac{\pi}{2} \right) = 0, \quad \text{for } \sigma = +1, \quad (4)$$

$$\text{and } \Psi \left( r, \frac{\pi}{2} \right) = 0, \quad \text{for } \sigma = -1,$$

$$\lim_{r \rightarrow 0} r^2 \frac{\partial \Psi(r, \theta)}{\partial r} = 0. \quad (5)$$

The discrete-spectrum wave function obeys the asymptotic boundary condition approximated at large  $r = r_{\max}$  by a boundary condition of the first type,

$$\lim_{r \rightarrow \infty} r^2 \Psi(r, \theta) = 0 \rightarrow \Psi(r_{\max}, \theta) = 0. \quad (6)$$

Here, the energy  $\epsilon \equiv \epsilon(r_{\max})$  plays the role of eigenvalues of the boundary problem (1)–(6) determined by a variational principle with an additional normalization condition in a finite interval  $0 \leq r \leq r_{\max}$ ,

$$\mathbf{\Pi}(\Psi, \epsilon) = 0, \quad (7)$$

$$2 \int_0^{r_{\max}} \int_0^{\pi/2} r^2 \sin \theta |\Psi(r, \theta)|^2 d\theta dr = 1,$$

where  $\mathbf{\Pi}(\Psi, \epsilon)$  is a symmetric functional defined by

$$\mathbf{\Pi}(\Psi, \epsilon) = 2 \int_0^{r_{\max}} \int_0^{\pi/2} \sin \theta \left( r^2 \left| \frac{\partial \Psi(r, \theta)}{\partial r} \right|^2 + \left| \frac{\partial \Psi(r, \theta)}{\partial \theta} \right|^2 + r^2 (U(r, \theta) - \epsilon) |\Psi(r, \theta)|^2 \right) d\theta dr.$$

In the Fano–Lee **R**-matrix theory [16, 17], a continuum-spectrum wave function  $\Psi(r, \theta)$  obeys the boundary condition of the third type at fixed values of energy  $\epsilon$  and radial variable  $r = r_{\max}$

$$\frac{\partial \Psi(r, \theta)}{\partial r} - \mu \Psi(r, \theta) = 0. \quad (8)$$

Here, the parameters,  $\mu \equiv \mu(r_{\max}, \epsilon)$ , determined by a variational principle, play the role of eigenvalues of a logarithmic normal derivative matrix of the solution of the boundary problem (1)–(5) and (8)

$$\mathbf{\Pi}(\Psi, \epsilon) = 2\mu r_{\max}^2 \int_0^{\pi/2} \sin \theta |\Psi(r_{\max}, \theta)|^2 d\theta. \quad (9)$$

Standard theorems [18] ensure the existence of a function  $\mu(r_{\max}, \epsilon)$  such that Eq. (8) is satisfied (at any finite  $r = r_{\max} < \infty$ ) [19].

## 3. REDUCTION OF THE 2D PROBLEM BY THE KANTOROVICH METHOD

Consider a formal expansion of the partial wave function  $\Psi_i^{Em\sigma}(r, \theta)$  of (1)–(5) with (6)/(8) corresponding to the eigenstate  $|m\sigma i\rangle$  using the finite set



of one-dimensional basis functions  $\{\Phi_j^{m\sigma}(\theta; r)\}_{j=1}^{j_{\max}}$

$$\Psi_i^{Em\sigma}(r, \theta) = \sum_{j=1}^{j_{\max}} \Phi_j^{m\sigma}(\theta; r) \chi_j^{(m\sigma i)}(E, r). \quad (10)$$

In Eq. (10), the functions  $\chi^{(i)}(r) \equiv \chi^{(m\sigma i)}(E, r)$ ,  $(\chi^{(i)}(r))^T = (\chi_1^{(i)}(r), \dots, \chi_{j_{\max}}^{(i)}(r))$  are unknown, and the surface functions  $\Phi(\theta; r) \equiv \Phi^{m\sigma}(\theta; r)$ ,  $(\Phi(\theta; r))^T = (\Phi_1(\theta; r), \dots, \Phi_{j_{\max}}(\theta; r))$  form an orthonormal basis for each value of the radius  $r$ , which is treated here as a parameter.

In the Kantorovich approach, the wave functions  $\Phi_j(\theta; r)$  and potential curves  $E_j(r)$  are determined as the solutions of the following one-dimensional parametric eigenvalue problem:

$$\left( -\frac{\partial}{\partial \theta} \sin \theta \frac{\partial}{\partial \theta} + r^2 \sin \theta V(r, \theta) \right) \Phi_j(\theta; r) = E_j(r) \sin \theta \Phi_j(\theta; r), \quad (11)$$

with the boundary conditions

$$\lim_{\theta \rightarrow 0} \sin \theta \frac{\partial \Phi_j(\theta; r)}{\partial \theta} = 0, \quad \text{for } m = 0, \quad (12)$$

$$\text{and } \Phi_j(0; r) = 0, \quad \text{for } m \neq 0,$$

$$\frac{\partial \Phi_j}{\partial \theta} \left( \frac{\pi}{2}; r \right) = 0, \quad \text{for } \sigma = +1, \quad (13)$$

$$\text{and } \Phi_j \left( \frac{\pi}{2}; r \right) = 0, \quad \text{for } \sigma = -1.$$

Here, the sign of  $z$  parity,  $\sigma = (-1)^{N_\theta}$ , is defined by the (even or odd) number of nodes  $N_\theta$  in the solution  $\Phi(\theta; r)$  with respect to the angular variable  $\theta$  in the interval  $0 < \theta < \pi$ . Since the operator on the left-hand side of (11) is self-adjoint, its eigenfunctions are orthonormal

$$\begin{aligned} & \left\langle \Phi_i(\theta; r) \left| \Phi_j(\theta; r) \right. \right\rangle_\theta \\ &= 2 \int_0^{\pi/2} \sin \theta \Phi_i(\theta; r) \Phi_j(\theta; r) d\theta = \delta_{ij}, \end{aligned} \quad (14)$$

where  $\delta_{ij}$  is the Kronecker symbol.

Note that the solutions of this problem with shifted eigenvalues,  $\tilde{E}_j(r, \gamma) = E_j(r, \gamma) - \gamma m r^2$ , correspond to the solutions of the eigenvalue problem for oblate angular spheroidal functions [13] with respect to the variable  $\eta = \cos \theta$ :

$$\begin{aligned} & \left( -\frac{\partial}{\partial \eta} (1 - \eta^2) \frac{\partial}{\partial \eta} + \frac{m^2}{1 - \eta^2} \right. \\ & \left. + \left( \frac{\gamma r^2}{2} \right)^2 (1 - \eta^2) \right) \Phi_j(\eta; r) = \tilde{E}_j(r) \Phi_j(\eta; r). \end{aligned} \quad (15)$$

It means that, for small  $r$ , the asymptotics of the eigenvalues  $E_j(r)$ ,  $j = 1, 2, \dots$ , at fixed values  $m$  and  $\sigma$  is defined by the values of the orbital quantum number,  $l = s, p, d, f, \dots$ :  $E_j(0) = l(l+1)$ ,  $l = 0, 1, \dots$ , where  $j$  runs  $j = (l - |m|)/2 + 1$  for even  $z$ -parity states,  $\sigma = +1 = (-1)^{l-|m|}$ , and  $j = (l - |m| + 1)/2$  for odd  $z$ -parity states,  $\sigma = -1 = (-1)^{l-|m|}$ . Taking into account that the number of nodes  $N_\theta$  of the eigenfunction  $\Phi(\theta; r)$  at fixed  $|m|$  and  $\sigma = (-1)^{N_\theta}$  as a function of the parameter  $r$  is preserved, we get a one-to-one correspondence between these sets, i.e.,  $N_\theta = l - |m|$ .

For large  $r$ , the asymptotics of eigenvalues  $E_j(r)$ ,  $j = 1, 2, \dots$ , at fixed values of  $m$  and  $\sigma$  is defined by the values of the transversal quantum number,  $N_\rho$ :

$$\begin{aligned} \lim_{r \rightarrow \infty} r^{-2} E_j(r, \gamma) &= \epsilon_{m\sigma j}^{\text{th}}(\gamma) \\ &= \gamma(2N_\rho + |m| + m + 1), \end{aligned} \quad (16)$$

where  $N_\rho = 0, 1, \dots$ , and  $j$  runs  $j = N_\rho + 1$ . The values of the transversal quantum number  $N_\rho$ , i.e., the number of nodes of the eigenfunction  $\Phi(\theta; r)$  in the subinterval  $0 < \eta < 1$  or  $-1 < \eta < 0$ , corresponding to the transversal variable  $\rho = r \sin \theta$  on a semiaxis, are expressed via the number of nodes  $N_\theta$  of the solution  $\Phi(\theta; r)$ :  $N_\rho = 1/2 \cdot N_\theta$  for the even  $z$ -parity states,  $\sigma = +1 = (-1)^{N_\theta}$ , and  $N_\rho = 1/2 \cdot (N_\theta - 1)$  for the odd  $z$ -parity states,  $\sigma = -1 = (-1)^{N_\theta}$ .

Such a transversal classification also reveals a violation of degeneracy of the states with azimuthal quantum numbers,  $\pm m$ , having the same module  $|m|$  that holds for the angular oblate spheroidal functions, i.e.,

$$\lim_{r \rightarrow \infty} r^{-2} \tilde{E}_j(r, \gamma) = \gamma(2N_\rho + |m| + 1). \quad (17)$$

Taking into account the above-mentioned correspondence rules between the quantum numbers  $l - |m|$ ,  $N_\theta$ ,  $N_\rho$  and the number  $j$  at fixed values of  $m$  and  $\sigma$ , we use the *unified number*  $j$  without pointing out explicitly a concrete type of quantum numbers. These rules are similar to the conventional correlation diagrams for potential curves of a hydrogen atom in a uniform magnetic field or a helium atom.

After substituting the expansion (10) into the variational problem (7)/(9) and using Eqs. (11)–(14), the solution of the above problem is transformed into the solution of an eigenvalue problem for a system of  $j_{\max}$  ordinary second-order differential equations for determining the energy  $\epsilon$  and the coefficients (radial wave functions)  $\chi^{(i)}(r)$  of expansion (10),

$$\left( -\mathbf{I} \frac{1}{r^2} \frac{d}{dr} r^2 \frac{d}{dr} + \frac{\mathbf{U}(r)}{r^2} + \mathbf{Q}(r) \frac{d}{dr} \right) \quad (18)$$

$$+ \frac{1}{r^2} \frac{dr^2 \mathbf{Q}(r)}{dr} \Big) \chi^{(i)}(r) = \epsilon_i \mathbf{I} \chi^{(i)}(r),$$

$$\lim_{r \rightarrow 0} r^2 \left( \frac{\partial \chi^{(i)}(r)}{\partial r} - \mathbf{Q}(r) \chi^{(i)}(r) \right) = 0.$$

Here,  $\mathbf{I}$ ,  $\mathbf{U}(r)$ , and  $\mathbf{Q}(r)$  are matrices of dimension  $j_{\max} \times j_{\max}$  whose elements are given by the relations

$$U_{ij}(r) = \frac{E_i(r) + E_j(r)}{2} \delta_{ij} + 2Zr \delta_{ij} \quad (19)$$

$$+ r^2 H_{ij}(r), \quad I_{ij} = \delta_{ij},$$

$$H_{ij}(r) = 2 \int_0^{\pi/2} \sin \theta \frac{\partial \Phi_i(\theta; r)}{\partial r} \frac{\partial \Phi_j(\theta; r)}{\partial r} d\theta,$$

$$Q_{ij}(r) = -2 \int_0^{\pi/2} \sin \theta \Phi_i(\theta; r) \frac{\partial \Phi_j(\theta; r)}{\partial r} d\theta.$$

The above matrix elements were calculated by means of the authors' combined symbolic–numerical code MATRM implemented in both MAPLE 8 and FORTRAN [20].

The discrete spectrum solutions obey the asymptotic boundary condition and orthonormal conditions

$$\lim_{r \rightarrow \infty} r^2 \chi^{(i)}(r) = 0 \quad \rightarrow \quad \chi^{(i)}(r_{\max}) = 0, \quad (20)$$

$$\int_0^{r_{\max}} r^2 (\chi^{(i)}(r))^T \chi^{(j)}(r) dr = \delta_{ij}.$$

For the continuum-spectrum solution  $\chi^{(i)}(r)$ , we can alternatively require that projections of (8) onto all adiabatic functions hold,

$$\left\langle \Phi_j(\theta; r) \left| \frac{\partial \Psi_i^{Em\sigma}(r, \theta)}{\partial r} - \mu_i \Psi_i^{Em\sigma}(r, \theta) \right. \right\rangle_{\theta} = 0, \quad (21)$$

$$r = r_{\max},$$

which leads to the third-type boundary conditions at fixed values of energy  $\epsilon > \epsilon_{m\sigma 1}^{\text{th}}(\gamma)$  and radial variable  $r = r_{\max}$

$$\left( \mathbf{R} - \mathbf{Q}(r) - \mu_i \right) \chi^{(i)}(r) \quad (22)$$

$$= \left( \frac{\partial \chi^{(i)}(r)}{\partial r} (\chi^{(i)})^{-1}(r) - \mathbf{Q}(r) - \mu_i \right) \chi^{(i)}(r) = 0.$$

From here,  $\mu_i$  and  $\chi^{(i)}(r_{\max})$  should be a set of eigenvalues  $\mathbf{\Lambda} = \{\delta_{ij} \mu_i\}_{i,j=1}^{N_o}$  corresponding to a set

of eigenvectors  $\chi(r) \equiv \{\chi^{(i)}(r)\}_{i=1}^{N_o}$  of the following eigenvalue problem at  $r = r_{\max}$

$$\frac{d\chi(r)}{dr} - \mathbf{Q}(r) \chi(r) = \chi(r) \mathbf{\Lambda}, \quad (23)$$

which is reformulated by averaging variational problem (9) to the following one:

$$\mathbf{\Pi}(\chi, \epsilon) - r_{\max}^2 \chi^T(r_{\max}) \chi(r_{\max}) \mathbf{\Lambda} = 0. \quad (24)$$

Here  $N_o$  is the number of the open channels (i.e., the energy  $\epsilon$  should belong to the interval  $\epsilon_{m\sigma N_o}^{\text{th}}(\gamma) < \epsilon < \epsilon_{m\sigma N_o+1}^{\text{th}}(\gamma)$ ), and  $j_{\max} > N_o$ .

After discretization, Eq. (24) becomes the following algebraic eigenvalue problem

$$\mathbf{\Pi} \tilde{\chi} = r_{\max}^2 \tilde{\chi}(r_{\max}) \tilde{\mathbf{\Lambda}}, \quad (25)$$

$$r_{\max}^2 \tilde{\chi}^T(r_{\max}) \tilde{\chi}(r_{\max}) = \mathbf{I}.$$

The nonsymmetric  $\mathbf{R}$  matrix obtained by the total set of eigenvalues  $\tilde{\mathbf{\Lambda}} = \{\delta_{ij} \tilde{\mu}_i\}_{i,j=1}^{j_{\max}}$  and eigenvectors  $\tilde{\chi} \equiv \{\tilde{\chi}^{(i)}\}_{i=1}^{j_{\max}}$  of the eigenvalue problem (25) reads

$$\mathbf{R} = r_{\max}^2 \tilde{\chi}(r_{\max}) \tilde{\mathbf{\Lambda}} \tilde{\chi}^T(r_{\max}) + \mathbf{Q}(r_{\max}) \quad (26)$$

and gives the relation between  $\chi(r)$  and its derivative at  $r = r_{\max}$

$$\frac{d\chi(r)}{dr} = \mathbf{R} \chi(r). \quad (27)$$

Note that, in the diagonal approximation  $i = j$  of the problem (18)–(20), the so-called adiabatic approximation, the number of nodes  $N_r$  of the solution  $\chi(r)$  with respect to the slow radial variable  $r$  on a semiaxis for small values of the parameter  $\gamma$  corresponds to the radial quantum number  $N_r = N - l - 1$  of a free hydrogen atom in the bound state characterized by a conventional set of quantum numbers  $(N, l, m, \lambda = (-1)^l)$  and the binding energy  $-\epsilon_j(\gamma = 0) = -\epsilon_j^{(0)} = Z/N^2$  (in Ry).

Recalling that the number of nodes  $N_{\theta}$  of the solution  $\Phi(\theta; r)$  with respect to the fast angular variable,  $\theta$ , at fixed  $|m|$  and  $\sigma = (-1)^{N_{\theta}}$  as a function of the slow parameter,  $r$ , is conserved, i.e.,  $N_{\theta} = l - |m|$ , we have a one-to-one correspondence between the quantum numbers  $(N, l)$  of the free atom at  $\gamma = 0$  and the adiabatic ones  $\{N_r, N_{\theta}\}$  of the perturbed atom at  $\gamma \neq 0$ .

For large values of the parameter  $\gamma$ , the adiabatic radial number  $N_r$  corresponds to the longitudinal quantum number  $N_{|z|}$  of a hydrogen atom in the strong magnetic field at fixed  $m$  and the sign of  $\sigma = \pm 1$ , i.e., the number of nodes of the solution  $\chi(|z|)$  with respect to the longitudinal variable  $z = r \cos \theta$  on a semiaxis. It means that the solution  $\chi(z)$  on

an axis is defined as follows:  $\chi_{m\sigma}(z) = (\chi_m(\rho, z) + \sigma\chi_m(\rho, -z))/\sqrt{2}$  or reduced to the solution  $\chi(|z|)$  of a conventional eigenvalue problem on a semiaxis, using the Neumann and Dirichlet boundary conditions at  $z = 0$  for the even  $\sigma = +1$  and odd  $\sigma = -1$  solutions, respectively.

Taking into account the above correspondence rules with such an adiabatic set  $[N_{|z|}N_\rho]$  and the asymptotic form of eigenvalues  $E_j(r)$  at large  $r$ , we can express the binding energy  $\mathcal{E}$  via the eigenvalues  $\epsilon$  of the problem (18)–(20) as follows:  $\mathcal{E} = (\epsilon_{m\sigma j}^{\text{th}}(\gamma) - \epsilon)/2$  (in a.u.), where  $\epsilon_{m\sigma j}^{\text{th}}(\gamma)$  is the true threshold shift (16) or the reduced one  $\epsilon_{m\sigma}^{\text{th}}(\gamma) = \gamma(|m| + m + 1)$ , respectively.

#### 4. ASYMPTOTIC FORM OF SOLUTION

We write system of differential equations (18) at fixed values  $m$ ,  $\sigma$  and energy  $\epsilon = 2E$  in the explicit form for  $\chi_{ji_o}(r) \equiv \chi_j^{(i_o)}(r)$ ,  $j = 1, \dots, j_{\text{max}}$ ,  $i_o = 1, \dots, N_o$ ,

$$\left( -\frac{1}{r^2} \frac{d}{dr} r^2 \frac{d}{dr} - \frac{2Z}{r} - \epsilon + \frac{E_j(r)}{r^2} + H_{jj}(r) \right) \chi_{ji_o}(r) = \sum_{j'=1, j' \neq j}^{j_{\text{max}}} \left( -H_{jj'}(r) - Q_{jj'}(r) \frac{d}{dr} - \frac{1}{r^2} \frac{dr^2 Q_{jj'}(r)}{dr} \right) \chi_{j'i_o}(r). \quad (28)$$

At large  $r$ , the asymptotic form of matrix elements expanded in inverse powers of  $r$  (i.e., without exponential terms) has the form (for details, see [20])

$$r^{-2} E_j(r) = E_j^{(0)} + \sum_{k=1} r^{-2k} E_j^{(2k)}, \quad (29)$$

$$H_{jj'}(r) = \sum_{k=1} r^{-2k} H_{jj'}^{(2k)},$$

$$Q_{jj'}(r) = \sum_{k=1} r^{-2k+1} Q_{jj'}^{(2k-1)},$$

$$r \gg \max(n_l, n_r)/(2\sqrt{\gamma}).$$

Here,

$$E_j^{(0)} = \gamma(2n + |m| + m + 1), \quad (30)$$

$$E_j^{(2)} = -2n^2 - 2n - 1 - 2|m|n - |m|,$$

$$H_{jj'}^{(2)} = (2n^2 + 2n + 2|m|n + |m| + 1)\delta_{|n_l - n_r|, 0}$$

$$- \sqrt{n+1}\sqrt{n+|m|+1}\sqrt{n+2} \times \sqrt{n+|m|+2}\delta_{|n_l - n_r|, 2},$$

$$Q_{jj'}^{(1)} = (n_r - n_l)\sqrt{n+1}\sqrt{n+|m|+1}\delta_{|n_l - n_r|, 1}.$$

In these formulas, the asymptotic quantum numbers  $n_l$ ,  $n_r$  denote transversal quantum numbers  $N_\rho$  and  $N'_\rho$ , related to the unified numbers  $j$ ,  $j'$  by the above-mentioned formulas  $n_l = j - 1$ ,  $n_r = j' - 1$ , and  $n = \min(n_l, n_r)$ .

Note that  $E_j^{(2)} + H_{jj}^{(2)} = 0$ ; i.e., at large  $r$ , centrifugal terms are eliminated in Eq. (28). It means that the leading terms of radial solutions,  $\chi_{ji_o}(r)$ , have the asymptotic form of Coulomb functions with zero angular momentum.

Let us consider the asymptotic solution following [21]

$$\chi_{ji_o}(r) = R(p_{i_o}, r)\phi_{ji_o}(r) + \frac{dR(p_{i_o}, r)}{dr}\psi_{ji_o}(r), \quad (31)$$

where  $R(p_{i_o}, r) = iF(p_{i_o}, r) + G(p_{i_o}, r)$ ,  $[F(p_{i_o}, r)$  and  $G(p_{i_o}, r)$  are the Coulomb regular and irregular functions] and satisfies the differential equation

$$\frac{d^2 R(p_{i_o}, r)}{dr^2} + \frac{2}{r} \frac{dR(p_{i_o}, r)}{dr} + \left( p_{i_o}^2 + \frac{2Z}{r} \right) R(p_{i_o}, r) = 0. \quad (32)$$

Then we can expand the functions  $\phi_{ji_o}(r)$  and  $\psi_{ji_o}(r)$  in series in inverse powers of  $r$

$$\phi_{ji_o}(r) = \sum_{k=0}^{k_{\text{max}}} \phi_{ji_o}^{(k)} r^{-k}, \quad \psi_{ji_o}(r) = \sum_{k=0}^{k_{\text{max}}} \psi_{ji_o}^{(k)} r^{-k}. \quad (33)$$

As a result of substitution of expansions (33) into (31) and (28), using (32), and equating coefficients of expansion for the same powers of  $r$ , we arrive at the set of recurrence relations with respect to unknown coefficients  $\phi_{ji_o}^{(k)}$  and  $\psi_{ji_o}^{(k)}$ :

$$(p_{i_o}^2 - 2E + E_j^{(0)})\phi_{ji_o}^{(k)} - 2p_{i_o}^2(k-1)\psi_{ji_o}^{(k-1)} \quad (34)$$

$$- (k-2)(k-3)\phi_{ji_o}^{(k-2)} - 2Z(2k-3)\psi_{ji_o}^{(k-2)}$$

$$+ \sum_{k'=1}^k (E_j^{(k')} + H_{jj}^{(k')})\phi_{ji_o}^{(k-k')}$$

$$\begin{aligned}
 &= \sum_{j'=1, j' \neq j}^{j_{\max}} \sum_{k'=1}^k \left[ ((2k - k' - 3)Q_{jj'}^{(k'-1)} \right. \\
 &\quad \left. - H_{jj'}^{(k')} \phi_{j' i_o}^{(k-k')} + (2p_{i_o}^2 Q_{jj'}^{(k')} + 4ZQ_{jj'}^{(k'-1)}) \psi_{j' i_o}^{(k-k')} \right], \\
 &\quad (p_{i_o}^2 - 2E + E_j^{(0)}) \psi_{j i_o}^{(k)} + 2(k-1) \phi_{j i_o}^{(k-1)} \quad (35) \\
 &\quad - k(k-1) \psi_{j i_o}^{(k-2)} + \sum_{k'=1}^k (E_j^{(k')} + H_{jj}^{(k')}) \psi_{j i_o}^{(k-k')} \\
 &= \sum_{j'=1, j' \neq j}^{j_{\max}} \sum_{k'=1}^k \left[ ((2k - k' + 1)Q_{jj'}^{(k'-1)} \right. \\
 &\quad \left. - H_{jj'}^{(k')} \psi_{j' i_o}^{(k-k')} - 2Q_{jj'}^{(k')} \phi_{j' i_o}^{(k-k')} \right].
 \end{aligned}$$

From the first four equations of the set in (34) and (35) for  $\phi_{i_o i_o}^{(0)}$ ,  $\phi_{j_0 i_o}^{(0)}$ ,  $\psi_{i_o i_o}^{(0)}$ , and  $\psi_{j_0 i_o}^{(0)}$ , we get the leading terms of the eigenfunction, the eigenvalue, and the characteristic parameter, i.e., initial data for solving the recurrent sequence (34) and (35),

$$\phi_{j_0 i_o}^{(0)} = \delta_{j_0 i_o}, \quad \psi_{j_0 i_o}^{(0)} = 0, \quad p_{i_o}^2 = 2E - E_{i_o}^{(0)}, \quad (36)$$

which corresponds to the leading term of  $\chi_{j i_o}(r)$  satisfying the asymptotic expansion series (33) at large  $r$ . Substituting these initial data to the next equations of the set in (34) and (35), we get a step-by-step procedure for determining the series coefficients  $\phi_{j i_o}^{(k)}$  and  $\psi_{j i_o}^{(k)}$ . Using the explicit asymptotic matrix elements (29), we get an explicit expression of these coefficients  $\phi_{j i_o}^{(k)}$  and  $\psi_{j i_o}^{(k)}$  via the values of the number of a state (or channel)  $i_o = n_o + 1$  and the number of current equation  $j = 1, \dots, j_{\max}$ . For example, at  $k = 0, 1$ , such elements take the form

$$\begin{aligned}
 \phi_{i_o i_o}^{(0)} &= 1, \quad \psi_{i_o i_o}^{(0)} = 0, \\
 \phi_{i_o-1 i_o}^{(1)} &= 0, \quad \psi_{i_o-1 i_o}^{(1)} = \frac{\sqrt{n_o} \sqrt{n_o + |m|}}{\gamma}, \\
 \phi_{i_o i_o}^{(1)} &= 0, \quad \psi_{i_o i_o}^{(1)} = -\frac{2n_o + |m| + 1}{\gamma}, \\
 \phi_{i_o+1 i_o}^{(1)} &= 0, \quad \psi_{i_o+1 i_o}^{(1)} = \frac{\sqrt{n_o+1} \sqrt{n_o + |m| + 1}}{\gamma}.
 \end{aligned}$$

Taking into account the region of convergence of the matrix elements, we find that the region of convergence of expansion (31), as follows from asymptotic form of matrix elements which do not depend on

$$p_{i_o}, \text{ is } r_{\max} \gg n_{i_o}/(2\sqrt{\gamma}) \text{ and } r_{\max} \gg Z(2n_{i_o} + |m| + 1)/(p_{i_o}\sqrt{\gamma}).$$

## 5. THE SCATTERING STATES AND PHOTOIONIZATION CROSS SECTIONS

The solution of the scattering problem,

$$\begin{aligned}
 \chi^{(p)}(r) &= i\chi^{(ph)}(r)(\mathbf{I} - i\mathbf{K}) \quad (37) \\
 &= \chi^s(r) + \chi^c(r)\mathbf{K},
 \end{aligned}$$

with  $N_o$  open channels for  $p_{i_o}^2 \geq 0$  at  $i_o = 1, \dots, N_o$ , is defined by means of the two independent fundamental asymptotic solutions  $\chi^s(r) = 2\Im(\chi(r))$  and  $\chi^c(r) = 2\Re(\chi(r))$  (corresponding to “regular” and “irregular” type) of Eqs. (28) and a reaction matrix  $\mathbf{K} = i(\mathbf{I} + \mathbf{S})^{-1}(\mathbf{I} - \mathbf{S})$ , where  $\mathbf{S} = (\mathbf{I} + i\mathbf{K})(\mathbf{I} - i\mathbf{K})^{-1}$  is the scattering matrix.

In this case, the regular and irregular functions satisfy the generalized Wronskian relation at large  $r$

$$\mathbf{Wr}(\mathbf{Q}(r); \chi^c(r), \chi^s(r)) = \frac{2}{\pi} \mathbf{I}_{oo}, \quad (38)$$

where  $\mathbf{Wr}(\bullet; \chi^c(r), \chi^s(r))$  is a generalized Wronskian with a long derivative defined by

$$\begin{aligned}
 \mathbf{Wr}(\bullet; \chi^c(r), \chi^s(r)) \quad (39) \\
 = r^2 \left[ (\chi^c(r))^T \left( \frac{d\chi^s(r)}{dr} - \bullet \chi^s(r) \right) \right. \\
 \left. - \left( \frac{d\chi^c(r)}{dr} - \bullet \chi^c(r) \right)^T \chi^s(r) \right],
 \end{aligned}$$

which will be used to control a desirable accuracy of the above expansion. Here,  $\mathbf{I}_{oo}$  is the unit matrix of dimension  $N_o \times N_o$ .

Using Eq. (27), we obtain the equation for the reaction matrix  $\mathbf{K}$  via  $\mathbf{R}$  matrix at  $r = r_{\max}$

$$\left( \mathbf{R}\chi^c(r) - \frac{d\chi^c(r)}{dr} \right) \mathbf{K} = \left( \frac{d\chi^s(r)}{dr} - \mathbf{R}\chi^s(r) \right), \quad (40)$$

and Eq. (38) is equivalent to

$$\begin{aligned}
 \mathbf{Wr}(\mathbf{Q}(r_{\max}); \chi^s(r_{\max}), \chi^c(r_{\max})) \quad (41) \\
 = \mathbf{Wr}(\mathbf{R}; \chi^s(r_{\max}), \chi^c(r_{\max})).
 \end{aligned}$$

Note that, when some channels are closed, the left and right matrices of (40) are rectangular matrices. Therefore, multiplying (40) on the left by the matrix  $(\chi^c(\rho))^T$ , we obtain the following formula for the reaction matrix  $\mathbf{K}$ :

$$\mathbf{K} = -\mathbf{X}^{-1}(r_{\max})\mathbf{Y}(r_{\max}), \quad (42)$$

where

$$\mathbf{X}(r) = (\chi^c(r))^T \left( \frac{d\chi^c(r)}{dr} - \mathbf{R}\chi^c(r) \right),$$

$$\mathbf{Y}(r) = (\chi^s(r))^T \left( \frac{d\chi^s(r)}{dr} - \mathbf{R}\chi^s(r) \right)$$

are square matrices of dimension  $N_o \times N_o$  and  $\mathbf{X}(r_{\max})$  should be a symmetric matrix, which follows from the condition  $\mathbf{W}\mathbf{r}(\mathbf{R}; \chi^c(r_{\max}), \chi^s(r_{\max})) = 0$ .

Let the matrices  $\mathbf{S}$  and  $\mathbf{K}$  have eigenvalues  $\exp(2i\delta_i)$  and  $\tan \delta_i$ , respectively. Then

$$\mathbf{S}\mathbf{B} = \mathbf{B}\exp(2i\delta), \quad \mathbf{K}\mathbf{B} = \mathbf{B}\tan \delta, \quad (43)$$

where  $\exp(2i\delta)$  and  $\tan \delta$  are diagonal matrices and  $\mathbf{B}$  can be taken to be real and normalized to

$$\mathbf{B}^T \mathbf{B} = \mathbf{I}_{oo}. \quad (44)$$

We denote the eigenstate wave function of continuum  $\Psi_i^{Em\sigma}(r, \theta)$  with energy  $2E$  (of ejected electron) above the first threshold  $\epsilon_{m\sigma 1}^{\text{th}}(\gamma) = \epsilon_{m\sigma}^{\text{th}}(\gamma) = \gamma(|m| + m + 1)$  by the following:

$$\Psi_i^{Em\sigma}(r, \theta) = \sum_{j=1}^{j_{\max}} \Phi_j^{m\sigma}(\theta; r) \hat{\chi}_{ji}^{(m\sigma)}(E, r), \quad (45)$$

where

$$\hat{\chi}^{(m\sigma)}(E, r) = \chi^{(ph)}(r) \mathbf{B} \quad (46)$$

$$\text{or } \hat{\chi}^{(m\sigma)}(E, r) = \chi^{(p)}(r) \mathbf{B} \cos \delta.$$

In this case, the eigenstate wave function  $\Psi_i^{Em\sigma}(r, \theta)$  is normalized to

$$\begin{aligned} & \left\langle \Psi_i^{Em\sigma}(r, \theta) \left| \Psi_{i'}^{E'm'\sigma'}(r, \theta) \right. \right\rangle \quad (47) \\ &= \sum_{j=1}^{j_{\max}} \int_0^{r_{\max}} r^2 dr \left( \hat{\chi}_{ji}^{(m\sigma)}(E, r) \right)^* \hat{\chi}_{ji'}^{(m'\sigma')}(E', r) \\ &= \delta(E - E') \delta_{mm'} \delta_{\sigma\sigma'} \delta_{ii'}. \end{aligned}$$

In terms of the above definitions, the photoionization cross sections  $\sigma^d(\omega)$  and  $\sigma^p(\omega)$  (for light polarized along the  $z$  axis and in the  $XOY$  plane, respectively) are expressed as

$$\begin{aligned} \sigma^d(\omega) &= 4\pi^2 \alpha \omega \sum_{i=1}^{N_o} \left| \hat{D}_{i, N_{|z|}, N_\rho}^{m'\sigma}(E) \right|^2 a_0^2, \quad (48) \\ \sigma^p(\omega) &= 4\pi^2 \alpha \omega \sum_{i=1}^{N_o} \left| \hat{P}_{i, N_{|z|}, N_\rho}^{m'\sigma}(E) \right|^2 a_0^2, \end{aligned}$$

where  $\hat{D}_{i, N_{|z|}, N_\rho}^{m'\sigma}(E)$  and  $\hat{P}_{i, N_{|z|}, N_\rho}^{m'\sigma}(E)$  are the matrix elements of the longitudinal and transverse moments, respectively,

$$\hat{D}_{i, N_{|z|}, N_\rho}^{m'\sigma}(E) \quad (49)$$

$$= \delta_{|m-m'|0} \left\langle \Psi_i^{Em'-\sigma}(r, \theta) \left| r \cos \theta \right| \Psi_{N_{|z|}, N_\rho}^{m\sigma}(r, \theta) \right\rangle$$

$$= \sum_{j=1}^N \sum_{j'=1}^N \int_0^{r_{\max}} r^2 dr \left( \hat{\chi}_{ji}^{(m'-\sigma)}(E, r) \right)^* \times D_{jj'}^{(m'm\sigma)}(r) \chi_{j'}^{(m\sigma)}(r),$$

$$\hat{P}_{i, N_{|z|}, N_\rho}^{m'\sigma}(E) \quad (50)$$

$$= \delta_{|m-m'|1} \left\langle \Psi_i^{Em'\sigma}(r, \theta) \left| \frac{r \sin \theta}{\sqrt{2}} \right| \Psi_{N_{|z|}, N_\rho}^{m\sigma}(r, \theta) \right\rangle$$

$$= \sum_{j=1}^N \sum_{j'=1}^N \int_0^{r_{\max}} r^2 dr \left( \hat{\chi}_{ji}^{(m'\sigma)}(E, r) \right)^* \times P_{jj'}^{(m'm\sigma)}(r) \chi_{j'}^{(m\sigma)}(r).$$

The longitudinal  $D^{(m\sigma)}(r)$  and transversal  $P^{(mm'\sigma)}(r)$  matrix elements are expressed as

$$\begin{aligned} & D_{jj'}^{(m'm\sigma)}(r) \\ &= \delta_{|m-m'|0} \left\langle \Phi_j^{m'-\sigma}(\theta; r) \left| r \cos \theta \right| \Phi_{j'}^{m\sigma}(\theta; r) \right\rangle_\theta, \\ & P_{jj'}^{(m'm\sigma)}(r) \\ &= \delta_{|m-m'|1} \left\langle \Phi_j^{m'\sigma}(\theta; r) \left| \frac{r \sin \theta}{\sqrt{2}} \right| \Phi_{j'}^{m\sigma}(\theta; r) \right\rangle_\theta. \end{aligned}$$

In the above expressions,  $\omega = E - E(N_{|z|}, N_\rho, \sigma, m)$  is the frequency of radiation,  $E(N_{|z|}, N_\rho, \sigma, m)$  is the energy of the initial bound state  $\Psi_{N_{|z|}, N_\rho}^{m\sigma}(r, \eta)$ ,  $E$  is the energy of the final continuum state  $\Psi_i^{Em\sigma}(r, \eta)$  such that  $N_o$  is the number of the open channels,  $\alpha$  is the fine-structure constant,  $a_0$  is the Bohr radius.

In our calculations, we used the following physical constants: inverse centimeter–Hartree relationship  $\text{cm}^{-1} = 4.55633 \times 10^{-6}$  a.u., Bohr radius  $a_0 = 5.29177 \times 10^{-11}$  m, and fine-structure constant  $\alpha = 7.29735 \times 10^{-3}$  [22]. Figure 1 displays the calculated photoionization cross sections  $\sigma^d(\omega)$  and  $\sigma^p(\omega)$  from

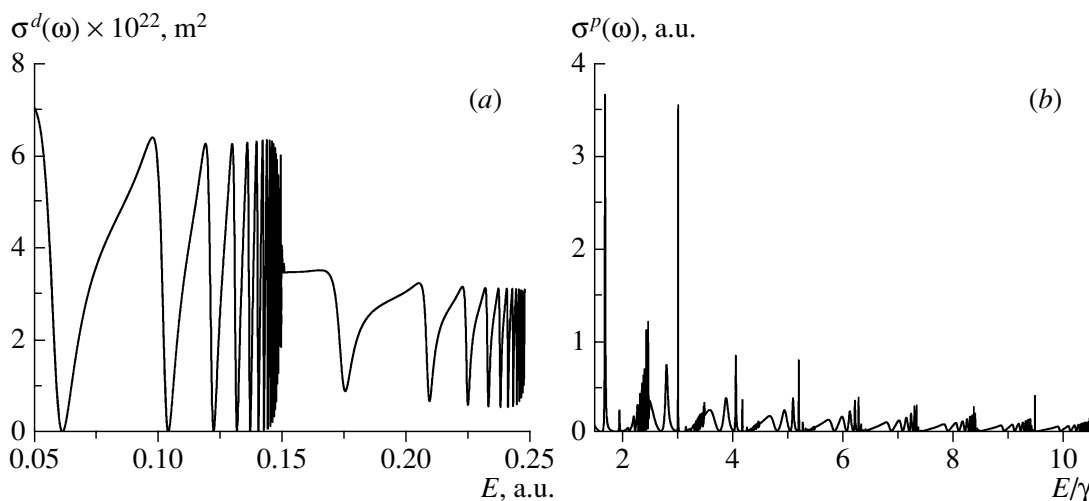


**Fig. 1.** Photoionization cross sections  $\sigma^d(\omega)$  (a) and  $\sigma^p(\omega)$  (b) from the ground state with  $\gamma = 0.1$  to the final state with  $\sigma = -1$  and  $m = 0$  at  $\gamma = 0.05$  to the final state with  $\sigma = +1$  and  $m = 1$ , respectively.

the ground state to the different continuous spectrum states. In Fig. 1a, we use the energy interval from  $E = 0.05$  to  $0.25$  a.u. for the final state with  $\sigma = -1$  and  $m = 0$ . The number of open channels is equal to 1 to 2. In Fig. 1b, we used the energy interval from  $E = 0.075$  to  $0.525$  a.u. for the final state with  $\sigma = +1$  and  $m = 1$ . The final-state energy  $E$  is measured relative to the zero-field ionization threshold. The number of open channels varies from 1 to 9. The calculated photoionization cross section is in good agreement with [12] between the thresholds, but not near them. Here, we show one of the goals of the elaborated approach to provide stable and economical calculations of the photoionization cross section having the true threshold behavior coinciding with [15].

## 6. CONCLUSIONS

A new efficient method for calculating wave functions of a hydrogen atom in a strong magnetic field is developed on the basis of the Kantorovich approach to parametric eigenvalue problems in spherical coordinates. The two-dimensional spectral problem for the Schrödinger equation at a fixed magnetic quantum number and parity is reduced to a spectral parametric problem for a one-dimensional equation by the angular variable and a finite set of ordinary second-order differential equations by the radial variable. The results are in good agreement with calculations by other authors. The developed approach is a good tool for calculating threshold phenomena in formation and ionization of (anti)hydrogen-like atoms and ions in magnetic traps. In the future, we will also calculate a manifold of the excited states in a layer with the principle quantum number  $N = 3$  of a hydrogen atom in

the magnetic field  $2.35 \times 10^4$  T and 6.1 T that may be interesting from our viewpoint for a laser-stimulated recombination in actually existing traps [23].

## ACKNOWLEDGMENTS

This work was partly supported by grants of the Russian Foundation for Basic Research (nos. 07-01-00660 and 08-01-00604-a), by CRDF BRHE grant REC-006 SR-006-X1/B75M06 Y3-P-06-08, by a grant of the President of the Bulgarian State Agency for Atomic Energy (2004), by grant no. I-1402/2004 of the Bulgarian Fund for Scientific Investigations, and by grant NFSAT-CRDF ARP1-3228-YE-04.

## REFERENCES

1. A. Rotondi, M. Amoretti, C. Amsler, et al., AIP Conf. Proc. **796**, 285 (2005).
2. N. Madsen, M. Amoretti, C. Amsler, et al., Phys. Rev. Lett. **94**, 033403 (2005).
3. W. Bertsche, A. Boston, P. D. Bowe, et al., AIP Conf. Proc. **796**, 301 (2005).
4. V. V. Serov, V. P. Kadjaeva, V. L. Derbov, and S. I. Vinitzky, Proc. SPIE **5773**, 195 (2005).
5. V. V. Serov, V. L. Derbov, and S. I. Vinitzky, Opt. Spectrosc. **102**, 557 (2007).
6. M. G. Dimova, M. S. Kaschiev, and S. I. Vinitzky, J. Phys. B **38**, 2337 (2005).
7. O. Chuluunbaatar et al., J. Phys. B **39**, 243 (2006).
8. J. R. Guest, J.-H. Choi, and G. Raithel, Phys. Rev. A **68**, 022509 (2003).
9. J. R. Guest and G. Raithel, Phys. Rev. A **68**, 052502 (2003).
10. J.-H. Choi, J. R. Guest, A. P. Povilus, et al., Phys. Rev. Lett. **95**, 243001 (2005).

11. C. C. Gerry and J. Laub, Phys. Rev. A **32**, 3376 (1985).
12. D. Delande, A. Bommier, and J. C. Gay, Phys. Rev. Lett. **66**, 141 (1991).
13. M. Abramowitz and I. A. Stegun, *Handbook of Mathematical Functions* (Dover, New York, 1972), p. 1037.
14. C. H. Greene, Phys. Rev. A **28**, 2209 (1983).
15. Q. Wang and C. H. Greene, Phys. Rev. A **44**, 7448 (1991).
16. U. Fano and C. M. Lee, Phys. Rev. Lett. **31**, 1573 (1973).
17. C. M. Lee, Phys. Rev. A **10**, 584 (1974).
18. R. Courant and D. Hilbert, *Methods of Mathematical Physics* (Springer, New York 1968), Vol. 1, p. 353.
19. J. Macek, Phys. Rev. A **30**, 1277 (1984).
20. S. I. Vinitisky et al., Program. Comput. Software **33**, 105 (2007).
21. M. Gailitis, J. Phys. B **9**, 843 (1976).
22. <http://physics.nist.gov/cuu/Constants/index.html>.
23. M. V. Ryabinina and L. A. Melnikov, AIP Conf. Proc. **796**, 325 (2005); Nucl. Instrum. Methods Phys. Res. B **214**, 35 (2004).





---

## ELEMENTARY PARTICLES AND FIELDS

### Theory

---

# Analytical and Numerical Calculations of Spectral and Optical Characteristics of Spheroidal Quantum Dots\*

A. A. Gusev<sup>1)\*\*</sup>, L. L. Hai<sup>1)</sup>, S. I. Vinitsky<sup>1)</sup>, O. Chuluunbaatar<sup>1)</sup>,  
V. L. Derbov<sup>2)</sup>, A. S. Klombotskaya<sup>2)</sup>, K. G. Dvyan<sup>3)</sup>, and H. A. Sarkisyan<sup>3)</sup>

Received July 17, 2012

**Abstract**—In the effective mass approximation for electronic (hole) states of a spheroidal quantum dot with and without external fields the perturbation theory schemes are constructed in the framework of the Kantorovich and adiabatic methods. The eigenvalues and eigenfunctions of the problem, obtained in both analytical and numerical forms, were applied for the analysis of spectral and optical characteristics of spheroidal quantum dots in homogeneous electric fields.

**DOI:** 10.1134/S1063778813080152

## 1. INTRODUCTION

Quantum dots (QDs) are considered to be promising as the elementary basis for the new generation of semiconductor devices [1, 2]. The unique opportunity to perform the energy level control and flexible manipulation in QDs is due to the full quantization of charge carrier energy spectra in these systems. This allows design and manufacturing of artificial structures with prescribed quantum physical characteristics [3]. That is why the scope of QDs potential applications is very wide, from heterostructure lasers to nanomedicine and nanobiology. An impressive example of such application is represented by QD lasers possessing low threshold current and high efficiency [3].

The peculiarities of physical processes in QDs are caused by both their composition and geometry. Electronic, kinetic, optical, and other properties of QDs have been investigated experimentally and theoretically in many papers [4–13]. Particularly, the optical absorption characteristics of QDs have been shown to be strongly correlated with their geometry, on the one hand, and with their physical–chemical properties, on the other hand. In one of the first publications on optical transitions in QD [14] the interband absorption of light was considered in the ensemble of weakly interacting spherical QDs implanted in a dielectric matrix. The dispersion of QD sizes was characterized in the framework of Lifshitz–Slezov

theory [15]. It was shown that in the absence of size dispersion, due to the full quantization of charge carriers energy spectra in QD, the absorption coefficient behaves like a delta function, and the absorption threshold frequencies depend on the peculiarities of electron and hole energy spectra. When the QD size dispersion is taken into account, the averaging procedure yields the absorption profile having finite width and height.

Recently several reports concerning the experimental implementation of narrow-band InSb QDs have appeared [16, 17], in which the dispersion law for electrons and light holes is non-parabolic and described according to the double-band mirror Kane model [18, 19]. For non-interacting band of heavy holes the dispersion law is considered as quadratic. The investigation of optical absorption peculiarities in InSb QDs with the transitions from light and heavy hole bands to the conduction band taken into account is an interesting problem. Interband transitions in an ensemble of cylindrical or spherical InSb QDs were considered theoretically in the dipole approximation with and without magnetic field, including exciton effects, by means of the perturbation theory and the adiabatic methods [20–22]. In our earlier work we elaborated the calculation schemes, symbolic-numerical algorithms (SNAs) and programs, based on the generalized Kantorovich method (KM) for numerical solving with required accuracy the boundary-value problems (BVPs) of discrete and continuous spectra describing the axial-symmetric models of quantum wells (QWs), quantum wires (QWr), and quantum dots (QDs) in external fields within the framework of the effective mass approximation [23–35]. Meanwhile, for the analysis and estimations of

\*The text was submitted by the authors in English.

<sup>1)</sup>Joint Institute for Nuclear Research, Dubna, Russia.

<sup>2)</sup>Saratov State University, Saratov, Russia.

<sup>3)</sup>Russian–Armenian (Slavonic) University, Yerevan, Armenia.

\*\*E-mail: [gooseff@jinr.ru](mailto:gooseff@jinr.ru)

the appropriate range of material parameters, spectral and optical characteristics of QDs at the first stage of investigation the approximate eigenvalues and eigenfunctions evaluated in the analytical form were applied [6–8, 14, 22]. It is a real challenge to specify the range of applicability of such approximations in the problems, depending on a few parameters [2], e.g., for impurity states of quantum wires in a homogeneous magnetic field [25].

With this aim in the present paper we report the formulation and MAPLE-environment implementation of algebraic schemes of the Lennard-Jones (LJ) and Rayleigh–Schrödinger (RS) perturbation theory (PT) [36], permissive in the nondiagonal and diagonal adiabatic approximations, respectively, to evaluate in numerical and in analytic forms the eigenvalues and eigenfunctions of models of spheroidal QDs in homogeneous magnetic and electric fields. To construct the required perturbation schemes, we choose such models of spheroidal QDs, in which the basis functions depending upon fast variables can be expressed in the analytic form. The region of the model parameters, for which the PT asymptotic series are applied, is estimated using the results of numerical calculations carried out with required accuracy. The efficiency of the schemes is demonstrated by the analysis of spectral characteristics of oblate and prolate spheroidal QDs and also spherical QDs with corresponding shape of confinement well with walls of infinite height under the influence of homogeneous electric fields (HEFs). We apply the developed approach to the analysis of spectral characteristics of oblate and prolate spheroidal QDs with parabolic and non-parabolic dispersion laws under the influence of HEFs, i.e., the quantum-confined Stark effect.

The paper is organized as follows. In Section 2 the calculation scheme for solving elliptic BVP describing spheroidal QDs in homogeneous electric fields using the Kantorovich method is presented. Section 3 is devoted to the description of the slow-variable PT schemes in nondiagonal adiabatic approximation and the comparison of the results with those of numerical calculation with given accuracy. In Section 4 the explicit PT scheme for evaluation of the basis functions of the fast variable for oblate spheroidal QDs in a homogeneous electric field is derived. Section 5 is devoted to the description of slow-variable PT schemes in the diagonal adiabatic approximation for spheroidal QDs in electric fields. The results evaluated here in the analytic form are compared with numerical ones to establish the range of their applicability. In Section 6 the absorption coefficient for an ensemble of spheroidal QDs with random dimensions of minor semiaxis and with parabolic and non-parabolic dispersion laws for holes and electrons under the influence of HEFs is found using the calculated eigenval-

ues and eigenfunctions. In Conclusion we summarize the results and discuss further applications.

## 2. STATEMENT OF THE PROBLEM

Let us consider an impurity localized in the center of a QD and take the electron–hole interaction into account. Then in the effective mass approximation of the  $\mathbf{k} \cdot \mathbf{p}$  theory the Schrödinger equation for the slow-varying envelope wave function  $\tilde{\Psi}(\tilde{\mathbf{r}}_e, \tilde{\mathbf{r}}_h)$  of an electron ( $e$ ) and a hole ( $h$ ) in a uniform magnetic field  $\mathbf{H}$  with the vector-potential  $\mathbf{A} = \frac{1}{2}\mathbf{H} \times \tilde{\mathbf{r}}$  and electric field  $\mathbf{F}$  in *oblate* and *prolate* QDs has the form [8]:

$$\left\{ \tilde{H}(\tilde{\mathbf{r}}_e, \tilde{\mathbf{r}}_h) - \tilde{E} \right\} \tilde{\Psi}(\tilde{\mathbf{r}}_e, \tilde{\mathbf{r}}_h) = 0, \quad (1)$$

$$\tilde{H}(\tilde{\mathbf{r}}_e, \tilde{\mathbf{r}}_h) = \sum_{i=e,h} \left\{ \frac{1}{2\mu_i} \left( \tilde{\mathbf{p}}_i - \frac{q_i}{c}\mathbf{A} \right)^2 - q_i(\mathbf{F} \cdot \tilde{\mathbf{r}}_i) + \tilde{U}_{\text{conf}}(\tilde{\mathbf{r}}_i) - \frac{q_i q_c}{\kappa |\tilde{\mathbf{r}}_i|} \right\} + \frac{q_e q_h}{\kappa |\tilde{\mathbf{r}}_e - \tilde{\mathbf{r}}_h|}.$$

Here,  $\tilde{\mathbf{r}}_i$  is the radius-vector,  $|\tilde{\mathbf{r}}_i| = \sqrt{\tilde{x}_i^2 + \tilde{y}_i^2 + \tilde{z}_i^2}$ ,  $\tilde{\mathbf{p}}_i = -i\hbar\nabla_{\tilde{\mathbf{r}}_i}$  is the momentum,  $\tilde{E}$  is the energy of the particles,  $q_e = -e$ ,  $q_h = +e$ , and  $q_c$  are the Coulomb charges of the electron, the hole, and the impurity center,  $\kappa$  is the dc permittivity,  $\mu_i = \beta_{e(h)}m_0$  is the effective mass of electron or hole,  $m_0$  is the mass of electron. For the model under consideration,  $\tilde{U}(\tilde{\mathbf{r}})$  is the potential of a spherical or axially-symmetric well

$$\tilde{U}(\tilde{\mathbf{r}}_i) = \{0, S(\tilde{\mathbf{r}}_i) < 0; \tilde{U}_0, S(\tilde{\mathbf{r}}_i) \geq 0\}, \quad (2)$$

bounded by the surface  $S(\tilde{\mathbf{r}}_i) = 0$  with walls of infinite height (infinite potential barrier model, IPBM) or finite height  $1 \ll \tilde{U}_0 < \infty$  (finite potential barrier model, FPBM). In Eq. (2)  $S(\tilde{\mathbf{r}}_i)$  depends on the parameters  $\tilde{a}$ ,  $\tilde{c}$ , which are semiaxes of a spheroidal QD,

$$S(\tilde{\mathbf{r}}_i) \equiv (\tilde{x}_i^2 + \tilde{y}_i^2)/\tilde{a}^2 + \tilde{z}_i^2/\tilde{c}^2 - 1. \quad (3)$$

Below we restrict ourselves to IPBMs of spheroidal QDs with possible influence of the uniform electric field  $\mathbf{F} = (0, 0, F)$ , the magnetic field being switched off,  $\mathbf{H} = 0$ , and the Coulomb interaction of the electron and the hole with the impurity center being absent,  $q_c = 0$ . In this case the wave function  $\tilde{\Psi}(\tilde{\mathbf{r}}_e, \tilde{\mathbf{r}}_h) = \tilde{\Psi}^e(\tilde{\mathbf{r}}_e)\tilde{\Psi}^h(\tilde{\mathbf{r}}_h)$  is factorized. So, we arrive at the 3D BVPs for unknowns  $\tilde{\Psi}^e(\tilde{\mathbf{r}}_e)$  and  $\tilde{E}^e$  or  $\tilde{\Psi}^h(\tilde{\mathbf{r}}_h)$  and  $\tilde{E}^h$ . The eigenvalues and eigenfunctions needed to evaluate the absorption coefficients (ACs) were calculated with prescribed accuracy by means of the program packages ODPEVP and KANTBP [28–30]. The models with nonzero values of these parameters were announced in [8, 25]. Throughout the paper we make use of the reduced atomic units [2, 5]:

$a_B^* = \kappa \hbar^2 / (\mu_p e^2)$  is the reduced Bohr radius,  $\tilde{E}_R \equiv Ry^* = \hbar^2 / (2\mu_p a_B^{*2})$  is the reduced Rydberg unit of energy, and the following dimensionless quantities are introduced:  $\tilde{\Psi}(\tilde{\mathbf{r}}) = a_B^{*-3/2} \Psi(\mathbf{r})$ ,  $2\hat{H} = \tilde{H} / Ry^*$ ,  $\mathcal{E} \equiv 2E = \tilde{E} / Ry^*$ ,  $2U(\mathbf{r}) = \tilde{U}(\tilde{\mathbf{r}}) / Ry^*$ ,  $\mathbf{r} = \tilde{\mathbf{r}} / a_B^*$ ,  $a = \tilde{a} / a_B^*$ ,  $c = \tilde{c} / a_B^*$ ,  $2\gamma_F = F / F_0^*$ ,  $F_0^* = Ry^* / (ea_B^*) = e / (2\kappa(a_B^*)^2)$ .

### 2.1. The BVP for SQDs in the Effective Mass Approximation

In cylindrical coordinates  $z, \rho, \varphi$  the solution of Eq. (1), periodical with respect to the azimuthal angle  $\varphi$ , is sought in the form of a product  $\Psi(\rho, z, \varphi) = \Psi^m(\rho, z) \exp(im\varphi) / \sqrt{2\pi}$ , where  $m = 0, \pm 1, \pm 2, \dots$  is the magnetic quantum number. The 3D BVP for spherical QDs (SQDs) at fixed values of  $m$  is reduced to 2D BVP with respect to *fast*  $x_f$  and *slow*  $x_s$  variables: *oblate*  $x_f = z$  (minor axis),  $x_s = \rho$  (major axis) and *prolate*  $x_f = \rho$  (minor axis),  $x_s = z$  (major axis) [27]:

$$\left( \hat{H}_f(x_f; x_s) + \hat{H}_s(x_s) + \check{V}_{fs}(x_f, x_s) - \mathcal{E}_t^m \right) \times \Psi_t^m(x_f, x_s) = 0. \quad (4)$$

Here,  $\hat{H}_s(x_s)$  is the operator of slow subsystem

$$\hat{H}_s(x_s) = -\frac{1}{g_{1s}(x_s)} \frac{\partial}{\partial x_s} g_{2s}(x_s) \frac{\partial}{\partial x_s} + \check{V}_s(x_s), \quad (5)$$

and  $\hat{H}_f(x_f; x_s)$  is the operator of fast subsystem

$$\hat{H}_f(x_f; x_s) = -\frac{1}{g_{1f}(x_f)} \frac{\partial}{\partial x_f} g_{2f}(x_f) \frac{\partial}{\partial x_f} + \check{V}_f(x_f; x_s). \quad (6)$$

For oblate spheroidal QD (OSQD)  $g_{1s}(x_s) = g_{2s}(x_s) = 1$ ,  $g_{1f}(x_s) = g_{2f}(x_s) = \rho$ ,  $\check{V}_f(x_f; x_s) = 0$ ,  $\check{V}_s(x_s) = m^2 / \rho^2$ ,  $\check{V}_{fs}(x_f, x_s) = 2\gamma_F z$ , while for prolate spheroidal QD (PSQD)  $g_{1s}(x_s) = g_{2s}(x_s) = \rho$ ,  $g_{1f}(x_s) = g_{2f}(x_s) = 1$ ,  $\check{V}_f(x_f; x_s) = m^2 / \rho^2$ ,  $\check{V}_s(x_s) = 2\gamma_F z$ ,  $\check{V}_{fs}(x_f, x_s) = 0$ . From (2) it follows that the boundary conditions for the eigenfunctions  $\Psi_t^m(x_f, x_s)$  of SQDs, corresponding to a well with walls of infinite height, have the form

$$\lim_{\rho \rightarrow 0} \left( \rho \frac{\partial \Psi_t^m(\rho, z)}{\partial \rho} \delta_{0m} + \Psi_t^m(\rho, z) (1 - \delta_{0m}) \right) = 0,$$

$$\Psi_t^m(\rho, z) \Big|_{\partial \Omega_2} = 0,$$

$$\Omega_2 = \left( \{\rho, z\} \left| \frac{\rho^2}{a^2} + \frac{z^2}{c^2} < 1 \right. \right),$$

$$\partial \Omega_2 = \left( \{\rho, z\} \left| \frac{\rho^2}{a^2} + \frac{z^2}{c^2} = 1 \right. \right).$$

The eigenfunctions  $\Psi_t^m(x_f, x_s)$  corresponding to the eigenvalues  $\mathcal{E}_t^m = \mathcal{E}_1^m < \mathcal{E}_2^m, \dots$  are subject to the normalization and orthogonality conditions

$$\int_{\Omega_2} \rho d\rho dz \Psi_t^m(\rho, z) \Psi_{t'}^m(\rho, z) = \delta_{tt'}.$$

Note, that at  $\gamma_F = 0$  the solutions are separated by the  $z$ -parity  $\sigma = \pm 1$  into two invariant subspaces  $\Psi_t^{m\sigma}$  corresponding to the eigenvalues  $\mathcal{E}_t^{m\sigma} = \mathcal{E}_1^{m\sigma} < \mathcal{E}_2^{m\sigma}, \dots$ , while at  $\gamma_F \neq 0$  the  $z$ -parity is violated.

### 2.2. Kantorovich or Adiabatic Reduction of the BVP

The solution  $\Psi_t(x_f, x_s) \equiv \Psi_t^m(x_f, x_s)$  of the above problem at fixed  $m$  is sought in the form of Kantorovich expansion

$$\Psi_t(x_f, x_s) = \sum_{j=1}^{j_{\max}} B_j(x_f; x_s) \chi_{jt}(x_s). \quad (7)$$

The set of appropriate trial functions is chosen as the set of eigenfunctions  $B_j(x_f; x_s)$  corresponding to the eigenvalues  $\hat{E}_j(x_s)$  of the Hamiltonian  $\hat{H}_f(x_f; x_s)$ , Eq. (6), depending parametrically on  $x_s \in \Omega(x_s)$ :

$$\hat{H}_f(x_f; x_s) B_j(x_f; x_s) = \hat{E}_j(x_s) B_j(x_f; x_s).$$

The eigenfunctions  $B_j(x_f; x_s)$  corresponding to the eigenvalues  $\hat{E}_j(x_s) = \hat{E}_1(x_s) < \hat{E}_2(x_s), \dots$  are subject to the normalization and orthogonality conditions with the weighting function  $g_{1f}(x_f)$  in the same interval  $x_f \in \Omega_{x_f}(x_s)$ :

$$\int_{x_f^{\min}(x_s)}^{x_f^{\max}(x_s)} B_i(x_f; x_s) B_j(x_f; x_s) g_{1f}(x_f) dx_f = \delta_{ij}. \quad (8)$$

The BVP for a set of second-order differential equations (ODEs) of the slow subsystem with respect to the unknown vector functions  $\chi_t(x_s) = (\chi_{1;t}(x_s), \dots, \chi_{j_{\max;t}}(x_s))^T$  corresponding to the unknown eigenvalues  $2E_t \equiv \mathcal{E}_t$ ,

$$\left( \mathbf{D} + \mathbf{E}(x_s) + \mathbf{W}(x_s) - \mathbf{I} \mathcal{E}_t \right) \chi_t(x_s) = 0, \quad (9)$$

$$\mathbf{D} = -\frac{1}{g_{1s}(x_s)} \mathbf{I} \frac{d}{dx_s} g_{2s}(x_s) \frac{d}{dx_s} + \mathbf{I} \check{V}_s(x_s),$$

$$\mathbf{W}(x_s) = \mathbf{U}(x_s) + \frac{g_{2s}(x_s)}{g_{1s}(x_s)} \mathbf{H}(x_s) + \frac{1}{g_{1s}(x_s)} \frac{dg_{2s}(x_s)}{dx_s} \mathbf{Q}(x_s) + \frac{g_{2s}(x_s)}{g_{1s}(x_s)} \mathbf{Q}(x_s) \frac{d}{dx_s}$$

satisfy the orthogonality and normalization conditions

$$\int_{x_s^{\min}}^{x_s^{\max}} (\chi_t(x_s))^T \chi_{t'}(x_s) g_{1s}(x_s) dx_s = \delta_{tt'}. \quad (10)$$

Here the effective potentials  $H_{ij}(x_s)$  and  $Q_{ij}(x_s)$  are defined by the formula

$$\begin{aligned} U_{ij}(x_s) &= U_{ji}(x_s) = \int_{x_f^{\min}(x_s)}^{x_f^{\max}(x_s)} \\ &\times B_i(x_f; x_s) \check{V}_{fs}(x_f, x_s) B_j(x_f; x_s) g_{1f}(x_f) dx_f, \\ H_{ij}(x_s) &= H_{ji}(x_s) \\ &= \int_{x_f^{\min}(x_s)}^{x_f^{\max}(x_s)} \frac{\partial B_i(x_f; x_s)}{\partial x_s} \frac{\partial B_j(x_f; x_s)}{\partial x_s} g_{1f}(x_f) dx_f, \\ Q_{ij}(x_s) &= -Q_{ji}(x_s) \\ &= - \int_{x_f^{\min}(x_s)}^{x_f^{\max}(x_s)} B_i(x_f; x_s) \frac{\partial B_j(x_f; x_s)}{\partial x_s} g_{1f}(x_f) dx_f. \end{aligned} \quad (11)$$

The basis functions of the fast subsystem and the matrix elements are calculated analytically. For OSQDs ( $x_f = z$ ,  $x_s = \rho$ )

$$\begin{aligned} B_i(x_f; x_s) &= B_i^\sigma(x_f; x_s) \quad (12) \\ &= \sqrt{\frac{a}{c\sqrt{a^2 - x_s^2}}} \sin \left( \frac{\pi n_o}{2} \left( \frac{x_f}{c\sqrt{1 - x_s^2/a^2}} - 1 \right) \right), \\ E_i(x_s) &= E_i^\sigma(x_s) = E_{i;0} \frac{a^2}{(a^2 - x_s^2)}, \\ E_{i;0} &= \frac{\pi^2 i^2}{4c^2}, \quad U_{ii}(x_s) = 0, \\ U_{ij}(x_s) &= U_{ij;0} \frac{\sqrt{a^2 - x_s^2}}{a}, \\ U_{ij;0} &= \frac{8\gamma_{FCij}(-1 + (-1)^{i+j})}{(i^2 - j^2)^2 \pi^2}, \\ H_{ii}(x_s) &= H_{ii;0} \frac{a^2 x_s^2}{(a^2 - x_s^2)^2}, \\ H_{ii;0} &= \frac{3 + \pi^2 i^2}{12a^2}, \\ H_{ij}(x_s) &= H_{ij;0} \frac{a^2 x_s^2}{(a^2 - x_s^2)^2}, \\ H_{ij;0} &= \frac{2ij(i^2 + j^2)(1 + (-1)^{i+j})}{a^2(i^2 - j^2)^2}, \end{aligned}$$

$$Q_{ij}(x_s) = Q_{ij;0} \frac{ax_s}{a^2 - x_s^2},$$

$$Q_{ij;0} = \frac{ij(1 + (-1)^{i+j})}{a(i^2 - j^2)}, \quad j \neq i.$$

For PSQDs ( $x_f = \rho$ ,  $x_s = z$ ) (at  $m = 0$  for nondiagonal potentials  $i \neq j$ )

$$\begin{aligned} B_{n_{pp}}^m(x_s) &= \frac{\sqrt{2}c}{a\sqrt{c^2 - x_s^2}} \quad (13) \\ &\times \frac{J_{|m|} \left( \sqrt{2E_{n_{pp}+1,|m|}}(x_s) x_f \right)}{|J_{|m|+1}(\alpha_{n_{pp}+1,|m|})|}, \\ E_i(x_s) &= E_{i;0} \frac{c^2}{(c^2 - x_s^2)}, \quad E_{i;0} = \frac{(\bar{J}_{|m|}^i)^2}{a^2}, \\ U_{ii}(x_s) &= 0, \quad U_{ij}(x_s) = 0, \\ H_{ii}(x_s) &= H_{ii;0} \frac{c^2 x_s^2}{(c^2 - x_s^2)^2}, \\ H_{ii;0} &= \frac{(1 + (\bar{J}_{|m|}^i)^2)}{3c^2}, \\ H_{ij}(x_s) &= H_{ij;0} \frac{c^2 x_s^2}{(c^2 - x_s^2)^2}, \\ H_{ij;0} &= \frac{2}{c^2} \left( \bar{J}_0^i \bar{J}_0^j \int_0^1 \frac{J_1(\bar{J}_0^i x)}{J_1(\bar{J}_0^i)} \frac{J_1(\bar{J}_0^j x)}{J_1(\bar{J}_0^j)} x^3 dx \right. \\ &\quad - \bar{J}_0^i \int_0^1 \frac{J_1(\bar{J}_0^i x)}{J_1(\bar{J}_0^i)} \frac{J_0(\bar{J}_0^j x)}{J_1(\bar{J}_0^j)} x^2 dx \\ &\quad \left. - \bar{J}_0^j \int_0^1 \frac{J_0(\bar{J}_0^i x)}{J_1(\bar{J}_0^i)} \frac{J_1(\bar{J}_0^j x)}{J_1(\bar{J}_0^j)} x^2 dx \right), \\ Q_{ij}(x_s) &= Q_{ij;0} \frac{cx_s}{c^2 - x_s^2}, \\ Q_{ij;0} &= \frac{2}{c} \bar{J}_0^j \int_0^1 \frac{J_0(\bar{J}_0^i x)}{J_1(\bar{J}_0^i)} \frac{J_1(\bar{J}_0^j x)}{J_1(\bar{J}_0^j)} x^2 dx, \quad j \neq i, \end{aligned}$$

where  $\alpha_{n_{pp}+1,|m|} = \bar{J}_{|m|}^{n_{pp}+1}$  are positive zeros of the Bessel function of the first kind [37].

For the interesting lower part of the spectrum  $\mathcal{E}_t$ :  $\mathcal{E}_1 < \mathcal{E}_2 < \dots$ , the number  $j_{\max}$  of the equations solved should be at least not less than the number of the energy levels of the problem (9) at  $a = c = r_0$ . To ensure the prescribed accuracy of calculation of the lower part of the spectrum discussed below with eight significant digits we used  $j_{\max} = 16$  basis functions in the expansion (8) and the discrete approximation of the desired solution by Lagrange finite elements of the fourth order with respect

**Table 1.** The convergence of eigenenergy  $\mathcal{E}_t$  vs number  $j_{\max}$  of basis functions at  $\gamma_F = 0$  (Fast and slow variables  $x_f = z$  and  $x_s = \rho$  (oblate spheroidal QD and spherical QD), number of nodes  $i = (n_{zo}, n_{\rho o})$ )

$j_{\max}$	$a = 2.5, c = 0.5$			$a = 2.5, c = 2.5$		
$(n_{zo}, n_{\rho o})$	(0, 0)	(0, 1)	(2, 0)	(0, 0)	(0, 1)	(2, 0)
$C$	12.73741	19.93621	96.69683*	1.468496	5.445665*	5.589461
1	12.76548	20.04602	96.75317*	1.590238	5.766612*	6.004794
2	12.76490	20.04133	96.75427	1.580243	5.340214	6.329334
4	12.76482	20.04074	96.75215	1.579273	5.316872	6.317204
16	12.76481	20.04065	96.75201	1.579140	5.314832	6.316562
Exact				1.579136	5.314793	6.316546

\* Diagonal approximation at  $j = 2$ .**Table 2.** The convergence of eigenenergy  $\mathcal{E}_t$  vs number  $j_{\max}$  of basis functions at  $\gamma_F = 0$  (Fast and slow variables  $x_f = \rho$  and  $x_s = z$  (prolate spheroidal QD and spherical QD), number of nodes  $i = (n_{\rho p}, n_{zp})$ )

$j_{\max}$	$c = 2.5, a = 0.5$			$c = 2.5, a = 2.5$		
$(n_{\rho p}, n_{zp})$	(0, 0)	(0, 2)	(1, 0)	(0, 0)	(0, 2)	(1, 0)
$C$	25.18473	34.42885	126.4245*	1.493612	5.131784	5.898668*
1	25.20174	34.53030	126.4565*	1.584433	5.680831	6.071435*
2	25.20129	34.52578	126.4573	1.579860	5.331101	6.324717
4	25.20121	34.52512	126.4561	1.579239	5.316732	6.317058
16	25.20120	34.52502	126.4561	1.579138	5.314828	6.316554
Exact				1.579136	5.314793	6.316546

\* Diagonal approximation at  $j = 2$ .

to the grid pitch  $\Omega_{h_s}^p(x_s) = [x_{s;\min}; x_{s;k} = x_{s;k-1} + h_s; x_{s;\max}]$ . The details of the corresponding computational scheme are given in [24].

The convergence of eigenenergies  $\mathcal{E}_t$  vs number  $j_{\max}$  of basis functions for oblate and prolate spheroidal QDs, and for spherical QD is shown on Tables 1 and 2 at  $\gamma_F = 0$  and  $m = 0$ . The considered QDs having the size comparable with de Broglie wavelength of composed particles with small effective masses are referred as quantum-size systems. In the spheroidal QDs having different length of minor and major axes the quantization procedure leads to different transversal and longitudinal spectra. Moreover, for PSQD ( $c = 2.5, a = 0.5$ ) the confinement in two variables ( $xy$ ) with the minor semiaxis  $a = 0.5$  leads to greater eigenvalues, than the confinement in one variable ( $z$ ) with the size-for-size minor semiaxis  $a = 0.5$  for PSQD ( $c = 2.5, a = 0.5$ ). Tables 1, 2 and 3–7 (see below) show that the expansions in basis functions (12) and (13) in cylindrical coordinates have better rate of convergence in the adiabatic limit of

strongly oblate and prolate QDs than for the benchmark spherical QDs with the known spectrum, which is not surprising. For lower states the crude adiabatic approximation (without  $H_{jj}(x_s)$ ) (CAA) provides a lower estimate, while the adiabatic approximation (AA) (with  $H_{jj}(x_s)$ ) (1) gives an upper estimate, such that at the ratio of minor to major semiaxis equal to  $1/5$  the bracket is approximated with the accuracy of  $\sim 0.1\%$ .

Below we present the analysis of the spectrum under the variation of parameters, which opens the questions about the additional symmetry of the problem, associated with the existence of exact and approximate integrals of motion [27, 38].

In Fig. 1 we show the eigenenergies of the lower part of the spectrum  $\mathcal{E}_t$ ,  $t = 1, \dots, 40$ , at  $m = 0$  for OSQD ( $c = 0.5, 1, 1.5, 2, a = 2.5$ ), SQD ( $c = 2.5, a = 2.5$ ), and PSQD ( $c = 2.5, a = 0.5, 1, 1.5, 2$ ) as functions of the dimensionless strength  $\gamma_F$  of the electric field. In spite of the fact that at  $\gamma_F = 0$  the

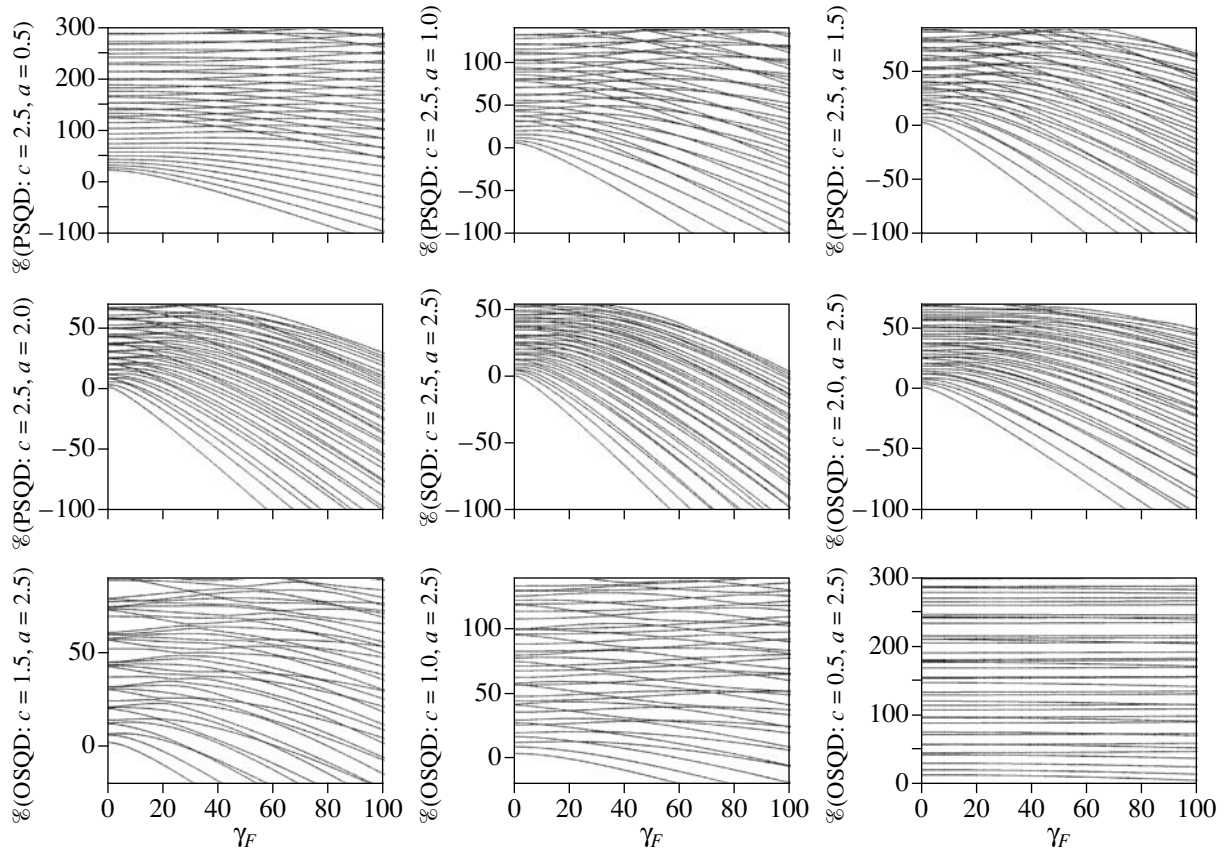


**Fig. 1.** Dependence of eigenenergies  $\mathcal{E}$  (in units of  $E_e$ ) of lower part of spectrum of electronic states of QDs at  $m = 0$  on electric field strength  $\gamma_F$  (in units of  $F_0^*$ ): for spherical quantum dot (SQD) with radius  $a = c = 2.5$ , oblate and prolate spheroidal quantum dots (OSQD and PSQD) at different minor semiaxis (for OSQD  $c = 0.5, 1, 1.5, 2$ ,  $a = 2.5$ , for PSQD  $c = 2.5$ ,  $a = 0.5, 1, 1.5, 2$ ).

eigenfunctions of SQD, OSQD, and PSQD have definite  $z$ -parity, and, therefore, exhibit additional integrals of motion and separation of variables in spherical and spheroidal coordinates systems, the spectrum of eigenvalues at fixed  $m$  is simple, i.e., nondegenerate, similar to the case  $\gamma_F \neq 0$ , when the eigenfunctions have no definite  $z$ -parity. At  $\gamma_F = 0$  a one-to-one correspondence rule  $n_{pp} + 1 = n_p = i = n = n_r + 1$ ,  $i = 1, 2, \dots$ , and  $n_{zp} = l - |m|$  holds between the quantum numbers  $(n, l, m, \hat{\sigma} = (-1)^{|m|}\sigma)$  of SQD with the radius  $r_0 = a = c$ , the spheroidal quantum numbers  $\{n_\xi = n_r, n_\eta = l - |m|, m, \sigma\}$  of PSQD with the major  $c$  and the minor  $a$  semi-axes, and the adiabatic set of quantum numbers  $[n_p = n_{pp} + 1, n_{zp}, m, \sigma]$  under the continuous variation of the parameter  $\zeta_{ac} = a/c$ . At  $\gamma_F = 0$  there is a one-to-one correspondence rule  $n_o = n_{zo} + 1 = 2n - (1 + \sigma)/2$ ,  $n = 1, 2, 3, \dots$ , and  $n_{po} = (l - |m| - (1 - \sigma)/2)/2$ , between the sets of spherical quantum numbers  $(n, l, m, \hat{\sigma} = (-1)^{|m|}\sigma)$  of SQD with the radius  $r_0 = a = c$  and spheroidal ones  $\{n_\xi = n_r, n_\eta = l - |m|, m, \sigma\}$  of OSQD with the major  $a$  and the

minor  $c$  semi-axes, and the adiabatic set of cylindrical quantum numbers  $[n_o = n_{zo} + 1, n_{po}, m, \sigma]$  under the continuous variation of the parameter  $\zeta_{ca} = c/a$ .

One can see that when the parameter  $\gamma_F$  increases, the eigenvalues  $\mathcal{E}_t$  decrease faster for SQD, slower for PSQD and even more slower for OSQD, because the influence of the electric field for OSQD at  $c = 0.5$  is essentially weaker than for PSQD at  $c = 2.5$ . With increasing  $\gamma_F$  a series of exact crossings of eigenenergies with different values of quantum numbers for PSQD and OSQD occur at  $\gamma_F \gtrsim 20$  and a series of avoided crossings for SQD occur at  $\gamma_F \gtrsim 10$ . With further growth of the parameter they first increase and then begin to decrease. Indeed, with the growth of  $\gamma_F$  the eigenfunctions with smaller number of nodes in the longitudinal variable  $z$  are localized (see Fig. 2) in the vicinity of the equilibrium point, and the corresponding eigenenergies decrease. Increasing the number of nodes is accompanied with delocalization of the wave functions, and the corresponding eigenenergies increase and then decrease again. For PSQD the density of states per unit energy for the eigenfunction with the same number

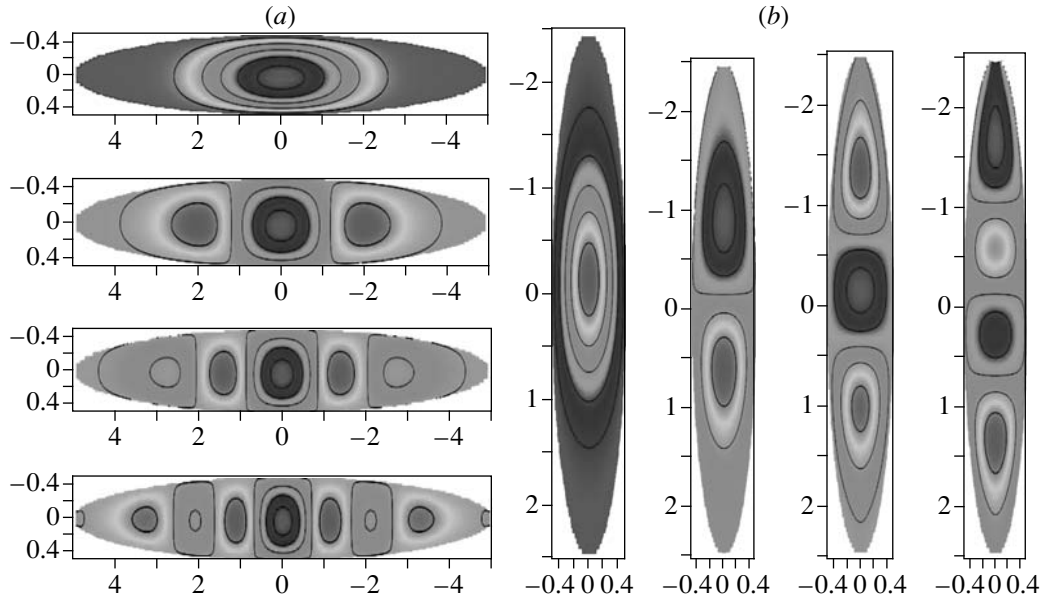


**Fig. 2.** (a) Eigenfunctions of sixth order of PT of 2D BVP for OSQD  $a = 5$ ,  $c = 0.5$  ( $t = n_{zo} = 0$ ,  $n = n_o = 1, 2, 3, 4$ ,  $m = 0$ ) in electric field  $\gamma_F = -10$  (weak asymmetry by  $z$ -axis i.e. by minor ellipsoid axis). (b) Eigenfunctions of sixth order of PT of 2D BVP for PSQD  $c = 2.5$ ,  $a = 0.5$  ( $t = n_{pp} = 0$ ,  $n = n_p = 0, 1, 2, 3, 4$ ,  $m = 0$ ) in electric field  $\gamma_F = -1$  (asymmetry by  $z$ -axis i.e. by major ellipsoid axis).

of nodes  $n_{pp}$  in the transverse variable  $\rho$  is greater (i.e., the separation between the adjacent energy levels is smaller) than the density of states for the function having the same number of nodes  $n_{zp}$  in the longitudinal variable  $z$ . For this reason in Fig. 1 one can see three crossing series of curves with different number of  $\rho$  nodes  $n_{pp} = 0, 1, 2$ , the lower of them (e.g., with  $a = 0.5$ ,  $n_{pp} = 0$ , and  $n_{zp}$  from 0 to 12) are decreasing at all  $\gamma_F \geq 0$ , while the upper ones (e.g., with  $a = 0.5$ ,  $n_{pp} = 0$ , and  $n_{zp}$  starting from 13) with the energies, exceeding that of the state ( $n_{pp} = 1$ ) without  $z$  nodes ( $n_{zp} = 0$ ), increase from the beginning and then start to decrease. Thus, at small  $\gamma_F$  the energy levels for the groups of states with even  $n_{pp} = 0, 2, \dots$  and odd  $n_{pp} = 1, 3, \dots$  number of nodes are repulsing and crossing.

For OSQD, on the contrary, the number of energy levels per unit energy for the eigenfunctions having the same number  $n_{\rho o}$  of  $\rho$  nodes is smaller (i.e., the separation between the adjacent levels is larger) than that for the eigenfunctions having the same number  $n_{zo}$  of  $z$  nodes. Therefore, in Fig. 1 one can see four crossing series of almost “parallel” curves with different number  $n_{zo} = 0, 1, 2, 3$  of  $z$  nodes.

For OSQD and PSQD the crossings of the energy levels that occur with increasing  $\gamma_F$  are similar to the exact crossings of the energy levels with decreasing  $c$  semiaxis in OSQD and PSQD without electric field ( $\gamma_F = 0$ ), i.e., we observe the accidental degeneracy, which is known to be generally associated with the

existence of an additional integral of motion [27] and with the separability of variables in oblate and prolate spheroidal coordinate systems. Thus, from our observations it follows that an additional approximate integral of motion should exist.

For SQD eigenfunction with different numbers of  $\rho$  and  $z$  nodes,  $n_\rho$  and  $n_z$ , and with increasing  $\gamma_F$  the series of crossings become mixed. Note, that the eigenenergies of the states with the same  $z$ -parity at  $\gamma_F = 0$  are repulsed with increasing  $\gamma_F$  (e.g., [ $t = 9$ ,  $n = 1$ ,  $l = 5$ ,  $\mathcal{E}_9(\gamma_F = 0) = 14.01$ ] and [ $t = 10$ ,  $n = 3$ ,  $l = 0$ ,  $\mathcal{E}_{10}(\gamma_F = 0) = 14.21$ ]), but the states with different  $z$ -parity are attracted (e.g., [ $t = 7$ ,  $n = 1$ ,  $l = 4$ ,  $\mathcal{E}_7(\gamma_F = 0) = 10.71$ ] and [ $t = 8$ ,  $n = 2$ ,  $l = 2$ ,  $\mathcal{E}_8(\gamma_F = 0) = 13.24$ ]). This fact should be also associated with the existence of approximate integrals of motion. Indeed, from Fig. 1 one can see that for SQD at  $a = c = 2.5$  with increasing  $\gamma_F$  the series of exact crossings appear.

### 3. THE PTLJ IN NONDIAGONAL ADIABATIC APPROXIMATION

We expand the potentials (12) and (13) of the BVP (9) and (10) in Taylor series in the vicinity of  $x_s = 0$ :

$$E_i(x_s) = E_{i;0} + \sum_{k=1}^{k_{\max}} \frac{E_{i;0}^{(k)}}{\tau^{2k}} x_s^{2k}, \quad (14)$$

$$\begin{aligned}
U_{ij}(x_s) &= U_{ij;0} + \sum_{k=1}^{k_{\max}} \frac{\tilde{U}_{ij;k}}{\tau^{2k}} x_s^{2k}, \\
H_{ij}(x_s) &= \sum_{k=1}^{k_{\max}} k \frac{H_{ij;0}}{\tau^{2k}} x_s^{2k}, \\
Q_{ij}(x_s) &= \sum_{k=1}^{k_{\max}} \frac{Q_{ij;0}}{\tau^{2k-1}} x_s^{2k-1},
\end{aligned}$$

where  $\tilde{U}_{ij;k} = \frac{(2k-3)!!}{(2k)!!} U_{ij;0}$  and the parameter  $\tau$  equals  $\tau = a$  for OSQD, and  $\tau = c$  for PSQD. Substitution of expansions (14) into Eq. (9) leads to the BVP for a set of ODEs of the slow subsystem with respect to the unknown vector functions  $\chi_t(x_s) = (\chi_{1;t}(x_s), \dots, \chi_{j_{\max;t}}(x_s))^T$  corresponding to the unknown eigenvalues  $2E_t \equiv \mathcal{E}_t$ :

$$\begin{aligned}
&\left( \mathbf{D}^{(0)} + (E_{i;0} - \mathcal{E}_t) + \tilde{V}_s(x_s) \right. \\
&+ \sum_{k=1}^{k_{\max}} \frac{E_{ii;0} + k H_{ii;0}}{\tau^{2k}} x_s^{2k} \Big) \chi_{i;t}(x_s) \\
&+ \sum_{j \neq i} \sum_{k=1}^{j_{\max}} \sum_{k=1}^{k_{\max}} \left( \frac{\tilde{U}_{ij;k}}{\tau^{2k}} x_s^{2k} + k \frac{H_{ij;0}}{\tau^{2k}} x_s^{2k} \right. \\
&\quad \left. + (2k-1) \frac{Q_{ij;0}}{\tau^{2k-1}} x_s^{2k-2} \right. \\
&\quad \left. + 2 \frac{Q_{ij;0}}{\tau^{2k-1}} x_s^{2k-1} \frac{d}{dx_s} \right) \chi_{j;t}(x_s) = 0,
\end{aligned} \quad (15)$$

where  $\tilde{U}_{ij;k}$  is given by the expansion (14) and  $\tilde{V}_s(x_s) = 0$  for OSDQ;  $U_{ij}(x_s) = 0$  and  $\tilde{V}_s(x_s) = \gamma_F z$  for PSDQ. We choose the unperturbed operator to have the eigenvalues and basis functions of 2D and 1D oscillators. For the OSQD (2D oscillator) with respect to the scaled slow variable  $x$  we have  $x_s = \rho = \sqrt{x/\sqrt{E_f}}$ , where  $E_f = (E_{i';0} + H_{i'i';0})/(4a^2) = \omega_{i'}^2/4$ , i.e., the adiabatic frequency, at given  $i' = n_o$

$$\begin{aligned}
L(n) &= \mathbf{D}^{(0)} - E^{(0)}, \\
\mathbf{D}^{(0)} &= - \left( \frac{d}{dx} x \frac{d}{dx} - \frac{x}{4} - \frac{m^2}{4x} \right), \\
E^{(0)} &\equiv E_{n,m}^{(0)} = n + (|m| + 1)/2, \\
\Phi_q^{(0)}(x) &= \frac{\sqrt{q!} x^{|m|/2} \exp(-x/2) L_q^{|m|}(x)}{\sqrt{(q + |m|)!}}, \\
\int_0^\infty \Phi_q^{(0)}(x) \Phi_{q'}^{(0)}(x) dx &= \delta_{qq'}.
\end{aligned} \quad (16)$$

Therefore, the action of the operators  $L(n)$  and  $x$  on the function  $\Phi_q^{(0)}(x) \equiv \Phi_{q,m}^{(0)}(x)$  is determined by the recurrence relations [37]

$$\begin{aligned}
L(n) \Phi_{q,m}^{(0)}(x) &= (q - n) \Phi_{q,m}^{(0)}(x), \\
x \Phi_{q,m}^{(0)}(x) &= -\sqrt{q + |m|} \sqrt{q} \Phi_{q-1,m}^{(0)}(x) \\
&\quad + (2q + |m| + 1) \Phi_{q,m}^{(0)}(x) \\
&\quad - \sqrt{q + |m| + 1} \sqrt{q + 1} \Phi_{q+1,m}^{(0)}(x), \\
x \frac{d\Phi_{q,m}^{(0)}(x)}{dx} &= -\sqrt{q + |m|} \sqrt{q} \Phi_{q-1,m}^{(0)}(x)/2 \\
&\quad - \Phi_{q,m}^{(0)}(x)/2 + \sqrt{q + |m| + 1} \sqrt{q + 1} \Phi_{q+1,m}^{(0)}(x)/2.
\end{aligned} \quad (17)$$

For PSQD (1D oscillator) with respect to the scaled slow variable  $x$   $x_s = x/\sqrt[4]{E_f}$ , where  $E_f = (E_{i';0} + H_{i'i';0})/c^2 = \omega_{i'}^2$ , i.e., the adiabatic frequency, at given  $i' = n_p$ , we have

$$\begin{aligned}
L(n) &= \mathbf{D}^{(0)} - E^{(0)}, \quad \mathbf{D}^{(0)} = -\frac{d^2}{dx^2} + x^2, \\
E^{(0)} &\equiv E_n^{(0)} = 2n + 1, \quad n = 0, 1, \dots, \\
\Phi_q^{(0)}(x) &= \frac{\exp(-x^2/2) H_q(x)}{\sqrt[4]{\pi} \sqrt{2^q} \sqrt{q!}}, \\
\int_{-\infty}^\infty \Phi_q^{(0)}(x) \Phi_{q'}^{(0)}(x) dx &= \delta_{qq'}.
\end{aligned} \quad (18)$$

Correspondingly, the action of operators  $L(n)$ ,  $x$  and  $d/dx$  on function  $\Phi_q^{(0)}(x)$  is determined by the recurrence relations [37]

$$\begin{aligned}
L(n) \Phi_q^{(0)}(x) &= 2(q - n) \Phi_q^{(0)}(x), \\
x \Phi_q^{(0)}(x) &= \frac{\sqrt{q}}{\sqrt{2}} \Phi_{q-1}^{(0)}(x) + \frac{\sqrt{q+1}}{\sqrt{2}} \Phi_{q+1}^{(0)}(x), \\
\frac{d}{dx} \Phi_q^{(0)}(x) &= \frac{\sqrt{q}}{\sqrt{2}} \Phi_{q-1}^{(0)}(x) - \frac{\sqrt{q+1}}{\sqrt{2}} \Phi_{q+1}^{(0)}(x).
\end{aligned} \quad (19)$$

The eigenfunctions (15) as functions of the new scaled variable  $x$  are sought in the form of expansion over the basis of the normalized functions  $\Phi_q^{(0)}(x)$ ,  $q = 0, 1, \dots$ , of the 2D or 1D oscillators with unknown coefficients  $b_{j,s}$ :

$$\begin{aligned}
\chi_{j;t}(x) &= \sum_{q=0}^{q_{\max}} b_{j,q;t} \Phi_q^{(0)}(x), \\
b_{j,q<0;t} &= b_{j,q>q_{\max};t} = 0.
\end{aligned} \quad (20)$$

Below we demonstrate that such expansions are appropriate for getting approximate solutions in the



**Table 3.** The convergence of eigenenergies  $\mathcal{E}_t$  of Eq. (23) vs order  $k_{\max}$  of approximation of effective potentials from (14) for  $j_{\max} = 4$  and  $q_{\max} = 60$  basis functions at  $\gamma_F = 0$  (Fast and slow variables  $x_f = z$  and  $x_s = \rho$  (oblate spheroidal QD and spherical QD), number of nodes  $i = (n_{zo} = n_o - 1, n_{\rho o})$ )

$k_{\max}$	$a = 2.5, c = 0.5$			$a = 2.5, c = 2.5$		
$(n_{zo}, n_{\rho o})$	(0, 0)	(0, 1)	(2, 0)	(0, 0)	(0, 1)	(2, 0)
8	12.66820	19.06745	96.71486	1.192415	2.998982	5.325360
12	12.74967	19.81383	96.75070	1.377572	4.088539	5.868629
20	12.78407	19.83842	96.75172	1.132323	5.084082	6.735687
$N(j_{\max} = 4)$	12.76482	20.04074	96.75215	1.579273	5.316872	6.317204

lower part of the BVP spectrum (9) and (10). Substitution of the expansion (20) into (15) yields the set of equations

$$\begin{aligned}
 & \sum_{q=0}^{q_{\max}} \hat{\mathbf{A}}_{ii} b_{i,q;t} \Phi_q^{(0)}(x) \\
 & + \sum_{j \neq i=1}^{j_{\max}} \sum_{q=0}^{q_{\max}} \hat{\mathbf{A}}_{ij} b_{j,q;t} \Phi_q^{(0)}(x) \\
 & = \sum_{q=0}^{q_{\max}} \kappa^{-2} \mathcal{E}_t E_f^{-1/2} b_{i,q;t} \Phi_q^{(0)}(x), \\
 & \hat{\mathbf{A}}_{ii} = \left( \mathbf{D}^{(0)} + \tilde{V}_s(x) E_f^{-3/4} \right. \\
 & \left. + \kappa^{-2} E_{i;0} E_f^{-1/2} + \kappa^{-2} \sum_{k=1}^{k_{\max}} \frac{E_{i;0} + k H_{ii;0}}{\tau^{2k} E_f^{(k+1)/2}} x^{2k} \right), \\
 & \hat{\mathbf{A}}_{ij} = \kappa^{-2} \sum_{k=1}^{k_{\max}} \left( \frac{\tilde{U}_{ij;k} + k H_{ij;0}}{\tau^{2k} E_f^{(k+1)/2}} x_s^{2k} \right. \\
 & \left. + \frac{Q_{ij;0}}{\tau^{2k-1} E_f^{k/2}} \left( (2k-1) x^{2k-2} + 2x^{2k-1} \frac{d}{dx} \right) \right),
 \end{aligned} \quad (21)$$

where  $\kappa = 2$  and  $\tilde{V}_s(x_s) = 0$  for OSQD;  $\kappa = 1$  and  $\tilde{V}_s(x) = \gamma_F x$  for PSQD. Applying the relations (17) or (19) to get first the derivatives of the basis functions, we get the expressions for the action of operators  $\hat{\mathbf{A}}_{ij}$ :

$$\hat{\mathbf{A}}_{ij} \Phi_q^{(0)}(x) = \sum_{q'=0}^{q_{\max}} \alpha_{ij;qq'} \Phi_{q'}^{(0)}(x) \quad (22)$$

and, hence, the algebraic eigenvalue problem with

respect to the unknown  $E_t$  and  $b_{j,q;t}$

$$\begin{aligned}
 & \sum_{q=0}^{q_{\max}} \alpha_{ii;q'q} b_{i,q;t} + \sum_{j \neq i=1}^{j_{\max}} \sum_{q=0}^{q_{\max}} \alpha_{ij;q'q} b_{j,q;t} \\
 & = \kappa^{-2} \mathcal{E}_t E_f^{-1/2} b_{i,q;t}.
 \end{aligned} \quad (23)$$

In the matrix form it reads as

$$\mathbf{A} \mathbf{B}_t = \kappa^{-2} \mathcal{E}_t E_f^{-1/2} \mathbf{B}_t, \quad \mathbf{B}_t^T \mathbf{B}_t = \delta_{tt'},$$

where  $\mathbf{B}_t = (b_{1,0;t}, b_{1,1;t}, \dots, b_{1,q_{\max};t}, b_{2,0;t}, \dots, b_{j_{\max},q_{\max};t})^T$  is a vector with dimension of  $j_{\max}(q_{\max} + 1)$ , and  $\mathbf{A}$  is a positive defined symmetric matrix having the dimensions  $(j_{\max}(q_{\max} + 1)) \times (j_{\max}(q_{\max} + 1))$  with the elements  $A_{(q_{\max}+1)(i-1)+q+1, (q_{\max}+1)(j-1)+q'+1} = \alpha_{ij;qq'}$ .

Note, that the approximation with nonzero elements on the diagonal of the matrix  $\mathbf{A} = \{\alpha_{ii;q'q}\}_{q',q=0}^{(q_{\max})} \delta_{i=i_0, j=i_0}$ , obtained by the action of the diagonal operator  $\hat{\mathbf{A}}_{ii}$ , Eq. (21), on the basis function  $\Phi_q^{(0)}(x)$ , Eq. (22), gives the diagonal adiabatic approximation (AA) of PTLJ solution (23), i.e.,  $\mathcal{E}_t \approx \mathcal{E}_{i;n}$ ,  $n = 0, 1, \dots$ , at each fixed  $i$ . Such adiabatic classification of the eigenenergies is used in tables discussed below.

The convergence of eigenenergies of Eq. (23) vs the order  $k_{\max}$  of approximation of the effective potentials (14) for  $j_{\max} = 4$  and  $q_{\max} = 60$  is shown in Tables 3 and 4 for OSQD, PSQD, and SQD at  $\gamma_F = 0$  and in Table 5 at  $\gamma_F = -10$  for PSQD and SQD. Table 4 shows that for PSQD we have upper estimate and monotonic convergence with increasing  $k_{\max}$  to the numerical results at  $j_{\max} = 4$ . Similar behavior is observed for OSQD, however, the accuracy of approximation of the effective potentials is worse, especially for the lowest effective potential  $i' = 1$ , corresponding to the ground state of the fast subsystem, because the upper estimates are violated. These tables show also that such expansions have faster

**Table 4.** The convergence of eigenenergies  $\mathcal{E}_t$  of Eq. (23) vs order  $k_{\max}$  of approximation of effective potentials from (14) for  $j_{\max} = 4$  and  $q_{\max} = 60$  basis functions at  $\gamma_F = 0$  (Fast and slow variables  $x_f = \rho$  and  $x_s = z$  (*prolate* spheroidal QD and spherical QD), number of nodes  $i = (n_{pp}, n_{zp})$ )

$k_{\max}$	$c = 2.5, a = 0.5$			$c = 2.5, a = 2.5$		
$(n_{pp}, n_{zp})$	(0, 0)	(0, 2)	(1, 0)	(0, 0)	(0, 2)	(1, 0)
8	25.17914	34.07677	126.4459	1.471911	4.270174	5.614892
12	25.19962	34.46884	126.4560	1.536121	4.716984	6.188144
20	25.20116	34.52202	126.4561	1.563492	5.182198	6.266533
$N(j_{\max} = 4)$	25.20121	34.52512	126.4561	1.579239	5.316732	6.317058

**Table 5.** The convergence of eigenenergies  $\mathcal{E}_t$  of Eq. (23) vs order  $k_{\max}$  of approximation of effective potentials from (14) for  $j_{\max} = 4$  and  $q_{\max} = 60$  basis functions at  $\gamma_F = -10$  (Fast and slow variables  $x_f = \rho$  and  $x_s = z$  (*prolate* spheroidal QD and spherical QD), number of nodes  $i = (n_{pp}, n_{zp})$ )

$k_{\max}$	$c = 2.5, a = 0.5$			$c = 2.5, a = 2.5$		
$(n_{pp}, n_{zp})$	(0, 0)	(0, 2)	(1, 0)	(0, 0)	(0, 2)	(1, 0)
8	20.22165	30.91336	125.3062	-19.67398	-5.378707	-1.784110
12	20.60733	32.37540	125.3316	-15.34850	-6.881266	-2.605091
20	20.65846	32.67445	125.3322	-12.19445	-2.204160	-1.336853
$N(j_{\max} = 4)$	20.66203	32.70877	125.3322	-10.84402	-1.511063	1.129039

convergence for strongly oblate or prolate spheroidal QDs than for spherical ones.

#### 4. PTRS FOR BVP FOR OSQD IN ELECTRIC FIELD BY FAST VARIABLES

To have an analytic representation of the matrix elements (11) for small  $\gamma_F$ , one can use  $\check{V}_f(x_f; x_s) = 2\gamma_F z$ ,  $\check{V}_{fs}(x_f, x_s) = 0$  as potentials for OSQD instead of the potentials (12) introduced in Section 2.1. Then we arrive at the Sturm–Liouville problem for the OSQD in fast variable expressed in the form

$$\left(-\frac{d^2}{dz^2} - \epsilon z - E_j(\rho)\right) B_j(z; \rho) = 0, \quad (24)$$

$$\langle B_i(\rho) | B_j(\rho) \rangle = \int_{-L(\rho)/2}^{L(\rho)/2} B_i(z; \rho) B_j(z; \rho) dz = \delta_{ij},$$

where  $\epsilon = \gamma_F$  is the electric field strength considered here as a formal parameter of the PT, implying a small interval  $\rho \in (0, L(\rho) = 2c\sqrt{1 - \rho^2/a^2})$  of the scalar

product  $\langle B_i(\rho) | B_j(\rho) \rangle$ . The solutions  $B_j^{(0)}(z; \rho)$  and  $E_j^{(0)}(\rho)$  of the unperturbed equation (at  $\epsilon = 0$ ) have the form

$$\{B_j^{(0)}(z; \rho), E_j^{(0)}(\rho)\} \quad (25)$$

$$= \begin{cases} \{B_j^s(z; \rho), E_j^s(\rho)\}, & \text{for even } j = 2, 4, \dots, \\ \{B_j^c(z; \rho), E_j^c(\rho)\}, & \text{for odd } j = 1, 3, \dots, \end{cases}$$

where

$$B_j^s(z; \rho) = \sqrt{2/L(\rho)} \sin(\pi j z / L(\rho)),$$

$$B_j^c(z; \rho) = \sqrt{2/L(\rho)} \cos(\pi j z / L(\rho)),$$

$$E_j^s(\rho) = (\pi j / L(\rho))^2, \quad E_j^c(\rho) = (\pi j / L(\rho))^2.$$

We seek for the eigenfunctions  $B_j(z; \rho)$  and the eigenvalues  $E_j(\rho)$  in the form of power expansions

$$B_j(z; \rho) = \sum_{k=0}^{k_{\max}} \epsilon^k B_j^{(k)}(z; \rho), \quad (26)$$

$$E_j(\rho) = \sum_{k=0}^{k_{\max}} \epsilon^k E_j^{(k)}(\rho).$$

Substituting Eq. (26) into Eqs. (24) and equating the coefficients at the same powers of  $\epsilon$ , we arrive at the system of inhomogeneous differential equations with respect to corrections  $E_j^{(k)}$  and  $B_j^{(k)}(z; \rho)$ :

$$\begin{aligned} & \left( -\frac{d^2}{dz^2} - E_j^{(0)}(\rho) \right) B_j^{(k)}(z; \rho) \\ & = \left( z + E_j^{(1)}(\rho) \right) B_j^{(k-1)}(z; \rho) \end{aligned} \quad (27)$$

$$\begin{aligned} & + \sum_{p=2}^k E_j^{(p)}(\rho) B_j^{(k-p)}(z; \rho), \\ & \sum_{p=0}^k \langle B_j^{(p)}(\rho) | B_j^{(k-p)}(\rho) \rangle = 0. \end{aligned}$$

In each  $k$ th order of the PT the solutions becoming zero at the boundary points ( $z = \pm L(\rho)/2$ ) are sought in the form

$$B_j^{(k)}(z; \rho) = \begin{cases} \sum_{\nu=0}^{\nu_{\max}} B_j^s(z; \rho) S_{\nu}^{(k)} z^{\nu} + (z^2 - (L(\rho)/2)^2) \sum_{\nu=0}^{\nu_{\max}-2} B_j^c(z; \rho) C_{\nu+2}^{(k)} z^{\nu}, & j = 2, 4, \dots, \\ \sum_{\nu=0}^{\nu_{\max}} B_j^s(z; \rho) C_{\nu}^{(k)} z^{\nu} + (z^2 - (L(\rho)/2)^2) \sum_{\nu=0}^{\nu_{\max}-2} B_j^c(z; \rho) S_{\nu+2}^{(k)} z^{\nu}, & j = 1, 3, \dots \end{cases} \quad (28)$$

Substituting Eq. (28) into the corresponding equation (27) of the  $k$ th order of the PT, and extracting the coefficients at  $B_j^s(z; \rho) z^{\nu}$  and  $B_j^c(z; \rho) z^{\nu}$ ,  $\nu = 0, \dots, \nu_{\max}$ , we arrive at the set of algebraic equations with respect to unknowns  $E_j^{(k)}(\rho)$ ,  $S_{\nu}^{(k)}$ , and  $C_{\nu}^{(k)}$ , for even  $j$ :

$$\begin{aligned} & -(-1)^j (\nu+1) (L(\rho)/2) \pi j C_{\nu+3}^{(k)} \\ & - (\nu+2)(\nu+1) S_{\nu+2}^{(k)} + (-1)^j \cdot 2(\nu+1) \pi j C_{\nu+1}^{(k)} \\ & - E_j^{(1)}(\rho) S_{\nu}^{(k-1)} - S_{\nu-1}^{(k-1)} - \sum_{p=2}^{k-1} E_j^{(p)}(\rho) S_{\nu}^{(k-p)} \\ & - E_j^{(k)}(\rho) \delta_{\nu,0} = 0, \\ & (\nu+1)(\nu+2) (L(\rho)/2)^2 C_{\nu+4}^{(k)} \\ & - (\nu+2)(\nu+1) C_{\nu+2}^{(k)} - (-1)^j \cdot 2(\nu+1) \pi j S_{\nu+1}^{(k)} \\ & - E_j^{(1)}(\rho) (C_{\nu}^{(k-1)} - (L(\rho)/2)^2 C_{\nu+2}^{(k-1)}) \\ & - C_{\nu-1}^{(k-1)} + (L(\rho)/2)^2 C_{\nu+1}^{(k-1)} \\ & - \sum_{p=2}^{k-1} E_j^{(p)}(\rho) (C_{\nu}^{(k-p)} - (L(\rho)/2)^2 C_{\nu+2}^{(k-p)}) = 0. \end{aligned}$$

For odd  $j$  the same unknowns are calculated using these equations with the replacement  $C^{(p)} \leftrightarrow S^{(p)}$ . The unknowns  $C_0^{(k)}$  for odd  $j$  are determined from the

respective conditions:

$$\begin{aligned} & \sum_{p=0}^k \sum_{\nu, \nu'} \left( S_{\nu}^{(p)} S_{\nu'}^{(k-p)} \langle B_j^s(\rho) | z^{\nu+\nu'} | B_j^s(\rho) \rangle \right. \\ & + [(C_{\nu}^{(p)} S_{\nu'}^{(k-p)} + S_{\nu}^{(p)} C_{\nu'}^{(k-p)}) \\ & + (L(\rho)/2)^2 (C_{\nu+1}^{(p)} S_{\nu'+1}^{(k-p)} \\ & + S_{\nu+1}^{(p)} C_{\nu'+1}^{(k-p)})] \langle B_j^s(\rho) | z^{\nu+\nu'} | B_j^c(\rho) \rangle \\ & + [(C_{\nu}^{(p)} C_{\nu'}^{(k-p)} - 2(L(\rho)/2)^2 C_{\nu+1}^{(p)} C_{\nu'+1}^{(k-p)} \\ & + (L(\rho)/2)^4 C_{\nu+2}^{(p)} C_{\nu'+2}^{(k-p)})] \langle B_j^c(\rho) | z^{\nu+\nu'} | B_j^c(\rho) \rangle \Big) = 0, \end{aligned} \quad (29)$$

and  $S_0^{(k)}$  for even  $j$  is calculated from the Eq. (29) with the replacement  $C^{(p)} \leftrightarrow S^{(p)}$ . This algorithm was implemented using the Maple environment. The run was performed until the maximal order of the PT  $k_{\max} = 8$ . Below we present the first few coefficients of the eigenvalue expansion, truncated by the terms proportional to  $\epsilon^6 = \gamma_F^6$

$$\begin{aligned} E_j(\rho) &= \frac{\pi^2 j^2}{(L(\rho))^2} \\ &+ \frac{(L(\rho))^4 (\pi^2 j^2 - 15)}{48 \pi^4 j^4} \epsilon^2 \\ &+ \frac{(L(\rho))^{10} (1980 - 210 \pi^2 j^2 + \pi^4 j^4)}{2304 \pi^{10} j^{10}} \epsilon^4, \end{aligned} \quad (30)$$

the eigenfunctions truncated by the terms proportional to  $\epsilon^2 = \gamma_F^2$

$$B_j(z; \rho) = \begin{cases} B_j^s(z; \rho) + \left( -\frac{(L(\rho))^2 z B_j^s(z; \rho)}{4\pi^2 j^2} + \frac{L(\rho)(z^2 - (L(\rho)/2)^2) B_j^c(z; \rho)}{4\pi j} \right) \epsilon, & j = 2, 4, \dots, \\ B_j^c(z; \rho) + \left( -\frac{(L(\rho))^2 z B_j^c(z; \rho)}{4\pi^2 j^2} - \frac{L(\rho)(z^2 - (L(\rho)/2)^2) B_j^s(z; \rho)}{4\pi j} \right) \epsilon, & j = 1, 3, \dots, \end{cases}$$

and the diagonal effective potentials, truncated by the terms proportional to  $\epsilon^6 = \gamma_F^6$

$$H_{jj}(z) = \left( \frac{dL(\rho)}{d\rho} \right)^2 \left( \frac{\pi^2 j^2 + 3}{12(L(\rho))^2} + \frac{(L(\rho))^4 (-2880 + 258\pi^2 j^2 + 7\pi^4 j^4)}{576\pi^6 j^6} \epsilon^2 \right. \\ \left. + \frac{L(\rho)^{10} (3510000 - 389880\pi^2 j^2 + 3321\pi^4 j^4 + 13\pi^6 j^6)}{27648\pi^{12} j^{12}} \epsilon^4 \right). \quad (31)$$

## 5. THE PTRS IN THE DIAGONAL ADIABATIC APPROXIMATION

The desired solutions of the original 2D BVP (4) are determined by the diagonal approximation of the Kantorovich expansion (7) at fixed  $m$

$$\Psi_{i;n}^m(x_f, x_s) \approx B_i(x_f; x_s) \chi_{i;n}(x_s).$$

The diagonal approximation of the BVP (9) and (10) in the slow variable has the form

$$\left( -\frac{1}{x_s^d} \frac{d}{dx_s} x_s^d \frac{d}{dx_s} + \frac{\tilde{m}}{x_s^2} + V_i(x_s) - \mathcal{E}_{i;n} \right) \quad (32) \\ \times \chi_{i;n}(x_s) = 0.$$

and the eigenfunctions satisfy the orthonormalization conditions on the semiaxis  $[x_s^{\min} = 0, x_s^{\max} = \infty)$  at  $d=1$  for the OSQD and on the axis  $(x_s^{\min} = -\infty, x_s^{\max} = \infty)$  at  $d=0$  for the OSQD

$$\int_{x_s^{\min}}^{x_s^{\max}} \chi_{i;n}(x_s) \chi_{i;n'}(x_s) (x_s)^d dx_s = \delta_{nn'}. \quad (33)$$

Here  $V_i(x_s) = \check{V}_s(x_s) + E_i(x_s) + DH_{ii}(x_s)$ , where the parameter  $D$  is  $D=0$  for the crude adiabatic ap-

proximation and  $D=1$  for the adiabatic approximation;  $\check{V}_s(x_s) = 0$ ,  $E_i(x_s)$  and  $H_{ii}(x_s)$ , Eqs. (30), (31), for OSQD and  $\check{V}_s(x_s) = 2\gamma_F z$ ,  $E_i(x_s)$  and  $H_{ii}(x_s)$ , Eq. (13), for PSQD;  $\mathcal{E}_{i;n}$  are the eigenenergies of a lower part of the spectrum  $\mathcal{E}_{i;0} < \mathcal{E}_{i;1} < \dots < \mathcal{E}_{i;n}$  enumerated in the ascending order by the number of nodes  $n = 0, 1, 2, \dots$  of the eigenfunctions  $\chi_{i;n}(x_s)$  at fixed adiabatic quantum numbers  $i = n_o$  for OSQD and  $i = n_p$  for PSQD. The potential function  $V_i(x_s)$  is expanded in powers of the small parameter  $\epsilon$

$$V_i^{[j_{\max}]}(x_s) = V_i^{(0)} + \kappa^{-2} \omega_i^2 x_s^2 \quad (34)$$

$$+ \kappa^{-2} \sum_{j=1}^{j_{\max}} V_i^{(j)}(x_s) \epsilon^j.$$

For OSQD at the values of the parameters  $d=1$ ,  $\epsilon = c^{-2}$ ,  $\kappa = 2$ ,  $\tilde{m} = m$  the coefficients  $V_i^{(j)}$  are determined by Taylor expansion of the effective potentials (30), (31) in the vicinity of the equilibrium point  $x_s = 0$ . With the accuracy up to order of  $O(\gamma_F^6)$  the coefficients  $V_i^{(j)}$  and  $\omega_i^2$  are expressed as:

$$V_i^{(0)} = \frac{\pi^2 n_o^2}{4c^2} + \gamma_F^2 \frac{c^4 (\pi^2 n_o^2 - 15)}{3\pi^4 n_o^4} + \gamma_F^4 \frac{4c^{10} (\pi^4 n_o^4 - 210\pi^2 n_o^2 + 1980)}{9\pi^{10} n_o^{10}}, \quad (35) \\ \omega_i^2 = \frac{\pi^2 n_o^2}{(ac)^2} + D \frac{3 + \pi^2 n_o^2}{a^4} + \gamma_F^2 \left( -\frac{8c^4 (\pi^2 n_o^2 - 15)}{3a^2 \pi^4 n_o^4} + D \frac{4c^6 (7\pi^4 n_o^4 + 258\pi^2 n_o^2 - 2880)}{9a^4 \pi^6 n_o^6} \right) \\ + \gamma_F^4 \left( -\frac{80c^{10} (\pi^4 n_o^4 - 210\pi^2 n_o^2 + 1980)}{9a^2 \pi^{10} n_o^{10}} + D \frac{16c^{12} (13\pi^6 n_o^6 + 3321\pi^4 n_o^4 - 389880\pi^2 n_o^2 - 3510000)}{27a^4 \pi^{12} n_o^{12}} \right), \\ V_i^{(j)} = \left( \frac{\pi^2 n_o^2}{(ac)^2} + jD \frac{3 + \pi^2 n_o^2}{a^4} + \gamma_F^2 \left( -\frac{4c^4 (\pi^2 n_o^2 - 15)}{3a^4 \pi^4 n_o^4} \delta_{i2} - D \frac{4c^6 (7\pi^4 n_o^4 + 258\pi^2 n_o^2 - 2880)}{9a^6 \pi^6 n_o^6} \delta_{i2} \right) \right)$$

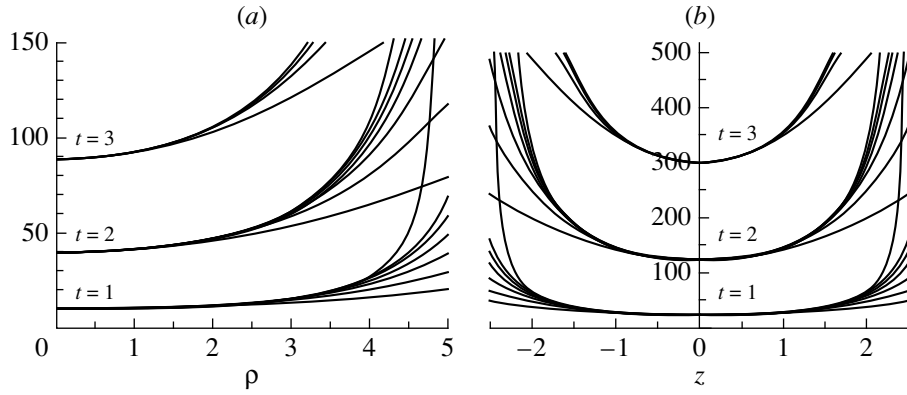


**Fig. 3.** Three potential functions  $V_i(x_s)$  for (a) oblate  $x_s = \rho$  and (b) prolate  $x_s = z$  spheroids and their power expansions till sixth order with account of adiabatic frequencies  $\omega_i$  and lower bound shifts  $V_i^{(0)}$ .

$$+ \gamma_F^4 \left( \frac{16c^{10}(\pi^4 n_o^4 - 210\pi^2 n_o^2 + 1980)}{9a^4 \pi^{10} n_o^{10}} \left( 10\delta_{i2} - 10\frac{\delta_{i3}}{a^2} + 5\frac{\delta_{i4}}{a^4} - \frac{\delta_{i5}}{a^6} \right) \right. \\ \left. + D \frac{16c^{12}(13\pi^6 n_o^6 + 3321\pi^4 n_o^4 - 389880\pi^2 n_o^2 - 3510000)}{27a^6 \pi^{12} n_o^{12}} \left( -4\delta_{i2} + 6\frac{\delta_{i3}}{a^2} - 4\frac{\delta_{i4}}{a^4} + \frac{\delta_{i5}}{a^6} \right) \right) x_s^{2j+2}.$$

For PSQD at the values of the parameters  $d = 0$ ,  $\varepsilon = 1$ ,  $\kappa = 1$ ,  $\tilde{m} = 0$  the coefficients  $V_i^{(j)}$  are sought in the form of a Taylor expansion in powers of  $\bar{x}_s = (x_s - x_0)$  and  $\gamma_F$  of the effective potentials  $V_i(x_s, \gamma_F) = E_j(x_s) + DH_{jj}(x_s) + \gamma_F x_s$ , Eq. (13). The expansion coefficients  $x_0 = \sum_k \tau_{2k+1} \gamma_F^{2k+1}$  are sought from the equilibrium condition

$$\left. \frac{\partial V_i(x_s, \gamma_F)}{\partial x_s} \right|_{x_s=x_0} = 0$$

at fixed  $\gamma_F$ . With the accuracy up to  $O(\gamma_F^5)$  the coefficients  $V_i^{(j)}$  and  $\omega_i^2$  are expressed as:

$$V_i^{(0)} = -2\tau_1 \gamma_F^2 - 2\tau_3 \gamma_F^4 + \alpha_{n_p, |m|}^2 / (a^2) \quad (36) \\ + D(1 + \alpha_{n_p, |m|}^2) / (3c^4) + \gamma_F^2 \tau_1^2 (\alpha_{n_p, |m|}^2 / (a^2 c^2) \\ + D(1 + \alpha_{n_p, |m|}^2) 2 / (3c^4)) \\ + \gamma_F^4 \tau_1 (\alpha_{n_p, |m|}^2 (\tau_1^3 + 2c^2 \tau_3) / (a^2 c^4) \\ + 2D(1 + \alpha_{n_p, |m|}^2) (\tau_1^3 + \tau_3 c^2) / (3c^6)), \\ \omega_i^2 = \left( \alpha_{n_p, |m|}^2 / (a^2 c^2) + D(1 + \alpha_{n_p, |m|}^2) / (3c^4) \right. \\ + \gamma_F^2 \tau_1^2 \cdot 6(\alpha_{n_p, |m|}^2 / (a^2 c^4) \\ + D(1 + \alpha_{n_p, |m|}^2) 2 / (3c^6)) \\ + \gamma_F^4 \tau_1 (\alpha_{n_p, |m|}^2 (15\tau_1^3 + 12c^2 \tau_3) / (a^2 c^6) \\ + D(1 + \alpha_{n_p, |m|}^2) (15\tau_1^3 + 8\tau_3 c^2) / (c^8)) \Big),$$

$$V_i^{(j)} = \left( + 2\gamma_F \tau_1 ((i+1)\alpha_{n_p, |m|}^2 / (a^2 c^{2i+2}) \right. \\ + D(i+1)^2 (1 + \alpha_{n_p, |m|}^2) / (3c^{2i+4})) \\ + 2\gamma_F^3 (i+1) \left( \alpha_{n_p, |m|}^2 ((2i^2 + 7i + 6)\tau_1^3 \right. \\ + 3\tau_3 c^2) / (3a^2 c^{2i+4}) \Big) + D(1 + \alpha_{n_p, |m|}^2) \\ \times ((2i^3 \tau_1^3 + 11i^2 + 20i + 12)\tau_1^3 \\ + 3(i+1)\tau_3 c^2) / (9c^{2i+6}) \Big) \bar{x}_s^{2i+1} \\ + \left( \alpha_{n_p, |m|}^2 / (a^2 c^{2i+2}) + D(1 + \alpha_{n_p, |m|}^2) \right. \\ \times (i+1) / (3c^{2i+4}) + \gamma_F^2 \tau_1^2 (i+2)(2i+3) \\ \times (\alpha_{n_p, |m|}^2 (a^2 c^{2i+4}) + D(1 + \alpha_{n_p, |m|}^2) \\ \times (i+2) / (3c^{2i+6})) + \gamma_F^4 \tau_1 (i+2) \\ \times (2i+3) \left( \alpha_{n_p, |m|}^2 ((2i^2 + 11i \right. \\ + 15)\tau_1^3 + 12c^2 \tau_3) / (6a^2 c^{2i+6}) \Big) \\ + D(1 + \alpha_{n_p, |m|}^2) ((2i^3 + 17i^2 + 48i \\ + 45)\tau_1^3 + 12(i+2)\tau_3 c^2) / (18c^{2i+8}) \Big) \bar{x}_s^{2i+2},$$

where  $\tau_{2k+1}$  is determined from the condition that the coefficient at  $\bar{x}_s$  is zero:

$$\tau_1 = \frac{3a^2c^4}{3c^2\alpha_{n_p,|m|}^2 + Da^2(1 + \alpha_{n_p,|m|}^2)}, \quad \tau_3 = -\frac{54a^6c^{10}(3c^2\alpha_{n_p,|m|}^2 + 2Da^2(1 + \alpha_{n_p,|m|}^2))}{(3c^2\alpha_{n_p,|m|}^2 + Da^2(1 + \alpha_{n_p,|m|}^2))^4}.$$

In Fig. 3 we show three potential functions  $V_i(x_s)$  for *oblate*  $x_s = \rho$  and *prolate*  $x_s = z$  spheroids and the convergence of the corresponding power expansions till the sixth order with account of *adiabatic frequencies*  $\omega_i$  and *lower bound shifts*  $V_i^{(0)}$ .

We choose the unperturbed operators of Eq. (32) at  $\varepsilon = 0$  in the expansion (34) in the form (16)–(19) with the eigenvalues and the basis functions of 2D and 1D oscillators given in Section 3 with respect to the scaled coordinate  $x$ ,  $x_s = \sqrt{2x/\omega_i}$  and  $\bar{x}_s = x/\sqrt{\omega_i}$ , where the adiabatic frequencies  $\omega_i$  are defined by Eqs. (35) and (36) (at fixed  $i' = n + 1$ ), respectively. According to (34), we seek for the eigenfunctions  $\chi_{i;n}(x_s)$  and the eigenvalues  $\mathcal{E}_{i;n}$  in the form of expansions in powers of  $\varepsilon$  with unknowns  $\Phi_n^{(k)}$  and  $E_n^{(k)}$ , omitting the notation  $m$  for brevity:

$$\chi_{i;n}(x_s) = \Phi_n^{(0)} + \sum_{k=1}^{k_{\max}} \Phi_n^{(k)}(x_s)\varepsilon^k, \quad (37)$$

$$\mathcal{E}_{i;n} = V_i^{(0)} + \sum_{k=0}^{k_{\max}} \mathcal{E}_{i;n}^{(k)} = V_i^{(0)} \quad (38)$$

$$+ \kappa\omega_i \left( E_i^{(0)} + \sum_{k=1}^{k_{\max}} E_n^{(k)}\varepsilon^k \right).$$

Substituting the expansions (34), (37), and (38) into Eq. (32) and equating the terms with the same power of the parameter  $\varepsilon$ , we arrive at the recurrence set of inhomogeneous equations of the PT with respect to the unknowns  $E_n^{(k)}$  and  $\Phi_n^{(p)}(x)$ :

$$L(n)\Phi_n^{(0)}(x) = 0 \equiv f^{(0)}(x), \quad (39)$$

$$L(n)\Phi_n^{(k)}(x) = \sum_{p=0}^{k-1} (E_n^{(k-p)} - V_i^{(k-p)})\Phi_n^{(p)}(x) \\ \equiv f^{(k)}(x), \quad k \geq 1,$$

with the initial conditions (16) and (18) for OSQD and PSQD, respectively. The solution of this problem is implemented in four steps.

Applying the relations (17) and (19), we expand the right-hand side  $f^{(k)}(x)$  and the solutions  $\Phi^{(k)}(x)$  of Eqs. (39) over the basis of normalized states  $\Phi_{n+s}^{(0)}(x)$ , Eqs. (16) and (18):

$$\Phi_n^{(k)}(x) = \sum_{s=-s_{\max}}^{s_{\max}} b_s^{(k)}\Phi_{n+s}^{(0)}(x), \quad f^{(k)}(x) = \sum_{s=-s_{\max}}^{s_{\max}} f_s^{(k)}\Phi_{n+s}^{(0)}(x). \quad (40)$$

Then a recurrent set of linear algebraic equations for unknown coefficients  $b_s^{(k)}$  and corrections  $E^{(k)}$  is obtained

$$s'b_s^{(k)} - f_s^{(k)} = 0, \quad s = -s_{\max}, \dots, s_{\max}, \quad (41)$$

where  $s' = s$  for OSQD and  $s' = 2s$  for PSQD. These equations are solved sequentially for  $k = 1, 2, \dots, k_{\max}$ :

$$f_0^{(k)} = 0 \rightarrow E^{(k)}; \quad b_s^{(k)} = f_s^{(k)}/s', \quad s = -s_{\max}, \dots, s_{\max}, \quad s \neq 0. \quad (42)$$

The initial conditions for this procedure are

$$b_s^{(0)} = \delta_{s0}, \quad E^{(0)} = (n + (|\tilde{m}| + 1)/2) \quad \text{or} \quad E^{(0)} = (n + 1)/2.$$

To obtain the normalized wave function  $\Phi_j(x)$  up to the  $k$ th order, the coefficients  $b_0^{(k)}$  are determined by the following relation:

$$b_0^{(k)} = -\frac{1}{2\langle 0|0\rangle} \sum_{p=1}^{k-1} \sum_{s'=-s_{\max}}^{s_{\max}} \sum_{s=-s_{\max}}^{s_{\max}} b_s^{(k-p)} \langle s|s'\rangle b_{s'}^{(p)}. \quad (43)$$

The above scheme implemented in Maple was applied to the evaluations of solutions in the analytical form up to the order  $k_{\max} = 6$  of the PTRS. The first four nonzero coefficients for the energy (38) *in the analytic form*, truncated by the terms proportional

to the sixth power of the electric field strength,  $\gamma_F^6$ , in the CAA take the form:

1) For OSQD in terms of minor  $c$  and major  $a$  semiaxes; the set of adiabatic quantum numbers  $[m, n_o = n_{zo} + 1, n_{\rho o}]$

$$\begin{aligned}
 V_{n_o}^{(0)} &= \frac{\pi^2 n_o^2}{4c^2} + \gamma_F^2 \frac{c^4(\pi^2 n_o^2 - 15)}{3\pi^4 n_o^4} + \gamma_F^4 \frac{4c^{10}(\pi^4 n_o^4 - 210\pi^2 n_o^2 + 1980)}{9\pi^{10} n_o^{10}}, \\
 \mathcal{E}_{n_o; n_{\rho o}}^{(0)} &= \left[ \frac{\pi n_o}{ac} - \gamma_F^2 \frac{4c^5(\pi^2 n_o^2 - 15)}{3a\pi^5 n_o^5} - \gamma_F^4 \frac{8c^{11}(2\pi^4 n_o^4 - 360\pi^2 n_o^2 + 3375)}{3a\pi^{11} n_o^{11}} \right] (2n_{\rho o} + |m| + 1), \\
 \mathcal{E}_{n_o; n_{\rho o}}^{(1)} &= \left[ \frac{1}{a^2} + \gamma_F^2 \frac{4c^6(\pi^2 n_o^2 - 15)}{\pi^6 n_o^6 a^2} + \gamma_F^4 \frac{16c^{12}(7\pi^4 n_o^4 - 1110\pi^2 n_o^2 + 10350)}{3\pi^{12} n_o^{12} a^2} \right] \\
 &\quad \times (2 + 6n_{\rho o} + 3|m| + 6n_{\rho o}^2 + |m|^2 + 6n_{\rho o}|m|), \\
 \mathcal{E}_{n_o; n_{\rho o}}^{(2)} &= (2n_{\rho o} + |m| + 1) \left[ \frac{3c}{2\pi a^3 n_o} (2 + 2n_{\rho o} + |m| + 2n_{\rho o}^2 + 2n_{\rho o}|m|) \right. \\
 &\quad - \gamma_F^2 \frac{2c^7(\pi^2 n_o^2 - 15)}{3\pi^7 n_o^7 a^3} (54 + 118n_{\rho o} + 16|m|^2 + 59|m| + 118n_{\rho o}^2 + 118n_{\rho o}|m|) \\
 &\quad - \gamma_F^4 \left( \frac{4c^{13}(1874\pi^4 n_o^4 - 273120\pi^2 n_o^2 + 2536425)}{9\pi^{13} n_o^{13} a^3} (2n_{\rho o} + |m| + 2n_{\rho o}^2 + 2n_{\rho o}|m|) \right. \\
 &\quad \left. \left. + \frac{224c^{13}(8\pi^4 n_o^4 - 1140\pi^2 n_o^2 + 10575)}{9\pi^{13} n_o^{13} a^3} |m|^2 + \frac{8c^{13}(326\pi^4 n_o^4 - 48480\pi^2 n_o^2 + 450675)}{3\pi^{13} n_o^{13} a^3} \right) \right],
 \end{aligned} \tag{44}$$

2) For PSQD in terms of minor  $a$  and major  $c$  semiaxes, the set of adiabatic quantum numbers  $[m, n_p = n_{\rho p} + 1, n_{zp}]$  and positive zeros  $\alpha_{n_p, |m|}$  of the Bessel functions of the first kind [37]

$$\begin{aligned}
 V_{n_p; n_{zp}}^{(0)} &= \frac{\alpha_{n_p, |m|}^2}{a^2} - \gamma_F^2 \frac{a^2 c^2}{4\alpha_{n_p, |m|}^2} + \gamma_F^4 \frac{a^6 c^4}{16\alpha_{n_p, |m|}^6}, \\
 \mathcal{E}_{n_p; n_{zp}}^{(0)} &= \left[ \frac{\alpha_{n_p, |m|}}{ac} + \gamma_F^2 \frac{3a^3 c}{4\alpha_{n_p, |m|}^3} - \gamma_F^4 \frac{9a^7 c^3}{16\alpha_{n_p, |m|}^7} \right] (2n_{zp} + 1), \\
 \mathcal{E}_{n_p; n_{zp}}^{(1)} &= \left[ \frac{3}{4c^2} + \gamma_F^2 \frac{27a^4}{16\alpha_{n_p, |m|}^4} - \gamma_F^4 \frac{105a^8 c^2}{64\alpha_{n_p, |m|}^8} \right] (2n_{zp}^2 + 2n_{zp} + 1), \\
 \mathcal{E}_{n_p; n_{zp}}^{(2)} &= \frac{3a}{16c^3 \alpha_{n_p, |m|}} (2n_{zp} + 1)(n_{zp}^2 + n_{zp} + 3) \\
 &\quad + \gamma_F^2 \left( \frac{5a^5}{64c\alpha_{n_p, |m|}^5} (2n_{zp} + 1)(25n_{zp}^2 + 25n_{zp} + 51) - \frac{a^4}{4\alpha_{n_p, |m|}^4} (30n_{zp}^2 + 30n_{zp} + 11) \right) \\
 &\quad - \gamma_F^4 \left( \frac{45a^9 c}{256\alpha_{n_p, |m|}^9} (2n_{zp} + 1)(23n_{zp}^2 + 23n_{zp} + 37) - \frac{3a^8 c^2}{8\alpha_{n_p, |m|}^8} (30n_{zp}^2 + 30n_{zp} + 11) \right).
 \end{aligned} \tag{45}$$

In Tables 6 and 7 we demonstrate how the approximate eigenvalues in the lower part of spectrum for OSQD and PSQD at  $m = 0$  and  $\gamma_F = 0$  converge to the values calculated numerically with required

accuracy in the crude adiabatic approximation with increasing of the PT order  $k$ . The accuracy was from 8 to 5 digits at  $n_{zo} = 0$ , from 10 to 8 digits at  $n_{zo} = 2$ , from 6 to 4 digits at  $n_{\rho p} = 0$ , and from 8

**Table 6.** Convergence of eigenvalues  $\mathcal{E}_{n_{zo}, n_{po}}^{(k_{\max})} = V_{n_{zo}}^{(0)} + \sum_{k=0}^{k_{\max}} \mathcal{E}_{n_{zo}, n_{po}}^{(k)}$  for *oblate* spheroid  $c = 0.5$ ,  $a = 5$  vs PT order  $k_{\max}$  at  $\gamma_F = 0$  (First line \* notes adiabatic shift  $V_{n_{zo}, n_{po}}^{(0)}$ . Last lines are results of numerical calculations (Num))

$k_{\max}$	$n_{zo} = 0, n_{po} = 0$	$n_{zo} = 0, n_{po} = 1$	$n_{zo} = 0, n_{po} = 2$	$n_{zo} = 0, n_{po} = 3$	$n_{zo} = 0, n_{po} = 4$
*	11.12624146	13.63951558	16.15278970	18.66606383	21.17933795
0	11.20624146	14.19951558	17.67278970	21.62606383	26.05933795
1	11.21006118	14.23389305	17.80647986	21.97365822	26.78126477
2	11.21026382	14.23433886	17.80254859	21.95100281	26.71094787
3	11.21028027	14.23441723	17.80242765	21.94908610	26.70256215
4	11.21028227	14.23443790	17.80265195	21.95065251	26.70959163
5	11.21028259	14.23444049	17.80264785	21.95052291	26.70875037
Num	11.21028268	14.23444147	17.80265065	21.95050805	26.70857727

$k_{\max}$	$n_{zo} = 2, n_{po} = 0$	$n_{zo} = 2, n_{po} = 1$	$n_{zo} = 2, n_{po} = 2$	$n_{zo} = 2, n_{po} = 3$	$n_{zo} = 2, n_{po} = 4$
*	92.59635079	100.1361731	107.6759955	115.2158178	122.7556402
0	92.67635079	100.6961731	109.1959955	118.1758178	127.6356402
1	92.67762403	100.7076323	109.2405589	118.2916826	127.8762825
2	92.67764654	100.7076818	109.2401221	118.2891654	127.8684695
3	92.67764715	100.7076847	109.2401176	118.2890944	127.8681589
4	92.67764718	100.7076850	109.2401203	118.2891137	127.8682457
5	92.67764718	100.7076850	109.2401203	118.2891132	127.8682422
Num	92.67764718	100.7076850	109.2401204	118.2891132	127.8682419

to 7 digits at  $n_{pp} = 1$ , respectively. Note, that the difference between the adiabatic shift  $V_i^{(0)}$  and the eigenvalues  $\mathcal{E}_{i;n} = V_i^{(0)} + \mathcal{E}_{i;n}^{(0)}$  in the zero order  $k = 0$  of the PT is small, but increases with growing  $n_{po}$  and  $n_{zp}$  for OSQD and PSQD, respectively. The shifts  $V_i^{(0)}$  give the main contribution and provide the lower adiabatic estimate of each set of eigenvalues, generated by the perturbed harmonic oscillator terms with adiabatic frequency  $\omega_i$ . From Tables 6 and 7 one can see that with increasing quantum numbers  $n_{zo}$  (or  $n_{pp}$ ), related to the fast variable, the accuracy of approximation of the lower part of the spectrum is increasing. This is because the accuracy of the Taylor approximations of potential function (34) in Eq. (32) is improved with increasing the number  $i = n_{zo} + 1 > 2$  (or  $i = n_{pp} + 1 > 2$ ), which is demonstrated in Fig. 3.

In Figs. 4 and 5 we show the eigenvalues  $\mathcal{E}$  of the lower part of the spectrum of oblate and prolate QDs versus the electric field strength within small (left panels) and large (right panels) intervals of  $\gamma_F$ , calculated in the crude adiabatic approximation (solid and dashed lines) to compare them with the

numerical results (dotted lines). One can see that the eigenvalues calculated using the PT (solid and dashed lines), corresponding to the eigenfunctions with smaller number of nodes along the electric field (i.e., with smaller  $n_{zo}$  for OSQD and  $n_{zp}$  for PSQD) and with greater number of nodes across the electric field (i.e., with greater  $n_{po}$  for OSQD and  $n_{pp}$  for PSQD), provide better approximation of the eigenvalues, calculated numerically with required accuracy (dotted lines). This property follows from the fact that such functions have better localization in the vicinity of the plane, passing through the QD center transverse to the electric field, i.e., in the region with minimal contribution of the electric field potential to the Hamiltonian of the system. As shown in the right panels of Figs. 4 and 5, the differences between the eigenvalues, calculated using the PT and the numerical method, increase faster in a smaller interval of  $\gamma_F$  for larger PSQD than for smaller OSQD, the size being measured along the direction of the electric field.

The range of the parameter values, for which the PT algorithms are valid, was estimated by means of numerical calculations using the KANTBP program



**Table 7.** Convergence of eigenvalues  $\mathcal{E}_{n_{pp}, n_{zp}}^{(k_{\max})} = V_{n_{pp}}^{(0)} + \sum_{k=0}^{k_{\max}} \mathcal{E}_{n_{pp}, n_{zp}}^{(k)}$  for *prolate* spheroid  $c = 2.5$ ,  $a = 0.5$  vs PT order  $k_{\max}$  at  $\gamma_F = 0$  (First lines \* notes adiabatic shift  $V_{n_{pp}, n_{zp}}^{(0)}$ . Last lines are results of numerical calculations (Num))

$k_{\max}$	$n_{pp} = 0, n_{zp} = 0$	$n_{pp} = 0, n_{zp} = 2$	$n_{pp} = 0, n_{zp} = 4$	$n_{pp} = 0, n_{zp} = 6$	$n_{pp} = 0, n_{zp} = 8$
*	25.05660430	32.75204608	40.44748787	48.14292965	55.83837144
0	25.17660430	34.31204608	45.36748787	58.34292965	73.23837144
1	25.18408925	34.42432034	45.88394944	59.80249498	76.41947535
2	25.18465987	34.42810718	45.87103269	59.69485535	76.04779441
3	25.18472054	34.42867746	45.87114189	59.68460238	75.99436976
4	25.18472960	34.42880826	45.87257549	59.69618640	76.05191800
5	25.18473139	34.42883580	45.87259458	59.69511288	76.04351256
Num	25.18472985	34.42884694	45.87265876	59.69512314	76.04210082

$k_{\max}$	$n_{pp} = 1, n_{zp} = 0$	$n_{pp} = 1, n_{zp} = 2$	$n_{pp} = 1, n_{zp} = 4$	$n_{pp} = 1, n_{zp} = 6$	$n_{pp} = 1, n_{zp} = 8$
*	126.3011119	143.9653618	161.6296118	179.2938617	196.9581117
0	126.4211119	145.5253618	166.5496118	189.4938617	214.3581117
1	126.4243727	145.5742742	166.7746086	190.1297223	215.7439616
2	126.4244810	145.5749929	166.7721571	190.1092932	215.6734198
3	126.4244860	145.5750400	166.7721661	190.1084455	215.6690025
4	126.4244863	145.5750447	166.7722178	190.1088627	215.6710754
5	126.4244864	145.5750452	166.7722181	190.1088459	215.6709435
Num	126.4244896	145.5750487	166.7722220	190.1088484	215.6709278

[30], as well as the condition that the mean value of the slow variable is smaller than the size of the major axis of OSQD or PSQD, i.e.,  $\rho \leq a$  or  $z \leq c$ , or known estimates of the distribution of nodes of Laguerre or Hermite polynomials [37]. To calculate also the approximate eigenfunctions of the lower part of the spectrum  $n = 0, \dots, n_{\max}$  with required numbers  $n$  of nodes in the interval  $\rho \in (0, a)$  (or  $z \in (-c, c)$ ) for OSQD (or PSQD), one should choose such value of parameter  $a = \sqrt{2x_0/\omega_i}$  (or  $c = x_0/\sqrt{\omega_i}$ ), that outside this interval  $x \in (x_0 = 4n + 2|m| + 2, \infty)$  (or  $|x| \in (x_0 = (2n + 1)^{1/2}, \infty)$ ) the Laguerre (or Hermite) polynomials have no nodes. As an example, in Fig. 2 we show contour plots in  $(z, x)$  and  $(x, z)$  plane of the first four eigenfunctions of OSQD and PSQD, respectively, that have a required number of nodes (crossings of the function plot with zero plane) in the interval  $\rho \in (0, a)$  and  $z \in (-c, c)$  at the values  $c = 0.5$ ,  $a = 5$ ,  $c = 2.5$ ,  $a = 0.5$ . One can see that the asymmetry with respect to  $z$ -axis of the eigenfunctions of PSQD is greater than that of OSQD, because the variation of well depth of PSQD is greater than of OSQD.

## 6. ABSORPTION COEFFICIENT FOR AN ENSEMBLE OF QDs

One can use the differences in the energy spectra to verify the considered models of QDs by calculating the absorption coefficient  $K(\tilde{\omega}^{ph}, \tilde{a}, \tilde{c}, u)$  of an ensemble of identical semiconductor QDs [14]. Since we do not discuss exciton effects in the present paper, the absorption coefficient may be approximately expressed as

$$\tilde{K}(\tilde{\omega}^{ph}, \tilde{a}, \tilde{c}, u) = \sum_{\nu, \nu'} \tilde{K}_{\nu, \nu'}(\tilde{\omega}^{ph}, \tilde{a}, \tilde{c}, u) \quad (46)$$

$$= \tilde{A} \sum_{\nu, \nu'} \tilde{I}_{\nu, \nu'}(u) \delta(\hbar \tilde{\omega}^{ph} - \tilde{W}_{\nu \nu'}),$$

$$\tilde{I}_{\nu, \nu'}(u) = \left| \int \tilde{\Psi}_{\nu}^e(\tilde{\mathbf{r}}; \tilde{a}, \tilde{c}, F, \mu_e) \tilde{\Psi}_{\nu'}^h(\tilde{\mathbf{r}}; \tilde{a}, \tilde{c}, F, \mu_h) d^3 \tilde{\mathbf{r}} \right|^2,$$

where  $\tilde{A}$  is proportional to the square of the matrix element in the Bloch decomposition,  $\tilde{\Psi}_{\nu}^e(u)$  and  $\tilde{\Psi}_{\nu'}^h$  are the eigenfunctions of the electron ( $e$ ) and the heavy hole ( $h$ ),  $\tilde{E}_{\nu}^e$  and  $\tilde{E}_{\nu'}^h$  are the energy eigenvalues for the electron ( $e$ ) and the heavy hole ( $h$ ), depending on the semiaxis size  $\tilde{c}, \tilde{a}$  for OSQD (or

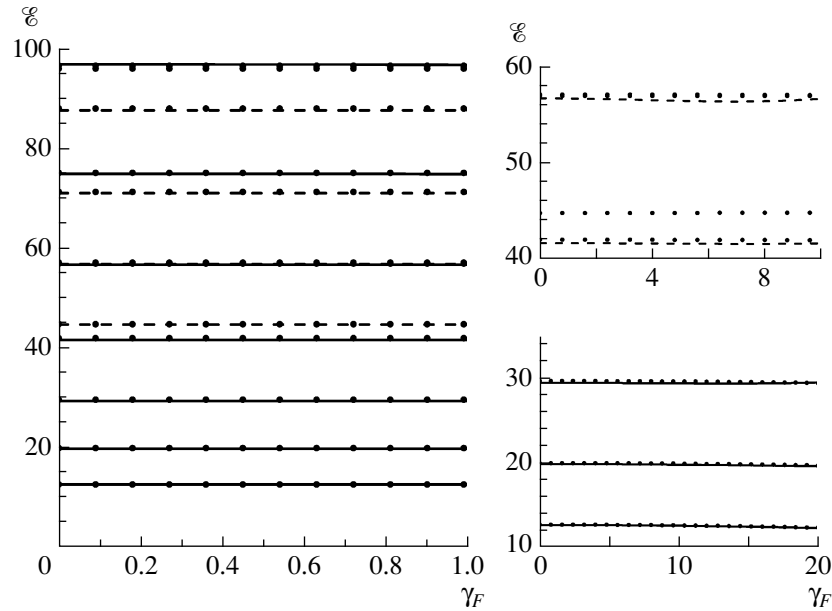


**Fig. 4.** Dependence of eigenenergies  $\mathcal{E}$  (in units of  $E_e$ ) of lower part of spectrum of electronic states of OSQDs ( $a = 2.5$ ,  $c = 0.5$ ) at  $m = 0$  on electric field strength  $\gamma_F$  (in units of  $F_0^*$ ). Solid and dashed lines are eigenenergies calculated by PTRS till 5 order in crude adiabatic approximation: seven solid lines ( $n_{zo} = 0$ ,  $n_{\rho o} = 0, 1, \dots, 6$ ) and four dashed lines ( $n_{zo} = 1$ ,  $n_{\rho o} = 0, 1, 2, 3$ ) are shown on left panel in interval  $\gamma_F \in (0, 1)$ ; the first three of solid lines ( $n_{zo} = 1$ ,  $n_{\rho o} = 0, 1, 2$ ) and the first two of dashed lines ( $n_{zo} = 1$ ,  $n_{\rho o} = 0, 1$ ) are shown on lower-right and upper-right panel, respectively, in bigger intervals  $\gamma_F \in (0, 20)$  and  $\gamma_F \in (0, 10)$ . Numerical solutions of Eqs. (4) at  $j_{\max} = 4$  are shown by points.

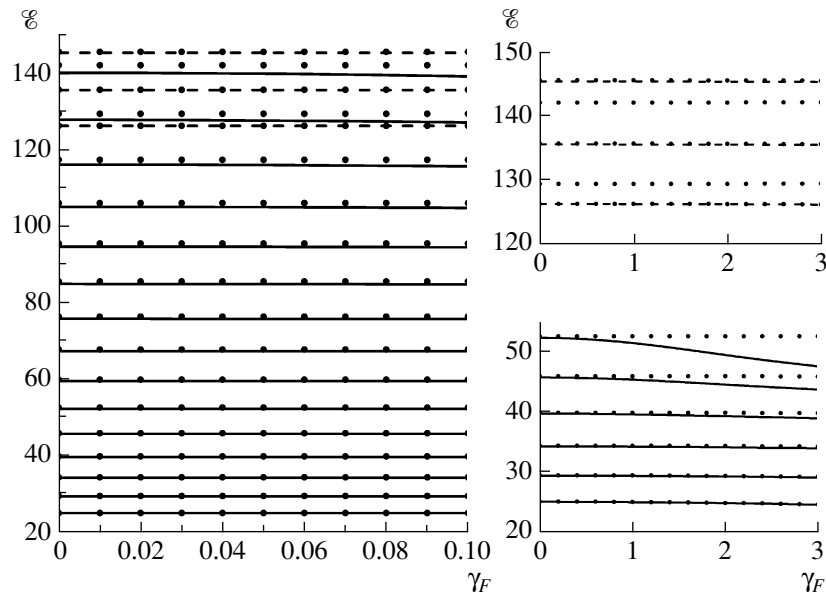


**Fig. 5.** Dependence of eigenenergies  $\mathcal{E}$  (in units of  $E_e$ ) of lower part of spectrum of electronic states of PSQDs ( $a = 0.5$ ,  $c = 2.5$ ) at  $m = 0$  on electric field strength  $\gamma_F$  (in units of  $F_0^*$ ). Solid and dashed lines are eigenenergies calculated by PTRS till 5 order in crude adiabatic approximation: fifteen solid lines ( $n_{\rho p} = 0$ ,  $n_{zp} = 0, 1, \dots, 14$ ) and three dashed lines ( $n_{\rho p} = 1$ ,  $n_{zp} = 0, 1, 2$ ) are shown on left panel in interval  $\gamma_F \in (0, 0.1)$ ; the first six of solid lines ( $n_{\rho p} = 0$ ,  $n_{zp} = 0, 1, \dots, 5$ ) are shown on lower-right panel and the dashed lines ( $n_{\rho p} = 1$ ,  $n_{zp} = 0, 1, 2$ ) are shown on upper-right panel in bigger interval  $\gamma_F \in (0, 3)$ . Numerical solutions of Eqs. (4) at  $j_{\max} = 4$  are shown by points.

$\tilde{a}, \tilde{c}$  for PSQD) and the adiabatic set of quantum numbers  $\nu = [n_{zo}, n_{\rho o}, m]$  and  $\nu' = [n'_{zo}, n'_{\rho o'}, m']$  ( $\nu = [n_{\rho p}, n_{zp}, m]$  and  $\nu' = [n'_{\rho p}, n'_{zp}, m']$ ), where  $m' = -m$ ,  $\tilde{E}_g$  is the band gap width in the bulk semiconductor,  $\tilde{\omega}^{ph}$  is the incident light frequency,  $\tilde{W}_{\nu\nu'} = \tilde{E}_g + \tilde{E}_\nu^e(\tilde{a}, \tilde{c}) + \tilde{E}_{\nu'}^h(\tilde{a}, \tilde{c})$  is the inter-band transition energy for which  $\tilde{K}(\tilde{\omega}^{ph})$  has the maximal value. We rewrite the expression (46) in the terms of frequency shift of the incident light  $\Delta\omega^{ph}/(2\pi) = (\hbar\tilde{\omega}^{ph} - \tilde{E}_g)/(2\pi\hbar)$  corresponding to the inter-band transition energy shift  $\Delta\tilde{W}_{\nu\nu'} = \tilde{W}_{\nu\nu'} - \tilde{E}_g = \tilde{E}_\nu^e(\tilde{a}, \tilde{c}) + \tilde{E}_{\nu'}^h(\tilde{a}, \tilde{c})$  for which  $\tilde{K}(\Delta\tilde{\omega}^{ph})$  has the maximal value, using dimensionless variables in the reduced atomic units

$$\tilde{K}(\Delta\tilde{\omega}^{ph}, \tilde{a}, \tilde{c}) = \tilde{A}\tilde{E}_g^{-1} \sum_{\nu, \nu'} \tilde{I}_{\nu, \nu'}(u) \delta[f_{\nu, \nu'}(u)], \quad (47)$$

$$f_{\nu, \nu'}(u) = \lambda_1 - \frac{2E_\nu^e(a, c) + 2E_{\nu'}^h(a, c)(\mu_h/\mu_e)}{2E_g},$$

where the parameter  $u$  will be defined below,  $\lambda_1 = (\hbar\tilde{\omega}^{ph} - \tilde{E}_g)/\tilde{E}_g$  is the energy of the optical interband transitions scaled to  $\tilde{E}_g$ ,  $2E_g = \tilde{E}_g/\tilde{E}_R^e$  is the dimensionless band gap width.

For GaAs the functions  $f_{\nu, \nu'}^{h \rightarrow e}(u)$  describing the ( $h \rightarrow e$ ) inter-band transitions have the form

$$f_{\nu, \nu'}^{h \rightarrow e}(u) = \lambda_1 - (2E_g)^{-1}(2E_\nu^e(a, c, \gamma_F) + 2E_{\nu'}^e(a, c, -(\mu_h/\mu_e)\gamma_F)(\mu_e/\mu_h)), \quad (48)$$

where  $\mu_e = 0.067m_0$  and  $\mu_h \equiv \mu_{hh} = 0.558m_0$  are the masses of electron and hole, respectively,  $\tilde{E}_g = 1430$  meV is the band gap width and  $\kappa = 13.18$  is the dc permittivity and  $E_R^e = e^2/(2\kappa a_B^e) = 5.275$  meV,  $a_B^e = \hbar^2\kappa/(\mu_e e^2) = 104$  Å,  $E_R^h = e^2/(2\kappa a_B^h) = 49$  meV,  $a_B^h = \hbar^2\kappa/(\mu_h e^2) = 15$  Å,  $2\gamma_F = F/F_0^*$ ,  $F_0^* = E_R^e/(ea_B^e) = e/(2\kappa(a_B^e)^2) = 5.04$  kV/cm.

For InSb the dispersion law for heavy holes ( $hh$ ) is parabolic while for electrons ( $e$ ) and light holes ( $lh$ ) it is non-parabolic and may be described by the Kane model [18, 19, 22] at  $\gamma_F = 0$ . The energy values in our notation are:

$$2\tilde{E}_\nu^{hh}(\text{InSb}) = 2\tilde{E}_{\nu'}^h(\tilde{a}, \tilde{c}), \quad (49)$$

$$2\tilde{E}_\nu^e(\text{InSb}) = 2\tilde{E}_\nu^{lh}(\text{InSb}) \quad (50)$$

$$= -\tilde{E}_g/2 + \sqrt{\tilde{E}_g^2/4 + \tilde{E}_g(2\tilde{E}_\nu^e(\tilde{a}, \tilde{c}))}.$$

As follows from Eqs. (49) and (50), to determine the energy spectrum and the wave function of the light hole and the electron one should solve the Klein-Gordon equation [39, 40], while for heavy hole the Schrödinger equation is applicable. The functions  $f_{\nu, \nu'}^{hh \rightarrow e}(u)$  and  $f_{\nu, \nu'}^{lh \rightarrow e}(u)$  describing the ( $hh \rightarrow e$ ) and the ( $lh \rightarrow e$ ) inter-band transitions have the forms

$$f_{\nu, \nu'}^{hh \rightarrow e}(u) = \lambda_1 - \left( 1/2 + \sqrt{1/4 + (2E_\nu^e(a, c)/(2E_g))} + (2E_g)^{-1} \cdot 2E_{\nu'}^e(a, c)(\mu_e/\mu_h) \right), \quad (51)$$

$$f_{\nu, \nu'}^{lh \rightarrow e}(u) = \lambda_1 - 2\sqrt{1/4 + (2E_\nu^e(a, c)/(2E_g))}, \quad (52)$$

where  $\mu_e = \mu_{lh} = 0.15m_0$  and  $\mu_h \equiv \mu_{hh} = 0.5m_0$  are the masses of electron, light, and heavy holes, respectively,  $\tilde{E}_g = 180$  meV is the band gap width,  $\kappa = 16$  is the dc permittivity, and  $E_R^e = E_R^{lh} = e^2/(2\kappa a_B^e) = 7.972$  meV,  $a_B^e = a_B^{lh} = \hbar^2\kappa/(\mu_e e^2) = 56.44$  Å,  $E_R^h = E_R^{hh} = e^2/(2\kappa a_B^{hh}) = 26.57$  meV,  $a_B^h = a_B^{hh} = \hbar^2\kappa/(\mu_h e^2) = 16.93$  Å.

For both electron and hole carriers the dimensionless energies  $2E_\nu^e = \tilde{E}_\nu^e/\tilde{E}_R^e$  and  $2E_\nu^h(\mu_h/\mu_e) = \tilde{E}_\nu^h/\tilde{E}_R^e$  are expressed in the same reduced atomic units  $\tilde{E}_R^e$ , and the overlap integral (46) between the eigenfunctions, corresponding to  $E_\nu^e(\gamma_F)$  and  $E_\nu^h(\gamma_F) = (\mu_e/\mu_h)E_\nu^e(-(\mu_h/\mu_e)\gamma_F)$ , takes the form

$$\tilde{I}_{\nu, \nu'}(u) = \left| \int (a_B^e)^3 \Psi_\nu^e(\mathbf{r}; a, c, \gamma_F, \mu_e) \Psi_{\nu'}^e(\mathbf{r}; a, c, -(\mu_h/\mu_e)\gamma_F, \mu_e) d^3\mathbf{r} \right|^2. \quad (53)$$

Now consider an ensemble of OSQDs (or PSQDs), differing in the minor semiaxis values  $c = u_o\tilde{c}$  (or  $a = u_p\tilde{a}$ ), determined by the random parameter  $u = u_o$  (or  $u = u_p$ ). The corresponding minor semiaxis mean value is  $\tilde{c}$  at fixed major semiaxis  $a$  (or  $\tilde{a}$  at fixed major

semiaxis  $c$ ), and the appropriate distribution function is  $P(u_o)$  (or  $P(u_p)$ ). Commonly, in this case the normalized Lifshits–Slezov distribution function [15] is used:

$$P(u) = \{3^4 e u^2 \exp(-1/(1 - 2u/3))/2^{5/3}/(u + 3)^{7/3}/(3/2 - u)^{11/3}, u \in (0, 3/2); 0, \text{otherwise}\} \quad (54)$$

having conventional properties  $\int P(u)du = 1$ ,  $\bar{u} = \int uP(u)du = 1$ . The absorption coefficients  $\tilde{K}^o(\tilde{\omega}^{ph}, \tilde{a}, \tilde{c})$  or  $\tilde{K}^p(\tilde{\omega}^{ph}, \tilde{a}, \tilde{c})$  of an ensemble of semiconductor OSQDs or PSQDs with different dimensions of minor semiaxes are expressed as

$$\tilde{K}^o(\tilde{\omega}^{ph}, \tilde{a}, \tilde{c}) = \int \tilde{K}(\tilde{\omega}^{ph}, \tilde{a}, \tilde{c}, u_o) P(u_o) du_o, \quad (55)$$

$$\tilde{K}^p(\tilde{\omega}^{ph}, \tilde{a}, \tilde{c}) = \int \tilde{K}(\tilde{\omega}^{ph}, \tilde{a}, \tilde{c}, u_p) P(u_p) du_p.$$

Substituting (47) into (55) and taking into account the known properties of the  $\delta$  function, we arrive at the analytical expression for the absorption coefficient  $\tilde{K}(\tilde{\omega}^{ph}, \tilde{a}, \tilde{c})$  of a system of semiconductor QDs with a distribution of random minor semiaxes:

$$\frac{\tilde{K}(\tilde{\omega}^{ph})}{\tilde{K}_0} = \sum_{\nu, \nu', s} \frac{\tilde{K}_{\nu, \nu'}(\tilde{\omega}^{ph})}{\tilde{K}_0}, \quad (56)$$

$$\frac{\tilde{K}_{\nu, \nu'}(\tilde{\omega}^{ph})}{\tilde{K}_0} = \tilde{I}_{\nu, \nu'}(u_s) \left| \frac{df_{\nu, \nu'}(u)}{du} \right|_{u=u_s}^{-1} P(u_s),$$

where  $\tilde{K}_0 = \tilde{A}^{-1} \tilde{E}_g$  is the normalization factor,  $u_s$  are the roots of the equation  $f_{\nu, \nu'}(u_s) = 0$ .

At  $\gamma_F = 0$  for IPBM we have the interband overlap  $\tilde{I}_{\nu, \nu'} = \delta_{n_{\rho o}, n'_{\rho o}} \delta_{n_{z o}, n'_{z o}} \delta_{m, -m'}$  for OSQD, or  $\tilde{I}_{\nu, \nu'} = (J_{1+|m|}(\alpha_{n_{\rho p}+1, |m|})/J_{1-|m|}(\alpha_{n_{\rho p}+1, |m|}))^2 \times \delta_{n_{z p}, n'_{z p}} \delta_{n_{\rho p}, n'_{\rho p}} \delta_{m, -m'}$  for PSQD, where  $\alpha_{n_{\rho p}+1, |m|}$  is the positive root of the Bessel function, and the selection rules  $m = -m'$ ,  $n_{z o} = n'_{z o}$ ,  $n_{\rho o} = n'_{\rho o}$ , or  $n_{\rho p} = n'_{\rho p}$ ,  $n_{z p} = n'_{z p}$  [27], while at  $\gamma_F \neq 0$  one should calculate the interband overlap (53) in accordance with the selection rules  $m = -m'$ ,  $n_{\rho o} = n'_{\rho o}$ , or  $n_{\rho p} = n'_{\rho p}$ , respectively. Note, that in the adiabatic limit and at small  $\gamma_F$  the contributions of non-diagonal matrix elements to the energy values are about 1% for IPBM of OSQD and PSQD; then in the Born–Oppenheimer approximation of the order  $b_{\max}$  for the AC we get

$$f_{\nu, \nu'}(u) = \lambda_1 - \sum_{j=0}^{f_{\max}} f_{\nu, \nu'}^{(j)} u^{j-2}. \quad (57)$$

The coefficients of the expansion (57) for parabolic dispersion law for small  $\gamma_F \neq 0$  were constructed using the expansions (44) and (45) and at  $\gamma_F = 0$  they

are given in [27]. In general case for the calculation  $f_{\nu, \nu'}(u)$  by formula (48), (51), or (52) we used the eigenvalues  $E_{\nu}^e(a, c)$  and  $E_{\nu'}^h(a, c)$  calculated numerically with given accuracy. After that we evaluated the coefficients of expansion like (57) by the method of least squares and by the polynomial interpolation in the case of parabolic and non-parabolic dispersion laws, respectively. Because of monotonic behavior of function  $f_{\nu, \nu'}(u)$  vs  $u$  in the case under consideration, we have only one root  $u_s$  of the equation  $f_{\nu, \nu'}(u_s) = 0$ , which was used in formula (56).

For the Lifshits–Slezov distribution Figs. 6 and 7 display the total absorption coefficients  $\tilde{K}(\tilde{\omega}^{ph})/\tilde{K}_0$  and the partial absorption coefficients  $\tilde{K}_{\nu, \nu'}(\tilde{\omega}^{ph})/\tilde{K}_0$ , that form the corresponding partial sum (56) over a fixed set of quantum numbers  $\nu, \nu'$  at  $m = -m' = 0$ . As a result of averaging (55) a series of curves with finite width and height are observed instead of a series of  $\delta$  functions. One can see that the summation over the quantum numbers  $n_o = n_{z o} + 1 = 1, 2, 3, 4, 5$  (or  $n_p = n_{\rho p} + 1 = 1, 2, 3$ ) enumerating the nodes of the wave function with respect to the fast variable gives the corresponding principal maxima of the total AC for the ensemble of QDs with distributed dimensions of minor semiaxis, while the summation over the quantum number  $n_{\rho o} = 0, 1, 2, 3, \dots, 8$  (or  $n_{z p} = 0, 1, 2, \dots, 15$ ) that labels the nodes of the wave function with respect to the slow variable leads to the increase of amplitudes of these maxima and to secondary maxima arising in the case of sparser energy levels of IPBM of OSQDs (or PSQDs).

In the regime of strong dimensional quantization the frequencies of the interband transitions ( $h \rightarrow e$ ) in GaAS between the levels  $n_o = 1, n_{\rho o} = 0, m = 0$  for OSQD or  $n_p = 1, n_{z p} = 0, m = 0$  for PSQD at the fixed values  $\tilde{a} = 2.5a_e$  and  $\tilde{c} = 0.5a_e$  for OSQD or  $\tilde{a} = 0.5a_e$  and  $\tilde{c} = 2.5a_e$  for PSQD, are equal to  $\Delta\tilde{\omega}_{100}^{ph}/(2\pi) = 16.9$  THz at  $\gamma_F = 0$  and  $\Delta\tilde{\omega}_{100}^{ph}/(2\pi) = 15.9$  THz at  $\gamma_F = 10$ , or  $\Delta\tilde{\omega}_{100}^{ph}/(2\pi) = 33.3$  THz at  $\gamma_F = 0$  and  $\Delta\tilde{\omega}_{100}^{ph}/(2\pi) = 31.5$  THz at  $\gamma_F = 2$ , where  $\Delta\tilde{\omega}_{100}^{ph}/(2\pi) = (2\pi\hbar)^{-1}(\tilde{W}_{100,100} - \tilde{E}_g)$  corresponds to the IR spectral region [7, 8], taking the band gap value  $(2\pi\hbar)^{-1}\tilde{E}_g = 346$  THz into account. In Fig. 7 one can see the quantum-confined Stark effect that consists in the reduction of the absorption energy (light frequency) at the expense of lowering the energy of both ( $e$ ) and ( $h$ ) bound states due to the electric field effect. The total ACs at  $F \neq 0$ ,

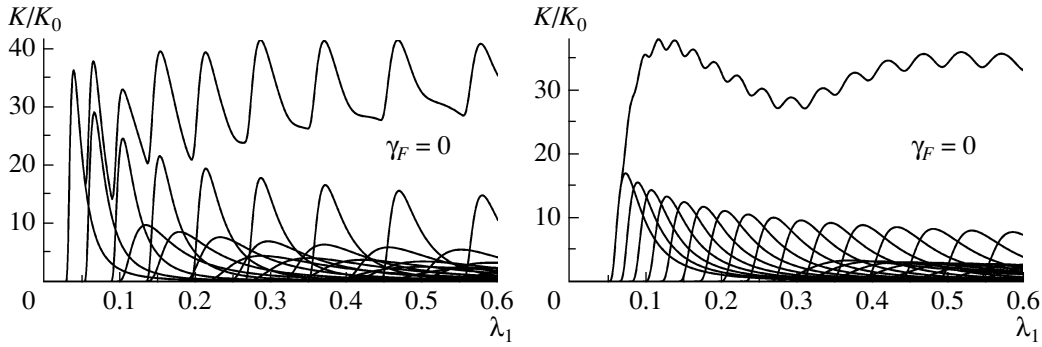


**Fig. 6.** Absorption coefficient  $K/K_0$ , Eq. (55), consisting of a sum of the first partial contributions vs the energy  $\lambda = \lambda_1$  of the optical interband transitions for the Lifshits–Slezov distribution, using the functions  $f_{\nu,\nu'}^{h \rightarrow e}(u)$  for GaAs ( $h \rightarrow e$ ) without electric field: for ensemble of OSQDs  $\bar{c} = 0.5$ ,  $a = 2.5$  (left panel) and for ensemble of PSQDs  $\bar{a} = 0.5$ ,  $c = 2.5$  (right panel).

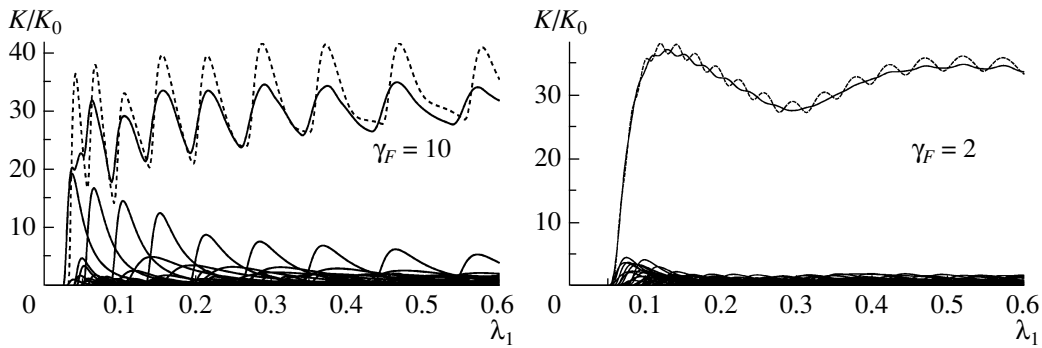


**Fig. 7.** The same as in Fig. 6, but in the presence of electric field  $2\gamma_F = F/F_0^*$ . For comparison, the corresponding absorption coefficient without electric field is given by dashed line.

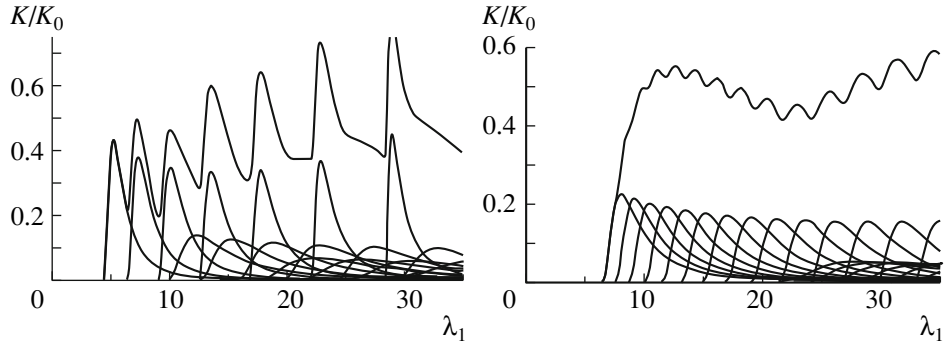


**Fig. 8.** The same as in Fig. 6, but for InSb ( $hh \rightarrow e$ ) inter-band transition.

shown by solid lines, qualitatively correspond to the total AC at  $F = 0$ , shown by dashed lines, but have lower magnitudes and smooth behavior, in spite of the additional contribution to the partial ACs of the overlap integral (53) from the interband transition  $n_{zo} \neq n'_{zo}$  or  $n_{zp} \neq n'_{zp}$  in OSQD or PSQD, also shown in Fig. 7.

At the same parameters of the QDs the frequencies of the interband transitions ( $lh \rightarrow e$ ) in InSb

are equal to  $\Delta\tilde{\omega}_{100}^{ph}/(2\pi) = 68.5$  THz for OSQD or  $\Delta\tilde{\omega}_{100}^{ph}/(2\pi) = 87.2$  THz for PSQD, while the frequencies of the interband transitions ( $hh \rightarrow e$ ) in InSb are equal to  $\Delta\tilde{\omega}_{100}^{ph}/(2\pi) = 78.6$  THz for OSQD or  $\Delta\tilde{\omega}_{100}^{ph}/(2\pi) = 102$  THz for PSQD. These values correspond to the infrared spectral region with longer wavelength, similar to [22], with the band gap value  $(2\pi\hbar)^{-1}\tilde{E}_g = 44$  THz taken into account. One

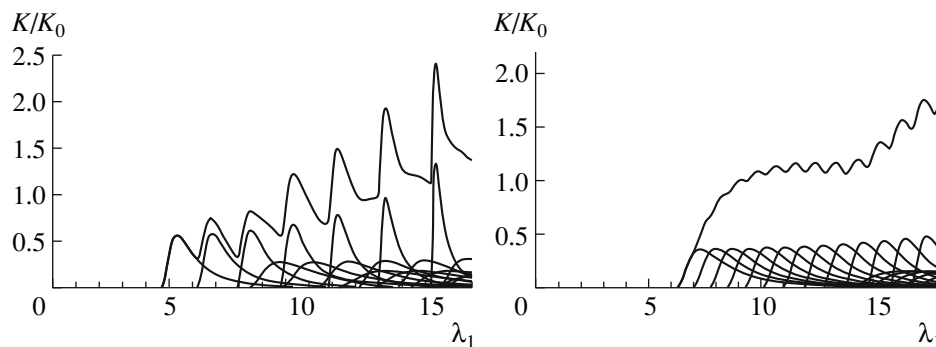


Fig. 9. The same as in Fig. 6, but for InSb ( $lh \rightarrow e$ ) inter-band transition.

can see that the behavior of total ACs for parabolic dispersion law for IPBM of InSb, shown in Fig. 8, is similar to that for GaAs (Fig. 6), while the behavior of AC for nonparabolic dispersion law, shown in Fig. 9, is essentially different. In particular, for OSQDs it grows faster with increasing  $\lambda_1$ , while for PSQDs it goes to a plateau before starting to grow. Indeed, with increasing quantum numbers  $n_{\rho o}$  or  $n_{zp}$  that characterize the excitation of slow motion, the maxima of partial ACs decrease for parabolic dispersion law, while for the non-parabolic one the maxima of partial ACs increase.

With decreasing semiaxis the threshold energy increases, because the “effective” band gap width increases, which is a consequence of the dimensional quantization enhancement. Therefore, the above frequency is greater for PSQD than for OSQD, because the OSQD implemented in two direction of the plane ( $x, y$ ) is effectively larger than that in the direction of the  $z$ -axis solely at similar values of semiaxes. Higher-accuracy calculations reveal an essential difference in the frequency behavior of the AC for interband transitions in systems of semiconductor OSQDs or PSQDs having a distribution of minor semiaxes, which can be used to verify the above models.

## 7. CONCLUSIONS

The 3D BVP for spheroidal quantum dots with respect to fast and slow variables of cylindrical coordinates was reduced by Kantorovich or adiabatic method to BVP for set of second-order differential equations (ODE) with effective potentials given in the analytic form with respect to the slow variable, using the basis function of fast variables, that depended on the slow variable as a parameter. Separation of variables of 3D BVP in spheroidal coordinates provides exact classification of energy eigenvalues by means of nodes of eigenfunctions which transform exactly to an adiabatic classification of eigensolutions of a

diagonal approximation of ODE at small parameter, i.e. ratio of minor and major semiaxes of oblate or prolate spheroid. The effective potential of a crude diagonal adiabatic approximation (CDAA) of the ODE has been approximated by power expansions by slow variable. Energy eigenvalues and eigenfunctions of the BVP for CDAA were sought in the form of expansions over eigenfunctions of 2D or 1D oscillator with *adiabatic frequencies* and power of small parameter by the PT. Required coefficients of these expansions were calculated in analytical form as polynomials of the sets of adiabatic quantum numbers.

To specify the region of the model parameters, in which the PT asymptotic series are valid, we have compared the PT results with those of numerical calculations carried out with required accuracy. The PT eigensolutions were used in analytic evaluation of the photoabsorption coefficient for ensembles of *oblate* and *prolate* spheroidal QDs with given random distribution of small semiaxes without and with small values of external electric fields. In general case for calculation  $f_{\nu,\nu'}(u)$  by formula (48), (51), or (52) we used eigenvalues calculated numerically with given accuracy and we evaluated the coefficients of expansion like (57) by the method of least squares and by the polynomial interpolation in the case of parabolic and nonparabolic dispersion laws, respectively. Note, in the case of numerical calculations of the photoabsorption coefficient the required derivatives of eigenenergies and eigenfunctions with respect to a parameter, e.g., the small semiaxis, can be calculated also with the help of the numerical algorithms [29, 35].

The elaborated methods, symbolic-numerical algorithms (SNAs) and programs [23–35] can be applied for solving the BVPs of discrete and continuous spectra of the Schrödinger-type equations and the analysis of spectral and optical characteristics of QWs, QWr's and QD's in external fields, as well as the spectra of models of deformed nuclei [41].

This work was partially supported by the RFBR grants nos. 10-02-00200 and 11-01-00523.

## REFERENCES

1. D. Bimberg, M. Grundman, and N. Ledentsov, *Quantum Dot Heterostructures* (Wiley, New York, 1999).
2. P. Harrison, *Quantum Well, Wires and Dots. Theoretical and Computational Physics of Semiconductor Nanostructures* (Wiley, New York, 2005).
3. Zh. I. Alferov, *Semiconductors* **32**, 1 (1998).
4. Li Bin et al., *Phys. Lett. A* **367**, 493 (2007).
5. G. Lamouche and Y. Lépine, *Phys. Rev. B* **49**, 13452 (1994).
6. H. A. Sarkisyan, *Mod. Phys. Lett. B* **16**, 835 (2002).
7. K. G. Dvovyan et al., *Nanoscale Res. Lett.* **4**, 106 (2009); *Proc. SPIE* **7998**, 79981F (2010).
8. K. G. Dvovyan et al., *Nanoscale Res. Lett.* **2**, 601 (2007).
9. S. López et al., *Physica E* **40**, 1383 (2008).
10. M. G. Barseghyan, A. A. Kirakosyan, and C. A. Duque, *Eur. Phys. J. B* **72**, 521 (2009).
11. A. Gharaati and R. Khordad, *Superlatt. Microstruct.* **48**, 276 (2010).
12. I. Filikhin, V. M. Suslov, and B. Vlahovic, *Phys. Rev. B* **73**, 205332 (2006).
13. I. Filikhin et al., *Physica E* **41**, 1358 (2009).
14. Al. L. Efros and A. L. Efros, *Sov. Phys. Semicond.* **16**, 772 (1982).
15. I. M. Lifshits and V. V. Slezov, *Sov. Phys. JETP* **8**, 331 (1959).
16. K. D. Moiseev et al., *Tech. Phys. Lett.* **33**, 295 (2007).
17. K. D. Moiseev et al., *Semiconductors* **43**, 1102 (2009).
18. E. O. Kane, *J. Phys. Chem. Sol.* **1**, 249 (1957).
19. B. Askerov, *Electronic Transport Phenomena in Semiconductors* (Nauka, Moscow, 1985; World Scientific, Singapore, 1994).
20. E. M. Kazaryan, A. V. Meliksetyan, and H. A. Sarkisyan, *Tech. Phys. Lett.* **33**, 964 (2007).
21. E. M. Kazaryan, A. V. Meliksetyan, and H. A. Sarkisyan, *J. Comput. Theor. Nanosci.* **7**, 486 (2010).
22. M. S. Atonyan et al., *Physica E* **43**, 1592 (2011).
23. V. L. Derbov et al., *Izv. Saratov Univ., Ser. Fiz.* **10** (1), 4 (2010).
24. A. A. Gusev et al., *Lect. Notes Comp. Sci.* **6244**, 106 (2010).
25. A. A. Gusev et al., *J. Phys. Conf. Ser.* **248**, 012047 (2010).
26. A. A. Gusev et al., *Phys. At. Nucl.* **73**, 331 (2010).
27. A. A. Gusev et al., *Phys. At. Nucl.* **75**, 1210 (2012).
28. O. Chuluunbaatar et al., *Comput. Phys. Commun.* **177**, 649 (2007).
29. O. Chuluunbaatar et al., *Comput. Phys. Commun.* **180**, 1358 (2009).
30. O. Chuluunbaatar et al., *Comput. Phys. Commun.* **179**, 685 (2008).
31. A. Gusev et al., *Lect. Notes Comp. Sci.* **4194**, 205 (2006).
32. O. Chuluunbaatar et al., *Comput. Phys. Commun.* **178**, 301 (2008).
33. O. Chuluunbaatar et al., *Lect. Notes Comp. Sci.* **4770**, 118 (2007).
34. A. A. Gusev et al., *Lect. Notes Comp. Sci.* **6885**, 175 (2011).
35. S. I. Vinitsky et al., *Progr. Comp. Software* **33**, 105 (2007).
36. J. E. Lennard-Jones, *Proc. R. Soc. London, Ser. A* **129**, 598 (1930); *J. Lond. Math. Soc.* **6**, 290 (1931); N. Mott and I. Sneddon, *Wave Mechanics and Its Applications* (Clarendon, Oxford, 1948).
37. M. Abramowitz and I. A. Stegun, *Handbook of Mathematical Functions* (Dover, New York, 1965). <http://dlmf.nist.gov/> NIST Digital Library of Mathematical Functions
38. K. Helfrich, *Theor. Chim. Acta* **24**, 271 (1972).
39. E. M. Kazaryan, L. S. Petrosyan, and H. A. Sarkisyan, *Physica E* **16**, 174 (2003).
40. M. Zoheir, A. Kh. Manaselyan, and H. A. Sarkisyan, *Physica E* **40**, 2945 (2008).
41. S. Cwiok et al., *Comput. Phys. Commun.* **46**, 379 (1987).





## ELEMENTARY PARTICLES AND FIELDS

### Theory

# Adiabatic Description of Nonspherical Quantum Dot Models\*

A. A. Gusev<sup>1)\*\*</sup>, O. Chuluunbaatar<sup>1)</sup>, S. I. Vinitzky<sup>1)</sup>, K. G. Dvovyan<sup>2)</sup>, E. M. Kazaryan<sup>2)</sup>,  
H. A. Sarkisyan<sup>2)</sup>, V. L. Derbov<sup>3)</sup>, A. S. Klombotskaya<sup>3)</sup>, and V. V. Serov<sup>3)</sup>

Received May 5, 2011

**Abstract**—Within the effective mass approximation an *adiabatic* description of spheroidal and dumbbell quantum dot models in the regime of strong dimensional quantization is presented using the expansion of the wave function in appropriate sets of single-parameter basis functions. The comparison is given and the peculiarities are considered for spectral and optical characteristics of the models with axially symmetric confining potentials depending on their geometric size, making use of the complete sets of exact and *adiabatic* quantum numbers in appropriate analytic approximations.

**DOI:** 10.1134/S1063778812100079

*Devoted to the blessed memory  
of professor Alexei Norairovich Sissakian*

## 1. INTRODUCTION

To analyze the geometrical, spectral, and optical characteristics of quantum dots in the effective mass approximation and in the regime of strong dimensional quantization following [1], many methods and models were used. We mention some of them, that are in the field of our interest: the exactly solvable models of spherical and cylindrical layer (toroid) impermeable wells [2, 3], the adiabatic approximation for a lens-shaped well confined to a narrow wetting layer [4], and a hemispherical impermeable well [5], molecular interaction and polarisability [6], the model of strongly oblate or prolate ellipsoidal impermeable well [7–9], as well as numerical solutions of the boundary value problems (BVPs) with separable variables in the spheroidal coordinates for wells with infinite and finite wall heights [10–15], Möbius [16] nanostructures, diffraction of waves by ribbons [17], scattering problems for toric [18] and coupled nonidentical microdisks [19].

Similar models were used for describing the energy spectra of deformed nuclei [20–26], atomic clusters deposited on planar surfaces [27], and low-energy barrier nuclear reactions [28–33]. However, thorough

comparative analysis of spectral and optical characteristics of models with different potentials, including those with non-separable variables, remains to be a challenging problem.

In the present paper we analyze spectral and optical characteristics of the following models: a spherical quantum dot (SQD), an oblate spheroidal quantum dot (OSQD), a prolate spheroidal quantum dot (PSQD), and a dumbbell QD (DQD). We make use of the Kantorovich method that reduces the problem to a set of ordinary differential equations (ODE) [34] by means of expanding the wave function in appropriate sets of single-parameter basis functions [35], similar to the well-known adiabatic method [36].

We present briefly a calculation scheme for solving elliptical BVPs with axially-symmetric potentials in cylindrical coordinates (CC), spherical coordinates (SC), oblate spheroidal coordinates (OSC), and prolate spheroidal coordinates (PSC). Basing on the symbolic-numerical algorithms (SNA) developed for axially-symmetric potentials [37–39], different sets of solutions are constructed for the parametric BVPs related to the fast subsystem, namely, the eigenvalue problem solutions (the terms and the basis functions), depending upon the slow variable as a parameter, as well as the matrix elements, i.e., the integrals of the products of basis functions and their derivatives with respect to the parameter. These terms and matrix elements form the matrices of variable coefficients in the set of second-order ODE with respect to the slow variable, which are calculated in special cases analytically and in the general case using the program ODPEVP [40]. The BVP for this set of ODEs is solved by means of the program KANTBP [41], while in the special cases crude diagonal estimations can be

\*The text was submitted by the authors in English.

<sup>1)</sup>Joint Institute for Nuclear Research, Dubna, Russia.

<sup>2)</sup>Russian–Armenian (Slavonic) University, Yerevan, Armenia.

<sup>3)</sup>Saratov State University, Russia.

\*\*E-mail: [gooseff@jinr.ru](mailto:gooseff@jinr.ru)

performed using the appropriate analytic approximations.

The efficiency of the calculation scheme and the SNA used is demonstrated by tracing the peculiarities of spectral and optical characteristics in the course of varying the aspect ratio of the prolate or oblate spheroid and dumbbell in the models of quantum dots with different confining potentials, such as the isotropic and anisotropic harmonic oscillator, the spherical and spheroidal well with finite or infinite walls approximated by smooth short-range potentials, as well as by constructing the adiabatic classification of the states.

The paper is organized as follows. In Section 2, the calculation scheme for solving elliptic BVPs with axially-symmetric confining potentials is briefly presented. Sections 3 and 4 are devoted to the analysis of the spectra and absorption coefficient of quantum dot models with three types of axially-symmetric potentials, including the benchmark exactly solvable models. In Conclusion we summarize the results and discuss the future applications.

## 2. PROBLEM STATEMENT

Within the effective mass approximation under the conditions of strong dimensional quantization, the Schrödinger equation for the slow envelope of the wave function  $\tilde{\Psi}(\tilde{\mathbf{r}})$  of a charge carrier (electron  $e$  or hole  $h$ ) in the models of QDs has the form [7, 8]

$$\begin{aligned} & \{\tilde{H} - \tilde{E}\}\tilde{\Psi}(\tilde{\mathbf{r}}) \\ & = \{(2\mu_p)^{-1}\tilde{\mathbf{P}}^2 + \tilde{U}(\tilde{\mathbf{r}}) - \tilde{E}\}\tilde{\Psi}(\tilde{\mathbf{r}}) = 0, \end{aligned} \quad (1)$$

where  $\tilde{\mathbf{r}} \in \mathbf{R}^3$  is the position vector of the particle having the effective mass  $\mu_p = \mu_e$  (or  $\mu_p = \mu_h$ ),  $\tilde{\mathbf{P}} = -i\hbar\nabla_{\tilde{\mathbf{r}}}$  is the momentum operator,  $\tilde{E}$  is the energy of the particle,  $\tilde{U}(\tilde{\mathbf{r}})$  is the axially-symmetric potential confining the particle motion in SQD, PSQD, or OSQD. In Model A,  $\tilde{U}(\tilde{\mathbf{r}})$  is chosen to be the potential of an isotropic or anisotropic axially-symmetric harmonic oscillator in Cartesian coordinates  $\mathbf{r} = \{x, y, z\}$ :

$$\tilde{U}^A(\tilde{\mathbf{r}}) = \mu_p \tilde{\omega}^2 (\zeta_1(\tilde{x}^2 + \tilde{y}^2) + \zeta_3 \tilde{z}^2)/2. \quad (2)$$

Here  $\zeta_1 = 1$ ,  $\zeta_3 = 1$  for a spherical QD or  $\zeta_1 = (\tilde{r}_0/\tilde{a})^4$ ,  $\zeta_3 = (\tilde{r}_0/\tilde{c})^4$  for a spheroidal QD, inscribed into a spherical one, where  $\tilde{a}$  and  $\tilde{c}$  are the semiaxes of the ellipse which transforms into a sphere at  $\tilde{a} = \tilde{c} = \tilde{r}_0 = \sqrt{\tilde{x}_0^2 + \tilde{y}_0^2 + \tilde{z}_0^2}$ ,  $\tilde{\omega} = \gamma_{\tilde{r}_0} \hbar / (\mu_p \tilde{r}_0^2)$  is the angular frequency, and  $\gamma_{\tilde{r}_0}$  is an adjustable parameter. We will use the value  $\gamma_{\tilde{r}_0} = \pi^2/3$  that follows from equating the ground state energies for the spherical oscillator and the spherical QD of Model B considered below.

If necessary, this definition can be replaced with a different one, e.g., the one conventional for nuclear physics [24–26].

For Model B,  $\tilde{U}(\tilde{\mathbf{r}})$  is the potential of a spherical or axially-symmetric well

$$\tilde{U}^B(\tilde{\mathbf{r}}) = \{0, S(\tilde{\mathbf{r}}) < 0; \tilde{U}_0, S(\tilde{\mathbf{r}}) \geq 0\}, \quad (3)$$

bounded by the surface  $S(\tilde{\mathbf{r}}) = 0$  with walls of finite or infinite height  $1 \ll \tilde{U}_0 < \infty$ . In Eq. (3)  $S(\tilde{\mathbf{r}})$  depends on the parameters  $\tilde{a}$ ,  $\tilde{c}$ , and  $0 \leq \tilde{c}_1 \leq 1$

$$S(\tilde{\mathbf{r}}) \equiv \frac{\tilde{x}^2 + \tilde{y}^2}{\tilde{a}^2} + \frac{(\tilde{z}^2 - \tilde{c}^2)(\tilde{z}^2 \tilde{c}_1^2 + 1 - \tilde{c}_1^2)^2}{\tilde{c}^2(\tilde{c}_1^2 \tilde{c}^2/4 + 1 - \tilde{c}_1^2)^2}. \quad (4)$$

At  $c_1 = 0$  we get a spheroidal quantum dot model, at  $0 < c_1 < 1$  it becomes a dumbbell QD with a symmetric double well, and at  $c_1 > 1$  we get a triple-well model.

For Model C,  $\tilde{U}(\tilde{\mathbf{r}})$  is taken to be a spherical or axially-symmetric diffuse potential

$$\tilde{U}^C(\tilde{\mathbf{r}}) = \tilde{U}_0 \left(1 - (1 + \exp(S(\tilde{\mathbf{r}})/s))^{-1}\right), \quad (5)$$

where  $s$  is the edge diffusiveness parameter of the function smoothly approximating the vertical walls of finite height  $\tilde{U}_0$ . Below we restrict ourselves by considering Model B with infinite walls  $\tilde{U}_0 \rightarrow \infty$  and Model C with walls of finite height  $\tilde{U}_0$ .

Throughout the paper we make use of the reduced atomic units [1, 8]:  $a_B^* = \kappa \hbar^2 / \mu_p e^2$  is the reduced Bohr radius,  $\kappa$  is the DC permittivity,  $\tilde{E}_R \equiv Ry^* = \hbar^2 / (2\mu_p a_B^{*2})$  is the reduced Rydberg unit of energy, and the following dimensionless quantities are introduced:  $\tilde{\Psi}(\tilde{\mathbf{r}}) = a_B^{*-3/2} \Psi(\mathbf{r})$ ,  $2\hat{H} = \tilde{H} / Ry^*$ ,  $2E = \tilde{E} / Ry^*$ ,  $2U(\mathbf{r}) = \tilde{U}(\tilde{\mathbf{r}}) / Ry^*$ ,  $\mathbf{r} = \tilde{\mathbf{r}} / a_B^*$ ,  $a = \tilde{a} / a_B^*$ ,  $c = \tilde{c} / a_B^*$ ,  $c_1 = \tilde{c}_1 / a_B^*$ ,  $r_0 = \tilde{r}_0 / a_B^*$ ,  $\omega = \gamma_{r_0} / r_0^2 = \hbar \tilde{\omega} / (2Ry^*)$ . For an electron with the effective mass  $\mu_p \equiv \mu_e = 0.067m_0$  at  $\kappa = 13.18$  in GaAs:  $a_B^* = a_B^e = 104 \text{ \AA} = 10.4 \text{ nm}$  and  $Ry^* = \tilde{E}_R^e = 5.275 \text{ meV}$ . For a heavy hole with the effective mass  $\mu_h = \mu_e / 0.12 = 0.558m_0$  the corresponding values are  $a_B^h = a_B^e (\mu_e / \mu_h) = 12.48 \text{ \AA} = 1.248 \text{ nm}$ , and  $\tilde{E}_R^h = \tilde{E}_R^e (\mu_h / \mu_e) = 46.14 \text{ meV}$ .

Note that for Model A with approximation of OSQD/PSQD by the anisotropic oscillator (2) the separation of variables in cylindric coordinates  $\mathbf{x} = (z, \rho, \varphi)$  is possible and additional integrals exist [42–44]. Similarly, for Model B the variables are separable in the oblate/prolate spheroidal coordinates  $\mathbf{x} = (\xi, \eta, \varphi)$  and the additional integrals of motion

The values of conditionally fast  $x_f$  and slow  $x_s$  independent variables, the coefficients  $g_{is}(x_s)$ ,  $g_{jf}(x_f)$  and the potentials  $\check{V}_f(x_f)$ ,  $\check{V}_s(x_s)$ ,  $\check{V}_{fs}(x_f, x_s)$ , in Eqs. (10)–(12) for SQD, OSQD, and PSQD in cylindrical (CC), spherical (SC), oblate and prolate spheroidal (OSC and PSC) coordinates with  $(d/2)^2 = \pm(a^2 - c^2)$ , + for OSC, – for PSC

	CC		SC	OSC and PSC
	OSQD	PSQD	SQD	OSQD and PSQD
$x_f$	$z$	$\rho$	$\eta$	$\eta$
$x_s$	$\rho$	$z$	$r$	$\xi$
$g_{1f}$	1	$\rho$	1	1
$g_{2f}$	1	$\rho$	$1 - \eta^2$	$1 - \eta^2$
$g_{1s}$	$\rho$	1	$r^2$	1
$g_{2s}$	$\rho$	1	$r^2$	$\xi^2 \pm 1$
$g_{3s}$	1	1	$r^2$	1
$\check{V}_f(x_f)$	$\omega^2 \zeta_3 z^2$	$m^2/\rho^2 + \omega^2 \zeta_1 \rho^2$	$m^2/g_{2f}$	$m^2/g_{2f} \pm (d/2)^2 g_{2f} \cdot 2E$
$\check{V}_s(x_s)$	$m^2/\rho^2 + \omega^2 \zeta_1 \rho^2$	$\omega^2 \zeta_3 z^2$	0	$\mp m^2/g_{2s} - ((d/2)^2 g_{2s} - 1) \cdot 2E$
$\check{V}_{fs}(x_f, x_s)$	0	0	$\check{V}(r, \eta)$	$\check{V}(\xi, \eta)$

are  $\hat{\Lambda}$ :  $[\hat{H}, \hat{\Lambda}] \equiv \hat{H}\hat{\Lambda} - \hat{\Lambda}\hat{H} = 0$ , i.e.  $\hat{H}_p$  and  $\hat{\Lambda}_p$  in PSQD

$$\hat{H}_p = -\frac{4}{d^2} \left[ \frac{1}{\xi^2 - \eta^2} \left( \frac{d}{d\xi} (\xi^2 - 1) \frac{d}{d\xi} + \frac{d}{d\eta} (1 - \eta^2) \frac{d}{d\eta} \right) + \left( \frac{1}{(\xi^2 - 1)(1 - \eta^2)} \right) \frac{d^2}{d\varphi^2} \right], \quad (6)$$

$$\hat{\Lambda}_p = \frac{1 - \eta^2}{\xi^2 - \eta^2} \frac{d}{d\xi} (\xi^2 - 1) \frac{d}{d\xi} + \frac{\xi^2 - 1}{\xi^2 - \eta^2} \times \frac{d}{d\eta} (1 - \eta^2) \frac{d}{d\eta} + \left( \frac{1}{\xi^2 - 1} - \frac{1}{1 - \eta^2} \right) \frac{d^2}{d\varphi^2}, \quad (7)$$

$\hat{H}_o$  and  $\hat{\Lambda}_o$  in OSQD

$$\hat{H}_o = -\frac{4}{d^2} \left[ \frac{1}{\xi^2 + \eta^2} \left( \frac{d}{d\xi} (\xi^2 + 1) \frac{d}{d\xi} + \frac{d}{d\eta} (1 - \eta^2) \frac{d}{d\eta} \right) - \left( \frac{1}{(\xi^2 + 1)(1 - \eta^2)} \right) \frac{d^2}{d\varphi^2} \right], \quad (8)$$

$$\hat{\Lambda}_o = -\frac{1 - \eta^2}{\xi^2 + \eta^2} \frac{d}{d\xi} (\xi^2 + 1) \frac{d}{d\xi} - \frac{\xi^2 + 1}{\xi^2 + \eta^2} \times \frac{d}{d\eta} (1 - \eta^2) \frac{d}{d\eta} - \left( \frac{1}{\xi^2 + 1} + \frac{1}{1 - \eta^2} \right) \frac{d^2}{d\varphi^2}. \quad (9)$$

Equation (9) is obtained by substituting  $\xi \rightarrow i\xi$ ,  $d \rightarrow -id$  from the known Eq. (7) derived in [45, 46].

Since the Hamiltonian  $\hat{H}$  in Eqs. (1)–(5) commutes with the  $z$ -parity operator of reflection in the plane  $z = 0$  ( $z \rightarrow -z$  or  $\eta \rightarrow -\eta$ ), the solutions are divided into even ( $\sigma = +1$ ) and odd ( $\sigma = -1$ ) ones. The solution of Eq. (1), periodical with respect to the azimuthal angle  $\varphi$ , is sought in the form of a product  $\Psi(x_f, x_s, \varphi) = \Psi^{m\sigma}(x_f, x_s) e^{im\varphi}/\sqrt{2\pi}$ ,

where  $m = 0, \pm 1, \pm 2, \dots$  is the magnetic quantum number. Note, that in the absence of magnetic fields the Hamiltonian commutes also with the inversion operator ( $\mathbf{r} \rightarrow -\mathbf{r}$ ) with the eigenvalues  $\hat{\sigma} = (-1)^m \sigma$  and the solutions can be divided into *gerade* ( $\hat{\sigma} = +1$ ) and *ungerade* ( $\hat{\sigma} = -1$ ) ones. Then the function  $\Psi^{m\sigma}(x_f, x_s)$  satisfies the following equation in the two-dimensional domain  $\Omega = \Omega_{x_f}(x_s) \cup \Omega_{x_s} \subset \mathbf{R}^2 \setminus \{0\}$ ,  $\Omega_{x_f}(x_s) = (x_f^{\min}(x_s), x_f^{\max}(x_s))$ ,  $\Omega_{x_s} = (x_s^{\min}, x_s^{\max})$ :

$$\left( \hat{H}_1(x_f; x_s) + \hat{H}_2(x_s) \right. \quad (10)$$

$$\left. + V(x_f, x_s) - 2E \right) \Psi^{m\sigma}(x_f, x_s) = 0.$$

The Hamiltonian of the slow subsystem  $\hat{H}_2(x_s)$  is expressed as

$$\hat{H}_2(x_s) = \check{H}_2(x_s) = -\frac{1}{g_{1s}(x_s)} \frac{\partial}{\partial x_s} g_{2s}(x_s) \frac{\partial}{\partial x_s} + \check{V}_s(x_s), \quad (11)$$

and the Hamiltonian of the fast subsystem  $\hat{H}_1(x_f; x_s)$  is expressed in terms of the reduced Hamiltonian  $\check{H}_f(x_f; x_s)$  and the weighting factor  $g_{3s}(x_s)$ :

$$\hat{H}_1(x_f; x_s) = g_{3s}^{-1}(x_s) \check{H}_f(x_f; x_s), \quad (12)$$

$$\check{H}_f(x_f; x_s) = -\frac{1}{g_{1f}(x_f)} \frac{\partial}{\partial x_f} g_{2f}(x_f) \frac{\partial}{\partial x_f} + \check{V}_f(x_f) + \check{V}_{fs}(x_f, x_s).$$

The table contains a detailed description of the conditionally fast  $x_f$  and slow  $x_s$  independent variables, the coefficients  $g_{1s}(x_s)$ ,  $g_{2s}(x_s)$ ,  $g_{3s}(x_s)$ ,  $g_{1f}(x_f)$ ,

$g_{2f}(x_f)$ , and the reduced potentials  $\check{V}_f(x_f)$ ,  $\check{V}_s(x_s)$ ,  $\check{V}_{fs}(x_f, x_s)$ , entering Eqs. (10)–(12) for SQD, OSQD, and PSQD in cylindrical ( $\mathbf{x} = (z, \rho, \varphi)$ ), spherical ( $\mathbf{x} = (r, \eta = \cos \theta, \varphi)$ ), and oblate/prolate spheroidal ( $\mathbf{x} = (\xi, \eta, \varphi)$ ) coordinates (CS, SC, and OSC/PSC) [47]. Note that in the table, using Eqs. (2), (5) in the reduced atomic units, the potential  $\check{V}(r, \eta)$  for OSQD/PSQD in SC is expressed for Model A as

$$\check{V}(r, \eta) = 2r^2 U^A(r, \eta) = \omega^2 r^4 (\zeta_1(1 - \eta^2) + \zeta_3 \eta^2),$$

and for Model C as

$$\begin{aligned} \check{V}(r, \eta) &= 2r^2 U^C(r, \eta) \\ &= 2r^2 U_0 \left( 1 - (1 + \exp((r^2((1 - \eta^2)/a^2 + \eta^2/c^2) - 1)/s))^{-1} \right), \end{aligned}$$

both having zero normal first derivatives  $\partial V(r, \eta)/\partial r$  in the vicinity of the origin  $r = 0$  (equilibrium point), similar to [29]. We do not use the CC for Model C, because the motion in this case is not restricted by two coordinates  $\rho$  and  $z$ . For Model B in the table  $\omega = 0$  and the potentials  $\check{V}(r, \eta) = \check{V}(\xi, \eta) = 0$  are zero, since in this case one should impose the Dirichlet boundary conditions  $\Psi^{m\sigma}(x_f, x_s)|_{\partial\Omega} = 0$  at the boundary  $\partial\Omega = \{\mathcal{R}^2 | S(x_f, x_s) = 0\}$  of  $\Omega$ , restricted by the surface  $S(\tilde{\mathbf{r}}) = 0$ , which is equivalent to the action of the potential (3).

The solution  $\Psi_i^{m\sigma}(x_f, x_s) \equiv \Psi_i^{Em\sigma}(x_f, x_s)$  of the problem (10)–(12) is sought in the form of Kantorovich expansion [34]

$$\begin{aligned} \Psi_i^{Em\sigma}(x_f, x_s) & \quad (13) \\ &= \sum_{j=1}^{j_{\max}} \Phi_j^{m\sigma}(x_f; x_s) \chi_j^{(m\sigma i)}(E, x_s). \end{aligned}$$

The set of appropriate trial functions is chosen as the set of eigenfunctions  $\Phi_j^{m\sigma}(x_f; x_s)$  of the Hamiltonian  $\check{H}_f(x_f; x_s)$  from (12), i.e., the solutions of the parametric BVP

$$\{\check{H}_f(x_f; x_s) - \check{\lambda}_i(x_s)\} \Phi_i^{m\sigma}(x_f; x_s) = 0, \quad (14)$$

in the interval  $x_f \in \Omega_{x_f}(x_s)$ , depending on the conditionally slow variable  $x_s \in \Omega_{x_s}$  as on a parameter. These solutions obey the boundary conditions

$$\begin{aligned} \lim_{x_f \rightarrow x_f^t(x_s)} \left( N_f^{(m\sigma)}(x_s) g_{2f}(x_f) \frac{d\Phi_j^{m\sigma}(x_f; x_s)}{dx_f} \right. & \quad (15) \\ \left. + D_f^{(m\sigma)}(x_s) \Phi_j^{m\sigma}(x_f; x_s) \right) &= 0 \end{aligned}$$

at the boundary points  $\{x_f^{\min}(x_s), x_f^{\max}(x_s)\} = \partial\Omega_{x_f}(x_s)$  of the interval  $\Omega_{x_f}(x_s)$ . In Eq. (15),  $N_f^{(m\sigma)}(x_s) \equiv N_f^{(m\sigma)}$ ,  $D_f^{(m\sigma)}(x_s) \equiv D_f^{(m\sigma)}$ , unless specially declared, are determined by the relations  $N_f^{(m\sigma)} = 1$ ,  $D_f^{(m\sigma)} = 0$  at  $m = 0$ ,  $\sigma = +1$  (or at  $\sigma = 0$ , i.e., without parity separation),  $N_f^{(m\sigma)} = 0$ ,  $D_f^{(m\sigma)} = 1$  at  $m = 0$ ,  $\sigma = -1$  or at  $m \neq 0$ . The eigenfunctions satisfy the orthonormality condition with the weighting function  $g_{1f}(x_f)$  in the same interval  $x_f \in \Omega_{x_f}(x_s)$ :

$$\begin{aligned} \langle \Phi_i^{m\sigma} | \Phi_j^{m\sigma} \rangle &= \int_{x_f^{\min}(x_s)}^{x_f^{\max}(x_s)} \Phi_i^{m\sigma}(x_f; x_s) & (16) \\ &\times \Phi_j^{m\sigma}(x_f; x_s) g_{1f}(x_f) dx_f = \delta_{ij}. \end{aligned}$$

Here  $\check{\lambda}_1(x_s) < \dots < \check{\lambda}_{j_{\max}}(x_s) < \dots$  is the desired set of real eigenvalues. The corresponding set of potential curves  $2E_1(x_s) < \dots < 2E_{j_{\max}}(x_s) < \dots$  of Eqs. (12) is determined by  $2E_j(x_s) = g_{3s}^{-1}(x_s) \check{\lambda}_j(x_s)$ . Note that for OSC and PSC the desired set of real eigenvalues  $\check{\lambda}_j(x_s)$  depends on the combined parameter,  $x_s \rightarrow p^2 = (d/2)^2 \cdot 2E$ , i.e., the product of spectral  $2E$  and geometrical  $(d/2)^2$  parameters of the problem (10). The solutions of the problem (14)–(16) for Models A and B are calculated in the analytical form [39], while for Model C this is done using the program ODPEVP [40]. Substituting the expansion (13) into Eq. (1), we get a set of ODEs for the slow subsystem with respect to the unknown vector functions  $\chi^{(m\sigma i)}(x_s, E) \equiv \chi^{(t)}(x_s) = (\chi_1^{(t)}(x_s), \dots, \chi_{j_{\max}}^{(t)}(x_s))^T$ :

$$\begin{aligned} \left( -\frac{1}{g_{1s}(x_s)} \frac{d}{dx_s} g_{2s}(x_s) \frac{d}{dx_s} + \check{V}_s(x_s) \right. & \quad (17) \\ \left. + V_{ii}(x_s) - 2E \right) \chi_i^{(t)}(x_s) &= - \sum_j V_{ij}(x_s) \chi_j^{(t)}(x_s). \end{aligned}$$

Here  $V_{ii}(x_s) = 2E_i(x_s) + H_{ii}(x_s)$ ,  $V_{ij}(x_s)$  are defined by the formula

$$\begin{aligned} V_{ij}(x_s) &= \frac{g_{2s}(x_s)}{g_{1s}(x_s)} H_{ij}(x_s) + \frac{1}{g_{1s}(x_s)} & (18) \\ &\times \frac{dg_{2s}(x_s) Q_{ij}(x_s)}{dx_s} + \frac{g_{2s}(x_s)}{g_{1s}(x_s)} Q_{ij}(x_s) \frac{d}{dx_s}, \\ H_{ij}(x_s) &= H_{ji}(x_s) \end{aligned}$$

$$\begin{aligned}
&= \int_{x_f^{\min}(x_s)}^{x_f^{\max}(x_s)} g_{1f}(x_f) \frac{\partial \Phi_i(x_f; x_s)}{\partial x_s} \frac{\partial \Phi_j(x_f; x_s)}{\partial x_s} dx_f, \\
&Q_{ij}(x_s) = -Q_{ji}(x_s) \\
&= - \int_{x_f^{\min}(x_s)}^{x_f^{\max}(x_s)} g_{1f}(x_f) \Phi_i(x_f; x_s) \frac{\partial \Phi_j(x_f; x_s)}{\partial x_s} dx_f,
\end{aligned}$$

and calculated analytically for Model B and by means of the program ODPEVP [40] for Model C, while the solutions of the BVPs for Eq. (17) with the boundary and orthonormalization conditions of the type (15), (16) with  $x_f \rightarrow x_s$  were calculated by means of the program KANTBP [41]. Note that for Model A in SC or CC and Model B in OSC or PSC, the variables  $x_f$  and  $x_s$  are separated so that the matrix elements  $\check{V}_{ij}(x_s) = 0$  are put into the r.h.s. of Eq. (17), and  $V_s(x_s)$  are substituted from the table. For the interesting lower part of the spectrum of Models A and B  $2E$ :  $2E_1 < 2E_2 < \dots < 2E_t$ , or of Model C  $2E$ :  $2E_1 < 2E_2 < \dots < 2E_t < U_0$ , the number  $j_{\max}$  of the equations solved should be at least not less than the number of the energy levels of the problem (17) at  $a = c = r_0$ . To ensure the prescribed accuracy of calculation of the lower part of the spectrum discussed below with eight significant digits, we used  $j_{\max} = 16$  basis functions in the expansion (8) and the discrete approximation of the desired solution by Lagrange finite elements of the fourth order with respect to the grid pitch  $\Omega_{h^s(x_s)}^p = [x_{s;\min}, x_{s;k} = x_{s;k-1} + h_s, x_{s;\max}]$ . The details of the corresponding computational scheme are given in [39].

### 3. SPECTRAL CHARACTERISTICS OF SPHEROIDAL AND DUMBBELL QDs

#### 3.1. Model A of OSQD and PSQD

In the exactly solvable Model A the variables are separable in spherical coordinates, and under the variation of the aspect ratio parameters  $\zeta_{ca} = c/a$  and  $\zeta_{ac} = \zeta_{ca}^{-1} = a/c$  for the oblate and prolate spheroids, determining the transverse  $\omega_\rho = \sqrt{\zeta_1} \omega$  and longitudinal  $\omega_z = \sqrt{\zeta_3} \omega$  frequencies of the circular and linear harmonic oscillators. The spectrum is given by the sum of energies  $2E_{n_\rho m} = 2\omega_\rho(2n_\rho + |m| + 1)$ ,  $n_\rho = 0, 1, \dots$ ,  $m = 0, \pm 1, \dots$  (with the eigenvalues being degenerate with respect to  $\lambda_\rho = 2n_\rho + |m|$  that numbers in ascending order the energy values of the states [48, 49], which is conventionally used in practice, see, for example, [21, 27]), and

$2E_{n_z} = 2\omega_z(n_z + 1/2)$ ,  $n_z = 0, 1, \dots$ , at  $\omega = \omega_{r_0} = \pi^2/(3r_0^2)$ ,  $\sqrt{\zeta_1} = r_0^2/a^2$ , and  $\sqrt{\zeta_3} = r_0^2/c^2$ . At  $a = c = r_0$  the independent variables are separable in the boundary problem for Eq. (1) in the spherical coordinates too, i.e., we have the energy spectrum of a spherical oscillator  $2E_{n_r l m}^{\text{osc}} = 2\omega_{r_0}(2n_r + l + 3/2)$ ,  $n_r = 0, 1, \dots$ ,  $l = 0, 1, \dots$ ,  $m = 0, \pm 1, \dots, \pm l$ , with the eigenvalues being degenerate with respect not only to  $m$ , but also to  $\lambda_r = 2n_r + l$  that numbers in ascending order the energy values of states, separated in parity  $\hat{\sigma} = (-1)^\lambda = (-1)^l = (-1)^m \sigma$ ,  $\sigma = (-1)^{l-m} = \pm 1$ . The energy spectrum of the spherical oscillator  $2E_{n_r l m}^{\text{osc}}$  coincides at  $a = c$  with

$$\begin{aligned}
2E(a, c) &= 2(E_{n_{zo}} + E_{n_{\rho o}, m}), \\
2E(c, a) &= 2(E_{n_{pp}, m} + E_{n_{zp}}),
\end{aligned} \tag{19}$$

which, respectively, defines the one-to-one correspondence between the sets of the quantum numbers  $n_{zo} = l - |m|$ ,  $n_{\rho o} = n_r$ ,  $m = m$  for OSQD and SQD and  $n_{pp} = n_r$ ,  $m = m$ ,  $n_{zp} = l - |m|$  for PSQD and SQD, that characterize the fast and slow subsystems at continuous variation of the parameters  $\zeta_{ca} = c/a$  and  $\zeta_{ac} = a/c$ . At decreasing the parameter  $\zeta_{ca}$  or  $\zeta_{ac}$  the degeneracy of the spectrum with respect to the quantum numbers  $n, l, m$  is removed.

Figure 1 illustrates the lower part of the equidistant energy spectrum  $\tilde{E}/\tilde{E}_R = 2E(a, c)$  and  $\tilde{E}/\tilde{E}_R = 2E(c, a)$  for even states  $\sigma = +1$  of the model of OSQD and PSQD with parabolic confining potentials (2), at  $m = 0$ , i.e., of an oblate and prolate spheroid, depending on the minor  $c$  or  $a$  and the major  $a$  or  $c$  semiaxes, respectively. At fixed values of the parity  $\sigma$  and the magnetic quantum number  $m$ , when the ratio of the frequencies  $\omega_\rho$  and  $\omega_z$  of the longitudinal and transverse oscillators is a rational number,  $\omega_\rho/\omega_z \in \mathcal{Q}$ , as illustrated, e.g., in Fig. 1, the exact crossings of the same-parity terms occur, after which above each energy level of OSQD (or PSQD), labelled with the quantum number  $n_{zo}$  (or  $n_{pp}$ ) of the fast subsystem, an equidistant spectrum appears with the energy levels labelled with the quantum number  $n_{\rho o}$  (or  $n_{zp}$ ) of the slow subsystem. Note that when the parameters tend to zero, the longitudinal energy of OSQD and the transverse energy of PSQD tend to infinity. However, since the variables are separable and the energy can be presented as a sum, the finite energies for a disc  $E_{n_{\rho o}, m}$  or a wire  $E_{n_{zp}}$  result from the subtraction of the longitudinal  $E_{n_{zo}}$  or transverse  $E_{n_{pp}, m}$  energy, respectively.

#### 3.2. Models B and C for Oblate Spheroidal QD

At fixed coordinate  $x_s$  of the slow subsystem, the motion of the particle in the fast degree of freedom

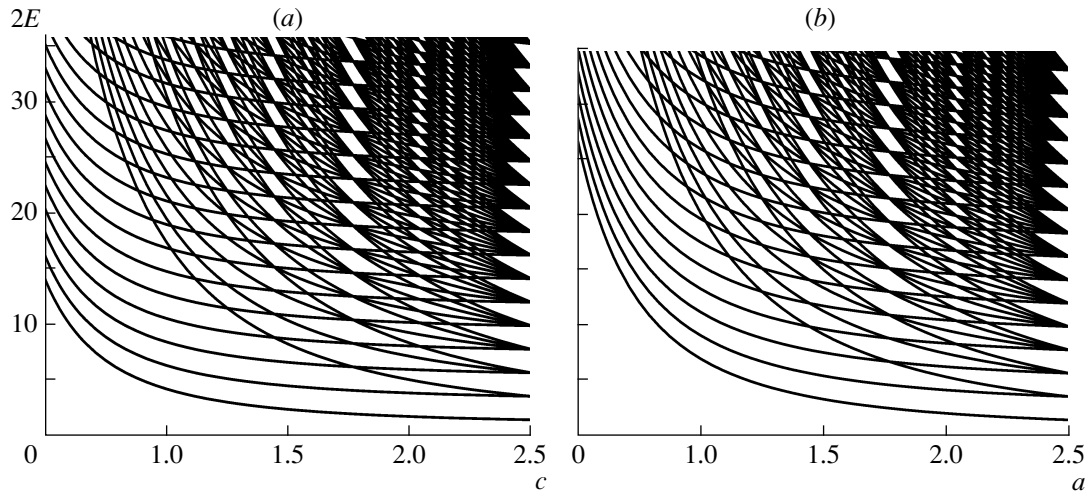


**Fig. 1.** Energies  $2E = \tilde{E}/E_R$  of even  $\sigma = +1$  lower states of Model A OSQD at  $a = 2.5$  (a) and PSQD at  $c = 2.5$  (b) versus  $c$  or  $a$ . The exact intersections of the energy levels take place at rational ratios  $R = \omega_\rho/\omega_z = (c/a)^2 \in \mathcal{Q}$  (a) and  $R = \omega_z/\omega_\rho = (a/c)^2 \in \mathcal{Q}$  (b) of the frequencies of transverse and longitudinal oscillators with  $R = 1, 4/5, 3/4, 2/3, 3/5, 1/2, 2/5, 1/3, 1/4, 1/5, \dots$

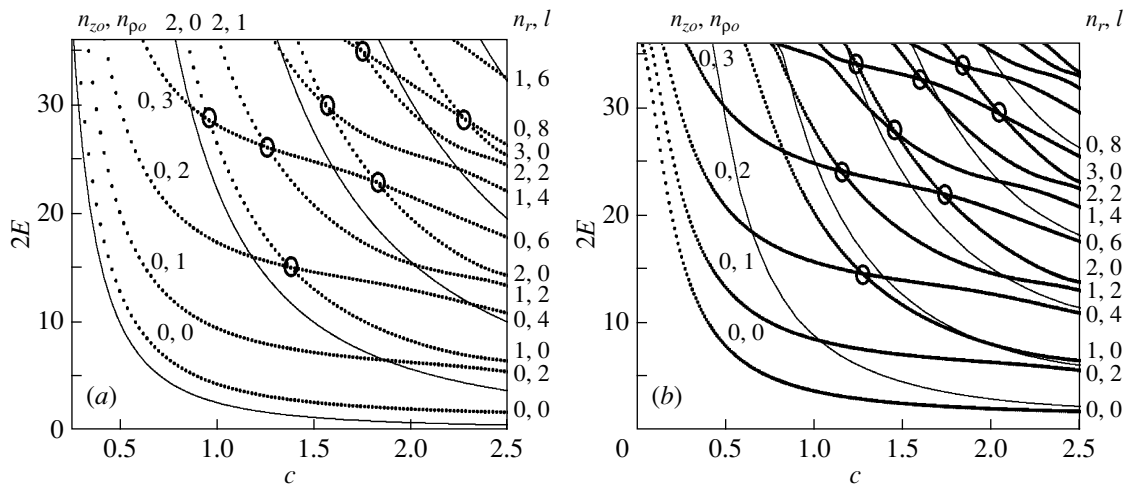


**Fig. 2.** Energies  $2E = \tilde{E}/E_R$  of even  $\sigma = +1$  lower states for OSQD versus the minor  $c$ ,  $\zeta_{ca} = c/a \in (1/5, 1)$  being the spheroid aspect ratio: (a) well with impermeable walls, (b) diffusion potential with  $2U_0 = 36$ ,  $s = 0.1$ , the major semiaxis  $a = 2.5$  and  $m = 0$ . The thin lines are minimal values  $2E_i^{\min} \equiv 2E_i(x_s = 0)$  of potential curves.

$x_f$  is localized within the potential well having the effective width

$$L(x_s) = 2c\sqrt{1 - x_s^2/a^2}, \quad (20)$$

where  $L = \tilde{L}/a_B^*$ . The parametric BVP for Eq. (12) at fixed values of the coordinate  $x_s$ ,  $x_s \in (0, a)$ , is solved in the interval  $x_f \in (-L(x_s)/2, L(x_s)/2)$  for Model C using the program ODPEVP, and for Model B the eigenvalues  $\tilde{E}_{n_o}(x_s)/\tilde{E}_R \equiv 2E_i(x_s)$ ,  $n_o = i = 1, 2, \dots$ , and the corresponding parametric eigenfunctions  $\Phi_i^\sigma(x_f; x_s)$ , are expressed in the ana-

lytical form:

$$2E_i(x_s) = \frac{\pi^2 n_o^2}{L^2(x_s)}, \quad \Phi_i^\sigma(x_f; x_s) \quad (21)$$

$$= \sqrt{\frac{2}{L(x_s)}} \sin\left(\frac{\pi n_o}{2} \left(\frac{x_f}{L(x_s)/2} - 1\right)\right),$$

where the even solutions  $\sigma = +1$  are labelled with odd  $n_o = n_{zo} + 1 = 2i - 1$ , and the odd ones  $\sigma = -1$  with even  $n_o = n_{zo} + 1 = 2i$ ,  $i = 1, 2, 3, \dots$ . The effective potentials (18) in Eq. (17) for the slow subsystem

are expressed analytically in terms of the integrals over the fast variable  $x_f$  of the basis functions (21) and their derivatives with respect to the parameter  $x_s$  including the states of both parities  $\sigma = \pm 1$ :

$$2E_i(x_s) = \frac{a^2 \pi^2 n_o^2}{4c^2(a^2 - x_s^2)}, \quad (22)$$

$$H_{ii}(x_s) = \frac{3 + \pi^2 n_o^2}{12} \frac{x_s^2}{(a^2 - x_s^2)^2},$$

$$H_{ij}(x_s) = \frac{2n_o n'_o (n_o^2 + n_o'^2)(1 + (-1)^{n_o + n'_o})}{(n_o^2 - n_o'^2)^2} \times \frac{x_s^2}{(a^2 - x_s^2)^2},$$

$$Q_{ij}(x_s) = \frac{n_o n'_o (1 + (-1)^{n_o + n'_o})}{(n_o^2 - n_o'^2)^2} \frac{x_s}{a^2 - x_s^2}, \quad n'_o \neq n_o.$$

For Model B at  $c = a = r_0$  the OSQD turns into SQD with known analytically expressed energy levels  $E_t \equiv E_{nlm}^{\text{sp}}$  and the corresponding eigenfunctions

$$2E_{nlm}^{\text{sp}} = \frac{\alpha_{n_r+1, l+1/2}^2}{r_0^2}, \quad (23)$$

$$\Phi_{nlm}^{\text{sp}}(r, \theta, \varphi) = \frac{\sqrt{2} J_{l+1/2} \left( \sqrt{2E_{nlm}^{\text{sp}}} r \right)}{r_0 \sqrt{r} |J_{l+3/2}(\alpha_{n_r+1, l+1/2})|} Y_{lm}(\theta, \varphi),$$

where  $\alpha_{n_r+1, l+1/2}$  are zeros of the Bessel function of semi-integer index  $l + 1/2$ , numbered in ascending order  $0 < \alpha_{11} < \alpha_{12} < \dots < \alpha_{iv} < \dots$  by the integer  $i, v = 1, 2, 3, \dots$ . Otherwise one can use equivalent pairs  $iv \leftrightarrow \{n_r, l\}$  with  $n_r = 0, 1, 2, \dots$  numbering the zeros of the Bessel function and  $l = 0, 1, 2, \dots$ , being the orbital quantum number that determines the parity of states  $\hat{\sigma} = (-1)^l = (-1)^m \sigma$ ,  $\sigma = (-1)^{l-m} = \pm 1$ . At fixed  $l$ , the energy levels  $\tilde{E}_{nlm}/\tilde{E}_R = 2E_t$ , degenerate with respect to the magnetic quantum number  $m$ , are labelled with the quantum number  $n = n_r + 1 = i = 1, 2, 3, \dots$ , in contrast to the spectrum of a spherical oscillator, degenerate with respect to the quantum number  $\lambda = 2n_r + l$ . Figures 2, 3 show the lower part of the non-equidistant spectrum  $\tilde{E}(\zeta_{ca})/\tilde{E}_R = 2E_t$  and the eigenfunctions  $\Psi_t^{m\sigma}$  from Eq. (13) for even states of OSQD Models B and C at  $m = 0$ . There is a one-to-one correspondence rule  $n_o = n_{zo} + 1 = 2n - (1 + \sigma)/2$ ,  $n = 1, 2, 3, \dots$ , and  $n_{\rho o} = (l - |m| - (1 - \sigma)/2)/2$ , between the sets of spherical quantum numbers  $(n, l, m, \hat{\sigma})$  of SQD with radius  $r_0 = a = c$  and spheroidal ones  $\{n_\xi = n_r, n_\eta = l - |m|, m, \sigma\}$  of OSQD with the major  $a$  and the minor  $c$  semiaxes,

and the adiabatic set of cylindrical quantum numbers  $[n_{zo}, n_{\rho o}, m, \sigma]$  at continuous variation of the parameter  $\zeta_{ca} = c/a$ . The presence of crossing points of the energy levels of similar parity under the symmetry change from spherical  $\zeta_{ca} = 1$  to axial, i.e., under the variation of the parameter  $0 < \zeta_{ca} < 1$ , in the BVP with two variables at fixed  $m$  for Model B is caused by the possibility of variable separation for Eq. (8) in the OSC [47], i.e., the r.h.s. of Eq. (17) equals zero, and by the existence of the integral of motion (9). The transformation of the eigenfunctions occurring in the course of a transition through the crossing points (marked by circles) in Fig. 2, is shown in Fig. 3 for Model B (marked by arrows) and similar for Model C. From the comparison of these figures one can see that if the eigenfunctions are ordered in accordance with the increasing eigenvalues of the BVPs, then for both Models B and C, the number of nodes [50] is invariant under the variation of the parameter  $c$  from  $c = a = 2.5$  to  $c = 0.5$  of the potentials (3) and (5). For Model B, such a behavior follows from the fact of separation of variables of the BVP with the potential (3) in the OSC, while for Model C further investigation is needed because the coordinate system, in which the variables of the BVP with the potential (5) are separable, is unknown. So, crossing and quasicrossing points will correspond to branching points in the complex plane of focal parameter  $d$ , like in the case of separable variables [51]. So, at small values of the deformation parameter ( $\zeta_{ca}$  for OSQD or  $\zeta_{ac}$  for PSQD) there are nodes only along the corresponding major semiaxis. For Model C at each value of the parameter  $a$  there is a finite number of discrete energy levels limited by the value  $2U_0$  of the well walls height. As shown in Fig. 2b, the number of levels of OSQD, equal to that of SQD at  $a = c = r_0$ , is reduced with the decrease of the parameter  $c$  (or  $\zeta_{ca}$ ), in contrast to Models A and B that have countable spectra, and avoided crossings appear just below the threshold.

### 3.3. Models B and C for Prolate Spheroidal QD

In contrast to OSQD, for PSQD at fixed coordinate  $x_s$  of the slow subsystem the motion of the particle in the fast degree of freedom  $x_f$  is confined to a 2D potential well with the effective variable radius

$$\rho_0(x_s; a, c) = a \sqrt{1 - x_s^2/c^2}, \quad (24)$$

where  $\rho_0(x_s) = \tilde{\rho}_0(x_s)/a_B^*$ . The parametric BVP for Eq. (12) at fixed values of the coordinate  $x_s$  from the interval  $x_s \in (-c, c)$  is solved in the interval  $x_f \in (0, \rho_0(x_s))$  for Model C using the program ODPEVP, while for Model B the eigenvalues  $\tilde{E}_{n_{pp}+1}(x_s)/\tilde{E}_R \equiv 2E_i(x_s)$ ,  $n_{pp} + 1 = i = 1, 2, \dots$ , and the corresponding parametric basis functions  $\Phi_i^{m\sigma=0}(x_f; x_s) \equiv$

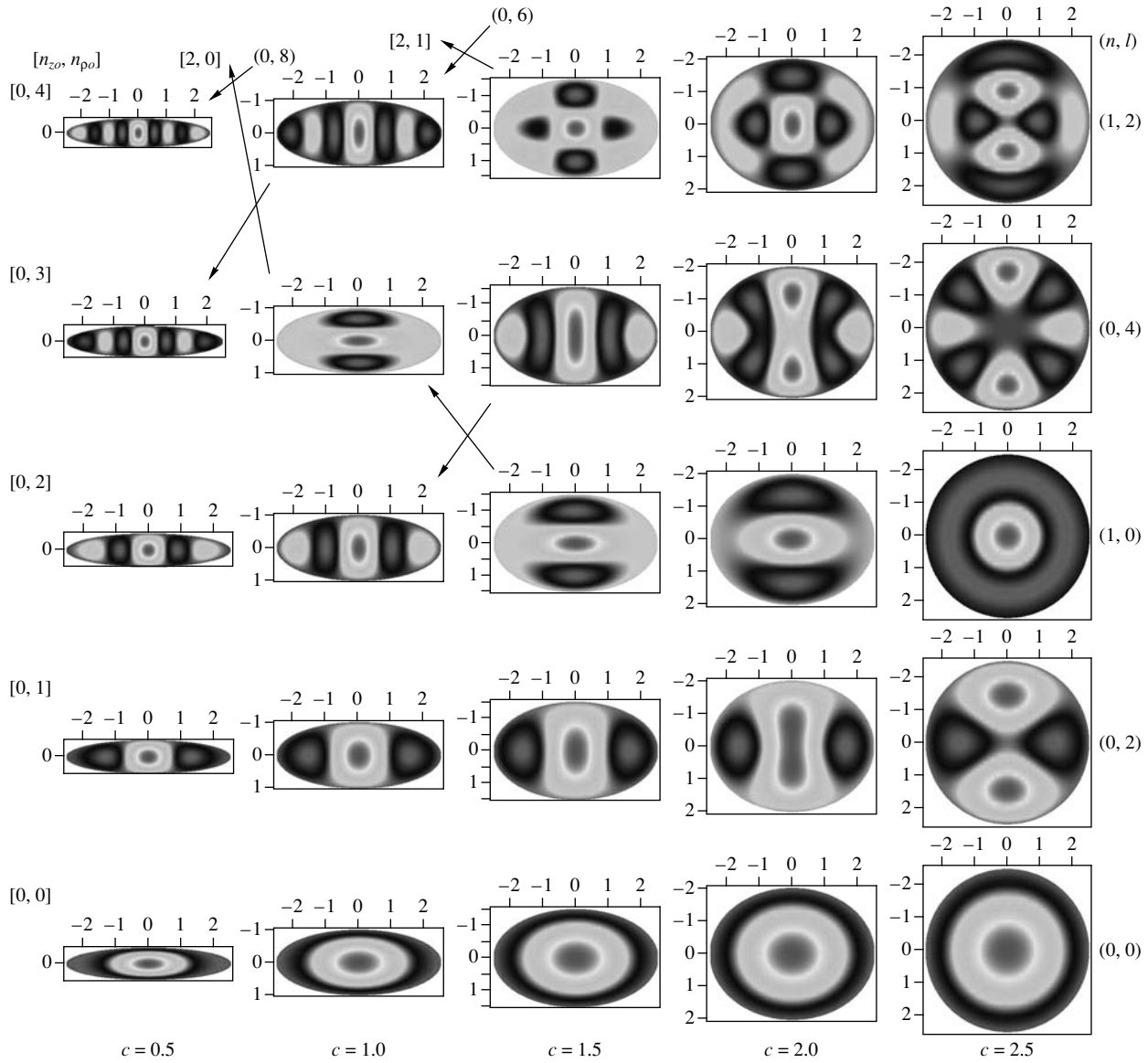


**Fig. 3.** Contour lines of the first five even-parity wave functions  $\sigma = +1$  in the  $xz$  plane of Model B of OSQD for the major semiaxis  $a = 2.5$  and different values of the minor semiaxis  $c$  ( $\zeta_{ca} = c/a \in (1/5, 1)$ ).

$\Phi_i^m(x_f; x_s)$  without parity separation are expressed in the analytical form:

$$2E_i(x_s) = \frac{\alpha_{n_{pp}+1, |m|}^2}{\rho_0^2(x_s)}, \quad (25)$$

$$\Phi_{n_{pp}}^m(x_s) = \frac{\sqrt{2}}{\rho_0(x_s)} \frac{J_{|m|} \left( \sqrt{2E_{n_{pp}+1, |m|}(x_s)} x_f \right)}{|J_{|m|+1}(\alpha_{n_{pp}+1, |m|})|},$$

where  $\alpha_{n_{pp}+1, |m|} = \bar{J}_{|m|}^{n_{pp}+1}$  are positive zeros of the Bessel function of the first kind  $J_{|m|}(x_f)$ , labeled in the ascending order with the quantum number  $n_{pp} + 1 = i = 1, 2, \dots$

The effective potentials (18) in Eq. (17) for the slow subsystem are calculated numerically in quadratures via the integrals over the fast variable  $x_f$  of the basis functions (25) and their derivatives with respect to the parameter  $x_s$ , and at  $m = 0$  may be presented in the analytical form:

$$2E_i(x_s) = \frac{(\bar{J}_0^i)^2}{\rho_0^2(x_s)}, \quad (26)$$

$$H_{ii}(x_s) = \left( \frac{\rho_0'(x_s)}{\rho_0(x_s)} \right)^2 \frac{(1 + \bar{J}_0^i)}{3},$$



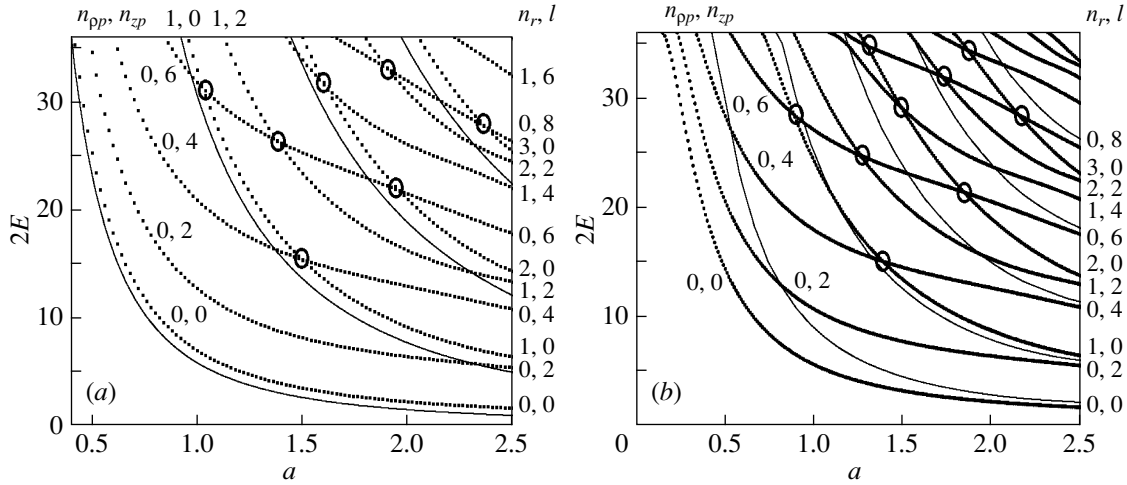


**Fig. 4.** Energies  $2E = \tilde{E}/E_R$  of even  $\sigma = +1$  lowest states for PSQD depending on the minor semiaxis  $a$  ( $\zeta_{ac} = a/c \in (1/5, 1)$  is the spheroid aspect ratio): (a) well with impermeable walls, (b) diffusion potential,  $2U_0 = 36$ ,  $s = 0.1$ , the major semiaxis  $c = 2.5$  and  $m = 0$ . Thin lines are minimal values  $2E_i^{\min} \equiv 2E_i(x_s = 0)$  of potential curves.

$$\begin{aligned}
 H_{ij}(x_s) &= 2 \left( \frac{\rho'_0(x_s)}{\rho_0(x_s)} \right)^2 \\
 &\times \left( \bar{J}_0^i \bar{J}_0^j \int_0^1 \frac{J_1(\bar{J}_0^i x)}{J_1(\bar{J}_0^i)} \frac{J_1(\bar{J}_0^j x)}{J_1(\bar{J}_0^j)} x^3 dx \right. \\
 &\quad - \bar{J}_0^i \int_0^1 \frac{J_1(\bar{J}_0^i x)}{J_1(\bar{J}_0^i)} \frac{J_0(\bar{J}_0^j x)}{J_1(\bar{J}_0^j)} x^2 dx \\
 &\quad \left. - \bar{J}_0^j \int_0^1 \frac{J_0(\bar{J}_0^i x)}{J_1(\bar{J}_0^i)} \frac{J_1(\bar{J}_0^j x)}{J_1(\bar{J}_0^j)} x^2 dx \right), \\
 Q_{ij}(x_s) &= -2 \frac{\rho'_0(x_s)}{\rho_0(x_s)} \bar{J}_0^j \int_0^1 \frac{J_0(\bar{J}_0^i x)}{J_1(\bar{J}_0^i)} \frac{J_1(\bar{J}_0^j x)}{J_1(\bar{J}_0^j)} x^2 dx, \\
 &\quad j \neq i.
 \end{aligned}$$

Figures 4, 5 illustrate the lower part of the non-equidistant spectrum  $\tilde{E}(\zeta_{ac})/\tilde{E}_R = 2E_t$  and the eigenfunctions  $\Psi_t^{m\sigma}$  from Eq. (13) of even states of PSQD Models B and C.

A one-to-one correspondence rule  $n_{pp} + 1 = n_p = i = n = n_r + 1$ ,  $i = 1, 2, \dots$ , and  $n_{zp} = l - |m|$  holds between the quantum numbers  $(n, l, m, \sigma)$  of SQD with the radius  $r_0 = a = c$ , the spheroidal quantum numbers  $\{n_\xi = n_r, n_\eta = l - |m|, m, \sigma\}$  of PSQD with the major  $c$  and the minor  $a$  semiaxes, and the adiabatic set of quantum numbers  $[n_p + 1, n_{zp}, m, \sigma]$  under the continuous variation of

the parameter  $\zeta_{ac} = a/c$ . The presence of crossing points of similar-parity energy levels in Fig. 4 under the change of symmetry from spherical  $\zeta_{ac} = 1$  to axial, i.e., under the variation of the parameter  $0 < \zeta_{ac} < 1$ , in the BVP with two variables at fixed  $m$  for Model B is caused by the possibility of variable separation for Eq. (6) in the PSC [47], i.e., r.h.s. of Eq. (17) equals zero, and by the existence of the additional integral of motion (7). For Model C, at each value of the parameter  $c$  there is also only a finite number of discrete energy levels limited by the value  $2U_0$  of the well walls' height. As shown in Fig. 4b, the number of energy levels of PSQD, equal to that of SQD at  $a = c = r_0$ , which is determined by the product of mass  $\mu_e$  of the particle, the well depth  $\tilde{U}_0$ , and the square of the radius  $\tilde{r}_0$ , is reduced with the decrease of the parameter  $\tilde{a}$  (or  $\zeta_{ac}$ ) because of the promotion of the potential curve (lower bound) into the continuous spectrum, in contrast to Models A and B having countable spectra. Note that the spectrum of Model C for PSQD or OSQD should approach that of Model B with the growth of the walls' height  $U_0$  of the spheroidal well. However, at critical values of the ellipsoid aspect ratio it is shown that in the effective mass approximation, both the terms (lower bound) and the discrete energy eigenvalues in models of the B type are shifted towards the continuum. Therefore, when approaching the critical aspect ratio values, it is necessary to use such models, as the lens-shaped self-assembled QDs with a quantum well confined to a narrow wetting layer [4], or, if the minor semiaxis becomes comparable with the lattice constant, to proceed to models beyond the effective mass approximation (see, e.g., [52]).

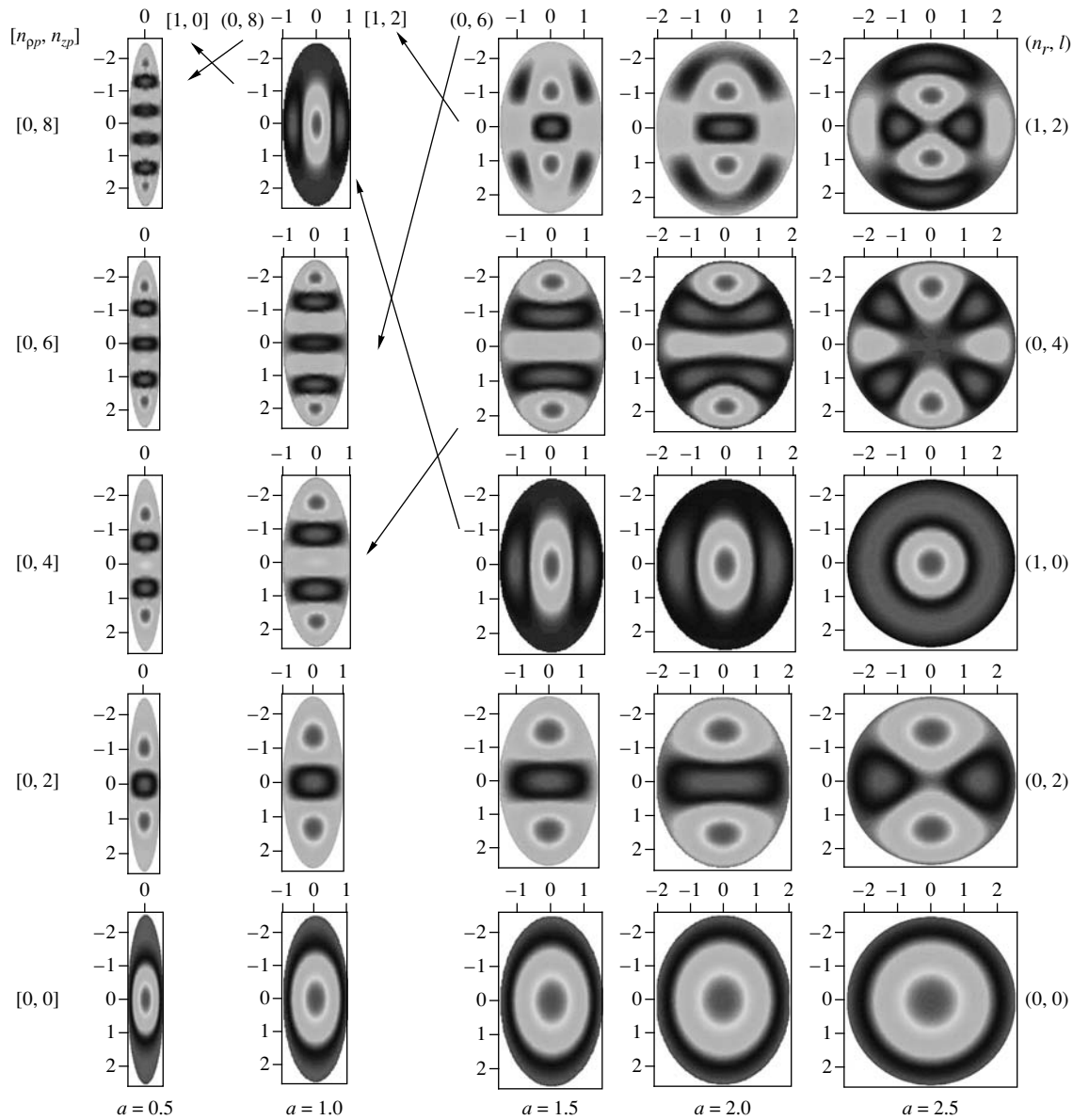


**Fig. 5.** Contour lines of the first five even-parity wave functions  $\sigma = +1$  in the  $xz$  plane of Model B of PSQD for the major semiaxis  $c = 2.5$  and different values of the minor semiaxis  $a$  ( $\zeta_{ac} = a/c \in (1/5, 1)$ ).

### 3.4. Models B for Dumbbell QD

For DQD at the fixed coordinate  $x_s$  of the slow subsystem the motion of the particle in the fast degree of freedom  $x_f$  is confined to a 2D potential double well at  $0 \leq c_1 \leq 1$  with the effective variable radius

$$\rho_0(x_s) \equiv \rho_0(x_s; a, c, c_1) \quad (27)$$

$$= \frac{a}{c} \sqrt{c^2 - x_s^2} \frac{x_s^2 c_1^2 + 1 - c_1^2}{c_1^2 c^2 / 4 + 1 - c_1^2}.$$

Figure 6 illustrates the transformation of the prolate spheroidal shape of QD with  $c = 2.5$  and  $a = 0.5$

considered in the previous section, into a “dumbbell”-type shape and the corresponding evolution of the lower part of the countable spectrum  $\tilde{E}(\zeta_{ac} = 1/5, c_1)/\tilde{E}_R = 2E_t$  of Model B versus the deformation parameter  $c_1$  at a few fixed values  $c_1 = 0, 0.25, \dots, 1.00$  from the interval  $0 \leq c_1 \leq 1$ . At  $c_1 = 0$  the discrete spectrum states are characterized by a set of exact spheroidal or adiabatic cylindrical quantum numbers,  $\{n_\xi, n_\eta, m, \sigma\}$  or  $[n_{pp}, n_{zp}, m, \sigma]$ . Typically, one can see exact crossing of energy levels having different parity ( $\sigma = \pm 1$ ) with the growth of the deformation parameter  $c_1$ , which leads, first, to the quasidegeneracy of these energy levels and

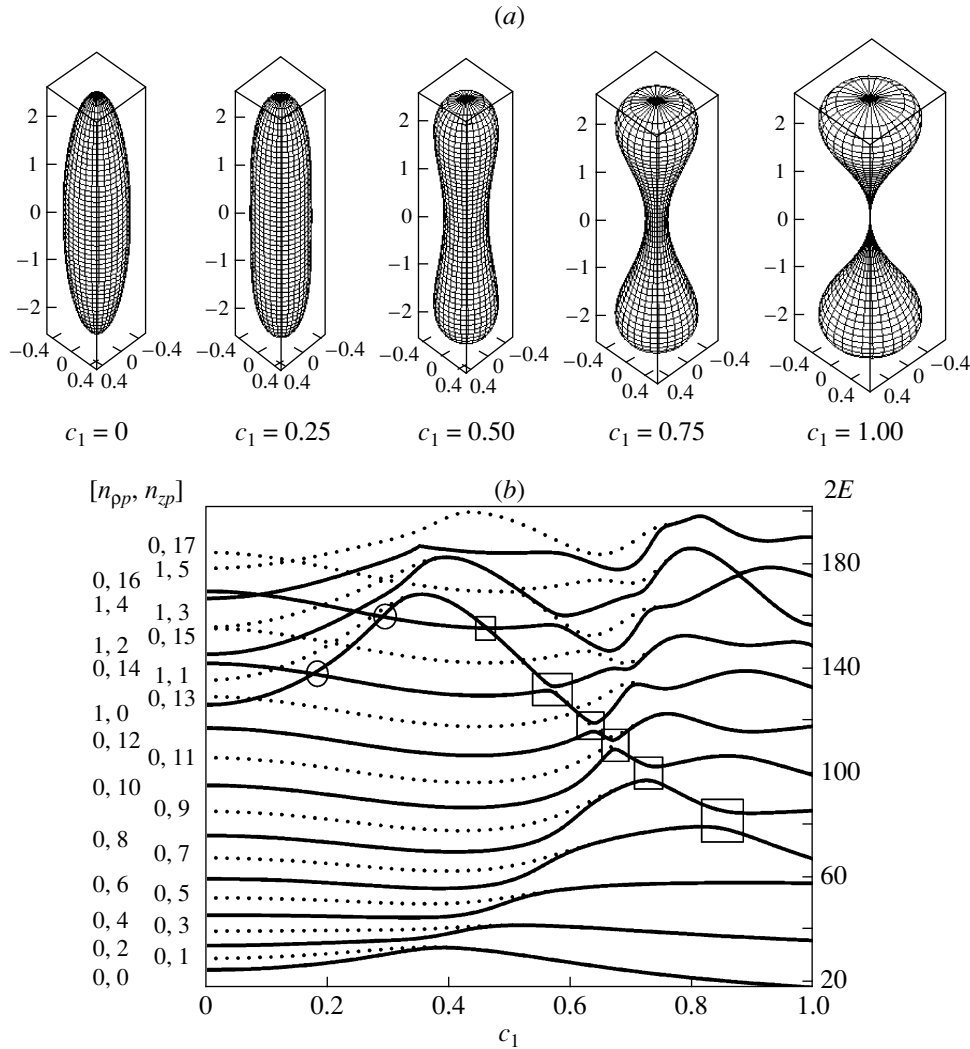


**Fig. 6.** (a) The profile in plane  $z\rho$  of closed surface generated by rotating of continuous curve  $\rho_0(z; a, c, c_1)$  from (4) about  $z$ -axis for  $c = 2.5$ ,  $a = 0.5$  versus  $c_1 = 0, 0.25, 0.50, 0.75, 1.00$ . (b) The energy levels of the even and odd states of DSQD for Model B generated by (4) for  $c = 2.5$ ,  $a = 0.5$  versus  $c_1$  classified at  $c_1 = 0$  by adiabatic quantum numbers  $n_{\rho\rho}$ ,  $n_{zp}$  and  $m = 0$  of PSQD.

then to their exact degeneracy at the critical value  $c_1 = 1$ . On the other hand, for small values of the deformation parameter  $c_1$  one observes, first, exact crossings (labelled with circles like in Fig. 4b above) of similar-parity energy levels, replaced with the avoided crossings (labelled with squares) for greater values of the deformation parameter approaching the critical value  $c_1 = 1$ . A similar picture was observed in the example of a 2D-Sinai billiard [53], a 2D-quantum billiard with the shape  $x^2 + y^2 + \epsilon x^3 = 1$  and the deformation parameter  $\epsilon > 0$ , possessing the so-called whispering gallery modes and considered in [54, 55], as well as in the unidirectional far-field emission of coupled nonidentical microdisks [19].

Figure 7 illustrates the evolution of the first five eigenfunctions with the increasing deformation pa-

rameter values  $c_1 = 0, 0.11, \dots, 0.99$ . The transformation of eigenfunctions when passing the avoided crossing points (labelled with squares) in Fig. 6b, is shown in Fig. 7 for Model B of DQD (labelled with arrows). Comparing these figures, one can see that if the eigenfunctions are ordered in accordance with the increasing eigenvalues of the BVPs, then the number of nodes is not invariant under the variation of the parameter  $c_1$  from  $c_1 = 0$  to  $c_1 = 1$  in the potentials (27). In particular, in Fig. 7 one can see that the eigenfunction of the state  $[n_{\rho\rho} = 0, n_{zp} = 6, m = 0, \sigma = +1]$  at  $c_1 = 0.99$  has the same number of nodes as the eigenfunction of the state  $[n_{\rho\rho} = 1, n_{zp} = 0, m = 0, \sigma = +1]$  at  $c_1 = 0$ . Above we could already observe this in Fig. 5 at  $a = 1$  (up-

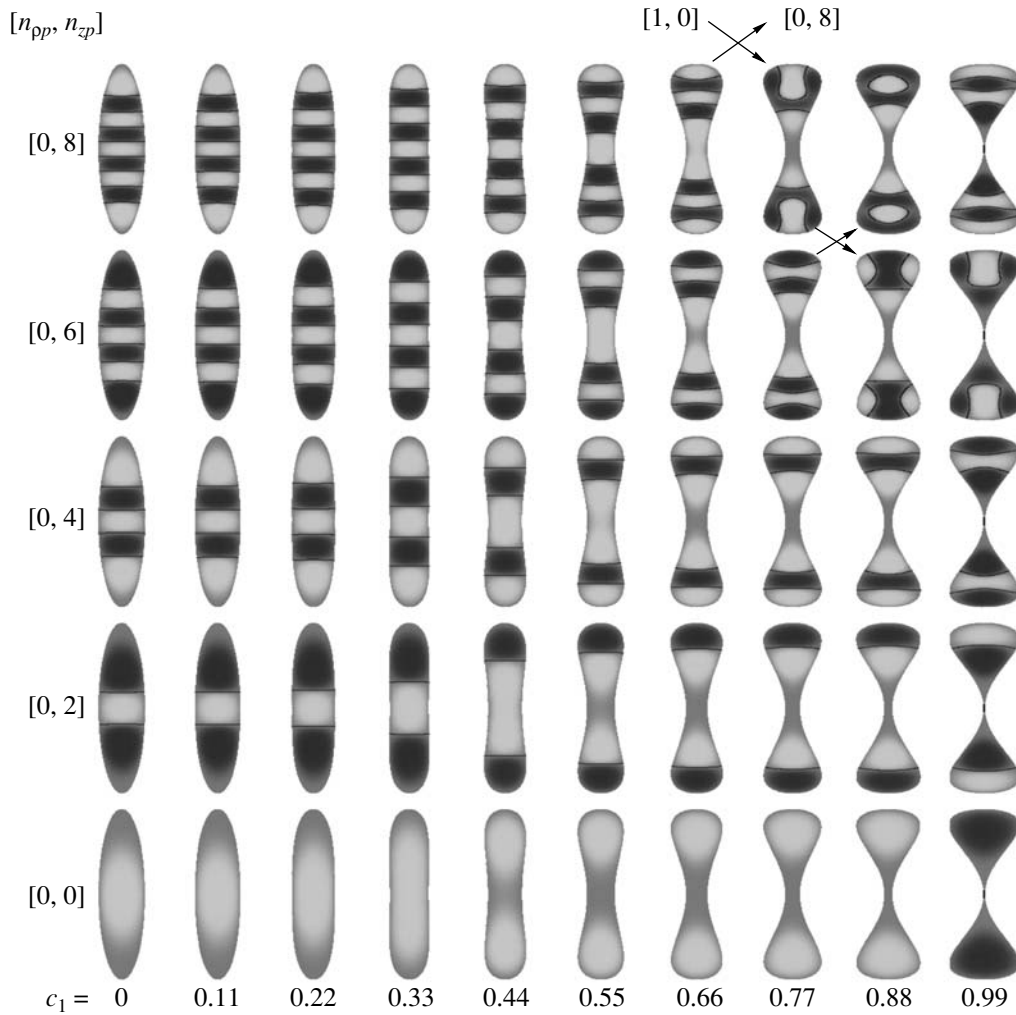


**Fig. 7.** Contour lines of the first five eigenfunctions of Model B of DSQD at  $a = 2.5$ ,  $c = 0.5$  and several values of  $c_1$ . Light and dark inflections are positive and negative values of eigenfunctions and lines are eigenfunction nodes. The adiabatic cylindrical quantum numbers  $[n_{pp}, n_{zp}]$  are given at  $m = 0$ . Crossing arrows mean the transformation of nodes of pair of eigenfunctions after passing value of parameter in which avoided crossing of corresponding pair of eigenvalues was taking place in Fig. 6b.

going arrow) after several exact and avoided crossings of the corresponding energy levels in Fig. 6b. At the same time, the eigenfunction of the state  $[n_{pp} = 0, n_{zp} = 8, m = 0, \sigma = +1]$  at  $c_1 = 0.99$  after avoided crossing of the corresponding energy levels in Fig. 6b has the same number of nodes as the eigenfunction of the state  $[n_{pp} = 6, n_{zp} = 0, m = 0, \sigma = +1]$  at  $c_1 = 0$ .

#### 4. ABSORPTION COEFFICIENT FOR AN ENSEMBLE OF QDs

One can use the mentioned differences in the energy spectra to verify the considered models of QDs by calculating the absorption coefficient  $K(\omega^{ph}, \tilde{a}, \tilde{c}, )$

of an ensemble of identical semiconductor QDs [56]:

$$\begin{aligned} \tilde{K}(\tilde{\omega}^{ph}, \tilde{a}, \tilde{c}) &= \sum_{\nu, \nu'} \tilde{K}_{\nu, \nu'}(\tilde{\omega}^{ph}, \tilde{a}, \tilde{c}) \quad (28) \\ &= \tilde{A} \sum_{\nu, \nu'} \tilde{I}_{\nu, \nu'} \delta(\hbar \tilde{\omega}^{ph} - \tilde{W}_{\nu \nu'}), \\ \tilde{I}_{\nu, \nu'} &= \left| \int \tilde{\Psi}_{\nu}^e(\tilde{\mathbf{r}}; \tilde{a}, \tilde{c}, ) \tilde{\Psi}_{\nu'}^h(\tilde{\mathbf{r}}; \tilde{a}, \tilde{c}, ) d\tilde{\mathbf{r}} \right|^2, \\ \tilde{W}_{\nu \nu'} &= \tilde{E}_g + \tilde{E}_{\nu}^e(\tilde{a}, \tilde{c}) + \tilde{E}_{\nu'}^h(\tilde{a}, \tilde{c}), \end{aligned}$$

where  $\tilde{A}$  is proportional to the square of the matrix element in the Bloch decomposition,  $\tilde{\Psi}_{\nu}^e(u)$  and  $\tilde{\Psi}_{\nu'}^h$  are the eigenfunctions of an electron ( $e$ ) and a heavy hole ( $h$ ),  $\tilde{E}_{\nu}^e$  and  $\tilde{E}_{\nu'}^h$  are the energy eigenvalues for an electron ( $e$ ) and a heavy hole ( $h$ ), depending on the semi-

axis size  $\tilde{c}, \tilde{a}$  for OSQD (or  $\tilde{a}, \tilde{c}$  for PSQD) and the adiabatic set of quantum numbers  $\nu = [n_{zo}, n_{\rho o}, m]$  and  $\nu' = [n'_{zo}, n'_{\rho o}, m']$  ( $\nu = [n_{\rho p}, n_{zp}, m]$  and  $\nu' = [n'_{\rho p}, n'_{zp}, m']$ ), where  $m' = -m$ ,  $\tilde{E}_g$  is the band gap width in the bulk semiconductor,  $\tilde{\omega}^{ph}$  is the incident light frequency,  $\tilde{W}_{\nu\nu'}$  is the inter-band transition energy for which  $\tilde{K}(\tilde{\omega}^{ph})$  has the maximal value. We rewrite the expression (28) using dimensionless quantities in reduced atomic units

$$\begin{aligned} \tilde{K}(\omega^{ph}, \tilde{a}, \tilde{c}) &= \tilde{A}\tilde{E}_g^{-1} \sum_{\nu, \nu'} \tilde{I}_{\nu, \nu'} \delta[f_{\nu, \nu'}(u)], \\ f_{\nu, \nu'}(u) &= \lambda_1 \\ &- (2E_g)^{-1} (2E_\nu^e(a, c) + 2E_{\nu'}^h(a, c)(\mu_h/\mu_e)), \end{aligned}$$

where the parameter  $u$  will be defined below,  $\lambda_1 = (\hbar\tilde{\omega}^{ph} - \tilde{E}_g)/\tilde{E}_g$  is the energy of the optical in-

terband transitions scaled to  $\tilde{E}_g$ ,  $2E_g = \tilde{E}_g/\tilde{E}_R^e = 1.43/(5.27 \times 10^{-3})$  is the dimensionless band gap width. For both electron and hole carriers the dimensionless energies  $2E_\nu^e = \tilde{E}_\nu^e/\tilde{E}_R^e$  and  $2E_{\nu'}^h(\mu_h/\mu_e) = \tilde{E}_{\nu'}^h/\tilde{E}_R^e$  are expressed in the same reduced atomic units  $\tilde{E}_R^e$ .

Now consider an ensemble of OSQDs (or PSQDs) with different values of the minor semiaxis  $c = u_o\tilde{c}$  (or  $a = u_p\tilde{a}$ ) determined by the random parameter  $u = u_o$  (or  $u = u_p$ ). The corresponding minor semiaxis mean value is  $\bar{c}$  at fixed major semiaxis  $a$  (or  $\bar{a}$  at fixed major semiaxis  $c$ ) and the appropriate distribution function is  $P(u_o)$  (or  $P(u_p)$ ). Conventionally, they use the normalized Lifshits–Slezov  $P(u) \equiv P^{LS}(u)$  [57] or Gaussian  $P(u) \equiv P^G(u)$  distribution functions ( $\int P(u)du = \int uP(u)du = 1$ ):

$$\begin{aligned} P^{LS}(u) &:= \{3^4 e u^2 \exp(-1/(1 - 2u/3))/2^{5/3}/(u + 3)^{7/3}/(3/2 - u)^{11/3}, u \in (0, 3/2); 0, \text{otherwise}\}, \\ P^G(u) &:= 1/\sqrt{2\pi}/\sigma \exp(-(u - 1)^2/(2\sigma^2)), \end{aligned}$$

where  $\bar{u} = \int uP^G(u)du = 1$  is the mean value of  $u$  and  $\sigma^2 = (\int (u - \bar{u})^2 P^G(u)du)$  is the variance. The absorption coefficient of an ensemble of semiconductor QDs with different dimensions of minor semiaxes is then expressed as

$$\begin{aligned} \tilde{K}^o(\omega^{ph}, \tilde{a}, \tilde{c}) &= \int \tilde{K}(\omega^{ph}, \tilde{a}, \tilde{c}, u_o) P(u_o) du_o, \\ \tilde{K}^p(\omega^{ph}, \tilde{a}, \tilde{c}) &= \int \tilde{K}(\omega^{ph}, \tilde{a}, \tilde{c}, u_p) P(u_p) du_p. \end{aligned}$$

Taking the known properties of the  $\delta$  function into account, we arrive at the analytical expression for the the absorption coefficient  $\tilde{K}(\omega^{ph}, \tilde{a}, \tilde{c})$  of a system of semiconductor QDs with a distribution of minor semiaxes:

$$\begin{aligned} \frac{\tilde{K}(\omega^{ph})}{\tilde{K}_0} &= \sum_{\nu, \nu', s} \frac{\tilde{K}_{\nu, \nu'}(\omega^{ph})}{\tilde{K}_0}, \quad (29) \\ \frac{\tilde{K}_{\nu, \nu'}(\omega^{ph})}{\tilde{K}_0} &= \tilde{I}_{\nu, \nu'} \left| \frac{df_{\nu, \nu'}(u)}{du} \right|_{u=u_s}^{-1} P(u_s), \end{aligned}$$

where  $\tilde{K}_0 = \tilde{A}^{-1}\tilde{E}_g$  is the normalization factor,  $u_s$  are the roots of the equation  $f_{\nu, \nu'}(u_s) = 0$ .

In particular, for Model B of OSQD or PSQD we have the interband overlap  $\tilde{I}_{\nu, \nu'} = \delta_{n_{\rho o}, n'_{\rho o}} \delta_{n_{zo}, n'_{zo}} \delta_{m, -m'}$  for OSQD,

$\tilde{I}_{\nu, \nu'} = (J_{1+|m|}(\alpha_{n_{\rho p}+1, |m|})/J_{1-|m|}(\alpha_{n_{\rho p}+1, |m|}))^2 \times \delta_{n_{zp}, n'_{zp}} \delta_{n_{\rho p}, n'_{\rho p}} \delta_{m, -m'}$  for PSQD, and the selection rules  $n_{zo} = n'_{zo}$ ,  $n_{\rho o} = n'_{\rho o}$ , and  $m = -m'$  or  $n_{\rho p} = n'_{\rho p}$ ,  $n_{zp} = n'_{zp}$  and  $m = -m'$ , respectively. Note that the contributions of non-diagonal matrix elements to the energy values are about 1% for OSQD and PSQD of Model B; then in the Born–Oppenheimer approximation of the order  $b_{\max}$  for the absorption coefficient we get

$$f_{\nu, \nu'}(u) = \lambda_1 - \sum_{j=0}^{b_{\max}} \tilde{E}^{(j)} u^{j-2}. \quad (30)$$

Here the coefficients  $\tilde{E}^{(j)}$  are defined by

$$\begin{aligned} \tilde{E}^{(j)} &= (2E_g)^{-1} E_{io}^{(j)} \omega_{\rho; n_o}^{2-j}(\bar{c})(1 + \mu_e/\mu_h) \quad (31) \\ \text{or } \tilde{E}^{(j)} &= (2E_g)^{-1} E_{ip}^{(j)} \omega_{z; n_{\rho p}}^{2-j}(\bar{a})(1 + \mu_e/\mu_h), \\ \omega_{\rho; n_o}(\bar{c}) &= \pi n_o/(a\bar{c}), \quad \omega_{z; n_{\rho p}}(\bar{a}) = \alpha_{n_{\rho p}+1, |m|}/(\bar{a}c), \\ E_{io}^{(0)} &= a^2/4, \quad E_{io}^{(1)} = (2n_{\rho o} + |m| + 1), \\ E_{io}^{(2)} &= (6n_{\rho o}|m| + 2 + 6n_{\rho o} + 6n_{\rho o}^2 \\ &\quad + |m|^2 + 3|m|)a^{-2}, \\ E_{io}^{(3)} &= 3(6n_{\rho o} + 3|m| + 2 + |m|^2 + 6n_{\rho o}^2 \\ &\quad + 6n_{\rho o}|m| + 4n_{\rho o}^3 + 6|m|n_{\rho o}^2 + 2|m|^2n_{\rho o})a^{-4}/2, \end{aligned}$$

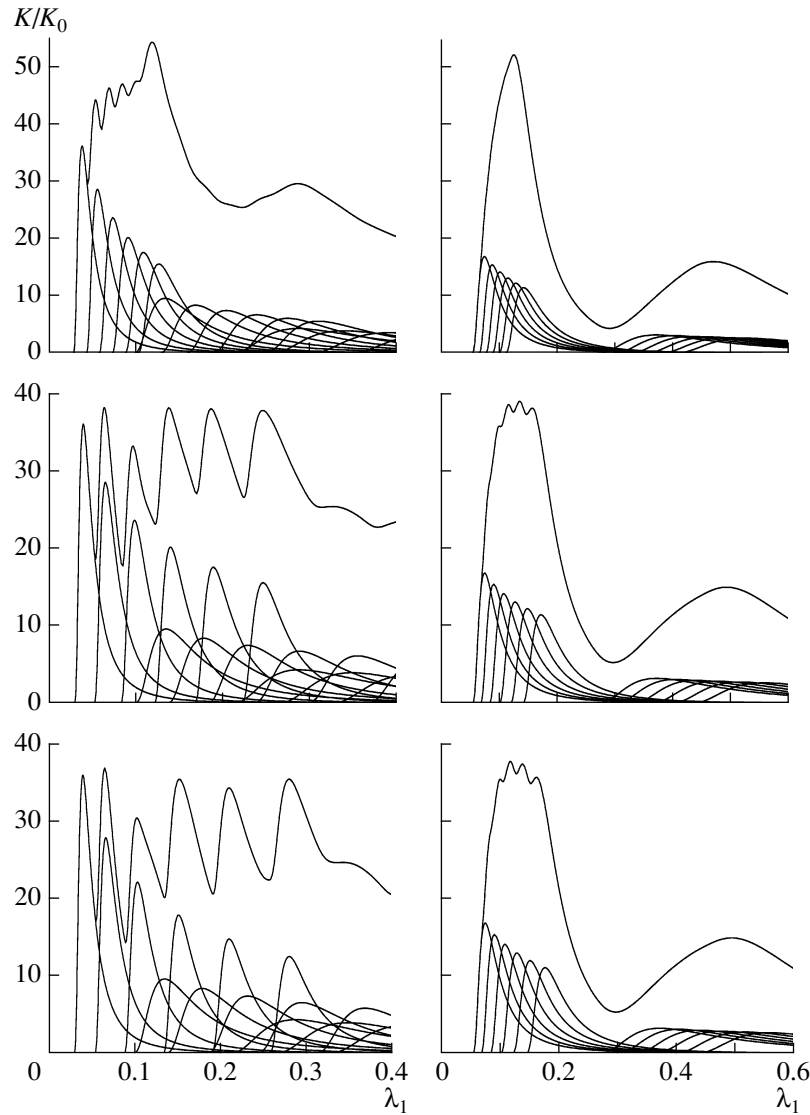


**Fig. 8.** Absorption coefficient  $K/K_0$  from (29) consists of a sum of the first partial contributions versus the energy  $\lambda = \lambda_1$  of the optic interband transitions for the Lifshits–Slezov distribution in first, second, and third (from top to bottom) Born–Oppenheimer approximations: (left panels) for ensemble of OSQDs  $\bar{c} = 0.5$ ,  $a = 2.5$  (summation by  $n_o = 1, 2, 3$ ,  $n_{\rho o} = 0, 1, 2, 3, 4, 5$ ,  $m = 0$ ), (right panels) for ensemble of PSQDs  $\bar{a} = 0.5$ ,  $c = 2.5$  (summation by  $n_p = 1, 2, 3$ ,  $n_{zp} = 0, 1, 2, 3, 4, 5$ ,  $m = 0$ ).

$$\begin{aligned} E_{ip}^{(0)} &= c^2, \quad E_{ip}^{(1)} = (2n_{zp} + 1), \\ E_{ip}^{(2)} &= +3(2n_{zp} + 2n_{zp}^2 + 1)c^{-2}/4, \\ E_{ip}^{(3)} &= 3(3n_{zp}^2 + 7n_{zp} + 2n_{zp}^3 + 3)c^{-4}/16. \end{aligned}$$

The coefficients of the order  $b_{\max} \geq 4$  are calculated by the perturbation theory algorithms [37, 38] using exact solutions of 2D and 1D oscillators with *adiabatic* frequencies  $\omega_{\rho; n_o}(\bar{c})$  and  $\omega_{z; n_{zp}}(\bar{a})$  from (31) that distinguish from conventional ones, for example,  $\omega_{\rho}$  and  $\omega_z$  used in Section 3.1 or in [21, 27]. The accuracy of such approximations up to  $b_{\max} = 5$  is about 4–6

decimal digits in comparison with the numerical results of the crude diagonal adiabatic approximation (CDAA) of Eq. (17) without  $H_{ii}(x_s)$  for the states from Fig. 2a at  $c = 0.5$  and Fig. 4a at  $a = 0.5$ . In the case  $a = c = 1$  the accuracy is only about two decimal digits in comparison with the CDAA of the exact spectrum Eq. (23) of Model B of SQDs [56].

Note that in Model B  $2E_{io}$  and  $2E_{ip}$  monotonically depend upon the parameter  $u$  and, therefore, the algebraic equation  $f_{\nu, \nu'}(u) = 0$  has the only solution in the considered domain of definition. Using the notations  $\lambda'_1 = \lambda_1$  for  $b_{\max} = 1$  and  $\lambda'_1 = \lambda_1 - E_{io}^{(2)}$ , or

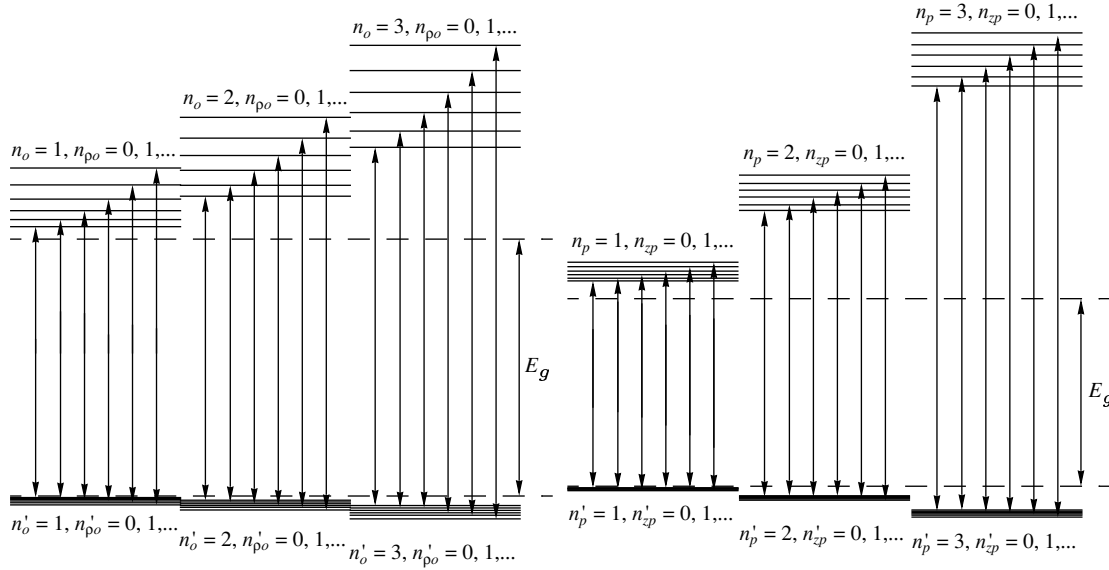


Fig. 9. Schematic plots of interband transition corresponding to Fig. 8.

$\lambda'_1 = \lambda_1 - E_{ip}^{(2)}$  for  $b_{\max} \geq 2$ , we rewrite this equation in the Born–Oppenheimer approximations up to the third order  $b_{\max} \leq 3$

$$f_{\nu,\nu}(u) = \lambda'_1 - \check{E}^{(0)}u^{-2} - \check{E}^{(1)}u^{-1} - \check{E}^{(3)}u = 0,$$

which has the required roots  $u_1 = u_1^{(b_{\max})}$ :

$$u_1^{(1,2)} = (2\lambda'_1)^{-1}(\check{E}^{(1)} + ((\check{E}^{(1)})^2 + 4\lambda'_1\check{E}^{(0)})^{1/2}),$$

$$u_1^{(3)} \approx u_1^{(2)} + \check{E}^{(3)}(u_1^{(2)})^4 / (2\check{E}^{(0)} + \check{E}^{(1)}u_1^{(2)}).$$

For the Lifshits–Slezov distribution Fig. 8 displays the total absorption coefficients  $\tilde{K}(\omega^{ph})/\tilde{K}_0$  and the partial absorption coefficients  $\tilde{K}_{\nu,\nu}(\omega^{ph})/\tilde{K}_0$ , that form the corresponding partial sum (29) over a fixed set of quantum numbers  $\nu$  at  $m = -m' = 0$ . One can see that the summation over the quantum numbers  $n_{zo}$  (or  $n_{pp}$ ) numerating the nodes of the wave function with respect to the fast variable gives the corresponding principal maxima of the total absorption coefficients for the ensemble of QDs with distributed dimensions of minor semiaxis, while the summation over the quantum number  $n_{po}$  (or  $n_{zp}$ ) that label the nodes of the wave function with respect to the slow variable leads to the increase of amplitudes of these maxima and to appearing secondary maxima in the case of sparser energy levels of Model B OSQDs (or PSQDs).

In the regime of strong dimensional quantization the frequencies of the interband transitions between the levels  $n_o = 1$ ,  $n_{po} = 0$ ,  $m = 0$  for OSQD or  $n_p = 1$ ,  $n_{zp} = 0$ ,  $m = 0$  for PSQD in the BO1, at the fixed values  $\tilde{a} = 2.5a_e$  and  $\tilde{c} = 0.5a_e$  for OSQD

or  $\tilde{a} = 0.5a_e$  and  $\tilde{c} = 2.5a_e$  for PSQD, are equal to  $\Delta\tilde{\omega}_{100}^{ph} = 1.64 \times 10^{13} \text{ s}^{-1}$  or  $\Delta\tilde{\omega}_{100}^{ph} = 3.32 \times 10^{13} \text{ s}^{-1}$  ( $\Delta\tilde{\omega}_{100}^{ph} = (2\pi\hbar)^{-1}(\tilde{W}_{100,100} - \tilde{E}_g)$  with the accuracy to 3% and 0.5%, respectively), corresponding to the infrared spectral region [7, 8]. With decreasing semiaxis the threshold energy increases, because the “effective” band gap width increases, which is a consequence of the enhancement of dimensional quantization. Therefore, the above frequency is greater for PSQD than for OSQD, because the OSQD implemented in two directions of the plane  $xy$  is effectively greater than that in the direction of the  $z$  axis solely at similar values of semiaxes. Higher-accuracy calculations reveal an essential difference in the frequency behavior of the absorption coefficient for interband transitions (see Fig. 9) in systems of semiconductor OSQDs or PSQDs having a distribution of minor semiaxes, which can be used to verify the above models.

## 5. CONCLUSIONS

The presented examples of the analysis of energy spectra of SQD, OSQD, PSQD, and DQD models with three types of axially symmetric potentials demonstrate the efficiency of the developed computational scheme and SNA. Only Model A (anisotropic harmonic oscillator potential) is shown to have an equidistant spectrum, while Models B and C (wells with infinite and finite wall height) possess non-equidistant spectra. In Model C, there is a finite number of energy levels. This number becomes smaller as the parameter  $a$  or  $c$  ( $\zeta_{ac}$  or

$\zeta_{ca}$ ) is reduced because the potential curve (lower bound) moves into the continuum. Models A and B have countable discrete spectra. This difference in spectra allows verification of SQD, OSQD, and PSQD models using the experimental data [2], e.g., photoabsorption, from which not only the energy level spacing, but also the mean geometric dimensions of QD may be derived [7, 12, 13]. The considered examples of calculating the absorption coefficient for ensembles of OSQDs or PSQDs with random minor semiaxes in Model B have proved the possibility of a similar verification. It is shown that there are critical values of the ellipsoid aspect ratio, at which in the approximation of effective mass the discrete spectrum of the models with finite-wall potentials turns into a continuous one. Hence, using the experimental data, it is possible to verify different QD models like the lens-shaped self-assembled QDs with a quantum well confined to a narrow wetting layer [4], or to determine the validity domain of the effective mass approximation, if a minor semiaxis becomes comparable with the lattice constant and to proceed opportunely to more adequate models such as [52].

Further development of the method, symbolic–numerical algorithms, and the software package is planned for solving the quasi-2D and quasi-1D BVPs with both discrete and continuous spectrum, which are necessary for calculating the optical transition rates, channeling and transport characteristics in the models like quantum wells or quantum wires and low-energy barrier nuclear reactions.

#### ACKNOWLEDGMENTS

The authors thank Profs. V.I. Furman, V.P. Gerdt, L.G. Mardoyan, G.S. Pogosyan, V.A. Rostovtsev for useful discussions and F.M. Peeters for remarks. This work was done within the framework of the Protocols nos. 3967-3-6-09/11 and 4038-3-6-10/13 of collaboration between JINR (Dubna), RAU (Erevan), and SSU (Saratov) in dynamics of low-dimensional quantum models and nanostructures in external fields. The work was supported partially by RFBR (grants nos. 10-01-00200 and 11-01-00523), and by the grant no. MK-2344.2010.2 of the President of Russian Federation.

#### REFERENCES

1. P. Harrison, *Quantum Well, Wires and Dots* (Wiley, New York, 2005).
2. K. M. Gambaryan, *Nanoscale Res. Lett.* **5**, 587 (2009).
3. V. A. Harutyunyan et al., *Physica E* **36**, 114 (2007).
4. A. Wojs et al., *Phys. Rev. B* **54**, 5604 (1996).
5. L. A. Juharyan et al., *Solid State Commun.* **139**, 537 (2006).
6. A. Michels, J. de Boer, and A. Bijl, *Physica* **4**, 981 (1937).
7. K. G. Dvovyan et al., *Nanoscale Res. Lett.* **2**, 601 (2007).
8. K. G. Dvovyan et al., *Nanoscale Res. Lett.* **4**, 106 (2009); *Proc. SPIE* **7998**, 79981F (2010).
9. Y. E. Kim and A. L. Zubarev, *Phys. Lett. A* **289**, 155 (2001).
10. G. Cantele et al., *J. Phys.: Condens. Matter.* **12**, 9019 (2000).
11. M. van den Broek and F. M. Peeters, *Physica E* **11**, 345 (2001).
12. F. Trani et al., *Phys. Rev. B* **72**, 075423 (2005).
13. A.-M. Lepadatu et al., *J. Appl. Phys.* **107**, 033721 (2010).
14. A. Bagga, P. K. Chattopadhyay, and S. Ghosh, *cond-mat/0406517v1*.
15. I. Filikhin et al., *Physica E* **41**, 1358 (2009).
16. J. Gravesen and M. Willatzen, *Phys. Rev. A* **72**, 032108 (2005).
17. P. M. Morse and P. J. Rubenstein, *Phys. Rev.* **54**, 895 (1938).
18. G. N. Afanasiev, *Sov. J. Part. Nucl.* **21**, 74 (1990).
19. J.-W. Ryu et al., *Phys. Rev. A* **79**, 053858 (2009).
20. S. Granger and R. D. Spencer, *Phys. Rev.* **83**, 460 (1951).
21. A. J. Rassey, *Phys. Rev.* **109**, 949 (1958).
22. Y. Ayant and R. Arvieu, *J. Phys. A* **20**, 397 (1987).
23. F. Brut and R. Arvieu, *J. Phys. A* **26**, 4749 (1993).
24. V. V. Pashkevich, V. M. Strutinsky, *Sov. J. Nucl. Phys.* **9**, 35 (1969).
25. J. Damgaard et al., *Nucl. Phys. A* **135**, 432 (1969).
26. J. Maruhn and W. Greiner, *Z. Phys. A* **251**, 431 (1972).
27. D. N. Poenaru et al., *Phys. Lett. A* **372**, 5448 (2008).
28. H. Hofmann, *Nucl. Phys. A* **224**, 116 (1974).
29. B. Buck and A. A. Pilt, *Nucl. Phys. A* **280**, 133 (1977).
30. S. G. Kadmsky and V. I. Furman, *Alpha Decay and Related Nuclear Reactions* (Energoatomizdat, Moscow, 1985) [in Russian].
31. K. Hagino et al., *Comput. Phys. Commun.* **123**, 143 (1999).
32. V. I. Zagrebaev and V. V. Samarin, *Phys. At. Nucl.* **67**, 1462 (2004).
33. V. I. Zagrebaev et al., *Phys. Part. Nucl.* **38**, 469 (2007).
34. L. V. Kantorovich and V. I. Krylov, *Approximate Methods of Higher Analysis* (Wiley, New York, 1964).
35. A. A. Gusev et al., *Math. Comp. Simul.* (in press); arXiv: 1005.2089 [cond-mat.mes-hall].
36. M. Born and X. Huang, *Dynamical Theory of Crystal Lattices* (Clarendon Press, Oxford, 1954).
37. O. Chuluunbaatar et al., *Lect. Notes Comput. Sci.* **4770**, 118 (2007).
38. S. I. Vinitzky et al., *Lect. Notes Comput. Sci.* **5743**, 334 (2009).
39. A. A. Gusev et al., *Lect. Notes Comput. Sci.* **6244**, 106 (2010).



40. O. Chuluunbaatar et al., *Comput. Phys. Commun.* **180**, 1358 (2009).
41. O. Chuluunbaatar et al., *Comput. Phys. Commun.* **177**, 649 (2007).
42. Yu. N. Demkov, *Sov. Phys. JETP* **9**, 63 (1959).
43. Yu. N. Demkov, *Sov. Phys. JETP* **17**, 1349 (1963).
44. L. A. Il'kaeva, *Vestn. Leningr. Univ.*, No. 22, 56 (1963).
45. H. E. Erikson and E. L. Hill, *Phys. Rev.* **75**, 29 (1949).
46. L. G. Mardoyan et al., Preprint No. P2-85-139, JINR (Dubna, 1985).
47. M. Abramowitz and I. A. Stegun, *Handbook of Mathematical Functions* (Dover, New York, 1965).
48. L. G. Mardoyan et al., *Quantum Systems with Hidden Symmetry* (Fizmatlit, Moscow, 2006) [in Russian].
49. E. G. Kalnins et al., *J. Math. Phys.* **43**, 3592 (2002).
50. R. Courant and D. Hilbert, *Methods of Mathematical Physics. Vol. 1* (Wiley, New York, 1989).
51. T. Oguchi, *Radio Sci.* **5**, 1207 (1970).
52. P. G. Harper, *Proc. Phys. Soc. London A* **68**, 874 (1955).
53. P. G. Akishin, F. Bosco, and S. I. Vinitisky, *Comput. Math. Appl.* **34**, 613 (1997).
54. J. E. Bayfield, *Quantum Evolution an Introduction to Time-Dependent Quantum Mechanics* (Wiley, New York, 1999), p. 207.
55. B. Crespi, G. Perez, and S.-J. Chang, *Phys. Rev. E* **47**, 986 (1993).
56. Al. L. Efros and A. L. Efros, *Sov. Phys. Semicond.* **16**, 772 (1982).
57. I. M. Lifshits and V. V. Slezov, *Sov. Phys. JETP* **8**, 331 (1959).

